Information for Contributors

Manuscripts

Send manuscripts to S. A. Goudsmit, Brookhaven National Laboratory, Upton, Long Island, New York.

Each article submitted will in general consist of (a) textual material, i.e., all material which is to be set in type, and (b) drawings or photographs from which zinc etchings or copper halftones will be made. Textual material will consist of an abstract, the body of the paper, tabular material, references, and figure captions. All of this material must be in English, typewritten (except mathematical expressions) double spaced with wide margins (for editorial instructions to the printer) on a durable, white paper, preferably letter size. The original copy, not the carbon, should be submitted.

For general style, spellings, abbreviations, and form, recent issues of this journal should be consulted.

The prime requisite is that the copy shall be clear to the typesetter, who is neither a physicist nor a mathematician.

Abstracts

An abstract must accompany each article. It should be adequate as an index and as a summary. As an index, it should give all subjects, major and minor, concerning which new information is presented. As a summary it should give the conclusions of the article and all numerical results of general interest.

Mathematical Expressions

All but the simplest mathematical expressions should be carefully printed in by hand. Be sure to distinguish between capital and small letters. Indicate clearly superscripts and subscripts by inverted carets and carets, respectively. Avoid complicated superscripts and subscripts. Avoid repetition of a complicated expression by representing it by some convenient symbol. Identify in the margin Greek letters and unusual symbols. Use fractional exponents instead of root signs. Use the solidus (/) for fractions wherever its use will save vertical space.

References

References should appear as footnotes, numbered consecutively, and arranged thus:

[1] H. Bethe, Phys. Rev. 47, 747 (1935).

[2] J. Frenkel, *Wave Mechanics* (Clarendon Press, Oxford, England, 1932), first edition, pp. 575, 645.

Tables

All but the simplest tabular material should be organized in tabular form rather than as a

THE PHYSICAL REVIEW

A journal of experimental and theoretical physics established by E. L. Nichols in 1893

VOLUME 100

Second Series

OCTOBER 1–DECEMBER 15, 1955

Published for the

AMERICAN PHYSICAL SOCIETY

by the

AMERICAN INSTITUTE OF PHYSICS

Incorporated

THE PHYSICAL REVIEW

A journal of experimental and theoretical physics established by E. L. Nichols in 1893

Published by the American Institute of Physics for the

AMERICAN PHYSICAL SOCIETY

Officers

President

R. T. BIRGE
University of California
Berkeley, California

Vice-President

E. P. WIGNER
Princeton University
Princeton, New Jersey

Secretary

K. K. DARROW
Bell Telephone Laboratories
Office:
Columbia University
New York 27, New York

Treasurer

G. B. PEGRAM
Columbia University
New York 27, New York

Local Secretary for the Pacific Coast

WILLIAM A. NIERENBERG
University of California
Berkeley, California

Managing Editor

S. A. GOUDSMIT
Brookhaven National Laboratory
Upton, Long Island
New York

BOARD OF EDITORS

Editor

S. A. GOUDSMIT

Assistant Editor

S. PASTERNACK

Associate Editors

1953–1955	*1954–1956*	*1955–1957*
W. A. FOWLER	P. G. BERGMANN	G. J. DIENES
KENNETH GREISEN	GREGORY BREIT	R. G. HERB
CHARLES KITTEL	F. J. DYSON	K. G. MCKAY
R. E. MARSHAK	P. KUSCH	J. R. PELLAM
W. K. H. PANOFSKY	R. SMOLUCHOWSKI	LEWI TONKS
V. F. WEISSKOPF	J. C. STREET	GREGOR WENTZEL

Manuscripts for publication should be submitted to S. A. GOUDSMIT, Brookhaven National Laboratory, Upton, Long Island, New York. The authors' institutions are requested to pay a publication charge of $25 per page which, if honored, entitles them to 100 free reprints. Instructions will be sent with galley proofs.

Proof and all correspondence concerning papers in the process of publication should be addressed to the Publication Manager, American Institute of Physics, 57 East 55 Street, New York 22, New York.

Subscription Price

United States and Canada $30.00
Elsewhere $32.00

Back Numbers[1]

Yearly back number rate when complete year is available:
Prior to 1949: $25.00
Thereafter: $33.00
Single copies: $3.00 each, prior to July, 1929;
$1.50 each, July, 1929–December, 1941;
$3.00 each, January, 1942–December, 1946;
$1.50 each, thereafter.
General index, 1893–1920: $4.00.
1921–1950: Paper binding, $10 (Members); $14 (Nonmembers)
Cloth binding, $12 (Members); $16 (Nonmembers)

Subscriptions, renewals, and orders for back numbers should be addressed to the American Institute of Physics, 57 East 55 Street, New York 22, New York.

Changes of address in the case of members of the American Physical Society should be addressed to the Treasurer; in the case of other subscribers to the American Institute of Physics.

[1] For Series 1 inquire of Physics Department, Cornell University, Ithaca, New York.

The Physical Review is published semi-monthly at Prince and Lemon Streets, Lancaster, Pennsylvania.

Entered as second-class matter March 6, 1947, at the Post Office at Lancaster, Pennsylvania, under the Act of March 3, 1879.

Acceptance for mailing at special rate of postage provided for in paragraph (d-2), section 34.40, P. L. & R. of 1948, authorized January 27, 1933.

Copyright 1955 by the American Physical Society

THE
PHYSICAL REVIEW

A journal of experimental and theoretical physics established by E. L. Nichols in 1893

SECOND SERIES, VOL. 100, No. 1 OCTOBER 1, 1955

Independent-Particle Model of the Nucleus. II. Weak Surface Coupling*

KENNETH W. FORD† AND CARL LEVINSON‡
Indiana University, Bloomington, Indiana
(Received May 9, 1955)

The role of weak surface coupling is discussed for multiparticle nuclear configurations. Matrix elements are given for the standard form of the coupling of nucleons to nuclear surface vibrations. Energy spacings, configuration interaction, magnetic moments, quadrupole moments, and $E2$ transition rates are discussed, with emphasis on features independent of special details of particle configurations. Magnetic moments, in particular, become orderly when account is taken of variations of surface coupling strength together with a directly induced configuration mixing. Experimental evidence favors the idea that a true weak coupling situation exists for many nuclei near closed shells. In these nuclei, collective quadrupole effects may be appreciable while all other collective effects are negligible.

I. INTRODUCTION

THE possibly important role in low-energy nuclear phenomena of coupling of nucleons to the nuclear surface has first been pointed out by Foldy and Milford[1] in connection with magnetic moments, and by Rainwater[2] in connection with quadrupole moments. The existence of such surface coupling is inescapable if the nucleons within the nucleus behave in any way like independent particles: the nucleus is certainly deformable, and the (linear) variation of independent particle energy with nuclear deformation leads to surface coupling. In this sense surface coupling and the collective model of the nucleus are automatic consequences of the shell model. In view of the strong evidence for the independent particle behavior of nucleons in the nucleus, the relative importance rather than the existence of surface coupling is in question. Elementary calculation indicates that surface coupling energies may be appreciable relative to direct particle coupling energies for deformations of only a few percent, and one is led to expect surface coupling to play a dominant role in heavy nuclei with more than a few nucleons outside closed shells. Very eloquent and complete discussions of the properties of strongly deformed nuclei have been given by Hill and Wheeler[3] and by Bohr and Mottelson,[4] the latter authors working from the very fruitful strong coupling approximation of Bohr.[5] Certain predictions of the strong coupling model, those regarding the nuclear rotational states,[6,6,7] have been startlingly well confirmed in two regions of the periodic table, comprising roughly neutron numbers 90 to 115 and 135 or more. The agreement with experiment has come in energy level ratios,[4,8] in transition rates,[4,8,9] and in correlations among energies, quadrupole moments,[7] transition rates,[4,10] and atomic isotope shifts.[11] Some important quantitative discrepancies remain,[10,12] but it seems to be well established that nuclei in these regions are very substantially deformed from the spherical shape, which is most easily explained in terms of strong coupling of nucleons to the nuclear surface.

* Supported in part by a grant from the National Science Foundation.
† Now on leave at Max Planck Institut für Physik, Göttingen, Germany.
‡ Now at Palmer Physical Laboratory, Princeton University, Princeton, New Jersey.
[1] L. L. Foldy and F. J. Milford, Phys. Rev. **80**, 751 (1950); F. J. Milford, Phys. Rev. **93**, 1297 (1954).
[2] J. Rainwater, Phys. Rev. **79**, 432 (1950).
[3] D. L. Hill and J. A. Wheeler, Phys. Rev. **89**, 1102 (1953); see also J. Griffin, Bull. Am. Phys. Soc. **30**, No. 3, 48 (1955).
[4] A. Bohr and B. R. Mottelson, Kgl. Danske Videnskab. Selskab, Mat.-fys. Medd. **27**, No. 16 (1953).
[5] A. Bohr, Kgl. Danske Videnskab. Selskab, Mat.-fys. Medd. **26**, No. 14 (1952).
[6] A. Bohr, *Rotational States of Atomic Nuclei* (E. Munksgaard, Copenhagen, 1954).
[7] K. W. Ford, Phys. Rev. **90**, 29 (1953).
[8] A. Bohr and B. R. Mottelson, Phys. Rev. **90**, 717 (1953).
[9] A. Bohr and B. R. Mottelson, Phys. Rev. **89**, 316 (1953).
[10] P. Stelson and F. K. McGowan, Phys. Rev. **99**, 112 (1955); A. W. Sunyar, Phys. Rev. **98**, 653 (1955); G. Temmer and N. P. Heydenberg, Phys. Rev. **98**, 1308 (1955).
[11] Wilets, Hill, and Ford, Phys. Rev. **90**, 1388 (1953).
[12] K. W. Ford, Phys. Rev. **95**, 1250 (1954).

In contrast, there is little experimental evidence for the existence in any nuclei of a weak (but appreciable) coupling of nucleons to nuclear surface. Some rather successful applications of the shell model have been made[13,14] near double closed shells without reference to surface coupling. One motivation in undertaking the present work was the desire to learn whether the existence of weak surface coupling near closed shells or in light nuclei could be detected. It is theoretically expected[3] that the nuclear surface tension, and therefore the strength of particle-to-surface coupling, should show a marked dependence on the shell structure, the coupling being a minimum near closed shells. An analysis of quadrupole moments in terms of single particle effect plus collective deformation[15] indicates that this is the case. More detailed studies[16] near the double closed shell nucleus Pb^{208} and, in a succeeding paper,[17] Ca^{40}, indicate that the effective surface tensions for these doubly-magic cores are at least several times the "hydrodynamic" values,[4] while deviations from pure rotational spectra indicate that the hydrodynamic values are approximately correct in the region of strong coupling.[18] Evidence so far, both theoretical and experimental, then leads to the interesting conclusion that the strength of surface coupling is self-reinforcing, being very strong when strong and almost negligible when weak.

Because of the variation of nuclear surface tension with shell structure, it seems reasonable to expect that there will exist nuclei for which a treatment of weak surface coupling with only one or two phonons of surface excitation included will be adequate. Previous work on weak surface coupling[4,19,20] is extended to several extra shell nucleons in this paper, a numerical example is given of the role of weak surface coupling for configurations $(7/2)^3$ and $(7/2)^2$, and nuclear moments and transition rates are discussed.

II. MATRIX ELEMENTS OF SURFACE INTERACTION

We follow the theory and notation of Bohr and Mottelson and Choudhury,[20] replacing the interaction constant times the radial integral of the surface interaction by an energy, k, whose order of magnitude is twice the kinetic energy of nucleons within the nucleus, and whose value should depend weakly on the angular quantum numbers of the extra nucleons. With this simplification, and the restriction to ellipsoidal surface vibrations, the particle-to-surface interaction becomes:

$$H_{\rm int}=-k[\hbar\omega/2C]^{\frac{1}{4}}\sum_i\sum_\mu(b_\mu+(-1)^\mu b_{-\mu}^*)\times Y_{2\mu}(\theta_i,\varphi_i), \quad (1)$$

where $\hbar\omega=\hbar(C/B)^{\frac{1}{2}}$ is the phonon excitation energy, B is the mass constant in the surface kinetic energy, C is the surface tension constant in the surface potential energy, b_μ and b_μ^* are destruction and creation operators for the phonons with spin two and Z-component of angular momentum μ, $Y_{2\mu}$ is a normalized spherical harmonic, and the index i labels the particles. As is well known, the average of $H_{\rm int}$ over a closed shell is zero, and in practice the sum extends only over those nucleons in unfilled shells. To simplify notation, we define,

$$\mathcal{Y}_{2\mu}=(\pi/5)^{\frac{1}{2}}Y_{2\mu}, \quad (2)$$

and

$$\gamma=(5\hbar\omega/2\pi C)^{\frac{1}{2}}=(5\hbar/2\pi B\omega)^{\frac{1}{2}}, \quad (3)$$

whence

$$H_{\rm int}=-k\gamma\sum_i\sum_\mu(b_\mu+(-1)^\mu b_{-\mu}^*)\mathcal{Y}_{2\mu}(\theta_i,\varphi_i). \quad (4)$$

The zero order nuclear states are taken to be shell model states of configuration α and angular momentum J, vector-coupled to surface excitation states of N phonons and angular momentum R, to yield total angular momentum I, which states we indicate by

$$|\alpha J;NR;IM\rangle. \quad (5)$$

Matrix elements of the interaction between such states can be evaluated according to the methods of Racah,[21,22] since both b_μ and $\mathcal{Y}_{2\mu}$ are tensor operators of rank 2 according to the definitions of Racah. The result is:

$$\langle\alpha J;NR;IM|H_{\rm int}|\alpha' J';N'R';IM\rangle = (-1)^{2J'+J+I+R+1}(k\gamma)W(RR'JJ';2I)(NR\|b\|N'R')\times(\alpha J\|\textstyle\sum_i\mathcal{Y}_2(\theta_i,\varphi_i)\|\alpha' J'), \quad (6)$$

where the double bar reduced matrix elements are defined as in references 21 and 22. Selection rules are: $\Delta N=1$, $\Delta R\leq 2$, $\Delta J\leq 2$, configurations α and α' differ at most in the quantum numbers of one particle, and for that particle, $\Delta l=0$ or 2, $\Delta j\leq 2$. Values of $(NR\|b\|N'R')$ are given in reference 20 up to $N'=3$ (Choudhury's reduced matrix elements should be multiplied by $(2R'+1)^{\frac{1}{2}}$ to give ours). Values of the one-particle matrix elements $(lsj\|\mathcal{Y}_2\|l'sj')$ have been given by Kerman[19] and Choudhury,[20] but their expressions can be very substantially simplified; namely,

$$(isj\|\mathcal{Y}_2\|l'sj')=\tfrac{1}{2}(2j+1)^{\frac{1}{2}}(j2-\tfrac{1}{2}0|j2j'-\tfrac{1}{2}), \quad \Delta l=0,\pm 2, \quad (7)$$

where $(j_1j_2m_1m_2|j_1j_2jm)$ is a Clebsch-Gordan co-

[13] J. P. Elliott and B. H. Flowers, Proc. Roy. Soc. (London) **A229**, 536 (1955).
[14] D. E. Alburger and M. H. L. Pryce, Phys. Rev. **95**, 1482 (1954).
[15] M. G. Mayer, Report of International Conference of Theoretical Physics, Kyoto and Tokyo, 1953 (Science Council of Japan, Tokyo, 1954). M. G. Mayer and J. H. D. Jensen, *Elementary Theory of Nuclear Shell Structure* (John Wiley and Sons, Inc., New York, 1955).
[16] W. True (to be published).
[17] C. Levinson and K. W. Ford, following paper [Phys. Rev. **100**, 13 (1955)].
[18] E. L. Church and M. Goldhaber, Phys. Rev. **95**, 626 (1954).
[19] A. K. Kerman, Phys. Rev. **92**, 1176 (1953).
[20] D. C. Choudhury, Kgl. Danske Videnskab. Selskab, Mat.-fys. Medd. **28**, No. 4 (1954).
[21] G. Racah II, Phys. Rev. **62**, 438 (1942); III, Phys. Rev. **63**, 367 (1943); IV, Phys. Rev. **76**, 1352 (1949).
[22] Simon, Van der Sluis, and Biedenharn, Oak Ridge National Laboratory ORNL-1679, 1954 (unpublished).

efficient.[23] This result is found as follows: the expressions of Choudhury and Kerman are proportional to the product of a Racah and a Clebsch-Gordan coefficient. By Eq. (2), p. x, in reference 22, this product may be set equal to a sum over three Clebsch-Gordan coefficients. But the sum has only two terms and two of the three coefficients can be written down explicitly since they involve spin ½. The reduction to (7) then follows easily.

For two-particle configurations, Eq. (44) of Racah II[21] may be used to give the reduced particle matrix elements. Several cases are to be distinguished:

(a) off diagonal:

$$(j_1j_2J\|\textstyle\sum_i\mathcal{Y}_2(i)\|j_1'j_2J') = (-1)^{j_2-j_1'-J}[(2J+1)(2J'+1)]^{\frac{1}{2}} \times W(j_1Jj_1'J';j_22)(j_1\|\mathcal{Y}_2\|j_1'), \quad (8)$$

where j is used as shorthand for all particle quantum number, e.g., nlj;

(b) diagonal, inequivalent particles:

$$(j_1j_2J\|\textstyle\sum_i\mathcal{Y}_2(i)\|j_1j_2J') = (-1)^{j_2-j_1-J}[(2J+1)(2J'+1)]^{\frac{1}{2}} \times[(j_1\|\mathcal{Y}_2\|j_1)W(j_1Jj_1J';j_22) + (j_2\|\mathcal{Y}_2\|j_2)W(j_2Jj_2J';j_12)]; \quad (9)$$

(c) diagonal, equivalent particles:

$$(j^2J\|\textstyle\sum_i\mathcal{Y}_2(i)\|j^2J') = 2(-1)^J[(2J+1)(2J'+1)]^{\frac{1}{2}} \times(j\|\mathcal{Y}_2\|j)W(jJjJ';j2). \quad (10)$$

For configurations of more than two particles, expansions of the particle wave functions in terms of fractional parentage coefficients become necessary. We state the result for the reduced particle matrix elements only for the special case of the configuration $(j)^n$ of equivalent particles. Then

$$(j^nJ\|\textstyle\sum_i\mathcal{Y}_2(i)\|j^nJ') = n(-1)^{j-J}[(2J+1)(2J'+1)]^{\frac{1}{2}} \times(j\|\mathcal{Y}_2\|j)\sum_{J_1}(-1)^{J_1} \times(J[J_1)W(jJjJ';J_12)(J_1]J'), \quad (11)$$

where $(J_1]J)$ is shorthand for the fractional parentage coefficient, i.e.,

$$(J_1]J) = (j^{n-1}J_1jJ]j^nJ). \quad (12)$$

Fractional parentage expansions of configurations of inequivalent particles have been discussed by Redlich[24] and by Meshkov[25] and are used in the succeeding paper.[17]

Fractional parentage methods may also be used to find the reduced surface matrix elements $(NR\|b\|N'R')$.

[23] E. U. Condon and G. H. Shortley, *The Theory of Atomic Spectra* (Cambridge University Press, London, 1951).
[24] M. Redlich, Ph.D. thesis, Princeton University, 1954 (unpublished).
[25] S. Meshkov, Phys. Rev. **91**, 871 (1953).

TABLE I. Two-phonon to three-phonon fractional parentage coefficients.

R \ R'	0	2	3	4	6
0		$(7/15)^{\frac{1}{2}}$			
2	1	$(4/21)^{\frac{1}{2}}$	$(5/7)^{\frac{1}{2}}$	$(11/21)^{\frac{1}{2}}$	
4		$(12/35)^{\frac{1}{2}}$	$-(2/7)^{\frac{1}{2}}$	$(10/21)^{\frac{1}{2}}$	1

Between 0 and 1 phonon,

$$(00\|b\|12) = 5^{\frac{1}{2}}. \quad (13)$$

Between 1 and 2 phonons,

$$(12\|b\|2R') = 2^{\frac{1}{2}}[5(2R'+1)]^{\frac{1}{2}}(00\|b\|12)W(022R';22) = [2(2R'+1)]^{\frac{1}{2}}. \quad (14)$$

Between 2 and 3 phonons,

$$(2R\|b\|3R') = 3^{\frac{1}{2}}[(2R+1)(2R'+1)]^{\frac{1}{2}}(00\|b\|12) \times W(0R2R';R2)(R_0^3(R)R_0R']R_0^3R') = [3(2R'+1)]^{\frac{1}{2}}(R_0^3(R)R_0R']R_0^3R'), \quad (15)$$

where $R_0=2$, the angular momentum of each phonon. The phonon fractional parentage coefficients may be found, following Racah III,[21] by means of the relations (required to make the total wave function symmetric):

$$\textstyle\sum_R(2R+1)^{\frac{1}{2}}W(22R'2;RR'')(2^2(R)2R']2^2R') = 0, \quad (16)$$

where R is summed over the allowed 2-phonon values 0, 2, 4; R' is the 3-phonon angular momentum; and R'' is 1 or 3, the unallowed 2-phonon angular momenta. Table I gives the two-phonon to three-phonon parentage coefficients.

III. DISCUSSION OF WEAK SURFACE COUPLING

A. Effective Scalar Interaction

The contribution of surface coupling to the nuclear energy takes a very simple form in the limit of strong coupling, giving the characteristic rotational states whose energies are independent of details of the particle structure. This is the limit of nuclear deformation large compared to amplitude of surface vibration, or of surface coupling energies large compared to interparticle interaction energies, or of surface rotation frequency slow compared to particle motion, so that the particle structure adjusts adiabatically to the surface shape. The opposite limit of weak coupling is also of special interest and simplicity, although of course it has no such marked consequences as the strong coupling limit. The weak coupling limit may be defined by mean deformation small compared to amplitude of surface vibration, by phonon energy large compared to spacing of particle levels, or by frequency of surface vibration large compared to particle frequencies, i.e., the adiabatic adjustment of the surface shape to the particle

structure. By the nature of the surface interaction (its relation to the kinetic energy of the nucleons), a weak coupling situation with particle energy spacings larger than phonon energies is not reasonable, and therefore configuration interaction is an essential part of weak coupling.[26]

In a one-phonon approximation, the energy shift of the configuration $\alpha J(I=J)$ is, by second-order perturbation theory,

$$\Delta E(\alpha J) = -\sum_{\alpha' J'} \frac{|\langle \alpha J; 00; IM|H_{\rm int}|\alpha' J'; 12; IM\rangle|^2}{\hbar\omega + E^{(0)}(\alpha' J') - E^{(0)}(\alpha J)}, \quad (16)$$

where $\hbar\omega$ is the phonon energy. In the weak coupling limit, $|E^{(0)}(\alpha' J') - E^{(0)}(\alpha J)| \ll \hbar\omega$, for many configurations. In the crudest approximation, the numerator in (16) is supposed to cut off before the denominator differs appreciably from $\hbar\omega$. Then

$$\Delta E(\alpha J) \cong -(\hbar\omega)^{-1} \sum_{\alpha' J'} |\langle \alpha J; 00; IM|H_{\rm int}|\alpha' J'; 1,2; IM\rangle|^2$$
$$= -(\hbar\omega)^{-1} \langle \alpha J; 00; IM|(H_{\rm int})^2|\alpha J; 00; IM\rangle. \quad (17)$$

As has been previously pointed out,[4,19] the surface interaction then reduces in this approximation to an effective scalar two body interaction—where the surface phonon plays a role analogous to the meson in the ordinary nucleon-nucleon force. Integration over surface coordinates in (17) gives the effective scalar potential, due to surface interaction,

$$V_s = -[(k\gamma)^2/\hbar\omega] \sum_{ij} \sum_{\mu} Y_{2\mu}^*(i) Y_{2\mu}(j), \quad (18)$$

where it is to be noted that self-energy terms $(i=j)$ are included.

There are several flaws in these arguments leading to (18) coming from the assumed localization of the surface interaction at the nuclear surface, i.e., $H_{\rm int} \sim \sum \delta(r_i - R)$ in a square well model. This means that the matrix elements in (16) depend so weakly on the radial quantum numbers of the nucleons that the convergence of the sum (16) is questionable. If the surface interaction is spread out over a reasonable edge thickness, then the principal quantum number dependence of the terms in (16) will produce the desired cutoff, but only at very high excited states. Thus the energy $E^{(0)}(\alpha' J') - E^{(0)}(\alpha J)$ in the denominator of (16) may not be ignored relative to $\hbar\omega$. This difficulty may be avoided as follows. We note that for a given principal quantum number n, there are a finite number of configurations α' which can mix with α, limited by the selection rules stated after Eq. (6). These form a complete set for the angular dependence of $H_{\rm int}$, and in the weak coupling limit, this set will occur within an energy region less than $\hbar\omega$. If the weak dependence of the radial part of $H_{\rm int}$ on angular quantum numbers is ignored, (16) may be approximated as

$$\Delta E(\alpha J) = -\sum_n f(n) \times \sum_{\alpha' J'}{}' \frac{|\langle \alpha J; 00; IM|H_{\rm int}'|\alpha' J'; 1\,2; IM\rangle|^2}{\hbar\omega + E^{(0)}(\alpha' J') - E^{(0)}(\alpha J)}, \quad (19)$$

where the primes on $H_{\rm int}$ and on the sum indicate that the radial dependence and radial quantum numbers respectively are not involved. Then for each n, the closure approximation may be applied to the angular sum in (19) with a suitable average energy denominator, $\hbar\omega + \Delta(n)$, to give

$$\Delta E(\alpha J) \cong -\{\sum_n [\hbar\omega + \Delta(n)]^{-1} f(n)\} \times \langle \alpha J; 00; IM|(H_{\rm int}')^2|\alpha J; 00; IM\rangle. \quad (20)$$

This expression differs from (17) in having $(\hbar\omega)^{-1}$ replaced by the curly bracket, and in having the radial dependence of $H_{\rm int}$ removed. The latter change is important, since in the delta function approximation of the radial dependence of $H_{\rm int}$, Eq. (17) leads to infinite self-energy terms in (18), while Eq. (20) leads properly to the relative magnitudes of mutual and self-energy given in (18).

Neither of the possible uncertainties in the scalar interaction (18) is significant for energy levels. The over-all strength of interaction is uncertain, but should be regarded as an adjustable parameter of the theory in any case. The relative size of the mutual- and self-energy terms has no effect on level spacings of a given configuration, since the self-energy terms affect all levels of a given configuration equally. Thus for spacings within a given configuration, the self-energy terms may be ignored altogether. Then this limiting form of the surface interaction may be treated exactly as an ordinary two-body force, except that only diagonal elements are to be taken, since the surface induced configuration mixing is already included.

For configuration $(j)^n$ of equivalent particles, the interaction (18) leads to simple expressions for the surface contribution to nuclear energy levels. We rewrite (18) as,

$$V_s = \epsilon_0 [\sum_{i>j} v_{ij} + \sum_i v_i], \quad (21)$$

where

$$v_{ij} = -\sum_\mu Y_{2\mu}^*(i) Y_{2\mu}(j) = -\sum_\mu (-1)^\mu Y_{2,-\mu}(i) Y_{2\mu}(j), \quad (22)$$

$$v_i = -\tfrac{1}{2} \sum_\mu (-1)^\mu Y_{2,-\mu}(i) Y_{2\mu}(i), \quad (23)$$

and ϵ_0 is the energy unit of the interaction, given roughly, as in (18) by $+2(k\gamma)^2/\hbar\omega$.

[26] See, however, a recent paper by G. Scharff-Goldhaber and J. Weneser [Phys. Rev. 98, 212 (1955)], who suppose that direct particle coupling energies may be larger than phonon energies.

The mutual interaction term v_{ij} has the form of the scalar product of two tensors of rank two, and can be treated by the standard Racah methods.[21] For the configuration $(j)^2$,

$$\langle j^2 J | v_{12} | j^2 J \rangle = | (j \| Y_2 \| j) |^2 W(jjjj; 2J), \quad (24)$$

a result already given by Kerman.[19] We note from (7)

$$(j \| Y_2 \| j) = -\frac{1}{8}\left[\frac{(2j-1)(2j+1)(2j+3)}{j(j+1)}\right]^{\frac{1}{2}}. \quad (25)$$

The Racah coefficient in (24) is not in general a monotonic function of J (for J even), but it is monotonic if j is not too large. Two-particle configurations and level orders from (24) are: $(3/2)^2$, 0, 2; $(5/2)^2$, 0, 2, 4; $(7/2)^2$, 0, 2, 4 and 6 degenerate; $(9/2)^2$, 0, 2, 4, 8, 6.

The reduced one-particle matrix element of (23) is

$$(j \| v_1 \| j) = \tfrac{1}{2}(2j+1)^{\frac{1}{2}}. \quad (26)$$

Therefore the matrix elements of the self-energy term, $\sum_i v_i$, are, for the configuration $(j)^n$,

$$\langle j^n J | \textstyle\sum_i v_i | j^n J \rangle = -n/8, \quad (27)$$

independent of J.

For more than two equivalent particles, the mutual interaction energy is,[21] in units of ϵ_0,

$$\langle j^n \alpha J | \sum_{i>j} v_{ij} | j^n \alpha' J \rangle = [n/(n-2)] \sum_{\alpha'' \alpha''' J'} (\alpha J \{ \alpha'' J')(\alpha''' J' \} \alpha' J) \times \langle j^{n-1} \alpha'' J' | \textstyle\sum v_{ij} | j^{n-1} \alpha''' J' \rangle, \quad (28)$$

where an abbreviated notation is used for the fractional parentage coefficients:

$$(\alpha'' J' \} \alpha J) = (j^{n-1}(\alpha'' J') j \alpha J \} j^n \alpha J). \quad (29)$$

Surface contributions to nuclear energy in the weak coupling limit are given in Fig. 1 for all configurations $(j)^n$ of equivalent particles through $j=7/2$ and for $(9/2)^3$. Configurations $(j)^{-n}$ are equivalent to $(j)^n$. The required parentage coefficients were taken from Edmonds and Flowers.[27] For the configuration $(5/2)^3$, $I=j=5/2$ lies lowest, in contrast to the strong-coupling limit where $I=j-1$ lies lowest for all j. For $(7/2)^3$, $I=j-1$ also lies lowest in the weak coupling limit,[28] although by a relatively small amount. Thus the occurrence in Ca^{43}, with configuration $(f_{7/2})^3$, of a ground state spin 7/2 must be attributed to interactions other than surface coupling (this nucleus is discussed in detail in a succeeding paper).[17]

[27] A. R. Edmonds and B. H. Flowers, Proc. Roy. Soc. (London) **A214**, 515 (1952). Among the coefficients of fractional parentage needed in our work, we noted several typographical errors in this paper. In first line of Table III, change $5/(14)^{\frac{1}{2}}$ to $(5/14)^{\frac{1}{2}}$ and $3/14$ to $3/(14)^{\frac{1}{2}}$. In last line of Table V, change $(5/22)^{\frac{1}{2}}$ to $-(5/22)^{\frac{1}{2}}$.

[28] A remark on p. 35 of reference 4 appears to be in error on this point.

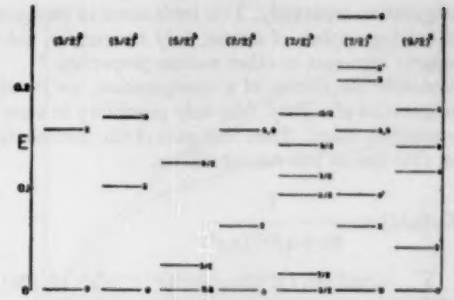

FIG. 1. Surface-induced energy spacings for simple configurations in weak coupling limit, in units of ϵ_0 [see Eqs. (18), (21), (24), and (28)]. For configuration $(7/2)^4$, primes on spins 2 and 4 indicate seniority 4 states.

Among the configurations shown in Fig. 1, only $(7/2)^4$ has more than one level of a given angular momentum. These levels are most conveniently classified according to seniority,[21,29] and, in fact, the inter-seniority matrix elements vanish for $(7/2)^4$. These matrix elements may be expanded in terms of the two particle matrix elements as,

$$(j^4 v_1 I | \sum_{i>j} v_{ij} | j^4 v_2 I) = 6 \sum_{J_2} \{ \sum_{J_3} (v_1 I \{ J_3) \times (J_3 \} v_2 I) | (J_2 \} J_3) |^2 \} (j^2 J_2 | v_{12} | j^2 J_2), \quad (30)$$

where v is the seniority quantum number, and the parentage coefficients are abbreviated in an obvious way: J_2 is two-particle angular momentum, J_3 is three-particle angular momentum. For $j=7/2$, and $v_1 \neq v_2$ ($I=2$ and 4), it has been verified[30] that the quantity in curly brackets vanishes. Therefore, for this configuration, seniority is a good quantum number for all scalar two-body operators. A more general result has not been found.

B. Configuration Interaction

The appropriate surface-induced potential (18), which springs from the assumption that many particle levels lie within an energy $\hbar\omega$, might appear inadequate in a particular nucleus, and one would be led to examine the perturbation expression (16) to see in greater detail the effect of specific configuration mixing induced by weak surface coupling. The interesting result is that for groups of equivalent particles, configuration mixing, like the self-energy contribution in (18), affects all levels of a given configuration equally, therefore the energy spacing[5] calculated from (18) are exactly the same as those calculated from only the diagonal elements in (16). That is, in the sum (16), all off diagonal (in *angular* quantum numbers) matrix elements give contributions independent of I. Moreover, this independence of I holds for the effect of each admixed

[29] B. H. Flowers, Proc. Roy. Soc. (London) **A212**, 248 (1952).
[30] C. Schwartz and A. de-Shalit, Phys. Rev. **94**, 1257 (1954).

configuration separately. This irrelevance of configuration mixing applies, of course, only to energies, not to magnetic moments or other nuclear properties.

Consider the mixing of a configuration, $\alpha=j^n$, with configuration $\alpha'=j^{n-1}j'$ (the only possibility in view of the selection rules). Then that part of the perturbation sum (16) due to this mixing will be,

$$\Delta E_{\alpha'}(\alpha\beta J)=-\frac{1}{\hbar\omega+\Delta E^{(0)}(\alpha,\alpha')}\times\sum_{\beta''J''J'}|\langle j^n\beta J;00;IM|H_{\rm int}|j^{n-1}(\beta''J'')j'J';12;IM\rangle|^2, \tag{31}$$

where β represents other quantum numbers possibly required to specify the states, e.g., seniority. Note that no other quantum number β' is required with J'. From the general formula (6) for the matrix elements of $H_{\rm int}$, one has

$$|\langle\alpha J;00;IM|H_{\rm int}|\alpha'J';12;IM\rangle|^2=5(2I+1)^{-1}(k\gamma)^2|(\alpha J\|\textstyle\sum_i\mathcal{Y}_2(i)\|\alpha'J')|^2. \tag{32}$$

Now one expands the antisymmetrized states,

$$\langle j^n\beta J|=\sum_{\beta_1J_1}\langle j^n\beta J[j^{n-1}(\beta_1J_1)j\beta J)\times\langle j^{n-1}(\beta_1J_1)j_n\beta J|, \tag{33}$$

and

$$|j^{n-1}(\beta''J'')j'J')=n^{-\frac{1}{2}}|j^{n-1}(\beta''J'')j_n'J')+\sum_{\beta'''J'''}a_{\beta''',J'''}|j^{n-2}j'(\beta'''J''')j_nJ'), \tag{34}$$

combinations of $(n-1)$ particles vector-coupled to the nth particle, and the subscripts n indicate the dependence only on the coordinates of the nth particle. Equation (34) is a straightforward generalization of a three-particle result of Redlich.[24] In this case the coefficients $a(\beta'''J''')$ do not concern us. The reduced matrix element in (32) becomes

$$(\alpha J\|\textstyle\sum_i\mathcal{Y}_2(i)\|\alpha'J')=n^{\frac{1}{2}}\langle j^n\beta J[j^{n-1}(\beta''J'')j\beta J)\times(j^{n-1}(\beta''J'')j_n\beta J\|\mathcal{Y}_2(n)\|j^{n-1}(\beta''J'')j_n'J'). \tag{35}$$

The right side of (35) may be reduced by means of Eq. (44) in Racah II.[21] The shift due to configuration interaction, Eq. (31), then becomes

$$\Delta E_{\alpha'}(\alpha\beta J)=-\left[\frac{(k\gamma)^2}{\hbar\omega+\Delta E^{(0)}(\alpha,\alpha')}\right]|(j\|\mathcal{Y}_2\|j')|^2\cdot5n\times\sum_{\beta''J''}|\langle j^{n-1}(\beta''J'')j\beta J]j^n\beta J)|^2\times\sum_{J'}(2J'+1)W^2(jj'JJ';2j). \tag{36}$$

The sum over J' in (36) is just $(2j+1)^{-1}$, by the orthogonality condition, while the normalization of the fractional parentage coefficients makes the sum over β'' and J'' equal to unity. Writing simply ϵ for the energy contained in the square brackets in (36), we obtain finally,

$$\Delta E_{\alpha'}(\alpha\beta J)=-5n\epsilon(2j+1)^{-1}|(j\|\mathcal{Y}_2\|j')|^2, \tag{37}$$

independent of J. It is to be noted that this result is not peculiar to the form of $H_{\rm int}$, but holds for all scalar operators of the one-particle form, $\sum_i f_i$. The result depends essentially on the inequivalence of j and j'. If J' could not take on all values consistent with vector coupling of J'' and j', then the sum over J' in (36) would retain a dependence on J. Thus for more complicated initial configurations, α, the result that the configuration interaction energy shift is independent of J need not remain true.

IV. NUMERICAL EXAMPLE: $f_{7/2}$ SHELL

As an example of the influence of weak surface coupling on the energies of multiparticle configuration, the surface interaction energy matrices have been numerically diagonalized for the configurations $(f_{7/2})^2$ and $(f_{7/2})^3$ [or equivalently, $(g_{7/2})^2$ and $(g_{7/2})^3$] including 1 or 2 phonons. Direct interparticle forces have been ignored, and configuration mixing has been ignored, in the example. As shown above, other configurations do not contribute to level splitting in the weak coupling limit, although they may become important when two phonons are important.

The calculation may conveniently be carried out in dimensionless form. The energy unit is $k\gamma$ [Eqs. (3) and (4)], the natural unit for expressing the interaction energy, and we define a dimensionless measure of the phonon energy, $\xi^{-1}=(\hbar\omega/k\gamma)$; ξ plays the role of coupling constant, and is related to the coupling constant x used in references 4 and 20 by

$$\xi=(8j)^{\frac{1}{2}}x. \tag{38}$$

The eigenvalues obtained by diagonalizing the energy matrices through one or two phonons are $\lambda=E/k\gamma$. These dimensionless results, λ *vs* ξ are given, for configurations $(7/2)^2$ and $(7/2)^3$ in Figs. 2 and 3 and Tables II and III. The translation to energy units de-

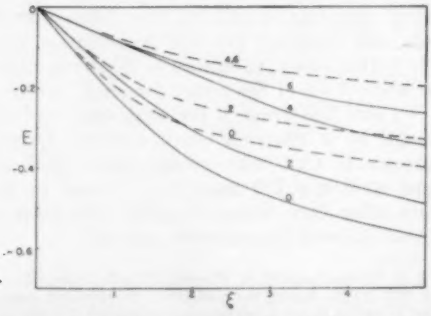

FIG. 2. Surface-induced energy shifts of levels of $(7/2)^2$ configuration. Dashed lines: one phonon included. Solid lines: two phonons included. Vertical scale, energy in units $k\gamma$ [see above Eq. (38)]. Horizontal scale, coupling strength ξ [see above Eq. (38)].

pends somewhat on one's assumptions about the parameters of the collective theory. For example, one may assume that the interaction constant, k, and the mass parameter, B, are known, and that all of the variation of phonon energy comes from the variation of effective surface tension, C. Thus, if we choose $k=40$ Mev, and $B=(3/8\pi)MR^2$, with $R=1.40\times10^{-13}A^{\frac{1}{3}}$ cm, or $\hbar^2/B=179A^{-\frac{5}{3}}$ Mev, and if C is eliminated in favor of $\hbar\omega$, we obtain the energy unit

$$k\gamma=478A^{-\frac{5}{6}}(\hbar\omega \text{ Mev})^{-\frac{1}{2}}, \tag{39}$$

and the coupling constant,

$$\xi=478A^{-\frac{5}{6}}(\hbar\omega \text{ Mev})^{-\frac{1}{2}}. \tag{40}$$

Table II gives the energies in the weak coupling limit, good in the linear regions of Figs. 2 and 3, roughly for $\xi<0.7$. The results of exact matrix diagonalization are given in Table III, for one, two, and, for the special case $I=0$, three phonons, and are plotted in Figs. 2 and 3. Because of the difficulties of exact matrix diagonalization, the results are incomplete. The lowest levels of spin 0, 2, 4, and 6 for $(7/2)^2$ are shown for one and two phonons included in Fig. 2. In order better to illustrate the range of validity, we show in Fig. 4 the energy shifts of the spin-zero state only, for one, two, and three phonons. It is evident from the figure that the one-phonon result is accurate for $\xi\lesssim0.8$, and the two-phonon result for $\xi\lesssim2$. The weak coupling two particle result differs from the strong coupling result principally in having a small spacing of the 4+ and 6+ states. Both weak- and strong-coupling results differ qualitatively from the results for short-range particle forces in having a smaller 0-2:2-4 ratio of spacings. The four-particle configuration, $(7/2)^4$ gives rise, in the weak-coupling limit, to the same surface-induced energy spacings as $(7/2)^2$.

The energy level order of the $(7/2)^3$ configuration due to weak surface coupling is 5/2, 7/2, 11/2, 3/2, 9/2, 15/2, while the lowest two states in strong coupling also are 5/2, 7/2. In Fig. 3, only the states of lowest spin, 3/2, 5/2, 7/2, have been calculated with two phonons. The surface-induced level spacings, for any

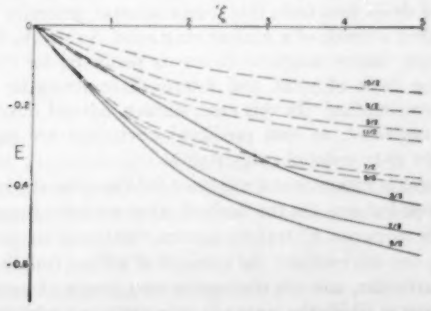

FIG. 3. Surface-induced energy shifts of levels of $(7/2)^3$ configuration. Dashed lines: one phonon included. Solid lines: two phonons included. Scales as in Fig. 2.

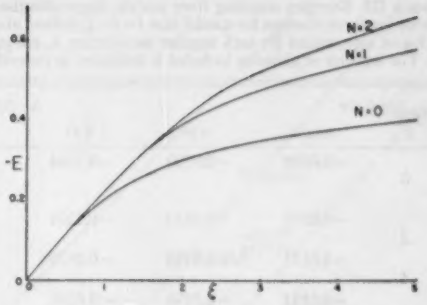

FIG. 4. Surface-induced energy of spin-zero state of $(7/2)^3$ configuration resulting from exact matrix diagonalization, including one, two, and three phonons. (*Note:* From top to bottom, the curves should read $N=3$, $N=2$, and $N=1$, respectively.)

TABLE II. Energies in weak coupling limit.

Configuration $(7/2)^2$		Configuration $(7/2)^3$	
I	λ[a]	I	λ[a]
0	−15/63	5/2	− 59/252
2	−11/63	7/2	− 55/252
4	− 5/63	11/2	− 5/36
6	− 5/63	3/2	− 71/588
		9/2	−157/1764
		15/2	− 5/84

[a] λ is the energy shift due to the surface-induced interaction in the weak coupling limit, in units $\xi(k\gamma)=(k\gamma)^2/\hbar\omega$.

strength of coupling, differ from the direct particle force induced spacing in having the $I=5/2$ state lower than the $I=7/2$.

Energy matrices involving both surface coupling and direct particle coupling have been diagonalized for the same two and three particle configurations, but since special assumptions about the particle matrix elements were made, the results are primarily of qualitative significance. The approximate method of adding together the separate particle and surface induced shifts differs from the result of simultaneous diagonalization principally in overestimating the shifts of the spin 0 (for two particles) or spin 7/2 (for three) states. These results have been used in an attempt to set an upper limit on the strength of surface coupling in the calcium isotopes.[17]

V. MOMENTS AND TRANSITION RATES

A. Magnetic Moments

The existence of surface coupling contributes to nuclear magnetic moments by (1) mixing particle configurations, and (2) contributing directly due to the sharing of the particle angular momentum with the core.[4] For weak coupling, the first effect is likely to be of greater significance, but *neither* effect is important compared to the configuration mixing induced by direct particle forces. This is because weak coupling affects magnetic moments only in second order. Let the wave function be a superposition of the states given in Eq.

TABLE III. Energies resulting from matrix diagonalization for pure particle configurations, $(7/2)^2$ and $(7/2)^3$, through one or two phonons (or three phonons for special case $I=0$). ξ, defined above Eq. (38) and approximated by (40), measures the strength of coupling. The lowest eigenvalues for each angular momentum, λ, are given in units of $k\gamma$, which is defined by Eq. (3) and approximated by Eq. (39). The number of phonons included is indicated in parentheses at the right of each row.

A. $(7/2)^2$ configuration

I \ ξ	0.1667	0.25	0.75	1.00	2.50	2.86	5.0	N
0	−0.0396	−0.0590	−0.1594		−0.3274		−0.3981	(1)
				−0.2233		−0.4643	−0.5737	(2)
				−0.2249		−0.5001	−0.6517	(3)
2	−0.0291	−0.0432	−0.1201		−0.2632		−0.3297	(1)
				−0.1679		−0.3792	−0.4896	(2)
4	−0.0132	−0.0198	−0.0570		−0.1455		−0.1989	(1)
				−0.0812		−0.2320	−0.3414	(2)
6	−0.0132	−0.0198	−0.0570		−0.1455		−0.1989	(1)
				−0.0789		−0.1888	−0.2622	(2)

B. $(7/2)^3$ configuration

I \ ξ	0.1667	0.25	0.75	1.00	2.50	2.86	5.0	N
5/2	−0.0390	−0.0580	−0.1570		−0.3235		−0.3941	(1)
						−0.4604	−0.5739	(2)
7/2	−0.0364	−0.0538	−0.1473		−0.3081		−0.3777	(1)
							−0.5215	(2)
11/2	−0.0232	−0.0344	−0.0970		−0.2230		−0.2859	(1)
3/2	−0.0201	−0.0300	−0.0850		−0.2009		−0.2615	(1)
				−0.1232		−0.3253	−0.4448	(2)
9/2	−0.0148	−0.0220	−0.0636		−0.1692		−0.2146	(1)
15/2	−0.0099	−0.0148	−0.0432		−0.1154		−0.1636	(1)

(5). Then for weak surface coupling but no direct coupling, there will be only one component with amplitude of order unity, which will have $N=0$. Amplitudes of $N=1$ states will be of first order in the coupling strength, while $N=2$ states and other $N=0$ states will be of second order. The magnetic moment operator,

$$\mu_z=\sum_i g_i j_{iz}+g_R R_z, \tag{41}$$

is diagonal with respect to N, the number of phonons. Therefore the off diagonal contributions and the $N=1$ contributions, both diagonal and off-diagonal, are of second order. With direct particle coupling, however, other $N=0$ states and correspondingly the off-diagonal contributions to μ, are introduced in first order in the strength of direct coupling.

We conclude that for weak surface coupling, deviations of nuclear magnetic moments from the pure state values (in some cases the Schmidt lines) are due principally to configuration mixing induced by direct particle forces. In strong coupling, surface induced deviations from the $(l+\frac{1}{2})$ Schmidt line may be of the same order as the shifts due to configuration mixing, but even in strong coupling, shifts away from the $(l-\frac{1}{2})$ Schmidt lines are expected to be due primarily to configuration mixing. The smallness of the collective corrections to magnetic moments has been confirmed by calculations in weak coupling with various assumptions about the strength of coupling and the degree of mixing.[31] Predicted deviations from this source amount generally to less than a tenth of a nuclear magneton. Table IV, for example, shows magnetic moments predicted for Ca^{43} on the basis of weak and intermediate strengths of surface coupling. (In this case, surface induced mixing was neglected, so that predicted deviations are only correct as to order of magnitude.)

There is experimental evidence for the general ideas expressed above. On the basis of other evidence (quadrupole moments, $E2$ transition rates, rotational energies, etc.), one can estimate the strength of surface coupling. In particular, one can distinguish two groups of nuclei for each of which the magnetic moment is insensitive to

TABLE IV. Magnetic and quadrupole moments of $(f_{7/2})^N$, $J=7/2$, for various strengths of surface coupling. The coupling parameter, ξ, is defined in Eq. (38) and approximated in Eq. (40). Surface-induced mixing is ignored.

ξ	No. of phonons included	$\Delta\mu_N$	μ	Q (barns)
0	0	0	−1.91	0
0.75	1	+0.03	−1.88	0.0280
2.5	1	+0.10	−1.81	0.0695
5	2	+0.17	−1.74	
$\to\infty$	strong coupling limit	+2.21	+0.30[a]	$(1/15)Q_0$[a]
$\to\infty$	strong coupling limit	+0.90	−1.01[a]	$(5/14)Q_0$[a]

[a] The first value given in the strong coupling limit is for $\Omega=K=5/2$ $I=7/2$, but this is not the lowest state. The second value is for $\Omega=K=I=5/2$, the lowest state. $I=7/2$ is also not lowest in weak coupling unless direct particle coupling is included.

[31] K. W. Ford, Phys. Rev. 92, 1094 (1953).

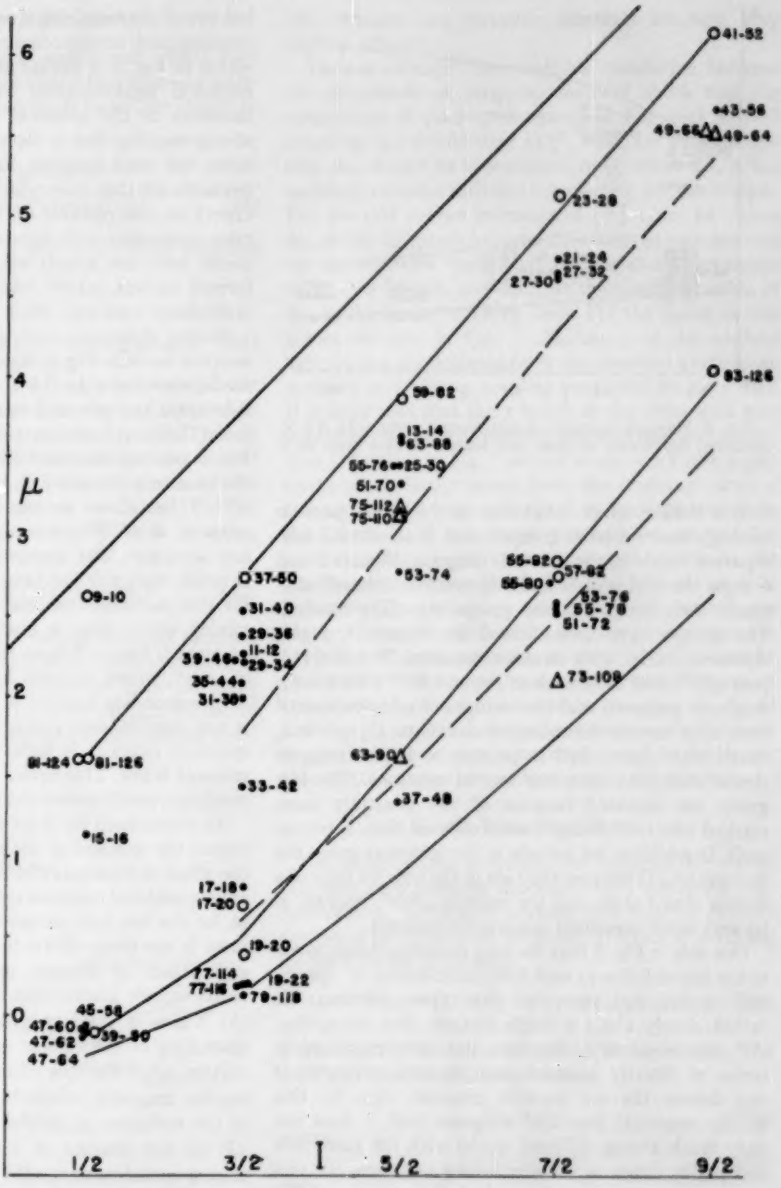

FIG. 5. Magnetic moments of odd-proton nuclei with $A>16$. Each point labeled by $Z-N$ of the nucleus. Open circles denote "spherical" nuclei, triangles denote "highly deformed" nuclei, and solid circles are nuclei which do not fit either extreme (see text for definitions). Outer solid lines are the Schmidt lines, giving the magnetic moments for pure configurations of equivalent protons. Inner solid lines are the "Blin-Stoyle Perks lines," drawn arbitrarily through the moments of spherical nuclei. Dashed lines are the "Bohr lines" giving the predicted position of the moments of highly deformed nuclei if the extra-particle g-factors are the same as for the spherical nuclei. Moments are taken from H. E. Walchli [Oak Ridge National Laboratory Report ORNL-1469, April 1, 1953 (unpublished)] and from the subsequent card file of the nuclear data group of the National Bureau of Standards.

the exact strength of surface coupling: I, the "highly deformed" nuclei, for which the collective contribution is given by the strong coupling limiting formula,[32]

$$\Delta\mu_{\text{collective}}=[I/(I+1)](g_R-g_J), \qquad (42)$$

where g_R and g_J are, respectively, the collective and particle g-factors; and II, the "spherical" nuclei, for which the surface coupling is sufficiently weak that

$$\Delta\mu_{\text{collective}}\ll\mu. \qquad (43)$$

The moments of the latter group should be determined almost entirely by the particle structure and the directly induced configuration mixing. The first group should show in addition the shift given by (42). If the shift (42) is larger than the fluctuations in the Blin-

[32] A. Bohr, Phys. Rev. 81, 134 (1951).

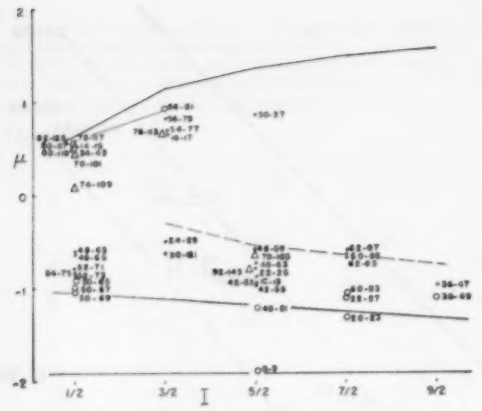

FIG. 6. Magnetic moments of odd-neutron nuclei with $A>16$. Notation, significance of lines, and sources of data same as in Fig. 5.

Stoyle Perks[23] effect (shift due to $l+\frac{1}{2}, l-\frac{1}{2}$ particle mixing), then nuclei in groups I and II should fall into separate bands in the Schmidt diagram. Figures 5 and 6 show the odd proton and odd neutron Schmidt diagrams with nuclei in these groups especially marked. The groups have been defined as follows: I, *highly deformed*, nuclei with neutron numbers $90\leq N\leq 113$, plus $_{92}U^{238}$ (the only nucleus beyond Bi^{209} with known magnetic moment) and the isotopes of $_{49}In$, because of their large measured quadrupole moments; II, *spherical*, nuclei with closed shell in protons or in neutrons, or closed shell plus or minus one in neutrons. The last group are included because of the generally more marked effect of closing a neutron shell than a proton shell. In addition, we include in the spherical group the isotopes of $_{81}Tl$ because they are in the near vicinity of a double closed shell, and the nucleus $_{41}Nb^{93}$, because of its very small measured quadrupole moment.

One sees in Fig. 5 that the $l+\frac{1}{2}$ moments lying closest to the Schmidt line at each spin value belong to "spherical" nuclei, and moreover that these moments lie rather closely along a single straight line (exception, $_9F^{19}$, whose moment, however, has been explained in terms of directly induced configuration mixing[12]). If one defines the net particle moment, Jg_J, by this wholly empirical line, and supposes that it does not vary much among different nuclei with the same spin and parity (there is no very strong argument for this assumption), then one may calculate by means of Eq. (42) the extra shift to be expected for strongly deformed nuclei. This leads to a revised "Bohr line," shown by the dashed line in Fig. 5. Four of the five known strongly deformed nuclei of the odd proton, $l+\frac{1}{2}$ type, lie very close to this line. The fifth, $_{63}Eu^{153}$, $I=5/2$, is displaced to the neighborhood of the opposite Schmidt line. All but two of the remaining moments lie between the weak-coupling and strong-coupling lines. For the $l-\frac{1}{2}$ moments in Fig. 5, a similar procedure is carried out. An empirical weak-coupling line is drawn through the moments of the spherical nuclei (solid line), and a strong-coupling line is then constructed (dashed line) using the weak-coupling line to define g_J. The "$d_{\frac{3}{2}}$" moments are then more widely scattered than one would expect on this picture. At spin 7/2, however, one obtains agreement with experiment in that the spherical nuclei have the largest moments, and the highly deformed nucleus, $_{73}Ta^{181}$, has the smallest moment (i.e., is displaced *outward*), while other nuclei lie between.

Similar data and analysis are shown for the odd-neutron nuclei in Fig. 6. Again the moments of spherical nuclei are closest to the $(l+\frac{1}{2})$ Schmidt line at every spin value and are used to define a weak coupling line (solid line). A strong-coupling line is defined as in Fig. 5 (dashed line) and the two lines enclose most of the moments. At spin 5/2, the highly deformed nucleus $_{70}Yb^{173}$ lies close to the strong-coupling line. The moment of $_{92}U^{235}$ is not close but is not known with any accuracy. The moment of $_8O^{17}$ lies very near the Schmidt line; this has been explained by the fact that for this particular nucleus, the kind of configuration mixing which gives a first order contribution to the moment is absent.[23] Note that the same should be true of $_{20}Ca^{41}$, whose moment has not yet been measured. A corresponding analysis of the $l-\frac{1}{2}$ moments in Fig. 6 is not possible. One notes, however, that at $I=\frac{3}{2}$, the spherical moment is high, while the highly deformed moment is low. This agrees with the fact that Eq. (42) predicts a small *inward* shift due to strong coupling.

As emphasized by Bohr and Mottelson,[4] one should expect the moment of the extra-particle structure and the effect of configuration mixing to vary considerably among nuclei of the same spin and parity, and especially so for the low spin values and $j=l+\frac{1}{2}$. Therefore one more in the many efforts to give an over-all qualitative explanation of nuclear magnetic moments perhaps needs further justification. Our main points are these: (1) There is good evidence against an appreciable quenching of the nuclear magnetic moment in nuclear matter. (2) Collective effects alone cannot account for nuclear magnetic moments, but can account for most of the *variations* of moments at each spin and parity. (3) In the absence of surface coupling, nuclei still show a considerable inward deviation from the Schmidt line, as pointed out by Blin-Stoyle and Perks[23] (except for special cases such as $_8O^{17}$ which are understood). We feel that this description brings new order into the over-all picture of magnetic moments. It should be emphasized, however, that we have only brought together the ideas of Bohr and of Blin-Stoyle and Perks, together with the observation that weak surface coupling has only a second order effect on magnetic moments.

[23] R. J. Blin-Stoyle and M. A. Perks, Proc. Phys. Soc. (London) **A67**, 885 (1954).

B. Quadrupole Moments

For weak surface coupling, quadrupole effects may still be relatively great, since the surface coupling interaction energy is itself of quadrupole form. The collective quadrupole operator,

$$Q_c = (3/5)(5/\pi)^{\frac{1}{2}} ZeR^2\alpha_0 = (3/5)\gamma ZeR^2(b_0+b_0^*), \quad (44)$$

contributes in first order, giving in the weak coupling limit, a quadrupole moment,

$$Q = (6/5)ZeR^2\gamma \times[I(2I-1)/(I+1)(2I+3)]^{\frac{1}{2}}\bar{A}_{\alpha I00}A_{\alpha I12}, \quad (45)$$

where γ is defined by (3), and $A_{\alpha JNR}$ is the amplitude of the state with particle configuration αJ coupled to N phonons of spin R to give the total spin I. Thus in lowest order, admixed particle states do not contribute.[4] Typical collective quadrupole moments predicted for Ca^{43} by this formula are shown in Table IV. The amplitudes in (45) are given in the weak coupling limit by $\bar{A}_{\alpha I00}=1$, and

$$A_{\alpha I12} = (k\gamma/\hbar\omega)5^{\frac{1}{2}}(\alpha I\|\textstyle\sum_i y_2(i)\|\alpha I). \quad (46)$$

Some of the reduced particle matrix elements required in (46) are given in Sec. II. The qualitative picture is that collective quadrupole moments may be comparable to or greater than the direct particle moments of extra-shell protons for a strength of coupling so weak that energies and magnetic moments are only very slightly affected.

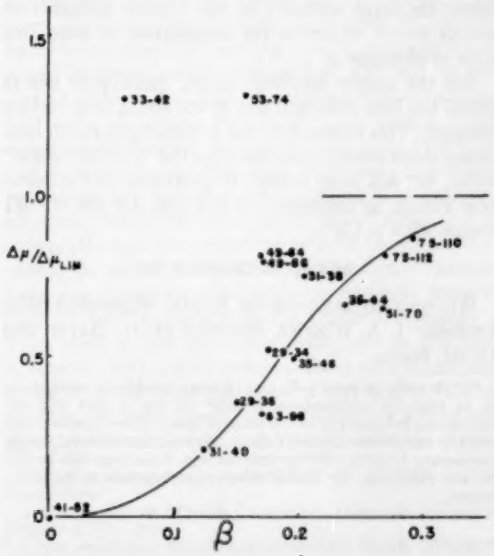

FIG. 7. Deviations of magnetic moments of odd-proton nuclei of $l+\frac{1}{2}$ type from the "Blin-Stoyle Perks line" (see Fig. 5) in units of predicted deviation for strong surface coupling *vs* the nuclear deformation β as deduced from the observed quadrupole moment (using the strong-coupling projection factor).

Various authors[34] have noted a correlation between the magnitude of magnetic moment shifts and the magnitudes of quadrupole moments. For weak surface coupling, $\Delta\mu_c$ should vary as Q^2, while for strong coupling, $\Delta\mu_c$ should be independent of Q, where $\Delta\mu_c$ is the magnetic moment shift due to collective nuclear motion. For the odd proton moments of $l+\frac{1}{2}$ type, we define $\Delta\mu_c$ as the difference between the observed moment and the moment of a "spherical" nucleus at the same spin value (see Fig. 5), and $\Delta\mu_{11m}$ as the predicted value of $\Delta\mu_c$ in the strong coupling limit. For the nuclei in this group, we plot in Fig. 7: $\Delta\mu_c/\Delta\mu_{11m}$ *vs* the nuclear deformation β calculated from the observed quadrupole moment *as if strong coupling were valid in every case.* If it were true that the g factor of the extra shell particle structure were a constant for given spin and parity, then the points in Fig. 7 should be along a curve which starts parabolically away from the origin at small β and approaches unity at large β. Indeed the best fit to the points is of this form, although an appreciable scatterer enters due to experimental errors in the quadrupole moments and to fluctuations in the particle g factors. In particular, two points fall far off the curve—those of $_{33}As^{75}$ and $_{53}I^{127}$. In both cases, the anomalously great magnetic moment deviation can be understood in terms of an unusually great mixing of nearly degenerate particle states—$f_{5/2}$–$p_{3/2}$ at $Z=33$ and $d_{3/2}$–$g_{7/2}$ at $Z=53$. A third anomaly is $_{63}Eu^{153}$, whose magnetic moment deviation appears to be far larger than that of any other nucleus, and is unexplained.

C. *E2* Transition Rates

For weak surface coupling, the collective $E2$ transition rate may compete favorably with the direct particle rate for extra-shell protons, and may be entirely dominant for extra-shell neutrons. The rate is governed by the reduced probability,

$$B_c(2) = (2I'+1)^{-1}\sum_{MM'm}|(f|Q_{2m}|i)|^2, \quad (47)$$

where I' and I are spins of initial and final states. The collective quadrupole operator is,

$$Q_{2m} = q\alpha_m, \quad (48a)$$

where

$$q = (3/4\pi)ZeR^2, \quad (48b)$$

and

$$\alpha_m = (\hbar\omega/2C)^{\frac{1}{2}}[b_m+(-1)^m b_{-m}^*]. \quad (48c)$$

This leads, in lowest order to

$$B_c(2) = (\pi/5)\gamma^2q^2 \times[\bar{A}_{0I1}A_{1I'}+(2I+1/2I'+1)^{\frac{1}{2}}\bar{A}_{1I'1}A_{0I'1'}]^2, \quad (49)$$

where A_{NJI} is the amplitude of the state with N

[34] H. Kopfermann, Naturwiss. **38**, 29 (1951); H. Miyazawa, Progr. Theoret. Phys. (Japan) **6**, 801 (1951).

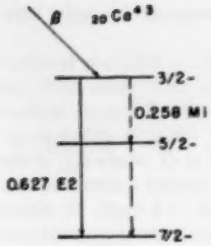

FIG. 8. Lowest states of Ca^{43} (reference 35).

phonons coupled to particle configuration J to give total spin I.

As an example we consider the lowest levels of Ca^{43}, $7/2-$, $5/2-$, $3/2-$, as shown in Fig. 8. According to the work of Lindqvist and Mitchell[35] the $3/2-$ state decays predominantly by crossover rather than cascade. (a) Assume the particle states are $f_{7/2}$, $f_{5/2}$, $p_{3/2}$ (all neutrons). Then in the absence of collective effects, the cascade should be more probable than the crossover by about 10^6. Even for protons instead of neutrons, the cascade should be favored by at least 10^2. The observed favoring of the crossover would require a strong surface coupling of unreasonably large magnitude. (b) Assume that the particle states are all $(f_{7/2})^3J$. Then for pure states, the $M1$ cascade is forbidden, and the $E2$ crossover is greatly inhibited (going only by recoil of the core). The $M1$ cascade will be greatly speeded up by small configuration mixing (although still small compared to the one-particle cascade of (a) above), and the $E2$ crossover will be greatly speeded up by weak surface coupling. We calculate crudely that the $M1$ rate, including particle mixing, is,

$$T_{M1}(3/2\rightarrow 5/2)\sim 3\times 10^{8}\ \text{sec}^{-1}, \tag{50}$$

while the $E2$ rate is,

$$T_{E2}(3/2\rightarrow 7/2)\cong 0.9\times 10^{11}(k\gamma^2/\hbar\omega)^2\ \text{sec}^{-1}. \tag{51}$$

If we choose the "standard" values for the interaction constant k and the mass constant B of the collective model in order to reduce the number of parameters to one, the phonon energy (or the effective surface tension), we obtain

$$T_{E2}(\text{crossover})/T_{M1}(\text{cascade})\sim(17\ \text{Mev}/\hbar\omega)^4, \tag{52}$$

i.e., the crossover will dominate for phonon energy less than about 17 Mev. This value corresponds to a very weak surface coupling. These arguments are crude, but provide the following information: (1) The observed dominance of the crossover transition is evidence for $(f_{7/2})^3$ configurations rather than one-particle configurations; (2) only a very weak surface coupling is sufficient to account for the dominance of the crossover; (3) the transition rates are perhaps slow enough to be measured—in particular, the $5/2$ state might have a measurable lifetime.[36]

[35] T. Lindqvist and A. C. G. Mitchell, Phys. Rev. **95**, 444 (1954) and Phys. Rev. **95**, 1535 (1954).

VI. CONCLUSION

In claiming success for any nuclear model, one must be wary of those results which are model-independent, or at least given by more than one model. For example, almost any alteration of the pure jj coupling shell model improves the calculated ft values of unfavored beta transitions, since the pure jj coupling ft values are nearly minimal, and almost any change of coupling scheme will increase the predicted ft value. Similarly, in assessing the evidence for collective phenomena in low-energy nuclear properties, it is important to note that many of the effects of surface coupling can be duplicated by direct interactions among extra shell nucleons moving in the field of a rigid core. For example, energy level orders as shown in Fig. 1 are qualitatively close to those predicted for direct short range attractive forces; and deviations of nuclear magnetic moments from the pure state value are in the same direction, due to surface coupling or due to direct interaction. Large quadrupole moments and the striking regularities of the properties of the strongly deformed nuclei receive at least much simpler and more direct explanation from the collective model—but the important large anomaly in the nuclear moments of inertia leaves uncertain the explanation of even this class of phenomena.

For the nearly spherical nuclei, quadrupole effects afford the best empirical test of the strength of surface coupling. This evidence favors a coupling strength near closed shells considerably less than the "hydrodynamic" value, but still large enough to give important quadrupole effects, as discussed, for example, for the $E2$–$M1$ competition in Ca^{43}.

ACKNOWLEDGMENTS

We wish to acknowledge helpful discussions with Professor J. A. Wheeler, Professor M. G. Mayer, and Dr. D. Inglis.

[36] *Note added in proof.*—R. van Lieshout has kindly pointed out to us that the experimental results[35] do not in fact give unambiguous information on the relative speed of the crossover and cascade transitions discussed above, because of accidental energy degeneracy between different gamma rays. Equations (50) to (52) remain valid, but the actual relative rates remain to be determined.

Independent-Particle Model of the Nucleus. III. The Calcium Isotopes*

CARL LEVINSON† AND KENNETH W. FORD‡
Indiana University, Bloomington, Indiana
(Received May 31, 1955)

The isotopes of calcium of mass number 41, 42, and 43 are analyzed using the methods given in papers I and II of this series. It is found that the experimental data on Ca^{41} and Ca^{43} is sufficient to predict the low-lying odd-parity levels of Ca^{42} as well as the magnetic moment. Detailed agreement between theory and experiment is obtained for the levels of Ca^{43} of spin and parity $7/2^-$, $5/2^-$, $3/2^-$, and $9/2^-$ and the experimental Schmidt line magnetic moment deviation of 0.595 nm is in agreement with a predicted deviation of 0.60 nm. The relative importance of particle forces and surface forces due to collective motion is investigated and it is concluded that for the isotopes investigated the surface forces are so weak as to have a negligible effect on the level spacings. As a measure of the upper limit of the strength of the surface forces the magnitude of $\hbar\omega$ (the surfon energy) is set at $\gtrsim 15$ Mev. An effective two-particle interaction potential is derived which differs to some extent from the two-particle scattering potential in that it has a longer range and is more shallow.

INTRODUCTION

IN this paper, we shall apply the methods outlined in papers I[1] and II[2] to the nuclei Ca^{41}, Ca^{42}, and Ca^{43}. The empirically determined single-particle levels of Ca^{41} determine the zero-order scheme and define the relevant cofigurations in Ca^{42} and Ca^{43} and their energy spacings. The experimental level scheme of Ca^{42} then serves to determine the necessary information about the two-body interaction which allows us to calculate the level scheme, wave functions, and magnetic moment of Ca^{43}. In order to apply these methods it is essential that the low-lying "single-particle" levels (i.e., $f_{7/2}$, $p_{3/2}$, $f_{5/2}$, $p_{1/2}$, $g_{9/2}$) of Ca^{41} be well represented by independent-particle wave functions. If the Ca^{40} core were truly inert and rigorously replaceable by a single-particle potential well, then the method described above would be exact. As a matter of fact, Ca^{40} has its first excited state at 3.75 Mev and core excitation states in Ca^{41} seem to appear at 2.6 Mev and higher. Since empirical information concerning the levels of Ca^{41} and Ca^{42} is used it is clear that some corrections due to core excitations are automatically included. For example, all corrections to the level spacing of Ca^{42} which can be interpreted as corrections due to core excitation that should be present for one of the extra core particles alone are already included since the empirical levels of Ca^{41} are used in setting up the problem. Similarly a large class of core excitation corrections to the level scheme of Ca^{43} are included since the potential has been adjusted to the empirical levels of Ca^{41} and Ca^{42}. This problem has been investigated in detail by Brueckner, Eden, and Francis[3] who find that in adjusting a two-body interaction to the empirical levels of Ca^{42} the core excitation corrections are automatically included for this problem. In the case of Ca^{43}, the approach again includes most of the corrections and one can expect a high degree of accuracy in the final results. If core excitation corrections are indeed small, then the empirically derived matrix elements for the Ca^{42} problem should be derivable from a two-body potential which fits the nucleon-nucleon scattering data. If, on the other hand, these corrections are appreciable then the effective potential may be somewhat different from the scattering one.

The only easy way to take explicit account of core excitations is through the collective model of coupling to nuclear surface oscillations. We have attempted to include such coupling in the calculations as a perturbation to the more detailed shell model treatment, but with the result that the closest agreement to experiment is obtained with zero additional surface coupling. This does not rule out, of course, that effects of a deformable core on the energies are already included in the semi-empirical approach outlined above. Diagonal contributions of weak surface coupling and of direct particle interaction are in fact indistinguishable in this approach. Off-diagonal contributions (configuration mixing) are, however, somewhat different.

I. LEVELS OF Ca^{41}

Ca^{41} consists of a doubly magic Ca^{40} core and a single neutron. According to the shell model, this neutron has an $f_{7/2}$ ground state and excited states of $p_{3/2}$, $f_{5/2}$, $p_{1/2}$, $g_{9/2}$, $d_{3/2}$ and $g_{7/2}$ in that order.[4] The first seven excited states of Ca^{41} are according to Braams at 1.947, 2.015, 2.469, 2.582, 2.611, 2.675, and 2.890 ± 0.010 Mev.[5] The ground state of Ca^{41} has an experimental shell model assignment of $f_{7/2}$.[5] The 1.95- and 2.47-Mev levels have experimental spin and orbital angular momentum

* Supported in part by a grant from the National Science Foundation.
† Now at Palmer Physical Laboratory, Princeton University, Princeton, New Jersey.
‡ Now on leave at Max Planck Institut für Physik, Göttingen, Germany.
[1] C. A. Levinson and K. W. Ford, Phys. Rev. **99**, 792 (1955). Referred to as I in the balance of this paper.
[2] K. W. Ford and C. A. Levinson, preceding paper [Phys. Rev. **100**, 1 (1955)]. Referred to as II in the balance of this paper.
[3] Brueckner, Eden, and Francis, Phys. Rev. (to be published).
[4] P. F. A. Klinkenberg, Revs. Modern Phys. **24**, 63 (1952).
[5] P. M. Endt and J. C. Kluyver, Revs. Modern Phys. **26**, 95 (1954).

values of $p_{3/2}$ and $p_{1/2}$.[6] These levels bracket the 2.01-Mev level which from shell model considerations we take to be the $f_{5/2}$ state. The $g_{9/2}$ level assignment is the hardest to make. In $_{39}Y^{89}$, the $p_{1/2}-g_{9/2}$ spacing is experimentally fixed at 0.913 Mev.[7] Y^{89} has a magic neutron core and closed proton subshells up to but not including $2p_{1/2}$ and one $2p_{1/2}$ proton. The levels are therefore close to single-particle levels and the spin of the excited state is fixed by the fact that it is isomeric. It is hard to say what this spacing corresponds to in Ca^{41} since the mass number A is so different. Two effects that are certainly present are: (a) the oscillator level spacing increases for Ca^{41} thus tending to increase the $p_{1/2}-g_{9/2}$ separation; (b) the spin-orbit interaction increases[8] thus tending to decrease the $p_{1/2}-g_{9/2}$ separation in Ca^{41} (i.e., $g_{9/2}$ is pushed down further and $p_{1/2}$ is pushed up further). As a guess the 2.89 Mev level in Ca^{41} was taken to be the $g_{9/2}$ state, thus corresponding to a $p_{1/2}-g_{9/2}$ separation of 0.42 Mev. The $g_{9/2}$ level is probably not lower than 2.89 Mev. It resulted that with the $g_{9/2}$ level taken at this value the spin 6, 4, and 2 states of Ca^{42} were not appreciably influenced by its presence. The effect of the $g_{9/2}$ level on the spin-zero state, while considerable, did not vary appreciably if the g level were raised up by one Mev. With the $g_{9/2}$ state at 2.89 Mev the spin-zero ground state in Ca^{42} contained a 9% admixture of the $g_{9/2}^2$ wave function.

In order to fix the position of the $g_{7/2}$ level in Ca^{41}, it was thought best to compute the $g_{9/2}-g_{7/2}$ doublet splitting from theoretical considerations and experiments designed to measure this splitting. Harvey[9] finds the energy discontinuity in neutron binding energy at magic number 50 (i.e., the $g_{9/2}-g_{7/2}$ splitting) to be 2 Mev for cores of 86 and 84 particles. We wish the splitting for a core of 40 particles. Assuming the spin-orbit splitting goes as A^{-1},[8] we get a splitting of 3.2 Mev for the Ca^{40} core. Alternately, taking the 2-Mev f-state splitting for Ca^{41} as given and assuming a $(2l+1)$ dependence on the splitting for fixed A, we get a $g_{9/2}-g_{7/2}$ splitting of 2.6 Mev. These values are sufficiently close for the purposes of this calculation, so we arbitrarily assigned a value of 3 Mev to the $g_{9/2}-g_{7/2}$ splitting and thus took the $g_{7/2}$ state of Ca^{41} to be at 5.89 Mev. The $2d_{3/2}$ state has 2 nodes to one node for the $1f_{7/2}$ state, thus giving a small overlap. In addition it is assumed to be far away in energy, and we therefore neglect its contribution to the calculation. Although the $g_{7/2}$ state is just as far away in energy from the $f_{7/2}$ state, it has only one node and almost exactly overlaps the $f_{7/2}$ state (see Fig. 1). Hence we keep it in the calculation. Higher excited single-particle states of the Ca^{41} odd neutron were neglected because they were supposed to be too far away in energy or else overlapped the $f_{7/2}$ state badly. Parity considerations also decrease the coupling between the f configurations and those in the next shell. Consider Ca^{42} with a zero-order f^2 configuration. In order to couple with f^2, the configurations in the next higher shell must have plus parity. This immediately dispenses with the fg, fs, and fd configurations and leaves the configurations g^2, gd, etc., which lie two times higher in energy then the odd-parity levels and in general have small interaction matrix elements with the f^2 configuration.

The states in Ca^{41} corresponding to core excitations have been discussed in the introduction and are neglected for the reasons referred to there.

II. LEVELS OF Ca^{42}

Schiffer[10] finds levels in Ca^{42} at 1.51±0.03, 1.95±0.07, 2.29±0.05, 2.59±0.07, 3.02±0.05, and 3.75±0.07 Mev.[11] The 1.51-Mev level has an experimental spin assignment of 2 from beta-gamma angular correlations.[12] To zero order the lowest states of Ca^{42} should correspond to an f^2 configuration with spins 0, 2, 4, and 6. (No odd spins due to the Pauli principle.) Any reasonable assumption for the interparticle forces together with any strength of surface coupling will give the level order 0, 2, 4, 6.[13] The third and fourth excited states of Ca^{42} were accordingly assumed to have spins 4 and 6. The identification of the spin-six level is the least certain since the lowest levels of the $f_{7/2}p_{3/2}$ configuration must lie nearby. However, the position of this level is sufficiently uncritical for the purposes of predicting the levels of Ca^{43} that an error of a few tenths of a Mev will not change the computed Ca^{42} levels appreciably. The experimental relative level spacings are shown in Fig. 2. In order to fix the absolute value of the ground-state energy of Ca^{42}, information on binding energies[14] was used. On the basis of the model used here, the two neutrons in Ca^{42} core are each bound to the core by the energies of the Ca^{41} nucleus. These

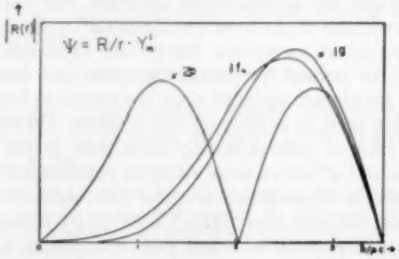

FIG. 1. Radial wave functions for the f, p, and g states of Ca^{41} where the central potential is constant and the nuclear wall is an infinite barrier.

[6] J. R. Holt and T. N. Marsham, Proc. Phys. Soc. (London) **A66**, 565 (1953).
[7] Evidence summarized by M. Goldhaber and R. D. Hill, Revs. Modern Phys. **24**, 179 (1952).
[8] D. R. Inglis, Revs. Modern Phys. **25**, 390 (1953).
[9] J. A. Harvey, Phys. Rev. **81**, 353 (1951).
[10] J. P. Schiffer, Phys. Rev. **97**, 428 (1955).
[11] Braams and Buechner find levels at 1.53, 1.84, and 2.43 Mev. This information reached the authors after the calculations had been performed. They would not change the results appreciably.
[12] D. T. Stevenson and M. Deutsch, Phys. Rev. **84**, 1071 (1951).
[13] Dieter Kurath, Phys. Rev. **91**, 1430 (1953).
[14] Summarized in reference 13.

bonds we call core bonds. In addition there is an extra binding due to the interparticle force. This binding is due to the particle bond. The ground state binding energy due to the core and particle bonds in Ca^{42} is simply the difference between the binding energies of Ca^{42} and Ca^{40} which is 19.8 Mev. Hence we take $E_0=-19.8$ Mev for Ca^{42}. Then the Hamiltonian H_0+V for the Ca^{42} problem has a lowest state at -19.8 Mev. It is more convenient to write $H_0=-16.6$ Mev$+\Delta H_0$ since the $f_{7/2}$ neutron in Ca^{41} has an 8.3-Mev binding energy. This makes $\Delta H_0=0$ for the $f_{7/2}^3$ configuration and positive for all other configurations. Our problem is then to find the eigenvalues of ΔH_0+V with lowest state at -3.2 Mev. The -3.2 Mev can be looked at as the contribution to the energy due to the particle bond alone.

III. SOLUTION OF THE TWO-BODY PROBLEM

As a first approximation we shall consider the effects of the $f_{5/2}$, $g_{9/2}$, and $g_{7/2}$ states on the zero-order $f_{7/2}^2$ configuration in Ca^{42}. As shown in Fig. 1, the radial dependence of the g state is almost identical to that of the f state. We shall assume they are identical and thus all radial integrals will be independent of l, the orbital quantum number.

We now make substitutions into Eq. (11) of I. The values of l_1, l_2 of interest are only f^2 and g^2, since the state fg has odd parity. It is easier to work with the expression

$$\beta(Jl_1l_2)=\frac{1}{\alpha(Jl_1l_2)}=\left\{\sum_{j_1'j_2'}\frac{|(l_1l_2J|j_1'j_2'l_1l_2)|^2}{E_J-H_0(l_1l_2j_1'j_2')}\right\}^{-1}. \quad (1)$$

Then, by a slight manipulation of Eq. (11) in I, we get

$$\begin{vmatrix}(f^2J|V|f^2J)-\beta(Jf^2) & (f^2J|V|g^2J)\\ (g^2J|V|f^2J) & (g^2J|V|g^2J)-\beta(Jg^2)\end{vmatrix}=0. \quad (2)$$

From the data given in Secs. I and II plus the values of LS–jj transformation coefficients,[15] one can easily evaluate the β's. Equation (2) represents four equations, one for each value of J. In order to get unique answers, we express our unknown matrix elements in terms of the four matrix elements V_J, where

$$(f^2J|V|f^2J)\equiv V_J \quad (3)$$

and $|f^2J)$ is a two-particle wave function in an LS representation for $l_1=l_2=3$, $S=0$, $L=J$. Now each V_J can be expressed in terms of four Slater parameters[16] and inversely the Slater parameters F^κ, ($\kappa=0, 2, 4, 6$) can be expressed in terms of V_J. The F^κ's are the radial integrals of the problem and are independent of l_1, l_2 as pointed out above. These relations can be written:

$$V_J=\sum_\kappa B_{J\kappa}F^\kappa, \quad F^\kappa=\sum_J A_{\kappa J}V_J. \quad (4)$$

$B_{J\kappa}$ is given in Condon and Shortley[16] and $A_{\kappa J}$ is given in Table I. We also need expressions for F^κ for $\kappa=1, 3, 5, 7, 8$. In general, F^κ is a smooth function of κ. In fact, for zero-range forces, $F^\kappa=(2\kappa+1)F^0$. Examples of Slater parameters appear in Kurath's[13] work. We therefore take the values of F^κ for $\kappa=1, 3, 5, 7, 8$ to be given by linear interpolation or extrapolation on the F^κ's for $\kappa=0, 2, 4, 6$, i.e.,

$$\begin{gathered}F^1=\tfrac{1}{2}(F^0+F^2), \quad F^5=\tfrac{1}{2}(F^4+F^6), \quad F^8=2F^6-F^4,\\ F^3=\tfrac{1}{2}(F^2+F^4), \quad F^7=\tfrac{1}{2}(3F^6-F^4).\end{gathered} \quad (5)$$

Now all the relevant Slater parameters can be expressed in terms of the four V_J's. The matrix elements $(g^2J|V|g^2J)$ can be expressed in terms of $F^\kappa\kappa=0, 2, 4, 6, 8$. The matrix elements $(g^2J|V|f^2J)$ can be expressed in terms of $F^\kappa\kappa=1, 3, 5, 7$. Hence we finally write all matrix elements in terms of V_J, $J=0, 2, 4, 6$ and then solve for V_J. The expressions for $(g^2J|V|g^2J)$ in terms[17] of F^κ and the other diagonal matrix elements[16] are given in the literature and the off-diagonal elements are given in Table II. Equation (2) can now be solved in a straightforward manner and one finds for the values

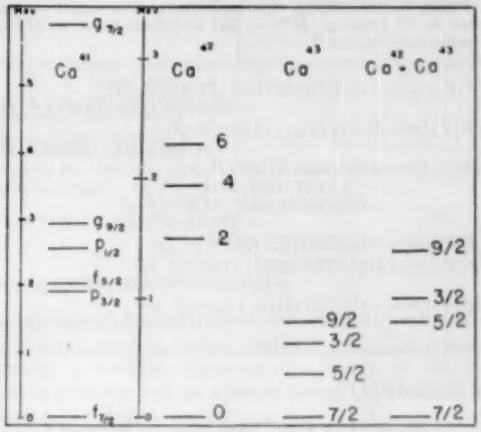

FIG. 2. The first three level diagrams on the left give the level spacings and spin assignments of Ca^{41}, Ca^{42}, and Ca^{43} which are taken as the "empirical" levels. The diagram on the right represents the predicted level spacings of Ca^{43} based on the empirical levels of Ca^{42} if configuration interaction is neglected.

TABLE I. Values of $A_{\kappa J}$ to three decimal places. $F^\kappa=\sum_J A_{\kappa J}V_J$.

κ \ J	0	2	4	6
0	−0.103	0.204	0.367	0.529
2	0.766	−1.457	−3.448	4.147
4	2.017	−5.034	1.845	1.181
6	2.276	4.716	0.940	−7.948

[15] G. Racah, Physica **16**, 651 (1950).

[16] E. U. Condon and G. H. Shortley, *The Theory of Atomic Spectra* (Cambridge University Press, Cambridge, 1951).

[17] G. H. Shortley and B. Fried, Phys. Rev. **54**, 739 (1938).

TABLE II. Off-diagonal matrix elements of a singlet central force in LS coupling. $R^{(\kappa)}(l_1l_2;l_3l_4)$ is defined as on p. 175 of Condon and Shortley.[14]

$$
\begin{aligned}
(f^2|V_J|fp) &= -(2/5)(42)^{\frac{1}{2}}W(3331;J2)R^{(2)}(f^2;fp)\\
&\quad -4(7/33)^{\frac{1}{2}}W(3331;J4)R^{(4)}(f^2;fp)\\
(f^2|V_J|p^2) &= (9/5)W(3311;J2)R^{(2)}(f^2;p^2)\\
&\quad +(4/3)W(3311;J4)R^{(4)}(f^2;p^2)\\
(f^2|V_J|g^2) &= -4W(4433;J1)R^{(1)}(f^2;g^2)\\
&\quad -(18/11)W(4433;J3)R^{(3)}(f^2;g^2)\\
&\quad -(180/143)W(4433;J5)R^{(5)}(f^2;g^2)\\
&\quad -(245/143)W(4433;J7)R^{(7)}(f^2;g^2)\\
(p^2|V_J|fp) &= -\tfrac{1}{2}6\sqrt{3}W(1131;J2)R^{(2)}(p^2;fp)\\
(g^2|V_J|fp) &= 12(3/77)^{\frac{1}{2}}W(4431;J3)R^{(3)}(g^2;fp)\\
&\quad +30/11(6/13)^{\frac{1}{2}}W(4431;J5)R^{(5)}(g^2;fp)\\
(g^2|V_J|p^2) &= -(12/7)W(4411;J3)R^{(3)}(g^2;p^2)\\
&\quad -(15/11)W(4411;J5)R^{(5)}(g^2;p^2)
\end{aligned}
$$

of V_J and $\beta(Jf^2)$.

$$
\begin{aligned}
&V_0=-3.33 \text{ Mev}, \quad \beta(0,f^2)=-4.20 \text{ Mev},\\
&V_2=-2.49 \text{ Mev}, \quad \beta(2,f^2)=-2.50 \text{ Mev},\\
&V_4=-2.10 \text{ Mev}, \quad \beta(4,f^2)=-2.16 \text{ Mev},\\
&V_6=-2.20 \text{ Mev}, \quad \beta(6,f^2)=-2.22 \text{ Mev}.
\end{aligned} \tag{6}
$$

We note that only V_0 differs much from the corresponding $\beta(0,f^2)$. The $\beta(J,f^2)$'s are the V_J's one would find if only the $f_{5/2}$ state were taken into consideration. In other words, it is the spin-zero ground state of Ca^{42} that is most affected by the presence of the states $g_{9/2}$ and $g_{7/2}$. The other states are hardly influenced at all.

In order to find the effect of the p states we need to know the radial integrals involved in the matrix elements like $(f^2J|V|fpJ)$ and $(f^2J|V|p^2J)$. An upper limit on these matrix elements can be established by assuming that the p state radial wave function is identical to the f state radial wave function. In this case, the matrix elements can be expressed in terms of the V_J's by the methods described above. In this limit, the p states still leave V_4 and V_6 unchanged and change V_2 from -2.49 Mev to -2.47 Mev. Since the overlap is only the order of 50 percent [see Fig. 1], we will take $V_2=-2.48$ Mev. The general accuracy of our calculation is such that more detailed investigation of this point is not necessary. In a similar fashion, it was estimated that V_0 is changed from -3.33 Mev to -3.25 Mev. The fact that V_0 sustained the greatest change again reflects the fact that the spin-zero ground state of Ca^{42} is the most strongly affected state by configuration interaction. Finally we list here our semiempirically determined values of V_J.

$$
\begin{aligned}
&V_0=-3.25 \text{ Mev}, \quad V_2=-2.48 \text{ Mev},\\
&V_4=-2.10 \text{ Mev}, \quad V_6=-2.20 \text{ Mev}.
\end{aligned} \tag{7}
$$

It is interesting to compute the diagonal matrix elements for the Ca^{42} configurations $f_{7/2}^2$ ($J=0$, 2, 4, 6) since the difference between these values and energies for these states is the energy due to configuration interaction. This comparison is shown in Fig. (3).

We can also fit a potential well to our empirically derived diagonal matrix elements. Let D_J be the diagonal element for spin J in a jj representation. We then have:

$$
\begin{aligned}
&D_0=-1.86 \text{ Mev}, \quad D_2=-1.27 \text{ Mev},\\
&D_4=-0.77 \text{ Mev}, \quad D_6=-0.31 \text{ Mev}.
\end{aligned} \tag{8}
$$

We have given graphs of D_J for various assumed potentials in I. It is important to notice that $(D_2-D_0)/(D_4-D_2)=1.18$ while $(E_2-E_0)/(E_4-E_2)=3.43$. We see that we must fit to two almost equal spacings and not to a ratio of 3.43 which would be the case if configuration interaction were neglected. In Table III are listed the best fits for potentials of the form $V_0\exp[-r^2/r_0^2]$. These tables were computed from Kurath's[13] evaluation of the Slater parameters for the above potential using oscillator wave functions which go as $r^l\exp[-r^2/r_n^2]$. The parameter $\lambda=r_0/r_n$ measures the ratio of the force range to the spread of the nuclear wave function. The best value of λ lies between 1.11 and 1.25. A good fit is obtained with $V_0=-14.4$ Mev, $\lambda=1.18$. If in addition we demand that this well have a bound state at zero energy thus approximating the singlet well binding strength we obtain an effective range ${}^1r_{eff}=4\times10^{-13}$ cm and $r_0=2.79\times10^{-13}$ cm.

On the other hand it seems more realistic to fix r_n at some value consistent with the radius of Ca. Kurath[13] has proposed a value of $r_n=2.9\times10^{-13}$ cm on the basis of best approximating a square well wave function whose constants are determined from the experimental evidence in the mass number 40 region. This value of r_n gives for the mean square radius, $\langle r^2\rangle^{\frac{1}{2}}$, 4.35×10^{-13} cm, which is to be compared with an "outside" radius of 4.95×10^{-13} cm for $A=43$, based on $R=r\times A^{\frac{1}{3}}$, with $r=1.41\times10^{-13}$ cm. Since $\lambda=1.18$, we find the range of the interparticle Gaussian potential is $r_0=3.42\times10^{-13}$

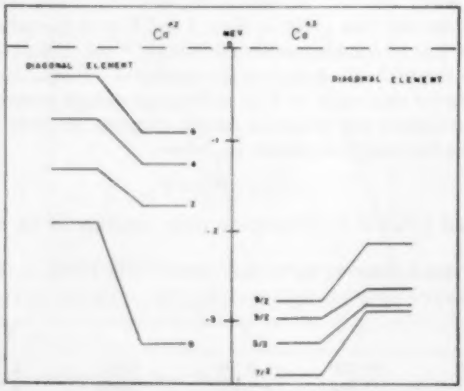

FIG. 3. The level diagrams on the outside represent the contribution due to diagonal matrix elements alone to the observed levels. The difference between these energies and the total energies is due to configuration interaction. The levels labeled by spin values are the observed levels.

cm. Combining this with the well depth of 14.4 Mev, we find a well depth parameter[18] $s=1.5$ (i.e., this potential is strong enough to bind two particles) and effective range of 3.82×10^{-13} cm. Fitting a Gaussian to low-energy singlet scattering data one finds $V_0=35$ Mev, ${}^1r_{eff}=2.7\times10^{-13}$ cm, and $r_0=1.78\times10^{-13}$ cm. If our results are correct we must conclude that the effective nuclear interaction potential in Ca^{42} is indeed not well represented by a Gaussian constructed to fit the low-energy scattering data but is better represented by a Gaussian which is about one-half as deep and two times longer-ranged. There are two possible explanations for this result:

(1) The presence of the core excitations which were neglected in the calculation cause the modifications. This effect is predicted theoretically[3] but it remains to be calculated for the case of Ca^{42}. In particular, collective core excitations should be in the direction to produce an effectively longer-range interaction. (Compare figures showing energy shifts in papers I and II.)

(2) The relative energies involved between the extra core particles are so great that a potential which fits low-energy scattering only is inappropriate.

It is a simple matter to investigate this second point further since, as shown by Talmi,[19] the independent-particle two-body wave functions corresponding to a harmonic oscillator central potential can be easily expressed in terms of the relative ($\mathbf{r}$) and center-of-mass ($\mathbf{R}$) coordinates of the two particles. The two-particle wave function can always be written in the form

$$\psi(\mathbf{r}_1,\mathbf{r}_2)=\sum_n a_n\phi_n(\mathbf{R})\chi_n(r), \qquad (9)$$

where ϕ and χ are themselves harmonic oscillator wave functions. If χ corresponds to a $1s$ state of relative motion, then one finds a probability distribution of relative energies given by:

$$p(\epsilon)d\epsilon=4(2/\pi)^{\frac{1}{2}}(\hbar\omega)^{-\frac{3}{2}}\exp[-2\epsilon/\hbar\omega]\epsilon^{\frac{1}{2}}d\epsilon, \qquad (10)$$

where ϵ is the center-of-mass kinetic energy of the two particles and $\hbar\omega$ is the characteristic energy spacing of the single-particle central oscillator well. The average energy is $\bar{\epsilon}=\frac{3}{4}\hbar\omega$. Equating the energy of the top particle in the well to a Fermi energy of 30 Mev, we find $\hbar\omega=8.6$ Mev for O^{17} and $\hbar\omega=6.7$ Mev for Ca^{41}. (Elliott and Flowers[20] use 7 Mev and Redlich[21] uses 10 Mev for O^{17}.) The average relative scattering energy then amounts to 6.45 Mev in O^{17} and 5 Mev in Ca^{41}. These numbers are *lower limits* on the average scattering energy since they are based on a $1s$ state of relative motion. Since the shape-independent analysis of pp scattering breaks down around 10 Mev, some shape dependence for the effective nuclear interaction is to be expected.

TABLE III. Diagonal matrix elements predicted for an $(f_{7/2})^2$ configuration with $J=0, 2, 4, 6$ using a Gaussian potential of the form $V_0\exp[-r^2/r_0^2]$ and an oscillator wave function of the form $\psi\sim r^l\exp[-r^2/r_n^2]$. The best value of V_0 is listed for the given values of λ ($\lambda=r_0/r_n$) such that the predictions agree most closely with the matrix elements deduced from the empirical analysis. All numbers but the dimensionless values of λ are in $-$Mev.

Empirical analysis	V_0	18.6	15.8	14.4	13.3	11.9
↓	λ	1.00	1.11	1.18	1.25	1.33
0.31	D_6	0.35	0.37	0.38	0.38	0.39
0.77	D_4	0.59	0.66	0.70	0.74	0.78
1.27	D_2	1.14	1.22	1.27	1.30	1.33
1.86	D_0	1.92	1.88	1.87	1.84	1.82

FIG. 4. Radial integrals F_G^κ and F_Y^κ for Gaussian and Yukawa interparticle potentials with infinite scattering lengths as a function of effective range.

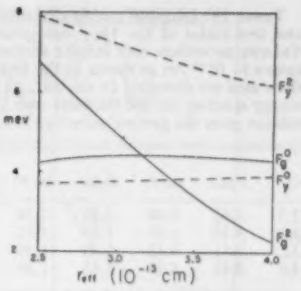

The shape dependence of the matrix elements can also be demonstrated by computing them with a Gaussian and a Yukawa potential, both adjusted to give the same effective range and scattering length. This calculation was performed for the $1p^2$ radial integrals. The scattering length of both potentials was chosen to be infinite, thus corresponding to a bound state at zero energy, and the results are plotted as a function of the effective range in Fig. 4. The integrals plotted are given by Swiatecki.[22] The parameter r_n giving the range of the nuclear wave function was taken to be 2.33×10^{-13} cm. ($r_n=\sqrt{2}a_0$ in Lane's notation[23]) following the results of Elliott in fitting Coulomb energy data in the $1p$ shell as reported by Lane.[23] Table IV gives the diagonal matrix elements for the states $1p_{3/2}{}^2J=0,2$ which are derived from the corresponding radial integrals. It is immediately seen that F^0 is not very shape dependent while F^2 has a considerable shape dependence for the larger effective ranges. For a very slowly varying potential all F^κ's are very much smaller than F^0, and for a delta function potential $F^\kappa=(2\kappa+1)F^0$. Thus, roughly speaking, the values of F^κ for $\kappa>0$ should be expected to increase as the potential is made to vary more rapidly with r. The trends in Fig. 4 can be interpreted as reflecting this. Longer effective ranges correspond to less rapidly varying

[18] J. M. Blatt and V. F. Weisskopf, *Theoretical Nuclear Physics* (John Wiley and Sons, Inc., New York, 1952), p. 55.
[19] I. Talmi, Helv. Phys. Acta **25**, 185 (1952).
[20] B. H. Flowers, lecture at University of Chicago, March, 1955 (unpublished).
[21] M. Redlich, Phys. Rev. **95**, 448 (1954).
[22] W. J. Swiatecki, Proc. Roy. Soc. (London) **A205**, 238 (1951).
[23] A. M. Lane, Proc. Phys. Soc. (London) **A68**, 197 (1955).

TABLE IV. Diagonal matrix elements in Mev for the spin zero and two states of the $1p_{3/2}^2$ configuration using Gaussian and Yukawa potentials with infinite scattering lengths and effective ranges in 10^{-13} cm as shown in the first column. The wave functions used are described in the text. Δ_G and Δ_Y are the first-order energy spacings for the Gaussian and Yukawa wells and the last column gives the percent difference in these spacings.

r_{eff}	$D_0(G)$	$D_0(Y)$	$D_2(G)$	$D_2(Y)$	Δ_G	Δ_Y	% difference
2.5	4.62	4.60	1.48	1.34	3 14	3.26	3.7
3.0	4.26	4.45	1.53	1.35	2.73	3.10	13
3.5	3.81	4.32	1.50	1.36	2.31	2.96	25
4.0	3.48	4.25	1.46	1.39	2.02	2.86	34

potentials and a Yukawa well varies more rapidly than a Gaussian. Configurations involving higher angular momenta also require radial integrals F^κ for higher values of κ in order to express their matrix elements. Hence energy levels corresponding to higher configurations should show an increasing shape dependence. From Fig. 4 and Table IV one sees that if the effective two-body singlet potential acting between $1p$ nucleons has an effective range near 2.7×10^{-13} cm (the singlet scattering effective range) then one can expect a slight shape dependence for the matrix elements. However, if for some reason the effective range of the internucleon potential in nuclear matter is closer to 4×10^{-13} cm, then the problem becomes considerably shape-dependent.

Comparing the empirical values of D_J with the predictions of the modified Gaussian wells in I, we see that the "singulated Gaussian" cannot possibly fit the data and the "hard core Gaussian" gives a best fit around $\lambda=0.79$. Especially for high l, the shape dependence of the results is sufficient to raise the hope that studies of nuclear energy levels may yield information on the shape of the potential. This point is under further study.

The wave functions for the four states of Ca^{42} can be written out in the L–S or jj coupling representations. The mixture parameters [defined in Eq. (16) of I for the case of jj coupling] resulting from the semiempirical values of V_J given above are given in Tables V and VI.

IV. Ca^{43} AND THE THREE-BODY PROBLEM

The level energies and spin assignments given by Lindqvist and Mitchell[24] supplied the necessary information about Ca^{42}. They find levels at 0.369, 0.627, and 0.81 Mev with spins 5/2, 3/2, and 9/2 in that order. The ground state spin of 7/2 and magnetic moment of -1.3152 ± 0.0002 nm come from the work of Jeffries.[25] Levels at 0.38 and 0.61 are seen by Braams.[26]

TABLE V. Mixture parameters for the spin 0, 2, 4, and 6 states of Ca^{42} in the L–S coupling representation based on the semiempirical analysis of the levels of Ca^{41} and Ca^{43}.

J	f^{1J}	$f^{3J}(J-1)$	$f^{3J}(J+1)$	g^{1J}	$g^{3J}(J+1)$
0	0.884	···	−0.315	−0.335	0.098
2	0.896	0.351	−0.276	0	0
4	0.872	0.455	−0.194	0	0
6	0.864	0.503	···	0	0

A very general test of the presence of configuration interaction independent of the exchange properties or space dependence of the two body potential was described in Sec. IV of I. If configuration interaction is small the relations between the levels of Ca^{42} and Ca^{43} should be simply given in terms of fractional parentage coefficients. One might name the levels of Ca^{43} predicted from those of Ca^{42}, assuming pure configurations, "projected" levels. As shown in Fig. 2, the projected levels of Ca^{43} are not in good agreement with the observed levels (although the level order is the same). This proves that there exists no two-body potential which can predict the observed level spacings of both Ca^{43} and Ca^{43} and give negligible configuration interaction within the framework of the independent particle model.

The two-body analysis of Sec. III of I can be generalized to include three bodies so that Ca^{43} could be treated in a manner similar to Ca^{42}. There result four equations for the same unknowns V_0, V_2, V_4, and V_6. In this case the coefficients in these equations involve the empirically given energies of the excited states of Ca^{41} and Ca^{43} instead of the states of Ca^{41} and Ca^{42}. One can solve for the V_J's and compare with those found from the Ca^{42} analysis. Alternatively one can eliminate the V_J's from the equations and obtain relations between the levels of Ca^{42} and Ca^{43}. These relations would then include the effects of configuration interaction. This approach will not be reported on further in this paper but instead a less elegant but more straightforward one is used.

TABLE VI. Mixture parameters of the states of Ca^{43} in a jj representation based on the semiempirical analysis of the levels of Ca^{41} and Ca^{42}.

J	$f_{7/2^2}$	$f_{7/2f5/2}$	$f_{5/2^2}$	$g_{5/2^2}$	$g_{7/2^2}$
0	0.87	···	0.34	−0.31	−0.15
2	0.948	−0.212	0.238	0	0
4	0.915	−0.369	0.170	0	0
6	0.794	−0.610	···	0	0

Since all the two-body matrix elements are given as linear functions of V_J, we can apply Eq. (15) of I and obtain all the three-body matrix elements as linear functions of V_J. It then remains to diagonalize the resulting Ca^{43} matrices of the Hamiltonian. Upon calculating the various matrix elements, it was found that most of the nondiagonal elements were quite small with some notable exceptions. A series of transformations was

[24] T. Lindqvist and A. C. G. Mitchell, Phys. Rev. **95**, 1535 (1954).

[25] C. D. Jeffries, Phys. Rev. **90**, 1130 (1953).

[26] C. M. Braams, Phys. Rev. **95**, 650 (1954).

then applied to the matrix in question to reduce the magnitude of the larger nondiagonal elements below a certain preassigned value. When this process was completed the eigenvalues were obtained by using second order perturbation formulas. The results of this calculation and comparison with the experiments are shown in Table VII and Fig. 3. The spacings and spin assignments agree remarkably well with the experimental results. The difference in binding energy between Ca^{43} and Ca^{40} is 27.8 Mev. Subtracting out the 3.57 Mev calculated for the particle forces and dividing by three leaves 8.08 Mev for the single-particle bond rather than the 8.3 Mev used for Ca^{42}. This can be interpreted to mean that the single-particle bond has a dependence on the number of nucleons A. If we assume the $1/A$ dependence discovered by Kurath[13] in his analysis of the binding energies in the $f_{7/2}$ shell, then the 8.3-Mev bond in Ca^{42} would be an 8.1-Mev bond in Ca^{43} which agrees quite well with the calculated results.

The almost exact agreement between experiment and theory is probably fortuitous. First, the perturbation method of obtaining eigenvalues is only accurate to about 0.02 Mev. Secondly, some errors in the "empirical" levels of Ca^{41} and Ca^{42} are probably present. (Position of $g_{9/2}$ state in Ca^{41}, spin 6 state in Ca^{42}, etc.) Thirdly, the odd-state tensor force discussed in I has been neglected. This error is considerably reduced by the small triplet admixtures in the final wave functions as shown in Table V. Consider the spin-zero state of Ca^{42}. In zero order (pure $f_{7/2}^2$) it contains a 43 percent triplet admixture but this decreases to a 10 percent admixture in the final wave function. Since the tensor force is a triplet interaction and gives no contribution in singlet states, its effect is greatly diminished compared to its effect on a zero-order state which is given in Fig. 4 of I.

TABLE VII. Comparison of calculated and experimental energies for Ca^{42} in Mev. The experimental energy for the $J=7/2$ state is normalized to the calculated result. The diagonal matrix elements are given in order to illustrate the effect of configuration interaction.

J	Experimental[a] energies	Calculated energies	Diagonal matrix elements
7/2	−3.57	−3.57	−2.84
5/2	−3.20	−3.19	−2.77
3/2	−2.94	−2.96	−2.63
9/2	−2.76	−2.77	−2.13

[a] See reference 24.

In order to investigate further the influence of triplet forces, the following idealized problem was solved: The Hamiltonian was taken to be

$$H=H_0+aP_S+bP_T, \tag{11}$$

where P_S and P_T are singlet and triplet projection operators, a and b are numbers measuring the singlet and triplet potential strengths, and H_0 has two single-particle levels $f_{7/2}$ and $f_{5/2}$ separated by an energy $\Delta/2$. The two-body two-by-two energy matrix for the spin-zero state was set up and the percent of triplet state admixture P was computed. P is a function of one parameter ρ, where $\rho=(b-a)/\Delta$. $P(\rho)$ is shown in Fig. 5. In the case of Ca^{42} we take $a=\beta(f^20)\sim-4$ Mev where $\beta(f^20)$ is given in Eq. (6). Δ is 4 Mev and $b=0$ which gives a 12% triplet admixture. Now if a repulsive triplet force is added, the amount of triplet admixture decreases. For instance, if $b=2$ Mev we get a 7% triplet admixture. As mentioned in I, scattering data implys that the triplet odd-state force (triplet even forces do not occur between neutrons due to the Pauli principle) is indeed repulsive. We conclude that the neglect of triplet forces in the calculation is a good approximation, owing to the fact that the predominantly singlet forces tend to create predominantly singlet wave functions.

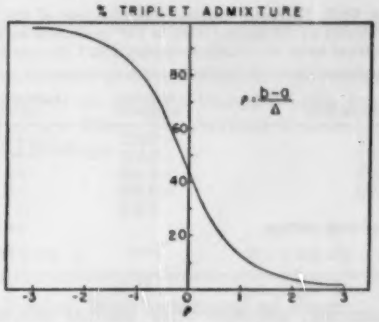

FIG. 5. Percent of triplet component (P) in the lowest spin zero wave function corresponding to the Hamiltonian of Eq. (11). ρ is defined just under Eq. (11).

The ground state of Ca^{43} was further investigated in order to find its magnetic moment. The general formulas for calculating three-body magnetic moments are given in Sec. V of I. The admixtures $f_{7/2}^2(2)f_{5/2}$, $f_{7/2}^2(4)f_{5/2}$ and $f_{7/2}^2(6)f_{5/2}$ (the number in parentheses gives the value of J to which $f_{7/2}^2$ is coupled before being coupled to $f_{5/2}$ to make a total J of 7/2) are the only ones which are coupled to the $f_{7/2}^3$ dominant mode by the magnetic moment operator defined in Eq. (19) of I. These admixtures are mainly responsible for the shift of the magnetic moment from the Schmidt line value given by $\langle f_{7/2}^3 7/2|\mu|f_{7/2}^3 7/2\rangle=-1.91$ nm because they contribute a value linear in the mixture amplitudes while other states can only give a contribution quadratic in the mixture amplitudes. The state $f_{5/2}^2(0)f_{7/2}$ was the only state not directly coupled to the $f_{7/2}^3$ state that gave an appreciable contribution to the magnetic moment. The magnitudes of the relevant mixture parameters and the contribution of each admixture to the magnetic moment (both diagonal and off-diagonal) are given in Table VIII.

We also include a small correction due to the motion of the core about the common center of mass of core and extra core particles, because it is easy to include

TABLE VIII. Magnetic moment contributions of the various admixed states to the ground state of Ca^{43} in nuclear magnetons. The empirical value is -1.315 (reference 25).

Admixed state	Mixture amplitude	Magnetic moment contribution
$7/2^3(2)5/2$	-0.025	$+0.033$
$7/2^3(4)5/2$	-0.081	$+0.211$
$7/2^3(6)5/2$	-0.108	$+0.271$
$5/2^3(0)7/2$	-0.209	-0.117
$7/2^3$	0.961	-1.764
Center-of-mass motion		$+0.061$
	Total	-1.305

approximately, although other omitted effects may contribute corrections of the same order of magnitude. The magnetic moment of a system composed of an extra core particle structure and a core is given by

$$\mu = g_c\langle I_c\rangle + g_J\langle I_J\rangle, \tag{12}$$

where g_c and g_J are the gyromagnetic ratios for the core and particle structure respectively and I_c and I_J are their total angular momenta about the center of mass of the system. This magnetic moment can be split up into two parts μ_1 and $\Delta\mu_c$, where

$$\mu_1 = g_J\langle I_c + I_J\rangle = g_J I_{\text{total}}, \quad \Delta\mu_c = (g_c - g_J)\langle I_c\rangle. \tag{13}$$

Now μ_1 is the part computed when one assumes the total angular momentum is associated with the particle structure and $\Delta\mu_c$ is the correction term associated with a nonvanishing value of I_c. g_c is taken to be Z/A and g_J is taken to be -0.377. $\langle I_c\rangle$ we approximate as $3\hbar/A$, since the dominant state ($^2F_{7/2}$, seniority 1) represents an orbital angular momentum of three units carried in effect by one particle. In this way, we obtain the crude estimate for $\Delta\mu_c$:

$$\Delta\mu_c = 0.061 \text{ nm}. \tag{14}$$

The agreement of the predicted and observed magnetic moments is nearly perfect and surely better than one could have expected. It shows, however, that the configuration mixing obtained for the ground state must be of the right order of magnitude.

Two low-lying levels in Ca^{43}, so far unobserved, may be predicted by using the same empirically determined matrix elements. These have spins 11/2 and 15/2, and predicted energies above the ground state,

$$E_{11/2} = 0.835 \text{ Mev}, \quad E_{15/2} = 1.00 \text{ Mev}.$$

V. SURFACE COUPLING

The results of II were employed to try to obtain a fit to the data with a combination of direct coupling and surface coupling. Best fits to energies and magnetic moment were obtained with zero surface coupling. A rough upper limit to the strength of coupling is expressed by

$$\hbar\omega \gtrsim 15 \text{ Mev}, \tag{15}$$

where $\hbar\omega$ is the surfon energy, and the mass parameter B and coupling parameter k are defined as in II. With stronger surface coupling, one can still approximately (but not well) fit the energies, but in order to do so it is necessary to reduce the strength of direct particle coupling. This in turn reduces the directly induced configuration mixing and causes the predicted magnetic moment shift to be appreciably less than the observed shift, in spite of the surface contributions to this shift. This argument applies in the region of weak surface coupling. Still stronger coupling has not been investigated closely, but intermediate coupling would predict such a large 0–2 spacing in Ca^{42} that the additional particle forces required would be unreasonably small. In the region of strong surface coupling, the surface induced 0–2 spacing would decrease again, but difficulties would arise in accounting for the relative spacings in Ca^{42} and for the level order in Ca^{43}. There is in any case no theoretical reason to expect strong surface coupling in these nuclei.

We conclude that the Ca^{40} core is an unusually rigid, undeformable, structure, like the analogous O^{16} core, for which the properties of O^{17} lead to the same conclusion.[25] The "hydrodynamic" value[26] of the surfon energy in Ca^{40} is about 4 Mev, to be compared with the limit in Eq. (15). As discussed in the introduction, however, it is not ruled out that some weak surface coupling is already included in our effective two-body potential, because of the semiempirical nature of the analysis. The only experimental test of the role of surface coupling in the calcium isotopes will be afforded by measurements of electric quadrupole effects, e.g., the $E2/M1$ ratios in γ decays in Ca^{43} or the ground-state quadrupole moment of Ca^{43}. Such data is not yet available. The problem of cascade *versus* crossover in the $3/2^- \rightarrow 7/2^-$ transitions in Ca^{43} is discussed in II.

VI. CONCLUSION

A remarkably accurate prediction of level spacings and magnetic moment of Ca^{43} has been made on the basis of the shell model perturbed by central two-body forces. Zero-order level spacings and interparticle interaction matrix elements were obtained empirically from Ca^{41} and Ca^{42}. The force was assumed to be central, two-body, and singlet for equivalent particles. The empirically determined potential appeared to be shallower and of longer range than that required to fit low-energy scattering. A study of the dependence of results on the radial shape of the potential suggests in a preliminary way that potentials with central repulsion may give a better simultaneous fit of scattering and of interparticle matrix elements in the nucleus than the Gaussian or Yukawa shapes. The analysis leads to the conclusion that surface coupling is not playing an important role in the calcium isotopes investigated. Configuration interaction is quite significant.

We have emphasized only energies and magnetic moments. Other important properties of the nuclear

states considered which will be significantly affected by configuration mixing are gamma decay rates and (p,d) or (d,p) cross sections, in addition, of course, to beta decay. These properties will need to be calculated, and similar analyses made of other nuclei in the vicinity before it can be concluded that the successful calculations reported here indeed represent an adequate description of the nuclear state.

It is a pleasure to acknowledge the many enlightening conversations we had with Professor Keith Brueckner, Dr. Richard Eden, Dr. Norman Francis, and Dr. Leonard Kisslinger.

PHYSICAL REVIEW VOLUME 100, NUMBER 1 OCTOBER 1, 1955

Gamma-Ray and Neutron Yields from the Proton Bombardment of Boron

J. K. Bair, J. D. Kington, and H. B. Willard
Oak Ridge National Laboratory, Oak Ridge, Tennessee

(Received June 21, 1955)

Yield curves of the gamma rays and neutrons resulting from the proton bombardment of boron have been measured for proton energies from approximately 2 to 5 Mev. Both the 0° and 90° yields for the $B^{11}(p,\gamma)C^{12}$ reaction have been measured for the ground state transition and for the transition to the 4.43-Mev state in C^{12}, as has the yield of the 2.14-Mev γ ray resulting from the inelastic scattering of protons on B^{11}. The neutron yield from $B^{11}(p,n)C^{11}$ is given at 0° and for almost 2π solid angle in the forward direction. New levels were observed in the C^{12} compound nucleus at 18.3, 18.39, 18.84, 19.2, 19.41, 19.66, 19.87, 20.25, 20.48, and 20.64 Mev. Preliminary data are given for the $B^{10}(p,n)C^{10}$ and $B^{10}(p,\gamma)C^{11}$ reactions.

I. INTRODUCTION

GAMMA-ray yield curves for B^{11} bombarded by protons have been reported by Huus and Day,[1] by Cochran, Ryan, Given, Kern, and Hahn,[2] and by Gove and Paul,[3] who give references to earlier data. In the present work, the γ-ray yields have been extended from the previous limit of 2.8 Mev to about 5-Mev proton bombardment energy for the reactions

$$B^{11}+p \rightarrow C^{12}+\gamma_0,$$

$$B^{11}+p \rightarrow C^{12*}+\gamma_1 \rightarrow C^{12}+\gamma_1+\gamma_2,$$

and

$$B^{11}+p \rightarrow B^{11*}+p' \rightarrow B^{11}+p'+\gamma_3.$$

Measurements were made at both 0° and 90° with respect to the bombarding proton beam.

Richards, Smith, and Browne[4] have found the threshold for the reaction

$$B^{11}+p \rightarrow C^{11}+n$$

to be 3.015 ± 0.003 Mev. Blaser, Boehm, Marmier, and Scherrer[5] have reported observation of the yield of C^{11} by a stacked foil technique. Neutron yield curves are given in the present paper for proton energies from threshold to approximately 5 Mev.

II. EXPERIMENTAL PROCEDURE

Protons from the ORNL 5.5 Mv Van de Graaff were magnetically analyzed by a 90° magnet whose slits were adjusted to about 0.1 percent energy resolution. A proton moment device was used to measure the magnetic field. Energy calibration is believed to be accurate within $\pm0.2\%$ relative to the $Li^7(p,n)Be^7$ threshold at 1.882 Mev.[6] An electrostatic strong focus lens system was used to focus the beam on targets located 15 to 25 feet from the magnet.

Thin boron targets were prepared by evaporating elemental boron of natural isotopic ratio on tantalum backings. Target thicknesses used for the data given here were about 30 kev at 3 Mev, although thinner targets were at times used. Target thicknesses were determined by measurements on the geometrical peak of the neutron yield from a very thin target, and then comparing the yield of this and the unknown target at a proton energy where the neutron yield was slowly varying. Similar targets of 96% B^{10} were available[6] and were used to check that the reactions measured were due to B^{11}. Although the B^{10} targets were free from serious impurities, considerable effort was necessary to produce suitable B^{11} targets. In addition to the usual fluorine contamination on the backing material, the first boron used contained an impurity, probably aluminum, which gave rise to a number of narrow resonances yielding high-energy γ rays and a rather intense low-energy γ ray of about 1 Mev. Targets made from natural boron of greater than 99% purity[7] were finally used for the γ-ray work and were quite satisfactory.

[1] Torben Huus and Robert B. Day, Phys. Rev. **91**, 599 (1953).
[2] Cochran, Ryan, Given, Kern, and Hahn, Phys. Rev. **87**, 672 (1952).
[3] H. E. Gove and E. B. Paul, Phys. Rev. **97**, 104 (1955).
[4] Richards, Smith, and Browne, Phys. Rev. **80**, 524 (1950).
[5] Blaser, Boehm, Marmier, and Scherrer, Helv. Phys. Acta **24**, 465 (1951).
[6] Herb, Snowden, and Sala, Phys. Rev. **75**, 246 (1949).
[6] Elemental B^{10} was obtained from the Stable Isotopes Division of this Laboratory.
[7] Varlocoid Chemical Company, 116 Broad Street, New York City.

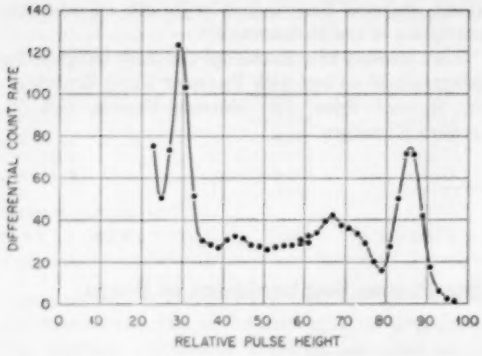

FIG. 1. $B^{10}(p,p')B^{10}$ and $B^{11}(p,p')B^{11}$ γ-ray spectrum as seen by NaI crystal spectrometer. $E_p=2.8$ Mev. The peak at a pulse height of 29 corresponds to the 0.72 Mev γ ray from scattering on B^{10}. The remaining three peaks are the usual single crystal peaks corresponding to the 2.14-Mev γ ray from scattering on B^{11}.

III. GAMMA-RAY MEASUREMENTS

A large 3-in. diameter, 3-in. high sodium iodide crystal in conjunction with a 3-in. photocathode photomultiplier tube, DuMont type K1197, was used as a detector for the proton-capture and inelastic-scattering γ rays. This combination has a resolution of 8% (full width at half maximum) for the Cs^{137} photopeak. Pulses from the photomultiplier were amplified using standard electronic techniques and recorded with a 20 channel pulse-height analyzer.[8] For the yield curves shown, the 20 channel analyzer was adjusted so as to cover only the region of the γ-ray spectrum of immediate interest, the datum plotted for a given proton bombarding energy (uncorrected for target thickness) is the reading in the channel corresponding to the maximum of the full energy peak corrected, if necessary, for the effect of any higher energy γ rays. This technique not only minimizes the effects of small changes in the over-all gain of the system, but simplifies measurements of the capture γ-ray yields since as the γ-ray energy changes due to changes in the bombarding proton energy, the peak in the spectrum merely moves from one channel to the next and can be easily followed.

Figure 1 gives a differential pulse height spectrum for the low-energy γ rays resulting from the bombardment of natural isotopic boron with 2.8-Mev protons. The peak at a pulse height of 29.5 is the 0.72-Mev γ ray from the reaction $B^{10}(p,p')B^{10*}$. The remaining peaks are the usual single crystal spectrometer peaks produced by the 2.14-Mev γ rays from the reaction $B^{11}(p,p')B^{11*}$, although the two-quantum escape peak (at a pulse height of 43) shows some effect of the target impurity previously mentioned. Energies were obtained by calibrating the crystal spectrometer with the known Cs^{137} and ThC'' γ rays, and agree with the previously measured level energies of 0.718 and 2.138 Mev in B^{10} and B^{11}, respectively,[9] and with the gamma-ray energies determined by Huus and Day.[1] It is to be noted that the full energy peak, at a pulse height of 86, is considerably accentuated over that obtained with the usual 1½ in. diameter crystal. The count rate corresponding to this peak (pulse height of 86) was plotted as a function of proton energy to obtain the B^{11} inelastic scattering γ-ray yield curves.

The lower curve (open circles) of Fig. 3 is the yield of the 2.14-Mev γ ray from the reaction $B^{11}(p,p')B^{11*}$ and was measured at 0° with respect to the proton beam and with the detector approximately 100 cm from the target. A similar curve taken at 90° differed in no essential respects and is not shown. Measurements of the 2.66-Mev resonance as well as higher energy resonances show the γ ray to be emitted isotropically. Neutron effects in the crystal could safely be neglected due to the intense yield of the inelastic scattering γ rays. Table I includes in Column 7 the energies of these γ-ray resonances, corrected for target thickness. No attempt was made to determine absolute γ-ray cross sections. However, the proton bombarding energy overlaps that of Huus and Day[1] sufficiently to permit normalization to their values.

Figure 2 shows a differential pulse-height curve of the B^{11} capture gamma rays for a bombarding proton energy (1.4 Mev) well below the threshold for neutron production. The maximum in the region of 17 pulse height units is due to the γ ray from the 4.43-Mev excited state in C^{12} and, when observed with narrower channels in the pulse-height analyzer, the usual three peaks were resolved. Peaks at 50 and 67 pulse-height units correspond to the capture transition to the 4.43-Mev state in C^{12} and to the ground state respectively.

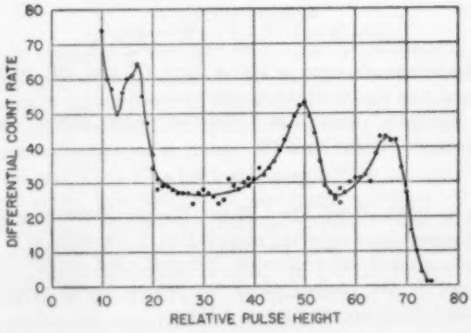

FIG. 2. $B^{11}(p,\gamma)C^{12}$ γ-ray spectrum as seen by 3 in.×3 in. NaI crystal spectrometer. $E_p=1.4$ Mev. The maximum at a pulse height of 17 is due to the γ ray from the 4.43-Mev excited state of C^{12}. The three peaks usually obtained with a single crystal spectrometer are not resolved due to the wide channel width. The maxima at pulse heights of 67 and 50 are due respectively to the ground state transition and the transition to the 4.43-Mev excited state. No structure was observed in these maxima even with considerably narrower channels.

[8] Kelley, Bell, and Goss, Oak Ridge National Laboratory Quarterly Progress Report ORNL-1278, 1951 (unpublished).

[9] F. Ajzenberg and T. Lauritsen, Revs. Modern Phys. **24**, 321 (1952), and Revs. Modern Phys. **27**, 77 (1955).

TABLE I. Characteristics of the observed levels in the C^{13} compound nucleus. Columns 2 through 7 give the proton energies at which maxima were observed in the yield respectively: of neutrons; γ rays to the 4.43-Mev level, as measured at 0°; the same γ ray as measured at 90°; the γ ray to the ground state, as measured at 0°; the same γ ray as measured at 90°; and the inelastic scattering γ ray. Column 8 gives an estimate of the width of the level at half maximum. Column 9 lists the energy of excitation in the compound nucleus.

1 Level	2 Neutrons Mev	3 γ_{1} 0° Mev	4 γ_{1} 90° Mev	5 γ_{0} 0° Mev	6 γ_{0} 90° Mev	7 γ_{0} Mev	8 Width Mev	9 Energy Mev
1	···	2.5	2.65	weak	···	···	0.3	18.3
2	···	···	···	···	···	2.66	0.046	18.39
3	3.17	3.12	3.14	weak	···	3.15	0.1	18.84
4	3.65	3.6	3.5	3.6	weak	3.4	0.5	19.2
5	···	···	···	···	···	3.78	0.05	19.41
6	4.05	···	···	···	···	···	0.2	19.66
7	···	weak	···	···	···	4.28	0.1	19.87
8	4.70	···	···	···	···	4.68	0.2	20.25
9	···	4.95	4.93	···	···	···	0.2	20.48
10	···	5.12	5.12	···	···	5.13	0.2	20.64

Measurements on these peaks with narrower channels did not resolve additional structure. Although the peaks are broad for these high-energy γ rays and one is uncertain as to their interpretation, they are in agreement with the energies expected from mass values and the kinetics of the reaction (15.95 Mev+11/12 E_p), and with this energy less that of the 4.43-Mev excited state in the C^{12} residual nucleus.

Due to the low intensity of the capture γ rays, neutron capture effects in the crystal itself are very troublesome above the neutron threshold. These effects can be minimized by neutron shielding between the source and crystal, provided such shielding does not seriously effect the gamma rays. A useful shield can be made by stirring as much finely divided lithium fluoride as possible into melted paraffin and casting the mixture into suitable shapes. For all the capture γ-ray yield curves given here, the crystal was located 3 in. to 5 in. from the target, the intervening space containing the neutron shield. Even with this neutron shielding, the number of neutron produced pulses, corresponding to γ-ray energies below 8 or 9 Mev, was sufficiently high to effectively prevent measurement of γ rays from the 4.43-Mev state in C^{12}. The background for the higher energy capture γ rays was negligibly small.

The yield of the capture γ rays as measured at 0° to the proton beam is given by the top two curves of Fig. 3. Measurements made at 90° are shown in the middle two curves. Open points indicate the transition direct to the ground state of C^{13}, whereas the solid points are essentially for the transition to the 4.43-Mev excited state. The data plotted for the "16" Mev gamma ray is the reading in the channel corresponding to the maximum in the pulse-height distribution. Data for the "12" Mev gamma ray have been corrected for the presence of the "16" Mev gamma ray by a method similar to that used by Gove and Paul.[3] For the large crystal used in this work, the "12" Mev gamma-ray data was corrected by subtracting ¼ of the count in the "16" Mev peak. Table I includes in columns 3, 4, 5, and 6 these data. A preliminary run (E_p=2 to E_p=5 Mev) on the B^{10} capture gamma rays at 90° to the proton beam, made for the purpose of checking any possible effects of the B^{10} content of the natural boron targets, indicated only a single, broad (one-half Mev) level at a proton energy of approximately 4 Mev.

IV. NEUTRON MEASUREMENTS

A conventional long counter was used to measure the neutron yield. Figure 4 shows typical curves of neutron yield as a function of bombarding proton energy, uncorrected for target thickness. The top curve (open points) was taken with the long counter at zero degrees with respect to the proton beam and 5 cm from the target; therefore, it gives the yield into somewhat less

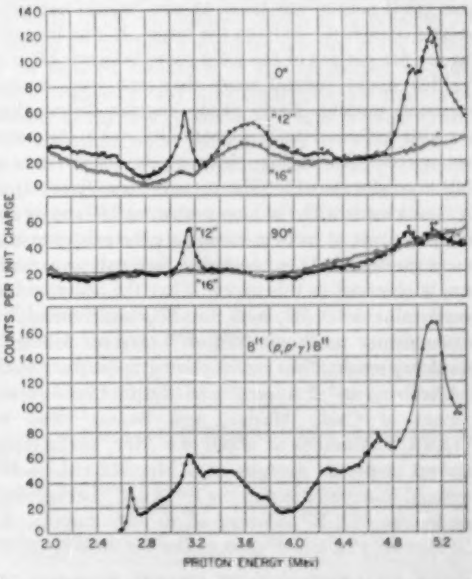

FIG. 3. Top pair of curves give the γ-ray yield from $B^{11}(p,\gamma)C^{12}$ in the forward direction. The middle pair of curves give similar data at 90°. Solid points represent the transition to the 4.43-Mev state in C^{13} and the open circles represent transitions to the ground state. The bottom curve is the 0° yield of 2.1-Mev γ rays resulting from the reaction $B^{11}(p,p')B^{11}$.

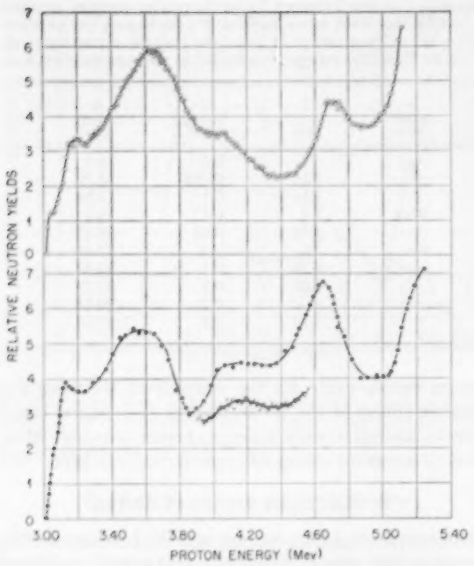

FIG. 4. Yield of neutrons from the $B^{11}(p,n)C^{11}$ reaction. Top curve: long counter at 0° and 5 cm from target. Middle curve: long counter at 0° and approximately 60 cm from target. Bottom curve: long counter at 15° and 40 cm from the target, region between $E_p=3.9$ and $E_p=4.55$ Mev only.

than 2π solid angle in the forward direction. The middle curve (solid points) was taken at zero degrees but with the long counter 60 cm from the target. It was thought that the flat portion of the yield curve between 4.0 and 4.4 Mev might conceal more than one level in the compound nucleus. Early crude angular distribution data also indicated such a possibility, with the most pronounced effect being observed in measurements made at angles near 15°. The bottom curve (crosses) of Fig. 4 was made with the long counter at 15° and 40 cm from the target to further investigate the existence of a second maximum. It is concluded that only one maximum is observed in this region. That the neutrons observed came from B^{11}, and not B^{10}, was verified by measurements made on 96% B^{10} targets. Although beta-decay results,[10] the recent photographic plate work of Ajzenberg and Franzen,[11] and the threshold measurement of Cook, Marion, and Bonner[9] lead to $B^{10}(p,n)C^{10}$ threshold at about 4.8 Mev, preliminary data up to proton energies of 6 Mev showed no B^{10} threshold observed through the $B^{11}(p,n)C^{11}$ background due to the 2% B^{11} content of the B^{10} targets. At 3.55 Mev the absolute 0° cross section for the $B^{11}(p,n)C^{11}$ reaction was measured to be 5.4±0.5 millibarns per steradian. [*Note added in proof.*—The value of this cross section is about one-third that observed by the group at Rice Institute (T. W. Bonner, private communication). It is quite possible that our targets were actually B_2O_3 instead of metallic boron, as suggested by Dr. Bonner. A check on the cross section will be made.]

Table I lists the proton energies of the observed levels, the corresponding excitation energies in the C^{12} compound nucleus, and an estimate of the width of the levels. Resonant energies are taken from the large solid angle yield curve (top of Fig. 4), since such a procedure minimizes any apparent energy shifts due to the angular distribution of the neutrons. Energies are corrected for target thickness.

V. DISCUSSION

In addition to the known resonance at 2.66 Mev, maxima are found in the $B^{11}(p,p'\gamma)B^{11}$ yield at 3.15, 3.4, 3.78, 4.28, 4.68, and 5.13-Mev proton bombarding energies. These levels are observed in both 0° and 90° yield curves with the same intensity. This isotropy, independent of energy and hence of the levels formed in the compound nucleus, could lead to the conclusion that the spin of the first excited state in B^{11} is $\frac{1}{2}$. Due to the curious accidental degeneracy of the Racah coefficient relating an $L=2$ transition between two states of $J=\frac{3}{2}$, there is some ambiguity in this assignment. However, in the case of $\frac{3}{2}\rightarrow\frac{3}{2}$, some admixture of the $L=1$ transition might be expected, which would remove the isotropy.

Capture γ-ray yield curves show resonances at proton energies of 2.6, 3.14, 3.6, 4.94, and 5.12 Mev. This lowest energy resonance was not apparent in the work of Huus and Day[1] since they give 90° yield curves only, and at this angle their maximum proton energy was barely above the maximum yield. There is no disagreement in the data. Gove and Paul[3] discuss a level at about this energy.

Neutron yield curves, Fig. 4, indicate resonances at proton energies of 3.17, 3.65, 4.05, and 4.70 Mev. Blaser[6] *et al.*, using a stacked foil technique and detecting C^{11}, have found maxima at 3.7, 5.18, 5.87, and 6.37 Mev. Their levels at 3.7 and 5.18 Mev evidently correspond to our level at 3.65 Mev and to the rise at the upper energy of our data, respectively. The low resolution of the stacked foil technique undoubtedly explains why our resonances at 3.17, 4.05, and 4.70 Mev are not apparent in their work.

Table I summarizes the data on the resonances in C^{12} as obtained from the present work.

The authors would like to express their thanks to Dr. Normal H. Lazar of this Laboratory for the large NaI crystal used in the γ-ray work.

[10] R. Sherr and J. B. Gerhart, Phys. Rev. **91**, 909 (1953).
[11] F. Ajzenberg and W. Franzen, Phys. Rev. **95**, 1531 (1954).

Collision Matrix for (n,d) and (p,d) Reactions*

R. G. THOMAS
Los Alamos Scientific Laboratory, University of California, Los Alamos, New Mexico
(Received April 27, 1955)

The contributions to (n,d), (p,d) reactions and their inverses from the pickup and stripping mechanisms are considered as corrections to the compound-nucleus or R-matrix theory of nuclear reactions. In an (n,d) reaction, for example, the R-matrix theory neglects the interaction of the incident neutron with the target-nucleus proton "tails" which extend beyond the nuclear radius. The pickup correction to the collision-matrix component, or reaction amplitude, appears as the matrix element of the neglected interaction involving an exact wave function and the approximate wave function of the compound-nucleus system not having the interaction; a distorted-wave Born approximation is used in which the former exact wave function is replaced by one of the latter type with the appropriate radiation condition. An explicit expression is given for the collision-matrix component which, together with the compound-nucleus contribution, can be substituted directly into the formulas of Blatt and Biedenharn for total reaction cross sections and angular distributions. In general, the angular distributions contain interference terms in addition to the straight pickup and compound-nucleus contributions. If the distorted neutron and deuteron spherical partial waves are assumed to depend only on the angular momenta, and not explicitly on the total spin and the channel spins, the formula of Tobocman is obtained for the pickup contribution, while Butler's formula is obtained if plane waves are used instead of distorted waves. There are discussions of the various approximations, the exchange terms, and the question of the nuclear radius.

I. INTRODUCTION

THE theories of deuteron stripping and formation by pickup, which were first formulated by Butler[1] and by Bhatia, Huang, Huby, and Newms[2] for applications at intermediate energies where it is possible to observe the angular distributions of the individual particle groups,[3] have been the subject of numerous theoretical studies.[4] However, it does not appear that any of these investigations have revealed how the compound-nucleus contribution to these deuteron reactions can be fitted into a general theory in a manner which is also useful for interpretations. The purpose of this note is to show formally how this can be done and to give an explicit form of the stripping or pickup contribution to the collision matrix which, together with the compound-nucleus contribution, can be substituted directly into the formulas of Blatt and Biedenharn[5] for the total reaction cross sections and angular distributions. The present derivation of the stripping or pickup contribution is also simpler than some of the previous ones in that the desired collision-matrix components are obtained directly by an application of Green's theorem to the wave equations involved, rather than by introducing Green's functions, such functions not being necessary for the usual approximate procedures (plane-wave or distorted-wave Born approximations). With the present results it is possible, for example, to interpret a stripping reaction in the vicinity of an isolated resonance of the compound nucleus,[6] which resonance may also contribute an appreciable number of reaction products, and it is possible to consider the distortion by the nucleus of the wave functions involved in the evaluation of the stripping contribution.[7] The present formulation should also be applicable to a more detailed interpretation of other "surface" or "direct" interactions, such as the (n,p) and (n,n') reaction mechanisms proposed by Austern, Butler, and McManus.[8]

Wigner, Eisenbud, and Teichmann[9] have developed a general theory of nuclear reactions, the R-matrix theory, which is particularly useful for considering reactions which proceed through one or two isolated

* Work performed under the auspices of the U. S. Atomic Energy Commission.

[1] S. T. Butler, Phys. Rev. **80**, 1095 (1950); Proc. Roy. Soc. (London) **A208**, 559 (1951); Phys. Rev. **88**, 685 (1952).

[2] Bhatia, Huang, Huby, and Newms, Phil. Mag. **43**, 485 (1952).

[3] The earlier work on deuteron reactions was primarily concerned with the excitation functions or with the angular distributions at high energies where the resolution of the individual particle groups is not of concern. See J. R. Oppenheimer and M. Phillips, Phys. Rev. **48**, 500 (1935); H. A. Bethe, Phys. Rev. **53**, 39 (1938); R. Serber, Phys. Rev. **72**, 1008 (1947); D. C. Peaslee, Phys. Rev. **74**, 1001 (1948); G. F. Chew and M. L. Goldberger, Phys. Rev. **77**, 470 (1950).

[4] P. B. Daitch and J. B. French, Phys. Rev. **87**, 900 (1952); R. Huby, Proc. Roy. Soc. (London) **A215**, 385 (1952); N. Austern, Phys. Rev. **89**, 318 (1953); E. Gerjuoy, Phys. Rev. **91**, 645 (1953); F. L. Friedman and W. Tobocman, Phys. Rev. **92**, 93 (1953); J. Horowitz and A. M. L. Messiah, Phys. Rev. **92**, 1326 (1953) and J. phys. et radium **14**, 695 (1953); N. C. Francis and K. M. Watson, Phys. Rev. **93**, 313 (1954); S. Yoshida, Progr. Theoret. Phys. (Japan) **10**, 1, 370 (1953); Fujimoto, Hayakawa, and Nishijima, Progr. Theoret. Phys. (Japan) **10**, 113 (1953); R. D. Dalitz, Proc. Phys. Soc. (London) **A66**, 28 (1953); M. Gell-Mann and M. L. Goldberger, Phys. Rev. **91**, 398 (1953); E. Clementel, Nuovo cimento **11**, 412 (1954); S. T. Butler and N. Austern, Phys. Rev. **93**, 355 (1954); W. Tobocman, Phys. Rev. **94**, 1655 (1954); J. Yocoz, Proc. Phys. Soc. (London) **A67**, 813 (1954); I. P. Grant, Proc. Phys. Soc. (London) **A67**, 981 (1954) and **A68**, 244 (1955). A review of the experimental material and of the theoretical work has been presented by R. Huby, Progr. Nuclear Phys. **3**, 177 (1953).

[5] John M. Blatt and L. C. Biedenharn, Revs. Modern Phys. **24**, 258 (1952).

[6] Berthelot, Cohen, Cotton, Faraggi, Grjebine, Levêque, Naggiar, Roclawski-Conjeaud, and Szteinsznaider, Compt. rend. **238**, 1312 (1954); Holmgren, Blair, Simmons, Stratton, and Stuart, Phys. Rev. **95**, 1544 (1954); Jones, McEllistrem, Douglas, Herring, and Silverstein, Phys. Rev. **98**, 241(A) (1954).

[7] Numerical evaluations of the effects of such distortions have been made by W. Tobocman and M. H. Kalos, Phys. Rev. **97**, 132 (1955).

[8] Austern, Butler, and McManus, Phys. Rev. **92**, 350 (1953).

[9] E. P. Wigner and L. Eisenbud, Phys. Rev. **72**, 29 (1947); T. Teichmann and E. P. Wigner, Phys. Rev. **87**, 123 (1952). Additional references on the development of this theory are cited in these papers.

levels of the compound nucleus. This theory is also readily applicable to the region of nuclear excitations where many levels overlap, provided that the signs of the reduced-width amplitudes $\gamma_{\lambda c}$, for the levels λ and channels c, are uncorrelated,[10] such a lack of correlations presumably being the case if the interactions in the internal, or compound-nucleus region, are relatively strong. In this application the compound nucleus is found to manifest many of the reaction properties which have been well known from the work of Weisskopf and his collaborators.[11] The salient features of such compound-nucleus reactions are the symmetry of the angular distributions and the Maxwellian nature of the energy distributions. In contrast, the stripping and pickup angular distributions are generally peaked forward and the energy distributions are concentrated at the higher energies. These departures could of course be attributed to correlations of the signs of the $\gamma_{\lambda c}$. However, in an examination of the derivation of the R-matrix theory one notices that the derivation assumes that the nuclear interactions are confined to an internal or compound-nucleus region of the configuration space and thereby neglects, for example, the interaction of an incident neutron, while it is in the external neutron channel, with the "tail" of the wave function of a proton from the target nucleus, which tail extends to infinity though in an exponentially decaying manner. The present theories of pickup (or stripping) do indeed suggest that it is just such interactions which give rise to the deuterons in an (n,d) reaction. Since the total neutron cross sections are satisfactorily described by the compound-nucleus theory and since they are observed to be an order of magnitude larger than the total (n,d) reaction contribution, it seems reasonable to use the R-matrix theory for the interpretation of the interaction of the incident neutron with the bulk of the nucleus and then to correct for the external interaction with the proton by a first-order perturbation calculation using the compound-nucleus wave functions as first approximations. The collision-matrix component $U_{n;d}$ referring to an (n,d) reaction appears then as a sum $U_{n;d}=\mathfrak{U}_{n;d}+\Delta U_{n;d}$, where $\mathfrak{U}_{n;d}$ represents the compound-nucleus contribution and $\Delta U_{n;d}$ the external pickup correction term. The cross section therefore contains terms proportional to $|\mathfrak{U}_{n;d}|^2$ for the straight compound-nucleus contribution, to $|\Delta U_{n;d}|^2$ for the pickup contribution, and to interference terms of the form $\mathfrak{U}_{n;d}\Delta U_{n;d}^*+$c.c. At nuclear excitations where the levels overlap, the interference terms will vanish if averaged over a sufficiently wide energy interval, provided that the signs of the $\gamma_{\lambda c}$ are uncorrelated.[10] On the other hand, these terms may be important in the vicinity of an isolated resonance level.

The pick-up term $\Delta U_{n;d}$ appears as the matrix element of the perturbing np interaction of the external region. This matrix element involves the wave function of the complete Hamiltonian which includes the perturbing interaction, and the wave function of the Hamiltonian with just the internal or compound-nucleus interactions. An approximation for its evaluation is the replacement of the former type wave function by one of the latter type with the same radiation condition, as in a Born approximation. Since the "distorted" waves of the compound nucleus are used rather than plane waves, this evaluation is expected to be more accurate than the usual "plane-wave" Born-approximation calculation. The distorted-wave method has been presented for general applications by Mott and Massey[12]; it has also been discussed and applied in various forms to stripping and pickup reactions by Horowitz and Messiah,[4] by Francis and Watson,[4] by Tobocman,[4] and by Kalos and Tobocman.[7] It was first noted by Francis and Watson,[4] that at nuclear excitations where the levels overlap, the complex potential representations of the nucleon-nucleus interaction[10,13] may be useful for constructing the external wave functions which are involved in the correction matrix element.

II. DERIVATION BY MEANS OF GREEN'S THEOREM

The derivation proceeds by considering the two wave equations

$$H\Psi=E\Psi, \tag{1a}$$

$$\mathcal{H}\Phi=E\Phi. \tag{1b}$$

Here H is the complete Hamiltonian and $\mathcal{H}=H-\Delta V$ is the Hamiltonian for the system not having the interaction ΔV between the neutron and proton in the external region, that is, in the region where both are situated at distances from the center of the residual nucleus which are larger than the nuclear radius a; Ψ and Φ are the respective wave functions with the hereinafter specified radiation conditions. By application of Green's theorem to the integral over the configuration space τ of the difference of (1a) multiplied on the left by Φ^* and the complex conjugate of (1b) multiplied on the right by Ψ, one obtains[14]

$$\int_\tau \Phi^*\Delta V\Psi d\tau=\int_S (\hbar^2/2M_a)\times(\Psi\,\mathrm{grad}_n\Phi^*-\Phi^*\,\mathrm{grad}_n\Psi)dS, \tag{2}$$

[10] R. G. Thomas, Phys. Rev. **97**, 224 (1955).

[11] V. F. Weisskopf, Phys. Rev. **52**, 295 (1937); V. F. Weisskopf and D. H. Ewing, Phys. Rev. **57**, 472, 935 (1940); H. Feshbach and V. F. Weisskopf, Phys. Rev. **76**, 1550 (1949); and, in particular, J. M. Blatt and V. F. Weisskopf, *Theoretical Nuclear Physics* (John Wiley and Sons, Inc., New York, 1952), Chaps. VIII and IX.

[12] N. F. Mott and H. S. W. Massey, *The Theory of Atomic Collisions* (Oxford University Press, London, 1949), Chap. VIII, Sec. 5.

[13] N. C. Francis and K. M. Watson, Phys. Rev. **92**, 291 (1953); Feshbach, Porter, and Weisskopf, Phys. Rev. **96**, 448 (1954); Lane, Thomas, and Wigner, Phys. Rev. **98**, 693 (1955).

[14] G. Breit, Phys. Rev. **58**, 1068 (1940); E. P. Wigner, Phys. Rev. **70**, 15 (1946).

provided that the surface S is far enough out so that the nuclear systems can be regarded as decomposed into groups of two-particle subsystems of reduced masses M_c; groups involving three or more subsystems are ignored.

For the consideration of an (n,d) reaction, the example to be used throughout, spherical waves of the following asymptotic form are substituted in (2):

$$\Psi_d=\sum_c(\delta_{cd}\mathcal{I}_c-U_{c;d}\mathcal{O}_c), \tag{3a}$$

$$\Phi_n=\sum_c(\delta_{cn}\mathcal{O}_c-\mathfrak{U}_{c;n}{}^*\mathcal{I}_c), \tag{3b}$$

where $\mathcal{I}_c$ and $\mathcal{O}_c$ are wave functions for the various channels c representing unit-flux *incoming* and *outgoing* waves, respectively; U and $\mathfrak{U}$ are the collision matrices associated with the Hamiltonians H and $\mathfrak{K}$, respectively. The radiation condition imposed on the solution Ψ_d is that only the deuteron channel d has an *incoming* wave, while the condition imposed on Φ_n is that only the neutron channel n has an *outgoing* wave. The Φ_n of (3b) is thus a solution which is the time-reversed of the usual type, such as (3a), having an *incoming* wave in only one channel.[12,15] The expansion of Φ_n is valid throughout the entire external part of the configuration space, whereas the expansion of Ψ_d is the asymptotic form which is valid only at distances far from the origin where even the interaction ΔV is negligible.

As in the work of Wigner and Eisenbud,[9] $\mathcal{I}_c$ and $\mathcal{O}_c$ wave functions are constructed for each channel c having a definite value of the channel spin j, which is a vector sum of the spins of the two particles of the group, and of the total spin J, which is a vector sum of j and the relative angular momentum $\hbar l$ of the two particles, and of the total spin component M along the beam direction; the channel subscript c thus refers to the set of quantities $\alpha jlJM$, where α denotes the nature of the pair and their respective states of excitation. These wave functions are therefore of the form

$$\mathcal{I}_{\alpha jlJM}=\sum_{\nu m}(jl\nu m|JM)\psi(\alpha j\nu)\times(i^lY_{lm}(\Omega_a))v_a{}^{-\frac{1}{2}}r_a{}^{-1}I_{al}(r_a), \tag{4a}$$

$$\mathcal{O}_{\alpha jlJM}=\sum_{\nu m}(jl\nu m|JM)\psi(\alpha j\nu)\times(i^lY_{lm}(\Omega_a))v_a{}^{-\frac{1}{2}}r_a{}^{-1}O_{al}(r_a). \tag{4b}$$

Here $\psi(\alpha j\nu)$ is the sum of the products of the wave functions of the two members of the pair α, which sum has a definite channel spin j, component ν; Y_{lm} is the spherical harmonic with the usual property $Y_{lm}{}^*=(-1)^mY_{l-m}$; and v_a is the relative velocity.[16] The radial functions in (4) are taken to be

$$I_{al}=(G_{al}-iF_{al})\exp(i\psi_{al})\sim\exp[-i(\rho_a-\eta_a\log 2\rho_a-\tfrac{1}{2}l\pi+\sigma_{a0})], \tag{5a}$$

$$O_{al}=I_{al}{}^*, \tag{5b}$$

where $\sigma_{a0}=\arg\Gamma(1+i\eta_a)$ and $\psi_{al}=\sum_{s=1}{}^l\tan^{-1}(\eta_a/s)$ are Coulomb phases, $\eta_a=Z_{1a}Z_{2a}e^2/\hbar v_a$ is the Coulomb field parameter, and $\rho_a=M_av_ar_a/\hbar=k_ar_a$; F and G are the usual regular and irregular external radial wave functions.

By substituting the expansions (3) into the right side of (2) with the surface S at infinity and by noting that the Wronskian $I(dO/d\rho)-O(dI/d\rho)=2i$, one immediately finds that

$$\Delta U_{n;d}=U_{n;d}-\mathfrak{U}_{n;d}=(i/\hbar)\int_\tau\Phi_n{}^*\Delta V\Psi_d d\tau. \tag{6}$$

The matrix element on the right gives the correction $\Delta U_{n;d}$ which is to be added to the compound-nucleus contribution $\mathfrak{U}_{n;d}$ in order to obtain the total collision matrix component $U_{n;d}$. As noted by Watson and by Breit and Bethe,[15] the use of a wave function having an incoming wave in only one channel, rather than the Φ_n of (3b), would not give $\Delta U_{n;d}$, but a sum over channels c of the products of the components $U_{c;d}$ and $\mathfrak{U}_{n;c}$.

III. APPROXIMATIONS AND EVALUATIONS OF THE COMPONENT SUMS

As mentioned in the Introduction, the basic approximation of the present approach is the replacement of the exact wave function Ψ_d in (6) by a solution with the same radiation condition to the partial Hamiltonian $\mathfrak{K}$. It is also assumed that the contributions to the matrix element (6) from the reaction channels of the Ψ_d and Φ_n solutions can be neglected; that is, these wave functions are approximated in the external region by

$$\Psi_d=\mathcal{I}_d-\mathfrak{U}_{d;d}\mathcal{O}_d, \tag{7a}$$

$$\Phi_n=\mathcal{O}_n-\mathfrak{U}_{n;n}{}^*\mathcal{I}_n. \tag{7b}$$

The second approximation neglects, for example, the possibility that a neutron, which is inelastically scattered by a compound-nucleus process, could on emergence pick up a proton to form a deuteron.[17] The inclusion of such contributions does not present any formal difficulties, but does make the final formulas more cumbersome. A third approximation is the neglect of the tensor np force which gives rise to the ^3D component of the deuteron wave function; this neglect may be justified by a plane-wave, Born-approximation cal-

[15] See K. M. Watson, Phys. Rev. **88**, 1163 (1952); G. Breit and H. A. Bethe, Phys. Rev. **93**, 888 (1954).

[16] The behaviors under the time-reversal operation K of the wave functions in (4) are

$$K\psi_{(\alpha j\nu)}=(-1)^{j-\nu}\psi_{(\alpha j-\nu)},\quad K(i^lY_{lm})=(-1)^{l-m}(i^lY_{l-m}).$$

This representation was suggested by L. C. Biedenharn and M. E. Rose, Revs. Modern Phys. **25**, 736 (1953), and differs from the one used by Wigner and Eisenbud. As noted by R. Huby, Proc. Phys. Soc. (London) **A67**, 1103 (1954), the use of the present representation requires that the Z coefficients in Eq. (4.6) of Blatt and Biedenharn for the differential cross sections be replaced by the coefficients $\bar{Z}(l_1J_1l_2J_2;jL)=i^{l_1-l_2-L}Z(l_1J_1l_2J_2;jL)$.

[17] According to calculations by B. H. Bransden, Proc. Phys. Soc. (London) **A65**, 738 (1952), such processes are likely to be important at energies above 200 Mev. See also W. N. Hess and B. J. Moyer, Phys. Rev. **96**, 859(A) (1954).

culation which shows that the contribution from this component is incoherent and therefore negligible compared with the ^3S contribution.[18] As in the work of Horowitz and Messiah,[4] it is assumed as a fourth approximation that the interaction ΔV between neutron and proton can be replaced by a zero-range (central-force) interaction[19]; if $\chi(\mathbf{r})$ is the wave function for the relative motion of the neutron and proton in the ground state of the deuteron, then

$$\Delta V(\mathbf{r})\chi(\mathbf{r}) = -(\hbar^2/M)(8\pi\alpha)^{\frac{1}{2}}\delta(\mathbf{r}), \tag{8}$$

where $\alpha^{-1}=(\hbar^2/MB)^{\frac{1}{2}}=4.4\times10^{-13}$ cm is the "radius" of the deuteron associated with its binding energy B, $\delta(\mathbf{r})$ is the three-dimensional delta function, and M is the nucleon mass.

The final bit of information needed for the evaluation of (6) is an expansion of the wave function of the target nucleus t in the external region of the configuration space where the contributions occur; that is, it is necessary to know the form of the proton "tails" which can be picked up. This wave function appears as one of the factors in the $\psi(\alpha j\nu)$ of (4) when the latter is used in (7b). The expansion is taken to be

$$\psi(tI_t i_t) = \sum (I_f \tfrac{1}{2} i_f i_p | j_p \nu_p)(j_p l_p \nu_p m_p | I_t i_t) \times \psi(\alpha_f I_f i_f)\psi(p\tfrac{1}{2}i_p)u(\alpha_f j_p l_p; r_p) r_p^{-1} \times [i^{l_p} Y_{l_p m_p}(\Omega_p)], \tag{9}$$

the sum being with respect to $\alpha_f j_p \nu_p l_p m_p i_f i_p$. Here I_t, i_t and I_f, i_f are the spins and components of the states of the target and final nucleus, respectively; $\psi(\alpha_f I_f i_f)$ is the wave function of the final nucleus in the excitation state α_f and $\psi(p\frac{1}{2}i_p)$ is the wave function representing the pickedup proton in the spin state i_p; l_p and m_p designate the orbital angular momenta and components of the proton tails; the channel spins j_p are the vector sums of the proton spin $\frac{1}{2}$ and I_f, and their components are ν_p; the $(i^{l_p}Y_{l_p m_p})$ are the angular parts of the proton wave functions and the $u(r_p)$ are r_p-times the radial parts, the latter being considered as real because they may be defined as scalar products.[20] It is convenient to express the radial parts as

$$u(\alpha_f j_p l_p; r_p) = \gamma(\alpha_f j_p l_p)(2M\epsilon a/\hbar^2)^{\frac{1}{2}} \times [W(-\eta_p, l_p+\tfrac{1}{2}; 2k_p r_p)/ W(-\eta_p, l_p+\tfrac{1}{2}; 2k_p a)]. \tag{10}$$

Here $\gamma(\alpha_f j_p l_p)$ is the reduced-width amplitude for the separation in the external region of the ground state of the target nucleus into a proton and a state α_f of the final nucleus; M is the nucleon mass; $W(-\eta, l+\frac{1}{2}; 2kr)$ is the exponentially decaying Whittaker function; $k_p=(2M\epsilon B_{pf}/\hbar^2)^{\frac{1}{2}}$ is the wave number associated with the binding energy B_{pf} of the proton in the ground state of the target to the state α_f of the final nucleus; $\eta_p=Z_f e^2 M\epsilon/\hbar^2 k_p$ is the corresponding Coulomb field parameter; $\epsilon=A_t-1/A_t$ is the ratio of the masses of the final and target nuclei.[21]

With the above information and approximations the matrix element (6) can readily be evaluated, the methods of Racah[22] being used to perform the sums over the various spin components. The result is that

$$\Delta U(nj_n l_n; dj_d l_d; J) = 2if(-1)^{I_f - I_t + J}(2I_t+1)^{\frac{1}{2}} \sum_{j_p l_p} (-1)^{l_p - i_p}(2j_p+1)^{\frac{1}{2}} \times \gamma(j_p l_p) W(\tfrac{1}{2}1 j_p j_d; \tfrac{1}{2} I_f) W(I_d l_p \tfrac{1}{2} j_d; j_p j_n) \times \bar{Z}(l_n j_n l_d j_d; J l_p) R(j_n l_n, j_d l_d; l_p J), \tag{11}$$

where

$$f=(3\alpha a/M\epsilon v_n v_d)^{\frac{1}{2}},$$

and the (dimensionless) radial integral is

$$R(j_n l_n, j_d l_d; l_p J) = i^{l_p - l_n + l_d}\int_a^\infty \frac{dr}{r}\cdot\frac{W(-\eta_p, l_p+\frac{1}{2}; 2k_p r)}{W(-\eta_p, l_p+\frac{1}{2}; 2k_p a)} \times [I_{l_n}(\sigma r) - \mathfrak{U}(nj_n l_n; nj_n l_n; J) O_{l_n}(\sigma r)] \times [I_{l_d}(r) - \mathfrak{U}(dj_d l_d; dj_d l_d; J) O_{l_d}(r)]; \tag{11a}$$

W is the Racah coefficient and the relation between the $\bar{Z}$ coefficient and the Z coefficient of Blatt and Biedenharn is given in reference 16. The angular distributions may be obtained by substitution of these collision-matrix components, together with those for the compound-nucleus contribution, into the formulas given by Blatt and Biedenharn,[5] and polarizations may be deduced from the formulas of Simon and Welton.[23] Since ΔU is symmetrical, this result applies also to (d,n) reactions; the modifications required for (p,d) and (d,p) reactions should be obvious.

The presence of the Racah and $\bar{Z}$ coefficients in (11) implies that there are selection rules. In addition to the

[18] R. D. Dalitz, reference 4; R. G. Thomas (unpublished).

[19] See G. Breit, Phys. Rev. **71**, 215 (1947) where the validity of such an approximation is investigated in detail in connection with the problem of the interaction of slow neutrons with bound protons.

[20] See Eq. (4) of Wigner and Eisenbud, reference 9.

[21] The dimension of the reduced-width amplitude used here is the square root of energy (see Sec. II of reference 10); it is normalized with respect to all configuration space, rather than just the internal region as in the resonance applications, the difference usually being negligible. In the expansion for a pickup neutron, which is involved in a (p,d) reaction, $\eta_p=0$ and $W(0, l+\frac{1}{2}; 2z) = (2z/\pi)^{\frac{1}{2}}K_{l+\frac{1}{2}}(z)$, where $K_{l+\frac{1}{2}}(z)$ is the modified Bessel function [see Sec. II-B of R. G. Thomas, Phys. Rev. **88**, 1109 (1952)].

[22] Biedenharn, Blatt, and Rose, Revs. Modern Phys. **24**, 249 (1952).

[23] A. Simon and T. A. Welton, Phys. Rev. **90**, 1036 (1953); Albert Simon, Phys. Rev. **92**, 1050 (1953). The remarks in footnote 16 concerning the modification in the convention for time reversal also apply to these papers; the i factors involving angular momentum exponents should be deleted and the Z coefficients replaced by $\bar{Z}$ coefficients. Polarizations in stripping and pickup processes have been investigated by W. B. Cheston, Phys. Rev. **96**, 1590 (1954), by J. Horowitz and A. M. L. Messiah, J. phys. radium **14**, 731 (1953), and by H. C. Newns, Proc. Phys. Soc. (London) **A66**, 477 (1953).

expected ones: $\mathbf{j}_n+\mathbf{l}_n=\mathbf{J}$; $\mathbf{j}_d+\mathbf{l}_d=\mathbf{J}$; $\frac{1}{2}+\frac{1}{2}=1$; $\frac{1}{2}+\mathbf{I}_f=\mathbf{j}_p$; $1+\mathbf{I}_f=\mathbf{j}_d$; $\frac{1}{2}+\mathbf{I}_i=\mathbf{j}_n$; $\mathbf{l}_p+\mathbf{j}_p=\mathbf{I}_i$; there are also the relations $\mathbf{j}_n+\mathbf{j}_d=\mathbf{I}_p$; $\frac{1}{2}+\mathbf{j}_d=\mathbf{j}_p$; $\mathbf{l}_n+\mathbf{l}_d=\mathbf{I}_p$. There is also the parity rule $l_n+l_d+l_p=$ even.

At intermediate and high energies where many partial waves l_n and l_d contribute to the pickup process, the cross section evaluations will in general be very tedious. Fortunately, some simplification is possible if it is assumed that the diagonal collision-matrix components in the radial integrals of (11) are independent of the total spin and of the channel spins, in which case the radial integrals depend only on l_n, l_d, and l_p. This simplification is quite reasonable for applications at excitation energies where the levels overlap. Indeed, at such excitations it is the practice to represent the neutron-nucleus or deuteron-nucleus interactions by models which depend on only the angular momentum, such as the strong-coupling or complex potential models (without a spin-orbit coupling dependence). With this simplification the sums over the total spin J and the channel spins j_n, j_d in the formulas of Blatt and Biedenharn can be evaluated using the unitary properties of the transformation coefficients and the Racah sum rules.[22] One finds that the pickup contribution to the (n,d) differential cross sections is given by

$$[d\sigma_{n;d}(\theta_d)/d\Omega_d]_{\text{pickup}} = \tfrac{1}{4}k_n^{-2}f^2\sum_{l_p}(2l_p+1)^{-2}\gamma(l_p)^2Q(l_p), \quad (12)$$

where

$$\gamma(l_p)^2=\sum_{j_p}\gamma(j_pl_p)^2,$$

and

$$Q(l_p)=\sum_{m=-l_d}^{l_d}\Big|\sum_{l_nl_d}(2l_n+1)(2l_d+1)\Big[\frac{(l_d-|m|)!}{(l_d+|m|)!}\Big]^{\frac{1}{2}} \times(l_nl_d00|l_p0)(l_nl_d0m|l_pm) \times R(l_n,l_d;l_p)P_{l_d}^{|m|}(\cos\theta_d)\Big|^2,$$

$$=(-1)^{l_p}(2l_p+1)\sum_L(-1)^LP_L(\cos\theta_d) \times\sum_{l_nl_n'l_dl_d'}(2l_n+1)(2l_n'+1)(2l_d+1)(2l_d'+1) \times(l_nl_d00|l_p0)(l_n'l_d'00|l_p0)(l_nl_n'00|L0) \times(l_dl_d'00|L0)W(l_nl_n'l_dl_d';Ll_p) \times R(l_n,l_d;l_p)R(l_n',l_d';l_p)^*.$$

Apart from a slight difference entering the factor f, this cross-section formula with the first alternative expression for the quantity $Q(l_p)$ is the same as the one derived by Tobocman.[4,7] The second alternative form of $Q(l_p)$ is obtained by forming the absolute square in the first and carrying out the sum over the deuteron angular momentum component m; for numerical work it is probably not as useful as the first. Note that the incoherence of the various contributing j_p and l_p terms is a consequence of the simplification.

The compound-nucleus contribution to the differential cross section can be obtained directly from the formulas of Blatt and Biedenharn. The interference terms can also be simplified if the pickup radial integrals are again assumed to be independent of J. By carrying out the J sum in the pickup factor, one finds that for a single compound-nucleus collision matrix component $\mathfrak{U}(nj_n'l_n';dj_d'l_d';J')$ these terms are given by

$$[d\sigma_{n;d}(\theta_d)/d\Omega_d]_{\text{interference}} =-\tfrac{1}{4}k_n^{-2}if(2I_i+1)^{-\frac{1}{2}}(-1)^{I_f+I_i+J'}(2J'+1) \times\sum_L(-1)^LP_L(\cos\theta_d)\sum_{j_pl_p}(-1)^{l_p}(2j_p+1)^{\frac{1}{2}} \times\gamma(j_pl_p)\sum_{l_nl_d}[(2l_n+1)(2l_d+1)/(2l_n'+1)(2l_d'+1)]^{\frac{1}{2}} \times(l_dl_d'00|L0)(l_nl_d00|l_p0)(l_n'l_d'00|l_p0)^{-1} \times\mathfrak{Z}(l_n'j_n'l_d'j_d';J'l_p)\mathfrak{Z}(l_nj_dl_n'l_d';l_pL) \times W(\tfrac{1}{2}1j_pj_d';\tfrac{1}{2}I_f)W(Il_p\tfrac{1}{2}j_d';j_pj_n') \times R(l_n,l_d;l_p)^*\mathfrak{U}(nj_n'l_n';dj_d'l_d';J')+\text{c.c.} \quad (13)$$

One-level formulas for the collision-matrix componenst have been given by Wigner and Eisenbud[9] and by Blatt and Biedenharn.[5]

Much simpler expressions are obtained for the straight pickup and the interference contributions if the plane-wave Born approximation is used rather than the distorted-wave Born approximation. These expressions are given in the Appendix.

IV. DISCUSSIONS

The reader may have noticed that the above development contains a flaw in the assertion that the R-matrix theory can be used to obtain the compound-nucleus contribution to the collision matrix component $U_{n;d}$ for a nuclear system not having the interaction ΔV between the neutron and proton when they are in the external region. For if ΔV were completely neglected in the R-matrix formalism the deuterons which appear at the nuclear surface would cease to interact there and consequently would appear at infinity as free neutrons and protons. This contribution to $U_{n;d}$ would thus vanish, and the "compound-nucleus" deuterons which appear at the nuclear surface would contribute instead to the component $U_{n;np}$. This difficulty may be resolved by noting that the effect of the interaction ΔV is not only to give the $\Delta U_{n;d}$ contribution of (6) but also to convert the above compound-nucleus component $U_{n;np}$ to a compound-nucleus component $U_{n;d}$, as implied in the development. It is evident then that the derivation

of the R-matrix theory does not entirely neglect ΔV but only that contribution from it which was used to calculate $\Delta U_{n;d}$.

There is also an exchange contribution to $U_{n;d}$ from the interactions of the external region. This contribution arises from additional terms in the expansion (9) corresponding to the dissociation of the target nucleus in the external region into a deuteron and a core of A_t-2 particles. The perturbing interactions are those between the incident neutron n_1 and both the neutron n_2 and the proton p of the deuteron when the deuteron is in the external region. As a result of these interactions the deuteron can be ejected and the recoiling neutron n_1 captured by the core. (The incident neutron could also pick up the core, forming the residual nucleus and leaving the deuteron behind.) A similar mechanism was considered by Austern, Butler, and McManus[8] for the contribution to (n,p) reactions from the external region, in which the incident neutron ejects a proton from the target and the recoiling neutron is subsequently captured by the core. Because of the fact that in the (n,d) exchange calculation there are essentially four interacting particles involved (the core and the nucleons n_1, n_2, p), rather than just the three particles of the direct term, the exchange term is considerably more difficult to compute. Fortunately, it may be negligible for a number of reasons: First, and perhaps the most significant, is that the reduced width (or probability) for the dissociation of the target into a deuteron and a core may be expected to be small compared with the proton reduced width since two particles are involved. Secondly, the radial wave function for the dissociation, which is involved in a "radial" integral similar to (11a), will decay rather more rapidly than a proton function, which is involved in the direct term, because deuteron binding energies are generally larger than proton binding energies and because a deuteron has twice the mass. Finally, the "radial" integral will also be relatively smaller because it involves two, rather than just one, exponentially decreasing function and because the momenta transfers involved are relatively larger.

In the calculation of the pickup contribution we have neglected the contribution from the interaction between the incident neutron and the core which takes place when the proton of the target and the core are separated by distances greater than the channel radius. One can associate with this interaction a mechanism in which the incident neutron ejects the core with the result that the freed proton can combine with the neutron to form a deuteron. This mechanism is essentially the same as the above-mentioned one considered by Austern *et al.*[8] However, there is an important difference in detail in that in the (n,p) case the ejected particle is a light one whereas in the (n,d) case it is a heavy one, that is, the roles of the proton and core are reversed; and it is this difference which leads one to believe that although the former mechanism is apt to be important, the latter is not. Unfortunately, we cannot give a really satisfactory justification for this remark, although the impulse type of approximation, such as the one used by Austern *et al.*, suggests that in an (n,d) reaction, the core ejection mechanism is apt to be less important than the pickup mechanism. First, the radial integral of the former involves two, rather than just one, exponentially decaying radial function and, secondly, the momentum transfer involved in producing forward deuterons is much larger in the ejection process than in the pickup process. In fact, according to such a calculation, the deuterons from the ejection process are concentrated in the backwards directions (as one would expect for a process which ejects the core in the forward directions), rather than in the forward directions, as in the pickup process.

It is well to emphasize that although the present approach utilizes distorted partial waves in the matrix elements, it is still a Born approximation evaluation and subject to the limitations of that approximation. In particular, the absolute magnitude of the calculated collision-matrix component $U_{n;d}$ of (11) can exceed unity in certain circumstances, thus violating the unitarity or flux-conservation requirement. If the waves involved in the radial integrals are not distorted by a sharp resonance, it is not likely that the absolute magnitude of those integrals will exceed unity, and it would then be sufficient to require that the factor $f\gamma(j_p l_p)$ of (11) be less than unity. Since the factor αa of f is of the order unity, this requirement is essentially that the geometric mean of the neutron and deuteron energies be greater than the reduced widths $\gamma(j_p l_p)^2$, these having an upper limit of a few Mev according to the sum rule. On the other hand, near a sharp resonance, the absolute value of the radial integral can become very large compared with unity because the irregular functions G, which are generated by the resonance, would be large. However, in such a case it is probably not necessary to include an external contribution to $U_{n;d}$ because the internal contribution dominates and, anyway, the channel radii for the resonant partial waves could be taken large enough to include in the "internal" region most of the "external" interaction so that there is effectively no "external" contribution to $U_{n;d}$ for those partial waves. The radial integrals could also be large if the binding and barrier of the picked-up proton are very small; the Whittaker function would then decay very slowly and contributions to the integral could arise from a large radial interval. The Born approximation will also be invalid if there is appreciable polarization of the deuteron by the Coulomb field, as expected at low deuteron energies.

Finally, it is appropriate to remark on the important matter of what value of the nuclear radius should be used in the external calculation. In order that the above Born approximation have some validity, it is clear that the radius should not be too small. On the

other hand, for the applicability, in the case of overlapping levels, of the compound-nucleus theory to the internal region, it is necessary that the radius be small enough for the signs of the reduced-width amplitudes to be uncorrelated, thus indicating that the interactions of that region are strong right up to the surface. In other words, the interactions of the internal region must be strong enough so that the multiple processes dominate, whereas those of the external region must be sufficiently weak so that multiple processes can be ignored (Born approximation). Clearly these requirements are not compatible with a unique boundary, and there is probably an intermediate region, or shell, which is not properly accounted for by either the compound-nucleus calculation or by the external perturbation calculation. Although there may be no simple way of dealing with this region, the observed near equality of the nuclear radii inferred from total neutron cross sections and stripping processes[24] is an indication that it may be small or not very important.

ACKNOWLEDGMENTS

The writer wishes to acknowledge the helpful discussions and suggestions received in connection with this work from N. Austern, G. Breit, A. M. Lane, W. Tobocman, K. M. Watson, and E. P. Wigner.

APPENDIX

The results of the text are, of course, much simpler if undistorted rather than distorted waves are used, that is, if the $\mathfrak{U}_{n;s}$ and $\mathfrak{U}_{d;d}$ of (7) are assumed to be unity, and if, in addition, the Coulomb fields are neglected. With these simplifications the various neutron and deuteron partial waves combine to form a simple exponential function, and the radial integrals corresponding to (11a) become simply the Fourier transforms of the radial functions $u(\alpha_f j_p l_p; r_p)$ of (9). By application of the wave equation and by an integration by parts, these transforms may be expressed as wronskians evaluated at $r=a$. Furthermore, if the compound-nucleus contribution is neglected, the cross section formula reduces to the relatively simple one which was originally given by Butler. Although these approximate methods do appear to give fairly accurate predictions of the angular distributions in circumstances where the Coulomb barriers are not strong, they are found to predict absolute yields that are much too large.[7,25]

In the plane-wave Born approximation, the pickup contributions ΔA to the (n,d) reaction amplitudes $A=\mathfrak{A}+\Delta A$ for initial and final channel spin states j_n,ν_n and j_d,ν_d, respectively, are

$$\begin{aligned}\Delta A(nj_n\nu_n;\,dj_d\nu_d)&=-4\pi^{\frac{1}{2}}fk_d(2j_n+1)^{\frac{1}{2}}(2j_d+1)^{\frac{1}{2}}(2I_i+1)^{\frac{1}{2}}\\&\times(-1)^{I_f-I_i-is+i_n+\nu_n}(\alpha^2+k_{pn}^2)^{-1}\\&\times\sum_{l_pl_pm_p}(-1)^{m_p-i_p}(2j_p+1)^{\frac{1}{2}}(2l_p+1)^{-\frac{1}{2}}\\&\times W(I_id_p\tfrac{1}{2}j_d;\,j_pj_n)W(\tfrac{1}{2}1j_pj_d;\,\tfrac{1}{2}I_f)\\&\times(j_nj_d\nu_n-\nu_d|l_pm_p)\gamma(j_pl_p)\mathfrak{W}_{l_p}Y_{l_pm_p}(\Theta,\Phi).\end{aligned}\tag{14}$$

In addition to the quantities already defined in connection with (11), there are the following: The characteristic stripping momentum transfer wave numbers are $\mathbf{k}_{pn}=\mathbf{k}_n-\frac{1}{2}\mathbf{k}_d$ and $\mathbf{k}_{pf}=\mathbf{k}_d-\epsilon\mathbf{k}_n$, so that

$$k_{pn}^2=k_n^2+\tfrac{1}{4}k_d^2-k_nk_d\cos\theta_d,$$

$$k_{pf}^2=\epsilon^2k_n^2+k_d^2-2\epsilon k_nk_d\cos\theta_d;$$

Θ is the angle between the direction of $\mathbf{k}_{pf}$ and the incident beam and may be obtained from the relation $\sin\Theta=(k_d/k_{pf})\sin\theta_d$. The Wronskian is

$$\mathfrak{W}_l=F_{l-1}(x)-(l+\Lambda)x^{-1}F_l(x),$$

where $x=k_{pf}a$, and Λ is the radius a times the logarithmic derivative at a of r times the radial part of the wave function of the proton bound to the target nucleus; when the Coulomb field is neglected, the expressions for $(l+\Lambda)$ in terms of $z=k_pa$ for the proton angular momenta l are

l	$l+\Lambda$
0	$-z$
1	$-z^2/(1+z)$
2	$-(z^2+z^3)/(3+3z+z^2)$
3	$-(3z^2+6z^3+z^4)/(15+15z+6z^2+z^3)$
4	$-(15z^2+15z^3+6z^4+z^5)/(105+105z+45z^2+10z^3+z^4)$

Butler's formula for straight pickup is obtained by summing the absolute square of the amplitudes (14) over all final channel spin states and averaging over all initial ones; it is

$$[d\sigma_{n;d}(\theta_d)/d\Omega_d]_{\text{pickup}}=k_d^2f^2(k_{pn}^2+\alpha^2)^{-2}\times\sum_{l_p}\gamma(l_p)^2\mathfrak{W}_{l_p}^2.\tag{15}$$

[24] J. R. Holt and T. N. Marsham, Proc. Phys. Soc. (London) **A66**, 1032 (1953). These authors show that the stripping radii are actually larger, as one would expect.

[25] R. G. Thomas, Phys. Rev. **91**, 453(A) (1953); Horowitz and Messiah, reference 4; Fujimoto, Kikuchi, and Yoshida, Progr. Theoret. Phys. (Japan) **11**, 264 (1954); G. Abraham, Proc. Phys. Soc. (London) **A67**, 273 (1954). The proportionality of stripping and pickup cross sections to the reduced widths $\gamma(l_p)^2$, which is also evident in (12), is brought out in these papers; see also A. M. Lane and D. H. Wilkinson, Phys. Rev. **97**, 1199 (1955).

Note that the angular dependent factors $Y_{l_p m_p}(\Theta,\Phi)$ in the amplitude expressions do not appear in (15).

The contributions to the reaction amplitudes from a particular collision-matrix component

$$\mathfrak{U}(nj_n'l_n';dj_d'l_d';J')$$

are given by

$$\begin{aligned}&\mathfrak{a}(nj_n'\nu_n';dj_d'\nu_d')\\&=-i\pi^{\frac{1}{2}}k_n^{-1}(2l_n'+1)^{\frac{1}{2}}(j_n'l_n'\nu_n'0|J'\nu_n')\\&\times(j_d'l_d'\nu_d'\nu_n'-\nu_d'|J'\nu_n')\\&\times\mathfrak{U}(nj_n'l_n';dj_d'l_d';J')Y_{l_d'\nu_n'-\nu_d'}(\Omega_d).\end{aligned}\quad(16)$$

By summing the absolute squares of the sum of terms from (16) and (14) over all possible ν_n', ν_d' and by dividing by the number of initial spin states, one obtains in addition to the straight pickup and resonance contributions, the interference contribution to the differential cross section which is

$$\begin{aligned}&[d\sigma_{n;d}(\theta_d)/d\Omega_d]_{\text{interference}}\\&=\tfrac{1}{2}ifk_dk_n^{-1}(-1)^{I_t+I_t+J'}(\alpha^2+k_{p_n}^2)^{-1}(2J'+1)\\&\times(2I_t+1)^{-\frac{1}{2}}\mathfrak{U}(nj_n'l_n';dj_d'l_d';J')\sum_{j_pl_p}(-1)^{j_p}\\&\times(2j_p+1)^{\frac{1}{2}}\gamma(j_pl_p)\mathfrak{W}_{l_p}W(I_dj_p\tfrac{1}{2}j_d';j_pj_n')\\&\times W(\tfrac{1}{2}1j_pj_d';\tfrac{1}{2}I_t)\bar{Z}(l_n'j_n'l_d'j_d';J'l_p)\\&\times\textstyle\sum_m[(l_n'l_d'0m|l_pm)/(l_n'l_d'00|l_p0)]\\&\times[(l_d'-|m|)!(l_p-|m|)!/(l_d'+|m|)!(l_p+|m|)!]^{\frac{1}{2}}\\&\times P_{l_d'}^{|m|}(\theta_d)P_{l_p}^{|m|}(\Theta)+\text{c.c.}\end{aligned}\quad(17)$$

The m sum extends from $-l_p$ to l_p, or from $-l_d'$ to l_d', whichever range is smaller.

The pickup reaction amplitude (14) was calculated for the deuteron ^1S wave function of the zero-range potential. For a Chew-type wave function of the form $\exp(-\alpha r)-\exp(-\beta r)$, where $\beta\approx 7\alpha$, (14), (16), and (17) should be multiplied by $\beta^{\frac{1}{2}}(\alpha+\beta)^{\frac{1}{2}}/(\beta^2+k_{p_n}^2)$, and (15) should be multiplied by its square.

PHYSICAL REVIEW VOLUME 100, NUMBER 1 OCTOBER 1, 1955

Reactions $C^{12}(d,n)N^{13}_{\text{ground state}}$ and $C^{12}(d,t)C^{11}$ up to $E_d=20$ Mev*

D. H. WILKINSON†
Brookhaven National Laboratory, Upton, New York
(Received May 31, 1955)

The course of the partial cross section for the direct formation of N^{13} in its ground state only in the reaction $C^{12}(d,n)N^{13}$ has been followed up to $E_d=20$ Mev by observing the N^{13} activity induced in a stack of polyethylene foils (only the ground state is stable against proton emission). The cross section falls appreciably less rapidly than would be expected for compound nucleus formation and also less rapidly than predicted by simple stripping theory. The cross section at $E_d=8$ Mev is 100 mb which is not so large relative to that for the mirror (d,p) reaction as is predicted by simple stripping theory. The reaction $C^{12}(d,t)C^{11}$ has been detected and its total cross section measured from its threshold ($E_d=14.5$ Mev) to $E_d=20$ Mev where it is 10 mb. The magnitude of this cross section indicates that this is a pickup reaction.

INTRODUCTION

THE many measurements of "stripping" angular distributions in recent years have given ample grounds for believing that (d,p) and (d,n) reactions induced by deuterons of energy greater than three or four Mev do not as a rule involve the strong formation of a compound nucleus but that the reactions proceed most frequently by a direct interaction in which a nucleon of the impinging particle simply severs its "deuteron bond" at the nuclear surface and attaches itself to the existing (and undisturbed) structure of the target nucleus thereby forming one or other of those states of the residual nucleus of which the target nucleus is a parent.[1] Although fair to good qualitative agreement between experimental and theoretical stripping patterns can usually be obtained (albeit by a somewhat cavalier approach to the problem of the nuclear radius), it is abundantly clear that neither the details of the patterns predicted by simple stripping theory nor the theoretical absolute cross sections are reproduced by experiment and that considerable refinements to the theory are needed. Examples of such refinements are the taking account of Coulomb effects, scattering of the incident deuteron wave, exchange effects, and boundary conditions for the outgoing particle.[2] As soon as such refinements are introduced the fit with experiment may, of course, be much improved since it is not usually clear which of many alternative procedures should be followed at each stage, and advantage may be taken of this uncertainty. Thus, although some empirical working recipe may emerge for the fitting of experimental angular distributions and reduced widths, we cannot feel confident that the particular constellation of param-

* Performed under the auspices of the U. S. Atomic Energy Commission.
† On leave from Cavendish Laboratory, Cambridge, England.
[1] S. T. Butler, Proc. Roy. Soc. (London) **A208**, 559 (1951).
[2] See, for example, W. Tobocman and M. H. Kalos, Phys. Rev. **97**, 132 (1955).

eters represented by that recipe necessarily reflects the physical conditions obtaining in the reaction. We must, therefore, look around for some other aspect of the experimental situation that will, in the first place, distinguish between reactions proceeding via a compound nucleus and via direct interaction and, secondly, provide another datum against which the refinements of stripping theory, adduced to explain angular distributions and reduced widths, may be tested.

When we consider the variation with deuteron energy of the partial cross section for the formation of the residual nucleus in a particular state, another way of distinguishing between compound nucleus formation and direct interaction becomes apparent since the considerations governing the energy dependence of the partial cross sections are entirely different in the two cases. If we have compound nucleus formation, a given residual state will be populated as the result of statistical competition between that state and all other energetically-accessible states of the residual nucleus, and so the energy-dependence of the partial cross section will be governed largely by more and more competing states becoming available as the excitation increases. In the case of stripping, there is a fixed set of really or potentially available residual states, namely those states which have appreciable fractional parentage coefficients for the target nucleus; whether a particular state is energetically accessible or not does not affect its potency as a "competitor" of the particular residual state in which we are interested. The various partial cross sections to the various residual states are now independent of each other. The "competition" between the states is fixed once and for all, in a manner essentially independent of the energy of the deuteron, by the fractional parentage coefficients that describe the relationship between the target and residual nuclei. The statistical aspect of the competition that characterizes decay following compound nucleus formation is wholly absent. In the stripping reaction the energy dependence of the partial (differential) cross section is governed largely by the instantaneous availability in the incident deuteron of a nucleon with the correct momentum for tacking onto the target nucleus so as to leave the residual nucleus in the desired state when the emergent nucleon leaves in a particular direction. (To compare with compound nucleus theory, we of course integrate the theoretical differential cross section over all angles.) Since the mechanisms governing the energy dependence of the partial cross sections are so different in the two cases, we may hope to distinguish quite sharply between the two possibilities, particularly when we bear in mind that the theoretical energy dependence derived from compound nucleus theory must be normalized to experiment at low deutron energies, since it is certainly there that the theory is valid if anywhere, while the normalization between stripping theory and experiment should be made rather in the region of high deuteron energy.

The reason why no such test has been made heretofore is probably that the taking of angular distributions on a particular group of product particles over a wide range of deuteron energies would be a most tedious business. An alternative approach is to study the excitation function for the production of a radioactive product nucleus. This as a rule is uninformative since the observed radioactive ground state may be reached not only directly in the particle transition but also by gamma-ray transitions from excited residual states. We do not know the relative populations of the several residual states to which the actual particle transitions take place; and these relative populations depend on the energy of the deuterons.

There is, however, one case at least, though possibly it is unique, where the residual radioactivity measures transitions to one state only of the product nucleus, and that is in the reaction $C^{13}(d,n)N^{13}$. N^{13} is a positron emitter of half-life 10 minutes, and since *all* excited states of N^{13} are energetically unstable against proton emission, we may be sure that the N^{13} positron activity measures only those neutron transitions that lead directly to the ground state except for the negligible fraction of cases where gamma-ray emission to the ground state of N^{13} successfully competes with proton emission following a neutron transition to an excited state.

It was therefore thought profitable to study the production of N^{13} in the deuteron bombardment of carbon over as wide a range of deuteron energy as possible. Since detailed measurements already exist up to $E_d=3$ Mev,[3] particular attention has been given to the region of higher deuteron energy up to 20 Mev available with the Brookhaven 60-in. cyclotron. It is known from isolated measurements of angular distributions in the reaction $C^{13}(d,p)C^{13}$ at 3.3 Mev[4] and 8 Mev[5] that the stripping process predominates in the region of present investigation, and it was therefore hoped that our results would display a clear discrimination against the form of cross section variation with deuteron energy to be expected on the compound nucleus model. It was also hoped that the results would show deviations from expectations based on the simple form of stripping theory that neglects the refinements detailed above, so that the results might provide a test of the applicability of those refinements.

The reaction $C^{13}(d,n)N^{13}$ is endothermic by only 281 kev and so proceeds almost throughout our range of deuteron energy; but a second reaction that produces a radioactive end product becomes possible above a deuteron energy of 14.5 Mev, to wit $C^{13}(d,t)C^{11}$ which has a Q value of -12.45 Mev. This reaction has not been reported in the literature and it was thought to be of interest to see whether it could be detected, since if it

[3] See F. Ajzenberg and T. Lauritsen, Revs. Modern Phys. **27**, 77 (1955).
[4] Holmgren, Blair, Simmons, Stratton, and Stuart, Phys. Rev. **95**, 1544 (1954).
[5] J. Rotblat, Nature **167**, 1027 (1951).

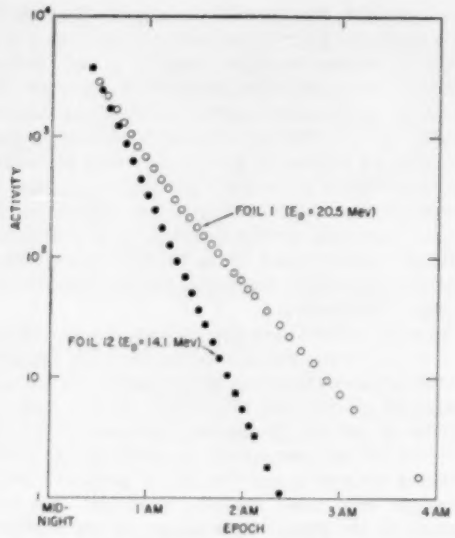

FIG. 1. Decay curves of polyethylene foils irradiated with deuterons of 14.1 Mev and 20.5 Mev. The former shows a pure exponential decay characteristic of N^{13} formed in the reaction $C^{12}(d,n)N^{13}$; the latter shows mixed N^{13} and C^{11} decay, the C^{11} coming from the reaction $C^{12}(d,t)C^{11}$ which has its threshold at deuteron energy of 14.5 Mev.

proceeds by a direct or pickup mechanism it provides a measure of the probability that a deuteron on coming near a nucleus should snatch out a nucleon from that nucleus rather than lose a nucleon to it. It was also hoped that in this case also the results might discriminate between a mechanism involving compound nucleus formation and one of direct interaction—in this case pickup. The situation is not so clear-cut as in the (d,n) reaction, because several excited states of C^{11} are stable against heavy particle breakup and by $E_d = 20$ Mev three of them have become energetically available. C^{11} is a positron emitter of half-life 20 minutes, and so its separation from the 10 minute N^{13} would not be possible unless the (d,t) reaction possessed a fair cross section.

The production of C^{11} in the bombardment of carbon with deuterons may be safely attributed to the (d,t) reaction below $E_d = 21.8$ Mev, at which energy the $C^{12}(d,dn)C^{11}$ reaction becomes possible. The production of C^{11} by several contaminant reactions such as $N^{14}(p,\alpha)C^{11}$ was also considered. Chemical analysis of the foils together with the known proton (H_2^+) content of the deuteron beam showed them to be wholly negligible.

EXPERIMENTAL METHOD

The experiment was performed by bombarding stacks of 4-mil polyethylene foils with about 1/100 microampere of 20-Mev deuterons for periods of the order of 30 minutes, during which time the beam current was held constant to better than 10%. The diameter of the beam was about 4 mm. After the bombardment the individual foils were trapped between aluminum sheets of thickness adequate to absorb the positrons of N^{13} and C^{11}, and the decay was followed over many half-lives by counting the annihilation quanta with an NaI(Tl) crystal. (Neither body gives nuclear gamma rays.)

Those foils for which the deuteron energy was below the threshold for C^{11} production showed an accurately exponential decay with a half-life of 10 minutes; others, above the threshold, showed an initially nonexponential decay, rapid at first but leveling off to a half-life of 20 minutes. Examples of such decays are shown in Fig. 1. The half-life displayed by the foil bombarded with deutrons of mean energy 14.1 Mev[6] is 10.08 ± 0.04 minutes, which figure accords well with the best recent value for N^{13} of 10.05 ± 0.03 min.[7] The foil bombarded with deutrons of mean energy 20.5 Mev clearly shows the mixed periods and eventually decays with a half-life of about 20 minutes; the values in the literature for for C^{11} are about 20.5 ± 0.1 minutes.[3]

All decay curves were analyzed to find the relative amounts of N^{13} and C^{11} present in each foil at the end of the irradiations, and these quantities were in turn

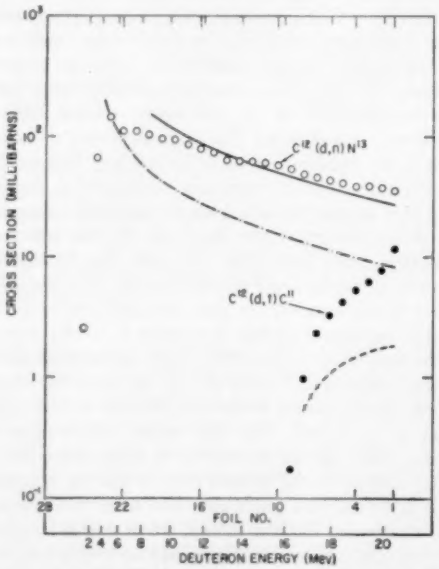

FIG. 2. Excitation functions for the reactions $C^{12}(d,n)N^{13}$ and $C^{12}(d,t)C^{11}$. The dashed-dotted curve shows the expected course of the (d,n) reaction if the reaction proceeds via compound nucleus formation (normalized at $E_d = 5$ Mev); the full curve is the prediction of simple stripping theory (normalized at $E_d = 14$ Mev). The dashed curve is the prediction based on compound nucleus formation for the reaction $C^{12}(d,t)C^{11}$ under the assumption that the reduced width for triton emission is as great as that for nucleon emission.

[6] We have used the range-energy relations of M. Rich and R. Madey, University of California Radiation Laboratory Report UCRL 2301 (unpublished).

[7] Churchill, Jones, and Hunt, Nature **172**, 460 (1953).

corrected for the finite duration of the bombardments. The surface densities of the polyethylene foils were determined by weighing small triangles cut from the bombarded region of each foil; they were constant to within 2 percent from foil to foil and no correction was necessary on account of variations in surface density. With these data, relative cross sections for the (d,n) and (d,t) reactions were computed. The absolute sensitivity of the detecting apparatus was computed and this enabled an absolute cross section scale to be established. This scale, however, was not set up with great care and may be in error by as much as 50 percent; the relative cross sections are established with very much better accuracy.

The results for the energy dependence of the two cross sections are displayed in Fig. 2. Little attention should be given to the two points of lowest energy for the (d,n) cross section since straggling is undoubtedly of importance here at the end of the deuteron range.

DISCUSSION

The chief feature of both cross sections is that they change smoothly with deuteron energy. It is known that the (d,n) cross section for low deuteron energies shows strong resonances[3]; none is revealed at high energies, although even for our higher energies the thickness of a foil represents about 500 kev of deuteron energy so the energy resolution is always very poor.

The most interesting feature of the cross section for the (d,n) reaction is that it varies so little with deuteron energy. The experimental variation has been compared with what may be expected on the basis of compound nucleus theory and simple stripping theory.

Although N^{14} is too light a nucleus for us to attempt to describe realistically by the usual thermodynamic methods, it is possible to construct an expression that represents fairly well the empirically observed level densities in odd-mass nuclei in this region; this is:

$$w(E)=0.3\exp[2(0.3E)^{\frac{1}{2}}],$$

where $w(E)$ is the level density (per Mev) at an excitation of E Mev. We use this expression and the usual formalism, and assume that the total cross section for compound nucleus formation is independent of deuteron energy in order to compute the variation with deuteron energy of the cross section for formation of N^{13} in its ground state. A fit was made at low deuteron energy for the reason given in the Introduction, and the result is shown as the dashed-dotted line of Fig. 2. It is clear that the theoretical falloff with deuteron energy is initially much faster than indicated by experiment.

The energy variation expected on stripping theory has been computed using the simple Born approximation formulation[4]; that is, we have taken

$$\sigma(\theta)=(k_p/k_d)G^2j_1^2(kR).$$

Here the symbols have their usual meaning as used in stripping theory; we use j_1 since we work entirely in the p shell. The slightly more complicated Butler formula[1] gives essentially similar predictions. The prediction of the above formula, after integration over angle, is compared with experiment as the full line of Fig. 2. Normalization has been performed in the higher-energy region since we expect stripping theory more nearly to hold for high deuteron energies. It is seen that the prediction of the simple stripping theory fits experiment fairly well over a rather wide range of deuteron energy, whereas the deviation of the prediction of compound nucleus theory from experiment is immediate.

However, the experimental cross section seems to fall less rapidly than simple stripping theory would suggest. This may be due in part to the influence of Coulomb effects which will oppose the entry of the proton into the nucleus at low energies but allow it free entry at high. It is clear that refinement to stripping theory is needed to explain the detailed course of the present cross section and, as remarked above, the same refinements must suffice for this task as are postulated in order to improve agreement between theory and experiment in other aspects of the stripping process.

It is interesting to compare the absolute cross section for the (d,n) reaction with that for the mirror reaction $C^{12}(d,p)C^{13}$ which has been measured by Rotblat[5] at $E_d=8$ Mev. Under the assumption of the charge symmetry of nuclear forces we may use the comparison of these two "mirror cross sections" as a further test of simple stripping theory. The total cross section for the (d,p) reaction was computed from Rotblat's data (which run from $\theta=15°$ to $\theta=160°$) by using simple stripping theory to extrapolate his differential cross section to small angles and assuming a constant cross section between $\theta=160°$ and $\theta=180°$. We then find that our measured (d,n) cross section at $E_d=8$ Mev is greater than the (d,p) cross section by a factor of 1.2. The ratio predicted by simple stripping theory is 2.0. In view of the possible error of about 50% in the (d,n) cross section, this discrepancy cannot be said to be very great. It may, however, be due in part to the presence of a "compound nucleus" component in the reactions. If we interpret the differential cross section at backward angles in Rotblat's data as due to such compound nucleus formation and assume a consonant contribution in the (d,n) case, the experimental stripping cross section ratio becomes 1.5 instead of 1.2. Another possible explanation is in terms of the differing importance for the two mirror reactions of the refinements to stripping theory referred to above. It might be naively argued that the (d,n) to (d,p) ratio predicted by simple stripping theory should be diminished owing to the opposition of the Coulomb barrier to the entry of the proton into the nucleus in the (d,n) case, and this change is in the sense indicated by experiment. If a suitably refined stripping theory correctly accounts for the form of the variation of cross section with energy, and if

[4] Bhatia, Huang, Huby, and Newns, Phil. Mag. 43, 485 (1952).

after these corrections and that for compound nucleus contribution a similar discrepancy yet remains, it is in the sense to correspond to a greater reduced width for neutrons (in C^{13}) than for protons (in N^{13}); i.e., "the neutrons stick out further than the protons." Such an effect has been suggested for heavier nuclei, though it would be very surprising to find it holding for so light a nucleus as $A=13$.

An estimate of the course of the cross section for the reaction $C^{12}(d,t)C^{11}$ was made on the basis of compound nucleus formation by assuming, as before, that the whole of the cross section for $C^{12}(d,n)N^{13}$ at low deuteron energies involves compound nucleus formation. On the assumption that the reduced width for triton emission is as great as that for neutron emission (the assumption of "preformed" tritons), we predict the dashed line of Fig. 2—in which the coming into play of successive residual states of C^{11} has been allowed for and the associated irregularities smoothed out. It is seen that even under the very unplausible assumption of the existence of preformed tritons, compound nucleus theory fails by an order of magnitude to explain the observed C^{11} formation. We are forced then to assume that this (d,t) reaction proceeds by some pickup mechanism and that we are indeed measuring the relative probability of the deuteron's losing a nucleon to the nucleus and removing one from it. As yet no sufficiently reliable theory of (d,t) pickup exists to warrant a comparison being made with these results. It is interesting to note that, at $E_d=3.3$ Mev, the angular distribution of the reaction $C^{13}(d,t)C^{12}$ is such as to suggest that a direct mechanism already predominates.[4]

It is interesting to compare these results with those of Cohen and Handley[9] on (p,t) reactions. These authors suggest that triton emission from a compound nucleus state has an inherent probability comparable with that for single nucleon emission. They base this argument on the rather flat angular distributions sometimes obtained which, they remark, tell against a pickup process. However, this conclusion is no longer valid when the energy of one or both the charged particles concerned is of the order of or below the Coulomb barrier; here a direct mechanism can give a sensibly isotropic angular distribution. It appears that considerable interest attaches to the resolution of this question of the mechanism by which tritons and similar complicated particles are emitted from nuclei in events of moderate to high energy.

[9] B. L. Cohen and T. H. Handley, Phys. Rev. **93**, 514 (1954)

PHYSICAL REVIEW VOLUME 100, NUMBER 1 OCTOBER 1, 1955

Many-Body Problem for Strongly Interacting Particles. II. Linked Cluster Expansion*

K. A. Brueckner
Indiana University, Bloomington, Indiana
(Received April 28, 1955)

An approximation method developed previously to deal with many particles in strong interaction is examined in further detail. It is shown that the series giving the interaction energy is a development in a sequence of linked or irreducible cluster terms each of which gives a contribution to the energy proportional to the total number of particles. Consequently the convergence of the expansion is independent of the total number of particles. The origin of this simple feature is illustrated by showing that a similar situation exists in the expansion of standard perturbation theory. The numerical convergence of the expansion is quantitatively discussed for the nuclear problem where it is shown that the correction arising from the first cluster term involving three particles is less than the leading term by a factor of about 10^{-4}. The smallness of the correction is largely a result of the action of the exclusion principle.

I. INTRODUCTION

In a previous paper[1] (to be referred to as I) we have given a method for reducing approximately the many body problem for strongly interacting particles to a problem of self-consistent fields. Some of the physical content and origin of the method were discussed there and the nature of certain correction terms which can be neglected for very many particles was discussed. We shall in this paper examine the structure of another type of correction term which arises from interaction of clusters of particles and in so doing exhibit the general structure of the expansion involved. This will also allow us to draw some general conclusions about the convergence and accuracy of the method.

In Sec. II, we shall briefly summarize the relevant formulas from I and describe some difficulties which appear in high-order terms in the expansion for the energy which can be removed by a simple modification of the many-body propagation function. In Sec. III, we show how similar terms appear to arise in the usual perturbation theory but that they cancel identically, in a manner simply related to the cancellation discussed in Sec. II. In Sec. IV, we summarize these results and show how they may be generalized into a simple pre-

* Supported in part by a grant from the National Science Foundation.
[1] K. A. Brueckner and C. A. Levinson, Phys. Rev. **97**, 1344 (1955).

scription for evaluating matrix elements or, equivalently, used to redefine the many-body propagator for the system. In Sec. V, we take as an example the nuclear case and discuss quantitatively the convergence of the method. In Sec. VI, we discuss the equation for the two-body reaction matrices which provide the leading approximation to the energy. Finally in Sec. VII, we summarize our results and make some concluding remarks.

II. FORMALISM

A. Structure of the Expansion for the Energy

In this section, we shall summarize the results of I and discuss some of the formal properties of the expansion. We use the formalism developed in I for dealing with identical particles. We shall compress the notation used there by introducing the following definitions:

$$\begin{aligned}
\mathbf{T}_i &= T_i \eta_i^* \eta_i, \\
\mathbf{v}_{ij,\,kl} &= \eta_i^* \eta_j^* v_{ij,\,k\mathfrak{m}} \eta_{\mathfrak{m}} \eta_k, \\
\mathbf{t}_{ij,\,kl} &= \eta_i^* \eta_j^* t_{ij,\,k\mathfrak{m}} \eta_{\mathfrak{m}} \eta_k, \\
\mathbf{I}_{ij,\,kl} &= \mathbf{t}_{ij,\,kl} - \mathbf{t}_{ij,\,ij}\delta_{ik}\delta_{jl} - \mathbf{t}_{ij,\,ji}\delta_{il}\delta_{jk}.
\end{aligned} \tag{1}$$

In this notation the equation for the operator t is

$$\mathbf{t}_{ij,\,kl} = \mathbf{v}_{ij,\,kl} + \sum_{mn} \mathbf{v}_{ij,\,mn} \frac{1}{e} \mathbf{t}_{mn,\,kl}, \tag{2}$$

where $1/e$ is the propagator for the many-body system. We have previously defined e to be the operator

$$e = E - \sum_i \mathbf{T}_i - \sum_{ij} \mathbf{t}_{a,\,ij}, \tag{3}$$

where

$$\mathbf{t}_{a,\,ij} = \tfrac{1}{2}(\mathbf{t}_{ij,\,ij} + \mathbf{t}_{ij,\,ji}), \tag{4}$$

which we shall still use for the present; in Sec. IV we shall show how a different definition may be advantageously introduced to simplify the structure of the expansion for the energy. In terms of these operators, the energy of the system is

$$E = (\phi_0, \sum_i \mathbf{T}_i + \mathbf{t}_{a,\,ij}\phi_0) + \tfrac{1}{2} \sum_{ijkl} (\phi_0, \mathbf{I}_{ij,\,kl} F_{kl} \phi_0), \tag{5}$$

where

$$\begin{aligned}
F &= 1 + \frac{1}{2}\frac{1}{e} \sum_{ijkl} \mathbf{I}_{ijkl} F_{kl}, \\
F_{kl} &= 1 + \frac{1}{2}\frac{1}{e} \sum_{mn \neq kl} \mathbf{I}_{mnrs} F_{rs}.
\end{aligned} \tag{6}$$

Equation (5) for the energy may be written more explicitly as an expansion in the incoherent or nondiagonal operators I. We use Eq. (6) for the F's and find for the leading terms in the expansion

$$\begin{aligned}
E - (\phi_0, \sum_i \mathbf{T}_i \phi_0) &= \sum_{ij} (\phi_0, \mathbf{t}_{a,\,ij}\phi_0) \\
&+ \tfrac{1}{2} \sum \left(\phi_0, \mathbf{I}_{ij,\,kl} \frac{1}{e} \mathbf{I}_{mn,\,rs} \phi_0 \right) \\
&+ \tfrac{1}{4} \sum \left(\phi_0, \mathbf{I}_{ij,\,kl} \frac{1}{e} \mathbf{I}_{mn,\,rs} \frac{1}{e} \mathbf{I}_{pq,\,tu} \phi_0 \right) \\
&+ \tfrac{1}{8} \sum \left(\phi_0, \mathbf{I}_{ij,\,kl} \frac{1}{e} \mathbf{I}_{mr,\,rs} \frac{1}{e} \mathbf{I}_{pq,\,tu} \frac{1}{e} \mathbf{I}_{ab,\,cd} \phi_0 \right).
\end{aligned} \tag{7}$$

In all of these terms the condition must be imposed on the summations that consecutive pairs of indices not be matched, this condition arising from the similar condition in the defining equation for F_{kl}. Let us now examine these terms in detail. The first term on the right hand side of Eq. (7) is that previously evaluated in detail elsewhere; it gives by far the largest contribution to the energy of a highly degenerate Fermi gas. We shall return to a discussion of its structure in more detail in Sec. VI. The second term vanishes identically since the product of the two nondiagonal operators with $mn \neq kl$ has no diagonal matrix element. The third term is the first correction term to the energy as given by the first term alone; it involves a cluster of three particles. A typical pairing of indices gives a term

$$\Delta E_3 = \tfrac{1}{8} \sum \left(\phi_0, \mathbf{I}_{ij,\,i'j'} \frac{1}{e} \mathbf{I}_{j'k,\,jk'} \frac{1}{e} \mathbf{I}_{i'k',\,ik} \phi_0 \right). \tag{8}$$

This term has what we shall call a typical linked or irreducible structure; each I is linked to the other two. As a consequence of this structure, this term cannot be written as a product of simpler terms; this result is a general feature of all linked terms. As we shall see it is criterion of linkage which characterizes the expansion and determines its convergence.

To determine the order of magnitude of these typical terms, it is convenient at this stage to introduce a method of counting the dependence on the total number of particles, N. We observe that the operators I contain a factor of $v^{-1} \sim N^{-1}$ which comes from the normalization of the wave functions. Each free summation over momentum states gives a factor of N since

$$\sum_{\mathbf{k}} \to \frac{v}{(2\pi)^3} \int d\mathbf{k} \sim N. \tag{9}$$

In determining the number of free summations we must of course take proper account of the Kronecker delta function on the total momentum contained in each operator I. Thus we can determine the N-dependence of a given term by a simple counting procedure. Application of these rules to the terms so far

discussed gives

$$E_1=\sum_{ij}(\phi_0,\mathbf{t}_{a,ij}\phi_0)\sim N^2(1/N)=N \tag{10}$$

as we expect. Similarly

$$E_2\sim N^4/N^3=N, \tag{11}$$

with three factors of N coming from the summation over i,j,k and one factor of N from the summation over i'.

In the next term of fourth order in the I's, we first find terms of a new structure arising.[2] In addition to a variety of linked cluster terms, we now find reducible or unlinked terms. These have the form

$$E_4^{(r)}=\sum\left(\phi_0,\mathbf{I}_{ij,\,e'j'}\frac{1}{e}\mathbf{I}_{kl,\,k'l'}\frac{1}{e}\mathbf{I}_{e'j',\,ij}\frac{1}{e}\mathbf{I}_{k'l',\,kl}\phi_0\right). \tag{12}$$

If ij and kl are summed independently, application of the counting rule gives

$$E_4^{(r)}\sim N^2. \tag{13}$$

On the other hand, for a typical linked term such as

$$\sum\left(\phi_0,\mathbf{I}_{ij,\,e'j'}\frac{1}{e}\mathbf{I}_{kl',\,k'e}\frac{1}{e}\mathbf{I}_{i'j',\,il'}\frac{1}{e}\mathbf{I}_{k'l',\,kl}\phi_0\right), \tag{14}$$

the counting rule shows a linear dependence on N. This result holds generally for a linked cluster; these are always of the order N or lower and hence depend at most on the same power of N as the leading term. Consequently the convergence of this series does not depend on N (as long as N is very large) except through the appearance of unlinked clusters. Before examining these in more detail, we write down some typical unlinked clusters of higher order which also depend on higher powers of N than the first. These are, for example,

$$E_6^{(r)}=\left(\phi_0,\mathbf{I}_{ij,\,e'j'}\frac{1}{e}\mathbf{I}_{e'k,\,ek'}\frac{1}{e}\mathbf{I}_{mn,\,m'n'}\times\frac{1}{e}\mathbf{I}_{k'j',\,kj}\frac{1}{e}\mathbf{I}_{m'n',\,mn}\phi_0\right)\sim N^3,$$

$$E_6^{(r)}=\left(\phi_0,\mathbf{I}_{ij,\,e'j'}\frac{1}{e}\mathbf{I}_{mn,\,m'n'}\frac{1}{e}\mathbf{I}_{e'j',\,ij}\frac{1}{e}\mathbf{I}_{e'e',\,e'e'}\times\frac{1}{e}\mathbf{I}_{m'n',\,mn}\frac{1}{e}\mathbf{I}_{e'e',\,e'e'}\phi_0\right)\sim N^3. \tag{15}$$

B. Reducible Clusters

The terms which cause difficulty since they are not linear in N all have a similar unlinked structure. Consequently they do not represent actual interaction energy; for example, in the fourth order term, the two pairs ij and kl are independent of each other with no interaction term linking them. They therefore arise in the expansion only because of an inadequacy in this approximation scheme. It is easy, however, to show that they may be eliminated by a very simple and natural redefinition of the propagator $1/e$. To see this, let us look elsewhere for similar unlinked terms in the energy. It is easy to see that these first appear in the second order term $t_{ij,\,ij}$. Let us examine a typical term

$$\mathbf{t}_{ij,\,ij}=\mathbf{v}_{ij,\,ij}+\mathbf{v}_{ij,\,e'j'}\frac{1}{e}\mathbf{t}_{e'j',\,ij}$$

$$=\mathbf{v}_{ij,\,ij}+\mathbf{v}_{ij,\,e'j'}\left(E-\sum_k\mathbf{T}_k-\sum_{kl}\mathbf{t}_{a,kl}\right)^{-1}\mathbf{t}_{e'j',\,ij}. \tag{16}$$

We can evaluate the propagator by making use of the fact that to a good approximation

$$E=\sum\mathbf{T}_k^{(0)}+\sum_{kl}\mathbf{t}_{a,kl}^{(0)}, \tag{17}$$

where by the superscript zero we mean evaluated in the ground state. Consequently the energy denominator is

$$E-\sum\mathbf{T}_i-\sum_{kl}\mathbf{t}_{a,kl}=e_{e'j'}+\sum_{kl\neq ij}(t_{a,kl}^{(0)}-t_{a,kl}), \tag{18}$$

where

$$e_{e'j'}=\mathbf{T}_i+\mathbf{T}_j+V_a(i)+V_a(j)-\mathbf{T}_{i'}-\mathbf{T}_{j'}-V_a(i')-V_a(j'), \tag{19}$$

and

$$V_a(i)=\sum_j\mathbf{t}_{a,ij}, \tag{20}$$

etc. The terms in $t_{a,kl}$, which do not refer explicitly to the excited particles i', j' have changed because of an implicit dependence of the operator for the kl pair on the excitation state of the unlinked ij pair. Explicitly, neglecting the second-order change in t,

$$\mathbf{t}_{a,kl}^{(0)}-\mathbf{t}_{a,kl}=\mathbf{v}_{kl,\,k'l'}\left(\frac{1}{e_{k'l'}}-\frac{1}{e_{k'l'e'j'}}\right)\mathbf{t}_{k'l',\,kl}$$

$$=\mathbf{v}_{kl,\,k'l'}\frac{1}{e_{k'l'}}\frac{1}{e_{k'l'e'j'}}(e_{k'l'e'j'}-e_{k'l'})\mathbf{t}_{k'l',\,kl}$$

$$=\mathbf{v}_{kl,\,k'l'}\frac{1}{e_{k'l'}}\frac{1}{e_{k'l'e'j'}}\mathbf{t}_{k'l',\,kl}e_{e'j'}. \tag{21}$$

Inserting this change into the propagator for the ij pair and expanding the propagator, the expression for $t_{ij,\,ij}$ breaks up into two terms

$$\mathbf{t}_{ij,\,ij}=\mathbf{v}_{ij,\,ij}+\mathbf{v}_{ij,\,e'j'}\frac{1}{e_{e'j'}}\mathbf{t}_{e'j',\,ij}$$

$$-v_{ij,\,e'j'}\frac{1}{e_{e'j'}}v_{kl,\,k'l'}\frac{1}{e_{e'j'k'l'}}\frac{1}{e_{k'l'}}t_{k'l',\,kl}e_{e'j',\,ij}. \tag{22}$$

The last term is identical except for sign with $E_4^{(r)}$

[2] The author is indebted to Professor J. Bardeen for pointing out the lack of a satisfactory treatment of these terms in other theories of the many-body system.

except that two of the I operators have been replaced by v operators. These, however, are equal to first order; thus we see that the N^2 terms cancel, leaving only the linked terms for irreducible clusters which are of no higher order than N. The two-body operator defined by the equation

$$\mathbf{K}_{ij,\,ij}=\mathbf{v}_{ij,\,ij}+\mathbf{v}_{ij,\,i'j'}\frac{1}{e_{i'j'}}\mathbf{K}_{i'j',\,ij}, \tag{23}$$

which differs from $t_{ij,\,ij}$ in that the unlinked terms are omitted from the propagator, is thus, although much simpler, a much better approximation to the leading term in the energy. It is similar to the result used in applications of these methods to the nuclear problem.[1,2]

Before going on to show that is possible to generalize this definition of the propagator for a general matrix element, we shall show how a similar simplification occurs in ordinary perturbation theory.

III. RELATION TO PERTURBATION THEORY

For simplicity in this section, we shall assume that the particles are distinguishable; the more general discussion closely follows the treatment we give here.

In the usual perturbation theory[4] the Hamiltonian is separated into the unperturbed Hamiltonian

$$H_0=\sum_i T_i, \tag{24}$$

and the perturbation

$$h=\sum_{ij} v_{ij} \tag{25}$$

(for simplicity we absorb a factor of $\frac{1}{2}$ into the v's). We take for the zeroth order wave functions a product of the eigenfunctions of H_0, for example plane waves normalized in a large box of volume v. The perturbation series for the energy then is

$$E=\sum_n E_n. \tag{26}$$

We introduce a compact notation to simplify the form of the perturbation expansion; we define

$$(\phi_0,\theta\phi_0)=\langle\theta\rangle \tag{27}$$

for any operator. We also let

$$\left(\phi_n,\frac{1}{\epsilon_0-\epsilon_n}\phi_n\right)=\left(\phi_n,\frac{1}{\epsilon_0-H_0}\phi_n\right)=\left(\phi_n,\frac{1}{a}\phi_n\right), \tag{28}$$

where the operator $1/a$ is

$$1/a=1/(\epsilon_0-H_0). \tag{29}$$

Using this notation it is then easy to show that the perturbation series for the energy is given by the development

$$E_n=\langle hS_{n-1}\rangle-\sum_{m=1}^{n-1}E_m\langle S_{n-m}\rangle, \tag{30}$$

where

$$S_n=\frac{1}{a}hS_{n-1}-\frac{1}{a}\sum_{m=1}^{n-1}E_mS_{n-m}. \tag{31}$$

The diagonal elements of S_n are not needed explicitly; they can, however, be fixed by the unit normalization condition

$$\sum_{m=0}^{n}S_mS_{n-m}=0 \quad n\neq 0 \tag{32}$$

together with

$$S_0=1. \tag{33}$$

We also introduce

$$u=h-\langle h\rangle, \tag{34}$$

which has vanishing matrix elements in the ground state. The expansion can then be written

$$E_0=\epsilon_0=\langle H_0\rangle,$$

$$E_1=\langle h\rangle,$$

$$E_2=\left\langle\frac{1}{a}h\frac{1}{a}h\right\rangle=\left\langle\frac{1}{a}u\frac{1}{a}u\right\rangle,$$

$$E_3=\left\langle\frac{1}{a}h\frac{1}{a}u\frac{1}{a}h\right\rangle,$$

$$E_4=\left\langle\frac{1}{a}h\left[\frac{1}{a}u\frac{1}{a}u-\left\langle\frac{1}{a}u\frac{1}{a}u\right\rangle\right]\frac{1}{a}h\right\rangle,$$

$$E_5=\left\langle\frac{1}{a}h\left[\frac{1}{a}u\frac{1}{a}u\frac{1}{a}u-\left\langle\frac{1}{a}u\frac{1}{a}u\frac{1}{a}u\right\rangle-\frac{1}{a}u\left\langle\frac{1}{a}u\frac{1}{a}u\right\rangle-\left\langle\frac{1}{a}u\frac{1}{a}u\right\rangle\frac{1}{a}u\right]\frac{1}{a}h\right\rangle. \tag{35}$$

The structure of these terms is extremely simple; we can obtain them by taking the nth order iterate of u

$$\left\langle a\left(\frac{1}{a}u\right)^n\right\rangle, \tag{36}$$

and subtracting all matrix elements of the same order in which matrix elements in the ground state of any subset of the u's appear, always remembering that a matrix element of the form

$$\left\langle\frac{1}{a}\quad\text{or}\quad\frac{1}{a}\right\rangle \tag{37}$$

is to be set equal to zero. This simple prescription suffices to define the full perturbation series for the energy.

We next note some simple properties of the expansion by examining the first few terms; we shall later generalize the results. Inserting the series for h and for u, the

[1] K. A. Brueckner, Phys. Rev. **97**, 1353 (1955).
[4] See, for example, L. I. Schiff, *Quantum Mechanics* (McGraw-Hill Book Company, Inc., 1949), Chap. VII.

expression for E_2 becomes

$$\sum_{n\neq 0}\sum_{ij}\sum_{kl}(\phi_0,v_{ij}\phi_n)\frac{1}{\epsilon_0-\epsilon_n}(\phi_n,v_{kl}\phi_0). \tag{38}$$

In the double sum over ij, kl, since matrix elements to the ground state are omitted, the matrix element will vanish unless $ij=kl$. This result also is apparent if we note that v_{kl} is in effect an operator exciting the pair kl from the ground state; this pair must be returned by v_{ij}. Thus

$$E_2=\sum_{n\neq 0}\sum_{ij}(\phi_0,v_{ij}\phi_n)\frac{1}{\epsilon_0-\epsilon_n}(\phi_n,v_{ij}\phi_0)=\sum_{ij}\left\langle \underset{a}{\frac{1}{}}v_{ij}\right\rangle, \tag{39}$$

which is the second term in the expansion for t_{ij}. We break down the third term

$$E_3=\sum_{ijklmn}\left\langle \underset{a}{\frac{1}{}}v_{ij}\underset{a}{\frac{1}{}}(v_{kl}-\langle v_{kl}\rangle)v_{mn}\right\rangle \tag{40}$$

in a similar way. In this term we can combine the indices ij, kl, mn in several ways. The simplest possibility is with all pairs the same, giving

$$E_3^{(1)}=\sum_{ijk}\left\langle \underset{a}{\frac{1}{}}v_{ij}\underset{a}{\frac{1}{}}(v_{ij}-\langle v_{ij}\rangle)v_{ij}\right\rangle. \tag{41}$$

We can also pair ij and mn and leave kl free; this gives

$$\left\langle \underset{a}{\frac{1}{}}v_{ij}\underset{a}{\frac{1}{}}(v_{kl}-\langle v_{kl}\rangle)v_{ij}\right\rangle. \tag{42}$$

This can be further reduced since unless k or l is equal to i or j, only the diagonal elements of $v_{kl}-\langle v_{kl}\rangle$ with respect to the ground state enter, giving zero. Thus we have a restriction on k,l so that

$$E_3^{(2)}=\sum_{ijk}\left\langle \underset{a}{\frac{1}{}}v_{ij}\underset{a}{\frac{1}{}}(v_{ik}-\langle v_{ik}\rangle+v_{jk}-\langle v_{jk}\rangle)v_{ij}\right\rangle. \tag{43}$$

Writing the matrix element out more explicitly, this is

$$E_3^{(2)}=\sum_{ijn}(\phi_0,v_{ij}\phi_n)\frac{1}{\epsilon_0-\epsilon_n}\times\sum_k[(\phi_n,v_{ik}\phi_n)-(\phi_0,v_{ik}\phi_0)+(i\to j)]\frac{1}{\epsilon_0-\epsilon_n}\times(\phi_n,v_{ij}\phi_0). \tag{44}$$

We now note that this term in E_3 can be combined with the second order term E_2 to give

$$E_2+E_3^{(2)}=\sum_{ijn}(\phi_0,v_{ij}\phi_n)\left\{\frac{1}{\epsilon_0-\epsilon_n}+\frac{1}{\epsilon_0-\epsilon_n}\times\sum_k[(\phi_n,v_{ik}\phi_n)-(\phi_0,v_{ik}\phi_0)+i\to j]\times\frac{1}{\epsilon_0-\epsilon_n}\right\}(\phi_n,v_{ij}\phi_0)$$
$$\cong\sum_{ij}(\phi_0,v_{ij}\phi_n)\{\epsilon_0+\textstyle\sum_k(\phi_0,(v_{ik}+v_{jk})\phi_0)-\epsilon_n-\sum_k(\phi_n,(v_{ik}+v_{jk})\phi_n)\}^{-1}(\phi_n,v_{ij}\phi_0). \tag{45}$$

Thus the effect of $E_3^{(2)}$ is to give the first correction term in the nonperturbation propagator $1/e$ in E_2.

The remaining term in E_3 arises from combining three different indices, corresponding to the involvement of three particles. This term is

$$E_3^{(3)}=\sum_{ijk}\left\langle \underset{a}{\frac{1}{}}v_{ij}\underset{a}{\frac{1}{}}v_{jk}v_{ki}\right\rangle, \tag{46}$$

which is the first term in the expansion of the three body cluster term.

The next term in the energy E_4 contains a variety of types of combinations of the matrix element of the v's; we shall consider here in detail only those terms which are similar to the unlinked clusters discussed in Sec. II. The general reductions are given in the Appendix. The terms of fourth order which we shall not discuss here are the following:

(1) fourth order interaction of v_{ij} (for a single pair).
(2) changes in the propagators of lower order terms.
(3) linked 4-body cluster.

The unlinked or reducible terms in E_4 are:

$$E_4^{(r)}=\sum_{ijkl}\left\{\left\langle \underset{a_{ij}}{\frac{1}{}}v_{ij}\underset{a_{ijkl}}{\frac{1}{}}\left(\underset{a_{ij}}{\frac{1}{}}v_{kl}+\underset{a_{kl}}{\frac{1}{}}v_{ij}\right)v_{kl}\right\rangle\right\}-\sum_{ijkl}\left\{\left\langle \underset{a_{ij}^2}{\frac{1}{}}v_{ij}v_{ij}\right\rangle\left\langle \underset{a_{kl}}{\frac{1}{}}v_{kl}v_{kl}\right\rangle\right\}, \tag{47}$$

where

$$a_{ij}=\epsilon_i+\epsilon_j-\epsilon_{i'}-\epsilon_{j'}, \tag{48}$$

etc. This we simplify using the identity

$$\frac{1}{a_{ij}}\frac{1}{a_{ijkl}}\left(\frac{1}{a_{ij}}+\frac{1}{a_{kl}}\right)-\frac{1}{a_{ij}^2}\frac{1}{a_{kl}}=\frac{1}{a_{ij}^2}\left(\frac{a_{ij}+a_{kl}}{a_{ijkl}}-1\right). \tag{49}$$

Since

$$a_{ijkl}=a_{ij}+a_{kl}, \tag{50}$$

these two terms cancel. We note that this is possible only when all of the matrix elements of the same general unlinked structure, are combined. Thus the unlinked terms (of order N^2) give zero, as we expected from the consideration of a similar cancellation in Sec. II. We shall not discuss the cancellations of the unlinked

terms of higher order; the proof has been explicitly constructed in fifth and sixth order and always involves a lengthy but trivial sequence of algebraic identities such as those of Eq. (49).

We proceed next to a more general statement of this result in the following section.

IV. LINKED PROPAGATOR

The results of the last two sections strongly suggest that the appearance of unlinked cluster terms in the energy expansion is everywhere spurious in that they are exactly canceled by similar terms appearing elsewhere in the expansion. Consequently the expansion is in each order linear in the total number of particles in that the contributions to the energy depend on N. The unlinked terms which cancel are always unphysical in that they cannot represent actual interaction energy; this situation is similar to that which exists in the S-matrix expansion of quantum field theory where similar unlinked terms can always be identified as contributing only to the phase of the wave function without giving real effects in the scattering.

In discussing these terms in Secs. II and III, we have shown that their omission results in a simple and reasonable definition of the propagator or energy denominator. The criterion of dropping unlinked terms is perhaps sufficient to apply to any given term in the energy expansion since the spurious terms can be easily recognized and dropped. It is however convenient to show that these conditions may be formulated more formally by defining what we shall call a linked propagator. We introduce a modified propagator $\not{p}$ with the following properties. Consider a typical expression involving the nondiagonal I operators and the propagator;

$$(\phi_0,\cdots \mathbf{I}_{kl,k'l'}\not{p}\mathbf{I}_{mn,m'n'}\cdots\phi_0). \tag{51}$$

We define the matrix element of $\not{p}$ in this case to be

$$\not{p}=[\sum_i (E_i-E_{i'})]^{-1}, \tag{52}$$

where the sum over i is to run over all terms linked to the left to the pair k',l'. For the energies E_i and E_i' we shall take

$$E_i=(\phi_0,\mathbf{T}_i+\sum_j \mathbf{t}_{c,ij}\phi_0),$$

$$E_{i'}=(\phi_{i'},\mathbf{T}_{i'}+\sum_j \mathbf{t}_{c,c'j'}\phi_{i'}). \tag{53}$$

If the energy difference is zero, then the matrix element of $\not{p}$ is to be set equal to zero. Since the states we consider are discrete, the omission of the single term in the matrix element is unambiguous. To show that this definition leads to the desired changes; first, it is obvious that the equation for $K_{ij,ij}$ now appears directly. In addition, in a typical unlinked term of fourth order, for example, we now have the matrix element

$$(\phi_0,\mathbf{I}_{ij,c'j'}\not{p}(c'j')I_{kl,k'l'}\not{p}(k'l')\times I_{c'j',ij}\not{p}(ij)I_{k'l',kl}\phi_0). \tag{54}$$

The propagator $\not{p}(ij)$ is for the ij and all linked pairs (in this case the $i'j'$ pair) in the ground state; hence the energy difference is zero and by the previous definition, this matrix element of the propagator is equal to zero. Thus this term is identically zero; this will be true for any such unlinked interaction.

This completes the specification of the expansion; it now has a quite simple form since it is a series in the linked or irreducible clusters alone. The great simplification of this result in comparison with the perturbation expansion, for example, is due to the immense compression of the series which is accomplished by the introduction of the K and I operators. The equation for K is nonlinear; it is the perturbation expansion of this operator which leads to the very complicated series of perturbation theory. It is worth noting, however, that the convergence of the perturbation series itself does not depend on N, each term in the series depending only on N linearly.

V. CONVERGENCE OF THE LINKED CLUSTER EXPANSION

To determine the extent to which the linked cluster expansion is sufficiently rapidly convergent to make it a useful approximation method, we shall examine the leading cluster terms. Since the convergence does not depend on N, we expect that the expansion will be characterized by other parameters of the system such as the density and the interaction strength and range. Thus we shall attempt to determine the dimensionless expansion parameter which governs the rate of convergence of the series; if this is sufficiently small, we expect that the leading term in the expansion will be an accurate representation of the many-body energy. As an explicit example we shall consider the nuclear system which has been studied elsewhere[1,3,5-7]; the convergence of the method has been investigated in these papers but only in a semiquantative way with the intent of establishing a rough upper limit on the magnitude of the correction terms.

We consider in detail the first cluster term involving more than two particles; this is

$$\Delta E_2=\tfrac{1}{8}\sum_{ijk i'j'k'}(\phi_0,\mathbf{I}_{ij,c'j'}\not{p}I_{k'l',k'i}\not{p}I_{i'j',kl}\phi_0). \tag{55}$$

In evaluating this we shall neglect all exchange terms; these are in general much smaller and also of opposite sign to the main term so that we over-estimate ΔE_2 by making this approximation. In evaluating ΔE_2 we shall take a simple form for the nondiagonal operators I, i.e.,

$$I_{ij,kl}=\frac{2\pi V_0}{\mu\Omega}[f(\mathbf{k}_i-\mathbf{k}_k)+f(\mathbf{k}_i+\mathbf{k}_k)]\times\delta(\mathbf{k}_i+\mathbf{k}_j,\mathbf{k}_k+\mathbf{k}_l), \tag{56}$$

[5] Brueckner, Levinson, and Mahmoud, Phys. Rev. **95**, 219 (1954).
[6] K. A. Brueckner, Phys. Rev. **96**, 908 (1954).
[7] Brueckner, Francis, and Eden, Phys. Rev. (to be published).

where

$$f(x)=1/(\mu^2+x^2), \tag{57}$$

and $V_0/\mu=0.25$, $v=$ total normalization volume. This result is a reasonable approximation to the actual nondiagonal operators I; it is the Born approximation matrix element given by a Yukawa well with Serber exchange mixture. In the propagator we use the approximate result for the energies

$$E_i=k_i^2/2M^*, \tag{58}$$

where $M^*=0.54M$ is the effective mass of a nucleon moving in the velocity-dependent nuclear potential.[3] Making these substitutions into Eq. (55), the energy shift ΔE_3 is

$$\Delta E_3=\tfrac{1}{3}(2M^*)^2\left(\frac{2\pi V_0}{\mu v}\right)^3\sum_{ijki'}[f(\mathbf{k}_i-\mathbf{k}_{i'})+f(\mathbf{k}_i+\mathbf{k}_{i'})]$$
$$\times(k_i^2+k_j^2-k_{j'}^2-k_{j'}^2)^{-1}[f(\mathbf{k}_i-\mathbf{k}_{i'})+f(\mathbf{k}_i+\mathbf{k}_{i'})]$$
$$\times(k_j^2+k_k^2-k_{j'}^2-k_{k'}^2)^{-1}$$
$$\times[f(\mathbf{k}_i-\mathbf{k}_{i'})+f(2\mathbf{k}_j+\mathbf{k}_k-\mathbf{k}_{i'})]. \tag{59}$$

The sum over $ijki'$ is not only over the momentum states but also over spins and isotopic spins. Since the operator I does not involve spin operators, the sum over the two spin and two isotopic spin values for the states ijk introduces a factor of $(4)^3$ (the summation over the spin states of i', j', k' gives unity). The summations over momenta can be replaced by integrations, using

$$\sum_{\mathbf{k}_i}\rightarrow\frac{v}{(2\pi)^3}\int d\mathbf{k}_i. \tag{60}$$

Introducing the variable

$$\mathbf{k}_i-\mathbf{k}_{i'}=\mathbf{x}, \tag{61}$$

we then find

$$\Delta E_3=8(\mu^*)^2\left(\frac{2\pi V_0}{\mu v}\right)^3\left[\frac{v}{(2\pi)^3}\right]^4\int_{k_f}d\mathbf{k}_i\int_{k_f}d\mathbf{k}_j\int_{k_f}d\mathbf{k}_k\int d\mathbf{x}$$
$$\times f^2(x)[x^2-(\mathbf{k}_i+\mathbf{k}_j)\cdot\mathbf{x}]^{-1}[x^2-(\mathbf{k}_j+\mathbf{k}_k)\cdot\mathbf{x}]^{-1}, \tag{62}$$

where we have dropped some small exchange terms depending on $f(x)^2f(\mathbf{x}+\mathbf{k}_i)$, etc., which are much smaller (for large k_i) than the main term. In this integral the restrictions arising from the exclusion principle are that

$$|\mathbf{k}_i'|=|\mathbf{k}_i-\mathbf{x}|\geqq k_f,$$
$$|\mathbf{k}_j'|=|\mathbf{k}_j-\mathbf{x}|\geqq k_f, \tag{63}$$
$$|\mathbf{k}_k'|=|\mathbf{k}_k-\mathbf{x}|\geqq k_f.$$

Let us now examine this 12-dimensional integral to see how simplifications can be made to reduce the problem of evaluation. We note that $f(x)^3$ is a very rapidly decreasing function of x for $x>\mu$, falling off as x^{-6}. Therefore, since the rest of the integrand is also largest for x small, it is reasonable to evaluate the integrals over $\mathbf{k}_i$, $\mathbf{k}_j$, $\mathbf{k}_k$ making the approximation that x is small. This integral is

$$\Delta=\int\frac{d\mathbf{k}_i d\mathbf{k}_j d\mathbf{k}_k}{x^2}\frac{1}{(k_i\mu_i+k_j\mu_j-x)}\cdot\frac{1}{(k_j\mu_j+k_k\mu_k-x)}, \tag{64}$$

where $\mu_i=\mathbf{k}_i\cdot\mathbf{x}/k_ix$, etc. The restriction from the exclusion principle restricts the angular range of integration; the condition is

$$\mu_i\leqq(k_i^2+x^2-k_f^2)/2k_ix, \tag{65}$$

and similarly for the other angular variables. Keeping only the leading terms in x, the integral over k_i, for example, is

$$2\pi\int_{k_f-x}^{k_f}k_i^2dk_i\int_{-1}^{(k_i^2+x^2-k_f^2)/2k_ix}\frac{d\mu_i}{k_i\mu_i+k_j\mu_j-x}. \tag{66}$$

For small x, we set $k_i=k_f$ except for the upper limit of the angular integration where we set

$$\frac{k_i^2+x^2-k_f^2}{2k_ix}\cong\frac{(k_i+k_f)(k_i-k_f)}{2k_ix}\cong\frac{k_i-k_f}{x}, \tag{67}$$

with these approximations, we find for the k_i integration

$$2\pi k_f\int_{k_f-x}^{k_f}dk_i\int_{-1}^{(k_i-k_f)/x}\frac{d\mu_i}{\mu_j+\mu_i}$$
$$=-2\pi k_fx[1+\mu_j\ln(1-1/\mu_j)]. \tag{68}$$

The integral over k_k gives a similar result; the remaining integral over k_j gives

$$\Delta=(2\pi k_f)^2 2\pi k_f^2$$
$$\times\int_{k_f-x}^{k_f}dk_j\int_{-1}^{(k_j-k_f)/x}[1+\mu_j\ln(1-1/\mu_j)]^2d\mu_j. \tag{69}$$

A change in the order of integration and a change of variable in the μ_j integration leads finally to

$$\Delta=(2\pi k_f)^3k_fx\int_0^1 dss\left[1+s\ln\frac{s}{1+s}\right]^2$$
$$=(2\pi k_f)^3k_fx(0.078). \tag{70}$$

Collecting these results we find

$$\Delta E_3=8(M^*)^2\left(\frac{2\pi V_0}{\mu v}\right)^3\left[\frac{v}{(2\pi)^3}\right]^4(2\pi k_f)^3$$
$$\times 0.078k_f\int_0^\infty 4\pi x^2f^3(x)dx. \tag{71}$$

Using Eq. (57) for $f(x)$, the integral over x is

$$\int f^3(x)x^2dx=\tfrac{1}{4}\mu^2. \tag{72}$$

Taking $4v(4/3\pi k_f^3)/(2\pi)^3=N$, the final result is

$$\Delta E_3=\left(\frac{M^*}{\mu}\frac{V_0}{\mu}\frac{1}{4\pi}\right)^3 0.468\frac{\mu}{M^*}k_f. \tag{73}$$

For typical values of the parameters, i.e., $M^*/\mu \sim 4$, $V_0/\mu = -\frac{1}{4}$, $k_f = 1.6\mu$, this gives

$$\Delta E_2 \cong -0.0071 \text{ Mev}, \tag{74}$$

which is to be compared with the leading term in $K_{ij,ij}$ which is about equal to 30 Mev per particle.

The very small effect of the correction term on the energy is due to the smallness of the effective expansion parameter

$$\beta = \frac{M^*}{\mu}\frac{V_0}{\mu}\frac{1}{4\pi} = 0.072. \tag{75}$$

It can be fairly easily shown that the four body cluster term is also given by an expression very similar to that for ΔE_3 except that it depends on β^4; consequently it is again the size of β which determines the next higher order correction. The smallness of the expansion parameter β is due in part to the size of $(V_0/\mu)(M^*/\mu)$ which is in this case of the order of unity. It is of course obvious that convergence cannot be expected for large values of this combination of constants. Even more important, however, is the factor of $1/(4\pi)$ which always appears paired with the mass and potential constants. This factor appears as the result of the restriction of the angular integrations by the exclusion principle; this restriction is important because the typical momenta near the Fermi limit are rather large compared with momenta for which the matrix elements of the interaction are large. We have made use of this fact in evaluating the integrals for ΔE_3. For much stronger potentials, however, this result would no longer hold and for the same Fermi momentum the angular integrations would be less affected by the exclusion principle.

Another important and striking feature of the result for the three- (and more-) body cluster is its linear dependence on the Fermi momentum. It is easily shown that the leading term in the energy depends on k_f^3; thus the relative importance of the higher-order cluster terms decreases as the Fermi momentum increases or, equivalently, as the density increases. The origin of this effect is obvious; as the Fermi momentum increases, the momentum transfers required to bring particles out of the Fermi gas to excited states increase. Since the matrix elements of the interaction decrease as the momentum transfers increase, excitations involving the multiple excitation of particles are inhibited. The effect is most pronounced for the high-order clusters for this reason.

VI. METHODS OF SOLVING THE $K_{ij,ij}$ EQUATION

We have shown that the linked cluster expansion converges very rapidly for forces of typical nuclear strength so that it is a very good approximation in this case to evaluate only the leading term in the expansion. The convergence may not be as rapid in other systems of physical interest; even in such cases, however, the leading term will give very useful semiquantitative information about the system. The equation for the matrix elements of $K_{ij,ij}$ as given by Eq. (23) is, in the ground state,

$$\mathbf{K}_{ij,ij} = \mathbf{v}_{ij,ij} + \mathbf{v}_{ij,i'j'}(E_i + E_j - E_{i'} - E_{j'})^{-1}\mathbf{K}_{i'j',ij}, \tag{76}$$

where

$$\begin{aligned} E_i &= (\phi_0, (\mathbf{T}_i + \textstyle\sum_k \mathbf{t}_{ei k})\phi_0) \\ &= (\phi_0, [\mathbf{T}_i + \tfrac{1}{2}\textstyle\sum_k(\mathbf{K}_{ik,ik} + \mathbf{K}_{ik,ki})]\phi_0), \end{aligned} \tag{77}$$

and

$$E_{i'} = (\phi(i'), [\mathbf{T}_{i'} + \tfrac{1}{2}\textstyle\sum_k(\mathbf{K}_{i'k,i'k} + \mathbf{K}_{i'k,ki'})]\phi(i')). \tag{78}$$

To a good first approximation, we can suppose that the coherent potential

$$V_c(i) = \tfrac{1}{2}\textstyle\sum_k(\mathbf{K}_{ik,ik} + \mathbf{K}_{ik,ki}) \tag{79}$$

acting on the ith particle depends only on the momentum state of the particle i and evaluate $V_c(i)$ as if particle i were always propagating on the energy shell. This is equivalent to the assumption that the potential acting on a particle is the same in virtual states as in real states. If we make this simplifying assumption, then we can write

$$\begin{aligned} \mathbf{K}_{ij,ij} = \mathbf{v}_{ij,ij} + \mathbf{v}_{ij,i'j'}[&T_i + T_j - T_{i'} - T_{j'} + V_c(i) + V_c(j) \\ &- V_c(i') - V_c(j')]^{-1}\mathbf{K}_{i'j',ij}, \end{aligned} \tag{80}$$

and

$$\begin{aligned} V_c(i) &= [\phi_0, \textstyle\sum_k(\mathbf{K}_{ik,ik} + \mathbf{K}_{ik,ki})\phi_0], \\ V_c(i') &= [\phi_0, \textstyle\sum_k(\mathbf{K}_{i'k,i'k} + \mathbf{K}_{i'k,ki'})\phi_0]. \end{aligned} \tag{81}$$

Equations (80) and (81) form a coupled system for the determination of $V_c(i)$; they are equivalent to a nonlinear integral equation for $V_c(i)$. In this approximation they have been solved as a self-consistency problem in applications of the methods to the nucleus.[8]

A more accurate treatment of the propagator in intermediate states is possible if account is taken of the fact that propagation off the energy shell is occurring. According to our rules for defining $\mathfrak{p}$, in an intermediate state with $i'j'$ excited, the equation for a typical term in $V_c(i')$ is

$$\begin{aligned} \mathbf{K}'_{i'k,i'k} = \mathbf{v}_{i'k,i'k} &+ \mathbf{v}_{i'k,i'k'} \\ &\times (E_i + E_j + E_k - E_{i'} - E_{j'} - E_{k'})^{-1}\mathbf{K}_{i'k',i'k}. \end{aligned} \tag{82}$$

This differs from the equation for $K_{i'k',i'k}$ on the energy shell in that

$$\begin{aligned} \mathbf{K}_{i'k,i'k} = \mathbf{v}_{i'k,i'k} &\\ + \mathbf{v}_{i'k,i'k'}(E_{i'} + E_k - E_{i'} - E_{k'})^{-1}&\mathbf{K}_{i'k',i'k}. \end{aligned} \tag{83}$$

The neglect of the difference between $K_{i'k,i'k}$ and $K'_{i'k,i'k}$ leads to a high order correction term in the energy. If the energy difference in the propagator is expanded out as a perturbation, i.e., if we take

$$\begin{aligned} \mathbf{K}'_{i'k,i'k} &= \mathbf{v}_{i'k,i'k} + \mathbf{v}_{i'k,i'k'}\frac{1}{e_{ik} + \Delta E}\mathbf{K}'_{i'k',i'k} \\ &\cong \mathbf{K}_{i'k,i'k} - \mathbf{v}_{i'k,i'k'}\frac{1}{e_{ik}}\Delta E\frac{1}{e_{ik}}\mathbf{K}_{i'k',i'k}, \end{aligned} \tag{84}$$

then the equation for the ground-state matrix element of $K_{ij,ij}$ is altered by the amount

$$\Delta K_{ij,ij} \cong v_{ij,i'j'} \frac{1}{e_{i'j'}} v_{i'k,i''k''} \frac{1}{e_{ik}} \times \Delta E \frac{1}{e_{ik}} K_{i''k'',i'k} \frac{1}{e_{i'j'}} K_{i'j',ij}. \quad (85)$$

Since the effect appears in such high order, the actual quantitative change is probably quite small. If greater accuracy is desired, this effect can be included at least approximately. It adds the complication that a self-consistent solution must be obtained for the effective potential V_e acting on a particle both off and on the energy shell. It is probably an excellent first approximation to neglect this effect and make the static approximation for V_e; this has been done in the actual applications of this method.

VII. CONCLUSIONS

We have considered in detail an approximation method which has been developed to deal with the problem of determining the interaction energy of a many-body system when the particle-particle forces are not weak. The usefulness of the method is determined by the convergence of an expansion which determines the interaction energy. We have primarily interested ourselves in this paper in a study of the structure of this expansion, particularly in the dependence of the convergence on the total number of particles (which we wish to take to be very large). We have shown that the convergence of the method does not depend on N, any dependence on higher powers of N than the first being spurious and exactly canceled by similar spurious terms appearing elsewhere in the expansion. This cancellation has been shown to occur in a precisely similar manner in the expansion of conventional perturbation theory, any nonlinear dependence on the total number of particles being again spurious. As a consequence the resulting expansion is in every order proportional to the total number of particles the total number thus appearing as a common factor for the entire series. The expansion is in a series of irreducible or linked clusters which involve a succession of transitions brought about by the nondiagonal transition operators of the theory. The convergence for the nuclear system has been investigated by a detailed examination of the first irreducible cluster (involving three particles) and shown to be extremely rapid, with the exclusion principle playing an important role in determining the rate of convergence.

Finally the problem of evaluating the two-body interaction operators has been briefly discussed; it is a sum over the diagonal part of these operators which provides the leading term in the interaction energy. It is shown that in the approximation the potential acting on a particle is the same in virtual as real states, the problem of solving for the potential reduces to the problem of self-consistency used in other applications. The accuracy of this approximation is discussed briefly and methods of improving on the approximation are described.

ACKNOWLEDGMENTS

The author is indebted to Dr. R. J. Eden for many helpful discussions.

APPENDIX

Reduction of Fourth-Order Perturbation Term

We shall show how the fourth-order perturbation term can be broken up into a variety of terms which can be identified either as modifications of the propagators of lower order clusters or as irreducible cluster terms. To make this identification possible we first expand the reaction matrix K_{ij} as given by Eq. (23) with the notation simplified for the case of distinguishable particles:

$$\langle K_{ij}\rangle = \langle v_{ij}\rangle + \left\langle v_{ij} \frac{1}{e_{ij}} K_{ij} \right\rangle, \quad (A1)$$

where to second order the modified propagator is

$$e_{ij} = \epsilon_i + \epsilon_j + \sum_k \left\{ \langle v_{ik}\rangle + \left\langle v_{ik} \frac{1}{a} v_{ik} \right\rangle - v_{ik} \frac{1}{a} v_{ik} + (i \rightarrow j) \right\}. \quad (A2)$$

Expanding the equation for K_{ij} we find for the fourth-order term

$$\begin{aligned}
\langle K_{ij}\rangle^{(4)} = & \sum_k \left\langle v_{ij} \frac{1}{a} v_{ij} \frac{1}{a} v_{ij} \frac{1}{a} v_{ij} \right\rangle \\
& + \sum_k \left\langle v_{ij} \frac{1}{a} (v_{ik} - \langle v_{ik}\rangle) \frac{1}{a} v_{ij} \frac{1}{a} v_{ij} \right\rangle \\
& + \sum_k \left\langle v_{ij} \frac{1}{a} v_{ij} (v_{ik} - \langle v_{ik}\rangle) \frac{1}{a} v_{ij} \right\rangle \\
& + \sum_k \left\langle v_{ij} \frac{1}{a} \left(v_{ik} \frac{1}{a} v_{ik} - \left\langle v_{ik} \frac{1}{a} v_{ik} \right\rangle \right) \frac{1}{a} v_{ij} \right\rangle \\
& + \sum_k \sum_l \left\langle v_{ij} \frac{1}{a} (v_{ik} - \langle v_{ik}\rangle) \frac{1}{a} (v_{il} - \langle v_{il}\rangle) \frac{1}{a} v_{ij} \right\rangle \\
& + \sum_k \sum_l \left\langle v_{ij} \frac{1}{a} (v_{ik} - \langle v_{ik}\rangle) \frac{1}{a} (v_{jl} - \langle v_{il}\rangle) \frac{1}{a} v_{ij} \right\rangle, \quad (A3)
\end{aligned}$$

omitting some terms which result from interchange of ij. We shall also need for comparison the expansion of the

modified propagator for the three-body cluster which is, to fourth order,

$$\sum_{ijmk}\left\{\left\langle \underset{a}{1}(v_{ij}-\langle v_{ik}\rangle)\underset{a}{1}v_{jm}-v_{mi}\right\rangle + \left\langle \underset{a}{1}\underset{a}{1}v_{ij}-v_{jm}-(v_{jk}-\langle v_{jk}\rangle)\underset{a}{1}v_{mi}\right\rangle\right\}. \quad \text{(A4)}$$

The perturbation expansion as given in Sec. III gives for the fourth-order term in the energy

$$E_4=\left\langle \underset{a}{1}\underset{a}{1}u-u-u-u\underset{a}{1}\right\rangle-\left\langle \underset{a}{1}u-u\underset{a}{1}\right\rangle\left\langle \underset{a}{1}u-u\underset{a}{1}\right\rangle. \quad \text{(A5)}$$

Inserting the expansion for u, this is

$$E_4=\sum_{ijmnrsv}\left[\left\langle \underset{a}{1}u_{ij}-u_{mn}\underset{a}{1}u_{rs}-u_{iv}\underset{a}{1}\right\rangle - \left\langle \underset{a^2}{1}u_{ij}-u_{mn}\underset{a}{1}\right\rangle\left\langle u_{rs}-u_{iv}\right\rangle\right]. \quad \text{(A6)}$$

The first simplification is that already noted in Sec. III, i.e.,

$$\sum_{ijmn}\left\langle \underset{a}{1}u_{ij}-u_{mn}\right\rangle=\sum_{ijmn}\left\langle \underset{a}{1}u_{ij}-u_{ij}\right\rangle\delta_{im}\delta_{jn} =\sum_{ij}\left\langle \underset{a}{1}u_{ij}-u_{ij}\right\rangle. \quad \text{(A7)}$$

Consequently the second term of Eq. (A6) is

$$\sum_{ijmn}\left\langle \underset{a^2}{1}u_{ij}-u_{ij}\right\rangle\left\langle \underset{a}{1}u_{mn}-u_{mn}\right\rangle = \sum_{ij\neq mn}\left\langle \underset{a^2}{1}u_{ij}-u_{ij}\right\rangle\left\langle \underset{a}{1}u_{mn}-u_{mn}\right\rangle + \sum_{ijk}\left\langle \underset{a^2}{1}u_{ij}-u_{ij}\right\rangle\left\langle \underset{a}{1}u_{ik}-u_{ik}\right\rangle, \quad \text{(A8)}$$

the first term of which is of order N^2. Before reducing the first term of Eq. (A6), we note a simple property of the matrix element. An expression in which a term u_{mn} is not linked to any other term is zero, since in this case the expectation value of the product reduces to the product of the expectation values, and the expectation value of u_{mn} in the ground state is zero. This rule greatly simplifies the possible terms; they can be classified according to the number of pairs of indices which are set equal. The simplest term is that with all pairs of indices equal, i.e.,

$$E_4^{(4)}=\sum_{ij}\left\langle \underset{a}{1}\underset{a}{1}u_{ij}-u_{ij}\underset{a}{1}u_{ij}-u_{ij}\right\rangle. \quad \text{(A9)}$$

This is the fourth-order iterate of u_{ij} which appears in the expansion of K_{ij}. The next term with one u_{mn} different is

$$E_4^{(3)}=\sum_{ijk}\left[\left\langle \underset{a}{1}\underset{a}{1}u_{ij}-u_{ij}\underset{a}{1}u_{ik}-u_{ij}\right\rangle + \left\langle \underset{a}{1}\underset{a}{1}u_{ij}-u_{ik}\underset{a}{1}u_{ij}-u_{ij}\right\rangle\right], \quad \text{(A10)}$$

together with terms in which u_{ik} is replaced by u_{jk}. These two terms are the first-order modification in the propagator of the third-order iterate of u_{ij} in the equation for K_{ij}. The next term has two u's the same:

$$E_4^{(2)}=\sum_{ij\neq mkl}\left[\left\langle \underset{a}{1}\underset{a}{1}u_{ij}-u_{kl}\underset{a}{1}u_{kl}-u_{ij}\right\rangle+\left\langle \underset{a}{1}\underset{a}{1}u_{ij}-u_{kl}\underset{a}{1}u_{ij}-u_{kl}\right\rangle\right] +\sum_{ijk}\left\langle \underset{a}{1}\underset{a}{1}u_{ij}-u_{ik}\underset{a}{1}u_{kj}-u_{ij}\right\rangle+\sum_{ijkl}\left\langle \underset{a}{1}\underset{a}{1}u_{ij}-u_{ik}\underset{a}{1}u_{jl}-u_{ij}\right\rangle. \quad \text{(A11)}$$

In $E_4^{(2)}$ we have not included terms which vanish because they involve matrix elements of u in the ground state or because they require intermediate transitions to the ground state. The various terms in $E_4^{(2)}$ have the following interpretation; the first two cancel with the unlinked term of Eq. (A8) as shown in Sec. III. The last two terms combine with the linked term in Eq. (A8) to modify the propagator of the second term in the expansion for K_{ij}. Finally we have the term with no u's the same but all linked; these are for example

$$\sum_{ijmkl}\left\langle \underset{a}{1}\underset{a}{1}u_{ij}-u_{ik}\underset{a}{1}u_{jm}-u_{ml}\right\rangle, \quad \text{(A12)}$$

which is the modification of propagator of the three-body cluster term, and

$$\sum_{ijkl}\left\langle \underset{a}{1}\underset{a}{1}u_{ij}-u_{jk}\underset{a}{1}u_{kl}-u_{li}\right\rangle, \quad \text{(A13)}$$

which is a term typical of the fourth-order irreducible clusters.

(d,n) Reactions in O^{16} and N^{14}†

J. B. MARION,* R. M. BRUGGER,‡ AND T. W. BONNER
The Rice Institute, Houston, Texas

(Received June 6, 1955)

The technique of observing neutron thresholds in (p,n) and (d,n) reactions has been applied to the reactions $O^{16}(d,n)F^{17}$ and $N^{14}(d,n)O^{15}$. A nuclear resonance absorption magnetometer, in conjunction with a 90° magnetic analyzer, was used to accurately measure the bombarding energies. The $Li^7(p,n)Be^7$ threshold was used as the primary calibration. The energy of the first excited state of F^{17} was found to be 0.499 ± 0.003 Mev; excited states in O^{15} were found at 6.20 ± 0.03, 6.841 ± 0.009, and 6.909 ± 0.009 Mev. Ten broad resonances in the forward yield of neutrons from the reaction $O^{16}(d,n)F^{17}$ have been found in the range of bombarding energies from 1.8 to 4.3 Mev. The cross section for the $N^{14}(d,n)O^{15}$ reaction increases with the deuteron energy in the range 1.1 to 4.5 Mev; a sharp rise in the cross section begins at a bombarding energy of 2.1 Mev. The absolute cross sections for the $O^{16}(d,n)F^{17}$ and $N^{14}(d,n)O^{15}$ reactions were measured.

I. INTRODUCTION

THERE is at present considerable interest in the similarity of the level structure of pairs of mirror nuclei, since the hypothesis of the charge symmetry of nuclear forces predicts that these structures should be identical, except for Coulomb effects. Theoretical analysis of the energy shifts of mirror excited states has met with success only in a qualitative manner.[1] Both theoretical and experimental difficulties are present: the magnitude of the energy shifts are critically dependent on the nuclear radius, and the radius varies with excitation energy in an unknown manner. Also, accurate determinations of the energy levels of both members of a mirror pair have been made in only a few cases. Magnetic analysis of inelastically scattered charged particles and of charged-particle groups from nuclear reactions allow accurate measurements of the energies of excited states. The levels of many nuclei, however, are inaccessible with this technique, and in most cases the best present information is derived from measurements of the energies of neutron groups or of γ rays from various reactions. Since these types of measurements are difficult to make with great accuracy, the level structures of some nuclei are known only to an order of magnitude less accurately than those of the mirror partners.

By measuring, as a function of bombarding energy, the ratio of the number of slow neutrons to the number of fast neutrons emitted in (p,n) and (d,n) reactions, it is possible to detect neutron thresholds corresponding to the ground states or to excited states of the residual nuclei. This technique[2] has been supplemented with a means of precisely determining the bombarding energy. In this manner, it is possible to accurately measure the excitation energy of the residual nucleus and thus provide information which may be used in the comparison of the level structures of pairs of mirror nuclei.

The method of measuring the ratio of the number of slow neutrons to fast neutrons with two paraffin-moderated BF_3 counters, one sensitive preferentially to slow neutrons ("slow counter") and the other almost energy-insensitive ("modified long counter"), is called the "counter ratio" technique, and it is applied here in the measurement of neutron thresholds in the reactions $O^{16}(d,n)F^{17}$ and $N^{14}(d,n)O^{15}$.

II. PRECISION MEASUREMENT TECHNIQUE

In order to establish the level structures of nuclei with considerable accuracy by measuring neutron threshold energies with the "counter ratio" technique, it is necessary to know precisely the energy of the bombarding particles. Since magnetic analysis of the charged-particle beam is used with the Rice Institute 6-Mev Van de Graaff accelerator, measurements of the radius of curvature of the particle orbit and the magnetic field strength suffice to determine the particle energy. A Pound magnetometer[3] is used to measure the field strength. This instrument utilizes a proton resonance absorption signal for field strengths up to about 7000 gauss and a lithium signal for higher strengths. The oscillator unit supplies a signal that is beat against the signal from a frequency meter,[4] and the beat frequency is displayed on an oscilloscope along with the resonance absorption signal in the conventional manner. The probe, which is fitted between the pole pieces of the analyzing magnet close to the accelerator vacuum tube, is connected by short leads to the oscillator. The frequency tuning and the operation of the frequency meter and the oscilloscope are carried out at the accelerator's remote control station.

The radius of curvature was determined by measuring the field strength at the threshold for the reaction $Li^7(p,n)Be^7$. The threshold energy for this reaction is

† Supported by the U. S. Atomic Energy Commission.

* National Science Foundation Predoctoral Fellow. Now Postdoctoral Fellow, Kellogg Radiation Laboratory, California Institute of Technology, Pasadena, California.

‡ Humble Oil and Refining Company Fellow in Physics. Now at Phillips Petroleum Company, Atomic Energy Division, Idaho Falls, Idaho.

[1] J. B. Ehrman, Phys. Rev. **81**, 412 (1951); R. G. Thomas, Phys. Rev. **88**, 1109 (1952).

[2] T. W. Bonner and C. F. Cook, Phys. Rev. **96**, 122 (1954).

[3] Manufactured by the Laboratory for Electronics, Inc., Boston, Massachusetts; Model 101.

[4] Manufactured for the U. S. Army Signal Corps by the Zenith Radio Corporation, Chicago, Illinois; Model BC-221-K.

1.8811±0.0005 Mev.[5] Over a period of several days, no change in the calibration could be detected which corresponded to an energy shift of more than 0.5 kev at the $Li^7(p,n)Be^7$ threshold. A typical calibration threshold is shown in Fig. 1. The deviation from linearity on the low-energy side of the threshold is due to the energy spread of the beam.

Since the average field strength experienced by a particle is not exactly that measured by the magnetometer, a systematic error could be introduced by using the calibration deduced from the $Li^7(p,n)Be^7$ threshold measurement over a large range of field strengths. In order to determine the magnitude of this systematic error, a number of well-known (p,n) thresholds[5-7] were measured. The difference between the known and the observed threshold energy [based on the $Li^7(p,n)Be^7$ calibration] was found to be an increasing function of field strength. Six (p,n) threshold measurements were made, which are listed in Table I, and the energy difference was plotted as a function of $H\rho$. For a given field strength, the energy correction for protons is twice that necessary for deuterons. The correction curve for protons determined in this manner is shown in Fig. 2. The correction at the highest field strengths used amounted to about 17 kev for protons, 9 kev for deuterons.

TABLE I. (p,n) Threshold calibration points.

	Target nucleus	Threshold energy (Mev)	Reference	Approximate $H\rho$ (Kilogauss-cm)	Mass No. of beam	Correction (kev)
A	Li^7	1.8811 ±0.0005	5	198	1	standard
B	Be^9	2.059 ±0.002	6	208	1	2
C	B^{11}	3.015 ±0.003	6	250	1	6.5
D	C^{13}	3.236 ±0.003	6	260	1	6
E	H^3	1.0203 ±0.0015	7	295	2	12
F	Li^7	1.8811 ±0.0005	5	398	2	16

Small errors in the application of this correction, together with the energy spread of the beam and the uncertainty in extrapolating the leading edge of a threshold to determine the threshold energy, limits the accuracy of the absolute measurement of energies to about ±4 kev. Energy differences of less than a few hundred kev may be measured somewhat more accurately.

Each of the measurements of the threshold energies reported herein was carried out on at least two different occasions, with separate calibrations of the radius of curvature. In no case was an energy spread of more than 3 kev noted among the runs, and in most cases nonsystematic shifts of about 1 kev were observed.

III. $O^{18}(d,n)F^{17}$

The energy of the first excited state of F^{17} has been measured with an accuracy of about 15 kev by two different methods. Ajzenberg[8] obtained an energy of 0.536±0.010 Mev for this level from the observation in a photographic plate of the ranges of the recoil protons from the reaction $O^{18}(d,n)F^{17}$ at a bombarding energy of 8 Mev. Warren *et al.*,[9] observed the γ radiation from this state in the reaction $O^{18}(p,\gamma)F^{17}$, and obtained a value of 0.487±0.015 Mev. In view of the rather large discrepancy between these two measurements, the $O^{18}(d,n)F^{17}$ reaction was investigated with the "counter ratio" technique.

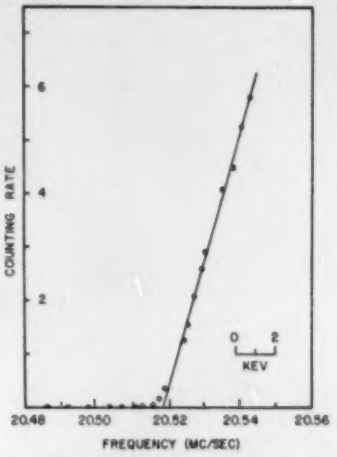

FIG. 1. Typical $Li^7(p,n)Be^7$ threshold calibration.

An oxygen target of about 25-kev thickness at a deuteron energy of 2 Mev was prepared by heating a clean tungsten blank at a temperature of 600°–800°C in an induction heater in the presence of tank oxygen at a pressure of about 25 mm of Hg. The counter ratio and the neutron yield in the forward direction were

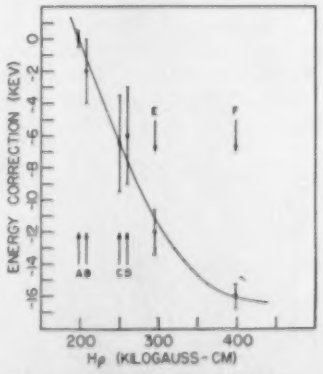

FIG. 2. Experimentally determined curve of the energy correction for protons.

[5] Jones, Douglas, McEllistrem, and Richards, Phys. Rev. **94**, 947 (1954).
[6] Richards, Smith, and Browne, Phys. Rev. **80**, 524 (1950).
[7] T. W. Bonner and J. W. Butler, Phys. Rev. **83**, 1091 (1951).
[8] F. Ajzenberg, Phys. Rev. **83**, 693 (1951).
[9] Warren, Laurie, James, and Erdman, Can. J. Phys. **32**, 563 (1954).

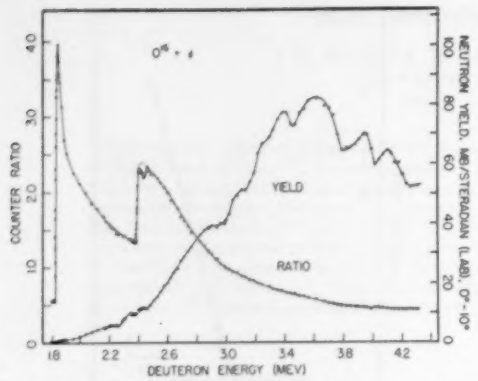

FIG. 3. $O^{16}(d,n)F^{17}$. Counter ratio and yield of neutrons in the forward direction as a function of bombarding energy.

measured in the range of deuteron energies from 1.8 to 4.3 Mev. The results are presented in Fig. 3, which shows the two thresholds that were observed and a number of resonances in the neutron yield. At a bombarding energy of 1.830 ± 0.004 Mev, threshold neutrons corresponding to the ground state of F^{17} were observed, and a sharp rise in the counter ratio results. The curve rises until the target thickness is reached and then decreases in the expected manner. The second sharp increase in the ratio, at a bombarding energy of 2.393 ± 0.004 Mev, is due to the emission of threshold neutrons leaving F^{17} in the first excited state.

For cases in which the number of neutrons emitted at an excited state threshold is large, it is possible to use either the counter ratio curve or the plot of the counting rate in the "slow counter" to determine the threshold energy. Figure 4 shows the extrapolation of the leading edge of the 2.393-Mev threshold observed with the "slow counter" to determine the threshold energy. These two thresholds establish the energy of the first excited state of F^{17} to be 0.499 ± 0.003 Mev.

The calculated Q-value for the ground state threshold is -1.626 ± 0.004 Mev, which is to be compared with a value of -1.622 ± 0.004 Mev, obtained by Bonner and Butler,[7] when their value is corrected for the most recent determination of the $Li^7(p,n)Be^7$ threshold.[8] The threshold energies, Q-values, and the excitation energies in F^{17} are summarized in Table II.

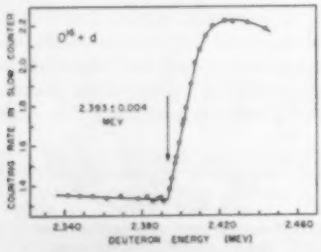

FIG. 4. $O^{16}(d,n)F^{17}$. Counting rate in the "slow counter" as a function of bombarding energy, showing the extrapolation of the leading edge of the 2.393-Mev threshold to obtain the threshold energy.

The slow decrease of the counter ratio above the second threshold is probably due to the emission of slow neutrons with $l=1$. The yield of such neutrons continues to rise for a greater energy interval than that for s-wave neutrons. Since the first excited state of F^{17} is $\frac{1}{2}^+$, s-wave neutron emission to this state would be possible only if the states of the compound nucleus were either 0^+ or 1^+. The resonance structure of the yield curve suggests that compound nucleus formation plays an important role at these low bombarding energies. Therefore, if 0^+ or 1^+ states are present in this energy region of the compound nucleus, they must be weak. At the peak of the ratio curve, at 2.42 Mev, a dip in the ratio occurs. That such a shape of the ratio curve should not be interpreted as an additional threshold may be seen by noting that only a single level occurs in the mirror nucleus, O^{17}, in this energy region. This dip is probably not the result of a decrease in the number of slow neutrons emitted, but of an increase of the number of fast neutrons at the corresponding resonance in the yield of neutrons in the forward direction. This dip in the ratio is taken to imply that neutron emission to the ground state is favored over emission to the excited state at the 2.42-Mev resonance. This would occur if s-wave emission were possible to the ground state at resonance, while it were not favored to the excited state. Since the ground state of F^{17} has spin $5/2^+$, this effect would result from the compound nucleus being in either a 2^+ or a 3^+ state, with an additional assumption that deuterons with $l\geq4$ are ineffective. Therefore, it is probable that the 9.7-Mev state of F^{18}, which is formed at the 2.42-Mev resonance, is a 2^+ or 3^+ state.

TABLE II. Neutron thresholds in the reaction $O^{16}(d,n)F^{17}$.

Threshold energy (Mev)			Excitation in F^{17} (Mev)	
Present work	Other measurement	Q-value (Mev)	Present work	Other measurement
1.830 ± 0.004	1.835 ± 0.005[a]	-1.626 ± 0.004	0	0
2.393 ± 0.004		-2.125 ± 0.004	0.499 ± 0.003	0.536 ± 0.010[b] 0.487 ± 0.015[c]

[a] See reference 7. The published value has been corrected; see text.
[b] See reference 8.
[c] See reference 9.

Figure 5 shows the level schemes of the mirror nuclei, O^{17} and F^{17}, up to excitations of 2 Mev. The O^{17} energies are from Sperduto *et al.*,[10] and the F^{17} energies are the values of Table II. The extreme downward shift in energy of the first excited state of F^{17}, compared with that of O^{17}, is probably associated with the change in boundary conditions on the wave

[10] Sperduto, Buechner, Bockelman, and Browne, Phys. Rev. **96**, 1316 (1954).

functions at the nuclear surface as a result of the anomalously low particle dissociation energy in F^{17}.[11]

The neutron yield in the forward direction from three separate runs, is shown in Fig. 3. The background, obtained by bombarding a clean tungsten blank, has been subtracted. The percentage background counting rate in the modified long counter decreased from 37% at 2.4 Mev to 6% at 4.0 Mev. Ten broad resonances were found between threshold and 4.3 Mev, some of which agree with those observed in the $O^{16}(d,p)O^{17}$ reaction.[12,13] The flattening of the yield curve immediately above the threshold for the F^{17} ground state was also observed by Bonner and Butler.[7] This effect is probably due to the resonance at 1.7 Mev, below the threshold for neutron emission, which is known from the $O^{16}(d,p)O^{17}$ reaction.[12] A summary of the resonances found, together with the corresponding excitation energies in F^{18} is given in Table III.

TABLE III. Resonances in $O^{16}+d$.

$O^{16}(d,n)$; $\theta=0°$–$10°$ E_d (Mev)	$O^{16}(d,p)$ E_d (Mev)	$^*F^{18}$ (Mev)
	1.7[a]	9.0
2.22	2.2[a]	9.5
2.34		9.6
2.42		9.7
	2.65[b]	9.9
2.89		10.1
	3.0[a]	10.2
	3.01[b]	
3.07		10.3
3.22	3.25[b]	10.4
3.38	3.43[b]	10.6
3.62		10.8
3.94		11.0
4.10		11.2

[a] See reference 12. Resonances in the integrated cross section.
[b] See reference 13. Resonances in the cross section at 50°.

IV. $N^{14}(d,n)O^{15}$

The reaction $N^{14}(d,n)O^{15}$ has been studied with the "counter ratio" technique described above. The target

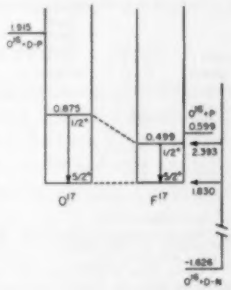

FIG. 5. Energy level diagrams for the first 2 Mev of excitation of the mirror nuclei, O^{17} and F^{17}.

was prepared by absorbing nitrogen gas in tantalum. This was accomplished by heating a 40-mil tantalum disk in an induction heater to about 1300°C for several minutes in the presence of 1 atmosphere of nitrogen. This target was approximately 60 kev thick at a deuteron energy of 1.9 Mev.

The counter ratio and the forward yield of neutrons is given in Fig. 6 for deuteron energies from 1.1 to 4.5 Mev. The counter ratio curve indicates thresholds at bombarding energies of 1.24±0.02 and 1.967±0.004 Mev. A closer examination of the region near 2.0 Mev was made with a 20-kev target and the results are shown in Fig. 7. An additional threshold was observed at 2.044±0.004 Mev. The threshold energies, Q-values, and excitation energies in O^{15} are listed in Table IV. The large error in determining the energy of the 1.24-Mev threshold was due to the large background counting rate at this low bombarding energy.

The threshold at 1.24±0.02 Mev implies an energy level in O^{15} at 6.20±0.03 Mev. This is in agreement with the determination of Evans, Green, and Middleton[14] using photographic plates (6.19±0.16 Mev), and with that by Bent *et al.*,[15] obtained from a pair-spectrometer investigation of the γ radiation from the deuteron bombardment of N^{14} (6.12±0.06 Mev). With the photographic plate method it was not possible to resolve the neutron groups corresponding to the 6.841- and 6.909-Mev states. The pair-spectrometer measurements indicated a single line at 6.81±0.04 Mev.

Table V lists the relative intensities of protons, neutrons, and γ rays from the deuteron bombardment of N^{14}. The bombarding energy at which the intensity was measured is given in each case. The relative intensities will be influenced by differences in angular distribution since the intensities are taken from measurements made at a single angle. Also, comparison of relative intensities from reactions produced at

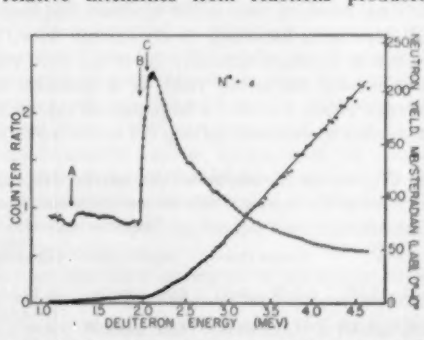

FIG. 6. $N^{14}(d,n)O^{15}$. Counter ratio and yield of neutrons in the forward direction as a function of bombarding energy.

[11] T. Lauritsen, Ann. Rev. Nuc. Sci. **1**, 67 (1952).
[12] N. P. Heydenburg and D. R. Inglis, Phys. Rev. **73**, 230 (1948).
[13] Van Patter, Simmons, Stratton, and Zipoy, Phys. Rev. **96**, 825(A) (1954).
[14] Evans, Green, and Middelton, Proc. Phys. Soc. (London) **A66**, 108 (1953).
[15] Bent, Bonner, McCrary, Ranken, and Sippel, Phys. Rev. **99**, 710 (1955).

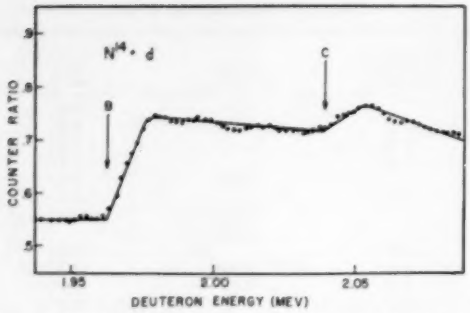

FIG. 7. $N^{14}(d,n)O^{15}$. Counter ratio as a function of bombarding energy near 2.0 Mev, showing the 1.967- and 2.044-Mev thresholds.

different bombarding energies is probably not valid in a quantitative sense, but the comparison should be at least qualitatively correct.

The N^{15} level at 7.314 Mev and the O^{15} level at 6.841 Mev appear to be the most intensely produced levels in these reactions. Because of this fact, it may be reasonable to associate these two states as mirror levels. If this is the case, the N^{15} level at 7.575 Mev and the O^{15} level at 6.909 Mev are also mirror states, and the O^{15} level corresponding to the 7.165-Mev state in N^{15} has not yet been detected. Such a level to which neutron emission near threshold is less than about 0.3 as intense as at the 2.044-Mev threshold (6.909-Mev state in O^{15}), would not have been detected in this experiment. The indication of a weak threshold at about 1.83 Mev (see Fig. 6) attributed to a small oxygen, contamination, could possibly be due to this missing state.

The yield of neutrons in the forward direction from the $N^{14}(d,n)O^{15}$ reaction is shown in Fig. 6. The background, obtained by bombarding a clean tantalum blank, has been subtracted. The background was 33% of the total counting rate in the modified long counter at 1.1 Mev and decreased to 3% at 4.5 Mev. The cross section increases smoothly up to 2.1 Mev where there is a sharp rise in the yield. It is probable that at energies above 2.1 Mev a large part of the neutron yield consists of neutrons leaving O^{15} in the 6.841-Mev state. This is consistent with the intensity measurements of Evans, Green, and Middleton,[14] made at a bombarding energy of 7.7 Mev.

TABLE IV. Neutron thresholds in the reaction $N^{14}(d,n)O^{15}$.

	Threshold energy (Mev)	Q-value (Mev)	Excitation of O^{15} (Mev) Present work	Other measurements
A	1.24 ±0.02	−1.08 ±0.02	6.20 ±0.03[a]	{6.19±0.16[a] 6.12±0.06[b]}
B	1.967±0.004	−1.719±0.004	6.841±0.009[a]	{6.81±0.04[c] 6.84±0.16[b]}
C	2.044±0.004	−1.787±0.004	6.909±0.009[a]	

[a] The error assignment includes the uncertainty in the ground state Q-value, calculated from the mass defect uncertainties listed by J. E. Drummond, Phys. Rev. 97, 1004 (1955).
[b] See reference 14.
[c] See reference 15.

V. MEASUREMENT OF ABSOLUTE CROSS SECTIONS

Since very little information is available concerning the absolute cross sections for the emission of neutrons in nuclear reactions, measurements were made to obtain this information for the reactions $O^{16}(d,n)$ and $N^{14}(d,n)$. It was necessary to determine the absolute cross section for each reaction at one or more bombarding energies, thereby calibrating the relative yield curve. This entails a knowledge of two factors: (1) the absolute number of neutrons emitted from the target per unit solid angle and microcoulomb of beam current, and (2) the number of target nuclei per cm^2 on the target.

The first factor was determined by comparing the counting rate from the target with that from a calibrated[16] Ra-Be source with a "long counter" of the type described by Hanson and McKibben.[17] The current integrator was calibrated by measuring the time necessary to record an integrating pulse when a known current was passed through the circuit. The amount of current was determined by measuring the voltage drop across a precision, wire-wound resistor with a Leeds and Northrup potentiometer.

TABLE V. Relative reaction intensities in $N^{14}+d$.

$*N^{15}$ (Mev)	Protons[a] (E_d=7.0 Mev)	Gamma rays[b] (E_d=4 Mev, thick target)	$*O^{15}$ (Mev)	Neutrons (thresh-old)	Neutrons[c] (E_d=7.7 Mev)	Gamma rays[b] (E_d=4 Mev, thick target)
5.280	0.8	~1.5[d]				
5.305	0.6	~1.5[d]	5.29	...	0.4	~1.5[d]
6.330	1	1	6.20	1	1	0.7
7.165	1.3	...	...	...		...
7.314	2.7	3.2	6.841	4.6	2.4	2.2
7.575	1.7	...	6.909	0.9		...

[a] See reference 10.
[b] See reference 15. Intensities of γ radiation from both $*N^{15}$ and $*O^{15}$ are relative to the 6.33-Mev γ ray from $*N^{15}$.
[c] See reference 14.
[d] These three γ rays could not be resolved; the total intensity was 4.4, given an intensity of ~1.5 for each if they are equally intense.

The determination of the number of target nuclei per cm^2 was simplified by using a gas target for the absolute cross section measurements. The target chamber was 0.5 inch in diameter and 1.5 inches in length and was constructed of iron; a 2.58 mg/cm^2 nickel foil covered the entrance hole to the chamber. Gas pressures of about ½ atmosphere were used. Since the deuteron bombardment of nickel produces an appreciable number of neutrons, backgrounds were taken with the gas removed from the target chamber.

The absolute cross sections were determined at a

[16] Calibrated to an accuracy of 4% by the U. S. Bureau of Standards, September, 1954.
[17] A. O. Hanson and J. L. McKibben, Phys. Rev. 72, 673 (1947).

deuteron energy of 3.33 Mev. The yield curves shown in Figs. 3 and 6 were normalized to the absolute values at this energy. The curves have not been corrected for the variation of the sensitivity of the modified long counter with neutron energy. The efficiency of the modified long counter in its position behind the "slow counter," is a maximum for neutrons with an energy of about 1.5 to 2 Mev and it has a lower efficiency for both lower and higher energy neutrons. The decrease in efficiency is about 40% for 5-Mev neutrons and is slightly greater for neutrons of energy less than about 0.3 Mev. Since the correction is complicated by the existence of more than a single neutron energy group, such a correction has not been attempted.

The estimated accuracy to which the absolute cross sections have been determined is $\pm 50\%$.

PHYSICAL REVIEW VOLUME 100, NUMBER 1 OCTOBER 1, 1955

Isotopic Spin Impurity in Light Nuclei. I. Core Impurity

WILLIAM M. MACDONALD*
Princeton University, Princeton, New Jersey
(Received April 25, 1955)

The introduction of isotopic spin impurity by the Coulomb mixing of different nuclear eigenstates of T^2 can occur both through the perturbation of the wave function for nucleons in a J, $T=0$ core by the Coulomb interaction of nucleons in the core, and through the perturbation of the wave function for nucleons outside the core by their Coulomb interaction with nucleons in the core and with each other. In this paper the core impurity, the sum of the squared amplitudes of higher isotopic spin eigenstates ($T\neq 0$), is calculated for the ground state of $N=Z$ even-even nuclei on the Fermi gas model. The core impurity is found to exceed by a large factor the isotopic spin impurity in the wave function for nucleons outside the core.

I. INTRODUCTION

THE total isotopic spin quantum number T^2 exists under the assumption of a "charge-independent" interaction between nucleons of the form $\sum'(a+b\tau_i\cdot\tau_j)$, where a and b are functions of space and spin and τ_i is the isotopic spin vector for the ith nucleon. The primed summation indicates that one sums over $i\neq j$. The present active interest in the isotopic spin quantum number for nuclei began primarily among the experimentalists and among those interested in cataloging and understanding the large amount of experimental information on light nuclei which is being accumulated at an increasing rate. For this purpose the isotopic spin quantum number provides selection rules on each of three types of nuclear reactions: (1) reactions involving absorption and emission of heavy particles, (2) β-decay, and (3) isomeric transitions. Selection rules for processes of type (1) are usually simple and forbid such reactions as (d,α) going from the ground state of an $N=Z$ nucleus to the $T=1$ states of the final $N=Z$ nucleus. Selection rules for the second process were given by Wigner[1] and are different for the Fermi and Gamow-Teller matrix elements.

$$\begin{aligned} &\text{Fermi:} && \Delta T=0, \\ &\text{Gamow-Teller:} && \Delta T=0,\pm 1, \quad 0\nleftrightarrow 0. \end{aligned}$$

Finally selection rules for electric dipole transitions were recently derived by Trainor[2] in supermultiplet theory and more generally by Christy,[3] Radicati,[4] and Gell-Mann and Telegdi.[5] We have discussed this selection rule in some detail and have shown it to be a sensitive test of the validity of the isotopic spin quantum number.[6]

The validity of the selection rules is affected only by a nuclear interaction which does not commute with T^2; i.e., by a "charge-dependent" nuclear potential, or by the Coulomb interaction. Consequently, before any conclusions can be drawn about the nuclear potential, the quantitative effect of the Coulomb force on the isotopic spin quantum number must be determined. The possibility of accounting for any observed violations of the above selection rules by ascribing them to the Coulomb potential would strongly suggest a nuclear interaction of the form $\sum'(a+b\tau_i\cdot\tau_j)$. Conversely, the observation of large departures from the isotopic spin selection rules which could not be explained by the Coulomb force would certainly imply the existence of charge-dependent nuclear interactions. Of course, in case Coulomb forces should be shown to give rise to considerable mixing of the states of different isotopic spin, the usefulness of the isotopic spin quantum number would be destroyed.

We are therefore interested in the extent to which one can assign a total isotopic spin quantum number T to the states of light nuclei for which $A\leq 20$. Specifically we want to know how much admixture (sum of the

* Present address: Department of Physics, University of Wisconsin, Madison, Wisconsin.
[1] E. P. Wigner, Phys. Rev. **56**, 519 (1939).
[2] L. E. H. Trainor, Phys. Rev. **85**, 962 (1952).
[3] R. F. Christy, Pittsburgh Conference on Medium Energy Nuclear Physics, 1952 (unpublished).
[4] L. A. Radicati, Phys. Rev. **87**, 521(L) (1952).
[5] M. Gell-Mann and V. L. Telegdi, Phys. Rev. **91**, 169 (1953).
[6] W. M. MacDonald, Phys. Rev. **98**, 60 (1955).

squared amplitudes) of states of different isotopic spin is introduced into a total isotopic spin eigenstate by the Coulomb interaction. We shall call the amount of admixture—"the isotopic spin impurity of the state."

In the shell model, the simplest nuclear state is the ground state of a nucleus consisting of closed shells in neutrons and protons. Although only a few of the nuclear states are of this kind, the ground state and certain low-lying states of a nucleus with one or more particles in open shells can be regarded as the states of a system consisting of a "core" of particles having $J, T=0$ and one or more particles in open shells. Since the isotopic spin states of the same spin and parity are separated by a rather large energy ~ 15 Mev, in lowest approximation the effect of the Coulomb interaction between core nucleons in promoting the isotopic spin impurity of the ground state of the core can be treated separately from the effect upon the isotopic spin state of the Coulomb interaction of the outside nucleons with each other and with the core.[7] (The effect of the outside nucleons on the isotopic spin eigenstate of the core can be taken into account approximately later, if necessary.)

In the present paper we shall determine the core impurity for the ground state of an $N=Z$ even-even nucleus on the Fermi gas model. The results we obtain consequently will be less dependent on the details of nuclear structure than later calculations on the shell model. The second source of isotopic spin impurity, in the wave function for nucleons in open shells, will be treated in a later paper using the jj-coupling model with harmonic oscillator wave functions. A recalculation on this model of core impurity for C^{12}, which in an $N=Z$ even-even nucleus and also has closed shells in neutrons and protons, will be in agreement with results to be found here.

The conclusion which we shall reach in these calculations on light nuclei ($A \leq 20$) is that the core impurity is much more important than the impurity of the state of the outside nucleons.[8] This result invalidates the basis for some earlier somewhat less rigorous calculations on the mixing of the isotopic spin states by the Coulomb potential.[7]

II. DECOMPOSITION OF THE COULOMB OPERATOR

The so-called Coulomb perturbation is usually understood to contain not only the Coulomb potential between protons but also the neutron-proton mass difference. In the isotopic spin formalism the perturbation is

$$H_C=\tfrac{1}{4}e^2\sum{}'(1-\tau_{\xi i})(1-\tau_{\xi j})r_{ij}^{-1}+(m_n-m_p)c^2T_\xi + \tfrac{1}{2}A(m_n+m_p)c^2, \quad (1)$$

where τ_ξ has the eigenvalue $(+1)$ for a neutron and (-1) for proton. The ξ-component of isotopic spin then has the eigenvalue $T_\xi=\frac{1}{2}(N-Z)$ for a nucleus with N neutrons and Z protons. The last two terms of Eq. (1) commute with T^2 and, in fact, can produce no mixing of states of either the same or different isotopic spin if these states are orthogonal. These two terms merely will produce relative displacements of the levels of different isobars. To determine the effect of the perturbation produced by the first term, which is the Coulomb potential, one must perform a decomposition into irreducible tensors in isotopic spin space. Each of these tensors has different transformation properties under rotations in isotopic spin space, and there will exist different selection rules on the matrix elements of these tensors. The decomposition can easily be made and the selection rules stated which are relevant for our discussion.

$$H_C=S+T^{(10)}+T^{(20)},$$

Scalar: $$S=\tfrac{1}{4}e^2\sum{}'(1+\tfrac{1}{3}\boldsymbol{\tau}_i\cdot\boldsymbol{\tau}_j)r_{ij}^{-1}, \quad \Delta T=0$$

Vector: $$T^{(10)}=-\tfrac{1}{4}e^2\sum{}'(\tau_{\xi i}+\tau_{\xi j})r_{ij}^{-1}, \quad \Delta T=0,\pm1,0\nrightarrow 0 \quad (2)$$

Tensor: $$T^{(20)}=\tfrac{1}{4}e^2\sum{}'(\tau_{\xi i}\tau_{\xi j}-\tfrac{1}{3}\boldsymbol{\tau}_i\cdot\boldsymbol{\tau}_j)r_{ij}^{-1}, \quad \Delta T=0,\pm1,\pm2,0\nrightarrow 0,1.$$

The quantity $T^{(ij)}$ is the jth component of a tensor of rank i.[9] The scalar part S commutes with T^2 and can be included in the nuclear Hamiltonian without affecting the validity of the isotopic spin. The tensor $T^{(20)}$ can only mix the $T=0$ with the $T=2$ state, and the large energy separation of these two multiplets will enable us to neglect $T^{(20)}$ in computing the impurity of $T=0$ states. One has to consider only $T=0$ states for the normal states of $N=Z$ nuclei for $A\leq 20$, and only the vector component of H_C therefore need be considered.

According to perturbation theory the perturbation H_p introduces into an eigenstate Ψ_0 the impurity p, defined as the sum of the squared amplitudes of different eigenstates

$$p=\sum\frac{|(\Psi_\nu,H_p\Psi_0)|^2}{(E_0-E_\nu)^2}. \quad (3)$$

By closure, an upper limit on p is

$$p\leq p_M=\frac{(\Psi_0,H_p^2\Psi_0)-|(\Psi_0,H_p\Psi_0)|^2}{(E_0-E_1)^2}. \quad (4)$$

Since the perturbation which we shall use,

$$\mathcal{C}\equiv T^{(10)}=-\tfrac{1}{4}e^2\sum_{i,j}{}'(\tau_{\xi i}+\tau_{\xi j})r_{ij}^{-1}, \quad (5)$$

has zero expectation in the $T=T_\xi=0$ ground state Ψ_0, the maximum impurity is

$$p_M=(\Psi_0,\mathcal{C}^2\Psi_0)/(E_0-E_1)^2. \quad (6)$$

[7] L. A. Radicati, Proc. Phys. Soc. (London) **A66**, 139 (1953); **A67**, 39 (1953).

[8] W. M. MacDonald, Phys. Rev. **98**, 234(A) (1955).

[9] E. P. Wigner, *Gruppentheorie* (Friedrich Viewag and Sohn, Braunschweig, 1931).

The energy difference E_0-E_1 which appears in Eq. (6) should be the energy separation of the ground state $T=0$ from the first excited state of the same spin J and parity but having $T=1$. The importance of the distinction between this energy and the separation of the $T=0$ and $T=1$ multiplets is obvious for the odd-odd nuclei where the first state of the $T=1$ multiplet is only a few Mev above the $T=0$ ground state. In most cases, however, the first $T=1$ state of the same spin and parity as the ground state is not known. We are now interested only in the nuclei with $N=Z$ and $A=4n$, however, and for these the first $T=1$ level lies quite high. In this case we can use the energy separation of the $T=0$ and $T=1$ multiplets since the first $T=1$ state with same spin and parity as the ground state cannot lie much higher. The energies $E(T=0)-E(T=1)$ are estimated from the energy separation of the ground state of the $T_z=0$ member of an isobaric triad from the ground states of the $T_z=1$ components. (See Table I.)

TABLE I. Energy separation in Mev of isotopic multiplets in $T_z=0$ even-even nuclei.

A	8 (Be^8)	12 (C^{12})	16 (O^{16})	20 (Ne^{20})
$E(T=1)-E(T=0)$	16.7	15.1	12.9	10.1

III. SIMPLE ESTIMATE OF ISOTOPIC SPIN IMPURITY

The matrix element of $\mathcal{C}^2$ can be estimated by a method which is similar to that used for deriving sum rules. The squared sum $\mathcal{C}^2$ can be written

$$\mathcal{C}^2=\frac{e^4}{64}\{2\sum_{i,j}{}'(\tau_{zi}+\tau_{zj})^2r_{ij}^{-2}+2\sum_{i,j,l}{}'(\tau_{zi}+\tau_{zj})(\tau_{zi}+\tau_{zl})\times r_{ij}^{-1}r_{il}^{-1}+\sum_{i,j,k,l}(\tau_{zi}+\tau_{zj})(\tau_{zk}+\tau_{zl})r_{ij}^{-1}r_{kl}^{-1}\},\quad(7)$$

where the primed summations indicate that different indices never assume the same value. The approximation is now made that the expectation values of the reciprocal separations r_{ij}^{-2}, $r_{ij}^{-1}r_{il}^{-1}$, and $r_{ij}^{-1}r_{kl}^{-1}$ are the same for every term of each of the three sums appearing in Eq. (7) and are respectively $\langle r_{12}^{-2}\rangle$, $\langle r_{12}^{-1}r_{13}^{-1}\rangle$, and $\langle r_{12}^{-1}r_{34}^{-1}\rangle$. Each of the three sums over the isotopic spin coordinates can be carried out explicitly to yield

$$\langle\mathcal{C}^2\rangle\approx\tfrac{1}{16}e^4A(A-1)\{\langle r_{12}^{-2}\rangle+(A-4)\langle r_{12}^{-1}r_{13}^{-1}\rangle-(A-3)\langle r_{12}^{-1}r_{34}^{-1}\rangle\}.\quad(8)$$

This expression vanishes for all r_{ij} constant and equal, as it must since then $\mathcal{C}=-\frac{1}{2}e^2r_{ij}^{-1}T_z=0$.

The averages appearing in Eq. (8) will be calculated by taking the nucleus to be spherical and of uniform density.

$$\langle r_{12}^{-2}\rangle=V^{-2}\int d\mathbf{r}_1d\mathbf{r}_2r_{12}^{-2};$$

$$\langle r_{12}^{-1}r_{13}^{-1}\rangle=V^{-3}\int d\mathbf{r}_1d\mathbf{r}_2d\mathbf{r}_3r_{12}^{-1}r_{13}^{-1};\quad(9)$$

$$\langle r_{12}^{-1}r_{34}^{-1}\rangle=V^{-4}\int d\mathbf{r}_1d\mathbf{r}_2d\mathbf{r}_3d\mathbf{r}_4r_{12}^{-1}r_{34}^{-1},$$

where $V=(4/3)\pi R^3$ is the nuclear volume and the integrations are performed by allowing the points $\mathbf{r}_1$, $\mathbf{r}_2$, $\mathbf{r}_3$, and $\mathbf{r}_4$ to move through the volume of a sphere of radius R. These integrations yield

$$\langle r_{12}^{-2}\rangle=(9/4)R^{-2}=2.25R^{-2};$$
$$\langle r_{12}^{-1}r_{13}^{-1}\rangle=(51/35)R^{-2}=1.457R^{-2};$$
$$\langle r_{12}^{-1}r_{34}^{-1}\rangle=(36/25)R^{-2}=1.44R^{-2}.\quad(10)$$

Inserting these average values in (8), we have finally

$$\langle\mathcal{C}^2\rangle=\frac{e^4}{16R^2}A(A-1)(0.76+0.017A).\quad(11)$$

This result is very interesting in its dependence on atomic number. From Eq. (7) one might have expected $\langle\mathcal{C}^2\rangle$ to be proportional to A^4R^{-2} but this result is proportional to $A(A-1)R^{-2}$ for A less than ~100. If one writes the impurity limit p_M in the form,

$$p_M=\frac{A(A-1)}{2}\frac{(e^2/R)^2}{8(E_0-E_1)^2}(0.76+0.017A),\quad(12)$$

an obvious interpretation is that the core impurity is just the effect of the perturbation of a single-nucleon wave function by another nucleon multiplied by the number of interacting pairs. Stated in this way, no account has been taken of the differences in interaction between nucleons in different orbits. For example, the Coulomb interaction between nucleons in an s orbit is obviously greater than that between nucleons in a p orbit and the perturbation of the single-particle orbits is consequently greater in the first case than in the second. Nevertheless, the qualitative idea suggested by Eq. (12) is correct as will be seen in the shell model calculations.

IV. THE FERMI GAS MODEL

This simple evaluation is completely independent of the symmetric structure of the nuclear wave function and does not even approximately take account of the fact that the ground states of $A=4n$ nuclei where $A\leq20$ are of a four-structure with four nucleons in each space state. This feature of Eq. (8) is a consequence of the separation of the space and isotopic spin dependence of the operator $\mathcal{C}^2$ in Eq. (7) by the introduction of $\langle r_{12}^{-2}\rangle$, $\langle r_{12}^{-1}r_{13}^{-1}\rangle$, and $\langle r_{12}^{-1}r_{34}^{-1}\rangle$. Although the use of such an approximation means that the coefficients of these averages in Eq. (8) are not really correct, one might expect that the value of $\langle\mathcal{C}^2\rangle$ given by (11) has not been affected much by this error. The reason is that Eq. (11) is mostly a consequence of the necessary condition that $\mathcal{C}=0$ for all the r_{ij} of Eq. (5) equal to the same constant ($r_{ij}=a$) and of the near equality of $\langle r_{12}^{-2}\rangle$, $\langle r_{12}^{-1}r_{13}^{-1}\rangle$, and $\langle r_{12}^{-1}r_{34}^{-1}\rangle$.

In order to obtain a more correct evaluation of $\langle \mathcal{C}^2 \rangle$ which includes the four-structure of the ground state wave function, we shall work with the single-particle model and use a formalism similar to that of Rosenfeld.[10] The expression for the density matrix $(i|g|f)$ found there, however, omit terms which are important for this problem. The extension of these methods to the evaluation of three- and four-particle operators has not been necessary previously.

We begin by describing the nuclear ground state by the wave function $\Psi(Q_1,\cdots,Q_A)$ which is antisymmetric in the coordinates Q_i, which represent three space coordinates, a spin coordinate, and an isotopic spin coordinate. In the single-particle model, the antisymmetric ground state wave function can be represented by

$$\Psi=\begin{vmatrix}\psi_1(Q_1)\cdots\psi_1(Q_A)\\ \cdots\\ \psi_A(Q_1)\cdots\psi_A(Q_A)\end{vmatrix}, \tag{13}$$

where $\psi_\mu(Q_\nu)$ is a single-particle wave function of the form

$$\psi_\mu(Q_\nu)=\phi_\mu(\mathbf{r}_\nu)u_\mu(\sigma_\nu,\tau_\nu). \tag{14}$$

The function $u_\mu(\sigma_\nu,\tau_\nu)$ is a spin and isotopic spin state while $\varphi_\mu(\mathbf{r}_\nu)$ is a space state. The whole development of the expectation values of two-, three-, and four-nucleon operators is quite general up to a point where the "density matrices" are actually evaluated, but from this point we use for the space states plane waves normalized in the nuclear volume and fill all momentum states up to some wave number k_m. This choice constitutes the use of the Fermi gas model.[11]

V. MATRIX ELEMENTS OF MULTIPLE-NUCLEON OPERATORS

Two-Nucleon Operators

Consider an operator $W_{12}(Q_1,Q_2)$ on the collective coordinates Q_1 and Q_2. The expectation value of W_{12} will be

$$\langle W_{12}(Q_1,Q_2)\rangle=\int_{Q_1}\cdots\int_{Q_A}\Psi^*(Q_1,\cdots,Q_A)\times W_{12}(Q_1,Q_2)\Psi(Q_1,\cdots,Q_A). \tag{15}$$

This equation can be rewritten by separating the space and spin coordinates (intrinsic spin and isotopic spin) in Q_1 and Q_2. Let s denote the "total" spin state of both nucleons and $\mathbf{r}_1$, $\mathbf{r}_2$ denote their space coordinates. Then

$$\langle W(Q_1,Q_2)\rangle=\sum_s\int_{Q_3}\cdots\int_{Q_A}d\mathbf{r}_1d\mathbf{r}_2\Psi^*\times(\mathbf{r}_1,\mathbf{r}_2,s;Q_3,\cdots,Q_A)W_{12}(Q_1,Q_2)\times\Psi(\mathbf{r}_1,\mathbf{r}_2,s;Q_3,\cdots,Q_A). \tag{16}$$

The summation over s is simply the operation of taking a trace over the 16-dimensional spin and isotopic spin space of the two nucleons. We can make a unitary transformation in this space to the representation in which the states are eigenstates of $\tau_{\xi1}$ and $\tau_{\xi2}$, the ξ components of the isotopic spin of the nucleons, and of σ_{z1} and σ_{z2}, the intrinsic spin. The Eq. (17) can be written then

$$\langle W(Q_1,Q_2)\rangle=\sum_{s,s'}\int d\mathbf{r}_1d\mathbf{r}_2(s|g(\mathbf{r}_1,\mathbf{r}_2)|s')(s'|W_{12}|s), \tag{17}$$

where s and s' are now quantum numbers for the total spin state of the two nucleons and $(s|g(\mathbf{r}_1,\mathbf{r}_2)|s')$ is the density matrix defined by

$$(s|g(\mathbf{r}_1,\mathbf{r}_2)|s')=\int_{Q_3}\cdots\int_{Q_A}\Psi^*(\mathbf{r}_1,\mathbf{r}_2,s;Q_3,\cdots,Q_A)\times\Psi(\mathbf{r}_1,\mathbf{r}_2,s';Q_3,\cdots,Q_A). \tag{18}$$

In the state Ψ given by Eq. (13), we shall take every space state to be completely occupied by four nucleons, two neutrons, and two protons, with each pair of like nucleons having opposite spins. We shall thus be treating the normal states of nuclei with $A=4n$, $T=T_\xi=0$. In writing the exchange terms which appear in $(s|g(\mathbf{r}_1,\mathbf{r}_2)|s')$, we shall make use of the total spin exchange operator (intrinsic spin and isotopic spin): $P_{\sigma\tau}{}^{(ij)}=\frac{1}{2}(1+\boldsymbol{\sigma}_i\cdot\boldsymbol{\sigma}_j)(1+\boldsymbol{\tau}_i\cdot\boldsymbol{\tau}_j)$. The density matrix is then

$$(s|g(\mathbf{r}_1,\mathbf{r}_2)|s')=[A(A-1)]^{-1}\times\Big(s\Big|\sum_{\mu,\nu}^{m}\phi_\mu^*(1)\phi_\nu^*(2)[\phi_\mu(1)\phi_\nu(2)-P_{\sigma\tau}{}^{12}\phi_\mu(2)\phi_\nu(1)]+\delta(s,s_{12})\sum_{\mu}^{m}|\phi_\mu(1)|^2|\phi_\mu(2)|^2(1-P_{\sigma\tau}{}^{12})\Big|s'\Big), \tag{19}$$

where s_{12} denotes the total spin state (spin and isotopic spin) of nucleons 1 and 2 for which the two nucleons do not both have the same spin and isotopic spin. The $\delta(s,s_{12})$ restricts the sum over spin states s to those states compatible with the requirement that the same single particle state cannot be occupied by both nucleons 1 and 2.

At this point, we introduce for the ϕ_ν of Eq. (19) plane waves normalized to volume $V=(4/3)\pi R^3$,

$$\phi_\mu=V^{-\frac{1}{2}}\exp(i\mathbf{k}_\mu\cdot\mathbf{r}), \tag{20}$$

with the free particle states being taken as dense in k-space. We can replace sums over k_μ, therefore, by integrals up to a maximum wave number k_m given by $k_m=(9\pi)^{\frac{1}{3}}/2r_0=1.523/r_0$, where $R=r_0A^{\frac{1}{3}}$. The sums which appear in (19) are then easily evaluated:

$$\sum_{\mu,\nu}^{m}|\phi_\mu(1)|^2|\phi_\nu(2)|^2=A(A-1)/16V^2,$$

$$\sum_{\mu,\nu}^{m}\phi_\mu^*(1)\phi_\nu^*(2)\phi_\mu(2)\phi_\nu(1)=[A(A-1)/16V^2]G^2(r_{12}),$$

$$G(r)\equiv\frac{3}{k_mr}j_1(k_mr)=3\left(\frac{\pi}{2}\right)^{\frac{1}{2}}\frac{J_{\frac{3}{2}}(k_mr)}{(k_mr)^{\frac{1}{2}}}. \tag{21}$$

[10] L. Rosenfeld, *Nuclear Forces* (Interscience Publishers, Inc., New York, 1948).

[11] H. Bethe and R. Bacher, Revs. Modern Phys. **8**, 82 (1936). See also reference 10.

The function $G(r_{12})$ is designated as the equivalent nucleon correlation function since it gives the probability of a certain relative separation of two nucleons of the same spin and isotopic spin.

If we insert the sums of Eq. (21) into Eq. (19), we obtain

$$(s|g(\mathbf{r}_1,\mathbf{r}_2)|s')=\left(s\left|\frac{1}{16V^2}[1-P_{\sigma\tau}{}^{12}G^2(r_{12})]\times\left[1+\frac{4}{A-1}\delta(s,s_{12})\right]\right|s'\right). \quad (22)$$

Three-Nucleon Operator

The derivation of the density matrices for three and four particle operators is very straightforward. Denote the permutations P of the symmetric group by

$$P=\begin{pmatrix}\cdots\alpha_i{}^P\cdots\\ \cdots\beta_i{}^P\cdots\end{pmatrix},$$

where the $\alpha_i{}^P$ designate only the numbers which are not permuted into themselves by P. Further, let δ_P be the sign of the transposition so that $\delta_P=\pm1$ according as P is even or odd. Then, if the expectation value of W_{123} is given by

$$\langle W_{123}\rangle=\sum_{s,s'}\int d\mathbf{r}_1d\mathbf{r}_2d\mathbf{r}_3\times(s|g(\mathbf{r}_1,\mathbf{r}_2,\mathbf{r}_3)|s')(s'|W_{123}|s), \quad (23)$$

the density matrix is just

$$(s|g(\mathbf{r}_1,\mathbf{r}_2,\mathbf{r}_3)|s')=\left(s\left|[1+\sum_P\delta_PP_{\sigma\tau}{}^P(\textstyle\prod_iG(r_{\alpha_i{}^P\beta_i{}^P}))]\times\left[1+\frac{4}{A-1}[\delta(s,s_{12})+\delta(s,s_{13})+\delta(s,s_{23})]+\frac{16}{(A-1)(A-2)}[\delta(s,s_{123})+\delta(s,s_{132})]\right]\right|s'\right), \quad (24)$$

where s_{123} is a permissible total spin state for three nucleons occupying the same space state. The permutations $P_{\sigma\tau}{}^P$ on the spin and isotopic spin are all the permutations belonging to the symmetric group on three symbols.

Four-Nucleon Operator

The matrix element for the four-nucleon operator is just

$$\langle W_{1234}\rangle=\sum_{s,s'}\int d\mathbf{r}_1d\mathbf{r}_2d\mathbf{r}_3d\mathbf{r}_4\times(s|g(\mathbf{r}_1,\mathbf{r}_2,\mathbf{r}_3,\mathbf{r}_4)|s')(s'|W_{1234}|s), \quad (25)$$

where the proper density matrix is

$$(s|g(\mathbf{r}_1,\mathbf{r}_2,\mathbf{r}_3,\mathbf{r}_4)|s')=\left(s\left|[1+\sum_P\delta_PP_{\sigma\tau}{}^P(\textstyle\prod_iG(r_{\alpha_i{}^P\beta_i{}^P}))]\times\left[1+\frac{4}{A-1}[\delta(s,s_{12})+\delta(s,s_{13})+\delta(s,s_{14})+\delta(s,s_{23})+\delta(s,s_{24})+\delta(s,s_{34})]+\frac{16}{(A-1)(A-2)}\times[\delta(s,s_{124})+\delta(s,s_{234})+\delta(s,s_{123})]+\frac{16}{(A-1)(A-2)}\times[\delta(s,s_{12})\delta(s,s_{34})+\delta(s,s_{13})\delta(s,s_{24})+\delta(s,s_{14})\delta(s,s_{23})]+\frac{64}{(A-1)(A-2)(A-3)}\delta(s,s_{1234})\right]\right|s'\right). \quad (26)$$

These expressions are rather lengthy, but the calculation of expectation values with these density matrices is greatly simplified in two ways. First, it will be noticed that all the permutations which are equivalent under the normal subgroup which leaves the operator invariant, contribute equal integrals to the expectation value. Therefore only one of the terms which are equivalent under this group need be considered, multiplied by the number of such terms. Secondly, a large number of terms will be found to contribute nothing to the expectation value when the sum over total spin states is evaluated.

VI. EVALUATION OF $\langle e^2\rangle$ FOR $T_i=0$, $A=4n$ NUCLEI

From Eq. (7), the squared Coulomb operator can be written as

$$e^2=\frac{e^2}{16}\{\sum_{i,j}{}'W_{ij}+\sum_{i,j,k}{}'W_{ijk}+\sum_{i,j,k,l}{}'W_{ijkl}\} \quad (27)$$

where

$$W_{ij}=(\tau_{fi}+\tau_{fj})^2r_{ij}{}^{-2},\ W_{ijk}=(\tau_{fi}+\tau_{fj})(\tau_{fi}+\tau_{fk})r_{ij}{}^{-1}r_{ik}{}^{-1},$$
$$W_{ijkl}=(\tau_{fi}+\tau_{fj})(\tau_{fk}+\tau_{fl})r_{ij}{}^{-1}r_{kl}{}^{-1}, \quad (28)$$

and primed summations indicate that different indices never assume the same value. From the complete antisymmetry of the nuclear wave function, it follows that

$$\langle e^2\rangle=\tfrac{1}{16}e^2\{\tfrac{1}{2}A(A-1)\langle W_{12}\rangle+A(A-1)(A-2)\langle W_{123}\rangle+\tfrac{1}{4}A(A-1)(A-2)(A-3)\langle W_{1234}\rangle\}. \quad (29)$$

The expectation value of each of the multi-nucleon operators is to be found using Eqs. (22), (24), and (26). In finding these expectation values, we shall omit the exchange terms containing integrals over the correlation function $G(r)$ and defer consideration of their magnitude and effect.

To terms of order $1/A$, the expectation value of W_{12} is

$$\langle W_{12}\rangle=\frac{1}{16V^3}\sum_{s,s'}\int \mathbf{dx}_1\mathbf{dx}_2(s|W_{12}|s')(s'|1|s). \quad (30)$$

The sum over the total spin states can be evaluated

$$\mathrm{Tr}W_{12}=32r_{12}^{-2},$$

and the result found:

$$\langle W_{12}\rangle=\langle r_{12}^{-2}\rangle. \quad (31)$$

Neglecting only terms of order A^{-1} in $\langle W_{12}\rangle$ implies that $\langle W_{123}\rangle$ must be correct up to terms of order A^{-2}.

$$\langle W_{123}\rangle=\frac{1}{64V^3}\sum_{s,s'}\int \mathbf{dx}_1\mathbf{dx}_2\mathbf{dx}_3(s|W_{123}|s')$$
$$\times\left(s'\left|1+\frac{4}{A-2}[\delta(s,s_{12})+\delta(s,s_{13})+\delta(s,s_{23})]\right|s\right). \quad (32)$$

In evaluating (26), the sums over total spin states give

$$\mathrm{Tr}W_{123}=64r_{12}^{-1}r_{13}^{-1},\quad \mathrm{Tr}[W_{123}\delta(s,s_{12})]=32r_{12}^{-1}r_{13}^{-1},$$
$$\mathrm{Tr}[W_{123}\delta(s,s_{13})]=0.$$

The expectation value is then

$$\langle W_{123}\rangle=\left(\frac{A+4}{A-2}\right)\langle r_{12}^{-1}r_{13}^{-1}\rangle. \quad (33)$$

Finding the expectation value $\langle W_{1234}\rangle$ is slightly more trouble since one must now carry all terms up to order A^{-3}. In this calculation some peculiar features arise from the fact that in some isotopic spin states for four nucleons W_{1234} is positive, and in others it is negative. In the case of W_{12} and W_{123}, only positive values were possible. A consequence of this fact is that $\mathrm{Tr}W_{1234}=0$. The expression which would give rise to a term in $\langle\mathcal{C}^2\rangle$ proportional to A^4 therefore vanishes here just as it did in the sum rule calculations.

The expectation value of $\langle W_{1234}\rangle$ is found from Eq. (26) to order A^{-3} to be

$$\langle W_{1234}\rangle=\frac{1}{256V^4}\sum_{s,s'}\int \mathbf{dr}_1\mathbf{dr}_2\mathbf{dr}_3\mathbf{dr}_4(s|W_{1234}|s')$$
$$\times\left(s'\left|1+\frac{4}{A-1}[\delta(s,s_{12})+\delta(s,s_{13})+\delta(s,s_{14})\right.\right.$$
$$+\delta(s,s_{23})+\delta(s,s_{24})+\delta(s,s_{34})]+\frac{16}{(A-1)(A-2)}$$
$$\times[\delta(s,s_{124})+\delta(s,s_{134})+\delta(s,s_{234})+\delta(s,s_{123})]$$
$$+\frac{16}{(A-1)(A-2)}[\delta(s,s_{12})\delta(s,s_{34})+\delta(s,s_{13})\delta(s,s_{24})$$
$$\left.\left.+\delta(s,s_{14})\delta(s,s_{23})]\right|s\right). \quad (34)$$

When the traces over spin and isotopic spin have been performed, the result is just

$$\langle W_{1234}\rangle=-\frac{4(A+5)}{(A-2)(A-3)}\langle r_{12}^{-1}r_{34}^{-1}\rangle. \quad (35)$$

Using now Eqs. (29), (31), (33), and (35), the expectation value of $\langle\mathcal{C}^2\rangle$ is just

$$\langle\mathcal{C}^2\rangle=\tfrac{1}{16}e^4A(A-1)\{\langle r_{12}^{-2}\rangle+(A+4)\langle r_{12}^{-1}r_{13}^{-1}\rangle$$
$$-(A+5)\langle r_{12}^{-1}r_{34}^{-1}\rangle\}. \quad (36)$$

When the average values from Eq. (10) are inserted, this becomes

$$\langle\mathcal{C}^2\rangle=\frac{e^4}{16R^2}A(A-1)\{0.878+0.017A\}. \quad (37)$$

As we expected, although the expression for $\langle\mathcal{C}^2\rangle$ in Eq. (36) appears to be rather different from the result given in Eq. (8), the insertion of numerical values for the averages yields results given by Eqs. (11) and (37) which are nearly the same.

VII. CORRELATION EFFECTS

The effect of correlations introduced by the Pauli principle on $\langle\mathcal{C}^2\rangle$ can be seen easily. The averages $\langle r_{12}^{-2}\rangle$, $\langle r_{12}^{-1}r_{13}^{-1}\rangle$, and $\langle r_{12}^{-1}r_{34}^{-1}\rangle$ which we have calculated by assuming a uniform distribution of nuclear matter completely neglects the effects of correlation embodied in the Pauli principle. For example, two nucleons in the same spin and isotopic spin state can never come into coincidence, and for such pairs of nucleons $\langle r_{12}^{-2}\rangle$ should be smaller. The effect of this correlation should be greatest on $\langle r_{12}^{-2}\rangle$ in fact, since contributions from the singularity are sharply reduced. The average $\langle r_{12}^{-1}r_{13}^{-1}\rangle$ is affected somewhat less because a correlation of nucleons 2 and 3 does not reduce the contributions from singularities of r_{12}^{-1} and r_{13}^{-1}. Since there is very little reduction of $\langle r_{12}^{-1}r_{34}^{-1}\rangle$ produced by any correlation of nucleons 1, 3 with nucleons 2, 4, this average is affected least of all.

A more physical way of seeing the effect of correlations on the averages proceeds from the physical interpretation of these quantities. The significance of $\langle r_{12}^{-2}\rangle$ lies in providing a measure of the density fluctuations in the nucleus. The quantity $\langle r_{12}^{-1}r_{13}^{-1}\rangle$ on the other hand correlates the "density" in one direction from a point with the "density" in another direction from that point. We may interpret $\langle r_{12}^{-1}r_{13}^{-1}\rangle$ as a measure of the "angular" uniformity about a point. The last quantity $\langle r_{12}^{-1}r_{34}^{-1}\rangle$ correlates the density at one point with that at another point. In this sense $\langle r_{12}^{-1}r_{34}^{-1}\rangle$ measures the uniformity in density of the nucleus. From the physical considerations one sees, therefore, that the effect of correlations will be greatest on $\langle r_{12}^{-2}\rangle$, less on $\langle r_{12}^{-1}r_{13}^{-1}\rangle$, and least of all on $\langle r_{12}^{-1}r_{34}^{-1}\rangle$.

Using this knowledge of the relative effects of correla-

tions on the averages appearing in Eqs. (8) and (36), one sees from these equations that the effect of correlations is to decrease the magnitude of $\langle \mathcal{C}^2 \rangle$. This result is reasonable when one realizes that the perturbation $\mathcal{C}$ produces an apparent attraction of neutrons and an apparent repulsion of protons. Since we actually evaluate $\langle \mathcal{C}^2 \rangle$, the effect of $\mathcal{C}$ on any pair of neutrons or protons can be regarded as a mutual repulsion. Now if the original wave function contains any correlation of this kind, the perturbation produced by $\mathcal{C}$ will be reduced. The Fermi gas model does provide a correlation between any pair of neutrons or protons which have the same spin. To the extent that this correlation coincides with the mutual repulsion produced by $\mathcal{C}$ will the effect of $\mathcal{C}$ in bringing in higher isotopic spin states be reduced.

The correlation terms in $\langle \mathcal{C}^2 \rangle$ will appear as a linear combination $f(A)$ of integrals involving $G(r)$, so that

$$\langle \mathcal{C}^2 \rangle = \tfrac{1}{16} c^4 \{ \langle r_{12}^{-2} \rangle + (A+4) \langle r_{12}^{-1} r_{13}^{-1} \rangle - (A+5) \langle r_{12}^{-1} r_{34}^{-1} \rangle - f(A) \}. \quad (38)$$

Clearly $f(A)$ cannot exceed the value of other terms in curly brackets even if $G(r)$ were unity for $r \leq R$. The short range of $G(r)$ causes the correlation integrals in $f(A)$ to decrease as $k_m R$ increases. The integral which decreases most slowly with increasing $k_m R$ is the correlation integral for r_{12}^{-2}, as we expected, and is

$$-V^{-2} \int d\mathbf{r}_1 d\mathbf{r}_2 r_{12}^{-2} G(r_{12}).$$

The ratio of $\langle r_{12}^{-2} \rangle$ to this integral is approximately $(k_m R) = (1.523 A^{\frac{1}{3}})$, and even for $A \sim 8$ the correlation terms would only reduce $\langle \mathcal{C}^2 \rangle$ by about one-third at the very most. Our values for maximum isotopic spin impurity are not presumed to be more accurate than this in any case.

VIII. IMPURITIES IN THE $T=0$ GROUND STATE OF $T=0$ EVEN-EVEN NUCLEI

The expression for $\langle \mathcal{C}^2 \rangle$ which has just been found may be used in Eq. (6) with the energy differences listed in Table I to find p_M, the upper limit on the isotopic spin impurity for the ground state of nuclei with $A=4n$ and $T_z=0$. (See Table II.) To be useful these values of p_M should be quite close to the actual value of the isotopic spin impurity for these states found from Eq. (3). We have actually verified that $p \approx p_M$ for the statistical model by explicitly writing the perturbation expansion of Eq. (3), using for the state Ψ_0 that given by Eq. (13), and for the excited states Ψ_r a Slater determinant of free-particle states with one nucleon excited to the continuum above the Fermi sphere.[12] In addition, the perturbation of a single-particle orbit found in this way agrees with that suggested by Eq. (12).

TABLE II. Statistical model estimate of isotopic spin impurity for ground states of nuclei with $A=4n$ and $T_z=0$.

Nucleus	Be^8	C^{12}	O^{16}	Ne^{20}
p_M	2.6×10^{-4}	7.5×10^{-3}	1.9×10^{-2}	3.9×10^{-2}

These values of core impurity, while small, are not negligible and should be detected, for example, in violations of the isotopic spin selection rule for electric dipole transitions. The core impurity is in fact much larger than the isotopic spin impurity produced by Coulomb distortion of the wave function for nucleons outside the core.[13]

We wish to remark that although the neglect of correlations in $\langle \mathcal{C}^2 \rangle$ gives a p_M which is an upper limit on isotopic spin impurity, one must not conclude that Eq. (37) represents an upper limit on the predictions of more detailed single-particle models. For even though a nuclear wave function of the form of Eq. (13) contains certain correlations, the individual-particle wave functions are smooth ($|\psi|^2 = V^{-1}$) and do not provide a positive internucleon correlation. A wave function, or set of wave functions, which describes a state of pronounced maxima or minima of the nuclear density in certain regions could increase $\langle r_{12}^{-2} \rangle$ and $\langle r_{12}^{-1} r_{13}^{-1} \rangle$ relative to $\langle r_{12}^{-1} r_{34}^{-1} \rangle$ and thus increase p. At the same time such a set of wave functions will not provide so large an overlap for all pairs of nucleons so that p can also decrease. This latter result is what we shall actually find when we calculate the isotopic spin impurity of the normal state of C^{12} on the jj-coupling model with harmonic oscillator wave functions.

ACKNOWLEDGMENTS

To Professor E. P. Wigner, I express my sincere thanks for suggesting this problem and for his guidance and advice during its investigation.

[12] Wm. M. MacDonald, Princeton dissertation, 1954 (unpublished).

[13] The large value of 2.5×10^{-3} obtained by Radicati (reference 8) for the isotopic spin impurity of the ground state of N^{14} is the result of an unrealistic representation of the Coulomb potential produced by the core nucleons (C^{12}). A more rigorous calculation gives 1×10^{-4} with his value of the energy separation.

Deuteron-Model Calculation of the High-Energy Nuclear Photoeffect*

K. G. DEDRICK
Stanford University, Stanford, California
(Received May 6, 1955)

The high-energy nuclear photoeffect has been calculated according to the "deuteron model" of Levinger. In this model, the photoprocess occurs when a neutron and a proton which are scattering one another inside the nucleus absorb the energy of the incident photon and escape from the nuclear potential well into the laboratory. The nuclear photoeffect cross section is then obtained by averaging the cross section for the above process over all possible neutron-proton pairs in the nucleus, assuming a nucleon momentum distribution. The electric dipole and quadrupole interactions of the radiation field with the neutron and proton are included, and the magnetic terms are neglected. The averaging over all neutron-proton pairs is performed by means of a random flight formulation of the problem. The analytical work involved may conveniently be done using either a zero-temperature Fermi ground-state nucleon momentum distribution or a Gaussian distribution. Numerical results for the energy and angle distributions of photoneutrons and photoprotons are presented in the case of the Gaussian distribution, for four photon energies between 50 and 125 Mev.

I. INTRODUCTION

LEVINGER'S[1] deuteron model for the high-energy nuclear photoeffect has been sufficiently successful in interpreting experimental data to warrant further calculations. This model assumes as a photon absorption process, the photodissociation of a neutron and a proton within the nucleus which interact through a short range potential and are scattering one another.[2] The neutron and proton absorb the photon energy and may then escape from the nucleus. The nuclear photoeffect cross section is obtained by averaging the cross section for the photodissociation of the quasi-deuteron over all possible neutron-proton pairs in the nucleus. Corrections may be made to this result for the scattering of the prospective photoparticle by other nucleons in the nucleus and consideration given to the effects of the Coulomb and centrifugal barriers at the nuclear surface.

Levinger[1] shows that the cross section for the photodissociation of the quasi-deuteron can be related to the cross section for the bound deuteron, and makes use of the deuteron photoeffect cross sections calculated by Schiff[3] and by Marshall and Guth.[4] We calculate instead the photodissociation cross section of a neutron and proton which are scattering one another and confined to a volume v which is later taken to be the volume of the nucleus under consideration. For initial and final state wave functions, triplet n-p scattering wave functions are fabricated to provide agreement with the phenomenological low-energy n-p interaction. Only the electric dipole and electric quadrupole contributions are calculated. The magnetic terms are neglected because they are expected to be small, and furthermore their neglect does not distort the angular dependence of the cross section in that there is no interference with the electric terms.

Deuteron-model calculations in the past[1,5] have handled the averaging over all quasi-deuterons in a manner which does not yield an analytical result. This average is dependent on the nuclear ground-state neutron and proton momentum distributions. Levinger assumes Fermi distributions with a temperature of 8 Mev, and Weil and McDaniel[5] use zero-temperature Fermi distributions.

The averaging is handled here by interpreting the kinematics as a random-flight problem involving the sum of four momentum vectors. It is necessary to choose ground-state nucleon momentum distributions that will submit to the repeated integrations which arise in the random-flight theory. The zero-temperature Fermi distribution and the Gaussian are satisfactory in this respect, and the averaging is performed for both. The analyses of other types of nuclear experiments like the "pickup" process[6] and the nuclear scattering of 320-Mev protons[7] suggest that the Fermi distribution does not give as good agreement with experiment as do smoother distributions. The distribution proportional[8] to $(p^2+a^2)^{-2}$, where p is the nucleon momentum and a^2 corresponds to 18 Mev, is found to give reasonable agreement with the "pickup" process experiments,[9] but does not give as good agreement with the proton scattering experiments[7] as does a Gaussian distribution with a $1/e$ value of 16 Mev. In view of this, numerical evaluation of the photoeffect calculation presented below has been done only in the case of the Gaussian momentum distribution.

Corrections for the collisions of the photoparticles with other nucleons inside the nucleus have not been included here. This effect mainly influences the low-

* Supported in part by the Office of Scientific Research, Air Research and Development Command.
[1] J. S. Levinger, Phys. Rev. **84**, 43 (1951).
[2] In Levinger's terminology, such a neutron and proton are referred to as a "quasi-deuteron."
[3] L. I. Schiff, Phys. Rev. **78**, 733 (1950).
[4] J. F. Marshall and E. Guth, Phys. Rev. **78**, 738 (1950).
[5] J. W. Weil and B. C. McDaniel, Phys. Rev. **92**, 391 (1953).
[6] G. F. Chew and M. L. Goldberger, Phys. Rev. **77**, 470 (1950).
[7] Cladis, Hess, and Moyer, Phys. Rev. **87**, 425 (1952).
[8] This is the "Chew-Goldberger" distribution. See reference 6.
[9] H. York, Phys. Rev. **75**, 1467(A) (1949).

energy photoparticles as the mean free path of a nucleon in nuclear matter is shorter for low-energy nucleons.[10]

In Sec. IV, account is taken of the reflections of photoneutrons from the edge of the nucleus where we expect a rapid change in nuclear potential and also a centrifugal barrier corresponding to the angular momentum of the photoneutron. In the case of photoprotons, the effect of the Coulomb barrier in reducing the penetration probability is also considered.

Tables of the numerical work are presented for photon energies of 50, 75, 100, and 125 Mev. These tables are not corrected for nuclear surface barrier penetrability, as it is necessary to specify a particular nucleus in calculating the penetrability. Directions for using the tables for a particular nucleus are presented in Sec. V.

II. QUASI-DEUTERON PHOTODISSOCIATION CROSS SECTION

The neutron and proton comprising the quasi-deuteron are assumed to interact through a short-range static potential of the kind usually assumed in explanations of the deuteron ground state and the low-energy n-p scattering. By virtue of this interaction, the neutron and proton can recoil against one another and absorb the energy of the photon. A direct calculation shows that without the n-p interaction, the cross section for the photon absorption is zero.

This calculation is very similar to the deuteron photoeffect calculations where one calculates the transition probability per unit time per unit incident photon flux from the deuteron ground state to a final state where the neutron and proton are nearly free, but still interact through the n-p potential. Just as in the deuteron photoeffect calculation, we obtain:

$$\sigma(\theta)=\frac{\sin^2\theta}{8\pi}[3\sigma_d+6(5\sigma_d\sigma_q)^{\frac{1}{2}}\cos\theta\cos\delta_2+15\sigma_q\cos^2\theta], \quad (1)$$

where

$$\sigma_d=\frac{4\pi^2}{3}\left(\frac{e^2}{\hbar c}\right)\frac{Mk_fE_\gamma'}{\hbar^2}|I_1|^2,$$
$$\sigma_q=\frac{\pi^2}{60}\left(\frac{e^2}{\hbar c}\right)\frac{Mk_f(E_\gamma')^3}{\hbar^4c^2}|I_2|^2; \quad (2)$$

θ is the angle of the photoparticle with respect to the direction of the incident photon, σ_d and σ_q are respectively the total electric dipole and electric quadrupole cross sections, M is the nucleon mass, k_f is the final nucleon momentum, E_γ' is the photon energy seen in the center-of-mass system, and

$$I_1\equiv\int_0^\infty R_1^*(r)r^2\psi_i(r)dr,$$
$$I_2\equiv\int_0^\infty R_2^*(r)r^4\psi_i(r)dr. \quad (3)$$

[10] Weil and McDaniel[3] show how collisions affect the photoparticle energy spectra.

In these expressions for I_1 and I_2, $R_1(r)$ is the radial part of the p state contribution to the final state wave function and $R_2(r)$ is the same for the d state. These final state radial functions are normalized to have the asymptotic form $R_l(r)\rightarrow\cos\delta_l\, j_l(k_fr)-\sin\delta_l\, n_l(k_fr)$, where the δ_l are the phase shifts.[11] In calculating the $R_l(r)$, we shall use the Serber force[12] which yields an interaction only for even values of l. This gives us the result that $R_l(r)=j_l(k_fr)$ for odd l. In calculating I_2, the r^4 factor in the integrand makes the details of $R_2(r)$ unimportant near $r=0$. Because of this, we use the asymptotic form[13]

$$R_2(r)\rightarrow\cos\delta_2\, j_2(k_fr)-\sin\delta_2\, n_2(k_fr).$$

The phase shift δ_2 is calculated by the Born approximation.[14]

For the initial state wave function ψ_i, we use the $l=0$ part of the n-p wave function in the triplet n-p potential. Neglect of the singlet interaction is not felt to be serious and considerably simplifies the calculation. Rather than start with the n-p potential where in general it is impossible to solve the wave equation, we make a choice for ψ_i which correctly gives the low-energy n-p scattering and in the limit of a negative value for the relative energy, becomes the deuteron bound-state solution for the Hulthén potential. This wave function is:

$$\psi_i(r)=(A/r)u_i(r)$$

where

$$u_i(r)=\frac{\sin(k_ir+\delta_0)}{\sin\delta_0}e^{-\beta r}.$$

From the "effective range" theories of Bethe[15] and Schwinger,[16] we use

$$k_i\cot\delta_0\cong-1/a_i+\tfrac{1}{2}r_{0i}k_i^2.$$

The effective range is r_{0i}, and a_i is the triplet scattering length. The parameter β is given by[17,18]

$$\beta=\frac{3}{2r_{0i}}\left[1+\left(1-\frac{16}{9}\frac{r_{0i}}{a_i}\right)^{\frac{1}{2}}\right].$$

Following Levinger, we choose the normalization factor A so that ψ_i is the s wave part of a plane wave Ψ_i which is normalized so that it yields one n-p pair in a volume v which is later taken to be the volume of the

[11] L. I. Schiff, *Quantum Mechanics* (McGraw-Hill Book Company, Inc., New York, 1949), Chap. V, Sec. 19.

[12] J. M. Blatt and V. F. Weisskopf, *Theoretical Nuclear Physics* (John Wiley and Sons, Inc., New York, 1952), p. 179.

[13] This approximation is used in references 3 and 4.

[14] Reference 11, p. 165.

[15] H. A. Bethe, Phys. Rev. **76**, 38 (1949).

[16] J. Schwinger, Phys. Rev. **72**, 742(A) (1947).

[17] A justification for using this formula for β is presented in the dissertation by the author, copies of which may be obtained from University Microfilms, 313 N. 1st St. Ann Arbor, Michigan. (Cat. No. 11171) (unpublished).

[18] Recent experiment shows $r_{01}=1.7\times10^{-13}$ cm, $a_1=5.39\times10^{-13}$ cm. (See reference 12, p. 71.)

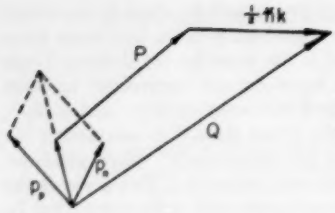

FIG. 1. The vector composition of the photoparticle momentum Q.

nucleus under consideration. This gives the result $A=v^{-\frac{1}{2}}\sin\delta_0$.

The results of calculation of I_1 and I_2 by Eq. (3) are lengthy algebraic expressions and are not included here.[19] The cross sections σ_d and σ_q follow directly through Eq. (2).

III. AVERAGING PROCESS

The averaging over-all quasi-deuterons is complicated by the dependence of the quasi-deuteron photodissociation cross section on the relative momentum of the neutron and proton, and on the photon energy that appears in the quasi-deuteron center of mass. This photon energy is given by a Doppler shift from the energy of the incident radiation and is dependent on the motion of the quasi-deuteron center of mass in the nucleus. The averaging is performed by interpreting the situation as a random flight problem involving four vectors. The momentum vector $\mathbf{Q}$ of a photoparticle in the laboratory is given by[20]

$$\mathbf{Q}=\mathbf{P}+\tfrac{1}{2}(\mathbf{p}_n+\mathbf{p}_p)+\tfrac{1}{2}\hbar\mathbf{k}. \tag{4}$$

The vector $(\mathbf{p}_n+\mathbf{p}_p)$ in Eq. (4) or Fig. 1, is the momentum of the center of mass of the quasi-deuteron, where $\mathbf{p}_n$ is the neutron momentum and $\mathbf{p}_p$ is the proton momentum. One-half of this must be added to $\mathbf{P}$, the momentum of the photoneutron or photoproton taken in the center-of-mass frame. In addition, each photoparticle receives a contribution $\frac{1}{2}\hbar\mathbf{k}$. We are interested in obtaining a distribution function which gives the probability $W(\mathbf{Q})d\mathbf{Q}$ that $\mathbf{Q}$ lies in the range $dQ_x dQ_y dQ_z \equiv d\mathbf{Q}$ about $\mathbf{Q}$.

The center-of-mass frame for the quasi-deuteron photodissociation will be taken as the quasi-deuteron center of mass. This means that the effect of the photon momentum in establishing the frame of reference is being neglected.

The random flight formulation consists in treating the momentum vectors in Eq. (4) as random variables. Chandrasekhar[21] gives the solution to random flight problems in a form convenient for our use. The calculation has been carried out in two steps. Let us take $\mathbf{Q}=\mathbf{Q}'-\frac{1}{2}\hbar\mathbf{k}$, where $\mathbf{Q}'=\mathbf{P}+\frac{1}{2}(\mathbf{p}_n+\mathbf{p}_p)$. We first calculate $W'(\mathbf{Q}')$ according to the random flight formalism, and then calculate $W(\mathbf{Q})$ by a reapplication of the same formalism. $W'(\mathbf{Q}')$ is given by[21]

$$W'(\mathbf{Q}')=\frac{1}{8\pi^3}\int \exp(-i\boldsymbol{\varrho}\cdot\mathbf{Q}')A'(\boldsymbol{\varrho})d\boldsymbol{\varrho}, \tag{5a}$$

where

$$A'(\boldsymbol{\varrho}')=\int\int\int \exp[i\boldsymbol{\varrho}\cdot(\mathbf{p}+\mathbf{q}_n+\mathbf{q}_p)]\tau_P(E_\gamma,\mathbf{q}_n,\mathbf{q}_p,\mathbf{P}) \times\tau_n(\mathbf{q}_n)\tau_p(\mathbf{q}_p)d\mathbf{P}d\mathbf{q}_n d\mathbf{q}_p, \tag{5b}$$

with $\mathbf{q}_n=\frac{1}{2}\mathbf{p}_n$ and $\mathbf{q}_p=\frac{1}{2}\mathbf{p}_p$. Similarly, $W(\mathbf{Q})$ is obtained from $W'(\mathbf{Q}')$:

$$W(\mathbf{Q})=\frac{1}{8\pi^3}\int \exp(-i\boldsymbol{\varrho}\cdot\mathbf{Q})A(\boldsymbol{\varrho})d\boldsymbol{\varrho}, \tag{6a}$$

$$A(\boldsymbol{\varrho})=\int \exp(i\boldsymbol{\varrho}\cdot\mathbf{p}_k)\tau_k(\mathbf{p}_k)d\mathbf{p}_k \times\int \exp(i\boldsymbol{\varrho}\cdot\mathbf{Q}')W'(\mathbf{Q}')d\mathbf{Q}', \tag{6b}$$

where we have introduced $\mathbf{p}_k=\frac{1}{2}\hbar\mathbf{k}$.

Knowledge of $W(\mathbf{Q})$ gives us not only the angular distribution of photoparticles but the energy distribution as well. Let us take Θ and Φ as the polar angles for the vector $\mathbf{Q}$. Then $d\mathbf{Q}$ is given by $d\mathbf{Q}=Q^2dQd\Omega$, where $d\Omega=\sin\Theta d\Phi d\Theta$ is the element of solid angle in $\mathbf{Q}$ space. Further, since the energy of the photoparticle above the bottom of the nuclear well is given nonrelativistically by $E_w=Q^2/(2M)$, we have

$$W(\mathbf{Q})d\mathbf{Q}=W(\mathbf{Q})(2M^3E_w)^{\frac{1}{2}}dE_w d\Omega. \tag{7}$$

The cross section $\sigma(\Theta,\Phi,E_w)$ per unit solid angle per unit energy of the photoparticle is then

$$\sigma(\Theta,\Phi,E_w)=W(\mathbf{Q})(2M^3E_w)^{\frac{1}{2}}. \tag{8}$$

If the depth of the nuclear potential well is V, the energy of the photoparticles in the laboratory is given by $E_L=E_w-V$. After the cross section $\sigma(\Theta,\Phi,E_w)$ is evaluated according to Eq. (8), the photoparticle energy scale must be shifted by an amount V which may be chosen from the analysis by Adair[22] of the results of neutron scattering experiments or on some other basis.

In calculating $W'(\mathbf{Q}')$ according to Eq. (5), we require the probability density $\tau_P(E_\gamma,\mathbf{q}_n,\mathbf{q}_p,\mathbf{P})$, given the values of E_γ, $\mathbf{q}_n$, and $\mathbf{q}_p$, that $\mathbf{P}$ will lie in the range $d\mathbf{P}$ about $\mathbf{P}$. The quasi-deuteron photodissociation cross section calculated in the previous section according to (1) and (2), may be written

$$\sigma_{np}(|\mathbf{p}_n-\mathbf{p}_p|, E_\gamma',\vartheta_P)$$

[19] See reference 17, pp. 37–38.

[20] Equation (4) is not quite correct for relativistic particle energies (i.e., for photon energies that are a sizable fraction of the nucleon rest energy). The approximation made in using Eq. (4) is consistent with others made in this work. A detailed development is presented in reference 17, in the Appendix, Sec. B.

[21] S. Chandrasekhar, Revs. Modern Phys. **15**, 8 (1943).

[22] Robert K. Adair, Phys. Rev. **94**, 737 (1954). A well depth of 40 Mev is suggested by this analysis.

where θ_P is the angle of the photoparticle in the quasi-deuteron center-of-mass system and E_γ' is the photon energy in the center-of-mass system. The cross section is dependent on the magnitude of $(\mathbf{p}_n-\mathbf{p}_p)$ and not on the direction since only the $l=0$ partial wave is included in the initial state wave function (moderate nucleon momenta). On multiplying σ_{np} by a delta function normalized to unity, which expresses conservation of energy in the photoprocess, we obtain τ_P.

$$\tau_P=\sigma_{np}\delta(|\mathbf{P}|-P_0)/P_0^2. \tag{9}$$

P_0 is the magnitude of the photoparticle momentum in the center of mass and is given by energy conservation between E_γ' and the initial relative energy between the neutron and proton. If we use the nonrelativistic Doppler formula to express E_γ' in terms of E_γ and introduce

$$\begin{aligned}\mathbf{r}&=\mathbf{q}_n-\mathbf{q}_p,\\ \mathbf{R}&=\mathbf{q}_n+\mathbf{q}_p,\end{aligned} \tag{10}$$

we find

$$P_0=\left[ME_\gamma\left(1-\frac{|\mathbf{R}|}{Mc}\cos\theta_R\right)+|\mathbf{r}|^2\right]^{\frac{1}{2}}. \tag{11}$$

Since σ_{np} depends on $\mathbf{r}$ through $|\mathbf{r}|$, and on $\mathbf{R}$ through the Doppler formula, it is seen that

$$\tau_P=\tau_P(|\mathbf{r}|,\mathbf{R},E_\gamma,\theta_P).$$

This suggests that the integrations indicated in (5) over $\mathbf{q}_n$ and $\mathbf{q}_p$ would be more easily performed if a transformation were made to the variables $\mathbf{r}$ and $\mathbf{R}$ as is Eq. (10). To do this, $\tau_n(\mathbf{q}_n)\tau_p(\mathbf{q}_p)d\mathbf{q}_nd\mathbf{q}_p$ must be replaced by $\tau_r(\mathbf{r})\tau_R(\mathbf{R})d\mathbf{r}d\mathbf{R}$. If τ_n and τ_p are of simple analytic form, this latter transformation is readily performed. τ_n and τ_p are closely related to the ground-state nucleon momentum distributions. The cross section σ_{np} may be expressed as a series of Legendre polynomials of order from zero to five in the angles of $\mathbf{P}$. The integration indicated in Eq. (5b) over these angles is readily carried out,[23] as is also the integration over P. The integration over the angles of $\mathbf{R}$ is complicated by the dependence of P_0 on θ_R as in Eq. (11) and the dependence of σ_{np} on E_γ' which is also a function of θ_R. A series expansion is made in powers of $(R\cos\theta_R)$ of σ_{np} and $j_n(\rho P_0)$ where the quadratic and higher terms are neglected.[24] Integration over θ_R then proceeds according to the same method used in the case of the angles of $\mathbf{P}$. Integration over the angles of $\mathbf{r}$ and $\boldsymbol{\rho}$ is done by using the results quoted in footnote 23.

[23] This integration, and many others to be done, make use of

$$\int\exp(i\mathbf{k}\cdot\mathbf{r})P_n(\cos\theta_r)d\Omega_r=4\pi i^nP_n(\cos\theta_k)j_n(kr).$$

Of occasional use also is

$$\int_0^\infty j_n(\alpha\rho)j_n(\beta\rho)\rho^2d\rho=\frac{\pi}{2\alpha\beta}[\delta(\alpha-\beta)+(-1)^{n+1}\delta(\alpha+\beta)].$$

[24] A justification for this approximation is given in reference 17, Appendix D.

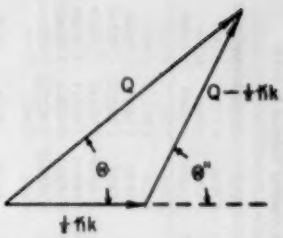

FIG. 2. Geometrical relation between Θ and Θ''.

The resulting expression for $W'(\mathbf{Q}')$ has yet to be integrated over r, R, and ρ, but first, specific forms for the ground state nucleon momentum distributions must be assumed. The integrations over R and ρ may be done by using the zero-temperature Fermi distribution and the Gaussian distribution. The result for $W'(\mathbf{Q}')$ is expressible in a series of Legendre polynomials. The coefficients in the case of the Gaussian distribution contain Gauss functions and Bessel functions of half-odd-integer order with an imaginary argument; in the case of the Fermi distribution, the coefficients are lengthy algebraic expressions. The integration over r is not done exactly, but is conveniently approximated numerically.

$W'(\mathbf{Q}')$ may be written

$$W'(\mathbf{Q}')=\sum_{n=0}^{5}B_n(|\mathbf{Q}'|)P_n(\cos\Theta'). \tag{12}$$

Next, $W(\mathbf{Q})$ must be obtained according to Eq. (6). For $\tau_k(\mathbf{p}_k)$ in Eq. (6b), we use $\delta(p_{kx})\delta(p_{ky})\delta(p_{kz}-\frac{1}{2}\hbar k)$, and readily obtain:

$$W(\mathbf{Q})=\sum_{n=0}^{5}B_n(|\mathbf{Q}-\tfrac{1}{2}\hbar\mathbf{k}|)P_n(\cos\Theta''), \tag{13}$$

where

$$|\mathbf{Q}-\tfrac{1}{2}\hbar\mathbf{k}|=Q[1+(\tfrac{1}{2}\hbar k/Q)^2-2(\tfrac{1}{2}\hbar k/Q)\cos\Theta]^{\frac{1}{2}}, \tag{14}$$

and

$$\cos\Theta''=\frac{\cos\Theta-(\tfrac{1}{2}\hbar k/Q)}{[1+(\tfrac{1}{2}\hbar k/Q)^2-2(\tfrac{1}{2}\hbar k/Q)\cos\Theta]^{\frac{1}{2}}}. \tag{15}$$

Figure 2 shows the geometrical relation between these quantities. Equation (13) states that to calculate $W(\mathbf{Q})$ for a given laboratory angle Θ and laboratory momentum Q with an associated energy E_w, we must calculate $\cos\Theta''$ and $|\mathbf{Q}-\frac{1}{2}\hbar\mathbf{k}|$ according to Eqs. (14) and (15) and substitute them into Eq. (13). The cross section $\sigma(\Theta,E_w)$ is then given by multiplying this result by $(2M^3E_w)^{\frac{1}{2}}$ as in Eq. (8). Numerical results in Table I are discussed in Sec. V.

IV. COULOMB AND CENTRIFUGAL BARRIER PENETRABILITIES

We assume that if a prospective photoparticle does not get through the Coulomb and centrifugal barriers on its first encounter, it does not get a second chance

TABLE I. Photoparticle yields assuming a Gaussian initial nucleon momentum distribution. Tabulated values are v times $\sigma(E_\omega,\Theta)$, where v is the nuclear volume in cubic centimeters. All entries are to be multiplied by 10^{-70}. The cross section $\sigma(E_\omega,\Theta)$ then has the units: cm²/Mev.

Photon energy Mev	E_ω, Mev	Laboratory angle—degrees 10	20	30	40	50	60	70	80	90	100	110	120	130	140	150	160	170
										Photoprotons								
50	43.20	108.9	132.8	164.7	195.5	216.9	223.6	214.7	192.5	161.9	128.3	96.01	68.28	46.46	30.61	19.96	13.43	9.981
	53.33	86.06	107.0	134.5	160.4	177.5	181.6	172.4	152.5	126.3	98.38	72.40	50.55	33.65	21.52	13.41	8.422	5.776
	64.53	58.79	74.54	95.02	113.9	125.8	127.9	120.2	105.1	85.99	66.20	48.17	33.26	21.84	13.66	8.150	4.729	2.876
	76.80	34.56	44.80	57.99	69.91	77.14	77.98	72.73	63.03	51.13	39.08	28.27	19.44	12.69	7.822	4.495	2.374	1.203
	90.13	17.38	23.14	30.49	37.03	40.88	41.18	38.19	32.90	26.56	20.24	14.64	10.08	6.577	4.019	2.232	1.063	0.4036
	104.53	7.421	10.21	13.76	16.88	18.69	18.81	17.40	14.95	12.06	9.199	6.681	4.624	3.030	1.843	0.9935	0.4241	0.0963
										Photoneutrons								
	43.20	46.44	62.07	85.44	112.9	140.0	162.5	177.1	181.9	176.9	163.3	143.5	120.3	96.18	73.56	54.20	39.47	30.27
	53.33	36.25	49.36	68.68	90.89	112.2	129.2	139.3	141.4	135.9	124.1	108.0	89.53	70.78	53.32	38.45	27.13	20.07
	64.53	24.78	34.30	48.15	63.75	78.30	89.40	95.48	96.02	91.48	82.91	71.66	59.09	46.40	34.62	24.56	16.88	12.08
	76.80	14.79	20.77	29.36	38.85	47.47	53.79	56.99	56.90	53.91	48.68	41.98	34.56	27.07	20.08	14.07	9.468	6.572
	90.13	7.685	10.93	15.53	20.52	24.95	28.09	29.59	29.42	27.82	25.13	21.70	17.90	14.02	10.37	7.201	4.756	3.212
	104.53	3.470	4.983	7.105	9.373	11.35	12.72	13.36	13.27	12.57	11.40	9.890	8.188	6.427	4.745	3.272	2.126	1.400
										Photoprotons								
75	30.49	27.86	35.32	45.63	56.23	64.57	68.74	67.92	62.44	53.56	43.00	32.42	23.13	15.84	10.70	7.459	5.650	4.797
	37.65	34.75	44.46	57.62	70.65	80.17	83.90	81.15	72.78	60.72	47.25	34.43	23.64	15.51	9.999	6.660	4.873	4.065
	45.55	39.13	50.55	65.71	80.17	89.93	92.59	87.78	76.94	62.58	47.39	33.53	22.30	14.10	8.709	5.516	3.837	3.086
	54.21	39.70	51.84	67.61	82.10	91.10	92.34	85.91	73.74	58.64	43.39	29.98	19.44	11.96	7.110	4.259	2.746	2.053
	63.62	36.25	47.88	62.71	75.84	83.29	83.21	76.08	64.06	49.95	36.26	24.60	15.69	9.461	5.458	3.077	1.774	1.149
	73.79	29.73	39.91	52.39	63.14	68.70	67.71	60.93	50.44	38.68	27.65	18.54	11.70	6.986	3.939	2.085	1.026	0.4917
	84.71	21.84	29.70	39.37	47.35	51.09	49.75	44.13	35.99	27.23	19.25	12.82	8.067	4.800	2.664	1.325	0.5251	0.1021
	96.38	14.33	19.87	26.59	31.95	34.20	32.94	28.86	23.26	17.42	12.23	8.124	5.125	3.056	1.673	0.7547	0.1778	···
	108.80	8.348	11.88	16.09	19.36	20.61	19.67	17.06	13.62	10.13	7.091	4.718	2.994	1.327	0.7211	0.3044	0.0342	···
										Photoneutrons								
	30.49	8.364	12.62	19.61	28.92	39.70	50.64	60.13	66.67	69.26	67.62	62.24	54.16	44.70	35.15	26.63	19.99	15.80
	37.65	9.813	15.07	23.54	34.55	46.89	58.87	68.62	74.57	75.85	72.50	65.32	55.62	44.86	34.37	25.24	18.23	13.84
	45.55	10.57	16.49	25.86	37.73	50.56	62.44	71.43	76.10	75.88	71.12	62.88	52.57	41.61	31.22	22.32	15.56	11.36
	54.21	10.40	16.48	25.90	37.52	49.63	60.28	67.71	70.79	69.31	63.86	55.58	45.80	35.73	26.38	18.46	12.48	8.775
	63.62	9.327	14.98	23.58	33.89	44.24	52.87	58.36	59.97	57.77	52.48	45.12	36.79	28.42	20.74	14.27	9.403	6.382
	73.79	7.603	12.29	19.47	27.75	35.75	42.06	45.68	46.23	43.94	39.47	33.64	27.25	20.92	15.14	10.29	6.632	4.359
	84.71	5.628	9.243	14.55	20.56	26.15	30.32	32.45	32.41	30.47	27.16	23.03	18.59	14.22	10.24	6.893	4.360	2.783
	96.38	3.781	6.258	9.828	13.75	17.26	19.73	20.86	20.64	19.27	17.10	14.47	11.67	8.914	6.390	4.237	2.602	1.581
	108.80	2.303	3.830	5.992	8.300	10.28	11.61	12.16	11.94	11.11	9.846	8.336	6.725	3.795	2.711	1.781	1.074	0.6319
										Photoprotons								
100	23.56	2.837	4.075	5.923	8.069	10.12	11.68	12.44	12.24	11.16	9.446	7.439	5.491	3.864	2.683	1.994	1.554	1.387
	29.09	4.846	6.860	9.786	13.04	15.96	17.90	18.47	17.56	15.42	12.50	9.389	6.574	4.373	2.890	2.048	1.663	1.534
	35.20	7.548	10.58	14.88	19.47	23.27	25.42	25.46	23.42	19.82	15.44	11.09	7.376	4.638	2.909	2.007	1.653	1.571
	41.89	10.74	14.98	20.83	26.79	31.35	33.40	32.52	29.00	23.72	17.81	12.27	7.787	4.642	2.755	1.834	1.513	1.466
	49.16	13.99	19.47	26.82	33.99	39.00	40.58	38.46	33.31	26.41	19.17	12.74	7.763	4.413	2.477	1.565	1.260	1.221
	57.02	16.71	23.24	31.80	39.76	44.78	45.57	42.12	35.49	27.34	19.27	12.41	7.326	4.008	1.870	1.252	0.9386	0.8765
	65.45	18.30	25.50	34.71	42.86	47.45	47.28	42.67	35.06	25.57	18.07	11.36	6.554	3.492	1.865	0.9412	0.6071	0.5052
	74.47	18.38	25.73	34.88	42.61	46.41	45.33	40.00	32.10	23.53	15.82	9.769	5.555	2.918	1.429	0.6586	0.3194	0.1793
	84.07	16.93	23.85	32.27	39.04	41.88	40.14	34.68	27.23	19.56	12.91	7.880	4.457	1.887	1.113	0.4507	0.1087	···
	94.25	14.29	20.31	27.48	32.96	34.86	32.82	27.81	21.40	15.10	9.833	5.960	3.375	1.776	0.8328	0.2895	···	···
	105.02	11.02	15.87	21.51	25.62	26.75	24.78	20.61	15.58	10.82	6.980	4.222	2.407	1.279	0.5941	0.1778	···	···
	116.36	7.747	11.36	15.47	18.33	18.92	17.26	14.12	10.51	7.208	4.618	2.798	1.627	0.8662	0.4004	0.1044	···	···

TABLE I.—(*Continued*).

Photon energy Mev	E_0, Mev	Laboratory angle—degrees 10	20	30	40	50	60	70	80	90	100	110	120	130	140	150	160	170
									Protoprotons—*Continued*									
100	128.29	4.937	7.423	10.20	12.05	12.32	11.09	8.941	6.563	4.458	2.846	1.733	1.009	0.5492	0.2532	0.0585	···	···
	140.80	2.829	4.411	6.150	7.267	7.374	6.564	5.227	3.795	2.560	1.634	1.002	0.5903	0.3247	0.1493	0.0312	···	···
	153.89	1.436	2.367	3.378	4.010	4.052	3.575	2.820	2.031	1.365	0.8737	0.5401	0.3218	0.1799	0.0818	0.0158	···	···
									Photoneutrons									
	23.56	0.6483	1.258	2.416	4.261	6.845	10.04	13.51	16.73	19.15	20.33	20.11	18.60	16.17	13.30	10.49	8.171	6.651
	29.09	0.9217	1.823	3.506	6.125	9.695	13.97	18.42	22.32	24.95	25.85	24.93	22.47	19.00	15.16	11.54	8.625	6.751
	35.20	1.252	2.522	4.840	8.349	12.98	18.31	23.60	27.90	30.43	30.75	28.92	25.41	20.94	16.24	11.96	8.597	6.463
	41.89	1.602	3.290	6.296	10.71	16.32	22.52	28.31	32.66	34.73	34.23	31.43	26.98	21.71	16.42	11.75	8.135	5.870
	49.16	1.917	4.018	7.669	12.85	19.20	25.88	31.75	35.71	37.05	35.67	32.03	26.92	21.23	15.72	10.30	7.341	5.086
	57.02	2.137	4.576	8.711	14.39	21.06	27.74	33.21	36.45	36.94	34.79	30.62	25.29	19.62	14.46	9.756	6.339	4.222
	65.45	2.216	4.851	9.203	14.99	21.50	27.68	32.36	34.69	34.54	31.76	27.49	22.39	17.15	12.96	8.278	5.241	3.364
	74.47	2.139	4.774	9.027	14.49	20.38	25.66	29.32	30.75	29.89	27.14	23.17	18.67	14.18	10.09	6.690	4.142	2.569
	84.07	1.920	4.362	8.210	13.00	17.92	22.08	24.69	25.37	24.23	21.70	18.33	14.66	10.87	7.826	5.133	3.119	1.874
	94.25	1.605	3.697	6.916	10.78	14.59	17.61	19.30	19.47	18.32	16.23	13.61	10.83	8.140	5.728	3.725	2.226	1.300
	105.02	1.251	2.905	5.390	8.273	10.99	13.01	13.99	13.90	12.92	11.35	9.471	7.512	5.631	3.946	2.545	1.499	0.8520
	116.36	0.9095	2.115	3.884	5.867	7.652	8.888	9.400	9.213	8.486	7.416	6.174	4.937	3.655	2.549	1.632	0.9471	0.5254
	128.29	0.6181	1.426	2.585	3.840	4.917	5.613	5.850	5.674	5.195	4.528	3.766	2.978	2.220	1.541	0.9779	0.5598	0.3034
	140.80	0.3931	0.8900	1.586	2.315	2.913	3.272	3.369	3.244	2.962	2.582	2.148	1.696	1.259	0.8685	0.5464	0.3086	0.1635
	153.89	0.2343	0.5140	0.8968	1.284	1.587	1.757	1.794	1.722	1.573	1.374	1.144	0.9012	0.6716	0.4560	0.2841	0.1582	0.0820
									Photoprotons									
125	40.06	1.952	3.213	5.071	7.168	9.050	10.27	10.54	9.775	8.190	6.164	4.134	2.449	1.295	0.6786	0.4796	0.5177	0.6208
	46.46	3.183	5.050	7.717	10.58	12.95	14.22	14.08	12.59	10.14	7.304	4.660	2.600	1.266	0.6080	0.4330	0.5119	0.6164
	53.33	4.725	7.313	10.90	14.56	17.32	18.45	17.67	15.26	11.84	8.201	5.007	2.644	1.195	0.5170	0.3549	0.4471	0.5868
	60.68	6.439	9.800	14.32	18.70	21.67	22.42	20.83	17.40	13.05	8.724	5.130	2.595	1.104	0.4255	0.2589	0.3324	0.4504
	68.50	8.101	12.19	17.53	22.42	25.36	25.55	23.04	18.67	13.56	8.786	5.013	2.462	1.007	0.3476	0.1613	0.1903	0.2661
	76.80	9.437	14.10	20.00	25.12	27.78	27.27	23.92	18.82	13.28	8.376	4.672	2.259	0.9110	0.2886	0.0765	0.0494	0.0747
	85.57	10.20	15.18	21.30	26.30	28.48	27.28	23.30	17.83	12.25	7.554	4.148	1.999	0.8138	0.2458	0.0135	···	···
	94.81	10.23	15.22	21.17	25.75	27.32	25.56	21.28	15.87	10.65	6.441	3.506	1.702	0.7102	0.2123	···	···	···
	104.53	9.534	14.21	19.64	23.56	24.53	22.44	18.23	13.27	8.716	5.191	2.816	1.387	0.5985	0.1816	···	···	···
	114.73	8.239	12.36	17.00	20.14	20.60	18.45	14.65	10.43	6.716	3.953	2.147	1.078	0.4816	0.1501	···	···	···
	125.39	6.594	9.994	13.73	16.08	16.18	14.20	11.04	7.692	4.871	2.843	1.551	0.7948	0.3670	0.1177	···	···	···
	136.53	4.869	7.507	10.33	11.99	11.88	10.23	7.792	5.328	3.326	1.930	1.060	0.5548	0.2634	0.0868	···	···	···
	148.15	3.310	5.225	7.226	8.335	8.147	6.897	5.155	3.465	2.137	1.236	0.6855	0.3655	0.1775	0.0597	···	···	···
									Photoneutrons									
	40.06	0.1016	0.4584	1.224	2.594	4.701	7.485	10.61	13.51	15.57	16.36	15.77	14.04	11.57	8.872	6.369	4.380	3.114
	46.46	0.1133	0.6185	1.664	3.464	6.124	9.489	13.08	16.19	18.14	18.55	17.42	15.12	12.17	9.110	6.359	4.221	2.876
	53.33	0.1119	0.7924	2.151	4.399	7.583	11.43	15.30	18.40	20.05	19.96	18.29	15.52	12.23	8.963	6.107	3.922	2.560
	60.68	0.0929	0.9609	2.635	5.294	8.898	13.04	16.96	19.82	21.01	20.39	18.26	15.19	11.76	8.471	5.655	3.826	2.207
	68.50	0.0567	1.101	3.049	6.021	9.870	14.07	17.78	20.20	20.86	19.77	17.35	14.19	10.84	7.698	5.054	3.071	1.847
	76.80	0.0086	1.191	3.327	6.458	10.33	14.32	17.61	19.47	19.62	18.20	15.70	12.66	9.364	6.725	4.358	2.590	1.500
	85.57	···	1.217	3.421	6.525	10.19	13.76	16.46	17.74	17.47	15.90	13.52	10.79	8.083	5.641	3.617	2.109	1.181
	94.81	···	1.174	3.309	6.202	9.455	12.44	14.50	15.25	14.71	13.18	11.08	8.769	6.330	4.530	2.879	1.651	0.8953
	104.53	···	1.070	3.012	5.541	8.251	10.58	12.03	12.38	11.72	10.36	8.628	6.792	5.035	3.474	2.190	1.237	0.6516
	114.73	···	0.9226	2.577	4.649	6.761	8.457	9.393	9.473	8.832	7.723	6.387	5.005	3.695	2.536	1.586	0.8831	0.4528
	125.39	···	0.7525	2.071	3.661	5.199	6.349	6.900	6.834	6.290	5.455	4.489	3.504	2.575	1.757	1.089	0.5983	0.2991
	136.53	···	0.5812	1.564	2.702	3.748	4.473	4.763	4.645	4.232	3.649	2.992	2.327	1.701	1.153	0.7079	0.3834	0.1871
	148.15	···	0.4255	1.108	1.869	2.531	2.954	3.089	2.974	2.690	2.311	1.889	1.463	1.063	0.7144	0.4342	0.2319	0.1106

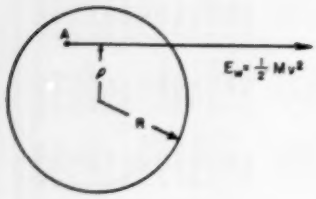

FIG. 3. Path of a photoparticle whose origin is at the point A in the nuclear fluid.

but is likely to collide with other nucleons with the result that the nucleus as a whole is excited. Further, we neglect refraction of the photoparticles in crossing the change in nuclear potential. This means that we neglect distortion of the photoparticle angular distribution developed in the last section, but expect that the energy spectrum will be modified.

The nuclear model considered is a sphere of uniformly distributed nuclear fluid which gives rise to a square potential well. In Fig. 3, we show such a nucleus and the path of a photoparticle whose origin is at the point A. This photoparticle has an angular momentum $Mv\rho$. From the standpoint of quantum mechanics, its square is given by $(Mv\rho)^2=l(l+1)\hbar^2$, where l is an integer. For 100-Mev photoparticles in a carbon nucleus, the largest value of l that occurs is about 8. For photoparticles with energies E_w measured above the bottom of the nuclear well, the yield of photoparticles which escape from the nucleus is given by;

$$I(E_w)=\sum_{l=0}^{l_{\max}} P_l T_l(E_w), \tag{16}$$

where P_l is the probability of occurrence of l, and $T_l(E_w)$ is the probability of escape from the nucleus of photoparticles with energy E_w and angular momentum quantum number l. The upper limit on the summation, $l_{\max}$, is the maximum value of l that occurs with given E_w and nuclear radius R.

The probability $T_l(E_w)$ may be calculated using[25]

$$T_l(E_w)=4S_lKR/[\Delta_l^2+(S_l+KR)^2],$$

where K is the wave number of the particle inside the nucleus associated with the energy E_w, and (Δ_l+iS_l) is the logarithmic derivative of the wave function of the photoparticle evaluated at the nuclear surface. Δ_l and S_l are given in terms of the regular and irregular Coulomb wave function F_l and G_l. The asymptotic expressions for F_l and G_l are respectively the real and imaginary parts of[26]

$$i\exp\{-i[kr-n\ln(2kr)-l\pi/2+\eta_l]\}$$
$$\times g(-l-in, l+1-in, -2ikr),$$

where

$$g(\alpha,\beta,z)=1+\frac{\alpha\beta}{z}+\frac{\alpha(\alpha+1)\beta(\beta+1)}{2!z^2}+\cdots,$$

and

$$\eta_l=\arg\Gamma(l+1+in).$$

The parameter n is defined by $Ze^2/\hbar v$, where v is the velocity of the particle outside the nucleus and k is the associated wave number. Three terms of the above series for $g(-l-in, l+1-in, -2ikr)$ are sufficient for our use as the expansion parameter $z=-2ikr$ evaluated at the nuclear radius R is large for the values of k encountered. Numerical substitutions in the resulting expression for T_l may be compared with the results obtained using the tables of Coulomb wave functions of Bloch *et al.*[27] In a particular case which provides a severe test of our formula for T_l, it is found that our results are a few percent high[28] for $l=0$ and $l=1$.

Since several values of l occur in the sum in Eq. (16), the sum may be approximated by an integral over ρ, where $(Mv\rho)^2=l(l+1)\hbar^2$ is used. Equation (16) becomes

$$I(E_w)\cong\int_0^R P(\rho)T(\rho,E_w)d\rho, \tag{17}$$

where $T(\rho,E_w)$ is $T_l(E_w)$ in which $l(l+1)$ has been replaced by $(Mv\rho/\hbar)^2$. The function $P(\rho)d\rho$ is the probability that ρ lies between ρ and $\rho+d\rho$.

Since the nucleons comprising the nucleus are assumed to be distributed uniformly within a sphere of radius R, we see that $P(\rho)=(3/R^3)\rho(R^2-\rho^2)^{\frac{1}{2}}$. There is a value ρ_0 of ρ at which the total Coulomb plus centrifugal barrier is equal to the laboratory energy $E_L=E_w-V$ of the photoparticle. For $R>\rho>\rho_0$, the penetrability $T(\rho,E_w)$ is small, and it can be shown[29] that for cases of interest, the contribution of the integral (17) from this region is small also and may be neglected. The integration may be done exactly and gives the average transmission probability for photoneutrons and photoprotons formed in the nucleus. Numerical work based on the resulting formula is given

TABLE II. Average proton barrier penetration probabilities for the carbon nucleus calculated by using a nuclear potential well depth of 40 Mev and 3.2×10^{-13} cm for the radius of the carbon nucleus.

Lab proton energy E_L (Mev)	Average penetration probability
10	0.5953
20	0.7924
30	0.8675
40	0.9052
50	0.9280
60	0.9425
70	0.9525
80	0.9600
90	0.9654
100	0.9661

[25] Reference 12, p. 360.
[26] Reference 11, p. 116.
[27] Block, Hull, Broyles, Bouricius, Freeman, and Breit, Revs. Modern Phys. **23**, 147 (1951).
[28] There is an error in Fig. 5.3 (p. 363) in reference 12. The T_l are shown much too small.
[29] See reference 17, p. 66.

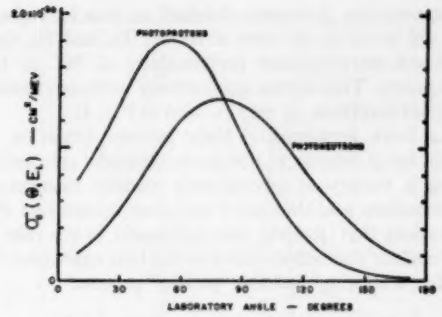

FIG. 4. The theoretical angular distributions of photoprotons and photoneutrons with laboratory energies $E_L=23.6$ Mev, from carbon irradiated by 75-Mev photons.

in Table II in the case of the carbon nucleus with a nuclear potential well depth of 40 Mev.

V. NUMERICAL RESULTS

The cross section $\sigma(\Theta,E_w)$ given by Eqs. (8) and (13) has been evaluated numerically in the case of the Gaussian ground state nucleon momentum distribution, where the $1/e$ value occurs at 16 Mev. The numerical work[20] is done for four photon energies, *viz.*, 50, 75, 100, and 125 Mev. For each photon energy, the cross section is evaluated at 10° intervals in the laboratory coordinate system and at a variety of values of the photoparticle energy E_w which is the energy taken with the bottom of the nuclear potential well as a reference. The results are presented in Table I and give the value of $v\sigma(\Theta,E_w)$, where v is the nuclear volume. These results are not intended to be descriptive of the photoeffect for a particular nuclide except where the Gaussian ground-state nucleon distribution parameters chosen ($1/e$ value at 16 Mev) represent to a better approximation the momentum distributions in some nuclides than others.

In applying the results of Table I to a particular nucleus, we must divide by the nuclear volume v which may be taken as $(4\pi/3)R^3$, where we may use $R=r_0A^{\frac{1}{3}}$, in which $r_0=1.4\times10^{-13}$ cm and A is the mass number. It is then necessary to multiply by NZ, the number of quasi-deuterons in the nucleus, since the calculation of Sec. III was done for one quasi-deuteron. Finally, the result must be multiplied by the escape probability calculated in Sec. IV.

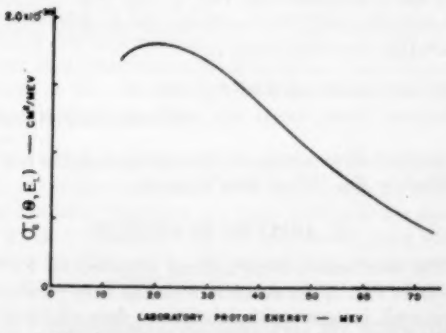

FIG. 5. The theoretical energy spectrum of photoprotons from carbon irradiated by 75-Mev photons. The yield is taken at a laboratory angle of 60°.

[20] The numerical work was performed on the I.B.M. Card-Programmed Calculator of the Stanford Computation Center.

As an example of the use of the tables, consider the photoeffect in carbon irradiated by 75-Mev photons. We calculate the angle distributions of 23.6-Mev photoprotons and photoneutrons and the energy distribution of photoprotons at the laboratory angle of 60°. The results are given in Figs. 4 and 5, respectively. To obtain the angle distributions of Fig. 4, we enter Table I with a photon energy of 75 Mev, and with an E_w value of $(40+23.6)=63.6$ Mev for both photoprotons and photoneutrons. The tabulated values are then multiplied by $(NZ/v)=2.61\times10^{38}$ cm^{-3}. In the case of protons, we then multiply by the value of the proton barrier penetration probability (0.825) which is obtained by graphically interpolating between values given in Table II. For neutrons, we multiply by (0.875) which is the appropriate barrier penetration probability. The energy distribution of 60° photoprotons of Fig. 5 is obtained from Tables I and II in essentially the same way.

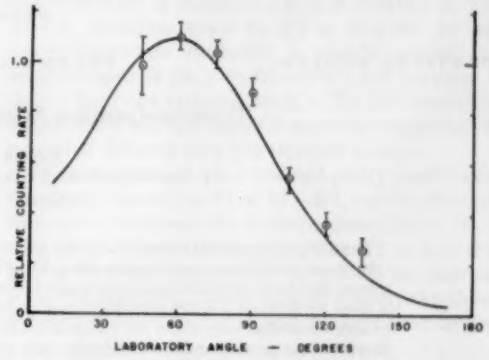

FIG. 6. Experimental data of Johansson[21] showing the yield of photoprotons with energies greater than 14 Mev obtained from carbon irradiated by the bremsstrahlung beam from a betatron operating at 65 Mev. The smooth curve is the calculated yield of 13.3-Mev photoprotons from carbon irradiated by 50-Mev photons. The normalization is at 60°.

VI. DISCUSSION

Experimental data which allow a detailed check of the calculations presented here are not available at present. In most experiments, the bremsstrahlung beam from a betatron or electron synchrotron is used and so the photoparticle yield is from many photon energies. The experimental apparatus of Weil and McDaniel[5] counts only those events due to 190-Mev photons out of a bremsstrahlung beam, and any data that may be taken in the future using a method such as theirs should

be very helpful in making a critical evaluation of our photoeffect calculations.

No numerical work was done at photon energies as high as 190 Mev and so comparison with the data of Weil and McDaniel is not possible. The bremsstrahlung experiment of Johansson[21] at 65 Mev is of interest since both photoneutrons and photoprotons which had reasonably well defined laboratory energies were observed. The angular distribution of the yield of photoprotons having energies greater than 14 Mev from carbon as observed by Johansson is shown in Fig. 6. By way of comparison, there is shown also on Fig. 6, our calculated results for 13.3-Mev photoprotons from carbon irradiated by 50-Mev photons. The two curves are normalized at 60° laboratory angle. In the case of photoneutrons, Johansson obtained no data for carbon, but did notice in the cases of Be, Al, Ta, and Tb, that neutrons were emitted preferentially at 90° in the laboratory. This agrees qualitatively with our results for photoneutrons, as may be seen in Fig. 4.

As more experimental data become available, it might be of interest to test deuteron-model calculation using a variety of ground-state nucleon momentum distributions and then see if the same momentum distributions that give the best agreement in the case of the nuclear photoeffect also give the best agreement for proton scattering[7] and the "pickup" process.[9]

[21] S. A. E. Johansson, Phys. Rev. **97**, 434 (1955).

ACKNOWLEDGMENTS

I wish to thank Professor L. I. Schiff for his very helpful advice in many parts of this calculation.

PHYSICAL REVIEW VOLUME 100, NUMBER 1 OCTOBER 1, 1955

Gamma-Gamma Angular Correlation in Ba^{134}

ERNEST D. KLEMA
Oak Ridge National Laboratory, Oak Ridge, Tennessee
(Received May 20, 1955)

The directional angular correlation of the 1367–605 kev γ-γ cascade in Ba^{134} has been measured with a coincidence scintillation spectrometer using NaI detectors. For a dilute cesium chloride aqueous solution source, the observed correlation function, after correcting for the finite angular resolution of the detectors, is given by $W(\theta)=1+(0.090\pm0.0086)P_2(\cos\theta)-(0.004\pm0.013)P_4(\cos\theta)$. From this result it is not possible to assign unambiguously a spin and parity to the 1972-kev level in Ba^{134}, from which the cascade originates. However, the present angular correlation data taken with internal conversion coefficient data for the transitions from this level indicate that it very probably has spin 3 and odd parity.

I. EXPERIMENTAL RESULTS

THE directional angular correlation of the 1367–605 kev γ-γ cascade in Ba^{134} has been measured with a coincidence scintillation spectrometer using NaI detectors in a series of 5 experiments with a total of 1.1×10^5 coincidence counts taken at 19 angular positions. The source was a dilute aqueous solution of cesium chloride.

The data were obtained as discussed previously[1] and were analyzed following the paper of Rose.[2] The γ-ray spectrum of the cesium chloride source is shown in Fig. 1. Each point on the curve out to a pulse height of 810 units contains 4096 counts, and the points for greater pulse heights contain 1024 counts each. The windows of the differential pulse-height analyzers were placed, as shown in Fig. 1, so that one was set on the full-energy peak of the 605-kev γ ray and the other accepted only the full-energy peak of the 1367-kev γ ray. Since the latter γ ray is the highest-energy one of the source, the measurement of the angular correlation of the 1367–605 kev cascade is a clean one and needs no correction for interference by the other cascades.

The true coincidence counting rate for the present experiment was of the order of 3.5×10^{-2} count/sec and the random rate was 15% of this. The correlation function obtained, after correcting for the finite angular resolution of the detectors, is

$$W(\theta)=1+(0.090\pm0.0086)P_2(\cos\theta)-(0.004\pm0.013)P_4(\cos\theta).$$

The errors given above are the standard deviations as defined by Eq. (30) of Rose's[2] paper.

II. ANALYSIS OF RESULTS

The most recent decay scheme proposed for Cs^{134} is given in Fig. 2.[3] In contrast with the ones previously advanced, it agrees with coincidence data obtained at this laboratory and with the relative intensities of the γ rays as measured by scintillation spectrometry here.[4]

[1] E. D. Klema and F. K. McGowan, Phys. Rev. **91**, 616 (1953).
[2] M. E. Rose, Phys. Rev. **91**, 610 (1953).
[3] Keister, Lee, and Schmidt, Phys. Rev. **97**, 451 (1955).
[4] R. C. Davis, private communication.

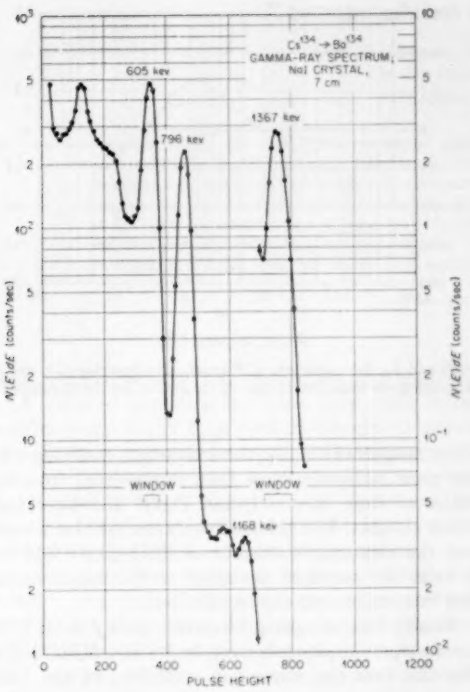

FIG. 1. Gamma-ray spectrum of the cesium chloride source. The brackets represent the positions of the windows of the differential pulse-height analyzers for the present experiment.

In the analysis of the present data, we consider spins 2, 3, 4, and 5 for the energy level at 1972 kev. We do this because there is no spin and parity assignment for this level which is consistent with all the experimental information, and we wish to point out what possible spins can be eliminated on the basis of angular correlation measurements alone. The 605-kev transition is known to be predominantly $E2$ radiation.[5] The lifetime of the 605-kev intermediate state of the cascade has been measured to be less than 3×10^{-9} sec.[6,7] Thus, it is probably a good assumption that the correlation is not affected by external fields and that the measurement yields the unperturbed correlation function.

The correlation functions expected theoretically, as calculated from the tables of Biedenharn and Rose,[8] if the 1367-kev transition is a pure multipole are shown in Table I. It is seen that the only one of these which cannot be ruled out by the present data is the one for the sequence $4(Q)2(Q)0$. If one assigns even parity to

[5] B. L. Robinson and L. Madansky, Phys. Rev. **84**, 604 (1951).
[6] R. E. Bell and H. E. Petch, Phys. Rev. **76**, 1409 (1949).
[7] *Note added in proof.*—A recent measurement by V. Z. Wintersteiger, [Bull. Inst. Nuclear Sci. "Boris Kidrich" (Belgrade) **4**, 79 (1954)] has shown the half-life to be less than 5×10^{-10} sec.
[8] L. C. Biedenharn and M. E. Rose, Revs. Modern Phys. **25**, 729 (1953).

TABLE I. Angular correlation coefficients A_2 and A_4 in $W(\theta)=1+A_2P_2(\cos\theta)+A_4P_4(\cos\theta)$ for the various sequences indicated.

Sequence	A_2	A_4
$2(D)2(Q)0$	0.2500	0
$2(Q)2(Q)0$	−0.0766	0.3264
$3(D)2(Q)0$	−0.0714	0
$3(Q)2(Q)0$	−0.2041	−0.0816
$4(Q)2(Q)0$	0.1020	0.0091
$4(O)2(Q)0$	−0.2678	0.0317
$5(O)2(Q)0$	0.1786	−0.0043

the 1972-kev level, the 1168-kev transition would be $E3$ or $E3+M4$ and the expected conversion coefficient for this transition would be far from that measured experimentally, as shown in Fig. 5 of reference 3. The 569-kev transition would be $M1$ or $E2+M1$. Its observed conversion coefficient is slightly outside the limits of those for the pure $E2$ and $M1$, but the value is nearly that to be expected for $M1$. The 1367 transition would be $E2$, and the observed conversion coefficient is somewhat different from the expected value.

The assignment of spin 4 and odd parity would make the 569-kev transition $E1$ or $E1+M2$, and its observed conversion coefficient lies between these limits. However, the 1168-kev transition would be $M3$ or $E4+M3$, and its observed coefficient is far outside of those expected for this case. Thus it is quite unlikely the above sequence is the correct one, and we next consider the

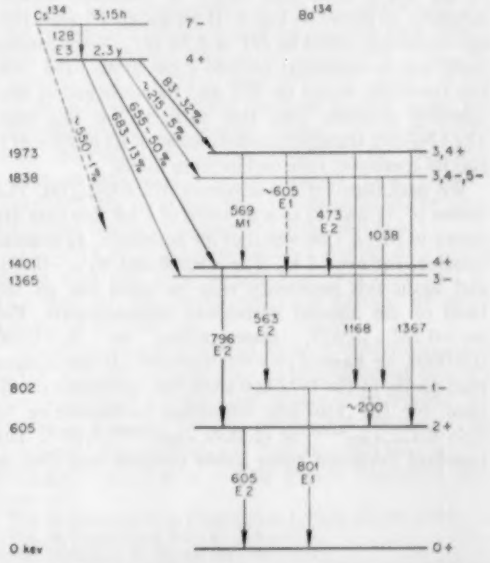

FIG. 2. Proposed decay scheme for Cs^{134} as given by Keister, Lee, and Schmidt, Phys. Rev. **97**, 451 (1955). The present data, taken with internal conversion data given in the above paper, indicate that the 1972-kev level very probably is 3^-.

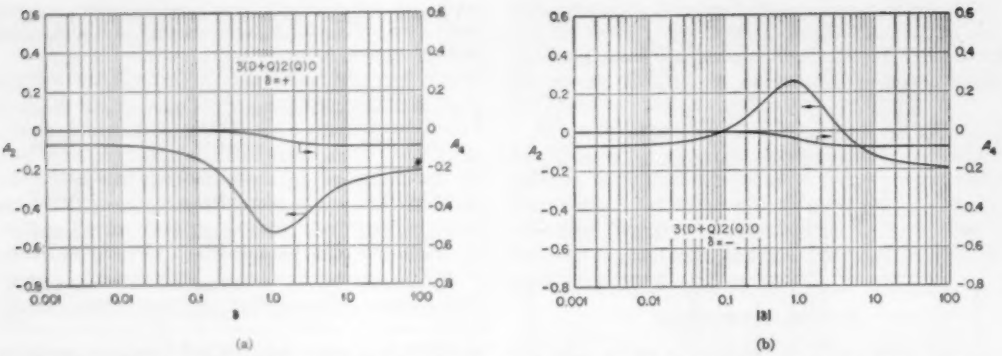

FIG. 3. Angular correlation coefficients, A_2, the coefficient of $P_2(\cos\theta)$ and A_4, the coefficient of $P_4(\cos\theta)$, as a function of δ, the mixing ratio giving the square root of the ratio of the intensity of the quadrupole radiation to that of the dipole, for the sequence $3(D+Q)2(Q)0$. (a) $\delta=+$; (b) $\delta=-$.

1367-kev transition to be mixed with spins 2 or 3 for the 1972-kev level.

For the sequence $2(D+Q)2(Q)0$ with δ positive, where δ^2 is the ratio of the intensity of the quadrupole radiation to the intensity of the dipole radiation, a value of A_2, the coefficient of $P_2(\cos\theta)$ in $W(\theta)$, of $+0.09$ corresponds to a value of A_4 of 0.31, and this possibility can be ruled out. For $\delta=-0.210_{-0.009}{}^{+0.012}$, corresponding to $A_2=0.090\pm0.0086$, we have $A_4=0.015\pm0.002$. This assignment cannot be ruled out on the basis of the angular correlation measurement. However, if we make the assignment 2^+ for the 1972-kev state, the intensity of the beta decay to it would be expected to be far lower than that which is measured experimentally, as shown in Fig. 1. If we assign 2^-, the 1168-kev transition would be $M1$ or $E2+M1$; its conversion coefficient is somewhat outside these limits. The 569-kev transition would be $M2$, and its coefficient is considerably different from that expected for this case. The 1367-kev transition would consist of $E1$ or $E1+M2$, and its coefficient falls within these limits.

We next consider the sequence $3(D+Q)2(Q)0$. The curves of A_2 and A_4 as a function of δ for this case are shown in Fig. 3. One sees that for positive δ, A_2 is never positive. For $\delta=-2.45$, $A_2=-0.090$ and $A_4=-0.070$, and again this possibility may be ruled out on the basis of the angular correlation measurements. For $\delta=-0.222_{-0.015}{}^{+0.011}$, corresponding to $A_2=0.090\pm0.0086$, we have $A_4=-0.004\pm0.001$. If one assigns even parity to the 1972-kev level, the conversion coefficient for the 1367-kev transition corresponding to $\delta=-0.222_{-0.015}{}^{+0.011}$ is $(1.1639_{-0.0076}{}^{+0.0071})\times10^{-3}$. The standard deviation given above includes only that of the measurement of A_2; the conversion coefficients for the pure multipoles have been interpolated from the tables of Rose, Goertzel, and Perry[9] and have been taken as exact. The difference between the above value and the measured coefficient of $(0.55\pm0.10)\times10^{-3}$ is 6 times the standard deviation of the measurement, and this assignment can be ruled out.

Finally if one assigns spin 3 and odd parity to the 1972-kev level, the sequence is given by $3^-(E1+M2)2^+(E2)0$. For this case the conversion coefficient of the 1367-kev transition corresponding to $\delta=-0.222_{-0.015}{}^{+0.011}$ is $(0.482_{-0.010}{}^{+0.012})\times10^{-3}$. This agrees with the measured value of $0.55\pm0.10\times10^{-3}$. On this assignment, the 569-kev transition is $E1$ or an $E1+M2$ mixture, and the value of δ^2 that corresponds to its observed conversion coefficient[3] of $10.5\pm1.6\times10^{-3}$ is 0.520 ± 0.093. The 1168-kev transition is $E2$ for this assignment. Its observed conversion coefficient is quite close to that expected for $E2$ radiation, the difference between the observed value and the theoretical value being less than twice the standard deviation of the measurement.

The above assignment of 3^- for the 1972-kev level and an $E1+M2$ mixture with $\delta=-0.222_{-0.015}{}^{+0.011}$ for the 1367-kev transition fits best all the experimental evidence, and it is concluded that it is probably correct.

III. ACKNOWLEDGMENTS

It is a pleasure to acknowledge the assistance of Wilma Stair, who transcribed the data from the tapes for the least-squares fittings.

[9] Rose, Goertzel, and Perry, Oak Ridge National Laboratory Report ORNL-1023 (unpublished).

Neutron-Induced Reactions in Fluorine*

JERRY B. MARION† AND ROBERT M. BRUGGER‡
The Rice Institute, Houston, Texas

(Received June 13, 1955)

By measuring the radioactivity produced when F^{19} is bombarded with monoenergetic neutrons, the excitation functions and absolute cross sections have been obtained for the $F^{19}(n,\alpha)N^{16}$ and $F^{19}(n,p)O^{19}$ reactions from energies at which the respective activities were first observed to 8.0 Mev. The occurrence of the (n,α) reaction was first observed at a bombarding energy of 3.1 Mev; the (n,p) reaction was first observed at 4.7 Mev. Several resonances were found in the (n,α) excitation function, while the (n,p) excitation function showed a single maximum at 7.5 Mev. For neutron energies up to 8.0 Mev, the (n,α) reaction cross section is larger than that for the (n,p) reaction by a factor of 2 or greater.

INTRODUCTION

MEASUREMENTS of the neutron total cross sections of most elements have been made in the neutron energy range from thermal energies to several Mev. These experiments are usually of the transmission type, and, consequently, it is not possible to deduce the process by which removal from the beam has occurred. Therefore, it is of interest to obtain the magnitudes of the individual contributions to the cross section. The total cross section is the sum of the elastic, inelastic, and reaction cross sections. For neutrons of energies less than about 20 Mev, the reaction cross section is composed of processes of the type (n,γ), (n,α), (n,p), and $(n,2n)$. Radiative capture is important only for low-energy neutrons, and $(n,2n)$ reactions are usually energetically impossible for neutrons of energies less than about 10 Mev. For neutrons in the energy range of a few Mev, (n,α) and (n,p) reactions are the most common neutron-induced reactions.

The excitation functions and absolute cross sections have been obtained[1–9] for the (n,p) reactions on N^{14}, O^{16}, Al^{27}, P^{31}, and S^{32}, and for the (n,α) reactions on Li^6, Be^9, B^{10}, N^{14}, Ne^{20}, and S^{32}. A preliminary report has been given[10] on the excitation function for the $F^{19}(n,\alpha)N^{16}$ reaction. Paul and Clarke[11] have measured the cross sections for (n,p), (n,α), and $(n,2n)$ reactions on many elements at a neutron energy of 14.5 Mev. Lillie[12] has studied the (n,p) and (n,α) reactions in oxygen and nitrogen at 14.1 Mev.

A common method of obtaining (n,p) and (n,α) reaction excitation functions is by observing, as a function of neutron energy, the pulse-height distribution in a gas counter filled with a gas that contains the nucleus to be used as a target. In some cases this is not convenient, and the reactions $O^{16}(n,p)N^{16}$, $Al^{27}(n,p)Mg^{27}$, $P^{31}(n,p)Si^{31}$, and $F^{19}(n,\alpha)N^{16}$ have been studied by observing the induced radioactivity as a function of neutron energy.

Resonances in the reaction $F^{19}(n,\alpha)N^{16}$ were first observed by Wilhelmy,[13] who bombarded an SF_6-filled ionization chamber with Po-Be and Rn-Be neutrons and observed the pulse height spectra. Peaks due to reactions on S and peaks caused by maxima in the energy distribution of the neutron sources were identified by performing the same experiment with the chamber filled with SO_2. The continuous nature of the energy spectra from these neutron sources made the interpretation of the results difficult; however, peaks were observed which, when corrected for the most recent determination of the Q-value for the $F^{19}(n,\alpha)N^{16}$ reaction,[14] can be attributed to resonances in the cross section at neutron energies of 4.4 and 4.9 Mev.

The $F^{19}(n,p)O^{19}$ reaction has been studied only to the extent that the cross section has been measured at 14.5 Mev. At this energy, Paul and Clarke[11] obtained a value of 135 ± 50 mb.

Since the half-life of N^{16} is 7.35 sec,[2,15] the observation of the induced radioactivity as a function of neutron energy provides a convenient means of examining the excitation function for the $F^{19}(n,\alpha)N^{16}$ reaction. The Q-value for this reaction is -1.49 Mev and that for the $F^{19}(n,p)O^{19}$ reaction is -4.00 Mev.[14] Therefore, the

* Supported by the U. S. Atomic Energy Commission.

† National Science Foundation Predoctoral Fellow; now Postdoctoral Fellow, Kellogg Radiation Laboratory, California Institute of Technology, Pasadena, California.

‡ Humble Oil and Refining Company Fellow in Physics; now at Phillips Petroleum Company, Atomic Energy Division, Idaho Falls, Idaho.

[1] C. H. Johnson and H. H. Barschall, Phys. Rev. **80**, 818 (1950).

[2] H. C. Martin, Phys. Rev. **93**, 498 (1954).

[3] R. L. Henkel, "Neutron cross sections," Atomic Energy Commission Report AECU-2040 (Technical Information Division, Department of Commerce, Washington, D. C., 1952), Supplement 3, 1954.

[4] R. Ricamo, Nuovo cimento **8**, 383 (1951).

[5] T. Hürlimann and P. Huber, Helv. Phys. Acta **28**, 33 (1955).

[6] F. L. Ribe, Phys. Rev. **87**, 205(A) (1952); Phys. Rev. **91**, 426(A) (1953).

[7] Allen, Burcham, and Wilkinson, Proc. Roy. Soc. (London) **A192**, 114 (1947).

[8] Petree, Johnson, and Miller, Phys. Rev. **85**, 155 (1952).

[9] Johnson, Bockelman, and Barschall, Phys. Rev. **82**, 117 (1951).

[10] Bostrom, Hudspeth, and Morgan, Phys. Rev. **99**, 643(A) (1955).

[11] E. B. Paul and R. L. Clarke, Can. J. Phys. **31**, 267 (1953).

[12] A. B. Lillie, Phys. Rev. **87**, 716 (1952).

[13] E. Wilhelmy, Z. Physik **107**, 769 (1937).

[14] F. Ajzenberg and T. Lauritsen, Revs. Modern Phys. **27**, 77 (1955).

[15] Bleuler, Scherrer, Walter, and Zünti, Helv. Phys. Acta **20**, 96 (1947).

(n,α) reaction can be investigated up to a neutron energy of about 4.2 Mev before the (n,p) reaction becomes possible. The half-life of O^{19} is 29 sec.[16] This is close enough to that for N^{16} so that precautions must be taken when attempting to determine the amount of N^{16} activity present at neutron energies above 4.2 Mev, and yet it is sufficiently long to make possible the separation of the two activities with little difficulty. The $(n,2n)$ reaction is not possible for neutron energies below 10.7 Mev and was not encountered in these experiments.

By observing the N^{16} and O^{19} activities produced when F^{19} is bombarded with monoenergetic neutrons from the p-T and d-d reactions, it has been possible to obtain the excitation functions and absolute cross sections for the $F^{19}(n,\alpha)N^{16}$ and $F^{19}(n,p)O^{19}$ reactions from energies at which the activities were first observed up to 8.0 Mev.

SAMPLE AND DETECTOR

In the investigation of neutron-induced reactions, it is desirable to have as large a neutron flux as possible and the greatest possible detection efficiency for measuring the effects of the reactions. If a charged-particle reaction is used as a neutron source, the size of the neutron flux is limited by the energy spread that can be tolerated and by the available charged-particle beam intensities. In order to obtain the largest possible number of target nuclei per cm^3, a solid, fluorine-containing sample was used in these experiments. The greatest possible efficiency for the detection of reactions produced in solid samples results when the sample and the detector are identical. In this manner a 4π geometry is obtained and the efficiency for the detection of decay electrons from induced radioactivity can be made almost 100% by biasing the detector to respond to all pulses greater than a certain small value. In order to investigate the neutron-induced radioactivity in F^{19}, a CaF_2 crystal was used. This crystal was found to be satisfactory both as a sample and as a detector.

The crystal was a 1 in. diam×1 in. cylinder of unactivated CaF_2 which was encased in a thin aluminum container. The inner surface of the aluminum was coated with MgO, which acted as a light reflector. Since CaF_2 fluoresces in the ultraviolet region, it was necessary to use a photomultiplier tube with a quartz window. An EMI 6255 tube with a 1 in.×1 in. photocathode surface was found to be quite satisfactory. Optical contact between the crystal and the quartz window was made with a thin layer of silicone fluid. The associated electronics were of the conventional type.

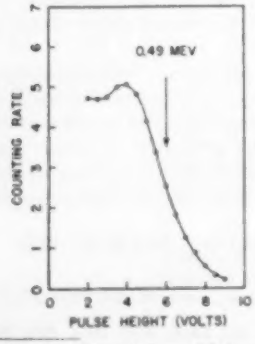

FIG. 1. Pulse-height distribution for the Cs^{137} γ ray that was obtained with the CaF_2 crystal. A channel width of 1 volt was used.

An energy calibration was obtained by observing the pulse-height distribution from the Cs^{137} gamma ray. This curve is shown in Fig. 1. Since the crystal contains elements of low Z, only a Compton scattering peak is prominent. The point at which the counting rate was one-half of the peak counting rate was taken to correspond to the maximum energy of the Compton electrons, 0.49 Mev, and is indicated by the arrow in Fig. 1. By comparing the pulse height of the Compton peaks obtained with the CaF_2 crystal and with a NaI crystal under the same conditions, the pulse height from CaF_2 was found to be smaller by a factor of 10 than that from NaI.

NEUTRON SOURCES

Neutrons of energies up to 4.9 Mev were obtained from the proton bombardment of a tritium target. This target [manufactured at the Oak Ridge National Laboratory, Oak Ridge, Tennessee] was prepared by absorbing tritium gas in a layer of zirconium metal evaporated onto a $\frac{3}{4}$ in. diam tungsten blank. The active area was $\frac{5}{8}$ in. in diameter. The target thickness was about 20 kev to 5-Mev protons. Although the target backing was cooled by an air stream, beam currents of less than 2 microamperes were used in order to prevent undue heating and possible loss of tritium. No indication of a decrease in the neutron flux was obtained over long periods of bombardment with 2 microamperes of 5-Mev protons.

With the p-T neutron source, an energy resolution of about 30 kev was obtained by placing the face of the CaF_2 sample-detector at a distance of 6 inches from the source. At a distance of 2.5 inches, the energy spread was increased to about 60 kev due to the decrease in neutron energy at the larger angles. Excitation functions were measured with the p-T source for both of these geometries.

The d-d reaction was used to produce neutrons of energies from 4.6 to 8.0 Mev. A gas deuterium target was used which was constructed from a $\frac{1}{2}$ in. diam ×1.5 in. platinum tube. The beam entered the target chamber through a $\frac{1}{4}$ in. hole which was covered with a 2.79 mg/cm^2 nickel foil. Deuterium pressures of about 10 inches of Hg were used. No decrease in pressure was observed over prolonged periods of bombardment with 2 microamperes of deuterons. With the face of the CaF_2 crystal placed at a distance of 2 inches from the

[16] A. M. Feingold, Revs. Modern Phys. 23, 10 (1951).

center of the target chamber, the total spread in neutron energy, resulting from the gas thickness, straggling in the foil, and the finite solid angle, amounted to about 100 kev.

EXPERIMENTAL PROCEDURE

Since N^{16} has a relatively short half-life, the simplest procedure for measuring the relative amounts of activity produced at different bombarding energies is to count the saturation activity during bombardment. This is made possible by the occurrence of high-energy electrons in the N^{16} decay scheme; 18% of the decays go to the ground state of O^{16} with a maximum electron energy of 10.4 Mev.[15] In order to discriminate against γ rays from inelastic neutron scattering, electrons from the radioactive decay of the nuclei produced in the (n,p) and (n,α) reactions on the aluminum container, the Ca of the crystal, and the Si of the phototube, and general background, the counter bias was set so that the pulse-height analyzer would respond only to those pulses corresponding to an energy greater than about 7.5 Mev. After saturation activity was reached, the number of counts was recorded for a given amount of charge collected at the neutron-producing target. The beam current was maintained constant to within 10 percent during both the buildup and counting periods. Changes in the counting rate caused by the small variations in the beam current were essentially averaged out by recording the number of counts obtained over a period of about 20 half-lives. In this manner it was possible to obtain a relative excitation function for the $F^{19}(n,\alpha)N^{16}$ reaction up to a neutron energy of 4.9 Mev, the maximum energy obtained from the p-T source.

When using the d-d reaction as the neutron source, it was not possible to continue the excitation function in the manner described above since the deuteron bombardment of the nickel foil of the gas target chamber produced γ-ray pile-up in the crystal to a pulse height greater than that obtained from the maximum-energy electrons. It was necessary, therefore, to determine the yield of radioactivity by observing the counting rate after the beam was cut off.

At each bombarding energy the N^{16} and O^{19} activities were allowed to reach equilibrium by bombarding for at least 4 minutes. At the end of this time, the deuteron beam was cut off by a compressed air-operated tantalum cup placed at a distance of about 8 feet from the deuterium target. As soon as the beam was stopped, a counting cycle was begun. This entailed counting the activity and then recording the data in alternate 10-sec intervals. To carry out this counting procedure, the bias was set so that the pulse-height analyzer would respond to all pulses corresponding to an energy greater than about 150 kev. Thus, it was possible to count essentially all of the decay electrons from both the N^{16} and O^{19} nuclei. A typical decay curve, taken at a neutron energy of 6.30 Mev, is shown in Fig. 2. The 2.3-min activity is due to the Al^{28} produced in the (n,p) reaction on the Si^{28} content of the phototube. The 9.6-min activity from the $Al^{27}(n,p)Mg^{27}$ reaction and the longer-lived activities from the (n,p) and (n,α) reactions on calcium do not appreciably affect the decay curve over the relatively short time interval for which observations were made. Subtraction of the 2.3-min activity revealed the 29-sec activity of O^{19}, and the subtraction of both of these activities left the 7.3-sec activity of N^{16}. At all bombarding energies for which the decay curve technique was used, the N^{16} activity was sufficiently intense to allow the decay to be followed for at least 7 half-lives in spite of the other activities which were present. At 6.30 Mev, for example, 75 percent of the initial activity was due to N^{16}. The extrapolation of the individual decay curves to the time at which the beam was turned off allowed the saturation activity to be determined. The decay curves were taken at approximately 100 kev intervals over the range of neutron energies from 4.6 to 8.0 Mev. Since there was some uncertainty in extrapolating the decay curves to zero time, the relative excitation functions obtained with the d-d source are probably accurate only to 10–15 percent.

Since the excitation functions obtained with both neutron sources were taken with respect to the beam current, these curves were corrected for the p-T and d-d cross sections. The p-T yield curve used was that

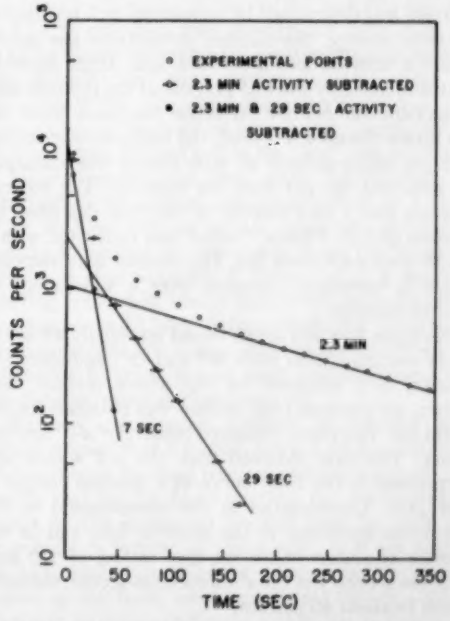

FIG. 2. Decay curve of the radioactivity induced in the CaF_2 crystal when bombarded by 6.30-Mev neutrons. Activities due to N^{16} (7 sec), O^{19} (29 sec), and Mg^{27} (2.3 min) are shown.

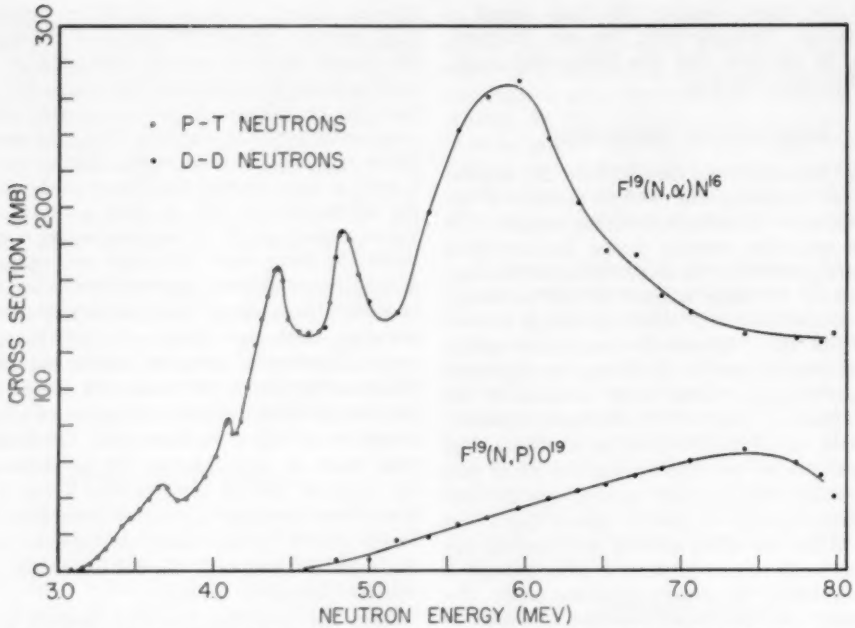

FIG. 3. Excitation functions and absolute cross sections for the reactions $F^{19}(n,\alpha)N^{16}$ and $F^{19}(n,p)O^{19}$. The energy resolution for the points obtained with the p-T neutron source is about 60 kev; for those obtained with the d-d source, the resolution is about 100 kev.

measured by Jarvis and Perry.[17] The curve for the d-d reaction was determined by measuring, as a function of deuteron energy, the number of neutrons per microcoulomb emitted into a forward solid angle equal to that subtended by the CaF_2 crystal at the position used to measure the relative excitation functions. Since the gas target chamber was used, the background counting rate per microcoulomb at each energy was measured by removing the gas from the chamber. The neutron detector was a long counter of the type described by Hanson and McKibben,[18] which was calibrated with a Ra-Be source of known flux. This counter has a response which is essentially constant over a wide range of neutron energies.

Since the bias was set to record essentially all of the decay electrons from both N^{16} and O^{19}, and since the neutron flux, obtained by the above method, was known, an absolute cross section was obtained for the excitation functions measured with the d-d neutron source. The data obtained with the p-T source was normalized to the (n,α) curve at a neutron energy of 4.86 Mev. Uncertainties in the measurement of the saturation activities, in the neutron flux, and in the number of counts below the bias setting of 150 kev, limit the accuracy of the absolute cross-section measurements to about 40 percent.

[17] G. A. Jarvis and J. E. Perry (unpublished).
[18] A. O. Hanson and J. L. McKibben, Phys. Rev. 72, 673 (1947).

To insure that the effects observed with the p-T source by counting the saturation activity during bombardment were due entirely to the $F^{19}(n,\alpha)N^{16}$ reaction, the neutron energy region accessible with p-T neutrons was reinvestigated in the following manner. A 1.5 in. diam$\times\frac{1}{4}$ in. cylinder of Teflon $[(CF_2)^n]$ was mounted on an anthracene crystal of the same diameter and $\frac{7}{16}$ in. in length. The Teflon was bombarded until saturation of the N^{16} activity was reached. After turning off the beam, the amount of activity was counted for 8 sec. Accurate reproduction of the time intervals was made possible by using a mechanical timer. In order to discriminate against any activity that might be present due to the (n,p) reaction, a bias setting equal to the energy of the maximum energy electrons in the O^{19} decay (4.8 Mev) was used. The excitation function so obtained reproduced in detail that measured with the previous technique, although the statistics were somewhat poorer. Since the only materials common to the two techniques were the fluorine and the silicon of the phototube, with its induced radioactivity of low energy, it was concluded that the effects observed were due only to the $F^{19}(n,\alpha)N^{16}$ reaction.

RESULTS

The excitation functions and absolute cross sections obtained in the manner described above for the reactions $F^{19}(n,\alpha)N^{16}$ and $F^{19}(n,p)O^{19}$ are shown in

Figs. 3 and 4. The data obtained with the p-T source shown in Fig. 3 were taken with the geometry that produced an energy spread of about 60 kev. Resonances are indicated at 3.70, 4.11, 4.42, and 4.86 Mev. A re-examination of this energy region was made with an energy resolution of 30 kev and the results are presented in Fig. 4. This data shows the peak observed at 3.70 Mev with the 60-kev resolution decomposed into at least 3 narrower resonances. The indication of structure on the low-energy side of the 3.70-Mev resonance (Fig. 3) appeared again in the 30-kev resolution data near an energy of 3.4 Mev. No 7.3-sec activity was observed below a neutron energy of 3.1 Mev.

The measurements made with the p-T and d-d sources overlap for neutron energies from 4.6 to 4.9 Mev and both sets of data indicate the resonance at 4.86 Mev. At higher energies, an additional maximum was observed with d-d neutrons at 5.9 Mev. It is probable that a number of resonances observed by Bostrom *et al.*[10] near 6 Mev are included in the broad resonance at 5.9 Mev. Since the energy resolution was about 100 kev for the d-d neutrons, only the gross structure of the excitation function could be detected. The resonance energies and peak cross sections are summarized in Table I.

For neutron energies above 4.7 Mev, 29-sec activity corresponding to the occurrence of the $F^{19}(n,p)O^{19}$ reaction was observed. The O^{19} yield was observed to increase smoothly up to a neutron energy of 7.5 Mev. Above this energy the yield decreased up to the maximum bombarding energy used. At the 7.5-Mev peak, the cross section for the (n,p) reaction is only one-half of that for the (n,α) reaction. The (n,p) excitation function shows no indication of the broad resonance at 5.9 Mev that was observed in the (n,α) reaction.

DISCUSSION

When a target nucleus is bombarded by neutrons with an energy of several Mev, compound nucleus formation may take place with many different values of the neutron angular momentum. Therefore, it is possible to form states of the compound nucleus with a wide range of J-values. Since these states are highly excited, the levels will be broad and overlapping. Neutron emission from such states is highly favored over other modes of decay, and, consequently, the resonance structure of the total cross section, evident for low-energy neutrons, is not prominent for neutrons of several Mev. Although neutron emission may occur with any of the large number of incoming angular momenta, charged particle emission, which is usually of lower energy, takes place predominately with low angular momentum. Therefore, selective emission will occur from those states with J-values that will allow the particles to be emitted with a small angular momentum value. Since the cross sections for reactions in which charged particles are emitted are an order of magnitude smaller than the elastic-plus-inelastic scattering cross section, resonances in the reactions leading to the emission of charged particles will not appreciably affect the total cross section. Because of this effect, it is possible to observe resonance structure in the compound nucleus by measuring the excitation functions for (n,α) and (n,p) reactions, even though the resonances frequently cannot be resolved in experiments that measure the neutron total cross section. In some cases, the J-values of the compound nucleus will be such that resonances can be observed both in the charged particle reaction cross sections and in the total cross section.

TABLE I. Resonances in the reaction $F^{19}(n,\alpha)N^{16}$.

Neutron energy (Mev)				Peak cross section (mb) (±40%)
30-kev resolution (p-T source)	60-kev resolution (p-T source)	100-kev resolution (d-d source)	Others[a] measurements	
3.4	3.4 (?)			
3.61±0.05				48
3.69±0.05	3.70±0.05			55
3.77±0.05				44
	4.11±0.05			90
	4.42±0.05		4.4	167
	4.86±0.05	4.9±0.1	4.9	186
		5.9±0.1		268

[a] See reference 13.

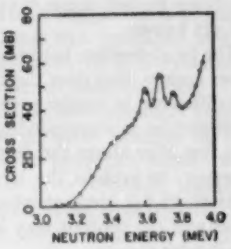

FIG. 4. Excitation function and absolute cross section for the reaction $F^{19}(n,\alpha)N^{16}$ obtained with the p-T neutron source. The energy resolution is approximately 30 kev.

Measurements have been made by Nereson and Darden[19] of the neutron total cross section for F^{19} from 3 to 12 Mev with an energy resolution of approximately 10 percent. In this energy range the total cross section is approximately 2 barns and is a smoothly varying function of energy except for the indication of a resonance at 4.4 Mev. It is probable that the group of resonances near this energy, observed in the $F^{19}(n,\alpha)N^{16}$ excitation function, are at least partially responsible for the total cross-section resonance.

Nereson and Darden obtained no evidence for a broad resonance at 5.9 Mev. Since a peak appeared at this energy in the (n,α) reaction excitation function but not in that for the (n,p) reaction, the J-values of the states of the compound nucleus must be such that α emission is favored at this energy. It is not possible to make any estimate of the spins or parities of these states on this basis, since α particles could be emitted, not only to the ground state of N^{16}, but to any of the

[19] N. Nereson and S. Darden, Phys. Rev. 94, 1678 (1954).

low-lying excited states,[14] the properties of which are not yet known.

The (n,α) reaction becomes energetically possible at a lower energy than does the (n,p) reaction, and, due to the difference in barrier penetration, the (n,α) reaction cross section is correspondingly higher for energies up to a few Mev above the (n,p) threshold. It is difficult, however, to explain the large difference in the cross sections at 8.0 Mev, at which energy both the α-particles and the protons may have energies greater than the barrier energy.

The cross sections obtained for the (n,α) and (n,p) reactions on F^{19} are of the same order of magnitude as the cross sections for reactions of this type on other nuclei.[1-9] The (n,α) reaction cross section measured at 3.9 Mev is 46 ± 18 mb, which is in good agreement with the value 37 ± 18 mb, obtained by Jelley and Paul[20] at this energy.

ACKNOWLEDGMENTS

The authors wish to express their appreciation of the continued assistance and encouragement given by Professor T. W. Bonner. Thanks are also due Dr. H. Bichsel for preparing and mounting the crystal.

[20] J. V. Jelley and E. B. Paul, Proc. Phys. Soc. (London) **A63**, 112 (1950).

PHYSICAL REVIEW VOLUME 100, NUMBER 1 OCTOBER 1, 1955

K-Capture - Positron Ratios for the First-Forbidden Transitions of Rb^{84} and the Relative Probabilities of *L*- and *K*- Electron Capture*

JOAN P. WELKER AND M. L. PERLMAN
Chemistry Department, Brookhaven National Laboratory, Upton, New York

(Received June 9, 1955)

The radiations from Rb^{84} have been investigated by means of scintillation coincidence spectrometer techniques in order to obtain the relative intensities of the various transitions. The energies and abundances of the radiations are 0.44-Mev β^- (5%), 0.81-Mev β^+ (10%), 1.70-Mev β^+ (9%), 0.89-Mev γ (64%), and 1.91-Mev γ (0.9%). [*Note added in proof.*—The β^- has been shown to be 0.91 Mev (2.5%).] Electron capture populates the level 1.91 Mev above the ground state, competes (54%) with the 0.81-Mev β^+ to populate the level 0.89 Mev above ground, and competes (21%) with the 1.70-Mev β^+ in effecting transitions to the ground state of Kr^{84}. The ratios of *K*-capture to positron emission for the transition to the 0.89-Mev level ($\Delta I=0$, yes) and to the Kr^{84} ground state ($\Delta I=2$, yes) are 5.15 ± 0.38 and 2.06 ± 0.36, respectively. These values are in qualitative agreement with theory. Nucleon configurations of the several states of Rb^{84}, Kr^{84}, and Sr^{84} are discussed. In the decay to the 0.89-Mev level an L/K-capture ratio of 0.12 ± 0.05 was obtained by use of a value, 0.65, for the fluorescence yield of krypton. Alternatively, an experimental value for the fluorescence yield, 0.62 ± 0.03, may be computed if the theoretical L/K-capture ratio is assumed.

THE radiations emitted in the decay of Rb^{84} have been studied by a number of investigators.[1-4] According to Huddleston and Mitchell,[4] two main positron groups are observed. The maximum energies and relative abundances were stated to be 1.63 Mev (0.39) and 0.82 Mev (0.58). A gamma ray of energy 0.89 Mev was found to be in coincidence with the lower energy positron group; the higher energy positrons were shown to represent a transition to the ground state of Kr^{84}. From the shape of the Fermi plot for the 1.63-Mev group, it was concluded that the transition is of the type $\Delta I=2$, yes. Moreover, since the spin-parity assignment for the ground state of Kr^{84}, an even-even nucleus, is $0+$,[5] the ground state of Rb^{84} was given the assignment $2-$. In agreement with this $2-$ designation and with the $2+$ designation for the first excited state[6] of Kr^{84}, the Fermi plot for the lower energy positron group was found by Huddleston and Mitchell to have an "allowed shape." These authors did not observe any appreciable negative beta emission, although Beckham and Pool[2] reported that negative beta decay to Sr^{84} occurs with a probability 16 percent as great as that for positron decay. It may be noted that negative beta decay should be exoergic to the extent of ~0.5 Mev.[6] Karraker and Templeton,[3] who also observed negative electrons and positrons, reported the principal mode of decay to be electron capture; in other respects their observations are in essential agreement with those of Huddleston and Mitchell. Further, a gamma ray of energy 1.89 Mev has been observed[7] in the radiations from Rb^{84}. The best value of the half-life obtainable from the literature is 34 days.[8]

As pointed out by Huddleston and Mitchell, the

* Research performed under the auspices of the U. S. Atomic Energy Commission.

[1] W. C. Barber, Phys. Rev. **72**, 1156 (1947).
[2] W. C. Beckham and M. L. Pool, Phys. Rev. **80**, 125 (1950).
[3] D. G. Karraker and D. H. Templeton, Phys. Rev. **80**, 646 (1950).
[4] C. M. Huddleston and A. C. G. Mitchell, Phys. Rev. **88**, 1250 (1952).
[5] G. Scharff-Goldhaber, Phys. Rev. **90**, 587 (1953).
[6] K. Way and M. Wood, Phys. Rev. **94**, 119 (1954).
[7] L. M. Langer and R. B. Duffield (private communication reported in reference 4).

assignment, 2−, for the ground state of Rb^{84} is consistent with the shell-model nucleon configurations, neutron $g_{9/2}$ and proton $f_{5/2}$. In this connection it may be noted that the measured spin of Rb^{85} is 5/2 and that the spins of Kr^{83} and Sr^{87} are 9/2.[8] Moreover, Stevenson and Deutsch,[9] from measurements of beta-gamma angular correlation, concluded that Rb^{86} has spin 2 and negative parity in accord with the nuclear magnetic moment result obtained by Bellamy.[10]

The probabilities of K-capture and positron emission for various types of transitions have been the subject of theoretical investigations.[11–14] For allowed transitions and first forbidden transitions of the type $\Delta I=2$, yes, the K-capture to positron probability ratios are independent of the nuclear matrix elements and thus of the type of interaction chosen. In the case $\Delta I=2$, yes, the K-capture to positron probability ratio is greater by a factor approximately three to six than that calculated for an allowed transition of the same energy and atomic number. However, in the cases in which $\Delta I=0$ or 1, yes, the probability ratios are dependent on the nuclear matrix elements but are not greatly different from the values to be expected for an allowed transition. Several investigations[15–17] of K-capture to positron ratios for allowed transitions have been reported and the results are in agreement with theory. On the other hand, very little experimental data exists for forbidden transitions; accurate measurements are available only for I^{126} ($\Delta I=2$, yes)[18] and As^{74} ($\Delta I=0$, yes).[19] The results for I^{126} are in good accord with theory,[12] and a careful comparison of the As^{74} value with the theoretical one is being made.[14] The study described in this paper was undertaken because Rb^{84} furnishes an opportunity for measurement of K-capture to positron ratios for first forbidden transitions of the types $\Delta I=2$ and 0.

EXPERIMENTAL METHODS AND RESULTS

Source Preparation and Purity

The Rb^{84} used in these experiments was produced by the reaction[8] $Br^{81}(\alpha,n)Rb^{84}$. The ammonium bromide target material, pressed onto the grooved face of a copper block and covered with a copper foil to degrade the energy of the helium ions, was irradiated in the external beam of the Brookhaven 60-inch cyclotron. Separation of the ammonium bromide from the rubidium activity was effected by the addition of freshly precipitated silver oxide to a water solution of the irradiated salt. The ammonium hydroxide formed was volatilized and the insoluble silver bromide, together with free silver and excess silver oxide, were removed by filtration. Precipitations of copper and zinc sulfides, ferric hydroxide, and barium sulfate were performed in order to free the rubidium from radioactive contaminants.[20] Approximately one microcurie of Rb^{84} was produced per microampere-hour of irradiation. The carrier-free rubidium activity was finally deposited on Mylar film, ~1 mg/cm² thick, and was covered with a thin layer of Zapon lacquer.

Unless otherwise stated, all the results reported in this paper and in the paper which follows were obtained with rubidium produced by the irradiation of a thick target with 14.5-Mev helium ions. The decay of one source was measured over a period of about 170 days with a proportional counter, the window of which was ~1.2 mg/cm² thick. The counter was filled to a pressure of one atmosphere with an argon-methane gas mixture. Rates were observed with the source uncovered, with a beta-stopping beryllium absorber, and with a beryllium and copper pair to stop beta particles and x-rays. The transmission of the beryllium absorber for krypton K x-radiation was determined experimentally to be 44.0% at normal incidence. The analysis of the count-rate data is shown in Fig. 1. Points labeled γ represent net rates observed through the beryllium-copper pair. The total x-ray points represent differences, corrected for the transmission of the beryllium, between the γ points and the rates observed through beryllium. The β points were computed by subtraction of the sum of the total x-ray and γ rates from the rates observed with no absorber. Although the β decay is clearly characterized by a half-life of 33.0±0.2 days, the γ and total x-ray decay points show that a long-lived component was present. Subtraction from the total x-ray rates of the amount of 83-day[21] Rb^{83} component shown in Fig. 1 yields the residual 33-day x-ray decay line.

At helium-ion energies of 14.5 Mev and less it is unlikely that Rb^{83} can be produced by the reaction $Br^{81}(\alpha,2n)Rb^{83}$; small amounts of Rb^{83} are produced, however, by the reaction $Br^{79}(\alpha,\gamma)Rb^{83}$.[22] Sources prepared from material irradiated with helium ions of higher energy contained, after a period of decay, large fractions of the 83-day x- and gamma-ray emitter, Rb^{83}; the beta decay of these sources nevertheless followed a

[8] P. F. A. Klinkenberg, Revs. Modern Phys. **24**, 63 (1952).
[9] D. T. Stevenson and M. Deutsch, Phys. Rev. **84**, 1071 (1951).
[10] E. H. Bellamy, Nature **168**, 556 (1951).
[11] Good, Peaslee, and Deutsch, Phys. Rev. **69**, 313 (1946).
[12] R. Nataf and R. Bouchez, J. phys. radium **13**, 190 (1952). References to earlier treatments are given in this paper.
[13] H. Brysk and M. E. Rose, Oak Ridge National Laboratory, Report ORNL 1830 (unpublished).
[14] Max Wolfsberg (private communication).
[15] King, Dismuke, and Way, Oak Ridge National Laboratory, Report ORNL 1450 (unpublished).
[16] J. K. Major and L. C. Biedenharn, Revs. Modern Phys. **26**, 321 (1954).
[17] R. Sherr and R. H. Miller, Phys. Rev. **93**, 1076 (1954).
[18] Marty, Langevin, and Hubert, J. phys. radium **14**, 663 (1953); M. L. Perlman and J. P. Welker, Phys. Rev. **95**, 133 (1954); Koerts, Macklin, Farrelly, van Lieshout, and Wu, Phys. Rev. **98**, 1230 (1955).
[19] Johansson, Cauchois, and Siegbahn, Phys. Rev. **82**, 275 (1951).
[20] Details of this chemical separation are given in one of the radiochemical procedures collected and distributed by H. L. Finston, Brookhaven National Laboratory, Upton, New York.
[21] S. V. Castner and D. H. Templeton, Phys. Rev. **88**, 1126 (1952).
[22] H. Morinaga, Phys. Rev. **99**, 655(A) (1955).

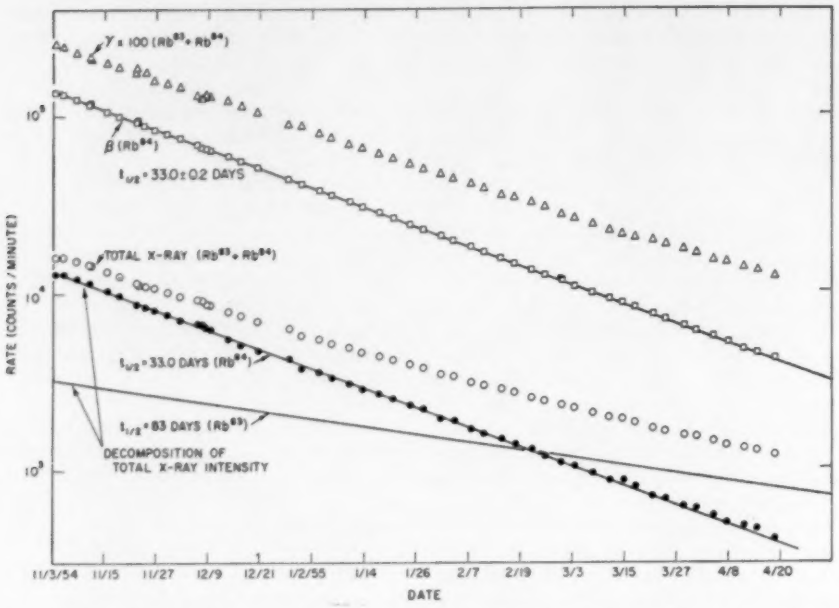
γ = 100 (Rb⁸³ + Rb⁸⁴)
β (Rb⁸⁴)
t1/2 = 33.0 ± 0.2 DAYS
TOTAL X-RAY (Rb⁸³ + Rb⁸⁴)
t1/2 = 33.0 DAYS (Rb⁸⁴)
t1/2 = 83 DAYS (Rb⁸³)
DECOMPOSITION OF TOTAL X-RAY INTENSITY
RATE (COUNTS / MINUTE)
10⁵
10⁴
10³
11/3/54 11/15 11/27 12/9 12/21 1/2/55 1/14 1/26 2/7 2/19 3/3 3/15 3/27 4/8 4/20
DATE

FIG. 1. Analysis of decay measurements taken with end-window proportional counter and suitable absorbers.

34-day half-life. The latter observation shows that there are very few particles emitted by Rb^{83} in agreement with the work of Castner and Templeton and with the expected decay energy.[6] The fact that no long-lived component was observed by Karraker and Templeton in rubidium sources prepared with 18-Mev helium ions is explainable; the Geiger-Müller detectors used by these authors are less sensitive to electromagnetic radiations than the end-window counter described above.

An independent determination of the relative contributions from Rb^{83} and Rb^{84} to the total x-ray intensity was made with a second source prepared from the target irradiated with 14.5-Mev helium ions. The x-ray intensity of this source, which was used in most of the experiments described below, was measured with a side-window proportional counter filled to a pressure of two atmospheres with a 95% argon-5% methane mixture. The area under the krypton K x-ray pulse-height distribution was evaluated as a function of time. Small corrections were applied to compensate for variations of the pulse-analyzer channel width between measurements. Subtraction from the experimental points of the 33-day line shown in Fig. 2 leaves residual rates which decay with an 83-day half-life. The relative x-ray intensities from Rb^{83} and Rb^{84} determined in the two ways differed by only 5%; the mean value was used in all calculations. From the work of Castner and Templeton, it is known that Rb^{83} decays at least in part to Kr^{83m}, 114-min half-life.[23] Because the sources used in this work did not emanate, as determined by test, the 83-day x-ray activity represented the sum of the contributions from Rb^{83} and from the Kr^{83m} in equilibrium with it.

Gamma-Ray Spectra

The gamma radiations were examined with a gray-wedge spectrometer and NaI(Tl) detectors. Various gamma-ray standards[23] were used to calibrate the energy scale. In addition to the K x-ray photoline, photopeaks were observed at energies 0.51, 0.89±0.02, and 1.91 ±0.05 Mev. Peaks at these energies were to have been expected on the basis of previously published information; it was found, however, that the intensity of the 0.51-Mev peak relative to that of the 0.89-Mev photoline increased as the fractional amount of Rb^{83} increased. Since there is no positron emission from Rb^{83}, it was concluded that a gamma ray of very nearly the same energy as annihilation radiation is associated with the decay of this nuclide.[24] It was observed that the ratio of the intensities of the 0.89- and 1.91-Mev photopeaks is independent of the source composition; therefore, the 1.91-Mev radiation is characteristic of Rb^{84}.

The pulse-height spectra shown in Figs. 3A and 3B

[23] *Nuclear Data*, National Bureau of Standards Circular 499 and Supplements (U. S. Government Printing Office, Washington, D. C., 1950).

[24] The decay scheme of Rb^{83} is discussed in detail by M. L. Perlman and J. P. Welker, following paper [Phys. Rev. **100**, 81 (1955)].

were obtained with a sliding channel pulse-height analyzer, a NaI(Tl) detector 1.5 inches in diameter and 1 inch long, and a source covered on both sides with beta-stopping beryllium absorbers. From the areas under the photopeaks and from the relative photopeak-efficiency curves of Bell,[28] the intensities of the 1.91- and 0.89-Mev gamma rays were calculated to be in the ratio $(0.0135\pm0.001)/1$.

Beta Spectra

Beta-ray spectra were investigated with a small anthracene scintillation detector only slightly greater in thickness than the range of the most energetic particles. A photograph of the pulse distribution from this detector as displayed by the gray-wedge spectrometer is given in Fig. 4. Three beta groups are seen to be present; the maximum energies are 1.70 ± 0.07, 0.81 ± 0.05, and 0.44 ± 0.05 Mev. The energy scale was calibrated by means of beta-ray standards[28]: P^{32} (1.701 Mev), Tl^{204} (0.765 Mev), and Na^{22} (0.542 Mev). There is no indication in the photographs of any internal-conversion electron line. The 0.81-Mev beta group was displayed alone in experiments in which coincidences with the 0.89-Mev gamma rays were required. It may be noted that the energy difference between the two higher energy groups agrees well with the observed gamma-ray energy, 0.89 Mev.

Experiments with a crude magnetic spectrometer indicated the presence of negative electrons, in abundance of the order one-fifth that of the positrons. On the basis of the coincidence results described in the next section of this paper, it is established that the two higher energy beta groups are positrons. Because the intensity of conversion electrons from the 0.89-Mev transition is expected to be approximately 1/200 that of the observed negative electrons, the negative particles must be the 0.44-Mev beta group. The abundance of these negative betas relative to that of the positrons was determined quantitatively by comparison of the rubidium source with a Na^{22} source. For the two sources in a defined geometry, the particle count rates were measured with an end-window proportional counter and the areas under the 0.51-Mev photopeaks were determined. The 0.51-Mev rubidium peak area was corrected

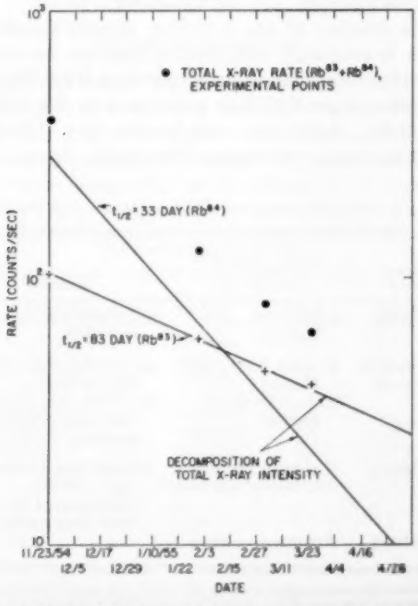
TOTAL X-RAY RATE (Rb^{83}+Rb^{84}), EXPERIMENTAL POINTS
$t_{1/2}$ = 33 DAY (Rb^{84})
$t_{1/2}$ = 83 DAY (Rb^{83})
DECOMPOSITION OF TOTAL X-RAY INTENSITY
RATE (COUNTS/SEC)
DATE
11/23/54 12/5 12/17 12/29 1/10/55 1/22 2/3 2/15 2/27 3/11 3/23 4/4 4/16 4/28

FIG. 2. Analysis of the decay of the K x-ray pulse distribution as observed with a proportional counter spectrometer.

[28] P. R. Bell (privately circulated data).

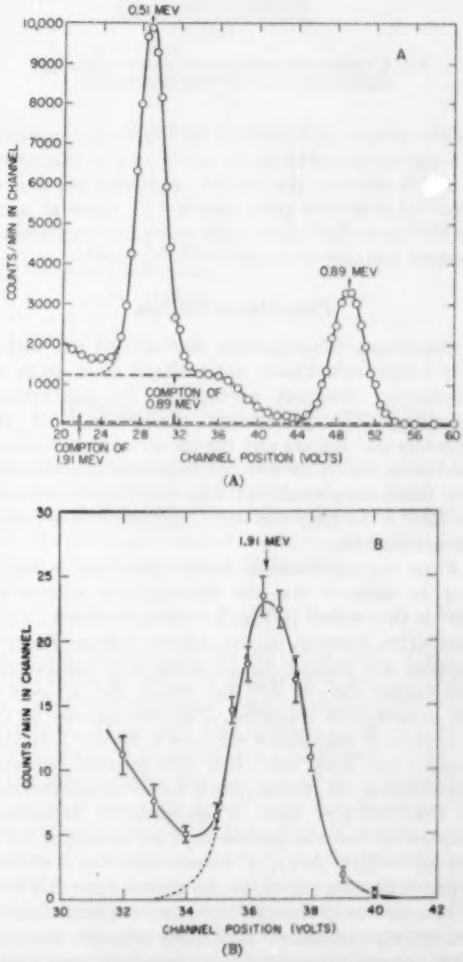

FIG. 3. Gamma rays emitted in the decay of Rb^{83} and Rb^{84}. Pulse-height distributions measured with a sliding channel scintillation spectrometer: A (high gain); B (low gain).

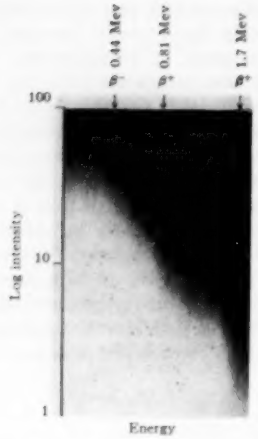

FIG. 4. Gray-wedge spectrometer record of beta-ray distributions from Rb^{84} (see reference 28).

for the amount of 0.525-Mev Rb^{83} radiation by means of a method described in the next section of this paper. It was found that the particle count rate per unit of corrected 0.51-Mev peak area is 1.25 times as great for Rb^{84} as for Na^{22}; or, in other words, the negatron-to-positron intensity ratio for Rb^{84} is 0.25 ± 0.10.

Coincidence Studies

Coincidence investigations were carried out with a gray-wedge coincidence spectrometer and pairs of scintillation detectors appropriate for the various radiations. The geometrical arrangements of the detectors and sources and the nature of the absorbers used were varied to suit the individual experiments. The coincidence resolution time was 0.1 microsecond. In Table I the results of these qualitative experiments are summarized.

From the experimental results presented so far, it may be deduced that the disintegration scheme for Rb^{84} is that shown in Fig. 5. A few comments on the qualitative features of the scheme follow. Positron emission and electron capture compete to populate the first excited state of Kr^{84} and should also compete in the ground-state transition. The observations of the radiations in coincidence with the 0.89- and 1.91-Mev gamma rays show that these two gammas represent transitions to the ground state of Kr^{84}. Positron emission to the 1.91-Mev level is energetically impossible. Because all observed gamma rays are accounted for in the $Rb^{84}\rightarrow Kr^{84}$ decay, it follows that the 0.44-Mev negative beta rays decay to the ground state of Sr^{84}.

In order to determine the relative abundances of the various transitions associated with the decay of Rb^{84}, several quantitative comparison coincidence measurements were performed. The intensity of the 0.525-Mev gamma rays of Rb^{83} relative to that of the annihilation quanta from Rb^{84} was determined by an experiment in 180° geometry in which the net number of (0.511, 0.511)-Mev coincidences per 0.511(0.525)-Mev quantum was compared with the number of (0.511, 0.511)-Mev coincidences per annihilation quantum from a Na^{22} source. Two NaI(Tl) scintillation detectors with sliding channel pulse-height selectors were used. One crystal and channel were kept fixed with respect to the source; with the other the areas under the "singles" and coincidence photopeaks were scanned. The result obtained on 12–17–54 for the intensity ratio of 0.525-Mev gamma rays to annihilation quanta, 0.77 ± 0.04, was then used together with the known half-lives of Rb^{83} and Rb^{84} to compute the relative amounts of these two radiations at other times. It is readily calculated that a negligible error is introduced into the Na^{22} measurement by the occurrence of coincidences of annihilation quanta with Compton events associated with the 1.28-Mev gamma ray.

In order to ascertain the fraction of the positrons which is followed by the 0.89-Mev radiation, the number of (0.511, 0.89)-Mev coincidences per 0.511 (0.525)-Mev quantum was compared with the number of (1.12, 0.89)-Mev coincidences per 1.12-Mev quantum from a Sc^{46} source. It is known that the two cascading Sc^{46} gamma radiations are of equal intensity.[23] In this experiment the geometry of the sources with respect to the detector for the 0.89-Mev radiations was maintained constant. The result, corrected for the 0.525-Mev gamma-ray intensity present at the time of measurement, is $I_{0.81\beta+}/I_{\text{total}\beta+}=0.505\pm0.026$.

The fraction of the 0.89-Mev gamma transitions which is associated with positron emission was determined by comparison of the number of (0.511, 0.89)-Mev coincidences per 0.89-Mev quantum with the number of (0.511, 1.28)-Mev coincidences per 1.28-Mev quantum from a Na^{22} source. The result, $I_{0.81\beta+}/I_{0.89\gamma}$

TABLE I. Results of coincidence experiments with $Rb^{83,84}$ mixture.

Selected event	Events observed in coincidence with selected event	Remarks[a]
Kr K x-ray	0.525-, 0.89-, 1.91-Mev γ's	0.525-Mev γ is associated with Rb^{83}
0.511(0.525)-Mev γ's[b]	K x-ray, 0.511-, 0.89-Mev γ's; 0.81-, 1.70-Mev β^+ spectra[c]	no γ's other than 0.89 Mev in coinc.; no [0.511, 0.511(0.525)]-Mev coinc. out of 180° geometry
0.89-Mev γ	K x-ray, 0.511-Mev γ; 0.81-Mev β^+ spectrum	no indication of coinc. with 1.02-Mev γ (stopover) or any γ other than annihil.
1.91-Mev γ	K x-ray	

[a] A detector-source-detector angle of ~135° was employed whenever necessary to eliminate (0.511, 0.511)-Mev annihilation coincidences.
[b] The photopeak distributions from these two radiations were not resolved from each other.
[c] Huddleston and Mitchell, reference 4, showed that the 1.70-Mev β^+ group is not in coincidence with a nuclear gamma ray and therefore represents a transition to the ground state of Kr^{84}.

$=0.150\pm0.011$, is based upon the fact that in the decay of Na^{22}, 90.0 ± 0.5 percent[17] of the 1.28-Mev quanta are associated with positrons.

To determine the fraction of the krypton K x-rays which is followed by the 0.89-Mev transitions, the number of K x-ray, 0.89-Mev gamma coincidences per K x-ray was compared with the number of (1.12, 0.89)-Mev coincidences per 1.12-Mev gamma quantum observed with a Sc^{46} source. A thin NaI(Tl) detector was used for the x-rays, and a thick NaI(Tl) scintillator was used for the 1.12-Mev gamma rays; however, the same crystal and geometry were employed for the detection of the 0.89-Mev radiations from both sources. The K x-ray "singles" rate was corrected for the intensity of 83-day x-rays present at the time of measurement. It should be noted that the result,

$$I_{\text{x-ray to 0.89 level}}/I_{\text{x-ray}}=0.71\pm0.03,$$

represents, independently of the fluorescence yield, the fraction of all electron capture which proceeds to the 0.89-Mev level, provided only that the ratio of L to K capture is the same for the various capture branches.

Most of these quantitative coincidence measurements were made twice; the errors attached to the above results were computed from errors assigned to the individual experiments. In all cases the differences between duplicate experiments were less than the combined individual errors.

INTERPRETATION OF Rb^{84} RESULTS

Transition Intensities

From the results of the quantitative coincidence experiments, from the ratio of negatrons to positrons, and from the intensity ratios of the gamma radiations, the intensities of all the transitions associated with Rb^{84} were computed. An L-capture to K-capture probability ratio of 0.10 is assumed.[13] The value for the fluorescence yield of krypton does not enter into these calculations. The transition intensities, together with the measured transition energies, were then used to compute the log ft values (Table II).

TABLE II. Abundances and comparative half-lives of the radiations from Rb^{84}.

Radiation	Abundance (percent)	log ft[a]	log fd[b]
EC to ground state	21 ±3	7.8	
EC to 0.89-Mev level	54.3±0.7	7.1	
EC to 1.91-Mev level	$0.9^{+0.3}_{-0.1}$	8.1	
0.81-Mev β^+	9.6±0.7	7.3	
1.70-Mev β^+	9.4±0.9	8.8	8.7
0.44-Mev β^-[c]	4.7±2.0	7.7	6.6
	Total 100		
0.89-Mev γ	64		
(1.02-Mev γ)	<0.3[d]		
1.91-Mev γ	0.9±0.1		

[a] The log ft values were computed from the monographs of S. A. Moszkowski, Phys. Rev. **82**, 35 (1951), and from the graphs given by E. Feenberg and G. Trigg, Revs. Modern Phys. **22**, 399 (1950).
[b] The log fd values for the unique transitions were calculated by the method of J. P. Davidson, Phys. Rev. **82**, 48 (1951).
[c] See reference 28.
[d] This upper limit was estimated from Fig. 3.

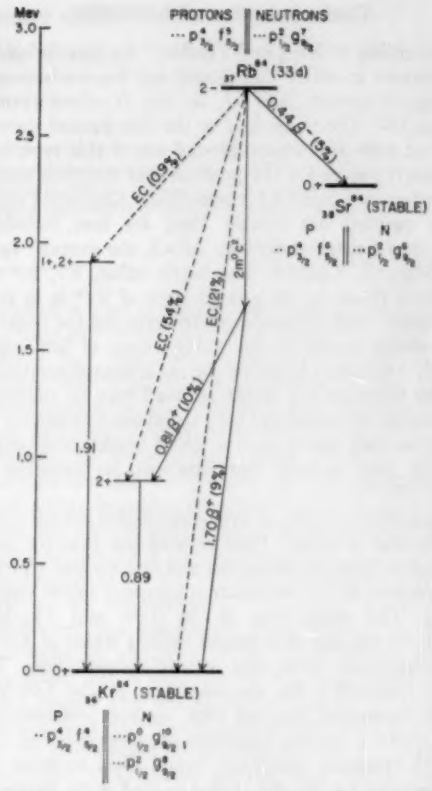

FIG. 5. The decay scheme of Rb^{84} (see reference 28).

K-Capture - Positron Ratios

For the transition to the 0.89-Mev level, which is characterized by spin change zero and parity change, the measured K-capture to positron-emission probability ratio is 5.15 ± 0.38. This result is to be compared with the value, 3.1, computed for an allowed transition of the same energy. For the ground-state transition, which is of the type $\Delta I=2$, yes, the K-capture to positron ratio observed is 2.06 ± 0.36; if the transition were an allowed one, the ratio would be 0.28. In both cases the measured ratios are larger than those computed for allowed transitions, and the increases are in agreement with the qualitative theoretical expectations for first forbidden transitions.[11–13] Quantitative comparisons will be made[14] on completion of the theoretical calculations for Rb^{84}.

Characterization of the Levels

According to King and Peaslee,[26] for first forbidden transitions in which $\Delta I=0$ and Δj, the nucleon spin change, is greater than ΔI, the log ft values average 7.55 ± 0.47. The transitions to the first excited state of Kr^{84} at 0.89 Mev above ground are of this type, and the logft values for the positron and electron-capture branches are 7.3 and 7.1, respectively. King and Peaslee have pointed out further that, for first forbidden transitions characterized by $\Delta I=2$, the average value for logf_1t is 8.5 ± 0.5. The logf_1t value, 8.7, for the positron decay to the ground state of Kr^{84} is in good agreement with this average; however, for the negative beta-decay branch to the ground state of Sr^{84}, logf_1t is 6.6. Arguments based on the nucleon configurations[27] of the three ground states involved may be employed to explain the relatively high transition probability for negative beta decay, and a set of tenable shell-model proton and neutron configurations is presented in Fig. 5.[28]

In a recent survey of even-even nuclei Scharff-Goldhaber and Weneser[29] have pointed out that the ratio of the energies of the second and first excited states is approximately 2.2 for neutron numbers below eighty-eight. The designation of the 0.89- and 1.91-Mev levels as the first and second excited states of Kr^{84} is in agreement with this general observation. The logft value, 8.1, for the transition to the 1.91-Mev level, considered together with the low probability of the stopover gamma transition as compared with that of the crossover transition, would seem to favor the designation 1+ for the second excited state. However, the designation 2+, which characterizes more than half of the second excited states investigated,[29] cannot be excluded.

RELATIVE PROBABILITY FOR THE CAPTURE OF L- AND K-ELECTRONS; THE FLUORESCENCE YIELD OF KRYPTON

The theory for the relative capture probability of L and K electrons has been thoroughly developed[13] for both allowed and forbidden transitions. The L/K-capture branching ratio for A^{37}, measured by Pontecorvo, Kirkwood, and Hanna,[30] is in agreement with theory; however, the results of Langevin[31] for Ge^{71}, 0.30 ± 0.02, and of Langevin and Radvanyi[32] for Kr^{79}, 0.25 ± 0.03, disagree with the theoretical predictions, 0.10 and 0.09, respectively. Because of the paucity of the experimental data, a measurement of the L/K-capture ratio for the transition to the 0.89-Mev level in Kr^{84} was undertaken.

Evaluation of the L/K-capture ratio depends on the relation,

$$[(EC_L+EC_K)/EC_K](f_s/\omega_K)+f_{\beta+}=1, \qquad (1)$$

where EC_L and EC_K refer to the probabilities of L- and K-electron capture, ω_K is the K-fluorescence yield of krypton, $f_{\beta+}$ designates the fraction of the 0.89-Mev level population that is supplied by positron emission, and f_s the fraction supplied by K-capture processes accompanied by fluorescence. Population of the 0.89-Mev level by gamma radiation from the 1.91-Mev state ($<0.5\%$) is neglected. The value for $f_{\beta+}$, 0.150 ± 0.011, was obtained as described earlier in this paper. The value for f_s, 0.48 ± 0.02, was determined from a measurement of the number of K x-ray, 0.89-Mev coincidences per 0.89-Mev quantum and from the absolute efficiency of the thin NaI(Tl) detector for krypton K x-rays. The latter efficiency is made up of several factors which were evaluated experimentally: the solid angle subtended by the detector at the source in the coincidence geometry, the fraction of the krypton x-ray pulse distribution accepted by the single channel analyzer, the transmission of the thin aluminum crystal cover, and the transmission of the beryllium beta-stopping absorber. The geometrical factor was determined by comparison of the x-ray count rate in the coincidence geometry with the count rate at a source-to-detector distance such that the solid angle subtended by the detector at the source could be accurately evaluated by mensuration. If, from the analysis of the experimental data carried out by Broyles, Thomas, and Haynes,[33] the value, 0.65, is taken for ω_K, then EC_L/EC_K is computed to be 0.12 ± 0.05. This result is in good agreement with the theoretical result, 0.10. It may be noted, that in order to obtain an L/K ratio about 0.27, an average of the values for Ge^{71} and Kr^{79}, ω_K would have to be 0.73, an unreasonably large value.

Conversely, Eq. (1) may be used to compute the krypton K-fluorescence yield if the theoretical L/K-capture ratio is assumed. The value thus obtained for ω_K is 0.62 ± 0.03.

ACKNOWLEDGMENTS

We are grateful to Dr. M. Wolfsberg, Dr. M. Goldhaber, Dr. S. Katcoff, and Dr. G. Friedlander for helpful and stimulating discussions.

[26] R. W. King and D. C. Peaslee, Phys. Rev. **94**, 1284 (1954).
[27] A. de-Shalit and M. Goldhaber, Phys. Rev. **92**, 1211 (1953).
[28] *Note added in proof.*—The authors are indebted to Dr. C. S. Wu and Miss N. Benczer, who has kindly informed them that unpublished results obtained in her laboratory with a magnetic lens spectrometer show that the negative beta radiations of Rb^{84} have a maximum energy of 0.910 Mev and an abundance $\frac{1}{4}$ that of the positrons. The small break in Fig. 4 which was interpreted to represent the end point of the negative beta spectrum is therefore probably spurious. The values obtained by Wu and Benczer change the negative beta abundance in the decay scheme from the quoted value, $4.7\%\pm2\%$, to 2.4%; and electron capture to the 0.89-Mev level increases from 54.3% to 55.5%. Other abundance changes are completely negligible. The value for logf_1t for the negative beta transition becomes 8.7 in excellent agreement with the value for the ground-state positron transition; and thus no special configuration arguments are required.
[29] G. Scharff-Goldhaber and J. Weneser, Phys. Rev. **98**, 212 (1955).
[30] Pontecorvo, Kirkwood, and Hanna, Phys. Rev. **75**, 982 (1949).
[31] M. Langevin, Compt. rend. **239**, 1625 (1954).
[32] M. Langevin and P. Radvanyi, Compt. rend. **238**, 77 (1954).
[33] Broyles, Thomas, and Haynes, Phys. Rev. **89**, 715 (1953).

Disintegration Scheme of Rb^{83}†

M. L. Perlman and Joan P. Welker
Chemistry Department, Brookhaven National Laboratory, Upton, New York

(Received June 9, 1955)

The decay of Rb^{83} has been determined to proceed by electron capture to an excited state of Kr^{83} which is 0.566 Mev above the ground state. This excited state is depopulated exclusively by emission of a 0.525-Mev gamma ray ($M1$) to the 0.041-Mev state, Kr^{83m}. Little or no electron capture direct to the 0.041-Mev level or to lower levels occurs. The spin-parity designation of the 0.566-Mev state is $p_{1/2}$, and that of the Rb^{83} ground state is $f_{9/2}$.

DURING the course of an investigation concerned with certain features of the decay[1] of Rb^{84}, sufficient information was obtained about the radiations of Rb^{83} to ascertain the disintegration scheme of this nuclide. According to published work[2,3] Rb^{83} has a half-life of 83 days; x-rays, conversion electrons corresponding to gamma rays of energies ~0.15 and ~0.45 Mev, and a gamma ray of energy ~0.8 Mev are reported to be emitted. The energy measurements are described as being crude.[3] At least a fraction of the decay proceeds to 114-min Kr^{83m}, as shown[3] by the growth of activity in rubidium fractions freshly separated from Sr^{83}. The level scheme of Kr^{83m} has been thoroughly investigated; the multipole orders of the electromagnetic radiations are established, and the spins and parities of the levels are known.[4] This information is summarized in Fig. 1.

EXPERIMENTAL METHODS AND RESULTS

The method of source preparation has been described in the paper which precedes this one.[1] Tests showed that the sources used in the following experiments did not emanate Kr^{83m}. As has been stated, decay measurements made with proportional counters and suitable absorbers confirmed the earlier observations that Rb^{83} disintegrates with the emission of K x-rays and of gamma rays, and that very little if any particle emission occurs. From the information shown in Fig. 1 of the preceding paper and with a knowledge of the particle to x-ray intensity ratio from Rb^{84}, it may be estimated that less than one percent of $Rb^{83} \rightarrow Kr^{83}$ events are associated with the emission of particles with energy exceeding 40 kev.

It has been noted also that a gamma ray of energy very nearly the same as that of annihilation radiation[1] is associated with the decay of Rb^{83}. The evaluation of the energy of this radiation was made from data obtained in a set of coincidence measurements in which Na^{22} and $Rb^{83,84}$ were compared. It was observed in the case of Na^{22} that the 0.511-Mev photopeak in coincidence with 0.511-Mev quanta was centered at the same position as the simultaneously recorded 0.511-Mev "singles" photopeak; in the case of the $Rb^{83,84}$, however, the "singles" peak, composed of annihilation radiation and the Rb^{83} gamma ray, was consistently a little higher in energy than the coincident photopeak. From the relative displacement of the two peaks and from a knowledge of the fraction of Rb^{83} gamma radiation present in the $Rb^{83,84}$ "singles" photopeak at the time of the measurement,[1] the energy of the Rb^{83} gamma ray was determined to be 0.525 ± 0.007 Mev. This radiation was found to be in coincidence with K x-rays and not in coincidence with annihilation radiation.[5] Several gray-wedge photographs of the gamma-ray spectra of $Rb^{83,84}$ were observed both with and without the requirement of coincidences with K x-rays and with 0.511 (0.525)-Mev gamma rays. There was no evidence for the emission, in the decay of Rb^{83}, of any gamma ray other than that of energy 0.525 Mev.

A determination was made of the fraction of Rb^{83} K-electron capture events which is associated with the emission of the 0.525-Mev gamma ray. The K x-ray, 0.525-Mev coincidence rate was compared with the K x-ray count rate. Two NaI(Tl) detectors and pulse-height selectors were employed. The result of this comparison measurement is independent of all x-ray efficiency factors. Apportionment of the x-ray rate between the 83-day Rb^{83} and the 33-day Rb^{84} was made by the methods described in the foregoing paper. Further, the Rb^{83} x-ray rate was corrected to take into account the fact that a part of the intensity, 0.22, is produced by internal conversion of gamma rays[6] from Kr^{83m}; the evaluation of this correction is described in the next section. For the coincidence-rate measurement, the area under the 0.525-Mev coincidence photopeak was scanned; small backgrounds associated with the radiations of Rb^{84} were evaluated and subtracted. The absolute efficiency of the detector and pulse-height selector for the 0.525-Mev quanta was measured by determination of the area of the 0.511-Mev annihilation

† Research performed under the auspices of the U. S. Atomic Energy Commission.

[1] J. P. Welker and M. L. Perlman, preceding paper [Phys. Rev. **100**, 74 (1955)].

[2] D. G. Karraker and D. H. Templeton, Phys. Rev. **80**, 646 (1950).

[3] S. V. Castner and D. H. Templeton, Phys. Rev. **88**, 1126 (1952).

[4] M. Goldhaber and R. D. Hill, Revs. Modern Phys. **24**, 179 (1952).

[5] Reference 1, Table I.

[6] I. Bergström, Phys. Rev. **81**, 638 (1951).

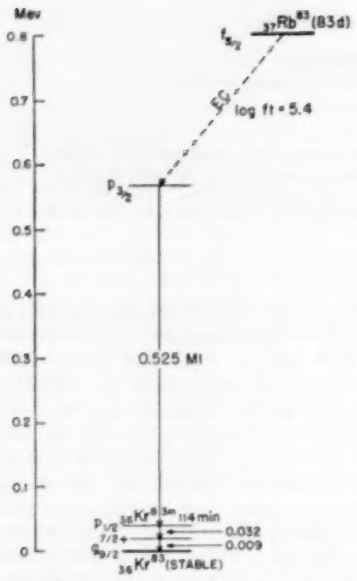

FIG. 1. The decay scheme of Rb^{83}.

photopeak from a calibrated Na^{22} source. The comparison experiment gave the result that 0.99 ± 0.10 of the electron-capture processes are followed by emission of the 0.525-Mev quanta.

DISCUSSION

The decay scheme shown in Fig. 1 was arrived at by combination of the experimental results given in this paper with information about the internal conversion[6] of the 32-kev transition in Kr^{83m} and about the growth of Kr^{83m} in freshly separated Rb^{83} fractions.[3] According to the compilation of Way and Wood[7] the disintegration energy of Rb^{83} is expected to be approximately 0.8 Mev; under this condition the ratio of L capture to K capture may be taken as 0.10.[8] The number of K vacancies per disintegration of Rb^{83} is expressed by the relation,

$$K_{vac}=0.91+0.26f. \quad (1)$$

The 0.91 vacancies are produced in the act of capture, f is the fraction of Rb^{83} disintegrations which populates the 0.041-Mev Kr^{83m} state, and 0.26 is the fraction of the 0.032-Mev Kr^{83m} transitions which produces a K vacancy.[6] The term $0.26f$ is evaluated as a function of K_{vac} from the growth curves of Castner and Templeton:

$$0.26f=(0.22\pm0.01)K_{vac}. \quad (2)$$

The solution of Eqs. (1) and (2) gives $K_{vac}=1.17$ and $f=1.00$. Three assumptions about the growth curves are implicit in Eq. (2): (a) the growth sources did not emanate Kr^{83}, (b) the count-rate measurements[9] were begun before appreciable growth had occurred, and (c) the count-rate data taken with a Geiger-Müller counter represent only the x-radiations. It should be noted that inaccuracy in any of these assumptions would tend to make f exceed 1.00, which would be an absurd result. Since each capture process in Rb^{83} populates the 0.041-Mev level and since 0.99 ± 0.10 of the capture events are in coincidence with 0.525-Mev quanta, capture followed by emission of 0.525-Mev gamma rays must populate the Kr^{83m} state. Moreover, little or no capture proceeds directly to the 0.041-Mev or to lower Kr^{83} levels. The allowed log ft value,[10] 5.4 ± 0.4, for the capture transition to the 0.566-Mev level is based on the decay energy estimated from the curves of Way and Wood.

The spin-parity assignments for the ground and first two excited states of Kr^{83} are well known.[4,6] Only two reasonable single particle assignments[11] remain for the 0.566-Mev Kr^{83} level, $p_{3/2}$ and $f_{5/2}$. If the level were characterized $f_{5/2}$, it should be depopulated more rapidly by $E1$ transitions to the 9-kev level than by $E2$ transitions to the 41-kev level, in contradiction of the experimental facts. The characterization $p_{3/2}$, on the other hand, is in agreement with the observation that all transitions from the 0.566-Mev level populate the 0.041-Mev level.

For the odd proton of Rb^{83} reasonable single particle characterizations are $f_{5/2}$, $p_{3/2}$, and, less probably, $p_{1/2}$ or $g_{9/2}$. Of these four $g_{9/2}$ is excluded because very little or no capture to the ground state of Kr^{83} occurs. Since the capture transition to the 0.041-Mev krypton state would be much more probable than that to the 0.566-Mev level if the assignment were $p_{3/2}$ or $p_{1/2}$, these two possibilities are excluded. Thus, $f_{5/2}$ would appear to be the designation for the ground state of Rb^{83}. The capture transition to the 0.566-Mev level of Kr^{83} is then allowed and the capture transitions to the other states of Kr^{83} are forbidden, which is in agreement with the experimental evidence. It may be noted that the ground-state assignments of the neighboring odd-even nuclides, Rb^{81} and Rb^{85}, are $p_{3/2}$ and $f_{5/2}$ respectively.[11,12]

[7] K. Way and M. Wood, Phys. Rev. **94**, 119 (1954).
[8] M. E. Rose and J. L. Jackson, Phys. Rev. **76**, 1540 (1949).
[9] Reference 3, Fig. 1.
[10] S. A. Moszkowski, Phys. Rev. **82**, 35 (1951).
[11] P. F. A. Klinkenberg, Revs. Modern Phys. **24**, 63 (1952).
[12] Hobson, Hubbs, Nierenberg, and Silsbee, Phys. Rev. **96**, 1450 (1954).

Gamma Rays Excited by Inelastic Scattering of Neutrons in Various Elements*

M. A. ROTHMAN, H. S. HANS,† AND C. E. MANDEVILLE
Bartol Research Foundation of The Franklin Institute, Swarthmore, Pennsylvania

(Received June 14, 1955)

Neutrons of energy 3.7 Mev have been inelastically scattered in a number of elements. The energies of the γ rays so excited have been measured by scintillation counting and pulse height analysis. In some cases, the cross sections for γ-ray excitation have been calculated.

INTRODUCTION

THE present measurements are a continuation of an earlier survey[1] of γ rays emitted when neutrons of intermediate energy are inelastically scattered by nuclei. Since the publication of the above mentioned report, other papers dealing with the same topic have appeared.[2,3] The γ-ray spectra resulting from inelastic scattering of neutrons of energy 3.7 Mev. by Al, Sb, As, Fe, Se, Si, and S are shown in Fig. 1. These measurements were performed in a geometry which has been previously described.[1] The quantum energies and cross sections are summarized in Table I.

DISCUSSION OF RESULTS

In the curves of Fig. 1, background of two types has been subtracted: (1) background proportional to the time (due mainly to radioactivity in the crystal); and (2) background proportional to the neutron flux. In the cases of silicon and arsenic, the scatterers were metallic powders contained in plastic rings.

TABLE I. Gamma rays excited by inelastic scattering of neutrons.

Element	Energy	Cross section
Aluminum	0.835±0.01 Mev	0.022 b/sterad at 90°
	1.02 ±0.01	0.041
	1.72 ±0.02	
	1.91 ±0.02	
	2.22 ±0.03	0.013
Antimony	1.00 ±0.04	0.075
Arsenic	0.815±0.01	
	1.02 ±0.01	
Iron	0.845±0.01	0.135
	1.23 ±0.01	
	1.80 ±0.02	0.024
	2.10 ±0.03	
Selenium	1.05 ±0.02	
	1.50 ±0.03	
Silicon	1.78 ±0.02	0.064
Sulfur	2.25 ±0.03	
Gold	...	<0.02

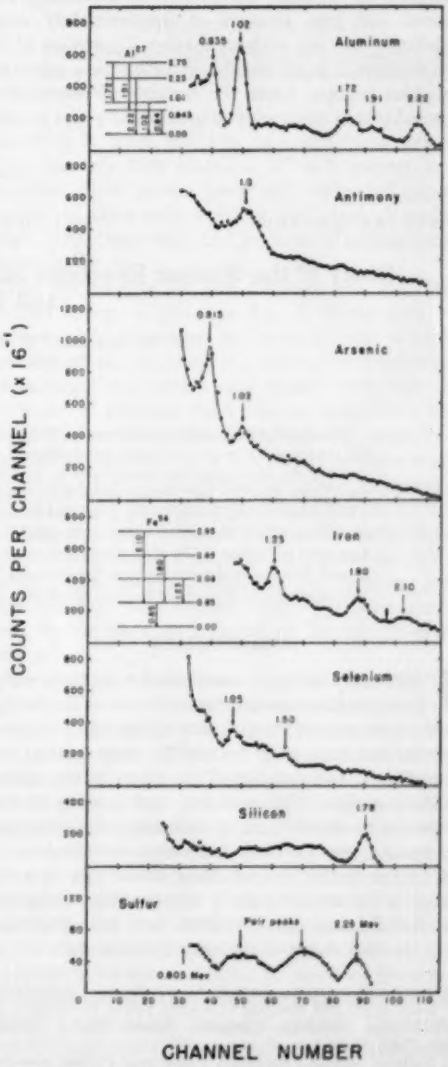

FIG. 1. Gamma rays (in Mev) resulting from inelastic scattering of neutrons of energy 3.7 Mev in various elements.

* Assisted by the U. S. Atomic Energy Commission.
† Fulbright fellow from the Muslim University of Aligarh, India.
[1] M. A. Rothman and C. E. Mandeville, Phys. Rev. **93**, 796 (1954). References to other papers published in 1953 and earlier, dealing with the same subject, may be found in this paper.
[2] Shapiro, Scherrer, Allison, and Faust, Phys. Rev. **95**, 751 (1954); R. M. Kiehm and Clark Goodman, Phys. Rev. **95**, 989 (1954); Scherrer, Allison, and Faust, Phys. Rev. **96**, 386 (1954).
[3] G. L. Griffith, Phys. Rev. **98**, 579 (1955).

Cross sections were determined by calibrating the NaI crystal with radioactive sources of known strength. Attenuation of neutrons and gamma rays in the scatterer was calculated, but no multiple scattering corrections were made. The scattering rings had radial and axial thicknesses of one inch. The incident neutron flux was calculated from the known cross section for the $d-d$ reaction. Cross sections are given in barns/steradian at 90°. Knowledge of the angular distribution of the γ rays is necessary to determine the total cross sections for production of these γ rays.

The cross sections have been corrected for isotopic abundance in all cases except that of antimony. This element has two isotopes of approximately equal abundance, so that without further knowledge of the level schemes, it is not possible to assign the γ ray to one particular isotope. From the breadth of the peak, it is probable that there are two unresolved γ rays present.

In the case of gold, no peaks were detected. The large attenuation of the gold scatterer would greatly cut down the yield of any γ rays produced. The figure given in the table is an estimated upper limit on the cross section for production of a 1-Mev γ ray.

The level scheme shown for Al is taken from Endt and Kluyver.[4] The γ-ray energies shown on the spectrum are within 1 percent of the energies obtained from the known levels.

The level scheme shown for Fe is based on the assumption that all the γ rays cascade through the 850-kev level.[5] The quantum energies given are taken from the Fe spectrum in Fig. 1 and agree well with measurements on the γ rays from Mn^{56} and Co^{56}.

[4] P. M. Endt and J. C. Kluyver, Revs. Modern Phys. **26**, 95 (1954).
[5] Jennings, Weddell, Alexeff, and Hellens, Phys. Rev. **98**, 582 (1955).

PHYSICAL REVIEW VOLUME 100, NUMBER 1 OCTOBER 1, 1955

Study of the Nuclear Reactions $Sc^{45}(p,n)Ti^{45}$, $Cu^{63}(p,n)Zn^{63}$, $Cu^{65}(p,n)Zn^{65}$, and $Zn(p,n)Ga$†

R. M. Brugger,* T. W. Bonner, and J. B. Marion‡
The Rice Institute, Houston, Texas

(Received June 22, 1955)

The counter ratio method has been applied to the (p,n) reactions for Sc^{45}, Cu^{63}, Cu^{65}, and Zn to determine the Q-values for the ground-state thresholds and to locate low-lying states in the residual nuclei. The thresholds for the (p,n) reactions were found to be 2.908 Mev for Sc^{45}, 4.215 Mev for Cu^{63}, 2.169 Mev for Cu^{65}, and 3.749 Mev for Zn^{65}. Other neutron thresholds were found corresponding to excited states in Ti^{45} at 0.743, 1.194, 1.347, 1.460, 1.876, 2.016, 2.430, and 2.555 Mev; in Zn^{65} at 0.191, 0.642, and 1.043 Mev; and in Zn^{65} at 0.78, 1.26, and 1.93 Mev. A threshold was found in the $Zn(p,n)Ga$ reaction which is probably due to a level in Ga^{65} at 0.170 Mev. Cross sections for the yield of neutrons in the forward direction were determined. The yields of neutrons from thin Sc^{45} and Cu^{63} targets were obtained for the proton energy region from the thresholds to 70 kev above these thresholds. McKibben nomographs are given for these two reactions.

INTRODUCTION

THE study of (p,n) reactions for medium weight elements has not been as extensive as for the light elements because of the difficulty of obtaining separated isotopes and because of the smaller cross sections near threshold. The knowledge of the levels in the residual nuclei is meager. The existence and spacing of these levels can be determined by measuring the energies of the neutron groups from the proton bombardment of the target nuclei several Mev above the threshold energy or by studying the γ rays accompanying these reactions. In some cases the levels have been determined from the beta decay of the next higher isobar.

A greater knowledge of medium-weight element (p,n) reactions as neutron sources is valuable because of the present interest in neutron scattering experiments in the 1–150 kev range. Because of the low center-of-mass velocity, the neutrons emitted near threshold from these reactions have energies of only a few kilovolts and the energy is approximately independent of angle in the forward direction. Although the yields are low, the beam currents obtainable with present-day Van de Graaff accelerators make the use of these sources possible in the kilovolt region. To obtain satisfactory resolution, thin targets and well resolved proton beams are necessary. Using these sources, experiments can be performed at zero degrees to the proton beam with neutron energies of a few kilovolts and only a small variation in energy with angle.

The counter ratio method which was first described by Bonner and Cook[1] employs two paraffin-moderated

† Supported in part by the U. S. Atomic Energy Commission.
* Humble Oil and Refining Company Fellow in Physics; now with Phillips Petroleum Company, Atomic Energy Division, Idaho Falls, Idaho.
‡ National Science Foundation Predoctoral Fellow; now Postdoctoral Fellow, Kellogg Radiation Laboratory, California Institute of Technology, Pasadena, California.

[1] T. W. Bonner and C. F. Cook, Phys. Rev. **96**, 122 (1954).

BF_3 counters. One counter (called the modified long counter) essentially determines the yield of neutrons of all energies from a reaction, while the second counter (called the slow counter) discriminates against fast neutrons in favor of slow neutrons. The ratio of the counting rate of the second counter to that of the first reveals not only thresholds corresponding to the ground states of the residual nuclei, but thresholds due to excited states as well. By applying this method to (p,n) reactions, the yield of neutrons in the forward direction and the existence and spacing of the low-lying states in the residual nuclei can be determined simultaneously.

Preliminary studies of the thick-target yield of neutrons from the proton bombardment of scandium by Hanson, Taschek, and Williams[2] showed that the $Sc^{45}(p,n)Ti^{45}$ reaction might be useful as a source of kilovolt neutrons, with a yield near threshold about 40 times that of the $V(p,n)$ reaction, another possible source of kev neutrons. They determined the threshold energy for the reaction to be 2.9 Mev and found that the cross section was roughly 30 millibarns near threshold. The threshold of 4.2 Mev for the $Cu^{63}(p,n)Zn^{63}$ reaction suggested that it might also give a satisfactory yield of neutrons near threshold.

The counter ratio method was also applied to the reactions: $Cu^{65}(p,n)Zn^{65}$, $Cu^{63}(p,n)Zn^{63}$, and $Zn(p,n)Ga$. Preliminary results with Cu^{65} have previously been obtained[3] with this technique. Only a rough measurement of the threshold of the $Zn^{68}(p,n)$ threshold has been reported.[4]

EXPERIMENTAL PROCEDURE

A procedure for the counter ratio method similar to that described by Marion, Brugger, and Bonner[5] was used in these experiments. This method involves the use of two BF_3 counters, one embedded in a paraffin cylinder 5 in. in diameter and 5 in. in length (modified long counter) and the second surrounded by a ring of paraffin ½ in. thick and 2 in. in length (slow counter). Both counters were placed at 0° with respect to the direction of the proton beam and subtended approximately the same solid angle at the target. A multiple target holder was used. The geometrical arrangement is shown in Fig. 1.

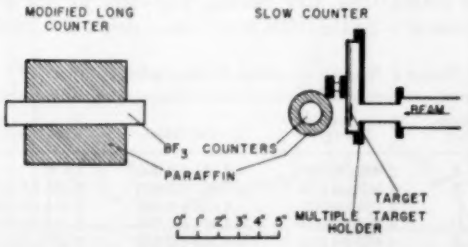

FIG. 1. Geometrical arrangement of the two counters and the target holder used in performing counter ratio experiments.

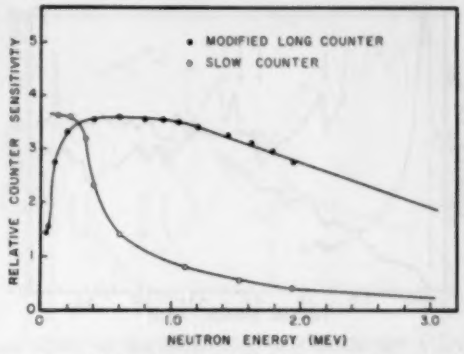

FIG. 2. Relative efficiencies as a function of the neutron energy of the slow counter and of the modified long counter in its position behind the slow counter.

The efficiency of the two counters as a function of neutron energy is given in Fig. 2. These data were determined by observing the counting rate in each of the counters as the energy of a beam of protons striking a LiF target was varied. The results were then compared to the absolute yield into the same cone determined by Taschek and Hemmendinger[6] in order to find the relative efficiency as a function of neutron energy. The efficiency of the modified long counter in its position behind the slow counter decreases rapidly for neutrons of energy less than 0.3 Mev. This is a desirable characteristic for detecting weak neutron thresholds with the counter ratio method; however, the neutron yields measured with this counter below 0.3 Mev are too small by as much as a factor of 2.5 for low-energy neutrons.

Pronounced resonances are obtained in most (p,n) reactions and the effects of these resonances are largely eliminated by using the counter ratio method.[1] However, in the case of the $Cu^{65}(p,n)$ reaction and to a smaller extent in the $Cu^{63}(p,n)$ reaction the effects of the resonances were not completely eliminated. At bombarding energies above the 2.97-Mev threshold of the first excited state of Zn^{65}, fluctuations in the counter ratio were observed that were too large to be attributed to statistics. The ratio of the number of neutrons emitted to the first excited state compared to the number emitted to the ground state would be expected to change from one resonance to another, because of the change in angular momentum and parity between successive levels of the compound nucleus. The fluctuations in the counter ratio are attributed to such changes.

[2] Hanson, Taschek, and Williams, Revs. Modern Phys. **21**, 635 (1949).
[3] C. F. Cook and T. W. Bonner, Phys. Rev. **94**, 807(A) (1954).
[4] Blaser, Boehm, Marmier, and Scherrer, Helv. Phys. Acta **24**, 441 (1951).
[5] Marion, Brugger, and Bonner, this issue [Phys. Rev. **100**, 46 (1955)].
[6] R. F. Taschek and A. Hemmendinger, Phys. Rev. **74**, 373 (1948).

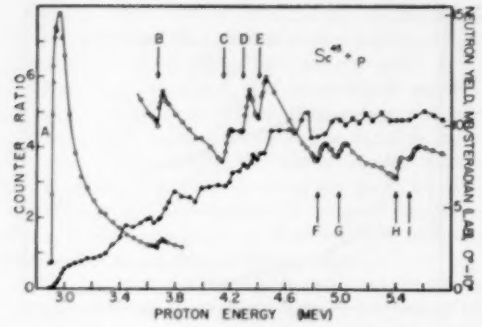

FIG. 3. The counter ratio (open circles) and the yield of neutrons in the forward direction measured by the modified long counter (solid circles) as a function of the proton energy for the $Sc^{45}(p,n)Ti^{45}$ reaction. *The counter ratios have been multiplied by 5 for proton energies above 3.6 Mev.*

Below the thresholds corresponding to the first excited states, there were no fluctuations observed that could not be attributed to statistics. To eliminate partially the fluctuations due to resonances, the data taken for Cu^{65} with a 35-kev target were averaged over 120 kev, while 120-kev targets were used for scandium and zinc. This averaging process increased the error in determining the threshold energies.

Values of the cross sections for the yield of neutrons in the forward direction in units of millibarns per steradian in the laboratory system were obtained for the proton bombardment of Sc^{45}, Cu^{63}, and Cu^{65}. A long counter similar to that described by Hanson and McKibben[7] was used to determine the cross sections. It was placed at zero degrees to the beam and 42 inches from the target and recorded the number of neutrons per microcoulomb of beam striking the targets. To eliminate variations in the efficiency of the long counter with neutron energy, weighed targets of Sc_2O_3, Cu^{63}, Cu^{65}, and LiF were bombarded at proton energies so that the emitted neutrons had an energy of about 0.60 Mev. This was not completely realized in the case of Cu^{63} because of a second group of neutrons emitted to the 0.191-Mev state of Zn^{63}. The differential cross section for the $Li^7(p,n)Be^7$ reaction which has been determined to an accuracy of about 10 percent by Taschek and Hemmendinger[8] was used as the standard to which the other reactions were compared.

For cross section determinations the target material was evaporated onto 2-mil pure aluminum backings. The amount of target material was determined by weighing the backings before and after an evaporation. A quartz spring with about 1 milligram per millimeter sensitivity, in conjunction with a telescope containing a calibrated eyepiece, was used to make the weighings. The weights of the Sc_2O_3, Cu^{63}, Cu^{65}, and LiF on the targets were 267, 323, 473, and 220 micrograms/cm², respectively.

[7] A. O. Hanson and J. L. McKibben, Phys. Rev. **72**, 673 (1947).

$Sc^{45}(p,n)Ti^{45}$

To study the yield of neutrons from the proton bombardment of scandium, targets were made by evaporating Sc_2O_3 from a V-shaped tungsten filament onto tungsten or weighted aluminum blanks. At temperatures close to the evaporating temperature (~1300°C) the Sc_2O_3 on the filament turned from white to black. The thickest target which was made (~120 kev thick) was dark grey in color, while the thinner targets were cream colored. Baker, Howell, Goodman, and Preston[8] reported making scandium targets by evaporating Sc_2O_3 from a carbon boat. In the process they reported that the oxide was reduced and metal targets were made. Targets that were made at the same time as the targets used in this experiment were also used to study the inelastic scattering of protons from scandium and the results[9] showed that the targets contained a considerable amount of oxygen. A scandium target evaporated onto a glass backing had a very high electrical resistance which also indicates that the oxide and not the metal was deposited.

Figure 3 shows the counter ratio and the yield of neutrons in the forward direction for scandium bombarded by protons of energies from 2.9 to 5.6 Mev. The target used was 120-kev thick to protons of 2.9 Mev and had a tungsten backing. The yield has been corrected for background obtained by bombarding a clean tungsten blank. The counter ratio shows the usual sharp rise at the ground-state threshold energy of 2.908 Mev (A) and other thresholds *B*, *C*, *D*, *E*, *F*, *G*, *H*, and *I* at higher energies due to eight excited states in Ti^{45}. Table I lists the threshold energies and the *Q*-values for the $Sc^{45}(p,n)Ti^{45}$ reaction and the excitation energies of the Ti^{45} states. The 120-kev target has essentially eliminated fluctuations due to resonances in the compound nucleus, by averaging the effects of a large number of resonances.

The ground-state threshold energy was measured to be 2.908±0.004 Mev yielding a *Q*-value for the reaction of −2.844±0.004 Mev; a mass defect of −25.87

TABLE I. Neutron thresholds in the reaction $Sc^{45}(p,n)Ti^{45}$.

Threshold	Threshold energy (Mev)	*Q*-value (Mev)	Ti^{45} (Mev)
A	2.908±0.004	−2.844±0.004	0
B	3.667±0.010	−3.587±0.010	0.743±0.011
C	4.129±0.007	−4.038±0.007	1.194±0.008
D	4.285±0.009	−4.191±0.009	1.347±0.010
E	4.400±0.010	−4.304±0.010	1.460±0.011
F	4.826±0.009	−4.720±0.009	1.876±0.010
G	4.969±0.012	−4.860±0.012	2.016±0.013
H	5.392±0.010	−5.274±0.010	2.430±0.011
I	5.520±0.007	−5.399±0.007	2.555±0.008

[8] Baker, Howell, Goodman, and Preston, Phys. Rev. **81**, 48 (1951).

[9] Gossett, Phillips, Schiffer, and Windham, this issue [Phys. Rev. **100**, 203 (1955)].

± 0.56 Mev and a mass of 44.97222 ± 0.00060 amu[10] are indicated for Ti^{45}. This threshold is in good agreement with the value of 2.9 Mev obtained by Hanson, Taschek, and Williams[2] and that estimated from the curve of Baker, Howell, Goodman, and Preston[8] as 2.87 Mev. A Q-value for the $Sc^{45}(p,n)Ti^{45}$ reaction can be calculated from the positron decay[11] of Ti^{45}. This calculation gives a Q-value of -2.822 ± 0.010 Mev, which is 0.022 Mev lower than that obtained from the threshold measurement. The higher thresholds are assigned errors depending on the estimated accuracy of extrapolating the leading edge of the threshold.

The differential cross section for the yield of neutrons in the forward direction was obtained at a proton energy of 3.53 Mev and was found to be 3.4 percent of that for the reaction $Li^7(p,n)Be^7$ at a proton energy of 2.30 Mev. The comparison was made for the same neutron energy to eliminate any energy dependence of the long counter efficiency. This gives a cross section for the $Sc^{45}(p,n)Ti^{45}$ reaction averaged over a proton energy from 3.41 to 3.53 Mev of 3.6 mb. The yield of neutrons into the forward cone of half-angle 10° is given by the right-hand ordinate of Fig. 3 in units of millibarns per steradian in the laboratory system.

The proton energy region from threshold to 0.070 Mev above threshold was investigated with a 2.7-kev target. The thickness of this target was determined by comparing the counting rate with that from a thicker weighed target. The amount of scandium oxide on the thin target was determined to be 29.5 micrograms/cm². Figure 4 shows the yield of neutrons measured by the slow counter from threshold to 0.070 Mev above threshold. The yield has been corrected for background. Since the counter sensitivity is essentially constant over this energy region, the yield has not been corrected for any variation in the counter sensitivity. The levels

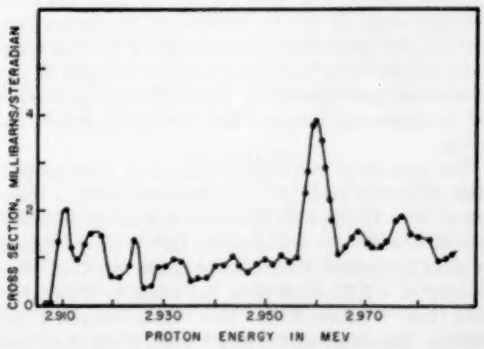

FIG. 4. The yield of neutrons in the forward direction as a function of the proton energy as measured by the slow counter for the $Sc^{45}(p,n)Ti^{45}$ reaction.

[10] Mass values of Sc^{45}, Cu^{63}, and Cu^{65} were taken from the tables of E. Segrè, *Experimental Nuclear Physics* (John Wiley and Sons, Inc., New York, 1953), Vol. 1, p. 745.

[11] Ter-Pogossian, Cook, Porter, Morganstern, and Hudis, Phys. Rev. **80**, 360 (1950).

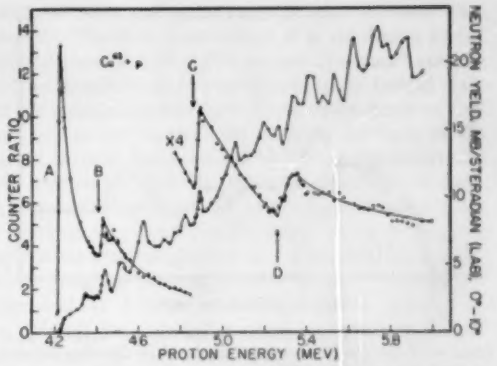

FIG. 5. The counter ratio showing thresholds at A, B, C and D and the yield of neutrons in the forward direction as a function of the proton energy as measured by the modified long counter for the $Cu^{63}(p,n)Zn^{63}$ reaction.

appear to be as wide as 6 kev and are spaced about 2–9 kev apart. The cross section near threshold was determined by comparing the counting rates to that for 3.53-Mev protons and then correcting for the change in counter sensitivity.

If the energy separation between levels is considerably greater than the level widths, the yield will become very small between resonances. In this case if the theoretical (p,n) threshold falls between two resonances, the experimental threshold would not appear until the proton energy reaches the next higher resonance, thus introducing a small error in the Q-value for the (p,n) reaction calculated from the neutron threshold.

$Cu^{63}(p,n)Zn^{63}$

The separated isotope of Cu^{63} (99.11 percent Cu^{63}) in the form of CuO was obtained from the Oak Ridge National Laboratory. The CuO was reduced to metallic copper and targets were made by evaporating the metal onto weighed aluminum blanks or onto tungsten blanks. Figure 5 shows the counter ratio and the yield of neutrons in the forward direction for a 17-kev Cu^{63} target. The yield has been corrected for background. The sharp rises at 4.215, 4.410, 4.868, and 5.265 Mev are attributed to the ground-state threshold and three excited state thresholds. The small dip and rise near 4.50 Mev is attributed to a resonance effect and not to a threshold. Table II lists the threshold energies and the Q-values for the $Cu^{63}(p,n)Zn^{63}$ reaction and the excitation energies in Zn^{63}.

The ground-state threshold energy of 4.215 ± 0.004 Mev yields a Q-value of -4.149 ± 0.004 Mev; a mass defect of -44.48 ± 1.86 Mev and a mass of 62.95223 ± 0.00200 amu[10] are indicated for Zn^{63}. A previous determination of the Q-value for this reaction by Strain[12] gave -4.04 ± 0.17 Mev, and that by Blaser, Boehm, Marmier, and Scherrer[4] gave -4.14 ± 0.1 Mev.

[12] C. V. Strain, Phys. Rev. **54**, 1021 (1938).

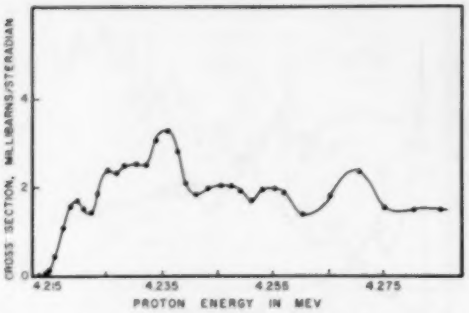

FIG. 6. The yield of neutrons in the forward direction as a function of the proton energy as measured by the slow counter for the $Cu^{63}(p,n)Zn^{63}$ reaction.

A preliminary determination by Cook and Bonner[3] gave -4.21 Mev. Recently Kington, Bair, Cohn, and Willard[10] have measured the threshold for the $Cu^{63}(p,n)Zn^{63}$ reaction to be 4.213 ± 0.008 Mev, which is in very good agreement with the present value. The Q-value calculated from the energy of the Zn^{63} positron decay of 2.36 Mev[14] gives better agreement than does that calculated with the value of 2.320 Mev.[15]

The cross section for the yield of neutrons in the forward direction was obtained by comparing the yield per nucleus of Cu^{63} bombarded by 4.74-Mev protons to that of Li^7 bombarded by 2.30-Mev protons. The cross section for neutrons emitted into the forward direction averaged over a proton energy from 4.71 to 4.74 Mev was 6.7 mb. The yield curve was normalized to this value of the cross section.

The region from threshold to 0.070 Mev above threshold was reinvestigated with a 3.6-kev target. Figure 6 shows the yield measured by the slow counter,

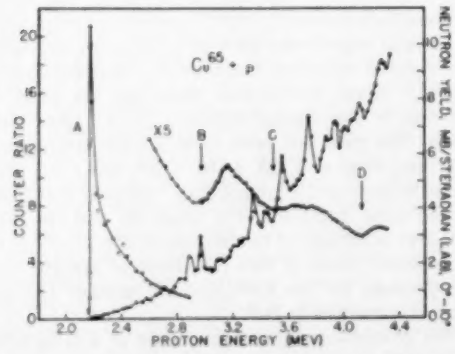

FIG. 7. The counter ratio (open circles) and the yield of neutrons in the forward direction as a function of the proton energy as measured by the modified long counter (solid circles) for the $Cu^{65}(p,n)Zn^{65}$ reaction.

[10] Kington, Bair, Cohn, and Willard, Phys. Rev. **99**, 1393 (1955).
[14] Huber, Medicus, Preiswerk, and Steffen, Helv. Phys. Acta **20**, 496 (1947).
[15] A. A. Townsend, Proc. Roy. Soc. (London) **A177**, 357 (1941).

corrected for background, but uncorrected for the small change in counter sensitivity in this energy region. The target thickness and the cross section were determined by the same methods used for the scandium reaction. The amount of Cu^{63} on the target was 85 micrograms/cm^2. The data of Fig. 6 indicates a complicated resonance structure. It is uncertain whether the observed widths of some of the resonances are level widths or are due to target thickness and to the spread in energy of the beam.

$Cu^{65}(p,n)Zn^{65}$

The separated isotope of Cu^{65} (98.2 percent Cu^{65}) in the form of CuO was reduced to metallic copper and evaporated onto weighed aluminum disks. Figure 7 shows the counter ratio and the yield of neutrons in the forward direction for a Cu^{65} target bombarded with protons. The data were taken with a target with a weight of 473 micrograms/cm^2 ($\sim$35 kev thick at

TABLE II. Neutron thresholds in the reaction $Cu^{63}(p,n)Zn^{63}$.

Threshold	Threshold energy (Mev)	Q-value (Mev)	$^*Zn^{63}$ (Mev)
A	4.215 ± 0.004	-4.149 ± 0.004	0
B	4.410 ± 0.010	-4.340 ± 0.010	0.191 ± 0.011
C	4.868 ± 0.010	-4.791 ± 0.010	0.642 ± 0.011
D	5.265 ± 0.014	-5.182 ± 0.014	1.043 ± 0.015

TABLE III. Neutron thresholds in the reaction $Cu^{65}(p,n)Zn^{65}$.

Threshold	Threshold energy (Mev)	Q-value (Mev)	$^*Zn^{65}$ (Mev)
A	2.169 ± 0.004	-2.136 ± 0.004	0
B	$2.97\ \pm0.03$	$-2.92\ \pm0.03$	0.78 ± 0.03
C	$3.45\ \pm0.03$	$-3.40\ \pm0.03$	1.26 ± 0.03
D	$4.13\ \pm0.02$	$-4.07\ \pm0.02$	1.93 ± 0.02

2.2 Mev). Above 2.95 Mev the counter ratio has been averaged over 120 kev to smooth out the fluctuations due to the pronounced resonances. This averaging increased the error in determining the energies of the second and third thresholds. Table III lists the threshold energies and Q-values for the $Cu^{65}(p,n)Zn^{65}$ reaction.

The ground-state threshold energy of 2.169 ± 0.004 Mev gives a Q-value of -2.136 ± 0.004 Mev; a mass defect of -47.54 ± 1.96 Mev and a mass of 64.94895 ±0.00210 amu[10] are indicated for Zn^{65}. This Q-value is in good agreement with that obtained by Cook and Bonner[3] of -2.12 ± 0.03 Mev, but lower by 0.030 Mev than the -2.166 ± 0.010 Mev value obtained by Shoupp, Jennings, and Jones[16] when their data are corrected for the accurate $Li^7(p,n)Be^7$ threshold energy. Kington, Bair, Cohn, and Willard[10] have recently measured the disintegration Q-value to be -2.137 ±0.005 Mev. The Q-value calculated from the positron decay of Zn^{65} is -2.129 ± 0.002 Mev,[17] 0.007 Mev

[16] Shoupp, Jennings, and Jones, Phys. Rev. **73**, 421 (1948).
[17] R. W. King, Revs. Modern Phys. **26**, 388 (1954).

lower than that calculated from the present threshold energy.

Crasemann[18] has studied the decay of Ga^{65}. The difference in energy between the two positrons reported indicates that the decay of Ga^{65} might leave Zn^{65} in excited states at 0.78 or 1.26 Mev. Since no high-energy γ rays were reported, this assignment is indefinite. No indication of low-lying states at 0.052, 0.092, or 0.114 Mev in Zn^{65} that would correspond to the γ rays of these energies reported by Crasemann were noticed in the counter ratio. Thresholds corresponding to these levels would not have been observed unless they were rather intense, since the total yield is low and the relative counter efficiencies would not have changed sufficiently to indicate a second group of neutrons if they appeared with nearly the same energy as the first group.

The cross section was obtained by comparing the yield per nucleus from a weighed Cu^{65} target bombarded with 2.75-Mev protons to the yield per nucleus

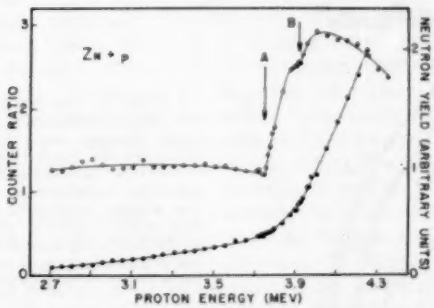

FIG. 8. The counter ratio (open circles) and the relative yield of neutrons in the forward direction as a function of the proton energy as measured by the modified long counter (solid circles) for the Zn(p,n)Ga reaction.

from Li^7 bombarded with protons of 2.30-Mev energy. The cross section for the yield of neutrons in the forward direction averaged over a proton energy from 2.71 to 2.75 Mev was 1.1 mb.

Zn(p,n)Ga

The threshold of the $Zn^{68}(p,n)Ga^{68}$ reaction was measured to be 3.4 ± 0.3 Mev by Marmier and Scherrer[4] using a cyclotron and stacked foils. In order to obtain a more precise value for this threshold, experiments were carried out with a normal Zn target. Figure 8 shows the counter ratio and yield of neutrons in the forward direction for a 120-kev natural zinc target bombarded by protons. Neutrons emitted below a proton bombarding energy of 3.7 Mev are due to Zn^{67}, which is 4.11 percent abundant in natural zinc and has a (p,n) threshold at 1.812 Mev,[19] and due to Zn^{70} (0.62 percent abundant) with a threshold at 1.47 Mev.[19] At 3.749 Mev and again at 3.921 Mev the ratio rises sharply. The first threshold at A is attributed to the ground state of Zn^{68} (18.56 percent abundant) and the second threshold at B is attributed to an excited state in the residual nucleus Ga^{68}. These assignments to Zn^{68} and not to Zn^{67} or Zn^{70} are made on the basis of the larger isotopic concentration of Zn^{68} in the target and the agreement with the expected threshold of Zn^{68}. The ground-state threshold at 3.749 ± 0.006 Mev gives a Q-value of -3.694 ± 0.006 Mev, which is in good agreement with the Q-value of -3.68 ± 0.20 Mev calculated from the positron decay[17] of Ga^{68}. The second threshold at 3.921 ± 0.006 Mev with a Q-value of -3.864 ± 0.006 Mev indicates an excited state of Ga^{68} at 0.170 ± 0.009 Mev above the ground state.

[18] B. Crasemann, Phys. Rev. **93**, 1034 (1954); **90**, 993 (1953).
[19] C. Trail and C. H. Johnson, Phys. Rev. **91**, 474(A) (1953).

$Sc^{45}(p,n)Ti^{45}$ and $Cu^{63}(p,n)Zn^{63}$ Reactions as Kilovolt Neutron Sources

At the present time the $Li^7(p,n)Be^7$ reaction, emitting neutrons at backward angles, is the most widely used source of kilovolt neutrons. The disadvantages of working at backward angles, using rotating targets, and the necessity of evaporating the target in the accelerator vacuum system are usually compensated by the many advantages of this reaction. The yield of neutrons even in the backward hemisphere is large and the threshold can be reached by most Van de Graaff accelerators. The energy resolution obtainable is one of the greatest advantages.

The energy of the neutrons emitted from either scandium or Cu^{63} changes rapidly the first few kilovolts above threshold. At a proton energy 4 kev above the scandium threshold, the neutron energy has reached 10 kev, and a 1-kev beam spread introduces about 2-kev spread in neutron energy. For 20-kev neutrons a proton beam spread of 1 kev introduces a spread in the neutron beam of 1 kev. For scandium, when 20-kev neutrons are emitted at 0°, 19.5-kev neutrons are emitted at 15° or only a 0.5-kev variation in neutron energy over this large angle. Thus samples subtending large angles could be used for neutron scattering or absorption without introducing a large energy spread.

Neutron sources obtained from the bombardment of heavier elements will have the advantage in experiments where background and room scattering into the detector are important. The number of neutrons emitted toward the detector as compared to the number emitted elsewhere is greatest when working at 0°. Further improvements in the energy resolution of Van de Graaff accelerators may make the doppler broadening the major limitation in resolution. Heavier nuclei such as Sc^{45} and Cu^{63} thus will be much superior to a light element such as Li^7.

The yield of neutrons in the forward direction for the scandium reaction just above threshold is about 1.5 mb per steradian. These cross sections are approximately 10 percent of the cross section per unit solid angle for

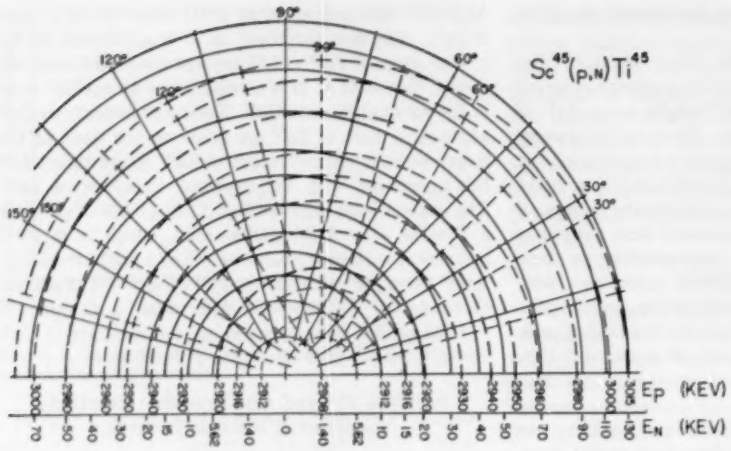

FIG. 9. A nomograph for the $Sc^{45}(p,n)Ti^{45}$ reaction. The upper energies and dotted circles are the proton energies in kilovolts. The lower energies and solid circles are the neutron energies in kilovolts. The solid radial lines are for angles in the laboratory system. The dotted radial lines are for angles in the center-of-mass system.

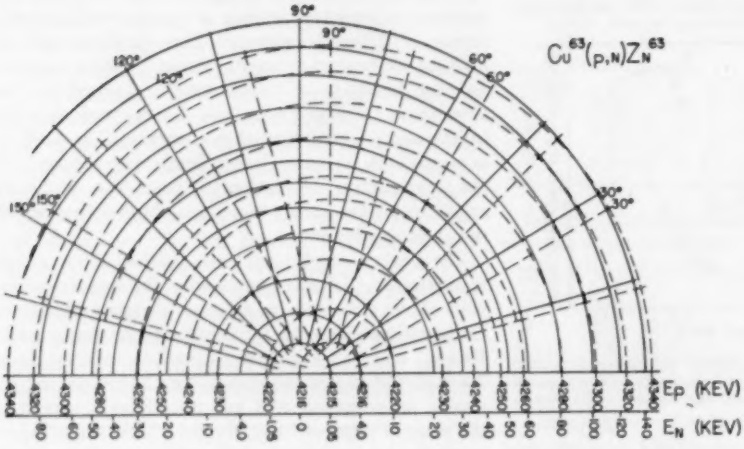

FIG. 10. A nomograph for the $Cu^{63}(p,n)Zn^{63}$ reaction. The upper energies and dotted circles are the proton energies in kilovolts. The lower energies and solid circles are the neutron energies in kilovolts. The solid radial lines are for angles in the laboratory system. The dotted radial lines are for angles in the center-of-mass system.

kev neutrons emitted at 120° from the $Li^7(p,n)Be^7$ reaction. The yields from Sc^{45} and Cu^{63} would still be adequate for neutron sources if large beam currents were used. There was no indication that target material was being lost when the targets were mounted in the poorly cooled multiple target holder and bombarded with 4 or 5 microamperes of beam. If the copper or Sc_2O_3 were evaporated onto thin backings and these were mounted flush to the thin, aircooled end of the accelerator vacuum system, the targets should be able to withstand 50 microamperes of beam.

The counter ratio for both Sc^{45} and Cu^{63} give no indication that there are low-lying states in Ti^{45} or in Zn^{63} below 190 kev. Thus the sources should be monoenergetic up to neutron energies of 200 kev. As may be seen from Fig. 4 the yield of neutrons from scandium varies rapidly with energy. However, the sharp resonances and low yields between resonances might be used to obtain a well-resolved neutron beam of discrete energy from a proton beam of 3- or 4-kev beam spread. By rotating the counter and scatterer from 0° to larger angles, neutrons could be obtained that would have energies that correspond to the gaps in the forward yield of neutrons. Thus a continuous variation in neutron energy could be obtained. Figures 9 and 10 are nomographs for these two reactions of the same type described by Hanson, Taschek, and Williams[2] for $Li^7(p,n)Be^7$.

Study of the Reactions $T^3(p,n)He^3$, $Li^7(p,n)Be^7$, $Be^9(p,n)B^9$, and $F^{19}(p,n)Ne^{19}$†

J. B. Marion,* T. W. Bonner, and C. F. Cook‡
The Rice Institute, Houston, Texas

(Received June 22, 1955)

A counter ratio study has been made of the (p,n) reactions on T^3, Li^7, Be^9, and F^{19}. The ground state threshold energy for the reaction $F^{19}(p,n)Ne^{19}$ was found to be 4.235±0.005 Mev. Other neutron thresholds were observed which indicated excited states in Be^7 at 0.434±0.004 Mev, in B^9 at 2.326±0.006 Mev and in Ne^{19} at 0.241±0.004 and 0.280±0.004 Mev. A broad maximum in the yield of slow neutrons from the bombardment of Be^9 was observed which could be due to the three-body breakup, $Be^9(p,pn)Be^8$, or to a broad, even parity state in B^9 at 1.4 Mev. The cross sections for the reactions $Be^9(p,n)B^9$, $B^{11}(p,n)C^{11}$, $C^{12}(p,n)N^{13}$, and $F^{19}(p,n)Ne^{19}$ were measured.

INTRODUCTION

THE accurate measurement of nuclear energy levels has been shown possible by using the "counter ratio" technique[1-3] for detecting the emission of slow neutrons near threshold in (p,n) and (d,n) reactions. This technique employs two paraffin-moderated BF_3 counters, one which is preferentially sensitive to low energy neutrons ("slow counter"), and one which is almost energy insensitive ("modified long counter"). A measure of the number of slow neutrons emitted in a reaction is obtained by observing, as a function of bombarding energy, the ratio of the counting rate in the slow counter to that in the modified long counter. Sharp increases in the counter ratio indicate the emission of slow neutrons leaving the residual nucleus in one of its energy states. Since the sensitivity of the modified long counter decreases rapidly for neutron energies less than about 0.3 Mev,[3] the rise in the counter ratio at a neutron threshold is enhanced. By arranging the two counters so that they subtend approximately the same solid angle at the target, irregularities in the ratio due to resonances for the production of neutrons are essentially eliminated.[1]

Since all (p,n) reactions on stable target nuclei have negative Q-values, it is possible to study with the counter ratio technique the low-lying level structure of the residual nuclei in such reactions. For reactions on odd-A light nuclei, these levels should be mirror to those of the target nuclei, and the latter have been investigated with precision inelastic scattering techniques. Therefore, the counter ratio method allows an accurate determination of nuclear energy levels which may be used in the comparison of mirror excited states. This technique has been applied to the (p,n) reactions on T^3, Be^9, Li^7, and F^{19} in order to investigate the level structures of He^3, B^9, Be^7, and Ne^{19}.

Since magnetic analysis of the charged-particle beam is used with the Rice Institute 6-Mev Van de Graaff accelerator, the bombarding energy is determined by measuring the field strength and the radius of curvature of the particle orbit. A nuclear resonance absorption magnetometer is used to measure the field strength, and the radius of curvature is determined by measuring the field strength at a number of well-known (p,n) thresholds. A detailed description of the technique used for precisely measuring the bombarding energy has been given previously.[2]

REACTION $T^3(p,n)He^3$

A counter ratio investigation was made of the reaction $T^3(p,n)He^3$, and the results are presented in Fig. 1. Since there are no known or expected low-lying levels in the He^3 nucleus, the ratio curve should be a smoothly decreasing function of the bombarding energy, and any irregularities that appear are probably characteristic of the counter ratio method and not of the He^3 nucleus. The target used in this experiment consisted of tritium gas adsorbed in a layer of Zr metal which had been evaporated onto a tungsten backing. This target was approximately 40 kev thick at a proton energy of 1 Mev. The counter ratio rises sharply at the threshold and then decreases smoothly until an energy of approximately 3.73 Mev is reached. At this bombarding energy, neutrons from the $T^3(p,n)He^3$ reaction have an energy

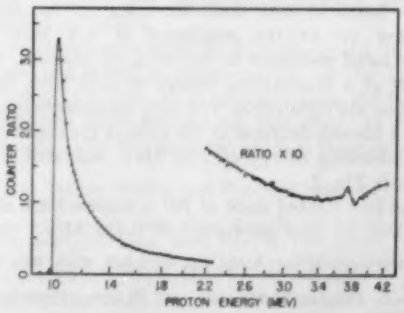

FIG. 1. $T^3(p,n)He^3$. Counter ratio as a function of bombarding energy.

† Supported in part by the U. S. Atomic Energy Commission.
* National Science Foundation Predoctoral Fellow; now postdoctoral Fellow at Kellogg Radiation Laboratory, California Institute of Technology, Pasadena, California.
‡ Now at Convair, Fort Worth, Texas.
[1] T. W. Bonner and C. F. Cook, Phys. Rev. **96**, 122 (1954).
[2] Marion, Brugger, and Bonner, this issue [Phys. Rev. **100**, 46 (1955)].
[3] Brugger, Bonner, and Marion, this issue [Phys. Rev. **100**, 84 (1955)].

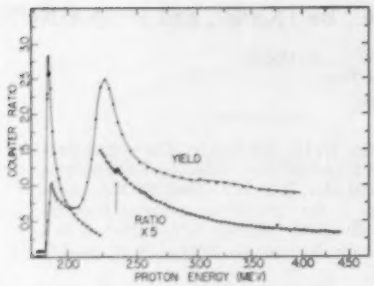

FIG. 2. $Li^7(p,n)Be^7$. Counter ratio and yield of neutrons in the forward direction as a function of bombarding energy.

of 2.95 Mev. This neutron energy corresponds to that for a resonance in the neutron total cross section for carbon.[4] Since the paraffin of the slow counter is interposed between the target and the modified long counter, the number of neutrons reaching the modified long counter will be reduced because of the greater scattering in carbon, and the counter ratio will rise. Therefore, the shape of the ratio curve will be approximately the same as the shape of the total cross section resonance. In the $T^3(p,n)He^3$ reaction, this is, indeed, seen to be the case. An additional resonance in this energy region, due to 2.08-Mev neutrons[4] ($E_p=2.80$ Mev), was not observed due to its very narrow width.

REACTION $Li^7(p,n)Be^7$

Since the yield of neutrons near threshold is quite large, and since the threshold energy is easily accessible with most present-day Van de Graaff accelerators, the threshold for the reaction $Li^7(p,n)Be^7$ has long been used as an energy calibration point for proton energies near 2 Mev. Consequently, the threshold energy has been measured quite accurately. The currently accepted value is 1.8811 ± 0.0005 Mev.[5] As was stated earlier,[2] this threshold was used as the primary calibration in these experiments.

The results obtained by the counter ratio technique in the bombardment of a 20-kev LiF target are presented in Fig. 2. The ratio rises sharply at the ground-state threshold and then decreases for bombarding energies up to the maximum of 4.4 Mev. The pronounced resonance in the yield of neutrons, which occurs at a bombarding energy of 2.30 Mev, has no effect on the ratio curve. The only significant departure from a smooth decrease in the ratio is the slight rise at a bombarding energy of 2.38 Mev, indicated by the arrow in Fig. 2.

The first excited state of Be^7 is known from several reactions to have an energy of 0.430 Mev.[6] Since a bombarding energy of 2.38 Mev should correspond to the threshold for neutron emission to this state, the energy region near 2.4 Mev was investigated more closely and under conditions slightly different from the normal counter geometry.[1-3] First, the slow counter was moved as close to the target as was possible, and the counter ratio was measured as a function of bombarding energy from 2.330 to 2.450 Mev. The results are shown in Curve "*A*" of Fig. 3, in which the experimental points are plotted on an expanded scale with a false zero. With points taken at an energy interval of approximately 2 kev, a significant increase occurs at a bombarding energy of 2.379 ± 0.003 Mev. After rising for about 20 kev (½target thickness), the ratio decreases in the expected manner.

In an attempt to improve the sensitivity to the neutrons from this weak threshold, this energy region was re-investigated after covering the exposed ends of the slow counter with thin brass tubing onto which had been painted a $\frac{1}{16}$-inch layer of boron, enriched to 96 percent B^{10}. Commercial "Nitroseal" was used as an adhesive for the boron. It was anticipated that the presence of the B^{10} would decrease the background due to the slow, "room" neutrons, and thereby enhance the effect of the threshold. The results are shown in Curve "*B*" of Fig. 3, where, again, the points are plotted on an expanded scale. The threshold occurs at an energy of 2.377 ± 0.003 Mev, but the amount of rise is only slightly greater than in the former case. This indicates that "room" neutrons are of little importance at this bombarding energy, even in the investigation of such weak thresholds.

The average of these two runs gives a threshold energy of 2.378 ± 0.004 Mev and a Q-value of -2.079 ± 0.004 Mev for this state. Since the ground state Q-value is -1.645 ± 0.001 Mev,[6] the first excited state of Be^7 has an energy of 0.434 ± 0.004 Mev, in excellent agreement with the previous measurements.

By measuring the increase in the counting rate in the slow counter at the ground state threshold and at the threshold for the emission of neutrons leaving Be^7 in the first excited state, the intensity of the first excited state threshold was found to be 1.8 ± 0.6 percent of that of the ground-state threshold. This is a slightly lower figure than was obtained by Willard and Preston,[7] who found a value of 3% using a similar method.

The relative intensities of the neutron groups emitted to the ground and first excited states of Be^7 have been measured by a number of investigators in the energy range from 2.5 to 4.4 Mev.[8,9] Above 3 Mev, the average intensity of the group emitted to the 0.43-Mev state is about 10 percent of that of the ground state group. At 2.52 Mev, the intensity of the

[4] Bockelman, Miller, Adair, and Barschall, Phys. Rev. **84**, 69 (1951).
[5] Jones, Douglas, McEllistrem, and Richards, Phys. Rev. **94**, 947 (1954).
[6] F. Ajzenberg and T. Lauritsen, Revs. Modern Phys. **27**, 77 (1955).
[7] H. B. Willard and W. M. Preston, Phys. Rev. **81**, 480 (1951).
[8] F. Ajzenberg and T. Lauritsen, Revs. Modern Phys. **24**, 321 (1952).
[9] R. Batchelor, Proc. Phys. Soc. (London) **A68**, 452 (1955).

low energy group at 0° is 2.8% of the intensity of the high energy group.[9] At a bombarding energy of 2.40 Mev, the ratio of the total cross sections of the two neutron groups was calculated to be 0.18±0.06%, by correcting for the difference in counter sensitivity[3] for the two groups and for the fact that the low energy group at this bombarding energy is emitted entirely into a forward solid angle less than that subtended by the counter.

The threshold corresponding to the 0.434-Mev state of Be^7 occurs while the system is under the influence of the 2.30-Mev resonance. The fact that neutron emission to this state is extremely weak is consistent with the recent analysis of Adair,[10] which indicates that the 2.30-Mev resonance is due to a 3^+ state in Be^8 at 19.2 Mev which is superimposed on a "background" of $(1,2)^-$ states. Since the ground states of Li^7 and Be^7 are $3/2^-$ and since the first excited state of Be^7 is $\frac{1}{2}^-$, protons with $l=1$ are most likely to form the 3^+ compound nucleus state, and neutrons emitted from this level to the first excited state of Be^7 must have $l=3$, while p-wave neutron emission to the ground state is possible. Since the yield of f-wave neutrons vanishes with zero slope at threshold, the number of these neutrons would not become appreciable until a considerable energy above threshold was reached. The fact that some neutrons are emitted to the first excited state near threshold is probably due to the background influence of the $(1,2)^-$ states, postulated by Adair, which would allow s-wave neutron emission near threshold from the 1^- states. The ratio curve rises to peak value above this threshold in approximately target thickness, indicating s-wave emission. Emission of p-wave neutrons would cause the rise to continue for a considerably larger energy interval, and d- and higher-wave emission would not occur near threshold with a measurable probability.

The yield curve of Fig. 2, as measured by the modified long counter at 0°, shows the rise at the ground state threshold caused by the emission of all of the neutrons into the forward cone. The subsequent decrease results from the opening of the cone to 180°. In addition to the well-known resonance at 2.30 Mev, there is some indication of a broad resonance at a bombarding energy of 3.2 Mev. This effect has also been observed by Bair *et al.*[11] It is possible that this broad resonance is at least partially responsible for the "background influence" on the yield near the 2.30-Mev resonance, mentioned earlier.

REACTION $Be^9(p,n)B^9$

The level structure of the Be^9 nucleus has been investigated with considerable accuracy up to excitations of a few Mev by observing inelastic proton scattering.[6,12] For excitations of less than 3 Mev, the existence of only one state, at 2.432±0.004 Mev,[12] has been definitely established. The possibility of additional states at 1.8 and 3.1 Mev has been reported.[13–16] Measurements by Ajzenberg and Buechner[17] on the reaction $Be^9(p,n)B^9$, using photographic plates, indicate a level in the mirror nucleus, B^9, at 2.37±0.04 Mev. No narrow states of lower excitation were found. A broad continuum of neutrons was observed,[17,18] attributed to the three-body breakup, $Be^9(p,pn)Be^8$, but the possibility of a broad state was not excluded.

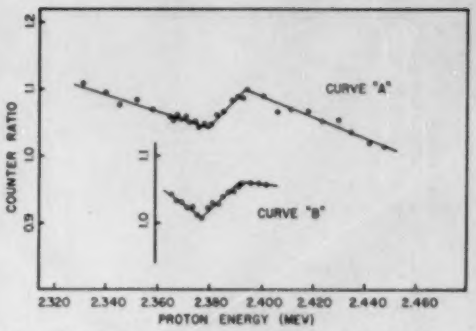

FIG. 3. $Li^7(p,n)Be^7$. Counter ratio as a function of bombarding energy in the region of the threshold corresponding to the first excited state of Be^7.

In order to obtain a more accurate value for the 2.37-Mev state and to investigate further the possibility of additional states, the reaction $Be^9(p,n)B^9$ was investigated with the counter ratio technique. An evaporated beryllium target, about 8 kev thick at a proton energy of 2 Mev, was used in the experiment. The counter ratio and the yield of neutrons in the forward direction were measured for proton energies from threshold to 5.8 Mev. The results are presented in Fig. 4. In addition to the ground state threshold, only one sharp threshold, at 4.645±0.005 Mev, was found. A rather broad rise in the ratio was observed to be centered about a bombarding energy of 3.6 Mev. These neutrons probably correspond to the continuous distributions previously found.[17,18] The threshold energies, Q-values, and excitation energies in B^9 are summarized in Table I.

The measurements made in this experiment do not allow an unambiguous interpretation of the broad maximum at 3.6 Mev. Slow neutrons from the three-body breakup could account for this effect, as could a broad state in B^9. The observed width of the maximum

[9] R. K. Adair, Phys. Rev. **96**, 709 (1954).
[10] Bair, Willard, Snyder, Hahn, Kington, and Green, Phys. Rev. **85**, 946 (1952).
[12] Gossett, Phillips, Schiffer, and Windham, this issue [Phys. Rev. **100**, 203 (1955)].
[13] C. J. Mullin and E. Guth, Phys. Rev. **76**, 682 (1949).
[14] Moak, Good, and Kunz, Phys. Rev. **96**, 1363 (1954).
[15] Almqvist, Allen, and Bigham, Phys. Rev. **99**, 631(A) (1955).
[16] L. L. Lee and D. R. Inglis, Phys. Rev. **99**, 96 (1955).
[17] F. Ajzenberg and W. W. Buechner, Phys. Rev. **91**, 674 (1953).
[18] Johnson, Ajzenberg, and Laubenstein, Phys. Rev. **79**, 187 (1950).

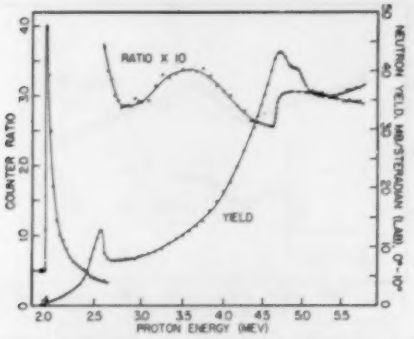

FIG. 4. $Be^9(p,n)B^9$. Counter ratio and yield of neutrons in the forward direction as a function of bombarding energy.

is approximately 1 Mev; the corresponding "state" would have the same width. Such a state in B^9 would be unstable to the emission of a proton to the ground state of Be^8, and a width of 1 Mev would indicate decay by s-wave proton emission.[19] This would imply even parity for the state, contrary to the systematics of the nuclei in the $p_{\frac{1}{2}}$ subshell, which indicate that all of these nuclei with unpaired $p_{\frac{1}{2}}$ particles have odd parity for the first excited state. An odd parity state at this energy that could decay by p-wave proton emission would have a width of approximately 0.3 Mev,[19] much narrower than the observed width of the maximum in the ratio curve. If the observed effect is due primarily to a broad state in B^9 and not to the three-body breakup, then this state probably has even parity and violates the shell model prediction.

An investigation has recently been made of the level structure of the mirror nucleus, Be^9, in this energy region. In a precision measurement of the protons inelastically scattered from Be^9, Gossett *et al.*[13] observed an asymmetric group of protons corresponding to an excitation in Be^9 of about 1.8 Mev. These data were not conclusive as to whether the protons arose from the three-body breakup or from a broad state in Be^9 which decays by s-wave neutron emission. A Be^9 state that decays by s-wave neutron emission must also have even parity.

Since unambiguous interpretations of these sets of data are not possible, it must be concluded that the observed effects are due either to the three-body breakup or to even-parity states in the mirror nuclei, Be^9 and B^9.

The threshold at 4.645 Mev rises to peak value in approximately 70 kev. Since the target thickness is considerably less than 70 kev, this slow rise is indicative either of level width or of the emission of threshold neutrons with $l=1$. The fact that the mirror state in Be^9 is quite narrow is strong evidence against the possibility of level width. Gossett *et al.*[13] report a width of $\leqslant 1$ kev for the Be^9 level. This state is known to decay mainly by neutron emission[20] and to have large spin, probably 5/2, 7/2, or 9/2, and odd parity.[12,21] The spin predicted by Inglis[22] is 5/2. The spin, parity, and level width should be the same for the B^9 state. Furthermore, the ratio curve does not decrease rapidly above threshold as it does above the ground state threshold. This implies that the yield of neutrons emitted to the 2.326-Mev state of B^9 is continuing to rise for a considerably larger energy interval above threshold than is to be expected for s-wave emission. This indicates that p-wave neutrons are largely responsible for the rise, and that the ratio is prevented from decreasing by the continued rise in the yield of neutrons with $l \geqslant 1$.

The 4.645-Mev threshold occurs near the resonance energy of 4.7 Mev, as is indicated in Fig. 4. The compound nucleus state involved is the 10.8-Mev level in B^{10}. If it is assumed that the larger part of the neutrons emitted near threshold have $l=1$ and that the B^9 state has spin 5/2, 7/2, or 9/2 and odd parity, then the resulting possible compound nucleus state has $J \leqslant 6^+$, and the incoming protons have odd angular momentum.

In an attempt to locate any higher energy state in B^9 which might be the analog of the reported 3.1-Mev state in Be^9, the ratio curve was extended to a bombarding energy of 5.8 Mev. No indication of additional thresholds was observed. This bombarding energy corresponds to an excitation energy in B^9 of 3.4 Mev and should be sufficiently high to include the region in which the threshold would be expected to occur. The fact that no threshold was observed does not exclude the possibility of the existence of a state or states, since there could be selection rules imposed by the compound nucleus states which would greatly reduce the probability of neutron emission near threshold. It may be stated, however, that no levels exist in this energy region for which the intensity of neutron emission near threshold is greater than about 0.2 of that for the 4.645-Mev threshold.

The yield curve of Fig. 4 shows the well-known resonance at a bombarding energy of 2.56±0.02 Mev and, superposed on a general rise, another broad

TABLE I. Neutron thresholds in the reaction $Be^9(p,n)B^9$.

Threshold energy (Mev)			Excitation energy in B^9(Mev)	
Present work	Other measurement	Q-value (Mev)	Present work	Other measurement
2.060±0.003	2.059±0.002[a]	−1.852±0.002[a]	0	0
3.6(?)		−3.25(?)	1.4(?)Γ≈1 Mev	
4.645±0.005		−4.178±0.005	2.326±0.006	2.37±0.04[b]

[a] Richards, Smith, and Browne, Phys. Rev. **80**, 524 (1950).
[b] See reference 17.

[19] R. F. Christy and R. Latter, Revs. Modern Phys. **20**, 185 (1948).

[20] G. A. Dissanaike and J. O. Newton, Proc. Phys. Soc. (London) **A65**, 675 (1952).
[21] F. L. Ribe and J. D. Seagrave, Phys. Rev. **94**, 934 (1954).
[22] D. R. Inglis, Revs. Modern Phys. **27**, 76 (1955).

maximum at 4.68±0.03 Mev. These resonances have been observed by Hahn *et al.*,[23] who obtained a resonance energy of 4.72±0.01 Mev for the latter peak. A close examination of the energy region near 5.0 Mev revealed the presence of a weak satellite to the 4.68-Mev resonance, located at a bombarding energy of 4.94±0.03 Mev.

REACTION $F^{19}(p,n)Ne^{19}$

The low-lying level structure of the F^{19} nucleus has been studied with great care by many investigators. The energies, spins, and parities of the first two excited states have been measured with considerable accuracy.[6] In order to establish the corresponding level structure of the mirror nucleus, Ne^{19}, about which no information had been previously obtained, the reaction $F^{19}(p,n)Ne^{19}$ was investigated with the counter ratio technique.

An evaporated AlF_3 target, which was about 7 kev thick at a proton energy of 4.5 Mev, was used in the experiment. The counter ratio and the forward yield of neutrons were measured from threshold to 5.9 Mev. The results are presented in Fig. 5. The ground-state threshold energy obtained was 4.235 ±0.005 Mev, in excellent agreement with that determined by Kington *et al.*,[24] who found a value of 4.240 ±0.008 Mev. In addition, two thresholds, corresponding to the first two excited states of Ne^{19}, were observed at 4.489±0.005 and 4.530±0.005 Mev. Both of these thresholds rise to peak value in an energy interval approximately equal to target thickness. The excitation energies in Ne^{19} are 0.241 and 0.280 Mev, respectively. Table II summarizes the threshold energies, Q-values, and excitation energies in Ne^{19}.

Since the first two excited states of F^{19} have energies of 0.110 and 0.197 Mev,[6] there is a considerable upward energy shift of the low-lying level structure between the mirror nuclei, F^{19} and Ne^{19}, with the nucleus of higher Z having levels of greater energy. In the light mirror nuclei ($A \leqslant 17$), there is no known case in which such an upward shift occurs for the first excited states. In the p-shell mirror nuclei, no such shift occurs even for the next two excited states within the accuracy to which these energy levels have been measured. Besides the case of F^{19} and Ne^{19}, it is perhaps significant that the only other well established departure from the rule that the energy levels of the mirror nucleus of higher Z lie lower also occurs in the d-shell. The second and third excited states of F^{17} have energies of 3.10 and 3.86 Mev, while the corresponding levels of O^{17} have energies of 3.06 and 3.85 Mev. Of the five well-known, low-lying pairs of levels in the d-shell mirror nuclei ($A=17$, 19), four exhibit the upward energy shift.

TABLE II. Neutron thresholds in the reaction $F^{19}(p,n)Ne^{19}$.

Threshold energy (Mev) Present work	Other measurement	Q-value (Mev)	Excitation energy in Ne^{19} (Mev)
4.235±0.005	4.240±0.008[a]	−4.022±0.005	0
4.489±0.005		−4.263±0.005	0.241±0.004[b]
4.530±0.005		−4.302±0.005	0.280±0.004[b]

[a] See reference 24.
[b] The error assignment is somewhat less than that determined from the errors in the Q-values since the energy of the excited state was obtained directly from an energy difference measurement.

[23] Hahn, Snyder, Willard, Bair, Klema, Kington, and Green, Phys. Rev. **85**, 934 (1952).
[24] Kington, Bair, Cohn, and Willard, Phys. Rev. **99**, 0000 (1955).

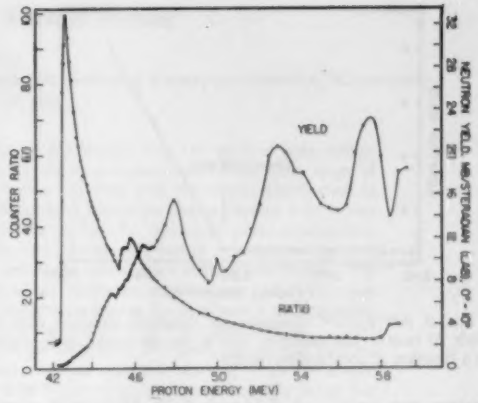

FIG. 5. $F^{19}(p,n)Ne^{19}$. Counter ratio and yield of neutrons in the forward direction as a function of bombarding energy, obtained with an AlF_3 target.

It was anticipated that the levels in Ne^{19} corresponding to the 1.35-Mev state and the reported state at 0.9 Mev in F^{19} might be observed, unless they were also shifted upward or were extremely weak near threshold. No indication of a threshold of intensity greater than 0.2 of that of the 4.489-Mev threshold was observed up to a bombarding energy of 5.8 Mev, corresponding to an excitation of 1.5 Mev in Ne^{19}.

At an energy of 5.82 Mev, an intense threshold was observed, due to the aluminum content of the AlF_3 target. In order to obtain a more accurate value for the threshold energy, this region was re-investigated using a thick aluminum target. The counting rate in the slow counter as a function of bombarding energy is shown in Fig. 6. The extrapolated point at which the yield rises above background is 5.816±0.008 Mev. This threshold energy is to be compared with the value of 5.792±0.010 Mev, obtained by Kington *et al.*[24]

The yield of neutrons in the forward direction from the reaction $F^{19}(p,n)Ne^{19}$, shown in Fig. 5, indicates several resonances. All of those resonances found below a bombarding energy of 5.2 Mev had been observed previously.[25] Since the yield curve was not taken with a very thin target, some of the resonances previously reported were not clearly resolved. Above 5.2 Mev,

[25] Willard, Bair, Kington, Hahn, Snyder, and Green, Phys. Rev. **85**, 849 (1952).

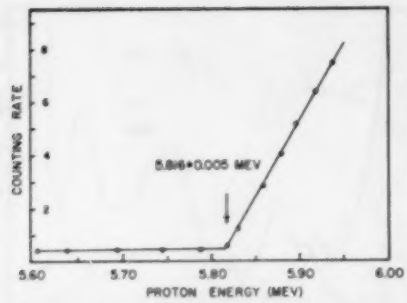

FIG. 6. $Al^{27}(p,n)Si^{27}$. Ground-state threshold obtained with a thick Al target. The counting rate in the slow counter is given as a function of bombarding energy.

strong resonances at 5.3 and 5.75 Mev and some indication of a resonance at 5.4 Mev were found. The excitation function for this reaction agrees well with that obtained by Blaser *et al.*,[25] who measured the Ne^{19} activity in a stacked foil experiment, except that the maximum at 5.75 Mev is much more pronounced in the present work.

MEASUREMENT OF ABSOLUTE CROSS SECTIONS

In order to obtain absolute cross sections for the production of neutrons in the proton bombardment of Be^9 and F^{19}, it was necessary to calibrate the relative yield curves that were obtained in the counter ratio studies. A Be^9 target of 171 $\mu g/cm^2$ and an AlF_3 target of 447 $\mu g/cm^2$ were prepared by techniques previously described.[3] The cross sections were determined by comparing the counting rates in a long counter[27] from the proton bombardment of these targets with that from a weighted LiF target, since the cross section for the reaction $Li^7(p,n)$ is well known.[28] In each case a bombarding energy was chosen so that the ground-state neutrons had an energy of approximately 0.6 Mev. In this manner, variations in the counter sensitivity with neutron energy were minimized.[3] At a bombarding energy of 2.52 Mev, the $Be^9(p,n)$ cross section was measured to be 11 mb/sterad, and at 4.74 Mev, the $F^{19}(p,n)$ cross section was 13 mb/sterad. Figures 4 and 5 show the cross sections for the emission of neutrons in these reactions into the forward cone of half-angle 10° in units of millibarns per steradian in the laboratory system. No corrections have been applied for the variations of the sensitivity of the modified long counter with neutron energy. The sensitivity of this counter[3] decreases rapidly for neutron energies below about 0.3 Mev, and, consequently, the measured cross sections near threshold are low by as much as a factor of 2. For the neutron energies encountered in these experiments, the counter sensitivity does not change appreciably above 0.3 Mev.

[25] Blaser, Boehm, Marmier, and Scherrer, Helv. Phys. Acta **24**, 465 (1951).
[27] A. O. Hanson and J. L. McKibben, Phys. Rev. **72**, 673 (1947).
[28] R. F. Taschek and A. Hemmendinger, Phys. Rev. **74**, 373 (1948).

TABLE III. Absolute cross sections for the reactions $B^{11}(p,n)$ and $C^{13}(p,n)$.

Reaction	Target thickness ($\mu g/cm^2$)	Proton energy (Mev)	Cross section (mb/sterad, lab system, 0°–10°)
$B^{11}(p,n)$	46	3.46	15
$C^{13}(p,n)$	190	3.70	6.7

REACTIONS $B^{11}(p,n)C^{11}$ AND $C^{13}(p,n)N^{13}$

A counter ratio study was made of the reactions $B^{11}(p,n)C^{11}$ and $C^{13}(p,n)N^{13}$ in an effort to locate neutron thresholds corresponding to the first excited states of the residual nuclei. These thresholds should have been observed at bombarding energies of 5.09 and 5.79 Mev, respectively. At these high energies, an increasing background of slow neutrons made difficult the detection of weak thresholds and the expected thresholds were not observed. Since thresholds with reasonable intensities could have been detected, it is not clear why these first excited state thresholds should be so weak that they were lost in the background. Excitation curves for the $B^{11}(p,n)$ reaction[26,29] and for the $C^{13}(p,n)$ reaction[26,30] have been given previously and they are not repeated here since good agreement was found with the earlier work. Absolute cross section measurements were made for these reactions with the techniques described above. The results are summarized in Table III.

[29] Bair, Kington, and Willard, quoted in reference 6.
[30] Bair, Kington, and Willard, Phys. Rev. **90**, 575 (1953).

Nuclear Radius and Nuclear Forces*

S. D. DRELL
Department of Physics and Laboratory for Nuclear Science, Massachusetts Institute of Technology, Cambridge, Massachusetts

(Received June 13, 1955)

The difference between the radius of the nuclear matter distribution and the nuclear force radius, $R_N \simeq 1.4A^{\frac{1}{3}} \times 10^{-13}$ cm, for heavy nuclei ($A > 100$) is interpreted as a consequence of the finite range of nuclear forces. Assuming that the nuclear matter distribution coincides with the charge distribution as determined at Stanford ($R_C = 1.12A^{\frac{1}{3}} \times 10^{-13}$ cm is the distance at which the charge density falls to one half value) we sum up the nuclear interactions of an incident nucleon for various proposed internucleon potentials, $V(r)$. We also evaluate contributions from the spin, charge, and matter polarizations induced in the nuclear distributions by the incident nucleon as a test of the convergence of these calculations. The aim here is to infer some features of nuclear forces which satisfy saturation requirements and at the same time give rise to an appreciable nuclear attraction for an incident nucleon at R_N. Analyses of the scattering of neutrons and protons by heavy nuclei suggest a nuclear attraction $\gtrsim 14$ Mev at a distance R_N.

These considerations are primarily sensitive to the long range behavior of the direct, central part of $V(r)$. The key point which emerges from them is that the nuclear forces must contain long range ($\sim$ meson Compton wavelength) direct, central attractions which will be felt by an incident nucleon at R_N before the shorter range repulsions (hard cores, many-body forces, or exchange interactions), which are responsible for saturation, become effective. Such interactions can be constructed phenomenologically, but are not found in recent meson-theoretically deduced potentials.

I. INTRODUCTION

THE discussion presented in this paper is concerned with the difference in nuclear radii as observed and interpreted in various experiments which measure different properties of the nuclear structure. It is limited to nuclei of large mass number, $A > 100$. The two classes of experiments of immediate concern here are the one group which measures the "nuclear force radius" (R_N) as opposed to that which determines the "radius of the charge distribution" (R_C) in nuclei.

By "nuclear force radius" is meant the radius at which an impinging nuclear particle (neutron, proton, etc.) first feels the influence of the nuclear forces. Analyses of neutron cross sections at various energies indicate a nuclear radius of roughly $1.4A^{\frac{1}{3}}$. (Unless specifically stated otherwise, all lengths in this paper are in units of 10^{-13} cm.)[1] The approximate $A^{\frac{1}{3}}$ variation of the radius expresses the well-known phenomenon of saturation of nuclear densities. More detailed considerations of the total, reaction, and elastic scattering cross sections of neutrons with kinetic energy in the range from thermal energies up to the order of 10 Mev as presented in the cloudy crystal ball analysis of Feshbach, Porter, and Weisskopf,[2,3] give radii which are slightly larger for intermediate mass nuclei with $A \sim 50$ and smaller for the heavy nuclei with $A \sim 200$. The optical analysis of Taylor[4] for high-energy total neutron cross sections in the energy range 50 to 400 Mev agrees with this conclusion. We take as a representation of the nuclear force radius

$$R_N = (1.26A^{\frac{1}{3}} + 0.75). \quad (1)$$

Equation (1) thus predicts radii of $1.45A^{\frac{1}{3}}$ for $A \sim 60$ and of $1.39A^{\frac{1}{3}}$ for $A \sim 200$.

This expression for the nuclear radius is obtained from a simple model which pictures the nuclear potential well to have sharp edges. For a rounded-off nuclear well, corresponding to a surface of finite thickness, we must know the depth of the potential well at the radius, R_N, in Eq. (1) before we can interpret this number. Toward this end, we may appeal to proton scattering cross sections. The analysis of Woods and Saxon[5] has shown that it is possible to fit the observed differential elastic scattering cross sections for $\sim$20-Mev protons on medium and heavy nuclei with a nuclear potential which decreases smoothly to zero in a distance ~ 2. A square-well model fails here because it predicts considerably too much large-angle relative to small-angle elastic scattering.

More important, however, for the discussion here is the presence of the Coulomb barrier. A proton with energy less than $\sim Z/A^{\frac{1}{3}}$ Mev incident on a nucleus of charge Z and mass number A must tunnel through the Coulomb barrier. Its probability of reaching the nuclear surface and of initiating a reaction is a very sensitive function of the height and width of the barrier. The

* This work was supported in part by the Office of Naval Research and the U. S. Atomic Energy Commission.

[1] J. M. Blatt and V. F. Weisskopf, *Theoretical Nuclear Physics* (John Wiley and Sons, Inc., New York, 1952), see Chap. 1, Sec. 4 for a qualitative discussion of the nuclear size as deduced from various experiments.

[2] Feshbach, Porter, and Weisskopf, Phys. Rev. **96**, 448 (1954). In this paper, the radius is actually taken to be $1.45A^{\frac{1}{3}}$.

[3] Later work (personal communication with V. F. Weisskopf) as discussed in the Brookhaven National Laboratory Report BNL-331 C-21, on the conference "Statistical aspects of the nucleus" held January 24–26, 1955 (see especially p. 16) reproduces a better fit with data on neutron scattering angular distributions and on cross sections for compound nucleus formation as a function of mass number if the radius is altered to a value in close agreement with Eq. (1).

[4] T. B. Taylor, Ph.D. thesis, Cornell, 1954 (Phys. Rev. to be published); also Phys. Rev. **92**, 577 (1954).

[5] R. G. Woods and D. S. Saxon, Phys. Rev. **95**, 577 (1954). Experimental and earlier theoretical analyses are referred to in this work.

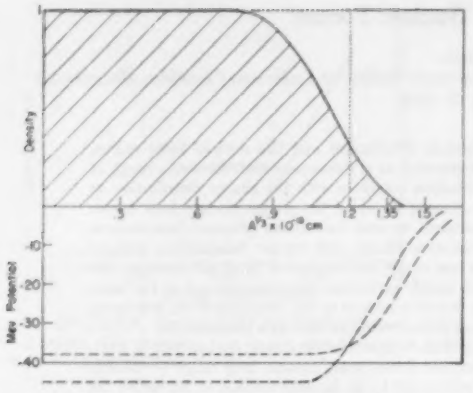

FIG. 1. The shaded region represents the charge distribution for Au (Ravenhall and Yennie, reference 13); the dotted line shows the uniform distribution with the same root mean square radius ($=1.2A^{\frac{1}{3}}$). The dashed lines show the nuclear wells (the depth gives the magnitude of the real part) which Saxon, Melkanoff, and Nodvik have used to match proton scattering data. The analytic form of these wells is $V_0/1+e^{(r-r_0)/a}$ with $a=0.49$, and $V_0=-38$ Mev $r_0=1.42A^{\frac{1}{3}}$ for the shallow curve (reference 5) and $V_0=-45$ Mev and $r_0=1.33A^{\frac{1}{3}}$ for the deep one (reference 8). The illustrated potentials and charge distributions are for Au.

observed cross sections thus give a relatively sensitive determination of the radius at which the attractive nuclear forces overcompensate the repulsive Coulomb barrier.[6] If the proton had to tunnel its way through a Coulomb barrier produced by the nuclear charge distribution with radius R_C, its cross section for formation of a compound nucleus would be much smaller than if the barrier stopped at the larger distance,[7] R_N. Saxon, Melkanoff, and Nodvik[5,8] have shown that it is possible to fit the data with a well of sloping sides and with the Coulomb barrier overcompensated by the nuclear forces at a distance slightly larger than R_N. The potential which they use is shown in Fig. 1. We assert then a basic premise for future discussions: an incident nuclear particle feels a nuclear force attraction which overcompensates the Coulomb barrier for protons at a distance from the center of the nucleus given by R_N of Eq. (1). For our purposes, it will suffice to approximate Eq. (1) to $R_N=1.4A^{\frac{1}{3}}$, and to require that the magnitude of the attractive nuclear forces at a distance R_N be at least 14 Mev.[8,9]

The above value of the nuclear force radius is to be contrasted with the radius of the proton, or electric charge, distribution, as determined by high-energy electron scattering at Stanford[10] and Michigan[11] and by the energy levels of μ-mesic atoms at Columbia.[12] The charge profile and size are both known from the recent work of Hofstadter, McIntyre, and collaborators[10] as analyzed by Ravenhall and Yennie.[13] The charge distribution is calculated to decrease to half-value at a radius of close to $R_C=1.12A^{\frac{1}{3}}$, with a surface thickness of 2.38 representing the distance between the 10 percent and 90 percent values of the density, for a mass number of $A=197$. [See Fig. 1.] It is not yet determined experimentally how the surface thickness scales with atomic number but this uncertainty will have no effect on the discussion here for heavy nuclei ($A>100$).

In this work, our aim is to infer some properties of nuclear forces on the basis of this difference between the charge and nuclear force radii. Although a complete nuclear force theory does not exist, it may still prove fruitful to study this difference in radii as a reflection of the effects of separated portions of the nuclear force.

It is generally agreed that the difference in radii is in part a measure of the finite range of nuclear forces. We observe that for medium-heavy nuclei, R_N-R_C is approximately equal to one meson Compton wavelength, or the characteristic nuclear force length. In this work, we adopt the interpretation that the difference between R_N and R_C is *entirely* a consequence of the finite nuclear force range, and we use the magnitude of this difference as a lever to learn some properties of the nuclear forces themselves.[14] That is, we *assume* that

[6] The presence of the Coulomb barrier is thus of value here in that it permits a "normalization" of the energy scale.

[7] For $Z=50$ and $E_p=5$ Mev, this reduction factor is of the order of three.

[8] Personal communication with Dr. D. S. Saxon and Dr. S. Mozkowski. More extensive calculations on elastic proton scattering from various nuclei, including Al, Cu, Ag, and Au, confirm the initial result of Woods and Saxon in reference 5 that the nuclear potential extends appreciably beyond the radius R_C. Some of these calculations are reported in the Brookhaven report (reference 3) in the session on "Elastic Scattering" by D. S. Saxon. In all cases, the best fit with experiment is achieved with a nuclear potential at least 14 Mev deep at $R_N=1.4A^{\frac{1}{3}}$.

[9] The analysis of J. S. Blair, Phys. Rev. **95**, 1218 (1954) on elastic α-particle scattering provides further evidence in support of a large nuclear force radius. He fits the experimental angular distributions of α particles elastically scattered by heavy nuclei [G. W. Farwell and H. E. Wegner, Phys. Rev. **95**, 1212 (1954)] with a nuclear model which assumes that the nucleus is opaque out to a radius of $1.5A^{\frac{1}{3}}$. Further work along these lines by Wall, Rees, and Ford with similar results is reported by D. S. Saxon in reference 3, pp. 51–52. See also Wall, Rees, and Ford, Phys. Rev. **97**, 726 (1955).

[10] Hofstadter, Fechter, and McIntyre, Phys. Rev. **92**, 978 (1953); Hofstadter, Hahn, Knudsen, and McIntyre, Phys. Rev. **95**, 512 (1954); Yennie, Wilson, and Ravenhall, Phys. Rev. **92**, 1325 (1953); Yennie, Ravenhall, and Wilson, Phys. Rev. **95**, 500 (1954).

[11] Pidd, Hammer, and Raka, Phys. Rev. **92**, 436 (1953).

[12] V. L. Fitch and J. Rainwater, Phys. Rev. **92**, 789 (1953); L. N. Cooper and E. M. Henley, Phys. Rev. **92**, 801 (1953).

[13] D. G. Ravenhall and D. R. Yennie, Phys. Rev. **96**, 239 (1954).

[14] To fix this point more clearly we consider a slowly moving proton which is incident on a heavy nucleus. We ask what factors help a proton which comes up against the high Coulomb barrier corresponding to radius R_C tunnel its way through as if the barrier were lower and cut off at the larger radius R_N. A first suggestion might be to take into account the polarizability of the proton in the electric field of the nucleus. This corresponds schematically to the proton tossing out its charge on a π^+ meson, coasting freely as a neutron, while the lighter π^+ meson bucks the barrier with greater ease, and then catching the π^+ back again. However, the effect of this induced electric dipole moment was calculated to be negligible with meson parameters adjusted to give the correct anomalous magnetic moments. (The entire magnetic moment contribution is itself negligible.) Along this line of thought we may consider that the proton throws out its π mesons to be caught by a nucleon inside the nucleus. This "forward pass" effect (as contrasted with the above "fumble") then contributes the nuclear force attraction to help balance the Coulomb barrier.

the *charge* distribution determined at Stanford coincides with the entire nuclear *matter* distribution. We then determine if various meson-theoretically inspired and phenomenological nuclear force theories which have been proposed are suitable to account for the radius difference, $R_N - R_C$.

The nuclear forces of primary interest in this work are those which satisfy the saturation requirements in heavy nuclei. It is a simple matter to write down attractive two-body forces extending over a range of the order of 1×10^{-13} cm which will account for $R_N - R_C$. However, we shall see that the dual demands that the nuclear forces account for saturation and at the same time give rise to an initial attraction of magnitude $\geqslant 14$ Mev for an incident nucleon at a distance R_N, provide severe requirements for the forces to satisfy. The reason for this is that the saturation phenomenon is an expression of the weakness of the average attraction experienced by a nucleon in nuclear matter. Only if the nuclear forces contain long-range direct, central attractions which will be felt by an incident nucleon at a distance R_N before the repulsions, which are responsible for saturation, become effective, can they completely account for the difference, $R_N - R_C$. Thus, the agents which serve to establish the saturation of nuclear forces, whether they be hard cores, many-body repulsions, and/or exchange potentials, must be characterized by a short range relative to the attractive interactions. This is the key point which emerges from our considerations.

Alternatively, the difference between R_N and R_C can be trivially explained on the basis of an entirely different approach to this problem which assumes that the neutron distribution extends beyond the proton one. Such proposals have been made by Johnson and Teller[15] and by Swiatecki[16] and are based on the excess in neutron number over proton number, and on Coulomb effects. In the absence of definite experimental information on the relative sizes of the neutron and proton distributions[17] in nuclei, these proposals provide equally valid approaches to an explanation of $R_N - R_C$. Further experimental as well as theoretical work is required in order to establish to what extent the radius difference can be explained simply on the basis of a larger matter than charge radius. As indirect evidence in support of the assumption of equal neutron and proton radii, we note the observations on the lighter nuclei[12,18] such as copper and titanium, which have roughly equal numbers of neutrons and protons, but for which the radius difference $(R_N - R_C)/A^{\frac{1}{3}}$ is essentially the same as for lead with a neutron to proton ratio of 1.5. We also note Williams[19] optical-model analysis of the 1.4-Bev neutron cross sections which indicates small matter radii in close agreement with R_C.

We assert then as a second basic premise for these discussions: the nuclear *matter* distribution coincides with the charge distribution as determined at Stanford. The best fit to Au is given in Fig. 1.

On the basis of the two preceding basic premises, we seek to establish features of the nuclear forces which are necessary to account for the observed difference in radii. At first sight, it may seem that a study of the difference between R_N and R_C in heavy nuclei is a rather indirect approach to the nature of nuclear forces. A study of the deuteron and of nucleon-nucleon scattering is surely more direct. However, the two-body problem in nuclear physics has proved to be very complicated and is nowhere near solution. It is evident, especially from the work of Lévy,[20] Brueckner and Watson,[21] and Blatt and Kalos,[22] that a fit to two-body data at various low and intermediate energies is quite sensitively affected by the introduction of infinite repulsive cores with different singlet and triplet ranges and by the depth and slope of the potential at the edge of the core. This means that the calculations of the two-body interactions are sensitive to regions of small particle separations (~ 0.4) where the static potential picture is certainly deficient. It also means that it is difficult to make an unambiguous choice of the exchange properties of the potential as well as of its profile for larger separations ($\sim \hbar/\mu c \simeq 1.4$). This point is clearly illustrated by the fact that the Lévy potential and the Brueckner-Watson potential both give a satisfactory account of themselves on low energy data, but are very different from one another insofar as concerns their exchange nature, tensor contributions, and space variation.[23]

On the other hand, a study of the nuclear radius difference can be used to cast light on one distinct feature of the nuclear force. Its main advantage is that, to lowest order, for two-body interactions it measures predominantly the effects of the long range behavior of the direct part of the central potential for heavy

[15] M. H. Johnson and E. Teller, Phys. Rev. **93**, 357 (1954).
[16] W. J. Swiatecki, Phys. Rev. **98**, 203-204 (1955).
[17] See however W. N. Hess and B. J. Moyer, Phys. Rev. **96**, 859(Å) (1954). W. N. Hess, University of California Radiation Laboratory Report UCRL-2670, 1954 (unpublished); L. N. Cooper and W. Tobocman, Phys. Rev. **97**, 243 (1955). The experiments of Hess and Moyer on the indirect pickup process provide qualitative indications of a 0.8 neutron surface layer in Pb which is not present in lighter elements with $N = Z = A/2$. However, the stripping analysis of Cooper and Tobocman suggests a neutron surface layer of 0.6 for mirror nuclei Mg^{25} and Al^{25}.
[18] Lyman, Hanson, and Scott, Phys. Rev. **84**, 626 (1951); A. E. Glassgold, Ph.D. thesis, Massachusetts Institute of Technology Physics Department, 1954 (unpublished).
[19] R. W. Williams, Phys. Rev. **98**, 1387, 1393 (1955) and personal communication, Coor, Hill, Hornyak, Smith, and Snow, Phys. Rev. **98**, 1369 (1955). Similar results are obtained from the scattering of 860-Mev protons. Chen, Leavitt, and Shapiro, Phys. Rev. **99**, 857 (1955).
[20] M. M. Lévy, Phys. Rev. **88**, 725 (1952).
[21] K. A. Brueckner and K. M. Watson, Phys. Rev. **92**, 1023 (1953).
[22] J. M. Blatt and M. A. Kalos, Phys. Rev. **92**, 1563 (1953).
[23] We note, for example, that the Lévy potential contains roughly four times as much direct central attraction as does the Brueckner-Watson potential and two-thirds as much long range tensor force. Henceforth, we shall mean by Brueckner-Watson potential the potential which they derive using only the gradient coupling version of pseudoscalar meson theory (no pair term).

nuclei, $A>100$; i.e., of $V_d(r)$ in an expression for the potential of the form

$$V(r)=V_d(r)+V_\tau(r)\boldsymbol{\tau}_1\cdot\boldsymbol{\tau}+V_\sigma(r)\boldsymbol{\sigma}_1\cdot\boldsymbol{\sigma}+V_{\sigma\tau}(r)\boldsymbol{\sigma}_1\cdot\boldsymbol{\sigma}\boldsymbol{\tau}_1\cdot\boldsymbol{\tau}+V_t(r)S_{12}+V_{t\tau}(r)\boldsymbol{\tau}_1\cdot\boldsymbol{\tau}S_{12}, \quad (2)$$

where S_{12} is the tensor force operator.

It measures only the effects of $V_d(r)$ because, to leading order in $A\gg1$, there are equal numbers of spin-up and spin-down particles in the nucleus, so that the last four terms of Eq. (2) average approximately to zero. They vanish identically in the sum over nuclear particles for spin zero nuclei. In general, their contributions are reduced by a factor of $A^{\frac{1}{3}}$. This is because there are $\sim A^{\frac{1}{3}}$ particles near the facing surface of the nucleus which interact strongly with the incident nucleon, in virtue of the short range of the nuclear forces, and all but one of a few of these $A^{\frac{1}{3}}$ particles will be paired in spin-up and spin-down states. Also, the second term of Eq. (2) is proportional to the neutron excess and is responsible for only a small contribution to the calculations following in comparison with the $V_d(r)$ term. This approach thus has the advantage of being primarily sensitive to one portion of the nuclear potential: the long-range behavior of $V_d(r)$, which determines at what distance from the nucleus an impinging nucleon first experiences an appreciable nuclear interaction. By the same token it cannot tell whether $V(r)$ falls precipitously up to the edge of a repulsive core or simply increases gradually as $r\to0$.

II. OUTLINE AND SUMMARY

In this section, we present a brief outline of the calculations performed and results obtained in the succeeding paragraphs.

Firstly, in Sec. III, we sum up the nuclear interactions of a nucleon outside the nucleus with the nucleons comprising the nucleus. In this calculation we neglect the influence of the external nucleon on the nuclear matter density, which we assume to correspond to the charge distribution measured at Stanford.[10] We also neglect the requirement of antisymmetrizing the wave function of the incident nucleon with those in the nucleus. To first order, it is only the direct (σ- and τ-independent) parts of the nuclear potential which are of importance. We consider in this work several different models of nuclear forces, all of which have in common the property of satisfying the saturation requirements in nuclei. Two of these models are rooted in meson field theory; one is the Lévy[20] potential of pseudoscalar meson theory, supplemented by sufficient three-body repulsions to meet the saturation requirements; the second is the Brueckner-Watson[21] potential, deduced on the basis of the gradient-coupling version of pseudoscalar meson theory, which is also consistent with the saturation requirements. Two more phenomenological models are also discussed. The Lévy and Brueckner-Watson models have in common the feature that the main contributions to the central forces result from two-meson exchanges so that the interaction is of characteristic range of the order of one-half of the meson Compton wavelength. We find that the direct part of the Brueckner-Watson potential is too small to account for the difference between R_N and R_C. The Lévy potential, on the other hand, has a very strong Wigner attraction; however, when enough three-body repulsion of the form predicted by the same meson theory as used in deducing the two-body attraction is introduced to be consistent with nuclear stability,[24] we find again that the difference between R_N and R_C cannot be accounted for. In contrast, a simple phenomenological Yukawa or Hulthén potential with a range of one meson Compton wavelength and a depth appropriate to the binding energy of the deuteron has the desired property. Calculations are presented for two different potentials of this type. In the course of these calculations we verify that our conclusions are insensitive to details of the assumed shape of the tail of the nuclear charge distribution.

In Sec. IV, we calculate the induced spin, charge, and matter polarization of the nuclear density due to the interactions with the approaching nucleon. These effects are found to be small for the incident nucleon at a distance $\gtrsim1.35A^{\frac{1}{3}}$ from the center of the nucleus and indicate the convergence of our calculations.

Section V is devoted to a consideration of the effect of taking into account the Pauli principle by antisymmetrizing the wave function of the incident nucleon with the nucleons in the nucleus. This effect serves to weaken the nuclear attraction due to direct terms, since the Pauli principle inhibits the close approach of two fermions, and to introduce exchange energies. Its contributions are shown to be small. These exchange contributions do not influence our conclusions which are presented in Sec. VI and may be summarized briefly as follows.

The observed difference between the nuclear force radius, R_N, and the charge radius, R_C, may be explained in either of two ways. On the one hand we may assume that the nuclear charge and matter distributions coincide, in which case the potential between nucleons must contain an appreciable amount of long range, direct, central attractive interaction. If we require that this same internucleon potential account for nuclear saturation, the repulsive cores, many-body repulsions, and/or exchange interactions which stabilize the nucleus against collapse must be of shorter range than the attractive interactions. Recent meson-theoretically deduced nuclear potentials are not consistent with these requirements. On the other hand, we may assume that the radius of the neutron distribution extends beyond the radius, R_C, of the proton distribution. Our calculations show that the matter distribution must extend

[24] S. D. Drell and K. Huang, Phys. Rev. **91**, 1527 (1953).

at least 10% beyond the charge radius if we accept the indications of meson field theory as manifest in the potentials of Lévy[20] or of Brueckner and Watson.[21]

We emphasize at this point that the nuclear radius, R_N, as used in this discussion, represents the distance at which an incident nucleon feels an appreciable nuclear attraction, 14 Mev. Our calculations are valid only for the incident nucleon "outside" of the nucleus, and tell nothing about the strength or shape of the nuclear interaction for a particle "inside" of the nucleus.

III. FIRST-ORDER INTERACTION ENERGY

In this section, we compute directly the interaction energy between a nucleon outside of the nucleus and the nucleons in the nucleus as a function of distance, making the following simplifying approximations:

(1) We neglect the influence of the external nucleon on those in the nucleus, which we take to be distributed according to the Stanford charge distribution.

(2) We treat the external nucleon as distinguishable; i.e., we ignore the requirement of the Pauli principle that its wave function be antisymmetrized with those in the nucleus.

(3) We assume that the interaction between a nucleon outside with one or a pair of nucleons inside nuclear matter is unchanged from what it would be if these (two or three) interacting nucleons were isolated from the rest of the nuclear matter.

Approximations (1) and (2) are analyzed and discussed in the following sections. Their effects are calculated in order to determine the regions of validity which they limit for our discussions here. Approximation (3) is an assumption as to the linearity of the nuclear force theory. We remark that, because of the short range character of nuclear forces, the important contributions to the interaction energy which we calculate below come from nucleons near the surface of the nucleus facing the incident particle. It is the nucleons in the region between $1.3A^{\frac{1}{3}}$ and $1.0A^{\frac{1}{3}}$ of the density distribution shown in Fig. 1, where the nuclear density is gradually increasing, which contribute most of the energy. Nonlinearities of the type discussed by Schiff,[25] which operate in regions of high density, may thus be relatively unimportant in these calculations. However, if present, such nonlinearities would have an important influence on the saturation conditions. Our point of view is to assume the linearity of the theory in calculating the interaction energy and in considering the saturation requirements on the two- and three-body potentials studied in this work.

We consider in this calculation only heavy nuclei ($A\sim 176$) so that we can replace the sum over nuclear particles by an integration over the nuclear density. As discussed in the last paragraph of Sec. I, it is consistent with our approximations to neglect the last four terms of Eq. (2). They average approximately to zero in the sum over nuclear coordinates. Upon summing over the charges of the nuclear particles, we obtain for Eq. (2)

$$V(r)=V_d(r)+[(2Z-A)/A]\langle\tau_{z1}\rangle V_\tau(r), \qquad (3)$$

with $\langle\tau_{z1}\rangle=\pm 1$ for incident proton or neutron, respectively.[26] The second term is seen to be proportional to the neutron excess. Since $(1-2Z/A)<1/5$ for most nuclei, its effect is reduced relative to the first term. A big contribution from the $V_\tau(r)$ term would reflect itself in a difference between neutron and proton radii of heavy nuclei. This difference suggests itself as a possible means of investigating the importance of Heisenberg (or charge exchange) forces in nuclei. For our purposes here we shall confine our attentions primarily to the first term, $V_d(r)$. We shall, however, briefly consider the second term in a discussion of the potential model of Brueckner and Watson which has a fair amount of Heisenberg force.

If we consider first just two-body interactions, the basic integral to be calculated is

$$E_n=\sum_{i=1}^{A} V_d(|\mathbf{R}_0-\mathbf{r}_i|)=\frac{A}{v}\int \rho(r)d\tau V_d(|\mathbf{R}_0-\mathbf{r}|), \quad (4)$$

where $\rho(r)$ is the nuclear matter density, $v=\int\rho(r)d\tau$ is the nuclear volume, and R_0 is the coordinate of the external nucleon.

The integral in Eq. (4) can be reduced to a canonical form for these calculations on the basis of the assumed spherical symmetry of the nuclear distribution. A simple change in variable in the polar angle integration gives directly

$$\int d\Omega V_d(|\mathbf{R}_0-\mathbf{r}|)=(2\pi/rR_0\mu^2)\int_{|R_0-r|\mu}^{(R_0+r)\mu} dyyV_d(y), \quad (5)$$

where $1/\mu=1.4$ is the meson Compton wavelength in units $\hbar=c=1$. Introducing Eq. (5) into (4) we have the interaction energy as a function of R_0 for a given potential, nuclear density, and A. We introduce the following notation to put the expression in dimensionless form:

$$\eta=\mu R_0/A^{\frac{1}{3}}; \quad x=\mu r/A^{\frac{1}{3}}$$

and use the experimental result for the charge density that it occupies a volume equivalent to a uniform distribution of radius $1.16A^{\frac{1}{3}}=0.83A^{\frac{1}{3}}/\mu$ cm. This gives finally

$$E_n=2.6(A^{\frac{1}{3}}/\eta)\int_0^\infty \rho(x)xdx\int_{A^{\frac{1}{3}}|\eta-x|}^\infty yV_d(y)dy, \quad (6)$$

where we have replaced to a very good approximation

[25] Such nonlinearities are contained in theories such as those given by Schiff [L. I. Schiff, Phys. Rev. 83, 1 (1951)].

[26] In Eq. (3), the charge dependent term is altered if we give up the basic premise No. II (coincidence of neutron and proton distributions). This situation is discussed later.

the upper limit of the integral in Eq. (5) by ∞, as permitted by the short range of the forces.

The evaluation of Eq. (6) is effected by a straightforward procedure of elementary and/or graphical integrations.

We consider as a first model of the potential, a saturating combination of short range direct and exchange forces with no repulsive cores. A simple prototype of this class of interactions replaces $V_i(r)$ in Eq. (2) (for all subscripts i) by a step function

$$V_i(r)=\lambda_i\epsilon_i(r);\quad \epsilon_i(r)=\begin{cases}1 & r<\rho_i\\ 0 & r>\rho_i\end{cases}. \tag{7}$$

The saturation conditions for such a potential include the requirement that $\lambda_d\geq 0$. This is because it is only the V_d term of Eq. (2) that operates for a nucleus in the collapsed state, and its coefficient must be positive to prevent the nuclear collapse that would accompany a negative A^2 contribution to the energy.[27] However, for $\lambda_d>0$, the energy of interaction calculated in Eq. (6) is positive, which means a net repulsion of the external nucleon by the nuclear force effects when it first gets within the force range. If we assume, for example, a range $\rho_d\sim 1$, a nucleon incident on a heavy nucleus would first feel the nuclear force effects when it approached within $(1.2A^{\frac{1}{3}}+1)\simeq R_N$, and at this distance the nuclear interaction would be repulsive rather than attractive. We learn from this example that if we have simple potentials wells and achieve saturation by means of suitable exchange mixtures, we cannot explain the difference between R_N and R_C, once we have assumed that the charge and matter radii coincide.

It is apparent, however, that if saturation is achieved through repulsive cores in addition to exchange mixtures, a net attraction can be obtained in Eq. (6). As an example of this, we consider the Brueckner-Watson[21] potential which is deduced from gradient-coupling pseudoscalar meson theory carried through fourth order in the coupling parameter and thereby allowing for one and two meson exchanges. In the deduction of this force the theory is supplemented in two ways: repulsive cores are introduced at short distances and multiple scattering arguments are appealed to in order to allow a selection of a particular set of the fourth order interactions. The fourth order interactions which are retained in the analysis of Brueckner and Watson are those for which two virtual mesons are simultaneously present in the intermediate states in a perturbation expansion. All fourth order contributions which arise as nonadiabatic, velocity-dependent corrections to the second order, one-meson exchange interaction are dropped.

We accept this potential as indicative in general features of what results from the gradient-coupling meson theory; i.e., from the pseudoscalar theory when the pair term is completely suppressed. It has the virtues of giving a reasonably satisfactory fit to low and intermediate energy two-body data and of predicting reasonable saturation behavior for heavy nuclei.[28] The main feature of concern to us here is the short range and moderate strength of the direct term, V_d, as illustrated in Fig. 2. In units $z=\mu r$ it reads[29]

$$\begin{aligned}V_d=&-\gamma z^{-4}\big[(4+4z+z^2)e^{-z}K_1(z)\\ &+z(2+2z+z^2)e^{-z}K_0(z)\big],\quad \text{for}\quad z>0.32;\\ =&+\infty,\qquad\qquad\qquad\qquad \text{for}\quad z\leq 0.32;\end{aligned} \tag{8}$$

with

$$\gamma=6(\mu/\pi)(g^2/4\pi)^2(\mu/2M)^4=1.73\ \text{Mev}.$$

The short range of the direct part is due to the fact that it arises from two-meson exchange and is thereby

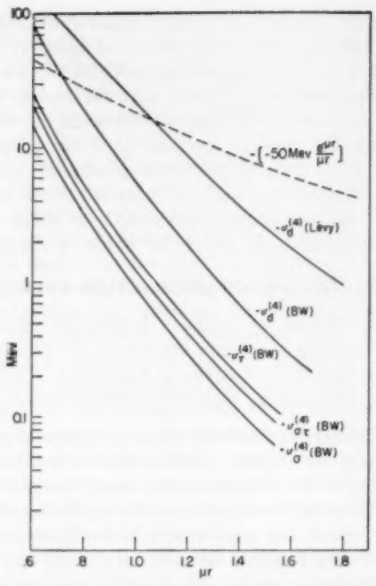

FIG. 2. Logarithmic plot of the magnitudes of the various contributions to the Lévy and Brueckner-Watson potentials as labeled vs distance. $-V_d^4$ (Lévy) represents Eq. (9) for the Lévy potential and $-V_d^4$ (Brueckner-Watson) represents Eq. (8) for the Brueckner-Watson potential. The two-meson exchange contributions to the Brueckner-Watson potential which are proportional to $\boldsymbol{\sigma}_1\cdot\boldsymbol{\sigma}$, $\boldsymbol{\tau}_1\cdot\boldsymbol{\tau}$ and $\boldsymbol{\sigma}_1\cdot\boldsymbol{\sigma}\boldsymbol{\tau}_1\cdot\boldsymbol{\tau}$ [see Eq. (2)] are represented by $+V_\sigma^{(4)}$ (Brueckner-Watson), $-V_\tau^{(4)}$ (Brueckner-Watson), and $V_{\sigma\tau}^{(4)}$ (Brueckner-Watson). The one-meson exchange terms, Eq. (27), and the additional two-meson exchange contributions to the tensor force are not indicated. The dashed line represents a Yukawa potential of sufficient depth to bind the deuteron.

[27] For a discussion of the various saturation conditions see reference 1, Chapter III.

[28] Brueckner, Levinson, and Mahmoud, Phys. Rev. **95**, 217 (1954); K. A. Brueckner, Phys. Rev. **96**, 908 (1954) and **97**, 1351 (1955).

[29] A repulsive core radius of 0.32 $(1/\mu)$ cm represents the appropriately weighted average of the singlet and triplet core radii in reference 21 (units corrected from reference 21 as indicated in reference 28).

approximately characterized by the range $1/2\mu$. The longer range contribution resulting from one meson exchange in the gradient coupling gives rise only to the long-studied tensor and V_{ss} terms and does not contribute in this first-order analysis.

Introducing Eq. (8) into Eq. (6), we have calculated the interaction energy as a function of the particle distance η. We have carried through these calculations both for the Stanford charge distribution and for the uniform distribution with the same root mean square radius ($\equiv 1.2A^{\frac{1}{3}}$) as drawn in Fig. 1 in order to test the sensitivity of our results to the tail of the charge distribution. The results are presented graphically in Fig. 3 and tabulated in Table I for an arbitrary nucleus of mass number $A=176$. The important point here is that, at a distance of $1.35A^{\frac{1}{3}}$, the nuclear attraction is 4.3 Mev, or less than one third of what is required to make the nuclear force radius appear to be this big. We conclude that the nuclear forces have contributed insufficiently in this case to make the nuclear force radius appear to be $R_N=1.4A^{\frac{1}{3}}$. It is seen that this conclusion applies to both calculations, with the Stanford and with the uniform charge distributions.

We observe that the energies obtained with the Stanford and with the uniform distributions correspond to each other much more closely for $R_0=1.35A^{\frac{1}{3}}$ than for $R_0=1.45A^{\frac{1}{3}}$. This may be understood in terms of the repulsive core and short range singular character of the internucleon potential. For large separations, the short range nature of the interactions weights heavily the energy contribution due to the portion of the matter distribution which extends beyond $1.2A^{\frac{1}{3}}$. However, for smaller separations the repulsive core is effective in preventing the matter distributions and incident nucleon from approaching to within $0.32/\mu$ cm of each other. The repulsive core in Eq. (8) has no influence in calculation for $R_0=1.45A^{\frac{1}{3}}$, since there is less than one percent of the matter distribution (Fig. 1) within a distance $0.32/\mu$ cm of an incident nucleon. It does, however, enter into the evaluation of the interaction energy for the incident nucleon at $1.40A^{\frac{1}{3}}$ and at $1.35A^{\frac{1}{3}}$, since the tail of the Stanford charge distribution extends out to these distances. For these cases, we have performed the calculations so as to obtain the maximum possible attraction by sharply cutting off the matter distribution at a separation of $0.32/\mu$ cm between the incident nucleon and the nucleus, and increasing its value uniformly in the region within 0.5 of the cutoff to preserve its normalization to A particles. By this procedure we avoid all repulsive contributions to the interaction arising due to the hard cores and at the same time take full advantage of the deepest portion of the internucleon attraction at the edge of the hard core. Various modifications of this procedure altered the calculated energies only by several percent. Also a decrease in the core radius to its minimum value (which applies for triplet states) of $0.30/\mu$ cm increased the attraction by less than 5%. On the basis of this discussion we feel that our conclusion above is safely insensitive to the shape of the tail of the charge distribution. We do not carry this analysis to smaller distances than $R_0=1.35A^{\frac{1}{3}}$ since the approximations represented in Eq. (6) do not warrant it. (This point is discussed more fully in the following sections.) In the final section, we discuss the A dependence of this result.

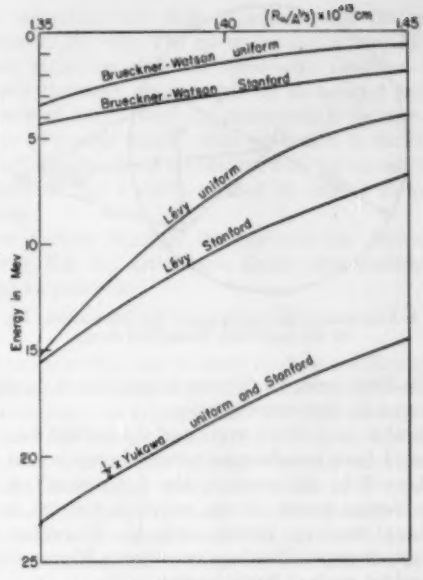

FIG. 3. Graph of results listed in Table I. The energies calculated with the Yukawa potential are reduced by a factor two in this graph.

From Fig. 2, it is clear that the V_t interaction term in the Brueckner-Watson potential contributes in Eq. (3) an energy which is less than 5 percent of that due

TABLE I. First-order interaction energies, Eq. (6), computed for the Brueckner-Watson potential, Eq. (8), the Lévy potential, Eq. (9), and the Yukawa potential, Eq. (16). The calculations were carried out for atomic number $A=176$ and for both the Stanford and equivalent uniform charge distributions shown in Fig. 1. The results of this table are graphed in Fig. 3.

R_0	Brueckner-Watson potential [Eq. (8)]		Lévy pot. [Eq. (9)]		Yukawa pot. [Eq. (16)]	
	Stanford	Uniform	Stanford	Uniform	Stanford	Uniform
$1.35A^{\frac{1}{3}}$	−4.3 Mev	−3.5 Mev	−15.6 Mev	−15.2 Mev	−45 Mev	−46 Mev
$1.40A^{\frac{1}{3}}$	−2.9 Mev	−1.4 Mev	−10.0 Mev	− 7.2 Mev	−35 Mev	−36 Mev
$1.45A^{\frac{1}{3}}$	−1.8 Mev	−0.64 Mev	− 6.9 Mev	− 3.9 Mev	−28 Mev	−29 Mev

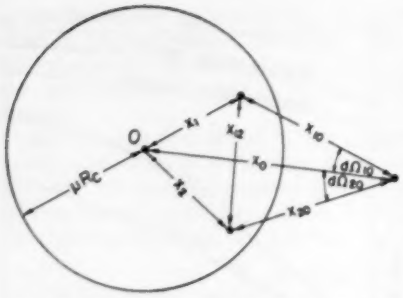

FIG. 4. Coordinates for carrying out the integrations, Eq. (12) for the three-body interaction energy.

to the direct term, V_d. We can thus neglect it insofar as concerns the first-order energies.

Another more dated version of the nuclear forces as deduced from pseudoscalar meson theory is that due to Lévy.[20] In this version, the "pair term" of the pseudoscalar meson theory, which is omitted in the gradient coupling version used by Brueckner and Watson, is responsible for a very strong Wigner attraction which reads to leading order

$$V_d=-\gamma z^{-2}K_1(2z), \quad z>0.38; \qquad +\infty, \quad z\leqslant 0.38; \tag{9}$$

with

$$\gamma=6(\mu/\pi)(g^2/4\pi)^2(\mu/2M)^2=151 \text{ Mev}.$$

As in the gradient coupling version, the main central force contribution results from two-meson exchanges and therefore is of range $\simeq 1/2\mu$. In both versions of the pseudoscalar theory, i.e., with or without the pair term, the longer-ranged single meson exchange terms give rise only to a tensor and V_{ST} part in Eq. (2).

In contrast with the Brueckner-Watson interaction, this nuclear force is sufficiently strong to give rise to an appreciable nuclear attraction at distances $R_N \sim 1.4A^{\frac{1}{3}}$. This is seen in Fig. 3 and Table I. The Lévy central potential is seen to be ~ 4 times stronger than the Brueckner-Watson at a distance ~ 1 and to give rise to ~ 4 times as strong a nuclear attraction. However, the Lévy potential is not a saturating interaction. One way of constructing a saturating nuclear force theory and still keeping Eq. (9) is to add three-body repulsive forces to provide the nuclear stability. The effect of such three-body repulsions will also be felt by the nucleon approaching the nuclear surface.

We will now outline the calculation of such three-body contributions to the nuclear force experienced by the incident nucleon. In this calculation, we will take the form of the three-body repulsion from the pseudoscalar meson theory with pair term, as previously studied:[24]

$$V_3=\beta\frac{K_1(\{r_{12}+r_{23}+r_{31}\}\mu)}{\mu^3 r_{12}r_{23}r_{31}}; \quad r_{ij}\equiv|\mathbf{r}_i-\mathbf{r}_j|; \tag{10}$$

i.e., we take the three-body force from the same theory that gives the two-body attraction, Eq. (9). We shall find that the minimum amount of three-body repulsion consistent with saturation essentially cancels the above calculated attraction due to the two-body forces.

Because of the complexity of this calculation we only outline the procedure here in the approximation of a uniform nuclear matter density. The essential difficulty here which is not present in the nuclear saturation problem is the following: in the saturation problem the usual procedure is to calculate the interaction energies between particles in an infinite nuclear medium of fixed density, whereas we must now take careful account of the nuclear surface since it is the distance from the surface that is the critical parameter.

We write first Eq. (10) in dimensionless form, denoting as in Fig. 4 by $x_0=\mu r_0$ the coordinate of the incident nucleon relative to the center of the nucleus:[21]

$$V_3=\beta\frac{K_1(x_{10}+x_{20}+x_{12})}{x_{10}x_{20}x_{12}}=\beta\int_1^\infty\frac{tdt}{(t^2-1)^{\frac{1}{2}}}\frac{e^{-x_{10}t}}{x_{10}}\frac{e^{-x_{20}t}}{x_{20}}\frac{e^{-x_{12}t}}{x_{12}}. \tag{11}$$

The interaction energy is then given by

$$E_{n_3}=[\tfrac{1}{2}A^2/(v\mu^3)^2]\int\int d\mathbf{x}_1 d\mathbf{x}_2\beta\times\int_1^\infty\frac{tdt}{(t^2-1)^{\frac{1}{2}}}\frac{e^{-x_{10}t}}{x_{10}}\frac{e^{-x_{20}t}}{x_{20}}\frac{e^{-x_{12}t}}{x_{12}}. \tag{12}$$

The procedure we found most direct for the evaluation of Eq. (12) develops as follows:

(1) Transform the volume integrals to integrals over the inter-particle separations and use the x_0 axis as the polar axis for the angular integrations; *viz.*,

$$\int\int d\mathbf{x}_1 d\mathbf{x}_2=\int_{x_0-x_1}^\infty x_{10}^2 dx_{10}\int_{x_0-x_2}^\infty x_{20}^2 dx_{20}\int d\Omega_{10}\int d\Omega_{20}, \tag{13}$$

with the limits on the polar angle integral expressed in terms of the nuclear radius R_C by

$$(x_0-x_{10})^2\leqslant x_{10}^2+x_0^2-2x_{10}x_0\cos\theta_{10}\leqslant(\mu R_C)^2, \quad (x_0-x_{20})^2\leqslant x_{20}^2+x_0^2-2x_{20}x_0\cos\theta_{20}\leqslant(\mu R_C)^2. \tag{14}$$

[20] A. Klein, Phys. Rev. **94**, 1061 (1954). He has presented a strong argument for the suppression of the pair term on the basis of the absence of strong S-wave pion nucleon scattering and the relation between this and the nuclear force problem. See also Phys. Rev. **89**, 1158 (1953) and reference 24.

[21] W. Magnus and F. Obberbettinger, *Special Functions of Mathematical Physics* (Chelsea Publishing Company, New York, 1949).

(2) Expand the exponential factor involving the separation x_{12} in a series of spherical harmonics with x_9 as the polar axis; *viz.*,[31]

$$\frac{e^{-x_{12}t}}{x_{12}}=4\pi\sum_{l,m}(x_{10}x_{20})^{-\frac{1}{2}}K_{l+\frac{1}{2}}(x_>t)I_{l+\frac{1}{2}}(x_<t)\times Y_l^m(\theta_{10})Y_l^{m*}(\theta_{20}), \quad (15)$$

with $x_>$ and $x_<$ the larger and smaller, respectively, of x_{10} and x_{20}.

(3) Observe that by cylindrical symmetry only the $m=0$ terms contribute, and for these

$$\int d\Omega_{10}Y_l^0=[(2l+1)\pi]^{\frac{1}{2}}\int_{\cos\Theta_{10}}^{1}d\mu P_l(\mu);$$

here $\cos\Theta_{10}$ is the solution of Eq. (14) with the equality on the right.

(4) Evaluate directly the first few l-terms.

The series in l converges rapidly in practice for the parameters of interest to us. For our hypothetical nucleus with $A^{\frac{1}{3}}=5.6$, the equivalent uniform nuclear radius is $\mu R_C=(6/7)A^{\frac{1}{3}}=4.8$. For the incident nucleon at a distance of $1.45A^{\frac{1}{3}}=R_0$, $x_0=5.8$ and the important values of x_{10} and x_{20} will be of the order of unity. As the integral representation Eq. (11) is peaked at $t\sim1$, the important arguments of the Bessel functions in Eq. (15) are also of the order of unity. The other two exponential factors in Eq. (12) weigh heavily against contributions from larger arguments. However, the Bessel function of imaginary argument in Eq. (15), $I_{l+\frac{1}{2}}(x_<t)$, is peaked at $x_<t\sim l$. This means that for large l, the peak in $I_{l+\frac{1}{2}}$ is beat down by the exponentials in the integrand in Eq. (12), and so the contribution of large l values to the energy in Eq. (12) is considerably reduced. It is this rapid convergence in l that supports the change in variable indicated in step 1.

Carrying out these calculations with the above indicated approximations and procedures we obtain for $A=176$ and $R_0=1.45A^{\frac{1}{3}}$ contributions of 1.9 Mev, 3.6 Mev, 1.2 Mev, and <0.5 Mev from the first $l=0$, 1, 2, and 3 values, so that the three-body energy contributions adds to 7 Mev, for $\beta=450$ Mev, as given by the full pair term of the pseudoscalar meson theory.[24] The corresponding two-body attraction for a uniform nucleus is seen in Table I to be only -3.9 Mev. It is possible to reduce the constant, β, of the three-body repulsion by no more than a factor of two consistent with the saturation requirement.[32]

The conclusion drawn from this calculation is that the Lévy potential supplemented by the minimal amount of three-body repulsion, of the form Eq. (10) as suggested by pseudoscalar meson theory, demanded for saturation also fails to account for the radius difference R_N-R_C. The reason for this is that the two-body attraction and the three-body repulsion have closely the same range as felt by an incident nucleon outside of the nucleus, and consequently balance each other to a large extent. This conclusion is unchanged by refining the above calculation with the actual charge density in Fig. 2 and is verified for smaller R_0 and A values.

As another example we calculate the interaction energy, Eq. (6), assuming a simple phenomenological Yukawa potential

$$V(r)=-50\text{ Mev }e^{-\mu r}/\mu r. \quad (16)$$

We consider this case in order to show specifically the importance of a long-range tail in the nuclear force as a possible source of explanation of the difference between R_N and R_C. The potential in Eq. (16) gives reasonable deuteron binding and together with various combinations of short-range many-body forces or of repulsive cores and exchange mixtures can be adjusted to meet saturation requirements. In fact, a qualitatively reasonable saturation results from the combination of Eq. (16) with the three-body repulsion of Eq. (10), with $\beta=450$ Mev. The calculations on the nuclear interaction energy, Eq. (6), using Eq. (16) are presented in Fig. 3 and Table I along with the preceding results. It is evident that with the longer range potential of Eq. (16) it is possible to account for the radius difference R_N-R_C.

Finally we consider briefly two phenomenological nuclear force models with long range potentials of the Yukawa type which have achieved some success in fitting data on low energy interactions of several nucleons. The potential used by Pease and Feshbach,[33]

$$V_P=-40\text{ Mev }e^{-1.3\mu r}/\mu r-28.6\text{ Mev }S_{12}e^{-0.81\mu r}/\mu r, \quad (17)$$

fits the observed properties of two-nucleon systems for energies up to ~15 Mev, as well as the binding energy of H^3. The first, or direct, term in Eq. (17) contributes an attractive interaction energy of -28 Mev for a nucleon at $R_0=1.35A^{\frac{1}{3}}$, with $A^{\frac{1}{3}}=5.6$. It is evident from this that an interaction of the type in Eq. (17) can account for the radius difference R_N-R_C. However, this is not a saturating force since the strong Wigner attraction would operate in heavy nuclei to collapse all of the A nucleons to within one meson Compton wavelength of one another. It is possible to counter this tendency with very short-range three-body repulsions which would not appreciably diminish the above calculated 28-Mev attraction and which at the same time would not affect the success of Eq. (17) in matching properties of the two nucleon system at low energy. However, the effect of such a modification of Eq. (17) on the calculated binding energy of H^3 remains to be studied.

[32] This result is established on the basis of the variation calculation discussed in reference 24. Brueckner, Levinson, and Mahmoud (reference 28) suggest a much smaller value of the constant, β, for saturation. However, their statement was based on the step functioned not on the trial function calculations of reference 24.

[33] R. L. Pease and H. Feshbach, Phys. Rev. **88**, 945 (1952).

Another two-body interaction which has met with noteworthy success in fitting data on two-body systems at low energies is the Rosenfeld mixture[34]

$$V_R = +40 \text{ Mev} \tau_1 \cdot \tau_2 [0.10 + 0.23 \sigma_1 \cdot \sigma_2] e^{-\mu r}/\mu r. \quad (18)$$

This is a saturating interaction. With this interaction, Inglis[35] and others have had considerable success in fitting observed level structures, moments, and transition matrix elements in their intermediate coupling studies in the p-shells of light nuclei. However, we see that there is no direct interaction in Eq. (18), so that the first-order contribution of the Rosenfeld mixture to the interaction energy vanishes. To this order Eq. (18) thus fails to account for the observed difference, $R_N - R_C$. This result is extended through second order interactions in the next section.

In summing up the calculations in this section we conclude that the inter-nucleon potential must contain a sizeable amount of long-range direct interaction, $V_d(r)$, if nuclear forces alone are to be held to account for $R_N - R_C$. The saturating character of the forces would then be a consequence of short range repulsions, due either to hard-core or many-body effects. Neither of the two meson-theoretically inspired potentials of Brueckner-Watson and of Lévy (with three-body repulsions for saturation) can explain the observed difference in radii unless it is assumed that the neutron distribution extends beyond the proton one. It must be added that the presently studied and applied versions of the pseudoscalar meson theory give no hint as to a possible source of any simple, central, Yukawa type potential with a range of roughly one meson Compton wavelength, corresponding to single meson interchange. The above analysis on the Lévy potential showed that a strong direct attraction of half that range, arising from two-meson exchange, can yield a sufficient energy contribution if saturation is achieved by shorter-range many-body repulsions than considered there. In this connection we note that Bonnevay[36] has shown that the meson-meson interaction, which the renormalization procedures introduce into meson theory, can serve as a source of central direct interactions of range $\sim 1/2\mu$. It is not established at present to what extent such a term is actually present, or whether a sufficient amount of this interaction to account for $R_N - R_C$ can be made consistent with nuclear saturation and with the information on two-body systems at low energy.

IV. INDUCED POLARIZATIONS

In this section, we calculate the second-order corrections to the interaction energy between the nucleus and the incident nucleon. These corrections result from the spin, charge, and matter polarizations which are induced in the nuclear distribution due to its interaction with the incident nucleon. Besides the second order effects due to the direct interaction term, V_d, which in general serve as small corrections to the first-order calculations of the previous paragraph, there are the more important contributions from the various exchange and tensor force terms of Eq. (2). These latter, as we have seen, contribute no first-order effects.

First we develop the techniques to calculate these effects. We wish to evaluate the change in the nuclear distribution resulting from interactions with the incident nucleon and then to determine the contribution of this change to the interaction energy. This is the same as evaluating the second order energy contribution

$$En_{(2)} = \sum_{(X)} \frac{|\langle X|V|g\rangle|^2}{E_g - E_X}, \quad (19)$$

where $|g\rangle$ and E_g are the ground-state eigenfunction and eigenvalue of the unperturbed nucleus and the sum extends over the excited states (X). Here again we treat the external nucleon as a distinguishable particle. The nucleus is idealized as a degenerate Fermi-Dirac gas. The excited states which contribute to the sum in Eq. (19) all correspond to a nucleon jumping out of a state, below the Fermi energy $E_F = k_F^2/2M$, which has momentum and energy k_l and $E_l = k_l^2/2M$, and up into a state above the Fermi level with k_u and $E_u = k_u^2/2M$, with appropriate spins and isotopic spins, σ and τ. Thus, introducing Eq. (2) into (19) and carrying out the elementary spin sums we obtain:

$$En_{(2)} = -2M \cdot 4 \cdot \sum_{k_l < k_F} \sum_{k_u > k_F} \cdot \left[\frac{V_d^2(\mathbf{k}_l, \mathbf{k}_u) + 3V_\tau^2(\mathbf{k}_l, \mathbf{k}_u) + 3V_\sigma^2(\mathbf{k}_l, \mathbf{k}_u) + 9V_{\sigma\tau}^2(\mathbf{k}_l, \mathbf{k}_u)}{(k_u^2 - k_l^2)} \right]. \quad (20)$$

For the equivalent uniform nucleus of radius $1.2A^{\frac{1}{3}}$, the Fermi energy corresponds to[37]

$$k_F = 1.77\mu. \quad (21)$$

In Eq. (20), we have omitted the tensor force terms, which we shall discuss separately below, and have introduced the notation

$$V(\mathbf{k}_l, \mathbf{k}_u) \equiv v^{-1} \int \rho(r) \exp[i(\mathbf{k}_l - \mathbf{k}_u) \cdot \mathbf{r}] V(\mathbf{r} - \mathbf{R}_0) d\mathbf{r} = V^*(\mathbf{k}_l, \mathbf{k}_u).$$

The numerical factors are computed for a "standard heavy nucleus" with equal numbers of up and down σ and τ states.

Before carrying out the coordinate integrations in Eq. (20), we effect the momentum sums by going over to the continuous limit of a momentum integral and

[34] L. Rosenfeld, *Nuclear Forces* (North Holland Publishing Company, Amsterdam, 1948), p. 234.
[35] D. R. Inglis, Revs. Modern Phys. **25**, 390 (1953); J. P. Elliott and B. H. Flowers, Proc. Roy. Soc. (London) (to be published).
[36] G. Bonnevay, Compt. rend. **16**, 1641 (1954).
[37] See, for example, reference 1, p. 143.

by replacing the integral over the unfilled states by the difference

$$\sum_{k_a>k_F} \rightarrow v(2\pi)^{-3}\int_{k>k_F} d\mathbf{k}$$

$$= v(2\pi)^{-3}\left[P\int_{\text{all } k} d\mathbf{k} - P\int_{k<k_F} d\mathbf{k}\right], \quad (22)$$

where P denotes the principal value of the integral to the right. We note next that the second term in the right member of Eq. (22) contributes nothing to the energy, Eq. (20), due to the oddness of the integrand, i.e.,

$$\int_{k'<k_F} d\mathbf{k}' P\int_{k<k_F} d\mathbf{k}\frac{\exp[i(\mathbf{k}-\mathbf{k}')\cdot\boldsymbol{\Delta}]}{k^2-k'^2}=0.$$

The momentum integrals then yield directly

$$\sum_{k_l<k_F}\sum_{k_a>k_F}\frac{\exp[i(\mathbf{k}_l-\mathbf{k}_a)\cdot\boldsymbol{\Delta}]}{k_l^2-k_a^2}$$

$$=\left(\frac{v}{8\pi^3}\right)^2\int_{k'<k_F} d\mathbf{k}' P\int_{\text{all } k} d\mathbf{k}\frac{\exp i(\mathbf{k}-\mathbf{k}')\cdot\boldsymbol{\Delta}}{k'^2-k^2}$$

$$=-\left(\frac{v}{8\pi^3}\right)^2\int_{k'<k_F} d\mathbf{k}'\frac{2\pi^2}{\Delta}\cos k'\Delta\cdot\exp i\mathbf{k}'\cdot\boldsymbol{\Delta}$$

$$=-(v^2k_F^2/16\pi^3\Delta^2)j_1(2k_F\Delta),$$

where j_1 is the regular spherical Bessel function of order unity. Collecting these results into Eq. (20), we have

$$En_{(2)}=-\frac{2Mk_F^4}{\pi^3}\int d\mathbf{r}\int d\mathbf{r}'\rho(r)\rho(r')\frac{j_1(2k_F|\mathbf{r}-\mathbf{r}'|)}{(2k_F|\mathbf{r}-\mathbf{r}'|)^2}$$

$$\times[V_d(\mathbf{r}-\mathbf{R}_0)V_d(\mathbf{r}'-\mathbf{R}_0)$$

$$+3V_\tau(\mathbf{r}-\mathbf{R}_0)V_\tau(\mathbf{r}'-\mathbf{R}_0)$$

$$+3V_\sigma(\mathbf{r}-\mathbf{R}_0)V_\sigma(\mathbf{r}'-\mathbf{R}_0)$$

$$+9V_{\sigma\tau}(\mathbf{r}-\mathbf{R}_0)V_{\sigma\tau}(\mathbf{r}'-\mathbf{R}_0)]. \quad (23)$$

It requires a "moderate" amount of work to carry through these integrals. The angular integrals can be achieved with the aid of the Poisson integral representation[21]

$$\frac{j_1(z)}{z^2}=\tfrac{1}{2}\int_0^1(1-u^2)du\frac{\cos uz}{z}, \quad (24)$$

and of the usual addition theorems. Equation (23) is then reduced to a manageable form for elementary and graphical integrations.

We discuss first, the application of Eqs. (23) and (24) to the Brueckner-Watson and Lévy potentials. Since the calculations are effected with standard techniques we present only results here. The two meson exchange part of the Brueckner-Watson potential is largely a direct interaction; the relative amounts of exchange terms are seen in Fig. 2. They contribute to Eq. (23) all told an energy of attraction which is about 0.1 Mev, or 3 percent of the first order contribution for the nucleon at $R_0=1.35A^{\frac{1}{3}}$, ($A^{\frac{1}{3}}=5.6$). Roughly half of this contribution comes from the direct term and half from the exchange terms, the contributions from which are enhanced by the spin factors. The two-meson part of the Lévy potential (the pair term) has no exchange terms and gives a second order correction of about 0.7 Mev or less then 5 percent of the first order contribution for the nucleon at $R_0=1.35A^{\frac{1}{3}}$, ($A^{\frac{1}{3}}=5.6$). For larger distances their energy contributions are, of course, relatively smaller and indeed entirely negligible. The smallness of these second-order contributions is a direct consequence of the extreme short range of these forces. We can qualitatively understand their magnitude by the following rough approximations in Eq. (23):

Because of the short range character of the potentials most of the energy contribution results when the coordinates, r and r' in Eq. (23), lie near the surface of the nucleus facing R_0. The factor depending on the particle separation within the nucleus, is replaced by its value at an average distance $|\mathbf{r}-\mathbf{r}'|\sim 1/\mu$, since this is the range of important coordinate values in the integral. Equation (23) then approximates to

$$En_{(2)}\approx -\frac{2Mk_F^4}{\pi^3}\frac{j_1(2k_F/\mu)}{(2k_F/\mu)^2}\left(\frac{v}{A}\right)^2$$

$$\times[U_d^2+3U_\tau^2+3U_\sigma^2+9U_{\sigma\tau}^2], \quad (25)$$

where $U_i=(A/v)\int\rho(r)V_i(\mathbf{r}-\mathbf{R}_0)d\mathbf{r}$ is the first-order interaction energy for a potential with coordinate dependence specified by $V_i(\mathbf{r}-\mathbf{R}_0)$, as in Eq. (4). Using the relation for the nuclear volume above Eq. (6) and Eq. (21), we simplify Eq. (25) to

$$En_{(2)}\approx -\frac{28}{\mu}\frac{j_1(2k_F/\mu)}{(2k_F/\mu)^2}[U_d^2+3U_\tau^2+3U_\sigma^2+9U_{\sigma\tau}^2]. \quad (26)$$

Equation (26) serves only to show the rough form and variation of the interaction energy. It is indeed untrustworthy for actual numerical comparison because the Bessel function is a sensitive function for arguments in the region of four as occur here.

Of greater significance in the discussion of the second order effects is the role of the tensor force terms. This is because pseudoscalar meson theory yields a long range (μ^{-1}) tensor force interaction as a consequence of single meson exchange. There are additional tensor contributions resulting from two-meson exchange in the Brueckner-Watson version, but these are of lesser importance due to their shorter range.[21] We note that there is very little by way of spin-dependent central

forces in both the Brueckner-Watson and Lévy potentials, and it is the large tensor force term of long range, μ^{-1}, that is responsible for the difference in behavior in the singlet and triplet states of the two-body system. This is of significance because it indicates that both of these potential models are making full use of the long-range tensor term (which appears from pseudoscalar meson theory in the characteristic combination with a spin-spin term)[38]

$$V=\frac{1}{3}\left(\frac{g^2}{4\pi}\right)\left(\frac{\mu}{2M}\right)^2\mu\tau_1\cdot\tau_2\left(\sigma_1\cdot\sigma_2+S_{12}\frac{3+3x+x^2}{x^2}\right)\frac{e^{-x}}{x};$$

$$x\equiv\mu r \quad (27)$$

for their spin dependence.

This term[39] contributes in second order an attractive interaction energy of $0.016(g^2/4\pi)^2$ Mev for $R_0=1.35A^{\frac{1}{3}}$; $A^{\frac{1}{3}}=5.6$. This amounts to 3.6 Mev for $g^2/4\pi=15$ as in the Brueckner-Watson potential, and 1.6 Mev for $g^2/4\pi=10$ as in the Lévy model. When the two-meson exchange parts of the tensor forces in the Brueckner-Watson model are included, the attraction decreases to 2.6 Mev for the same choice of R_0 and A. At a distance of $R_0=1.4A^{\frac{1}{3}}$, these interaction energies decrease by 40% to values of 1.5 Mev and 0.9 Mev, respectively, for the Brueckner-Watson and Lévy potentials. Henley and Ruderman[40] have shown that higher-order contributions due to multiple meson scattering at a source serve only to increase the tensor force by 7 percent, so there is at present no known way of appreciably increasing the effect of this term on a field theoretic basis.

In the cases of both of the nuclear potentials which are rooted in the pseudoscalar meson theory, it thus seems clear that one cannot attribute the difference (R_N-R_C) to the finite range of nuclear forces, alone. In the Brueckner-Watson model, the sum of the effects of the short range direct forces of attraction and of the longer range tensor forces add up to 7 Mev at a distance of $1.35A^{\frac{1}{3}}$, with $A=5.6$, and thus serve merely to cut down the Coulomb barrier for protons from a height of 14 Mev to +7 Mev at this distance. For the Lévy potential the total nuclear attraction is only ~2 Mev.

Finally, we note briefly the results of calculations on the second-order interaction energies using the various phenomenological potentials discussed in the preceding section. The results are presented as before for $R_0=1.35A^{\frac{1}{3}}$ and $A^{\frac{1}{3}}=5.6$. For the Yukawa potential, Eq. (16), the second-order energy gives an 8 percent correction to the first-order result, serving to increase the attraction by 3.5 Mev. The second order contributions for the Pease-Feshbach potential, [Eq. (17)], come to −2.5 Mev, or a 10 percent increase in the first-order result. The total second-order contributions in the case of the Rosenfeld force amount to an attraction of −1.4 Mev only.

These results give an idea of the role of the second-order contributions in this work.[41] Of special importance here are their general orders of magnitude, which are small, and the feature that they do not provide the necessary attractions in the field theory cases to account for R_N-R_C.

V. ANTISYMMETRIZATION

We analyze here the effects which are introduced when we modify our work to obey the requirement of the Pauli principle that the wave function of the system, incident nucleon plus nucleus, be antisymmetric in all coordinates.

These effects do not manifest themselves directly as simple potential terms but as exchange modifications of the scattering amplitudes and cross sections. We shall show, however, that these modifications are of quite minor importance for our work, and that their effects can be simulated by slight alterations of the energies calculated in the preceding sections.

Before displaying the relevant formalism for effecting the antisymmetrization, we note the following general features:

1. The first-order interaction energy calculated in Sec. III for the direct term, $V_d(r)$, of Eq. (2), is decreased in magnitude in general. This is because the Pauli principle inhibits the close approach to two fermions. The magnitude of the reduction factor is roughly given by

$$1-(1/4)\exp[-(R_0-R_C)/\lambda], \quad (28)$$

where the factor (1/4) represents the fraction of possible exchanges, since states with different spin and/or isotopic spin are mutually orthogonal. The exponential factor serves as a rough estimate of the overlap in the exchange of a nuclear particle at the nuclear surface, R_C, with the external nucleon at R_0; the length $\lambda\sim1/\mu$

[38] See, for example, G. Wentzel, *Quantum Theory of Wave Fields* (Interscience Press, New York, 1950).

[39] The calculational problems encountered in evaluating the second order energy, Eq. (19), with a potential of the form in Eq. (27) are most readily surmounted by expressing the bracket in Eq. (27) in terms of differentials

$$(\ )\to\sigma_1\cdot\nabla\sigma_2\cdot\nabla$$

and by carrying out the indicated differentiations only at the very end. In place of Eq. (23), one has an expression of the form

$$\lim_{R'\to R_0}(\nabla R'\cdot\nabla R_0)^2\int d\mathbf{r}\int d\mathbf{r}'\rho(r)\rho(r')\frac{j_1(2k_F|\mathbf{r}-\mathbf{r}'|)}{(2k_F|\mathbf{r}-\mathbf{r}'|)^2}$$

$$\times V(\mathbf{r}-\mathbf{R}_0)V(\mathbf{r}'-\mathbf{R}').$$

[40] E. M. Henley and M. A. Ruderman, Phys. Rev. **92**, 1036 (1953).

[41] These second-order calculations indicate the nature of the limitations on the conclusions drawn below Eq. (7). Thus a potential of the form $(a+b\sigma_1\cdot\sigma\tau_1\cdot\tau)\exp(-\mu r)/\mu r$ is a saturating interaction provided $a\geq0$ and $a+b\geq0$, and can account for R_N-R_C if $b\sim50$ Mev and $a\leq b/10$. However such a pathological potential would predict among other things much too large a deuteron binding energy.

corresponds to the barrier penetration distance of a particle bound by ~10 Mev in a square well. In that, we assign the maximum penetration length, λ, to all nuclear particles including those bound deeply in the well, we overestimate the exchange correction in Eq. (28). For $R_0=1.35A^{\frac{1}{3}}$, with $A^{\frac{1}{3}}=5.6$, the factor expressed by Eq. (28) equals ~0.9 and serves to decrease the energies in Sec. III by roughly 10%. It is thus a small effect and contributes only in the direction of strengthening our conclusions.

2. The second-order interaction energies due to polarization as calculated in Sec. IV are all quite small. The exchange corrections to these are negligible since, aside from other factors, they are reduced by the same exponential as in Eq. (28).

3. The one important effect of the antisymmetrization procedure is to give rise to *first*-order contributions to the interaction energy from the exchange potentials in Eq. (2). In particular, for the Brueckner-Watson and Lévy potentials, we need consider only the long-range V_{rr} term of Eq. (2) as contained in Eq. (27) since this is the only term of any significance. However, we find that this term contributes an attraction of less than one Mev for $R_0=1.35A^{\frac{1}{3}}$; $A^{\frac{1}{3}}=5.6$.

In order to outline a development of this result, we formulate the problem of the scattering of a nucleon by a nucleus of A particles. If we take as the nuclear Hamiltonian

$$h_A=\sum_{i=1}^{A} t_i+\sum_{i>j=1}^{A} V_{ij},$$

with eigenvalues ϵ_i and eigenfunctions $g_i(1\cdots A)$ which are antisymmetric under particle interchanges, the Schrödinger equation for the nucleus plus an incident nucleon reads

$$\left(h_A+t_s+\sum_{i=1}^{A} V_{is}-E\right)\Psi=0. \tag{29}$$

Let us assume first of all that the incident nucleon is distinguishable so that we can write the formal scattering solution of Eq. (29) as[42]

$$\Psi=g(1\cdots A)\varphi(s)+\frac{1}{E-h_A-t_s}\sum_{i=1}^{A} V_{is}\Psi, \tag{30}$$

for the nucleus initially in the ground state, g, and the incident nucleon initially in the plane wave state, $\varphi(s)$. The outgoing wave contour is understood in the propagator in Eq. (30). By projecting Eq. (30) onto appropriate nuclear eigenstates we obtain the scattering amplitudes for different processes.

[42] This is similar to the development in N. Francis and K. M. Watson, Phys. Rev. **92**, 291 (1953).

In particular, for elastic scattering we have

$$\begin{aligned}(g,\Psi)&\equiv\int g^*(1\cdots A)\Psi(s;1\cdots A)d\mathbf{1}\cdots d\mathbf{A}\\&=\varphi(s)+(E-\epsilon-t_s)^{-1}\left(g,\sum_{i=1}^{A} V_{is}\Psi\right)\\&=\varphi(s)+(E-\epsilon-t_s)^{-1}\Bigg[\left(g,\sum_{i=1}^{A} V_{is}g\right)\\&\quad+\sum_{n,n'}{}'\left(g,\sum_{i=1}^{A} V_{is}g_n\right)\\&\quad\cdot\frac{1}{(E-\epsilon_n-t_s)\delta_{n,n'}-\left(g_n,\sum_{i=1}^{A} V_{is}g_{n'}\right)}\\&\quad\cdot\left(g_{n'},\sum_{i=1}^{A} V_{is}g\right)\Bigg](g,\Psi),\end{aligned} \tag{31}$$

with the sum on n and n' extending over all nuclear states except the ground state. The first term in the brackets in the right member of Eq. (31) corresponds to the first order interaction energy calculations of Sec. III. It contributes the potential scattering[43] amplitude

$$f_D=\int\varphi_f^*(s)\left(g,\sum_{i=1}^{A} V_{is}g\right)(g,\Psi)d\mathbf{S}. \tag{32}$$

We investigate this term further in order to calculate the Pauli exchange corrections to it. Due to the equiva-

[43] The second term gives all of the compound elastic effects in the terminology of reference 2. The induced polarization contributions which we calculated in Sec. IV correspond to a second order approximation to the second term which neglects the potential term in the intermediate energy denominator and replaces the kinetic energy operator, t_0, by its value for the incident particle before (or after) scattering in state $\varphi(s)$. The first of these two approximations is judged to be good in consequence of the smallness of the second order relative to the first order interaction energies for the direct terms, $V_d(r)$. The second approximation corresponds to making the optical approximation that a given potential can represent the scattering. It is rigorous in the adiabatic limit of slow incident particles (<50 kev). It also applies to calculations for the incident nucleon "outside" of the nucleus so that the nucleon can be considered to be moving freely with its initial kinetic energy. Incident nucleons of kinetic energy $\gtrsim$20 Mev can be localized to within 10^{-13} cm so that this approximation should be valid in the energy range above 20 Mev for calculations of interaction energies at distances up to within 10^{-13} cm of the surface; i.e., to within $1.4A^{\frac{1}{3}}$ for $A^{\frac{1}{3}}=5.6$. As the initial nuclear effect will be one of attraction, the incident nucleon will be speeded up, thereby increasing the magnitude of the energy denominator and decreasing the contribution of this term. We have no quantitative criterion for the validity of this second approximation at lower energies. Here we must rely on the smallness of the calculated second order corrections and on the results of the cloudy crystal ball analysis which indicate that the potential scattering predominates for elastic processes (except in the immediate vicinity of a resonance). The average elastic cross section is primarily due to potential scattering from an impenetrable sphere whose radius coincides quite closely to the radius of the potential well. (See Fig. 1 of reference 2.)

lence of the nuclear particles we can replace the sum, $\sum_{i=1}^{A} V_{is}$, by one term, AV_{is}. Representing the nuclear ground-state function by a Slater determinant of independent particle orbitals and spin functions in Eq. (32), we have

$$f_D=\sum_b \int \varphi_f^*(s)\varphi_b^*(1)V_{1s}\varphi_b(1)(g,\Psi)d\mathbf{S}d\mathbf{1}, \quad (33)$$

where the sum on b extends over the A filled single particle states of the nucleus. Now we can simply include the exchange scattering by replacing the product $\varphi_f^*(s)\varphi_b^*(1)$ by the antisymmetrized product[44] $[\varphi_f^*(s)\varphi_b^*(1)]-[\varphi_f^*(1)\varphi_b^*(s)]$ so that the scattering amplitude, including exchange, becomes

$$f=\sum_b \int [\varphi_f^*(s)\varphi_b^*(1) - \varphi_f^*(1)\varphi_b^*(s)]V_{1s}\varphi_b(1)(g,\Psi)d\mathbf{S}d\mathbf{1}.$$

In terms of an effective potential for the scattering of the incident nucleon, we have then

$$\mathcal{U}_{eff}(s)=\sum_b \int [\varphi_b^*(1)V_{1s}\varphi_b(1) - (\varphi_f^*(s))^{-1}\varphi_f^*(1)\varphi_b^*(s)V_{1s}\varphi_b(1)]d\mathbf{1}. \quad (34)$$

We calculate $\mathcal{U}_{eff}(s)$ now for the term of interest

$$V_{1s}=\tfrac{1}{4}(g^2/4\pi)(\mu/2M)^2\mu\boldsymbol{\tau}_1\cdot\boldsymbol{\tau}_s\boldsymbol{\sigma}_1\cdot\boldsymbol{\sigma}_s \times(\exp|\mathbf{x}_1-\mathbf{x}_s|)/|\mathbf{x}_1-\mathbf{x}_s| \quad (35)$$

in Eq. (27). The tensor term averages to zero and, as we have seen, the first, or non-exchange, term in Eq. (34) gives no first-order energy contribution for exchange potentials. For elastic exchange scattering, the spin factors in Eq. (35) give $\frac{1}{4}$ and the effective potential is from Eq. (34)

$$\mathcal{U}_{eff}(s)=-0.95\ \text{Mev}\sum_b \int e^{i\mathbf{k}\cdot(\mathbf{r}_s-\mathbf{r}_1)}\left(\frac{u_b^*(s)}{u_b^*(1)}\right) \times\left(u_b^*(1)\frac{e^{-\mu|\mathbf{r}_s-\mathbf{r}_1|}}{\mu|\mathbf{r}_s-\mathbf{r}_1|}u_b(1)\right)d\mathbf{1}, \quad (36)$$

where u_b is the spatial part of the wave function of a particle bound in the nucleus. The numerical constant is calculated for a coupling constant of $g^2/4\pi=15$ in Eq. (35) as in the Brueckner-Watson potential; it is replaced by 0.64 Mev for the parameters in the Lévy potential. The following series of approximations overestimate the magnitude of $\mathcal{U}_{eff}(s)$ and thereby provide an upper bound for the effective exchange potential of Eq. (36):

1. replace $e^{i\mathbf{k}\cdot(\mathbf{r}_s-\mathbf{r}_1)}$ by unity;

2. replace the ratio of bound state space functions, $u_b(s)/u_b(1)$ by its maximum value, corresponding to the particle in the highest filled nuclear level, bound by an energy E_{BE}. The function $u_b(s)$ in this state has the largest penetration distance outside of the nucleus. In the denominator, we insert for the wave function inside the nucleus, $u_b(1)$, its value near the nuclear surface where the density is low.

Introducing these approximations into Eq. (36) and summing over the bound states, we obtain then for the effective interaction energy

$$\mathcal{U}_{eff}(s)=-0.95\ \text{Mev}(A/v)\int \rho(\mathbf{r})\frac{e^{-\mu|\mathbf{r}_s-\mathbf{r}|}}{\mu|\mathbf{r}_s-\mathbf{r}|} \times\exp[-(2ME_{BE}/\mu^2)^{\frac{1}{2}}\mu|\mathbf{r}_s-\mathbf{r}|]d\mathbf{r}.$$

Integrating over the nuclear distribution we obtain an exchange attraction of 0.3 Mev for the incident nucleon at $r_s=R_0=1.35A^{\frac{1}{3}}$, with $A^{\frac{1}{3}}=5.6$ and for a binding energy $E_{BE}=10$ Mev. This result corresponds closely to that obtained below Eq. (28). If we include inelastic spin-flip scatterings as well as elastic processes, the spin factor in Eq. (35) gives $\frac{3}{4}$ and the effective exchange attraction increases to 0.9 Mev. These numbers are given for the coupling constant $g^2/4\pi=15$ used in the Brueckner-Watson potential and are reduced by one third for the Lévy potential.

This rough approximation to the exchange energy is an overestimate of its effect. It is clear, however, that it is of little qualitative importance in our development.

VI. CONCLUSION

To summarize, we have studied the difference between the nuclear force radius, R_N, and the radius of the charge distribution, R_C, for heavy nuclei, $A>100$. From the analyses of neutron[2-4] and proton[5,8] cross sections we take $R_N\simeq 1.4A^{\frac{1}{3}}$ as the distance at which an incident nuclear particle feels an appreciable nuclear attraction, $\gtrsim 14$ Mev. From the electron scattering work at Stanford[10,13] we take the charge distribution for gold as drawn in Fig. 1, which decreases to half-value at $R_C=1.12A^{\frac{1}{3}}$. The surfaces of the nuclear potential and charge distributions are seen to be similar in Fig. 1 but with the nuclear potential extending roughly 25 percent beyond the charge distribution.

The aim of this work has been to infer some properties of nuclear forces from the difference, R_N-R_C, if it is *assumed* that the nuclear charge and matter distributions coincide. We have considered various nuclear force models which are motivated by meson theory or by phenomenological analyses to see if they can simultaneously satisfy the saturation requirements in heavy nuclei and can account for the radius difference, R_N-R_C. This radius difference is to a large extent a measure of the long range behavior of the direct (σ- and τ-independent) part of the central interaction

[44] S. Altshuler, Phys. Rev. **91**, 5 (1953).

potential between nucleons. Our calculations show that the nuclear forces must contain long range direct central attractions with short range repulsive interactions if they are to account for both $R_N - R_C$ and saturation.

Such forces can be constructed phenomenologically. However, the two nuclear force models based on pseudoscalar meson theory, which have met with success in fitting low energy data on two-body systems, fail to meet these requirements. The Brueckner-Watson[21] potential (gradient coupling theory; no pair term) has too little direct central attraction to account for $R_N - R_C$. Using this potential and calculating the effects of induced polarizations and of antisymmetrization as well as the direct interaction [Eq. (6)] we have obtained a total nucleon-nucleus energy of attraction of less than 8 Mev, or roughly half of what we require to make the nuclear radius appear to be only as large as $1.35A^{\frac{1}{3}}$, for $A=176$. The difficulties in handling the repulsive core behavior of the potential for small distances and the calculations in Sec. IV of the second order energies arising from the induced polarizations caution us not to extend these calculations to smaller separations between the nucleon and nucleus. It is thus not possible for us to give a quantitative answer to the question: how far beyond the charge distribution does the neutron distribution have to extend if we use the Brueckner-Watson potential and require $\sim$14 Mev of attraction at $R_N = 1.4A^{\frac{1}{3}}$ in order to explain the difference in radii, $R_N - R_C$? However, if we disregard the above warnings to caution, we can carry out the calculations and estimate that the neutron distribution must extend at least 10% beyond the charge distribution,[45] corresponding to a neutron surface layer 0.7–1.0 thick for $A^{\frac{1}{3}} = 5.6$.

These calculations with the Brueckner-Watson potential were also applied to lighter nuclei in order to test the dependence of our results on atomic number. For a mass number $A=120$, we took the matter distribution to be the same as the Stanford charge distribution shown in Fig. 1; i.e., we assumed that the matter and charge distributions scaled together between $A=176$ and $A=120$. The nuclear attraction in this case was evaluated to be $\sim$9 Mev at $R_0 = 1.35A^{\frac{1}{3}}$ in comparison with the less than 8 Mev for $A=176$. The reason for this increase of roughly 1 Mev in the attraction is simply this: the separation between the nuclear matter and an incident nucleon at $R_0 = 1.35A^{\frac{1}{3}}$ decreases with $A^{\frac{1}{3}}$. For a singular inter-nucleon potential the accompanying increase in interaction energy more than compensates for the decrease due to the fact that there are fewer particles in the nucleus which interact with an incident nucleon. The above figure of 9 Mev is qualitatively but not quantitatively ($\pm 15\%$) reliable because one begins to encounter the same difficulties as mentioned in the preceding paragraph with decreasing A values. It is still significantly less than the 14 Mev of attraction required at $R_N = 1.4A^{\frac{1}{3}}$ to account for the observed radius and indicates the validity of our conclusions for $A \gtrsim 100$.

Further extrapolating the Stanford charge distribution (Fig. 1 for $A=197$) down to $A \sim 60$ and calculating at $R_0 = 1.4A^{\frac{1}{3}}$, because of the aforementioned difficulties in handling the repulsive cores for smaller distances, we obtain with the Brueckner-Watson potential less than half of the 14 Mev required to account for the observed difference, $R_N - R_C$.

The Lévy[20] potential has a strong, direct attraction due to the "pair" term which is sufficient in strength and range to explain the radius difference. However, when the three-body repulsions resulting from the "pair" term, and required for nuclear stability[24] are included, the attraction is balanced at large distances and it is no longer possible to account for $R_N - R_C$. In addition there is strong evidence especially from the work of Klein[20] for the damping of the pair term which is the source of the strong direct interaction in the Lévy potential. Without the pair term, there is only a weak direct central attraction of range $\sim 1/2\mu$ corresponding to double meson exchange in the gradient coupling version of pseudoscalar meson theory.[21,40] We note that the only clue at present as to a possible source of additional central attractions (also of range $\sim 1/2\mu$) in presently studied and applied versions of pseudoscalar meson theory comes from the meson-meson interaction introduced into meson theory by the renormalization program.[24] However, the role of this term has yet to be fully explored.

An alternative explanation of the radius difference assumes that the nuclear charge and matter distributions do not coincide, but that the radius of the neutron distribution extends beyond the radius, R_C, of the proton distribution.[15,16] The difficulties which face this explanation were pointed out in Sec. I. In particular, the optical analysis by Williams[39] of the reaction cross sections (total minus coherent elastic) for 1.4-Bev neutrons and 860-Mev protons incident on various medium and heavy nuclei indicates nuclear matter distributions in close agreement with the Stanford charge distribution. His results cannot be understood if the neutron radius is appreciably larger than the radius, R_C, of the charge distribution. They can, however, be explained, as Williams points out, in terms of a decrease in the effective range of the nucleon-nucleon interaction at high energies.[46]

[45] The charge dependent contribution from the second term in Eq. (2) is relatively unimportant in this consideration since V_τ is reduced in magnitude relative to V_σ by a factor of $\sim$4, as seen in Fig. 2. As mentioned in footnote 26, Eq. (3) is not valid for neutrons which form a surface layer since it is derived on the basis of a uniform proton-neutron mixture. For the surface neutrons Eq. (2) is replaced by $V_\sigma \pm V_\tau$ with the $+$ ($-$) sign obtaining for incident neutrons (protons). However, because of the small ratio of V_τ to V_σ in the Brueckner-Watson potential, the charge dependent contribution is unimportant here.

[46] This point will be discussed more fully in a note now in preparation. For large impact-parameter collisions in which the incident nucleon is only slightly deflected, one can show that

We wish to emphasize, however, that the aim of this work is not to argue the equality or inequality of the size of the neutron and proton distributions in nuclei but to show that, if one *assumes* their identity, then a special class of nuclear forces with long range attractions and short range repulsions is required to account for both the radius difference, $R_N - R_C$, and nuclear stability. Nuclear forces deduced from current meson theory and in accord with saturation requirements are not of this type.

the effective interaction potential decreases at high energy in proportion to $(1-v^2/c^2)^{\frac{1}{2}}=M/E$ if the interaction results from a (pseudo) scalar field. This is in contrast with the electromagnetic interaction in which the so-called "scalar potential" is the time component of a Lorentz four-vector and in which the above factor does not appear. This effect seems capable of qualitatively accounting for Williams' results if the large nuclear radius at low energies is interpreted as a consequence of the nuclear force attractions.

ACKNOWLEDGMENTS

It is a pleasure to acknowledge constructive comments by C. P. Schwartz and V. F. Weisskopf, and in particular to thank R. W. Williams for numerous valuable discussions on the nuclear radius situation at different energies.

PHYSICAL REVIEW VOLUME 100, NUMBER 1 OCTOBER 1, 1955

Gamma-Ray Branching in Sr^{89}

W. S. Lyon and R. R. Rickard
Oak Ridge National Laboratory, Oak Ridge, Tennessee
(Received June 17, 1955)

The decay of strontium-89 has been found to proceed through Y^{89m} to the extent of 0.02%.

STRONTIUM-89 (53 day) has been reported as a pure beta emitter in the tabulated nuclear data.[1] Various investigators have attempted to find gamma radiation accompanying Sr^{89} with no success. With the advent of NaI gamma-ray spectrometers, however, the limits of detection for gamma rays have been decreased sufficiently to enable many previously undetected small gamma-ray branchings to be observed. Since a 14-sec Y^{89m} isomeric state is known, it was of interest to see what fraction, if any, of the Sr^{89} decay proceeds through this level.

Approximately 1 Mc of strontium-89 was obtained from the Operations Division, Oak Ridge National Laboratory and put through chemical purification.[2] Strontium and barium carriers were added and the mixed barium-strontium nitrates precipitated with fuming nitric acid. The nitrates were dissolved in a few ml of H_2O and reprecipitated by the addition of fuming nitric acid. Upon dissolution of the precipitate, Fe^{+3} carrier was added and $Fe(OH)_3$ was precipitated by the addition of NH_4OH. The supernate from this scavenging was neutralized with HNO_3, acidified with acetic acid, buffered with ammonium acetate, and $BaCrO_4$ precipitated by addition of Na_2CrO_4. The $BaCrO_4$ was filtered off, the supernate was made basic with NH_4OH and the strontium was precipitated as the oxalate by addition of ammonium oxalate. The precipitate was filtered, washed, and mounted on a card for counting.

The Sr^{89} source was examined on a 3 in.×3 in. NaI(Tl) gamma-ray spectrometer, and a photopeak corresponding to a gamma ray of energy 0.91 Mev was observed. The total number of gamma-ray processes in the source was obtained by integration of the gamma peak and dividing by an appropriate efficiency factor in the usual manner.[3]

The total number of Sr^{89} disintegrations in the source was obtained by dissolving the strontium oxalate and absolute beta counting an aliquot of this solution. The ratio γ/total β^- was found to be 2×10^{-4}. Using this fractional branching, the log ft value for the 0.55-Mev beta group which must precede the gamma ray was calculated[4] to be 12.7. This corresponds to a $\Delta I=2$, no, transition and is in agreement with spin and parity changes deduced from tabulated nuclear data,[1] i.e., a 5/2+ level in Sr^{89} and a 9/2+ level in the Y^{89m} isomer.

Acknowledgment is made to S. A. Reynolds who suggested the problem, and to G. N. Case who performed much of the chemistry.

[1] Hollander, Perlman, and Seaborg, Revs. Modern Phys. **25**, 469 (1953).
[2] C. D. Coryell and N. Sugarman, *Radiochemical Studies: The Fission Products* (McGraw-Hill Book Company, New York, 1951), National Nuclear Energy Series, Plutonium Project Record, Vol. III, p. 1460.
[3] B. Kahn and W. S. Lyon, Nucleonics **12**, No. 6, 26 (1953).
[4] S. A. Moszkowski, Phys. Rev. **82**, 35 (1951).

Photonuclear Yields of N^{17}†

DARYL REAGAN*
High-Energy Physics Laboratory, Stanford University, Stanford, California
(Received June 3, 1955)

Yields of N^{17} from several elements have been measured as functions of electron energy and converter thickness for bombardments from the Stanford linear electron accelerator. After correction for the electron-produced part of the yield, the $O^{18}(\gamma,\rho)$ and $F^{19}(\gamma,2\rho)$ yields can be fitted (within statistics) to isochromats characteristic of 25- and 40-Mev photon energies, indicating integrated cross sections of 0.067 and 0.0037 Mev barn, respectively.

The neon and sodium yields are similar, one to the other, in their energy dependence, and indicate a N^{17} photoproduction cross section of the order of 3×10^{-30} cm² in the 100-Mev region, rising to the neighborhood of 3×10^{-29} cm² at 200 Mev.

The cross sections estimated for N^{17} photoproduction in magnesium and aluminum rise from about 2×10^{-30} cm² in the 80- to 180-Mev region to around 3×10^{-29} cm² at 400 Mev.

Estimating the N^{17} cross section to be about 1 percent of the total photoabsorption cross section leading to $A=17$ isobar production at high energies gives order of magnitude agreement with photomeson cross sections. This is consistent with the idea that direct photonuclear cross sections are small at high energies, and that the large apparent photonuclear cross section is due to indirect processes involving photomesons.

INTRODUCTION

THE energy dependences of the (γ,n) and (γ,ρ) cross sections have been measured for many elements with betatrons[1–5] for photon energies up to about 25 Mev. With synchrotrons, the detailed work has been extended to 330 Mev,[6] but only the total photoneutron production cross sections have been measured.

Experiments identifying specific photoreactions at 320-Mev synchrotron energy for a few elements in the copper-arsenic region established that the more complex reactions occur very much less frequently than the (γ,n) and (γ,ρ) reactions.[7] These experiments further established yield surfaces which specify approximately the yield for those photoreactions involving the emission of more than two nucleons. For a given isotope, the yield surface is a ridge, parallel to the valley of nuclear stability, peaked at about ½ mass unit toward the neutron-deficient side. The slope of the ridge peak is about 35 percent per mass unit. The ridge profile for constant number of emitted nucleons is approximately gaussian, dropping to half in 0.65 unit of atomic number.

Since the copper-arsenic experiments employed chemical separations, it would require a program of very large magnitude to continue this work, evaluating the yields as a function of energy, in order to establish photon cross sections for the reactions covering the available energy range.

The properties of N^{17}, a delayed neutron emitter, make it possible to identify small N^{17} yields resulting from complex reactions quickly and easily. Thus, for a few photonuclear reactions leading to N^{17} production, it is feasible to measure the energy dependence of the yields and to infer roughly the photonuclear cross sections as a function of energy.

In the work to be described, N^{17} yields due to bombardments of electrons and their bremsstrahlung radiation were measured, the two effects being empirically separated. Yields were measured for the elements oxygen through aluminum, for several electron energies in the range 80–415 Mev. The photon cross sections inferred from the results are compared with other results in this field.

PROPERTIES OF NITROGEN-17

Produced yields of N^{17} were measured by counting delayed neutrons. The decay scheme of N^{17}, as reported by Alvarez,[8] is as follows:

$$N^{17}\rightarrow O^{17*}+\beta^-, \quad t_{\frac{1}{2}}=4.2 \text{ sec},$$

$$O^{17*}\rightarrow O^{16}+{}_0n^1, \quad t_{\frac{1}{2}}=\theta(10^{-21}) \text{ sec},$$

$$\searrow\ O^{16*}+{}_0n^1\rightarrow\alpha+{}_6C^{13}+{}_0n^1\ (\sim1 \text{ percent}).$$

Nitrogen-17 is one of only two known nuclides in the low-Z region that emit neutrons having a measurable apparent half-life. The other, Li^9, emits neutrons having an apparent half-life of 0.168 sec. A feature of the experiment is the decay plot of the neutron count made each time a yield was measured. This allowed an estimate to be made of contamination due to Li^9 or any other (unknown) delayed-neutron emitter having a half-life much different from 4 sec, to moderated neutrons left over from the accelerator burst, or to pile-up

† The research reported here was supported by the joint program of the Office of Naval Research and the U. S. Atomic Energy Commission.
* Now at the University of California Radiation Laboratory, Livermore, California.
[1] Johns, Katz, Douglas, and Haslam, Phys. Rev. **80**, 1062 (1950).
[2] J. Halpern and A. K. Mann, Phys. Rev. **83**, 370 (1950).
[3] L. Katz and A. G. W. Cameron, Phys. Rev. **84**, 1115 (1951).
[4] Montalbetti, Katz, and Goldemberg, Phys. Rev. **91**, 659 (1953).
[5] R. Nathans and J. Halpern, Phys. Rev. **93**, 437 (1954).
[6] L. W. Jones and K. M. Terwilliger, Phys. Rev. **91**, 699 (1953).
[7] Halpern, Debs, Eisinger, Fairhall, and Richter, Laboratory of Nuclear Sciences, Massachusetts Institute of Technology (unpublished); also Phys. Rev. **97**, 1327 (1955).
[8] L. W. Alvarez, Phys. Rev. **75**, 1127 (1948).

TABLE I. Targets.

Material	Physical size	Thickness (moles/cm²)	Thickness (radiation lengths)	Remarks
Polystyrene	$\frac{1}{32}$-in. sheet	6.00×10^{-3}	0.0017	C^{11} monitor and ends of capsules
Water	Note[a]	2.12×10^{-4} [O^{16}]	0.0504	$O^{18}(\gamma,p)N^{17}$
O_2	Note[b]	1.15×10^{-4} [O^{16}]	0.027	Compare Ne
LiF	Note[a]	6.22×10^{-2}	0.040	$F^{19}(\gamma,2p)N^{17}$
Ne	Note[b]	2.93×10^{-3}	0.020	Ne→N^{17}
NaCl	Note[a]	4.12×10^{-2}	0.1094	$Na^{23}(\gamma,\alpha,2p)N^{17}$
Mg	$\frac{33}{64}$-in. thick	0.153	0.1457	Mg→N^{17}
Al	$\frac{1}{4}$-in. thick	0.491	0.140	$Al^{27}(\gamma,2\alpha,2p)N^{17}$
Cu converter	0.0446-in. thick	0.0159	0.0758	Radiator
Cu scatterer	0.1915-in. thick	0.068	0.325	Background estimate
Al collector foils, etc.[c]	...	...	0.003	Effective as additional converter

[a] Contained in polystyrene capsule $\frac{1}{8}$-in. thick by approximately 3-in. diameter. The polystyrene caps are $\frac{1}{32}$-in. thick.
[b] Contained in commercial type M.V. flask at 550 lb/in.²
[c] The aluminum collector foils in the monitor, mylar exit window, ZnS scintillator, and the air path between the accelerator exit and the target totaled about 0.003 radiation length. The ZnS scintillator was used as an aid in beam alignment.

of β or γ pulses. The rarity of radioactive neutron emitters and the relative insensitivity of the counters to electron and γ radiation resulted in background counting rates lower by several orders of magnitude than those commonly encountered in work of this type. This, in turn, permitted detection of the extremely small yields of N^{17} which resulted from the more complex photonuclear reactions investigated.

EXPERIMENTAL EQUIPMENT

1. Electron Beam

The x-rays which initiated the reactions were radiated by electrons from the Stanford Mark III accelerator which produces electrons in pulses about 1-μsec long, 60 times a second.[9,10] With suitable adjustments, the energy of the electrons can be varied over the range from about 50 Mev to the full energy of the machine which, at the time of this experiment, was 415 Mev.

In the end station of the accelerator,[11] the electrons are magnetically analyzed and electrons of improper energy are rejected by tungsten scrapers. The remaining electrons are again magnetically deflected in such a way that beam contamination by x-rays and soft electrons is minimized. The analyzing-magnet current is measured by a shunt and potentiometer. The energy calibration was made by a floating-wire technique. For this experiment, the electron beam was monochromatic to about 2 percent, and was about $\frac{3}{4}$ inch in diameter.

The beam intensity at the target varies with energy, ranging from about 10^8 electrons per pulse at 80 Mev to nearly 10^{10} at 415 Mev, under good running conditions. Low-beam intensity at low energies reduced the accuracy of data-taking to the point that it was unprofitable to operate below about 100 Mev.

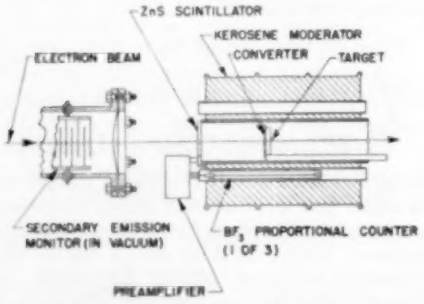

FIG. 1. Schematic cross section of the target assembly.

2. Target Assembly

A cross section of the counting and monitoring equipment installed in the bombardment area is shown in Fig. 1. A secondary-emission beam monitor[12] was installed at the end of the deflecting-system vacuum plumbing. The charge accumulated on its collector foils during a bombardment was measured by an automatic electronic slide-back electrometer in the counting area. A circuit similar to the one used is described by Littauer.[13] The performance of a prototype of the

TABLE II. Experimental program.

Period number	Purpose	Time (sec)	Interval (sec)
1	Bombardment	0 to 6.67	6.67
2	Wait; decay of short-lived activities and moderation of beam simultaneous neutrons	6.67 to 7.11	0.44
3	Count in scaler No. 1	7.11 to 12.21	5.10
4	Count in scaler No. 2	12.21 to 17.61	5.40
5	Count in scaler No. 3	17.61 to 22.99	5.38
6	Count in scaler No. 4	22.99 to 29.20	6.21
7	Wait	29.20 to 30.00	0.80

[9] R. B. Neal, Stanford University Microwave Laboratory Report No. 185 (unpublished).
[10] Chodorow, Ginzton, Hansen, Kyhl, Neal, and Panofsky, Rev. Sci. Instr. **26**, 134 (1955).
[11] W. K. H. Panofsky and J. A. McIntyre, Rev. Sci. Instr. **25**, 287 (1954).
[12] G. W. Tautfest and H. R. Fechter, Rev. Sci. Instr. **26**, 229 (1955).
[13] R. Littauer, Rev. Sci. Instr. **25** 148 (1954).

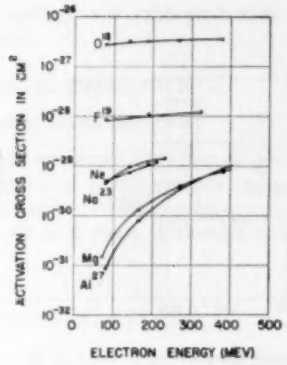

FIG. 2. Qualitative yield curves. Activation cross section is defined in the text.

monitor was checked[14] against a Faraday-cup beam collector, and its response was found to be linear with beam intensity and independent of beam energy over the 125- to 250-Mev range. The shape of the $O^{18}(\gamma,p)N^{17}$ yield curve (see Fig. 3) supports the assumption that its response is uniform over the range 80–400 Mev.

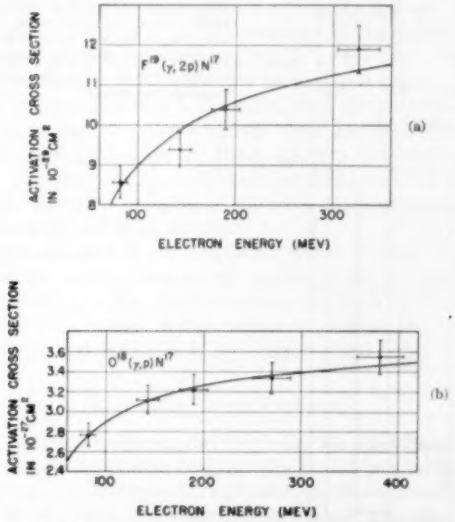

FIG. 3. Yields from the $O^{18}(\gamma,p)N^{17}$ and $F^{19}(\gamma,2p)N^{17}$ reactions, as functions of radiating electron energy. The solid lines are isochromats of characteristic energy 25 and 40 Mev, corresponding to integrated cross sections of 0.067 and 0.0037 Mev-barn, respectively.

The neutron moderator-counter assembly, used in detecting the N^{17} neutrons, was fabricated from iron tubing and a standard 55-gal oil drum and was filled with kerosene. Three B^{10}-enriched boron-trifluoride counters were inserted in the assembly as shown in Fig. 1.

[14] G. W. Tautfest (private communication).

3. Targets

Table I indicates the main features of the targets bombarded.

The $C^{12}(\gamma,n)C^{11}$ yield was used as a standard for calibrating the beam monitor,[15] and as a check on x-ray contamination of the beam. The $O^{18}(\gamma,p)N^{17}$ yield was used as a secondary standard. Relative yields from high-pressure oxygen and neon gases in "identical" containers (commercial type MV flasks) together with the background counting rate resulting from the bombardment of a similar flask containing argon, served to establish the neon yield relative to the oxygen yield. The flask bottoms, approximately 0.2-radiation-length

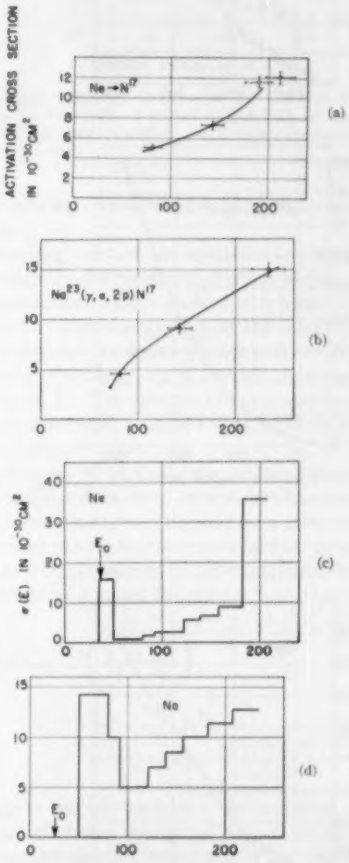

FIG. 4. Experimental N^{17} activation points for neon and sodium are plotted in the upper graphs. The lower graphs are the photon cross sections, which were calculated as indicated in the text. The activation cross sections indicated by the solid lines are reconstructions from the photon cross sections shown. The photon cross sections for energies below 80 Mev were chosen arbitrarily.

[15] Barber, George, and Reagan. Phys. Rev. 98, 73 (1955).

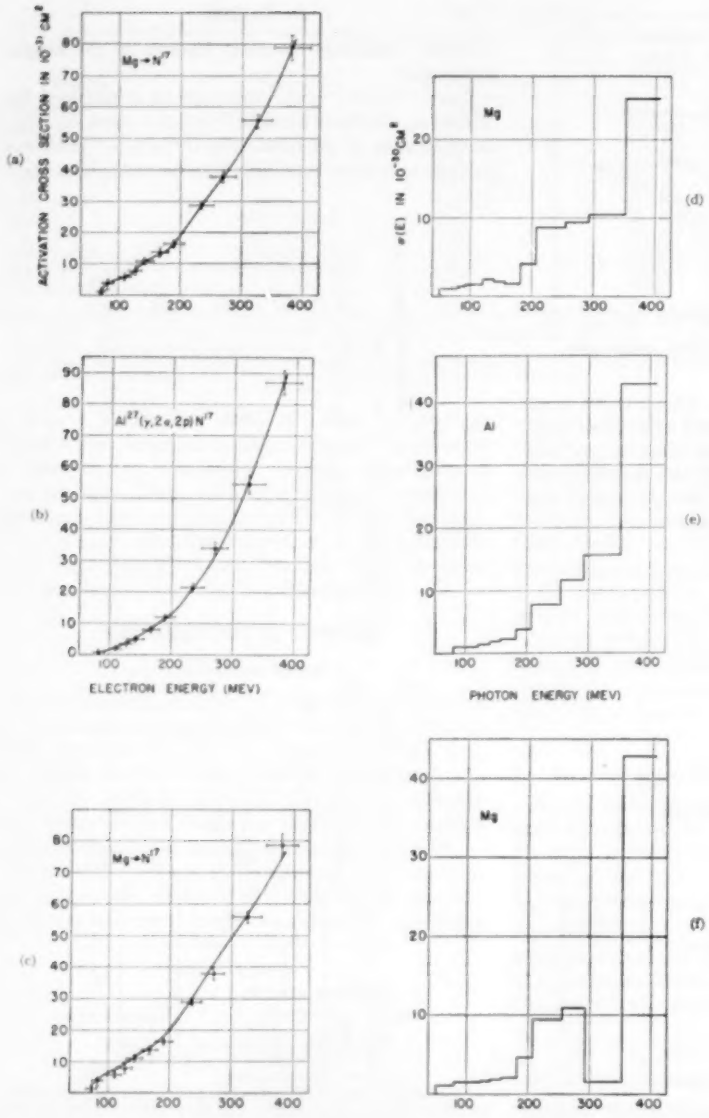

FIG. 5. Graphs a, b, and c show activation points for N^{17} yields in magnesium and aluminum. Graphs d, e, and f are the calculated photon cross sections, from which the solid lines in a, b, and c have been reconstructed. The third cross-section curve is actually the slightly modified result of an early aluminum run, and is included to illustrate the effects of moderate errors in data upon the photon cross section results.

thick, served as radiators for x-ray production in these experiments.

4. Counting Equipment

Figure 1 shows a cross section of the neutron-counting system. The neutrons emitted by the decay of the excited O^{17} have an energy of approximately 1 Mev,[18] and come out of the target isotropically, only rarely suffering a collision in the target. About 1.8 percent of them are slowed down in the kerosene moderator and react with B^{10} in a proportional counter, producing a pulse big enough to be counted. The pulses are amplified by a Los Alamos type 501 preamplifier and are transmitted by coaxial cable to the counting area. Here they are amplified by a Los Alamos type 501 amplifier and fed to a motor-driven cam-operated switching assembly, which programs the bombarding and counting cycle as indicated in Table II. The experimental sequence enables activity as a function of time to be plotted for over five half-lives. This permits more confident identification of the activity and an estimate

[18] E. Hayward, Phys. Rev. 75, 917 (1949).

on background. The system was calibrated with a radium-beryllium source.

EXPERIMENTAL YIELDS OF N^{17}

1. Activation Cross Sections

Figure 2 shows the measured N^{17} photon yield qualitatively as a function of Z and electron energy. Figures 3–5 show the measured activation cross sections, with estimated errors for each point. Activation cross section is defined as

$$A(E_\gamma)=\frac{Y(E_\gamma)}{N_e(E_\gamma)N_T'[X_C+(X_T/2)]}, \quad (1)$$

where E_γ is the energy of incident electrons in Mev; $A(E_\gamma)$ is the activation cross section measured at E_γ in cm^2; $Y(E_\gamma)$ is the number of N^{17} atoms produced by x-rays; $N_e(E_\gamma)$ is the number of incident electrons; N_T' is the target density in atoms cm^{-3}; and X_C is the converter thickness and X_T the target thickness; both X_C and X_T are measured in radiation lengths.

The yield of N^{17} has been corrected for background and for direct electron production. The beam-dependent part of the background exhibits a 4-sec period and is probably largely due to N^{17} produced in the fluorine of the BF_3 counters by large-angle x-rays from the target. Electron production will be discussed below.

The errors indicated in the ordinates of the activation points in Figs. 3–5 do not include those due to possible inaccurate evaluation of direct electron production. The indicated error in each point includes errors due to beam intensity variations, statistics, and voltmeter readings on the beam monitor.

The abscissas of the activation points in Figs. 3–5 show the approximate energy spread of the electrons contributing to the bremsstrahlung spectrum for each point. This spread is due mainly to energy loss by radiation and ionization in the converter and target.

2. Photon Cross Sections

Calculations were carried out using the yield curves to evaluate the photon cross sections for N^{17} production as a function of energy for each element above fluorine. To do this, first a bremsstrahlung curve[17] was calculated for each electron-bombardment energy used in the experiment, as illustrated in Fig. 6.

The low-energy part of the spectrum is taken as identical to the thin-target spectrum of an electron of energy E_m, where E_m is defined as

$$E_m=E_\gamma-\tfrac{1}{2}[(X_T+\tfrac{1}{2}X_C)E_\gamma+E_I], \quad (2)$$

where E_γ = energy of incident electrons, and E_I is the average ionization loss in the converter $+\frac{1}{2}$ the target. The electron energy E_m is roughly the mean energy of

[17] H. A. Bethe and W. Heitler, Proc. Roy. Soc. (London) **A146**, 83 (1934).

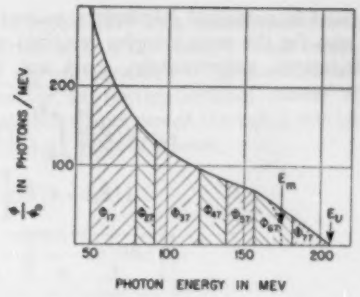

FIG. 6. Photon intensity distribution for 207-Mev electrons passing through 44.6 mils of copper and $\frac{1}{4}$ inch of aluminum. The areas Φ_i, are proportional to the bremsstrahlung integrals mentioned in the text.

radiating electrons contributing to the photon spectrum in the target.

The low-energy part of the spectrum is a reasonable approximation to the weighted average of the spectra of the electrons that radiate photons which pass through the target. The high-energy part of the modified spectrum is constructed by drawing a tangent to the mean-energy bremsstrahlung curve, which intersects the energy axis at E_γ. The spectra thus constructed have errors small compared to errors that arise from other sources in the experiment.

The evaluation of photon cross sections consists in unscrambling the data from several bombardments at different electron energies. The yield for a given reaction due to photons arising from electron bombardment of a converter and target as used in this experiment is given, to terms linear in X_C and X_T, by

$$Y(E_\gamma)=N_e(E_\gamma)N_T'\left(X_C+\frac{X_T}{2}\right)\times\int_0^{E_\gamma}\sigma(E)\phi(E,E_\gamma)dE, \quad (3)$$

where $\sigma(E)$ is the photonuclear-reaction cross section as a function of photon energy; $\phi(E,E_\gamma)$ is the appropriate bremsstrahlung spectrum; and E is the photon energy in Mev. Substituting Eq. (3) in (1),

$$A(E_\gamma)=\int_0^{E_\gamma}\sigma(E)\phi(E,E_\gamma)dE; \quad (4)$$

or, approximately,

$$A(E_\gamma)=\sum_{i=1}^{p}\sigma_i\int_{E=E_{i-1}}^{E_i}\phi(E,E_\gamma)dE, \quad (5)$$

where σ_i is the average value of $\sigma(E)$ in the range E_{i-1} to E_i, and E_0 is the energetic threshold for the reaction $[\sigma(E)=0, E\leq E_0]$. The approximation of Eq.

(5) was used in numerical calculations to evaluate σ_i step by step for the more complex reactions studied. The calculations, unfortunately, could not lead to unique values for σ_i, due to errors in the measurements of $A(E_\gamma)$, as will be shown.

Solving (5) for σ_1 and σ_2, we have

$$\sigma_1 = A(E_1)\left[\int_{E_0}^{E_1}\phi(E,E_1)dE\right]^{-1}, \tag{6}$$

$$\sigma_2 = \frac{A(E_2)-A(E_1)\left[\int_{E_0}^{E_1}\phi(E,E_2)dE \Big/ \int_{E_0}^{E_1}\phi(E,E_1)dE\right]}{\int_{E_1}^{E_2}\phi(E,E_2)dE}. \tag{7}$$

Since $E_2 > E_1$, then $\phi(E,E_2) > \phi(E,E_1)$ for all E, and the coefficient of $A(E_1)$ in Eq. (7) is greater than unity. It can be shown that, in general,

$$\sigma_j = \frac{A(E_j)-Q}{\int_{E_{j-1}}^{E_j}\phi(E,E_j)dE}, \tag{8}$$

where Q is greater than $A(E_{j-1})$. So σ depends upon a difference in activation yield that is weighted unfavorably as far as accuracy in σ is concerned. Reference to the activation cross-section curves shows that the errors in activation cross section are quite comparable to the differences between adjacent A's. The result is that, in evaluating σ, almost inevitably one comes to an energy region where σ oscillates violently from large to small or negative values as one computes the higher energy σ's. To force the σ's into a reasonable pattern, the A's were adjusted during the calculation of σ in order that σ would not become negative or oscillate violently. Many σ curves were calculated, more or less consistent with the data and the requirements of regularity. Of these, five have been plotted in Figs. 4 and 5. These have been chosen largely for their suggestiveness. To show their compatibility with the activation data, each activation curve has been reconstructed from σ and plotted with the corresponding experimental points.

The error possible in any single σ_j is very large—several hundred percent. For example, by revising A_{j-1} downward a few percent, and A_j upward a few percent, one can, in most cases, double or treble σ_j. However, such a manipulation will be reflected in changes in the neighboring σ_j's. In particular, σ_{j-1} and σ_{j+1} will become much smaller. Further, if σ_{j+1} does not become negative, then σ_{j+2} probably will if further changes in neighboring A's are not made. Assuming, therefore, some relatively smooth energy dependence for σ, the error in the average value of σ taken over three or four neighboring σ_j's is of the order of 50 percent.

3. Comments

The oxygen and fluorine yields, shown in Fig. 3, fit well with yield curves computed for narrow σ resonances at 25 and 40 Mev. The reaction energetic thresholds are 15.8 Mev for $O^{18}(\gamma,p)N^{17}$ and 23.5 Mev for $F^{19}(\gamma,2p)N^{17}$. The integrated cross sections necessary to account for the yields, assuming the narrow resonances, are 0.067 Mev-barn for oxygen and 0.0037 Mev-barn for fluorine. The indicated errors on the oxygen and fluorine yields would allow up to about one-third of the area under the cross-section curves to occur well above the resonance region. This redistribution, attributing more yield to the region of higher energy and lower x-ray intensity of the bremsstrahlung spectra, would require an upward revision of up to 30 percent to the integrated cross sections. Under this arrangement, the photon cross section for the oxygen reaction could have an average value of not more than 2×10^{-25} cm^2 in the 50- to 400-Mev energy region.

The neon- and sodium-yield points, taken as they were for bombardment energies above 90 Mev only, cannot give any direct information about the σ values below 90 Mev. It is clear, however, that there is an energy region below 90 Mev having appreciable σ. The σ's computed for Ne and Na embody two somewhat different assumptions for the nature of σ at lower energies. Since the yield curves are so closely similar (when errors are taken into account) each σ should be regarded as a possibility for either element.

The magnesium and aluminum curves were investigated in the greatest detail and are shown in Fig. 5. Unfortunately, the evaluation of the direct electron effect is very poor in the case of magnesium, and is lacking in the case of aluminum. The relative error from this source could be as great as 20 percent. The qualitative features of the total yield (of which the given yields are a fixed fraction, 0.76) must, however, reflect those of the true photon activation curve. The striking feature of these curves is their increasing slope in the region above meson threshold. This is fairly conclusive evidence for a σ that is larger above meson threshold than below, and which remains, on the average, large over a very broad energy region. For the low-energy magnesium and aluminum runs, the counting rates were low, only slightly above background. The errors are thus relatively large. It is possible, therefore, that either magnesium or aluminum may have a low-energy σ behavior qualitatively like any in Fig. 5.

4. Direct Electron Production

Of the electrons in each bombardment, 90 percent passed through the target with energy loss of only a few percent of their initial energy. These electrons, and many of the degraded electrons, possessed enough energy to produce N^{17} by a direct process without the intervention of an x-ray. Blair[18-20] has computed the ratio of electron-produced to photon-induced nuclear reactions for an electron-initiated shower after the parent electrons have passed through a thin converter. For the energy range of interest,

$$R=N_C'Z^2r_0^2F, \tag{9}$$

with

$$F=\frac{2\pi\left(\frac{k}{E_\nu}\right)\left\{\left[\frac{k}{E_\nu}+\frac{E_\nu}{k}\right]\left[\frac{\phi_1(\gamma)}{4}-\frac{1}{3}\ln Z\right]-\frac{2}{3}\left[\frac{\phi_2(\gamma)}{4}-\frac{1}{3}\ln Z\right]\right\}}{\left[1+\frac{k^2}{E_\nu^2}\right]\ln\frac{2Ek}{\mu c^2E}+C}; \tag{10}$$

where R is the ratio of x-ray-produced to electron-produced reactions at depth N_C'; Z is the atomic number of the converter; $r_0^2=7.83\times10^{-26}$ cm^2; k is the recoil energy of the electron; E_ν is the initial energy of the electrons; $E=E_\nu-k$ is the excitation energy of the nucleus; μc^2 is the rest energy of the electron (0.511 Mev); $\gamma=100\,\mu c^2EZ^{-\frac{1}{3}}/E_\nu k$; and $\phi_1(\gamma)$ and $\phi_2(\gamma)$ are as plotted by Bethe and Heitler[17]; C is $-2(k/E_\nu)$ for electric-dipole interaction, 0 for the magnetic-dipole interaction, and $8k^2/3(E^2)$ for the electric-quadrupole interaction.

For the lithium-fluoride target at 240-Mev electron energy, the total yield was measured as a function of converter thickness. The results appear in Fig. 7. The first measured point is for the target with no copper converter. The effective converter thickness for this is taken to be the thickness of the monitor foils, vacuum window, and scintillator, plus half the thickness of the target, since, on the average, each x-ray produced in the target passes through half of the target. The other points were taken with copper converters up to 0.0446-inch thick, about 0.07 radiation length. The yield axis intercept of the curve gives directly the electron-produced part of the yield. It is $51/173=0.295$ times the total yield at maximum converter thickness (to terms linear in X, and neglecting electron degradation in the target). The ratio R, for the maximum converter thickness, is then $(1-0.295)/0.295=2.4\pm0.3$.

The weighted sum of $N_C'Z^2r_0^2$ for the maximum converter thickness plus half the target thickness is 0.78. This gives an experimental value of $\bar{F}$ of $3.06\leq0.4$. Here $\bar{F}$ is a mean value of F averaged over E and all possible multipole coupling terms. The fit of the yield curve with a 40-Mev isochromat (see Fig. 3) suggests that a suitable E for Eq. (10) is 40 Mev. The computed values for F from Eq. (10) are, with $E=40$ Mev and $E_\nu=240$ Mev, for electric dipole $F\leqq4.7$; magnetic dipole, $F\leqq4.15$; and electric quadrupole, $F\leqq0.8$. Each F value increases with E, the electric-quadrupole term having a greater slope than the dipole terms. The quadrupole term is about 3 for $E=100$ Mev with $E_\nu=240$ Mev.

It appears, then, on the basis of Blair's theory and considering the experimental error, that either electric- or magnetic-dipole interaction could possibly account for the yield, and certainly a combination of these with electric-quadrupole interaction could be made to fit the data.

The direct electron effect was evaluated in several additional cases by measuring the yield with and without the 46.6-mil copper converter. This work was done during the latter part of the experiment, at a time when the beam intensity and stability of the accelerator were somewhat below par. Consequently, the measurements suffered in accuracy. The oxygen effect was measured at 90 Mev, leading to an $\bar{F}$ value of 2.36_{-1}^{+2}. This value was applied to all oxygen data to obtain the estimate of the photon yield shown in Fig. 3.

For fluorine, in addition to the data at 240 Mev, the simplified evaluation was made at 92, 258, and 355 Mev, leading to $\bar{F}$ values of 4.7 ± 0.6, 3.0 ± 0.5, and 3.0 ± 0.4, respectively. The photon activation curve for fluorine (Fig. 3) reflects these variations in $\bar{F}$, which substantially flattened the raw curve. The errors are such, however, as to make it doubtful whether the change in shape of the activation curve was really justified. In magnesium at 258 Mev, $\bar{F}$ was found to be 2.15 ± 0.5.

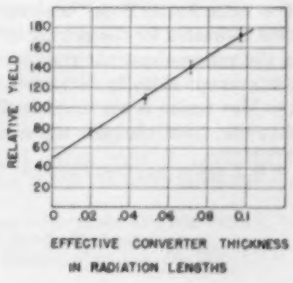

FIG. 7. Total N^{17} yield from fluorine as a function of effective converter thickness.

[18] J. S. Blair, Phys. Rev. **75**, 907 (1949).
[19] J. S. Blair (unpublished mimeographed notes).
[20] J. S. Blair (private communications to Richard Wilson and K. L. Brown).

Any x-ray contamination of the electron beam would be reflected in a lower measured value of $\bar{F}$.

The correction applied to the yield curves for the direct electron effect ranged from 20 to 34 percent, and was constant with energy except in the case of fluorine. The neon correction was somewhat arbitrarily taken as equal to that for oxygen.

DISCUSSION

As a survey of the general features of the energy dependence of specific photonuclear reactions of varying complexity, the yield data suggest that the resonance-shape characteristic of the (γ,n), (γ,p), (γ,np), etc., reactions persist in even more complex reactions, including, possibly, reactions involving the emission of about six nucleons, as exemplified by the $Na^{23}(\gamma,\alpha,2p)N^{17}$ reaction. The magnesium yield—probably mostly due to $Mg^{24}(\gamma,\alpha,3p)N^{17}$—suggests that a broad resonance might exist even in this case, extending from the reaction threshold to meson threshold. It is possible that generally for the more complex reactions the σ resonances are broader, as well as smaller in amplitude, than those of the simpler reactions. The breadth of the resonance for the more complicated reactions, as well as the indicated increase of σ even below meson threshold, would confirm the emission of energetic particles as suggested by LeCouteur.[21]

It is of interest to estimate the total photonuclear cross section in the energy region above the giant resonance for a nuclide having an atomic number ≈ 10 by summing the partial cross sections due to the various processes.

Assuming the yield surface found by Halpern *et al.*[7] to apply in low-Z cases and over a wide energy range, the N^{17} yield from a given nuclide having $A>19$ would represent roughly 1 percent of the total $A=17$ yield due to high-energy photon bombardment. An estimate of the total photodisintegration cross section can then be formed by summing the photon cross sections in Figs. 4 and 5 (representing ΔA's of 3, 6, 7, and 10), adding terms determined by interpolation for missing ΔA's, and multiplying by 100. This gives a value of the order of 3×10^{-27} cm^2 as total photonuclear cross section in the 50- to 150-Mev region, and an increase to at least 10^{-26} cm^2 at 400 Mev, taking into account the many reactions contributing at the higher energies. The value 3×10^{-27} cm^2 is already 15 times the upper limit estimated for the average $O^{18}(\gamma,p)N^{17}$ cross section in the region above the resonance. The upper limit on the average $F^{19}(\gamma,2p)N^{17}$ cross section in the 50- to 150-Mev region is ten times smaller still. This confirms that the more complex reactions compete effectively with the simpler reactions in the higher-energy region. If the constant ΔA yield profiles are actually broader or narrower in this region of the periodic table than those measured by Halpern *et al.*,[7] or if the peak of the yield profile for constant ΔA is shifted relative to the position found by Halpern's group, this estimate might be off by a factor of the order of 10 either way. In any case, the cross section for the emission of seven or more nucleons at 200 to 400 Mev is considerably larger than that for the emission of only one or two.

Previous cross-section evaluations for complex photonuclear reactions have been made with x-rays from synchrotrons, using photographic plate techniques. The average value for the cross section for the photoproduction of stars of three or more prongs in silver is given by Miller.[22] For the 242- to 322-Mev photon-energy interval, it is $(8\pm1)\times10^{-27}$ cm^2; in the 161- to 242-Mev interval $(7\pm1)\times10^{-27}$ cm^2. The corresponding total photon absorption figures in aluminum from the data presented here would be of the order of 8×10^{-27} and 6×10^{-27} cm^2, respectively. Applying a factor of four to correct for the differences in nucleon numbers in silver and aluminum makes the total absorption cross section reported here roughly four times the star-production cross section reported by Miller. This is a reasonable agreement, considering the errors and the differences in choice of data.

Previous workers[23] have shown that the charged pion photoproduction cross sections for low-Z nuclei are of the order of 10^{-28} cm^2 per nucleon. The pion yields are found to be proportional to A^1, indicating possibly that a charged photomeson produced in the nuclear interior is usually absorbed immediately within the parent nucleus. The resulting highly excited nucleus would then decay by nucleon emission; the whole process appearing to be a photonuclear reaction. The order-of-magnitude agreement of the meson photoproduction cross sections and the total high-energy nuclear photoabsorption cross section estimated here leaves open the possibility that the "photonuclear" process at high-photon energies is predominantly a mesonic, rather than a nuclear effect.

The author wishes to acknowledge with thanks the contributions to this work of Professor W. K. H. Panofsky, who suggested the problem and directed its execution; Professor R. A. Ogg, Jr., who prepared several special targets in the early phases of the work; Mrs. P. B. Hanson, T. McKinney, J. Van Mierlo, and K. Wilson, who were responsible for the efficient operation of the accelerator; and Mrs. I. Machein, who performed a large part of the data reduction.

[21] K. J. LeCouteur, Proc. Phys. Soc. (London) **A63**, 259 (1950).

[22] R. D. Miller, Phys. Rev. **82**, 260 (1951).

[23] R. E. Marshak, *Meson Physics* (McGraw-Hill Book Company, Inc., New York, 1952), pp. 98–109.

Angular Distribution of n-p Scattering at 17.9 Mev

A. GALONSKY AND J. P. JUDISH
Oak Ridge National Laboratory, Oak Ridge, Tennessee
(Received June 27, 1955)

The angular distribution of protons bombarded by 17.9±0.1-Mev neutrons was measured at 11 angles from 2.5° to 50° in the laboratory system. At each angle the energy spectrum of protons producing a coincidence of pulses in two proportional counters and a NaI(Tl) crystal was measured in the NaI crystal. Each spectrum has a peak less than 25% wide at half-maximum and a small low-energy tail caused by Coulomb scattering of the protons in the detector. The error in each yield was between 2 and 3% for angles from 2.5° to 45° and 8% at 50°. A least squares fit to the data gives 1.08±0.03 for the ratio of the n-p scattering cross sections at neutron angles 180° and 90° cm.

INTRODUCTION

THERE have been several measurements of the n-p scattering angular distribution with neutrons of 14.1 Mev. Each of three most recent investigations[1–3] has revealed a small anisotropy. The best value of $\sigma(180°)/\sigma(90°)$ is 1.05±0.02. At 27.2 Mev the effect is much larger—$\sigma(180°)/\sigma(90°)=1.28\pm0.10$.[4] The only measurement between 14.1 and 27.2 Mev gave the inconclusive result $\sigma(150°)/\sigma(90°)=1.06\pm0.16$ for neutrons between 18 and 21 Mev.[5] The value found in this experiment for $\sigma(180°)/\sigma(90°)$ is 1.08±0.03 for 17.9-Mev neutrons.

EXPERIMENTAL

Deuterons accelerated to 1.96 Mev by the 2.5-Mv electrostatic generator entered a 1.5-in. long tritium gas target through a 0.05-mil nickel foil. At the normal operating pressure of one atmosphere of tritium the shift in the $T(p,n)He^3$ threshold and the rise of the yield curve showed that the deuteron energy in the tritium target was 1.7±0.1 Mev. Hence, the neutrons produced at 0° in the $T(d,n)He^4$ reaction have energies of 17.9±0.1 Mev. Since the gas is contained in a steel cylinder with a 0.010-in. wall, a 0.05-mil nickel entrance window, and a 0.004-in. platinum beam-stop, contamination of the forward beam by energy-degraded neutrons is negligible.

Experience showed that currents above 2 μa produced pinholes in the nickel window. At the average operating current of 1 μa no pinholes were produced, but there was still a small heat-leak of about 1.5% per hour. After several hours the target was replenished with tritium from a uranium storage vessel.

A long propane recoil counter biased above d-d neutrons was the neutron flux monitor. In a 3-week test with a Po-Be source the counting rate of this monitor followed the Po decay curve to within ±0.5%. During this time the bias setting varied by ±0.5% and the voltage[6] by ±0.02%.

The n-p angular distribution was obtained by counting with a triple coincidence telescope[7] the number of protons ejected from a polyethylene radiator as a function of angle made with the 17.9-Mev neutrons incident on the radiator. The proton counts were normalized to the propane monitor counts, and at least 6 runs were made at each of 10 angles from 0° to 45°. (With the telescope set at 0° the average angle is 2.5°, but this angle will be referred to as 0°.)

Figure 1 shows the tritium gas target, the polyethylene radiator, the two proportional counters, and the NaI spectrometer. The housing is a steel can with a 0.030-in. thick hemisphere between the tritium and radiator to produce a constant attenuation of the neutrons as the telescope is rotated about an axis through the radiator. The distance of the radiator to the center of the tritium was 4.3 in.; of the NaI aperture to the radiator, 3.9 in. The entire can was filled to 0.5 atmos of an argon +3% CO_2 mixture. With this arrangement there is no foil or counter-wire in the path of the protons from radiator to NaI crystal. A 180° field-tube served to delineate the active length of each counter at 1 in. and to reduce by $\frac{1}{3}$ the number of argon recoils detected by the proportional counters. The thickness of the NaI crystal, 2.5 mm, is sufficient to stop a 20-Mev proton. Using 15-Mev protons from the $He^3(d,p)He^4$ reaction Trail and Johnson[7] found that the full width at half-maximum of the NaI coincidence spectrum was 3%. Alignment of the apparatus was achieved in two steps: first, visually with the aid of plumb bobs, and then more accurately by observing the pulse height difference in the NaI spectrometer for supposedly equal proton recoil angles, $+\theta$ and $-\theta$. This method is quite sensitive, for, if the true zero angle is in error by 1°, the pulse heights at ±45° will differ by 6.7%.

To adjust for the collection time of the porportional counter pulses, the NaI pulses were delayed before entering the coincidence circuit. In order to choose the

[1] H. H. Barschall and R. F. Taschek, Phys. Rev. **75**, 1819 (1949).
[2] Allred, Armstrong, and Rosen, Phys. Rev. **91**, 90 (1953).
[3] John D. Seagrave, Phys. Rev. **97**, 757 (1955).
[4] Brolley, Coon, and Fowler, Phys. Rev. **82**, 190 (1951).
[5] E. M. Baldwin, Phys. Rev. **83**, 495 (1951).
[6] The voltage supply was a 1–5-kv model 400*B* manufactured by the John Fluke Company, Seattle, Washington.
[7] C. C. Trail and C. H. Johnson, Phys. Rev. **95**, 1363 (1954).

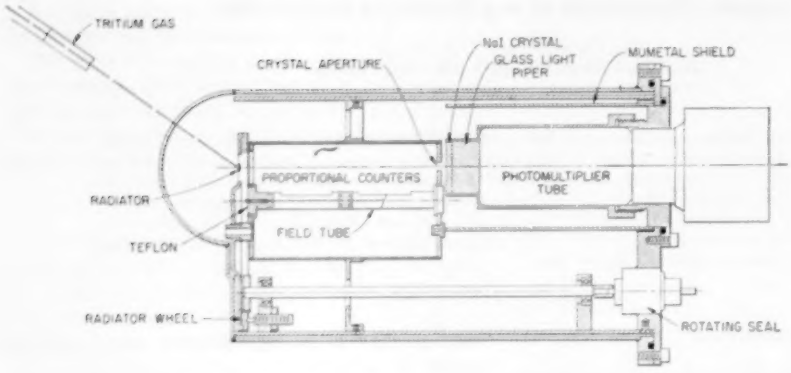

FIG. 1. The $T(d,n)He^4$ neutron source, radiator, and triple coincidence telescope detector. (Approximately to scale.)

proper delay-time, curves of coincidence counts *vs* delay-time were obtained for several proton energies from 4.5 to 17.9 Mev. With increasing delay-time each of the curves rose sharply to a flat plateau and then fell sharply. The width of the plateaus was 1.1 ± 0.1 μsec. Because of the dependence of proportional counter pulse height on proton energy, the plateaus shifted to longer delay-times with increasing proton energy. The shift was slight enough compared to the plateau width so that a 0.6 μsec delay could be used for all of the above-mentioned energies and, therefore, for all recoil angles between 0° and 45°. At 50°, however, a 0.3-μsec delay was used so that the operating point would stay closer to the middle of the plateau.

Since the protons lost an average of about 1% of their energy in each proportional counter, their coincidence spectra were very broad, in qualitative agreement with the Symon-Landau theory.[8] To insure that all protons would be counted, the proportional counter biases were set at half the height of the low-energy cutoff when the telescope was set at 0°. At other angles the pulses were, of course, higher.

The noncoincidence counting rates of the two proportional counters and the NaI spectrometer were approximately constant with angle at 1500, 1200, and 300 counts/sec, respectively. These rates are so low that corrections for accidental coincidences and dead time are each less than 1%. The corrections were not made since only the relative angular distribution was investigated.

It was the intention to take an equal number of counts at $\pm\theta$ in order to reduce the errors caused by small misalignments. However, almost all of the background coincidences, presumably from the $F^{19}(n,p)$, (n,d), and (n,α) reactions, were found to originate in the teflon insulator (see Fig. 1). Because of the difference in neutron flux on the Teflon at $\pm\theta$, a higher statistical accuracy could be achieved in a given time by orienting the telescope as in Fig. 1, i.e., with the Teflon away from the neutron source. The observed difference in the backgrounds (e.g., a factor of 1.5 for ±45°) could be explained by this mechanism. Approximately $\frac{3}{4}$ of the data were taken with the Teflon on the far side of the tritium, $\frac{1}{4}$ on the near side. The NaI coincidence spectra taken on the far side are shown in Fig. 2 for proton recoil angles ranging from 0° to 50°. Backgrounds, which varied from 5% under the 0° peaks to 40% under the 50° peak, have been subtracted.

A polyethylene radiator 0.016 in. thick was used for the angles 0° to 30°. In order to maintain sharp spectra a 0.008-in. radiator was used from 35° to 50°. These radiators were mounted inside the telescope-can on a wheel which also contained a 0.003-in. radiator, an α-particle source for testing purposes, and a blank and a carbon target for measuring background. The wheel could be turned without breaking the vacuum through a bellows-type rotating seal.

Aside from radiator thickness, the angular resolution of the system, ±3°, was the major factor in broadening the peaks. Since $E_p=E_n\cos^2\theta$, where E_p and E_n are the recoil proton and incident neutron energies, respectively, it is unimportant (in regard to the proton spectra) to have good angular resolution near 0°, but very important at large angles. For example, a ±3° resolution produces a width at half-maximum of 2% at 5° and 20% at 45°. An increased efficiency without sacrifice of energy resolution was achieved by the well-known device of using a rectangular, rather than a circular, radiator and NaI aperture. For the dimensions chosen, 0.2 in.×0.4 in. for both radiator and aperture, the angular acceptance is not appreciably increased except for angles less than ~10°, where the proton energy is almost constant with angle.

Calculations of single and multiple[9] Coulomb scattering in the radiator and A-CO_2 showed that there was a negligible effect on the NaI spectra. Some of the protons initially recoiling at the proper angle to be detected are scattered in the radiator and gas so that they do not hit the NaI crystal. There is compensation, however, from

[8] Bruno Rossi, *High-Energy Particles* (Prentice-Hall, New York, 1952), pp. 29 ff.

[9] H. S. Snyder and W. T. Scott, Phys. Rev. **76**, 220 (1949).

protons initially recoiling at other angles. For the proton energies, radiator thicknesses, and gas pressure used in this experiment more than 99.5% of the protons were deflected by less than 4°. In such a small angular range the yield of n-p scattering is so nearly linear with angle that the compensation is essentially perfect. The compensating protons, coming from closely neighboring recoil angles, have nearly the same energy as the direct protons and fall within the peaks of the NaI spectra. The small but discernible tails (see Fig. 2) which occur on the low-energy side of the peaks are attributed to penetration of the slit over the NaI crystal and to scattering in the walls of the proportional counters. Approximate calculations of these effects agreed with the observed tails, but no correction was applied to the data because the complicated geometry demanded that several simplifying assumptions be made. In addition, the number of counts observed in the first few channels below the peak compared to that in the peak was always less than 1% per channel and was often 0% within the statistical uncertainty. However, at each angle a 1% uncertainty was assigned to the yield to cover the possible error in the number of channels included in the peak. As a check on the effects of radiator thickness and counter-gas pressure spectra were obtained with a statistical accuracy of 4% with 0.008-in. radiator at 0°, of 5% with a 0.003-in. radiator at 45°, and of 7% at 45° with the A-CO_2 pressure reduced from the usual value of $\frac{1}{2}$ atmos to $\frac{1}{8}$ atmos. In all three cases the shapes of the spectra and the yields agreed with the other data taken at 0° and 45°.

Since three different radiators were used in this experiment, it was necessary to have an accurate comparison of their weights. Each radiator was cut into a 0.2-in.×0.4-in. rectangle, weighed on a microbalance, and then attached to a $\frac{3}{4}$-in. tantalum disk by gentle heating on a hotplate. Each tantalum disk was then cemented over a hole in the radiator wheel. There was no weight change after the heating. The number of hydrogen atoms is directly proportional to the weight. No area measurements are required and no assumption need be made as to the uniformity in thickness of the polyethylene foils. This method also eliminates the usual slit in front of the radiator.

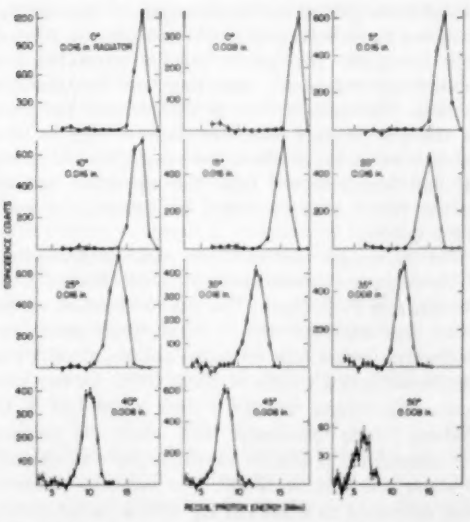

FIG. 2. NaI coincidence spectra taken with the telescope oriented as in Fig. 1. These spectra comprise about $\frac{1}{4}$ of all the data. Backgrounds, which varied from 5 percent under the 0° peaks to 40% under the 50° peak, have been subtracted.

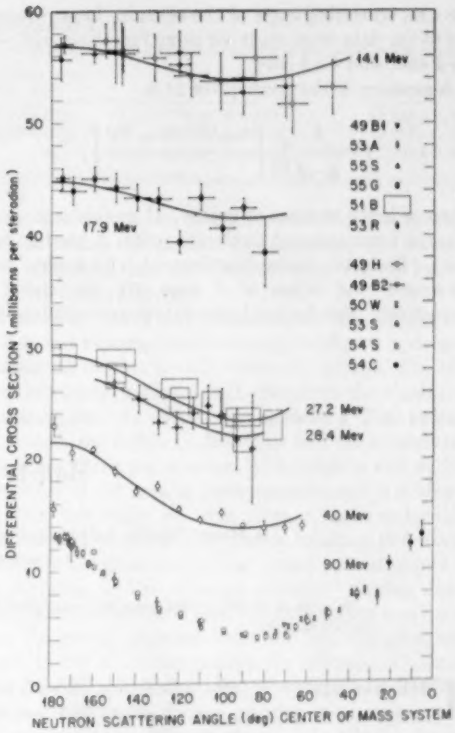

FIG. 3. This drawing was prepared by J. L. Fowler for use in a forthcoming review article. The curves for the 14.1- and 17.9-Mev data were obtained from least squares analyses assuming distributions of the form $1+k\cos^2\theta$. The other curves were drawn visually. 49B1—H. H. Barschall and R. F. Taschek, Phys. Rev. **75**, 1819 (1949). 53*A*—Allred, Armstrong, and Rosen, Phys Rev. **91**, 90 (1953). 55*S*—J. D. Seagrave, Phys. Rev. **97**, 757 (1955). 55*G*—Present work. 51*B*—Brolley, Coon, and Fowler, Phys. Rev. **82**, 190 (1951). 53*R*—Remley, Jentschke, and Kruger, Phys. Rev. **89**, 1194 (1953). 49*H*—J. Hadley *et al.*, Phys. Rev. **75**, 351 (1949). 49*B2*—K. Brueckner *et al.*, Phys. Rev. **75**, 555 (1949). 50*W*—Roger Wallace, Phys. Rev. **81**, 493 (1950). 53*S*—Selove, Strauch, and Titus, Phys. Rev. **92**, 724 (1953). 54*S*—R. H. Stahl and N. F. Ramsey, Phys. Rev. **96**, 1310 (1954). 54*C*—Owen Chamberlain and James W. Easley, Phys. Rev. **94**, 208 (1954).

RESULTS

The yields, converted to the c.m. system by the relativistic transformation, are plotted in Fig. 3 against

the c.m. scattering angle of the neutron. Least squares fits to the data were made for three functions: $\sigma(\theta)\sim 1$, $1+k\cos\theta$, and $1+k\cos^2\theta$.

A measure of the goodness of fit is

$$s^2=\frac{1}{n-2}\sum_{i=1}^{n}\left[\frac{\sigma_{\text{calc}}(\theta_i)-\sigma_{\text{exp}}(\theta_i)}{\epsilon_i}\right]^2,$$

where n is the number of points—11 in this case—and ϵ_i is the error assigned to the ith point. A good fit has $s^2\approx 1$. For the three functions—1, $1+k\cos\theta$, and $1+k\cos^2\theta$—the values of s^2 were 3.0, 2.0, and 1.4, respectively. For the two latter functions $k=0.08\pm 0.04$ and 0.08 ± 0.03, respectively. In order to compare the data at 17.9 Mev with those at other neutron energies, $1+(0.08\pm 0.03)\cos^2\theta$ was taken to be the best fit, and the relative yields measured here were normalized to the total cross section of 535 mb. There is no intention to imply that symmetry about 90° has been observed.

ACKNOWLEDGMENTS

The authors are indebted to C. H. Johnson and C. C. Trail for the loan of their telescope and for many helpful discussions. The constant advice and encouragement of J. L. Fowler were invaluable and are gratefully acknolwedged.

PHYSICAL REVIEW VOLUME 100, NUMBER 1 OCTOBER 1, 1955

Half-Life of Tritium*

W. M. JONES
Los Alamos Scientific Laboratory, University of California, Los Alamos, New Mexico
(Received June 13, 1955)

A value of 12.262±0.004 years has been found for the tritium half-life by measurement of the He^3 growth in two samples.

THE availability at this laboratory of sufficient amounts of tritium gas of about 99.5 percent isotopic purity has made possible a more precise determination of the tritium half-life by measurement of the amount of He^3 produced in a known length of time from a known initial amount of tritium gas.

Half-life determinations were made on two samples. Sample I was sealed off in a 200 cc cylindrical lime glass vessel, and Sample II in a similar Pyrex vessel. A blank mixture of He^4 and H_2, in proportions approximating the final He^3/T_2 ratio in Sample II, was put into a lime glass vessel and stored for about the same length of time and in the same manner as Sample I. Each vessel was well baked out and provided with two break-off seals in series in order to prevent contact of the gas with material other than clean glass, and in order to check possible diffusion through the first break-off seal during the decay. Each vessel was enclosed in an evacuated Pyrex sheath, also provided with a break-off seal, and stored at liquid nitrogen temperature for the duration of the decay period. The low temperature storage minimized diffusion of the gases, especially helium, into the vessel walls. Lime glass was employed in Sample I since it is considerably less permeable to helium than Pyrex.[1] The He^3 contents of Samples I and II were determined within a few days of each other. The He^4 in the blank was then separated to prove the effectiveness of the storage and separation methods. The separation of tritium (hydrogen) from He^3 (He^4) was made with a small palladium thimble, operated at 350°C and causing negligible holdup. The gas to be separated communicated with the inside of the palladium thimble by means of a Kovar tube, welded to the palladium. The arrangement insured that the gases to be separated would not come in contact with hot glass. The gas undergoing separation was exposed only to mercury, clean glass, and the palladium thimble. The contact time of tritium with hot glass on the low pressure side was short enough so that diffusion or exchange effects were negligible. After the gas had been removed from the separation system, further traces were recovered by heating the walls of the system.

The tritium gas used had been enriched in a system of Hertz pumps constructed by R. M. Potter, J. R. Mosley, and F. J. Dunn. The gas to be sealed up for decay was analyzed with a mass spectrometer immediately after passage through a palladium valve and compressed into a volume of about 100 cc for measurement. This volume included a limb of the $\frac{3}{4}$ in. I. D. Trubore tubing manometer with which the pressure was measured. The volume was calibrated with mercury to about one part in 50 000. The meniscus positions were estimated to 0.001 cm Hg with a cathetometer, which was intercompared with a standard meter bar suspended between the limbs of the manometer. The temperature was estimated to 0.005° with a mercury-in-

* This paper is based on work performed under University of California contract with the U. S. Atomic Energy Commission.
[1] S. Dushman, *Vacuum Technique* (John Wiley and Sons, Inc., New York, 1949), p. 536.

TABLE I. Summary of experimental data.

Sample	Initial T_2, cc	He^3, cc	Decay time, mean solar days	Final T_2 plus $\frac{1}{2}$ He^3, cc	$T_{\frac{1}{2}}$, years
I	78.204±0.020	20.178±0.003	892.76±0.02	78.197±0.020	12.265±0.004
II	105.245±0.025	18.016±0.003	578.09±0.02	105.285±0.025	12.259±0.004
				accepted value	12.262±0.004

glass thermometer taped to the measuring volume and insulated from the room. The thermometer was graduated to 0.02°, and its calibration was checked against a standard platinum resistance thermometer. The average temperature of the gas exceeded the measured temperature slightly due to radioactive heating. The calculated correction averaged about 0.03°. After measurement, practically all the tritium was transferred into the decay vessel through a capillary lead-in with a mercury Toepler pump. The lead-in was sealed off, and the very small amount of gas not transferred was measured and then analyzed on a mass spectrometer. The helium was measured in a volume of about 35 cc, which was known to one part in 15 000. Pressure and temperature measurements were similar to those above. Appropriate reduction of pressures to international cm Hg were made. Corrections for gas imperfections were made using the virial coefficient data for H_2 and He^4 summarized by Keyes.[2] Comparison of data for H_2 and D_2 [3] indicates that isotope effects in the virial coefficients may for present purposes be neglected.

The initial and final tritium and the helium were analyzed on a Consolidated-Nier mass spectrometer, using a high-pressure leak. Several independent analyses were made. The instrument was well baked out, sometimes with high purity tritium gas flowing through, in order to minimize memory and exchange effects. Analyses were continued until there were no changes in the indicated composition. This sometimes required two hours or more and replacement of sample. Making some allowance for absolute errors, an uncertainty of about 0.02 percent is estimated for the initial and for the final amounts of tritium due to the mass spectrometer analysis. The tritium isotopic content of the initial tritium in Sample II was checked to 0.01 percent on a different mass spectrometer, using a molecular leak. Corrections for the small amounts of non-isotopic impurities, amounting to a few hundredths of a percent, were made on the basis of known mixtures of small amounts of such gases with hydrogen. The mass spectrometer was calibrated with these mixtures at approximately the time of analysis.

Since the initial tritium to be used for decay was measured as a function of time as it passed through the palladium thimble, the average time at which the tritium sample started to decay was known. Similarly, in the final separation of tritium and He^3, the average time at which the tritium was separated was known. It is estimated that the effective decay time is known to a half-hour or better.

Following the He^3-T_2 separations, the separation system was exposed to several samples of pure hydrogen in order to remove possible traces of tritium. The He^4 was then separated from the hydrogen in the blank and analyzed on the mass spectrometer. The helium recovered was 0.001_6 cc less than had been measured out in the blank preparation. This result is well within the errors of the several measurements and is evidence for the adequacy of the storage and separation procedure. The probability that a recoiling He^3 would penetrate the glass of the decay vessel was estimated to be negligible. In this estimate collisional slowing down was taken into account, and the assumption was made that the energy required for entry into the glass was equal to the activation energy for diffusion. Columns 2 and 5 of Table I show that the material balance is within experimental error.

Results

The experimental data for the two samples is summarized in Table I. The amounts of gases are expressed in cc NTP, corrected for gas imperfections.

TABLE II. Comparison with other determinations.

Observer	Half-life, yr	Method
Novick[a]	12.1±0.5	He^3 growth.
Jenks, Ghormley, and Sweeton[b]	12.46±0.1	Steady state rate of diffusion of He^3 from a thin quartz capsule containing tritium oxide.
Jones[c]	$12.41^{+0.15}_{-0.25}$	Absolute counting.
Present data	12.262±0.004	He^3 growth.

[a] A. Novick, Phys. Rev. **72**, 972 (1947).
[b] Jenks, Ghormley, and Sweeton, Phys. Rev. **75**, 701 (1949); Jenks, Sweeton, and Ghormley, Phys. Rev. **80**, 990 (1950).
[c] W. M. Jones, Phys. Rev. **83**, 537 (1951).

Comparison with Other Data

The present value is compared with other determinations in Table II.

ACKNOWLEDGMENTS

I wish to thank R. M. Potter, J. R. Mosley, and F. J. Dunn for the use of a system of Hertz pumps in enriching tritium for Sample II, and R. M. Potter for providing the enriched tritium for Sample I.

[2] F. G. Keyes, *Temperature* (Reinhold Publishing Corporation, New York, 1941), p. 41.
[3] Wooley, Scott, and Brickwedde, J. Research Natl. Bur. Standards **41**, 379 (1948).

Slow Neutron Resonances of Manganese, Bismuth, and Selenium*

L. M. Bollinger, D. A. Dahlberg,† R. R. Palmer,‡ and G. E. Thomas
Argonne National Laboratory, Lemont, Illinois

(Received January 13, 1955; revised manuscript received May 9, 1955)

The apparatus associated with the Argonne fast neutron "chopper" and techniques that have been developed for its use in neutron transmission measurements are described. Of particular importance is the application of a boron-loaded liquid scintillation counter for the efficient detection of slow neutrons. The nature of the data that are obtained is illustrated by the results given for bismuth, selenium, and manganese. Several techniques for finding neutron resonance parameters and their application to the above data are are discussed. Resonance widths are found for the first two levels in bismuth. For the levels in selenium the measurements give only $\sigma_0\Gamma^2$. A complete set of parameters is obtained for the first three manganese resonances. The abnormally large ratio of neutron width to level spacing for manganese produces an unusual shape for the cross-section curve in the neighborhood of the second resonance which is interpreted as being caused by interference between the second and third resonances. For this interpretation we obtain $J=2$ for $E_0=337$ ev, $J=3$ for $E_0=1080$ ev, and $J=3$ for 2360 ev.

I. INTRODUCTION

THE use of the time-of-flight method for slow neutron experiments has been thoroughly treated in the literature.[1,2] In particular, the characteristics of the Argonne fast mechanical neutron velocity selector in its initial state of development was described by Selove.[3] During the past two years, however, almost all of the original equipment has been replaced and new techniques have evolved for obtaining data of high quality. The purpose of the present paper is to describe these improvements in our system and to give illustration of the data that can be obtained with it. The bulk of the results that are being accumulated will be reported in following papers.

The Argonne fast neutron velocity selector has been used only for the measurement of the neutron transmission of materials, that is, for the determination of total neutron cross sections. In these experiments, a short burst of collimated neutrons from the Argonne heavy-water pile (CP-3′) is passed by a mechanical shutter (usually termed a neutron "chopper") at a known time. The time that elapses between the emission of this burst and the detection of a neutron at a known distance from the chopper provides a measure of the energy of that neutron. The energy distribution of the neutron beam passed by the chopper is measured by recording counting rate as a function of flight time; because of the small counting rates obtained, these rates are registered on a multichannel differential flight-time analyzer. The transmission of a sample as a function of energy is measured by dividing the counting rate distribution, corrected for background, from the chopper into the corresponding distribution that is obtained when the sample is placed in the neutron beam.

The essential properties of the three basic components required for neutron transmission experiments, namely the chopper, detector, and flight-time analyzer, are listed in the following section as an introduction to a discussion of their use in our measurements.

II. APPARATUS

Chopper

The chopper used for the present measurements is similar in design to that described by Selove.[3] Its slit system consists of 6 slits running parallel to the axis of rotation. The neutron beams issuing from these slits overlap on the axis of rotation for all flight paths greater than a few meters giving the neutron intensity patterns shown in Fig. 1.

Detector

Two kinds of neutron detectors were used. A bundle of counters filled with BF_3 at 2-atmosphere pressure, as described in reference 3, was used for measurements at all energies, that is, from thermal energies to the upper energy limit set by the resolution of the system. The location of the counters relative to the neutron beam is indicated in Fig. 1.

For neutrons with energies greater than about 100 ev, a successful model of the new boron-loaded liquid scintillation neutron detector[4] has been put into operation.[5] This counter,[6] using a counting liquid consisting of 4 g per liter of 2–5, diphenoloxyzol and 16 mg per liter of diphenylhexatriene in equal volumes of phenylcyclohexane and enriched trimethyl borate, has a mean neutron capture time of 0.4 μsec. The 2-inch

* This work was done under the auspices of the U. S. Atomic Energy Commission.

† Now at Stanford University, Stanford, California.

‡ On leave from Beloit College, Beloit, Wisconsin.

[1] L. J. Rainwater and W. W. Havens, Jr., Phys. Rev. **70**, 136 (1946); W. W. Havens, Jr., and L. J. Rainwater, Phys. Rev. **83**, 1123 (1951); A. W. Merrison and E. R. Wiblin, Proc. Roy. Soc. (London) **A215**, 278 (1952).

[2] Seidl, Hughes, Palevsky, Levin, Kato, and Sjöstrand, Phys. Rev. **95**, 476 (1954).

[3] W. Selove, Rev. Sci. Instr. **23**, 350 (1952).

[4] C. O. Muehlhause and G. E. Thomas, Jr., Nucleonics **11**, No. 1, 44 (1953).

[5] G. Thomas and L. Bollinger, Phys. Rev. **91**, 452 (1953).

[6] The properties of boron-loaded liquid neutron counters will be described in detail elsewhere.

diameter by 4-inch long quartz cell that contains the scintillating liquid is mounted in the neutron beam as shown in Fig. 1. For our measurements, the most important characteristic of the liquid counter is its high neutron-counting efficiency ϵ, which is given approximately by $\epsilon = 1.0E^{-0.13}$ for $10 < E < 10\,000$ ev. This efficiency is about 15 times that of our gas counters at 1000 ev. The liquid counter has the serious drawback, however, of being sensitive to γ rays and high-energy neutrons. The high background that results from this property sets a lower energy limit of usefulness for the counter as will be discussed in a following section.

100-Channel Time Analyzer

The primary emphasis in the design of the flight-time analyzer was on stability and reliability of performance. The resulting instrument records data in 100 channels, with the counts arriving in each channel being stored in a scale of 4 scaler and a mechanical register. Channel widths ranging from 1 to 20 μsec are available. The start of operation of the first channel can be delayed by times equivalent to integral units of 10 channels up to 90 channels; thus, the total range that can be covered is 190 channels. The basic principles of operation of the system assure that all 100 channels are of exactly equal widths, a property that was unique at the time of its construction.[7] As another consequence of these principles, however, only one detector count can be recorded for each burst of neutrons, a limitation that is unimportant for the counting rates normally used.

Associated with the time analyzer are circuits which have the dual purposes of protecting the chopper from mechanical damage and of monitoring the over-all operation of the velocity selector to insure that meaningful data are being accumulated. By using these circuits, a large fraction of the data obtained with the system is collected at night without an operator in attendance.

3. TECHNIQUES OF MEASUREMENT

Insofar as the equipment described above differs from that of reference 3, the changes were made for the primary purpose of improving the resolution of the selector. Lesser objectives were to improve the energy calibration of the system and to decrease the statistical and absolute uncertainties of transmission data obtained with it.

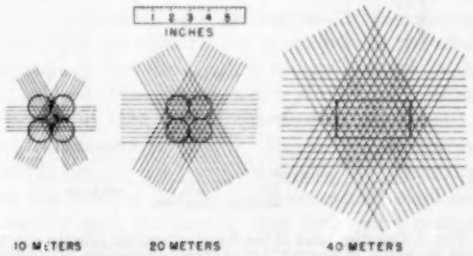

FIG. 1. Neutron intensity patterns formed under static conditions. The heavy solid lines show the outlines of the counter active areas.

[7] Bollinger, Harris, and Schumann, Phys. Rev. **87**, 184 (1952).

Resolution

The resolving power of the velocity selector depends on the length of the neutron flight path and on the over-all intensity *vs* time distribution of the system for monoenergetic neutrons. For our system the effects that are significant in determining the width of this intensity distribution are the duration of the burst of neutrons from the chopper and the lifetime of a neutron in the detector. In the case of the liquid counter, the neutron lifetime in the counter, namely 0.4 μsec, is negligibly small. For the BF_3 system, however, this lifetime can be of importance; it is the time required for a neutron to traverse the 29-cm length of the counters and varies with energy as $t = (21E^{-\frac{1}{2}})\mu$sec, where E is in ev. It is expected that future improvements in neutron scintillation detectors will make it unnecessary to use gas counters, but at the present time, the length of these gas counters is a primary source of resolution broadening for low-energy measurements.

For high-energy neutrons, however, the fundamental limitation to resolution is set by the burst width of the chopper. Attempts to reduce this width by turning the rotor at significantly higher speeds (25 000 rpm) have resulted in mechanical failure; the speed is therefore limited to 17 500 rpm. When using the scintillation detector, not only the neutron burst width but also its shape is rapidly determined by measuring an intensity *vs* time distribution for pile γ rays. One such determination is given in Fig. 2, where it is seen that, for full

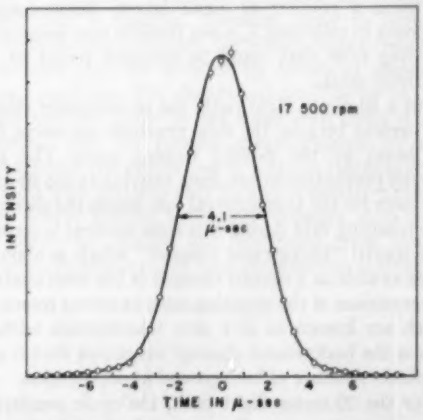

FIG. 2. Chopper resolution function. The data points were obtained by recording counting rate *vs* time for pile γ rays with the chopper run at a greatly reduced speed so as to eliminate the effect of the time analyzer channel width. The burst width measured in this way is found to be independent of γ-ray energy.

speed operation, the width of the neutron burst is 4.1 μsec.

The important gains in the resolving power of our system have been achieved by using neutron flight paths that are longer than the 10-meter distance originally employed. In the present measurements three detection stations, giving flight paths of 10, 20, and 40 meters, were used. The BF_3 gas conters were used at 10 and 20 meters whereas the highly efficient liquid scintillation neutron detector was installed 40 meters from the chopper. Typical examples of the high resolution data that have been obtained with this long flight path are given in Figs. 4, 5, 6, and 7. These data show that the boron-loaded liquid scintillation neutron detector has become a useful tool for neutron time-of-flight measurements; the flight path of 40 meters was feasible for our system only because of its high efficiency.

The highest resolving powers that can be obtained with the velocity selector for the 10, 20, and 40 meter flight paths are 0.5, 0.25, and 0.12 μsec/meter, respectively, where these values refer to the full width of the resolution function at half maximum. For the two shorter flight paths the resolution widths become somewhat greater at low energies because of neutron flight times in the BF_3 counters.

Background and Second-Order Effects

The increased resolving power obtained with the longer flight paths is gained at the expense of reduced counting rates, relatively higher background rates, and second-order effects. The important features of these several effects are illustrated in Fig. 3.

The second-order effect to be considered here consists of an ambiguity as to whether a detector pulse is caused by a fast neutron or by a slow neutron from the proceding cycle. The elimination of the low-energy neutrons by using a counter of small lateral dimensions, as proposed in reference 3, is not feasible here because the counting rates that could be obtained would be prohibitively small.

For a 10-meter flight path, the second-order effect is not present because the slow neutrons are swept from the beam by the rapidly turning rotor. The rotor thereby prevents neutrons from arriving at the 10-meter detectors for the time interval just before the slits open. The counting rate during this time interval is recorded in a special "background channel" which is about 20 times as wide as a normal channel of the time analyzer. A comparison of the counting rates at strong resonances which are known to give zero transmission with the rate in the background channel has shown that it gives a reliable measure of background at all energies.

For the 20-meter flight path, the cycle overlapping effect comes into play. Corrections for both background and second-order counting rates can be made with accuracy for samples that have no resonance structure in the second-order energy range. The data required to make these corrections are: the shape of the time dependence of the second-order contribution, the number of counts recorded in the background channel, and the time independent background. This latter background is measured by blocking the neutron beam issuing from the chopper at regular intervals and recording the total counting rate with the beam so blocked. This cyclic counting operation is automatically performed for 44 seconds of a 4-minute cycle. To the background measured in this way is added a small contribution for the high-energy neutrons which, under normal operation, pass through the 16-inch steel rotor.

The background and overlap problems for the 40-meter flight path are similar to those at 20 meters, but the greater magnitude of these effects at 40 meters sets a more severe limitation on the samples that can be profitably studied. In particular, the time-independent background of the liquid counter is greater than its counting rate due to chopper neutrons with energies less than 100 ev; measurements are, therefore, usually limited to energies greater than 100 ev. Second-order neutrons do not constitute a serious source of background above this energy because the counting rate produced in the liquid detector by a $1/E$ neutron beam varies approximately as neutron velocity V as contrasted with the constant counting rate obtained from a $1/V$ detector.[3] Since a knowledge of the variation

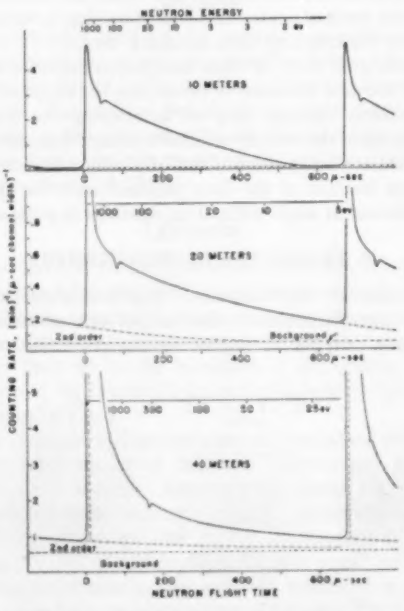

FIG. 3. Counting rates of the Argonne neutron velocity selector with the heavy water pile CP-3 as the primary source of neutrons. The small transmission dips observed at 337 and 2360 ev are caused by manganese resonances, the manganese being an impurity in the aluminum of either the pile tank wall or the neutron flight tube windows.

with energy of the second-order counting rate is required, however, the 40-meter flight path is used primarily for samples that have no neutron resonance structure at low energies. An example of the raw data that are obtained with the liquid counter and an illustration of the way in which a prominent resonance is used to determine the first-order contribution is given in Fig. 4.

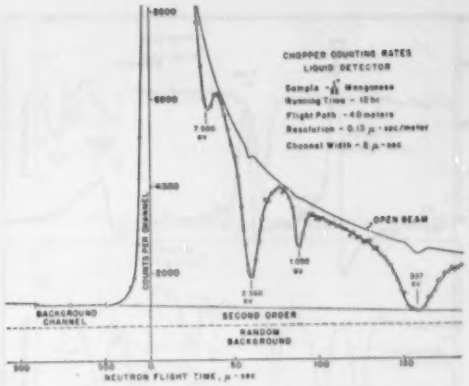

FIG. 4. Raw data obtained with the liquid detector. The first order contribution is accurately given by a linear interpolation between the counting rates at the "background" channel and that at the minimum caused by the 337-ev resonance.

Accuracy of Cross-Section Measurements

In addition to lack of resolution and statistical accuracy, an important source of error in our transmission measurements is an instability in the over-all sensitivity of the detection systems. The ratio of counting rate of the detector to that of the pile power monitor may drift by about 3% during a 24-hour period for the BF_3 detection system and by a somewhat lesser amount for the liquid counter. To eliminate systematic errors of this kind, an automatic sample-changing system has been developed which periodically switches the velocity selector from measurements on the sample to open-beam measurements, with a total cycle time of 4 minutes. The two sets of data are alternately recorded on different halves of the time analyzer. Measurements of this kind usually cover a wide energy range with poor resolution. The high-resolution data that are obtained without repeated alternation are then normalized to the low-resolution data by requiring, for a particular sample, that the two sets of transmissions, averaged over a wide energy range, shall be equal. It has been found that data obtained by the sample alternation technique are reproducible and that they are in good agreement with other careful measurements.

Energy Calibration

The principal systematic error that limits the accuracy with which neutron velocities, and hence energies, can be measured with the present velocity selector is an uncertainty as to the zero of time for the neutrons. Two sources of error cause the zero-time uncertainty. The more subtle effect is that the transmission of the slit system is greater for neutrons that enter it while the slits are opening than for those entering while they are closing. The magnitude of the effect depends on the velocity of a neutron relative to the rotor speed. Thus, the mean time of the initial neutron intensity *vs* time distribution depends somewhat on the relative neutron velocity. This shift in the neutron distribution has not been investigated experimentally, but it is believed that, for the experimental conditions normally used, the zero in time varies with neutron energy by less than 1 μsec.

A second source of error in the energy calibration is in the determination of the time zero for fast neutrons, for which the intensity distribution is not influenced by the sweeping action of the rotor slits. This time calibration is made by measuring, with a scintillation counter, the zero time for pile γ rays; to this γ-ray zero is added a small constant time that is equal to the mean difference between the arrival of a neutron at the counter and the formation of a detector pulse. Using the above procedure, zero time determinations are reproducible to about 0.2 μsec and are believed to be in error by less than 0.5 μsec.

4. RESULTS

For the range of energies that is of primary interest for the measurement of neutron cross sections by the time-of-flight method, namely, from 5 to 5000 ev, the instrumental resolution width is generally not narrow enough to permit a direct observation of the detailed shape of resonance structure. A fruitful interpretation of the data is possible, therefore, only in terms of assumed resonance shapes, for which shapes resonance parameters may be deduced by means of somewhat indirect methods. The shapes required for an analysis of this kind are given by the single-level Breit-Wigner formulas. For the present measurements we need consider only the simple case of a target material which interacts with neutrons only by way of radiative capture or by *s*-wave eleastic scattering processes, with which are associated capture and scattering cross sections σ_c and σ_s. In this case the total cross section is given by[8]

$$\sigma=\sigma_c+\sigma_s,$$

with

$$\sigma_c=\sigma_0\frac{\Gamma_\gamma}{\Gamma}\left(\frac{E_0}{E}\right)^{\frac{1}{2}}\frac{1}{1+x^2}, \tag{1}$$

$$\sigma_s=4\pi R^2+\sigma_0\frac{\Gamma_n}{\Gamma}\left[1+\left(2\frac{R}{\lambda_0}\frac{\Gamma}{\Gamma_n}\right)x\right]\Big/(1+x^2), \tag{2}$$

[8] H. A. Bethe, Revs. Modern Phys. 9, 115 (1937).

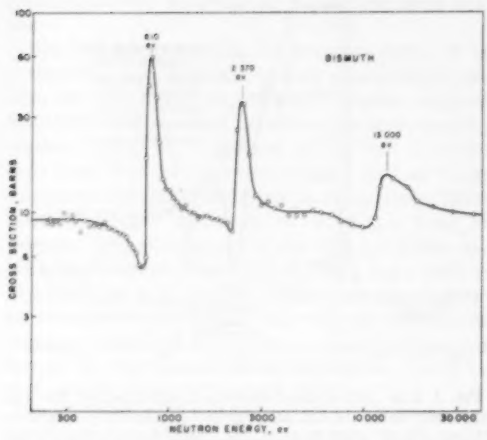

FIG. 5. Total neutron cross section of bismuth. The measurements were made with a 40-meter flight path, for which the resolution is 0.12 μsec/meter.

where

$$\Gamma=\Gamma_n+\Gamma_\gamma,$$
$$x=(2/\Gamma)(E-E_0), \qquad (3)$$
$$\sigma_0=4\pi\lambda_0^2 g\Gamma_n/\Gamma.$$

Here E is the kinetic energy of the neutron. The constants E_0 and $2\pi\lambda_0$ are the neutron energy and wave length at exact resonance, Γ, Γ_γ, and Γ_n are the total, γ-ray, and neutron widths, and σ_0 is the cross section at exact resonance. The statistical factor g is given by

$$g=\tfrac{1}{2}(2J+1)/(2I+1)=\tfrac{1}{2}[1\pm 1/(2I+1)],$$

where I is the spin of the target nucleus and J is the spin of the compound nuclear state.

Of the data which follow, those for bismuth and selenium illustrate measurements for which resonance parameters can be deduced only by an indirect analysis, assuming the resonance formulas given above to be applicable. For the manganese data, on the other hand, the experimental resolution width was narrow enough for a direct observation of resonance shapes.

Bismuth

The total neutron cross section of bismuth has been studied over the range of energy from 2 to 20 000 ev. For the measurements at low energies, resolution was sacrificed in favor of the high absolute accuracy of cross section that is obtained by using a 10-meter flight path and the automatic sample changing system described in an earlier section. Two runs of this kind showed no measurable change in cross section between 1.5 and 20 ev. The average values obtained for this interval were 9.30±0.05 and 9.34±0.05 barns, where the errors given are standard statistical errors; each measurement was also subject to possible systematic errors of about ±0.05 barn.

For the measurements above 200 ev, our best resolution and several sample thicknesses were used since resonances had previously been observed[9] at about 800 and 2400 ev. Some of the data obtained are given in Fig. 5. It is seen that the existence of resonances at 810 and 2370 ev is firmly established and that other resonance structure is observed in the neighborhood of 13 kev. This latter peak has been studied at higher resolution with an electrostatic generator[10] and has been found to consist of two resonances, which are at about 12 and 16 kev.

For the first two resonances, parameters may be deduced either by using the area above transmission dips or by curve fitting the shape of the tails of resonances. A straightforward application of the usual area method,[11] which assumes a symmetrical resonance of the form $\sigma=\sigma_0(1+x^2)^{-1}$, is not accurate for the bismuth resonances because their shapes are very asymmetric. For any shape, however, if all parameters but one are known, the unknown parameter must have a value such as to give a calculated transmission curve above which the area is equal to the experimentally measured area. In the case of predominantly scattering resonances, all parameters except Γ are often approximately known, so that the equal area criteria may be used to find Γ by the following procedure: A resonance shape is assumed. For this shape, a transmission curve is calculated for assumed constants Γ, Γ_γ, R, and g, with Γ_γ, R, and g being considered to be known and Γ unknown. The area above the calculated transmission dip is compared with that above the experimentally measured dip over some energy range that is wide enough to eliminate resolution errors. If the two areas are not equal, a new value of Γ is chosen and the procedure of comparison is repeated. This process of successive approximation rapidly leads to a Γ for which the calculated transmission area is satisfactorily close to the measured area. The process is most useful for $\Gamma_\gamma \ll \Gamma$, for which case the final value of Γ is insensitive to the assumed Γ_γ; the final Γ is also insensitive to R if the areas are

TABLE I. Parameters of bismuth resonances. The widths Γ are for $g=\frac{1}{2}$.

E_0 (ev)	Sample (g/cm²)	$\sigma_0\Gamma$ (barn-ev)	$\sigma_0\Gamma^2$ (barn-ev)	Γ ev	Type of data
810	2.37		38 900	4.93±0.7	Area
	10.35		55 000	5.85±0.35	Area
		9400		5.86±0.5	Wing
			Average	5.8 ±0.3	
2370	2.37		224 000	20 ±4	Area
	10.35		159 000	17 ±1.5	Area
		7660		14 ±3	Wing
			Average	17 ±1.5	

[9] L. M. Bollinger and S. P. Harris (private communication).
[10] H. W. Newson (private communication).
[11] Melkonian, Havens, and Rainwater, Phys. Rev. **92**, 702 (1953).

measured between energy limits that are symmetrically located relative to E_0.

The foregoing technique has been applied to the data obtained with the two thinner samples used, namely 2.37 and 10.35 g/cm², at both the 810 and 2370 ev resonances. In these calculations the resonance shape used was that of *s*-wave scattering with the parameters $g=\frac{1}{2}$, $R=0.86\times10^{-12}$ cm, and $\Gamma_\gamma=0.04$ ev; Doppler effect was neglected. The results obtained, which are listed in Table I, show that these are almost entirely scattering resonances; our results are, therefore, almost independent of the value assumed for Γ_γ. Moreover, the resonances are wide enough to justify neglect of Doppler effect.

The strong asymmetry, caused by interference between the potential and resonance scattering amplitudes, that is observed for the bismuth resonances affords an alternative procedure for finding resonance parameters. From Eq. (2), it is clear that the magnitude of the interference term (the $[E-E_0]^{-1}$ term) in the scattering cross-section relationship is proportional to $\sigma_0\Gamma R/\lambda_0$. Moreover, the magnitude of the interference term becomes greater than that of the $(E-E_0)^{-2}$ term at a sufficiently large distance from E_0; hence the shape of the wings of scattering resonances allows a determination of $\sigma_0\Gamma R/\lambda_0$.

In curve fitting the present data, the technique described by Kato *et al.*[12] was used. In the wings of each resonance, measured cross sections σ_t were plotted in the form of $[\sigma_t-\frac{1}{4}\sigma_0\Gamma^2(E-E_0)^{-2}]$ *vs* $(E-E_0)^{-1}$, giving a straight line for which the slope is $\sigma_0\Gamma R/\lambda_0$ and the intercept of the cross-section axis is $4\pi R^2$. Since, for the bismuth data, the cross-section term varying as $(E-E_0)^{-1}$ is much larger than the $(E-E_0)^{-2}$ term, the latter may be calculated for an aprroximate value of $\sigma_0\Gamma^2$ without introducing a significant error. For both resonances, corrections were made for the effect of the neighboring level. The results obtained are given in Table I. In determining $\sigma_0\Gamma$ from a measured value of the slope, R was taken to be that value given by the intercept. The two values obtained for R were 0.88×10^{-12} and 0.89×10^{-12} cm for the 810 and 2370 ev resonances, respectively. These values are not very different from that given by the relationship $R=1.45\times10^{-13}A^{\frac{1}{3}}$, which gives $R=0.86\times10^{-12}$ cm for bismuth. It should be noted that the widths obtained from the area data and from the wing shapes, as listed in Table I, are in satisfactory agreement.

TABLE II. Resonance parameters of selenium.

E_0 (ev)	$\sigma_0\Gamma^2$ (barn-ev²)
27.1	53
211	1410
270	3520
383	920

[12] Kato, Hughes, and Levin, Phys. Rev. **93**, 931 (1954).

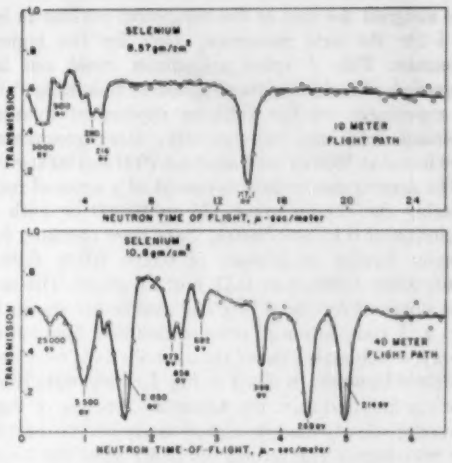

FIG. 6. The neutron transmission of selenium as observed with 10- and 40-meter flight paths.

Selenium

There are no previously reported measurements of the neutron cross section of selenium within the energy range 1 to 1000 ev. Some of the results obtained in the present investigation are given in Fig. 6. In other runs, a 1.24-g/cm² sample was studied with a 0.35-μsec/meter resolution over the energy range 20 to 2000 ev and a 10.8-g/cm² sample was used for low-resolution measurements above 2 ev; no additional resonance structure was observed in these latter data. The above data have been previously reported in the form of cross section *vs* energy in *Neutron Cross Sections*.[13]

For all the selenium transmission dips for which a measurable area was obtained the sample was essentially thick, i.e., $n\sigma_0\gg1$, hence only $\sigma_0\Gamma^2$ may be obtained. Further, in this case the isotopic assignment of the resonances is not known, so that values of resonance parameters cannot be found for an assumed Γ_γ. The rather meager results that can be obtained, values of $\sigma_0\Gamma^2$ which refer to the element selenium rather than to a particular isotope, are summarized in Table II.

Manganese

The prominence of the low-energy neutron resonances in manganese has made them a favorite subject for investigation. The 337- and 2360-ev resonances[14] were carefully studied by Muehlhause and co-workers,[15]

[13] *Neutron Cross Sections*, U. S. Atomic Energy Commission Report AECU-2040, Supplement 3 (Office of Technical Services, Department of Commerce, Washington, D. C., 1954).

[14] Rainwater, Havens, Wu, and Dunning, Phys. Rev. **71**, 65 (1947).

[15] Harris, Hibdon, and Muehlhause, Phys. Rev. **80**, 1014 (1950).

who assigned the spin of the compound nucleus to be $J=3$ for the first resonance, $J=2$ for the higher resonance. This J value assignment could not be reconciled with the results obtained at Oak Ridge[16] in an experiment on the radiative capture of thermal polarized neutrons. Subsequently, other resonances were found at 1080 ev[2] and at about 7000 and 9000 ev.[17]

The present measurements consist of a series of runs covering the energy range 175 to 10 000 ev with a resolution of 0.12 μsec/meter. Data were obtained for samples having thicknesses of 0.029, 0.030, 0.034, 0.065, 0.098, 0.099, 0.20, 0.51, and 7.6 g/cm^2. The raw data obtained for the 0.51-g/cm^2 sample are shown in Fig. 4. A compilation of cross section as a function of energy, which makes use of the data obtained for many sample thicknesses, is given in Fig. 7. These data show that the first and third resonances are, because of their characteristic asymmetry, almost surely s-wave scattering resonances. The second resonance may not be so directly interpreted, however, for it exhibits the unusual effect of having a higher cross section on the low energy than on the high energy side.

The manganese data provide two kinds of information that are useful in attempting to understand the resonance structure, namely, meaningful cross sections at most energies and areas above transmission dips which give measures of either $\sigma_0\Gamma$ or $\sigma_0\Gamma^2$. The data

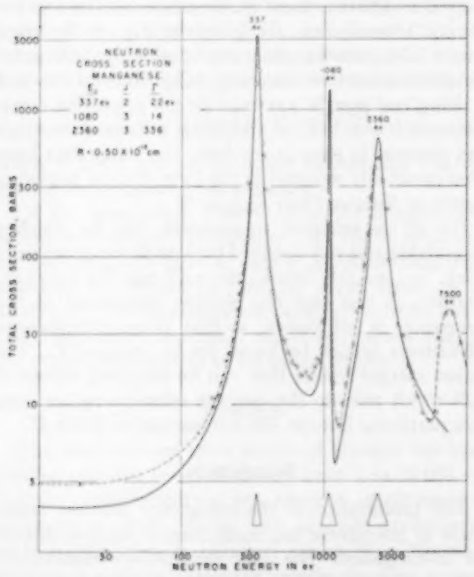

FIG. 7. Total neutron cross section of manganese as a function of energy. The solid line is the theoretical cross section for the parameters listed on the figure. The three data points below 150 ev are those given by Muehlhause and co-workers in reference 15.

[16] L. D. Roberts and S. Bernstein, Phys. Rev. **93**, 917 (1954).
[17] H. Marshak and H. W. Newson, Phys. Rev. **98**, 1162 (1955).

TABLE III. Manganese resonance parameters. All values are for $\Gamma_\gamma=0.6$ ev.

E_0 (ev)	$10^{-4}\sigma_0\Gamma$ (b−ev)	$10^{-4}\sigma_0\Gamma^2$ (b−ev^2)	J	Γ (ev)	Γ_n/Γ	$\Gamma_nE_0^{-\frac{1}{2}}$ (ev$^{\frac{1}{2}}$)
337 ±3		144 ±10	2	21.5 ±0.8	0.97	1.44 ±0.05
1080 ±20		2.8 ± 0.7	3	14.5 ±1.5	0.96	0.42 ±0.05
2360 ±60	219 ±10		3	340 ±16	1.00	6.99 ±0.35

obtained for the seven thinnest samples were used for the area analysis of the 337- and 2360-ev resonances. Numerical integrations of the areas above calculated transmission dips due to scattering resonances showed that for these two manganese resonances the usual relationships relating transmission areas to $\sigma_0\Gamma$ and $\sigma_0\Gamma^2$ are valid when $n\sigma_0$ is small. It was necessary to use the data obtained with a thicker sample, the 0.51-g/cm^2 sample, for the 1080-ev resonance and the anomalous shape of its transmission dip indicates a need to use the special treatment applied to the bismuth data. Values of $\sigma_0\Gamma$ and $\sigma_0\Gamma^2$ that are given by the above area analyses are listed in Table III.

For the case of the unusually wide manganese resonances at 337 and 2360 ev, the instrumental resolution was narrow enough to make the measured peak cross sections meaningful. The data given in reference 15 shows that for both of these levels $\Gamma_n/\Gamma\approx 1$; thus, for each E_0, the possible values of σ_0, as given by Eq. (3), are determined almost entirely by the two possible J assignments for the compound nuclear state, depending only slightly on the γ-ray width. Tentatively assuming Γ_γ for both resonances to be 0.6 ev, which is the value given in reference 15 for $E_0=337$ ev, the possible theoretical values are compared in Table IV with the measured peak cross sections, σ_m. These experimental cross sections were corrected for resolution distortion but the effect of Doppler broadening was ignored because for manganese Doppler width is much narrower than the level width.

For convenience in making resolution corrections when Doppler effect may be neglected, a series of curves were constructed from which one may make a direct determination of σ_m/σ_0, the ratio of the measured to the true-peak cross section. In these calculations a resolution function similar to that of Fig. 2 was used and resonance shapes were approximated by the symmetrical form $\sigma=\sigma_0(1+x^2)^{-1}$. First, curves were prepared giving σ_m/σ_0 as a function of w/Γ for several values of $n\sigma_0$, where w is the resolution width. Then, to eliminate the need for employing a method of successive approximation, these curves were used to construct two other sets of curves. One set, which is reproduced in Fig. 8, gives σ_m/σ_0 as a function of $\sigma_m w/\sigma_0\Gamma$ with $n\sigma_m$ as the parameter; the other gives σ_m/σ_0 vs $\sigma_m w^2/\sigma_0\Gamma^2$. Since σ_m and either $\sigma_0\Gamma$ or $\sigma_0\Gamma^2$ can be experimentally determined and w is known, the resolution correction σ_m/σ_0 may be read directly from the appropriate curve.

Returning to the results of Table IV, the errors

associated with the resolution corrected cross sections include errors introduced by an estimated 10% uncertainty in the resolution width. The agreement between the corrected cross sections and one particular set of theoretical values is good enough in the case of the 337-ev resonance, to show quite unambiguously that $J=2$. The uncertainty in the value of Γ_γ for this resonance cannot weaken this conclusion. The value used, namely 0.6 ev, is probably an upper limit; it was obtained by equating the measured thermal capture cross section to the contribution expected from the resonances at 337 and 2360 ev without taking into account the effects of levels at negative energies. For values of Γ_γ less than 0.6 ev our conclusion that $J=2$ for $E_0=337$ becomes even stronger.

The inference that there is a resonance in the neighborhood of 2360 ev for which $J=3$ is equally certain in spite of a possibility that the observed transmission dip could be caused by more than one resonance. The conclusion can be otherwise only if too large a correction was made for resolution broadening. The resolution correction factor used was determined by the magnitude of the apparent $\sigma_0\Gamma$ for the resonance, i.e., by the transmission area obtained for a thin sample. For such a sample, an assumption that the area is caused by two or more resonances can only result in a larrer correction for resolution broadening, making the conclusion that $J=3$ even more certain.

The anomalous shape of the 1080-ev resonance suggests that we have here an example of the previously unobserved phenomenon of interference between two s-wave neutron scattering resonances. To examine the credibility of such an interpretation, consider the well-known multilevel neutron scattering cross-section relationship[8]:

$$\sigma_s=\sum_J g_J\left|R+\sum_r \tfrac{1}{2}\lambda_r\Gamma_{nr}(E-E_0+\tfrac{1}{2}i\Gamma_r)^{-1}\right|^2, \quad (4)$$

where the index r refers to each resonance.[18] For the special case of interest here, the interference between two resonances of the same J, Eq. (4) gives for the cross section:

$$\sigma_{sJ}=4\pi g\left\{R^2+\sum_{r=1}^{2}\left[\frac{\lambda^2(\Gamma_n/\Gamma)^2}{1+x^2}\left(1+\frac{2R\Gamma}{\lambda\Gamma_n}x\right)\right]_r +2\lambda_1\lambda_2\frac{\Gamma_{n1}\Gamma_{n2}}{\Gamma^2}\frac{(x_1x_2+1)}{(x_1^2+1)(x_2^2+1)}\right\}, \quad (5)$$

where x is defined in Eq. 3. It will be observed that the first three terms of Eq. (5) are the single-level scattering terms, whereas the last term is an interference term which becomes negligibly small when resonances are widely separated relative to their widths. An important qualitative feature of the interference term is that it is negative in the energy region between the resonances and positive outside of this range.

If the 1080-ev resonance is an s-wave scattering resonance, its proximity to both the first and third levels necessarily leads us to expect to see the effects of interference with one or the other; we may determine with which by comparing the measured cross-section curve with theoretical curves calculated for the two possible sets of J values. Assuming first that $J=3$ for the 1080 ev resonance, its width Γ was obtained by equating the area above the experimental transmission dip to that above a theoretical dip, as was described for the bismuth resonances; the details of the analysis are given in Fig. 9. The result obtained is $\Gamma=14.5\pm1.5$ ev. Using approximately the widths that have been deduced for the first three resonances, the cross section contributed by them has been calculated and is shown as the solid line in Fig. 7. It is seen that this curve is in good qualitative agreement with the data. The most

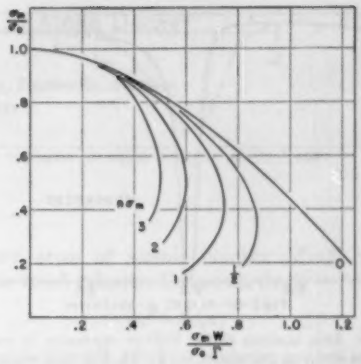

FIG. 8. Resolution corrections for resonance peak cross sections.

TABLE IV. Comparison of measured peak cross sections σ_m with the two theoretically possible values. Γ_n/Γ was taken from Table III. For the 2360-ev resonances, the results for samples of approximately equal thickness were averaged.

E_0 (ev)	$\left(n\frac{\text{atoms}}{\text{cm}^2}\right)$	σ_m (barns)	Corrected σ_m (barns)	Theoretical σ_0 (barns) $J=2$	$J=3$
337	4.03×10^{20}	1910±190	2610±460		
	4.16	2000±200	2790±480		
	4.62	2300±250	3400±700		
		weighted average	2830±370	3120	4370
2360	4.27×10^{20}	484±50	807±200		
	8.02	445±40	692±130		
	11.63	436±20	680±90		
		weighted average	702±85	459	643

[18] The authors are indebted to Professor Wigner for having pointed out that Eq. (4) is not valid when level widths become comparable to level spacing and that, for this reason, the present data might be more propertly treated in terms of the very general Wigner theory as given, for instance, by E. Wigner and L. Eisenbud in Phys. Rev. 72, 29 (1947). Comparative calculations have shown, however, that for the present case the two theories give nearly the same results. Equation (4) is used here because of its greater familiarity to most readers.

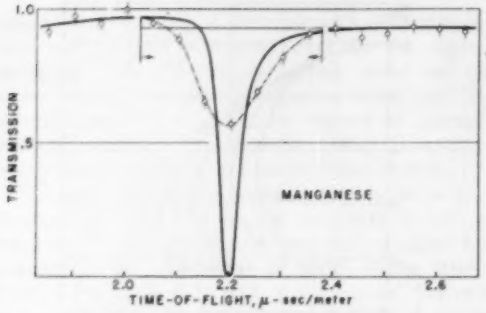

FIG. 9. Area analysis of the 1080-ev resonance in manganese. The solid line was calculated for $\Gamma=14$. For this width the area above the theoretical curve is almost equal to that above the experimental points within the energy limits E_1 to E_2.

important feature of the calculated curve, the high cross section below the second resonance and the low cross section above it, is very insensitive to the values used for R and Γ.

For the alternative possibility, that $J=2$ for the second resonance, a satisfactory value of Γ cannot be obtained because, unlike the case $J=3$, the theoretical transmission curve does not fit the data in the off-resonance region. If, however, we use the same value of $\sigma_0\Gamma^2$ as obtained previously, for the present case we have $\Gamma=17$ ev. For this value the cross section due to the first three resonances has again been calculated. The curve obtained, which is omitted from Fig. 7 to avoid confusion, is entirely unlike the experimental curve in the neighborhood of $E_0=1080$ ev; in particular, at the minima at 800 and 1250 ev the calculation gives 4.4 and 19 barns, respectively, as contrasted with measured cross sections of about 16 and 7 barns. This marked qualitative disagreement cannot be significantly improved by an adjustment in the values used for the radius and the widths. In view of the good qualitative agreement between theory and experiment for $J=3$ and the strong disagreement for $J=2$, it is concluded that $J=3$ for the resonance at 1080 ev.

Although the qualitative agreement between the calculated cross section, as given by the solid line in Fig. 7, and the data is good enough to allow us to conclude that $J=3$ for the second resonance, the quantitative agreement is not good. It is felt, however, that the discrepancies need not be attributed to a failure of the theory. It is likely that a more complete treatment, taking into account all resonances, in particular unknown levels at negative energies, and a minor adjustment of the parameters that were used, would give satisfactory agreement with the measured data. In the latter connection it should be mentioned that the value $R=5.0\times10^{-13}$ cm gives a significantly better fit than $R=1.45A^{\frac{1}{3}}\times10^{-13}=5.5\times10^{-13}$ cm; an even smaller R would probably give further improvement.

The unusually large ratio of neutron width to level spacing in manganese is of special interest not only because of the interference effects discussed above, but also for its bearing on the validity of the "cloudy crystal ball" theory of nuclear reactions.[19] This theory assumes that in a nuclear collision the formation of a compound nucleus is governed by a potential well of the form $V=V_0(1+\zeta i)$. One consequence of this assumption is a prediction that the ratio of the average reduced neutron width to average level spacing per J value $\bar{\Gamma}_n^0/\bar{D}$ depends on the target nuclear radius, and hence on the atomic weight A. In particular, for $V_0=-42$ Mev and $\zeta=0.03$, a curve of $\bar{\Gamma}_n^0/\bar{D}$ *vs* A is expected to have relatively narrow maxima in the neighborhood of $A=55$ and $A=155$ with a broad minimum between the two peaks. Systematic experimental investigations have shown that there is, in fact, a sharp maximum[20] at $A=52$ and a broader maximum[21] at about $A=155$.

In obtaining a value of $\bar{\Gamma}_n^0/\bar{D}$ for manganese from the present data it seems worthwhile to use all information up to 10 kev. The transmission dip observed at 7.5 kev was not treated above because it has been shown to be caused by two resonances.[17] If the area data for a thin sample is used as though the dip were caused by a single resonance, however, an apparent width is obtained which is, to a good approximation, the sum of the widths of the two resonances; the value given for this width is 575 ev. Using this value and the reduced widths for the first three resonances, with D assumed to be equal to twice the average level spacing, we obtain 10×10^{-4} $(\text{ev})^{-\frac{1}{2}}$ for $\bar{\Gamma}_n^0/\bar{D}$. This result, which is uncertain by a factor of two, is about 20 times larger than that observed in the minima between $A=55$ and $A=155$ and confirms the existence of a peak value for $\bar{\Gamma}_n^0/\bar{D}$ near $A=55$.

[19] Feshbach, Porter, and Weisskopf, Phys. Rev. **96**, 448 (1954).
[20] R. Cote and L. M. Bollinger, Phys. Rev. **98**, 1162 (1955).
[21] Carter, Harvey, Hughes, and Pilcher, Phys. Rev. **96**, 113 (1954).

Theory of Atomic Perturbation in Alpha Decay*

H. M. SCHWARTZ
Department of Physics, University of Arkansas, Fayetteville, Arkansas
(Received April 11, 1955)

A method for calculating the probabilities of internal atomic excitation in alpha decay is outlined and compared with earlier work by other authors.

I. INTRODUCTION

THE theory of inner shell atomic perturbation in alpha decay has been discussed by Migdal[1] and by Levinger.[2] For ionization in the K shell their results differ appreciably. It is the purpose of this note to outline a treatment, applicable both to the inner and outer shell electrons, and which is shown to lead to results that are essentially equivalent to those given by Migdal.[3]

It is also shown that the discrepancy with corresponding results in reference 2 is largely eliminated when one removes one simplifying assumption made therein.

II. PRESENT METHOD

The underlying idea of the present method is to invoke the relative smallness of the charge of the alpha particle rather than its relative slowness, and thus apply standard time-dependent perturbation theory, taking proper account of the nuclear recoil, and change of charge that transpires at the instant of alpha emission. By treating the problem in a coordinate system moving with the recoiling nucleus, the only time-dependent part of our Hamiltonian operator is the perturbation potential,[4]

$$V(t)=-2e^2\sum_i|\mathbf{r}_i-\mathbf{v}t|^{-1} \tag{1}$$

($\mathbf{r}_i$=position vector of the ith electron and $\mathbf{v}$=velocity of alpha particle in the moving system); and the eigenfunctions of the unperturbed Hamiltonian have the form

$$u_n=\exp\left(\frac{im}{\hbar}\mathbf{v}_n\cdot\sum\mathbf{r}_i\right)u_n^{Z-2}, \tag{2}$$

where u_n^{Z-2} is the corresponding eigenfunction for a stationary atom of atomic number $(Z-2)$ and $\mathbf{v}_n$ =nuclear recoil velocity. Consequently, if

$$u_0^Z=Sc_nu_n \tag{3}$$

is the wave function of the atomic state of the parent atom at the instant of alpha decay, then the probability of finding the atomic state $u_n(\neq u_0)$ at $t=\infty$ is to first order:

$$\left|c_n+\frac{1}{\hbar i}\int_0^\infty\exp\left[\frac{i}{\hbar}(E_n-E_0)t\right]V_{n0}(t)dt\right|^2, \tag{4}$$

where E_n is the energy in the state u_n and V_{nm} is the matrix of the operator $V(t)$ relative to the complete orthonormal system $\{u_n\}$.

In using the expression (1) for $V(t)$ it is assumed that the alpha particle has zero angular momentum relative to the nucleus. That the result is not essentially changed within the present approximation, when the angular momentum is $Lh>0$, can be seen by considering the potential

$$V_a(t)=-2e^2\sum_i|\mathbf{r}_i-\mathbf{a}-\mathbf{v}t|^{-1},$$

where

$$a\equiv|\mathbf{a}|\sim Lh/M_av \quad (M_a=\text{mass of alpha particle}).$$

Indeed, if r_0, v_0 represent average inner electron radius and velocity respectively, we have

$$\frac{a}{r_0}\sim\frac{Lh}{M_av}\left(\frac{\hbar}{mv_0}\right)^{-1}\sim L(m/M_a)(v_0/v)\ll1,$$

and

$$\int V_au_n^*u_0d\tau=\int Vu_n^*(\mathbf{r}_i+\mathbf{a})u_0(\mathbf{r}_i+\mathbf{a})d\tau$$
$$=\int u_n^*u_0Vd\tau[1+O(a/r_0)].^5$$

The numerical evaluation of the c_n under simplifying assumptions concerning the atomic wave functions and with the approximation[6] $v_n=0$ in (2) has been treated in connection with the corresponding problem in beta decay.[1,2,7] The second term in (4) can be evaluated under the assumption of central-field approximation for

* This work is supported in part by the U. S. Atomic Energy Commission.

[1] A. Migdal, J. Phys. (U.S.S.R.) 4, 449 (1941).

[2] J. S. Levinger, Phys. Rev. 90, 11 (1953).

[3] The restriction in reference 1 to *inner* shell excitation derives only from the expansion of the time integral in the transition probability formula in powers of the ratio of alpha particle to atomic electron velocities. But this expansion though useful when applicable, is not necessary, as is indicated in Sec. II.

[4] Because of its relatively large mass one can approximately treat the departing alpha particle as a uniformly moving center of force. See for instance, N. F. Mott, Proc. Cambridge Phil. Soc. 27, 553 (1927). The effect of the initial variation of the alpha-particle velocity has been estimated by G. W. Schafer (private communication, W. Rubinson).

[5] See reference 2, p. 21.

[6] See the relevant discussion in Sec. III.

[7] H. M. Schwartz, J. Chem. Phys. 21, 45 (1953).

the atomic wave functions, the analysis involving results given by Condon and Shortley.[8] Results of such calculations will be presented in a subsequent note.

III. COMPARISON WITH REFERENCE 1

Formula (13) of reference 1 (the second equation) is approximately identical with our formula (4). Since $v=v_n+v_n$ is approximately equal to v_n and since the energy associated with our u_n is

$$E_n^{Z-2}+(m/2)v_n^2,$$

it is seen that there is approximate equality for the second terms of the formulas in question. As to our c_n, to see that they are within our approximation essentially equal to the C_n^0 of reference 1, it is only necessary to observe, recalling the expression (2), that we have

$$\frac{mv_n}{\hbar}r_0\sim\frac{v}{Z}\,\frac{mr_0}{\hbar}\sim\frac{1}{Z}\,\frac{v}{v_0}\ll 1.$$

Incidentally, formula (15) of reference 1, which is obtained by integration by parts of the time integral in (4) and neglect of terms assumed to be of the order of $(v/v_0)^2$, results from the substitution for c_n of an approximation which is apparently derived by Migdal from first-order time-independent perturbation theory. This approximation also follows at once from the following formula:

$$\int u_m^{Z'*}u_n^{Z}d\tau\equiv(u_m^{Z'},u_n^{Z})=\frac{1}{E_n^{Z}-E_m^{Z'}}(u_m^{Z'},[H_Z-H_{Z'}]u_n^{Z}),$$

whose derivation is immediate. Here H_Z denotes the Hamiltonian operator of an atom of atomic number Z and a fixed number of electrons, independent of Z.

IV. COMPARISON WITH REFERENCE 2

The result (37) of reference 2 differs from (4) essentially in the occurrence in that formula of the potential (40) of reference 2

$$H(t)=-2e^2[x^2+y^2+(z-v_nt)^2]^{-\frac{1}{2}}-(Z-2)e^2[x^2+y^2+(z+v_nt)^2]^{-\frac{1}{2}}$$

rather than our potential (1) (for a single electron). However, the derivation of (37) involves taking as time-independent the wave functions which enter in the formation of the matrix elements. If, instead, we note that by the definition of the $u_n(t)$ involved in the derivation of the exact formula (36) (notation and formulas as in reference 2), they have in the *zeroth* approximation the form $u_n^{Z-2}(x,y,z+v_nt)$, it is seen that

$$\left(\frac{\partial H}{\partial t}\right)_{n0}=\int\int\int dxdydz'u_n^*(x,y,z')\times u_0(x,y,z')\left[\frac{\partial H}{\partial t}\right]_{z=z'-v_nt}$$
$$=\int\int\int dxdydzu_n^*(x,y,z)u_0(x,y,z)\times\left(\frac{\partial V}{\partial t}-(Z-2)e^2v_n\cdot\frac{\partial}{\partial z}\frac{1}{r}\right)$$
$$=\left(\frac{\partial V}{\partial t}\right)_{n0}+U_{n0}. \tag{5}$$

Here $V(t)$ is the potential (1) (specialized for a single electron and alpha particle velocity direction along the positive z-axis), disregarding the negligible difference between v and v_n; U is defined in (5); and the matrix elements are now taken with respect to the time-independent wave functions $u_n^{Z-2}(x,y,z)$. If we substitute (5) in the first part of (37) and integrate the time integral by parts, we obtain

$$a_n(t)=(i\hbar\omega)^{-1}\left[e^{i\omega t}\left(\frac{\partial V}{\partial t}\right)_{n0}+U_{n0}\right]_0^t-(i\hbar\omega^2)^{-1}\int_0^t e^{i\omega t}\left(\frac{\partial^2V}{\partial t^2}\right)_{n0}dt.$$

We see that except for the first term we have indeed H replaced by V. As to the first term, considering the approximation of retaining only that term, and inasmuch as it has no limit for $t\to\infty$ (U being time-independent), we have to evaluate the time average of the probability in question,

$$\lim_{t\to\infty}\frac{1}{t}\int_0^t|a_{n0}(t)|^2dt.$$

Assuming for simplicity that the wave functions are real, one finds for this limit the value

$$(e^2/\hbar^2\omega^2)\left(\frac{\partial}{\partial z}\frac{1}{r}\right)_{n0}^2[(2v_n-(Z-2)v_n)^2+(Z-2)^2v_n^2],$$

and this is seen to be of the same order of magnitude though somewhat smaller as the corresponding expression (15) in reference 1.

V. COMPARISON WITH EXPERIMENTS

The numerical results obtained in references 1 and 2 for ionization in the K shell seem to admit of meaningful comparison with recent experimental findings for Po^{210}.[9] Migdal's approximation of retaining the first

[8] E. U. Condon and G. Shortley, *Theory of Atomic Spectra* (Cambridge University Press, London, 1935); second edition (1951).

[9] W. C. Barber and R. H. Helm, Phys. Rev. **86**, 275 (1952); A. Lagasse and J. Doyen, Compt. rend. **239**, 700 (1954).

term in the series obtained by integration by parts is more nearly valid for the most tightly bound electrons, and the use of hydrogenic wave functions is less in error for these electrons. Though the relativistic correction is likely to be large here, it seems reasonable to expect that the overall error would not be much larger than a factor of two. The experimental findings are discussed in reference 2. It can be concluded that the probable experimental result is of the order of 10^{-6} K-ionizations per alpha. This is consistent with the theoretical result in reference 1. The reservation relative to the dependence of the experimental result on the estimate of the internal conversion coefficient for the gamma ray of Po^{210}, voiced in reference 2, is apparently removed by the result of a x-ray-electron coincidence experiment reported by Lagasse and Doyen.[9]

PHYSICAL REVIEW VOLUME 100, NUMBER 1 OCTOBER 1, 1955

Complex Alpha and Gamma Spectra of $Cf^{250,252}$†

FRANK ASARO, FRANK S. STEPHENS, JR., B. G. HARVEY, AND I. PERLMAN
Radiation Laboratory and Department of Chemistry, University of California, Berkeley, California

(Received June 17, 1955)

The alpha and gamma spectra of Cf^{250} and Cf^{252} have been investigated with an alpha-particle spectrograph and an alpha-particle gamma-ray coincidence counter. Alpha groups of 6.112 (84.5%) and 6.069 Mev (15.5%) belonging to Cf^{252} were found, as were groups of 6.024 (83%) and 5.980 Mev (17%), belonging to Cf^{250}. L x-rays and gamma rays of 42 (0.014%) and 100 kev (0.01$_4$%) were assigned to Cf^{252}. Other gamma rays were assigned to odd-mass californium isotopes. The results are evaluated with respect to the current theory and systematics of complex alpha spectra and excited states of even-even nuclei.

I. INTRODUCTION

IN the heavy element region, the alpha-decay characteristics of even-even nuclei show marked regularities with respect to energy level separations and the selective alpha particle population to the various states. The level spacings correlate well with the Bohr-Mottelson[1–3] formulation for collective rotational motion in highly deformed nuclei, and the alpha population to the ground and first even state follow simple alpha decay predictions closely. There are small but significant departures, however, from the simple theory.[4,5]

On the other hand, the alpha population to the second even states varies considerably from the expectations of simple alpha-decay theory.[4,6] The ratio of the predicted to the observed population follows a regular pattern which has been treated in terms of the spheroidal model by various authors.[7]

The present work was undertaken to determine to what extent the trends just mentioned would continue in the californium isotopes Cf^{250} and Cf^{252}. These are beta-stable isotopes with half-lives of ~10 years and ~2 years, respectively.[8,9]

II. METHODS AND APPARATUS

A high-resolution spectrograph[10] was used to measure the separation between the alpha groups to the ground and first even states and their relative intensities. The transmission of the instrument, however, was 4×10^{-6} so that in the weak sources available only the strongest alpha lines were observed.

The L x-ray intensity of the $Cf^{250,252}$ mixture was determined from alpha—L x-ray coincidences. The measurements were made by coincidence counting because the gamma-ray background was comparable to the intensity of L x-rays in the sample whereas the coincidence background was negligible. The alpha detector was zinc sulfide which detected not only alpha particles but also spontaneous fission particles. Compared with the alpha—L x-ray coincidences, however, the spontaneous fission coincidence contributions were very small.

The gamma-ray spectrum of the californium isotopes was also measured in coincidence with alpha particles. These coincidence measurements were necessary because of the relatively large numbers of gamma rays

† This work was performed under the auspices of the U. S. Atomic Energy Commission.

[1] F. Asaro and I. Perlman, Phys. Rev. **87**, 393 (1952); **91**, 763 (1953).

[2] A. Bohr and B. R. Mottelson, Phys. Rev. **89**, 316 (1953); **90**, 717 (1953); Kgl. Danske Videnskab Selskab, Mat.-fys. Medd. **27**, No. 16 (1953).

[3] A. Bohr, *Rotational States of Atomic Nuclei* (Ejnar Munksgaard, Copenhagen, 1954).

[4] I. Perlman and F. Asaro, Ann. Revs. Nuclear Sci. **4**, 157 (1954).

[5] P. Falk-Vairant and J. Teillac, Compt. rend. **236**, 914 (1953).

[6] Asaro, Stephens, Thompson, and Perlman, Phys. Rev. **98**, 19 (1955).

[7] J. O. Rasmussen, Jr., University of California Radiation Laboratory Unclassified Report UCRL-2431, December, 1953 (unpublished); R. F. Christy, Phys. Rev. **98**, 1205 (1955); P. O. Fröman, Kgl. Danske Videnskab. Selskab, Mat.-fys. Medd. (to be published); B. Segall and J. O. Rasmussen, Jr. (to be published).

[8] Ghiorso, Thompson, Choppin, and Harvey, Phys. Rev. **94**, 1081 (1954).

[9] Diamond, Magnusson, Mech, Stevens, Friedman, Studier, Fields, and Huizenga, Phys. Rev. **94**, 1083 (1954).

[10] F. L. Reynolds, Rev. Sci. Instr. **22**, 749 (1951); Asaro, Reynolds, and Perlman, Phys. Rev. **87**, 277 (1952).

from the spontaneous fission branching of the californium isotopes compared to those accompanying the alpha decay.

For alpha-gamma coincidence counting the alpha particle and fission fragment detector was a $\frac{1}{32}$-inch thick thallium-activated potassium iodide crystal optically coupled to a DuMont-6292 photomultiplier tube. The crystal counting area was masked to a rectangle $\frac{5}{16}\times\frac{1}{4}$ inch with 0.002-inch platinum foil. The output of the photomultiplier tube, after shaping and amplification, was fed into a single-channel pulse-height analyzer. The analyzer selected only the pulses caused by alpha particles and these were fed into a coincidence unit with 2-microsecond resolving time. In some cases the analyzer was adjusted to select only the pulses caused by spontaneous fission fragments. The gamma rays were detected with a $1\times1\frac{1}{2}$ inch thallium-activated sodium iodide crystal optically coupled to a DuMont-6292 tube. The output of the photomultiplier tube after shaping and amplification was fed into the coincidence unit of 2-microseconds resolving time and simultaneously into a 50-channel pulse-height analyzer. The 50-channel analyzer (8-microsecond resolving time) was gated by coincidence pulses from the 2-microsecond unit. This latter unit served to reduce the chance coincidence rate. In all runs the chance coincidences were determined experimentally and subtracted from the total coincidences.

To secure better resolution between the alpha particles and spontaneous fission fragments, the region between the sample and the alpha particle detector was evacuated.

The alpha-particle and gamma-ray detectors each subtended about 20% of 4π in the alpha-gamma coincidence measurements. In the alpha—L x-ray coincidence measurements, the zinc sulfide detector subtended about 40% and the gamma detector subtended about 30% of 4π.

III. SOURCE PREPARATIONS

The californium had been produced by intensive neutron irradiation of lower elements, initially Pu^{239}.[11,12] The pertinent reactions which resulted in the californium preparation are as follows:

$$\begin{array}{l} Cm^{244}(n,\gamma)Cm^{245}(n,\gamma)\cdots Cm^{249} \\ \qquad\qquad\qquad\qquad\quad \downarrow\beta^- \\ \qquad\qquad\qquad\qquad\quad Bk^{249}(n,\gamma)Bk^{250} \\ \qquad\qquad\qquad\qquad\quad \downarrow\beta^- \qquad \downarrow\beta^- \\ Cf^{249}(n,\gamma)Cf^{250}(n,\gamma)Cf^{251}(n,\gamma)Cf^{252}(n,\gamma)Cf^{253}. \\ \qquad\qquad\qquad\qquad\qquad\qquad\qquad\qquad\quad \downarrow\beta^- \end{array}$$

The isotopes listed are beta stable except those designated as β^- emitters. Of the alpha activity in the sample, about 85% was due to Cf^{252} and 15%, Cf^{250}. The Cf^{249} could be estimated from the irradiation history to contribute only about 0.04% to the alpha activity. (The mass of Cf^{249} is only about tenfold lower than that of Cf^{250} but its half-life is 400 to 500 years whereas the half-life of Cf^{250} is 10 years.) Despite the low activity of Cf^{249}, it has prominent gamma rays which showed up in the gamma-ray spectrum which will be mentioned. Similarly, the Cf^{251} and the alpha branching of Cf^{253} can be estimated to be in even lower intensity.

After chemical purification of the californium fraction, part of the activity was electroplated on to a 0.0005-inch platinum plate.[13] The plate had been masked so that the activity could deposit only on a rectangular area $\frac{1}{32}\times\frac{1}{4}$ inch. The electrolytic deposit was dried and heated to a dull red color to drive off volatile matter. This sample, containing 1.2×10^5 alpha disintegrations per minute, was used as the alpha-particle spectrograph source.

The alpha-gamma coincidence source was prepared by evaporating to dryness a few drops of lactic acid solution containing 1.4×10^5 alpha disintegrations per minute on a 0.0005-inch platinum plate. The alpha—L x-ray source was prepared by evaporating to dryness a few drops of concentrated nitric acid containing about 2000 alpha disintegrations per minute on a 0.0005-inch aluminum plate.

IV. EXPERIMENTAL RESULTS

Alpha Spectra

The electroplated sample of mixed californium isotopes described above was exposed in the alpha-particle spectrograph for 141 hours. The alpha particles were detected by direct track counting of the photographic plate which was the receiver in the spectrograph. A graph of the alpha spectrum is shown in Fig. 1. The alpha-particle energies were determined by comparison with Em^{220} α_0 which has been measured by Briggs[14] as 6.282 Mev. The groups at 6.112 ± 0.005 and 6.024 ± 0.005 Mev were assigned to Cf^{252} and Cf^{250}, respectively, in accordance with earlier measurements with ionization chambers. Thompson *et al.* reported early values of 6.15 and 6.05 Mev[8,11,15] and

[11] Thompson, Ghiorso, Harvey, and Choppin, Phys. Rev. **93**, 908 (1954).
[12] Harvey, Thompson, Ghiorso, and Choppin, Phys. Rev. **93**, 1129 (1954).
[13] Harvey, Choppin, and Thompson (unpublished).
[14] G. H. Briggs, Proc. Roy. Soc. (London) **A157**, 183 (1936).
[15] Ghiorso, Thompson, Higgins, Harvey, and Seaborg, Phys. Rev. **95**, 293 (1954).

later revised them to 6.13 and 6.04 Mev.[16] Diamond *et al.*[9] reported alpha-particle energies of 6.12±0.01 and 6.03±0.01 Mev, and Magnusson *et al.*[17] reported values of 6.117±0.010 and 6.033±0.010 Mev for these isotopes.

Among even-even alpha emitters in this region there are prominent alpha groups some 40 kev lower in energy than the most abundant groups[4] and in an abundance of 15 to 30%.[4,6] By analogy, the groups at 6.069 and 5.980 Mev are assigned to Cf^{252} and Cf^{250}, respectively. The existence of complex structure in both Cf^{252} and Cf^{250} was determined previously from L x-ray-alpha particle coincidence measurements by Diamond *et al.*[9] Magnusson *et al.*[17] reported the energy separations to be between 40 and 45 kev.

In order to determine the energy of the first excited state of the product nucleus one must add to the 43-kev separation between the alpha groups of Cf^{252}, a nuclear recoil energy difference of 0.7 kev. Thus the energy becomes 44 kev. Similarly, in the case of Cf^{250} decay, a 43.6-kev separation in alpha-particle energy corresponds to a 44-kev first excited state energy in the daughter nucleus. To simplify their description, the alpha groups to the ground state are designated α_0, and those for the 44-kev states are designated α_{44} (an alpha group to an excited state of x kev would thus be called α_x).

The intensities of the alpha groups were determined by integrating the area under the peaks. Although the alpha particles from the electroplated sample were resolved quite well considering the objective of obtaining high transmission, there appears to be an appreciable tailing on the low-energy side of the peaks. This tailing was estimated from α_{44} of Cf^{250}, by assuming that all of the alpha peaks on the photographic plate had very nearly the same shape. After resolving the peaks in this manner intensities for Cf^{252} α_{44} and Cf^{250} α_{44} were 15.8% and 17.5%, respectively. From the spectrograph measurements, the abundance of Cf^{250} alpha activity at the time of the run was 14.2% of the total alpha activity. The remaining 85.8% was due to Cf^{252}. The weighted average of the $Cf^{250,252}$ α_{44} groups was then 16.0%. This number will be useful for comparison with the alpha–L x-ray coincidence work discussed next.

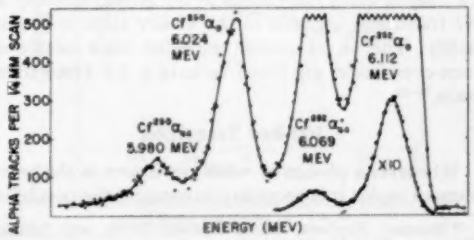

FIG. 1. Alpha spectra of Cf^{250} and Cf^{252}.

V. COINCIDENCE STUDIES

Alpha–L X-Ray Coincidences

The abundance of an alpha group in an even-even nucleus which populates the first excited state can be determined indirectly from the intensity of L x-rays since the corresponding gamma ray transition is by far the most prominent and is heavily converted in the L shell. The intensity is best measured by determining the alpha–L x-ray coincidence rate per alpha disintegration. The corrections which must be applied to the raw data to obtain the total population of the first excited state are the following: (1) allowance for fluorescence yield of the L x-rays; (2) conversion in M, N . . . shells; (3) geometry factor; (4) L x-ray attenuation between source and detector. The geometry factor was determined by measuring the coincidence rate of the alpha particles of Am^{241} with its 60-kev gamma ray whose abundance is known.[18] In order to minimize some of the uncertainties in the other correction factors, Cm^{242} was used as a standard for comparison. The alpha population to the first excited state for this isotope is known fairly accurately[19] and its alpha–L x-ray coincidence rate was measured under the same experimental conditions. The population of the first excited state defines the total electron vacancies and from the conversion electron spectrum[20] the number of L-shell vacancies can be calculated. The measured L x-ray intensity must then be brought into agreement with this value by correcting for fluorescence yield and L x-ray absorption. These two factors were dissociated by accepting the calculated[21] fluorescence yield, thereby ending up with an effective absorber thickness to produce the required attenuation of the particular L x-rays from Cm^{242} decay. Now the desired values for the californium isotopes could be obtained by applying these corrections in reverse fashion. Since the Cm^{242} was used as a standard, the errors are only those of second-order nature in extrapolating fluorescence yields and x-ray attenuation factors over two units of atomic number.

The results of these measurements and calculations gave 15.5% as the weighted average for the abundances of the α_{44} groups of Cf^{250} and Cf^{252}. This is to be compared with the 16.0% value from direct alpha track counting already cited. The complete independence of the two methods lends some confidence to the alpha–L x-ray coincidence counting method which can be applied to sources of this type which are too weak to obtain the alpha spectrum.

[16] Thompson, Ghiorso, Harvey, and Choppin (unpublished data, 1954).
[17] Magnusson, Studier, Fields, Stevens, Mech, Friedman, Diamond, and Huizenga, Phys. Rev. **96**, 1576 (1954).
[18] Beling, Newton, and Rose, Phys. Rev. **86**, 797 (1952).
[19] Asaro, Thompson, and Perlman, Phys. Rev. **92**, 694 (1953).
[20] T. O. Passell, Ph.D. thesis, University of California Radiation Laboratory Unclassified Document UCRL-2528, March, 1953 (unpublished).
[21] B. B. Kinsey, Can. J. Research **A26**, 404 (1948).

TABLE I. Alpha-particle gamma-ray coincidence results.

Exp. No.	42-kev gamma-ray[a] Energy (kev)	Abundance ($\times10^{-6}$)	67-kev radiation Energy (kev)	Abundance	100-kev gamma ray Energy (kev)	Abundance ($\times10^{-6}$)	K-ray maximum abundance ($\times10^{-6}$)	~180-kev gamma ray Energy (kev)	Abundance	Other radiations Energy (kev)	Abundance
1	43	1.5	66–73	2.6	99	1.3	5	~190	>8[b]	[c]	...
2	41	1.3	67	4.3	96	1.0	7	[c]		[c]	...
3	~40	1.5	70	1.2	99	1.4	9	~180	22	[c]	...
4	~40	1.4	63–67	2.5	100	1.4	7	~180	8	350–400	3
Best value[d]	42[a]	1.4	...	...	100	1.3	7	...	...	350–400	3

[a] This energy value is not as accurate as that derived from the separation of the peaks in the alpha spectrum.
[b] The gamma-ray peak would have been just partially observed in this experiment.
[c] These gamma rays would not have been observed in this experiment.
[d] The contribution of gamma rays of 99[kev] produced by Cf^{250} decay would be less than 10% of any of californium gamma rays.

Magnusson *et al.*[17] reported abundances of about 10% for both of these groups from L x-ray alpha-particle coincidence measurements using the abundance of Pu^{238} α_{44}, 24%, as a standard. A later value of 28%[22] for the abundance of Pu^{238} α_{44} would then raise the californium abundances of Magnusson[17] to about 12%.

Gamma Rays

Four measurements of the alpha-particle gamma-ray coincidence spectrum were made. The energies and abundances of the observed radiations are shown in Table I. A graph of the results of Exp. 2 are shown in Fig. 2.

Spontaneous fission fragment gamma-ray coincidence measurements were also taken. With our detection system, a gamma-ray "continuum" was observed which rose to a plateau at 125 → 200 kev and then decreased continuously out to several Mev. Superimposed on the continuum was a peak at ~63 kev which might well have been due to platinum K x-rays produced in the platinum sample mounting by the fission gamma rays. Figure 3 shows the fission fragment-photon coincidences in the region of interest. From this spectrum it seems unlikely that any of the gamma rays shown in Table I are a result of the spontaneous fission process.

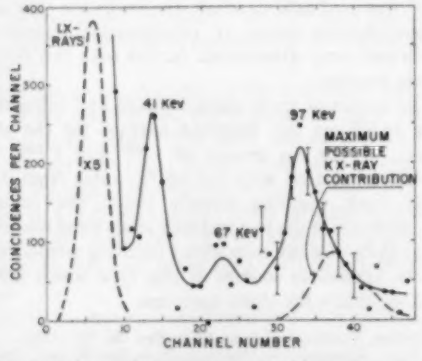

FIG. 2. Alpha-particle gamma-ray coincidence spectrum of $Cf^{250,252}$ from experiment 2 (see Table I).

44-kev Transition

The "42-kev" gamma ray is interpreted as belonging to the highly converted transitions of 44 kev leading from the first excited states to the ground states in both Cf^{250} and Cf^{252} decay. The energy measurement from the alpha data is somewhat better than the gamma-ray value, so the 44-kev value is preferred. The abundance of this gamma ray is 1.4×10^{-4} per alpha particle (Table I). With the weighted abundance of the alpha groups to the 44-kev levels of 16%, the conversion coefficient is 1.1×10^{3}. Since this value is nearly the same as found for the analogous transition in Cf^{246},[22] it is reasonable to assume that the corresponding conversion coefficients of Cf^{250} and Cf^{252} will not differ markedly. Therefore, as the sample activity is predominantly Cf^{252}, the measured conversion coefficient applies principally to Cf^{252}. By comparing this conversion coefficient with theoretical values[24,25] it is found that the transition can only be $E2$. The observed value is about a factor of 3 lower than the calculated value[25] for an $M2$ transition but conversation of parity requires that gamma transitions to the ground state of an even-even nucleus from states populated by alpha emission be electric transitions.

Inasmuch as the 44-kev state of Cm^{248} (populated by Cf^{252} alpha decay) de-excites to the ground state by an $E2$ transition, the spin of the 44-kev state is 2, even parity. This is, of course, expected since nearly all even-even nuclei are found to have a 2+ first excited state.[26–28]

100-kev Transition

Whenever a photon of ~100 kev is seen in the heavy element region it is necessary to consider the possibility

[17] F. Asaro and I. Perlman, Phys. Rev. **94**, 381 (1954).

[22] Hummel, Stephens, Asaro, Chetham-Strode, and Perlman, Phys. Rev. **98**, 22 (1955).
[24] Gellman, Griffith, and Stanley, Phys. Rev. **85**, 944 (1952).
[25] Rose, Goertzel, and Swift (privately circulated tables).
[26] M. Goldhaber and A. W. Sunyar, Phys. Rev. **83**, 906 (1951).
[27] Horie, Umezawa, Yamaguchi, and Yoshida, Progr. Theoret. Phys. (Japan) **6**, 254 (1951).
[28] G. Scharff-Goldhaber, Phys. Rev. **90**, 587 (1953).

that it may be a K x-ray or a gamma ray or both. For curium, the K x-ray group should produce a peak of approximately 108 kev and it is seen from Fig. 2 that most of the peak at ~100 kev lies at too low an energy. However, the peak does tail on the high-energy side, and it seems likely that it is not produced by a single photon. In order to get a reasonable minimum value for the intensity of the gamma ray, a peak centering on the K x-ray energy of 108 kev was resolved. The shape of the subtracted peak was obtained by weighting the different components of the K x-ray group according to the relative intensities observed for uranium.[29]

The intensity of the 100-kev gamma ray after subtracting the maximum possible K x-ray contribution was $1.3\times10^{-2}\%$ of the total californium alpha particles. The group attributed to K x-rays has a corresponding maximum intensity of $7\times10^{-3}\%$. The best energy of the gamma ray is 99 kev; it would be 101 kev if the K x-ray subtraction is not made.

This gamma ray probably represents a transition from the second even spin state[30] to the first even spin state of each of the isotopes, Cf^{252} and Cf^{250}. This assignment is made by analogy with other even-even alpha emitters in this region.[4,31] For example, the gamma spectra of Cm^{242} [19] and Pu^{238},[22] have gamma rays of about 100 kev which are known to decay from the second to the first even states. Because of the preponderance of Cf^{252} in the sample, the measured energy and abundance of the gamma ray apply principally to Cf^{252} decay. As these values are much the same as found in Cf^{246} decay,[24] however, Cf^{250} would be expected to show in its decay a gamma ray of similar energy and abundance.

Other Radiations

Radiations of approximately 67, approximately 180, and approximately 350 → 400 kev were also observed.

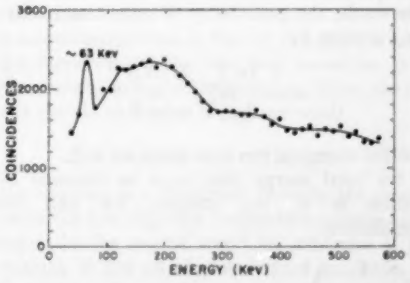

FIG. 3. Partial spontaneous fission fragment gamma-ray coincidence spectrum of $Cf^{250,252}$.

[29] Extrapolation of curves given by A. H. Compton and S. K. Allison, *X-Rays in Theory and Experiment* (D. Van Nostrand Company, Inc., New York, 1935), p. 641.

[30] The term *even spin states* refers to the sequence of 2+, 4+, 6+ excited states which is characterized as a rotational band based on the 0+ ground state of an even-even nucleus in this region.

[31] F. Asaro and I. Perlman, Phys. Rev. **91**, 763 (1953).

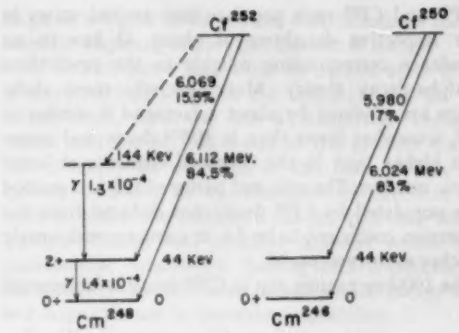

FIG. 4. Alpha-decay schemes of Cf^{250} and Cf^{252}.

The 67-kev radiation is probably due in large part to platinum K x-rays arising from the fluorescence excitation of the sample backing plate by the higher energy gamma rays.

A sample of highly enriched Cf^{249} which had grown into previously purified Bk^{249} containing small amounts of Cf^{250} and Cf^{252} was separated and subjected to alpha-gamma coincidence counting. Two gamma rays of 340 and 395 kev with abundances of 16 and 60%, respectively, relative to the Cf^{249} alpha activity, were observed. These gamma rays correspond well with the 350 → 400 kev radiations seen in the mixed californium isotopes (see Table I). Since the alpha activity due to Cf^{249} in this sample is estimated to be ~0.04%, the observed intensities of these gamma rays, 0.03%, is not out of line. The gamma ray at 180 kev is not accounted for by the Cf^{249} but could possibly come from the Cf^{251} or Cf^{253}. From estimations of the amounts of Cf^{251} and Cf^{253}, their alpha-emission half-lives, and alpha-particle energies, it seems barely possible for Cf^{253} to have an alpha group in as large an abundance as the 180-kev gamma ray but quite reasonable for Cf^{251}.

VI. DISCUSSION AND SUMMARY

Cf^{250} and Cf^{252} have alpha and gamma spectra which are typical of heavy element even-even alpha emitters. Their decay schemes are shown in Fig. 4. In both decays the most abundant alpha group goes to the ground state of the daughter nucleus. The decay of Cf^{249}, however, indicates a different type of spectra in which the most abundant alpha group populates an excited state in the daughter nucleus which then decays to the ground state by one or more gamma transitions. A corollary to this effect is that the ground-state alpha groups in the even-even decay have hindrance factors of about 1, whereas the ground-state transitions for odd mass emitters may be hindered[32] by many orders of magnitude.

[32] "Hindrance" or "hindrance factor" as used here is defined as the ratio of the expected abundance from alpha-decay theory to the experimental abundance.

Cf^{250} and Cf^{252} each populate first excited states in their respective daughters of about 44 kev in an abundance corresponding roughly to the predictions of alpha-decay theory. More precisely these alpha groups are hindered by about a factor of 3, similar to Cf^{246}, somewhat lower than in 100^{254} decay and somewhat higher than in the decay of elements of lower atomic number. The spin and parity of the first excited state populated by Cf^{254} decay was deduced from the conversion coefficient to be 2+ in common with nearly all other even-even nuclei.

The 100-kev gamma ray in Cf^{252} decay is interpreted as the transition from the second even state to the first even state. The energies of the first and second states are such that they can be interpreted as a Bohr-Mottelson rotational band with a consequent spin of 4+ for the second even state. The alpha decay to the second even state as deduced from the abundance of the 100-kev gamma ray is lower by over two orders of magnitude from the predictions of spin-independent alpha-decay theory. This hindrance factor is very similar to that of Cf^{246} and appears to follow the general trends observed for corresponding transitions in other even-even nuclides.

PHYSICAL REVIEW VOLUME 100, NUMBER 1 OCTOBER 1, 1955

Double K Capture and Single K Capture with Positron Emission

ROLF G. WINTER
Pennsylvania State University, University Park, Pennsylvania
(Received April 29, 1955)

Transition probabilities are estimated for double K capture and for single capture with single positron emission. With real neutrino emission, the mean lives for both processes should be greater than 10^{21} years. Without real neutrino emission, as with Majorana neutrinos, the mean life for K capture in conjunction with positron emission is about 10^{15} years in the allowed approximation. Double K capture, however, is then at least a third-order process because an additional step is necessary to remove the energy, with the result that the mean life exceeds 10^{19} years.

I. INTRODUCTION

FOUR possible types of double beta processes[1] are double negatron emission, double positron emission, double negatron capture, and single capture with single positron emission. Double negatron emission probabilities have been calculated with various theories, while double positron probabilities are given, except for the Coulomb distortion of the wave functions of each of the emitted electrons, by similar calculations. Most experiments have been searches for these double emission processes.

One published experiment[2] and some private speculation, however, involved attempts to detect double capture or single capture with single positron emission. Double capture will be the only energetically possible transition if the mass difference between the parent atom and the isobaric atom with atomic number less by two lies between 0 and $2mc^2$. Either double capture or one capture and one positron emission can occur if the atomic mass difference is between $2mc^2$ and $4mc^2$. Both of these processes and double positron emission can occur if the difference is greater than $4mc^2$.

It is the purpose of this note to exhibit rough estimates of the transition probabilities for double capture and for single capture with positron emission.

[1] See references in Rolf G. Winter, Phys. Rev. **99**, 88 (1955).
[2] Berthelot, Chaminade, Levi, and Papineau, Compt. rend. **236**, 1769 (1953).

II. DIRAC NEUTRINOS

If the neutrino is a Dirac particle, double capture probabilities can be calculated from a second order perturbation. Both steps consist of the capture of a K negatron and the emission of a neutrino. The calculation is like that used by Goeppert-Mayer,[3] except that K negatrons are captured rather than free negatrons being emitted. If one intermediate nuclear state s, about mc^2 above the initial state i, contributes most of the result, the probability of transition to the final state f is given by

$$w_{if}=\frac{2\pi}{\hbar}\rho\left|\sum_s\frac{H_{is}H_{sf}}{mc^2+E_\nu}\right|^2, \tag{1}$$

where the energy of the first neutrino is E_ν.

If the total energy that must be removed by the neutrinos is E, one obtains, for unit volume normalization,

$$\rho\left(\sum_s\frac{1}{mc^2+E_\nu}\right)^2 = (2\pi^2\hbar^3c^3)^{-2}\int_0^E(E-E_\nu)^2E_\nu^2\frac{dE_\nu}{(mc^2+E_\nu)^2}. \tag{2}$$

If the lepton spin sums and nuclear wave function

[3] M. Goeppert-Mayer, Phys. Rev. **48**, 512 (1935).

integrals are a maximum, the Fermi beta-decay matrix elements for K capture become

$$H_{is}\simeq H_{sf}\simeq g(Z^3/\pi a^3)^{\frac{1}{2}}, \tag{3}$$

where a is the Bohr radius, Z the atomic number, and $g=2\times10^{-49}$ erg cm^3 is the Fermi coupling constant.

Integrating (2) and substituting the result and (3) into (1), one finds, with $E=mc^2\epsilon$, that

$$w_{if}\simeq\frac{m^3g^4Z^6}{2\pi^5\hbar^7a^6}\left[\frac{\epsilon^5}{3}+4\epsilon^3+4\epsilon-2(\epsilon+2)(\epsilon+1)\ln(1+\epsilon)\right]. \tag{4}$$

For $Z=30$, (Berthelot *et al.*[2] investigated Zn) and $\epsilon=2$, w_{if} becomes 4×10^{-25} per year. As might be expected, this result lies in the same neighborhood as low-energy double negatron emission probabilities in the Dirac neutrino theory.

The calculation for one K capture followed by one positron emission is similar. The first neutrino with energy $E_{\nu 1}$, the second neutrino with energy $E_\nu-E_{\nu 1}$, and the positron with energy $E_\beta=E-E_\nu$ remove the total energy E. Therefore, instead of (2), one must calculate

$$(2\pi^2c^3\hbar^3)^{-3}\int_0^{E-mc^2}(E-E_\nu)[(E-E_\nu)^2-m^2c^4]^{\frac{1}{2}}dE_\nu\times\int_0^{E_\nu}\frac{(E_\nu-E_{\nu 1})^2E_{\nu 1}^2dE_{\nu 1}}{(mc^2+E_{\nu 1})^2}. \tag{5}$$

The K capture matrix element H_{is} is still approximated by (3), but the positron emission matrix element is given by

$$H_{sf}\simeq gf^{\frac{1}{2}}(E_\beta,Z). \tag{6}$$

Here $f^{\frac{1}{2}}(E_\beta,Z)$ is the Coulomb correction in the positron wave function.

The second integration in Eq. (5) can only be carried through numerically. The resulting transition probability is strongly energy dependent, but lies in the same range as the above double K capture result.

III. MAJORANA NEUTRINOS

If the neutrino is a Majorana particle, the neutrino emitted in the first step of a double beta process can be reabsorbed in the second step.[4] Its existence is then only virtual, it has all of phase space available, and therefore it usually produces a large increase in the transition probability.

Since, however, the neutrino is not actually emitted, it cannot carry away any energy. In general, then, double capture without real neutrino emission cannot bring the system to an available state; it is necessary to go to a higher order process that includes a mechanism for disposing of the right amount of energy.

Of course, there may exist an excited state of the product nucleus to which the transition can go. The initial state, however, has a completely negligible width, and the excited states of the product nucleus will generally have widths of less than 10^{-2} ev and spacings of about 10^5 ev. Therefore the existence of a state to which the transition can go with only double capture without real neutrino emission would be a monumental coincidence. Barring such a coincidence, the necessity of a third step to balance the energy leads to a large decrease in transition probability.

Double K capture with one internal bremsstrahlung appears to be the dominant process. The transition probability is

$$w_{if}=\frac{2\pi}{\hbar}\frac{\omega^2}{2\pi^2c^3\hbar}\left|\sum_t\sum_s\frac{H_{ft}H_{ts}H_{si}}{(E_t-E_i)(E_s-E_i)}\right|^2, \tag{7}$$

where ω is the angular frequency of the emitted gamma ray. The expression

$$\sum_s H_{ts}H_{si}/(E_s-E_i) \tag{8}$$

corresponds to the capture of one K negatron with the emission of a bremsstrahlung photon and a virtual Majorana neutrino and brings the system to a state of energy E_t. The final step, given by H_{ft}, consists of the capture of the second K negatron and the absorption of the virtual neutrino.

Since the virtual neutrino can have any energy, one cannot approximate its wave function by a constant over the region of the nucleus. For optimum overlap, the nuclear matrix elements are, if the nuclear radius is R,

$$\frac{3}{4\pi R^3}\int_{r<R}e^{ik\cdot r}d\tau. \tag{9}$$

Otherwise, there is no difference between the calculation of (8) and the calculation of single bremsstrahlung matrix elements[5,6]; the result is

$$\frac{ge}{mc}\left(\frac{\pi\hbar}{\omega}\right)^{\frac{1}{2}}\Psi_{K1}(0)\frac{3}{4\pi R^3}\int_{r<R}e^{ik\cdot r}d\tau, \tag{10}$$

where $\Psi_{K1}(0)$ is the wave function, evaluated at the nucleus, of the electron that is captured. The remainder of the calculation is the same as that used by Furry.[4] The term H_{ft} is the usual matrix element for allowed K capture except for the use of (9) for the integration over the nuclear functions and is given by

$$g\Psi_{K2}(0)\frac{3}{4\pi R^3}\int_{r<R}e^{ik\cdot r}d\tau. \tag{11}$$

[4] W. H. Furry, Phys. Rev. **56**, 1184 (1939).

[5] P. Morrison and L. I. Schiff, Phys. Rev. **58**, 24 (1940).

[6] Richard E. Cutkosky, dissertation, Carnegie Institute of Technology, 1953 (unpublished).

If one intermediate nuclear state contributes most of the result, the sum over t is simply an integration over the phase space of the virtual neutrino which does not cut off until the neutrino wavelength is of the order of the nuclear radius. Since most of the contribution to this integral comes from the high energy (about $100mc^2$) end, it is reasonable to use for E_t-E_i merely the neutrino energy, or chk. The term $\Psi_{K1}(0)\Psi_{K2}(0)$ can range from a maximum of

$$2\Psi_K^2(0)\simeq 2Z^3/\pi a^3, \tag{12}$$

down to zero in case of complete cancellation in the spin sum, depending on the particular form of the interaction; the maximum value will be used here. The sum over t is now a count of the number of cells in phase space available to the virtual neutrino and contributes

$$\frac{1}{2\pi^2}\int_0^\infty k^2 dk, \tag{13}$$

where, of course, all of the above k dependent terms must be included before the integration is performed.

Collecting the above estimates, one finds that the transition probability becomes

$$w_{if}\simeq \frac{81}{16\pi^6}\frac{g^4}{R^4 m^5 c^8 \hbar^2}\frac{e^2}{\hbar c}\frac{Z^6}{a^6}\omega. \tag{14}$$

If $\hbar\omega=2mc^2$, $Z=30$, and $R=6\times10^{-13}$ cm, $w_{if}\simeq10^{-18}$ per year. This result, which is smaller by 10^{-4} than allowed emission probabilities, might be expected; in ordinary K capture, inner bremsstrahlung occurs once in about 10^4 captures.

Of course, double capture without real neutrino emission can proceed with any third-order process that includes a mechanism for removing energy. Competition with inner bremsstrahlung photon emission can come from electron conversion, depending on the angular momentum that must be removed. Another class of processes involves double capture to a virtual state of the final nucleus followed by, for instance, gamma emission. Such processes, however, are considerably less probable. For double K capture followed by electric quadrupole gamma emission, a calculation much like the above, with similar approximations, gives for the transition probability

$$\frac{243}{4\pi^6}\frac{g^4}{m^2c^{10}\hbar^2}\frac{e^2}{\hbar c}\frac{Z^6}{a^6}\omega^5, \tag{15}$$

or 10^{-32} per year for $\hbar\omega=2mc^2$ and $Z=30$. This result can also be understood by means of a qualitative argument. Allowed double electron emission with Majorana neutrinos should have transition probabilities of about 10^{-14} per year.[6,7] Here, since no real state is available after only double capture, one might imagine virtual transitions with a probability of 10^{-14} per year. If the energy difference between the initial state and the virtual state is roughly mc^2, the virtual state can exist for about $\hbar/mc^2\simeq10^{-21}$ sec. Electric quadrupole transition probabilities are, for $2mc^2$ energy, of the order of 10^{12} per second. Therefore, the probability that there is gamma emission from the virtual state rather than return to the initial state is 10^{-21} sec$\times10^{12}$ per sec or 10^{-9}. Therefore the probability of a third order transition consisting of a double beta process followed by gamma emission is $10^{-9}\times10^{-14}$ per year or 10^{-23} per year.

It can be seen from these arguments, or from more rigorous calculation, that in other double beta theories that do not give neutrinos in the final state,[8,9] just as in the Majorana-Furry theory, double capture lifetimes should exceed double emission lifetimes by similar factors.

If single capture in conjunction with single positron emission is energetically possible, one can again consider a second order process, for now the positron can remove the energy. The transition probability has the form (1), the lepton spin sum can be at most, instead of (12),

$$2f^1(E_\beta,Z)(Z^3/\pi a^3)^1, \tag{16}$$

and the sum over the states of the virtual neutrino and the integration of its wave function over the nucleus appear as above. The density of final states involves only the states of the positron of definite energy, and is

$$(2\pi^2c^3\hbar^3)^{-1}m^2c^4\epsilon(\epsilon^2-1)^1, \tag{17}$$

where ϵ is the total energy of the positron in units of mc^2. The result is

$$w_{if}\simeq \frac{81}{16\pi^6}\frac{m^2g^4}{ch^6R^4}\frac{Z^3}{a^3}f(E_\beta,Z)\epsilon(\epsilon^2-1)^1. \tag{18}$$

In the Zn^{64} transition for which Berthelot *et al.*[2] showed experimentally that $w_{if}\lesssim10^{-16}$ per year, the kinetic energy available to the single positron should, according to the decay of Cu^{64}, be only 0.08 Mev. The result for w_{if} is then 10^{-15} per year.

All of the above estimates of transition probabilities are upper limits. The nuclear matrix elements, which occur in each calculation to the fourth power, are certainly less than unity, and there will be some cancellation in the lepton spin sums.

---

[7] H. Primakoff, Phys. Rev. **85**, 888 (1952).
[8] Bruno Touschek, Z. Physik **125**, 108 (1948–1949).
[9] Rolf G. Winter, Phys. Rev. **83**, 1070 (1951).

Inner Bremsstrahlung from A^{37}*

TORSTEN LINDQVIST† AND CHIEN-SHIUNG WU
Columbia University, New York, New York

(Received December 20, 1954)

The continuous gamma-ray spectrum (inner bremsstrahlung), accompanying orbital electron capture in A^{37}, has been reinvestigated by the method of scintillation spectroscopy with particular emphasis on the low energy region. The absorption between the source and the NaI crystal is only due to two one-mil Al foils. After correcting for NaI crystal detection efficiency, the geometrical factor, the ratio of photoelectric cross section to total cross section, Compton electron backscattering, iodine x-ray escape, absorption and resolution, it is found that the intensity of the extremely low-energy photons is much greater than can be accounted for by Morrison and Schiff's treatment. A better agreement can be obtained if one considers the p-electron capture, and takes the Coulomb effect into consideration as shown by Glauber and Martin.

INTRODUCTION

THE continuous gamma-ray spectrum (inner bremsstrahlung) accompanying orbital electron capture was first investigated theoretically by Morrison and Schiff.[1] Later Jauch[2] extended the theoretical investigation with minor revisions. However, both studies take account only of the K-electron capture. Recent investigations[3-5] on the distribution of inner bremsstrahlung from electron capture processes in Fe^{55}, Cs^{131}, and Ge^{71} all have shown that the aforementioned calculations are not adequate in interpreting the low-energy region of the distribution. The observed distributions show a large increase in intensity at low energies instead of dropping to zero intensity as called for by Morrison and Schiff's predictions. The region where the deviation from Morrison and Schiff's prediction becomes noticeable is different for different elements.

Earlier experiments[6,7] on the inner bremsstrahlung from A^{37} have concentrated their efforts on the determination of the maximum available energy but very little attention has been paid to its distribution in the low-energy region. Therefore it was highly desirable to reinvestigate this nuclide with emphasis on the shape of the spectrum particularly in the low-energy region.

A^{37} decays to Cl^{37} by pure electron-capture with a half-life of 34 days. There are no β^- or β^+ and no γ rays. According to the shell model it is a $d_{3/2} \rightarrow d_{3/2}$ transition, i.e., an allowed transition. The decay energy has been calculated from the threshold energy[8] of the $Cl^{37}(p,n)A^{37}$ reaction to be 816 ± 4 kev which is in good agreement with the value 815 ± 20 kev determined from the maximum energy of the inner bremsstrahlung.[5,6] The ratio of the total number of bremsstrahlung photons to the total number of K-captures is given for $1S$ capture by

$$\int_0^k \frac{N(k)dk}{N_e} = \frac{\alpha}{12\pi}\left(\frac{W_0}{m_0c^2}\right)^2,$$

where W_0 is the maximum disintegration energy. It is proportional to W_0^2, and therefore the intensity of the A^{37} inner bremsstrahlung is expected to be relatively high.

I. GLAUBER-MARTIN THEORY[9]

This theory takes into consideration (1) both magnetic and electric radiation, (2) both S- and P-electron capture, (3) all effects of the Coulomb field. It is shown that the electric dipole radiation accompanying the capture of p-electrons is primarily responsible for the large intensity increase at low energies. The electric dipole radiation is relatively more important for larger nuclear charge. In Table I are listed the isotopes whose inner bremsstrahlung has been investigated experi-

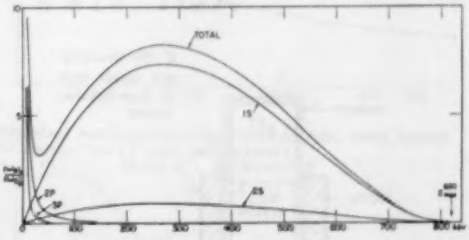

FIG. 1. The distribution of the bremsstrahlung radiations from $1S$-, $2S$-, $2P$-, and $3P$-electron capture in A^{37} according to the Glauber-Martin theory.

$$\frac{(\omega_k)dk}{(\omega_c)_{1S}} = \frac{\alpha}{\pi}\left(\frac{Z^2\alpha^2}{2}\right)\left[1-\frac{x-(E_1-E_{1S})}{x_{max}}\right]^2 I_1(x)dx,$$

where x is in $(Z^2 \cdot Ry)$ units; x_{max} is the upper limit of the photon energy; and $I_1(x)$ is a theoretical function tabulated in P. C. Martin's thesis.

* This work was supported by the U. S. Atomic Energy Commission.

† Now at Physics Department, University of Uppsala, Sweden.

[1] P. Morrison and L. I. Schiff, Phys. Rev. **58**, 24 (1940).

[2] J. M. Jauch, Oak Ridge National Laboratory ORNL-1102, 1951 (unpublished).

[3] L. Madansky and F. Rasetti, Phys. Rev. **94**, 407 (1954).

[4] B. Saraf, Phys. Rev. **94**, 642 (1954).

[5] B. Saraf, Phys. Rev. **95**, 97 (1954).

[6] Anderson, Wheeler, and Watson, Phys. Rev. **90**, 606 (1953).

[7] Emmerich, Singer, and Kurbatov, Phys. Rev. **94**, 113 (1954).

[8] Richards, Smith, and Browne, Phys. Rev. **80**, 524 (1950); Schoenfeld, Duborg, Preston, and Goodman, Phys. Rev. **85**, 873 (1952).

[9] R. J. Glauber and P. C. Martin, Phys. Rev. **95**, 572 (1954).

TABLE I. Some pertinent information on the inner bremsstrahlung from the electron capture process in Fe^{55}, Cs^{131}, Ge^{71}, and A^{37}.

Isotope	E_{max} kev	E_K kev	E_t kev	Reference
Fe^{55}	220	5.9	60	3
Cs^{131}	350	33	100–150	4
Ge^{71}	230	10	40–60	5
A^{37}	820	2.8	30	Fig. 7

mentally. E_t denotes the region below which there is a deviation from Morrison and Schiff's prediction. E_K is the K-ionization potential.

In Fig. 1 is shown the distribution of the radiations from $1S$-, $2S$-, $2P$-, and $3P$-electron capture according to the Glauber-Martin theory. The general expression for the radiative l-events $(\omega_k)_l$ per $1S$-electron capture $(\omega_c)_{1S}$ is

$$\frac{(\omega_k)_l dk}{(\omega_c)_{1S}} = \frac{\alpha}{\pi}\left(\frac{Z^2\alpha^2}{2}\right)^2\left[1-\frac{x-(E_l-E_{1S})}{x_{\max}}\right]^2 I_l(x)dx \quad (1)$$

or

$$\frac{(\omega_k)_l dk}{(\omega_c)_{1S}} = \frac{\alpha}{\pi}\frac{Z^2\alpha^2}{2m}\left[1-\frac{x-(E_l-E_{1S})}{x_{\max}}\right]^2 I_l\left(\frac{k}{\tfrac{1}{2}Z^2\alpha^2 m}\right)dk, \quad (1')$$

where x is the photon energy given in units of $Z^2Ry = Z^2 \times 13.5$ ev; $I_l(x)$ is a theoretical function tabulated in Martin's thesis[10]; $x_{\max}$ is the upper limit of the photon energy. In the case of radiation from $1S$-capture, Eq. (1) reduces to the old Morrison-Schiff theory:

$$\frac{(\omega_k)_{1S}dk}{(\omega_c)_{1S}} = \frac{\alpha}{\pi}\left[1-\frac{x}{x_{\max}}\right]^2\frac{k}{m}d\left(\frac{k}{m}\right)$$

$$= \frac{\alpha}{\pi}\left(\frac{W}{m}\right)^2\left[1-\frac{k}{W}\right]^2\frac{k}{W}d\frac{k}{W}. \quad (2)$$

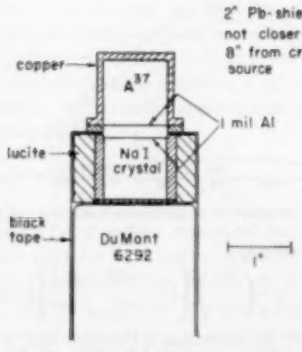

FIG. 2. Experimental arrangement.

[10] P. C. Martin, thesis, Harvard University, May, 1954 (unpublished).

For the radiation from $2S$-capture, one only takes $\frac{1}{8}$ of the $1S$-intensity. For the $2P$- and $3P$-captures, the function $I_l(x)$ is more complicated. The results shown in Fig. 1 are taken from a table given in Martin's thesis.[10] Fig. 1 shows also the sum of all contributions for the case of A^{37}. The marked increase in intensity starts at about 30 kev.

II. EXPERIMENTAL ARRANGEMENT

The experimental arrangement is shown in Fig. 2. The A^{37} gas is contained in a copper cylinder of diameter 1 in., height 1 in., with a 1-mil Al window. The NaI crystal, of diameter 1 in. and height 1 in., is permanently canned in an aluminum container with a MgO reflector

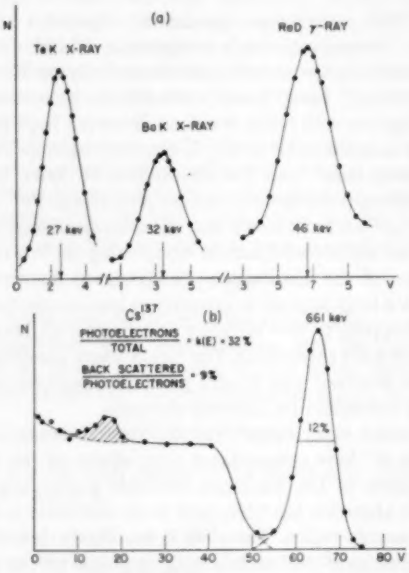

FIG. 3. (a) The low-energy calibrations. (b) An example of a complete gamma-ray spectrum used to determine the ratio of photo cross section to total cross section.

on its side wall. The top surface through which the radiation enters is covered with a 1-mil Al foil only. The total amount of absorbing material between source and crystal is 2 mils of Al. The gas container is placed as close to the crystal as possible. Since the source has a finite volume it was impossible to obtain all the correction curves with this geometry. As an approximation it was assumed that a point-source located in the center of an identical gas-container would represent the proper geometry. The crystal is mounted on a DuMont 6292 photomultiplier-tube. The arrangement gives a resolution of 12% at the gamma-ray energy 661 kev. The pulses are amplified in a nonblocking linear amplifier and the spectrum is analyzed with a pulse-height analyzer. The energy calibration is carried out by using

x-radiations of Te, Ba, and Hg and gamma-radiations of RaD, Hg^{203}, Cr^{51}, I^{126}, Au^{198}, Cu^{64}, Na^{22}, Cs^{137}, etc. The linearity throughout the region used is good. Figure 3(a) shows some of the low-energy calibrations.

III. SCINTILLATION TECHNIQUE APPLIED TO CONTINUOUS GAMMA-RAY SPECTRUM

In order to interpret the experimental data from a scintillation spectrometer measurement, it is necessary to study carefully the various effects in the crystal and from the surrounding material. These effects combine to affect the observed experimental spectrum. Therefore it is very difficult to analyze correctly in this manner. However, in the few cases where a theoretical prediction of its distribution exists, it is preferable to apply all the corrections due to the crystal effects to the theoretical distribution and compare it with the experimentally observed spectrum. The corrections applied to the theoretical distribution as shown in Fig. 4 are the following:

A. γ-Detection Efficiency Including the Geometrical Factor

For source-crystal distances of the order of magnitude used in this experiment, namely $\frac{1}{2}$ in., the geometrical factor becomes very important. For instance, when the efficiency for a normally incident beam on this particular crystal at 600 kev is 70%, it is only 40% for a source-crystal distance of $\frac{1}{2}$ in. The γ-efficiency curve used is shown in Fig. 5(a), which is taken from Novey, since our geometrical arrangement is very similar to his. The resulting distribution after the efficiency correction is shown as curve A in Fig. 4.

B. Fractions of Photons Detected with Full Energy

Because of the presence of the Compton effect, all photons are not detected with their full energy. The ratio of photo cross section to total cross section is energy-dependent and should be determined for a number of energies throughout the region under identical conditions; for example, see Fig. 3(b). The region below 250 kev is not covered with experimental points, but fortunately the contribution from Compton electrons for energies below 250 kev is small. The curve obtained [Fig. 5(b)] can be checked together with the γ-efficiency curve by measuring the relative intensity of two γ rays where the intensity ratio is well known from other experiments. This was done by using the two γ rays of I^{126} of 380 kev and 650 kev, their intensity ratio being determined as 1:1.[11] The agreement with this ratio was rather good. The distribution curve due to the contribution of these full-energy pulses is shown as curve B in Fig. 4.

[11] M. L. Perlman and Joan P. Welker, Phys. Rev. **95**, 133 (1954).

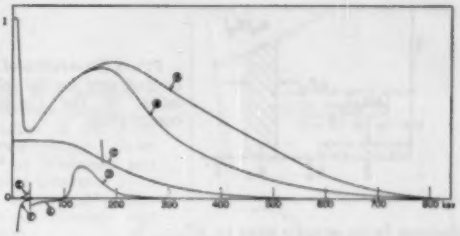

FIG. 4. Corrections to the theoretical distribution. NaI crystal; 1 in. diam.×1 in. height; source-crystal $\frac{1}{2}$ in. (a) Theoretical curve corrected for γ efficiency. (b) The distribution curve due to photoelectrons. (c) The Compton-electrons. (d) Backscattered photons. (e) Escape-effect. (f) Absorption.

C. Compton Electrons

The fraction of photons detected with energy less than their full energy can also be determined from Fig. 5(b). If the fraction of photons detected with full energy is $p(E_\gamma)$, it is obvious that the fraction of photons detected with less than full energy is $[1-p(E_\gamma)]$. This correction becomes very important when there are photons of high energy present as in this case.

The number of photons of energy E_γ absorbed in the crystal is $N_a(E_\gamma)$. The number of Compton-electrons ranging from energy zero to E_γ^e, where E_γ^e is the maximum Compton-electron energy (the Compton peak), is $N_a(E_\gamma)[1-p(E_\gamma)]$. The probability[12] that such a Compton-electron will have an energy between E and $E+dE$ is a function $C(E,E_\gamma)$. The total number of Compton-electrons at energy E due to all incoming

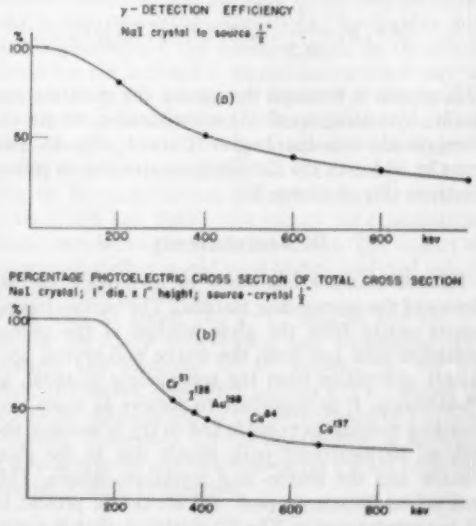

FIG. 5. (a) γ-detection efficiency. (b) The percentage of the photoelectric cross section of the total cross section *vs* energy.

[12] K. Lidén and N. Starfelt, Arkiv Fysik **7**, No. 36 (1954).

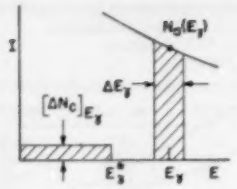

FIG. 6. Illustration of the method used for the calculation of the Compton contribution.

photons from energy zero to $E_{\gamma,\max}$ is

$$N_c=\int_0^{E_{\max}} C(E,E_\gamma)N_a(E_\gamma)[1-p(E_\gamma)]dE_\gamma.$$

By examining carefully a few cases of the entire distribution of the scintillation spectrum of a single γ ray at various energies we find that the Compton-electron distribution for a certain γ energy is approximately constant over the energy-range $0-E_\gamma^*$. We can therefore approximate the function $C(E,E_\gamma)$ to be

$$C(E,E_\gamma)=C(E_\gamma)=1/E_\gamma^*, \quad 0<E<E_\gamma^*$$
$$C(E,E_\gamma)=0, \quad E>E_\gamma^*.$$

In order to obtain the Compton-electron distribution, we performed a step-by-step integration. One starts out at the highest energy and takes the $N_a(E_\gamma)$ from curve (see Fig. 6). Then one looks up the corresponding $[1-p(E_\gamma)]$ and chooses a suitable value of ΔE_γ, the smaller the better. One then calculates $[\Delta N_c]_{E_\gamma}$, the ordinate of the Compton distribution from 0 to E_γ^* due to photons of energy between E_γ and $E_\gamma+\Delta E_\gamma$, by the relation

$$[\Delta N_c]_{E_\gamma}=\frac{1}{E_\gamma^*}\cdot N_a(E_\gamma)[1-p(E_\gamma)]\Delta E_\gamma.$$

This process is repeated throughout the spectrum and finally, by adding up all the contributions, we get the Compton-electron distribution (Curve *C*, Fig. 4). This must be added to the distribution curve due to photoelectrons (Fig. 4, Curve *B*).

D. Backscattering

Here it becomes important to investigate the influence of the surrounding material. The backscattering results partly from the glass window of the photomultiplier-tube and from the source and crystal containers and partly from the surrounding material, as Pb-shielding. It is important to remove as much surrounding material as possible and to try to measure the residual backscattered peak mostly due to the glass window and the source- and crystal-containers. This residual backscattered peak will always be present in all the measurements. The Pb shielding, that is necessary for the measuring of the weak inner bremsstrahlung, should be kept at a distance so as not to increase the backscattering. In this experiment it was found that 2-in. Pb shielding at a distance of 6 in. from the source-crystal did increase the backscattering, but when the shielding was removed to a distance of 8 in. the increase in backscattering was negligible. Another effect that has to be taken into consideration is the fluorescence radiation from the Pb shielding. A thick aluminum lining of the Pb shielding is provided to take care of this effect. It is not advisable to put a Cu absorber close to the source- and crystal-containers to attenuate this radiation, since the backscattering thus produced is undesirable.

The correction for the backscattering is of course very difficult to calculate accurately. It is shown by an auxiliary experiment that at the energy of 661 kev and with proper geometry, the backscattered peak was about 9% of the photo peak. Considering the energy dependence of the Compton cross section, the γ efficiency and the original spectral intensity, it is estimated that the average number of backscattered photons is equal to 9% of the number of photoelectrons from photons of energy of 200 kev$\rightarrow E_{\max}$. The energy range for the backscattered photons is around 110 kev $-$ 200 kev with a tail to the high-energy side due to the 90°-scattered photons. [$E_{90°}$ for 800 kev=310 kev]. This estimation leads to the curve *D* on Fig. 4.

E. *K* X-Ray Escape Effect

This correction has been calculated by Novey,[13] and since this is a surface effect the correction is not dependent on the thickness of the crystal. The correction is shown as curve *E* on Fig. 4.

F. Absorption

Of course the experimental arrangement should be arranged to reduce this effect to a minimum. In our case there is a limit since the source is in gas form. The total absorbing material between the source and the crystal is a 1-mil Al foil of the window of the gas container and a 1-mil Al foil on top of the crystal. The absorption effect does not show up until 30 kev and is shown as curve *F* in Fig. 4.

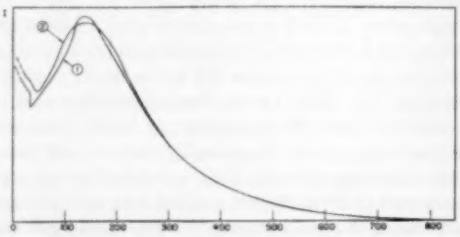

FIG. 7. The correction for the resolution of the system. Curve 1 is the total theoretical distribution, N_{theor}, obtained from Fig. 4. Curve 2 is the distribution, $N_{\text{res.}}$ obtained by correcting N_{theor} for resolution as described in Sec. III(G).

[13] T. B. Novey, Phys. Rev. **89**, 672 (1953).

G. Effect of the Resolution of the System

The correct way to carry out this correction is to treat the theoretical distribution according to the known resolving power of the system and then to compare the resultant curve with the experimental one. If the continuous spectrum is considered to consist of a number of monochromatic γ rays it is obvious that each "γ ray", E_γ, is recorded as a Gaussian distribution, $g(E)$,

$$g(E)=[2\pi KE_\gamma]^{-\frac{1}{2}}\exp[-(E_\gamma-E)^2/2KE_\gamma],$$

where $K=W^2(E_\gamma)/2E_\gamma \ln 2$ and $W(E_\gamma)=$ half-width at half-intensity. N_{res}, the theoretical distribution corrected for resolution, is therefore obtained by integrating:

$$N_{res}(E)=\int_0^{E_{max}} N_{theor}(E_\gamma)g(E)dE_\gamma.$$

This operation was carried out by graphical integration and the correction is shown in Fig. 7. At energies above 300 kev the corrected and the uncorrected curve coincide.

H. Background

This correction is carried out on the experimental points and includes the tube-noise, the amplifier-noise and the background radiation. This correction is shown as "noise-level" in Fig. 8. The noise-level varies drastically with the room temperature, so all the measurements were taken in an air-conditioned room with a minimum temperature variation.

IV. RESULTS

In Fig. 8 is shown the final theoretical curve together with the experimental points. The experiment was repeated in two runs with different gain on the amplifier.

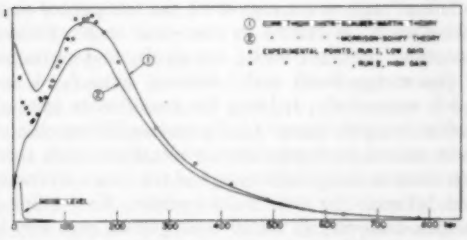

FIG. 8. Inner bremsstrahlung from A^{37}. (1) Theoretical distribution according to the Glauber-Martin theory after correction for the experimental factors. (2) Theoretical distribution according to the Morrison-Schiff theory after correction for the experimental factors. ○—Experimental points, Run I, low gain. ●—Experimental points, Run II, high gain.

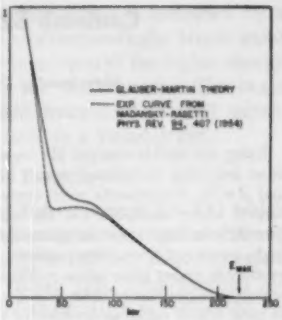

FIG. 9. A comparison of the experimental distribution of the inner bremsstrahlung from Fe^{55} by Madansky and Rasetti (reference 3) to the theoretical prediction of Glauber and Martin.

The peak-counting rate at 150 kev in Run I is 3100 counts/min, and the experimental points are normalized to the theoretical curve by taking the average ratio of three points above 250 kev. The peak-counting rate in Run II is 750 counts/min and the exp points are matched to Run I at 90 kev.

The agreement down to 100 kev is excellent. Because of the low Z-value of A^{37} ($Z=18$), the contribution due to the $2P$ electron capture does not become important until below 30 kev. The experimental distribution curve does reach a maximum around 150 kev as predicted and then drops down to 30 kev. From there it suddenly swings up rapidly. In fact, this occurs exactly where the effect of the $2P$ electron-capture should show up as predicted by the Glauber and Martin calculation.

The experimental points below 120 kev do not lie exactly on the theoretical curve. This may be due partially to the accumulated errors introduced by the various corrections and partially to the simplifications used in the theoretical calculations. As Glauber and Martin pointed out, the screening effect on the distribution was not included in the calculation but it may be appreciable in the low-energy region. For comparison, we tried to fit the experimental distribution of the inner bremsstrahlung from Fe^{55} by Madansky and Rasetti[4] to the theoretical prediction of Glauber and Martin (Fig. 9). We observed that the agreement was excellent to about 100 kev. Below that energy the experimental points were below the predicted values. The neglect of the screening effect would yield higher predicted values at the low-energy region.

We wish to thank Dr. P. C. Martin and Dr. F. Pollock for many enlightening and stimulating discussions, and Professor W. W. Havens, Jr., for his constant interest. One of the authors (T. L.) wishes to express his appreciation to the Department of Physics, Columbia University, for the opportunity of working in its laboratories and to acknowledge a grant from the Swedish Atomic Committee.

Coulomb Excitation of Rare-Earth Nuclei with Alpha Particles*

N. P. HEYDENBURG AND G. M. TEMMER
Department of Terrestrial Magnetism, Carnegie Institution of Washington, Washington, D. C.
(Received May 16, 1955)

Using our doubly charged He beam at 6 Mev we have excited most low-lying (rotational) states in the nuclei between $Z=60$ and $Z=73$. Assignments were made with isotopically enriched targets where available. On the whole the predictions of the "strong coupling" approximation of the unified model are strikingly borne out by our observations. All 2^+ first-excited states of even-even nuclei lying below ~600 kev were observed, some of which were previously unknown. Two excited states were found in most odd-A nuclei as revealed by direct and/or cascade radiation to the ground state as well as coincidence measurements. The positions of the first two rotational levels agree with the simple interval rule in all established cases within the experimental accuracy. The majority of these states are not found in beta-ray spectroscopy. The reduced electric-quadrupole transition probabilities for all these transitions were measured and found to be some 50 to 100 times greater than those expected for an independent particle. Good agreement was found with some values of these quantities available from direct lifetime observations, giving us confidence in the correctness of both the theoretical expression for the total excitation cross section, and the experimental approach for its determination. A systematic decrease in these transition probabilities is evident in even-even nuclei upon approaching the closed-neutron shell at $N=82$; a corresponding increase in the energy of the 2^+ levels reflects the common origin of both phenomena, namely the decrease of the intrinsic deformation of the nuclei. However, the absolute magnitude derived for this deformation depends upon which manifestation is used.

Some evidence for a difference in splitting constants $\hbar^2/2\mathcal{I}$ between even-even, even-odd, and odd-even nuclei is found. Within the rather large uncertainties the transition probabilities do not seem to show a corresponding variation.

I. INTRODUCTION

DURING our initial survey of gamma radiation emitted by nuclei under low-energy alpha-particle bombardment,[1,2] it became apparent that some of the most strongly excited gamma rays occurred in the rare-earth region, mainly between neodymium ($Z=60$) and tantalum ($Z=73$). Some of the energy levels thus excited were known from beta- and gamma-ray spectroscopy; some of them had not been observed previously.

In a few cases the lifetimes of these transitions had been determined by fast coincidence techniques to be about 50 to 100 times faster than predicted on the basis of single-particle estimates. These so-called "fast $E2$" transitions have been known for some time[3]; they are, of course, particularly well suited to study by Coulomb excitation, since the cross section for this $E2$ process is then about 50 to 100 times greater than expected for "normal" $E2$ transitions. In fact, it was pointed out[4] before the discovery of Coulomb excitation that the latter process would especially favor the speeded-up electric quadrupole transitions which play such a prominent role in the unified description of the nucleus.

In one of our previous communications,[5] we have reported preliminary results on the rare-earth region, with particular emphasis on the level spacings observed in nuclei of odd mass number and their bearing on rotational interpretation. In the meantime, we were able to obtain most of the presently available enriched isotopes[6] in this region. This has led to confirmations (and some revisions) of previous level assignments, and has made it possible to obtain absolute cross-section measurements in most cases. From these measurements we can derive reduced transition probabilities, which can be compared with those derived from lifetime measurements.[7,8] Satisfactory agreement in the few cases where overlap of the two methods exists has given us confidence in our general approach. Trends in the sizes of the transition matrix elements bear out the general predictions of the "strong coupling" approximation of the unified model, to be discussed in Sec. IV.

What we observe, in general, can be summarized as follows: only one energy level, the first-excited state with spin 2^+, is excited in even-even nuclei, without exception. In odd-A nuclei, we usually find excitation of two energy levels with presumed spins I_0+1 and I_0+2, respectively, I_0 being the ground-state spin, all parities being the same.[9] Ideally we should then observe three gamma rays, representing transitions from these two states to the ground state, and the (cascade) transition between the two excited states. For technical reasons, however, we see all three gamma rays only in two cases (Eu^{153} and Ta^{181}); most of the time the cascade radiation is hidden by the very much stronger radiation

* A preliminary account of the results in this paper has been presented at the 1955 Annual Meeting of the American Physical Society at New York City [N. P. Heydenburg and G. M. Temmer, Phys. Rev. **98**, 1198(A) (1955)].

[1] G. M. Temmer and N. P. Heydenburg, Phys. Rev. **93**, 351 (1954).

[2] N. P. Heydenburg and G. M. Temmer, Phys. Rev. **93**, 906 (1954).

[3] M. Goldhaber and A. W. Sunyar, Phys. Rev. **83**, 906 (1951).

[4] A. Bohr and B. R. Mottelson, Kgl. Danske Videnskab. Selkab, Mat.-fys. Medd. **27**, No. 16 (1953).

[5] G. M. Temmer and N. P. Heydenburg, Phys. Rev. **94**, 1399 (1954).

[6] Obtained from the Isotopes Division, Oak Ridge National Laboratory, Oak Ridge, Tennessee.

[7] F. K. McGowan, Phys. Rev. **80**, 923 (1950); **85**, 151 (1952); **87**, 542 (1952).

[8] A. W. Sunyar, Phys. Rev. **95**, 626 (1954); **98**, 653 (1955).

[9] A. Bohr, dissertation, Copenhagen, 1954 (unpublished); also *Beta- and Gamma-Ray Spectroscopy*, edited by K. Siegbahn (North-Holland Publishing Company, Amsterdam, 1955), Chap. 17.

of only slightly lower energy from the first excited state. In some cases we only see one gamma ray, which may be associated with one of the three possibilities just mentioned; the other two lines may be hidden by lines from other contaminating isotopes or by the strong characteristic x-radiation excited directly by the incident charged particles, or following the internal conversion of Coulomb-excited gamma radiation. In the detailed discussion which follows in Sec. III we shall present evidence or arguments supporting one or another of these possibilities. In some odd nuclei no lines whatsoever were observed (La^{139}, Pr^{141}, Nd^{143}, Sm^{147}, Sm^{149}).

We have been able to assign all observed lines in $_{60}$Nd, $_{62}$Sm, $_{64}$Gd, and $_{72}$Hf by means of enriched isotopes; no problem exists in the monoisotopic, odd-A elements $_{65}$Tb, $_{67}$Ho, $_{69}$Tm, and $_{73}$Ta. The case of $_{63}$Eu is almost certainly settled even though it consists of two about equally abundant isotopes. The element $_{71}$Lu consists predominantly of isotope 175 (97.4 percent), the balance being occupied by the odd-odd isotope 176. Assignments in this case could be made plausible on the basis of abundance.

This leaves the even-Z elements $_{66}$Dy, $_{68}$Er, and $_{70}$Yb, for which no enriched isotopes are as yet available. We shall nevertheless present our results obtained with natural targets of these elements, since they will become useful as soon as assignments can be made. Because of the systematic behavior of the first-excited states of even-even nuclei[10,11] some fairly consistent identification of gamma rays can be made even for these poly-isotopic elements.

II. EXPERIMENTAL METHOD

A. Alpha-Particle Beam

We have previously described the general features of our experimental setup.[12] Throughout this work we used the doubly charged helium beam produced when singly-charged helium ions lose their second electron upon passing through an oxygen gas stripper[13] mounted some 300 kev below our rf ion source. The nominal beam energy was kept at 6 Mev by running the electrostatic generator at 3.15 Mev. The beam energy is believed to be known to ± 50 kev; the precise energy calibration of the beam must await comparison with some sharp resonances in this energy range determined elsewhere, or the completion of our electrostatic analyzer. The beam energy is known to sufficient accuracy for our present purposes. Most of our previously reported work[1,2,5,14] was done with our He^+ beam which is limited to energies below about 3.6 Mev. Although many of the levels discussed in this paper could be reached with this lower energy beam, the yield of gamma rays in the 200-kev region is increased by a factor of about 40, with correspondingly larger gains in intensity (and hence in accuracy) for higher energy levels, upon shifting to the 6-Mev beam. The beam currents we used ranged from 0.05 to 0.10 microampere, and were integrated in a Faraday cup.

B. Targets

We used thick oxide targets (except for Ta) which were prepared by compressing of the order of 100 mg of the salts into a standard one-half inch wide depression in a small aluminum target cup, thus assuring reproducible thicknesses of material to be traversed by the gamma radiation before it enters the scintillation crystal. An empirically determined self-absorption correction was applied to all observed gamma yields. The geometry was kept rigorously fixed by a tight-fitting Lucite spacer between the target cup and the front face of the aluminum can containing the $1\frac{3}{4}$ in.$\times 2$ in. NaI(Tl) crystal. In many cases we inserted from 0.010 in. to 0.025 in. of copper absorber between target and crystal to attenuate strong x-radiation or interfering low-energy gamma radiation from the targets, for which proper correction was, of course, made. For a schematic diagram of our experimental arrangement, we refer to Fig. 1 in reference 12. Since the solid angle subtended by the detector at the target is nearly 2π, no correction was necessary for anisotropy in the gamma emission.

We obtained an empirical conversion factor from the oxides to equivalent pure-element targets by comparing the gamma-ray yields of ordinary HfO_2 and Ta_2O_5 with metallic Hf and Ta targets. The ratio found in both cases was 0.50. We have assumed that the same ratio applies to all rare-earth oxides of the form X_2O_3, where X represents any rare-earth element. Changes in this factor over the interval $Z=60$ to $Z=73$ are expected to be small; consequently, all observed yields were multiplied by 2.0. As noted previously,[14] the only other major effect ascribable to the presence of oxygen in the target is the appearance of a gamma-ray line at 342 kev. We were able to show by means of a Ba_2CO_3 target enriched to 9 percent in O^{18}, that this line results from the $O^{18}(\alpha,n\gamma)Ne^{21}$ reaction, O^{18} having a natural abundance of 0.20 percent. Since the yield of this line was found to be rather independent of element over the rare-earth region, and is of course unaffected by isotopic enrichment, it serves as a valuable intensity marker for the intercomparison of the various targets. In the few instances where a Coulomb-excited line fell close to 340 kev, we were able to perform a satisfactory subtraction of the oxygen contribution. As a check, we also observed these gamma rays from 3-Mev proton excitation.

C. Energy and Intensity Measurements

The gamma-ray energies, determined by calibrating our system with a number of reference sources listed previously,[12] are believed to be reliable to ± 1 percent.

[10] G. Scharff-Goldhaber, Phys. Rev. **90**, 587 (1953).
[11] P. Stähelin and P. Preiswerk, Nuovo cimento **10**, 1219 (1953).
[12] N. P. Heydenburg and G. M. Temmer, Phys. Rev. **94**, 1252 (1954).
[13] J. W. Bittner, Rev. Sci. Instr. **25**, 1058 (1954).
[14] G. M. Temmer and N. P. Heydenburg, Phys. Rev. **96**, 426 (1954).

The absolute thick-target yields were obtained as follows: first, a thin source of Au^{198} calibrated in a 4π absolute beta counter at the National Bureau of Standards,[15] was placed at the target position, and the intensity under the photoelectric peak produced by the 411-kev gamma ray was determined. Knowing the absolute disintegration rate of the source we immediately obtain the effective photopeak efficiency of our system for a gamma ray of this energy (8.87 percent). The relative effective photopeak efficiencies for gamma rays of different energies were determined by referring to some semiempirical results obtained by a Swiss group.[16] We can then calculate all the transition probabilities in the manner to be described below. We find good agreement with the known transition probability[17] for the 136-kev transition in tantalum, as well as with those obtained from lifetime measurements where available.

We should like to point out that at no time did we find evidence of continuous gamma radiation (bremsstrahlung)[18] produced by alpha particles in the targets, so that no correction had to be made for such an effect. This is evident from our pulse-height distributions[1,14] and is in keeping with the dependence of the bremsstrahlung cross section on charge and mass of the projectile.[18] Direct background radiation from our generator was also found negligible; the only background for which we had to correct was that produced by Coulomb-excited gamma rays of higher energy than the one of interest.

D. Extraction of Transition Probabilities

The thick-target yields were reduced to thin-target cross sections as follows: We start with the expression for the $E2$ Coulomb excitation cross section as given by Alder and Winther[19]

$$\sigma=(2\pi^2/25)(m^2v_f^2/Z_2^2e^2\hbar^2)g_2(\xi)B(E2), \qquad (1)$$

where $g_2(\xi)$ is a numerically tabulated function of the adiabatic parameter

$$\xi=\frac{Z_1Z_2e^2}{\hbar}\left(\frac{1}{v_f}-\frac{1}{v_i}\right),$$

v_f is the final projectile velocity after collision, v_i is the initial projectile velocity, $B(E2)$ is the sought-after reduced $E2$ (upward) transition probability, ΔE is the energy of the excited state above the ground state, Z_1 and Z_2 are the charges of the projectile and target nucleus, respectively, and m is the projectile mass.

The adequacy of expression (1) for the total excitation cross section has been recently demonstrated theoretically[20,21] and supported experimentally.[1,14] For the sake of simplicity we shall use the approximation $\Delta E/E\ll 1$, a condition which is rather well satisfied for our bombarding energy, and level energies below $\sim$300 kev [for $\Delta E>300$ kev, expression (1) was used]; upon inserting numerical constants appropriate for alpha particles, Eq. (1) can be written

$$\sigma(E)\cong(15.1E/Z_2^2)g_2(\xi)B(E2), \qquad (2)$$

where $B(E2)$ is expressed in 10^{-48} cm^4,[22] $\sigma(E)$ in barns, and E in Mev, and ξ is now given by

$$\xi\cong(Z_1Z_2e^2/\hbar v)(\Delta E/2E). \qquad (3)$$

Expression (2) must now be integrated along the track of the slowing-down incident particle. We make the following assumptions[23] concerning the dependence of the stopping power on particle energy and the atomic number Z_2 of the target:

(a) the stopping power, dE/dx, varies as $E^{-\frac{1}{2}}$;

(b) the stopping power *per atom* varies as $Z_2^{\frac{1}{2}}$.

These assumptions are in keeping with experiments on the stopping powers at low energies.[24–26] Since $g_2(\xi)$ is a very steep function of projectile energy, most of the yield is produced at the beginning of the alpha-particle track, and the thick-target yields turn out to be rather insensitive to the details of assumption (a) (see below). Since the range in atomic numbers for the targets studied here is small, not much error can be introduced by any slight departures from assumption (b). If we denote by a subscript zero those quantities referring to the incident particle energy, we obtain the following expression for the thick target yield:

$$Y=N\sigma(E_0)\left[\frac{E_0y(\xi_0)}{(dE/dx)_0}\right], \qquad (4)$$

where $y(\xi_0)$ stands for a numerical integral given by

$$y(\xi_0)=\tfrac{3}{2}\xi_0^{5/3}\frac{1}{g_2(\xi_0)}\int_{\xi_0}^{\infty}\frac{g_2(\xi)}{\xi^{8/3}}d\xi, \qquad (5)$$

and N is the number of target atoms per cc. The factor in brackets occurring in Eq. (4) evidently represents an equivalent target thickness. $\sigma(E)$ is given by Eq. (2) [or Eq. (1) when $\Delta E>300$ kev]. In Table I, we list some representative numerical values of the function

[15] We are indebted to L. Cavallo and H. H. Seliger for this calibration.
[16] Maeder, Müller, and Wintersteiger, Helv. Phys. Acta **27**, 3 (1954).
[17] Alder, Bohr, Huus, Mottelson, Winther, and Zupančič, Revs. Modern Phys. (to be published).
[18] C. Zupančič and T. Huus, Phys. Rev. **94**, 205 (1954).
[19] K. Alder and A. Winther, Phys. Rev. **96**, 237 (1954); see also reference 17.
[20] G. Breit and P. B. Daitch, Phys. Rev. **96**, 1447 (1954).
[21] L. C. Biedenharn and C. M. Class, Phys. Rev. **98**, 691 (1955).
[22] It is understood throughout this paper that the quantity $B(E2)$ has been divided by e^2.
[23] Suggested by T. Huus and B. R. Mottelson (private communication).
[24] C. B. Madsen, Kgl. Danske Videnskab. Selskab, Mat.-fys. Medd. **27**, No. 13 (1953).
[25] Chilton, Cooper, and Harris, Phys. Rev. **93**, 413 (1954).
[26] J. Lindhard and M. Scharff, Kgl. Danske Videnskab. Selskab, Mat.-fys. Medd. **27**, No. 15 (1953).

TABLE I. Numerical values of the thick-target function $y(\xi_0)$ vs the adiabatic parameter ξ_0. $y(\xi_0)$ is defined in Eq. (5).

ξ_0	0.0	0.1	0.2	0.3	0.4	0.6	0.8	1.0	1.2	1.4	1.6	1.8	2.0
$y(\xi_0)$	0.400	0.366	0.260	0.213	0.178	0.135	0.108	0.0903	0.0768	0.0674	0.0602	0.0579	0.0540

$y(\xi_0)$ for a series of values of ξ_0.[27] It turns out that if we had assumed a *constant* stopping power instead of assumption (a), the value of $y(0)$, where the maximum discrepancy is to be expected, would have been 0.500 instead of 0.400. The value of $(dE/dx)_0$ we used for tantalum was 197 Mev-cm²/g. Stopping powers for the other targets were computed from this value according to assumption (b) above, and are found in Table II.

Upon inserting (2) into expression (4) we can solve for $B(E2)$; using appropriate numerical constants, we obtain:[28]

$$B(E2)=\frac{AZ_2^2(dE/dx)_0Y}{9.06E_0^2g_2(\xi_0)y(\xi_0)}\times10^{-48}\ \text{cm}^4, \qquad (6)$$

where A is the atomic weight of the target, $(dE/dx)_0$ the stopping power of the target (for alphas) in Mev-cm²/g, E_0 the incident energy in Mev, and Y is the yield of excited nuclei per incident particle. All other quantities were defined above.

Some remarks are in order concerning the meaning of $B(E2)$. In accordance with a convention adopted in a review article on Coulomb excitation,[17] we shall denote by $\epsilon B(E2)$ for a given gamma ray, the quantity obtained when inserting the experimental thick-target yield of gamma radiation into expression (6). The quantity ϵ, which is of necessity always less than unity, contains the following factors which must still be removed before we arrive at a theoretically meaningful transition probability:

(a) The total internal conversion coefficient α_t; the experimental quantity $\epsilon B(E2)$ must be multiplied by $(1+\alpha_t)$ to obtain the total excitation of a given level. This is an important correction for almost all rare-earth levels we observe. Unfortunately, empirical information in this transition-energy region on K-conversion as well as K/L conversion ratios is scanty,[3,7,8] and theoretical tabulations presently available require rather daring extrapolation.[28,29] A further complication exists in the case of odd-A transitions which involve mixtures of $M1$ and $E2$ radiation; knowledge of this mixture is essential for a determination of internal conversion, and is very scarce in the rare-earth region, especially since many of the transitions are seen only in Coulomb excitation. A number of the transitions have been observed by Huus[30] using conversion-electron detection, so that in principle, at least, total conversion coefficients could and should be determined experimentally.

(b) In the case of odd-A nuclei, where the second rotational state is often excited, a branching correction must also be made. As was mentioned above, the cascade transition from second- to first-excited state is usually not observed, but its strength (corrected for internal conversion) must be added to the direct ground-state transition in order to give a true representation of the total excitation of the second level. In the case of Ta^{181}, for instance, the 167-kev cascade is stronger than the direct 303-kev transition.[17] These branching ratios are of special theoretical interest, since they are connected with the gyromagnetic ratio of collective flow, g_R[4,9] a quantity which is not otherwise obtainable (see Sec. IV-B below). Unfortunately, our results are meager on this score, because of insufficient resolution of scintillation counters. It is hoped that methods capable of higher resolution, such as internal-conversion spectrometry and possibly bent-crystal spectrography will contribute more of these branching ratios. In view of the existing uncertainties discussed above, we only feel justified in reporting values of $\epsilon B(E2)$ *uncorrected* for either (a) or (b) except for the few cases where comparison can be made with values obtained from lifetime measurements.[7,8] Whenever total internal conversion coefficients and branching ratios become available from experiment in the future, the factor ϵ can readily be removed.†

E. Accuracy

A few words should be said concerning the reliability of our quantities $\epsilon B(E2)$. Uncertainties due to counting statistics alone are always negligible. While it is difficult to ascertain the errors inherent in the reduction of our results, we feel that in view of such evidence as the rather good agreement of our results with lifetime measurements, our error in the absolute value of any given transition probability can be conservatively fixed at ±30 percent. The relative error between the isotopes of one element or even neighboring elements is estimated at ±15 percent. In general, lines giving rise to stronger photopeaks are inherently more reliable than weak lines; lines that are more completely resolved from their neighbors also yield better values.

III. RESULTS

In Table II we have collected our experimental results for the rare-earth region. We list, in turn: the element;

[27] We are indebted to T. Huus for furnishing these values.
[28] Rose, Goertzel, Spinrad, Harr, and Strong, Phys. Rev. **83**, 79 (1951); Rose, Goertzel, and Swift (privately circulated tables).
[29] Gellman, Griffith, and Stanley, Phys. Rev. **85**, 944 (1952).
[30] T. Huus (private communication).

† *Note added in proof.*—A. W. Sunyar has kindly furnished estimates of the total $E2$ conversion coefficients for our even-even transitions (cf. reference 8). Using these, we have evaluated nuclear deformations for even-even nuclei, which have recently been published in this Journal [Phys. Rev. **99**, 1609 (1955), especially Fig. 1].

TABLE II. Summary of results on Coulomb excitation of rare-earth nuclei by 6-Mev alpha particles. For explanation of symbols used in the column headings, see text. Entries in parentheses are tentative assignments.

Element	A	Abundance (%)	I_0	E_γ (kev)	ξ_0	$g_3(\xi_0)$	$\gamma(\xi_0)$	$(dE/dx)_0$[a] (Mev-cm²/g)	$aB(E2)$ (10^{-48} cm⁴)
$_{60}$Nd	145	78.60[b]	7/2	70	0.0925	1.08	0.368	224	~0.03
	146	17.2	0+	455	0.640	0.200	0.126	224	0.84
	148	89.85[b]	0+	300	0.412	0.49	0.171	224	1.50
	150	5.6	0+	128	0.169	0.96	0.283	224	1.24
$_{62}$Sm	148	72.73[b]	0+	562	0.826	0.086	0.105	218	2.06
	150	68.04[b]	0+	337	0.480	0.385	0.154	218	2.32
	152	26.8	0+	122	0.166	0.97	0.288	218	1.36
	154	22.7	0+	82	0.112	1.05	0.350	218	0.48
$_{63}$Eu	(151)	47.8	5/2	310	0.447	0.436	0.162	218	0.64
	153	52.2	5/2	82	0.114	1.05	0.348	218	0.36
				105[c]	0.259	0.80	0.229	218	0.15[c]
				187	0.259	0.80	0.229	218	0.49
$_{64}$Gd	154	2.15	0+	123	0.173	0.96	0.282	213	2.10
	155	72.28[b]	(7/2)	145	0.204	0.90	0.258	213	0.112
	156	20.5	0+	89	0.125	1.02	0.332	213	1.24
	157	69.68[b]	(7/2)	131	0.184	0.93	0.272	213	0.083
	158	24.9	0+	79	0.111	1.06	0.350	213	1.02
	160	21.9	0+	76	0.107	1.07	0.355	213	~1
$_{65}$Tb	159	100	3/2	79[c]	0.194	0.92	0.265	212	0.19[c]
				136	0.194	0.92	0.265	212	0.041
$_{66}$Dy[d]	161	97.6	(7/2)	76	0.110	1.06	0.351	208	0.23[d]
	162		0+						
	163		(7/2)						
	164		0+						
	(161)	43.9	(7/2)	166	0.240	0.84	0.239	208	0.29[d]
	(163)		(7/2)						
$_{67}$Ho	165	100	7/2	94	0.138	1.01	0.318	207	0.54
				206	0.312	0.69	0.206	207	0.036
$_{68}$Er[d]	162	100	0+	79	0.118	1.04	0.341	206	0.48[d]
	164		0+						
	166		0+						
	167		7/2						
	168		0+						
	170		0+						
	(167)	22.9	7/2	172	0.256	0.81	0.230	206	0.081[d]
$_{69}$Tm	169	100	1/2	109[c]	0.182	0.94	0.275	205	1.12[c]
$_{70}$Yb[d]	170	85.7	0+	78	0.120	1.03	0.340	202	0.28[d]
	172		0+						
	173		5/2						
	174		0+						
	176		0+						
	(171)	14.3	1/2	110	0.169	0.96	0.286	202	0.20[d]
	(173)	16.1	5/2	180	0.276	0.77	0.221	202	0.086[d]
$_{71}$Lu	175	97.4	7/2	114	0.177	0.96	0.280	201	0.72
				250	0.402	0.51	0.175	201	0.20
	(176)	2.6	>9	180	0.280	0.76	0.220	201	(1.14)
$_{72}$Hf	176	59.45[b]	0+	87	0.137	1.01	0.320	198	0.56
	177	59.08[b]	?	112	0.176	0.96	0.280	198	0.77
				250	0.408	0.50	0.172	198	0.55
	178	31.73[b]	0+	90	0.142	1.00	0.311	198	0.85
	179	53.32[b]	?	119	0.187	0.92	0.272	198	0.67
				260	0.424	0.47	0.169	198	0.056
	180	44.20[b]	0+	93	0.146	0.99	0.309	198	0.78
$_{73}$Ta[e]	181	100	7/2	136	0.218	0.88	0.241	197	0.70
				167[c]	0.504	0.353	0.149	197	~0.13[c]
				303	0.504	0.353	0.149	197	0.15

[a] Stopping power for pure element.
[b] Isotopically enriched target used; all other assignments from natural targets.
[c] Cascade radiation from second rotational state, whose ΔE is used in computation of ξ_0.
[d] Preliminary assignments until enriched isotopes become available; see text.
[e] Metallic target; all others are oxides of the form X_xO_y (except HfO_2).

mass number of the responsible isotope; relative abundance (either in the natural, or the enriched sample where used); spin of the ground state, I_0; gamma-ray energy in kev (equal to level energy except where otherwise noted); ξ_0; $g_2(\xi_0)$; $y(\xi_0)$; $(dE/dx)_0$ in Mev-cm^2/g; and $\epsilon B(E2)$ in 10^{-48} cm^4.[22] The last five quantities were defined in Sec. II-B. The quantities $\epsilon B(E2)$ listed have been corrected for the presence of oxygen in the targets and brought up to 100 percent, using the appropriate abundances. $(dE/dx)_0$ refers to the stopping power in the pure elements. For targets where no enriched isotopes were available, the abundance correction is made as described below in more detail for the various elements.

A. Lanthanum ($Z=57$)

This element is monoisotopic and consists of the nucleus La^{139}.[21] A careful search failed to reveal the 166-kev transition which is known from the decay of Ce^{139} (or any others). Internal conversion data ascribe an $M1$ character to this radiation.[22] Recent results from low-temperature nuclear alignment of Ce^{139} support this assignment, although a small amount of $E2$ admixture seems indicated.[23] From the negative Coulomb excitation results we can conclude that the $E2$ transition probability (if any) is about two orders of magnitude smaller than in the stronger rare-earth cases, i.e., of the order of the single-particle transition strength. The fact that La^{139} contains a magic number of neutron ($N=82$) is undoubtedly related to this observation.

B. Cerium ($Z=58$)

This element consists entirely of even-even isotopes, the predominant one again having 82 neutrons (Ce^{140}, 88.5 percent) and a known first-excited 2^+ state at 1.61 Mev. We therefore observe no gamma rays from Ce (1.6 Mev is far too high an energy to be excited with 6 Mev alphas) as pointed out previously[2]; the low-energy gamma rays we saw are undoubtedly due to rare-earth impurities.

C. Praseodymium ($Z=59$)

A careful re-examination of monoisotopic Pr^{141} did not yield the 145-kev gamma ray known from the beta decay of Ce^{141}. As in the case of La^{139}, low-temperature nuclear alignment experiments have been carried out on Ce^{141} which establish the transition as $M1$, with an $E2$ admixture of about 4 percent.[24] Pr^{141} is another "magic" nucleus with 82 neutrons. Our negative result again shows the single-particle character of this $7/2^+ \rightarrow 5/2^+$ transition, with no effective competition to $M1$ radiation from $E2$ radiation.

D. Neodymium ($Z=60$)

For this element we had enriched targets of both odd-A isotopes Nd^{143} and Nd^{145}, and the even-even isotope Nd^{148}. This permitted us to assign new 2^+ first-excited states to Nd^{148} and Nd^{150} at 300 kev and 128 kev, respectively, as well as to observe the 455-kev state in Nd^{146}. The newly found transitions are shown in Fig. 1. Because of the rapid rate of change of excitation energy with neutron number in this region, we could excite no levels in Nd^{142} and Nd^{144}. A gamma transition of 70 kev, rather weak compared to most rare-earth transitions, was found associated with Nd^{145}, while no gamma rays at all were found to belong to Nd^{143}. The transitions in Nd^{145} and Nd^{150} have since been studied with protons as well.[25]

The trend in the values of $\epsilon B(E2)$ as we go from Nd^{146} to Nd^{150} is worthy of note. The internal conversion corrections are small except for the 128-kev transition whose intensity should be multiplied by a factor of about 2. We see the monotonic increase in the matrix elements as we move away from the closed neutron shell at $N=82$, an effect which can be related to the decrease in excitation energy of the first-excited states (see Sec. IV). A particularly large break in excitation energy occurs between neutron numbers 88 and 90 (300 kev to 128 kev). As we shall see in Sec. III-E this break also exists in samarium.

E. Samarium ($Z=62$)

Figure 2 shows the pulse-height distribution produced by gamma rays of 122 and 82 kev from the first-excited states of the even-even nuclei Sm^{152} and Sm^{154}, respectively, as obtained with a natural target of Sm_2O_3.

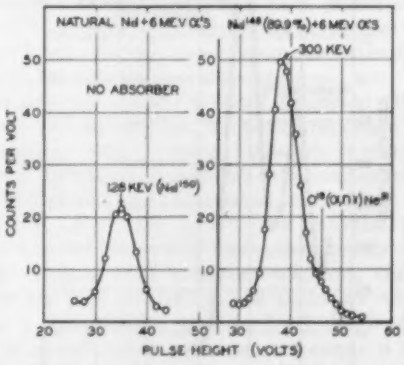

FIG. 1. Coulomb excitation of $_{60}$Nd with 6-Mev alphas. Pulse-height distributions: ordinary Nd (left) showing 128-kev line from Nd^{150} (5.6 percent); Nd enriched to 89.9 percent Nd^{148} (right) showing 300-kev line in that isotope. Location of 342-kev gamma from O$^{18}(\alpha,n\gamma)$Ne^{21} is indicated (see Sec. II-B). Both are newly discovered energy levels; 455-kev level in Nd^{146} observed but not shown. No absorber used.

[21] Except for a negligible amount of the odd-odd nucleus La^{138} (0.089 percent).
[22] C. R. Pruett and R. G. Wilkinson, Phys. Rev. **96**, 1340 (1954).
[23] Ambler, Hudson, and Temmer (private communication).
[24] Ambler, Hudson, and Temmer, Phys. Rev. **97**, 1212 (1955), and Phys. Rev. (to be published).
[25] Simmons, Van Patter, Famularo, and Stuart, Phys. Rev. **97**, 89 (1955).

Figure 3 similarly shows the de-excitation gamma radiation of the first-excited 2^+ states at 562 kev and 337 kev in enriched targets of Sm^{148} and Sm^{150}, respectively. Although the 337-kev line is superimposed upon the 342-kev "oxygen" line (see Sec. II-B), its intensity can easily be found by subtracting the oxygen contribution of a neighboring rare-earth oxide. The dotted curve illustrates the magnitude of this contribution. Our observation of these four lines again confirms the spin and parity of the first-excited states in these nuclei as 2^+ and illustrates the systematic trend of their excitation energies. A particularly large jump in excitation energy is again found between neutron number 88 and 90 (337 kev to 122 kev), just as in neodymium (Sec. III-D). Additional evidence has been pointed out for a major rearrangement at neutron number 88, such as an abrupt change in the ratio of second to first-excited state energies in even-even nuclei from a value near 2 to a value near 3.33,[35] the latter being the ratio predicted by the "strong coupling" approximation of the unified model (see Sec. IV).

Although we had available enriched targets of both odd-A isotopes of Sm ($A=147$ and $A=149$), we observe no gamma rays associated with these nuclei. We can set an upper limit on the intensity of any levels in the odd nuclei of Sm of about 2 percent of that of the levels in the even-even nuclei.

It is again interesting to note the trend in the quantity $\epsilon B(E2)$ for the four even nuclei. We must remember the internal conversion correction (Sec. II-E), which raises $\epsilon B(E2)$ for the 122-kev transition by a factor of about 2, and that for the 82-kev transition

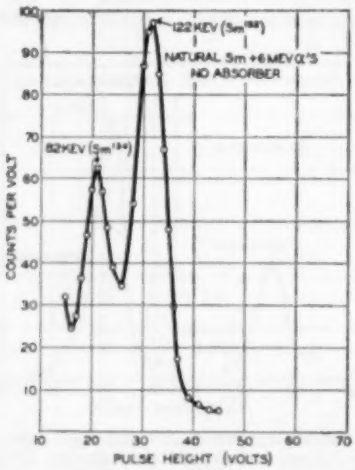

FIG. 2. Coulomb excitation of $_{62}$Sm with 6-Mev alphas. Pulse-height distribution for ordinary Sm showing first-excited state gamma transitions at 82 kev in Sm^{154} (22.7 percent) and at 122 kev in Sm^{152} (26.8 percent). No absorber used.

[36] G. Scharff-Goldhaber and J. Weneser, Phys. Rev. **98**, 212 (1955).

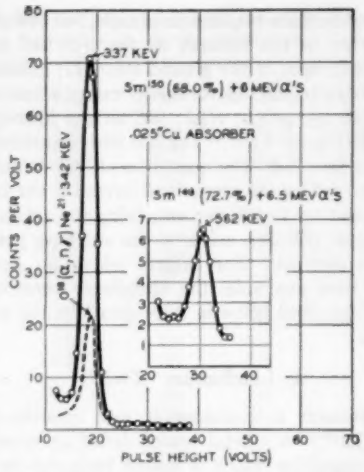

FIG. 3. Coulomb excitation of $_{62}$Sm with alphas. Pulse-height distributions: enriched Sm^{150} (68.0 percent)+6-Mev alphas showing 337-kev transition (left); enriched Sm^{148} (72.7 percent) +6.5-Mev alphas showing 562-kev transition (right). Dashed curve indicates amount of 342-kev radiation contributed by the $O^{18}(\alpha,n\gamma)Ne^{21}$ reaction (see Sec. II-B). 0.025 in. Cu absorber used.

by a factor of about 8. The transition probability is then seen to vary inversely with the excitation energy.

The case of Sm^{152} is of special importance, because the lifetime of the 122-kev transition has actually been measured by fast coincidence techniques.[8] From the value of the half-life ($=1.4\times10^{-9}$ second), corrected for internal conversion (Sunyar estimates $\alpha_t=1.27$[8]), and Weisskopf's formula for the probability for electric quadrupole radiation,[37] we obtain a *downward* $B(E2)$ of 0.66.[38] This corresponds to an *upward* $B(E2)$ of 3.3 the statistical factor $(2I_f+1)/(2I_i+1)$ being 5 in this case. Using our value for $\epsilon B(E2)$ of 1.36, we obtain $B(E2)=3.1$ after multiplication by $(1+\alpha_t)$; this is in very gratifying agreement with the value obtained from the lifetime measurement.

F. Europium ($Z=63$)

Europium consists of two odd-A isotopes, Eu^{151} (47.8 percent) and Eu^{153} (52.2 percent). Our early investigation of Eu targets[3] revealed three gamma rays at 82 kev, 105 kev, and 187 kev. Figure 4 shows the gamma-ray spectra observed through varying thicknesses of absorber. By using two NaI crystals and two single-channel pulse-height selectors in coincidence, one set on the photopeak of the 82-kev line and the other at varying pulse-height settings, we obtained a coincidence maximum at about 105 kev, showing that some of the 82-kev radiation was indeed in cascade with the 105-kev gamma ray, and establishing the decay scheme shown in the insert of Fig. 4. This represents a well-

[37] V. F. Weisskopf, Phys. Rev. **83**, 1073 (1951).

[38] $E2$ transition probabilities always expressed in units of 10^{-48} cm^4.

developed rotational spectrum, as we shall discuss below. Although we have shown that all three gamma rays belong to the same nucleus we could not identify the responsible isotope, since enriched Eu^{153} is as yet unavailable. However, in the meantime the 82-kev transition[39] has been looked for and found to be very weakly excited in the conversion-electron spectrum following the beta decay of Sm^{153},[39,40] so that the assignment of the system of levels to Eu^{153} is almost certain. Note that the quantity $\epsilon B(E2)$ for the 105-kev cascade radiation is computed using a value of ξ_0 appropriate for an excitation energy of 187 kev.

Recently we discovered an additional gamma ray of 310 kev, which we have temporarily assigned to the isotope Eu^{151}, mainly because some slight evidence for a 0.265-kev gamma ray (determined by absorption) following the decay of Gd^{151} is found in the literature.[41] Note that the two Eu isotopes are also straddling the gap between $N=88$ and $N=90$, a fact which might be related to the existence of a strong rotational spectrum in one but not the other nucleus.

G. Gadolinium ($Z=64$)

Figure 5 shows the gamma-ray spectra from ordinary Gd and the odd-A isotopes Gd^{155} and Gd^{157}. The 123-kev line belongs to Gd^{154},[42] whose natural abundance is only 2.15 percent. The large composite peak at around 80 kev is due to the even-even isotopes Gd^{156}, Gd^{158}, and Gd^{160}, whose first-excited state energies are known to be 89 kev, 79 kev,[42] and 76 kev,[30] respectively. The shifts in the peak position, and changes in peak width as well as height in the three targets of Fig. 5 are satisfactorily accounted for by their isotopic compositions; for instance, the target enriched in Gd^{155} contains 17.7 percent Gd^{156}, 2.9 percent Gd^{158}, and 0.81 percent Gd^{160}. This explains the narrower half-width of the photopeak from this target, as well as its peak value of 87 kev. We were able to obtain transition probabilities for all isotopes but Gd^{152} (0.20 percent) and Gd^{160}; the latter has a value of about the same order as Gd^{158}, but could not be accurately determined with the enriched targets at our disposal.

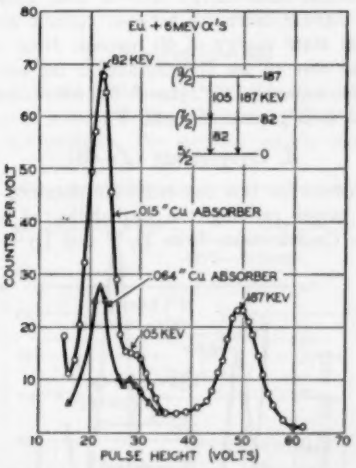

FIG. 4. Coulomb excitation of $_{63}Eu$ with 6-Mev alphas. Pulse-height distribution for ordinary Eu shows lines at 82 kev, 105 kev, and 187 kev. 0.015 in. Cu absorber used; low-energy portion of spectrum also shown as seen through 0.064 in. Cu absorber. Coincidence experiment establishes decay scheme shown as insert. Excited isotope is probably Eu^{153} (see Sec. III-F), 310-kev line also observed (not shown).

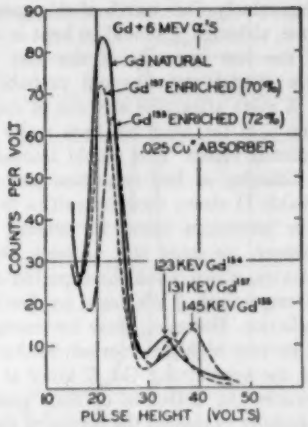

FIG. 5. Coulomb excitation of $_{64}Gd$ with 6-Mev alphas. Pulse-height distributions: ordinary Gd showing 123-kev state in Gd^{154} (2.15 percent); enriched Gd^{155} (72.3 percent) showing state at 145 kev; enriched Gd^{157} (69.7 percent) showing state at 131 kev. Large composite peak around 80 kev is due to varying amounts of Gd^{156} (89 kev), Gd^{158} (79 kev), and Gd^{160} (76 kev) in the three targets. Note low intensity of 131-kev and 145-kev lines (see Sec. III-G). 0.025 in. Cu absorber used.

The two new lines in the odd-A isotopes at 131 kev and 145 kev represent an unexpected departure from the so-called "strong coupling" situation in rotational spectra; unexpected because we found well-developed rotational levels in odd-A nuclei on either side of $_{64}Gd$, namely in $_{63}Eu^{153}$ and $_{65}Tb^{159}$. The transition probabilities in Gd^{155} and Gd^{157} are about twenty times weaker than in their even-even neighbors, and the companion lines expected in odd nuclei are missing. Using a ground-state spin $I_0=7/2$,[43] the predicted ratio of second- to first-rotational state energy is 2.22;‡ if the discovered lines represent the first rotational states, the companion states should lie at 291 kev and

[39] N. Marty, Compt. rend. **238**, 2516 (1954).
[40] E. L. Church (private communication).
[41] R. E. Hein and A. F. Voigt, Phys. Rev. **79**, 783 (1950).
[42] E. L. Church and M. Goldhaber, Phys. Rev. **95**, 626 (1954).
[43] $I_0 \geq 5/2$ according to K. Murakawa, Phys. Rev. **96**, 1543 (1954).

‡ *Note added in proof.*—Recent hyperfine structure evidence shows the spin of the odd Gd nuclei to be 3/2 [F. A. Jenkins and D. R. Speck, Bull. Am. Phys. Soc. **30**, No. 5, 27 (1955)]; the appropriate ratio is then 2.40, and the situation is similar to Tb^{159} (Sec. III-H).

322 kev, respectively. Our search of this energy region revealed none, although it should be kept in mind that because of the low intensity of the first rotational states, these second states would probably be undetectable. A more attractive way out of the dilemma is to assume that the observed lines really represent *second* rotational states. This would immediately remove the difficulty of low transition probability. A glance at Table II shows their intensities to be of the order of the intensities found for second rotational states. However, we must still account for the first rotational states, which would be expected at 59 kev, and 65 kev, respectively.§ We found no direct evidence for such radiation. However, these low-energy gamma rays would be very highly converted; furthermore, the nearness of the very strong Gd K x-ray at about 44 kev complicates the detection of such gamma rays. We have carefully examined the profile of the K x-ray in the target enriched in Gd^{155} where a 65-kev line might be expected, and conclude that such a line might indeed be hidden in the tail of the x-ray peak. A strong piece of evidence in this direction is the fact that the K x-ray line from the odd-A targets was considerably (~50 percent) stronger than from the ordinary Gd target. Since the direct excitation of target x-rays is of course independent of isotopic composition, and since approximately the same visible amount of gamma radiation producing K x-rays following internal conversion exists in all three Gd targets, the excess K x-radiation from the odd-A targets is most easily explained by the presence of a strongly converted gamma transition which is itself hidden in the wing of the x-ray peak. For a similar situation where the facts are actually established we refer to the next element, Tb^{159} (Sec. III-H). The most direct confirmation of the correctness of our interpretation of the odd Gd spectra will, as in the case of Tb, have to come from an observation of internal conversion electrons.

The lifetime of the 123-kev transition in Gd^{154} is known directly.[8] Again using Sunyar's estimate for the total internal conversion coefficient ($\alpha_t = 1.42$),[8] we calculate an upward transition probability $B(E2) = 3.4$. From our excitation data we obtain a value of 5.1. This represents a larger discrepancy than found in the other cases where comparison is possible. The most likely reason for this is to be found in the fact that our result here was obtained from natural Gd, of which Gd^{154} constitutes only 2 percent.

H. Terbium ($Z = 65$)

The gamma-ray spectrum we observe for monoisotopic Tb^{159} is shown in Fig. 6. The two transitions at 79 kev and 136 kev do not fit a rotational scheme; however, the energy difference of 57 kev together with the 136-kev gamma ray constitute a perfect rotational spectrum, with an energy ratio of 2.39. The theoretically expected ratio for the case of ground-state spin $I_0 = \frac{3}{2}$ is 2.40. It turns out that Huus[30] finds a very strong conversion-electron line at 57 kev in Tb. We have checked the ratio of intensities of the 79-kev and 136-kev gamma ray and found it to remain constant between 3-Mev and 6-Mev bombarding energy. Had the 79-kev gamma ray originated at a 79-kev level, this intensity ratio would have changed by a factor of about three in favor of the 136-kev radiation. This proves that the 79-kev line originates at the 136-kev level and is the cascade to the 57-kev level. Hence the level scheme shown in the insert of Fig. 6 is established. It represents a perfect example of a rotational spectrum. In computing $\epsilon B(E2)$ for the 79-kev cascade radiation, we used the value of ξ_0 appropriate for an excitation of 136 kev.

The reason for our inability to detect the 57-kev gamma radiation is its high internal conversion and its nearness to the 46-kev x-radiation, which is itself enhanced by the internal conversion process. In spite of very careful examination of the 57-kev region with critical absorbers we were not able to detect the radiation from the first rotational state. The cascade radiation is so clearly resolved in this case for two reasons: (a) the second rotational state has a comparatively low energy so that it is strongly Coulomb-excited; (b) the ground-state spin of $\frac{3}{2}$ is the lowest one giving rise to an ordinary rotational spectrum,[9] with the maximum second-to-first state energy ratio of 2.40. This means that we have a difference between cascade and first-rotational state energy of 40 percent. Note that we were also able to see the cascade in the next most favorable cause of Eu^{153} ($I_0 = 5/2$), where the latter difference is 29 percent (Sec. III-F).

I. Dysprosium ($Z = 66$)

Our results for this element were obtained from a natural target pending the availability of enriched isotopes. Contributions from Dy^{156} and Dy^{158} can be

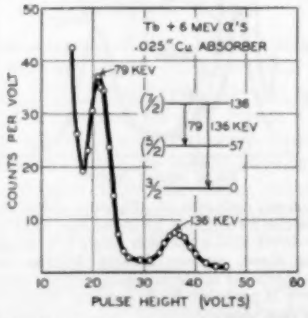

FIG. 6. Coulomb excitation of $_{65}Tb^{159}$ with 6-Mev alphas. Pulse-height distribution shows gamma rays at 79 kev and 136 kev, whose relative intensity is *independent* of bombarding energy, establishing decay scheme shown as insert (see Sec. III-H). 0.025 in. Cu absorber used.

§ *Note added in proof.*—With $I_0 = 3/2$, these values are 55 and 60 kev, respectively.

neglected because of their low abundances (0.05 and 0.09 percent, respectively). This leaves a total of about 53 percent for the even-even isotopes 162 and 164, and about 44 percent for the odd-A isotopes 161 and 163. The only excited state known definitely in Dy is the 86-kev level in Dy^{160} whose lifetime is known,[7] but which we did not observe in natural Dy (only 2.3 percent Dy^{160}). We find a strong, undoubtedly composite peak at around 76 kev, which we shall temporarily assume to belong to both even-even isotopes (Dy^{162} and Dy^{164}) and both odd-A isotopes for the purpose of calculating $\epsilon B(E2)$ It is reasonable to expect little change in the position of the first-excited states of the even-even nuclei in view of such behavior of these states in elements on both sides of Dy (see Gd and Hf, Secs. III-G and III-O). Hence there is little doubt that the line at 166 kev must belong to one or both odd-A isotopes, and represents their second rotational state. We temporarily make our abundance correction as if both Dy^{161} and Dy^{163} share the 166-kev level. We assume a tentative value of $I_0=7/2$ for these nuclei.[44]

J. Holmium ($Z=67$)

Figure 7 shows the gamma spectrum observed in monoisotopic Ho^{165}, and its level scheme. This again represents a well-developed rotational spectrum for a nucleus of spin 7/2. The 94-kev first-excited state is probably the one previously found in the decay of Dy^{165}, although its spin assignment is more likely to be 9/2 than 5/2.[45]

K. Erbium ($Z=68$)

Our results for this element are again based on bombardment of a natural target because of unavailability of enriched isotopes. The element mainly consists of

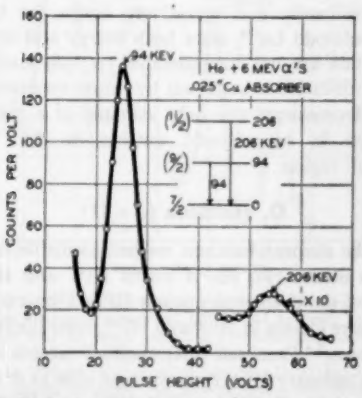

FIG. 7. Coulomb excitation of $_{67}Ho^{165}$ with 6-Mev alphas. Pulse-height distribution shows transitions at 94 kev and 206 kev. Decay scheme shown as insert. 0.025 in. Cu absorber used.

[44] K. Murakawa and T. Kamei, Phys. Rev. **92**, 325 (1953).
[45] M. Goldhaber and R. D. Hill, Revs. Modern Phys. **24**, 179 (1952).

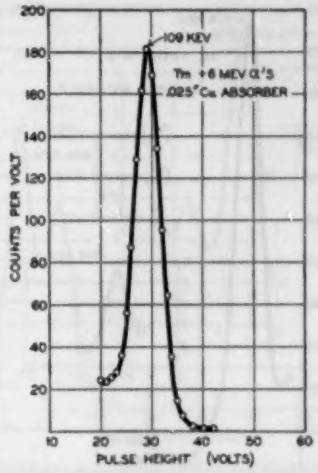

FIG. 8. Coulomb excitation of $_{69}Tm^{169}$ with 6-Mev alphas. Pulse-height distribution shows a single peak at 109 kev, probably representing a cascade transition from a 120-kev level (see Sec. III-L). This nucleus has $I_0=\frac{1}{2}$. 0.025 in. Cu absorber used.

the three even-even isotopes Er^{166}, Er^{168}, and Er^{170}, and the single odd isotope Er^{167}. As in the case of dysprosium discussed above, one expects the first-excited states of the even-even nuclei to lie close together around 80 kev. We again associate the level at 172 kev with the second rotational level of the single odd-A nucleus Er^{167}, having spin $I_0=7/2$. Using the appropriate ratio of 2.22, the first rotational level should occur at 78 kev. Hence, we shall ascribe the large photopeak at 79 kev to *all* isotopes of Er until further clarification. The only known level in any abundant even-even isotope of Er is the 81-kev state of Er^{166}, whose lifetime is also known. We calculate the *upward* transition probability from McGowan's lifetime (1.7×10^{-9} sec)[7] to be 5.3, whereas we get from our excitation data a value of $B(E2)=4.4$, using Sunyar's estimate for the total conversion coefficient ($\alpha_t=8.1$). This near agreement shows that the photopeak at 79 kev must be due to most isotopes of Er in approximate proportion to their abundances. If, for example, the 79-kev peak belonged entirely to Er^{166} (33.4 percent natural abundance), we would calculate $B(E2)=13.2$. In fact, lifetime measurement of a 91-kev state in Er^{164} [8] yields a transition probability of the same order [$B(E2)up=5.05$], supporting this conclusion.

L. Thulium ($Z=69$)

The pulse-height spectrum for the monoisotopic element Tm^{169} is shown in Fig. 8. A single peak at 109 kev is observed. Huus[30] observes two conversion-electron peaks corresponding to transitions at 111 kev and 119 kev. He believes from a study of the shape of the excitation of the 111-kev radiation, that the latter originates from a level at about 120 kev, indi-

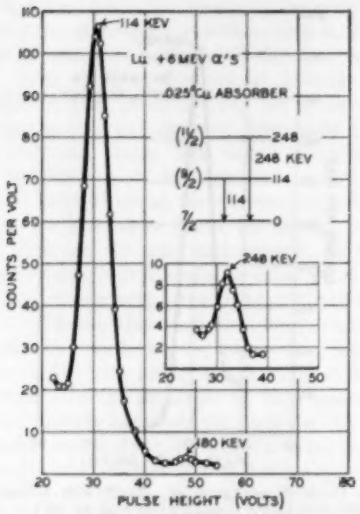

FIG. 9. Coulomb excitation of $_{71}Lu^{175}$ with 6-Mev alphas. Pulse-height distribution shows transitions at 114 kev and 248 kev (at lower gain), leading to decay scheme shown in the insert (see also reference 50). Small peak at 180 kev is arbitrarily assigned to Lu^{176} (2.6 percent). 0.025 in. Cu absorber used.

cating a first-excited state at about 9 kev. This scheme receives some support from existing data on the decay of Yb^{169}.[46] Our scintillation detector could not resolve two lines at 111 kev and 119 kev. However, from the position of the peak we seem to excite predominantly the (cascade?) radiation of 109 kev. Now the ground-state spin of Tm^{169} is $\frac{1}{2}$, and hence we do not expect a conventional rotational spectrum.[9] We have previously studied three of these spin $\frac{1}{2}$ nuclei[47]; some very precise data have recently appeared concerning W^{183}, having spin $\frac{1}{2}$.[48] All these cases illustrate the special features of the rotational system when decoupling of the odd-particle spin from the intrinsic nuclear deformation axis takes place. The nearness of the first-excited state to the ground state fixes the value of the decoupling parameter a[9] at about -0.75 and yields a "splitting constant" $\hbar^2/2\mathcal{I}$ in keeping with that of even-even neighbors. Our transition probability for the 109-kev transition was computed using a value of ξ_0 appropriate for an excitation energy of 120 kev.

M. Ytterbium ($Z=70$)

The case of Yb is similar to those of Dy and Er. Again only natural targets were available. Only one excited state is known, the 84.1-kev level of Yb^{170}, whose lifetime has been measured.[49] The four even-even isotopes of mass numbers 170 through 176 are all fairly abundant and are again expected to have first-excited states around 80 kev. The fact that the composite peak lies at 78 kev is evidence for the existence of states at somewhat lower energies in Yb^{172}, Yb^{174}, and Yb^{176}. Pending further work with separated isotopes, we shall once again divide the photopeak at 78 kev among these four even nuclei and the odd-A isotope Yb^{173}, whose spin is 5/2. We ascribe the gamma ray at 180 kev to the second rotational state of Yb^{173}, so that the first rotational state should lie at about 79 kev. The other odd-A isotope Yb^{171} has spin $I_0=\frac{1}{2}$, so that we anticipate unconventional behavior as in Tm^{169} (see Sec. III-L). We have arbitrarily assigned the line at 110 kev to Yb^{171} for the present time. Using the total internal conversion estimate from Sunyar's tabulation[8] ($\alpha_t=7.4$) and the lifetime of the 84-kev transition in Yb^{170},[49] we calculate an upward $B(E2)$ of 5.07, whereas we get a value of 2.3 from our data. This discrepancy seems to indicate that the line at 78 kev predominantly belongs to only some of the five isotopes which we have assumed to share its intensity equally; in fact only about 40 percent of the isotopes (by abundance) would account for the observed strength.

N. Lutetium ($Z=71$)

The pulse-height distribution for this element is shown in Fig. 9. The abundance of the odd-A nucleus Lu^{175} accounts for 97.4 percent of the element, the remaining 2.6 percent belonging to the odd-odd nucleus Lu^{176}. The photopeaks at 114 kev and 250 kev constitute another example of a well-developed rotational spectrum for a nucleus of spin $I_0=7/2$. Gamma rays of nearly the same energy have recently been found in the decay of Yb^{175},[50] the only case where a second rotational state of an odd-A element was seen in beta decay.

We arbitrarily and tentatively assign the 180-kev line to odd-odd Lu^{176}, since both energy and intensity of this line are not unreasonable for this nucleus. If this identification is borne out by future measurements, it would constitute the only example of a rotational transition in an odd-odd nucleus in the "strong coupling" region.

O. Hafnium ($Z=72$)

For the element hafnium we had available enriched isotopes of the two odd-A nuclei Hf^{177} and Hf^{179}, as well as of the even-even nucleus Hf^{176}. First-excited 2^+ states were known in Hf^{178} and Hf^{180}; their lifetimes are also known.[7,8] From our three enriched targets, coupled with an ordinary Hf target, we were able to determine the quantities $\epsilon B(E2)$ for Hf^{176}, Hf^{178}, and Hf^{180}. From the lifetimes and estimates of total internal conversion coefficients,[8] we calculate the following *upward* transi-

[46] Martin, Jensen, Hughes, and Nichols, Phys. Rev. **82**, 579 (1951).
[47] N. P. Heydenburg and G. M. Temmer, Phys. Rev. **95**, 861 (1954).
[48] Murray, Boehm, Marmier, and DuMond, Phys. Rev. **97**, 1007 (1955).
[49] Graham, Wolfson, and Bell, Can. J. Phys. **30**, 459 (1952).
[50] J. P. Mize (private communication); also Mize, Bunker, and Starner, Bull. Am. Phys. Soc. **30**, No. 3, 71 (1955).

tion probabilities:

$$Hf^{176}: B(E2)=4.9\ ;\quad Hf^{180}: B(E2)=4.4.$$

Using our Coulomb-excitation results, we obtain

$$Hf^{176}: B(E2)=4.3;\quad Hf^{180}: B(E2)=5.1,$$

in rather satisfactory agreement with the former values.

The gamma-ray spectra obtained from the odd-A isotopes of Hf are shown in Figs. 10 and 11, together with the inferred level schemes. The photopeaks in the 100-kev region show the contributions of the residual amounts of the even-even isotopes, as well as the first rotational states of the odd isotopes. Note the shift of the lower-energy peak from 90 kev in the Hf^{177} sample, whose even-even constituent is predominantly Hf^{178} (31.7 percent), to 93 kev in the Hf^{179} sample, whose even-even component is almost pure Hf^{180} (44.2 percent). The peaks shown in the 300-kev region in Figs. 10 and 11 represent, in addition to the ever-present 342-kev line from O^{15} (see Sec. II-B), the second rotational states of Hf^{177} and Hf^{179} at 250 kev and 260 kev, respectively.[51] Their intensities are seen to differ considerably (about a factor of 10) simply by comparing them with their neighboring "oxygen lines," which are of identical height. Unfortunately, the ground state spins of the odd Hf isotopes are not known,[52] but if they are the same for both nuclei, the difference in the strengths of the second rotational states is rather unexpected. At the same time, the first-excited state transitions in the two odd nuclei are of quite comparable intensities. Recent precision spectroscopy

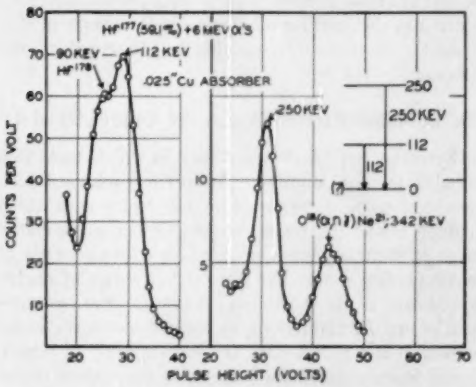

FIG. 10. Coulomb excitation of $_{72}Hf$ with 6-Mev alphas. Pulse-height distribution for enriched Hf^{177} (59.1 percent) shows lines at 112 kev and (at lower gain) 250 kev belonging to Hf^{177}. One also sees 90-kev transition in Hf^{178} (31.7 percent) and 342-kev line due to $O^{18}(\alpha,n\gamma)Ne^{21}$ reaction (see Sec. II-B). Decay scheme for Hf^{177} shown as insert (see also reference 53). Note relative heights of 250-kev and "oxygen" peaks (compared to Fig. 11). 0.025 in. Cu absorber used.

[51] Lines at somewhat lower energies have been reported by McClelland, Mark, and Goodman, Phys. Rev. **97**, 1191 (1955).

[52] E. Rasmussen, Naturwiss. **23**, 69 (1935).

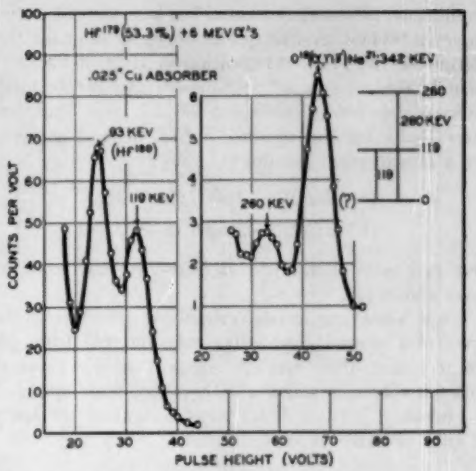

FIG. 11. Coulomb excitation of $_{72}Hf$ with 6-Mev alphas. Pulse-height distribution for enriched Hf^{179} (53.3 percent) shows lines at 119 kev and (at lower gain) 260 kev belonging to Hf^{179}. One sees 93-kev transition in Hf^{180} (44.2 percent) and 342-kev line due to $O^{18}(\alpha,n\gamma)Ne^{21}$ reaction (see Sec. II-B). Decay scheme for Hf^{179} shown as insert. Note relative heights of 260-kev and "oxygen" peaks (compare to Fig. 10). 0.025 in. Cu absorber used.

of Lu^{177} by Marmier and Boehm[53] has confirmed the two levels in Hf^{177}, although some discrepancies exist concerning multipolarities of gamma-ray transitions. Using their very accurate energy values of 112.97 kev and 249.69 kev for the first and second rotational states of Hf^{177}, we can obtain a value for the ground-state spin I_0 as well as for the splitting constant $\hbar^2/2\mathcal{I}$ from the expression for rotational states (see Sec. IV). The spin value is 3.76, which is close to 7/2 and deviates from that half-integer in the direction to be expected from small vibration-rotation interaction effects,[4,9] which tend to depress higher rotational states slightly; in fact, an upward shift of 1.5 kev of the second rotational states level would yield a spin of exactly 7/2. The splitting constant in this interpretation is 11.87 kev, which is less than the 15 kev obtained from the neighboring 2^+ states at 90 kev. This again represents a trend in odd-even alternation which is observed throughout the rare-earth region, as will be seen in Fig. 13. On the other hand, Marmier and Boehm[53] favor a $p_{\frac{1}{2}}$ configuration for the ground state in keeping with shell-model predictions. If we use their spin assignments of 5/2 and 3/2 for first and second excited states, respectively, we can insert their energy values into the expression for an anomalous rotation spectrum[9] and extract values for the decoupling parameter a and splitting constant $\hbar^2/2\mathcal{I}$. They are:

$$a=1.98;\quad \hbar^2/2\mathcal{I}=27.95\ \text{kev}.$$

The latter value is definitely too large to accord with neighboring even-even nuclei; in fact the 2^+ states

[53] P. Marmier and F. Boehm, Phys. Rev. **97**, 103 (1955).

should then be found at around 180 kev, instead of the observed 90 kev. Sunyar quotes an *upper* limit for the lifetime of the 112-kev transition in Hf^{177} of 5×10^{-10} second.[8] When combined with his estimate for the total internal conversion coefficient of 2.7, this leads to *lower* limits for the upward $B(E2)$, depending upon the assumed spins, as follows:

(a) $B(E2)>2.2$ for $7/2\rightarrow9/2$;

(b) $B(E2)>5.2$ for $1/2\rightarrow5/2$.

Our excitation data yield $B(E2)=2.8$, and seem to favor choice (a).

While these arguments certainly do not constitute proof of a ground-state assignment different from $p_{\frac{1}{2}}$, we feel that they strongly support a conventional rotation spectrum starting with ground-state spin 7/2 (or possibly 5/2). A direct measurement of the spins of Hf^{177} and Hf^{179} is sorely needed.

P. Tantalum ($Z=73$)

This element is well-known to possess a simple rotational spectrum.[84] We have measured the intensities of the 136-kev and 303-kev transitions mainly as an internal check and normalization point for comparing intensities and transition probabilities. The 167-kev cascade was seen only feebly, but we were able to obtain a pronounced coincidence peak at 167 kev when examining the coincidence spectrum between 136-kev radiation and the rest of the gamma spectrum, as described above under europium (Sec. III-F). It is interesting to note that the K x-radiation emitted from the tantalum target at about 61 kev, as shown in Fig. 1 of a previous communication,[1] is almost entirely accounted for by the internal K-conversion of the 136-kev gamma ray, so that no more than a few percent of the x-ray peak can be ascribed to direct target excitation. This explains the differences in behavior of the excitation curves given in Fig. 2 of the previous reference[1] for proton and alpha-particle bombardment: the x-radiation maintains a constant ratio to the gamma radiation for alpha particles (even up to 6 Mev), whereas it increases with energy relative to the gamma ray in the case of proton bombardment.

IV. DISCUSSION

A. Review of the Unified Model

The sixteen stable elements from praseodymium through tantalum which we have studied in this paper constitute a continuous series of nuclei more or less removed from the closed shells for both protons at $Z=50$ and $Z=82$, and for neutrons at $N=82$ and $N=126$. It is just in this region that nuclei are expected to depart farthest from the spherical shape owing to the presence of a large number of nucleons outside of closed shells. The existence of large static quadrupole moments in this region of mass numbers has long pointed in this direction; the occurrence of electric-quadrupole transitions with probabilities up to two orders of magnitude greater than encompassed by the transition of a single particle, as revealed by Coulomb excitation or lifetime measurements, points in the same direction. As Bohr and Mottelson point out,[4] the existence of rotational energy levels with positions given by the simple quasi-molecular expression

$$E=(\hbar^2/2\mathcal{I})[I(I+1)-I_0(I_0+1)], \tag{7}$$

connected by fast $E2$ transitions, is a direct consequence of the large deformations known to exist in these nuclei, "large" being quantitatively interpreted as large compared to the zero-point oscillations of the nuclear surface shape, inherent in this quantum phenomenon. If this condition is fulfilled, a preferred axis of deformation (z-axis) exists in the nucleus, and the peculiar quantized flow of nuclear matter leading to a rather simple rotational spectrum is an inevitable consequence.

Since we have a preferred axis, we can define an intrinsic measure of the departure of the nuclear surface from the spherical shape with respect to that axis, the so-called intrinsic quadrupole moment Q_0. This quantity can be defined for all nuclei, even if their spin is 0 or $\frac{1}{2}$. The quantity $\mathcal{I}$ occurring in Eq. (7) above is proportional to Q_0^2, as is also the quantity $B(E2)$ measured in our experiments. Thus large deformations imply low-lying excited states and large transition probabilities. It turns out both from our work and Sunyar's that the values of Q_0 one obtains from (7) are always larger, by a factor of about two, than those obtained from $B(E2)$, pointing to the need for refinement in the simple model. A similar discrepancy can also be discerned in the region of $A\sim100$.[55,56]

B. Coulomb Excitation and the Unified Model

The rather straightforward way in which transition probabilities are obtained from Coulomb-excitation cross sections, and the complete uniformity with which all stable nuclei are treated, make this method probably the most desirable one available today for the study of the properties of the first few excited states of nuclei. In addition to its special suitability for the measurement of fast $E2$ transitions, as pointed out in the introduction, it is a favorite for the investigation of experimental features having a bearing on the unified model in one further respect: it is in the very nature of the unified model to predict trends and properties transcending any specific nuclear species. Hence, the possibility of studying all nuclei under precisely the same conditions eliminates many sources of error inherent in the conventional methods of nuclear spectroscopy where

[84] T. Huus and C. Zupančič, Kgl. Danske Videnskab. Selskab, Mat.-fys. Medd. **28**, No. 1 (1953).

[55] K. W. Ford, Phys. Rev. **95**, 1250 (1954).

[56] G. M. Temmer and N. P. Heydenburg, Phys. Rev. **98**, 1308 (1955) and to be published.

moving from one nucleus to the next may entail an entirely different decay scheme, caused by vast differences in beta-decay energy, degree of forbiddenness of the beta transitions, spins and parities of parent nuclei, not to mention the complete lack of these pieces of information in a large number of cases.

The absence of positive excitation results for the three nuclei having 82 neutrons (La^{139}, Ce^{140}, Pr^{141}) illustrates the lack of enhanced electric-quadrupole transitions for nearly spherical nuclei.

Recently some low-lying gamma-ray transitions in Eu^{153} and Gd^{155} were found to have electric-dipole character.[40,42] A few words are in order concerning the complete absence of these transitions in our work. The intrinsic Coulomb-excitation probability of $E1$ transitions[19,57] is about three hundred times *greater* than the quadrupole excitation for transitions of ~ 100 kev and $Z=64$; however, the reduced $E1$ transition probability $B(E1)$ is expected to be very much *smaller* than that of a single proton. Remembering that the $E2$ transitions we observe are about one-hundred times stronger than those of a single particle, we would not expect to observe $E1$ transitions in spite of their being *a priori* favored by the Coulomb-excitation process. A number of $E1$ transitions have recently been discovered in the strong-coupling region beyond Pb^{206} with transition probabilities about three orders of magnitude below the single-particle strength.[58] Our negative result can be used to set a limit of about this order of magnitude for any $E1$ transitions leading to the ground state.

1. Even-Even Nuclei

Starting with Nd^{146}, we were able to excite all first-excited 2^+ states lying below about 600 kev, the latter limit being dictated merely by the intrinsic Coulomb-excitation mechanism as embodied by the function $g_2(\xi)$ defined in Sec. II-D. We have added a number of new cases to the growing systematics of the *positions* of first-excited states of even-even nuclei. A plot summarizing the results in this paper on even-even nuclei excited with 6-Mev alpha particles is shown in Fig. 12. The excitation energy of the first-excited state is plotted as a function of the neutron number N. The sharp rise toward the left where we approach the closed shell at $N=82$ is very apparent. A number of the levels were previously unknown (open circles). In the cases of Dy, Er, and Yb no detailed results are as yet available, as discussed in Sec. III, and the points are shown at positions representing an average over the even-even isotopes. A plot of the reciprocal of the transition probabilities would have a very similar appearance to the curve in Fig. 12. Because of the existing uncertainties in total internal conversion coefficients we refrain from presenting such a plot; we have already pointed out the monotonic variations with neutron number which exist

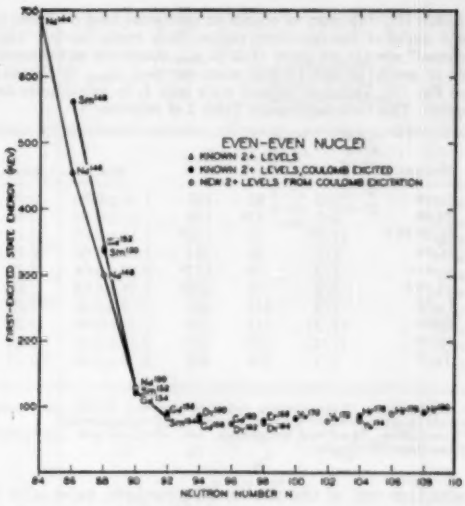
EVEN-EVEN NUCLEI
▲ KNOWN 2+ LEVELS
● KNOWN 2+ LEVELS,COULOMB EXCITED
○ NEW 2+ LEVELS FROM COULOMB EXCITATION
FIRST-EXCITED STATE ENERGY (kev)
NEUTRON NUMBER N

FIG. 12. Summary of results on even-even rare-earth nuclei. Energies of first-excited (2^+) states *vs* neutron number. (△)—known states, not Coulomb-excited; (●)—known states, Coulomb-excited; (○)—new states discovered by Coulomb excitation. Levels for elements where no enriched isotopes are available (Dy, Er, Yb) shown at an average position. See also references 10 and 11.

in the quantity $B(E2)$ in the region of rapid change, i.e., neutron number $N=86$ to $N=92$, as represented by elements Nd and Sm. Here the internal conversion correction is not too important. The same trend can still be discerned in the three even-even Gd nuclei, again after proper allowance is made for internal conversion.

On the whole, the transition probabilities observed here are from 50 to 100 times larger than one calculates from the single-particle formula of Weisskopf.[57]

2. Odd-A Nuclei

In the nuclei of odd mass number that we have examined we were usually able to observe or infer the existence of two excited states, as is expected from the $E2$ character of the excitation process and the spins and parities associated with rotational levels. No rotational energy levels in the odd nuclei (except in Ta) were known when we began this investigation. There is a difference in the reliability of our results between odd-Z (odd-even) and odd-N (even-odd) nuclei, because of the fact that the former all occur as monoisotopic elements (with the exception of Eu) and permit unique assignments to be made. In Table III, we have collected the information on level spacings for all odd nuclei, listing the first-excited state energy E_{I_0+1}, the second-excited state energy E_{I_0+2}, their observed ratio ρ_{exp} and predicted ratio ρ_{theor} for the given (or assumed) ground-state spin I_0. It must be pointed out that much greater precision in energy determination than is available with scintillation counters is required in order to have

[57] C. J. Mullin and E. Guth, Phys. Rev. **82**, 141 (1951).
[58] Stephens, Asaro, and Perlman, Phys. Rev. **96**, 1568 (1954).

TABLE III. Summary of results on rotational level positions in odd-A nuclei of the rare-earth region. Only nuclei having "conventional" spectra are listed ($I_0>\frac{1}{2}$). ρ_{exp} stands for experimental ratio of second-to-first excited state energies; ρ_{theor} is obtained from Eq. (7). Values of ground state spin I_0 in parentheses are assumed. This table supersedes Table I of reference 5.

Nucleus	I_0	E_{I_0+1} (kev)	E_{I_0+2} (kev)	ρ_{exp}	ρ_{theor}
$_{63}Eu^{153}$	5/2	82	187	2.28±0.04	2.29
$_{65}Tb^{159}$	3/2	57[a]	136	2.39±0.05	2.40
$_{66}Dy^{161,163}$ [b]	(7/2)	76	166[b]	2.18±0.04	2.22
$_{67}Ho^{165}$	7/2	94	206	2.19±0.04	2.22
$_{68}Er^{167}$ [b]	7/2	79	172[b]	2.18±0.04	2.22
$_{70}Yb^{173}$ [b]	5/2	78	180[b]	2.31±0.04	2.29
$_{71}Lu^{175}$	7/2	114	250	2.19±0.04	2.22
$_{72}Hf^{177}$	(7/2)	112	250	2.23±0.04	2.22
$_{72}Hf^{179}$	(7/2)	119	260	2.18±0.04	2.22
$_{73}Ta^{181}$	7/2	136	303	2.23±0.04	2.22

[a] Inferred from 79-kev cascade radiation (see Sec. III-H); conversion electrons directly observed by T. Huus (private communication).
[b] Conclusions, based on systematics, are tentative (see appropriate sections above for details).

a sensitive test of the rotational structure, especially if such small departures from the simple formula (7) as are expected from vibration-rotation interaction effects (about 1–2 kev in this region) are to be detected. The case of Hf^{177}, discussed in Sec. III-O above, is a case in point.[60] Very precise conversion-line data are also available in some odd transuranic elements (see, for instance, the case of Np^{237} as known from the alpha decay of Am^{241}).[60,61] However, our results on level positions certainly bear out the predictions of the unified model in zeroth approximation very well. No more than two levels were observed in any odd-A nucleus.

There is considerable variation in the values of $\epsilon B(E2)$ for second rotational states, as well as in the ratio of second to first-excited state transition probabilities. As we have pointed out above, the possibility (and even certainty) of $M1$ cascade competition in returning to the ground state will profoundly affect the value of $\epsilon B(E2)$ for the second rotational states. In fact, in the famous case of Ta^{181}, where the composition of the 136-kev transition has been experimentally determined by angular correlation measurements,[61] the $M1$ component outweighs the (enhanced) $E2$ component by about 6 to 1; the cascade between second and first-rotational state probably represents a similar situation. Now if we calculate the branching ratio for the de-excitation of a second rotational state, via cascade or direct crossover, to the ground state, from the theoretical expressions furnished by the unified model for $E2$ transitions only, we find that the cascade path is weaker than the crossover, the exact extent depending on spins, transition energies, and conversion coefficients. Any indication that the observed cascade transition is stronger than the crossover is evidence of additional transition probability provided by $M1$ radiation. The two cases where we are able to observe the cascade radiation directly illustrate this point. The cascade at 105 kev in Eu^{153} is rather weak compared to the 187-kev crossover transition, as can be seen from Table II. [Fig. 4 gives a distorted impression of this ratio, because of the effect of the Coulomb-excitation correction contained in $g_2(\xi)$.] The situation is reversed in the case of Tb^{159}, where the 79-kev cascade is about five times stronger than the 136-kev crossover. Internal conversion correction increases this ratio even further. Note that the actual value of $\epsilon B(E2)$ for the 136-kev transition in Tb^{159} is only about one tenth that for the 187-kev transition in Eu^{153}. We see that the true transition probabilities to these second rotational states, as represented by the sum of the crossover and cascade radiations, are more nearly equal. This is to be expected, since this probability is supposedly a function of Q_0^2 only, and the deformations in the two nuclei in question are certainly comparable. In the remaining odd-A nuclei, where we do not observe the cascade directly, we can infer its importance from the size of $\epsilon B(E2)$ for the direct $E2$ cross-over transition. When the latter is strong, the cascade transition is weak which means, as we pointed out above, that the contribution of $M1$ radiation to the cascade is reduced. From the variation in $\epsilon B(E2)$ for the second rotational states (see Table II) we see that this contribution can vary considerably from nucleus to nucleus. According to the unified model[4] the $M1$ transition probability is governed by the quantity $(g_\Omega - g_R)^2$ where g_Ω and g_R stand for the gyromagnetic ratios of the intrinsic particle configuration and the collective rotational flow, respectively; they also determine the static magnetic moment in the ground state. Variations in $(g_\Omega - g_R)$ are presumably to be ascribed to fluctuations in g_Ω, since g_R is not expected to change radically from one nucleus to the next.

Strictly speaking we should diminish $\epsilon B(E2)$ of the first-rotational state by the amount contributed by cascade from the second-rotational state, which leads to the same gamma ray. In practice, however, this gives rise to an unimportant correction because of the relatively weak excitation of the second state when using alpha particles, whose $g_2(\xi)$ falls off rapidly with excitation energy ΔE (see relative photopeak heights in Figs. 4, 6, 7, 9, and 10).

This discussion of odd-A nuclei should not be terminated without recalling the few instances where the possibility of discrepancy with the general behavior expected from the unified model exists at present.

(a) As mentioned in Sec. III-D, the case of Nd^{145} is exceptional in that we find a weak, but low-energy transition at 70 kev with no apparent companion lines. The complete absence of any observable transitions, such as in Nd^{143}, Sm^{147}, and Sm^{149} is more in keeping with the approach to a closed-shell structure in this region; the low energy line in Nd^{145}, while not necessarily

[60] Milsted, Rosenblum, and Valadares, Compt. rend. **239**, 259 (1954).
[61] P. P. Day, Phys. Rev. **97**, 689 (1955).
[61] F. K. McGowan, Phys. Rev. **93**, 471 (1954).

representing a transition to the ground state, must nevertheless be considered an exception.

(b) Several interpretations of the situation in the odd isotopes of Gd have been presented in Sec. III-G. However, until further direct evidence becomes available concerning possible first excited states of Gd^{155} and Gd^{157}, we must class these nuclei as exceptions, especially since they are bracketed both as to proton number and neutron number by nuclei showing standard rotational bands (Eu^{153} and Tb^{159}).

(c) In Sec. III-O we have pointed to the fact that the second rotational states in Hf^{177} and Hf^{179} at 250 kev and 260 kev, respectively, differ in transition probability by about an order of magnitude. This factor is subject to very little error. At the same time the first rotational transitions (reflecting the nuclear deformation) are quite comparable. Unfortunately, the spins of the ground states of these nuclei are not known with certainty.[82] If they are the same, as might be indicated by the similarity of the level positions, the difference observed for the second states would, in the framework of the unified model, imply very different $M1$ transition probabilities for the cascade transitions in the two nuclei (see beginning of this section). However, the spins and coupling schemes might well be different in the two isotopes (as in Yb^{171} and Yb^{173}).

In addition, we should keep in mind the definite discrepancy which exists between the values of Q_0 obtained from the position of rotational states, and the values derived from the size of the reduced transition probabilities: nuclei seem more deformed when judging from the location of their excited states, i.e., the latter lie at an energy which is lower by a factor of about four than would be expected from the observed transition strengths.

3. *Comparison of Even and Odd Nuclei*

An important question in connection with collective effects concerns possible even-A—odd-A differences in deformation. Spectroscopic quadrupole moments obviously cannot throw any light on that subject. As we pointed out earlier, one approach uses level positions as an index of deformation. In Fig. 13, we have plotted the "splitting constants" $\hbar^2/2\mathcal{I}$ for all rare-earth nuclei of interest, distinguishing even-even, even-odd, and odd-even nuclei, by appropriate symbols. The spins of the odd nuclei we used are either known, or assumed in accordance with the entries given in Table III. For the elements Dy, Er, and Yb we have obtained the splitting constants from what we expect to be the second rotational states, in the odd nuclei, as discussed in Sec. III. Tentative values are represented by open symbols. There seems to be a grouping into the three above-mentioned classes: even-odd nuclei have splitting constants falling consistently lowest; odd-even nuclei are next with somewhat higher $\hbar^2/2\mathcal{I}$; finally, even-even nuclei are lying highest. All three groups show a tendency to coalesce toward the higher neutron

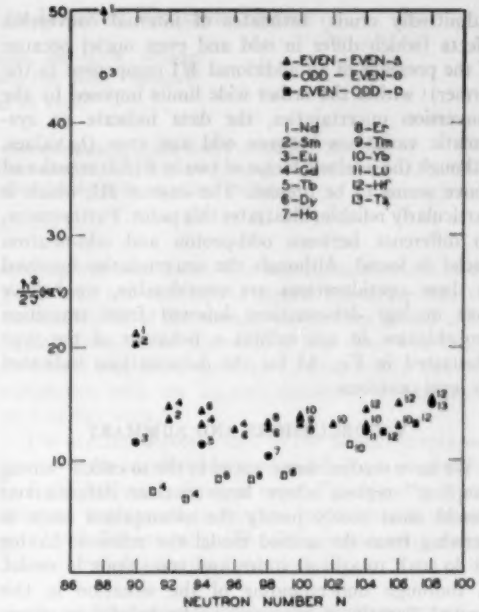

FIG. 13. Summary of results on rotational-level parameters in rare-earth nuclei. "Splitting constants" $\hbar^2/2\mathcal{I}$ vs neutron number, as obtained from Eq. (7). Solid symbols represent definitive results, open symbols represent tentative assignments. (△)—even-even nuclei; (⊡)—even-odd nuclei; (⊙)—odd-even nuclei. Nuclei are identified by numbers in the figure.

numbers. Incidentally, the fact that this plot has the neutron number N as abcissa (and no proton parameter) does not affect these conclusions, since most of the low odd-A points are bracketed in Z on both sides; for instance, low $_{65}Tb^{159}$ occurs at the *same* neutron number ($N=94$) as $_{64}Gd^{158}$ and $_{66}Dy^{160}$ which lie higher, etc.

Let us now examine the other index of deformation, the reduced transition probabilities. As we have seen above, the quantity $B(E2)$ to the first-rotational states in odd-A nuclei is least influenced by cascade or branching effects, and hence reflects most accurately the quadrupole-transition probability, and intrinsic quadrupole moment Q_0. The expression for the reduced *upward* transition probability to the first rotational state of an odd-A nucleus of spin I_0 is given by

$$B(E2)=(15/16\pi)e^2Q_0^2[I_0/(I_0+1)(I_0+2)]; \quad (8)$$

for the values of I_0 which occur in the rare earth nuclei (3/2, 5/2, 7/2) this quantity is about $0.05\ e^2Q_0^2$. For the $0^+\rightarrow 2^+$ transition in even-even nuclei, we get a value $0.10\ e^2Q_0^2$ (from a different expression). Hence, according to the unified model, we expect a variation of about a factor of two between even and odd nuclei in $B(E2)$ having identical intrinsic quadrupole moments. An examination of the experimental values $\epsilon B(E2)$ in Table II, reveals the following trends after we make

(admittedly crude) estimates of internal conversion effects (which differ in odd and even nuclei because of the presence of an additional $M1$ component in the former): within the rather wide limits imposed by the conversion uncertainties, the data indicate no systematic variations between odd and even Q_0 values, although the intrinsic factor of two in $B(E2)$ mentioned above seems to be present. The case of Hf, which is particularly reliable, illustrates this point. Furthermore, no difference between odd-proton and odd-neutron nuclei is found. Although the uncertainties involved in these considerations are considerable, we believe that nuclear deformations inferred from transition probabilities do not exhibit a behavior of the type illustrated in Fig. 13 for the deformations indicated by level positions.

V. CONCLUSIONS AND SUMMARY

We have studied many nuclei in the so-called "strong coupling" region, where large nuclear deformations should most nearly justify the assumptions made in deriving from the unified model the relations having to do with rotational states and transitions in nuclei. A thorough understanding of the situation in this limited domain is expected to be helpful in disentangling nuclear properties in those regions where one or more of these assumptions are no longer valid, namely where "intermediate coupling" or "weak coupling" regimes prevail. It is therefore gratifying to find that, on the whole, the unified model is successful in accounting for most of the main features which are observed when strongly deformed nuclei are excited by the electric field of relatively slow charged particles. By way of recapitulation, we here collect together those features:

(1) Over-all uniformity in behavior is found as we move from one nucleus to the next, without much regard to specific constitution such as evenness or oddness of proton of neutron number, spin, etc.

(2) We find systematic occurrence of rotational states obeying a simple quasi-molecular interval rule. In keeping with the $E2$ character of Coulomb excitation we observe one excited state only, having spin 2^+ in even-even nuclei, and generally two excited states in odd-A nuclei. While no individual spin assignments were made to the two states in the various cases, we know that their parities must equal the ground state parity, and that the values of the spins must be limited to fall within two units of the ground-state spin I_0. The particular sequence I_0, I_0+1, I_0+2, demanded by the unified model, could be definitely established only by angular distribution measurements. However, the intensities of cascade and crossover radiations in most cases seem to point to different spins for the two excited states. The fact that none of the second-excited states are found to be directly excited in beta decay points toward some degree of forbiddenness for such a transition, and a spin difference of at least two units between these states and the ground state. All this still allows a sequence which is the inverse of the one given above, but we shall favor the normal sequence on the basis of agreement with the theory.

(3) We find systematic occurrence of electric-quadrupole transitions having probabilities of the order of one hundred times those which would be accounted for by the $E2$ transition of a single proton. Significant variations of this quantity are found where variations in the excited-state positions occur as well, in such a direction as to support the view that both reflect a decrease in nuclear deformation upon approaching a closed-shell configuration.

However, a few examples of possibly exceptional behavior in odd-A nuclei have been found and were summarized at the end of Sec. V-B(2).

The main contribution of Coulomb excitation to the understanding of the rotational level structure probably lies in the odd-A nuclei; essentially no lifetime information is available for them, and their level structure is generally inaccessible by other means. Accurate measurements of level energies, branching ratios and internal conversion coefficients (to determine $M1$–$E2$ mixture ratios) can yield a wealth of information concerning details of nuclear structure not otherwise obtainable. It is evident from our results that much remains to be done along these lines.

We have found to our surprise that some of the simple properties encountered in the strong-coupling region can still be found for nuclei of much lower mass number, especially in the even-even nuclei. Some results on Rh, Pd, Ag and Cd have already been published[47,54] while additional information on even lighter but still deformed nuclei will be the subject of a subsequent publication.

VI. ACKNOWLEDGMENTS

We are greatly indebted to the following persons for their cooperation in supplying us with the indispensable materials of this research: to C. P. Keim (Oak Ridge National Laboratory) for all enriched isotopes used; and to F. H. Spedding (Ames Laboratory), and E. L. Weise (National Bureau of Standards) for a number of high-purity rare-earth oxides. A number of people have kindly informed us of results prior to publication concerning decay schemes of various nuclei covered in this research. Finally, it is a pleasure to recall the many fruitful discussions with A. Bohr, B. R. Mottelson, and T. Huus during a most pleasant stay at the Institute for Theoretical Physics in Copenhagen.

$V^{51}(p,n)Cr^{51}$ Reaction as a 5- to 120-kev Neutron Source

J. H. Gibbons, R. L. Macklin, and H. W. Schmitt
Oak Ridge National Laboratory, Oak Ridge, Tennessee

(Received June 27, 1955)

The $V^{51}(p,n)Cr^{51}$ reaction provides a usable source of monoenergetic neutrons from 5 to 120 kev. The yield indicates resonances in Cr^{52} with an average spacing of less than 2 kev in this evergy range. A preliminary measurement was made of the angular distribution of eleven of the more prominent peaks.

THE $V^{51}(p,n)Cr^{51}$ reaction has been recognized as a source of monoenergetic neutrons for many years,[1,2] but has not been extensively used. In connection with a series of experiments on the Oak Ridge National Laboratory 2.5-Mv Van de Graff, we have run a forward yield curve using a 1 kev thick natural vanadium (99.76 percent V^{51}) target. Such targets may be readily prepared by vacuum evaporation from tungsten if care is taken to avoid the tungsten oxide which evaporates at a lower temperature. The neutron yield curve at high energies has been reported.[3]

At proton energies from 1.55 to 1.65 Mev many resonances were observed (Fig. 1), with an average spacing less than 2 kev. The experimental width of the peaks was just that of the target, indicating that the natural widths of the resonances (and the spread of the proton beam) were appreciably less than 1 kev. The threshold was determined as 1.5656 ± 0.0015 Mev by calibration with the $Li(p,n)$ threshold, in agreement with earlier work.[2,4]

The neutron detector used in the measurements was a set of three paraffin-surrounded BF_3 counters grouped in a 45° half-angle forward cone. The response of the counters is expected to vary no more than 20 percent over the 5–120 kev range. The background, as measured below threshold, was negligible (see Fig. 1). Some of the

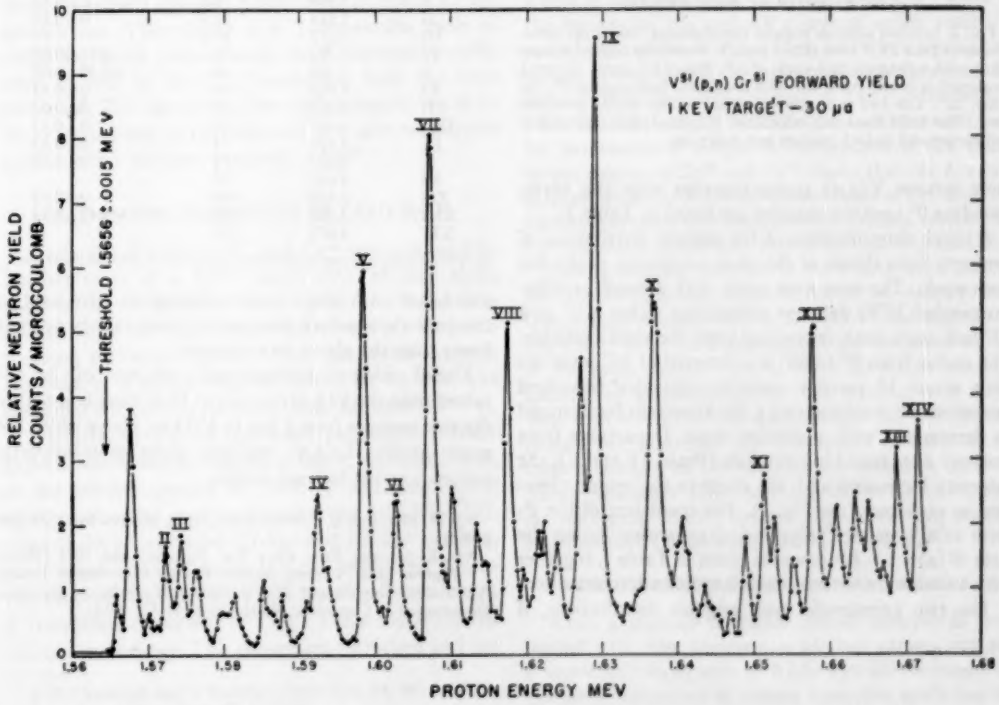

FIG. 1. $V^{51}(p,n)Cr^{51}$ forward neutron yield. Target thickness was 1.0 kev. Proton beam current was about 30 μa.

[1] Hanson, Taschek, and Williams, Revs. Modern Phys. **21**, 635 (1949).
[2] Stelson, Preston, and Goodman, Phys. Rev. **80**, 287 (1950).
[3] Baker, Howell, Goodman, and Preston, Phys. Rev. **81**, 48 (1951).
[4] R. V. Smith and H. T. Richards, Phys. Rev. **74**, 1257 (1948).

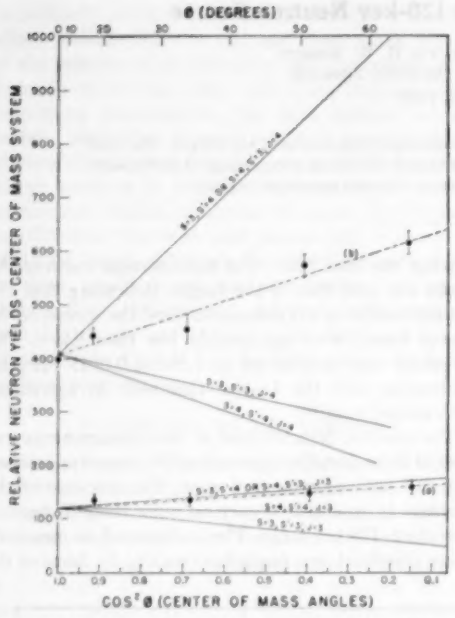

FIG. 2. Selected neutron angular distributions. Curve (a) corresponds to peak IV, Curve (b) to peak V. Points for curve (a) were taken with a detector half-angle of 22°. Points for curve (b) are a combination of two runs, one with a detector half-angle of 9°, the other, 22°. The two runs gave identical results within probable error. The solid lines are calculated (Channel Spin formalism) and correspond to $l=1$ protons and neutrons.

more intense $V(p,n)$ peaks together with the corresponding 0° neutron energies are listed in Table I.

A rough determination of the angular distribution of neutrons from eleven of the more prominent peaks has been made. The runs were made with a small paraffin-surrounded $B^{10}F_3$ detector subtending either a 9° or a 22° half-angle cone, depending upon the yield available. The region from 0° to 60° was covered at 15° intervals with about 10 percent counting statistics (standard deviation) after subtracting a 20–30 percent background as determined with a shadow cone. Departures from isotropy were found in two cases (Peaks IV and V), the intensity increasing with the angle to the proton direction in each case (see Fig. 2). The coefficient of the P_2 term in a Legendre polynominal expansion fitting the data $W(\phi)\sim 1+AP_2(\cos\phi)$ is given in Table I, together with an estimate of the uncertainty in its determination.

The two anisotropic peak angular distributions, if considered as dominated by single resonances, can be fitted with reasonable channel spin mixtures,[5] assuming the initial and final nuclei have spins of 7/2 and the same parity, as predicted by the shell model. Peak IV can be fitted for p wave protons and neutrons assuming spin $J=3$ or 4 for the compound nucleus, while Peak V is well fitted only for $J=4$. The channel spin pairs are shown unmixed in Fig. 2. No reasonable fits were found for either angular distribution using the j-j coupling model.[6]

The absolute yield of Peak VII (1-kev target) was estimated, using a McKibben long counter standardized with a Po-B neutron source of given yield, to be 380 (±10 percent) neutrons per steradian per microcoulomb near 0°. Another estimate was obtained from an activation experiment in which the 25-minute beta activity of I^{128}, induced by neutron bombardment of NaI(Tl) crystals, was measured. Published iodine cross sections,[7] also based on a long counter calibration, were used to compute the absolute yield and a value twenty percent lower than the above was obtained.

TABLE I. $V^{51}(p,n)Cr^{51}$ neutrons: Selected peaks. The figures in the last column represent the coefficient A, of the angular distribution $W(\phi)\sim 1+AP_2(\cos\phi)$.

Peak	E_p(Mev)	0°E_n(kev)	A
I	1.568	4.8	0±0.13
II	1.573	11.3	0±0.13
III	1.575	13.6	...
IV	1.592	34	−0.21±0.07
V	1.598	40	−0.30±0.05
VI	1.603	45	0±0.13
VII	1.607	50	0±0.13
VIII	1.617	61	0±0.13
IX	1.629	74	0±0.13
X	1.637	82	0±0.13
XI	1.651	97	...
XII	1.658	104	0±0.13
XIII	1.669	116	−0.11±0.13
XIV	1.672	119	...

Useful yields of monoenergetic neutrons can be obtained from the $V(p,n)$ reaction at 15 or more reasonably discrete energies from 5 kev to 120 kev, above which the more prolific $Li(p,n)$ reaction gives monoenergetic neutrons at the forward angles.

[5] J. M. Blatt and L. C. Biedenharn, Revs. Modern Phys. 24, 258 (1952).
[6] G. R. Satchler, Proc. Phys. Soc. (London) A66, 1081 (1953).
[7] *Neutron Cross Sections*, Atomic Energy Commission Report AECU-2040 Supplement No. 2 (Office of Technical Services, Department of Commerce, Washington, D. C., 1953).

Radioactivity of the Cerium-137 Isomers

A. R. Brosi and B. H. Ketelle
Chemistry Division, Oak Ridge National Laboratory, Oak Ridge, Tennessee

(Received June 20, 1955)

A cerium isotope with an 8.7-hr half-life has been assigned to Ce^{137} and shown to decay by electron capture with about 3% of the captures to a 445-kev level in La^{137}. The 34.5-hr decay period previously characterized as electron capture of Ce^{137} is an isomeric transition from a 255-kev level in Ce^{137}. Spin assignments consistent with the experimental data indicate that the transition between ground states of La^{137} and Ba^{137} should be allowed. However, the K or L electron capture half-life of La^{137} was found to be greater than 10^9 years.

I. INTRODUCTION

A RADIOACTIVE decay period of 36 hr was assigned to Ce^{137} by Chubbock and Perlman[1] who reported decay by electron capture through a 280 kev level in La^{137}. Stover[2] confirmed the work of Chubbock and Perlman but found the gamma energy to be 240 kev. In a search for an isomeric transition in Ce^{137} Hill[3] confirmed the mass assignment of the 36 hr period by the use of enriched isotopes and found the K/L conversion ratio of a 257-kev gamma ray to be about 4. Keller and Cork,[4] who also used enriched isotopes, confirmed the mass assignment and gave an energy of 253.4 kev for the gamma ray. They found a K/L conversion ratio of about 10. In the present work the K conversion coefficient as well as the K/L conversion ratio has been measured. This has led to a new assignment of the 36 hr decay period and to the discovery of a new radioactive species which has been assigned to Ce^{137}.

II. ISOMERIC TRANSITION IN CERIUM-137

A mixture of Ce^{137}, Ce^{139}, and Ce^{141} was produced by bombardment of a BaF_2 target with 48-Mev alpha particles in the Berkeley 60-in. cyclotron. The cerium fraction from the target was identified and purified with a cation exchange column.[5] The conversion electron spectrum of a source prepared from this material was measured with a thin magnetic lens spectrometer.

The intensity of the K conversion peak of the 255-kev gamma was measured relative to the K conversion peak of the 166-kev gamma of Ce^{139}. A NaI scintillation spectrometer was used to measure the relative intensities of the unconverted 255 kev and 166-kev gammas. From these intensity ratios and the published[6] K conversion coefficient (0.2 ± 0.05) of the 166-kev gamma, a K conversion coefficient of 5.5 ± 1.5 was found for the 255-kev gamma ray. This conversion coefficient and the K/L conversion ratio of 2.3 ± 0.2 indicate that the 255-kev gamma is emitted in an $M4$ transition.[7,8]

An $M4$ isomeric transition in Ce^{137} is expected from the systematics of energy level spacings.[9] X-ray gamma-ray coincidence measurements show that the 255-kev gamma is not coincident with capture x-rays and thus support the conclusion that it is emitted from an isomeric level. This conclusion is confirmed by the fact that the x-rays associated with the 34.5-hr period are cerium rather than lanthanum x-rays. This was shown by using a xenon filled proportional counter, linear amplifier and pulse analyzer. Both the $K\alpha_1$, and the $K\beta$ x-rays of lanthanum are critically absorbed. Escape of the fluorescent $K\alpha$ and $K\beta$ x-rays of xenon results in pulse height peaks at about 5 kev and 9 kev when either cerium or lanthanum x-rays are counted. However, the ratio of the intensity of the peak at 5 kev to the peak at 9 kev should be about 10 times greater for cerium than for lanthanum K x-rays. A comparison of the pulse-height spectra of Ce^{139} and Ce^{137} shows that the K x-rays emitted with a 34.5 hr half-life are those of Ce. The conversion electrons and unconverted gamma of the 255-kev transition also decay with a 34.5 ± 0.5 hr half-life.

Cerium samples enriched in Ce^{136} have been used to confirm the mass assignment of the 34.5-hr decay period. One sample was enriched to 30% Ce^{136} and another to 6% Ce^{136}. Both were bombarded for the same period at the same neutron flux in the Oak Ridge National Laboratory graphite reactor. The samples were measured with a scintillation spectrometer and the 255-kev gamma ray activities per microgram of each of the cerium isotopes in the samples are shown in Table I. These data show that the yields of the 34.5-hr isomer per microgram of Ce^{136} are the same in the two samples and therefore the isomeric transition is in Ce^{137}.

III. ELECTRON CAPTURE DECAY OF Ce^{137}

When a mixture of stable cerium isotopes is bombarded with slow neutrons, a 445-kev gamma ray and x-rays which decay with an 8.7-hr half-life are produced. Chemical separation of cerium from rare earth impuri-

[1] J. B. Chubbock and I. Perlman, Phys. Rev. **74**, 982 (1948).
[2] B. J. Stover, Phys. Rev. **81**, 8 (1951).
[3] R. D. Hill, Phys. Rev. **82**, 449 (1951).
[4] H. B. Keller and J. M. Cork, Phys. Rev. **84**, 1079 (1951).
[5] B. H. Ketelle and G. E. Boyd, J. Am. Chem. Soc. **69**, 2800 (1947).
[6] C. H. Pruett and R. G. Wilkinson, Phys. Rev. **96**, 1340 (1954).
[7] Rose, Goertzel, Spinrad, Harr, and Strong, Phys. Rev. **83**, 79, (1951).
[8] M. E. Rose (privately distributed L conversion coefficients).
[9] M. Goldhaber and R. D. Hill, Revs. Modern Phys. **24**, 179 (1952).

TABLE I. Neutron capture yields referred to isotopic assays.

	255 kev counts/min μg				455 kev counts/min μg			
	Ce^{136}	Ce^{138}	Ce^{140}	Ce^{142}	Ce^{136}	Ce^{138}	Ce^{140}	Ce^{142}
Isotopic enrichment No. 1	9.8	430	4.5	71	30.8	1,340	14.2	220
Isotopic enrichment No. 2	10.1	6	0.8	21	31.0	18.3	2.4	64

ties shows that the activity is associated with a cerium isotope. The data in Table I show that the amount of the 445-kev gamma emitter formed is proportional to the amount of Ce^{136} bombarded and therefore, the transition must occur in the decay of Ce^{137}. The 445-kev gamma is in prompt coincidence with K x-rays which are not critically absorbed in the xenon proportional counter. These facts show that Ce^{137} decays by electron capture with at least some of the captures to a 445-kev level in lanthanum.

Decay curves of the x-rays and the 445-kev gamma ray show that the 8.7-hr electron capture process is the daughter of the 34.5-hr isomeric transition. When the parent and daughter are in equilibrium, the relative number of 255-kev and 445-kev transitions indicates that 3% of the electron captures are to the 445-kev level in La^{137}. An approximate K conversion coefficient of 0.02 for the 445-kev transition was computed from intensity ratios and indicates an $M1$ or $E2$ transition.

Approximate cross sections of Ce^{136} for pile neutrons have been computed from the yields. These give 20 barns for capture to the ground state and 2 barns for capture to the isomeric state of Ce^{137}. These cross sections are known within a factor of two and are in reasonable agreement with 25 barns$\pm$100% given by Pomerance[10] for the thermal neutron absorption cross section of cerium-136.

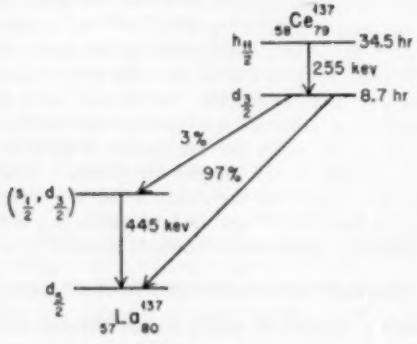

FIG. 1. Cerium-137 decay scheme.

[10] H. S. Pomerance, Phys. Rev. **88**, 442 (1952).

IV. DISCUSSION

On the basis of the single-particle model[11] an isomeric transition between $h_{11/2}$ and $d_{\frac{1}{2}}$ levels is probable in Ce^{137}. In the 79-neutron isotopes of Te, Xe, and Ba the single-particle predictions have been verified and isomeric transitions from $h_{11/2}$ levels to $d_{\frac{1}{2}}$ levels are known. In the case of Ce^{137} the K conversion coefficient and the K/L conversion ratio indicate an $M4$ transition for the decay of the 255-kev isomeric state. Therefore, the isomeric state is shown as an $h_{11/2}$ level in the decay scheme proposed for Ce^{137} in Fig. 1. Although it seems quite clear that the isomeric transition is to a $d_{\frac{1}{2}}$ level, it is not as certain that the ground state of Ce^{137} is a $d_{\frac{1}{2}}$ level. The ground states of many of the odd-neutron isotopes near the end of the 82-neutron shell are $s_{\frac{1}{2}}$ levels. The systematics of energy level spacing[9] do not lead to a definite prediction concerning the ground state of Ce^{137}. However, no experimental evidence for a $d_{\frac{1}{2}}-s_{\frac{1}{2}}$ transition following decay of the isomer was found. The fact that electron capture to the 445-kev and to the ground state of La^{137} is allowed can also be used as an argument against an $s_{\frac{1}{2}}$ ground state for Ce^{137}.

Of the single-particle levels available for assignment to the ground state of La^{137} only $d_{\frac{1}{2}}$ fits the experimental observations. Since the spin of Ba^{137} is known to be $d_{\frac{1}{2}}$, a transition between the ground states of La^{137} and Ba^{137} should be allowed. However, no evidence of K or L x-rays which could be attributed to electron capture decay of La^{137} was found. Because of the high x-ray counting efficiency of the detectors used in this work the lower limit for the K or L electron capture half-life for La^{137} must be increased from 400 years[1] to 10^6 years. The long half-life of La^{137} may mean that the energy available for the transition is very low. On the other hand, this may be another case where the probability of a transition is reduced because it occurs between a state with a mixed configuration and a pure single particle state.[12]

We are indebted to Dr. G. B. Rossi for arranging the cyclotron bombardment and to members of the Stable Isotopes Division of Oak Ridge National Laboratory for samples of enriched cerium isotopes and for isotopic assays.

[11] M. G. Mayer, Phys. Rev. **78**, 16 (1950).
[12] A. de-Shalit and M. Goldhaber, Phys. Rev. **92**, 1211 (1953).

Precision Energy Measurements of the Gamma Rays Following the Decay of Bi^{207}†

AVIVI I. YAVIN AND FRED H. SCHMIDT
Department of Physics, University of Washington, Seattle, Washington

(Received June 13, 1955)

The external conversion spectrum of the two intense gamma rays of Pb^{207} has been examined by means of a high resolution spectrometer. The 1.06-Mev gamma ray was found to consist of a single component of energy 1063.43±0.50 kev. The energy of the ground state transition was found to be 568.85±0.30 kev.

INTRODUCTION

THE usefulness of 8.0-yr Bi^{207} as an energy standard in beta- and gamma-ray spectroscopy has been pointed out by Alburger,[1] who made a precision measurement of the energy of electrons from the strongly-converted 1.06-Mev transition in Pb^{207}. However, Prescott[2] found an excess of coincidences between lead x-rays and the 1.06-Mev gamma ray, and accordingly suggested the existence of a closely spaced pair of nuclear levels giving rise to two gamma rays at very nearly 1.06 Mev. One of these was postulated to be a prompt transition, and the other the well-known 0.84-second isomeric decay. Very recently, Lazar and Klema[3] re-examined the gamma-ray spectrum with a scintillation-coincidence spectrometer and found no evidence for the existence of more than one transition at 1.06 Mev.

The work herein reported consisted of a search for a closely spaced pair of gamma rays near 1.06 Mev and precision measurements of the energies of both the 1.06- and the 0.57-Mev gamma rays.

EXPERIMENTAL METHOD AND RESULTS

The Bi^{207} was made in the University of Washington sixty-inch cyclotron by bombarding lead with 22-Mev deuterons for approximately 3000 microampere-hours. About 9 months after the bombardment was completed, the bismuth was separated from the lead following Alburger's[4] method. An external conversion source was prepared in the same manner as described by Keister, Lee, and Schmidt.[5] In order for the thorium radiator foil to subtend a maximum solid angle at the source material, a copper foil was placed between the source capsule and the radiator to absorb the K and L conversion electrons from the 1.06-Mev transition.

The photoelectric external conversion spectrum was measured in a uniform field solenoidal beta-ray spectrometer equipped with a ring focus.[6] Two runs were made: one with the spectrometer set at a nominal transmission of 4 percent utilizing a thorium foil radiator of 12.5 milligrams per cm^2 surface density, and a second with the spectrometer set at a nominal transmission of 2 percent utilizing a thorium foil radiator of 3.5 milligrams per cm^2 surface density. In each case, the radiators were of appropriate diameters (0.25 inch and 0.056 inch, respectively) to give optimum luminosity and momentum resolution. The inverse momentum resolution was approximately 1.5 percent and 0.4 percent full width at half-maximum for the two settings, respectively.

With the larger radiator and greater transmission, the peak counting rate of the K photoconversion line was 3 counts per second above background. The region from ~80 kev below to ~80 kev above the 1.06-Mev line was examined carefully. From this run we can state that no gamma ray exists in this region with an intensity greater than 10 percent of the 1.06 and differing by more than 10 kev in energy.

At the higher resolution setting with a 3.5 mg/cm^2 thorium radiator, the intensity of the 1.06-Mev K photoconversion line was only ~0.2 count/sec above a background of ~0.9 count/sec. These data are plotted in Fig. 1; the solid line is the transmission curve of the spectrometer as determined by the F line of thorium B. The results indicate that there is no other gamma ray differing in energy by more than

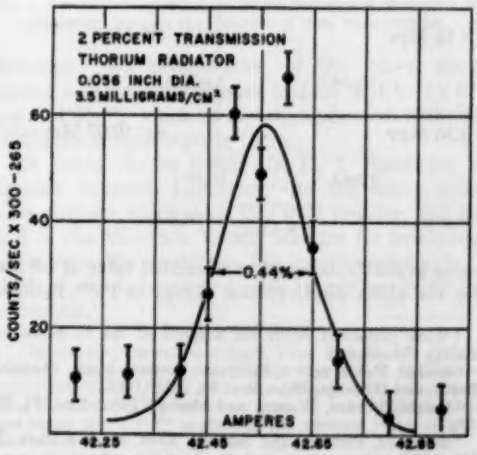

FIG. 1. K photoconversion line of the 1.06-Mev gamma ray at the higher resolution.

† Supported in part by the U. S. Atomic Energy Commission.
[1] D. E. Alburger, Phys. Rev. **92**, 1257 (1953).
[2] J. R. Prescott, Proc. Phys. Soc. (London) **A67**, 540 (1954).
[3] N. H. Lazar and E. D. Klema, Phys. Rev. **98**, 710 (1955).
[4] D. E. Alburger and G. Friedlander, Phys. Rev. **81**, 523 (1951).
[5] Keister, Lee, and Schmidt, Phys. Rev. **97**, 451 (1955).
[6] F. H. Schmidt, Rev. Sci. Instr. **23**, 361 (1952).

5 kev and with an intensity greater than 50 percent of the 1.06-Mev line.

The F line of thorium B was used to recheck the earlier precision calibration[7] of the spectrometer. The instrument is known to be linear to a very high degree.[7]

At the higher resolution the K photoconversion line of the 0.57-Mev gamma ray was ~0.6 count/sec above background. We conclude that two nearly equal energy gamma rays do not exist in the region of the 0.57-Mev gamma ray either.

Upon adding the 109.79-kev binding energy of thorium[8] to the measured energy of the K photoconversion electrons, we obtain 1063.43±0.50 kev and 568.85±0.30 kev, respectively, for the energies of the two gamma rays. The former is to be compared with the measurement of Alburger,[1] *viz.*, 1063.9±0.3 kev.

[7] D. I. Meyer and F. H. Schmidt, Phys. Rev. **94**, 927 (1954).
[8] Hill, Church, and Mihelich, Rev. Sci. Instr. **23**, 523 (1952).

Lazar and Klema[3] have shown that the 1.06−0.57 Mev cascade have relative gamma intensities of 0.77±0.06 and 1.00, respectively. Bi^{207} is thus particularly useful as a test source in gamma-ray coincidence spectroscopy. The 975.9-kev K conversion electrons[1] from the 1.06-Mev transition, together with the coincident 0.57 gamma ray, have proved to be of particular use in this laboratory for energy calibration of beta-gamma coincidence scintillation spectrometers.

ACKNOWLEDGMENTS

We wish to thank T. J. Morgan and the cyclotron crew for the long deuteron bombardment, J. R. Penning for help with the chemical separation, and H. R. Maltrud for assistance with the tedious hours of operation of the beta-ray spectrometer.

PHYSICAL REVIEW VOLUME 100, NUMBER 1 OCTOBER 1, 1955

Electron Capture Decay of Am^{244} and the Spontaneous Fission Half-Life of Pu^{244}†

P. R. Fields, J. E. Gindler, A. L. Harkness, M. H. Studier, J. R. Huizenga, and A. M. Friedman
Argonne National Laboratory, Lemont, Illinois

(Received June 30, 1955)

The branching ratio (electron captures/beta particles) of Am^{244} was determined as 0.039±0.003%. An enriched Pu^{244} sample was isolated from neutron irradiated Am^{243}, and the spontaneous fission half-life of Pu^{244} was found to be $(2.5\pm0.8)\times10^{10}$ years.

A CONSIDERATION of the closed energy cycle[1]

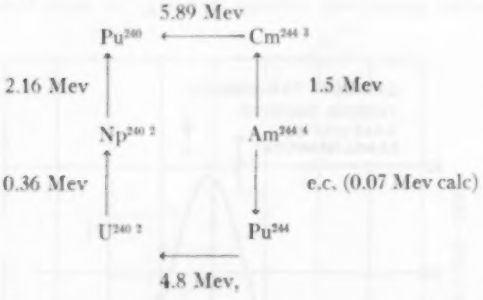

using available data and an estimated value of 4.8 Mev for the alpha disintegration energy of Pu^{244}, indicates that Am^{244} may be slightly unstable toward electron capture decay. The fact that Pu^{244} is apparently beta stable[1,5] suggests that Am^{244} is analogous to Am^{242} and is probably unstable toward electron capture decay. Evidence of electron capture decay for Am^{244} can be found in the Materials Testing Reactor (MTR) irradiations of plutonium. The Pu^{242} to Pu^{244} ratios in several MTR irradiations of plutonium (Table I) indicated that Pu^{244} was being produced more rapidly than would be predicted from the path

$$Pu^{242}(n,\gamma)Pu^{242}(n,\gamma)Pu^{244},$$

and that some Pu^{244} was probably being formed by the alternate path

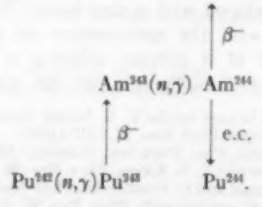

† Work performed under the auspices of the U. S. Atomic Energy Commission.
[1] Studier, Fields, Sellers, Friedman, Stevens, Mech, Diamond, Sedlet, and Huizenga, Phys. Rev. **93**, 1433 (1954).
[3] Knight, Bunker, Warren, and Starner, Phys. Rev. **91**, 889 (1953).
[5] Hollander, Perlman, and Seaborg, Revs. Modern Phys. **25**, 611 (1953).
[6] Ghiorso, Thompson, Choppin, and Harvey, Phys. Rev. **94**, 1081 (1954).
[1] Inghram, Hess, Fried, and Pyle, private communication.

TABLE I. The Pu^{244}/Pu^{242} ratios in MTR irradiated plutonium

Sample No.	Integrated flux	Pu^{244}/Pu^{242}
1	4×10^{21}	5.28×10^{-5}
2	1.1×10^{22}	3.84×10^{-4}
3	1.4×10^{22}	5.26×10^{-4}

In order to determine the electron capture branching ratio of Am^{244} and to prepare some enriched Pu^{244} samples, Am^{243} was irradiated in the Argonne heavy water reactor and in the MTR.

Approximately one milligram of Am^{243} was irradiated for two days in the heavy water reactor and later also irradiated for three weeks in the MTR. The plutonium formed in the irradiation was isolated from the Am^{243} with a Dowex A-1 anion resin column and TTA (thenoyltrifluoroacetone) extractions. Table II shows the amount of Pu^{244} and Cm^{244} formed in the irradiations and Table III gives the isotropic composition of the plutonium fractions. An average branching ratio (electron captures/beta particles) of 0.039 $\pm$0.003% was obtained from the two experiments. The largest source of error in the determination is the uncertainty in the Cm^{244} half-life (18.4$\pm$0.5 yr).[6] Complete recovery of plutonium was assumed, and in

TABLE II. Results of irradiating *ca* 1 mg of Am^{243}.

Reactor	μg Pu^{244} formed	μg Cm^{244} formed
CP-5	3.75×10^{-5}	8.95×10^{-2}
MTR	1.42×10^{-3}	39.15

view of the fact that the recovery of plutonium after the first step in the purification could be followed by the alpha pulse analyzer, this assumption is probably fairly reliable. From the branching ratio and the half-life for beta emission (25 min)[4] an electron capture half-life of 44.5 days was calculated. A mass spectrometric analysis of the irradiated Am^{243} showed less than 0.001% Am^{244}. If Am^{244} has a long-lived ground state similar to Am^{242}, then the branching of Am^{244} to this state is less than 0.002%. The figure 0.002% was calculated by also taking into consideration the fact that on the average approximately one-half of the Am^{243} was in the MTR for about one year before it was isolated and reirradiated for the present experiment.

TABLE III. Isotopic composition of plutonium formed from irradiation of *ca* 1 mg of Am^{243}.

Plutonium isotope	CP-5 reactor	MTR
Pu^{238}	17.8 $\pm$0.2[a]	<2.1
Pu^{239}	13.0 $\pm$0.2[a]	8.1$\pm$0.2
Pu^{240}	67.5 $\pm$0.3	70.4$\pm$0.4
Pu^{241}	0.052$\pm$0.004	1.7$\pm$0.1
Pu^{242}	1.63 $\pm$0.09[a]	4.2$\pm$0.2
Pu^{244}	0.058$\pm$0.004	13.5$\pm$0.3

[a] The larger percentages of Pu^{238}, Pu^{239}, and Pu^{242} were due to the fact that the plutonium was contaminated with some of the original irradiated plutonium. The amount of Pu^{244} introduced by this contamination was negligible.

[5] Friedman, Harkness, Fields, Studier, and Huizenga, Phys. Rev. **95**, 1501 (1954).

In the MTR irradiation sufficient enriched plutonium was formed to measure the spontaneous fission half-life of Pu^{244}. A total of 110 fissions in 50 356 minutes was observed using a sample containing 0.0064 microgram of Pu^{244}. After correcting for the counter background (0.00033 counts/minute), and the spontaneous fission rates due to the Pu^{240} [7,8] and Pu^{242} [9] in the sample, a spontaneous fission half-life of $(2.5\pm0.8)\times10^{10}$ years was calculated for Pu^{244}.

Figure 1 shows a plot of the logarithm of the spontaneous fission half-lives of even-even plutonium isotopes as a function of the mass number A as proposed by

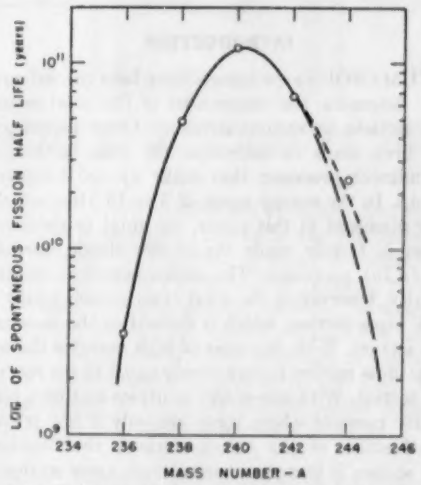

FIG. 1. A plot of the spontaneous fission half-lives of the even-even plutonium isotopes as a function of their mass number.

Huizenga.[10] An extrapolation of this curve would predict a spontaneous fission half-life of $1.5-2\times10^{10}$ years of Pu^{244}, which is in fair agreement with the experimental value reported here.

We would like to thank Mr. D. J. Henderson of Argonne National Laboratory for the many alpha pulse analyses which made this work possible, and the staff of the Materials Testing Reactor for irradiating our sample. We would also like to acknowledge J. F. Mech of this Laboratory for his help in purifying the americium.

[7] Chamberlain, Farwell, and Segrè, Phys. Rev. **94**, 156 (1954).

[8] E. M. Kinderman, Atomic Energy Commission Declassified Report HW-27660, April, 1953 (unpublished). The more recent value of $1.51\times10^{3}\pm2\%$ fissions per gram per hour for the spontaneous fission rate of Pu^{240} as given in this reference was used in the calculations.

[9] M. H. Studier and A. Hirsch (private communication).

[10] J. R. Huizenga, Phys. Rev. **94**, 158 (1954).

Nonelastic Scattering Cross Sections for Fast Neutrons*†

H. L. Taylor, O. Lönsjö, and T. W. Bonner
The Rice Institute, Houston, Texas

(Received June 16, 1955)

Measurements have been made of the nonelastic cross sections of neutrons in Be, C, Al, Ti, Cr, Fe, Ni, Cu, Ag, Sn, Pb, and Bi. These cross sections include all processes except elastic scattering. The experiments have been carried out with monoenergetic neutrons of 3.5, 4.7, 7.1, 12.7, and 14.1 Mev. The neutrons were produced with a Van de Graaff accelerator using the nuclear reactions: $T^3(p,n)He^3$, $D(d,n)He^3$, and $T^3(d,n)He^4$. Cross sections were determined from transmissions through spherical shells which were 3.8 cm in radius and 2 cm thick. A new type of neutron detector which gives energy information about neutrons and is insensitive to γ radiation was placed at the center of the spherical shell and was used as a biased detector of neutrons. The results of these experiments show that the nonelastic neutron cross section for 12.7- and 14.1-Mev neutrons is nearly geometrical and is closely approximated by $\sigma=\pi(R+\lambda)^2$, where $R=1.4\times10^{-13}A^{\frac{1}{3}}$. The nonelastic cross sections are roughly constant in the energy range 5 to 14 Mev; below about 5 Mev the cross sections begin to decrease.

The elastic cross sections can be obtained by subtracting the nonelastic cross sections from the total cross sections. The variations with energy of the nonelastic and elastic cross sections are quite different.

Data with 12.7-Mev neutrons and low counter bias, give the relative number of γ rays given off per inelastic collision of these neutrons. The number of γ rays decreases rapidly with increasing atomic number and there are less than 5% as many γ rays from Bi as from Al, Ti, Cr, and Fe.

INTRODUCTION

NUMEROUS experiments have been carried out to determine the magnitudes of the total neutron cross sections in various elements. Other experiments have been made to determine the cross sections for the different processes that make up the total cross sections. In the energy range of 3 to 15 Mev, which is to be discussed in this paper, the total neutron cross section is largely made up of the elastic, inelastic, and $(n,2n)$ processes. The experimentally measured quantity, however, is the total cross section minus the elastic cross section, which is defined as the nonelastic cross section. With neutrons of high energies the nonelastic cross section is very nearly equal to the reaction cross section. With low-energy neutrons and with intermediate energies where there are only a few possible excited states of the struck nucleus, the nonelastic cross section is less than the reaction cross section by the amount of the compound elastic scattering. Early experiments[1] with a radium-beryllium source of neutrons placed inside a spherical absorber qualitatively measured the cross section for inelastic scattering of neutrons in the absorber. More recent experiments[2,3] with 14-Mev neutrons and threshold detectors gave results which are in general agreement with the present cross sections.

Another method for estimating the inelastic scattering cross section has been to determine the neutron spectrum by the exposure of photographic plates to neutrons.[4,5] Measurements by Graves and Rosen with 14- to 15-Mev neutrons indicate that for all elements from aluminum to bismuth almost all the inelastically scattered neutrons have an energy of less than 5 Mev. This method is good for finding the energy distribution of the inelastically scattered neutrons but is not adapted for accurate quantitative values of the cross section.

If a monoenergetic source of neutrons is surrounded by a sphere of a material with which the neutrons could interact only by elastic scattering, a biased detector, whose energy discrimination was not sufficiently sharp to resolve the small loss of energy from elastic scattering, would count at the same rate with the scatterer on as with the scatterer off. If, however, the neutrons are inelastically scattered with sufficient loss of energy such that they will not be detected, then they have been effectively absorbed in a transmission experiment.

It is more convenient to place the detector inside the spherical scatterer which subtends a small solid angle from a source so that all the neutrons incident on the scatterer have very nearly the same energy. A general proof for the validity of such an interchange of source and detector has been given by Bethe.[6]

The general theory for calculating nonelastic cross sections by transmission through a thick spherical shell has been worked out by Bethe, Beyster, and Carter[7] and has been used in analyzing the experimental results reported herein. The purposes of the present research were to adapt a new scintillation type detector to a useful form and to measure the nonelastic scattering

* Supported in part by the U. S. Atomic Energy Commission.

† Preliminary report of these results was given at the Pittsburgh Conference on Medium Energy Nuclear Physics, June, 1953 (unpublished); Birmingham Conference on Nuclear Physics, July, 1954 (unpublished); and Phys. Rev. **94**, 807(A) (1954).

[1] Dunning, Pegram, Fink, and Mitchell, Phys. Rev. **48**, 265 (1935); Seaborg, Gibson, and Grahame, Phys. Rev. **52**, 408 (1937); D. C. Grahame and G. T. Seaborg, Phys. Rev. **53**, 795 (1938).

[2] Gittings, Barschall, and Everhart, Phys. Rev. **75**, 1610 (1949).

[3] Phillips, Davis, and Graves, Phys. Rev. **88**, 600 (1952).

[4] P. H. Stetson and Clark Goodman, Phys. Rev. **82**, 69 (1951); E. R. Graves and L. Rosen, Phys. Rev. **89**, 343 (1953).

[5] B. G. Whitmore and G. E. Dennis, Phys. Rev. **84**, 296 (1951); B. G. Whitmore, Phys. Rev. **92**, 654 (1953).

[6] H. A. Bethe, Los Alamos Report LA-1428, 1952 (unpublished).

[7] Bethe, Beyster, and Carter, Los Alamos Report LA-1429 (unpublished).

cross sections of elements of various atomic weights as a function of energy from 3.5 to 14.1 Mev.

APPARATUS

The scattering samples were thick spherical shells with a standard size of 7.62 cm outside diameter with a 2 cm wall thickness. There was a hole of 1.62-cm diameter through the shell for the insertion of the light pipe to the counter. The spheres were machined to a tolerance of less than 0.002 cm from commercially available materials. The one exception to the standard size was the chromium sphere which was 7.15 cm in outside diameter with a 2-cm wall.

The neutron detectors were made of an organic scintillator which gave light pulses from recoil protons caused by neutron scattering in the scintillator.[8] The light pulse is proportional to the range of the ionizing particle in the scintillator.[9] In order to count neutrons and not γ rays, it was necessary to make pulses due to Compton electrons a factor of 2 to 3 smaller than the neutron pulses. The plastic scintillator[10] was made into spheres of such size that an electron passing through the diameter of the scintillating sphere would give less than half as large a pulse as neutrons from the source. Anthracene crystals were used in the first experiments. A plastic scintillator was substituted for the anthracene detector since the pulse size in anthracene varies as much as 15% with the direction of the neutrons. The plastic scintillators and the detectors made from them did not show directionality of response.

In order to have a high counting rate it is desirable to use a scintillator with a large volume. For the 12.7- and 14-Mev neutron detector, it would have been possible to use a scintillation sphere 2 cm in diameter and still discriminate against γ-ray pulses. A 1 cm diameter scintillator was used and was large enough to give an adequate counting rate. The maximum pulse due to γ rays in this scintillator is produced by a 2.5-Mev electron which will have a range of 1 cm in the plastic. Such a pulse is the same size as that of a 6-Mev recoil proton.

An adequate counting rate for 7.1-Mev neutrons was obtained with a single sphere with a diameter of 6.5 mm. An electron of 1.6 Mev will just traverse the sphere and produce a pulse in the scintillator equal to half that from a 7-Mev recoil proton.

For the 4.7-Mev neutron detector, it was necessary to use spheres with a diameter of 2.5 mm. The range of a 0.75-Mev electron is 2.5 mm; an electron of this energy produces a pulse 45% as large as a 4.7-Mev recoil proton in the scintillator. A single sphere of 2.5-mm diameter did not give a satisfactory counting rate, so a detector was constructed using four such spheres. Two

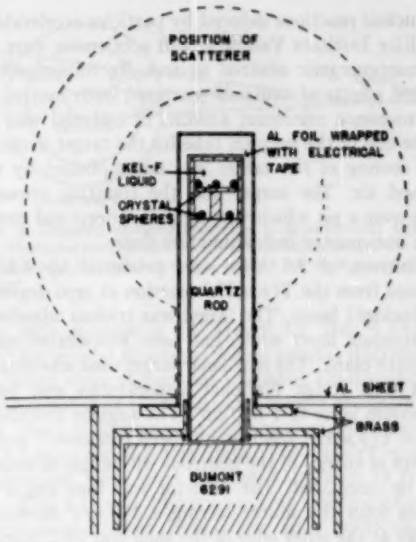

FIG. 1. Diagram of neutron detector showing spherical scintillators, quartz light pipe, and position of the scattering sample.

spheres were placed in each of two layers, the upper layer being supported on a glass disk and positioned so that the spheres were not directly above the spheres in the lower layer. To improve optical coupling and to place electron stopping material between the spheres, the volume of the detector was filled with Kel-F fluid[11] ($Cl_3F_3C_6$). A fluid containing no hydrogen was used to avoid production of recoil protons in the fluid. The minimum energy of an electron which passes through two spheres and the intervening Kel-F is 4 Mev.

The 3.5-Mev neutron detector was constructed of scintillation spheres with a diameter of 1.5 mm. An electron of 0.5 Mev produces a pulse equal to 50 percent of the pulse from a 3.5-Mev proton and has a range of 1.5 mm in the scintillator. Eight spheres were arranged at quadrant points of each of two layers in a glass tube of 10 mm inside diameter. Spheres in the upper layer were supported by a glass disk and were not directly over the spheres of the lower layer. The sealed volume was filled with Kel-F fluid. Only electrons with energies greater than 3 Mev could traverse two spheres and the minimum intervening material. The 3.5-Mev detector and mounting to hold the spherical absorbers is illustrated in Fig. 1. The detectors were constructed on a quartz rod of such a length as to place the geometrical center of the detector at the center of the scattering shell. The detector and quartz were wrapped with 0.0005 inch aluminum foil and scotch electrical tape and optically coupled to the Dumont 6291 photomultiplier tube by silicone vacuum grease.

[8] McCrary, Taylor, and Bonner, Phys. Rev. **94**, 808(A) (1954).
[9] J. B. Birks, Phys. Rev. **84**, 364 (1951); Taylor, Jentschke, Remley, Eby, and Kruger, Phys. Rev. **84**, 1034 (1951).
[10] Obtained from Nuclear Enterprises, Ltd., 1124 Grosvenor Avenue, Winnipeg, Canada.
[11] Manufactured by W. M. Kellogg Company, Chemical Manufacturing Division, Jersey City, New Jersey.

Nuclear reactions induced by particles accelerated in the Rice Institute Van de Graaff accelerator were used as monoenergetic neutron sources. To minimize background effects of neutrons scattered from matter near the source, a minimum amount of material was used at the end of the vacuum tube for the target mounting, and cooling of the target was accomplished by compressed air. The target and the counting apparatus were over a pit which was eight feet deep and covered by a one-quarter inch aluminum floor.

Neutrons of 3.5 Mev were produced by 4.2-Mev protons from the $T(p,n)He^3$ reaction at zero degrees to the incident beam. The target was tritium adsorbed in a zirconium layer which had been evaporated onto a tungsten blank. The particular target used was obtained from Oak Ridge National Laboratories and had a zirconium layer of 1 mg/cm². The angular distribution of the $T(p,n)He^3$ reaction has been measured[12] and the change of energy of the neutrons with angle of emission can be calculated. The detector was four and a half inches from the source, giving a 110-kev decrease in energy at the outer edge of the shell and 10% illumination decrease at the outer edge of the shell.

The $D(d,n)He^3$ reaction was used as the source for the 4.7-Mev and 7.1-Mev neutrons with bombarding energies of 1.47 and 3.8 Mev, respectively. The gas chamber was 3.8 cm long, 1.3 cm in diameter, and had a beam entrance aperture of 0.6 cm diameter covered by a 0.0001 inch nickel foil. About 0.3 atmos of deuterium gas was used as a target. The detector for the 4.7-Mev neutrons was placed 4 inches from the center of the target; the detector-to-target distance was increased to 12 inches in the experiments with 7.1-Mev neutrons; with such geometry there is a decrease of 50 kev in the energy of the neutrons at the maximum subtended half-angle and a decrease in illumination[13] of 9 percent.

The $T(d,n)He^4$ reaction was used as the source for 12.7-Mev and 14.1-Mev neutrons. The detector was placed 8 inches from the source at 160° to the direction of the incident beam of 675-kev energy to get 12.7-Mev neutrons and at 90° with respect to the 350-kev beam for the 14.1-Mev neutrons.

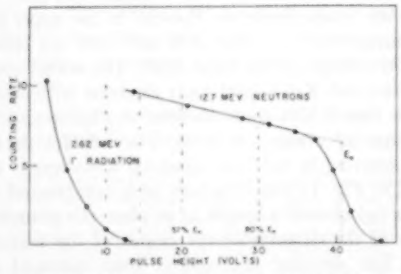

FIG. 2. Pulse-height distribution curve for 12.7-Mev neutrons in 1 cm scintillator and pulse height distribution of γ rays of maximum effective energy.

[12] Willard, Bair, and Kington, Phys. Rev. **90**, 865 (1953); G. A. Jarvis (private communication).
[13] Henkel, Perry, and Smith (private communication).

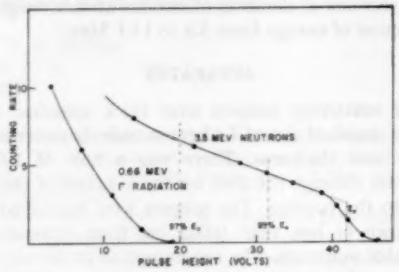

FIG. 3. Pulse height distribution curve for 3.5-Mev neutrons in eight 1.5 mm diameter scintillators and pulse distribution of γ rays of maximum effective energy.

DATA

Figure 2 shows the pulse distribution curve of the neutron detector for 12.7-Mev neutrons and that obtained from the 2.62-Mev γ radiation from a Th C″ source. Figure 3 gives the similar pulse distribution curve which was obtained with 3.5-Mev neutrons and 0.66-Mev γ radiation. The pulse height distribution curve for neutrons is not quite flat, since the pulse height depends on the range of the particle producing the pulse and not its energy.

The pulse-height distribution curves in Figs. 2 and 3 are typical experimental curves which also indicate the relative size of neutron pulses and maximum possible γ-ray pulses. Theoretically the curve should drop off sharply at the upper end as indicated by the E_0 dotted line.

A bias value corresponding to 80% of the energy of the source neutrons was used for the cross-section determination at 12.7 and 14.1 Mev and a value of 85% at 3.5, 4.7, and 7.1 Mev. Data were also obtained with a lower bias in all the experiments. The efficiency of detection as a function of neutron energy was measured for each detector, and the results for the 3.5-Mev neutron detector are shown in Fig. 4 when biased at 85% of the 3.5-Mev energy. The efficiency of detection curves for the other neutron detectors were similar in shape to that given in Fig. 4.

The cross-section data were taken by measuring counting rates with the scatterer in position and removed. The ratio of the counting rate with the scatterer in position to the counting rate without the scatterer is the experimental transmission. Results of these transmissions are given in Table I; each transmission is a mean of 6 to 20 separate experiments. Simultaneously with the 80% or 85% bias, a transmission using a lower bias was taken to find the dependence of the transmission on the choice of bias point.

Figure 5 shows the geometry of the experimental arrangement. The transmission must be corrected because of the uncompensated elastic scattering due (1) to the decreased efficiency of detecting the elastically scattered neutrons of slightly less energy because of energy loss to the struck nucleus, (2) a decrease in the efficiency of detecting neutrons of lower energy from the source which are emitted at an angle ϕ, and (3) the nonuniform illumination of the spherical scatterers.

The detector for neutrons of 3.5, 4.7, and 7.1 Mev was placed at zero degrees with respect to the direction of the accelerator beam on the target and subtended a very small solid angle at the source as indicated in Fig. 5. Thus the neutrons detected when the scatterer was not in position were emitted from the source at essentially zero degrees. When the scatterer was in position, the neutrons which did not reach the detector because of elastic scattering in the portion of the shell directly between the source and detector, at point A in Fig. 5 are assumed to equal (except for small corrections) the number of neutrons elastically scattered towards the detector by the rest of the spherical shell. Such elastically scattered neutrons will not have exactly the same energy as the incident neutrons and, as indicated by Fig. 4, will not have the same probability of being detected. The fraction of the incident neutrons so scattered is $(1-e^{-N\sigma_e})$, where N is the number of nuclei per square centimeter of the scatterer and σ_e is the elastic scattering cross section. The value of σ_e is obtained by subtracting an assumed value of nonelastic scattering cross section σ_n from the total scattering cross section σ_t. When necessary in view of later calculations, the assumed σ_n was revised. The energy lost by a neutron depends on the angle θ through which it is scattered. The number of elastically scattered neutrons as a function of angle of scattering is needed in order to make corrections (1), (2), and (3) listed above.

Angular distributions have been studied with neutrons with energies of 1.0 Mev,[14] 4.1 Mev,[15] and 14 Mev[16] for several elements. Where angular distribution data for an element were not available, the distribution for the element of nearest atomic weight available was used. The 4.1-Mev angular distributions were used for the 3.5-Mev and 4.7-Mev data. The 14-Mev angular distributions were used for the 12.7- and 14.1-Mev data. The 4.1- and 14-Mev angular distributions are similar in that they both show large scattering at small angles. Therefore, since no angular distributions were available near 7 Mev, the effects expected from both 4- and 14-Mev angular distributions were calculated for the 7.1-Mev data and a linear interpolation was made to get the effect expected from 7-Mev angular distributions. The errors introduced by this approximation are quite small except in the case of the very light elements, Be and C, where the error was considered to be too large to make the results very useful. In the case of lead the correction for source energy spread and illumination is 3.7% of the number of elastically scattered neutrons with 4-Mev angular distributions, 1.4% with 14-Mev distributions, and 3.0% for the interpolated value at 7 Mev.

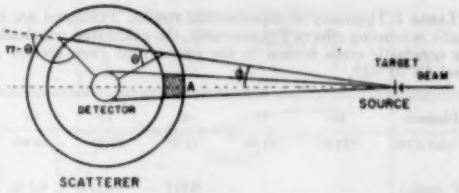

FIG. 5. Diagram showing geometry of experimental arrangement. Neutrons emitted at an angle ϕ to the direction of the beam are elastically scattered through angle θ or $\pi-\theta$ to reach the detector.

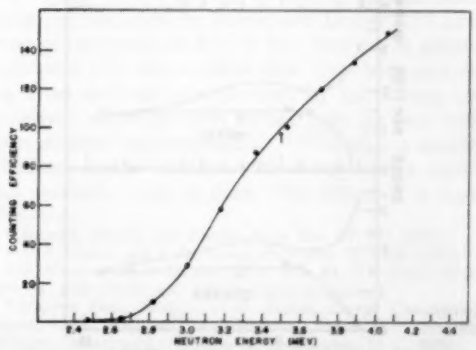

FIG. 4. Relative efficiency as function of neutron energy for detector biased at 85% energy for 3.5-Mev neutrons.

The transmissions, corrected for uncompensated elastic scattering are given as T (corrected) in Table I. The difference between the experimental transmission and the corrected transmissions are smaller at the higher energies and with heavier nuclei. Considerable errors may result for light nuclei, especially in the case of Be and C where the corrections are large and the angular distributions do not extend past 90° for 14-Mev neutrons.

The nonelastic cross sections were calculated from an expression derived by Bethe, Beyster, and Carter which takes account of multiple scattering in the shell:

$$(1-T)=(1-T_0)\frac{\sigma_n}{\sigma_n+\sigma_{el}P_m},$$

where T = experimental transmission (corrected), $T_0 = e^{-N\sigma_t}$, P_m = escape probability of the neutron, σ_n = nonelastic cross section, σ_e = elastic cross section, σ_{el} = elastic

[14] M. Walt and H. H. Barschall, Phys. Rev. **93**, 1062 (1954).
[15] M. Walt and J. R. Beyster, Phys. Rev. **98**, 677 (1955).
[16] J. H. Coon and R. W. Davis, Phys. Rev. **94**, 786(A) (1954), and private communication.

TABLE I. Summary of experimental results. Tabulated are the experimental transmission T (expt.), the transmissions corrected for elastic scattering effects T (corrected), the calculated nonelastic cross section σ_n, the total scattering cross section σ_t, and the ratio of the nonelastic cross section to the geometrical cross section for each element. The nuclear radius is calculated from the relation $R=1.4\times10^{-13}A^{\frac{1}{3}}$.

Element	Be	C	Al	Ti	Cr	Fe	Ni	Cu	Ag	Sn	Pb	Bi
$N/cm^2\times10^{22}$	24.0	16.06	12.37	11.38	16.05	16.91	18.18	16.90	11.72	7.40	6.59	5.62
						3.5 Mev						
T (expt.)			0.877	0.832	0.776	0.773	0.717	0.734	0.758	0.845	0.876	0.883
T (corrected)			0.913	0.857	0.813	0.807	0.747	0.767	0.775	0.857	0.891	0.896
σ_n			0.68 ±0.05	1.24 ±0.05	1.14 ±0.04	1.14 ±0.04	1.48 ±0.04	1.45 ±0.04	2.03 ±0.07	2.00 ±0.09	1.58 ±0.07	1.73 ±0.06
σ_t			2.40	3.67	3.90	3.47	3.35	3.45	4.18	4.28	7.70	7.76
$\sigma_n/\pi(R+\lambda)^2$			0.49	0.70	0.62	0.60	0.76	0.72	0.81	0.73	0.44	0.48
						4.7 Mev						
T (expt.)			0.872	0.828	0.758	0.738	0.703	0.704	0.749	0.826	0.831	0.848
T (corrected)			0.912	0.854	0.797	0.777	0.741	0.737	0.769	0.838	0.851	0.867
σ_n			0.70 ±0.05	1.32 ±0.06	1.32 ±0.03	1.38 ±0.05	1.54 ±0.06	1.69 ±0.04	2.14 ±0.07	2.33 ±0.07	2.25 ±0.07	2.39 ±0.06
σ_t			2.20	3.40	3.70	3.72	3.55	3.72	4.01	4.00	7.40	7.48
$\sigma_n/\pi(R+\lambda)^2$			0.56	0.81	0.78	0.79	0.87	0.91	0.88	0.92	0.66	0.70
						7.1 Mev						
T (expt.)			0.889	0.848	0.782	0.758	0.743	0.754	0.770	0.844	0.825	0.851
T (corrected)			0.914	0.865	0.809	0.783	0.770	0.779	0.782	0.851	0.833	0.857
σ_n			0.74 ±0.05	1.21 ±0.04	1.22 ±0.04	1.35 ±0.04	1.33 ±0.06	1.37 ±0.05	2.01 ±0.07	2.12 ±0.06	2.67 ±0.07	2.66 ±0.07
σ_t			1.88	3.18	3.50	3.44	3.60	3.73	4.12	4.08	5.60	5.60
$\sigma_n/\pi(R+\lambda)^2$			0.63	0.83	0.81	0.86	0.84	0.82	0.91	0.92	0.85	0.84
						12.7 Mev						
T (expt.)	0.821	0.892	0.873	0.871	0.810	0.786	0.773	0.768	0.806	0.860	0.842	0.867
T (corrected)	0.871	0.910	0.876	0.873	0.813	0.789	0.776	0.771	0.808	0.861	0.843	0.868
σ_n	0.49 ±0.08	0.56 ±0.10	1.06 ±0.07	1.17 ±0.06	1.26 ±0.07	1.36 ±0.05	1.35 ±0.05	1.49 ±0.05	1.75 ±0.10	1.97 ±0.09	2.58 ±0.09	2.47 ±0.14
σ_t	1.60	1.30	1.69	2.37	2.60	2.67	2.83	3.10	4.41	4.61	5.15	5.05
$\sigma_n/\pi(R+\lambda)^2$	0.92	0.91	1.11	0.91	0.95	0.98	0.96	1.01	0.88	0.94	0.90	0.86
						14.1 Mev						
T (expt.)	0.855	0.899	0.886	0.872	0.802	0.786	0.761	0.777	0.804	0.870	0.843	0.866
T (corrected)	0.909	0.918	0.890	0.873	0.804	0.788	0.763	0.779	0.806	0.871	0.844	0.867
σ_n	0.57 ±0.08	0.51 ±0.08	0.91 ±0.05	1.17 ±0.04	1.33 ±0.04	1.38 ±0.03	1.45 ±0.05	1.44 ±0.04	1.78 ±0.05	1.82 ±0.06	2.52 ±0.09	2.50 ±0.07
σ_t	1.55	1.34	1.73	2.28	2.45	2.60	2.72	2.96	4.34	4.68	5.48	5.46
$\sigma_n/\pi(R+\lambda)^2$	0.72	0.86	0.99	0.94	1.02	1.02	1.05	1.00	0.91	0.88	0.89	0.88

transport cross section $=(\sigma_t-\sigma_n)S$, and

$$S=\frac{\int\sigma_e(\theta)(1-\cos\theta)d\theta}{\int\sigma_e(\theta)d\theta}.$$

To use this formula it is necessary to assume a value of σ_n and use it in the equation. The nonelastic cross section σ_n is subtracted from the known σ_t to determine σ_e. The P_m values have been calculated by Bethe, Beyster, and Carter, and in this experiment had values which extended from 0.65 to 0.84. A trial and error process of successive approximations is necessary to

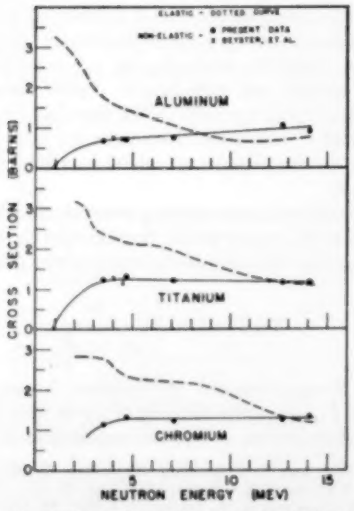

FIG. 6. Nonelastic (solid curve) and elastic (broken curve) cross sections in Al, Ti, and Cr.

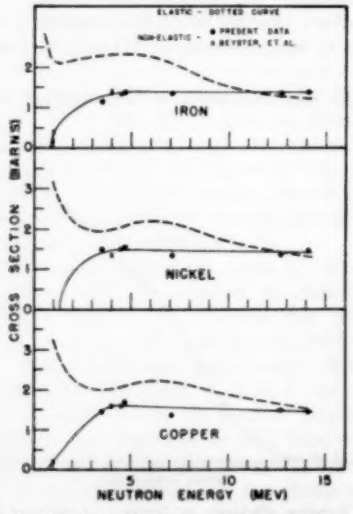

FIG. 7. Nonelastic (solid curve) and elastic (broken curve) cross sections in Fe, Ni, and Cu.

achieve the final result. The calculated nonelastic cross sections σ_n are given in Table I. These cross sections are too small by an amount depending on the number of inelastically scattered neutrons which are still counted by the biased detector. In general this is a small effect and an estimate of its magnitude can be obtained by comparing the cross sections calculated from the data with lower energy bias.

Data taken with 3.5-Mev neutrons and a bias of 57% of the maximum energy instead of 85% gave an average decrease in the cross section of 11% for the elements chromium through bismuth. In most cases the energy of the first excited state is large enough so that inelastically scattered neutrons will have a very low efficiency for being counted when using the 85% bias. For example inelastically scattered neutrons from iron will lose 0.845 Mev or greater energy and will have a relative efficiency for being counted of 2% or less.

With 4.7-Mev neutrons, data were taken with a bias of 70% as well as 85% of the energy. The average decrease in cross section with the 70% bias was 7%, indicating about 7% of the neutrons inelastically scattered to energies between 2.9 and 3.8 Mev. Silver is the only element with energy levels below about 0.6 Mev. The probability of detection of 4.1-Mev neutrons was 50%. Therefore, neutrons exciting levels of 0.6 Mev or less would contribute less than 50% of their cross section to the observed value.

With 12.7-Mev neutrons a bias point corresponding to 57% of the source neutron energy gave cross sections which were an average of only 4% smaller than for the 80% bias. This result indicates that only 4% of the inelastically scattered neutrons have an energy between 7.2 and 10.2 Mev in agreement with the photoplate-experiments of Graves and Rosen that most of the inelastically scattered neutrons have energies less than 5 Mev.

DISCUSSION

The results of the nonelastic cross sections are shown in Figs. 6, 7, 8, and 9. Recent data of Beyster, Henkel, and Nobles[17] at 1.0, 4.0, and 4.5 Mev are also included. Data just published by Graves and Davis[18] with neutrons of energies from 13.5 to 14.7 Mev are in general agreement with our 14.1-Mev data. The elastic scattering cross sections were obtained by subtracting the nonelastic scattering cross section from the best total cross sections that are available.[19–22] There is a marked difference in the variation with energy of the elastic and nonelastic cross sections. This difference is most

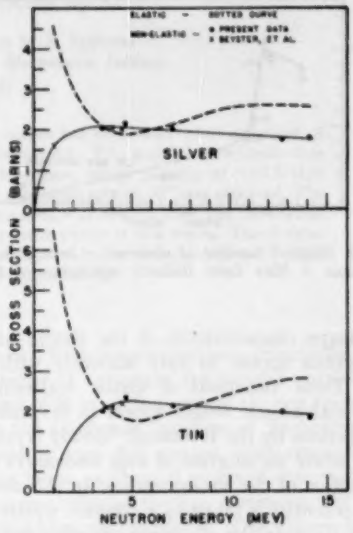

FIG. 8. Nonelastic (solid curve) and elastic (broken curve) cross sections in Ag and Sn.

marked in the case of Ag and Sn where the elastic cross section becomes larger as the energy increases from 5 to 14 Mev. In this same energy interval the nonelastic cross section decreases. In all the elements studied, except for Cu, the nonelastic cross section is greater than the elastic cross section at some particular energy.

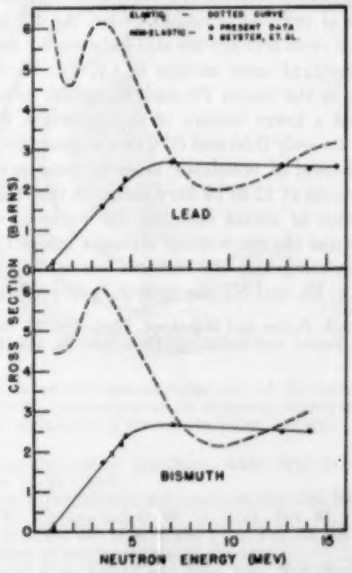

FIG. 9. Nonelastic (solid curve) and elastic (broken curve) cross sections in Pb and Bi.

[17] Beyster, Henkel, and Nobles, Phys. Rev. **97**, 563 (1955).
[18] E. R. Graves and R. W. Davis, Phys. Rev. **97**, 1205 (1955).
[19] N. Nereson and S. Darden, Phys. Rev. **89**, 775 (1953); Phys. Rev. **94**, 1678 (1954); and private communication.
[20] *Neutron Cross Sections*, U. S. Atomic Energy Commission Report AECU 2040 and 3 supplements (Technical Information Division, Department of Commerce, Washington, D. C., 1952).
[21] Bonner, Alba, Fernandez, and Mazari, Phys. Rev. **97**, 985 (1955).
[22] McCrary, Taylor, and Bonner (unpublished data on Cr).

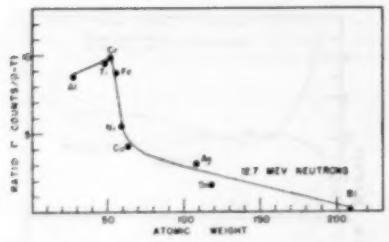

FIG. 10. Relative number of observed γ rays with energies greater than 3 Mev from inelastic scattering of 12.7-Mev neutrons.

The shape characteristics of the elastic scattering cross sections appear to vary smoothly with atomic weight. These variations of elastic scattering cross sections with atomic weight appear to fit qualitatively the predictions by the Weisskopf "cloudy crystal ball" model,[23] where the location of wide resonances appears as a function of the nuclear radius. In this model the nuclear potential is taken as a complex square well of the form $V=V_0(r)(1+i\zeta)$, where ζ is some real number which gives the absorption necessary to account for the formation of a compound nucleus. Feshbach, Porter, and Weisskopf[22] fitted the total cross sections up to about 3 Mev with this model using a ζ equal to 0.03. The large nonelastic cross sections obtained in the present experiments require a larger ζ at higher energies.

Comparison of the measured nonelastic cross section to the geometrical cross section is shown in Table I. The nuclear radius R was calculated from the relation: $R=1.4\times10^{-13}A^{\frac{1}{3}}$. The nonelastic cross sections for 12.7- and 14.1-Mev neutrons are very nearly equal to the geometrical cross sections: $\pi(R+\lambda)^2$. At 4.7 Mev the nonelastic cross sections are still between 0.8 and 0.9 of the geometrical cross section in Cr, Fe, Ni, Cu, Ag, and Sn; in the nuclei Pb and Bi, which have closed shells and a lower density of energy levels, the cross sections are only 0.66 and 0.70 of the geometrical.

Comparison of nonelastic cross sections and elastic cross sections at 12 to 14 Mev indicates that there is an interference of waves entering the nucleus, suffering only a phase change without stronger interaction, and then interfering with the incident waves. At 14.1 Mev for Al, Cr, Fe, and Ni, the ratio $\sigma_n/\pi(R+\lambda)^2$ is greater than one. At this energy these elements have an elastic cross section which is less than the nonelastic cross section. Similarly, it is noticed that for Pb and Bi at 14 Mev the ratio $\sigma_n/\pi(R+\lambda)^2$ is particularly low, and the elastic cross section is greater than the nonelastic cross section. Both these results can be explained by interference effects.

[23] Feshbach, Porter, and Weisskopf, Phys. Rev. **90**, 166 (1953); Feshbach, Porter, and Weisskopf, Phys. Rev. **96**, 448 (1954).

γ RADIATION FROM INELASTIC SCATTERING OF 12.7-MEV NEUTRONS

When the 12.7-Mev data were taken, one of the channels of the pulse-height analyzer was set to count pulses with heights between 10 and 14 volts, as indicated by dotted lines on Fig. 2. Some of these pulses were produced by γ rays with an energy greater than 3 Mev. This channel corresponded to the largest pulses from neutrons with energies of from 5.2 to 6.3 Mev. Since the results of Graves and Rosen show that there are very few inelastically scattered neutrons of this energy, any increase in the counts in this channel with the sphere in position are due largely to γ radiation produced in the scatterer. There are more counts in this channel for many elements with the scatterer on than with the scatterer off. This increase in counting above the expected neutron counts was attributed to γ rays produced by the inelastic scattering in the sphere. The ratio of γ counts to the neutron absorption $(1-T)$ is plotted as a function of atomic weight in Fig. 10. The fact that more high-energy γ rays are observed from lighter elements than for the heavier ones is explained by the fact that $(n,2n)$ reactions have higher cross sections for heavier elements and comprise a greater portion of the nonelastic cross section than for the lighter elements. This follows because in an $(n,2n)$ reaction, γ radiation above 3 Mev is not expected. The $(n,2n)$ cross section for 12.7 Mev neutrons is not known for most of the elements studied. The results with Bi indicate that nearly all the nonelastic cross section of 2.5 barns is due to the $(n,2n)$ cross section. The $(n,2n)$ reaction is energetically impossible in aluminum and so this cross section must be zero. The experimental results indicate a small cross section for $(n,2n)$ reactions in Ti, Cr, and Fe, which all give about the same amount of γ radiation as aluminum. Less γ radiation is observed from Ni, Cu, Ag, and Sn, and indicates a considerable cross section for the $(n,2n)$ reactions in these elements for 12.7-Mev neutrons.

Scattering of 22-Mev α Particles by C^{12}†*

V. K. RASMUSSEN,‡ D. W. MILLER, AND M. B. SAMPSON
Department of Physics, Indiana University, Bloomington, Indiana

(Received May 4, 1955)

The elastic and inelastic scattering of 22-Mev α particles by carbon has been observed at a number of angles. Groups corresponding to the excitation of C^{12} to the known 4.4-, 7.7-, and 9.6-Mev levels were found. There was no evidence for the higher states reported by others, except possibly at ~12.7-Mev excitation. A strong angular dependence and a marked lack of symmetry around 90° was observed. The excitation function for $E_\alpha = 20.4$ to 22.6 Mev indicates a resonance at $E_\alpha = 21.85 \pm 0.1$ Mev, and the angular asymmetry indicates that there is at least one other level of opposite parity in this region. The Q-value for the second excited state was measured to be -7.64 ± 0.07 Mev. By looking for the appropriate C^{12} recoil ions it was established that this state decays to $Be^8 + \alpha$ with >80% probability.

I. INTRODUCTION

THE inelastic scattering of 22-Mev α particles by C^{12} was chosen as the subject for preliminary investigation with the Indiana University heavy-particle spectrometer because of the simplicity of the level scheme below 10-Mev excitation and the availability of target materials. It was hoped that information might also be obtained concerning some of the levels that have been reported above 10 Mev, and that the angular distribution for various α groups might be determined.

The present information about the level scheme of C^{12} has been summarized by Ajzenberg and Lauritsen.[1] There are well-established levels at 4.431 ± 0.013 Mev and 9.613 ± 0.012 Mev, the energies quoted having been obtained from observation of the $N^{14}(d,\alpha)$ reaction.[2] The existence of a level around 7.5 Mev has, until recently, been open to some question. It is now clearly established and its location given as 7.68 ± 0.03 Mev.[3] A very broad ($\Gamma = 1.6$ Mev) level at 9.7 Mev is reported by Jackson and Wanklyn.[4] Between 10- and 16-Mev excitation almost all of the available information is from the $B^{11}(d,n)$ reaction, which indicates several levels in this energy region.[5]

II. EXPERIMENTAL PROCEDURE

A. Spectrometer

The Indiana University heavy-particle spectrometer is of the point-focusing type with the magnetic field varying as $1/\sqrt{r}$, as introduced by Siegbahn and Svartholm.[6] With some exceptions, principally that the mean radius of curvature for focused particles is 20 in. instead of 16 in., it is a copy of the one designed and built at the California Institute of Technology.[7] The spectrometer may be rotated with respect to the cyclotron beam, so that all angles of observation from 45° counter-clockwise through a minimum of 12½° to 145° clockwise are available. The target chamber, made from two short 15 in. i.d. steel cylinders joined by a sliding O-ring seal, allows these changes to be made continuously without breaking the vacuum (see Fig. 1).

A null-reading, magnetic-balance type of fluxmeter is used to measure the magnetic field. Matched agate knife edges and V-blocks[8] are used to support both the balance beam and weight. The main parts of this balance are located between the counter and the

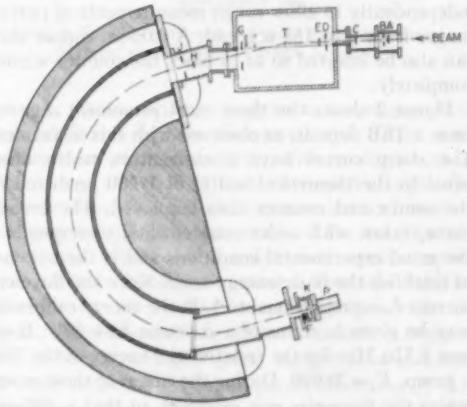

FIG. 1. Schematic cross-sectional view of the target chamber and magnetic spectrometer at the minimum laboratory angle of 12½°. For explanation of the various letters, see text.

† Supported by the joint program of the Office of Naval Research and the U. S. Atomic Energy Commission.

* Parts of this work have been reported previously by Rasmussen, Miller, Carmichael, and Sampson, Phys. Rev. **92**, 852(A) (1953) and Miller, Rasmussen, and Sampson, Phys. Rev. **95**, 649(A) (1954).

‡ Now at the Bartol Research Foundation, Swarthmore, Pennsylvania.

[1] F. Ajzenberg and T. Lauritsen, Revs. Modern Phys. **27**, 77 (1955).

[2] R. Malm and W. W. Buechner, Phys. Rev. **81**, 519 (1951).

[3] Dunbar, Pixley, Wenzel, and Whaling, Phys. Rev. **92**, 649 (1953).

[4] J. D. Jackson and D. I. Wanklyn, Phys. Rev. **90**, 381(A) (1953).

[5] V. R. Johnson, Phys. Rev. **86**, 302 (1952).

[6] K. Siegbahn and N. Svartholm, Arkiv. Mat. Astron. Fysik. **33A**, Nos. 21, 24 (1946).

[7] Snyder, Rubin, Fowler, and Lauritsen, Rev. Sci. Instr. **21**, 852 (1950); W. Whaling and C. W. Li, Phys. Rev. **81**, 150 (1951). See also R. Malm and D. R. Inglis, Phys. Rev. **95**, 993 (1954) for a description of another magnet of this type.

[8] Obtained from Voland and Sons, Inc., New Rochelle, New York.

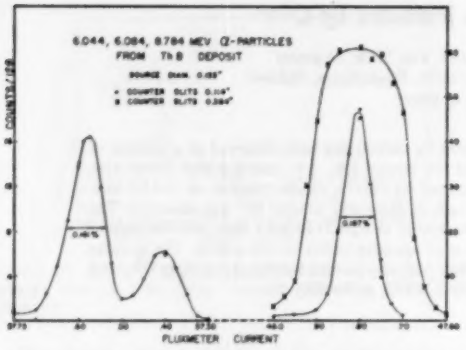

FIG. 2. Natural α groups from a ThB deposit, taken with two different counter slit openings. $K_f = 20\,070$.

magnet exciting coils. The fluxmeter coil proper, supported by an aluminum tube, extends a minimum of two inches into the field region from the edges of the magnet poles. This fluxmeter has, in general, been quite satisfactory, although small temperature effects are observed and there is a noticeable nonlinearity at high fields. The latter effect is a result either of small changes in field shape or of a local inhomogeneity in the field.

Focused particles are detected by a thin-window proportional counter (P in Fig. 1). Adjustable slits (K) allow the counter aperture to be varied. Aluminum foils (F) of nominal thickness 1, 2, 4, 9, 19, 48, and 75 mg/cm^2 can be moved in front of the counter independently to allow rough measurements of particle ranges from 1 to 158 mg/cm^2. A 0.06-in. copper sheet can also be inserted so as to block the counter window completely.

Figure 2 shows the three most prominent α groups from a ThB deposit, as observed with this instrument. The sharp curves have a momentum width about equal to the theoretical width[9] of 1/600 predicted for the source and counter sizes employed. The broader curve, taken with wider counter slits, corresponds to the usual experimental conditions and is the one used to establish the basic energy scale. Since the fluxmeter current I_f is proportional to $1/B$, the energy calibration may be given in terms of a constant $K_f = EI_f^2$. If one uses 8.776 Mev for the (relativistic) energy of the ThC′ α group, $K_f = 20\,070$. During the course of these experiments the fluxmeter was modified, so that a different constant (given in the captions) is to be used for some of the later figures.

B. Cyclotron Beam Focusing

The external cyclotron beam passes through a focusing magnet, the cyclotron shielding, and an analyzing magnet before it reaches the target chamber. The focusing magnet, designed by Professor N. Svartholm and Dr. F. E. Steigert, consists of two consecutive 12° sector magnets which give opposite deflections and produce radial focusing with minimum beam displacement. It changes the divergent incident beam into one that is slightly converging. The homogeneous-field analyzing magnet provides a 32° beam deflection and brings the beam to a focus approximately at the set of slits marked C in Fig. 1. The slits marked B limit the vertical extent of the beam. Under usual operating conditions, the beam at the target position is $\sim\frac{1}{32}$ in. high and $\sim\frac{5}{16}$ in. wide with a horizontal angular divergence of $\sim 1°$. At times, the beam spot has been found to be much narrower than this, apparently as a result of variations in cyclotron operating conditions. The energy and spread in energy of the useful beam are determined partly by the cyclotron fringing field and partly by the analyzing magnet. As estimated from the widths of scattered peaks, the spread in energy of the useful α-particle beam varies from $\sim$75 to $\sim$150 kev, depending on cyclotron conditions. The mean energy of the beam may also vary by an appreciable amount from day to day. These variations were limited to a certain extent by placing a set of adjustable slits between the cyclotron and the focusing magnet.

C. Targets

For experiments of this nature thin target backings are required. After some preliminary attempts to use gold or aluminum leaf, backings made by evaporating a semitransparent layer of aluminum onto thin ($\sim$1400 A) Zapon lacquer films were adopted. By keeping the film on the metal frame upon which it was originally picked up, it was possible to get very smooth targets which stood up quite well under bombardment after minor initial wrinkling at the beam spot. About 0.1 mg/cm^2 of carbon was added to these films by spraying them with a dilute colloidal suspension of graphite in water or water-alcohol mixture.[10] The total thickness of the targets and, in some cases, the backing thickness (which proved to be almost negligible) were measured by observing the energy loss of ThC′ alphas. It was also possible in this way to estimate the target uniformity, which was generally satisfactory although not quite as good as desired.

III. RESULTS

A. Observed α Groups

The elastic α group and groups corresponding to the excitation of C^{12} to its first three excited states were found at a number of angles. Typical curves are given in Fig. 3. These curves were taken with the $\frac{1}{2}$% "window" of Fig. 2. Almost all of the observed width of each peak is due to the variation of the emitted

[9] D. L. Judd, Rev. Sci. Instr. **21**, 213 (1950).

[10] Aquadag, a product of the Acheson Colloids Corporation, was used. Their alcohol suspension would probably have been more satisfactory.

particle energy over the finite acceptance angle of the spectrometer. Target thickness and inhomogeneiety and the energy spread of the incident beam also contribute to some extent to the observed peak widths. No detailed analysis of the separate contributions has been attempted, although the effect of varying single factors has been observed.

It seemed of interest to attempt a fairly accurate measurement of the location of the state at ~7.7 Mev. An angle (79° lab) was chosen at which the α groups leaving C^{12} at 7.7 Mev and 4.43 Mev fell close to the calibration points furnished by a ThB deposit. The beam energy was calculated from the location of the 4.43 group. The lower energy α group then gave a calculated level energy of 7.64±0.07 Mev, with the largest part of the probable error resulting from the widths of the peaks. Corrections for target thickness and relativistic effects were made, although the net result of these was small (~25 kev) since they also come into the beam-energy determination.

Since work in this laboratory and elsewhere[11,12] suggested a possible 7-Mev level in C^{12} (distinct from the 7.68-Mev state) which decayed either by γ-ray or pair emission, a search for the corresponding α group was undertaken. Weak groups were observed at some angles, but the shift with angle indicated that C^{12} was not the scattering nucleus. If such a level in C^{12} exists, it is excited in this reaction with less than 0.005 times the intensity of the 4.4-Mev level at a laboratory angle of 55°.

No other extended search for levels below 10 Mev was made. However, a search for the higher levels reported in the $B^{11}(d,n)$ reaction[5] was carried out at forward angles. The continuum of alphas from $C^{12*}\rightarrow Be^{8}+\alpha$ made the detection of weak alpha groups difficult. As a result, no evidence for the higher states was found except for one group at 12½° (lab) (see Fig. 4) which may correspond to a C^{12} excitation of around 12.7 Mev. Other groups would have been observed if they had an intensity greater than about 5–10% that of the group to the 9.61-Mev state. The very broad group at 12¼° results from the scattering of alphas by hydrogen contamination in the target (this group did not interfere at other angles, since it cannot occur at angles >15°). The continuum of α's from Be^{8} also would have obscured the very broad level at ~9.7 Mev reported in the $C^{12}(n,n')3\alpha$ reaction by Jackson and Wanklyn.[4] It is only possible to say that such a broad level is excited with less than ⅓ the probability of the sharp 9.6-Mev level.

B. Angular Distributions

It became apparent early in the course of these investigations that none of the observed α groups was isotropic. Cross sections at quite a few angles were obtained before it was discovered that there were significant variations in intensity with small changes in beam energy as well as with changes in angle. To check on these effects, thick-target excitation functions (discussed below) were then run, and the results made it clear that significant angular data would require closer control of the beam energy than was feasible. However, certain qualitative statements about the angular distributions can be made for incident α energies of ~22 Mev, the angles given being c.m. angles and the cross sections being in mb per 4π steradians.

(a) None of the four α groups investigated is symmetric around 90°.

(b) The α groups leaving C^{12} excited to 4.43 and 9.61 Mev show a fairly smooth variation of cross section with angle. The 4.43 group rises to a backward (150°) maximum about 5 times as high and a forward (30°) maximum about 3 times as high as the minimum of ~100 mb at 115°. A forward (30°) maximum over 10 times the flat (~60 mb) distribution from 70° to 120° is observed for the 9.61 group.

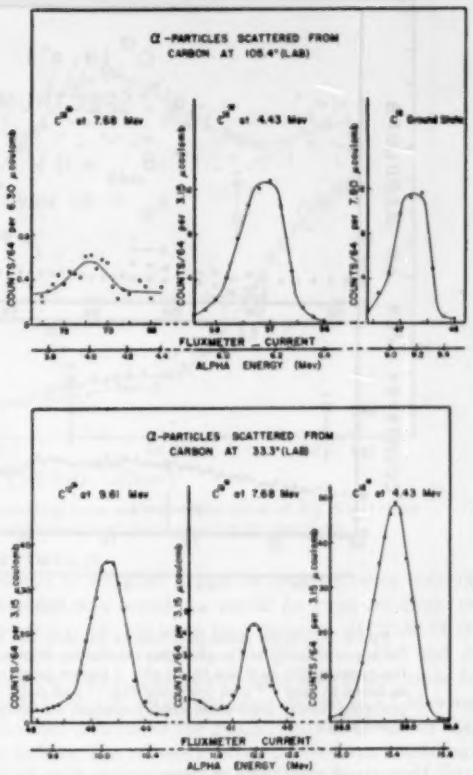
α-PARTICLES SCATTERED FROM CARBON AT 105.4° (LAB)
C¹² at 7.68 Mev
C¹² at 4.43 Mev
C¹² Ground State
COUNTS/64 per 6.50 μcoulomb
COUNTS/64 per 3.15 μcoulomb
COUNTS/64 per 7.60 μcoulomb
FLUXMETER — CURRENT
ALPHA ENERGY (Mev)
α-PARTICLES SCATTERED FROM CARBON AT 33.3° (LAB)
C¹² at 9.61 Mev
C¹² at 7.68 Mev
C¹² at 4.43 Mev
COUNTS/64 per 3.15 μcoulomb
FLUXMETER — CURRENT
ALPHA ENERGY (Mev)

FIG. 3. Typical elastic and inelastic α groups scattered from carbon at the angles noted. $K_f = 20\,070$.

[11] N. S. Wall and J. R. Rees (private communication).
[12] G. Harries and W. T. Davies, Proc. Phys. Soc. (London) **A65**, 564 (1952); G. Harries, *ibid.* **A67**, 153 (1954).

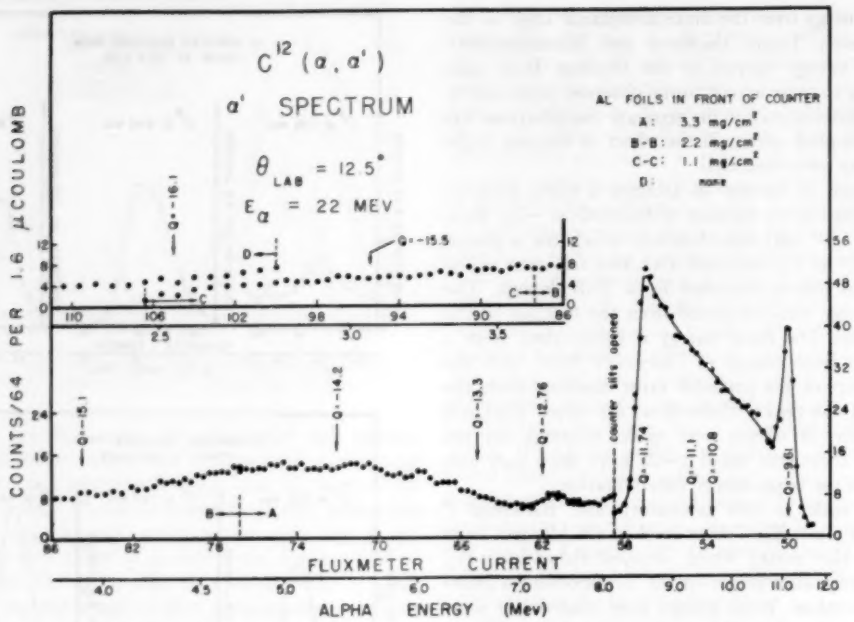

FIG. 4. Search for states in C^{12} above 9.6 Mev. See text for detailed discussion. States reported by others should fall approximately at the positions marked by arrows. The break near fluxmeter current 58 resulted from opening the counter slits to 0.614 in. to give a higher counting rate. Aluminum foils were placed in front of the counter as noted to stop C^{13} ions (compare Fig. 7) and singly-charged α particles. The double curve between 100 and 106 probably results from some doubly-charged α's being missed with the 1.1 mg/cm² foil in front of the counter. $K_f = 27\,850$.

(c) Very rapid variations of cross section with angle are exhibited by the elastic group and that leaving C^{12} excited to 7.7 Mev, changes by a factor of 5 or more for angular changes of 10°–15° being observed. The elastic cross section is ~1000 mb at 60°, while from 75° to 150° it averages ~40 mb. The 7.7-Mev cross section varies from ~3 mb to ~25 mb with an average value of ~15 mb.

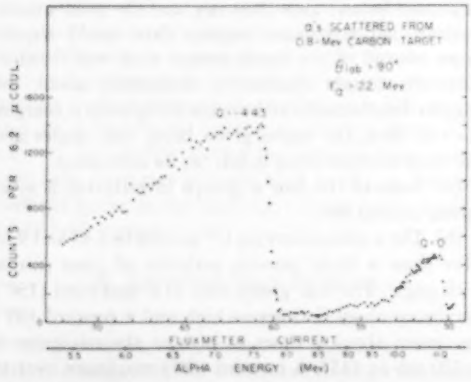

FIG. 5. Alpha particles scattered elastically and inelastically ($Q = -4.43$ Mev) from a semithick carbon target. $K_f = 27\,990$.

C. Excitation Function

The variation with energy of the cross section for elastic scattering and for inelastic scattering to the first excited state was obtained for beam energies between 20.4 and 22.6 Mev. A semithick target, of thickness 2.6 mg/cm² or 0.75 Mev for 22-Mev α's at normal incidence, was prepared in the same manner as the thin targets. The spectrometer was located at 90°, with the acceptance aperture closed down to give somewhat better resolution. The target was placed at 45° to the beam and was observed in reflection, i.e., the side on which the beam was incident also faced the spectrometer. Incident beam energies of 22.65, 22.40, and 22.0 Mev were obtained by small displacements of the cyclotron dees and the deflector. An energy of 21.4 Mev was obtained by placing an aluminum foil in the path of the beam just outside the cyclotron. Typical curves obtained in this manner are shown in Fig. 5. The data was analyzed by the method of Snyder *et al.* (reference 7, p. 866) to give the excitation functions of Fig. 6. No attempt was made to correct for straggling in energy loss or angle, and the target was not perfectly smooth and homogeneous. For these, and possibly other reasons, the various runs do not join together as smoothly as might be desired. However, the method used to obtain large changes in beam energy was so

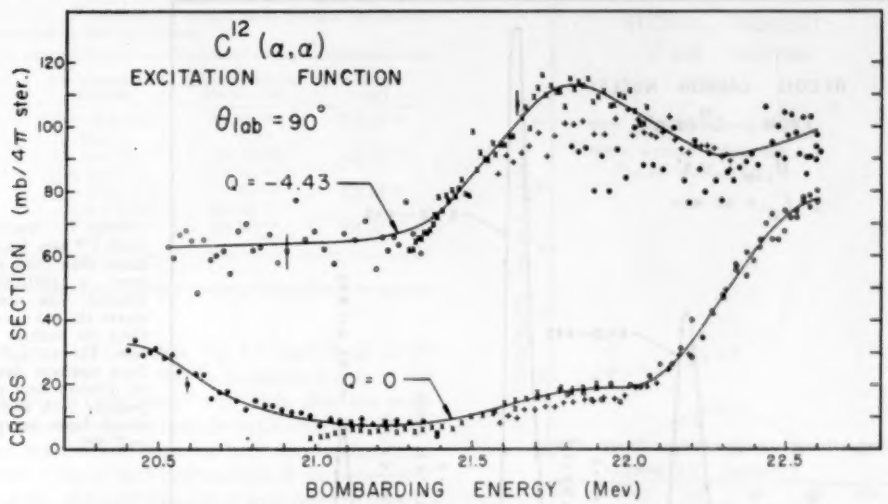

FIG. 6. Excitation functions for $C^{12}(\alpha,\alpha)C^{12}$ and $C^{12}(\alpha,\alpha')C^{12*}$ resulting from analysis of the curve of Fig. 5 and three other similar curves. The solid curves represent our best estimate of the true excitation functions.

hazardous to proper cyclotron dee adjustment that it seemed better not to attempt to repeat the experiment. It should be noted that the initial 200-kev rise of Fig. 5 does not represent the effective resolution for the excitation function, since an α particle that loses 90 kev in the target before being elastically scattered loses more energy before emerging and appears 200 kev lower in the observed spectrum.

D. C^{12} Recoils

At forward angles, even with the 1.8-mg/cm² mica counter window used in the early part of these experiments, pulses very large compared to maximum α pulses were observed. The range of these particles was small compared to that of an α particle of the same $B\rho$, suggesting that these were C^{12} recoil ions.

Since the mica window was cutting off at about 12-Mev ion energy (in the sense that the pulses became so small that they were difficult to distinguish from alphas), a 1.1 mg/cm² nickel window with pinholes filled by very thin Zapon lacquer was substituted. The cut-off with this window was below 8.45 Mev. The 6^+, 5^+, and 4^+ charge states of these ions were then found at lab angles of 12½° and 24° for both elastic recoils and for recoils which had been excited to 4.43 Mev. Typical curves are shown in Fig. 7. By changing the angle between the target and the direction of observation, and noting the shift of the low-energy side of the peak, it was found that an "Aquadag" target that was 40-kev thick for 8.8-Mev α's was approximately 0.5-Mev thick for 13.6-Mev carbon ions. Information on the intensity ratios of ions with various energies in different charge states is given in Table I.

Portions of the spectrum where recoils that had been excited to 9.6 Mev should be observed were scanned. Nothing was found, as would be expected from the instability of this state to α emission. Because of the astrophysical interest in the 7.7-Mev state[3] and its mode of decay, a more extended search was made for recoil C^{12} nuclei which had been excited to 7.7 Mev and had then decayed to the ground state of C^{12} rather than to $Be^8+\alpha$. The intensity to be expected was determined by observing the corresponding inelastic α group (both singly and doubly charged) in the backward direction. This gives the predicted curve of Fig. 8, assuming 100% decay of the 7.7-Mev state to the ground state of C^{12}. A similar experiment comparing the observed recoil C^{12} ions that had been excited to the 4.43-Mev state and the corresponding inelastic backward α's gave agreement to within 6%, thus checking the experimental method. The recoil C^{12} ions starting in the 7.7-Mev state would have an energy of 11.76 Mev, which is well above the cutoff for the nickel window (a clean peak for 8.45-Mev C^{12} recoil ions was obtained with a similar window).

TABLE I. Relative number of C^{12} ions in various charge states.[a]

C^{12} energy (Mev)	Ionic charge 6+	5+	4+	3+
11.3[b]	15	50	32	3
12.4[c]	22	57	21	...
13.1[b]	26	53	22	...
14.6[c]	29	52	...	...
15.6[c]	44	(37)	19	...

[a] For this data, the spectrometer was looking at the "Aquadag" face of the target.
[b] Data obtained in the course of a single run. Probable error, ±5%.
[c] Data collected over the course of several days running. Probable error, ±10%, but considerably larger errors cannot be ruled out. The value in parentheses is especially questionable.

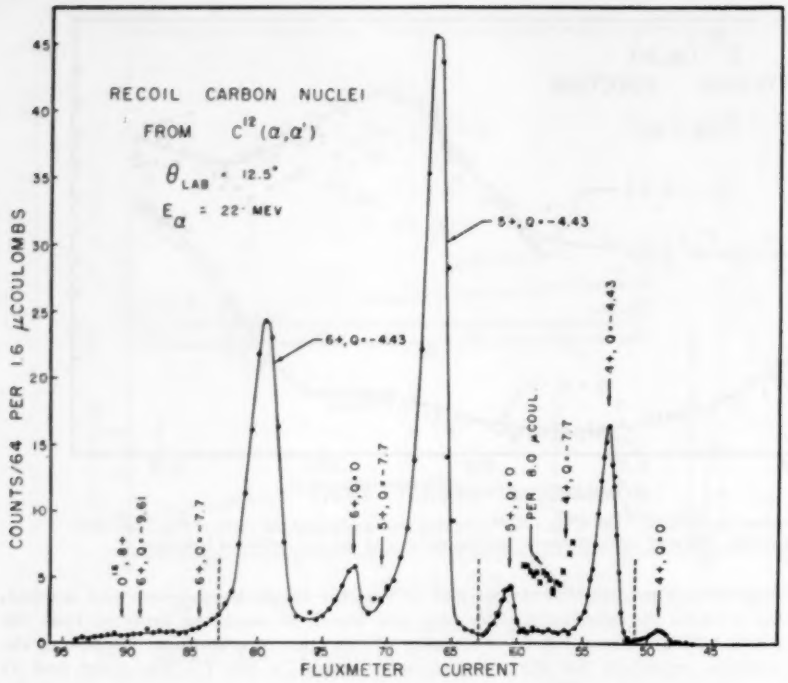

FIG. 7. Spectrum of recoil C^{12} ions. Only pulses larger than those resulting from α particles were counted. The arrows indicate the calculated locations for various possible ions. The vertical dashed lines represent data taken on different days and thus possibly with slightly different beam energies. $K_f = 27\,800$.

As shown in Fig. 8, no evidence for recoil C^{12} ions starting in the 7.7-Mev state was found. The background counts that were obtained in this region most probably represent C^{12} nuclei that have undergone large changes in energy or angle in the target, although a few singly charged α's may have been counted also.

IV. DISCUSSION

At the rather high energies involved, it is not clear that the excitation function of Fig. 6 has any significant bearing on the properties of the compound nucleus, O^{16}. On the other hand, there does not seem to be any other picture of the reaction process that will explain the features of this data, so that the compound nucleus point of view will be adopted with the reservation that it may be completely irrelevant. On this basis, then, the inelastic scattering indicates a resonance at $E_\alpha = 21.85 \pm 0.1$ Mev (O^{16*} excitation = 23.55 Mev) with a width of around 0.4 Mev. The lack of symmetry around 90° in the angular distributions shows that there is at least one other level, of opposite parity, in the neighborhood of 22 Mev (which the data easily allows). However, Wolfenstein's calculations[13] would indicate that there cannot be a large number of additional levels, since this should result in symmetry about 90°. Interference between a few close levels could also result in the sensitive dependence of the angular distributions on energy that was noted. The additional detail shown by the elastic-scattering data would be expected from the interference between resonance and other possible modes of scattering. This can, in principle, give additional information, but the accuracy of the present data is obviously not great enough to justify a detailed theoretical analysis. To illustrate the possible difficulties of such a calculation, it might be pointed out that rather high angular momentum transfers are possible, the barrier height being equal to the available center-of-mass kinetic energy for $L \sim 7$.

The level observed by Newson[14] should occur at $E_\alpha = 22.40$ Mev, where the inelastic curve of Fig. 6 shows a slight dip. The energy difference would seem to be outside experimental error; possibly this higher level is one that cannot be formed by two $J = 0$ particles.

One rather striking feature of the present experiment is the contrast between the ease with which the first three excited states of C^{12} are observed and the failure to find what would seem to be well-established higher levels starting $\sim$1.5 Mev above 9.61 Mev. In this connection, it should be noted that there is sufficient energy available to excite C^{12} to 16.5 Mev while the barrier for s-wave α particles is $\sim$3 Mev. We have been unable to discover any reason for this apparent cutoff.

From the recoil data given in Fig. 8 and from other similar data, it is estimated that there is a greater

[13] L. Wolfenstein, Phys. Rev. **82**, 690 (1951).

[14] H. W. Newson, Phys. Rev. **51**, 620 (1937).

TABLE II. Calculated lifetimes for 7.7-Mev state of C^{12} for various possible spin and parity assignments. See text for assumptions employed in the calculations.

Spin and parity	Electromagnetic radiation	Electromagnetic lifetime (sec)	α lifetime (sec)
0^+	3.25-Mev $E2$	8×10^{-13}	7×10^{-17}
	7.7-Mev γ	10^{-11}	
1^-	7.7-Mev $E1$[a]	3×10^{-15b}	4×10^{-15}
	3.25-Mev $E1$	4×10^{-14b}	
2^+	3.25-Mev $M1$	10^{-15}	5×10^{-12}
	7.7-Mev $E2$[a]	9×10^{-13}	
3^-	3.25-Mev $E1$	4×10^{-14b}	5×10^{-7}

[a] Not observed.
[b] Includes inhibition by an arbitrary factor of 10^2 because of the isotopic-spin selection rule.

than 80% probability that the 7.7-Mev state of C^{12} will decay to $Be^8+\alpha$. This is in contradiction to the recent work of Uebergang[15] who finds that the state decays predominantly by cascade γ radiation (7.7-Mev γ radiation has not been observed[16]). It may be that these two modes of decay have probabilities of the same order of magnitude, although this would seem rather unlikely. In an effort to clarify this point, calculations of the relative probabilities for the emission of an α particle (leaving Be^8 in its 0^+ ground state) and for decay by electromagnetic radiation have been made and are summarized in Table II.[17] The radius of the system $Be^8+\alpha$ was taken as $1.45(8^{\frac{1}{3}}+4^{\frac{1}{3}})\times10^{-13}$ cm and the reduced width, γ_α^2, of the decaying C^{12} state was taken as $\hbar^2/\mu R$. Lifetimes for γ radiation were calculated from the formulas given by Blatt and Weisskopf[18] and that for nuclear pair emission (the 0^+ to 0^+ transition) was estimated from the measured value for the O^{16} pair state[19] and the W^5 theoretical dependence.[20] The probabilities for electric-dipole transitions were reduced by an (arbitrary) factor of 10^2, to allow for the isotopic spin selection rule forbidding $\Delta T=0$ transitions in $N=Z$ nuclei.[21] The only spins and parities of the C^{12} state that must be considered are either even-even or odd-odd.[22]

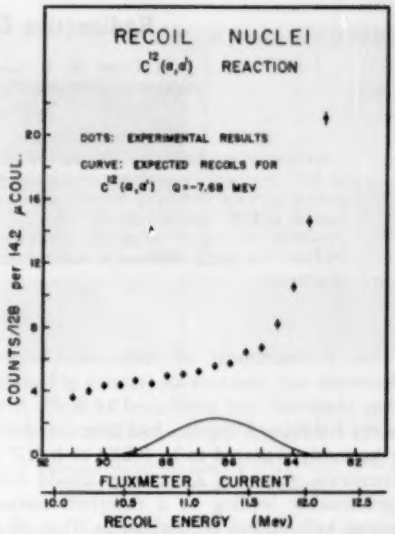

FIG. 8. Search for recoil carbon ions which had been excited to 7.7 Mev and then decayed to the ground state. The dots represent experimental points, while the solid curve represents the shape of the curve expected judging from the corresponding observed backward inelastic α's. The rapid rise at the right is a tail of 6^+, $Q=-4.43$ recoils. Background counts in this region are scattered C^{13} ions plus possibly a few singly-charged alpha particles (compare with Fig. 7). $K_f=27\,960$.

Since observed α widths vary from the limit $\hbar^2/\mu R$ to ~0.001 of that limit,[23] and since γ-ray widths vary from somewhat larger to very much smaller than the values given by the Blatt and Weisskopf formulas, we conclude from Table II only that spin and parity assignments of 0^+, 1^-, or 2^+ for the 7.7-Mev state of C^{12} are all consistent with the experimentally indicated competition between α and γ decay.[24]

V. ACKNOWLEDGMENTS

The authors would like to express their appreciation to Mr. O. E. Johnson for aid in construction of the magnetic spectrometer, and to Dr. B. M. Carmichael, Dr. N. S. Wall, and Mr. J. R. Rees for aid in taking the data. Helpful discussions of the results with Professor E. J. Konopinski, Dr. N. S. Wall, Dr. N. C. Francis, and Professor K. W. Ford are also gratefully acknowledged.

[15] R. G. Uebergang, Australian J. Phys. **7**, 279 (1954).
[16] Beghian, Halban, Husain, and Sanders, Phys. Rev. **90**, 1129 (1953).
[17] Similar results were reported by E. E. Salpeter, Phys. Rev. **98**, 1183(A) (1955).
[18] J. M. Blatt and V. F. Weisskopf, *Theoretical Nuclear Physics* (John Wiley and Sons, Inc., New York, 1952).
[19] Devons, Goldring, and Lindsey, Proc. Phys. Soc. (London) **A67**, 134 (1954).
[20] J. R. Oppenheimer and J. Schwinger, Phys. Rev. **56**, 1066 (1939).
[21] L. A. Radicati, Phys. Rev. **87**, 521 (1952); M. Gell-Mann and V. L. Telegdi, *ibid.* **91**, 169 (1953).
[22] Our observation of this state in C^{13} rules out 0^- completely, and other even-odd or odd-even states could not decay to the 0^+ ground state of Be^8. Decay into three alphas, it would seem, would involve considerably smaller barrier penetration probabilities since the available energy would be more evenly distributed among the three alpha particles. One would also expect decay to the "tail" of the broad 2^+ first excited state of Be^8 at ~2.9 Mev to be quite weak.
[23] See, for example, R. W. Hill, Phys. Rev. **90**, 845 (1953); J. W. Bittner and R. D. Moffat, *ibid.* **96**, 374 (1954).
[24] J. Seed, Phil. Mag. **46**, 100 (1955), has recently reported a $\gamma-\gamma$ correlation experiment which indicates a definite preference for 0^+. However, he also states that he cannot definitely rule out 3^+ or 4^+, in which case it would seem difficult to rule out 1^- or 2^+.

Radioactive Decay of Ruthenium-97†

J. M. Cork, M. K. Brice, L. C. Schmid, and R. G. Helmer
Department of Physics, University of Michigan, Ann Arbor, Michigan

(Received June 6, 1955)

Ruthenium enriched in mass 96 was irradiated for short and long periods in the pile and the radioactivity of Ru^{97}, produced by neutron capture, was studied by magnetic and scintillation spectrometers. Several gamma rays not previously reported were found to exist. The observed gamma rays in Tc^{97}, following K capture in Ru^{97}, have energies of 109.1, 216.1, 325.1, and 570 kev. A long-lived metastable state in Tc^{97} decays by the emission of gamma rays whose conversion electrons indicate gamma energies of 90.2 and 99.2 kev. The multipolarities of most of the transitions are determined and a satisfactory nuclear level scheme is proposed.

BY the bombardment of ruthenium with both deuterons and neutrons an activity of half-life 2.8 days was observed[1] and attributed to Ru^{97}. A single gamma ray following K capture had been noted with an energy variously reported to be 0.230[1] or 0.217[2] Mev. This transition, following K capture, should occur in Tc^{97}, presumably leading to a reported[3] metastable level whose half-life has been given as 90 to 95 days. A gamma ray with an energy somewhere between 96 and 108 kev had been found to be associated with Tc^{97m}.

In the present investigation a specimen of ruthenium, enriched in mass 96 from its normal 5.7 percent up to 95.5 percent, was irradiated in the maximum flux of the Argonne heavy water pile. In order to distinguish the lines due to Ru^{97}, both short (3-day) and long (30-day) irradiations were made. Radioactive sources were studied in photographic magnetic and scintillation spectrometers. Strong electron conversion lines were observed indicating the presence of several gamma rays not previously reported. Since the separated Ru^{96} specimen contained about 1% of Ru^{102}, the well-known gamma rays for Ru^{103} were found to be present but weak. There was also a very weak iridium impurity in the separated Ru isotope, so that its well-known spectrum was faintly observed. The half-life of the Ru^{97} activity was followed through more than eight octaves and was found to be 2.44 days, or 58.6 hours.

TABLE I. Energies and relative intensities of the electron lines from Ru^{97}.

Electron energy, kev	Designation	Intensity	Energy sum, kev
15.1	Auger KL_1L_1		
15.5	Auger KL_2L_2		
17.9	Auger KLM		
20.1	Auger KMM		
69.2	$K(Tc^{97m})$		90.2
78.2	$K(Tc^{97m})$		99.2
88.1	K	3	109.1
89.0	$L(Tc^{97m})$		92.0
97.8	$L(Tc^{97m})$		100.8
106.1	L	1	109.1
195.3	K	100	216.3
213.1	L	14	216.1
215.4	M		215.9
303.9	K	8	325.0
322.2	L	1	325.2
549	K		570

The energies of the observed electron conversion lines, exclusive of those due to Ru^{103} and Ir^{192}, are presented in Table I. The interpretation of each line is given in the second column and where possible the relative intensities are presented in column 3. From these observations it can be concluded that there are at least four gamma rays associated with the 2.44-day radiation, with energies of 109.1, 216.1, 325.1, and 570 kev. These energies were also observed as peaks with the scintillation spectrometer on "singles" studies, with the exception of the 109.1, which does, however, appear in strong coincidence with the 216.1. Coincidences between the 216.1- and 325.1-kev gammas are not observed. The spectrum in coincidence with the Tc K x-rays is identical with the "singles" spectrum out to 400 kev; coincidence work with the 570-kev peak was inconclusive because of its extreme weakness. Curve A of Fig. 1 shows the "singles" spectrum and curve B shows the spectrum in coincidence with the 216.1-kev gamma ray. The photopeaks and conversion lines for these four gamma rays, observed over a period of time, all appear to die out with the same half-life. The absence of an annihilation peak at 511 kev in the scintillation spectrum and the negative result of a search for positrons with the magnetic double-focusing spectrometer indicate that Ru^{97} decays principally, if not entirely, by K capture.

In the specimen irradiated for 30 days, the long-lived Ru^{103} and the Ir^{192} electron lines appeared relatively much stronger in comparison with the lines due to the 2.44-day Ru^{97}. However, certain new lines were evident which were not due to either of the above contaminants but which appeared to have a long half-life. Successive exposures showed that after the Ru^{97} short-lived activity died out, there still remained two pairs of electron lines with energy differences characteristic

† This investigation received the joint support of the Office of Naval Research and the U. S. Atomic Energy Commission.

[1] Sullivan, Sleight, and Gadrow, Phys. Rev. **70**, 778 (1946).
[2] Mei, Huddleston, and Mitchell, Phys. Rev. **79**, 429 (1950).
[3] Hollander, Perlman, and Seaborg, *Table of Isotopes*, Berkeley, 1952 [Revs. Modern Phys. **25**, 469 (1953)].

of the K and L work functions for Tc. Figure 2 shows (a) a plate made after the 3-day irradiation, (b) one made immediately following the 30-day irradiation, and (c) one made two weeks after the 30-day irradiation, when the 2.44-day activity had largely died out. It seems likely therefore that this is the radiation previously observed[3] to be associated with a metastable Tc^{97m}, whose half-life was noted to be from 90 to 95 days. No attempt was made to verify this half-life, or that of the ground state of $Tc^{97}(\sim 10^4 Y)$.

The energies of these gamma rays are 90.2 and 99.2 kev, and their K/L conversion ratios are both approximately unity. They are of about equal intensity as judged by the density of their K conversion lines, and are both highly converted, as they hardly appear in the

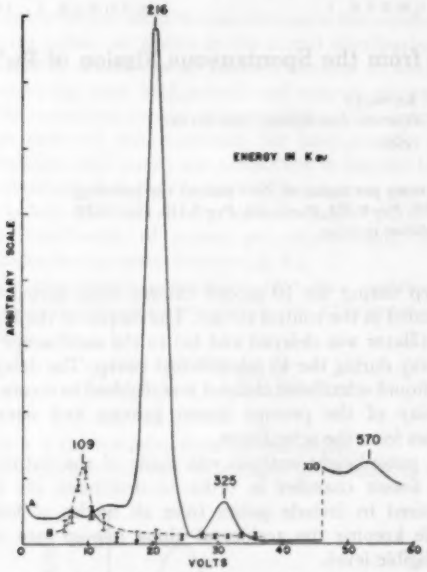

FIG. 1. Singles and coincidence spectra for Tc^{97} with the scintillation spectrometer.

scintillation spectrum. The high conversion coefficient, low K/L ratio, and long half-life indicate that these are high-order multipole transitions, probably $E3$ or $M4$. According to shell theory the ground state of Tc^{97} is expected to be a $g_{9/2}$ level and the first excited state a $p_{1/2}$ level. The difference in energy of these two gamma rays, namely 9 kev, suggests the existence of two low-lying states such as $g_{9/2}$ and $7/2+$, as has been reported[4] to exist in Tc^{99m}.

The relative intensities of the electron lines associated with the 2.44-day activity were determined from microphotometer traces of the photographic plates, corrected for variations in radius and emulsion sensitivity with energy. The K/L ratios for the 109.1-, 216.1-, and 325.1-kev gammas are 3.0 ± 0.6, 7.3 ± 0.3,

[4] Mihelich, Goldhaber, and Wilson, Phys. Rev. 83, 216 (1951).

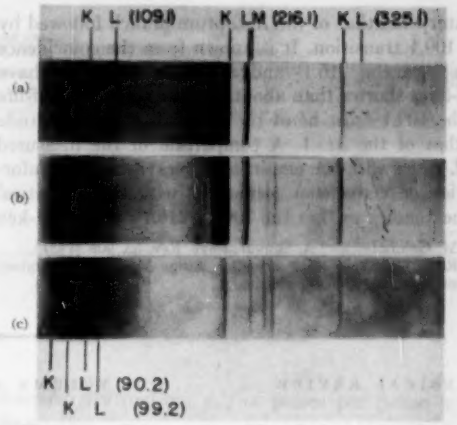

FIG. 2. Internal conversion spectra of Tc^{97} and Tc^{97m} for short- and long-period irradiations.

and 6.7 ± 0.6, respectively. The 109.1-kev gamma has a high conversion coefficient, as it appears only weakly in the scintillation spectrometer although strong conversion lines are observed. Measurements of the relative intensities of both the photopeaks and K conversion lines of the 216.1- and 325.1-kev gammas indicate that the ratio of their K conversion coefficients must be approximately unity. The fact that the 216.1-kev gamma is much stronger than the 109.1, both converted and unconverted, shows that the 216.1 follows the 109.1 and is supplied by an additional K capture branch whose degree of forbiddenness is no

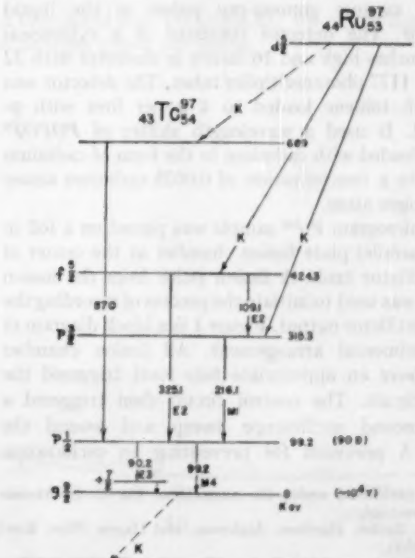

FIG. 3. Nuclear level scheme for Tc^{97}.

greater than that of the K capture branch followed by the 109.1 transition. It is known from the coincidence data that the 216.1- and 325.1-kev radiations have half-lives shorter than about 10^{-6} sec, and the half-life of the 109.1 must be of the same order of magnitude as that of the 325.1. A comparison of the measured K/L ratios with the empirical curves[5] and of the information on conversion coefficients with the theoretical values[6] indicates that the 109.1-, 216.1-, and 325.1-kev transitions are, respectively, $E2$, $M1$, and $E2$. The 570-kev gamma probably follows another weak K capture branch, but its terminal level is uncertain. A nuclear level scheme for Tc^{97} consistent with the above information is shown in Fig. 3.

Note added in proof.—A consideration of the expected half-lives for the 9-, 90.2-, and 99.2-kev transitions indicates the possibility of interchanging the order of the 9- and 90.2-kev gammas. The 9-kev transition would then be interpreted as $E3$ and the 90.2-kev transition as of lower multipole order.

[5] M. Goldhaber and A. Sunyar, Phys. Rev. **83**, 906 (1951).
[6] Rose, Goertzel, and Perry, Oak Ridge National Laboratory Report ORNL-1023 (unpublished).

PHYSICAL REVIEW VOLUME 100, NUMBER 1 OCTOBER 1, 1955

Distribution of the Number of Prompt Neutrons from the Spontaneous Fission of Pu^{240}†

J. E. HAMMEL AND J. F. KEPHART
Los Alamos Scientific Laboratory, University of California, Los Alamos, New Mexico
(Received June 16, 1955)

A measurement of the distribution of the number of neutrons per fission of Pu^{240} yielded the following probabilities, P_n, for 0,1,2, etc. neutrons: $P_0=0.062$, $P_1=0.198$, $P_2=0.374$, $P_3=0.228$, $P_4=0.114$, $P_5=0.027$, $P_6=0.000$. The measurement was made with a liquid scintillation counter.

THE distribution in the number of prompt neutrons emitted in the spontaneous fission of Pu^{240} has been investigated by means of a large liquid scintillator of high efficiency for the detection of neutrons.

The neutron detector was similar to the one described by Cowan *et al.*,[1] where neutrons are detected by cadmium capture gamma-ray pulses in the liquid scintillator. The detector consisted of a cylindrical tank 16 inches high and 16 inches in diameter with 32 DuMont 1177 photomultiplier tubes. The detector was filled with toluene loaded to 4 g per liter with *p*-terphenyl. It used a wavelength shifter of *POPOP*[2] and was loaded with cadmium in the form of cadmium octoate[3] to a concentration of 0.0025 cadmium atoms per hydrogen atom.

A 45-microgram Pu^{240} sample was placed on a foil in a small parallel plate fission chamber at the center of the scintillator tank. A fission pulse from the fission chamber was used to initiate the process of recording the liquid scintillator output. Figure 1 is a block diagram of the experimental arrangement. All fission chamber pulses above an appropriate bias level triggered the control circuit. The control circuit then triggered a 40-microsecond oscilloscope sweep and wound the camera. A provision for preventing an oscilloscope sweep during the 10 second camera wind period was included in the control circuit. The output of the liquid scintillator was delayed and fed to the oscilloscope for display during the 40 microsecond sweep. The delay in the liquid scintillator channel was required to insure the display of the prompt fission gamma and neutron pulses from the scintillator.

A pulse-height analysis was made of the output of the fission chamber in order to determine the bias required to include pulses from all modes of fission while keeping the accidental alpha pile-up rate to a negligible level.

All pulses in the scintillation detector of energy greater than that equivalent to a 350-kev gamma ray were accepted. The gain of the over-all system associated with the liquid scintillator was frequently checked by observing the 4.43-Mev gamma ray from C^{12} (obtained from the $Be^9(\alpha,n)C^{12}$ reaction).

In the 4197 fissions recorded, a total of 7029 pulses were observed. The background was determined by randomly triggered oscilloscope sweeps. The average background rate was found to be 0.123 ± 0.008 pulses per 40 microsecond sweep, and no significant deviation from a Poisson distribution in time was observed. By using 2.20 ± 0.03 for the average number of prompt neutrons per spontaneous fission[4,5] of Pu^{240} the efficiency of the scintillation detector for fission spectrum neutrons was determined. The efficiency, α, thus obtained was, together with its probable error, 0.716 ± 0.012.

† Work performed under the auspices of the U. S. Atomic Energy Commission.
[1] Cowan, Reines, Harrison, Anderson, and Hayes, Phys. Rev. **90**, 493 (1953).
[2] Hayes, Rogers, and Ott, J. Am. Chem. Soc. **77**, 1850 (1955).
[3] A. Ronzio, U. S. Atomic Energy Commission Report AECU-2924 (unpublished).
[4] Terrell, Diven, and Martin, (private communication).
[5] Carter, Haddad, Hand, and Smith (unpublished report).

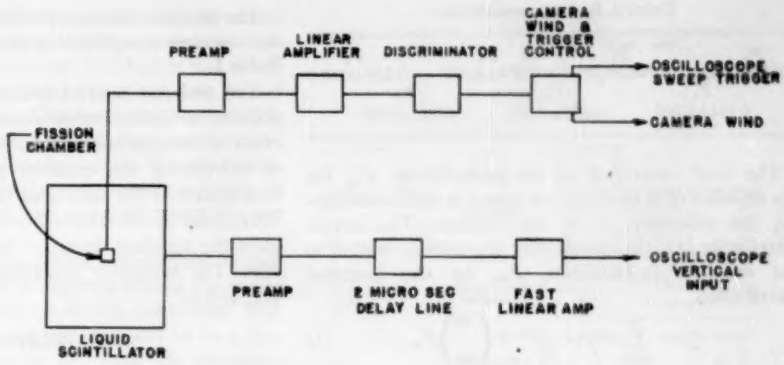

FIG. 1. Experimental arrangement.

The conversion from the distribution in the number of counter pulses per fission to the actual distribution in the number of neutrons per fission consists of corrections for resolving time, background, and counter efficiency.

The correction for the finite resolving time must be made prior to the correction for background. The probability that pulses are unresolved is derived from the observed time distribution of the capture gamma-ray pulses with the background included. $F(t)$, the time distribution of pulses per microsecond, after normalization to unity is shown in Fig. 2.

The elementary probability that two pulses are unresolved when they are within the 40 microsecond sweep is:

$$s=\tau\int_{0}^{40\ \mu\text{sec}}[F(t)]^2dt, \tag{1}$$

where τ is the resolving time for two pulses.

An application of this elementary probability to the observed distribution, q_n', of pulses per fission gives the relation

$$q_n=\left[q_n'-\binom{n+1}{2}q_{n+1}s\right]\Big/\left[1-\binom{n}{2}s\right], \tag{2}$$

where q_n is now the distribution corrected for resolving time. $\binom{n}{2}$ is the binomial coefficient $n!/2!(n-2)!$.

The background correction is then made considering the probability, B_m, of m background pulses per sweep. The q_n found by means of relation (2) are related to the actual distribution of neutron pulses, Q_n, by

$$q_n=\sum_{m=0}^{n}B_mQ_{n-m}. \tag{3}$$

A solution of Eqs. (3) yields, Q_n, the actual distribution of neutron pulses per fission.

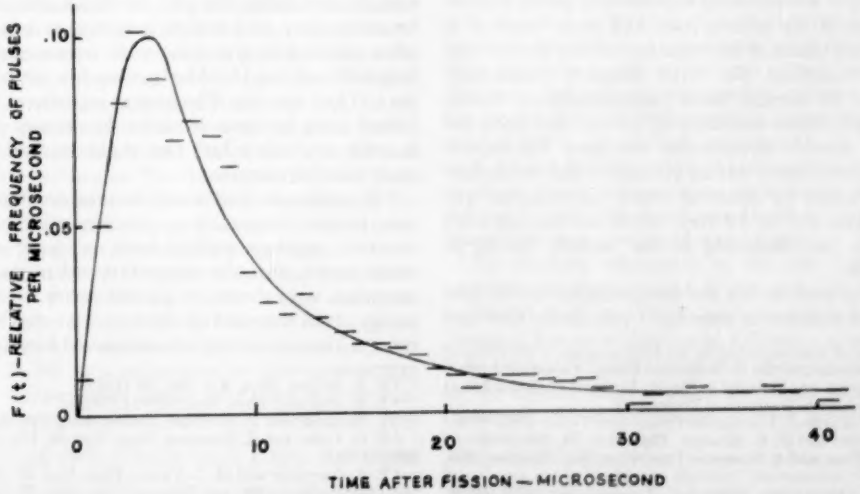

FIG. 2. Time distribution of pulses per microsecond.

TABLE I. Emission probabilities.

P_0	P_1	P_2	P_3
0.062±0.006	0.198±0.017	0.374±0.022	0.228±0.024
P_4	P_5	P_6	
0.114±0.022	0.027±0.013	0.000±0.005	

The final conversion to the probabilities, P_m, for the emission of m neutrons per fission is made considering the efficiency, α, of the counter. The actual distribution, Q_m, in the number of pulses is related to the emission probabilities, P_m, by the binomial distribution,

$$Q_n = \sum_{m=n}^{\infty} \alpha^n (1-\alpha)^{(m-n)} \binom{m}{n} P_m. \quad (4)$$

The inverse of the expression may be readily obtained, yielding

$$P_m = \sum_{n=m}^{\infty} (\alpha-1)^{(n-m)} \alpha^{-n} \binom{n}{m} Q_n. \quad (5)$$

The resultant emission probabilities obtained through the conversion outlined in the foregoing are given in Table I.

The probable errors attached to the emission probabilities in Table I were obtained by calculating the effect of independent variations in the parameters used in calculating the emission probabilities. The root sum square of the variations in the emission probabilities caused by one standard deviation in the parameters gave the standard deviation in the emission probabilities. The variations considered were those on α, s, B_m, and q_n'.

ACKNOWLEDGMENTS

The authors wish to express their gratitude for the assistance received in conversations with B. C. Diven, N. J. Terrell, and H. C. Martin of this Laboratory. For aid in the machine calculations, we are indebted to N. J. Terrell and Max Goldstein.

PHYSICAL REVIEW VOLUME 100, NUMBER 1 OCTOBER 1, 1955

Nuclear Scattering of Low-Energy Photons*

J. L. BURKHARDT†
Department of Physics and Laboratory for Nuclear Science, Massachusetts Institute of Technology, Cambridge, Massachusetts

(Received June 28, 1955)

The elastic photon scattering cross sections at 90° for lead, indium, cadmium, and copper have been measured between 0.5 and 3.0 Mev. Besides the expected Rayleigh scattering by bound electrons and Thomson scattering by the nucleus, a scattering component due to nuclear excitation is evident in the cross sections. The mechanism of this scattering is discussed.

NUCLEAR scattering of photons has been the subject of several recent experiments, partly because of interest in the process itself and partly because it represents a means of investigating nuclear photon capture cross sections. The latter reason is particularly important at energies below particle-emission thresholds, where elastic and inelastic photon scattering are the only possible photonuclear reactions. The experiment reported below was an attempt to observe nuclear photon capture by means of elastic scattering at very low energies (0.5 to 3.0 Mev) where the capture cross section is just beginning to rise toward the dipole resonance.

Previous work in this low-energy region has all been done with radioactive sources,[1-7] principally Co^{60} and Na^{24}. Fuller and Hayward,[8] starting at slightly higher energies and continuing over the dipole resonance, use bremsstrahlung as a radiation source, as was done in other experiments in and above the resonance region.[9,10] Stearns[11] used the 17.6-Mev gamma ray resulting from the $Li^7(p,\gamma)$ reaction. The present experiment was performed using bremsstrahlung as the primary radiation in order to obtain a high flux of photons and continuously variable energies.

The continuous spectrum of the bremsstrahlung, however, makes it impossible to determine whether a given scattered quantum resulted from an elastic or an inelastic event, since the energy involved in the capture transition is in doubt by the difference between the energy of the scattered quantum and the electron beam energy. This uncertainty was minimized here by biasing

* This work was supported by the joint program of the Office of Naval Research and the U. S. Atomic Energy Commission. Part of the material was included in the Ph.D. thesis of the author at the Massachusetts Institute of Technology.

† National Science Foundation Predoctoral Fellow 1952-1954.

[1] E. Pollard and D. E. Alburger, Phys. Rev. **74**, 926 (1948).
[2] P. B. Moon and A. Storruste, Proc. Phys. Soc. (London) **A66**, 585 (1953).
[3] W. G. Davey, Proc. Phys. Soc. (London) **A66**, 1059 (1953).
[4] K. Ilakovac, Proc. Phys. Soc. (London) **A67**, 601 (1954).
[5] R. R. Wilson, Phys. Rev. **90**, 720 (1953).
[6] T. D. Strickler, Phys. Rev. **92**, 923 (1953).
[7] L. Goldzahl and P. Eberhard, Compt. rend. **240**, 965 (1955).
[8] E. G. Fuller and E. Hayward, Phys. Rev. **94**, 732 (1954); **95**, 1106 (1954).
[9] E. R. Gaerttner and M. L. Yeater, Phys. Rev. **76**, 363 (1949).
[10] Dressel, Goldhaber, and Hanson, Phys. Rev. **77**, 754 (1950).
[11] M. B. Stearns, Phys. Rev. **87**, 706 (1952).

the scintillation counters used as detectors to record only those scattered photons with energy greater than 85% of the peak incident energy. Still higher bias would of course further reduce the uncertainty, but at too great a cost in intensity. The measured scattering is thus elastic, or very nearly so, and the term "elastic" will be used hereafter in the above sense. Since radiation widths increase very strongly with transition energy, it seems likely that most of the observed transitions are indeed elastic.

For the energies below 3 Mev investigated in this experiment, the presence of electrons around the nuclei under investigation leads to serious difficulties. The nuclear scattering cross sections turn out to be a few microbarns per steradian at 90°, while the electronic Compton scattering cross sections are of the order of a few tenths of a barn per steradian per atom. The Compton scattering is strongly degraded in energy at 90° and hence can be biased out, but it still can cause pileup in the relatively slow NaI scintillation counters. Elastic Rayleigh scattering by the K electrons, which cannot be separated experimentally from the other elastic scattering, is also appreciable in this energy region. This effect and others will be discussed extensively in Sec. III.

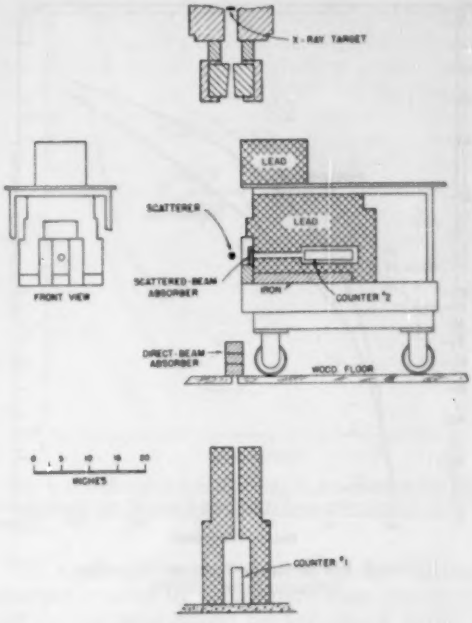

FIG. 1. Experimental arrangement.

I. EXPERIMENTAL PROCEDURE

The experiment was performed using the Electrical Engineering Department Van de Graaff generator at M.I.T.[12] The electron beam from the generator was focused on a water-cooled, $\frac{1}{4}$-inch thick gold target at the base of the accelerating tube, the target being grounded through a microammeter by which beam current was measured. Bremsstrahlung produced in the target proceeded through a lead and steel collimator to the scatterer, then through some lead absorbers and another collimator to scintillation counter No. 1, used as a monitor (see Fig. 1). Scintillation counter No. 2 was located under twenty inches of lead shielding at the end of a collimator pointed at the scatterer. To reduce pile-up by preferentially absorbing the low energy Compton component of the scattered radiation, one to three $\frac{1}{4}$-inch lead sheets were placed over the entrance to this latter collimator. The absorber in the direct beam ranged from two to ten inches of lead, depending on the machine energy, and was used to reduce the incident bremsstrahlung flux to countable proportions.

Four scatterers of identical dimensions were used: indium ($Z=49$) to compare with isomer excitation results[13]; cadmium ($Z=48$) to compare with indium, lead ($Z=82$) as a representative heavy element, and copper ($Z=29$) as a representative light-intermediate element. Various other metals were tried, but no startling differences appeared and only these four were investigated systematically. Scattering from aluminum ($Z=13$), the lightest element attempted, was indistinguishable from background. The scatterers were cylindrical, 1.9 cm in diameter and 3.0 cm long.

NaI scintillation crystals, $1\frac{3}{4}$ in. in diameter and 2 in. long, were mounted on DuMont 6292 photomultiplier tubes and sealed in light-tight containers. The resolution of these counters (width at half maximum of the photopeak divided by γ-ray energy) was 10% at 1.33 Mev and 5% at 2.76 Mev; they were connected through standard circuitry to a ten-channel pulse-height analyzer. An exceptionally stable high voltage power supply[14] was used with the photomultiplier tubes, because the output of these tubes is roughly proportional to the seventh power of the high voltage and the width of each channel of the ten-channel analyzer was usually set at about 3% of the maximum pulse height. The high voltage (about 1200 volts) was found to vary by less than 0.01% over periods of many hours.

The absolute efficiencies of the two scintillation counters were measured at 1.33 Mev and 2.76 Mev with calibrated Co^{60} and Na^{24} sources supplied by the National Bureau of Standards. Efficiency is here taken to be the fraction of the number of gamma rays incident on the crystal which produce an output pulse in the photopeak of the scintillation counter spectrum. The

[12] J. G. Trump and R. J. Van de Graaff, J. Appl. Phys. **19**, 599 (1948).

[13] Burkhardt, Winhold, and Dupree, Phys. Rev. **100**, 199 (1955); J. Goldemberg and L. Katz, Phys. Rev. **90**, 308 (1953).

[14] Quarterly Progress Report, Neutron and Gamma Ray Shielding Group and Electronic Nuclear Instrumentation Group, Massachusetts Institute of Technology, March 31, 1951 (unpublished), p. 36.

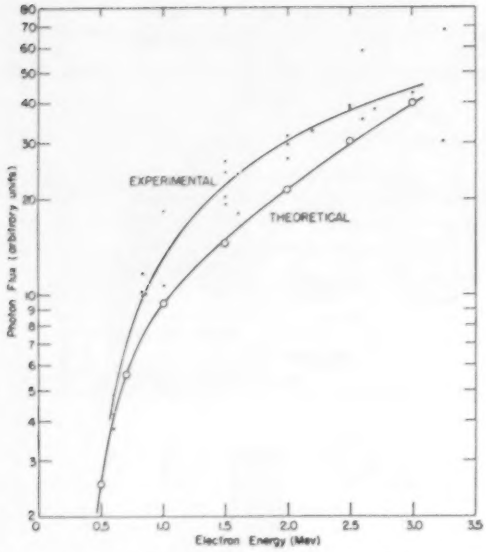

FIG. 2. Photon flux in the upper 15% of the bremsstrahlung spectrum.

measured efficiencies agreed fairly well with values calculated by a method similar to that of Maeder *et al.*,[15] so the calculated curve was normalized to the experimental points and used in all subsequent work.

Originally it was intended that scattered and direct counting rates should be determined simultaneously, the ratio being, within constants, the differential scattering cross section. This procedure was used for a time, but it proved simpler to measure the primary spectrum directly, without the scatterer interposed. Most of the data on scattered and direct flux were therefore taken separately and standardized against current and exposure time, using the ten-channel analyzer in both cases. Careful experiments were made to check the proportionality of counting rates to current at all energies, in order to be certain that pile-up in the scintillation crystals was not causing spurious counts. The energy scales of the counters were calibrated with γ rays from Cs^{134} (0.59 and 0.80 Mev), Na^{22} (0.51 and 1.28 Mev), Co^{60} (1.17 and 1.33 Mev), and Na^{24} (1.38 and 2.76 Mev). The Na^{24} has a half-life of 14.9 hours and was made as needed in the M.I.T. cyclotron; the remaining isotopes are long-lived. There appear to be no suitable sources with simple spectra and well-established γ-ray energies in the region from 1.5 to 2.5 Mev, so the Compton (2.35 Mev) and pair (1.74 Mev) peaks in the scintillation counter spectrum of the Na^{24} 2.76-Mev γ ray were used as secondary standards in this region. The counter output was found to be strictly linear with γ-ray energy, as expected, a fact which aided in the calibration at intermediate energies.

[15] Maeder, Muller, and Wintersteiger, Helv. Phys. Acta **27**, 3 (1954); M. J. Berger and J. A. Doggett, Phys. Rev. **99**, 663(A) (1955).

II. RESULTS

The number of counts recorded in the direct beam monitor per unit electron beam current per unit time for various electron energies is shown in Fig. 2. The small black points are experimental data; they have been corrected for the attenuation by the lead absorber in the beam, but not for the efficiency of the counter. The attenuation correction was made using the absorption coefficients of White[16] which differ very slightly from those of Davisson and Evans[17] below 1 Mev. By calculation and experimental check, it was shown that the experimental geometry was sufficiently good to justify the use of these coefficients without adjustment. As might be expected, the attenuation correction is somewhat sensitive to the value of the absorption coefficients. The fractional error in the correction factor C is given very closely by

$$\Delta C/C=[\Delta(\mu x)/\mu x]\ln C,$$

where μ is the absorption coefficient and x the thickness of the absorber. The values of C range from 40 to more than 10^7, and a reasonable estimate for the maximum fractional error in μx is 3%. Thus the maximum fractional error in C is around 50%. For most of the points C was of the order of 10^5, corresponding to an error of about 35%, which is consistent with the spread of the data. The line drawn through the experimental points was used in calculating the cross sections; it is considered good to within roughly 20%, on the basis of the above discussion.

The theoretical curve in Fig. 2 is based on a computation of the bremsstrahlung flux from the particular thick target used in this experiment. This computation was made as follows. The Bethe-Heitler thin target bremsstrahlung formula[18] was corrected for the use of the Born approximation by applying a factor derived from Sommerfeld's exact calculation.[19,20] This corrected thin target spectrum, which has a finite value at the short wave limit, was integrated to give a thick target spectrum, taking account of energy loss along the path of the electron. Only those electrons and photons with energy greater than 85% of the incident electron energy were considered, so screening could be neglected and the divergence at the low-energy end of the bremsstrahlung spectrum caused no difficulty. The thick target spectrum thus derived was corrected for self-

[16] G. R. White, National Bureau of Standards Report NBS-1003, 1952 (unpublished).

[17] C. M. Davisson and R. D. Evans, Revs. Modern Phys. **24**, 79 (1952).

[18] H. A. Bethe and W. Heitler, Proc. Roy. Soc. (London) **A146**, 83 (1934).

[19] W. Heitler, *The Quantum Theory of Radiation* (Oxford University Press, London, 1954), third edition, Sec. 25; J. C. Jaeger, Nature **140**, 108 (1937).

[20] J. W. Motz and W. Miller, Phys. Rev. **96**, 544 (1954); Motz, Miller, and Cialella, Phys. Rev. **96**, 1344 (1954).

absorption in the gold target, and its angular distribution was predicted from the electron scattering theory of Snyder and Scott.[21] The latter theory was modified crudely to correct for energy loss in the target and deviations from the small-angle approximation. Finally a correction for the efficiency of the counter as a function of energy led to the curve plotted in the figure. Considering the approximate nature of the calculation, the agreement is indeed gratifying. This computation is taken only as a rough substantiation of the shape and magnitude of the measured curve.

It is interesting to note that the group at the National Bureau of Standards found the measured thick target bremsstrahlung fluxes in this energy region to be in excess of computed values by about a factor of two.[20] Their calculation did not correct for the use of the Born approximation; had this correction been made, the discrepancy would match that shown in Fig. 2 almost exactly.

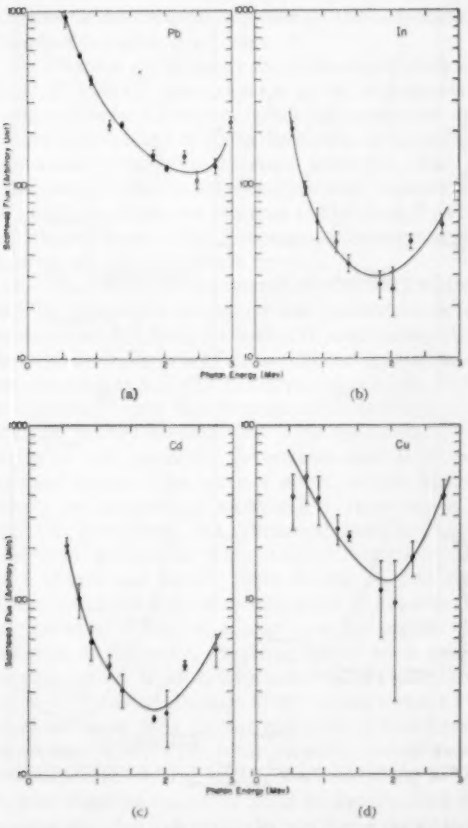

FIG. 3. Scattered photon flux.

[21] H. S. Snyder and W. T. Scott, Phys. Rev. **76**, 220 (1949); see B. Rossi, *High Energy Particles* (Prentice-Hall, Inc., New York, 1952), Sec. 2.17.

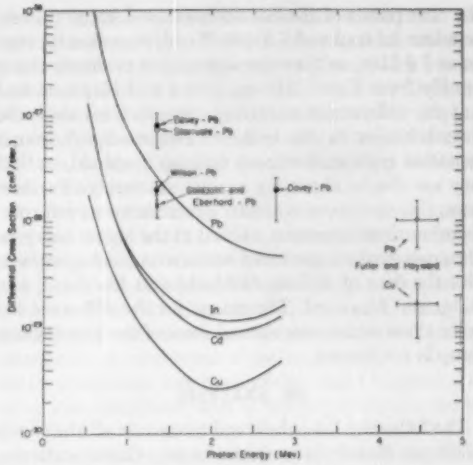

FIG. 4. Differential photon scattering cross sections at 90°. The points shown on the graph are taken from references 3, 5, 7, 8, and 22.

The number of events (corrected for the thin lead absorber) recorded by the scattered beam counter per unit electron beam current per unit time is shown in Fig. 3, plotted as a function of the weighted mean photon energy in the interval being counted. This weighted mean was determined from the shape of the scattered pulse-height spectrum measured on the ten-channel analyzer. Almost every point in the figure is the result of two or more (up to twenty) individual runs, each point representing from forty minutes to five hours total counting time. The plotted points are weighted averages of the individual runs, and the errors on the points are standard deviations computed from the spread of the individual values entering into each average. In copper, cadmium, and indium these errors are primarily of statistical origin; but in lead, where the counting rates were higher, they arise mainly from variations in discriminator settings from run to run. The lines drawn through the data were used for subsequent calculations.

Dividing the scattering curves of Fig. 3 by the experimental bremsstrahlung flux of Fig. 2 and correcting for counter efficiencies, solid angles, the number of atoms in each scatterer, and absorption in the scatterers, we arrive at the differential elastic scattering cross sections at 90° which are plotted in Fig. 4. Data of Wilson,[5] Goldzahal and Eberhard,[7] Davey,[8] and Storruste,[22] for scattering of γ rays from sources, and that of Fuller and Hayward[3] for a bremsstrahlung experiment very similar to the one reported here, are shown for comparison. (Fuller and Hayward's points were measured at 120°; their data have been converted to 90° using their assumed angular distribution proportional to $1+\cos^2\theta$.)

[22] A. Storruste, thesis, University of Oslo, 1950 (unpublished), as reported in reference 3.

The next points of the last authors are 7.9×10^{-28} cm^2/steradian for lead and 7.5×10^{-29} cm^2/steradian for copper at 7.4 Mev, so the cross sections are evidently rising steadily from 2 to 3 Mev on. Fuller and Hayward find that the differential scattering cross sections show the same behavior as the indium[13] and rhodium[23] isomer excitation cross sections near neutron threshold, so that they are clearly observing nuclear scattering. Furthermore, this scattering evidently proceeds by way of compound nucleus formation, at least at the higher energies. The cross sections measured here are in good agreement with the data of Wilson, Goldzahl and Eberhard, and Fuller and Hayward. The reason for the difference between these measurements and those of the Birmingham group is not known.

III. ANALYSIS

The following list is believed to contain all the effects which can contribute to elastic or near-elastic scattering as measured in this experiment: a. Rayleigh scattering by bound electrons. b. Compton scattering by bound electrons. c. Raman scattering by bound electrons. d. Thompson scattering by the nucleus. e. Delbruck scattering in the nuclear Coulomb field. f. Bremsstrahlung in the scatterer from photo-, Compton-, or pair-electrons. g. Scattering resulting from nuclear excitation. The first three processes are evidently closely related; they correspond to scattering by a bound electron which ends up in its original state, a continuum state, or an excited bound state, respectively. The last effect in the list constitutes the original objective of the experiment; in order to estimate its magnitude, the other contributions must be subtracted from the measured cross sections. These other contributions will now be discussed briefly.

a. No complete calcualtion of the Rayleigh scattering at relativistic energies has been published. The work of Franz,[24] based on the Fermi-Thomas atom model and the approximation of small-angle scattering, has been used by Moon[25] to predict scattering at all angles. However, large-angle scattering involves much greater momentum transfer than forward scattering and hence depends on components of the electronic momentum distribution which were neglected in the Franz calculation. Bethe has computed the atomic form-factor for Rayleigh scattering by the K shell using Dirac wave functions,[26] but in the approximation of nonrelativistic momentum transfer. Levinger[26] shows that this approximation introduces large errors when the momentum transfer approaches mc, but his correction is given in the form of an expansion which diverges beyond this point. Since the momentum transfer Δq for 90° scattering is

$$\Delta q/mc = 1.41(E_\gamma/mc^2),$$

it is seen that Levinger's expansion diverges over the entire energy range considered in this experiment. Moreover, Brown and Woodward[27] have shown that the use of the first Born approximation (plane wave intermediate state), implicit in the derivation of a form-factor, also introduces large errors. The second term in the Born expansion is found to be larger than the first for $\Delta q > 2.83\ mc$, but the succeeding terms decrease as powers of $Z/137$. The ratio of the second term to the first turns out to be inversely proportional to Z, and hence the second term is of greater importance in copper than in lead, but the reverse proves to be true for Levinger's correction. The magnitude of the difference between experiment and the uncorrected theory is shown in Fig. 5, where the cross sections are plotted to larger scale. (Note that Bethe's form factor takes account of the two K electrons only, the whole L shell being estimated to contribute only $\frac{1}{8}$ as much as the K shell.)

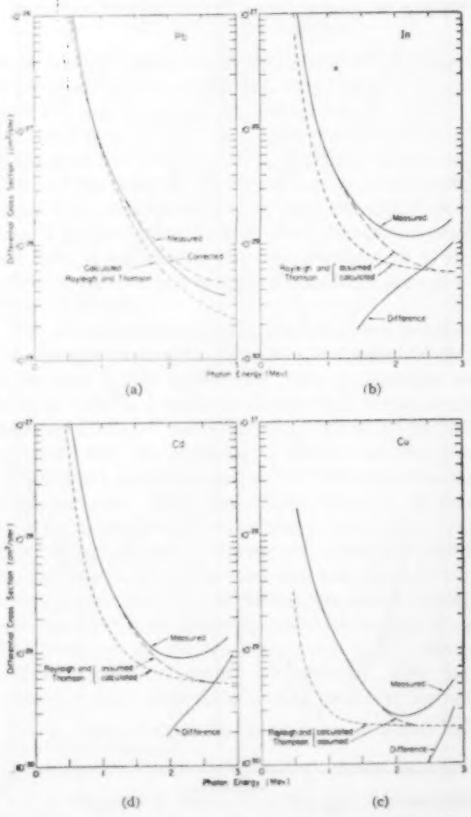

FIG. 5. Analysis of cross sections. The calculated Rayleigh plus Thompson cross sections, due to Bethe, are taken from reference 26.

[23] C. S. del Rio and V. L. Telegdi, Phys. Rev. **90**, 439 (1953).
[24] W. Franz, Z. Physik **95**, 652 (1935); **98**, 314 (1935).
[25] P. B. Moon, Proc. Phys. Soc. (London) **A63**, 1189 (1950).
[26] J. S. Levinger, Phys. Rev. **87**, 656 (1952).
[27] G. E. Brown and J. B. Woodward, Proc. Phys. Soc. (London) **A65**, 977 (1952).

b. Ordinary Compton scattering at 90° from free electrons produces photons of lower energies than those counted in this experiment. However, the Doppler shift for photons scattered from tightly bound electrons can bring them within the accepted interval. Even though this shifted part is but a small fraction of the total Compton scattering, its effect to the measured scattering may be appreciable because of the very large Compton cross section. The magnitude of this effect, calculated from the work of Franz,[28] was found to be negligible ($<2\%$) in all cases except lead, but substantially all of the correction to the lead curve shown in Fig. 5 is due to this modified Compton scattering.

c. Between the high-frequency cutoff of the Compton distribution (caused by the electron binding) and the Rayleigh line, a series of Raman lines should appear which must also be considered as a possible correction. However the only lines of appreciable intensity are those for which either the initial or final electron state is in the K shell, and the Pauli principle forbids virtually all of these in the elements considered. The correction is therefore negligible in all cases.

d. Thomson scattering by the nucleus has a cross section $(Z^2/1836A)^2$ times as large as the corresponding cross section for an electron. Since the wavelength of a 3-Mev photon is still 50 times the nuclear radius of lead, one would expect pure Thomson scattering, with no Compton effect by the individual protons. Thomson and Rayleigh scattering are coherent and in phase,[29] so the calculated curves in Fig. 5 represent a coherent superposition of these two effects.

e. The differential cross section for Delbruck scattering (by virtual pair production and annihilation in the nuclear Coulomb field) for lead at 0° was calculated by Rohrlich and Gluckstern[30] to be 0.59 and 9.2 millibarns per steradian at 1.33 and 2.62 Mev, respectively. Bethe and Rohrlich[31] show that the angular distribution is very strongly peaked forward, but their approximate formulas are only applicable for extreme relativistic energies and angles of the order of mc^2/E_γ or less. If their results are extrapolated graphically to large angles (a doubtful procedure), the differential cross section in lead at 90° is found to be about 3×10^{-31} cm²/steradian at 1.33 Mev and twenty times smaller at 2.62 Mev. These values are completely negligible. If however the suggestion of Wilson[8] is adopted and the angular distribution of diffraction scattering from a black sphere of radius $\hbar/mc$ is used, normalized to the calculated value at 0°, the cross section at 90° in lead turns out to be of the same order as that measured in this experiment. But Wilson's procedure certainly overestimates the scattering at large angles, since scattering in the forward direction can occur much farther out from the nucleus than that at large angles, and hence the forward peaking must be greater than the above estimate. The Delbruck scattering is of course coherent with the other elastic scattering, although the relative phases are unknown. At any rate, it seems likely that the Delbruck contribution to the measured scattering at 90° is small, if not negligible, in lead, and since it is proportional to Z^4, it is surely negligible in the remaining elements, even on Wilson's model.

f. The bremsstrahlung flux incident on the scatterer produces large numbers of photoelectrons, electron-positron pairs, and Compton-scattered electrons, all of which can radiate energy while slowing down in the scatterer. The pair electrons lose too much energy in formation to contribute to the measured cross section, because of the restriction of the measurements to near-elastic scattering. But both photo- and Compton-electrons can contribute, and a rough calculation shows that the effective cross section is about 3×10^{-30} cm²/steradian in lead at 2 and 3 Mev. This small correction has been included in Fig. 5. Since the bremsstrahlung cross section is proportional to Z^2, and the Compton and photoelectric cross sections to Z and Z^5, respectively, the correction is negligible in the lighter elements.

IV. INTERPRETATION

A comparison of the measured cross section curves in Fig. 5 with the theoretical Rayleigh plus Thomson cross sections shows fairly good agreement at low energies in lead, but progressively poorer agreement with decreasing atomic number. It should be emphasized that the measured data are plotted absolutely; they have not been normalized to the theoretical curves. In view of the uncertainties in the Rayleigh scattering calculation, the agreement in lead may be fortuitous, but it is encouraging to note that Storruste's[32] value ($\sim2\times10^{-26}$ cm²/steradian) for lead at 0.41 Mev agrees very well with both the Bethe curve and the present experiment. This evidence lends added confidence to the absolute normalization of the measured curves.

It is clear that the Rayleigh calculations are not sufficiently complete to be useful in the analysis of these data. It seems reasonable, on the other hand, to say that the low-energy ends of the measured cross sections represent the true Rayleigh plus Thomson scattering. The fact that the correction for the Born approximation is greater for smaller Z (see Sec. IIIa) adds support to this assumption, as does a recent exact calculation of lower energy Rayleigh scattering in mercury.[33] The low-energy portions of the indium, cadmium, and copper cross-section curves were therefore extrapolated arbitrarily to meet the (constant) Thomson cross section, as shown by the "assumed Rayleigh plus Thomson" curves in Fig. 5. The difference between these assumed curves and the measured data is then taken as a rough

[28] W. Franz, Ann. Physik **29**, 721 (1937).
[29] A. M. Cormack, Phys. Rev. **94**, 1397 (1954).
[30] F. Rohrlich and R. L. Gluckstern, Phys. Rev. **86**, 1 (1952).
[31] H. A. Bethe and F. Rohrlich, Phys. Rev. **86**, 10 (1952).
[32] A. Storruste, Proc. Phys. Soc. (London) **A63**, 1197 (1950).
[33] Brown, Peierls, and Woodward, Proc. Roy. Soc. (London) **A227**, 51 (1954); Brenner, Brown, and Woodward, Proc. Roy. Soc. (London) **A227**, 59 (1954).

representation of the contribution of internal nuclear scattering. The lack of definite curvature at the high energy end of the lead data hardly justifies such treatment in that case.

It is of interest to speculate on whether the nuclear absorption at these energies is the result of nuclear levels in this region or merely the effect of the long tail of the dipole resonance. Scattering by the tail of a higher energy resonance would be coherent with the Rayleigh and Thomson scattering, and exactly out of phase, whereas scattering by narrow levels which are completely covered by the incident spectrum would effectively add incoherently. Levinger[34] estimated the magnitude of the dipole resonance scattering at low energies by the use of the dipole sum rule and dispersion theory and found that the scattering amplitude at 3 Mev is only five to ten percent of the Thomson scattering amplitude for the elements studied in this experiment. Thus it is evident that the scattering cannot be totally caused by the tail of the dipole resonance.

One can use Weisskopf's estimates for single-particle gamma transition matrix elements[35] to predict the amount of scattering to be expected from energy levels in the region of irradiation, although the uncertainties in these estimates prevent detailed numerical comparison between theory and experiment. It is found that the measured nuclear scattering is consistent in magnitude, energy dependence, and A-dependence with predicted scattering from single-particle levels on the assumption that the transitions are predominantly electric quadrupole, with a possible magnetic dipole contribution. Electric dipole transitions would lead to too much scattering by a factor of $\sim 10^2$ while multipoles higher than $E2$ predict too little. Since experimental lifetimes for isomeric states differ by large factors from the single-particle estimates,[36] it is not possible to assign multipolarities to the scattering on the basis of the above comparison; the intention is rather to give an idea of the strengths of the transitions involved.

If the scattering actually occurs from narrow levels, the correction made for self-absorption in the scatterer may be in error, since that correction was made with the usual atomic absorption coefficients. Radiation scattered from a narrow level is shifted off resonance by nuclear recoil and hence not further attenuated by resonance absorption, but the incident spectrum seen by atoms inside the scatterer may be depleted in narrow regions around the resonance energies because of the large nuclear absorption of these energies. Rough calculations indicate that, as an upper limit, this effect could increase the nuclear component of the scattering by a factor of three over the measured data, the actual estimated value being much less.

The nuclear scattering from indium can also be compared with the known cross section[13] for photoexcitation of the isomeric state In^{115m}. If the angular distribution of the nuclear scattering is assumed isotropic (reasonable within a factor of the order of two), then the total nuclear elastic scattering cross section at 3 Mev is approximately ten times greater than the measured isomer excitation cross section at that energy, which fact correlates with the expectation that isomer production should be strongly suppressed because of the large spin change required. This point is discussed further in reference 13.

A final point of some interest is the apparent difference between the scattering from indium and cadmium. The curves of Fig. 4 show this difference, but the manner in which they were obtained from the actual data is not sufficiently reliable to draw a definite conclusion. However, if the original scattering data (Fig. 3, corrected for the number of atoms/cm^2 and self-absorption in the scatterer) is examined, it is found that every point in indium is above the corresponding point in cadmium, and although most of the individual differences are not statistically significant, the total effect is. Bethe's Rayleigh scattering formula is roughly proportional to Z^7, so that one would expect indium to differ from cadmium by a factor of 1.14 below roughly 1.2 Mev, and the average measured ratio of the first four points is 1.28 ± 0.19. But Thomson scattering is proportional to only Z^2 (ratio 1.04), and at the high-energy end, where this is the predominant background, the measured ratio is 1.40 ± 0.17. The indium and cadmium scatterers were checked by x-ray scattering analysis and found to have no measurable impurities, so the measured difference is not attributable to contamination. One is therefore led to the conclusion that either a significant difference exists between the self-absorption by nuclear levels in the two scatterers, or else that the nuclear elastic scattering cross section in indium is greater than that in cadmium by something of the order of 40%, perhaps because of the presumably higher level density in odd-A indium in predominantly even-A cadmium.

V. ACKNOWLEDGMENTS

The author expresses his appreciation to the many people who have contributed to this work. He is particularly indebted to Dr. P. T. Demos for advice and encouragement, to Dr. E. J. Winhold for active participation in all phases of the experiment work, and to K. A. Wright and Professor J. G. Trump for making available the Van de Graaff generator facilities and for many kindnesses.

[34] J. S. Levinger, Phys. Rev. **84**, 523 (1951).
[35] J. M. Blatt and V. F. Weisskopf, *Theoretical Nuclear Physics* (John Wiley and Sons, Inc., New York, 1952), p. 654.
[36] M. Goldhaber and A. W. Sunyar, in *Beta- and Gamma-Ray Spectroscopy*, edited by K. Siegbahn (North-Holland Publishing Company, Amsterdam, 1955), Chap. XVI(II).

Photoexcitation of the Isomeric State of Indium-115*

J. L. BURKHARDT,† E. J. WINHOLD,‡ AND T. H. DUPREE
Department of Physics and Laboratory for Nuclear Science, Massachusetts Institute of Technology, Cambridge, Massachusetts
(Received June 21, 1955)

The cross section for photoexcitation of In^{115m} has been measured between 1 and 14 Mev. The cross section is found to rise to a narrow peak at 8 Mev, 2 Mev wide, of maximum value 1.2 mb. This peak is interpreted as the result of competition from neutron emission by the excited nucleus. Clear evidence for sharp levels in the excitation cross section is found below 2 Mev and the integrated cross sections for two levels are determined approximately.

THE excitation of nuclei to isomeric states by photon irradiation is interesting because it gives several types of information about the electromagnetic interactions of nuclei. If a nucleus has an isomeric state of conveniently measurable half-life, it is possible to study the inelastic photon scattering process by measuring the production of the isomer. Below particle emission thresholds, where elastic and inelastic photon scattering are the only possible photonuclear reactions, one can sometimes estimate crudely the expected branching ratio for isomer production and thus obtain an indication of the size and shape of the photon capture cross section. The behavior of the isomer excitation cross section near photoneutron threshold should show whether or not competition plays a role in nuclear photon scattering. And finally, at low energies the cross section might be expected to give information about the level structure of the nucleus being studied. All of the above points have been investigated by other workers in the past.[1-5]

The matrix element for direct excitation of an isomer is of course exceedingly small, this being the criterion for the existence of the isomeric state. Instead, isomer production must proceed by way of an excited intermediate state (only isomeric states of the target nucleus will be considered), although a compound nucleus in the sense of the statistical theory may not necessarily be formed. The excited intermediate state itself can decay in several ways: by particle emission with or without accompanying photon emission, if the energy is high enough, or by photon emission alone, directly or by cascade to the ground or isomeric state of the target nucleus.

In the experiments to be described below, the isomer chosen for study was In^{115m}, previously investigated in similar experiments at Notre Dame[5] and Saskatchewan.[4] The relatively long half-life (4.5 hours) and strongly converted gamma ray of this isomer make possible the use of standard Geiger-counting techniques, whose absolute efficiency can be determined with fair reliability. Also the large natural abundance (96%) of In^{115} is important because of the small cross section for the isomer-excitation reaction, while the absence of stable neighboring indium isotopes eliminates confusion from other possible reactions leading to In^{115m}. The spin of the ground state is 9/2, positive parity, and that of the isomeric state is 1/2, negative parity; the 0.335 Mev isomeric transition is thus magnetic 2^4-pole. The conversion coefficient is known experimentally and predicted theoretically to be very nearly unity.[6]

I. EXPERIMENTAL PROCEDURE

A. High Energy Experiment

Two essentially separate experiments have been performed. In the first, two 2-mil indium foils were activated in each run by placing them on either side of a 5-mil tantalum radiator in the external analyzed electron beam of the Massachusetts Institute of Technology linear accelerator. This stacked-foil technique was used to obtain the highest possible yields from thin-target bremsstrahlung and also to facilitate background subtraction. Since the electron beam was to a first approximation unchanged in passing through the three foils, the electrodisintegration plus background activities in the two indium foils were approximately identical and the difference in activity was caused by forward-directed bremsstrahlung made in the tantalum foil. Runs were made at a series of electron energies from 2 Mev to 14 Mev, the high current output of the accelerator (approximately 0.2 μa analyzed beam) and the favorable exposure geometry making possible the low energy runs where activities were small. The lowest point (1.88Mev) was taken using only the Van de Graaff injector at a current of 1.25 μa. Exposures ranged from 15 to 90 minutes. To decrease radiation contamination, the electron beam collimators fitted to the linear accelerator were made of carbon. The beam cross section was 0.5 in. by 1 in., and the energy resolution of the analyzer was 3%. Beam current was measured by stopping the elec-

* This work was supported by the joint program of the Office of Naval Research and the U. S. Atomic Energy Commission. Portions of the material were included in the Ph.D. thesis of the first author and the S.B. thesis of the third author at Massachusetts Institute of Technology.
† National Science Foundation Predoctoral Fellow 1952-1954.
‡ Present address, Department of Physics, University of Pennsylvania, Philadelphia, Pennsylvania.
[1] E. Guth, Phys. Rev. **59**, 325 (1941).
[2] W. C. Miller and B. Waldman, Phys. Rev. **75**, 425 (1949).
[3] A. G. W. Cameron and L. Katz, Phys. Rev. **84**, 608 (1951).
[4] J. Goldemberg and L. Katz, Phys. Rev. **90**, 308 (1953).
[5] C. S. del Rio and V. L. Telegdi, Phys. Rev. **90**, 439 (1953).
[6] Hollander, Perlman, and Seaborg, Revs. Modern Phys. **25**, 537 (1953) and references therein.

trons in a carbon Faraday cage, shielded against secondary emission and grounded through a low impedance dc amplifier. To suppress ionization currents the Faraday cage was placed inside an evacuated chamber, with a thin aluminum window to admit the electron beam, the foils under exposure being placed between the vacuum chamber and the linear accelerator exit port. An excellent account of an almost identical experiment on copper has been given by Berman and Brown.[7]

As a check on the reliability of the exposure technique, several runs were made using a more conventional geometry. A thin foil of thorium was placed in front of enough graphite to absorb the electron beam, and this assembly was placed inside the analyzer vacuum chamber at the end of the collimator, with provision made for measuring beam current. Since the low atomic number of carbon makes it a very poor radiator, the radiation produced by this target was essentially thin-target bremsstrahlung from the thorium. Several runs were then made with indium foils placed outside the vacuum chamber in this bremsstrahlung beam, and the results agreed with those obtained with stacked foils. Because the broad angular distribution of the radiation at low energies made it difficult to intercept all the bremsstrahlung with the indium foil (separated from the radiator by approximately one inch of carbon), this technique was less satisfactory than the stacked foil method and was therefore abandoned.

Since inelastic neutron scattering can also produce In^{115m},[8,9] an experiment was performed to check the remote possibility that the observed activity differences between front and rear foils might be caused by neutrons made in the radiator or elsewhere in the target room. Obviously this effect could only occur at high energies, above neutron threshold. A single indium foil was placed behind a four-inch lead target in the undeflected beam of the accelerator and exposed for 15 minutes at 2 μa and 13.5 Mev. The copious neutron flux thus produced gave rise to some neutron capture activity (54 minute In^{116m}) but no observable inelastic scattering. The upper limit thus placed on the ratio of (n,n') to (n,γ) assured that the neutron-produced activity in the separate foils was negligible, and hence that the neutron contribution to the rear-front difference was negligible to a higher order.

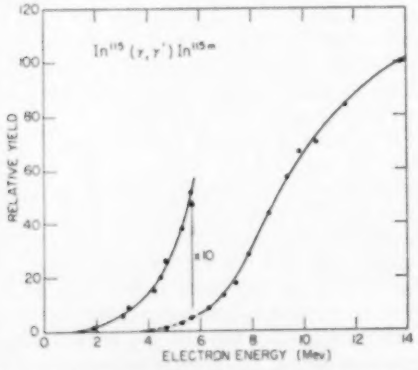

FIG. 1. Activation curve for the photoexcitation of In^{115m}, using thin-target bremsstrahlung.

The activated foils were counted on standard end-window Geiger counters. Activity was plentiful at the higher energies, but below 4.5 Mev the net counting rates were generally below background, so that statistical errors on individual points became large. Above 5 Mev, these errors are estimated to be less than $\pm 5\%$; at lower energies they may become as high as $\pm 20\%$, but in this region other corrections probably mask the statistical errors anyway. To determine the absolute efficiency of the Geiger counting procedure an activated indium foil was counted first in the standard manner and then in a 4π methane flow counter. Knowing this efficiency and the decay scheme of the isomer one can determine the true number of disintegrations occurring in the foil and hence, with the use of the bremsstrahlung spectrum, the magnitude of the activation cross section.

B. Low-Energy Experiment

The second experiment was performed with the Electrical Engineering Department Van de Graaff generator in Building 28 at Massachusetts Institute of Technology. Thick target bremsstrahlung was produced by stopping the electron beam in a $\frac{1}{4}$-inch thick water-cooled gold target at the base of the accelerating tube. Single 12-mil indium foils were exposed immediately below the aluminum window at the end of the tube, approximately one inch from the target. The target and tube extension were electrically connected and the current to them measured by a microammeter, all runs being made with 200 microamperes beam current. Machine energy was measured with a generating voltmeter whose linear voltage scale was calibrated against the beryllium and deuterium photoneutron thresholds and is estimated to be accurate to within ± 50 kv. A very satisfactory check on its accuracy was obtained by comparison with the energies of Na^{24}, Co^{60}, and Cs^{134} gamma rays, using scintillation counters.

The activation curve for In^{115m} produced by thick-target bremsstrahlung was obtained with the above apparatus between 1 and 2 Mev, using the same counting technique as in the high-energy experiment. Counting errors were less serious for the present experiment because of the high electron beam current employed. The bremsstrahlung spectrum of the machine was measured in a separate experiment reported elsewhere.[10]

[7] A. I. Berman and K. L. Brown, Phys. Rev. **96**, 83 (1954).
[8] Goldhaber, Hill, and Szilard, Phys. Rev. **55**, 47 (1939).
[9] S. G. Cohen, Nature **161**, 475 (1948).
[10] J. L. Burkhardt, Phys. Rev. **100**, 192 (1955).

II. RESULTS AND DISCUSSION

A. High-Energy Experiment

In the linear accelerator experiment several corrections to the raw activity data were needed, besides the trivial normalizations to standard beam current, exposure time, and foil mass. The electrodisintegration contributions to the activities in the foils are different in that the electron beam energy is lower in the rear foil than in the front, and the self-induced photodisintegration activities (produced in each foil by bremsstrahlung from the same foil) differ for the same reasons. Corrections for these effects were made using the energy-loss data of Paul and Reich[11] and Goldwasser *et al.*,[12] in conjunction with the electrodisintegration theory of Blair[13] and experiments of Scott *et al.*[14] and Brown and Wilson.[15] These energy corrections were relatively unimportant at high energies, but below about 4 Mev their magnitude increased considerably, amounting to roughly a factor of two on the individual foil activities at 2 Mev. The large correction arises from the fact that the total foil thickness for the three foils (0.186 g/cm^2) corresponds to an average energy loss of about 0.25 Mev for 2 Mev incident electrons. No correction was needed for background activities produced by photon contamination of the electron beam because these activities were equal in the two foils.

With the above corrections the activation curve plotted in Fig. 1 was obtained. It shows the relative yield of In^{115m} produced by the bremsstrahlung radiation from one indium and one tantalum foil bombarded with electrons of various energies. This activation curve was differentiated numerically using the Bethe-Heitler extreme relativistic bremsstrahlung spectrum, including screening,[16] at 0.5-Mev intervals, and the resulting cross section is shown in Fig. 2. The uncertainty of the cross section in the peak region is $\sim 30\%$, assuming the Bethe-Heitler spectrum is correct. The position of the peak is sensitive to the exact shape of the activation curve and is thus uncertain by about ± 1 Mev. The full width at half-maximum, likewise sensitive to the activation curve shape, is 2 Mev, with an estimated uncertainty of ± 1 Mev. The low-energy end of the cross-section curve may be overestimated somewhat by the use of the extreme relativistic bremsstrahlung formula.

The above cross section compares reasonably well in the location of the peak, but not in width or magnitude, with that of the Saskatchewan group[4] which finds a peak value of 2.2×10^{-27} cm^2 (corrected to an internal conversion coefficient of unity) at 9 Mev with a width of 9 Mev. That the narrower width is more plausible can be seen from the following considerations. First, it is apparent from both experiments that the peaked shape does not coincide with the dipole resonance maximum, but rather that the isomer excitation seems to peak near the (γ,n) threshold around 9 Mev. Neutron emission should be much more probable than photon emission when both are energetically possible, so that one would expect the isomer excitation cross section to fall off rapidly above photoneutron threshold, forming a sharp peak as observed in this experiment. Further evidence in support of this view is contributed by the Rh^{103m} excitation cross section measured at Chicago,[5] which has a width of 3 Mev, and the photon scattering cross sections investigated at the National Bureau of Standards,[17] which show clearly the effects of neutron emission competition.

With this explanation of the peak in terms of competition, it would seem that the photon capture cross section should be smooth in the neighborhood of the neutron threshold, because capture and emission are then not directly related. Since the photoneutron cross section is a good representation of the capture cross section just above threshold, one would therefore expect the total photon capture cross section below neutron threshold to join smoothly on to the extrapolated photoneutron curve. Using the Saskatchewan In^{115} (γ,n) cross section,[4] it appears that the peak value of the photon capture cross section to be expected just below neutron threshold should be roughly 50×10^{-27} cm^2. To compare this value with the measured cross section, one must estimate the fraction of excited nuclei which decay into the isomeric state. Since low multipole photon transitions are strongly favored when suitable spin states are available, a nucleus excited out of a $9/2+$ state is much more likely to return to that state than to a nearby $\frac{1}{2}-$ state. By analogy with some measured isomer/ground state ratios in (γ,n) reactions, Goldemberg and Katz estimate as $\frac{1}{3}$ the fraction going to the isomer by photon de-excitation in In^{115}. This estimate seems unconvincing, however, since selection rules and statistical factors for neu-

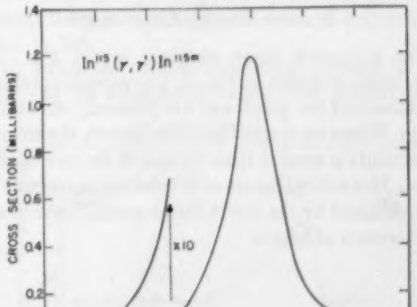

FIG. 2. Cross section for the photoexcitation of In^{115m}.

[11] W. Paul and H. Reich, Z. Physik. **127**, 429 (1950).
[12] Goldwasser, Mills, and Hanson, Phys. Rev. **88**, 1137 (1952).
[13] J. S. Blair, Phys. Rev. **75**, 907 (1949).
[14] Scott, Hanson, and Kerst, Phys. Rev. **94**, 763 (1954).
[15] K. L. Brown and R. Wilson, Phys. Rev. **93**, 443 (1954).
[16] H. A. Bethe and W. Heitler, Proc. Roy. Soc. (London) **A146**, 83 (1934).
[17] E. Hayward and E. G. Fuller, Phys. Rev. **95**, 1106 (1954).

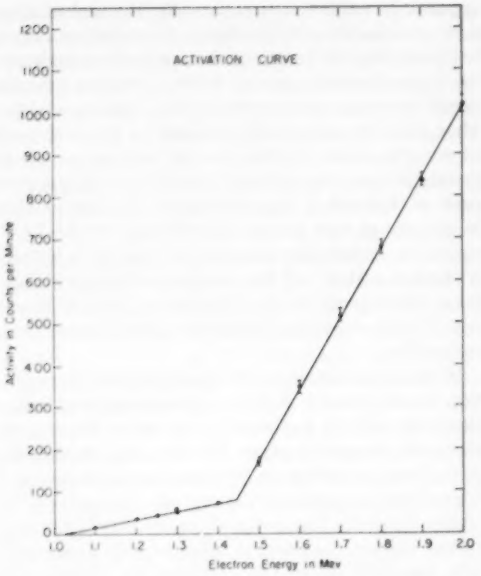

FIG. 3. Activation curve for the photoexcitation of In^{115m} at low energies, using thick-target bremsstrahlung.

tron and photon de-excitation are quite different. Moreover, Telegdi estimates the isomer/ground state ratio in rhodium to be $\frac{1}{4}$, and Rh^{103m} is only an $E3$ isomer, considerably less forbidden than the $M4$ In^{115m} case. His 12 millibarns peak measured cross section thus leads to about 50×10^{-27} cm² for the capture peak in rhodium, in good agreement with the above expectation. It would appear that a branching ratio of the order of 1/50 for In^{115} near the peak of the isomer cross section is by no means out of the question. Since the branching ratio is very likely energy-dependent, one cannot deduce a curve for the photon absorption cross section *versus* energy.

B. Low Energy Experiment

The activation curve obtained in the low energy experiment is shown in Fig. 3. The experimental errors are shown on the graph and are primarily statistical in origin. Where no vertical bar is indicated, the estimated uncertainty is smaller than the size of the corresponding point. This activation curve is excellent agreement with that obtained by the Notre Dame group,[2] both in shape and location of breaks.

In order to obtain a cross section from the activation curve of Fig. 3, it is necessary to know the thick-target bremsstrahlung spectrum from the particular target used in this experiment. Since this spectrum should be a relatively smooth function of energy, it is evident that the cross section between 1 and 2 Mev consists mainly of sharp lines at 1.02 ± 0.05 Mev and 1.45 ± 0.05 Mev, with the possibility of some smaller unresolved levels and/or a continuous contribution as well. The only reason for repeating these results, all of which were obtained by the Notre Dame group earlier, is that the shape and intensity of the bremsstrahlung spectrum used here has been measured,[10] and it is thus possible to obtain values for the integrated cross sections of the two levels detected. Assuming that only these levels are important, it is found that $\int\sigma dE$ for the 1.02-Mev level is 2×10^{-32} Mev-cm², and that for the 1.45-Mev level is 1×10^{-32} Mev-cm², where σ is the cross section for photoexcitation of the isomer, not the photon capture cross section. The estimated uncertainty of these values is of the order of a factor of four, resulting primarily from the difficulty of measuring the slope of the bremsstrahlung spectrum accurately.

For sharp lines of the sort excited in this experiment, one would expect an integrated photon-capture cross section of the order of $\lambda^2\Gamma$, where λ is the wavelength of the resonance x-rays and Γ the partial width of the level for decay directly to the ground state. If the fraction of the excited nuclei which decay into the isomeric state is called β, it is then expected that $\int\sigma dE$ as measured here should be of the order of magnitude of $\lambda^2\Gamma\beta$. Thus for the 1.45-Mev level, using the experimental integrated cross section, $\Gamma\beta$ should be about 10^{-12} Mev.

In the absence of detailed knowledge of the level scheme and transition matrix elements of In^{115}, one can only comment that this number appears reasonable, indicating that the observed transition is relatively improbable. (For example, Γ might be expected to be of the order of millivolts, making β about 10^{-9}.) It is interesting to note that Varma and Mandeville[18] found a level in In^{115} at 1.42 Mev, but they did not observe direct transitions between it and the ground state or any transitions connecting it with the isomeric state. In fact, none of the levels they observed connects directly or by cascade to both the ground and isomeric states with measurable intensity, which fact agrees with the small value of $\Gamma\beta$ quoted above and the absence of evidence in the isomer excitation cross section for the several other levels shown in their paper.

[10] J. Varma and C. E. Mandeville, Phys. Rev. **97**, 977 (1955).

Magnetic Analysis of the $Be^9(p,p')^*Be^9$ and $Be^9(p,pn)Be^8$ Reactions*

C. R. Gossett,† G. C. Phillips, J. P. Schiffer, and P. M. Windham
The Rice Institute, Houston, Texas

(Received June 20, 1955)

The energy distribution of protons from the bombardment of Be^9 with protons has been investigated by precision magnetic analysis in the region of excitation from the ground state through the 2.43-Mev state. A broad distribution of protons was found with a cutoff corresponding to a Q of -1.675 ± 0.002 Mev in Be^9. The asymmetry of the observed group and the proximity of the observed Q-value to the separation energy of a neutron from Be^9 suggests that the group consists of protons from the three body disintegration $^*B^{10} \rightarrow Be^8+p+n$, but the possibility of inelastic scattering to a state in Be^9 cannot be excluded. An excitation energy of 2.432 ± 0.004 Mev was found for the inelastic proton group from the known state, and a natural width $\leqslant 1$ kev is ascribed to this state from experiments conducted at optimum resolution.

FOR some time the 2.43-Mev state of Be^9 has been believed to be the first excited state of this nucleus. However, a possible state at about 1.7 or 1.8 Mev of excitation has recently been reported.[1,2] These reports are based upon scintillation spectrometer and low resolution magnetic spectrometer studies of the charged particle reactions leading to states in Be^9. In order to investigate this region of excitation in Be^9 with an instrument of greater precision, The Rice Institute annular magnet has been employed to obtain spectra of the protons scattered from this nucleus. The region of excitation from the ground state through the 2.43-Mev state was examined.

The apparatus and techniques are those described in an earlier paper[3] with the exception of changes in the incident beam alignment procedures which have sufficiently lowered the background so that the detection of weak particle groups has become possible. These changes consisted of completely defining the width of the beam by slits in tubing external to the magnet gap, and utilizing the traveling slit[3] only to determine the position and angle of the incident beam with respect to the target and to shield the target and target slits from particles which have suffered small-angle scattering at the external defining slits. The position measurements were made electrically, by determining the edges of the beam with the insulated traveling slit, rather than by direct definition of the beam by this slit. An order of magnitude reduction in the background level has been accomplished by these means.

BROAD PROTON GROUP

Figure 1 is a plot of the proton spectrum obtained with the annular magnet. The region of excitation from the ground state to about 1.4 Mev has been omitted from the plot as the background in this region showed no structure. In addition to groups corresponding to the ground state and 2.43-Mev state, a broad distribution of protons appears. In order to establish that this proton group is associated with the Be^9 nucleus, the high energy edge of the group was observed at three different bombarding energies. The results of these experiments are shown in Fig. 2, with a scale showing excitation in Be^9, and also in Table I, which lists the computed Q values. The agreement of these Q values establishes conclusively that this group is associated with the interaction of the incident protons and Be^9 nuclei.

The arrows of Fig. 1 indicate the points where the background level was normalized. These points represent the range of momenta accepted in a single exposure of a plate. The normalization is necessary since the background level, while statistically constant over a single plate, differed from plate to plate due to the alignment procedure. The plates on which the background was constant were corrected to an average value, and the plates upon which the broad distribution appeared were matched to the adjoining plates to give a smooth distribution. All of these corrections were such that they could not materially affect the shape of the distribution.

Three possible mechanisms can be reasonably considered to explain the observed broad distribution: the two-stage process $Be^9(p,n)B^9(p)Be^8$, the three-body breakup $Be^9(p,pn)Be^8$, and the inelastic scattering to a state in Be^9.

The two-stage process proceeding through a state in B^9 can be eliminated: while this process would

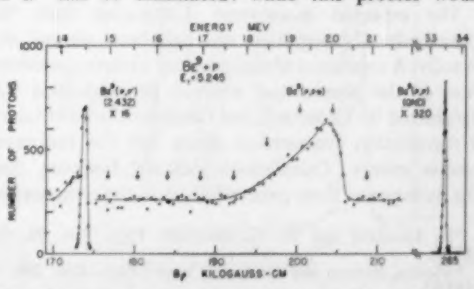

FIG. 1. Spectrum of protons from the Be^9+p reaction. Bombarding energy 5.245 Mev. The target was a 15 microinch Be foil.

* Supported by the U. S. Atomic Energy Commission.
† Now at the Naval Research Laboratory, Washington, D. C.
[1] Moak, Good, and Kunz, Phys. Rev. **96**, 1363 (1954); Almquist, Allen, and Bigham, Phys. Rev. **99**, 631(A) (1955).
[2] L. L. Lee and D. R. Inglis, Phys. Rev. **99**, 96 (1955).
[3] Gossett, Phillips, and Eisinger, Phys. Rev. **98**, 724 (1955).

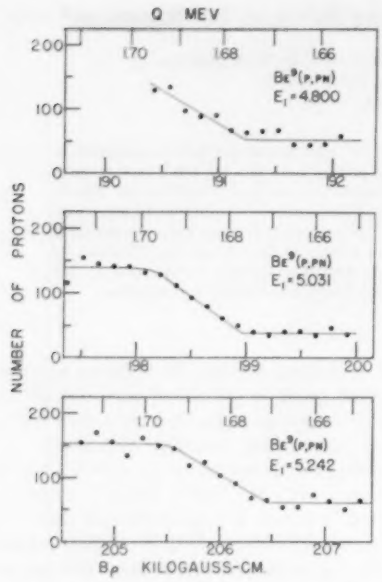

FIG. 2. High energy cut-off of the broad group, $B^{10} \rightarrow p+n+Be^8$, at different bombarding energies. The top scale of each plot represents excitation energy in the nucleus Be^9.

produce an asymmetric distribution, the energy of the proton group would not behave with change of bombarding energy as the observed group does. Moreover, this hypothesis would require, for the proton group observed, the existence of a state in B^9 below 1 Mev. The work of Ajzenberg and Buechner[4] and of Marion, Bonner, and Cook[5] indicate that no such state exists.

A possible explanation of the spectrum in Fig. 1 is that a three-body mechanism is operative. The observed broad distribution and the proximity of the observed Q-value to the neutron separation energy both favor this hypothesis. Such three-body effects were observed in the work of Ajzenberg and Buechner[4] on the $Be^9(p,n)B^9$ reaction. Their results show a continuum of neutrons which rise sharply towards lower energies. They suggested that these neutrons are due to the three-body breakup.

The expected momentum distribution from the three-body disintegration has not been worked out exactly. A treatment of this problem without consideration of the proton and neutron penetrabilities was considered by Uhlenbeck and Goudsmit,[6] who obtained a distribution symmetrical about half the maximum proton energy. Calculations indicate, however, that the inclusion of these penetrabilities in the computation will considerably affect the results, peaking the proton distribution towards higher momenta. However, the low energy side of the proton distribution function does not increase as rapidly with energy as was observed.

Although the momentum distribution is not easily calculated for this problem, it may readily be shown that the maximum energy protons for the three-body breakup correspond to zero relative velocity between the neutron and the Be^8 nucleus. While this information validates the calculation of the Q value in the usual manner,[5] it indicates that the line shape analysis,[7] normally applied to discrete groups, does not apply in this case, since this situation is more analogous to a neutron threshold, and would thus be expected to show the $E^{l+\frac{1}{2}}$ dependence generally observed for neutrons. Unfortunately, the statistical errors for the leading edge of the observed distribution are not sufficiently accurate to permit other than a linear fit. However, such a penetrability argument could be the explanation for the discrepancy between the Q value observed by the annular magnet, -1.675 ± 0.002 Mev, and that observed by Mobley and Laubenstein,[8] who obtained a Q value of -1.666 ± 0.002 Mev for the (γ,n) threshold. The discrepancy is well explained if p-wave neutrons are assumed.

TABLE I. Summary of observed Q values for the broad group.

Bombarding energy (Mev)	Q value (Mev)
4.7996	−1.6752
5.0308	−1.6768
5.2423	−1.6712
5.2445	−1.6758
5.2537	−1.6776
Mean:	-1.675 ± 0.002

The published evidence for the existence of a state in Be^9, in the region of the broad group observed with the annular magnet was based on the reaction $Li^7(He^3,p)Be^9$ and $B^{11}(d,\alpha)C^{12}$. The observed groups could be due to the three-body decay schemes: $B^{10} \rightarrow p+n+Be^8$ and $C^{13} \rightarrow \alpha+n+Be^8$. It may be shown that in these three-body disintegrations the Q value observed for the maximum energy charged particles corresponds to the binding energy of a neutron in Be^9. The earlier spectra[1,2] all exhibit distributions which can be interpreted as continua, not inconsistent with a three-body breakup.

The possibility of explaining the observed group by inelastic scattering to a state in Be^9 cannot be excluded. Whereas a Breit-Wigner resonance shape will not explain the distribution function, it is possible to fit the shape with a state of about 150-kev width when effects of the neutron threshold are considered. This large

[4] F. Ajzenberg and W. W. Buechner, Phys. Rev. **91**, 674 (1954).
[5] Marion, Bonner, and Cook, this issue [Phys. Rev. **100**, 91 (1955)].
[6] G. E. Uhlenbeck and S. Goudsmit, *Zeeman, Verhandlungen* (M. Nyhoff, The Hague, 1935), pp. 201–211.
[7] K. F. Famularo and G. C. Phillips, Phys. Rev. **91**, 1195 (1953).
[8] R. C. Mobley and R. A. Laubenstein, Phys. Rev. **80**, 309 (1950).

value would imply that this width is due to s-wave neutrons emission, so that the state would be $\frac{1}{2}+$, contrary to the independent particle model prediction.‡ Thus, if such a state in Be^9 exists at about 1.7 Mev of excitation it must have the unique property of lying partly in the bound, electromagnetic, region and partly in the virtual region of excitation and is probably a $\frac{1}{2}+$ state. The fact that the rather rapid low-energy fall-off of the group cannot be entirely accounted for by simple arguments based on barriers under the three-body hypothesis might perhaps be regarded as favoring this latter mechanism, although a quantum treatment of the three-body problem might show otherwise.

No definite conclusions can be made at present as to which of the latter two mechanisms are responsible for the observed line shape. A further study of this level, perhaps through the $B^{11}(d,\alpha)Be^9$ reaction, as observed by Lee and Inglis,[2] but with the available low background, high resolution spectrometer could establish the mechanism responsible for the observed group.

TABLE II. Summary of observed Q values for 2.43 state of Be^9.

Bombarding energy (Mev)	Q value (Mev)
4.6117	−2.4321
5.2434	−2.4325
5.2434	−2.4276
5.2445	−2.4321
5.2537	−2.4354
Mean:	−2.432±0.004

2.43-MEV STATE OF Be^9

A study of the well known 2.43-Mev state of Be^9 was conducted in conjunction with the study of the three-body disintegration. A summary of the Q values obtained in five bombardments is contained in Table II. On the basis of a systematic analysis of the possible sources of error, an error of ±0.004 Mev is assigned. A comparison with other values[9–11] reported for this state is contained in Table III.

Since the observed protons of the group corresponding to this state had energies of about 1.05 and 1.45 Mev for the 4.61- and 5.25-Mev bombardments, respectively, it was necessary to consider the possible energy losses in the surface contaminant layers of the Be^9 foil. Fortunately, in this case a means of evaluating this loss was available. The α-particle group from the $Be^9(p,\alpha)^*Li^6$ group, leaving Li^6 in the 2.187 state, appeared in the momentum region near the proton group from the 2.43 state of Be^9. Since the energy loss of the α particles in the contaminant layer was a factor of 8 greater than that of the protons for the energies observed, it was possible to obtain a fairly sensitive estimate of the thickness of the contaminant layer from the difference between the observed Q value for the α group and that observed by Browne *et al.*[9] The losses for the protons were then computed for this thickness and the Q values corrected accordingly. It was found that corrections of less than 1 kev were required for protons in cases where reasonably fresh foils were used. In one extreme case, where the foil had been bombarded a number of times previously and showed quite heavy discoloration, a correction of only 3 kev was indicated.

TABLE III. Comparison of observed Q values (Mev) with other determinations.

Experiment	Reported value	Reference
$Be^9(p,p')^*Be^9$ mag spec	−2.432±0.004	Present work
$Be^9(p,p')^*Be^9$ elec spec	−2.433±0.005	9
$B^{11}(d,\alpha)^*Be^9$ mag spec	−2.422±0.005	10
$B^{11}(d,\alpha)^*Be^9$ mag spec	−2.431±0.006	11

The observed width, shown in Fig. 1, of the proton group from the 2.43-Mev state, as compared to the width of the proton group from the ground state, was that to be expected from the additional energy loss of the lower energy protons in the foil. Since this method did not provide a very adequate means of

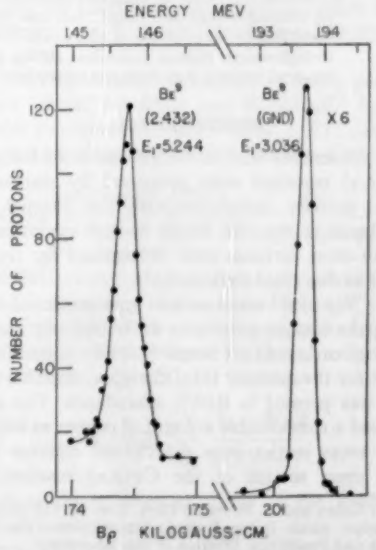

FIG. 3. Comparison of observed widths of proton groups for scattering from the 2.43 Mev and ground states of Be^9.

‡ *Note added in proof.*—Calculations by T. Lane (private communication) yield evidence for an S state at about this energy in Be^9.

[9] Browne, Williamson, Craig, and Donahue, Phys. Rev. **83**, 179 (1951).

[10] Van Patter, Sperduto, Huang, Strait, and Buechner, Phys. Rev. **81**, 233 (1951).

[11] R. B. Elliott and D. J. Livesay, Proc. Roy. Soc. (London) **A224**, 129 (1954).

TABLE IV. Observed cross sections at $E_p = 5.245$ Mev.

Particle group	σ mb/steradian	Angle of observation degrees
Ground state	23 ±10	174.2±1.9
Broad group	1.2	172.3±1.9
2.43-Mev state	3.6± 1.1	170.7±1.9

determining the natural width of the state, a more sensitive method was devised. For this experiment a very thin beryllium target was evaporated onto a carbon foil. The proton group for the 2.43 state was then observed with a bombarding energy of 5.25 Mev, and the ground state group observed at a bombarding energy of 3.00 Mev, computed to give the protons the same energy loss in the physical thickness of the target. The results of this experiment are shown in Fig. 3. Both groups show a thickness at half maximum of 3.2 kev.

All controllable quantities were adjusted to produce equal effects on the two proton groups. Three factors then remain which could affect the observed widths; these are: the natural width of the state, changes in the spectrometer width, and changes in the energy spread of the incident beam at the two different energies. Since it is believed that each of these factors should produce a greater observed width for the group from the 2.43-Mev state, it is concluded that this state has no observable natural width. An upper limit of 1 kev may be set for the natural width to take into account any factors which may not have been considered.

Since the 2.43-Mev state of Be^9 is about 766 kev unbound to neutron emission, an appreciable width would be expected for this state, if low angular momentum neutron emission were possible. The fact that a narrow width is observed for the proton group implies that a high centrifugal barrier exists for the neutrons. Calculations indicate that a lower limit of $J = 5/2$ may be set for the state on this basis.

An estimate may be made of the cross sections for the proton groups of Fig. 1. The values and the angle at which they were observed are listed in Table IV. These values should be accurate to approximately ±30%, except in the case of the broad group, where the cross section is somewhat indeterminate from our data.

PHYSICAL REVIEW VOLUME 100, NUMBER 1 OCTOBER 1, 1955

(p,γ) Cross Sections

BERNARD L. COHEN
Oak Ridge National Laboratory, Oak Ridge, Tennessee
(Received June 27, 1955)

Several (p,γ) cross sections were measured by activation with protons from 8 to 22 Mev. The dependences on incident energy and target mass are very slight, whereas a compound nucleus model would predict variations by many orders of magnitude. It seems probable, therefore, that the observed reactions are due to high-energy gamma transitions taking place prior to compound nucleus formation. The magnitudes involved indicate that these transitions have single-particle dipole matrix elements.

EXPERIMENTAL

CROSS sections and excitation functions for several (p,γ) reactions were measured by stacked foil-induced activity techniques with the internal circulating beam of the Oak Ridge 86-inch cyclotron. The absolute cross sections were determined by the ratio method as described previously.[1]

The $C^{12}(p,\gamma)N^{13}$ cross section was measured by observing the 10-min activity in an isotopically enriched[2] sample of carbon-12. A small (~10%) correction was applied for the activity from the (p,n) reaction on C^{13} which was present in 0.05% abundance. The sample contained a considerable amount of copper as impurity, so the cross section was determined relative to the known cross section of the $Cu(p,n)$ reaction.[3] The amount of copper impurity was determined by an activation analysis carried out in the Oak Ridge graphite reactor. The (p,γ) excitation function could not be extended to high energies because a 10-min activity from $Cu^{63}(p,pn)Cu^{62}$ is induced in copper by protons above 15 Mev.

The $Fe^{54}(p,\gamma)Co^{55}$ cross section was determined by comparing the activity of 18-hr Co^{55} with that of 44-min Mn^{51} produced by the (p,α) reaction, in an isotopically enriched[2] sample of $Fe^{54}{}_2O_3$. This measurement was not possible above the threshold of the $Fe^{56}(p,2n)$ reaction (~15 Mev) since that reaction also leads to Co^{55}. The cross section for the $Fe^{54}(p,\alpha)$ reaction was measured by bombarding stacks of natural iron foils and comparing the Mn^{51} activity in the low-energy foils with the Co^{55} activity in the high-energy foils, where the $(p,2n)$ cross section is known.[1]

The cross section and excitation function for the $Ni^{60}(p,\gamma)Cu^{61}$ activity was measured by bombarding

[1] B. L. Cohen and E. Newman, Phys. Rev. **99**, 718 (1955).
[2] Enriched stable isotopes were obtained from the Isotope Research and Production Division of this laboratory.
[3] Blaser, Boehm, Marmier, and Peaslee, Helv. Phys. Acta **24**, 3 (1951).

metal foils of isotopically enriched Ni^{60} and comparing the 3.3-hour activity of Cu^{61} with the 36-hour activity of Ni^{57}. The latter is produced by a (p,pn) reaction on Ni^{58}, which was present in 1.5% abundance. Only small corrections were necessary for the Cu^{61} activity induced by (p,n) and $(p,2n)$ reactions on Ni^{61} and Ni^{62} since these were present in only 0.02 and 0.01% abundances respectively.

The cross section for $Zn^{64}(p,\gamma)Ga^{65}$ was determined by measuring excitation functions for the 250-day Zn^{65} activity in stacks of natural zinc foils. At high energies, this is produced by the (p,pn) reaction on Zn^{66}, but below the threshold for that reaction, it is produced principally as the daughter of Ga^{65} from (p,γ) on Zn^{64}. The absolute values were obtained by comparison with the known cross section for $Zn^{66}(p,pn)$ at high energy.[1] It was also necessary to subtract a small background from neutron capture in Zn^{64}. In general, the measured cross sections are accurate to within 20%.

TABLE I. (p,γ) cross sections.

Reaction	Q (Mev)	Incident proton energy (Mev)	Cross section (mb)	$\frac{\sigma(p,\gamma)}{\sigma_p}$ ($\times 10^{27}$)
$C^{13}(p,\gamma)N^{14}$	1.9	11	1.8	2.5
		5	2.5	4.4
$Fe^{54}(p,\gamma)Co^{55}$	4.6	11	0.33	0.46
$Ni^{60}(p,\gamma)Cu^{61}$	5.5	22.5	0.9	0.8
		21	0.9	0.8
		16	0.7	0.8
		10	0.9	1.1
$Zn^{64}(p,\gamma)Ga^{65}$	6	11	1.2	1.6
		8	1.3	2.1
$Bi^{209}(p,\gamma)Po^{210}$	5.0	22.5	0.26[a]	0.23
		20	0.43[a]	0.40
		15	0.63[a]	0.95
		10	0.17[a]	1.54

[a] From reference 4.

RESULTS

The measured (p,γ) cross sections are listed in Table I. The measurements for bismuth by Kelly[4] are also included. The last column of Table I was obtained by dividing the measured cross sections by the theoretical reaction cross sections for protons (σ_p). It is a measure of the competition between gamma-ray and particle emission.

THEORY AND DISCUSSION

In considering nuclear reactions in this energy region, it is interesting first to investigate whether the results can be explained by compound nucleus theory. In order for a (p,γ) reaction to be observed, the compound nucleus which is formed after capture of the proton must de-excite electromagnetically to a level from which heavy particle emission is not energetically possible; that is, to a level within the particle binding energy, $B(\sim 6$ Mev), of the ground state.

This can happen either by a direct transition to one of these levels accompanied by emission of a high-energy gamma ray, or by a cascade process involving one or more intermediate levels. In the latter process, after each transition the probability is very large ($>99\%$) that a particle rather than another gamma ray is emitted, so that cascade processes could only be important if emission of quanta with energies about half the incident proton energy were hundreds of times more probable than emission of those with about the full incident proton energy. Measurements of energy distributions of gamma rays from proton bombardment of copper have been carried out by Gugelot with 18-Mev protons[5]; it was found that the probability does not increase nearly that fast with decreasing gamma-ray energy. It therefore can be concluded that the (p,γ) reactions observed here are not the result of cascade processes, but rather of single high-energy gamma-ray transitions to levels within the particle binding energy of the ground state.

It will be assumed here that all transitions are electric dipole. This is probably reasonably correct, and in any case, roughly the same conclusions would be reached regardless of the type of transitions. For simplicity, selection rules will be neglected. Since, in all cases, only ratios of cross sections will be discussed, this is equivalent to assuming that the same fraction of all possible transitions are allowed in each reaction. While this is not generally true, it should almost certainly not lead to large errors.

The problem of radiative capture of heavy particles has been treated by Blatt and Weisskopf.[6] For the case under consideration, their formula (7.23), page 649 for the gamma emission width, Γ_γ, reduces to

$$\Gamma_\gamma \approx 1.5\times 10^{-6}\frac{D(E_p+B)}{D_0}\int_{E_p}^{E_p+B}\frac{E^3\,dE}{D(E_p+B-E)}, \quad (1)$$

where D denotes level spacing, E_p is the incident proton energy, E is the energy of the emitted gammas, and D_0 is the level spacing at low excitation energies. Applying (approximately) the theorem of the mean, and defining the level density, ω, as $1/D$, (1) becomes

$$\Gamma_\gamma \approx 1.5\times 10^{-6}\frac{N}{D_0}\frac{(E_p+B/2)^3}{\omega(E_p+B)}, \quad (2)$$

where N is the number of states of the compound nucleus with energy less than B.

[4] E. Kelly, University of California Radiation Laboratory Report UCRL-1044 (unpublished).

[5] P. C. Gugelot, Brookhaven Conference on Statistical Aspects of the Nucleus, Brookhaven National Laboratory Report BNL-331, 1955 (unpublished).

[6] J. M. Blatt and V. F. Weisskopf, *Theoretical Nuclear Physics* (John Wiley and Sons, Inc., New York, 1952).

The width for emission of a particle, Γ_π (where π is generally a neutron or a proton) is proportional to[7]

$$\Gamma_\pi \propto \frac{\int_0^{\epsilon_\pi} \sigma_\pi E\omega(\epsilon_\pi - E)dE}{\omega(E_p+B)} = \frac{F_\pi}{\omega(E_p+B)}, \quad (3)$$

where σ_π is the cross section for capture of particle π in an inverse process, ϵ_π is the maximum energy avilable for emission of particle π, and F_π is defined by the numerator. The last is identical (within a constant multiplier) with the F_π of Blatt and Weisskopf who present curves of its dependence on energy and mass (reference 6, p. 373).

If we neglect emission of all particles except that which is most probably emitted (which for bismuth is a neutron and in all other cases considered here, a proton), the cross section for a (p,γ) reaction may be written[6]

$$\sigma(p,\gamma) = \sigma_p(\Gamma_\gamma/\Gamma_\pi). \quad (4)$$

Thus the quantity listed in the last column of Table I is, from (2), (3), and (4),

$$\frac{\sigma(p,\gamma)}{\sigma_p} = \frac{\Gamma_\gamma}{\Gamma_\pi} \propto \frac{(E_p+B/2)^2}{F_\pi}. \quad (5)$$

Data on the energy dependence of $\sigma(p,\gamma)/\sigma_p$ are available from Table I for Ni^{60} and Bi^{209}. In comparing Eq. (7) and the curves of reference 6 with the data, it is immediately evident that large discrepancies exist. For example, in Ni^{60}, the ratio between the cross sections at 10 and 22.5 Mev should be about 100 as compared with an observed ratio of 1.3. In Bi^{209}, this ratio should be about 10^5 as compared with an observed ratio of 6.7.

While the theoretical derivation may appear to be on a somewhat uncertain basis, its results are qualitatively clear and reasonable. The essential difference between Γ_γ and Γ_π is that, for the latter, the number of final states increases exponentially with increasing incident energy, whereas for the former, the number of final states is a constant, consisting of the set of states with excitation energy less than B. The fact that the number of final states available for particle emission increases exponentially (rather than according to a power law, for example) would seem to be guaranteed by the fact that the observed energy spectra of emitted particles are Maxwellian with a low and slowly varying temperature. It is therefore difficult to understand how the ratio can be as independent of energy as is indicated in Table I.

Similar difficulties are encountered in investigating the dependence of the cross section on atomic number (Z). From (2), (3), and (4), this is

$$\frac{\sigma(p,\gamma)}{\sigma_p} \propto \frac{1}{D_0}\frac{N}{F_\pi}. \quad (6)$$

The quantity D_0 varies rather slowly with Z, increasing by about a factor of ten from carbon to bismuth. The value of N can be estimated from level spacings found in slow neutron capture. This is about 100 times greater for bismuth (neglecting closed shell effects which do not enter into proton capture in bismuth) than for Fe, Ni, and Zn. However, F_π is smaller for these than for bismuth by a factor of about 10^5. Thus, $\sigma(p,\gamma)/\sigma_p$ should be smaller for bismuth by at least a factor of 1000, whereas the observed cross sections are about equal. While there is considerably more uncertainty in (1) as regards the dependence on Z than on E_p, such a large discrepancy would not be expected.

Since there seems to be great difficulty in explaining the experimental results by a compound nucleus interaction, other possibilities should be considered.

Weisskopf[8] has suggested that direct, single particle transitions may take place to bound states. If such transitions occur with the full single particle matrix element, their probability per unit time, P, is given by[6]

$$P = 2(E/20\ \text{Mev})^3(A^{\frac{1}{3}}/4)^2\times 10^{19}/\text{sec}. \quad (7)$$

The time of interaction between the incident particle and the nucleus, τ, is given, approximately, by the nuclear radius divided by the velocity; since the emitted gamma-ray energy is approximately the same as the incident proton energy, this is

$$\tau \approx (20\ \text{Mev}/E)^{\frac{1}{2}}(A^{\frac{1}{3}}/4)\times 10^{-22}\ \text{sec}. \quad (8)$$

The probability for such a transition to occur in a nuclear encounter is τP. Since this is just the quantity $\sigma(p,\gamma)/\sigma_p$, (7) and (8) give

$$\frac{\sigma(p,\gamma)}{\sigma_p} = \left(\frac{E}{20\ \text{Mev}}\right)^{5/2}\frac{A}{32}\times 10^{-3}. \quad (9)$$

The absolute values of $\sigma(p,\gamma)/\sigma_p$ given by (9) are in satisfactory agreement with the observed values from Table I. The theoretical values seem to be too large by a small factor, but this can be explained by the fact that the interaction time, τ, is less than given by (8) because of competition from formation of a compound nucleus.

There is no evidence in the data for the increase of $\sigma(p,\gamma)/\sigma_p$ with energy or target nucleus mass predicted by (9); in fact, there seem to be trends in the opposite direction. However, this can be explained by variation in the matrix elements.

The author is greatly indebted to V. F. Weisskopf and J. S. Levinger for their very helpful suggestions and criticisms, and to R. S. Livingston for his constant encouragement.

[7] See, for example, V. F. Weisskopf, Phys. Rev. 52, 295 (1937). Also, reference 6.

[8] V. F. Weisskopf (private communication).

Electro- and Photodisintegration Cross Sections of Cu^{63}

M. B. Scott, A. O. Hanson, and D. W. Kerst
Department of Physics, University of Illinois, Urbana, Illinois

(Received June 20, 1955)

Highly monoergic electrons from a 22-Mev betatron have been used to study the Cu^{63} activity in a pair of 2-mil copper foils separated by a 10-mil copper radiator. The ratio of the photodisintegration to electrodisintegration in the foils decreases by less than 10% in the region from 14 to 20 Mev. The measured value of F at 20 Mev is 8.6 in reasonable agreement with the extrapolation of previous measurements at higher energies and with the value of 8.38 expected on the basis of simple virtual photon calculations. Analysis of the excitation curves gave a $Cu^{63}(\gamma,n)$ cross section of 80×10^{-27} cm^2 which is 20% below most previous measurements.

INTRODUCTION

MOST investigations of (γ,n) reactions have been carried out using the bremsstrahlung spectra of electron accelerators. Activation curves are experimentally obtained by varying the kinetic energy of the electrons reaching the target (i.e., the maximum gamma-ray energy) and by observing the activity induced in samples per unit of irradiation. These activation curves are converted into cross sections with the aid of theoretical expressions for the shape of the bremsstrahlung spectrum. There is some uncertainty in the choice of a theoretical shape, associated with the questions of multiple traversals of the target by the electrons and the use of integrated (over angle) spectra as opposed to forward direction spectra.

In addition to the problem of the choice of a spectrum, the interpretation of the monitor response to arrive at unit irradiation for the various energies presents difficulties. Here one must make assumptions as to the interactions of the radiation of different energy with the material of the monitor and as to the degree of equilibrium established between the primary (gamma ray) and the secondary (electron-positron) radiation. From these assumptions one may deduce the number of photons of a particular energy band per unit of irradiation at each energy used. In the present experiment electrons free from gamma rays and of homogeneous energy are focused onto a small spot upon a copper foil stack and the emerging electrons are trapped in a Faraday cage. The monitor interpretation now presents little difficulty, since electrons of all energies give the same response to charge measuring devices, while gamma rays are not measured at all. Further, it is evident that the proper spectrum to use in interpreting this experiment is the integrated spectrum for single traversal. Multiple traversal is ruled out and the short path length from the origin of the gamma rays to their absorption acts to integrate the spectrum, at least the forward hemisphere of it. There remain, of course, experimental uncertainties, accentuated by the fact that the cross section depends on the derivatives of the activation curve and some residual doubt concerning the accuracy of the radiation expression itself.

One disadvantage of the present experiment is that to find the (γ,n) activity, the electrodisintegration activity which is due to the electrons passing through the sample must be subtracted from the total activity. Apart from energy losses and absorption, the (γ,n) activity will be proportional to the depth in the stack. Thus the intercept of the activity at zero depth will give the electrodisintegration probability while the slope of activity *versus* depth will give the product of the radiation and photodisintegration probabilities. The complication of this picture by the energy losses will be considered in more detail under the analysis of the data.

The technique of observing the variation of electron-induced radioactivity with depth in a stack of foils has been used previously in this laboratory.[1,2] Brown and Wilson[3] have made extensive measurements with stacks of foils of Cu, Zn, Ag, and Ta in order to investigate the nature of the interaction of the electromagnetic field with these nuclei. Their results are expressed in terms of the ratio of the bremsstrahlung induced activity to that produced directly by the electrons. The present work extends these results to lower energies for Cu.

Since the work was started, Berman and Brown,[4] hereafter referred to as BB, have reported on the measurements of the (γ,n) and $(\gamma,2n)$ cross sections in Cu^{63} using electron beam techniques very similar to that described here. Their work is done with less energy resolution but extends up to 36 Mev.

EXPERIMENTAL ARRANGEMENT AND PROCEDURE

Absolute and relative measurements were made of the activity induced in a stack of copper foils irradiated by monoenergetic electrons at half-Mev intervals from the Cu^{63} (γ,n) threshold to 22 Mev.

The stack consisted of an entrance and exit detector (whose activity was measured after irradiation) with or without a 10 mil radiator between the detector foils. The entrance and exit detectors were about 2 mils thick (true thickness 46.9 mg/cm^2) and 1 in.$\times\frac{3}{4}$ in. in dimension.

Irradiations employed the external electron beam of

[1] Skaggs, Laughlin, Hanson, and Orlin, Phys. Rev. **73**, 420 (1948).
[2] L. H. Lanzl and A. O. Hanson, Phys. Rev. **83**, 951 (1951).
[3] K. L. Brown and R. Wilson, Phys. Rev. **93**, 443 (1954).
[4] A. I. Berman and K. L. Brown, Phys. Rev. **96**, 83 (1954).

the 22-Mev betatron. A permendur peeler was used to increase the useful maximum energy of the electron beam. The emerging beam was collimated, and removed to a distance of about 10 feet where it was refocused by a magnetic lens to concentrate the electrons relative to gamma rays and neutrons. The focusing current was adjusted visually and photographically to bring the beam to a line focus (about $\frac{1}{4}$ in. by $\frac{3}{4}$ in. in dimensions) at the point where the copper foil stack was to be placed.

The foil stack lay deep in the mouth of a brass lined, aluminum Faraday cage (Fig. 1). The space in and around the Faraday cage and the foils was continuous with the vacuum of the betatron donut, so that prior to passing through the foils, and being trapped in the Faraday cage, the electrons were not retarded or scattered by any windows.

The charge collected by the Faraday cage passed to a vibrating reed electrometer which measured the voltage on a condenser shunted by a resistance so as to relax with the same time constant as the Cu^{62} activity. The voltage on the condenser (from a few tenths volt to one volt on one microfarad) measured on a potentiometer immediately after the betatron was turned off was thus proportional to the integrated exposure corrected for decay up to that time.

Various tests were made as to the performance of the equipment used. For example, to demonstrate that only electrons were being detected by the Faraday cage, the beam was blocked by aluminum of thickness calculated to stop the electrons. It was observed that the condenser then charged at less than one ten thousandth of its previous rate. Placing lead in the bottom of the aluminum Faraday cage to produce more bremsstrahlung from the electron beam showed no effect on the ratio of foil activity to measured irradiation.

Brass liners were added to the inside of the chamber until no effect due to backing the copper foils with material to scatter the emerging beam could be detected. Absence of this effect would indicate that no appreciable part of the beam current was being lost due to scattering out or through the Faraday cage. Tests for collection of charge in the cable connecting the Faraday cage with the electrometer circuit, made by disconnecting the cable at the Faraday cage and leaving it in place, were negative. To determine if electrons were missing the center of the foil, or if neutron or gamma ray background was causing activity in the foils, side foils were irradiated inside the Faraday cage but out of the electron beam which showed no net count. Also a foil exposed in the usual way had a $\frac{3}{8}$-in. hole punched out of its center after irradiation and the remaining area showed a negligible count over cosmic ray background.

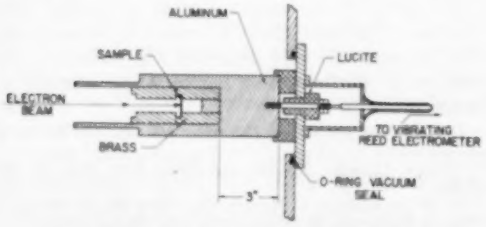

FIG. 1. Faraday cage and foil holder.

The activity in the entrance and exit detector foils were counted simultaneously between two pairs of Geiger counters during the intervals 2–6 and 7–13 minutes after the end of the irradiation. Foils were interchanged during the 6–7 minute interval so as to eliminate a small difference in counting efficiency of the pairs of counters.

The average counting efficiency of this arrangement was established at two energies by the comparison of the count of the Geiger counters on the exit foil, with the simultaneous count of the entrance foil in a 4π scintillation counter (foil sandwiched between two anthracene crystals), due account being taken of the measured ratio of exit activity to entrance activity.

The counting efficiency of the pairs of Geiger counters relative to the 4π counter was found to be nearly 55 percent.

Since the 55% measured counting efficiency was felt to be high by comparison with the 25–30% (estimated) geometrical solid angle covered by the counters, further tests were made with a Sr-Y^{90} source. This source consisted of a spot ($\frac{1}{8}$ in. in diameter) of activity between two 0.002 in. copper foils of the same size and served as a counting standard for the Geiger counters. The total rate at which electrons emerged from this source was determined by means of the 4π scintillation counter as well as by a 2π gas proportional counter. The efficiency of the pairs of Geiger counters using this Sr-Y^{90} source was found to agree with that using Cu^{62} sources.

It was found that the measured angular distribution was nearly of the form $\cos\theta$ where θ is measured from the normal to the plane of foil. This distribution, attributed to multiple scattering in the copper, was quantitatively sufficient to explain the observed Geiger counter efficiency.

In determining the absolute energy scale, we rely on a Cu^{63} (γ,n) threshold taken with thick gold radiators and thick copper detectors. The energy calibration in the region required for the interpretation of this experiment is based essentially upon the copper threshold which was taken to be 10.62 Mev, consistent with previous magnetic calibrations of the electron beam at 9.60 and 15.70 Mev[5] but perhaps somewhat lower than indicated by recent measurements elsewhere.[6,7] Small

[5] Goldwasser, Mills, and Hanson, Phys. Rev. **88**, 1137 (1952).
[6] M. Birnbaum, Phys. Rev. **93**, 146 (1954).
[7] Recent comparisons of the $Cu^{63}(\gamma,n)$ threshold with the $N^{14}(\gamma,n)$ and $F^{19}(\gamma,n)$ thresholds at Saskatoon indicated a value of 10.72 Mev. Katz, Penfold, and Spicer (private communication).

changes in this threshold serve only to move the energy scale of Figs. 3, 4, and 5 by a corresponding amount.

Since we intended to analyze the data using the photon difference method of analysis, we undertook to reduce the effects of energy scale drift by taking consecutively, alternating points (i.e., those 1 Mev apart) with frequent reversal of direction of traversal of the activation curve to fill in the intermediate points. Such a typical sequence of runs might be 17, 18, 19, 20, 20.5, 19.5, 18.5, 17.5, 16.5, 17 Mev for example. In all, two sets of about fifty runs each, taken three months apart, were combined to give the final data.

The observed count in each run was corrected for the observed background, dead time losses, and the decay of the Cu^{62} activity. Initially the Cu^{62} half-life was taken to be 10.0 minutes. In the subsequent analysis the half-life obtained from the observed ratio of the counts in the 2–6 minute periods to that in the 7–13 minute periods was 9.55±0.15 minutes. This shorter half-life was at first attributed to a small amount of the 5 minute neutron induced Cu^{66} activity but this seemed to be excluded by the negative results with foils placed just out of the beam. This shorter half-life is in qualitative agreement with half-life of 9.73±0.02 minutes reported by Berman and Brown.[4]

The absolute value of the cross section reported here is corrected to the observed half-life but nearly the same cross section is obtained by assuming a 10-minute period and enough 5-minute activity to account for the shorter period.

A further correction to the observed absolute count as measured by the scintillation counter arises from the self-absorption of the positrons in the copper sample. This absorption can be estimated as 7½% by the exponential approximation used by Baker and Katz[8] to fit their measurements on Cu foils up to 20 mil thick. However, measurements carried out on ½ mil to 2 mil foils specifically for this purpose led to a 4% absorption in the 2 mil foil which was used in this work. Subsequent calculations based on the two group diffusion theory of Bethe, Rose, and Smith using the positron energy spectrum of Cu^{62} indicated an even lower absorption of 2.5%.[9] This correction is not very sensitive to the minimum energy of positrons detected by the scintillation counter which was estimated to be 70 kev. The loss of positrons below this energy could introduce an error of less than 0.2% in the counter efficiency.

In a typical run the betatron was operated at 19.44 Mev and the charge remaining on the shunted condenser after the 10-minute irradiation was 1 microcoulomb. The two mil (46.9 mg/cm²) entrance foil inserted between the two anthracene crystals gave a net count of 72 140 in the interval between 2 and 6 minutes after the end of the irradiation. This would be 21.1% of the total count on the basis of a 10-minute half-life. This observed activity in the entrance foil is a mixture of electron and bremsstrahlung induced activity which can be separated by the use of the activity of the exit foil. In this example the electron produced activity is 0.890 of total activity of the entrance foil. A discussion of this analysis is found in the next section.

[8] R. G. Baker and L. Katz, Nucleonics 11, 14 (1953).
[9] M. B. Scott (unpublished report).

ANALYSIS OF DATA

Since the entrance and exit foils are behind different thicknesses of material, the ratio of the (γ,n) activity A_γ to the electrodisintegration activity A_e will be different in the two foils. The measured values of the activity of the entrance and exit foils, A_0 and A_1 respectively, can thus be used to separate A_γ and A_e. In order to do this accurately, however, it is necessary to allow for the energy loss and straggling of the electrons in the foil stack since the activities are strongly energy dependent.

For a given incident energy E_0, the electrodisintegration activity $A_e(E_0,x)$ at a depth x was calculated in terms of a linear attenuation coefficient $k(E_0)$ as defined by the relation,

$$A_e(E_0,x)=A_e(E_0,0)[1-k(E_0)x]$$
$$=\int_{E_t}^{E_0} A_e(E)P(x,E_0,E)dE, \quad (1)$$

where E_t is the (γ,n) threshold energy, E is the energy of an electron at a depth x whose incident energy was E_0. $A_e(E_0,0)$ or $A_e(E)$ is the measured electrodisintegration activity per unit thickness as obtained from the activity in the entrance foil extrapolated to zero thickness. $P(x,E_0,E)$ is the probability of finding an electron at a depth x having an energy E in a small unit energy interval. Since the energy loss distribution at a depth x can be represented by a group around the most probable energy loss having an half-width at half-maximum of about 0.1 of the energy loss, it was found unnecessary to calculate the effect of this distribution near the most probable energy in detail. On the other hand it was found that it was necessary to consider large individual energy losses arising from production of bremsstrahlung and from electron-electron collisions. The function P was therefore taken to be,

$$P(x,E_0,E)=\alpha\left(B_0+\frac{B_1}{E_p-E}+\frac{C}{(E_p-E)^2}\right). \quad (2)$$

The first two terms in the Eq. (2) represent the radiation straggling based on a trapezoidal approximation to the bremsstrahlung intensity curve. The third term is the familiar energy loss distribution associated with Rutherford scattering. $P(x,E_0,E)$ is taken as zero for energies E greater than a cutoff energy (E_p-E_c). This cutoff energy is chosen so that the

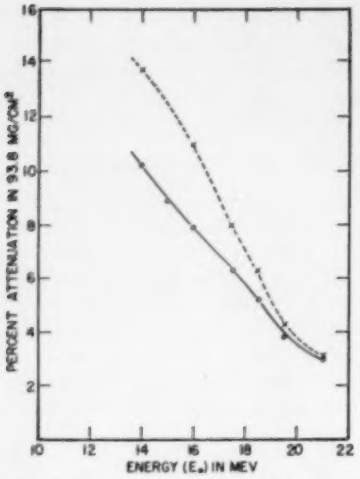

FIG. 2. Calculated attenuation coefficient $k(E_0)$ for a unit thickness of 4 mils (93.8 mg/cm²), as a function of the incident energy. The crosses represent the approximate attenuation found by assuming all electrons lost the average total energy loss.

average energy loss calculated by the relation

$$\langle E_0-E\rangle_{Av}=\frac{\int_{E_T-E_c}^{0}(E_0-E)P(x,E_0,E)dE}{\int_{E_T-E_c}^{0}P(x,E_0,E)dE} \tag{3}$$

gives the correct average total energy loss in a thickness x. α is chosen to normalize P to one electron. B_0, B_1, C and $1/\alpha$ are approximately proportional to x. The activity $A_e(E_0,0)$ was expressed in the form $a_i(E-E_i)^{n_i}$ to permit analytic integration of Eq. (1) and (3). a_i, E_i, and n_i are chosen to fit segments of an experimental curve of dA_e/dE against E. Values of n_i used were 2, 1½, 1, and ½, and the segments were joined to make A_e and dA_e/dE continuous.

The calculated values of k for a unit thickness of 4 mils (nominal) or 93.8 mg/cm² are shown as circles in Fig. 2, together with values of k based upon the mean energy loss and the derivative dA_e/dE. It is clear from the figure that the use of the mean energy loss (neglect of straggling) is a poor approximation near the threshold.

In the linear approximation the activity per unit thickness due to electrodisintegration is

$$dA_e/dx=(1-kx)A_e(E_0,0). \tag{4}$$

Since the photodisintegration activity arises from bremsstrahlung produced at all depths from 0 to x, the effective depth is just $x/2$ and the photon induced activity can be expressed as

$$dA_\gamma/dx=[1-(kx/2)]xg(E_0,0)A_e(E_0,0), \tag{5}$$

where $g(E_0,0)$ is ratio of the photodisintegration activity behind a unit thickness to the electrodisintegration activity. In terms of these relations the activity in the entrance and exit foils are

$$A_0(E_0)=\int_0^t\left(\frac{dA_e}{dx}+\frac{dA_\gamma}{dx}\right)dx$$
$$=\left(1+\frac{g-k}{2}t-\frac{gkt^2}{6}\right)A_e(E_0)t. \tag{6}$$

$$A_1(E_0)=\int_{T+t}^{T+2t}\left(\frac{dA_e}{dx}+\frac{dA_\gamma}{dx}\right)dx$$
$$=\left\{1+\frac{g-k}{2}(3t+2T)\right.$$
$$\left.-\frac{gk}{6}(7t^2+9tT+3T^2)\right\}A_e(E_0)t, \tag{7}$$

where t is the thickness of the detector foils and T is the thickness of the radiator foil. These two equations are solved for the unknowns A_e and g. The activity due to electrodisintegration per unit thickness is

$$A_e(E_0)=\frac{A_0(E_0)}{1+\dfrac{(g-k)t}{2}-\dfrac{gkt^2}{6}}. \tag{8}$$

An idea of the importance of the various terms is gained by noting that for thickness in units of 4 mils t, T, g, and k have magnitudes of 0.5, 5, 0.5, and 0.1, respectively.

The (γ,n) activity per unit thickness squared is

$$A_\gamma(E_0)=g(E_0)A_e(E_0)=N_{Cu^{63}}\int_0^{E_0}\phi\sigma(\gamma,n)dE_\gamma, \tag{9}$$

where ϕ is the radiation cross section of Bethe-Heitler for a thin target. The cross section for electrodisintegration is simply $A_e/N_{Cu^{63}}$, while $\sigma(\gamma,n)$ can be found from the equation above by the usual photon difference method.[10] The appropriate radiation spectrum for this purpose is one integrated over angle and normalized to one electron.

In order to determine the mode by which the nucleus is excited (namely electric dipole, magnetic dipole or electric quadrupole modes),[11] Blair pointed out that it is convenient to form the ratio

$$F=\frac{A_\gamma}{A_e N r_0^2 Z(Z+1)}. \tag{10}$$

[10] L. Katz and A. G. W. Cameron, Can. J. Phys. **29**, 518 (1951).
[11] J. S. Blair, Phys. Rev. **75**, 907 (1949).

This ratio as averaged over the observed $\sigma(\gamma,n)$ for Cu^{63} has been calculated and is presented in the work of Brown and Wilson.[3] Their calculation has been extended to lower energies in the present work. The value of F in terms of the quantities previously defined is simply $F=16.28g$, where g is the corrected ratio for a thickness of 93.8 mg/cm².

RESULTS AND DISCUSSION

In the simplest approximation of no energy loss the difference between the activity in the exit foil and the entrance foil is simply that produced by bremsstrahlung generated in the entrance and radiator foils. In order to obtain sufficient bremsstrahlung produced activity for accurate analysis it was necessary to use a radiator about 10 mils thick. In this case the corrections for energy loss are rather large and it is important that these be made accurately. The ratio of the observed activity in the exit foil to that in the entrance foil is shown in Fig. 3. The upper set of corrected points assumes all electrons in the material lose energy uniformly and that the energy at any depth in the foil is just the initial energy reduced by the average total energy loss due to ionization and radiation. The upper straight line and the open circles in the figure represent the same ratio after correcting for the energy loss in the material using the energy loss spectrum in the manner previously described. It is apparent that the points near threshold are particularly sensitive to different treatments of the energy loss. The normalized ratio of A_γ to A_e is shown as F in Fig. 4. It can be seen that this ratio at 21 Mev is not very sensitive to the manner in which the energy loss correction is made. The values observed are reasonably consistent with the extrapolation of those found by Brown and Wilson. As pointed out by them the experimental points lie closest to the theoretical values for magnetic dipole mode of absorption, but that it is more likely that these results point to a small admixture of electric quadrupole absorption with the predominant giant electric dipole resonance. Although it would be of interest to look for a change in the ratio at energies below the giant resonance, pointing more specifically to the type of interaction which is predominant in that region, it is unfortunate that the ratio is not sensitive to the mode of excitation in this region. It is also the region in which experimental measurements as well as the theoretical calculations are most unreliable.

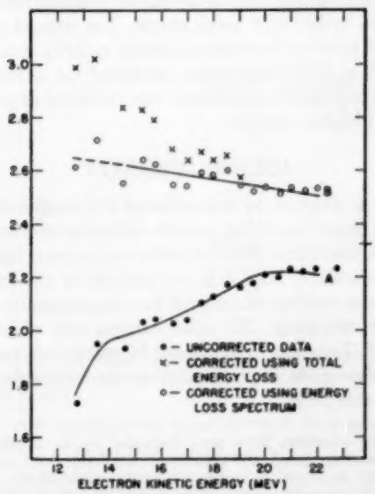

FIG. 3. Ratios of the activities in the exit foils to those in the entrance foils. The crosses represent the ratios as corrected assuming all electrons lost the average total energy loss.

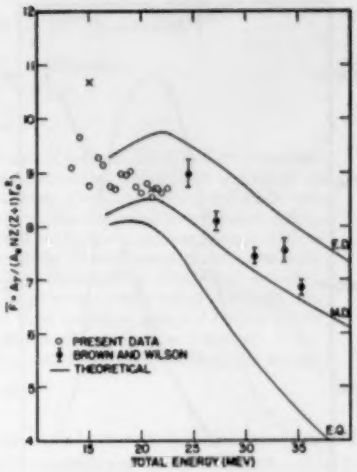

FIG. 4. Experimental values of F as obtained from the corrected values of the exit to entrance ratio. The two crosses are taken from the data which were corrected on the basis of the uniform energy loss used in Fig. 3. The solid lines represent the theoretical values of F for excitation of electric dipole, magnetic dipole, and electric quadrupole modes respectively.

The electrodisintegration cross section is determined with good accuracy since it depends largely on the activity in the first foil. This cross section is shown as curve 1 of Fig. 5.

The photodisintegration cross section is obtained from the corrected photon induced activity A_γ by the photon difference method. This photon-induced activity is proportional to the product of $\sigma(e,e'n)$ and F as shown in Fig. 4. Since F does not vary much in the energy region used in this work it is interesting to note that in the region around 20 Mev $\sigma(e,e'n)$ also represents the photon induced activity behind 0.175 g/cm² of copper. When increased to represent the corrected activity behind 0.3325 g/cm² as used by BB we get good agreement with the value of 3.3×10^{-28} indicated in Fig. 4 of their paper.

The photoneutron cross section is obtained from the activity A_γ by the photon difference method using the

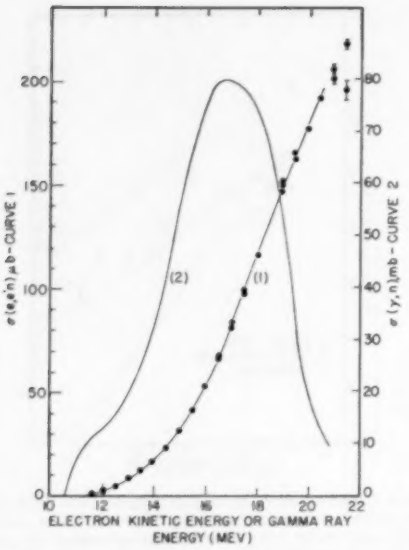

FIG. 5. The electrodisintegration activity as a function of the kinetic energy of the electron, normalized so as to represent the electrodisintegration cross section, is shown as curve 1. The statistical errors are less than the size of the points except where they are shown. The photodisintegration activity is proportional to the product of curve 1 by F as given in Fig. 4. The (γ,n) cross section as obtained from this product by the photon difference method is shown as curve 2.

total photon spectrum of Bethe and Heitler.[12] This cross section is shown as curve 2 of Fig. 5. This cross section includes the following corrections in addition to those for energy loss: (1) photon absorption in the stack (+1%), (2) multiple scattering in the stack (−2%), (3) Cu^{63} K capture transitions not detected in scintillation counter (+2%), (4) extrapolation of total count to zero thickness from 0.002 inch (+4%). The extraction of the electron beam became less reliable at higher energies so one cannot be very certain of the accuracy of the cross section at energies above 19 Mev.

It does appear to be significant that the photoneutron cross section is somewhat smaller and narrower than obtained by the earlier work using the x-ray beams. The maximum of 80 mb is less than values around 100 mb obtained in such work.[10,13–15] It is however, in better agreement with values around 85 mb obtained with 17.6-Mev rays.[16,17] The integral of the cross section at 20 Mev is 0.41 Mev barn as compared to 0.6 and greater,[16] but this work is not particularly suited for the determination of this integral because of the low maximum energy available. BB obtain a value of 0.55 Mev barn for the integrated cross section up to 34 Mev which also is below that measured previously. Their value of this integral can be obtained from the activity at the high energy without a detailed knowledge of the shape of the cross section and should therefore be more reliable than most previous values. Thus the lower maximum cross section found in this work and the lower integrated cross section found by BB agree that the previously measured cross sections are high by more than 10%.

A discrepancy of the order of 10% in the absolute cross section could arise from systematic errors in the measurement of the photon flux by means of ionization chambers.[18] It could also be that the discrepancy arises in the determination of the total number of active atoms produced. The latest measurements made use of scintillation counters which completely enclose the foils. These techniques reduce many of the systematic errors which arise in determining the effective solid angle and in correcting for absorption and scattering in the sample. In the present work the main sources of error are those associated with the absolute measurement of charge with the Faraday cage, the determination of the absolute counting rates, and the determination of F. These errors are estimated to be 3% in each case yielding an over-all estimated error of about 5%.

SUMMARY

The electrodisintegration cross section and the photodisintegration cross section have been determined in the energy range of 12 to 20 Mev. The maximum value of the (γ,n) cross section is about 20% lower than that obtained earlier with x-ray beams. The ratio of photon induced activity to electron induced activity was found to be 5 to 10% above that predicted for a magnetic dipole excitation in agreement with the trend of previous work at higher energies.

ACKNOWLEDGMENTS

It is a pleasure to acknowledge the cooperation of T. J. Keegan in setting up and operating the betatron and the associated electron beam equipment. Han Sah was particularly helpful in the analysis of the first run and in the making of many of the measurements of the counter efficiency. We also express our thanks to Dr. J. S. Laughlin of Memorial Hospital in New York City who made a permendur peeler available to us during this period.

[12] See for example B. Rossi, *High Energy Particles* (Prentice-Hall, Inc., New York, 1952), p. 48.
[13] B. C. Diven and G. M. Almy, Phys. Rev. **80**, 407 (1950).
[14] V. E. Krohn and E. F. Schrader, Phys. Rev. **87**, 685 (1952).
[15] Karl Strauch, Ann. Rev. Nuc. Sci. **2**, 108 (1952).
[16] S. Shimizu, Mem. Coll. Sci., Univ. Kyoto **25**, 325 (1949).
[17] J. H. Carver and E. Kondaiah, Phil. Mag. **45**, 988 (1954).
[18] These questions have been discussed by L. D. Marinelli, Ann. Rev. Nuc. Sci. **3**, 249 (1953).

Alpha-Alpha Angular Correlations in $B^{11}(p,\alpha\alpha)He^4$†*

E. H. Geer,‡ E. B. Nelson, and E. A. Wolicki‡
State University of Iowa, Iowa City, Iowa

(Received June 16, 1955)

The angular correlation in the reaction $B^{11}(p,\alpha\alpha)He^4$ has been measured between the alpha particle emitted from C^{12} and one of the break-up alpha particles from Be^8. The measurement was made in a plane at 90 degrees to the proton beam with bombarding energies of 163 and 290 kev. Thin targets of natural boron were used, and the alpha particles detected with thin scintillation counters. The theoretical correlation functions in the laboratory system were obtained by a numerical integration of the center-of-mass angular correlation functions over the 2.9-Mev level in Be^8. The probability for decay of the C^{12} state was assumed to have the same energy dependence for different angular momenta of the emitted alpha particle. This energy variation was obtained from the energy spectrum of the alpha particles. Using the two lowest values of angular momentum for the first alpha particle, the 163-kev data were found to be consistent with a 2+ state in C^{12}, and 2+ but not 0+ or 4+ in Be^8. The data at 290 kev are not consistent with a pure state of spin 1− or 2− or 3+ in C^{12}. They are in agreement with a pure state of 2+ or with a superposition of states at this energy.

INTRODUCTION

THE excited states in C^{12} produced by the proton bombardment[1] of B^{11} decay primarily by alpha emission to the first excited state of Be^8. This state immediately breaks up into two more alpha particles whose maximum energy in the laboratory system is about the same as that of the first alpha particle. The energy relations between the states under consideration are shown in Fig. 1. The alpha particle which results from the decay of C^{12} will be called α_1, the more energetic of the Be^8 break-up alpha particles will be called α_2, and the remaining one α_3. The comparison of the experimental curves with the theoretical correlation functions calculated under different assumptions for the spins and angular momenta will be expected to yield information about the first excited state in Be^8 and the compound states in C^{12}.

Any state in Be^8 which breaks up into two alpha particles must have both even spin and even parity. The spins and relative energies of the lower levels can be predicted from an alpha particle model by analogy with the molecular rigid rotator.[2] Inglis[3] suggests that the first excited state at 2.9 Mev may be described by a mixture of central- and alpha-model wave functions, with the latter providing the state with its unusually large width. In either case, the spin of the first excited state is predicted to be 2. The experimental determination of the spin of this level has not been easy. Alpha-alpha scattering experiments at present show a gap in just this energy region.[4] Telegdi,[5] studying the photodisintegration of C^{12} in photographic emulsions, observed the energy spectrum of the alpha particles. Using only the lowest possible values of angular momentum for the first alpha particle, he found his spectrum consistent with equal parts of electric quadrupole and magnetic dipole absorption and a spin of 2 but not 0 for the first excited state in Be^8. Treacy[6] has measured the energy spectrum of alpha particles from the reaction $B^{10}(d,\alpha)Be^8$ and computed the expected spectra for spins 0 and 2. The experimental spectrum was in better agreement with the curve for a spin of 2. A recent experiment[7] by Hanna, LaVier, and Class finds that the beta-alpha angular correlation from Li^8 through the 2.9-Mev level is isotropic for electron energies from 1 to 10 Mev. If, as is usually supposed, the spin of Li^8 is 2, then the spin of the state in Be^8 must be either 0 or 2. However, this experiment is consistent with a Be^8 spin of 4 and a Li^8 spin of 3.

The levels in C^{12} will be designated by the proton energy needed to produce them by bombarding B^{11}. The 5 kev wide resonance at 163 kev yields alpha

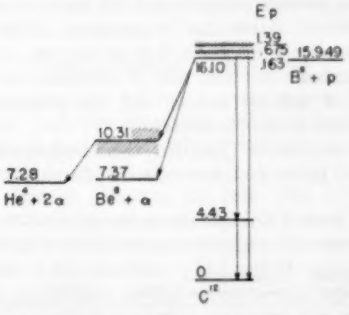

FIG. 1. Energy relationships in the reaction $B^{11}(p,\alpha\alpha)He^4$. Energies are plotted vertically in Mev, with the ground state of C^{12} taken as zero.

† This work was supported in part by the U. S. Atomic Energy Commission.

* Based on a thesis submitted by E. H. Geer in partial fulfillment of the requirements for the degree of Doctor of Philosophy in the Department of Physics of the State University of Iowa.

‡ Now at the Naval Research Laboratory, Washington, D. C.

[1] F. Ajzenberg and T. Lauritsen, Revs. Modern Phys. **27**, 77 (1955).

[2] J. A. Wheeler, Phys. Rev. **52**, 1083 (1937).

[3] D. R. Inglis, Revs. Modern Phys. **25**, 390 (1953).

[4] Phillips, Russell, and Reich [Bull. Am. Phys. Soc. **30**, No. 5, 14 (1955)] have studied alpha-alpha scattering from 3 to 6 Mev. Phase-shift analyses are consistent with a level in Be^8 at 2.9 Mev of width 0.8 Mev and spin 2+.

[5] V. L. Telegdi, Phys. Rev. **84**, 600 (1951).

[6] P. B. Treacy, Phil. Mag. **44**, 325 (1953).

[7] Hanna, LaVier, and Class, Phys. Rev. **95**, 110 (1954).

transitions[8] to the ground and first excited states of Be^8 as well as gamma rays[9] in C^{12}. A study[10] of the angular distribution of the alpha particles to the ground state of Be^8 indicates that the compound state in C^{12} corresponding to the 163-kev proton resonance has a spin of 2 with even parity. This is in agreement with the angular correlation[11] of the 11.7- and 4.4-Mev gamma rays. The variation of the asymmetry of the alpha angular distribution with bombarding energy is explained by interference with a weak state of odd parity and spin 1. The yield of long range alpha particles has a very broad resonance at 1.4 Mev which presumably contributes this background.

The width of the resonance at 675 kev allows one[12] to place an upper limit of 1 on the proton angular momentum. Since the ground state of B^{11} has a spin of $\frac{3}{2}$ and odd parity, and no alpha particles to the ground state of Be^8 or 16-Mev gamma rays are observed, certain restrictions can be placed on the values of spin and parity for this state. If the state is formed by s-wave protons, states of $1-$ or $2-$ are possible. $1-$ would provide both 12- and 16-Mev gamma rays by $E1$ transitions, contrary to the observations. If the state is formed by p-wave protons, states of $0+$, $1+$, $2+$, or $3+$ would be possible. The anisotropy of the gamma rays eliminates $0+$. $M1$ transitions from a $1+$ state could occur to either the $0+$ ground state or the $2+$ first excited state of C^{12}. $2+$ would yield alpha particles to the ground state of Be^8.

The angular distributions of gamma rays[13] and alpha particles[14] in the region above 675 kev show an asymmetry about 90 degrees to the proton beam which is approximately constant as a function of proton energy. French explains this on the assumption that the 675-kev and 1.4-Mev states are both formed by s-wave capture, and that there is interference with an even parity level at 2.6 Mev, whose contribution will be nearly constant over the range of energies observed. Recent work at Glasgow,[15] however, on the gamma-ray angular distributions using only one multipole is best explained on the assumption of $2+$ for the 675-kev state. This possibility is usually not considered because of the absence of alpha-particle transitions to the ground state of Be^8, but the authors point out that, if one assumes the same ratio of ground state to first excited state transitions as in the case of the 163-kev resonance, the ground state group would be weaker than the observed limits. Table I shows a compilation [1,12,13,15,16] of the known characteristics of these resonances in C^{12}.

In the past few years, several investigators have found indications of states in Be^8 other than the one at 2.9 Mev with excitation less than 6 Mev. Malm and Inglis[17] and Titterton[18] have discussed their existence. The observations by Malm and Inglis on the energy spectrum of alpha particles from $B^{11}(p,\alpha)Be^8$ at two different bombarding energies have been carefully made with magnetic analysis and show no indication of the disputed levels. Since this is the same reaction as is being studied here, it is assumed that the contributions of other states, if they exist, are negligible in comparison with the contribution from the state of 2.9 Mev.

PLAN OF THE EXPERIMENT

In the measurement of an angular correlation, two detectors observe the cascade radiations from a decaying source. In this experiment, the source is made by the bombardment of a boron target by protons. The direction relative to the target of one of the scintillation detectors was fixed at 90 degrees to the proton beam. The other detector was constrained to move in a plane at 90 degrees to the beam and with an angle ϕ between its direction and that of the first counter. The coincidence counting rate $C(\phi)$ between these two detectors does not give the angular correlation function $W(\phi)$ directly. $C(\phi)$ depends also on the number of reactions produced per second, n, the solid angles of the counters $d\Omega_1$ and $d\Omega_2$, and their efficiencies, ϵ_1 and ϵ_2:

$$C(\phi)=n\epsilon_1\epsilon_2 d\Omega_1 d\Omega_2 W(\phi). \quad (1)$$

The efficiencies can be measured as a function of the energy of the alpha particles. The magnitudes of the solid angles in the center-of-mass system are related to the alpha particle energies, and the transformation to the laboratory system can be calculated. Although the actual number of reactions, n, is not known, in practice the coincidence counting rate is normalized to a fixed number of monitor counts, and the proportionality factor remains as a parameter.

In the reaction $B^{11}(p,\alpha\alpha)He^4$, there are two successive processes. In the first, the emission of an alpha particle

TABLE I. Characteristics of resonances in C^{12}.

Energy (kev)	Width (kev)	Long range alphas?	16-Mev gammas?	Spin	Parity	References
163	5	yes	yes	2	+	1
675	300	no	no	2(3)	−,+?(+)	11,14,15
1400	1200	yes	yes	1	−	11,15
2000	150	yes	no	0?		11,12
2600	300	yes	?	2?	+	11,12

[8] H. von Ubisch, Kgl. Norske Videnskab. Selskabs, Fork. **15**, No. 9 (1942).
[9] R. Tangen, Kgl. Norske Videnskab. Selskabs, Fork. **19**, No. 1 (1946); A. H. Morrish, Phys. Rev. **76**, 1651 (1949).
[10] Thomson, Cohen, French, and Hutchinson, Proc. Phys. Soc. (London) **A65**, 745 (1952).
[11] Hubbard, Nelson, and Jacobs, Phys. Rev. **77**, 378 (1952).
[12] T. Huus and R. B. Day, Phys. Rev. **91**, 599 (1953).
[13] Given, Farney, Hahn, and Kern, Phys. Rev. **95**, 483 (1954); H. E. Gove and E. B. Paul, Phys. Rev. **97**, 104 (1955).
[14] A. P. French, private communication.
[15] Grant, Flack, Rutherglen, and Deuchars, Proc. Phys. Soc. (London) **A67**, 751 (1954).
[16] E. B. Paul and R. L. Clarke, Phys. Rev. **91**, 463 (1953); Beckman, Huus, and Zupančič, Phys. Rev. **91**, 606 (1953).
[17] R. Malm and D. R. Inglis, Phys. Rev. **92**, 1326 (1953); see also Holland, Inglis, Malm, and Mooring, Phys. Rev. **99**, 92 (1955).
[18] E. W. Titterton, Phys. Rev. **94**, 206 (1954).

from the excited C^{12} gives the daughter Be^8 nucleus a momentum equal and opposite to that of the alpha particle, and one third of the energy of the disintegration process appears in the recoil motion. Figure 2 is a diagram of the velocities involved in these processes. A lower limit on the angle between the detectors is set by the fact that below about 130 degrees in the laboratory it becomes energetically possible to detect coincidences between α_2 and α_3. For angles of 130 degrees or greater, no confusion will arise in interpreting all of the coincidences observed as between the first alpha particle and the more energetic of the break-up particles.

Thin targets of natural boron on thin backings were used so that the alpha particles could be observed both from the face of the target and through the back of the target with little loss in energy. The counters moved in the plane normal to the proton beam, so that the maximum angle between them was 180 degrees. The counters were made as nearly identical as possible. Thus each of the two correlated alpha particles could be detected in either of the detectors with equal probability, and the observed coincidence counting rate was simply twice as large at all angles as it would

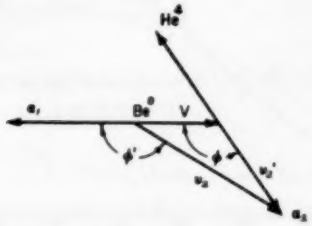

FIG. 2. Velocity diagram for the process $C^{12} \rightarrow Be^{8*}+\alpha_1$; $Be^{8*} \rightarrow \alpha_2+He^4$.

have been had each counter been able to detect only one of the two particles.

EXPERIMENTAL APPARATUS

The measurement of the angular correlation was performed using the State University of Iowa Cockcroft-Walton accelerator. Figure 3 shows the target chamber. It is shaped like a pillbox, with the beam entering through a hole in one face. This half of the chamber is bolted on the machine, and the fixed counter is a part of it. The movable counter is a part of the other half of the chamber, which rotates on the first. The thin target used in this experiment is represented by the diagonal line in the center of the chamber. Its face is at 45 degrees to the incident beam and to the movable counter. As the movable counter rotates through 50 degrees, the fixed counter views the target face at an angle varying from +25 degrees to −25 degrees. The counting rate from a polonium alpha source placed at the center of the chamber showed no asymmetry as the movable counter was rotated.

The backings for the boron targets were prepared by

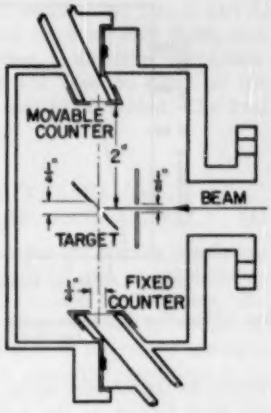

FIG. 3. Target chamber used in the alpha-alpha angular correlation experiment.

evaporating about 10 $\mu g/cm^2$ of aluminum on thin zapon films. The boron evaporated on the aluminum had about 5-kev stopping power for the protons used, as determined from the width of the yield curve of the resonance at 163-kev bombarding energy.

The alpha particles were detected by thin NaI flakes. These were connected to RCA 5819 photomultiplier tubes by Lucite light pipes, about six inches long and half an inch in diameter. The apertures in front of the crystals were quarter inch diameter holes in brass caps. The holes were covered with 25-microinch nickel foils in order to stop the protons scattered from the target. The foils placed a lower limit of 1 Mev on the energy of the alpha particles detectable by the system. The photomultipliers were selected for low noise level.

The efficiency of the detectors as a function of energy was measured with alpha particles from a polonium source. The energy of the alpha particles was reduced by weighed nickel and aluminum foils. The energy loss was computed from the proton data for dE/dx in aluminum and copper, assuming doubly charged helium ions. Figure 4 shows the foil holder. The six foils were placed as close as possible to the detectors in order that the effect of multiple scattering should be a minimum. The two counters were found to have similar efficiencies and an energy resolution of about 20

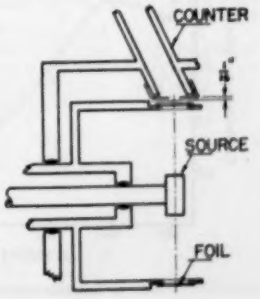

FIG. 4. Foil holder used in determining the efficiency of the detectors as a function of alpha-particle energy.

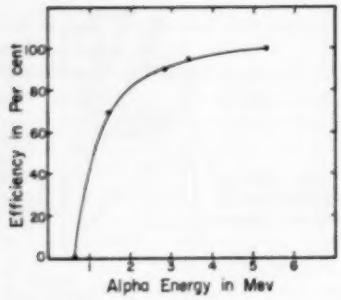

FIG. 5. Variation with alpha energy of the mean efficiency of the two detectors.

percent for the 5.3-Mev alpha particles. This resolution was good enough at the lower energies so that the efficiency remained fairly constant down to a steep cutoff to zero at about 1 Mev. Figure 5 shows the variation with alpha energy of the mean efficiency of the two counters.

The outputs from the photomultipliers were connected directly to the inputs of the Atomic Instrument Company Model 204B amplifiers. The reaction was monitored by the counting rates from both of the counters. The two monitors agreed with each other within the statistical errors throughout the runs. Coincidences were measured by an Atomic Instrument Company Model 502 coincidence circuit.

SUMMARY OF DATA

The yield of alpha particles from the reaction $B^{11}(p,\alpha\alpha)He^4$ was measured as a function of bombarding energy and found to be in substantial agreement with the more accurate measurements of von Ubisch.[8]

Figures 6 and 7 show the relative coincidence counting rates as a function of the laboratory angle between the counters for the two proton bombarding energies used: 163 and 290 kev. These numbers were obtained by dividing the number of coincidences minus the estimated number of accidentals by the number of counts in the monitor.

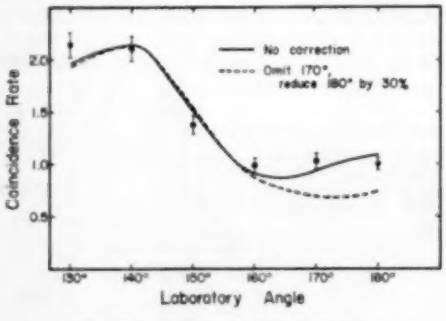

FIG. 6. Angular correlation at 163 kev.

At 163 kev, a typical counting rate in the individual channels was about 15 per second. The maximum coincidence counting rate was about 7 per hundred seconds, and the accidental rate was negligible. At 290 kev, the individual channels had rates between 80 and 130 counts per second, and the accidental rate measured by inserting a four microsecond delay line in one of the channels was found to agree with that calculated from the counting rates and the resolving time of the coincidence circuit.

THEORY

The theoretical expression for the angular correlation function is, apart from constant factors, the transition probability from the initial state, consisting of a boron nucleus and a proton approaching it with momentum $\mathbf{p}$ and spin $\mathbf{i}$, to the final state, consisting of a helium nucleus and the two emitted alpha particles. Table II shows the symbols used in the following discussion. The j and m symbols refer to the spins and magnetic quantum numbers of the nuclear states, and the L

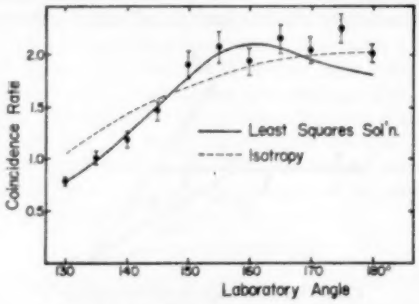

FIG. 7. Angular correlation at 290 kev.

and μ symbols refer to the total angular momentum and magnetic quantum numbers of the absorbed or emitted particles. The channel spin $\mathbf{s}$ is the vector sum of the spins of the boron nucleus and the incident proton. Under the Bohr compound-nucleus assumption, the matrix $\mathbf{D}$ for the whole transition may be expressed as the product of three independent transformation matrices, $\mathbf{A}$, $\mathbf{B}$, and $\mathbf{C}$. These correspond, respectively, to the formation of the compound C^{12} nucleus, of the intermediate state with the first alpha particle emitted into a solid angle Ω_1, and of the final state with the second alpha particle emitted into a solid angle Ω_2. The wave function of the final state is now:

$$(j_2 m_2 \Omega_2 \Omega_1 | \mathbf{D} | jm\mathbf{ps}) = (j_2 m_2 \Omega_2 | \mathbf{C} | j_1 m_1)(j_1 m_1 \Omega_1 | \mathbf{B} | j_0 m_0)(j_0 m_0 | \mathbf{A} | jm\mathbf{ps}). \quad (2)$$

The axis of quantization will be chosen to be along the direction of the proton beam, and thus the polar angle θ of both counters will be 90 degrees. The direction of emission of the first alpha particle is chosen as the axis from which the azimuthal angle ϕ is measured, so

TABLE II. Symbols used in the theoretical discussion.

B^{11} + proton		C^{12*}	α_1 + Be^{8*}		α_2 + He^4	
j,m	$i,\pm\frac{1}{2}$	j_0,m_0	0	j_1,m_1	0	j_2,m_2
s			L_1,μ_1		L_2,μ_2	

that the angle between the counters is given by the azimuthal angle of the second alpha particle. The dependence of the nuclear matrix elements on the direction of emission of the alpha particles may be expressed in spherical harmonics, Y_L^μ, with the dependence on magnetic quantum numbers appearing in Clebsch-Gordan coefficients.

For the formation of the compound nucleus in C^{12},

$$(j_0m_0|\mathbf{A}|jmps)=\sum(j\tfrac{1}{2}mi|sm_0)\mathbf{A}(j_0js)\times(ls0m_0|j_0m_0)(ls0m_0|ps). \quad (3)$$

Here $\mathbf{A}(j_0js)$ is the reduced matrix element, and the magnetic quantum number of the orbital angular momentum of the incident protons is zero because of the choice of the axis of quantization. We only consider the lowest possible value of angular momentum for the formation of the state. For this geometry, $(ls0m_0|ps)$, apart from constant factors, reduces to $(2l+1)^{\frac{1}{2}}$.

For the second transition,

$$(j_1m_1\Omega_1|\mathbf{B}|j_0m_0)=\sum Y_{L_1}^{\mu_1}(\Omega_1)(j_1L_1m_1\mu_1|j_0m_0)\mathbf{B}(j_0j_1L_1), \quad (4)$$

and for the breakup of Be^8,

$$(j_2m_2\Omega_2|\mathbf{C}|j_1m_1)=\sum Y_{L_2}^{\mu_2}(\Omega_2)(j_2L_2m_2\mu_2|j_1m_1)\mathbf{C}(j_1j_2L_2). \quad (5)$$

In this case, the spin j_2 of He^4 is zero, so the Clebsch-Gordan coefficient reduces to 1.

In the following we will assume that j, j_1, j_2, and L_2 are constant, so that terms involving only them, such as $\mathbf{C}(j_1j_2L_2)$, will be common to all terms of the summation. All such factors will have no effect on the angular correlation, and will be discarded. The final state wave function is now

$$(j_2m_2\Omega_2\Omega_1|\mathbf{D}|jmps)=\sum(2l+1)^{\frac{1}{2}}Y_{L_2}^{\mu_2}(\Omega_2)Y_{L_1}^{\mu_1}(\Omega_1)(L_2L_1\mu_2\mu_1|j_0m_0)\times(ls0m_0|j_0m_0)(j\tfrac{1}{2}mi|sm_0)\mathbf{A}(sj_0)\mathbf{B}(j_0L_1). \quad (6)$$

Table III presents the computed angular correlation functions in the center of mass for each set of conditions considered. ϕ is the angle between the detectors. The value of n indicates the power of $\cos\phi$ by which the sum of all the terms indicated in the row to the right is to be multiplied. Each numerical coefficient is to be multiplied by the variable in whose column it occurs. For example, in the case of spin 2− in C^{12} and 2+ in Be^8, the angular correlation is

$$W(\phi)=1+0.25B^2+B\cos\beta+\cos^2\phi(-1+3.5B^2-6B\cos\beta)+\cos^4\phi(-3.75B^2+5B\cos\beta).$$

The only unknown quantities are the values of the matrix elements for the decay of C^{12*} for different angular momenta of the first alpha particle. The ratio of the squares of the reduced matrix elements $|\mathbf{A}(2)/\mathbf{A}(1)|^2$ for values of the channel spin equal to 1 and 2 at the 163-kev resonance has been measured to be 0.42 ± 0.02 by Thomson *et al.*[10] We define $Be^{i\beta}=\mathbf{B}(L+2)/\mathbf{B}(L)$ where L is the lowest value of angular momentum possible for the first alpha particle, and β is the difference in phase between the two partial waves. Similarly, if three values of angular momentum are possible, $Ce^{i\gamma}=\mathbf{B}(L+4)/\mathbf{B}(L)$.

TABLE III. Theoretical angular correlation functions.

j_0	j_1	L_1	s	n	const	B^2	$B\cos\beta$	C^2	$C\cos\gamma$	$BC\cos(\beta-\gamma)$
2+	0	2	1,2	0	+ 1					
	2	0,2,4	1	0	+ 1	+40/7	+4(10/7)$^{\frac{1}{2}}$	+9/56	−3(14)$^{-\frac{1}{2}}$	−(6/7)5$^{\frac{1}{2}}$
				2	0	−120/7	−6(10/7)$^{\frac{1}{2}}$	−45/28	+15(14)$^{-\frac{1}{2}}$	+(39/7)5$^{\frac{1}{2}}$
				4	0	+90/7	0	+225/56	0	−(45/7)5$^{\frac{1}{2}}$
			2	0	+ 3	0	0	+21/8	+21(14)$^{-\frac{1}{2}}$	0
				2	0	+30/7	−6(10/7)$^{\frac{1}{2}}$	−15/28	−195(14)$^{-\frac{1}{2}}$	+(69/7)5$^{\frac{1}{2}}$
				4	0	0	0	+45/8	+210(14)$^{-\frac{1}{2}}$	−(15)5$^{\frac{1}{2}}$
	4	2,4,6	1	0	+ 3	+1080/11	+36(10/11)$^{\frac{1}{2}}$	+105/88	−3(35/22)$^{\frac{1}{2}}$	−(90/11)7$^{\frac{1}{2}}$
				2	− 30	−18360/11	−486(10/11)$^{\frac{1}{2}}$	−2940/88	+57(35/22)$^{\frac{1}{2}}$	+(2025/11)7$^{\frac{1}{2}}$
				4	+ 75	+95670/11	+1824(10/11)$^{\frac{1}{2}}$	+24990/88	−273(35/22)$^{\frac{1}{2}}$	−(13335/11)7$^{\frac{1}{2}}$
				6	0	−149940/11	−1470(10/11)$^{\frac{1}{2}}$	−61740/88	+315(35/22)$^{\frac{1}{2}}$	+(26355/11)7$^{\frac{1}{2}}$
				8	0	+72030/11	0	+46305/88	0	−(15435/11)7$^{\frac{1}{2}}$
			2	0	+ 49	0	0	+12705/352	+(231/4)(35/22)$^{\frac{1}{2}}$	0
				2	− 10	+810/11	−414(10/11)$^{\frac{1}{2}}$	−2940/352	−(8691/4)(35/22)$^{\frac{1}{2}}$	+(7965/44)7$^{\frac{1}{2}}$
				4	+105	−3780/11	+1596(10/11)$^{\frac{1}{2}}$	+83790/352	+(49959/4)(35/22)$^{\frac{1}{2}}$	−(54495/44)7$^{\frac{1}{2}}$
				6	0	+4410/11	−1470(10/11)$^{\frac{1}{2}}$	−202860/352	−(89145/4)(35/22)$^{\frac{1}{2}}$	+(114975/44)7$^{\frac{1}{2}}$
				8	0	0	0	+169785/352	+(48510/4)(35/22)$^{\frac{1}{2}}$	−(72765/44)7$^{\frac{1}{2}}$
2	2	1,3	2	0	+ 1	+ 0.25	+1			
				2	− 1	+ 3.5	−6			
				4	0	− 3.75	+5			
3	2	2,4	2	0	+ 10	+ 4	+8(5/2)$^{\frac{1}{2}}$			
				2	+ 0.8	−48	−90(5/2)$^{\frac{1}{2}}$			
				4	− 10.8	+44	+82(5/2)$^{\frac{1}{2}}$			
1	2	1,3	1	0	+ 2	+ 3	−2(6)$^{\frac{1}{2}}$			
				2	+ 6	− 6	+24(6)$^{\frac{1}{2}}$			
				4	0	+15	−30(6)$^{\frac{1}{2}}$			

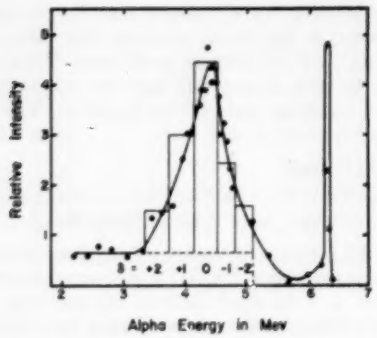

FIG. 8. Energy spectrum of alpha particles from $B^{11}(p,\alpha\alpha)He^4$ measured by Whaling showing continuum subtraction and division of the level into five parts. δ is the ratio of the displacement in energy from the center of the level to the half-width at half-maximum. The sections of the histograms are centered at $\delta=0,\pm1$, and ±2; their heights are proportional to the area under the experimental curve between the vertical lines.

These transition matrices have absorbed all of the energy dependent factors including the penetrability for different values of angular momentum of the alpha particles, and the phases of the alpha particle wave functions in a Coulomb field. A theoretical calculation of these energy dependences is made particularly difficult in this case because the nuclear potential seen by an alpha particle decaying from C^{12} is not a simple square well, and it does not have a unique radius. The next section will be concerned with the problems which arise from the fact that the level in Be^8 is not in fact a sharp level as has been assumed in this section. In general, it will be expected that the parameters B, C, $\cos\beta$, and $\cos\gamma$ will vary with the energy of the first alpha particle as it decays to the different parts of the 2.9-Mev level. For the purpose of this discussion, it has been assumed that this variation can be neglected, and the matrix elements can be considered as constant unknowns in the analysis.

COMPUTATIONS

The correlation function observed in the laboratory differs from that computed in the center of mass because of the large motion of the recoiling Be^8 nucleus[19] (see Fig. 2). This causes both the angle between the alpha particles and the differential solid angle into which the second alpha particle is emitted to be transformed into a different angle and solid angle in the laboratory. If the level in Be^8 were sharp, this correspondence would be unique. The observed correlation is due to contributions from the various parts of the broad level, and it was necessary to make a numerical integration before obtaining a theoretical curve which could be compared with the experimental results. At the time when these analyses were first being made, Whaling's[20] data on the energy spectrum from the reaction $B^{11}(p,\alpha\alpha)He^4$ at 1 Mev were the only ones available. Since subsequent measurements at similar or lower bombarding energies are in substantial agreement with them, his data have been used here. Measurements at higher energies show proportionately more background from the simultaneous breakup of C^{12} into three alpha particles. Whaling's alpha-particle spectrum, shown in Fig. 8, has a narrow peak due to transitions to the ground state of Be^8, which is much more prominent at his bombarding energy than at those used in this experiment. The broad peak is due to the state at 2.9 Mev and is superimposed on the continuum of break-up alpha particles. The exact shape of their spectrum will depend on the angular correlation as well as the smearing due to the level width. For the purpose of this analysis, a constant background up to the maximum α_2 energy was subtracted under the peak. It is recognized that the amount subtracted was too small, since for every α_1 there are two break-up particles. This approximation thus probably gives undue prominence to the center of the level. The level shape, thus determined, was further approximated by a histogram in five sections. These were labeled by δ, which is the ratio of the displacement in energy from the center of the level to the half-width at half-maximum. The sections were centered at $\delta=0$, ±1, and ±2. A graph of this division is shown in Fig. 8.

The correlation observed in the laboratory results from an integration over the contributions from the whole level. If $C(\phi')$ is the $\alpha_1-\alpha_2$ coincidence counting rate in the laboratory per unit solid angle in both counters, and w_δ is the weight of the part of the level labeled by δ, then,

$$C(\phi')d\Omega_1'd\Omega_2'=n\epsilon_1d\Omega_1\sum_\delta\epsilon_2(\phi_\delta)d\Omega_2W(\phi_\delta)w_\delta. \quad (7)$$

Note that ϵ_1 and $d\Omega_1$ are the same in the center-of-mass and laboratory systems since the C^{12} nucleus is nearly at rest. $W(\phi)$ are the center-of-mass angular correlation functions which appear in Table III.

$$C(\phi')=n\epsilon_1\sum\epsilon_2(\phi_\delta)\frac{d\Omega_2(\phi_\delta)}{d\Omega_2'(\phi')}\times W(\phi_\delta)w_\delta=\text{const}\sum\frac{\epsilon_2 w}{f}W(\phi), \quad (8)$$

where f is the ratio of differential solid angle in the laboratory to that in the center of mass. Negligible error is introduced if the efficiency for detection of the first alpha particle is taken to be one. The second alpha particle changes energy so rapidly that it virtually cannot be observed for center-of-mass angles less than 90 degrees, corresponding to about 130 degrees in the laboratory. The energy of α_2 was computed as a function of the laboratory angle between α_2 and α_3, and it was

[19] These relationships have also been computed by H. Glättli Nuovo cimento **12**, 174 (1954).

[20] C. W. Li and W. Whaling, Phys. Rev. **81**, 661 (1951); and W. Whaling, private communication.

found that observable coincidences between α_2 and α_3 will occur only at 130 degrees and then only for transitions to the uppermost part of the level. Here the energy is still quite small, and it was estimated that there would be a contribution of less than 4 percent to the coincidence counting rate at this angle. No α_2–α_3 coincidences will be observed at larger angles.

All of the center-of-mass angular correlations discussed in the section on theory for the case of $j_1=2$ reduce to the form:

$$W(\phi)=1+a\cos^2\phi+b\cos^4\phi, \qquad (9)$$

where the coefficients are functions of two unknown parameters. This general correlation function was integrated over the level and a least-squares solution made to the experimental data for the unknowns a, b, and a normalization parameter. Then for any set of conditions the definitions of a and b yielded the values of the theoretical parameters directly. Separate solutions had to be made for functions with more than two unknown parameters, or with higher powers of $\cos\phi$.

The correction to the observed correlation function due to the finite size of the counter apertures was small compared to the statistical errors of the points. The resolution function for circular apertures was calculated by numerical integration, dividing the circles into ten sections, and assuming no variation with θ. The half-width at half-maximum of a triangle which fits this resolution function was 5.25 degrees. Using the formulas of Church and Kraushaar,[21] a correlation function at 163 kev is modified as follows:

without correction: $W(\phi)=-1.926\cos^2\phi+1.230\cos^4\phi$,
with correction: $W(\phi)=-1.972\cos^2\phi+1.280\cos^4\phi$.

Transitions to the ground state of Be^8 can also contribute to the angular correlation. The alpha particles from the decay of C^{12} have an energy of 6 Mev and are detected with 100 percent efficiency. The energy released in the decay of the ground state of Be^8 is so small, 95 kev, that the major contribution to the energy of the break-up particles is from the recoil of Be^8. Their energies range from 1.0 to 2.0 Mev, so that these alpha particles are detectable, although with low efficiency. Because of their small component of velocity from the center-of-mass decay, all the break-up alpha particles are emitted in the laboratory in the direction opposite to the emission of the first alpha particle, within a cone of half-angle about 10 degrees. This means that only the data at angles of 170 degrees or greater will be affected.

The data at 290-kev bombarding energy were analyzed by the method of least squares in terms of the center-of-mass angles excluding the data at 170, 175, and 180 degrees. The resulting curve, shown in Fig. 7, lies below the experimental points at these angles. The coefficients are:

using all data: $a=+1.54\pm0.29$ $b=-1.17\pm0.26$,

omitting 170, 175, and 180 degree points:

$$a=+2.08 \quad b=-1.74.$$

Although the errors are large, it is not necessary for their interpretation that these coefficients be known more precisely.

Fewer experimental points were available for the correlation at 163-kev bombarding energy, so a correction to the experimental data was estimated. The angular correlation was measured in two different sets of runs. The efficiency for detection of the break-up alpha particles from the ground state was increased by about 40% in the second measurement. No difference within the statistical uncertainty of the points was observed in the shape of the curve for angles greater than 130 degrees. If the number of coincidences due to the ground state transitions had been greater than 30% of the total number of observed coincidences at 180 degrees, the second curve would have been higher than the first by an amount outside of the combined errors of observation. The curve shown in Fig. 6 is the least-squares solution to the data after a 30% contribution at 180 degrees has been subtracted. Assuming no correction to the data due to the ground-state group, the coefficients of the general correlation at a proton energy of 163 kev are

$$a=-1.97\pm0.56 \quad b=+1.28\pm0.95,$$

and, with the point at 170 degrees omitted, and the point at 180 degrees reduced by 30%

$$a=-1.84 \quad \text{and} \quad b=1.04.$$

DISCUSSION

A. Correlation at 163 kev

An immediate conclusion can be drawn from the data at 163 kev. Since the angular correlation is strongly anisotropic, the spin of the 2.9-Mev level in Be^8 cannot be zero.[22]

Assuming 2+ for the spins and parities of the C^{12} and Be^8 states, possible angular momenta for the first alpha particle are 0, 2, and 4. If only the contributions of angular momenta 0 and 2 are considered, the relative amplitudes and phases for the first alpha particle of the s- and d-partial waves provide two parameters, and the normalization a third. On comparing the coefficients of the least squares fits to the experimental data with those of the theoretical correlation function (see Table III), we obtain the following values for B and $\cos\beta$:

no correction for ground-state transitions:

$$B=1.01, \cos\beta=0.44,$$

180-degree point reduced by 30%:

$$B=0.80, \cos\beta=0.60.$$

[21] E. L. Church and J. J. Kraushaar, Phys. Rev. **86**, 419 (1952).

[22] F. Ajzenberg and T. Lauritsen, Revs. Modern Phys. **24**, 321 (1952) quote Nelson and Wolicki on this point, using unpublished data from this experiment.

Either of these cases fits the experimental data satisfactorily, and the values of B and $\cos\beta$ are not unreasonable. Any additional terms due to the inclusion of the higher angular momentum would fit at least as well, but, since there are so few angles at which data were taken, any improvement would be meaningless. This certainly does not mean that an angular momentum of 4 does not contribute to the reaction, but that these data are insufficient to determine the amount of its contribution.

Table III also gives the angular correlation function for the case of a spin of 4 for the 2.9-Mev state in Be^8. The state in C^{12} is again assumed to be 2+. Here the possible values of angular momentum for the first alpha particle are 2, 4, and 6. The spin of 4 in Be^8 introduces terms in $\cos^4\phi$ and $\cos^3\phi$ into the correlation function. Using only the two lowest values of angular momentum, the theoretical expressions were evaluated for each angle at which observations were made, and the resulting equations were solved by the method of least squares for the parameters B^2, $\cos\beta$, and the normalization. Here B and $\cos\beta$ compare the partial waves of $L_1=4$ with $L_1=2$, in accordance with the definitions in the section on theory. The curve calculated on the basis of the least-squares fit increased towards 180 degrees instead of decreasing, badly disagreeing with the experimental curve. This disagreement was found regardless of the reduction assumed for the 180-degree point. A second solution was made including all three values of angular momentum. This gives two additional parameters in the solution, corresponding to the new amplitude and phase, and the expression in Table III shows that there is also a term in $BC\cos(\beta-\gamma)$ which involves all the other theoretical unknowns. It was impossible to separate the components of this term in the solution, so that, with the normalization parameter, there were a total of six unknowns. Since there are only six experimental data, a solution has meaning only in so far as the parameters have reasonable values. This was not the case. B^2 was found to be negative and very small. If we assume that it should actually be small and positive, it is still found that $L_1=6$ is more probable than $L_1=2$, and roughly ten times as probable as $L_1=4$. Although the potential barrier for high angular momentum is probably small, $L_1=6$ is not expected to predominate in this manner.

There are two kinds of errors that enter into the calculations. First, there are such errors as arise from the inaccuracies of the measurement of the angular correlation, the estimation of the correction at large angles, the errors of the efficiency measurement that enter into the integration of the correlation function over the level, and the error in the relative contributions of the two values of channel spin measured by Thomson *et al.*[16] The second kind of error is the type inherent in the use of this theoretical analysis: namely, the assumption that the matrix elements for different angular momenta do not differ violently in their variation with energy, and that their values averaged over the level are meaningful. The use of thin targets allowed us to measure the angular correlation at the peak of the 163-kev resonance, and we have assumed that no other state in C^{12} contributed. Within this context, the present data are in qualitative disagreement with a choice of 0 or of 4 for spin of the 2.9-Mev level in Be^8, and we conclude that the spin is 2.

B. Correlation at 290 kev

The state in C^{12} responsible for the correlation at 290 kev may be either the resonance at 675 kev or the one at 1.4 Mev. We first consider the case where the correlation is due only to the 675-kev resonance. We assume pure s-wave capture if the state is 2−, and pure p-wave capture if the state is 3+, and either $j_1=2$ or 4 for the 2.9-Mev level in Be^8. The calculated correlations for all of these cases (see Table III) become zero at 180 degrees. Thus the observed nearly isotropic correlation is in clear disagreement with a pure 2− or 3+ state in C^{12} at 290 kev. We can however not reject a pure 2+ state at 675 kev as suggested by the Glasgow group,[15] since a choice of $B=+0.41$ and $\cos\beta=0$ fits our experimental angular correlation using their value for channel spin ratio.

Instead of the 675-kev state, the broad resonance at 1.4 Mev might be responsible for the correlation at 290 kev. Table III gives the angular correlation function for s-wave proton capture, a pure 1− state in C^{12}, and spin 2+ in Be^8. For no real value of the parameter B does the computed correlation agree with the observations. It is, however, possible to obtain qualitative agreement with the observed data using a mixture of 2− and 1− states, even if only the lowest values of angular momentum are considered for the alpha particles.

The angular correlation at 290 kev may be compared with the results of an experiment performed by Dissanaike.[23] He measured the energy spectrum of the alpha particles from this reaction with magnetic analysis as a function of bombarding energy from 250 to 1400 kev. The spectrum had the same form over the region investigated. From the velocity diagram, Fig. 1, it is clear that the angle between α_1 and α_2 is uniquely related to the energy of α_2 for a sharp level. Dissanaike has assumed that the energy spectrum of the first alpha particle is given by a Breit-Wigner curve and has then computed the energy spectrum of the break-up alpha particles corresponding to isotropic emission of the first alpha particle. By assuming an angular correlation function $W(\phi)$, and performing an integration over the level, he was able to infer the energy spectrum of the break-up alpha particles. The spectrum was consistent with a correlation of $1+3\cos^2\phi$, corresponding to a 1− level and $L_1=1$, and also with a 2−

[23] G. A. Dissanaike, Ph.D. thesis, Downing College, Cambridge, 1953 (unpublished).

level if both p- and f-wave alpha particles were considered, using an f/p wave amplitude ratio of 0.6, $\cos\beta=-1$, giving $W=1+7\cos^2\phi-8\cos^4\phi$. In comparing the results of the two experiments, it should be mentioned that the energy spectrum is not sensitive to the form of the angular correlation near 180 degrees, since the available solid angle is smallest there.

CONCLUSION

The alpha-alpha angular correlation at 163 kev is consistent with a pure state of spin 2 in C^{12} and 2+ but not 0+ or 4+ for the first excited state in Be^8. The nonresonant angular correlation at 290 kev cannot be explained on the basis of a pure state with spin 2− or 3+, corresponding to the 675-kev resonance, or 1−, corresponding to the 1.4-Mev resonance. The correlation is satisfactorily explained either by a mixture of these two states or by the assumption of a spin of 2+ for the 675-kev state alone.

ACKNOWLEDGMENTS

The authors are grateful to Professor F. Coester and Dr. Isidore Hauser for many discussions concerning the theory, and to Mr. Gyan Mohan and Mr. Theodore Stecher for their assistance with the computations. We also wish to express our appreciation to Professor A. P. French of the Cavendish Laboratory for discussing the experiment with us and making available the Cambridge results.

PHYSICAL REVIEW VOLUME 100, NUMBER 1 OCTOBER 1, 1955

Decay of Cr^{48}†

R. VAN LIESHOUT,* D. H. GREENBERG, L. A. CH. KOERTS, AND C. S. WU
Department of Physics, Columbia University, New York, New York
(Received May 5, 1955)

The nuclide Cr^{48} has been produced by spallation of Ni. It decays by electron capture only with a half life of 23 hours and emits gamma rays of 116 kev ($M1$) and 305 kev ($E2$) of equal intensity, which are in coincidence. The genetic relationship with 16.2-day V^{48} establishes the mass assignment. The total decay energy of Cr^{48} can be estimated as 1.45±0.20 Mev. Two alternative decay schemes are proposed.

1. INTRODUCTION

THE nuclide Cr^{48} has been reported[1] as a spallation product, decaying by electron capture only, with a half-life of 23 hours. It was identified by the growth and decay of its daughter V^{48}. The radiations from Cr^{48} were detected with an end window type Geiger-Muller tube; no appreciable amount of positrons was found in Cr^{45}.

The ground state of V^{48} very probably has a spin 4 or 5 and even parity. This can be concluded from the spins of the levels in Ti^{48} and the decay properties[2] of V^{48}. The relatively short period of Cr^{48} indicates an allowed transition even for decay energies as large as 6 Mev. Now since Cr^{48} should have a ground state spin 0 with even parity, this implies that the decay goes by way of an excited state in V^{48} with spin 0 or 1 and even parity. In this mass region, low lying states with widely different spin values are known to exist in various odd-odd nuclides (Sc^{44}, Sc^{46} and Mn^{52}); presumably they arise from different couplings of the $f_{7/2}$ proton with the $f_{7/2}$ neutron.[3]

The decay of Cr^{48} should therefore be accompanied by at least one gamma ray, possibly leading to a metastable state of V^{48}.

2. SAMPLE PREPARATION

Cr^{48} can be produced in good yield by the interaction of high energy particles with a target material of considerably greater mass number (so called "spallation" reactions). For such reactions the yield is relatively independent of the mass and charge number (A,Z) of the target material chosen,[4] provided that ΔA is not too large ($\lesssim$10 for 380-Mev protons) and that ΔZ is not too small. These considerations suggest the choice of natural nickel (68% Ni^{58}) as the target material.

It should be pointed out that in such an irradiation Cr^{49} and Cr^{51} will also be produced, the Cr^{49} in about equal yield (estimated) as Cr^{48} and the Cr^{51} in about twenty times greater yield (estimated). The Cr^{49} with only a 42-min half-life can be allowed to die, and the

† Partially supported by the U. S. Atomic Energy Commission and by the joint program of the Office of Naval Research and the U. S. Atomic Energy Commission.
* On leave from the Institute for Nuclear Research, Amsterdam, The Netherlands.
[1] Rudstam, Stevenson, Folger, Phys. Rev. **87**, 358 (1952).
[2] Nuclear data mentioned in this paper without further reference are taken from:
K. Way *et al.*, *Nuclear Data*, National Bureau of Standards Circular No. 499 (U. S. Government Printing Office, Washington, D. C. 1950); Hollander, Perlman, and Seaborg, Revs. Modern Phys. **25**, 469 (1953). The yearly compilations in Nuclear Science Abstracts **6**, 24B (1952); **7**, 24B (1953); **8**, 24B (1954).
[3] R. W. King and D. C. Peaslee, Phys. Rev. **90**, 1001 (1953).
[4] E. Belmont and J. M. Miller, Phys. Rev. **95**, 1554 (1954).

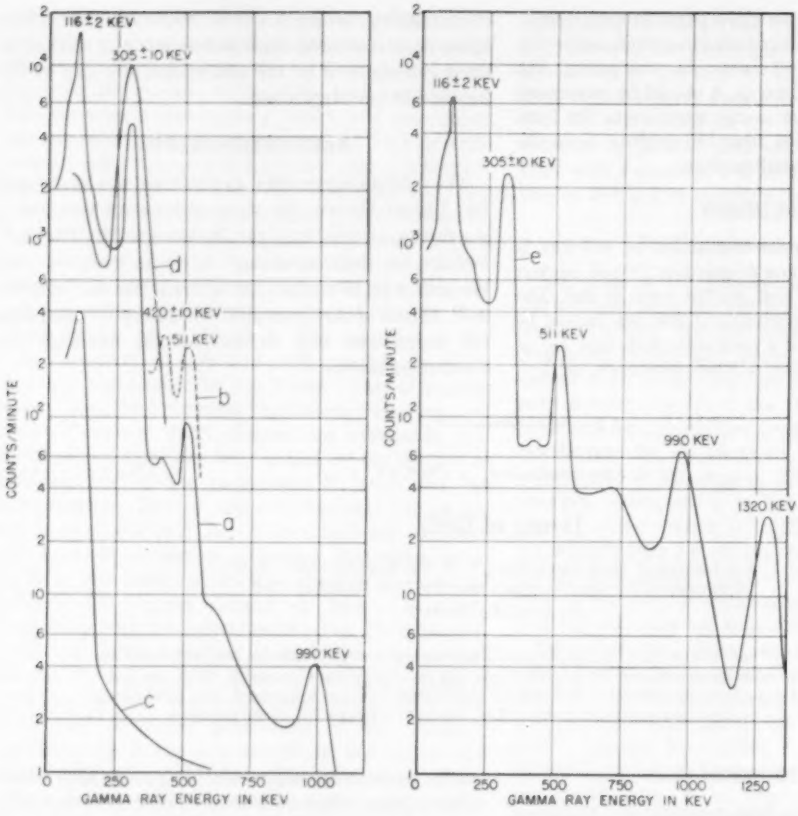

FIG. 1. Gamma spectrum of Cr^{48}. Curve *a* shows the spectrum taken with the source at $\frac{3}{4}$ in. from the detector, for curve *b* this distance is $\frac{1}{4}$ in. Curves *c* and *d* show the spectrum in coincidence with the 0.305 γ and 0.116 γ_1 respectively. Curve *e* was taken 2 days later and shows the characteristic radiations of V^{48} growing in.

Cr^{51}, though produced in far greater yield than the Cr^{48}, will contribute only a few percent to the total gamma activity of the sample at the end of the irradiation because of its long half-life (27 days) and particular decay scheme (electron capture with a γ ray in 10% of the disintegrations).

The targets, consisting of powdered nickel metal wrapped in thin aluminum foil, were irradiated with the 380-Mev circulating proton beam of the Nevis cyclotron for about two hours. After irradiation, the powder was dissolved in nitric acid, the chromium was oxidized to chromate with persulfate, and then was extracted as peroxychromic acid with ethyl acetate. To purify the sample it was extracted twice more. After the final extraction the chromium was reduced with hydrazine to the +3 state and precipitated as the hydroxide. For the gamma-ray spectrometer samples about 1 mg of chromium +3 carrier was added initially, while for the beta-ray spectrometer sample the procedure was followed using 50 μg of carrier and the sample mounted by evaporating the final solution to dryness on a thin film.

The high purity of the sample was shown by the fact that no annihilation radiation could be detected after sufficient time had been allowed for the decay of Cr^{49}. It is to be expected that any impurity would be on the neutron deficient side of the stability line because of the relatively low neutron number of Ni^{58}.

3. GAMMA-RAY SPECTRUM

The gamma ray spectrum of the chemically separated Cr fraction was studied with an energy- and efficiency-calibrated single-channel scintillation spectrometer (resolution 9% at 661 kev). For periods up to a few hours after the end of the bombardment the spectrum showed an appreciable amount of annihilation radiation decaying with a half-life of the order of 1 hour. The same short period was also found in the decay curve followed with an end window Geiger-Muller counter. It is attributed to the presence of 42-min Cr^{49}.

Curve *a* of Fig. 1 shows the gamma-ray spectrum at ~8 hours after the end of the bombardment. Prominent peaks are evident at 116±2 (γ_1) and at 305±10 kev (γ_2), there is a much smaller peak at 420±10 kev and a small annihilation peak. No other gamma rays are seen in the decay of Cr^{48}; the bump at the low-energy side of γ_1 is at the correct energy for the associated escape peak. This run was taken with the source at a distance of

$\frac{3}{4}$ inch from the crystal. The dotted curve *b* shows the region above 350 kev with the source at only $\frac{1}{4}$ inch distance. This demonstrates that the peak at 420 kev arises mainly from pile up of the two strong gamma rays.

The peak at 305 kev is not due to Cr^{51}. The intensity is too high by about an order of magnitude, the energy compared to that of the 0.325 line in pure Cr^{51} consistently turned out to be lower by about 20 kev and its intensity relative to γ_1 did not change appreciably over the first few days. The 325-kev line due to the Cr^{51} contamination was seen only after a few days.

The relative intensities of γ_1 and γ_2 were determined within 12 hr after the end of the bombardment by comparison with Se^{75}. In the region above 250 kev the relative efficiency of the scintillation spectrometer was determined by a method described in an earlier paper.[5] The intensity of γ_1 is 90±15% of that of γ_2. It is also possible to give an upper limit of 2% for any positrons in the decay of Cr^{48} and a rough upper limit of 2% for a cross over gamma ray of 420 kev.

For one of the sources used the evolution of the scintillation spectrum was followed for a period of three weeks. The characteristic radiations of V^{48} were seen to grow in (compare Fig. 1, curve *e*). The height of the various peaks was compared to those of standard sources of Se^{75}, Cr^{51}, Na^{22}, Bi^{207}, and Co^{60}. After the peak heights of γ_1 and γ_2 are corrected for the Compton contributions due to the other gamma rays, their decay yielded a half-life of 23±1 hour for Cr^{48} over a period of 6 half-lives. The growth and decay of the peaks due to V^{48} over a period of three weeks was compatible with the expected genetic relationship between γ_1 and γ_2 on the one hand and the 0.511-, 0.99-, and 1.32-Mev lines on the other hand.

The occurrence of a strong sum pulse at 420 kev (see Fig. 1) in contrast to the absence of a sum pulse at 230 kev, indicates that γ_1 and γ_2 are probably in cascade. A coincidence experiment, using the selective coincidence scintillation spectrometer described in an earlier paper,[5] was performed. Curve *c* and *d* of Fig. 1 show that γ_1 and γ_2 are indeed in coincidence and the dropping off of the counting rate at higher energy shows that there are no other coincident gamma rays. In addition the coincidence spectrum of Se^{75} was studied under the same conditions. From a comparison of the results of these two coincidence experiments the intensity of γ_1 is 95±10% of that of γ_2. Since the resolving time of the coincidence apparatus is $\sim 10^{-7}$ sec, it is clear that the delay between γ_1 and γ_2 is certainly less than 10^{-8} sec.

TABLE I. Decay properties of Cr^{48}.

	23±1 hour No $\beta^+(0.511\gamma < 1\%)$		β 16.2-day V^{48}	
	Energy	Rel. int.	α	
γ_1	116±2 kev	95±10	0.02±1	*M*1
γ_2	305±10 kev	100	0.006±3	*E*2
	γ_1 and γ_2 are in coincidence No other γ's			

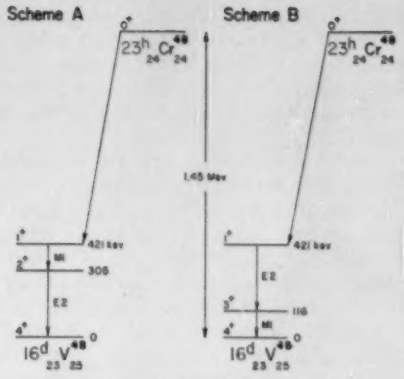

FIG. 2. Proposed decay schemes for Cr^{48}.

4. CONVERSION ELECTRON SPECTRUM

The conversion electron spectrum, studied in the Columbia solenoidal spectrometer, showed peaks corresponding to γ_1 and γ_2, but no other peaks of comparable intensity. The intensities of these two conversion peaks were compared to that due to the well-known 0.56-Mev gamma transition in Bi^{207}. The same two sources of Cr^{48} and Bi^{207} were then compared for their gamma intensities with the efficiency-calibrated scintillation spectrometer. This comparison gave conversion coefficients of $\alpha=0.02$ for the 116-kev transition and $\alpha=0.006$ for the 305-kev transition, the uncertainty amounting to 50%. This is only compatible with a dipole transition for γ_1 and a quadrupole for γ_2.

5. DISCUSSION

Taking the experimental lower limit of $\sim$50 for the ratio of electron capture to positron emission and using the graphs by Feenberg and Trigg,[6] an upper limit of 1.25 Mev can be placed on the energy difference between the initial and final states in the capture process. Assuming log $(2J_f+1)ft \geq 4.5$ for an allowed capture process (a super-allowed transition is not expected in this case), a lower limit of 0.85 Mev is found for this same energy difference.

The combined gamma (95±10) and conversion electron intensities (2±1) of γ_1 are practically equal to the total intensity of the 305-kev transition (101). The approximate equality of the two cascading gamma rays indicates that there is no appreciable electron capture to the intermediate level. This excludes an allowed transition to the intermediate state. Since only even parity states are expected in V^{48}, the intermediate level can therefore be populated only by a second or higher forbidden electron capture transition. This indi-

[5] Koerts, Macklin, Farrelly, van Lieshout, and Wu, Phys. Rev. 98, 1230 (1955).

[6] E. Feenberg and G. L. Trigg, Revs. Modern Phys. 22, 399 (1950).

cates that the electron capture takes place to the 421-kev level exclusively. From this, it follows that the mass difference between Cr^{48} and V^{48} lies between 1.25 and 1.65 Mev, compatible with the predictions of beta decay energy systematics in this region.[7] The various decay properties of Cr^{48} are listed in Table I.

The conversion coefficients limit the multipolarity of γ_1 to fairly pure $M1$ and that of γ_2 to $E2$. The order of emission of γ_1 and γ_2 is not known, but in either case rather severe restrictions can be placed on the possible spin values of the various states.

The total angular momentum carried away by the allowed electron capture process and by the gamma cascade is $J \leq 4$. This fixes the ground state spin of V^{48} as 4 and the spin of the 421-kev level as 1; spins 2 or 3 can be chosen respectively for the intermediate level for case A or case B (see Fig. 2). The branching ratio of the two possible γ transitions from the 421-kev level can be calculated using the nomogram published by Montalbetti[8] which is based on the formulas of Blatt and Weisskopf. For scheme A, the upper limit on the intensity of the cross over relative to the 116-kev transition is $\sim 1 \times 10^{-5}$, for scheme B its upper limit relative to the 305-kev transition is $\sim 1 \times 10^{-6}$. Neither of the two excited states is expected to have a half life of over 10^{-7} sec; thus the decay of Cr^{48} does not seem to lead to a metastable state of V^{48}.

From our data for the various gamma-ray intensities, it follows that for a 380-Mev proton bombardment of Ni the cross section for the production of 27-day Cr^{51} is 18 ± 2 times the cross section for the production of 23-hour Cr^{48} (assuming 10% K capture to the 0.32-Mev level in V^{51}).

[7] K. Way and M. Wood, Phys. Rev. **94**, 119 (1954).
[8] R. Montalbetti, Can. J. Phys. **30**, 660 (1953).

ACKNOWLEDGMENTS

The authors are indebted to Dr. J. M. Miller of the Chemistry Department for valuable suggestions concerning the chemical problems and to Miss B. Farrelly for her help in part of the experiments.

One of the authors (R.v.L.) wishes to thank the Netherlands Organization for Pure Research (Z.W.O.) for a grant.

PHYSICAL REVIEW VOLUME 100, NUMBER 1 OCTOBER 1, 1955

Excitation Function for the Reaction $Be^9(N^{14}, \alpha n)F^{18}$

H. L. REYNOLDS AND A. ZUCKER
Oak Ridge National Laboratory, Oak Ridge, Tennessee
(Received June 27, 1955)

The cross section for the production of F^{18} by nitrogen bombardment of beryllium was measured as a function of energy. The cross section varies from 100 to 200 millibarns at energies from 15 to 30 Mev. Below the barrier, the cross section falls off with decreasing energy in a manner which indicates a barrier penetration by the entire nucleus.

A SURVEY of nitrogen-induced nuclear reactions produced in light elements by 26-Mev nitrogen ions from the Oak Ridge National Laboratory 63-Inch Cyclotron was made by Reynolds, Scott, and Zucker.[1] The excitation functions of three nitrogen-induced reactions in carbon which result in radioactive residual nuclei were reported previously.[2] In this paper the excitation function of the reaction $Be^9(N^{14}, \alpha n)F^{18}$ is reported for energies from 6 to 29 Mev.

The experimental method is similar to that described previously.[2] Thick targets of beryllium metal were bombarded in the deflected nitrogen beam at various maximum nitrogen energies. The energy of the incident beam was varied by placing nickel foils in front of the targets. Bombardments were made in two ways. In the first method, a disk with twelve holes on the periphery, eleven of which contained beryllium and appropriate absorbers, was rotated through the beam at approximately 5 rpm. A Faraday cup was placed beyond the disk so that for each rotation of the disk the current passing through the empty hole was measured and integrated, thus determining the number of particles striking each target. Fluctuations in beam intensity were averaged out since bombardments lasted for 30 minutes or longer. After bombardment the targets were removed and the amount of 112-minute F^{18} activity was measured with shielded Geiger counters which were calibrated by standard procedures.[2]

In the second method, targets were bombarded individually inside the Faraday cup. The energy absorbers were placed inside the cup to avoid making corrections for electron charge exchange in the foils. The results from the two methods are in good agreement, as shown by the yield curve in Fig. 1. The points indicated by dots were obtained with the rotating disk while the crosses represent data obtained from the direct bombardments in the Faraday cup. The probable error in

[1] Reynolds, Scott, and Zucker, Proc. Natl. Acad. Sci. **39**, 975 (1953).
[2] H. L. Reynolds and A. Zucker, Phys. Rev. **96**, 1615 (1954).

the absolute yield is about 20%, mainly due to inaccuracies in Geiger-counter calibration. At energies below 10 Mev the errors are probably larger due to energy straggling, the 600-kev spread in the beam energy, and poorer statistics at low counting rates. The energy of the incident nitrogen ions was determined by passing the nitrogen beam into hydrogen gas and measuring the range of elastically scattered protons at zero degrees to the incident beam.[3]

The smooth curve drawn through the yields was differentiated to obtain the cross section as a function of energy, as shown in Fig. 2. The range of nitrogen in Be^9 was obtained by using the known range of nitrogen

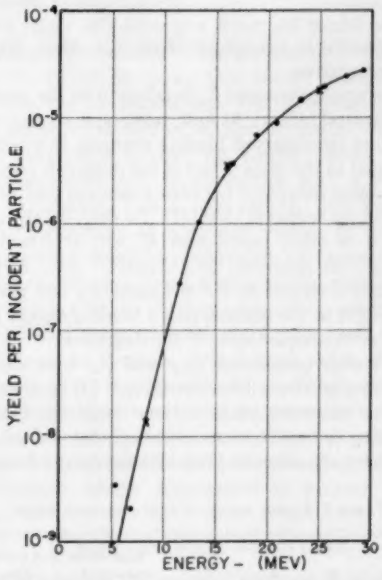

FIG. 1. Yield of the reaction $Be^9(N^{14},\alpha n)F^{18}$ as a function of energy. The dots represent runs made with the rotating disk; the crosses represent data obtained from direct bombardment in a Faraday cup.

in nickel[3] and the relative stopping power in nickel and beryllium for protons of equal velocity.

Since this reaction is detected by the F^{18} activity, it is not known if the other reaction products are He^5, or He^4 and a neutron, or both. No other reactions leading to radioactive products have been observed from the nitrogen bombardment of Be^9. This is to be expected because of the low Q-values for other reactions of this type. Of course, there are other competing reactions in

[3] Reynolds, Scott, and Zucker, Phys. Rev. **95**, 671 (1954).

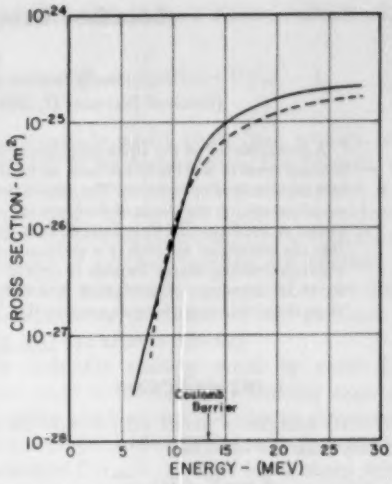

FIG. 2. Absolute cross section for the reaction $Be^9(N^{14},\alpha n)F^{18}$ as a function of the nitrogen ion energy. Solid line: experimental; dashed line: calculated.

beryllium, but they lead to stable residual nuclei which are not observed in this type of experiment.

It can be seen, from Fig. 2, that the cross section rises exponentially as the energy increases until the Coulomb barrier is reached. The shape of the curve suggests a barrier penetration phenomenon. The total cross section for the formation of the compound nucleus Na^{23} was computed from the relation

$$\sigma_T = \pi\lambda^2 \sum_l (2l+1) P_l \xi_l.$$

The penetrabilities P_l for charged-particle reactions were taken from Feshbach *et al.*[4] The sticking probability ξ_l is assumed to be unity. At maximum energy, l values as high as 13 enter into the cross section. The values for nuclear radii, 3.8×10^{-13} cm for Be^9 and 3.9×10^{-13} for N^{14}, used in this calculation were obtained from the fast neutron scattering data of Coon *et al.*[5] The dashed line in Fig. 2 represents the computed total cross section, divided by seven for purposes of normalization so that a visual comparison with the data can be made. The similarity between the data and the total cross section calculation indicates that the reaction rate is determined primarily by the entrance barrier penetration of the nuclei. The fact that the ratio of this reaction cross section to the total cross section remains nearly constant over this large an energy region is unexpected since there are many competing reactions possible.

[4] Feshbach, Shapiro, and Weisskopf, U. S. Atomic Energy Commission Report NYO-3077, 1953 (unpublished).

[5] Coon, Graves, and Barschall, Phys. Rev. **88**, 562 (1952).

Localized Orbitals in Nuclear Structure

R. K. NESBET*
Massachusetts Institute of Technology, Cambridge, Massachusetts
(Received December 17, 1954; revised manuscript received May 25, 1955)

A generalization of the alpha-particle model of nuclear structure is developed, in which even-even nuclei or inner cores of odd nuclei are built up from localized spatial cells occupied either by two neutrons or by two neutrons and two protons. The analysis used is based on general properties of solutions of Hartree-Fock equations and on the effects of configuration interaction for a neutron-proton system governed by a Hamiltonian of the form $\Sigma K(i)+\Sigma Q(i,j)$. It is not necessary to specify the operators K and Q exactly, except that the interaction operator Q is assumed to be primarily an attractive interaction of short range. A semi-empirical binding energy formula is derived which gives close agreement with observed binding energies for stable even-even nuclei lighter than Ca^{40}. For a reasonable value of a parameter not determined by these data, the energy formula predicts that Ti^{44} should be unstable.

1. INTRODUCTION

BINDING energies of nuclei with $N=Z=2m$ agree closely with the formula

$$E=mK_\alpha+kQ_{\alpha\alpha'}, \tag{1}$$

where K_α is the binding energy of a free α particle, k is the maximum total number of contacts between contiguous spheres in a cluster of m uniform spheres, and $Q_{\alpha\alpha'}$ is the energy of contact between any two contiguous spheres. This energy formula and the geometrical model of a cluster of rigid spheres are the basis of the α-particle model of nuclear structure.[1]

If nuclei for which $N=Z+2=2m$ can be thought of as clusters of rigid α-particle spheres with an additional rigid sphere which represents a neutron pair, then binding energies should be given by

$$E=(m-1)K_\alpha+K_r+(k-\bar{k})Q_{\alpha\alpha'}+\bar{k}Q_{\alpha r}. \tag{1'}$$

Here $\bar{k}$ is the number of spheres contiguous to the neutron pair, K_r is the internal energy of a neutron pair, and $Q_{\alpha r}$ is the energy of interaction between a neutron pair and a contiguous α particle. Observed binding energies of such nuclei agree closely with this formula. Table I lists calculated and observed binding energies for light even-even nuclei, expressed as mass defects $M-A$ in millimass units.

The unstable nuclei He^6, Be^8, and Be^{10} have been omitted since their observed masses deviate markedly from the energy formulas. The integers k and $\bar{k}$ for given m are determined from the simple geometrical model of a cluster of m rigid spheres. Parameter k ("contiguity") is the maximum number of contacts between contiguous spheres for given m. Parameter $\bar{k}$ is the maximum number of spheres in contact with any one sphere—a neutron pair is assigned to this position of maximum contiguity because parameter $Q_{\alpha r}$ is found to be greater in magnitude than $Q_{\alpha\alpha'}$. Both $Q_{\alpha r}$ and $Q_{\alpha\alpha'}$ are negative.

The energy parameter K_α is taken to be the mass defect of neutral helium. At first, parameter K_r was calculated from the observed binding energies. It was found to be equal to the mass defect of the deuteron, corrected for the mass difference between a neutron and neutral hydrogen, to within 0.15 mMU. To simplify the determination of other parameters K_r was arbitrarily set equal to this quantity, 15.575 mMU[2] (i.e., 2.015575 mass units if treated as the rest mass of a free system). This assigns to the neutron pair a binding energy equal to that of the triplet state of the deuteron.

The energy parameters $Q_{\alpha\alpha'}$ and $Q_{\alpha r}$ were assigned values obtained from formulas (1) and (2) by averaging over the observed mass defects listed in Table I. Calculated energies were obtained by substituting these energy parameters back into the energy formulas.

TABLE I. Atomic masses of light even-even nuclei.

Nucleus	m	k	$\bar{k}$	Mass defect $M-A$ (mMU) calculated	observed
He^4	1	0			3.873[a]
C^{12}	3	3		3.9	3.804[a]
C^{14}	4	6	3	7.6	7.682[a]
O^{16}	4	6		0.1	0.000[a]
O^{18}	5	8	4	5.0	4.857[b]
Ne^{20}	5	8		− 1.2	− 1.223[b]
Ne^{22}	6	12	4	− 1.4	− 1.642[b]
Mg^{24}	6	12		− 7.6	− 7.372[b]
Mg^{26}	7	16	6	−10.6	− 9.198[b]
Si^{28}	7	16		−14.0	−14.233[b]
Si^{30}	8	19	7	−15.8	−16.763[b]
S^{32}	8	19		−17.8	−17.817[b]
S^{34}	9	22	8	−21.0	−21.227[c]
A^{36}	9	22		−21.7	−21.070[c]
A^{38}	10	25	8	−24.9	−25.122[c]
Ca^{40}	10	25		−25.5	−24.580[c]
Ca^{42}	11	27	10	−28.9	−27.964[c]
Ca^{44}	12	33	8, 8	−33.0	−30.80[c]
Ti^{44}	11	29		−31.9	···

[a] C. W. Li, Phys. Rev. **83**, 512 (1951).
[b] C. W. Li, Phys. Rev. **88**, 1038 (1952).
[c] K. T. Bainbridge, *Experimental Nuclear Physics*, edited by E. Segrè (John Wiley and Sons, Inc., New York, 1953), Vol. I, Part V. Data from Table 16, pp. 745–758.

* Staff Member, Lincoln Laboratory, Massachusetts Institute of Technology, Cambridge, Massachusetts.

[1] W. Wefelmeier, Z. Physik **105**, 557 (1937); L. Hafstad and E. Teller, Phys. Rev. **54**, 681 (1938); J. Wheeler, Phys. Rev. **52**, 1083 (1937); E. Teller and J. Wheeler, Phys. Rev. **53**, 778 (1938); D. M. Dennison, Phys. Rev. **57**, 474 (1940); H. H. Haefner, Revs. Modern Phys. **23**, 228 (1951).

[2] C. W. Li, Phys. Rev. **83**, 512 (1951).

The energy parameters are assigned the following values:

$$\begin{aligned} K_\alpha &= \ \ 3.873\ \text{mMU}, \\ K_\nu &= \ \ 15.575\ \text{mMU}, \\ Q_{\alpha\alpha'} &= -2.57\ \text{mMU}, \\ Q_{\alpha\nu} &= -3.95\ \text{mMU}. \end{aligned} \tag{2}$$

In the case $m=5$ the geometrical structure assumed in earlier work[1] has contiguity $k=9$, appropriate to a trigonal bipyramid. This causes an anomoly in the calculated results for both Ne^{20} and O^{18} which can be resolved by using the contiguity appropriate to a tetragonal pyramid, $k=8$.

This paper will develop a structural model of nuclei and discuss the validity of energy formulas such as (1) and (1′). It will be shown that energy expressions of this form can be derived from the energy mean value of a linear combination of determinantal functions which takes into account the largest effects of configuration interaction, in connection with a Hartree-Fock calculation. This is only strictly true when the single determinant of minimum energy is invariant under spatial rotations; otherwise the energy mean value includes a rotational energy which cannot necessarily be described by the formulas under consideration. The fact that the parameters K_α, K_ν, $Q_{\alpha\alpha'}$, and $Q_{\alpha\nu}$ can be taken to be constant over a large range of nuclei follows from the argument to be given here if energy effects due to distortion of the structural units (α particles or neutron pairs) are small and if rotational energy effects are small for the Hartree-Fock functions of minimum energy appropriate to nuclear ground states.

2. NUCLEAR WAVE FUNCTIONS

If it is assumed that nuclear structure is determined by a Hamiltonian operator of the form

$$H' = \sum_{i=1}^{A} K'(i) + \sum_{i>j} Q'(i,j), \tag{3}$$

then the empirical correlations of the α-particle model suggest that eigenfunctions of this operator may be found by methods similar to those used in molecular spectroscopy. The corresponding molecular Hamiltonian is

$$H_m = -\sum_{\alpha=1}^{N} \frac{\hbar^2}{2M_\alpha}\nabla_\alpha^2 + \sum_{\alpha>\beta} \frac{e^2 Z_\alpha Z_\beta}{r_{\alpha\beta}} + E_e(\mathbf{r}_\alpha, \cdots), \tag{4}$$

where $E_e(\mathbf{r}_\alpha, \cdots)$ is the total electronic energy for a given configuration of nuclei. The Hamiltonian (4) describes the motion of nuclei only; all effects of electronic motion have been replaced by a potential function E_e, which can depend only on the relative separations of the nuclei. Hence if $T(\alpha) = -(\hbar^2/2M_\alpha)\nabla_\alpha^2$ then

$$H_m = \sum_{\alpha=1}^{N} T(\alpha) + U(r_{\alpha\beta}, \cdots). \tag{5}$$

The α-particle model arises from analogy between (3) and (5). If the nuclear interaction potential $Q'(i,j)$ represents an attraction at short range which is essentially the same for any two nucleons, a nuclear wave function will have maximum amplitude when the spatial coordinates of any four particles are identical, if the four possible spin-isotopic spin variables are different. By antisymmetry, a cluster of four particles is the largest that can arise in this way.

The molecular analogy would be valid if these clusters could be treated as interacting mass points, held rigidly apart at definite relative distances. This structural property of molecules arises from the form of the potential $U(r_{\alpha\beta}, \cdots)$, which has a sharp minimum value at certain internuclear distances, and becomes a repulsion at distances still very large compared with the effective nuclear radii. In contrast, the nuclear interaction operator $Q'(i,j)$ is presumably attractive for all internucleon separations small enough that specifically nuclear effects predominate over the Coulomb interaction. Even if $Q'(i,j)$ should have a "hard core" and a minimum value for some nonzero separation, this would determine the average relative separation of nucleons within an α-particle cluster rather than the intercluster separation. For reasonable values of the kinetic energy the nucleons making up an α-particle cluster have appreciable probability density in regions occupied by neighboring α particles. The rigid intercluster separations required by the α-particle model must be attributed to the exclusion principle, acting through the requirement that a wave function be totally antisymmetric in the coordinates of indistinguishable particles (fermions). This does not rule out a possible structural similarity between nuclei and molecules, but it indicates that it is fallacious to apply the perturbation methods of molecular spectroscopy to nuclei without further *a priori* analysis.

A systematic way of constructing totally antisymmetric wave functions can be developed from analysis of general properties of solutions of Hartree-Fock equations and the effects of configuration interaction.[2] An approximate wave function is built up by linear superposition of Slater determinants (*detors*) chosen from a complete set of single-particle functions (*orbitals*). The orbitals from which a given detor is constructed will be called the *occupied orbitals* of that

[2] L. Brillouin, *Les Champs self-consistent de Hartree et de Fock* (Hermann et Cie., Paris, 1934), No. 159 in series: Actualités Scientifiques et Industrielles; C. Møller and M. S. Plesset, Phys. Rev. **46**, 618 (1934); R. K. Nesbet, Proc. Roy. Soc. (London) **A230**, 312 (1955).

detor. In order to reduce the effects of configuration interaction, the complete set of orbitals can be chosen to include a subset of A orbitals (for a system of A nucleons) which are occupied orbitals of a detor Φ_0 of minimum energy. These orbitals satisfy Hartree-Fock equations of the form

$$\mathcal{H}_0\phi_i = \sum_{j=1}^{A} \epsilon_{ij}\phi_j; \quad i=1,\cdots,A. \tag{6}$$

Here $\mathcal{H}_0$ is an Hermitian operator (the *single-particle Hamiltonian* for Φ_0) constructed from the occupied orbitals of Φ_0. Under any unitary transformation of the occupied orbitals, Φ_0 is invariant except for a unit phase factor and $\mathcal{H}_0$ is invariant. Since $\mathcal{H}_0$ is Hermitian, there is some unitary transformation which diagonalizes the matrix $[\epsilon_{ij}]$, so the Hartree-Fock equations (for a single detor Φ_0) can be put into the canonical form

$$\mathcal{H}_0\phi_i = \epsilon_i\phi_i. \tag{7}$$

From Eqs. (7) it is clear that if $\mathcal{H}_0$ is invariant under some group of symmetry operations (which may include spin or isotopic spin rotations as well as rotation or inversion in ordinary space) then the canonical occupied orbitals of Φ_0 can be classified as basis elements of irreducible representations of this group. Moreover, since $\mathcal{H}_0$ is invariant under this group, the occupied orbitals must transform into themselves under all operations of the group. More precisely, the occupied orbitals span a unitary representation of the symmetry group. Occupied orbitals which satisfy Eqs. (6) span reducible representations in general, but in the canonical form (7) the representations are irreducible. In more physical language, the occupied orbitals of Φ_0 fill closed shells with respect to the invariance group of $\mathcal{H}_0$.

There is no *a priori* reason, however, why the group of $\mathcal{H}_0$ should be the full rotation-inversion group. This means that the canonical Hartree-Fock orbitals cannot in general be assigned an angular quantum number l or j, unless the occupied orbitals fill closed l-shells or j-shells, respectively.

The ground-state eigenfunction of the many-particle Hamiltonian H' can be expanded as a linear combination of detors chosen from a complete set. Consider the complete set of detors obtained from the Hartree-Fock detor Φ_0 by replacing occupied orbitals by other orbitals from a complete orthonormal set. Let $H_{\nu 0}$ be a matrix element of the many-particle Hamiltonian between Φ_0 and some other detor Φ_ν chosen from the complete set. It can be shown[3] that under the conditions (6) or (7) all matrix elements $H_{\nu 0}$ vanish unless Φ_ν is obtained from Φ_0 by replacing just two occupied orbitals. This is true if any unitary transformation of orbitals is made which does not mix occupied orbitals with the remaining members of the complete set. By second-order perturbation theory, if the Hartree-Fock detor is not degenerate, the coefficients of perturbing detors in expansion of an exact wave function are

$$\frac{-H_{\nu 0}}{H_{\nu\nu}-H_{00}} = \frac{-1}{H_{\nu\nu}-H_{00}}\left\{\int d\tau_1 \int d\tau_2 \phi_j(1)\phi_{k\nu}^*(2) \times Q'(1,2)\phi_j(1)\phi_k(2) - \int d\tau_1 \int d\tau_2 \phi_j(1)\phi_{k\nu}^*(2) \times \phi_{k\nu}^*(2)Q'(1,2)\phi_k(1)\phi_j(2)\right\}. \tag{8}$$

Here detor Φ_ν is obtained from Φ_0 by replacing two occupied orbitals ϕ_j,ϕ_k by orthogonal orbitals $\phi_{j\nu}$, $\phi_{k\nu}$. If $Q'(i,j)$ is a potential operator of short range spatial dependence then the integrals in the numerator of (8) will be large only when the orbitals ϕ_j, $\phi_{j\nu}$, ϕ_k, and $\phi_{k\nu}$ are all spatially dense in a volume comparable to that occupied by a single α particle. Since all four orbitals must be orthogonal there can only be a limited number of orbitals $\phi_{j\nu}$ and $\phi_{k\nu}$ with this property which do not also have so many nodes in the region occupied by ϕ_j and ϕ_k that the energy differences $H_{\nu\nu}-H_{00}$ become large.

The numerators of (8) can be maximized by making a transformation of occupied orbitals which localizes them as much as possible, and by choosing the unoccupied orthogonal orbitals to be similarly localized. Properties of a special class of such transformations of occupied orbitals have been analyzed in detail by Lennard-Jones *et al.*, with reference to molecular electronic wave functions.[4]

Except for effects due to degeneracy, it should be a good approximation to neglect all coefficients (8) arising from simultaneous changes of orbitals which are orthogonal primarily because of spatial localization. If the occupied orbitals of Φ_0 can be transformed into sets of two (for neutron pairs) or four (for α-particle structures) which have similar spatial localization, then a set of localized spatial cells are defined. The approximation suggested here is to neglect all terms (8) arising from substitutions which mix orbitals in different spatial cells. This approximation will be used in Sec. 3 to derive an energy formula which includes (1) and (1′) as special cases.

There are two types of degeneracy which can lead to significant energy effects. The first is due to localization of the wave function as a whole. For bound states the Hartree-Fock detor Φ_0 will be constructed from quadratically integrable orbitals and will itself be quadratically integrable with a fixed center of mass. Hence Φ_0 is not invariant under translation. No finite linear combination of quadratically integrable detors can be an eigenfunction of total linear momentum; this introduces a spurious kinetic energy of localization, since the mean

[4] J. E. Lennard-Jones, Proc. Roy. Soc. (London) **A198**, 1, 14 (1949); G. G. Hall and J. E. Lennard-Jones, Proc. Roy. Soc. (London) **A202**, 155 (1950); J. E. Lennard-Jones and J. A. Pople, Proc. Roy. Soc. (London) **A202**, 166 (1950); and later papers in this series.

value of the kinetic energy of the mass center, $T(\mathbf{P})$, cannot vanish for a localized function. Following Inglis,[5] the Hamiltonian (3) should be replaced by

$$H=H'-T(\mathbf{P})=\sum_{i=1}^{A} K(i)+\sum_{i>j} Q(i,j). \tag{9}$$

This defines new operators K and Q. Interactions in $T(\mathbf{P})$ which involve more than two particles have been neglected. In the nonrelativistic case

$$T(\mathbf{P})=\frac{1}{2M}\mathbf{P}^2=-\frac{\hbar^2}{2M}\sum_i \nabla_i^2-\frac{\hbar^2}{M}\sum_{i>j}(\nabla_i)\cdot(\nabla_j),$$

where M is the total mass of the system.

Since H and $T(\mathbf{P})$ commute, it is adequate to calculate eigenfunctions of H rather than of H'. The modified Hamiltonian H can have integrable eigenfunctions, expressed as wave packets in the coordinates of the center of mass.

It is much more difficult to deal with the energy effect due to orientation, when the Hartree-Fock detor is not invariant under rotation. There is then a spurious rotational kinetic energy and a potential energy due to centrifugal distortion. In principle this energy can be recovered by averaging an oriented function over all directions. One procedure for doing this is to expand all orbitals in terms of a single orthonormal set of orbitals which are eigenfunctions of angular momentum, expressed as radial functions multiplied by spherical harmonics and by the elementary spin and isotopic spin eigenfunctions. Any detor constructed from the original orbitals can be represented as a linear combination of detors whose occupied orbitals are eigenfunctions of angular momentum. By standard vector-coupling methods linear combinations of detors of this kind can be formed which are eigenfunctions of total angular momentum. Unless the occupied orbitals of Φ_0 and of the perturbing detors of greatest weight in configuration interaction can each be approximated by a relatively small number of different functions from the set of angular momentum eigenfunctions, this expansion procedure can become too complicated to be practically useful.

The kinetic energy of rotation cannot be represented by an operator which commutes with the total Hamiltonian. Even an approximate rotational operator such as

$$T(\mathbf{L})=\sum_{\mu}\frac{1}{2\sum M_i\rho_{\mu i}^2}L_\mu^2,$$

where $\rho_{xi}^2=x_i^2+y_i^2$, etc.; $\mu=x, y, z$, cannot be represented as a sum of one- and two-particle operators. Hence Inglis' method for dealing with $T(\mathbf{P})$ cannot be used with $T(\mathbf{L})$. For this reason the energy formulas to be derived in Sec. 3 do not take account of this energy of orientation.

[5] D. R. Inglis, Phys. Rev. 51, 531 (1937).

3. ENERGY FORMULA

An expression will be derived for the total energy of an approximate nuclear wave function Ψ_0 constructed from some detor Φ_0 of minimum energy. It is assumed that the occupied orbitals of Φ_0 can be transformed into spatially localized orbitals which define a set of localized spatial cells. Each spatial cell is occupied by no more than four particles.

The following notation will be used for integrals, where the integration includes summation over all discrete variables[6]:

$$(Q|^{i}_{j}|^{k}_{l})\equiv\int d\tau_1\int d\tau_2\phi_i^*(1)\phi_k^*(2)Q(1,2)\phi_j(1)\phi_l(2),$$

$$(R|^{i}_{j}|^{k}_{l})\equiv(Q|^{i}_{j}|^{k}_{l})-(Q|^{i}_{l}|^{k}_{j}),$$

$$(K|^{i}_{j})\equiv\int d\tau_1\phi_i^*(1)K(1)\phi_j(1).$$

The approximate wave function Ψ_0 is a linear combination of detors which will be denoted $\Phi_{\alpha\beta}$. Index β specifies a particular localized spatial cell. Index α determines a pair of indices k, l for two occupied orbitals in cell β of the Hartree-Fock detor Φ_0. The occupied orbitals $\phi_{k\beta}$ and $\phi_{l\beta}$ of Φ_0 are replaced by two orbitals $\phi_{h\alpha\beta}$ and $\phi_{l'\alpha\beta}$ in the detor $\Phi_{\alpha\beta}$. Detors Φ_α which differ from Φ_0 by only a single orbital are omitted from Ψ_0, since Φ_0 is assumed to have minimum energy and this implies that all matrix elements $H_{\alpha 0}$ vanish. Coefficients c_α of the detors $\Phi_{\alpha\beta}$ can be estimated by the perturbation formula (8). The coefficients can be determined more exactly by minimizing the energy of

$$\Psi_0=c_0\Phi_0+\sum_{\alpha>0}c_\alpha\Phi_{\alpha\beta}.$$

The energy mean value for Ψ_0 is

$$\begin{aligned}E&=\sum_\alpha|c_\alpha|^2H_{\alpha\alpha}+2\,\mathrm{Re}\sum_{\alpha>\alpha'}c_\alpha^*c_{\alpha'}H_{\alpha\alpha'}\\&=\sum_\beta K_\beta+\sum_{\beta>\beta'}Q_{\beta\beta'},\end{aligned}\tag{10}$$

where

$$\begin{aligned}K_\beta=\sum_\alpha|c_\alpha|^2\Big[&\sum_j(K|^{i\alpha\beta}_{j\alpha\beta})+\sum_{j>j'}(R|^{i\alpha\beta}_{j\alpha\beta}|^{i'\alpha\beta}_{j'\alpha\beta})\Big]\\&+2\,\mathrm{Re}\sum_{\alpha>\alpha'>0}c_\alpha^*c_{\alpha'}\delta_{\beta\beta'}H_{\alpha\beta,\alpha'\beta}\\&+2\,\mathrm{Re}\sum_{\alpha>0}c_\alpha^*c_0(R|^{h\alpha\beta}_{h\beta}|^{l\alpha\beta}_{l\beta}).\end{aligned}$$

[6] This notation differs from the usual Dirac notation in that indices referring to complex conjugate orbitals, not acted upon by the operator, are raised and placed after the operator as superscripts. Thus $(ik|Q|jl)$ is written $(Q|^{i}_{j}|^{k}_{l})$. This notation is used here to be consistent with reference 8, where it was introduced to facilitate a general discussion of the configuration interaction problem.

and

$$Q_{\beta\beta'}=\sum_{\alpha}|c_{\alpha}|^{2}\sum_{j}\sum_{j'}(R|{}^{k\alpha\beta}{}_{j\alpha\beta}|{}^{j'\alpha\beta'}{}_{j'\alpha\beta'}). \quad (11)$$

Matrix elements $H_{\alpha\beta,\alpha'\beta}$ either vanish or are of the form $(R|{}^{k\alpha\beta}{}_{k\beta}|{}^{l\beta}{}_{l\alpha'\beta})$ or $(R|{}^{k\alpha\beta}{}_{k\alpha'\beta}|{}^{l\alpha\beta}{}_{l\alpha'\beta})$. These expressions follow from the usual formulas for matrix elements between detors,[7] taking account of the fact that any two detors $\Phi_{\alpha\beta}$ and $\Phi_{\alpha'\beta'}$ of the set under consideration must differ by four orbitals when $\beta\neq\beta'$ and $\alpha,\alpha'\neq 0$.

It should be emphasized that only three assumptions have been made in deriving this formula:

First, it is assumed that occupied orbitals of the detor of minimum energy can be transformed into orbitals which are spatially localized and represent spatial cells occupied by four or less particles. The degree of localization must be sufficient to allow neglect of quantities of the form (8), in which the numerators are double-exchange integrals (integrals involving four orthonormal orbitals), when the orbitals are taken from two different spatial cells.

Second, the approximate wave function Ψ_0 will in general be an oriented function. Energy effects arising from orientation (which introduces a spurious kinetic energy of rotation and a change in potential energy due to centrifugal distortion) cannot be represented by an expression of the form (10). Hence to use this energy formula without modification it must be assumed that energy effects due to orientation are small.

Third, it is assumed that except for degeneracies arising from orientation all detors which have zero coefficients in the second-order perturbation expansion of Ψ_0 can be neglected in configuration interaction.

The first assumption would seem to be a natural consequence of an attractive nuclear interaction potential of short range. Particles are prevented from collapsing together by the increase of kinetic energy as spatial orbitals become more concentrated or have nodes in regions of high density. The exclusion principle acts through the requirement that all orbitals be orthogonal. The structure of minimum energy would be one which superimposed as many particles as possible in spatial orbitals without nodes in their regions of greatest density. Except for spin or isotopic spin orthogonality, the orbitals should be mutually orthogonal primarily because maximum spatial densities occur in different spatial cells. A "hard core" in the interaction potential would not change this qualitative behavior, except possibly to make individual spatial cells less compact.

The terms of the energy formula (10) can be classified into those occurring within the same cell, between contiguous cells, and between distant cells. For an interaction operator of sufficiently short range, the interaction energy $Q_{\beta\beta'}$ between spatial cells which are not contiguous should be negligible. If the structure within each spatial cell, due to the large binding energy of attracting particles in superimposed spatial orbitals, is insensitive to the structure of other spatial cells, then the parameters K_β will depend only on the type of particle occupying cell β, and parameter $Q_{\beta\beta'}$ for contiguous cells should depend only on the nature of the two cells. For light even-even nuclei, these further assumptions reduce the energy formula (10) to the two expressions (1) and (1′), which are found to be consistent with observed nuclear binding energies over the range of data given in Table I.

A test of internal consistency is given by considering the consequences of assuming that $Q(i,j)$ is strictly spin- and charge-symmetric. In this case there is no distinction between neutron and proton, and for $N=Z$ the detor Φ_0 will be a spin and charge singlet. The occupied orbitals of Φ_0 can be represented as a number of localized orthogonal spatial functions, each multiplied by the four orthogonal spin-isotopic spin functions. In configuration interaction, coefficients c_α will be equal for all of the six degenerate detors which can be constructed from Φ_0 by double substitution of orbitals with the same spatial factor. This is also true for the set of twelve degenerate detors obtained by double substitution of orbitals with two different spatial factors. Since all c_α are equal in either of these cases, the approximate eigenfunction will also be a spin and charge singlet. If $N=Z+2$, neither Φ_0 nor Ψ_0 can be exact eigenfunctions of total isotopic spin, but the deviation from isotopic spin eigenfunctions depends on integrals over orbitals in two different spatial cells. Under the assumptions already made in deriving formula (10) these quantities can be neglected.

If $Q(i,j)$ is the charge-symmetric operator

$$Q(i,j)=[a_0+a_\sigma\sigma_i\cdot\sigma_j+a_\tau\tau_i\cdot\tau_j+a_{\sigma\tau}(\sigma_i\cdot\sigma_j)(\tau_i\cdot\tau_j)]\bar{Q}_{ij},$$

then explicit expressions can be derived for the energy parameters of formulas (1) and (1′).

By (11), for the single detor Φ_0,

$$\begin{aligned}
K_\alpha&=2(K_p|{}^{\alpha}{}_{\alpha})+2(K_n|{}^{\alpha}{}_{\alpha})\\
&\quad+(6a_0-6a_\sigma-6a_\tau-18a_{\sigma\tau})(\bar{Q}|{}^{\alpha}{}_{\alpha}|{}^{\alpha}{}_{\alpha}),\\
K_\nu&=2(K_n|{}^{\nu}{}_{\nu})+(a_0-3a_\sigma+a_\tau-3a_{\sigma\tau})(\bar{Q}|{}^{\nu}{}_{\nu}|{}^{\nu}{}_{\nu}),\\
Q_{\alpha\alpha'}&=16a_0(\bar{Q}|{}^{\alpha}{}_{\alpha}|{}^{\alpha'}{}_{\alpha'})\\
&\quad-(4a_0+12a_\sigma+12a_\tau+36a_{\sigma\tau})(\bar{Q}|{}^{\alpha}{}_{\alpha'}|{}^{\alpha'}{}_{\alpha}), \quad (12)\\
Q_{\alpha\nu}&=8a_0(\bar{Q}|{}^{\alpha}{}_{\alpha}|{}^{\nu}{}_{\nu})\\
&\quad-(2a_0+6a_\sigma+6a_\tau+18a_{\sigma\tau})(\bar{Q}|{}^{\alpha}{}_{\nu}|{}^{\nu}{}_{\alpha}),\\
Q_{\nu\nu'}&=(4a_0+4a_\tau)(\bar{Q}|{}^{\nu}{}_{\nu}|{}^{\nu'}{}_{\nu'})\\
&\quad-(2a_0+6a_\sigma+2a_\tau+6a_{\sigma\tau})(\bar{Q}|{}^{\nu}{}_{\nu'}|{}^{\nu'}{}_{\nu}).
\end{aligned}$$

The indices α, ν refer to localized spatial orbitals. Similar relations are obtained for Ψ_0, if Φ_0 is a spin and isotopic spin eigenfunction. If α and ν cells are spatially similar these formulas imply that

$$Q_{\alpha\alpha'}=2Q_{\alpha\nu}. \quad (13)$$

[7] E. U. Condon and G. H. Shortley, *The Theory of Atomic Spectra* (The University Press, Cambridge, 1951), pp. 169–174.

This relation holds for the approximate wave function Ψ_0 if in the case $N=Z+2$ the deviation of Φ_0 and Ψ_0 from eigenfunctions of total isotopic spin is neglected.

The relation (13) does not agree with the semi-empirical parameter values (2). The simplest charge-dependent operator which might be considered is

$$Q(i,j)=S(i,j)+e_ie_jC(i,j),$$

where $S(i,j)$ is charge-symmetric and $C(i,j)$ is an ordinary potential. The symbol e is a charge operator with dimensionless eigenvalues 1 and 0, respectively, in proton and neutron states. This allows for the ordinary Coulomb interaction but does not exclude some other charge-dependent effect of short range. If configuration interaction is neglected and α- and ν-localized orbitals are spatially identical, Eqs. (11) and (12) require that

$$Q_{\alpha\alpha'}=S_{\alpha\alpha'}+4(C|^{\alpha}{}_{\alpha}|^{\alpha'}{}_{\alpha'})-2(C|^{\alpha}{}_{\alpha'}|^{\alpha'}{}_{\alpha}),$$
$$Q_{\alpha\nu}=\tfrac{1}{2}S_{\alpha\alpha'}.$$

Then from the parameter values (2),

$$(C|^{\alpha}{}_{\alpha}|^{\alpha'}{}_{\alpha'})-\tfrac{1}{2}(C|^{\alpha}{}_{\alpha'}|^{\alpha'}{}_{\alpha})=1.44\text{ mMU}. \quad (14)$$

For comparison, the Coulomb repulsion energy between two electron charges 10^{-13} cm apart is 1.54 mMU. This establishes the consistency of the values (2) found for energy parameters with the assumption that the interaction operator $Q'(i,j)$ is a charge-symmetric attraction of short range, modified by the ordinary Coulomb potential.

If $S(i,j)$ were an ordinary potential, then

$$(\bar{S}|^{\alpha}{}_{\alpha}|^{\alpha'}{}_{\alpha'})-\tfrac{1}{4}(\bar{S}|^{\alpha}{}_{\alpha'}|^{\alpha'}{}_{\alpha})=-0.494\text{ mMU}. \quad (15)$$

If $S(i,j)$ were a pure Majorana operator,

$$(\bar{S}|^{\alpha}{}_{\alpha'}|^{\alpha'}{}_{\alpha})-\tfrac{1}{4}(\bar{S}|^{\alpha}{}_{\alpha}|^{\alpha'}{}_{\alpha'})=-0.494\text{ mMU}. \quad (15')$$

Another relationship which can be derived from (12), assuming a δ-function potential and neglecting configuration interaction, is

$$Q_{\nu\nu'}=\tfrac{1}{2}Q_{\alpha\nu}+4(a_\nu-a_\alpha)(\bar{Q}|^{\nu}{}_{\nu}|^{\nu'}{}_{\nu'}). \quad (16)$$

This is still valid when a Coulomb potential is included. If $a_\nu=a_\alpha$, then

$$Q_{\nu\nu'}=\tfrac{1}{2}Q_{\alpha\nu}=-1.32\text{ mMU}. \quad (17)$$

Mass defects for the unstable nucleus Ti^{44} and its isobar Ca^{44} have been calculated using the value -1.32 mMU for $Q_{\nu\nu'}$ and are included in Table I. If 1.10 mMU is subtracted from the energy of Ti^{44} for the two electrons included in the neutral atom the calculated mass defects become equal for these two isobars. The structure of maximum contiguity for $m=11$ (number of spatial cells) is rather unsymmetrical and might not correspond to a possible model. If so, the value $k=29$ is too large and the mass difference between Ti^{44} and Ca^{44} would be even larger than that calculated. Since contiguity increases more rapidly than the number of spatial cells in this range there should be no stable nuclei heavier than Ca^{40} for which $N=Z$, since it is energetically profitable to expand an α cell into two contiguous ν cells in a structure of sufficiently high contiguity. This follows from the energy parameters (2), which indicate that the binding energy between two α cells is less in magnitude than that between a ν cell and an α cell.

4. STRUCTURE OF ODD NUCLEI

If a single neutron is added to a structure of α cells and neutron pairs, then by orthogonality the additional orbital must have a node in each cell already occupied, or else it must be outside all cells. The additional orbital can be concentrated in a region of small volume or superimposed on occupied cells only at the expense of an increase in kinetic energy. The fact that He^5 is not stable indicates that the kinetic energy due to an extra node in an orbital concentrated within an α cell more than compensates for the potential energy of interaction between this orbital and the wave function describing the α cell. Hence in general an additional neutron must be thought of as occupying a diffuse orbital.

If the core structure (α and ν cells) is oriented, then the orientation must be resolved by vector-coupling or by averaging over a sphere. Vector-coupling will project the entire function Ψ_0 onto an irreducible representation of the rotation group (an eigenfunction of angular momentum). This process may cause some mixing between a single diffuse orbital and the core structure. In some cases it may be possible to describe the vector-coupled angular momentum eigenfunction in terms of a single diffuse orbital orthogonal to the spherically symmetrical core obtained by spherically averaging an oriented core.

Occupied orbitals of a detor of lowest energy should fall into two categories: the majority can be transformed into a localized structure, leading to important configuration interaction effects and a core energy given by formula (10). The remaining occupied orbitals are diffuse. Since the numerator of (8) is relatively small for diffuse orbitals, configuration interaction will be less important for these orbitals unless there are degeneracies or near degeneracies which also make the denominator of (8) small.

In correlating the binding energies of light nuclei by formula (10), it was not found possible to obtain a consistent parametrization of energies for localized cells other than α particles and neutron pairs. This is consistent with the relative magnitude of binding energies between charged and uncharged particles in contiguous cells found in Sec. 3. It seems reasonable that the relatively strong Coulomb interaction (14) between contiguous cells can be balanced by the nuclear attractive potential (15) only when enough neutrons and protons are present to make α cells possible. A single neutron orbital should be diffuse because of the kinetic

energy effect, and protons not in α cells are assigned to external diffuse orbitals because of the Coulomb repulsion.

The physical model of nuclear structure described here is consistent with the α particle and neutron pair energy formulas as well as with the currently accepted form of the independent-particle model, for light nuclei. The latter has been used largely to correlate nuclear spins and moments, and attributes these effects to a relatively small number of particles in diffuse orbitals outside a spherically symmetrical core. The present analysis indicates that when configuration interaction is taken into account the core may be adequately described as a structure built up from localized cells. The fact that this structure will in general be oriented rather than spherically symmetrical, and must be resolved into spherical symmetry by an operation which is difficult to describe either mathematically or physically, should be taken into account when using the independent-particle model.

If the independent-particle model is based on the Hartree-Fock equations, there is a systematic way to estimate and calculate the effects of configuration interaction. Any restriction on the exact solution of Hartree-Fock equations for a single detor introduces configuration interaction effects.[8] Unless these are shown to be small, the independent-particle approximation may lead to a fallacious interpretation of nuclear structure.

One form of the Hartree-Fock method is based on minimizing the energy of a certain linear combination of detors which is an eigenfunction of total angular momentum. Occupied orbitals are constrained to be eigenfunctions of angular momentum (either with space and spin angular momentum treated separately, in *LS*-coupling, or together, in *jj*-coupling). One possible explanation of the correlation of nuclear binding energies given by the α-particle or neutron pair model is that except for the light nuclei, He^6, Be^8, and Be^{10}, energy effects due to orientation are small compared with the effect of localization of spatial cells. When this is true, it may be a bad approximation to constrain orbitals in the independent-particle model to be eigenfunctions of angular momentum, unless the occupied orbitals of the detor of lowest energy, under this constraint, fill closed shells of spherical harmonics which allow a transformation to localized orbitals. In *jj*-coupling, spatial shells of spherical harmonics are filled only if for given l both j-shells, $j=l\pm\frac{1}{2}$, are filled and if all functions in both j-shells have the same radial factors.

5. DISCUSSION

If the argument of Sec. 4 is valid, then heavier nuclei should consist of a core which can be described by the neutron pair model, with binding energy given by formulas similar to (1) and (1′) with a correction for the Coulomb repulsion between distant orbitals, together with a relatively small number of external diffuse orbitals. It should be possible to account for the stability properties of heavier nuclei on the basis of the neutron pair model and the values of energy parameters found for light nuclei.

The values found for individual integrals in Sec. 3 [(14), (15), and (15′)] indicate that the nuclear attractive potential must die away very rapidly at distances greater than the radius of an α particle. Hence the energy formulas (1) or (1′) lead to the nuclear saturation property if the internal energy of an α cell is independent of the total number of particles present. This requires that the internal energy of an α cell be sufficiently sensitive to distortion of the cell to prevent the effective radius from being altered by interaction with neighboring cells. The balance between kinetic and potential energy must be such that contiguous cells are kept separate.

A sufficient condition for instability of an infinite nucleus built entirely from neutron pairs, assumed to be a closed-packed structure of rigid spherical ν cells, is

$$2K_\nu+23Q_{\nu\nu'}>K_\alpha+12Q_{\alpha\nu}. \tag{18}$$

This follows from the energy change required to condense two interior ν cells into a single α cell. With energy parameters other than $Q_{\nu\nu'}$ taken from (2), this implies

$$Q_{\nu\nu'}>-3.24\ \text{mMU}, \tag{19}$$

or from (16), for a δ-function interaction,

$$(a_\tau-a_\nu)(\bar{Q}|^{\nu}{}_{\nu}|^{\nu'}{}_{\nu'})>-0.48\ \text{mMU}. \tag{20}$$

Apart from this condition the energy formulas (1) and (1′) give no information on the exchange character of the nuclear interaction, since they are based on a model which incorporates the saturation property *ab initio*.

The relationship between parameter K_ν and the binding energy of the deuteron, pointed out in Sec. 1, which could be interpreted to mean that the singlet state of the neutron pair has the same binding energy as the triplet state of the deuteron, was found only after K_ν had been derived without reference to the deuteron. This does not necessarily imply that a stable neutron pair must exist, for the ν cell occurs within a larger nucleus and is stabilized by interaction with its environment. Presumably an isolated neutron pair would decay rapidly by β emission into a deuteron. The apparent equality of binding energies is not easily explained. For the purposes of this paper K_ν is to be considered a purely empirical parameter defined only for observed nuclei heavier than C^{12}.

The author is indebted to Dr. N. Kemmer for discussions on several problems connected with this work. He is also grateful to the National Science Foundation for the grant of a Predoctoral Fellowship. This paper is part of a doctoral dissertation submitted to the University of Cambridge, England.

[8] R. K. Nesbet, Proc. Roy. Soc. (London) **A230**, 312 (1955).

d,p Reactions from C^{12} and C^{13}†

J. N. McGruer, E. K. Warburton, and R. S. Bender
University of Pittsburgh, Pittsburgh, Pennsylvania

(Received June 21, 1955)

Observations have been made of the proton groups resulting from the deuteron bombardment of a carbon target enriched to 60% in C^{13}. A total of twenty-four such groups was observed, of which eleven have been assigned to levels in C^{13} and thirteen to levels in C^{14}. The experimental angular distributions are compared with the predictions of stripping theory. The excitation values for twelve previously unreported levels have been obtained with probable errors of ±0.02 Mev. These levels are at 7.47, 9.50, and 9.90 Mev in C^{13} and at 6.59, 7.35, 8.32, 9.80, 10.43, 10.50, 12.60, 12.85, and 12.96 Mev in C^{14}.

INTRODUCTION

A STUDY has been made of the $C^{12}(d,p)C^{13}$ and $C^{13}(d,p)C^{14}$ reactions. The apparatus used has been previously described.[1] A collimated beam of 14.8-Mev deuterons is incident upon the target. Outgoing particles are magnetically analyzed and are detected by a CsI(Tl) crystal. Data were obtained at eleven angles lying between 9.8° and 86.6° in the laboratory system. The observed angular distributions are shown and Butler-type calculations are used when possible to determine the angular momentum transfer and parity change of the reactions.

EXPERIMENTAL PROCEDURE

The target used in obtaining most of the data here presented was elemental carbon enriched to 60% in C^{13} and was prepared by cracking methyl iodide on a thin tantalum strip.[2] Targets of natural carbon were used as aids in identifying particle groups and assigning them to the proper isotope. The elemental carbon targets

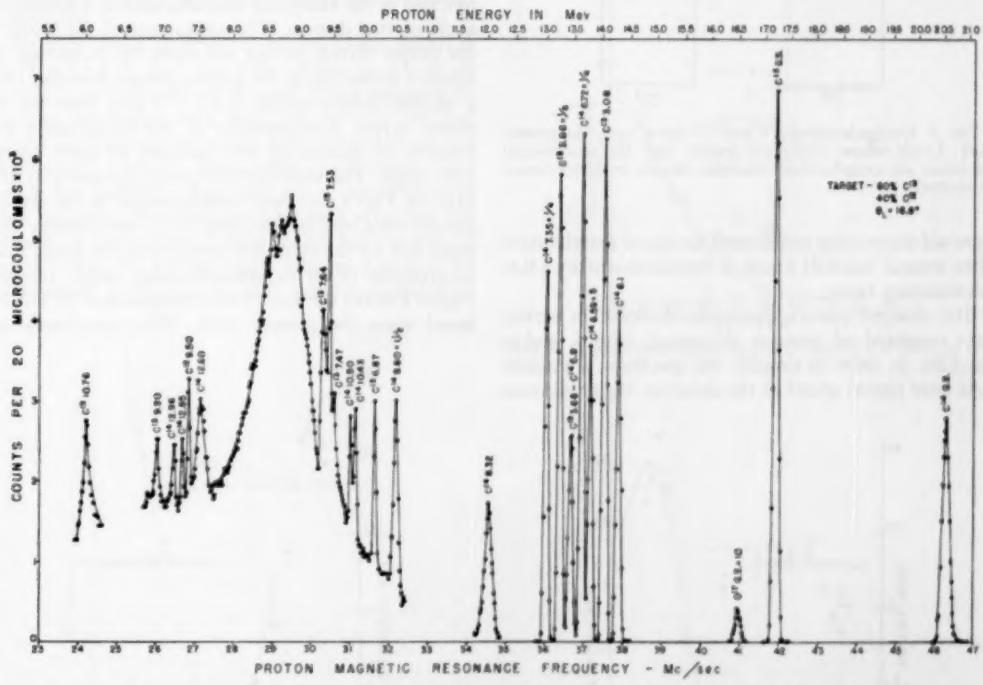

FIG. 1. Proton spectrum observed at 16.6° from a 60% C^{13} target bombarded by 14.8-Mev deuterons. The peaks are labeled by the state of the residual nucleus to which they belong.

† Work done in the Sarah Mellon Scaife Radiation Laboratory and assisted by the joint program of the Office of Naval Research and the U. S. Atomic Energy Commission.

[1] Bender, Reilley, Allen, Ely, Arthur, and Hausman, Rev. Sci. Instr. 23, 542 (1952); see also Levine, Bender, and McGruer, Phys. Rev. 97, 1249 (1955).

[2] We are indebted to T. Lauritsen for furnishing the target.

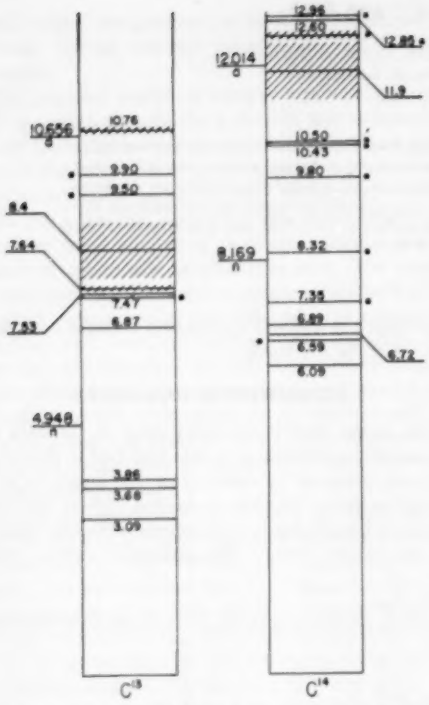

FIG. 2. Energy levels of C^{13} and C^{14} based upon the present work. Levels whose widths are greater than the experimental resolution are cross-hatched. Asterisks denote levels previously unreported.

were self-supporting and showed no sign of deterioration after several hundred hours of bombardment by a 0.5-microampere beam.

The charged particle spectrum observed in survey runs consisted of protons, deuterons, tritons, and α particles. In order to simplify the spectrum, aluminum foils were placed ahead of the detector, their thickness

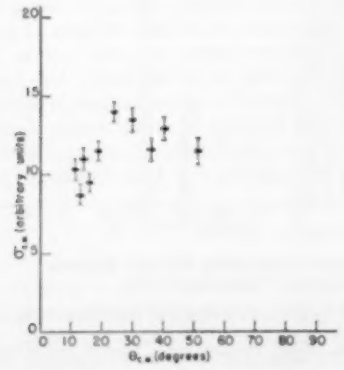

FIG. 3. Angular distribution of the $C^{13}(d,p)C^{13}$ 9.50-Mev level.

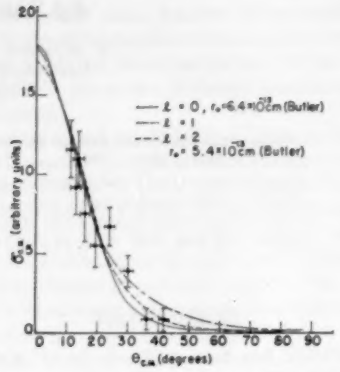

FIG. 4. Angular distribution of the $C^{13}(d,p)C^{14}$ 12.85-Mev level.

being chosen so as to ensure that only protons would be detected.

RESULTS

A. Energy Levels

Figure 1 shows the number of protons observed as a function of the analyzing magnetic field at a laboratory angle of 16.6 degrees. The assignment of the levels to the proper carbon isotope was made by comparing the relative intensities of the proton groups resulting from a natural carbon target (1.1% C^{13}) and from the enriched target. Confirmation of the assignments was possible by measuring the variation in recoil energy with angle. The small proton group appearing at 16.5 Mev in Fig. 1 has been demonstrated to be the O^{17} ground state both by the variation in recoil energy with angle and by the increased intensity of the group upon substitution of an oxygen-containing target (mylar). Figure 2 shows the energy level diagrams of C^{13} and C^{14} based upon the present work. Three previously un-

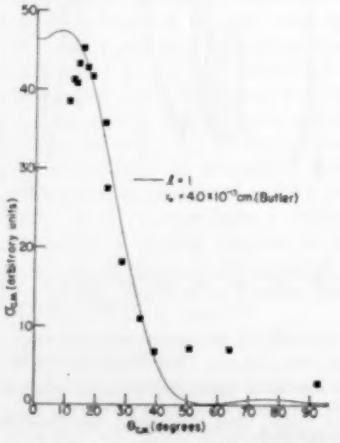

FIG. 5. Angular distribution of the $C^{13}(d,p)C^{13}$ ground state.

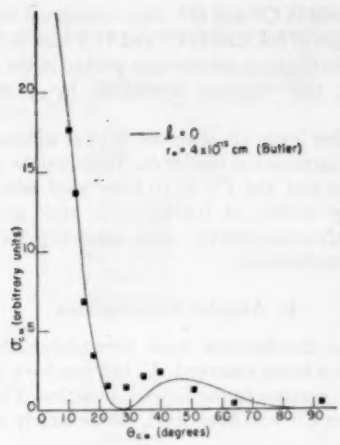

FIG. 6. Angular distribution of the $C^{13}(d,p)C^{13}$ 3.09-Mev level.

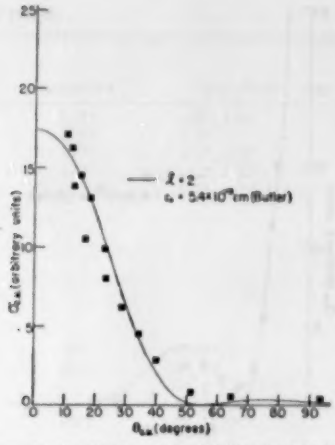

FIG. 8. Angular distribution of the $C^{13}(d,p)C^{13}$ 3.86-Mev level.

reported levels were found in C^{13} and nine in C^{14}. In addition, two levels in C^{13} previously reported[3] at 7.67 and 7.75 Mev are thought to have been more accurately located at 7.53±0.02 Mev and 7.64±0.02 Mev respectively.

The very broad asymmetric proton group shown in Fig. 1 at ~8.75 Mev has been shown to consist of contributions from both $C^{12}+d$ and $C^{13}+d$ reactions by scanning the region with both natural and enriched targets. Both groups are broad, have full widths at half maximum of 1.10±0.3 Mev, occur at the same value of outgoing particle energy, and are of approximately equal intensity. However, since no such structure has appeared in scanning the same region with targets of Ag, Al, or Be, the groups would thus not appear to be instrumental in nature. If they are associated with

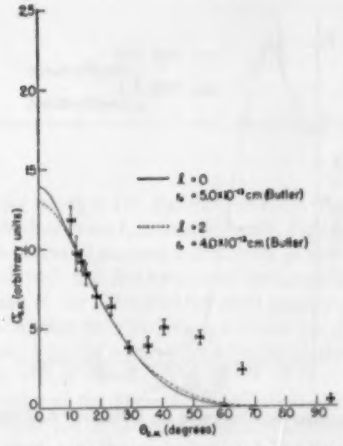

FIG. 9. Angular distribution of the $C^{13}(d,p)C^{13}$ 6.87-Mev level.

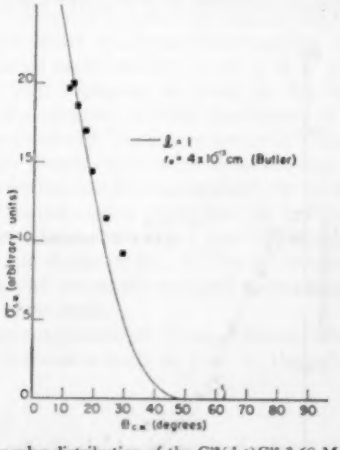

FIG. 7. Angular distribution of the $C^{13}(d,p)C^{13}$ 3.68-Mev level.

[3] F. Ajzenberg and T. Lauritsen, Revs. Modern Phys. **27**, 77 (1955).

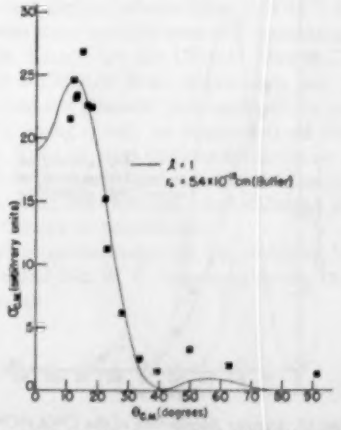

FIG. 10. Angular distribution of the $C^{13}(d,p)C^{14}$ ground state.

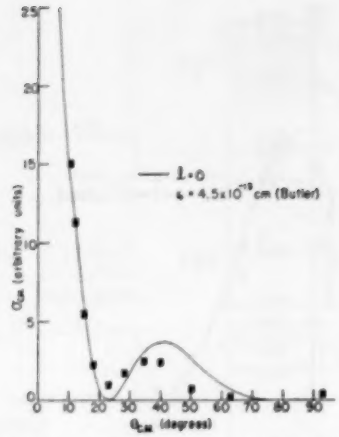

FIG. 11. Angular distribution of the $C^{13}(d,p)C^{14}$ 6.09-Mev level.

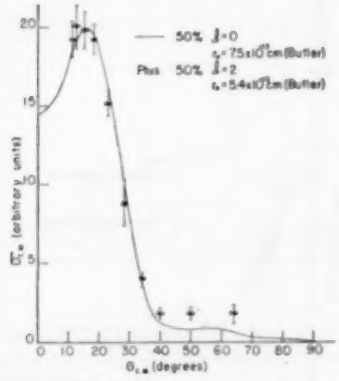

FIG. 12. Angular distribution of the $C^{13}(d,p)C^{14}$ 6.59-Mev level.

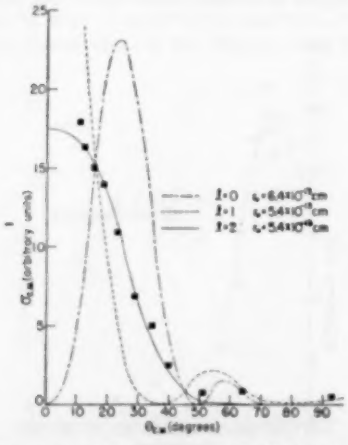

FIG. 13. Angular distribution of the $C^{13}(d,p)C^{14}$ 6.72-Mev level (Butler).

energy levels in C^{13} and C^{14}, they correspond to excitation energies of 8.4 Mev in C^{13} and 11.9 Mev in C^{14}. The angular distributions are strongly peaked in the forward direction; this suggests formation by a stripping process.

Two other levels are observed to have widths greater than the instrumental resolution. These are the C^{13} 7.64-Mev level and the C^{12} 12.60-Mev level which have laboratory widths of 0.070 ± 0.015 Mev and 0.130 ± 0.020 Mev respectively after correcting for instrumental contributions.

B. Angular Distributions

Angular distributions have been obtained for all twenty-four levels observed. All but one have distributions with maxima in the forward direction. The exception is the C^{13} 9.50-Mev level, whose nearly isotropic

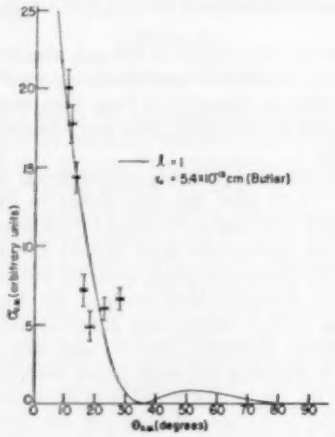

FIG. 14. Angular distribution of the $C^{13}(d,p)C^{14}$ 6.89-Mev level.

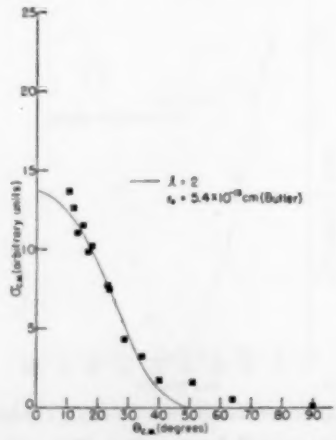

FIG. 15. Angular distribution of the $C^{13}(d,p)C^{14}$ 7.35-Mev level.

TABLE I. Summary of results obtained.

Reaction	E_L (Mev)	Level width (Mev)	l_n	$r_0 \times 10^{-13}$ cm	Spin (parity)[a]	Spin (parity)[b]	$\sigma(\theta)$ mb/sterad (±50%)
$C^{13}(d,p)C^{14}$	0		1	4.0	$1/2^-$	$1/2^-, 3/2^-$	26
	3.086		0	4.0	$1/2^+$	$1/2^+$	103
	3.685		1	4.0	$3/2^-$	$1/2^-, 3/2^-$	16
	3.855		2	5.4	$5/2^+$	$3/2^+, 5/2^+$	152
	6.868		0, 2	5.0, 4.0	$3/2^+, 5/2^+$	$(1/2^+, 3/2^+, 5/2^+)$	3.6
	7.470±0.02						~0.8
	7.533±0.02						9.6
	7.641±0.02	0.070±0.015					7.5
	8.4 +0.30	1.10 ±0.30					100
	9.500±0.02						1.6
	9.897+0.02						2.2
	10.759±0.02						4.5
$C^{13}(d,p)C^{14}$	0		1	5.4	0^+	$0^+, 1^+, 2^+$	10
	6.091		0	4.5	(1^-)	$0^-, 1^-$	62
	6.589±0.02		0, 2	7.5, 5.4		$(0^-, 1^-, 2^-, 3^-)$	1.6
	6.723		2	5.4		$1^-, 2^-, 3^-$	74
	6.894		1	5.4	(0^-)	$0^+, 1^+, 2^+$	22
	7.346±0.02		2	5.4		$1^-, 2^-, 3^-$	56
	8.321±0.02						2.2
	9.800±0.02						7.1
	10.433±0.02						~1.9
	10.505±0.02						~1.4
	11.9 ±0.30	1.10 ±0.30					90
	12.601±0.02	0.130±0.020					6.3
	12.854±0.02						1.0
	12.958±0.02						1.9

[a] As given by F. Ajzenberg and T. Lauritsen, Revs. Modern Phys. 27, 77 (1955).
[b] Present work.

distribution (Fig. 3) suggests that it is formed through the compound nucleus N^{14}.

Comparison of experimental angular distributions with the stripping theory of Butler can yield information about the orbital angular momentum transfer of the captured neutron (l_n). On the basis of the present work, using 14.8-Mev incident deuterons, stripping theory is usually quite definite in the assignment of l_n to levels having excitations less than the neutron binding energy of the final nucleus. However, for continuum states, the theoretically predicted angular distributions for different values of l_n lie too close together to permit a choice to be made between $l_n=0$, 1, or 2. A typical result for high excitation is shown in Fig. 4, which compares the observed angular distribution of the C^{14} 12.85-Mev level with the theory for $l_n=0$, 1, and 2.

Figures 5 through 9 show the observed angular distributions for the first five states of C^{13}, the solid curves being the Butler curves which best fit the data. For the 6.87-Mev level $l_n=0$ and 2 provided equally good fits. Both are shown in Fig. 9. The C^{13} results are in agreement with previously assigned[3] values of spin and parity for these levels.

A similar comparison of the experimental and stripping distributions is made in Figs. 10 through 15 for the first six states of C^{14}. For most of these levels it was possible to determine l_n unambiguously. Figure 13 compares the observed angular distribution of the C^{14} 6.72-Mev level with the Butler curves for $l_n=0$, 1, and 2. In the case of the C^{14} 6.59-Mev level equally good fits to the data were provided by $l_n=0$ and $l_n=2$. A 50% admixture of the two provided a better fit than either one alone, and is shown in Fig. 12.

The results of the present investigation are summarized in Table I. The values of absolute differential cross section listed are those determined at the forward maximum for those levels which showed maxima, and at the lowest angle of observation ($\theta_L=9.8°$) for those levels whose cross sections were still increasing toward zero angle. Except for the C^{13} 7.47 Mev and the C^{14} 10.43 and 10.50-Mev levels which were not resolved at all angles, the absolute cross sections are uncertain to ±50%, owing chiefly to uncertainty of the target thickness. Relative cross sections are probably good to ±10%. Spin and parity assignments which were arrived at by choosing between not very different stripping curves are shown in parentheses.

We wish to acknowledge the help received from Dr. A. J. Allen and Mr. W. F. Vogelsang during the course of this project.

Momentum Dependence of Phase Shifts

CHARLES J. GOEBEL, ROBERT KARPLUS, AND MALVIN A. RUDERMAN*
Radiation Laboratory and Physics Department, University of California, Berkeley, California
(Received June 23, 1955)

A lower limit is found for the momentum derivative of the scattering phase shifts of a relativistic neutral two-particle system when the interaction is of finite range.

SOME restrictions on the momentum dependence of the phase shifts for a nonrelativistic scattering problem have been discussed recently by Wigner.[1] In this note we derive a somewhat stronger restriction for the phase shifts for the relativistic scattering of neutral particles confined to a single channel. The latter condition essentially means that we are dealing with a first-quantized field.

The proof is based upon the unitarity of the partial S-matrix referring to a single phase shift and to the completeness, outside some radius a_0, of the asymptotic wave functions describing the scatterer and scattered particle in the center-of-mass system in a given state of angular momentum. We shall restrict our discussion to S-waves; analogous theorems are valid for other angular momenta.

For nonrelativistic S-wave scattering, unitarity and completeness have been shown[2,3] to lead to the conclusion that $S(k)e^{2ika}[a>a_0]$, if it has an analytic continuation,[4] is a regular function of k for $\mathrm{Im}\,k>0$ as long as no bound states are present. If there are no branch points, Ning Hu[3] has shown that one can therefore write

$$S(k)=e^{2i\delta(k)}=e^{-2ika}\prod_s \frac{k-k_s^*}{k-k_s}\frac{k+k_s}{k+k_s^*}, \quad (1)$$

$$a>a_0, \quad \mathrm{Im}k_s<0.$$

The k_s for different s are not assumed to be necessarily distinct. The form of Eq. (1) is dictated by the absence of poles in the upper half plane and by the condition

$$S(k)=e^{2i\delta(k)}=e^{-2i\delta(-k)}=S^*(-k). \quad (2)$$

For a relativistic particle the energy is a double-valued function, $E=\pm(k^2+\mu^2)^{\frac{1}{2}}$; in general the scattering amplitude depends both on k and E so that cuts must be introduced in the k-plane along the imaginary k axis from $i\mu$ to $i\infty$ and $-i\mu$ to $-i\infty$. Following Hu,[3] we can write

$$S(k,E)=e^{-2ika}\prod_s \frac{(k_s+k_s^*)(E-E_s^*)-(E_s^*-E_s)(k-k_s^*)}{(k_s+k_s^*)(E-E_s)-(E_s-E_s^*)(k-k_s)}. \quad (3)$$

$S(k)$ has a pole at $k=k_s$, $E=E_s=(k_s^2+\mu^2)^{\frac{1}{2}}$ but need not have a pole at $k=k_s$, $E=-E_s$; we have $S^*(k,E)=S(-k,E)$ in accord with unitarity but there is no simple relation between $S(k,E)$ and $S(k,-E)$. But for a real field (neutral particles only) $S(k,E)=S(k,-E)$, so that for every factor in Eq. (3) contributing a pole at k_s, E_s there is one contributing a pole at k_s, $-E_s$. When the pair of factors with E_s are multiplied, Eq. (3) reduces to the form of Eq. (1).

We may solve Eq. (1) for the phase shift and obtain

$$\delta(k)=-ak+\textstyle\sum_s \tan^{-1}\alpha_s(k)=-ak+\sum_s \theta_s(k), \quad (4)$$

where we have introduced the angle

$$\theta_s(k)=\tan^{-1}\alpha_s(k), \quad (5)$$

and the function $\alpha_s(k)$,

$$\alpha_s(k)=2k\ \mathrm{Im}k_s/(k^2-|k_s|^2). \quad (5')$$

The properties of the derivative of $S(k)$ with respect to k, denoted by a dot, are related to those of the derivatives of θ and α,

$$\dot\delta=-a+\sum_s \dot\theta_s=-a+\sum_s \frac{\dot\alpha_s}{1+\alpha_s^2}. \quad (6)$$

Because the poles of S are all in the lower half-plane, however, $\dot\alpha$ is always positive,

$$\dot\alpha_s=(-2\ \mathrm{Im}k_s)\frac{k^2+|k_s|^2}{(k^2-|k_s|^2)^2}>0, \quad (7)$$

whence

$$\dot\delta>-a. \quad (8)$$

Actually, the properties of α_s permit a still stronger statement on the lower limit of $\dot\delta$. By comparing Eqs. (5') and (7), we may conclude that

$$\dot\alpha_s>|\alpha_s|/k. \quad (9)$$

But this implies that θ_s has the lower limit

$$\theta_s>\frac{1}{k}\frac{|\alpha_s|}{1+\alpha_s^2}=\frac{1}{2k}|\sin 2\theta_s| \quad (10)$$

and that, in turn, $\dot\delta$ has to be greater than $-a$ by a positive definite amount

$$\dot\delta>-a+\frac{1}{2k}\sum_s|\sin 2\theta_s|\geq -a+\frac{1}{2k}|\sin 2(\delta+ka)|. \quad (11)$$

* This work was supported in part by the U. S. Atomic Energy Commission.

[1] E. P. Wigner, Phys. Rev. **98**, 145 (1955).
[2] W. Heisenberg, Z. Naturforsch. **1**, 608 (1946).
[3] Ning Hu, Phys. Rev. **74**, 131 (1948).
[4] N. G. van Kampen, Phys. Rev. **89**, 1072 (1953) and Phys. Rev. **91**, 1267 (1953).

The last part of the inequality can be easily deduced by induction, starting with a sum over two terms,

$$|\sin(\theta_1+\theta_2)| = |\sin\theta_1\cos\theta_2+\cos\theta_1\sin\theta_2| \leq |\sin\theta_1||\cos\theta_2|+|\sin\theta_2||\cos\theta_1| \leq |\sin\theta_1|+|\sin\theta_2|. \quad (12)$$

Equation (11) above corresponds to Eq. (5a) of reference 1, but differs in that the oscillating term always makes a positive contribution.

When bound states are present $S(k)$ of Eq. (1) has simple poles in the upper half-plane at $k=ik_\lambda$ such that the energy of the bound state is $(\mu^2-k_\lambda^2)^{\frac{1}{2}}$. Then the *rhs* of Eq. (1) will have a factor

$$\prod_\lambda \frac{k+ik_\lambda}{k-ik_\lambda} \quad (13)$$

and Eq. (11) becomes

$$\dot{\delta} > -a+\frac{1}{2k}|\sin(2\delta+2ka)| - \sum_\lambda \frac{k_\lambda}{k^2+k_\lambda^2}. \quad (14)$$

Another inequality which can be stronger than Eq. (11) and is valid for real fields even if inelastic processes enter at higher k, follows from an application of Cauchy's theorem to $\exp[2i\delta(k)+2ika]$. Since the integrand has no poles in the finite half-plane if there are no bound states, Cauchy's theorem yields

$$e^{2i[\delta(k)+ka]} = \frac{P}{\pi i}\int_{-\infty}^{\infty}\frac{dt}{t-k}e^{2i[\delta(t)+ta]}. \quad (15)$$

By differentiating Eq. (15) logarithmically and using $\delta(k)=-\delta(-k)$, we obtain

$$\dot{\delta}(k) = -a+\frac{1}{\pi}\int_{-\infty}^{\infty}\frac{dt\,\sin^2[\delta(t)-\delta(k)+at-ak]}{(t-k)^2} > -a. \quad (16)$$

The integrand of the right-hand side is always positive. Therefore a knowledge of $\delta(k)$, even over a limited region of k, contributes a lower limit to the entire integral in Eq. (16).[5]

For the partial S-matrix of Eq. (3), which describes the scattering of a charged relativistic particle, even the inequality (8) will not hold in general; it does not seem possible, therefore, to apply the inequalities (8), (12), and (16) to the scattering of charged mesons. Furthermore the possibility of charge exchange makes even Eq. (3) inadequate for the S-wave scattering of π^0 mesons by nucleons. Under the transformation $E\rightarrow -E$ the partial S-matrix $e^{2i\delta_3}$ for $\pi^+ + p \rightarrow \pi^+ + p$ becomes that for $\pi^- + p \rightarrow \pi^- + p$.[6] In a charge-independent theory, for instance, $\pi^- + p \rightarrow \pi^0 + n$ can take place, $e^{2i\delta_3(-E)}$ cannot be unitary, and $\delta_3(-E)$ cannot be real.

Nevertheless some information about the range of interaction can be inferred for the meson-nucleon system. Completeness and unitarity give the relation

$$\int_{-\infty}^{\infty} dk e^{ikr} S[k, +(k^2+\mu^2)^{\frac{1}{2}}] + \int_{-\infty}^{\infty} dk e^{ikr} S[k, -(k^2+\mu^2)^{\frac{1}{2}}] = 0,$$

where $S[k, +(k^2+\mu^2)^{\frac{1}{2}}]$ may be the partial S-matrix for $\pi^\pm + p \rightarrow \pi^\pm + p$ or $\pi^- + p \rightarrow \pi^0 + n$. Charge independence relates the charge exchange amplitude to the two elastic amplitudes, and the π^+ amplitude becomes the complex conjugate of that for π^- when the sign of the energy is changed. Completeness, unitarity, and charge independence lead to the single relation

$$2e^{2i\phi_3(k)}+e^{2i\phi_1(k)} = \frac{P}{\pi i}\int_{-\infty}^{\infty}\frac{2e^{2i\phi_3(l)}+e^{2i\phi_1(l)}}{l-k}dl, \quad (17)$$

where

$$\phi_3(k)=\delta_3(k)+ka \quad \text{and} \quad \phi_1(k)=\delta_1(k)+ka.$$

Differentiating both sides of Eq. (17) with respect to k and then setting $k=0$, we obtain

$$2\dot{\delta}_3(0)+\dot{\delta}(0)+3a = \pi\int_{-\infty}^{\infty}\frac{2\sin^2\phi_3(l)+\sin^2\phi_1(l)}{l^2}dl. \quad (18)$$

With Orear's extrapolated phase shifts,

$$\delta_3 = -0.11\frac{k}{\mu c} \quad \text{and} \quad \delta_1 = +0.16\frac{k}{\mu c}, \quad (19)$$

the complete neglect of the positive definite integral yields $a \geq 0.02(\hbar/\mu c)$.

A stronger limit on a is easily obtained if we use a linear approximation to the S-wave phase shifts.[7] The integration in Eq. (18) can be carried out, with the result

$$2\phi_3(0)+\phi_1(0) = 2|\phi_3(0)|+|\phi_1(0)|. \quad (20)$$

From this we can infer

$$a \geq 0.11(\hbar/\mu c). \quad (21)$$

[5] If multiple processes occur at momenta greater than k, Eq (16) still holds with the $\sin^2(\ )$ of the integrand replaced by $e^{-2\delta_2}\sin^2(\ )+e^{-\delta_2}\sinh(\delta_2)$, where δ_2 is the imaginary part of δ.

[6] M. Goldberger, Phys. Rev. **99**, 979 (1955). We are indebted to Professor Goldberger for furnishing us a copy of his paper before publication.

[7] J. Orear, Phys. Rev. **96**, 176 (1954).

Cross Sections in Deuterium at High Energies

R. J. GLAUBER
Lyman Laboratory of Physics, Harvard University, Cambridge, Massachusetts
(Received May 27, 1955)

Recent measurements at high energies indicate that the total cross sections for collisions of both nucleons and π mesons with deuterons are noticeably smaller than the sums of the corresponding cross sections for free neutrons and protons. A formalism for calculating the cross sections of the deuteron is developed, based on the assumption that the interactions of the incident particle with the neutron and proton may individually be treated by the general methods of diffraction theory. The nonadditivity of the free-particle cross sections is shown to be due largely to "eclipses" in which either the neutron or the proton lies in the shadow cast by the other, an effect in which quantum mechanical diffraction plays an important role. Simple representations of the high-energy interactions and the ground-state wave function of the deuteron are found to lead to cross-section defects of the magnitude observed.

I. INTRODUCTION

IT has often been suggested that in collisions with incident particles of sufficiently high energy the neutron and proton comprising a deuteron may be considered as independent scatterers. For de Broglie wavelengths much smaller than the deuteron radius, it is argued, interference effects vanish, and any cross section should equal the sum of the corresponding neutron and proton cross sections measured separately. Recent measurements of nucleon attenuation at 1.4 Bev (where $\lambda=0.1\times10^{-13}$ cm) seem, on the contrary, to reveal a substantial lack of additivity of the neutron and proton cross sections, in deuterium.[1,2] Measurements with incident protons and incident neutrons both indicate that the deuteron cross section is less than the sum of the free-particle cross sections. The measured differences, although obviously subject to uncertainty, amount to 9 mb and 6 mb respectively, values to be compared with $\sigma(n,p)=42$ mb and $\sigma(p,p)=48$ mb.

A very similar situation has been found to arise in measurements[3] of interactions of π mesons with hydrogen and deuterium at 800 Mev (where $\lambda=0.2\times10^{-13}$ cm). The observations, which we shall discuss later in detail, furnish support for the hypothesis of charge symmetry and show that the deuteron cross section is once again smaller than the sum of the free-particle cross sections. The measured differences in this case are 6 mb and 4 mb, values to be compared with the magnitudes $\sigma(\pi^-,p)=41$ mb and $\sigma(\pi^+,p)=18$ mb.

Some simple considerations may be of help in indicating the nature of the effect. At these energies the attenuation of the incident amplitude by incoherent processes such as meson production may be schematically represented as due to a certain amount of absorption of the incident wave by the nucleons. Since the incident wavelengths in these cases are evidently much smaller than the ranges of interaction, the nucleons may be thought of as casting fairly well-defined shadows. It is then clear that absorption or scattering by either nucleon is reduced when it enters the shadow of the other. Astronomers have long been familiar with a time-reversed analog of this effect; the decrease in luminosity of binary star systems during eclipses.

To observe the mechanism of the effect more closely we may begin by considering an elementary model. We represent the regions of interaction surrounding the nucleons as black spheres, each of which will then have a total cross section (comprising absorption and diffraction scattering) equal to twice its absorption (i.e., geometrical) cross section. The effect of eclipsing is most easily seen on the total absorption cross section of the system. This is because absorptions by the two nucleons are mutually exclusive events, and because no interference effects are involved, conditions which are both lacking in the consideration of scattering. To find the deviation of the total absorption cross section from the sum of the two absorption cross sections, we must correct for the fact that those particles whose initial trajectories cross both regions of interaction are absorbed in the first and not the second.

The geometrical cross section of the first nucleon will be $\sigma_1/2$, where σ_1 is its total cross section. We require the probability that a straight line passing through the first region of interaction also intersects the second. We shall assume, for the moment, that the interaction ranges are small compared with the average value of $|\mathbf{r}|$, the separation of the nucleons. Then, since the probability density of the second nucleon is isotropic[4] about the first, the required probability is $\frac{1}{2}\sigma_2\langle 1/4\pi r^2\rangle_d$ which is the average solid angle subtended by the second region, as viewed from the first. The correction to the absorption cross section of the system arising from collisions in which the shadow of region 1 falls on region 2 is thus $-\frac{1}{2}\sigma_1\sigma_2\langle 1/4\pi r^2\rangle_d$. An identical correction comes from collisions in which the regions are interchanged. Hence we have

$$\sigma_{abs}=\tfrac{1}{2}\sigma_1+\tfrac{1}{2}\sigma_2-(\sigma_1\sigma_2/8\pi)\langle 1/r^2\rangle_d \qquad (1)$$

[1] Coor, Hill, Hornyak, Smith, and Snow, Phys. Rev. **98**, 1369 (1955).
[2] Chen, Leavitt, and Shapiro (private communication). See also Phys. Rev. **95**, 663(A) (1954).
[3] Dr. O. Piccioni has kindly supplied these data.
[4] We neglect the *d*-state admixture and the effects of spin in the deuteron.

for the absorption cross section. The total cross section of the system is most simply found by appealing to the fact that, whatever their configuration may be, the total cross section of the black interaction regions equals twice their absorption cross section. We therefore have the expression for the total cross section

$$\sigma_d=\sigma_1+\sigma_2-(\sigma_1\sigma_2/4\pi)\langle 1/r^2\rangle_d. \tag{2}$$

Assuming that the deuteron has a radius of the order of the triplet effective range $r_e=1.7\times10^{-13}$ cm, it is easily verified that the correction term has the appropriate order of magnitude, 6 to 9 mb for nucleon scattering. We shall return to a more quantitative discussion of the effect at a later point.

Although the representation of the interaction regions as black spheres has been helpful in the foregoing derivation, it must be emphasized that the evidence available to date is not sufficiently detailed to support such a model firmly. While meson production may indeed represent a considerable absorption, the spatial distributions of opacity remain unknown within wide limits. Nor can we exclude the possibility of coherent scattering taking place within the interaction regions. For these reasons then, in examining the effect further, we shall avoid placing any strong restrictions on the nature of the interactions involved.

II. CALCULATION OF THE TOTAL CROSS SECTION

In the energy region of interest, incident particles have wavelengths considerably smaller than their ranges of interaction with nucleons. If it may be assumed that the energies of interaction of the incident particles with the nucleons are smaller than the incident kinetic energies, the collisions may be described by methods which are essentially those of diffraction theory.[5] In the diffraction approximation we assume that the incident plane wave sweeps, virtually undeviated, through the region of interaction, and emerges suffering only a position-dependent change of phase and amplitude.

If we let $\mathbf{b}$ be an impact-parameter vector in the plane perpendicular to the direction of incidence, the scattering process may be characterized by a function $\chi(\mathbf{b})$ which represents the change of phase, at a point $\mathbf{b}$ of the emerging wave front caused by passage through the region of interaction. The decrease of amplitude due to incoherent processes is represented by allowing $\chi(\mathbf{b})$ to assume complex values ($\mathrm{Im}\chi<0$). The coherent scattering at small angles is then given by[5,6]

$$f(\mathbf{k}',\mathbf{k})=\frac{k}{2\pi i}\int e^{i(\mathbf{k}-\mathbf{k}')\cdot\mathbf{b}}\{e^{-i\chi(\mathbf{b})}-1\}d^{(2)}\mathbf{b}, \tag{3}$$

in which $\mathbf{k}$ is the initial propagation vector and $\mathbf{k}'$ the deflected one. The integration is carried out over a plane perpendicular to the direction of incidence. We shall find it convenient to employ the abbreviation

$$\Gamma(\mathbf{b})=1-e^{-i\chi(\mathbf{b})}. \tag{4}$$

Then for axially symmetric regions of interaction centered at $\mathbf{b}=0$, the scattering amplitude reduces to

$$f(\mathbf{k}',\mathbf{k})=ik\int_0^\infty J_0(|\mathbf{k}-\mathbf{k}'|\delta)\Gamma(\delta)\delta d\delta. \tag{5}$$

We shall assume that the interactions of the incident particles with nucleons are completely characterized by functions $\chi(\mathbf{b})$ or $\Gamma(\mathbf{b})$ defined separately for the neutron and proton. In the work that follows, we make use of the scattering amplitudes only at or near the forward direction $\mathbf{k}'=\mathbf{k}$. It is this restriction which justifies the neglect of recoil effects implicit in the use of (3) and (5) for the description of scattering by isolated nucleons.[7]

In discussing scattering by deuterons and more complicated systems, the possibility of excitation of the system requires explicit treatment of its internal degrees of freedom. For this purpose a generalization of the diffraction procedures already outlined has been developed. While the application of the method is sufficiently direct in the present context, we shall return to a fuller discussion of its mathematical basis along with certain more general procedures in future work.

We may formulate the problem in a general way by considering the scattering by a bound system of nucleons whose individual velocities are small compared with the velocity of the incident particle. The nucleons may then be considered frozen in their instantaneous positions, say $\mathbf{r}_1\cdots\mathbf{r}_A$, during the particle's passage through the system. Assuming that the incident particle interacts with the nucleons through two-body forces, the total phase change of the emerging wave, $\chi_{\mathrm{tot}}(\mathbf{b})$, will be the sum of the phase changes produced by the individual nucleons. If the projections of the coordinates $\mathbf{r}_1\cdots\mathbf{r}_A$ on a plane perpendicular to the direction of incidence are $\mathbf{q}_1\cdots\mathbf{q}_A$, we may write

$$\chi_{\mathrm{tot}}(\mathbf{b},\mathbf{q}_1\cdots\mathbf{q}_A)=\sum_{j=1}^{A}\chi_j(\mathbf{b}-\mathbf{q}_j). \tag{6}$$

The function Γ analogous to (2) is then

$$\Gamma_{\mathrm{tot}}(\mathbf{b},\mathbf{q}_1\cdots\mathbf{q}_A)=1-\exp[-i\textstyle\sum_j\chi_j(\mathbf{b}-\mathbf{q}_j)]. \tag{7}$$

[5] G. Molière, Z. Naturforsch. **2a**, 133 (1947); Fernbach, Serber, and Taylor, Phys. Rev. **75**, 1352 (1949).

[6] If the interaction is due to a potential $V(r)$, the phase function $\chi(\mathbf{b})$ is given by $(\hbar v)^{-1}\int_{-\infty}^{\infty}V(\mathbf{z}+\mathbf{b})dz$, where $\mathbf{z}$ is the component of $\mathbf{r}$ in the direction of propagation and v is the incident velocity.

[7] Recoil effects are in fact easily included in a somewhat more general formulation of the method outlined in the succeeding paragraphs, but the corrections they represent for $\mathbf{k}'$ different from $\mathbf{k}$ are characteristically quite small. This is because the assumptions inherent in the diffraction approximation restrict the scattering predominantly to small angles. The forwardness of the scattering does not, however, exclude the possibility of internal excitation of scatterers containing more than one nucleon. To find the coherent scattering amplitude we must exclude the latter explicitly.

If the nucleons were rigidly fixed in their instantaneous positions, substitution of this expression in (3) would yield the scattering amplitude. Since the nucleons are not fixed in position the quantity $\Gamma_{tot}(\mathbf{b},\mathbf{q}_1\cdots\mathbf{q}_A)$ is to be regarded as an operator inducing transitions of the nuclear system as well as deflections of the scattered particle. In particular, if we are interested in elastic scattering, we must employ the diagonal element of $\Gamma_{tot}(\mathbf{b},\mathbf{q}_1\cdots\mathbf{q}_A)$ in the nuclear ground state.[6] For the reasons previously stated,[7] we may ignore the recoil momentum of the nucleus as a whole by letting its center of mass remain fixed at the origin. Then the elastic scattering amplitude is

$$F(\mathbf{k}',\mathbf{k})=\frac{ik}{2\pi}\int e^{i(\mathbf{k}-\mathbf{k}')\cdot\mathbf{b}}d^{(2)}\mathbf{b}$$
$$\times\int|\psi(\mathbf{r}_1\cdots\mathbf{r}_A)|^2\Gamma_{tot}(\mathbf{b},\mathbf{q}_1\cdots\mathbf{q}_A)\prod_j d\mathbf{r}_j, \quad (8)$$

where the $\mathbf{r}$-integrations are over the configuration space of the $A-1$ independent nucleon positions.

To apply this approximation to scattering by deuterons, we introduce the relative coordinates

$$\mathbf{r}=\mathbf{r}_1-\mathbf{r}_2, \quad \mathbf{q}=\mathbf{q}_1-\mathbf{q}_2, \quad (9)$$

and let $\phi(\mathbf{r})$ be the wave function of the deuteron ground state. Then the elastic scattering amplitude according to (8) reduces to

$$F(\mathbf{k}',\mathbf{k})=\frac{k}{2\pi i}\int e^{i(\mathbf{k}-\mathbf{k}')\cdot\mathbf{b}}$$
$$\times\left\{\int|\varphi(\mathbf{r})|^2 e^{-i[\chi_1(\mathbf{b}+\mathbf{q}/2)+\chi_2(\mathbf{b}-\mathbf{q}/2)]}d\mathbf{r}-1\right\}d^{(2)}\mathbf{b}, \quad (10)$$

where use has been made of the normalization

$$\int|\varphi(\mathbf{r})|^2 d\mathbf{r}=1.$$

Now the expression $\exp\{-i[\chi_1+\chi_2]\}$ may be written in the form

$$\exp\{-i[\chi_1(\mathbf{b}+\tfrac{1}{2}\mathbf{q})+\chi_2(\mathbf{b}-\tfrac{1}{2}\mathbf{q})\}$$
$$=[1-\Gamma_1(\mathbf{b}+\tfrac{1}{2}\mathbf{q})][1-\Gamma_2(\mathbf{b}-\tfrac{1}{2}\mathbf{q})], \quad (11)$$

so that the scattering amplitude may be resolved into the terms

$$F(\mathbf{k}',\mathbf{k})=\int|\varphi(\mathbf{r})|^2 d\mathbf{r}\left(\frac{ik}{2\pi}\right)\int e^{i(\mathbf{k}-\mathbf{k}')\cdot\mathbf{b}}\Gamma_1(\mathbf{b}+\tfrac{1}{2}\mathbf{q})d^{(2)}\mathbf{b}$$
$$+\int|\varphi(\mathbf{r})|^2 d\mathbf{r}\left(\frac{ik}{2\pi}\right)\int e^{i(\mathbf{k}-\mathbf{k}')\cdot\mathbf{b}}\Gamma_2(\mathbf{b}-\tfrac{1}{2}\mathbf{q})d^{(2)}\mathbf{b}$$
$$+\frac{k}{2\pi i}\int|\varphi(\mathbf{r})|^2 d\mathbf{r}$$
$$\times\int e^{i(\mathbf{k}-\mathbf{k}')\cdot\mathbf{b}}\Gamma_1(\mathbf{b}+\tfrac{1}{2}\mathbf{q})\Gamma_2(\mathbf{b}-\tfrac{1}{2}\mathbf{q})d^{(2)}\mathbf{b}. \quad (12)$$

[6] We neglect the influence of nuclear spins in the present work.

This expansion separates the scattering into the amplitudes contributed by the nucleons individually plus a term representing the corrections due to the presence of two nucleons. The $\mathbf{b}$-integrations of the first two terms, after translation of their origins in the $\mathbf{b}$-plane, indeed reduce to the neutron and proton scattering amplitudes given by (1).

Since our interest centers, for the present, on the total cross section, and this may be found from the forward scattering amplitude, we specialize at once to the case $\mathbf{k}=\mathbf{k}'$, and introduce the abbreviations

$$F(0)=F(\mathbf{k},\mathbf{k}), \quad f(0)=f(\mathbf{k},\mathbf{k}). \quad (13)$$

Then, introducing the individual forward scattering amplitudes via (3) and (4), we have

$$F(0)=f_1(0)+f_2(0)+\frac{k}{2\pi i}\int|\varphi(\mathbf{r})|^2$$
$$\times\Gamma_1(\mathbf{b}+\tfrac{1}{2}\mathbf{q})\Gamma_2(\mathbf{b}-\tfrac{1}{2}\mathbf{q})d^{(2)}\mathbf{b}d\mathbf{r}. \quad (14)$$

To find the total cross section of the deuteron, we make use of the fact that the attenuation of the incident beam may be described as a destructive interference with the coherent amplitude scattered in the forward direction. This relates the total cross section to the imaginary part of the forward amplitude in the familar way:

$$\sigma_d=(4\pi/k)\ \mathrm{Im}F(0), \quad (15)$$

and for the individual nucleons

$$\sigma_j=(4\pi/k)\ \mathrm{Im}f_j(0). \quad (16)$$

Then, taking the imaginary part of $F(0)$ as given by (14), we find the general expression for the deuteron cross section:

$$\sigma_d=\sigma_1+\sigma_2-2\ \mathrm{Re}\int|\varphi(\mathbf{r})|^2$$
$$\times\Gamma_1(\mathbf{b}+\tfrac{1}{2}\mathbf{q})\Gamma_2(\mathbf{b}-\tfrac{1}{2}\mathbf{q})d^{(2)}\mathbf{b}d\mathbf{r}. \quad (17)$$

The relation of the two-particle term to the "eclipse" corrections mentioned in the introduction may be seen in a general way at this point. The functions $\Gamma(\mathbf{b})$ defined by (4) go to zero for impact parameters lying outside the range of interaction. The integral over $\mathbf{b}$ in the two-particle term therefore vanishes except when the relative position of the nucleons is such that the region of interaction about one casts its "shadow" on the other.

Since the wave function of the deuteron is spherically symmetrical to a good approximation, it is convenient to express the two-particle term in a way which takes advantage of this. As a first step we calculate the term for a spherically symmetric wave function in which the neutron and proton remain a fixed distance ρ apart;

that is, we take

$$|\varphi(\mathbf{r})|^2=(4\pi\rho^2)^{-1}\delta(|\mathbf{r}|-\rho). \tag{18}$$

The $\mathbf{r}$-integration in (17) may then be separated into an integration over z, the component of $\mathbf{r}$ in the direction of incidence, and an integration of $\mathbf{q}$ over the perpendicular plane. The z-integration is easily carried out. Writing $S(\rho)$ for the two-nucleon correction in this case, we have

$$\sigma_d=\sigma_1+\sigma_2+S(\rho), \quad \rho \text{ fixed} \tag{19}$$

where

$$S(\rho)=-(2\pi\rho^2)^{-1}\,\mathrm{Re}\int d^{(2)}\mathbf{b}d^{(2)}\mathbf{q}\Gamma_1(\mathbf{b}+\tfrac{1}{2}\mathbf{q})\Gamma_2(\mathbf{b}-\tfrac{1}{2}\mathbf{q})$$

$$\times\int_{-\infty}^{\infty}\delta\{(q^2+z^2)^{\frac{1}{2}}-\rho\}dz=-\frac{1}{\pi\rho}\int_{|\mathbf{q}|<\rho}\frac{d^{(2)}\mathbf{q}}{(\rho^2-q^2)^{\frac{1}{2}}}$$

$$\times\mathrm{Re}\int\Gamma_1(\mathbf{b}+\tfrac{1}{2}\mathbf{q})\Gamma_2(\mathbf{b}-\tfrac{1}{2}\mathbf{q})d^{(2)}\mathbf{b}. \tag{20}$$

This result for a fixed distance between the nucleons may now be employed to find the correction to the cross section for any spherically symmetric representation of the deuteron wave function. The correction in the general case, which we represent as $\delta\sigma$, is obtained by averaging $S(\rho)$ over the radial distribution function.

$$\sigma_d=\sigma_1+\sigma_2+\delta\sigma, \tag{21}$$

$$\delta\sigma=\int_0^\infty|\varphi(\rho)|^2S(\rho)4\pi\rho^2d\rho. \tag{22}$$

For neutron-proton separations $\mathbf{r}$ much larger than the interaction ranges, $S(r)$ reduces to

$$S(r)\sim-(\pi r^2)^{-1}\,\mathrm{Re}\int\Gamma_1(\mathbf{b}+\tfrac{1}{2}\mathbf{q})\Gamma_2(\mathbf{b}-\tfrac{1}{2}\mathbf{q})d^{(2)}\mathbf{b}d^{(2)}\mathbf{q},$$

or, introducing $\mathbf{q}_1=\mathbf{b}+\mathbf{q}/2$, $\mathbf{q}_2=\mathbf{b}-\mathbf{q}/2$,

$$S(r)\sim-(\pi r^2)^{-1}\,\mathrm{Re}\left\{\int\Gamma_1(\mathbf{q}_1)d^{(2)}\mathbf{q}_1\int\Gamma_2(\mathbf{q}_2)d^{(2)}\mathbf{q}_2\right\}.$$

The latter integrals are proportional to the individual forward scattering amplitudes given by (3) and (4), so that $S(r)$ reduces to

$$S(r)\sim(4\pi/k^2r^2)\,\mathrm{Re}\{f_1(0)f_2(0)\}. \tag{23}$$

This is of course an asymptotic expression, valid at large distances, but its r-dependence is roughly correct down to the radii of the interaction regions themselves. Hence, if there is a sufficiently small probability that the interaction regions overlap, we have

$$\delta\sigma=(4\pi/k^2)\,\mathrm{Re}\{f_1(0)f_2(0)\}\langle r^{-2}\rangle_d. \tag{24}$$

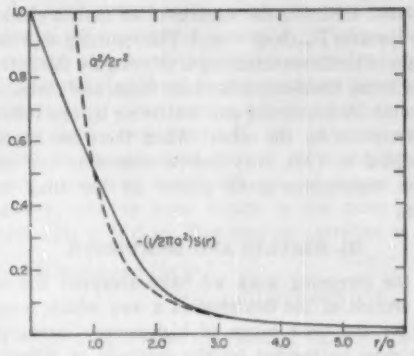

FIG. 1. The function $S(r)$, which represents the correction to the total cross section when the neutron-proton separation is held at the fixed value r, is plotted in units of $2\pi\sigma^2$. The dashed curve represents the asymptotic form the function assumes at large distances.

A further simplification may be achieved if it is assumed that the high-energy interactions are purely absorptive. The absorption, which represents incoherent processes such as meson production is, of course, always accompanied by elastic diffraction scattering. This assumption, that the incident wave suffers no real shift of phase, but only a decrease of amplitude (i.e., $\chi_j(\mathbf{b})$ is purely imaginary), implies that the scattering amplitudes (3) are purely imaginary. We then have $f_j(0)=(ik/4\pi)\sigma_j$, and substitution of these relations in (24) yields

$$\delta\sigma=-(1/4\pi)\sigma_1\sigma_2\langle r^{-2}\rangle_d. \tag{25}$$

This is just the expression found in the introductory considerations, which treated the interaction regions as black spheres. It is evident now, however, that the result is substantially more general. The interactions need not be perfectly opaque and indeed the opacity of a nucleon may be distributed arbitrarily within ranges small compared with the size of the two-body system. It must be mentioned, though, that the absorption of the system is no longer given in general by (1), since the absorption and total cross sections are no longer simply related by a factor of two.

It is instructive to calculate the absorption and scattering cross sections separately. Their sum, of course, furnishes a check on the total cross sections discussed thus far. The correction to the absorption cross section is still given by the argument of the introduction, but employing the individual absorption cross sections σ_{1a} and σ_{2a} instead of geometrical areas.

$$\delta\sigma_{\mathrm{abs}}=-(1/2\pi)\sigma_{1a}\sigma_{2a}\langle r^{-2}\rangle_d. \tag{26}$$

The considerations required to find the scattering are rather more lengthy. It is necessary to take account of all scattering processes involving breakup of the deuteron as well as the elastic collisions. This is accomplished by integrating the scattered intensity over

angles and summing the squares of all matrix elements of the operator $\Gamma_{tot}(\mathbf{b},\mathbf{q}_1\cdots\mathbf{q}_A)$. The resulting expression is a sum of terms representing scattering by the individual nucleons, interference between them, and corrections due to double scattering and scattering by one followed by absorption by the other. When these are summed and added to (26), they indeed reduce to the much simpler expressions given above for the total cross section.

III. RESULTS AND DISCUSSION

In the foregoing work we have analyzed the total cross section of the deuteron in a way which remains valid for the wide range of high-energy interactions which may be treated by the methods of diffraction theory. While it is anticipated that the actual interactions of high-energy incident particles with neutrons and protons will be found to have this character, too few observations exist as yet to permit conclusive analysis of the data. In particular, lacking measurements of the differential cross sections for elastic scattering, very little can as yet be said concerning the phase change functions $\chi_j(\mathbf{b})$, or the "shadow" functions $\Gamma_j(\mathbf{b})=1-\exp[i\chi_j(\mathbf{b})]$, which figure in the general results (20) and (22). We shall therefore confine ourselves for the present to the use of simple models for the high-energy interactions. In this way rough estimates of the effect may be reached along with comparisons of the relative magnitudes involved.

The experimental total cross sections[1,2] for nucleon-nucleon encounters at 1.4 Bev are

$$\sigma(p,p)=48 \text{ mb} \quad \text{and} \quad \sigma(n,p)=42 \text{ mb}.$$

Two attenuation measurements have also been performed with deuterium. With a beam of incident protons, a subtractive experiment[2] involving deuterium- and hydrogen-bearing targets yields $\sigma(p,[d-p])=33$ mb which is 9 mb smaller than $\sigma(p,n)=\sigma(n,p)$. The subtractive measurement added to $\sigma(p,p)$ indicates a proton-deuteron cross section $\sigma(p,d)=81$ mb. With neutrons incident on deuterium,[1] the total cross section of the deuteron is found to be $\sigma(n,d)=84$ mb, a value whose closeness to the corresponding result for protons strongly supports the hypothesis of charge symmetry. If it is assumed then that the free neutron-neutron cross section is the same as $\sigma(p,p)$ given above, the sum of the free-particle cross sections $\sigma(n,n)+\sigma(n,p)$ is found to exceed $\sigma(n,d)$ by 6 mb. As a further consequence of charge symmetry, these differences of 9 mb and 6 mb must be considered as two measurements of the same number. Since they are differences of experimental cross sections, their errors may of course be relatively large, but it will be of interest to see whether or not the results predicted lie in the range they indicate.

Since little more is known about nucleon interactions at 1.4 Bev than is contained in the above total cross section measurements, we shall employ them to define the radii of opaque regions of interaction. The black-sphere model to which we thus return is at least roughly consistent with measurements[3] made at somewhat lower energies of the relative proportions of elastic and inelastic processes occurring in proton-proton scattering. Since the neutron and proton cross sections are not very different, we shall simplify the calculations by assuming their regions of interaction identical. The radius $a=0.85\times10^{-13}$ cm corresponds to a mean nucleon-nucleon cross section $2\pi a^2=45.4$ mb.

Whether this interaction range may be considered small or not depends in large measure on the form assumed for the deuteron wave function. As we shall see, the experimental data such a wave function must be required to fit, leave the radial distribution function quite undetermined at small neutron-proton separations. In particular for models which concentrate the probability densities at small distances, it will be necessary to use the general formulation of the result given by (20) and (22).

The functions $\Gamma_j(\mathbf{b})$ for the black-sphere interactions assume the particularly simple form

$$\Gamma_1(\mathbf{b})=\Gamma_2(\mathbf{b})=\begin{cases}1, & b<a\\ 0, & b>a.\end{cases} \tag{27}$$

With the aid of these, the function $S(r)$, which represents the correction to the total cross section when the neutron-proton separation is held at the fixed value r, is easily found. Introducing the variable

$$x=r/2a, \tag{28}$$

we have for $x\leqslant 1$:

$$S(r)=-2\pi a^2\{1+(4/3\pi)(x^{-1}-x)K(x) -(4/3\pi)(x^{-1}+x)E(x)\} \tag{29}$$

and for $x\geqslant 1$:

$$S(r)=-2\pi a^2\{1+(4/3\pi)(x^2-1)K(x^{-1}) -(4/3\pi)(x^2+1)E(x^{-1})\}, \tag{30}$$

where the functions K and E are the complete elliptic integrals of the first and second kind, respectively. A graph of $-(1/2\pi a^2)S(r)$ is given in Fig. 1, where it is compared with the asymptotic form $a^2/2r^2$, which is valid at large distances. It may be seen that the asymptotic form deviates widely from the correct function only for radii r smaller than the range of interaction a.

The deviation of the total cross section from the sum of the free-particle cross sections is found by averaging the function $S(r)$ over the radial distribution function of the deuteron. For this purpose we shall discuss three possible models of the deuteron, selected to illustrate different ways in which the probability density may behave at small distances. The constants which any representation of the deuteron wave function must be chosen to fit are: the triplet effective range $r_e=1.7$

[3] Smith, McReynolds, and Snow, Phys. Rev. 97, 1186 (1955).

$\times 10^{-13}$ cm, and the binding energy, which may also be stated in terms of the parameter α, the logarithmic derivative of the radial wave function at large distances, $\alpha=(1/4.31)\times 10^{13}$ cm^{-1}.

If the interaction which binds the deuteron is represented as a square-well potential, its radius is found to be 2.07×10^{-13} cm. The value of $S(r)$ averaged over the radial distribution function appropriate to this potential yields $\delta\sigma=5.7$ mb, a value quite consistent with the smaller of the two measurements. The value found by employing the asymptotic result (25) exceeds this by about 20%, an error which corresponds to a probability of only 4% that the neutron-proton separation is less than 0.85×10^{-13} cm. The use of the asymptotic approximation must therefore be restricted to distributions which are less concentrated at small distances.

A model of the deuteron somewhat more in keeping with the original proposals of the meson theory would be based on a potential which becomes singular as $1/r$ near the origin and decreases exponentially at large distances. The Hulthén potential, $V(r)\sim\lambda(e^{\lambda r}-1)^{-1}$ for which the wave function is proportional to $e^{-\alpha r}\times(1-e^{-\lambda r})/r$, represents a convenient choice of this type. The parameter λ is found to be 1.21×10^{13} cm^{-1}, a value which corresponds to an increased concentration of the wave function near the origin. The mean value of $S(r)$, in this case, yields $\delta\sigma=-7.2$ mb, which lies between the measured values of the cross-section defect.

A third type of deuteron model which has recently received considerable discussion is based on the assumption of a "hard core" in the low-energy neutron-proton interaction. The particles are assumed subject to an infinite repulsive potential which prevents their approach closer than a distance r_c. An example of this model is furnished by one of the computations of Blatt and Kalos based on a core of radius $r_c=0.531\times 10^{-13}$ cm surrounded by a potential of the type proposed by Lévy, with parameters providing an approximate fit to the known constants for the triplet state.[10] The average value of $S(r)$ in this case gives $\delta\sigma=-4.5$ mb. The asymptotic approximation (25), as may be expected, is more accurate here than in the square-well case. Since the radial distribution lies almost entirely in the region $r>a$, the asymptotic estimate is on the low side, by about 10%.

The value 4.5 mb for the cross-section defect in the hard-core example considered is smaller than either of the measured values, 9 mb and 6 mb, though perhaps not small enough to exclude this model in view of the various uncertainties involved. However, since the case is one in which the asymptotic approximation is serviceable, certain general remarks may be made about the dependence of the result on the form assumed for the high-energy interactions. In particular, the validity of the asymptotic expression (25) for arbitrary interactions of a purely absorptive character indicates that the result should not be very sensitive to variations in the opacity distributions which leave the total cross sections unchanged. If the interactions are assumed to be refractive as well as absorptive, the forward scattering amplitudes are no longer purely imaginary, and we must return to the more general relation (24) to find $\delta\sigma$. This may be rewritten as

$$\delta\sigma\sim-(1/4\pi)\{\sigma_1\sigma_2-(4\pi/k)^2\times\mathrm{Re}f_1(0)\,\mathrm{Re}f_1(0)\}\langle r^{-2}\rangle_d, \quad (31)$$

from which it is evident that similar signs for the real parts of the forward scattering amplitudes would result in a decrease of the predicted effect, and hence a strong need for a more compact deuteron model. For models in which the probability density is substantially more concentrated, however, the asymptotic approximation becomes less accurate and the influence of other assumptions concerning the interactions can only be found by recalculating the general expression (22). While the black-sphere model we have employed in the absence of scattering data may well prove inaccurate, it seems clear that an effect of the magnitude observed may be explained with other strongly absorptive interactions by suitably adjusting the radial distribution of the deuteron.

A test of consistency may be made on the radial distribution required by analysis of the similar effect which is found to occur in collisions of π mesons with deuterons. The total cross sections at 800 Mev for collisions of $\pi^{\pm}$ mesons with protons are[3]

$$\sigma(\pi^-,\hat{p})=41\text{ mb},\quad \sigma(\pi^-,\hat{p})=18\text{ mb}, \quad (32)$$

while subtractive measurements performed with deuterium- and hydrogen-bearing targets yield

$$\sigma(\pi^+,[\hat{d}-\hat{p}])=35\text{ mb},\quad \sigma(\pi^-,[\hat{d}-\hat{p}])=14\text{ mb}. \quad (33)$$

These results, which involve probable errors of about 2 mb, may be added in pairs to yield the deuteron cross sections

$$\sigma(\pi^+,\hat{d})=53\text{ mb},\quad \sigma(\pi^-,\hat{d})=55\text{ mb}.$$

The agreement of these results offers further support for the hypothesis of charge symmetry, so that the cross sections (32) and (33) must be interpreted as implying that the deuteron cross section is less than the sum of the free-particle cross sections by about 5 mb. In the absence of other data on meson interactions at this energy, we may merely remark that the assumption of purely absorptive interactions, together with the use of the deuteron wave functions employed above, furnishes estimates of the effect in the range from 1 to 3 mb. A larger effect may be due to nonvanishing refractive effects or concentration of the density distribution of the deuteron at smaller radii.

[10] J. M. Blatt and M. H. Kalos, Phys. Rev. **92**, 1563 (1953). The wave function employed corresponds to the parameters listed on line 2 of Table I. The core radius is the smallest reported upon. We are indebted to Mr. J. Bernstein for supplying the tables.

In concluding we may mention still another factor whose possible influence on the effect may be of interest. We have assumed from the outset that the complex phase changes brought about by the passage of a wave through the two regions of interaction are additive. When the interaction regions overlap, any nonlinearity in the superposition of their fields may imply nonadditivity of the phase changes. This too would contribute to the observed cross-section defect, but its analysis must clearly follow a more complete investigation of the linear effects. The author is greatly indebted to Dr. Anatole Shapiro for calling the measurements of the effect to his attention, and to C. Sommerfield and J. Bernstein for aid with some of the calculations.

PHYSICAL REVIEW VOLUME 100, NUMBER 1 OCTOBER 1, 1955

A Theory of New Particles

RYOYU UTIYAMA
Institute for Advanced Study, Princeton, New Jersey
(Received May 31, 1955)

A tentative scheme is developed to formulate the behavior of the new unstable particles. This scheme is a straightforward generalization of the usual charge-independent meson theory. The selection rules for isotopic spin are identical with those suggested by Gell-Mann. Owing to the particular form of the interaction assumed in this scheme, we can derive a new selection rule which seems to be of some use in interpreting the metastability of the new particles.

1. INTRODUCTION

SEVERAL attempts[1] to interpret the contradictions between the copious productions of the new particles and their metastabilities have been published. Among these attempts the "two-coupling-constant theory," due to Pais, seems most successful. In this theory the production processes are due to an interaction with a large coupling-constant while the other small coupling-constant is responsible for decay processes. Pais' recent theory[1] based on the four-dimensional ω space seems especially attractive. However there may remain, of course, other kinds of formalisms within the framework of the "two-coupling-constant theory."

In the present paper, the details of a theory of the baryons and mesons will be presented. In this theory particles will be distinguished by (a) isotopic spin I, (b) curious particle constant A, and (c) intrinsic spatial parity ϵ in addition to the usual mass, spin, and charge. The theory is constructed so that the selection rules involving I, I_3, and A are identical with those proposed by Gell-Mann.[2] In addition we will show that it is natural to introduce an additional selection rule involving the intrinsic parity ϵ. This last aspect was briefly discussed in a paper by Tobocman and the author.[2]

In the usual formalism, the neutron and the proton are described by a spinor $\psi^\alpha(\alpha=1,2)$ in a three-dimensional τ space. Similarly the charged and neutral mesons are described by a vector $\boldsymbol{\phi}$ (or a symmetric spinor of the second rank $\chi^{\alpha\beta}=\chi^{\beta\alpha}$ $(\alpha,\beta=1,2)$) in τ space. The interaction Lagrangian between the two fields in the usual charge-independent theory is

$$g\boldsymbol{\phi}\bar{\psi}\gamma_5\boldsymbol{\tau}\psi=\sum_{\alpha,\beta=1,2}g\chi^{\alpha\beta}\bar{\psi}\gamma_5\tau_{\alpha\beta}\psi. \tag{1.1}$$

Here $\tau_{\alpha\beta}$ and $\chi^{\alpha\beta}$ are defined as follows:

$$\tau_{11}=\tau_{22}{}^{\dagger}=i(\tau_1+i\tau_2),\quad \tau_{12}=\tau_{21}=-i\tau_3,$$

and

$$\chi^{11}=\chi^{22*}=-(i/2)(\phi_1-i\phi_2),\quad \chi^{12}=\chi^{21}=(i/2)\phi_3.$$

Now we consider a straightforward generalization of (1.1), namely

$$g\sum_n\sum_{\alpha_1\alpha_2\cdots\alpha_n=1,2}\chi^{(\alpha_1\cdots\alpha_n)}\bar{\psi}\gamma_5\cdot T_{(\alpha_1\cdots\alpha_n)}\psi. \tag{1.2}$$

Here $\chi^{(\alpha_1\cdots\alpha_n)}$ is a symmetric spinor of the nth rank in τ space and is assumed to describe a meson field with the ordinary spin 0 and τ spin $n/2$, and ψ is a wave function corresponding to some assembly of baryons with ordinary spin $\frac{1}{2}$ and various values of τ spin. $T_{(\alpha_1\cdots\alpha_n)}$ is some square matrix which is considered to be a generalization of the usual τ matrix.

In this treatment, we shall include only three kinds of meson fields: the ordinary π-meson field $(\chi_{(\tau)}{}^{\alpha\beta}$ or $\boldsymbol{\phi})$,[3] the θ-meson field with τ spin $\frac{1}{2}(\chi_{(\theta)}{}^{\alpha})$, and the τ-meson field with τ spin $\frac{1}{2}$ $(\chi_{(\sigma)}{}^{\alpha})$. As to the baryons we shall include the nucleon field $(\psi_{(N)}{}^{\alpha})$, the Λ particle with τ spin 0 $(\psi_{(\Lambda)})$, the Σ particles with τ spin 1 $(\psi_{(\Sigma)}{}^{\alpha\beta})$, and the cascade particle Y with τ spin $\frac{1}{2}$ $(\psi_{(Y)}{}^{\alpha})$. Con-

[1] A. Pais, Physica **19**, 869 (1953); A. Pais, Proc. Nat. Acad. Sci. **40**, 484 (1954); M. Gell-Mann and A. Pais, Proceedings of the International Physics Conference, Glasgow, July, 1954 (Pergamon Press, London, 1955); T. Nakano and R. Utiyama, Progr. Theoret. Phys. (Japan) **11**, 411 (1954); T. Nakano and K. Nishijima, Progr. Theoret. Phys. (Japan) **10**, 581 (1953).

[2] R. Utiyama and W. Tobocman, Phys. Rev. **98**, 780 (1955). In the present paper this will be cited as U.T.

[3] Indices α, β, $\cdots$ are spinor indices in τ space. The ordinary spinor indices of baryons are omitted.

sequently the strong interaction Lagrangian (1.2) has the form

$$L_{\text{int}}^{(S)}=g\sum_{\alpha,\beta=1,2}[\bar{\psi}\gamma_5\cdot T_{\alpha\beta}^{(\tau)}\psi\cdot\chi_{(\tau)}^{\alpha\beta}+\bar{\psi}\gamma_5\cdot T_a^{(\theta)}\psi\cdot\chi_{(\theta)}^{\alpha}+\bar{\psi}\gamma_5\cdot T_a^{(\tau)}\psi\cdot\chi_{(\tau)}^{\alpha}]+(\text{Hermitian conj.}). \quad (1.3)$$

The structure of the three kinds of T-matrices can be determined by the requirements that (1.3) be invariant under Lorentz transformations, gauge transformations and under rotations in τ space (charge independence).

On account of our special assumption that the strong coupling between the meson-family and the baryons is a γ_5 interaction, a new selection rule involving the intrinsic parities can be derived which may be of some use in interpreting the metastability of the new particles. The selection rule derived from the invariance under τ rotations is sufficient to interpret the metastability of all the known particles. However, if more new particles are discovered in future, more selection rules may be necessary to guarantee the singular metastability of the newcomers. The intrinsic parity rule mentioned above may be of use in this connection.

In the following sections, we shall give explicit expressions for the T-matrices and derive the above-mentioned new selection rule. Further we shall consider the possible types of electromagnetic and weak interactions.

2. ROTATION-INVARIANCE IN τ SPACE

The total Lagrangian density is written as

$$L=L_B+L_M+L_{\text{int}}^{(S)}, \quad (2.1)$$

$$L_B=i\bar{\psi}(\gamma^\mu\partial_\mu+\mathbf{M})\psi, \quad L_M=-(\partial_\mu\chi^*\cdot\partial^\mu\chi+\chi^*\mu^2\chi),$$

where χ and χ^* are defined by

$$\chi^*=(\chi_{(\tau)}^{*\alpha\beta},\chi_{(\theta)}^{*\alpha},\chi_{(\tau)}^{*\alpha}), \quad \chi=\begin{pmatrix}\chi_{(\tau)}^{\alpha\beta},\\ \chi_{(\theta)}^{\alpha},\\ \chi_{(\tau)}^{\alpha},\end{pmatrix},$$

and μ^2 stands for

$$\mu^2=\begin{pmatrix}\mu_{(\tau)}{}^2E_2 & & 0\\ & \mu_{(\theta)}{}^2E_2 & \\ 0 & & \mu_{(\tau)}{}^2E_2\end{pmatrix},$$

where E_n is an $(n\times n)$ unit matrix.

As to the wave functions of baryons, we shall take the following representation:

$$\psi=\begin{pmatrix}\psi_{(N)}{}^\alpha\\ \psi_{(\Lambda)}\\ \psi_{(\Xi)}{}^{\alpha\beta}\\ \psi_{(Y)}{}^\alpha\end{pmatrix}, \quad \bar{\psi}=i\psi^*\gamma_4=(\bar{\psi}_{(N)}{}^\alpha,\bar{\psi}_{(\Lambda)},\bar{\psi}_{(\Xi)}{}^{\alpha\beta},\bar{\psi}_{(Y)}{}^\alpha). \quad (2.2)$$

In this case, the mass operator $\mathbf{M}$ has the form

$$\mathbf{M}=\begin{pmatrix}M_{(N)}E_2 & & & 0\\ & M_{(\Lambda)}E_1 & & \\ & & M_{(\Xi)}E_4 & \\ 0 & & & M_{(Y)}E_2\end{pmatrix}.$$

Under an infinitesimal rotation in τ space ψ and χ are assumed to be transformed in the following way:

$$\psi\to\psi'=(1+(i/2)\sum_{j,k=1}^{3}\epsilon_{jk}D^{jk})\psi$$

$$\chi\to\chi'=(1+(i/2)\sum_{j,k=1}^{3}\epsilon_{jk}\mathfrak{D}^{jk})\chi \quad (2.3)$$

$$(\epsilon_{jk}=-\epsilon_{kj}, \quad j,k=1,2,3).$$

Here D and $\mathfrak{D}$ are respectively given by

$$D=\begin{pmatrix}D(\frac{1}{2}) & & & \\ & D(0) & & \\ & & D(1) & \\ & & & D(\frac{1}{2})\end{pmatrix}$$

and

$$\mathfrak{D}=\begin{pmatrix}D(1) & & 0\\ & D(\frac{1}{2}) & \\ 0 & & D(\frac{1}{2})\end{pmatrix},$$

where $D(l)$ ($l=0$, or $\frac{1}{2}$ or 1) stands for an irreducible Hermitian representation matrix of $(2l+1)$ degree for the generator of the τ-rotation group.

Now let us assume charge independence for the strong interaction, namely, we assume the invariance of the Lagrangian under any τ rotation. Then we get the following relation

$$\delta L_{\text{int}}^{(S)}=\delta(g\cdot\bar{\psi}\gamma_5\mathbf{T}\psi\cdot\chi)=0,$$

where $\mathbf{T}$ means[4]

$$(T_{\alpha\beta}^{(\tau)},T_a^{(\theta)},T_a^{(\tau)}),$$

and $\mathbf{T}\cdot\chi$ the scalar product of $\mathbf{T}$ and χ.

Substituting (2.3) into the above equation, we get

$$\mathbf{T}\mathfrak{D}^{jk}=[D^{jk},\mathbf{T}],$$

or equivalently

$$\sum_{\alpha',\beta'=1}^{2}T_{\alpha'\beta'}^{(\tau)}(\alpha'\beta'|D^{jk}(1)|\alpha\beta)=[D^{jk},T_{\alpha\beta}^{(\tau)}],$$

$$\sum_{\alpha'=1}^{2}T_{\alpha'}^{(\theta)}(\alpha'|D^{jk}(1/2)|\alpha)=[D^{jk},T_a^{(\theta)}] \quad (2.4)$$

and

$$\sum_{\alpha'=1}^{2}T_{\alpha'}^{(\tau)}(\alpha'|D^{jk}(1/2)|\alpha)=D^{jk},T_a^{(\tau)}].$$

Now in our particular representation shown in (2.2), the T-matrices can be split into various rectangular submatrices in the following way:

$$T=\begin{pmatrix}(\frac{1}{2}|T|\frac{1}{2}) & (\frac{1}{2}|T|0) & (\frac{1}{2}|T|1) & (\frac{1}{2}|T|\frac{1}{2})\\ (0|T|\frac{1}{2}) & (0|T|0) & (0|T|1) & (0|T|\frac{1}{2})\\ (1|T|\frac{1}{2}) & (1|T|0) & (1|T|1) & (1|T|\frac{1}{2})\\ (\frac{1}{2}|T|\frac{1}{2}) & (\frac{1}{2}|T|0) & (\frac{1}{2}|T|1) & (\frac{1}{2}|T|\frac{1}{2})\end{pmatrix}, \quad (2.5)$$

[4] α and β are not matrix suffices but spinor indices taking values 1 or 2. Each T is an 8×8 matrix whose matrix indices are omitted.

where $(l|T|l')$ is a $(2l+1)\times(2l'+1)$ rectangular matrix.

By virtue of the relations (2.4) the zero submatrices of T's are given by

$$\begin{aligned}&(l|T^{(\tau)}|l')=0 \quad \text{for} \quad l-l'\neq\pm 1 \text{ or } 0,\\ &(l|T^{(\theta)}|l')=0 \quad \text{for} \quad l-l'\neq\pm\tfrac{1}{2},\\ &(l|T^{(\tau)}|l')=0 \quad \text{for} \quad l-l'=\pm\tfrac{1}{2}\end{aligned} \tag{2.6}$$

(see Appendix).

Since L_B and L_M are invariant under transformation (2.3), we get the conservation-law of τ angular momentum:

$$\frac{\partial}{\partial\chi^\alpha}[\bar\psi\gamma^\alpha D^{jk}\psi-i\{\chi^*\mathfrak{D}^{jk}\partial^\alpha\chi-\partial^\alpha\chi^*\cdot\mathfrak{D}^{jk}\chi\}]=0. \tag{2.7}$$

In particular, we have

$$I_Z=\int\left[\bar\psi\gamma^0 D_Z\psi+i\left(\chi^*\mathfrak{D}_Z\frac{\partial\chi}{\partial t}-\frac{\partial\chi^*}{\partial t}\mathfrak{D}_Z\chi\right)\right]dx$$

$$=\text{const.}\qquad D_Z=D^{12},\quad \mathfrak{D}_Z=\mathfrak{D}^{12}. \tag{2.8}$$

3. GAUGE INVARIANCE AND ELECTROMAGNETIC INTERACTION

To introduce the electromagnetic interaction, (2.1) must be replaced by the following expressions:

$$\begin{aligned}&L_B\to L_B'=i\bar\psi\{\gamma^\alpha(\partial_\alpha-ieCA_\alpha)+\mathbf{M}\}\psi,\\ &L_M\to L_M'=-\{(\partial_\alpha-ieC'A_\alpha)\chi\}^*\\ &\qquad\times\{(\partial^\alpha-ieC'A^\alpha)\chi\}-\chi^*\psi^2\chi.\end{aligned} \tag{3.1}$$

L_B' and L_M' are invariant under the following infinitesimal gauge transformation:

$$\begin{aligned}&\psi\to\psi'=[1+ie\lambda(x)C]\psi,\\ &\chi\to\chi'=[1+ie\lambda(x)C']\chi.\end{aligned} \tag{3.2}$$

Here C and C' are defined as follows:

$$C=D_Z+A,\quad C'=\mathfrak{D}_Z+A',$$

and in that particular representation in which D_Z and $\mathfrak{D}_Z$ are diagonal, C, C', A, and A' have the forms[5]

$$C=\begin{pmatrix}1 & & & & & & & & \\ & 0, & & & & & & & \\ & & 0, & & & & & 0 & \\ & & & 1 & & & & & \\ & & & & 0 & & & & \\ & & & & & -1, & & & \\ & & & & & & 0 & & \\ & & & & & & & -1 & \\ & & & & & & & & \end{pmatrix}=D_Z+\tfrac{1}{2}\begin{pmatrix}E_2 & & & \\ & 0_1 & & 0 \\ & & 0_2 & \\ & 0 & & -E_2\end{pmatrix},$$

$$C'=\begin{pmatrix}1 & & & & & & & & \\ & 0 & & & & & & & \\ & & -1, & & 0 & & & & \\ & & & 1 & & & & & \\ & & & & 0, & & & & \\ & & & & & 1 & & & \\ & & & & & & 0 & & \\ & 0 & & & & & & & \end{pmatrix}=\mathfrak{D}_Z+\begin{pmatrix}0_3 & & 0 \\ & \tfrac{1}{2}E_2 & \\ 0 & & \tfrac{1}{2}E_2\end{pmatrix}. \tag{3.3}$$

[5] These representations of C and C' correspond to the following representations of ψ and χ:

$$\psi=\begin{pmatrix}\text{proton}\\ \text{neutron}\\ \hline \Lambda^0\\ \hline \Sigma^+\\ \Sigma^0\\ \Sigma^-\\ \hline \Gamma^0\\ \Gamma^-\end{pmatrix},\qquad \chi=\begin{pmatrix}\pi^+\\ \pi^0\\ \pi^-\\ \hline \theta^+\\ \theta^0\\ \hline \tau^+\\ \tau^0\end{pmatrix}.$$

Now $L_{\text{int}}{}^{(S)}$ must be invariant under the transformation (3.2). From this requirement, we have

$$\mathbf{T}C'=[C\cdot\mathbf{T}],$$

or

$$[A\cdot\mathbf{T}]-\mathbf{T}A'=\mathbf{T}\cdot\mathfrak{D}_Z-[D_Z,\mathbf{T}]=0$$

on account of (2.4). Thus, we have the following representation for T-matrices:

$$T^{(\tau)}=\begin{pmatrix}N_2 & & \\ & N_4 & \\ & & N_2'\end{pmatrix},$$

$$T^{(\theta)}=T^{(\tau)}=\begin{pmatrix}0_2 & N_{2\times4} & 0_2\\ & 0_4 & N_{4\times2}\\ 0_2 & & 0_2\end{pmatrix}, \tag{3.4}$$

where N_i and $N_{i\times k}$ stand for $i\times i$ and $i\times k$ submatrices having nonvanishing elements respectively.

The conservation of charge is now expressed by

$$Q=e\int\left[\bar\psi\gamma^0C\psi+i\chi^*C'\left(\frac{\partial}{\partial t}-ieC'A_0\right)\chi\right.$$

$$\left.-i\left\{\left(\frac{\partial}{\partial t}-ieC'A_0\right)\chi\right\}^*C'\chi\right]dx=\text{const.} \tag{3.5}$$

If we omit the electromagnetic interaction, (3.5) becomes

$$Q=\int\left[\bar\psi\gamma^0C\psi+i\left\{\chi^*C'\frac{\partial\chi}{\partial t}-\frac{\partial\chi^*}{\partial t}C'\chi\right\}\right]dx=\text{const.} \tag{3.6}$$

From (3.6) and (2.8), we have the law of conservation of A for the strong coupling:

$$\int\left[\bar\psi\gamma^0A\psi+i\left\{\chi^*A'\frac{\partial\chi}{\partial t}-\frac{\partial\chi^*}{\partial t}A'\chi\right\}\right]dx=\text{const.} \tag{3.7}$$

Since every transition process must conserve the total charge Q, the conservation of A for the strong coupling is synonymous with that of I_Z for such a coupling.

Besides the gauge transformation, our Lagrangian is invariant under the phase transformation of baryon-fields

$$\psi\to\psi e^{i\alpha},\quad \bar\psi\to\bar\psi e^{-i\alpha},\quad \alpha=\text{const.}$$

Here it must be noted that all the baryon fields are assumed to be complex functions. From this invariance, we get the conservation of the number of baryons.

4. INVERSION-INVARIANCE AND THE SELECTION-RULE

It is easily seen that our Lagrangian is invariant under the proper Lorentz group. As to spatial inversion, however, some care is needed. As Yang and Tiomno[6] pointed out, spinor fields have four possible transformation characters under inversion in ordinary space:

$$\psi(x) \to \epsilon\gamma_4\psi(-x),$$

$$(A)\ \epsilon=1,\quad (B)\ \epsilon=-1,\quad (C)\ \epsilon=i,\quad (D)\ \epsilon=-i. \quad (4.1)$$

Since the θ meson is assumed in the present paper to be a scalar field owing to its decay mode, and since we assume that the strong coupling interaction is a γ_5 interaction, we are forced to introduce baryon fields with various intrinsic parities.

Now let us consider any element of the S-matrix

$$\langle f|S|i\rangle=(\Psi_f^*\cdot S\Psi_i)$$

which is rewritten under inversion as

$$\langle f|S|i\rangle=[(I\Psi_f)^*\cdot ISI^{-1}\cdot(I\Psi_i)].$$

Here I is a unitary operator representing inversion. Now suppose that Ψ_i and Ψ_f are the eigenstates of I, i.e.,

$$I\Psi_i=\eta_i\Psi_i,\quad I\Psi_f=\eta_f\Psi_f,\quad \eta=+1 \text{ or } -1,$$

and that S is invariant under inversion (no external field is present), namely,

$$ISI^{-1}=S. \quad (4.2)$$

Then we get

$$\langle f|S|i\rangle=\eta_i\eta_f\langle f|S|i\rangle$$

or

$$\eta_i=\eta_f. \quad (4.3)$$

$$T_n^{(\chi)}=i\begin{pmatrix} 0 & 1 & 0 & 0 & 0 \\ 0 & 0 & 0 & 0 & 0 \\ 0 & 0 & 0 & \sqrt{2} & 0 \\ 0 & 0 & 0 & 0 & \sqrt{2} \\ 0 & 0 & 0 & 0 & 0 \end{pmatrix}=T_{22}^{(\chi)\dagger}$$

$$T_{11}^{(\chi)}=-i\begin{pmatrix} 1/2 & 0 & 0 & 0 \\ 0 & -1/2 & 0 & 0 \\ 0 & 0 & 1 & 0 \\ 0 & 0 & 0 & -1 \end{pmatrix}=T_{22}^{(\chi)}$$

FIG. 1. Representation of $T^{(\chi)}$.

$$T_1^{(\theta)}=i\begin{pmatrix} O_2 & 1 & 0 & 0 \\ 0 & O_1 & 0 & \\ 0 & 0 & O_3 & \begin{matrix}\sqrt{2} & 0\\ 0 & 1\\ 0 & 0\end{matrix} \\ 0 & 0 & 0 & O_2 \end{pmatrix}$$

$$T_2^{(\theta)}=i\begin{pmatrix} O_2 & 0 & 0 & 0 \\ 0 & 1 & 0 & \\ 0 & 0 & O_3 & \begin{matrix}0 & 0\\ 1 & 0\\ 0 & \sqrt{2}\end{matrix} \\ 0 & 0 & 0 & O_2 \end{pmatrix}$$

FIG. 2. Representation of $T^{(\theta)}$.

This is nothing but the usual conservation law of parity.[7] (4.2) is a trivial relation in ordinary meson theory. However, in our case this requirement gives rise to some restrictions on the form of the interaction.

By using (3.4), $L_{\text{int}}^{(S)}$ can be written in the following way:

$$L_{\text{int}}^{(S)}=g\sum_{a,b,b'}\chi_{(a)}\bar{\psi}_{(b)}\gamma_5 T_{(a,b,b')}\cdot\psi_{(b')}, \quad (4.4)$$

where $\chi_{(a)}$ means some kind of meson, $\psi_{(b')}$ and $\bar{\psi}_{(b)}$ stand for some kinds of baryons, and finally $T_{(a,b,b')}$ stands for some rectangular submatrix shown in (3.4).

Now (4.2) is equivalent to

$$\int IL_{\text{int}}^{(S)}(\chi)I^{-1}d^4x=\int L_{\text{int}}^{(S)}(\chi)d^4x,$$

and from this relation, we get

$$-\epsilon_a\epsilon_b^*\epsilon_{b'}=1. \quad (4.5)$$

Here ϵ_a is equal to ±1 and means the intrinsic parity of $\chi_{(a)}$, ϵ_b and $\epsilon_{b'}$, (ϵ^* is a complex conjugate of ϵ) are the intrinsic parities of baryons introduced in (4.1).[8] If the ordinary nucleon is assumed to be a type-A spinor, the spinors of type-C and -D can be excluded from consideration on account of (4.5). From (4.4) and (4.5), we see that some of the submatrices in (3.4) must be put equal to zero. If we assume the parity assignment as shown in the table which was given in the paper of U. T., the representation of T-matrices is given by

[6] C. N. Yang and J. Tiomno, Phys. Rev. **79**, 495 (1950); S. Watanabe, Sci. Papers Inst. Phys. Chem. Research (Tokyo) **39**, 157 (1941); Wick, Wightman, and Wigner, Phys. Rev. **88**, 101 (1952).

[7] Of course in η the parity due to the orbital angular momentum is included.

[8] In the present paper the intrinsic parity is defined in the following way; (i) spinor field is transformed under inversion as

$$\psi(x)\to\epsilon\gamma_4\psi(-x),$$

(ii) tensor or scalar field is transformed as

$$A_{\mu\nu\cdots\lambda}(x)\to\epsilon(-1)^n A_{\mu\nu\cdots\lambda}(-x);$$

n=the number of suffices which are not equal to 4 among μ, ν, $\cdots\lambda$. In both cases, ϵ is called the intrinsic parity of the field considered.

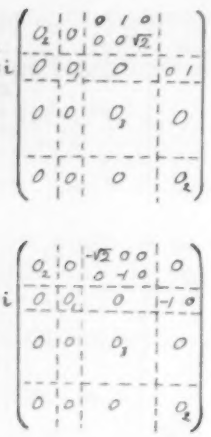

FIG. 3. Representation $T^{(7)}$.

Figs. 1, 2, and 3. In obtaining these representations, some use has been made of the assumed invariance under charge conjugation.

Since $L_{\text{int}}^{(S)}$ satisfies relation (4.5), we have the following relation for any transition exclusively depending on $L_{\text{int}}^{(S)}$:

$$\epsilon_i(-1)^{n_i}=\epsilon_f(-1)^{n_f}. \tag{4.6}$$

Here ϵ is the product of the intrinsic parities of all the particles present, n is the total number of all the kinds of mesons present, and i and f indicate the initial and final quantities respectively. The relation (4.6) is easily verified by considering any particular Dyson-Feynman diagram and supposing that at every vertex of the diagram the relation (4.5) is valid.

This new rule is essentially due to the particular choice of the interaction Lagrangian and, of course, does not contradict the validity of the usual parity law (4.3).

5. ELECTROMAGNETIC INTERACTION AND WEAK INTERACTION

The Lagrangian of the electromagnetic interaction introduced in Sec. 3 is

$$L^{(1)}{}_{\text{el. mag}}=eA_\mu\bar{\psi}\gamma^\mu C\psi+ieA_\mu\{-\chi^*C'\partial^\mu\chi+\partial^\mu\chi^*C'\chi\}-e^2A_\mu A^\mu\chi^*C''\chi. \tag{5.1}$$

The matrices C and C' are diagonal in the particular representation in which χ and ψ have the representations shown in footnote 5. Therefore transitions due to (5.1) do not give rise to any change of characters of baryons and mesons. In other words, the conservation of A and the ϵ rule (4.6) are also valid for these transitions.

In the usual meson theory, besides (5.1), we have another kind of electromagnetic interaction, namely, the so-called "Pauli-type interaction":

$$\tfrac{1}{4}\mu\bar{\psi}[\gamma^\mu\gamma^\nu]\psi F_{\mu\nu},\quad F_{\mu\nu}=\partial_\mu A_\nu-\partial_\nu A_\mu,$$

μ = the magnetic moment of nucleons.

Similarly, we can introduce in the present framework the following gauge invariant electromagnetic interaction:

$$L^{(2)}{}_{\text{el. mag}}=\tfrac{1}{4}\mu\bar{\psi}[\gamma^\mu\gamma^\nu]U\psi F_{\mu\nu}, \tag{5.2}$$

where the matrix U is an (8×8)-matrix and plays a similar role to that of our T-matrices.

This U-matrix is not necessarily diagonal but the requirements of the conservation of A and the ϵ rule (4.6) lead to the following representation of U:

(i) if Σ^0 and Λ^0 have the same intrinsic parity,

$$U=\begin{pmatrix}\mu_1 & 0 & & & & & & 0\\ 0 & \mu_2 & & & & & & \\ & & \mu_3 & 0 & a & 0 & & \\ & & 0 & \mu_4 & 0 & 0 & & \\ & & a & 0 & \mu_5 & 0 & & \\ & & 0 & 0 & 0 & \mu_6 & & \\ & & & & & & \mu_7 & 0\\ 0 & & & & & & 0 & \mu_8\end{pmatrix},$$

where the μ_i's and a are some real constants;

(ii) if Σ^0 and Λ^0 have the opposite parities, U is diagonal.

In the case (i) a fast γ decay of Σ^0 to Λ^0 is possible if the value of a is suitably chosen.

So far, we have discussed only the strong and electromagnetic interactions. For both types of interactions the ϵ rule (4.6) and the conservation of A-values and of the number of baryons are always valid.

Now let us discuss the possible types of weak interactions. These we define in the following way; a weak interaction is one which violates the ϵ rule or the conservation of A-values or both. However, the requirements of gauge-invariance and of the conservation of the number of baryons should be also satisfied, for this interaction.

We shall discuss separately the following three possible cases.

(i) A is conserved but ϵ rule is violated.

The interaction Lagrangian is

$$L_1^{(W)}=f[\bar{\psi}\mathbf{V}\psi\cdot\chi+\text{Hermitian conj.}], \tag{5.3}$$

where

$$\mathbf{V}=(V_{\alpha\beta}{}^{(\tau)},V_\alpha{}^{(\theta)},V_\alpha{}^{(\tau)}),$$

and

$$f\ll g.$$

Each V-matrix can be determined (to some extent) by the requirements of the gauge invariance and of the conservation of A. Namely, by using the notation of Sec. 3, these two requirements lead to

$$\mathbf{V}C'=[C,\mathbf{V}]\quad\text{(gauge invariance)} \tag{5.4}$$

TABLE I. Assignments of τ spin and intrinsic parity.

Particle	P, N	Λ^0	$\Sigma^+, \Sigma^0, \Sigma^-$	Y^0, Y^-	π^+, π^0, π^-	θ^+, θ^0	τ^+, τ^0
Spatial spin	1/2	1/2	1/2	1/2	0	0	0
Spatial parity	A (+)	B (−)	A (+)	B (−)	P.S. (−)	S. (+)	P.S. (−)
τ-spin	1/2	0	1	1/2	1	1/2	1/2
A-value	1/2	0	0	−1/2	0	1/2	1/2
Wave function	$\psi_{(N)}{}^{\alpha}$	$\psi_{(\Lambda)}$	$\psi_{(\Sigma)}{}^{\alpha\beta}$	$\psi_{(Y)}{}^{\alpha}$	$\chi_{(\pi)}{}^{\alpha\beta}$	$\chi_{(\theta)}{}^{\alpha}$	$\chi_{(\tau)}{}^{\alpha}$
			ψ			χ	

and

$$\mathbf{V}A'=[A,\mathbf{V}] \quad \text{(conservation of } A\text{)}. \tag{5.5}$$

Furthermore since (5.3) is a non-γ_5 interaction, $\mathbf{V}$ has the following property:

$$\begin{aligned}&(A|V^{(\pi)}|A)=(B|V^{(\pi)}|B)=0,\\ &(A|V^{(\tau)}|A)=(B|V^{(\tau)}|B)=0,\\ &(A|V^{(\theta)}|B)=(B|V^{(\theta)}|A)=0.\end{aligned} \tag{5.6}$$

These conditions (5.4)–(5.6) lead to a concrete representation for the V-matrix. For example, in our particular case, as shown in Table I, the representation of $V^{(\tau)}$ is given in Fig. 4, where a and b are some complex numbers while c must be a pure imaginary constant. (ii) ϵ rule is valid but A value is not conserved.

The interaction Lagrangian is

$$L_2{}^{(W)}=f[\bar{\psi}\gamma_5\mathbf{W}\psi\cdot\chi+\text{Hermitian conj.}]. \tag{5.7}$$

In this case, $\mathbf{W}$ must satisfy the following relations:

$$\mathbf{W}C'=[C,\mathbf{W}], \tag{5.8}$$

$$\mathbf{W}A'\neq[A,\mathbf{W}], \tag{5.9}$$

$$\begin{aligned}&(A|W^{(\pi)}|B)=(B|W^{(\pi)}|A)=0,\\ &(A|W^{(\tau)}|B)=(B|W^{(\tau)}|A)=0,\\ &(A|W^{(\theta)}|A)=(B|W^{(\theta)}|B)=0.\end{aligned} \tag{5.10}$$

(5.9) is just the formal expression of the following postulate: we must put equal to zero all those matrix elements which allow transitions conserving the A-value. (iii) ϵ rule and conservation of A are violated.

In this final case, the Lagrangian is

$$L_3{}^{(W)}=f[\bar{\psi}\mathbf{Y}\psi\cdot\chi+\text{Hermitian conj.}]. \tag{5.11}$$

The $\mathbf{Y}$-matrices must have the following properties:

$$\begin{aligned}&\mathbf{Y}C'=[C,\mathbf{Y}],\\ &\mathbf{Y}A'\neq[A,\mathbf{Y}],\\ &(A|Y^{(\pi)}|A)=(B|Y^{(\pi)}|B)=0,\\ &(A|Y^{(\tau)}|A)=(B|Y^{(\tau)}|B)=0,\\ &(A|Y^{(\theta)}|B)=(B|Y^{(\theta)}|A)=0.\end{aligned} \tag{5.12}$$

From (5.8)–(5.10) and (5.12), we can derive concrete representations for $\mathbf{W}$ and $\mathbf{Y}$.

$$V_{11}^{(\pi)}=\begin{pmatrix} 0_2 & 0 & 0 & 0\\ 0 & 0 & 0\ 0\ a & 0\\ 0 & b\\ & 0 & 0_3 & 0\\ & 0\\ 0 & 0 & 0 & 0_2\end{pmatrix}=V_{22}^{(\pi)\dagger}$$

$$V_{12}^{(\pi)}=\begin{pmatrix} 0_2 & 0 & 0 & 0\\ 0 & 0 & 0\ c\ 0 & 0\\ 0\\ 0 & c & 0_3 & 0\\ 0\\ 0 & 0 & 0 & 0_2\end{pmatrix}=V_{21}^{(\pi)}$$

$$=-V_{12}^{(\pi)\dagger}$$

FIG. 4. Representation of $V^{(\pi)}$.

ACKNOWLEDGMENTS

The author wishes to express his gratitude to Professor J. R. Oppenheimer, Professor A. Pais, Professor C. N. Yang, and Dr. W. Tobocman for valuable discussions on the present paper. It is also a pleasure to acknowledge my indebtedness to Professor J. R. Oppenheimer and the Institute for Advanced Study for their kind hospitality.

APPENDIX[9]

We shall explain briefly how to get the representation of T-matrices. As an example, let us consider the second equation of (2.4):

$$\sum_{\alpha'=1}^{2} T_{\alpha'}{}^{(\theta)}(\alpha'|D^{(\frac{1}{2})}(\tfrac{1}{2})|\alpha)=[D^{(\frac{1}{2})},T_{\alpha}{}^{(\theta)}]. \tag{2.4}$$

Now let us take a particular representation for $D^{(\frac{1}{2})}$ as given in Sec. 3. In such a representation the D's are

[9] The method here developed is quite similar to what was presented by Bhabha in his paper: H. J. Bhabha, Revs. Modern Phys. 17, 200 (1945).

given by the following expressions: put

$$D_P=D^{23}+iD^{31},\quad D_q=D^{23}-iD^{31},\quad D_Z=D^{12};$$

then

$$(l,m|D_P|l,m-1)=(l,m-1|D_q|l,m)=[(l+m)(l-m+1)]^{\frac{1}{2}},\quad (A.1)$$

$$(l,m|D_Z|i,m)=m,\quad m=l,l-1,\cdots-(l-1),-l,$$

where $(l,m|D|l',m')$ means an (m,m')-element of a $(2l+1)\times(2l'+1)$-rectangular-submatrix of D. Furthermore, $(\alpha'|D(\frac{1}{2})|\alpha)$ is represented in the following way:

$$(\alpha|D^{23}(\tfrac{1}{2})|\beta)=(\alpha|\tau_1|\beta),\quad \text{etc.},$$

where the τ's are defined by

$$\tau_1=\begin{pmatrix}0 & 1/2\\ 1/2 & 0\end{pmatrix},\quad \tau_2=\begin{pmatrix}0 & -i/2\\ i/2 & 0\end{pmatrix},\quad \tau_3=\begin{pmatrix}1/2 & 0\\ 0 & -1/2\end{pmatrix}.\quad (A.1)'$$

For the sake of convenience, let us rewrite (2.4) as follows:

$$[D_P\cdot T_1]=0,\quad (A.2),\qquad [D_P,T_2]=T_1,\quad (A.3)$$

$$[D_q\cdot T_1]=T_2,\quad (A.4),\qquad [D_q,T_2]=0,\quad (A.5)$$

$$[D_Z\cdot T_1]=\tfrac{1}{2}T_1,\quad (A.6),\qquad [D_Z,T_2]=-\tfrac{1}{2}T_2,\quad (A.7)$$

where the representation (A.1)′ has been used. Substituting (A.1) into (A.6) and (A.7), we get

$$(m-m'-\tfrac{1}{2}),\ (l,m|T_1|l',m')=0,$$
$$(m-m'+\tfrac{1}{2}),\ (l,m|T_2|l',m')=0.$$

Therefore the nonvanishing elements of T_1 and T_2 have the forms

$$(l,m|T_1|l',m-\tfrac{1}{2})\neq 0,\quad (l,m|T_2|l',m+\tfrac{1}{2})\neq 0.\quad (A.8)$$

From (A.2) we have

$$[(l+m)(l-m+1)]^{\frac{1}{2}}\cdot(l,m-1|T_1|l',m-\tfrac{3}{2})=[(l'+m-\tfrac{1}{2})(l'-m+\tfrac{3}{2})]^{\frac{1}{2}}\cdot(l,m|T_1|l',m-\tfrac{1}{2}).\quad (A.9)$$

By putting $m=-l$ or $l'+\frac{3}{2}$ in (A.9), this equation becomes

$$[(l'-l-\tfrac{1}{2})(l'+l+\tfrac{3}{2})]^{\frac{1}{2}}\cdot(l,-l|T_1|l',-l-\tfrac{1}{2})=0$$

or

$$[(l+l'+\tfrac{3}{2})(l-l'-\tfrac{1}{2})]^{\frac{1}{2}}\cdot(l,l'+\tfrac{1}{2}|T_1|l',l')=0.$$

Thus, if

$$l'=l\pm\tfrac{1}{2},\quad (A.10)$$

we have

$$(l,-l|T_1|l+\tfrac{1}{2},-l-\tfrac{1}{2})\neq 0,$$
$$(l,l|T_1|l-\tfrac{1}{2},l-\tfrac{1}{2})\neq 0.$$

Similarly, from (A.5) we can derive the relation (A.10). Accordingly, the nonvanishing elements of T-matrices take the forms

$$f_1^{\pm}(l,m)\equiv(l,m|T_1|l\pm\tfrac{1}{2},m-\tfrac{1}{2}),$$
$$f_2^{\pm}(l,m)\equiv(l,m|T_2|l\pm\tfrac{1}{2},m+\tfrac{1}{2}).\quad (A.11)$$

By substituting (A.11) into (A.2) and (A.5), the following recursion formula can be derived:

$$(l-m+1)^{\frac{1}{2}}\cdot f_1^{+}(l,m-1)=(l-m+2)^{\frac{1}{2}}\cdot f_1^{+}(l,m),$$
$$(l+m)^{\frac{1}{2}}\cdot f_1^{-}(l,m-1)=(l+m-1)^{\frac{1}{2}}\cdot f_1^{-}(l,m),$$
$$(l+m)^{\frac{1}{2}}\cdot f_2^{+}(l,m)=(l+m+1)^{\frac{1}{2}}\cdot f_2^{+}(l,m-1),$$
$$(l-m+1)^{\frac{1}{2}}\cdot f_2^{-}(l,m)=(l-m)^{\frac{1}{2}}\cdot f_2^{-}(l,m-1).$$

Therefore, we have the solution

$$f_1^{+}(l,m)\propto(l-m+1)^{\frac{1}{2}},$$
$$f_1^{-}(l,m)\propto(l+m)^{\frac{1}{2}},$$
$$f_2^{+}(l,m)\propto(l+m+1)^{\frac{1}{2}},$$
$$f_2^{-}(l,m)\propto(l-m)^{\frac{1}{2}}.$$

Substituting these into (A.3) and (A.4), we get the final solution

$$f_1^{+}(l,m)=a_l(l-m+1)^{\frac{1}{2}},$$
$$f_1^{-}(l,m)=b_l(l+m)^{\frac{1}{2}},$$
$$f_2^{+}(l,m)=-a_l(l+m+1)^{\frac{1}{2}},$$
$$f_2^{-}(l,m)=b_l(l-m)^{\frac{1}{2}},$$

where a_l and b_l are arbitrary complex constants only depending on l. For example, in our case we have

$$T_1^{(0)}=\begin{pmatrix}0 & 0 & b & 0 & a & 0 & 0 & 0\\ 0 & 0 & 0 & 0 & 0 & a\sqrt{2} & 0 & 0\\ 0 & c & 0 & 0 & 0 & 0 & 0 & d\\ e\sqrt{2} & 0 & 0 & 0 & 0 & 0 & f\sqrt{2} & 0\\ 0 & e & 0 & 0 & 0 & 0 & 0 & f\\ 0 & 0 & 0 & 0 & 0 & 0 & 0 & 0\\ 0 & 0 & g & 0 & h & 0 & 0 & 0\\ 0 & 0 & 0 & 0 & 0 & h\sqrt{2} & 0 & 0\end{pmatrix}.$$

On account of the gauge invariance, c, e, g, and h must vanish, Further, the ϵ rule makes a and d vanish because of our parity assignments.

East-West Asymmetry of Positive and Negative Mesons at the Geomagnetic Equator*

F. B. HARRIS,† *Massachusetts Institute of Technology, Laboratory for Nuclear Science, Cambridge, Massachusetts*

AND

I. ESCOBAR V.,‡ *Universidad Mayor de San Andrés, La Paz, Bolivia*

(Received June 22, 1955)

The intensities of positive and negative μ mesons at zenith angles of 45° in the east-west plane and at the vertical have been measured at atmospheric depth 548 g cm^{-2} near the geomagnetic equator. The data are analyzed through use of the empirical production spectrum and unidimensional equation for μ-meson production employed by Sands and by Olbert. A careful theoretical discussion is given, taking into account in detail the various effects arising both from the variation of the geomagnetic cutoff with direction of incidence of the primaries and from the curvature of the trajectories of the mesons in the earth's magnetic field after their production in the atmosphere. It is found that, to bring the 45° and vertical data into accord, it is necessary to assume an rms angle of production of the parent π mesons of 14°±2°. It is then possible to express the production spectrum, at any geographical location, by the single equation $G(R')=A[R'+a(M_c)]^{-n}$, where M_c is the cutoff magnetic rigidity for the primaries in a given direction of incidence at that location. The data do not indicate the presence of any appreciable number of negatively charged particles in the primary cosmic radiation.

I. INTRODUCTION

THE various directional asymmetries observed in the secondary cosmic radiation arise through two principal mechanisms. The first of these is the action of the magnetic field of the earth upon the primary particles. The second is the curvature, in the same magnetic field, of the trajectories of the secondary particles after their production in the atmosphere.

Fortunately, it is possible mathematically to consider the two processes as taking place consecutively, rather than concurrently. That is, the depth of the atmosphere is sufficiently small in comparison with the radii of curvature of those primary trajectories which are of interest that the primaries can be considered to undergo all of their deflection outside the atmosphere and to follow rectilinear trajectories after their entrance into the atmosphere. The secondaries however, much degraded in energy with respect to their primary parents, have considerable curvature in the magnetic field. The depth of the atmosphere is small enough compared with the radius of the earth that the portion of the earth's surface above which the secondary phenomena occur can be considered plane.

We shall follow Sands[1] and Olbert[2-4] in employing an empirical differential range spectrum of μ mesons at production of the form

$$G(R')=A(a+R')^{-n}, \tag{1}$$

where R' is the range of the μ meson at production. Sands derived values for the three constants of Eq. (1) on the basis of data on the vertical intensity at one latitude. Olbert reasoned that since very high-energy μ mesons can come only from high-energy primaries, i.e., those which are not affected by the earth's magnetic field, the spectrum for large values of R' must be independent of position on the earth, provided the primary radiation in the neighborhood of the earth is isotropic. Now the only one of the three empirical constants in the foregoing expression to which $G(R')$ is insensitive at large ranges is a, so that if indeed the empirical expression for the production spectrum does have this same general form at all locations on the earth, the constants A and n must be the same everywhere. He thus extended Eq. (1) to apply to the vertical direction at various geomagnetic latitides, a becoming a function of geomagnetic latitude. His values of the various parameters were based on more complete data than were Sands'.

The purpose of this paper is threefold: (a) to extend the range of applicability of Eq. (1) to include not only any location on the earth and any altitude, but also any direction of observation, (b) to relate a more precisely to the geomagnetic cutoff, and (c) to develop a theory whereby the intensities of positive and negative μ mesons in a given direction may be separately computed and the primary and secondary effects on the east-west asymmetries understood.

II. GEOMAGNETIC EFFECTS

The behavior of a particle in a magnetic field *in vacuo* depends exclusively upon its magnetic rigidity M, or ratio of momentum to charge. The magnetic rigidity in Bv is numerically equal to the momentum in Bev/c for singly charged particles, but of course not for multiply charged particles.

For a given direction of incidence at a particular

* Supported in part by the joint program of the Office of Naval Research and the U. S. Atomic Energy Commission.

† Now at Utica College of Syracuse University, Utica, New York.

‡ Now at the Centro Brasileiro de Pesquizas Físicas, Rio de Janeiro, Brazil.

[1] M. Sands, Phys. Rev. **77**, 180 (1950).

[2] S. Olbert, Phys. Rev. **92**, 454 (1953).

[3] S. Olbert, Technical Report No. 61, Laboratory for Nuclear Science, Massachusetts Institute of Technology, 1954 (unpublished).

[4] S. Olbert, Phys. Rev. **96**, 1400 (1954).

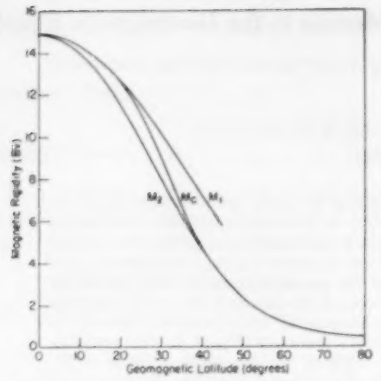

FIG. 1. The three critical magnetic rigidities, M_1, M_2, and M_c, in the vertical direction, uncorrected for eccentricity of the earth's dipole, as functions of geomagnetic latitude λ. At a given latitude, particles of all rigidities greater than M_1 arrive vertically, while no particles of rigidities less than M_2 can arrive. M_c is a tentative equivalent "cutoff" rigidity producing, as nearly as possible, the same secondary effects as the true rigidity spectrum of primaries

location on the earth, the terrestrial magnetic field acts as a rigidity filter on the primary radiation. No particles having rigidity less than M_2, computed from either the Störmer cone or the simple shadow cone,[5,6] can reach the earth in the given direction. Particles of all rigidities greater than M_1, computed from the main cone,[7,8] can arrive from that direction. Between M_1 and M_2, in the so-called "penumbra," some rigidities are allowed, others forbidden, the region ranging from mostly forbidden at the equator to mostly allowed at the poles. If, at a certain location, a given direction is accessible to particles of a certain rigidity, particles of that rigidity will arrive at the top of the atmosphere in that direction with the same intensity as that which they would have in the absence of the magnetic field.[9,10]

Since experimentally what is observed in the penumbra is some sort of "average" or effective intensity having a value between zero and the full intensity, in practice it is customary to define an effective "cutoff rigidity" M_c at a given location and in a given direction, above which all particles are assumed to arrive with full intensity and below which the intensity is zero. M_c is naturally intermediate in value between M_1 and M_2, coinciding with M_1 at very low latitudes and with M_2 at very high latitudes. Curves of M_1 and M_2,[11] and a tentative curve of M_c, at the vertical as functions of geomagnetic latitude are shown in Fig. 1, under the assumption of a centrally located magnetic dipole. In the east-west plane at the equator, the Störmer and main cones very nearly coincide, so that the simple Störmer theory holds approximately.

Actually the true field of the earth is much better represented by a dipole located at 342 km from the center.[12] For most purposes, the simplest procedure is to consider first the symmetrical case, and then make corrections for the eccentricity of the dipole.

The magnitudes of the several critical rigidities mentioned above depend inversely upon the square of the radius of the earth. Hence, the most important correction which must be made upon the symmetrical case is that due to the fact that the actual distance from the observer on the surface of the earth to the eccentrically placed dipole is not equal to the radius of the earth. The fractional correction to one of the critical rigidities is given by the relation

$$(\Delta M/M) = -0.106 \cos\lambda \cos(\omega - 18.2°), \quad (2)$$

where λ is the geomagnetic latitude and ω the geomagnetic longitude.

A second but rather less important correction is due to the fact that the magnetic vertical, again because of the eccentric position of the dipole, does not coincide with the gravitational vertical. This correction can be applied properly only by referring all directions to a new meridian plane, which has been rotated through an angle θ_m with respect to the geographical meridian plane, about an axis parallel to the axis of the earth's dipole. This angle can be computed as follows:

$$\sin\theta_m = 0.053 \sin(\omega - 18.2°), \quad (3)$$

where a positive result indicates that the new reference plane lies east of the meridian plane. It is seen that the angle of rotation varies from zero to about 3°. *At the vertical*, one can derive the following approximate expression for the fractional correction due to this effect, useful except at very high latitudes:

$$(\Delta M/M) = -0.027 \sin(\omega - 18.2°) \cos^3\lambda. \quad (4)$$

Thus we have, at the vertical, the following general expression:

$$M = M_0[1 - 0.106 \cos(\omega - 18.2°) \cos\lambda - 0.027 \sin(\omega - 18.2°) \cos^3\lambda], \quad (5)$$

where here M represents the corrected value of one of the critical rigidities, either M_1, M_2, or M_c, and M_0 represents its uncorrected value (i.e., computed for the case of a centrally located dipole).

Geomagnetic latitude λ can be computed from the following expression:

$$\sin\lambda = \cos 78.5° \cos(\Omega - 69.0°) \cos\Lambda + \sin 78.5° \sin\Lambda, \quad (6)$$

where Λ and Ω are geographic latitude and longitude, respectively. The geomagnetic longitude ω can be computed from a similar expression as follows:

$$\cos(\omega - 69.0°) = (\cos\lambda)^{-1} \times [\sin 78.5° \cos(\Omega - 69.0°) \cos\Lambda - \cos 78.5° \sin\Lambda]. \quad (7)$$

In both the above formulas, west longitude and north latitude are considered positive.

III. INTENSITY OF μ MESONS IN THE ATMOSPHERE

(a) Discussion

The intensity of μ mesons observed in a given direction at a given atmospheric depth at a given

[5] C. Störmer, Z. Astrophys. **1**, 237 (1930).
[6] E. J. Schremp, Phys. Rev. **54**, 158 (1939).
[7] G. Lemaître and M. S. Vallarta, Phys. Rev. **49**, 719 (1936).
[8] G. Lemaître and M. S. Vallarta, Phys. Rev. **50**, 493 (1936).
[9] G. Lemaître and M. S. Vallarta, Phys. Rev. **43**, 87 (1933).
[10] W. F. G. Swann, Phys. Rev. **44**, 224 (1933).
[11] For curves of proton energies corresponding to M_1 and M_2 in various directions, see M. S. Vallarta, Phys. Rev. **74**, 1837 (1948).
[12] J. Bartels and S. Chapman, *Geomagnetism* (Oxford University Press, London, 1940), p. 651.

location on the earth depends upon a large number of factors. The observed μ mesons comprise contributions from π mesons decaying in flight at all atmospheric levels above the point of observation. Their energy at production is greater than that at observation by an amount determined by the ionization loss experienced in transit, and the fraction of those produced at a given level arriving at the level of observation is influenced by the survival probability of μ mesons.

The π mesons decaying at any particular level have in turn been produced in nuclear interactions at all levels above that at which they decay. In addition to the considerations mentioned above for the case of μ mesons, the number of π mesons succeeding in giving birth to μ mesons depends also upon the cross section for nuclear interaction of π mesons.

The number of π mesons produced at a given level depends, of course, upon the intensity and composition of the nucleonic component at that level. If the primary particles are all of one sign, the character of the nucleonic component at the top of the atmosphere is determined, to a good order of approximation, only by the one parameter M_c, the effective cutoff rigidity. With Olbert,[3] we shall consider that this meson-producing component is then absorbed exponentially in the atmosphere with a mean free path of 121 g cm^{-2}.

The intensity of μ mesons in a given direction will thus depend not only upon the quantity of intervening material, but also upon the value of M_c in that direction. Since the survival probability depends chiefly upon linear spatial distance traversed, the intensity will depend also upon zenith angle due to the different density distribution found at an angle (if equal masses of intervening air are considered). For the same reason, it will depend upon the temperature distribution in the atmosphere above the point of observation. This last effect has been considered in some detail by Olbert.[2,3]

If one examines in more detail the problem of the paths of μ mesons in the atmosphere, it becomes evident that the above analysis must be modified to take into account the fact that their trajectories are appreciably curved due to the action of the terrestrial magnetic field after their production. In other words, the μ mesons observed in a certain direction have arisen from various points along a curved trajectory stretching back from the point of observation. Proceeding upward along this trajectory, the curvature is toward the east for positive mesons and toward the west for negatives. This problem was first studied by Rossi,[13] and later by Johnson[14] and Bowen.[15]

Olbert's computations,[3,4] for mesons having ranges between 100 and 6000 g cm^{-2} at sea level, assume that the parent π mesons decay instantaneously and that the direction of the primary particle is preserved in the π- and μ-meson production processes. Even with this simplification, the curvature of path profoundly complicates the computation of the μ-meson intensities, especially at directions other than the vertical.

Let us consider, for example, mesons arriving from some zenith angle in the east. The positives come in along a trajectory which bends farther away from the vertical as one moves upward, while the negatives follow a trajectory which bends closer to the vertical at the higher altitudes. Comparing positives and negatives born at the same altitude, one sees that the negatives on the average have traversed a shorter distance and a smaller mass of air than the positives, giving rise to two effects: (a) the negatives on the average have lower energies at birth than the positives, and (b) the survival probability of the negatives is greater on the average than that of the positives. Both these effects tend to favor the negatives. It must be borne in mind that the mesons observed come from all points of the trajectory, and that therefore the total number will depend upon a summation of all such contributions. The positive trajectory is longer than the negative, i.e., a greater mass of air is available in which the positives may be produced than the negatives. However, at mountain altitudes, this last effect is masked by the first two. All these effects are reversed in the west, and the net result is to favor the positives in that direction.

In the east, again due to the curvature, the negative mesons arise on the average from primaries incident at angles somewhat nearer the vertical than the angle of observation, while the reverse is true of the positives. Thus, the primaries which produce the negatives have, on the average, passed through less absorbing material than those which produce the positives. Like the effects discussed in the preceding paragraph, this effect favors negatives in the east and positives in the west.

It has been noted above that intensities in different directions are different because of different values of M_c. This effect is such as to favor the west over the east for both positives and negatives, since M_c is always greater in the east than in the west for predominantly positive primaries. There is another, but very much smaller, effect of this kind, involving particles of *opposite* sign observed in the *same* direction. The negatives arise on the average from primaries incident in more westerly directions than the positives, that is, from directions where M_c is smaller. Hence, this effect tends to favor negative mesons in *all* directions, except very near the western horizon, where the negative trajectories intersect the earth.

Another quantity which affects the relative numbers of positive and negative mesons observed is what will be called the "positive excess at production." This is defined as the *difference* between the numbers of positives and negatives produced, divided by the *average* of the two numbers. It will be a function not only of

[13] B. Rossi, Atti. accad. nazl. Lincei **15**, 62 (1932).
[14] T. H. Johnson, Phys. Rev. **59**, 11 (1941).
[15] I. S. Bowen, Phys. Rev. **45**, 349 (1943).

the energy of meson produced, but also presumably will vary with the energy of the producing particle.

It can easily be seen that, because of the complexity of the phenomena involved, the *observed* "positive excess" in a given direction is only very indirectly related to that at production. Even at the vertical, where the discrepancy is least serious, the observed excess depends to a considerable extent upon small terms in the expression for the μ-meson intensities. The procedure, adopted by some investigators, of speaking in terms of a positive excess defined *for a given zenith angle* as

$$2(W_+ + E_+ - W_- - E_-)/(W_+ + E_+ + W_- + E_-),$$

where W_+, for example, represents intensity of positives in the west, is to be discouraged, as this quantity is of but doubtful significance.

Another quantity not susceptible of direct physical interpretation is the east-west asymmetry defined as $2(W-E)/(W+E)$ for positives, negatives, or the natural mixture of both. In the last case (i.e., the natural mixture), it does approximate the effect due purely to the asymmetry of the primaries, although not exactly.

Since there are so many variables involved in the problem, naturally much more information can be gleaned from a study of the positives and negatives separately at various angles and at various energies. Groetzinger and McClure[16] measured the east-west asymmetries of positive and negative mesons for two different zenith angles at Mt. Evans, Colorado (geomagnetic latitude 49° N) and Chicago (51° N). Both these locations are considered to be above the knee of the latitude curve, that is, they are sufficiently far north so that the cutoff rigidity M_c is low enough in all directions to admit essentially all primaries important in producing the observed secondary cosmic radiation. Thus the asymmetries observed should be due only to the various effects of the curvature of the secondaries in the atmosphere after production. The experimental data are indeed consistent with such an interpretation, there being an asymmetry of positives toward the west, and a nearly equal asymmetry of negatives toward the east, of approximately the expected magnitude.

If the same observations are made at or near the equator, there is superposed upon the above asymmetries the effect of the large primary asymmetry at that latitude.

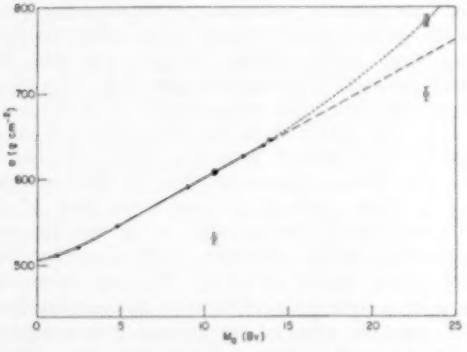

FIG. 2. The parameter a occurring in the expression for the production spectrum $G(R')$, as a function of cutoff rigidity M_c. The solid curve was derived from Olbert's results in the vertical direction. His points are shown by solid circles. The dashed curve represents the tentative extrapolation of this curve used in the early stages of the analysis.

The values of a_W and a_E obtained with the uncorrected theory are shown by hollow circles. The solid diamond indicates the value of a_W under the assumption that the latter lies on the curve, while the hollow diamond indicates the value derived for a_E on the basis of the same assumption. The dotted curve then represents the corresponding extension of Olbert's curve.

[16] G. Groetzinger and G. W. McClure, Phys. Rev. **77**, 777 (1950).

(b) Differential Range Spectrum of μ Mesons at Production

The number of mesons (positive and negative) of range between R' and $R'+dR'$ produced in a given direction at a given level of the atmosphere per gram of material, per steradian of solid angle, per second will here be represented by $G(R')\exp(-y/L)dR'$, where $G(R')$ is the differential μ-meson production spectrum of Eq. (1), y is the quantity of matter in g cm^{-2} intervening between the point of production and the top of the atmosphere *in the direction of production*, and L is the absorption mean free path of the nucleonic component in g cm^{-2}. G depends, of course, upon the composition of the incident radiation, and hence upon latitude, longitude, zenith angle, and azimuth. Implicit in this representation is the assumption that the composition of the nucleonic component does not change significantly as it passes down through the atmosphere, but that it is merely attenuated exponentially.

To the extent that the spectrum of the primary radiation is really describable in terms of the single cutoff rigidity M_c, it is evident that a is a function of M_c only. This relationship is shown in Fig. 2 for the range of cutoff rigidities covered by Olbert's work. The ordinates of the points shown were taken from Olbert,[3,4] while the abscissas were computed by us, using Eq. (5), for the actual flight path followed in taking the data[17] upon which Olbert's figures are based. The values of the other two parameters have been taken, at least tentatively, directly from Olbert, *viz.*: $A=7.31\times10^4$ g^{-2+n} cm^{2-2n} sec^{-1} sterad^{-1}, $n=3.58$.

Since we are here interested in the intensities of positive and negative mesons individually, it is necessary to consider two production spectra, which will be designated by $G_\sigma(R'+a)$, where σ is simply the sign of the meson, ±1. These are related to the positive excess at production $\delta(R',a)$ and the total production spectrum

[17] M. Conversi, Phys. Rev. **79**, 750 (1950).

$G(R'+a)$ as follows:

$$G_\sigma(R'+a)=\tfrac{1}{2}[1+\tfrac{1}{2}\sigma\delta(R',a)]G(R'+a). \quad (8)$$

(c) Definitions

Before proceeding to a consideration of the intensities, it will be convenient here to define and explain certain of the quantities which will enter into the discussion:

H—depth of atmosphere at point of observation (g cm^{-2}).
B—local horizontal terrestrial magnetic field (Gauss).
$\rho(Z)$—density of atmosphere at vertical height Z above point of observation (g cm^{-3}).
L—absorption mean free path of nucleonic component (taken to be 121 g cm^{-2}).
μ—rest mass of the μ meson (1.07×10^{8} ev/c^2).
τ—lifetime of the μ meson (2.10×10^{-6} sec).
q—charge of the meson ($\pm e$, the electronic charge).
R—residual range of meson at point of observation (g cm^{-2} air equivalent).
S—arc length upward along trajectory of meson from point of observation (g cm^{-2}).
Z—vertical height in the upward direction from point of observation (g cm^{-2}).
Θ—zenith angle of observation in east-west plane (considered positive if east of the vertical).
θ—zenith angle at point on trajectory, i.e., angle between tangent to curve and vertical at that point.
p—momentum of meson on arrival.
p'—momentum of same meson at distance S along its trajectory.
$w_\sigma(S,R)$—probability of survival until observation of a σ meson produced at distance S on trajectory which would arrive at point of observation with range R.

(d) Computation of the Intensities at the Equator

In the discussion which follows, three assumptions have been made: (a) π mesons decay instantaneously, (b) π meson and μ-meson production is collimated along the direction of flight of the original producing particle, and (c) multiple scattering of μ mesons in air is negligible.

For a detailed discussion of the range of validity of the above model, see reference 3. We shall return to these assumptions later.

In our case, we are interested specifically in the intensities of positive and negative μ mesons at various zenith angles in the east-west plane. In view of the above model of μ-meson production, we may write for these intensities

$$i_\sigma(R,\Theta) = \int_0 G_\sigma(R+S+a)\exp\left(-\frac{H-Z}{L}\sec\theta\right)w_\sigma(S,R)dS, \quad (9)$$

where the exponential expresses the absorption of the producing radiation, and the angle θ is *not* assumed to remain constant along the trajectory. The integration is carried from zero out to a point at which the survival probability has reduced the integrand essentially to zero.

It is possible to reduce Eq. (9) to the following form (see Appendix for details):

$$i_\sigma(R,\Theta)=C\cos^{n-1}\Theta J_1[1+\tfrac{1}{2}\sigma\bar{\delta}(R,a_1)]$$
$$\times\left[1-\left(\frac{J_2}{J_1}\right)\left(\frac{\Delta}{H}\right)+\tfrac{1}{2}\left(1+\frac{1}{n}\right)\left(\frac{J_2}{J_1}\right)^2\left(\frac{\Delta}{H}\right)^2\right]$$
$$\times\left[1-\sigma\gamma\tan\Theta\left(\frac{J_4}{J_1}\right)-\sigma\gamma\left(\frac{J_6}{J_1}\right)\left(\frac{1}{H}\frac{da}{d\theta}\right)_\Theta\right], \quad (10)$$

where the following abbreviations have been made: (a) $C=\frac{1}{2}A(nH)^{-n}$, (b) $a_1=a(\Theta)$, as distinguished from $a=a(\theta)$, (c) $\gamma=e\tau B/\mu$. The quantity $\bar{\delta}(R,a_1)$ is the average positive excess at production of mesons arriving in direction Θ with residual range R.

For computational purposes it was found convenient to express a_1 as $a_1+\Delta$, where a_1 is an arbitrarily chosen central value of a, presumably intermediate between the values expected in the directions to be considered, and Δ is a smaller quantity which is a function of Θ.

The J's which appear in Eq. (10) are all functions of R and $\cos\Theta$. They have been computed[18] for Chacaltaya [see Part IV, Sec. (b)], and are shown for $\pm45°$ in Fig. 3 and for the vertical in Fig. 4. At 45° a value of 621 g cm^{-2} was used for a_1, while at the vertical it was 640 g cm^{-2}. The quantity J_4 is absent

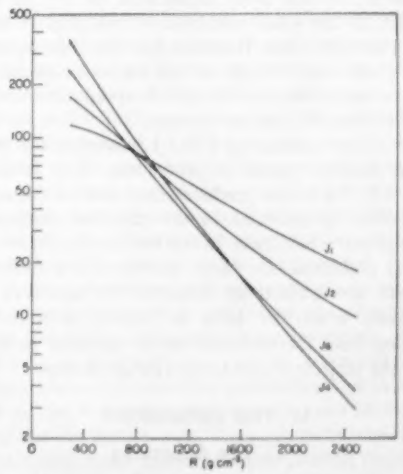

FIG. 3. The functions $J_i(R,\cos\Theta)$, in terms of which the intensities $i_\sigma(R,\Theta)$ are expressible, computed for $\Theta=\pm45°$.

[18] F. B. Harris, thesis, Massachusetts Institute of Technology, January, 1955 (unpublished).

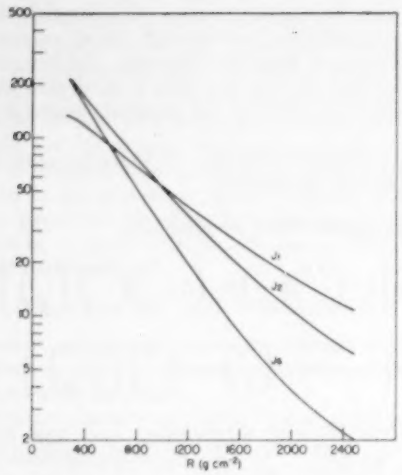

FIG. 4. The functions $J_i(R, \cos\Theta)$, in terms of which the intensities $i_e(R,\Theta)$ are expressible, computed for $\Theta=0°$.

at the vertical because there the term in which it occurs vanishes identically.

The constant C does not affect *comparative* intensity measurements taken at the same observatory. In addition, since the cosine is an even function of the angle, the multiplier $\cos^{n-1}\Theta J_1(R, \cos\Theta)$ does not enter into east-west asymmetry measurements based on the differential intensities.

Because of the complexity of the theory, and because the survival probability and the curvature effects are expressible in terms of the same integrals (see Appendix), it has been impractical to try to keep separate all the *effects* which come into play in determining the intensities. However, Eq. (10) does separate, for a given zenith angle in the east-west plane, the various *causes* leading to the observed asymmetries and the observed positive excesses.

The factor containing $\bar{\delta}(R,a_t)$ expresses the effect of the positive excess at production. The factor in which (J_2/J_1) occurs produces that part of the asymmetry directly traceable to the east-west asymmetry of the primary radiation. In the last factor, the term in (J_4/J_1) embodies the effect purely of the difference between the trajectories followed by positives and negatives, while the term in (J_6/J_1) is a hybrid, resulting from the variation in the primary radiation along the trajectory due to the change in slope.

IV. THE EXPERIMENT

(a) The Apparatus

A schematic end view of the apparatus used in the experiment to be described is shown in Fig. 5. The pieces marked I, II, III, and IV are long thin slabs of iron, each wound with several layers of heavy enameled wire. Sections I and II together form a complete magnetic circuit, being closed at the ends of the slabs by two pieces of the same material (not shown in the figure). Sections III and IV form a similar but separate magnetic circuit. In operation a magnetic field of 17 000 gauss is maintained, having one sense in I and III, and the opposite sense in II and IV.

The counters, marked A, B, C, D, and X in the figure, have a 20 in. effective length, and are of $\frac{9}{16}$ in. and $\frac{13}{16}$ in. i.d., respectively. Those having the same literal designation have their outputs connected directly together.

The entire ensemble, magnets and counters, and another identical ensemble are mounted on axes parallel to those of the counters. The twin units can be swung separately to the vertical or to $22\frac{1}{2}°$, $45°$, or $67\frac{1}{2}°$ from the vertical in either direction. The entire apparatus, in addition, can be rotated about a vertical axis and set at any desired azimuth.

In each case two threefold coincidences, (A,B,D) and (A,C,D), and two fourfold coincidences, (A,B,D,X) and (A,C,D,X), are counted. By taking directly the difference between readings of corresponding threefold and fourfold coincidences, one obtains the anticoincidence rates $(A,B,D,-X)$ and $(A,C,D,-X)$, i.e., for the former, those events in which there are simultaneous counts in A, B_1 or B_2, and D, but no simultaneous count in any of the counters X. The two anticoincidence counting rates above will be referred to as channel I counting rate and channel II counting rate, respectively.

The apparatus tends to select either positive or negative particles, depending upon the direction of the current. Groetzinger and McClure,[16] with a closely

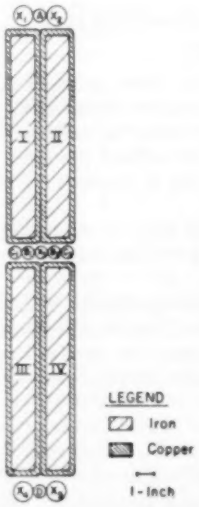

FIG. 5. End view of one of the two identical magnet arrangements. The smaller circles represent $\frac{5}{8}$ in. Geiger tubes, the larger ones 1-in. tubes. For clarity, the iron end pieces completing the two magnetic circuits (*viz.*, I–II and III–IV) have been omitted from the figure.

similar apparatus, found the probability of traversal of a particle of the wrong sign to be negligible.

The sensitivity of a counter telescope to μ mesons of various ranges is describable in terms of an "acceptance function" $r(R)$. This function is so defined that, if the intensity of such particles $i_\sigma(R)$ is constant over the opening angle of the telescope, the number of particles per second having ranges between R and $R+dR$ counted by the telescope is given by

$$dN_\sigma(R)=r(R)i_\sigma(R)dR. \tag{11}$$

Evidently, in our case there are two such functions, $r_1(R)$ and $r_2(R)$, one for each channel. They are shown in Fig. 6.

In their computation, an approximate analytical expression for the range-momentum relation in iron and copper was used for those particles entering the apparatus in a plane perpendicular to the axes of the counters. For those particles entering at an angle to this plane, it was assumed that this angle remains constant during the motion, and that the projection of the trajectory in the plane is the same as the trajectory of a particle entering parallel to the plane and having the same average radius of curvature in the magnetic field. A large number of these trajectories was computed, and the necessary multiple integrations actually performed numerically.

The computation of Fig. 6 also took into account the effect of multiple scattering of the mesons in the material of the magnets. If one considers the paths of mesons known to pass through the two points A and B, separated by a distance x, the lateral distribution in space at the midpoint can be shown to be Gaussian, and it is possible to derive an expression for the mean square lateral displacement.[19] The spreading due to scattering was considered to be superposed upon the deflection due to the curvature in the magnetic field. The acceptance function is not very sensitive to the exact value of the mean square displacement, the effect being to "smear out" the acceptance function, making the peak lower and spreading it out laterally. An approximate value of mean square displacement was chosen for each value of range of the incident particle, assuming that the particles are incident at an "average" angle with the plane perpendicular to the magnetic field in the equipment. It can be shown that this angle is about $13\frac{1}{2}°$.

Also included in Fig. 6 for comparison are the two other acceptance functions, $r_1'(R)$ and $r_2'(R)$, which apply when there is no field in the iron. Note that these latter represent the sensitivity of the instrument to particles of *either* sign, not to those of one sign exclusively. They are due entirely to scattering. The zero-field counting rates are approximately *one-sixth* the *sum* of positive and negative counting rates in a given direction.

[19] See, e.g., B. Rossi, *High-Energy Particles* (Prentice-Hall, Inc., New York, 1952), p. 72.

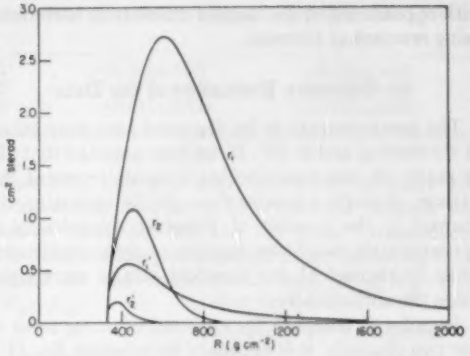

FIG. 6. Acceptance functions of one magnet assembly. r_1 and r_2 apply to particles of one sign only accepted by channels I and II, respectively, with field in the magnets *on*. r_1' and r_2' apply to particles of *any* sign accepted by channels I and II, respectively, with field in the magnets *off*.

(b) Description of the Experiment

The apparatus has been operated at the Laboratorio de Física Cósmica on Mt. Chacaltaya, Bolivia since May, 1952. Certain data pertinent to this laboratory appear below:

$\Lambda=16.4°$ S,	$\gamma=4.8\times10^{-2}$,
$\Omega=68.0°$ W,	$H=548$ g cm^{-2},
$\lambda=4.9°$ S,	mean annual air pressure $=403$ mm Hg,
$\omega=68.0°$ W,	altitude $=5210$ m (17 100 ft),
$B=0.27$ gauss,[20]	mean annual air temperature $=-2.2°$C.

The equipment was oriented with the counter axes magnetic north-south so that the two units could be inclined either magnetic east or west of the vertical. Measurements have been made at the various east and west zenith angles permitted by the equipment, as well as at the vertical, for positives, negatives, and with zero field in the magnets. In the east-west measurements, particles of a given sign were always counted at corresponding angles in east and west simultaneously, in order to reduce the effect of short-term variations in total cosmic-ray intensity on the asymmetries.

In these measurements, the two units can be inclined either toward or away from each other, the roles played by the two being thus easily interchangeable. These positions are designated ∧ and ∨, respectively. In addition, there exist two other possibilities, for in either the ∧ or the ∨ position, the apparatus can be rotated 180° about the vertical axis. The equipment is operated approximately equal times in the four possible positions, a change being made about every 80 hours. For the vertical measurements, the two telescopes were operated

[20] U. S. Coast and Geodetic Survey, *Magnetic Observations in the American Republics* (U. S. Department of Commerce, Washington, D. C., 1946), Serial 677.

with opposite signs, the magnet currents in both units being reversed at intervals.

(c) Tentative Evaluation of the Data

The measurements to be discussed here were taken at the vertical and at 45°. It has been assumed that all, or nearly all, the anticoincidence counts represent the passage of single μ mesons through the apparatus. In channel I, the number of threefold coincidences is approximately twice the number of anticoincidences, while in channel II the threefold rate is some eight times the anticoincidence rate.

In order to compute the expected counting rates in our two channels, it is necessary to integrate Eq. (11) over all values of R. To do so, it is convenient to choose an average value of $\bar{\delta}(R,\Theta)$ weighted, say, according to $r(R)J_1(R,\cos\Theta)$. This quantity will be denoted by $\delta_1(\Theta)$ or $\delta_2(\Theta)$, depending upon the channel to which we refer. It has been tacitly assumed that since the cone of acceptance of the telescope is symmetrical about the direction of inclination of the magnet assembly, Θ, the effect of the variation in intensity over the cone cancels out, at least in first order, and that therefore the effective intensity is that at zenith angle Θ.

After the integrations over the acceptance function, mentioned in the preceding paragraph, the various terms occurring in the expression for $i_\epsilon(R,\Theta)$ are found to have their counterparts in the expressions for the expected counting rates.[18] In our case, these counting rates will be represented by $W_\pm$, $E_\pm$, $V_\pm$, W_0, E_0, and V_0 for each channel, W, E, and V indicating 45° west, 45° east, and vertical, respectively, and the $\pm$ and 0 indicating polarity of the field in the iron or its absence.

The terms involving the derivative are very small and can be evaluated approximately using the curve of Fig. 2, extrapolated as shown to higher values of M_c in order to include directions east of the vertical. At Chacaltaya, the quantity $(da/d\theta)/H$ has the following approximate values: 0.075 (45° west), 0.216 (vertical), and 0.613 (45° east).

Before proceeding to a comparison of the data with the theoretical expressions it must be noted that even if (Δ/H), δ_1, and δ_2 are known for each direction the observed counting rates will differ from those predicted by the theory in two principal ways:

First, there is a small number of spurious events which succeed in triggering the proper combination of counters. In events of this type, the incoming particle may pass through two of the three counters necessary for a coincidence, while the third counter is triggered by another particle ejected at an angle by the incoming particle, either in a nuclear disintegration or in a knock-on process. Alternatively, the first particle may pass through one counter and its product through two, etc. Hence the number of such counts should be practically independent of the direction, presence, or absence of the magnetic field in the iron. In addition, it should be roughly the same for both channels.

Second, a normalizing constant must be employed to correct for the error introduced in the computation of the acceptance functions by the many approximations it was necessary to make. Another fact which will affect the normalizing constant is that a certain fraction of the particles passing through the proper three counters to cause a coincidence also produce knock-ons which trigger the anticoincidence counters, thus causing these events to be disregarded. The normalization is not necessarily the same for the two channels, nor for the zero-field case.

We shall assume that both these effects are present in some degree. It will also be assumed that δ_1 and δ_2 are unknown in all directions, that Δ (and therefore a) is unknown at 45° east and west, but that the value given by Fig. 2 for the vertical is correct.

From measured single and twofold coincidence rates, obtained by monitoring the equipment while in operation, it can be shown that corrections to the threefold and fourfold rates due to accidental coincidences and to counter dead time are entirely negligible.

There is a sufficient number of independent counting rates to evaluate the spurious counting rate, the normalization factors, and all the above unknowns. In fact, the problem is somewhat overdetermined, there being several counting rates not needed for the determination of the above quantities. This procedure yields the values of a shown on Fig. 2, plotted at $M_c=10.6$ and 23.3 Bv respectively, the corrected 45° west and east values at Chacaltaya. (The vertical value is 13.5 Bv, corresponding to $a=640$ g cm^{-2} on the curve.) The internal consistency of the data is excellent, as the superfluous counting rates are entirely compatible with the others, well within the experimental errors.

(d) Positive Excesses at Production

With the aid of Eq. (10), one can easily construct the observed positive excess in a given direction, as follows:

$$\epsilon(R,\Theta)=2\frac{i_+(R,\Theta)-i_-(R,\Theta)}{i_+(R,\Theta)+i_-(R,\Theta)}, \tag{12}$$

or, after simplification and neglecting certain very small terms in the denominator,

$$\bar{\delta}(R,a_i)=\epsilon(R,\Theta)+2\gamma\tan\Theta\frac{J_4(R,\cos\Theta)}{J_1(R,\cos\Theta)}$$
$$+2\gamma\frac{J_6(R,\cos\Theta)}{J_1(R,\cos\Theta)}H^{-1}(da/d\theta)_\theta. \tag{13}$$

Corresponding expressions for $\delta_1(\Theta)$ and $\delta_2(\Theta)$, involving $\epsilon_1(\Theta)$ and $\epsilon_2(\Theta)$, the observed excesses computed directly from the counting rates, and also involving the *integrals* of the J's, can be derived.[18] It

TABLE I. Positive excesses observed (ϵ) and at production (δ).

Direction	ϵ_1	δ_1	ϵ_2	δ_2
45° west	+0.300±0.017	+0.172±0.021	+0.301±0.067	+0.121±0.069
45° east	−0.104±0.021	+0.103±0.028	−0.212±0.089	+0.070±0.092
vertical	+0.073±0.008	+0.091±0.008	+0.075±0.028	+0.100±0.028

is worth noting that δ_1 and δ_2 can then be determined from the counting rates independently of the normalization, and are almost independent of the spurious rates, provided the latter are small. The ϵ's and δ's for the various directions are shown in Table I. The errors in the δ's shown are those corresponding to the statistical probable errors combined with an allowance for a possible 10% error in the computation of the numerical terms. However, the computations are seriously affected by the presence of small terms in the expression for the intensities of positives and negatives in a given direction.

V. MODIFICATIONS TO THE THEORY

Both a_W and a_E lie significantly below Olbert's curve (and its extrapolation, admittedly very uncertain). Physically, this means that all the intensities, both west and east, are rather higher than one would have expected in comparison with the vertical intensities. Of course, the points shown have been computed on the assumption that $\Delta_V=0$, or in other words that $a_V=640$ g cm^{-2}. However, a change in the value assumed for a_V does not improve this situation appreciably. We have investigated this possibility and have found that, even if one assumes that the curve of Fig. 2 lies much higher or lower, the computed values of a_W and a_E will be raised or lowered by a very nearly equal amount, and will therefore not be brought much nearer the curve.

Since all our 45° counting rates have in effect been normalized to the vertical, we must seek some effect or effects which come into play at 45° in a different way from that at the vertical. The first such effect which comes to mind is the possible existence of negative primaries. The cutoff at the vertical as a function of geomagnetic latitude is the same for primaries of either sign, while east and west about the (corrected) vertical are interchanged for the two types of particles. Hence, asymmetries in the east-west plane at the equator would be reduced by the presence of any considerable number of negative primaries, below what would be expected assuming the primaries to be exclusively positive in sign. Applied to our case, this means that a_W would lie above the curve derived from vertical data on the latitude effect, and a_E would lie below it. This is not adequate to explain the observed discrepancies.

In fact, disregarding the vertical data for the moment, one can compute, independently of the normalization, the asymmetries of positives and negatives on the assumption that a is really given by the curve and extrapolation of Fig. 2, i.e., that the western and eastern values are 609 and 746 g cm^{-2} respectively. The results of this procedure are shown below, $\mathbf{A}_\pm$ being defined in the conventional way as $2(W_\pm-E_\pm)/(W_\pm+E_\pm)$:

	Computed	Experimental
$\mathbf{A}_+$ (channel I)	+0.447	+0.505±0.018
$\mathbf{A}_-$ (channel I)	+0.049	+0.110±0.018
$\mathbf{A}_+$ (channel II)	+0.534	+0.569±0.037
$\mathbf{A}_-$ (channel II)	+0.030	+0.069±0.040

No error has been indicated for the calculated values, although this is presumably fairly large, due to the fact that the extrapolation of Fig. 2 is quite arbitrary. In view of this last fact, the above agreement must be considered good. If one hypothesizes that a certain fraction of the primaries is negatively charged, one may speculate as to the possible effect of this admixture on the calculated asymmetries. For example, in the event that the negative primaries may be considered completely symmetrical in all their properties to the positive component of the radiation (that is, same rigidity spectrum, same multiplicity of π-meson production, negative excess at production of secondaries instead of positive excess, etc.), that portion of the μ-meson intensity due to the positive fraction of the primary radiation can be computed as described above, while for that portion due to the negative fraction W_+ and E_- are interchanged, etc.

Focussing attention on channel I, under the above conditions one computes by the method of the preceding paragraph the values 0.403 and −0.007 for the two asymmetries if the fraction of negative primaries is 10%, and 0.359 and −0.063 if it is 20%. In other words, as one assumes increasing numbers of negative primaries, the agreement with the experimental data becomes progressively poorer. The situation in channel II is not materially different. We take this as a strong indication for the absence of any considerable number of negatively charged particles in the primary cosmic radiation.

The second factor which can operate to make our normalization procedure give an erroneous result is the fact that we do not really observe the intensity at angle Θ, but rather the average of the intensities taken from two cones of directions, one slightly to one side of Θ, the other slightly to the opposite side. A Taylor's series expansion about Θ yields the intensity

at angle $\Theta \pm \theta_1$:

$$i(\Theta \pm \theta_1) = i(\Theta)\left[1 \pm \left(\frac{1}{i}\frac{di}{d\theta}\right)_\Theta \theta_1 + \tfrac{1}{2}\left(\frac{1}{i}\frac{d^2i}{d\theta^2}\right)_\Theta \theta_1^2 \pm \cdots\right]. \quad (14)$$

If we interpret θ_1 as the magnitude of the angle which the central direction of the cone of observation makes on each side with the direction Θ, the observed intensity is the average of the two intensities of Eq. (14), or

$$\bar{i} = i(\Theta)\left[1 + \tfrac{1}{2}\left(\frac{1}{i}\frac{d^2i}{d\theta^2}\right)_\Theta \theta_1^2 + \cdots\right]. \quad (15)$$

The term involving the first derivative cancels out in the averaging, and the fractional magnitude of the effect on the intensity at Θ is therefore $\frac{1}{2}(i^{-1}d^2i/d\theta^2)\theta_1^2$. The next term (that in the fourth power of θ_1) and all higher even power terms are negligible.

Biehl, Neher, and Roesch[21] investigated the zenith angle dependence of the local cosmic radiation in the east-west plane at the geomagnetic equator over Peru. From their curves for atmospheric depth 310 g cm^{-2} and 20.8 cm of lead absorber, one can make a crude estimate of the effect in our case. In channel I of our apparatus it is of the order of 0.4% to 2.0%, while in the other channel the effect is about three times as large. In neither case is the effect large enough to account for the unexpectedly large counting rates at 45°.

The third possible explanation is that the assumptions involved in the highly simplified model of μ-meson production here employed must be re-examined. It is possible that the meson-producing component of the cosmic radiation does not vary strictly exponentially with atmospheric depth, especially in the uppermost part of the atmosphere. If this is the case, it is difficult to estimate the effect on our computations. However, at these altitudes, very considerable proportions of the observed mesons arise at *all* levels above that of observation, and it is hard to imagine that such an effect could account for more than one or two percent in the normalization.

The effect of the scattering of the mesons will be similar to that discussed in connection with θ_1, but it is even smaller, the root-mean-square scattering angle being of the order of only 3°.

A significantly larger effect results from the lack of collimation in the production of mesons. Observations in photographic emulsions at high altitudes[22] indicate that most π mesons having minimum ionization produced in nuclear events are collimated in a cone of about 15° half-angle about the direction of the primary particle.

The maximum angle of emission in the laboratory system of a μ meson whose parent π meson has momentum p_π can be calculated straightforwardly. The parent of our "typical" μ meson has $p_\pi/m_\pi c = 20$ (very approximate), corresponding to a maximum angle of emission of about 1°. This is negligible in comparison with the spreading which occurs in the primary collision.

Thus μ mesons produced at angle θ at a certain point along the trajectory leading to detection in the apparatus arise from primaries not in the direction θ, but rather in a cone of directions surrounding that of the trajectory at that point. Let us, for simplicity, consider only the variation in the east-west plane, at least for the inclined directions. For a pair of angles $\theta \pm \theta_2$ distributed symmetrically about θ, the intensities of the primary radiation at a certain point are proportional to

$$\exp\left[-\left(\frac{H-Z}{L}\right)\sec(\theta \pm \theta_2)\right],$$

where, however, we have neglected the small variation of a between $\theta-\theta_2$ and $\theta+\theta_2$. This function can be expanded in a series about θ, and the resulting two intensities averaged. As before, the term in the first derivative vanishes, and we can write for the over-all average of the intensities over the cone of incidence of the primaries

$$\bar{i} = i(\theta)\left\{1 + \tfrac{1}{2}\left(\frac{H-Z}{L}\right)\sec\theta \times\left[\left(\frac{H-Z}{L}\right)\sec\theta(\sec^2\theta - 1) - (2\sec^2\theta - 1)\right]\theta_2^2\right\}, \quad (16)$$

where now θ_2 must be interpreted as the root-mean-square angle of spread in the production of π mesons, projected into the east-west plane. At the vertical, the situation is slightly different because of the cylindrical symmetry about that direction, and we must use the root-mean-square angle in space.

Examination of Eq. (16) indicates that one needs some sort of average value of both $(H-Z)/L$ and $(H-Z)^2/L^2$. The appropriate ones are the averages weighted according to the relative numbers of mesons produced at various heights, or, to a high order of approximation, according to the function $\Psi(Z,R,\cos\Theta)$ defined in the Appendix. If one computes the numerical values of these two averages for a residual range of 600 g cm^{-2} (central value for channel I) and substitutes the trigonometrical factors for the vertical and for 45°, one obtains the fractional effects (on the intensities one would have in the case of perfect collimation) as follows:

$$-0.85\theta_2^2 \text{ (vertical)}; \quad +0.14\theta_2^2 \text{ (45°)}.$$

The coefficient at the vertical is always negative, but its magnitude is to some extent a function of R because of the dependence of the "distribution-in-production height" of observed mesons on R.

[21] Biehl, Neher, and Roesch, Phys. Rev. **76**, 914 (1949).
[22] Brown, Camerini, Fowler, Heitler, King, and Powell, Phil. Mag. **40**, 862 (1949).

At 45°, however, the situation is more complex. Here, at high altitudes the curve of primary intensity *vs* zenith angle is concave downward, while at lower altitudes a point of inflection intervenes, and the curve is concave upward. Hence, for low residual ranges, where the distribution function favors the lower altitudes, the coefficient is positive, while for higher ranges (greater than about 700 g cm^{-2}) the coefficient is negative.

It is interesting to note that Olbert actually determined the production spectrum of μ-mesons *produced in the vertical direction*, rather than the production spectrum corresponding to primaries *incident at the vertical*. It is the latter quantity which is of more fundamental interest. Olbert's spectrum, which can be derived from it through application of the correction given above, is usable to a good order of approximation provided one considers vertical data only. However, when one tries to apply his production spectrum to data at zenith angles other than zero there will be serious discrepancies. Since the vertical effect is negative, our "real" production spectrum will differ from Olbert's "effective production spectrum at the vertical" in that the normalizing constant A will be somewhat greater.

As before noted, the correction does depend on R, and therefore it is not strictly correct to apply a simple numerical correction to Olbert's constant A in order to find its "true" value. Evidently, there will be some effect on the constants n and a as well. We suggest that it would be highly advisable, when sufficient data exist, to repeat Olbert's computation of the μ-meson spectrum, taking this last effect into account in detail.

We shall be content for the present to modify Olbert's normalization in such a way that his spectrum coincides with the "true" one for range $R=600$ g cm^{-2}. It is worthy of note at this point that, at least to a first order of approximation, the much smaller effects due to θ_1 and to scattering of the mesons in air can be lumped together with θ_2. Another effect, which is important at the vertical but not at 45°, is that due to the distribution of the solid angle to the north and south of the east-west plane. The root-mean-square angle between the incoming trajectory and the east-west plane is about 16½°, and its effect, too, can be approximately lumped with θ_2.

Let it be assumed, for the moment, that a_W actually lies on the Olbert curve. It is then possible to compute, within certain accuracy, using the channel II zero-field data at the vertical and at 45° west, the spurious rates at the vertical and at 45°. One can then derive from the channel I data with field, vertical and 45°, both the root-mean-square angle of production of π mesons needed to bring the 45° and vertical data into accord and the corresponding value of a_E. The angle needed is 14°±2°, a value certainly not inconsistent with the observations of Brown *et al.*,[22] and the value of a_E obtained is 785±5 g cm^{-2}, a point lying not too far from the tentative extrapolation of the curve used until now.

We consider this result, taken conjointly with the foregoing considerations, to be sufficient justification for assuming that a_W actually does lie on the curve. One would, of course, not expect perfect agreement with the *extrapolated* portion of the curve, as it is highly arbitrary. Olbert's curve has been extended in Fig. 2 to include the point at 45° east, obtained as described above.

We are now in a position to attempt the crude modification of Olbert's production spectrum mentioned above. Using the angle 14° characteristic of the π-meson production, which brought about the best agreement of our results with Olbert's work, one finds for the "θ_2 effect" at the vertical at sea level -5.4%. (This figure does not include any possible effect due to the finite opening angle of the equipment used in obtaining the data upon which Olbert's computations are based.) We may now conclude that, in order to obtain the "true" production spectrum, at least in the region of range $R=600$ g cm^{-2}, we must modify Olbert's constant A as follows:

$$A'=A/(1-0.054). \tag{17}$$

We find thus that A must be increased from 7.31 to 7.73×10^4. Now, according to Olbert,[2,3] the average depth of production of mesons arriving at sea level with range 600 g cm^{-2} is about 213 g cm^{-2}, and since sea level corresponds to an atmospheric depth of 1033 g cm^{-2}, the average range of such particles at *production* is some 820 g cm^{-2} greater than that at *observation*, or about 1400 g cm^{-2}. Hence we conclude that the "true" production spectrum $G(R')$, at least in the vicinity of $R'=1400$ g cm^{-2}, is given approximately by

$$G(R')=7.73\times10^4[R'+a(M_e)]^{-2.55} \quad (\text{g}^{-2}\ \text{cm}^2\ \text{sec}^{-1}\ \text{sterad}^{-1}), \tag{18}$$

where $a(M_e)$ is given by Fig. 2. Note that Eq. (18) is now considered to hold *anywhere on the earth's surface and in any direction of incidence.*

It is now possible to compute a new set of theoretical counting rates for our apparatus, based on the corrected production spectrum and the values of a_W and a_E taken from the correct $a(M_e)$ curve of Fig. 2, and corrected for the θ_2 effect. The latter is slightly different for channel II from the values given above, due to the fact that the "typical" meson has a different range. These theoretical counting rates are shown, for both channels, in Table II.[23] Also shown are the experimental rates, corrected for spurious counts and the equipment normalization. It was necessary to recompute the normalization factors, which are shown, together with the original spurious rates, in Table III.[23] Table II

[23] Certain of the quantities in Tables II and III differ slightly from their counterparts in reference 18, because the method of evaluating some of the parameters of the theory has since been somewhat improved from a statistical standpoint.

TABLE II. Comparison of experimental and theoretical counting rates. (All in hr^{-1}.)

Channel	Direction	Sign	Theoretical counting rate (corrected)	Experimental counting rate (corrected and normalized)	Notes
I	45° west	+	16.31	16.31±0.27	a,b
I	45° east	+	9.73	9.73±0.19	a,b
I	45° west	−	12.05	12.05±0.21	a,b
I	45° east	−	10.78	10.78±0.20	a,b
I	45° west	○	4.42	4.30±0.14	
I	45° east	○	3.12	3.14±0.12	
I	vertical	+	26.24	26.24±0.49	a,b
I	vertical	−	24.40	24.40±0.46	a,b
I	vertical	○	7.86	8.05±0.35	
II	45° west	+	3.27	3.18±0.16	b
II	45° east	+	1.77	1.77±0.13	b
II	45° west	−	2.42	2.35±0.14	b
II	45° east	−	2.19	2.19±0.14	b
II	45° west	○	0.53	0.45±0.13	c
II	45° east	○	0.36	0.35±0.12	
II	vertical	+	5.17	5.42±0.39	b
II	vertical	−	4.80	5.03±0.39	b
II	vertical	○	0.91	1.10±0.40	c

[a] Data used in the determination of a_E and also the root-mean-square angle of π-meson production, needed in the correction of the theory. Apparent perfect agreement is, therefore, to be expected here.
[b] *Comparative* values of positive and negative counting rates, but not *absolute* values, used for determination of positive excesses.
[c] Data used for approximate determination of spurious counting rates.

indicates which of the data have been used to compute the various parameters of the theory. The values of the positive excesses at production shown in Table I are not affected by the above corrections.

It is clear from Table II that the theory is adequate to explain all the observed counting rates. Work is soon to be undertaken on an analysis of data taken at zenith angles of 22½° and 67½°. It is hoped that the results of this analysis will provide confirmation of the theory developed in this paper.

For the purpose of comparison with other experiments the conventionally measured east-west asymmetries **A** for positives, negatives, sum of positives and negatives, and zero-field are tabulated in Table IV. It is noteworthy that, where the statistical accuracy admits of direct comparison, the asymmetry of the sum of positives and negatives agrees very well with the asymmetry measured with zero field, thus confirming our interpretation that the particles detected in the latter case consist of a "natural mixture" of positives and negatives scattered in the iron of the magnets. Both these figures can be compared, at least qualitatively, with the results of Biehl, Neher, and Roesch.[21] They found, over Peru, a total asymmetry which increased with increasing absorber thickness (i.e., with increasing energy of the observed particles), and which decreased with increasing atmospheric depth. Their result at 45°, with 20.8 cm of lead absorber at 310 g cm^{-2} atmospheric depth, most nearly approximates the conditions of our data, with a total asymmetry of 0.304±0.015. Our data were taken at rather greater atmospheric depth, but corresponded to particles of rather higher energy, and in channel I the sum of positives and negatives gave 0.321±0.017.

TABLE III. Normalization factors and spurious counting rates.

Spurious counting rate—either channel	
vertical	1.01 ±0.35 hr^{-1}
45°	0.50 ±0.10 hr^{-1}
Normalization factor—vertical or 45°	
channel I (field on)	0.830±0.011
channel I (field off)	0.790±0.014
channel II (field on)	0.979±0.029
channel II (field off)	0.977±0.158

We are grateful to Professor Bruno Rossi, under whose guidance this work was performed.

APPENDIX

The purpose of this appendix is to outline the derivation of Eq. (10) of the text.

The change in direction of a μ meson due to curvature in the earth's magnetic field as we proceed upward a distance dS' along its trajectory is

$$d\theta=(\sigma eB/p')(dS'/\rho). \tag{19}$$

This expression yields, upon integration,

$$\theta-\Theta=\sigma\gamma\alpha, \tag{20}$$

where the following abbreviations have been made:

$$e\tau B/\mu=\gamma, \tag{21}$$

$$\frac{1}{\tau c}\int_0^S \frac{\mu c}{p'(R+S')}\times\frac{dS'}{\rho(Z')}=\alpha. \tag{22}$$

The probability of survival of the meson from the point of production to the point of observation can also be expressed in terms of the latter quantity, as follows:

$$w_e(S,R)=\exp(-\alpha). \tag{23}$$

It is convenient in what follows to refer all computations to a "zero-order trajectory," i.e., we expand all variables, their functions, and integrals about the values they would have if the mesons came in along a straight line trajectory in the direction in which they are observed. The subscript t will be used to indicate such quantities.

In order to evaluate α, it is convenient also to have an analytical expression for the range-momentum relation of μ-mesons in air, and we shall here employ that found by Olbert[2]:

$$\mu c/p'=\psi(R')=\eta(b+R')^{-1}-\kappa. \tag{24}$$

The values of the constants in Eq. (24) are as follows: $\eta=53.5$ g cm^{-2}, $b=56$ g cm^{-2}, $\kappa=2.07\times10^{-3}$.

Now dS is given by $dZ\sec\theta$, and also approximately, for angles θ near Θ,

$$\sec\theta=\sec\Theta(1+\tan\Theta\sigma\gamma\alpha). \tag{25}$$

If one expands $\psi(R')$ about the "zero-order trajectory," one obtains

$$\psi(R')=\psi(R_i')+(S'-S_i')\psi'(R_i'), \tag{26}$$

where $R_i'=R+S_i'=R+Z'\sec\Theta$.

By means of Eqs. (20), (24), (25), and (26) it is possible to obtain,[18] after considerable manipulation and substitution, the following expression:

$$\alpha=\alpha_0+\tfrac{1}{2}\tan\Theta\sigma\gamma\alpha_0^2-\tan\Theta\sigma\gamma \times\int_0^{\alpha_0(Z)}\left[\frac{\int_0^{Z'}\alpha_0(Z'')dZ''}{Z'+l}\right]d\alpha_0-\lambda_0\sec\Theta, \tag{27}$$

where

$$l=(R+b)\cos\Theta, \tag{28}$$

$$\alpha_0=(\eta/\tau c)\int_0^Z(Z'+l)^{-1}[dZ'/\rho(Z')], \tag{29}$$

$$\lambda_0=(\kappa/\tau c)\int_0^Z[dZ'/\rho(Z')]. \tag{30}$$

It is to be noted that the quantity γ giving the magnitude of the local magnetic field is quite small (never more than about 6×10^{-2}) compared with unity and that also, due to the small magnitude of κ, the integral λ_0 is quite small compared with α_0. Thus λ_0 can be considered to be of the order of $\gamma\alpha_0$. The function α_0 itself is of the order of unity. Therefore, in the derivation of Eq. (27), terms of the order of $\gamma^2\alpha_0$ and $\gamma\lambda_0$, and all smaller terms, have been neglected.

The integral α_0 is a function of vertical height Z, and depends parametrically upon the quantity l defined in Eq. (28) above. In other words, for a given location on the earth's surface, a family of curves of α_0 *vs* Z can be constructed with l as a parameter.[18] These curves then serve, at least in the east-west plane, for computations at any zenith angle. Note that l is symmetrical about the vertical.

The other integral λ_0 is simply a function of Z, and a single curve is adequate to express the relationship at any particular location on the earth.[18]

Both integrals depend on the density distribution in the atmosphere above the point of observation. Hence, since

$$\frac{1}{\rho(Z')}=\left(\frac{\Re}{\mathfrak{M}g}\right)\frac{T(Z')}{H-Z'}, \tag{31}$$

where $T(Z')$ is the absolute temperature, $\Re$ is the universal gas constant, $\mathfrak{M}$ is the average molecular weight of air, and g is the acceleration of gravity, they likewise can be considered functions of the *temperature* distribution in the atmosphere, and computed as follows:

TABLE IV. East-west asymmetry A conventionally measured

Type of measurement	Channel I	Channel II
positive particles	$+0.505\pm0.018$	$+0.569\pm0.037$
negative particles	$+0.110\pm0.018$	$+0.069\pm0.040$
positives+negatives	$+0.321\pm0.017$	$+0.330\pm0.069$
zero field	$+0.312\pm0.044$	$+0.244+0.405$

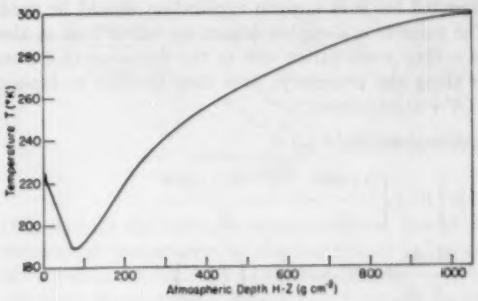

FIG. 7. Annual mean temperature of the atmosphere in the equatorial regions as a function of atmospheric depth $H-Z$.

$$\alpha_0=(\eta/\tau c)(\Re/\mathfrak{M}g) \times\int_0^Z(Z'+l)^{-1}(H-Z')^{-1}T(Z')dZ', \tag{32}$$

$$\lambda_0=(\kappa/\tau c)(\Re/\mathfrak{M}g)\int_0^Z(H-Z')^{-1}T(Z')dZ'. \tag{33}$$

It is more convenient to work with the temperature than directly with the density, as the former is known directly from meteorological data. The temperature distribution is a function of geographic latitude, and it is therefore not possible to compute universal curves for α_0 and λ_0. The distribution is, however, quite constant throughout the equatorial regions. It is shown for this region in Fig. 7, as taken from Olbert.[3]

Equation (9) can be rewritten as

$$i_s(R,\Theta)=\tfrac{1}{2}\int_0^H[1+\tfrac{1}{2}\sigma\delta(R',a)] \times G(R'+a)\exp\left(-\frac{H-Z}{L}\sec\theta-\alpha\right)\sec\theta dZ. \tag{34}$$

The positive excess at production δ is a number rather less than unity, and presumably does not vary very rapidly with R' and a. Therefore, any difference in δ along the curved path from that computed along the zero-order trajectory must be negligible, and we have $\delta(R',a)=\delta(R_i',a_i)$. Eqs. (25) and (27) can be substituted into Eq. (34), and the small terms in γ removed from the exponential through use of the expansion $e^x\approx1+x$.

It is advisable, for computational purposes, to expand the function $G(R'+a)$ about the value it takes on when a is equal to some arbitrarily chosen central value a_1, in terms of the deviation of the true value of a from this central value.

To this end, we write

$$a_i=a_1+\Delta(\Theta). \tag{35}$$

The choice of a_1 in a practical case is dictated by considerations of convenience. If a is known in the vertical direction, that figure might be a good choice for a_1. At any rate, some value intermediate between those

expected for a in a given application should be used. The value of a along the trajectory differs from a_1 also to a very small extent due to the deviation of θ from Θ along the trajectory. It is then possible to expand $G(R'+a)$ as follows:

$$G(R'+a)=G(R_t'+a_1)\times\left\{1-\zeta_1\left[\frac{\Delta\cos\Theta}{H}+\frac{(S'-S_t')\cos\Theta}{H}+\frac{1}{H}\frac{da}{d\theta}(\theta-\Theta)\cos\Theta\right]+\tfrac{1}{2}\left(1+\frac{1}{n}\right)\times\zeta_1^2\left[\left(\frac{\Delta\cos\Theta}{H}\right)^2+\frac{2(S'-S_t')\Delta\cos^2\Theta}{H^2}\right]\right\}, \quad (36)$$

where ζ_1 is the following function:

$$\zeta_1=nH[Z+(R+a_1)\cos\Theta]^{-1}. \quad (37)$$

After substitution of Eq. (36) into Eq. (34), and some further manipulation and simplification, one obtains an expression of the following form for the intensities:

$$i_\sigma(R,\Theta)=\tfrac{1}{2}A(nH)^{-n}\cos^{n-1}\Theta\int_0^H[1+\tfrac{1}{2}\sigma\delta(R_t',a_t)]\times\Psi(Z,R,\cos\Theta)[1+\text{other terms}]dZ, \quad (38)$$

where

$$\Psi(Z,R,\cos\Theta)=\zeta_1^n\exp\left[-\left(\frac{H-Z}{L}-\lambda_0\right)\sec\Theta-\alpha_0\right]. \quad (39)$$

Now $\frac{1}{2}\delta$ is quite small compared to unity, and hence if we define a weighted average of δ as

$$\bar{\delta}(R,a_t)=\frac{\int_0^H\Psi(Z,R,\cos\Theta)\delta(R_t',a_t)dZ}{\int_0^H\Psi(Z,R,\cos\Theta)dZ}, \quad (40)$$

we may write to an excellent order of approximation

$$i_\sigma(R,\Theta)=\tfrac{1}{2}A(nH)^{-n}\cos^{n-1}\Theta[1+\tfrac{1}{2}\sigma\bar{\delta}(R,a_t)]\times\int_0^H\Psi(Z,R,\cos\Theta)[1+\text{other terms}]dZ. \quad (41)$$

The integral in Eq. (41) can be evaluated numerically term by term, and the result, after further manipulation,[18] is Eq. (10) of the text.

PHYSICAL REVIEW VOLUME 100, NUMBER 1 OCTOBER 1, 1955

Scattering of Pions by Hydrogen at 165 Mev*

H. L. ANDERSON AND M. GLICKSMAN†
Institute for Nuclear Studies, The University of Chicago, Chicago, Illinois

(Received April 13, 1955)

Measurements of the elastic scattering of both positive and negative pions, and of the charge exchange scattering of negative pions were carried out at each of five angles, at 165 Mev using a liquid hydrogen target. In addition, the total cross sections for positive and negative pions were measured by the transmission method. Integration of the differential measurements gave total cross sections of 199±11 mb for the positive, and 69.8±3.8 mb for the negative pions. The corresponding cross sections obtained by transmission were 188.2±5.4 mb and 67.5±1.5 mb, respectively.

A least squares analysis was carried out on the seventeen data to determine the most probable values of the phase shifts, limiting the analysis to s and p waves. Seven solutions were found, three being of the Fermi type, the others of the Yang type. The Fermi type solutions gave α_{33} near 63°, α_3 near −20°, with the other phase shifts small.

INTRODUCTION

MUCH of the knowledge which we now have about the nature of the interaction between pions and nucleons has come from experiments on the scattering of pions by protons. In interpreting these experiments, the practice has been to carry out a phase shift analysis[1–7] of the data so as to be able to specify the magnitude of the interaction in each of the possible states of the pion-proton system. This program has been hampered considerably by the lack of sufficiently complete and accurate data in general, and of positive pion data above 135 Mev, in particular. Because of this, it was possible to obtain good fits to the experimental data with a number of different phase shift solutions, so that the whole analysis remained somewhat ambiguous.

The present work is part of a program to improve the knowledge of the phase shifts by carrying out more careful measurements with both π^+ and π^- pions. This report covers the experiments carried out at 165 Mev and includes a phase shift analysis of these data.

* Research supported by a joint program of the Office of Naval Research and the U. S. Atomic Energy Commission.

† Present address: RCA Laboratories, Princeton, New Jersey.

[1] Anderson, Fermi, Martin and Nagle, Phys. Rev. **91**, 155 (1953) (Quoted as *A*).
[2] Bodansky, Sachs, and Steinberger, Phys. Rev. **93**, 1367 (1954).
[3] Fermi, Metropolis, and Alei, Phys. Rev. **95**, 1581 (1954).
[4] de Hoffmann, Metropolis, Alei, and Bethe, Phys. Rev. **95**, 1586 (1954).
[5] R. L. Martin, Phys. Rev. **95**, 1606 (1954).
[6] M. Glicksman, Phys. Rev. **94**, 1335 (1954).
[7] J. Orear, Phys. Rev. **96**, 176 (1954).

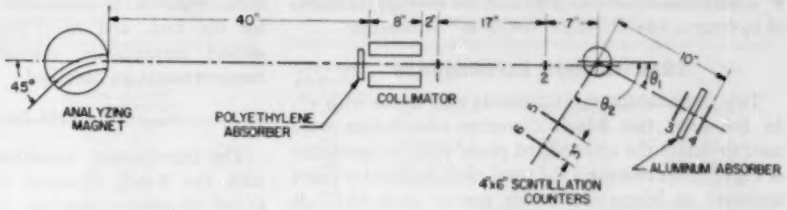

FIG. 1. Arrangement for the elastic scattering of pions by hydrogen. Distances shown are for π^+. For π^- counters 3 and 5 were 10.3 in. and counters 4 and 6 were 20.2 in. from the center of the hydrogen.

EXPERIMENTAL ARRANGEMENT

The arrangement was essentiaily the same as that used in previous work from this laboratory.[1,6,8,9] Details of the geometry for the elastic scattering are given in Fig. 1. Counters 1 and 2 were plastic scintillators $\frac{1}{4}$ inch thick and 2 inches$\times 2\frac{1}{16}$ inches for the π^+ experiment. For the π^- measurement these were reduced in width from $2\frac{1}{16}$ inches to $1\frac{1}{2}$ inches. Counters No. 3, 4, 5, and 6 were the 4 inch$\times$6 inch liquid scintillators described previously.[1] The use of four such counters made it possible to observe the scattered pions at two angles simultaneously. Proton contamination in the π^+ beam was removed by a 1.48-g/cm^2 polyethylene filter placed at the entrance to an 8-inch collimator in front of counter No. 1.

The charge exchange scattering $\pi^- + P \rightarrow \pi^0 + N$ was observed by detecting the gamma rays from the π^0 decay using the anticoincidence technique of Glicksman.[6] The geometry for this experiment is shown in Fig. 2.

In addition to the angular distribution measurements, a transmission measurement was made to obtain the total cross sections in an independent way. The geometry for this is shown in Fig. 3. Counters 3 and 4 were liquid scintillators in Lucite cells having an 8-inch diameter sensitive area.

PION BEAMS

The energy of the pion beams was determined from a range curve in copper using the transmission geometry (Fig. 3) with the hydrogen target removed. For π^+ the mean range was reached by the insertion of 75.3 g/cm^2 of copper in the beam. To obtain the correct value of the range this should be increased by 1.7 g/cm^2 to take into account the multiple scattering of the pions in traversing the copper. This correction was not applied in our previous work.[1,6,8,9] The copper equivalent of the final counters was 4.1 g/cm^2. This includes the addition of 0.3 g/cm^2 to account for the path obliquity in the counters. Thus, the total range was taken to be 81.1 g/cm^2 of Cu. According to Aron's tables,[10] using 6.72 as the ratio of proton to pion mass, we find that pions with this range have an energy of 166.6 Mev. When the hydrogen was in place they lost 1.7 Mev in arriving at the center of the hydrogen so that the energy there was 164.9 Mev. Analysis of the range curve showed, further, an energy spread of 3.7 Mev. With π^- the amount of copper needed to reach the mean range was 74.8 g/cm^2. This was sufficiently close to the result obtained with π^+ that we adopted 165 Mev with an energy spread of ± 6 Mev for both π^+ and π^- experiments.

The muon content of the beam at the center of the hydrogen was estimated, from an analysis of the range curve, to be 4.5 ± 1.0 percent for both π^+ and π^-. The electron content of the beams was negligible.

It was necessary to survey the distribution of the pion beams in space in order to determine the average thickness of hydrogen traversed and to average properly the solid angle subtended by the counters at the hydrogen. This was done by means of a small scintillator $\frac{1}{4}$ inch$\times\frac{1}{4}$ inch in area which could be moved across the beam. From such data we were able to determine that the mean thickness of hydrogen traversed was $(3.699 \pm 0.074) \times 10^{23}$ atoms/cm^2 for π^+. In the case of

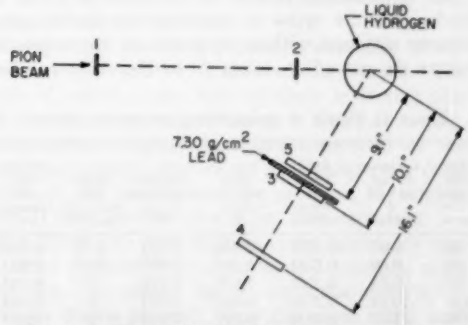

FIG. 2. Arrangement for observing the charge exchange scattering of negative pions in hydrogen.

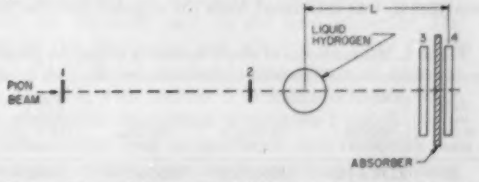

FIG. 3. Transmission method for measuring the total cross section of pions in hydrogen. $L = 19.75$ in. for π^-; $L = 13.31$ in. for π^+.

[8] Fermi, Glicksman, Martin, and Nagle, Phys. Rev. **92**, 161 (1953).

[9] M. Glicksman, Phys. Rev. **95**, 1045 (1954).

[10] W. A. Aron, University of California Radiation Laboratory Report, UCRL-1325 (unpublished).

π^- a narrower beam was used and the average thickness of hydrogen was $(3.778\pm0.038)\times10^{23}$ atoms/cm².

TRANSMISSION EXPERIMENTS

Two transmission measurements were made with π^+. In the first, two 8-inch diameter scintillators were used to detect the transmitted pions with the geometry of Fig. 3. This measures the total cross section for pions scattered at laboratory angles greater than 16.7°. A copper absorber of thickness 8.37 g/cm² was inserted between the last two counters so that the scattered protons would not be counted. The ratio of the quadruple coincidence rate with and without hydrogen was found to be

$$R_1=\frac{(Q/D)_{\mathrm{H}}}{(Q/D)_{\mathrm{No\ H}}}=\frac{0.8384\pm0.0019}{0.8929\pm0.0013}=0.9390\pm0.0025.$$

In a second measurement using 4 inch×6 inch counters with 8.78 g/cm² of aluminum absorber we obtained

$$R_2=\frac{0.7694\pm0.0011}{0.8196\pm0.0012}=0.9388\pm0.0019.$$

In this case, the measurement included pions scattered at laboratory angles greater than 15.4° on the average.

Under the assumption that the muons in the beam do not interact, and neglecting the effects of multiple Coulomb scattering and of $\pi-\mu$ decay in the liquid hydrogen, the cross section is given by

$$\sigma=-\frac{1}{N}\log_e\left\{R-\frac{r}{T}(1-R)\right\}, \qquad (1)$$

where N is the number of hydrogen atoms/cm², r is the ratio of muons to pions in the beam and T is the transmission for pions of the counter and copper absorber assembly used to detect the transmitted particles. For the π^+ measurements $r/T=0.052\pm0.011$.

For the first measurement the cross section turned out to be $(179.4\pm8.3)\times10^{-27}$ cm², whereas the second measurement gave $(179.9\pm6.8)\times10^{-27}$ cm². The total scattering cross section is obtained by adding the contribution of those pions which are scattered by the hydrogen into the solid angle subtended by the detecting counters. This contribution, excluding the Coulomb scattering, was estimated from the angular distribution measurements. It amounted to $(9.3\pm2.3)\times10^{-27}$ cm² for the first, and to $(7.9\pm1.5)\times10^{-27}$ cm² for the second transmission measurement. Combining the measurements we obtained

$$\sigma_{\mathrm{total}}(\pi^+)=(188.2\pm5.4)\times10^{-27}\ \mathrm{cm}^2.$$

The transmission measurement with π^- was made with the 8-inch diameter scintillators and a 10.26 g/cm² aluminum absorber. In two measurements we obtained

$$R_3=\frac{0.80259\pm0.00040}{0.82180\pm0.00038}=0.97662\pm0.00066,$$

$$R_4=\frac{0.79536\pm0.00028}{0.81476\pm0.00025}=0.97619\pm0.00046.$$

Using $r/T=0.055\pm0.012$ we obtained a cross section of $(66.8\pm1.5)\times10^{-27}$ cm² excluding pions scattered by angles less than 11.4°. This contribution, obtained from the angular distribution measurements, amounted to $(0.7\pm0.1)\times10^{-27}$ cm² so that the total interaction cross section of π^- with hydrogen was found to be

$$\sigma_{\mathrm{total}}(\pi^-)=(67.5\pm1.5)\times10^{-27}\ \mathrm{cm}^2.$$

These total cross sections are in good agreement with those measured by Ashkin *et al.*[11]

ELASTIC SCATTERING OF POSITIVE PIONS

Measurements of the angular distribution of the scattered pions were made at five different laboratory angles. Using the arrangement of Fig. 1, the scattering was observed at two angles at the same time. Due to the low intensity of the positive pion beam, it was necessary to use large detecting counters rather close to the target in order to obtain acceptable counting rates. This complicated the reduction of the data because the finite size of the detectors and of the target, as well as the variation of the differential cross section with angle had to be taken into account.

The experimental results are collected in Table I, which gives the ratios of quadruple to double coincidences with and without hydrogen in the target, as well as the net effect, taken to be the difference be-

TABLE I. Measurements of elastic scattering of positive pions.

Lab angle θ (degrees)	$(Q/D)_{\mathrm{H}}$ ×10³	$(Q/D)_{\mathrm{No\ H}}$ ×10³	$(Q/D)_{\mathrm{net}}$ ×10⁶	$\left(\frac{d\sigma}{d\Omega}\right)_{\mathrm{lab}}$ (10^{-27} cm²/sterad)
30	3234±145	1399±132	1835±196	28.8±3.4
60	1467± 90	557± 70	910±114	12.1±1.6
90	1474± 89	720± 76	754±117	10.0±1.6
120	1490± 91	384± 60	1106±109	15.6±1.8
150	1493± 88	561± 66	932±110	18.5±2.4

TABLE II. Details of the scattering arrangement for π^+.

Laboratory angle θ (degrees)	Distance to last counter d (inches)	Solid angle $\Delta\Omega$ (steradians)	Geometrical factor G	Multiple scattering factor M	Aluminum absorber (g/cm²)	Detection efficiency ϵ
30	9.94	0.2307	0.964	0.952	8.78	0.876
60	9.89	0.2281	1.016	0.980	2.59	0.937
90	9.87	0.2266	1.039	0.979	0	0.964
120	10.14	0.2180	0.982	0.973	0	0.964
150	12.32	0.1530	0.992	0.975	0	0.964

[11] Ashkin, Blaser, Feiner, Gorman, and Stern, Phys. Rev. **96**, 1104 (1954).

TABLE III. Differential cross sections for 165 Mev π^+ in center of mass system.

Cosine center of mass angle $\cos\chi$	Differential cross section $(d\sigma/d\omega)^+$ (10^{-27} cm^2/sterad)
0.7851	18.7±2.2
0.2793	9.8±1.3
−0.2618	10.7±1.7
−0.6767	21.4±2.5
−0.9209	30.3±3.9

TABLE IV. Observed counting rates in the measurement of the charge exchange scattering.

Lab angle (degrees)	$(Q'/D)_H$ $\times 10^6$	$(Q'/D)_{H_2O-H}$ $\times 10^4$	$(Q'/D)_{net}$ $\times 10^4$
30	254.3±6.8	64.1±4.2	190.2±8.0
60	141.9±6.4	21.4±3.4	120.5±7.3
90	118.2±4.7	20.5±2.6	97.7±5.4
120	136.9±5.2	35.7±3.9	101.2±6.5
150	181.0±6.0	60.5±4.5	120.5±7.5

tween the two. The errors shown are the standard deviations obtained from the total counts observed. The net quadruples to doubles ratio is

$$(Q/D)_{net} = Nf\epsilon M\sigma(\theta)\Delta\Omega G. \quad (2)$$

In this equation, N is the average number of hydrogen atoms per cm^2 traversed by the beam, f is the fraction of pions in the beam, ϵ is the efficiency of the detector for pions, M is the factor which corrects for the effect of multiple scattering in the target, and $\sigma(\theta)$ is the differential cross section in the laboratory. The solid angle, $\Delta\Omega$, and G, a geometrical factor dependent on $\sigma'(\theta)$ and $\sigma''(\theta)$, are tabulated in Table II. The calculation of $\Delta\Omega$ and G is described in the companion paper.[12] The distance d from the center of the counter to the center of the beam is included in the table, since the beam survey showed a 0.12-inch displacement of its center toward the counters. The counter was 4 inches×6 inches. The effective length of the beam in the target was 3.74 inches, and its cross section was 2 inches×2 inches.

At angles 30° and 60° absorbers were introduced between the last two counters so that the scattered protons would not be recorded. The detection efficiency was calculated taking into account the nuclear interaction of the scattered pions with the materials in their path. For aluminum we used a cross section of 490 millibarns for this and for carbon, 330 millibarns, based on some transmission measurements we had carried out. The efficiencies which were deduced taking these values are listed in Table II.

The multiple scattering correction was made following the method described in the companion paper.[12] The factor M, which is the ratio of single scattering plus in-scattering minus out-scattering to single scattering, was estimated roughly from our knowledge of the energy and angular dependence of the scattering cross section. It will be seen from the values of M listed in Table II that the correction is not very important.

The differential cross sections in the laboratory system were deduced from the observed counting rates using Eq. (2), taking for N the value 3.699×10^{23} hydrogen atoms per cm^2, for f the value 0.955, and for the other quantities, their values as given in Table II. This is the way in which the results listed in the last column of Table I were obtained. The errors quoted were obtained by assigning uncertainties of 2 percent in N, 1 percent in f, 2 percent in ϵ, 2 percent in M, 3 percent in $\Delta\Omega$, and 2 percent in G, and compounding these with the counting errors in the standard way.

Numerical integration of these differential cross sections leads to the value

$$2\pi\int\frac{d\sigma}{d\Omega}d\Omega = (199\pm11)\times10^{-27}\text{ cm}^2.$$

This result is somewhat higher, but not outside the experimental error, than that obtained from the transmission measurement.

The transformation of these results to the center of mass system is given in Table III.

We also fitted these data to an expression of the form

$$d\sigma/d\omega = a + b\cos\chi + c\cos^2\chi, \quad (3)$$

obtaining, by the method of least squares, the values,

$$a^+ = 8.85\pm1.18 \text{ millibarns/steradian}$$
$$b^+ = -3.66\pm1.76 \text{ millibarns/steradian}$$
$$c^+ = 21.11\pm3.40 \text{ millibarns/steradian.}$$

CHARGE EXCHANGE SCATTERING OF NEGATIVE PIONS

The measurement of the charge exchange scattering cross sections is complicated by the fact that we cannot observe the neutral pions directly. At best, we can observe the gamma rays into which they decay. This has been done with the anticoincidence arrangement of Fig. 3. The arrangement is not sensitive to charged particles incident on it. Its sensitivity to gamma rays is due principally to the electron pairs which are produced, for the most part, in the lead converter. The data for this experiment are collected in Table IV. In this table Q' is the quadruple coincidence of counters 1, 2, 3, and 4, with counter 5 in anticoincidence, while D is the double coincidence of counters 1 and 2.

In our earlier work we used such data to deduce the differential cross sections for the production of gamma rays by means of a formula analogous to Eq. (2). For the efficiency we used the value calculated for the average gamma-ray energy. This is not quite correct, as Bodansky, Sachs, and Steinberger[3] have shown. The

[12] Anderson, Davidon, Glicksman, and Kruse, following paper [Phys. Rev. 100, 279 (1955)].

TABLE V. Efficiency for detecting gamma rays.

Gamma ray energy E_γ Mev	Efficiency ϵ for lab angle 30° or 150°	90°
30	0.133	0.130
60	0.363	0.352
90	0.502	0.490
150	0.638	0.628
200	0.676	0.671

gamma rays are emitted over a broad energy spectrum, extending to low energies where the efficiency of the detector is falling rapidly. As a consequence, the efficiency for the average gamma rays is not a good approximation to the average efficiency. In the present work we have, due largely to the insistence of Dr. Jay Orear, attempted to take the energy dependence of the efficiency explicitly into account, in the manner of Bodansky, Sachs, and Steinberger.[2] In this we have been only moderately successful, due to our lack of knowledge of this dependence.

In what follows, we recapitulate the analysis given by Bodansky, Sachs, and Steinberger,[2] in order to make clear the way in which we preferred to deal with the problem.

The differential cross section for neutral pion production in the center of mass system is written as an expansion in Legendre polynomials

$$d\sigma_0/dw_0=\sum_l a_l P(\alpha), \tag{4}$$

where $\cos^{-1}\alpha$ is the center of mass angle of π^0 emission with respect to the incident π^-. In the system in which the π^0 is at rest, the γ rays are emitted isotropically with energy equal to $\frac{1}{2}$ the rest energy of the π^0,

$$E_0=\mu_0c^2/2. \tag{5}$$

Since two gamma rays are emitted for each π^0 decay, the number emitted into solid angle dw_0 in the rest system of the π^0 will be

$$(1/2\pi)(d\sigma_0/dw_0)dw_0,$$

but in the solid angle dw' of the center of mass system the number of gamma rays will be

$$(1/2\pi)(d\sigma_0/dw_0)(dw_0/dw')dw'.$$

The Lorentz transformation from this system in which the π^0 is at rest to the center of mass system gives

$$dw_0/dw'=1/(\gamma-\eta x)^2, \tag{6}$$

where $\gamma\mu_0c^2$ is the energy and $\eta\mu_0c$ is the momentum of the π^0 in the center of mass system, while $\cos^{-1}x$ is the angle of emission of the γ ray with respect to the direction of the π^0 in this system. Thus,

$$\frac{d}{dw}\frac{d}{dw'}\sigma_\gamma(\alpha,x)=\frac{1}{(\gamma-\eta x)^2}\frac{1}{2\pi}\sum_l a_l P_l(\alpha). \tag{7}$$

The number of gamma rays emitted at angle $\cos^{-1}y$ with respect to π^- direction in the center of mass system may be obtained from this by using the addition theorem

$$P_l(\alpha)=\frac{4\pi}{2l+1}\sum_m Y_l^{m*}(x)Y_l^m(y). \tag{8}$$

Then

$$\frac{d}{dx}\frac{d\sigma_\gamma}{dw}=\int\frac{1}{(\gamma-\eta x)^2}\frac{1}{2\pi}\sum_l a_l\frac{4\pi}{2l+1}\times\sum_m Y_l^{m*}(x)Y_l^m(y)d\xi', \tag{9}$$

where $d\xi'$ is the element of polar angle associated with dw'.

$$\frac{d}{dx}\frac{d\sigma_\gamma}{dw}=\sum_l a_l P_l(y)(\gamma-\eta x)^{-2}P_l(x). \tag{10}$$

Transforming to the laboratory system, the factor analogous to (6) is

$$dw/d\Omega=(\gamma_0-\eta_0 z)^{-2}, \tag{11}$$

where η_0/γ_0 is the velocity of the center of mass and $\cos^{-1}z$ is the angle in the laboratory at which the γ rays were observed. We obtain

$$\frac{d}{dx}\frac{d\sigma_\gamma}{d\Omega}=(\gamma_0-\eta_0 z)^{-2}\sum_l a_l P_l(y)(\gamma-\eta x)^{-2}P_l(x). \tag{12}$$

The energy of the gamma rays observed at z depends on the coordinates x and y according to the relation

$$\begin{aligned} E&=E_0(\gamma_0+\eta_0 y)(\gamma-\eta x)^{-1},\\ y&=(\gamma_0 z-\eta_0)(\gamma_0-\eta_0 z)^{-1}, \end{aligned} \tag{13}$$

so that the observed counting rate will be given by

$$\left(\frac{Q}{D}\right)^\gamma=C(\gamma_0-\eta_0 z)^{-2}\sum_l a_l k_l \bar{a}_l(z)P_l(y), \tag{14}$$

where

$$k_l=\int(\gamma-\eta x)^{-2}P_l(x)dx$$

is the same factor evaluated in A which gives the intensity of the gamma rays belonging to the spherical harmonic of order l. For the present experiment the values are 2, 1.297, and 0.6769, for k_0, k_1, and k_2, respectively.

The explicit dependence of the efficiency on the γ-ray energy occurs in the expression for the average efficiency,

$$\bar{a}_l(z)=k_l^{-1}\int\epsilon(x,z)(\gamma-\eta x)^{-2}P_l(x)dx. \tag{15}$$

$\epsilon(x,z)$ can be found if $\epsilon(E)$ is known through the use of Eqs. (13).

The factor C is the product of the factors $Nf\Delta\Omega GM$

TABLE VI. Apparent center of mass cross sections for gamma rays due to charge exchange scattering.

Laboratory angle θ (degrees)	$(Q/D)^0\times10^4$	Solid angle $\Delta\Omega$ (sterad)	Geometrical factor G	Multiple scattering factor M	$(\gamma_0-\eta_0 z)^2$	Efficiency $\bar{\epsilon}_0$	$\frac{\bar{\epsilon}_1}{\bar{\epsilon}_0}$	$\frac{\bar{\epsilon}_2}{\bar{\epsilon}_0}$	Apparent center of mass cross section for gammas due to π^0 $\frac{d\sigma^0}{dw}$ (mb/sterad)
30	188.4±8.0	0.0885	0.986	0.989	0.6911	0.558	1.172	1.265	7.49±1.20
60	118.7±7.3	0.0872	1.006	0.992	0.8336	0.536	1.189	1.295	5.88±1.00
90	96.2±5.4	0.0867	1.015	0.990	1.0498	0.505	1.209	1.340	6.36±1.05
120	100.2±6.5	0.0872	0.993	0.989	1.2910	0.490	1.218	1.350	8.55±1.43
150	119.7±7.5	0.0885	0.995	0.989	1.4832	0.472	1.235	1.392	11.97±2.00

which have the same meaning and which are evaluated in the same spirit as the corresponding factors in Eq. (2). Strictly speaking, C depends on l and x and should be incorporated in the integrand of (15). However, in view of the much larger uncertainties involved in estimating $\epsilon(E)$ it would be meaningless to attempt to take this dependence into account. We found it convenient to define an "apparent" cross section for gamma-ray production in the center of mass system

$$\left(\frac{d\sigma_\gamma}{dw}\right)_z^* = \frac{(Q/D)_z{}^\gamma(\gamma_0-\eta_0 z)^2}{Nf\Delta\Omega\epsilon_0(z)MG}, \tag{16}$$

so that we could express the measurements in a form which was convenient for machine calculation of the phase shifts.

$$\left(\frac{d\sigma_\gamma}{dw}\right)_z^* = a_0k_0P_0(y)+a_1k_1\frac{\bar{\epsilon}_1(z)}{\bar{\epsilon}_0(z)}P_1(y) + a_2k_2\frac{\bar{\epsilon}_2(z)}{\bar{\epsilon}_0(z)}P_2(y), \tag{17}$$

limiting the expansion to $l=2$ on the supposition that only s and p waves contribute to the scattering.

In determining the efficiency of our counting arrangement for gamma rays we followed the same general procedure described in A. However, instead of using Wilson's[13] calculations to give the transmission and multiple scattering of the electrons in lead, we carried out some experiments using electrons from our betatron.

The trasmission and multiple scattering of electrons of various energies up to 90 Mev were measured as a function of thickness of lead using a counting geometry similar to that used in the pion scattering work. Further details of these experiments are given in the companion paper.[12] This enabled us to determine the efficiency, especially at low energy, somewhat more reliably than using Wilson's calculations. Nevertheless, these improvements did not remove the major uncertainties in our knowledge of the efficiency and this remains the weakest aspect of our work.

In Table V the efficiency of our counting arrangement for gamma rays is given as a function of gamma-ray energy. The values differ slightly for laboratory angles 30° (or 150°) and 90°, so that the values for 60° (or 120°) could be reckoned by interpolation. From these results the values of $\bar{\epsilon}_0$, $\bar{\epsilon}_1$, and $\bar{\epsilon}_2$ were calculated by numerical integration using Eq. (15). Values of $\bar{\epsilon}_0$ and of the ratios $\bar{\epsilon}_1/\bar{\epsilon}_0$ and $\bar{\epsilon}_2/\bar{\epsilon}_0$ appropriate for the present experiment are tabulated in Table VI.

The counting rates given in the last column of Table IV include a small contribution due to the radiative capture process

$$\pi^-+p\rightarrow n+\gamma.$$

We were able to estimate this contribution from the knowledge of the inverse process,[14] deducing the formula

$$(d\sigma/dw)_{\gamma\rightarrow\gamma}=0.072-0.024\cos^2\chi \text{ mb/sterad}$$

by detailed balance. This correction has been included in tabulating the quantity $(Q/D)^0$ in Table VI.

The apparent cross section for the production of gamma rays due to the charge exchange process was calculated using these results by means of Eq. (16). We took $N=3.778\times10^{22}$ atoms/cm^2, $f=0.955$, and other factors as listed in Table VI. Errors were assigned as follows: 1 percent for N, 1 percent for f, 3 percent for $\Delta\Omega$, 15 percent for $\bar{\epsilon}_0$, and 2 percent for MG.

In accordance with Eq. (17) we were able to write the following five relations connecting the experimental results and the coefficients a_0, a_1, and a_2.

Lab angle

$$30^\circ \quad 7.49\pm1.20=2a_0+1.214a_1+0.392a_2, \tag{18a}$$

$$60^\circ \quad 5.88\pm1.00=2a_0+0.488a_1-0.306a_2, \tag{18b}$$

$$90^\circ \quad 6.36\pm1.05=2a_0-0.342a_1-0.389a_2, \tag{18c}$$

$$120^\circ \quad 8.55\pm1.43=2a_0-1.023a_1+0.118a_2, \tag{18d}$$

$$150^\circ \quad 11.97\pm2.00=2a_0-1.461a_1+0.704a_2. \tag{18e}$$

When these equations are solved by the method of least squares the following values are obtained:

$$a_0=\ 3.70\pm0.28,$$
$$a_1=-1.05\pm0.66,$$
$$a_2=\ 3.66\pm1.49.$$

[13] R. R. Wilson, Phys. Rev. 84, 100 (1951).

[14] M. Gell-Mann and K. M. Watson, Ann. Rev. Nuc. Sci. 4, 219 (1954).

TABLE VII. Measurements of the elastic scattering of negative pions.

Lab angle (degrees)	$(Q/D)_{\Pi}$ $\times 10^6$	$(Q/D)_{\pi_0\,\Pi}$ $\times 10^6$	$(Q/D)_{\rm corr}$ $\times 10^6$
−29.4	531.7±9.2	451.6±8.3	80.1±12.4
30.0	286.1±8.0	213.6±7.5	72.5±11.0
60.0	77.8±3.0	42.6±2.2	35.2± 3.7
90.0	48.1±2.2	24.4±2.4	23.7± 3.3
120.0	48.2±2.2	24.5±1.7	23.7± 2.8
150.0	81.7±3.6	45.5±2.3	36.2± 4.3

The coefficients a^0, b^0, c^0 appropriate to Eq. (3) are simply related to these and have the values

$$a^0 = 1.87\pm0.76,$$
$$b^0 = -1.05\pm0.66,$$
$$c^0 = 5.49\pm2.24.$$

We can also calculate the integrated value of the cross section due to charge exchange

$$\sigma^0 = \int\left(\frac{\partial\sigma^0}{\partial w}\right)dw = 4\pi a_0 = (46.5\pm3.5)\times10^{-27}\ \text{cm}^2.$$

The error given here is smaller than it would be if we had not neglected the correlation on the errors assigned to the efficiencies among the relations (8).

ELASTIC SCATTERING OF NEGATIVE PIONS

This experiment was carried out in a manner similar to that for the positive pions. Because of the higher flux which was available it was possible to use a better-defined geometry. This simplified the reduction of the data. The experimental data are given in Table VII. The errors given are the standard deviations due to statistics alone.

A small percentage of the counting rate recorded in the last column of Table VII is due to the gamma-ray production process. This was obtained by estimating the efficiency of this arrangement for detecting gamma rays, and using the data of the gamma-ray measurements. This contribution was subtracted in obtaining the value $(Q/D)^-$ due to the elastic scattering of negative pions alone, given in the second column of Table VIII. Proceeding as for the positive pions we calculated the differential cross sections in the laboratory given in the last column of Table VIII. The error given includes an error of 1 percent in the value of N, an error of 1 percent in the value of f, and errors of 2 percent of ϵ_- and of 2 percent in $\Delta\Omega$.

The total cross section for the elastic scattering of negative pions was calculated by a numerical integration of these results to have the value

$$\sigma(\pi^-\rightarrow\pi^-) = (22.5\pm1.5)\times10^{-27}\ \text{cm}^2.$$

Adding to this the value $(46.5\pm3.5)\times10^{-27}$ cm² due to charge exchange and the value $(0.80\pm0.20)\times10^{-27}$ cm² due to radiative capture, the total cross section for negative pions obtained in this way is found to have the value

$$\sigma_{\rm total}(\pi^-) = (69.8\pm3.8)\times10^{-27}\ \text{cm}^2,$$

in reasonable agreement with the result of the transmission measurement.

The differential cross sections for the elastic scattering for the center of mass system are given in Table IX.

PHASE SHIFT ANALYSIS

As in the earlier work,[1] a phase shift analysis of the data was carried out using an electronic computer. We are grateful to Donald Flanders and to Jean Hall of the Argonne National Laboratory for the opportunity to use the AVIDAC for this purpose. As before, the cross sections were expressed in terms of the phase shifts, limiting the analysis to include only s and p waves in states of isotopic spin $\frac{1}{2}$ and $\frac{3}{2}$. Starting with an initial set of six phase shifts, the machine computes the sum

$$M(\alpha_1,\alpha_3,\alpha_{11},\alpha_{13},\alpha_{31},\alpha_{33}) = \sum_{i=1}^{17}\frac{\Delta_i^2}{\epsilon_i^2} \qquad (19)$$

where α_1, $\cdots$, α_{33} are the six phase shifts with the notation of A, ϵ_i is the experimental error, and Δ_i is the deviation of the calculated from the observed cross section. The machine then proceeds to vary each phase angle in turn, seeking the set which gives the minimum value of M. It first varies α_1 by either plus or minus 1 degree, computes the corresponding value of M, and selects the altered or original value of the phase angle according to which gave the smaller M. It then proceeds to vary the next angle, and the next in order, until no further decrease in M is obtained. The variation is then reduced to $\frac{1}{2}$ degree and the same procedure is re-

TABLE VIII. Scattering of negative pions in the laboratory system.

Lab angle θ (degree)	$(Q/D)^-\times10^6$	Solid angle $\Delta\Omega$ (steradians)	Geometrical factor G	Multiple scattering factor M	Aluminum absorber (g/cm²)	Detection efficiency ϵ_-	Differential cross section in laboratory system $d\sigma^-/dw$ (10^{-27} cm²/sterad)
30	70.2±8.3	0.0570	0.991	0.979	8.78	0.835	4.21±0.53
60	31.1±3.7	0.0562	1.004	0.984	2.59	0.907	1.71±0.21
90	20.2±3.3	0.0559	1.009	0.986	0	0.939	1.07±0.13
120	20.0±2.8	0.0562	0.996	0.986	0	0.939	1.08±0.16
150	31.7±4.3	0.0570	0.997	0.987	0	0.939	1.67±0.24

TABLE IX. Differential cross sections for elastic scattering of negative pions in the center of mass system.

Cosine of center mass angle $\cos\chi$	Differential cross section $(d\sigma/d\omega)^-$ $(10^{-27}$ cm^2/sterad)
0.7851	2.74±0.34
0.2793	1.38±0.17
−0.2618	1.14±0.19
−0.6767	1.48±0.22
−0.9209	2.74±0.39

peated. The variation is reduced by a factor of two at each stage until it is 2^{-7} degrees. When the machine is unable to reduce M further using this variation it prints out the final set of α's and the corresponding cross sections and stops.

In the present work we required the solution to fit 17 different measurements instead of 9 as previously. These were the differential cross sections for the positive (Table III), negative (Table IX), and charge exchange [Eq. (18)] scattering processes, measured at each of five angles, and the total cross sections of positive and negative pions, obtained from transmission measurements.[15] Thus, the experimental knowledge was more completely exploited here than was possible previously.[3-6]

For the initial values of the phase shifts, we chose sets obtained from the construction of Ashkin diagrams.[16] Such construction utilizes only a part of the experimental data and leads to a multiplicity of possible solutions. The multiplicity can be as large as 16, not counting those solutions which differ only in that the signs of all the phase shifts are reversed. In our construction of these diagrams, we varied the input data as liberally as possible within the limits allowed by the experimental error so as to obtain as many starting sets as was reasonable.

In the Ashkin construction the phase shifts are obtained from the intersection of two circles. Thus, one starts out by finding two possible values for α_3, in the present case, −18.5 degrees and −27 degrees. Each of these leads to two possible sets of values for the pair, α_{33} and α_{31}. That for which α_{33} is large and α_{31} is small is known as the Fermi solution. The other, known as the Yang form, may be obtained from the first by means of the transformation

$$\alpha_{33}' = \eta_3 - \alpha_{33}, \qquad \alpha_{31}' = \eta_3 - \alpha_{31}, \tag{20}$$

where

$$\eta_3 = \text{angle of } (2e^{2i\alpha_{33}} + e^{2i\alpha_{31}}).$$

This solution is characterized by an α_{31} which is larger than α_{33}. Each of the four possible solutions for this isotopic spin $\frac{3}{2}$ state leads to two solutions for α_1, and these in turn to possibilities which correspond to the Fermi and Yang sets for the isotopic spin $\frac{1}{2}$ state. It frequently happens that some of the possibilities are not allowed by the data. In the present case we found some 12 possibilities which appeared to be acceptable. These are displayed in Table X. With these as the starting point, the machine found the solutions shown in the same table.

It will be seen that 7 solutions remain even when all the experimental data is included and a least squares fit is demanded. For a given solution, the value of M may serve as a measure of the goodness of the fit. In the usual theory of least squares, where the measurements are truly independent, the errors truly statistical,

TABLE X. Phase shifts at 165 Mev.

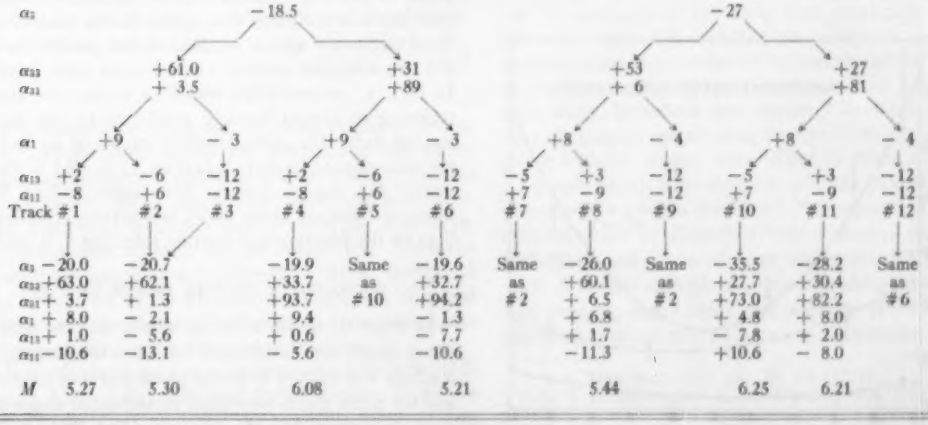

[15] For a variety of reasons the numbers actually fed into the computer differed in minor ways from the final values listed in the tables. The effect on the final results should not be significant.

[16] J. Ashkin and S. H. Vosko, Phys. Rev. **91**, 1248 (1953).

TABLE XI. Calculated cross sections compared with observed values[a] for 165 Mev. Here $\lambda^2=8.874\times10^{-27}$ cm².

Quantity	Lab angle	Expt value	Error	Calculated values Solution #1	#2	#6	#8	#10	#11
$4\lambda^{-2}d\sigma^+/d\omega$	30	8.43	0.99	9.20	9.00	9.02	9.26	9.17	9.38
	60	4.40	0.59	4.02	4.12	4.12	3.98	4.02	4.00
	90	4.79	0.77	4.31	4.38	4.38	4.26	4.20	4.25
	120	9.63	1.12	8.60	8.41	8.42	8.62	8.31	8.64
	150	13.66	1.76	12.79	12.34	12.37	12.87	12.34	12.94
$36\lambda^{-2}d\sigma^-/d\omega$	30	11.10	1.37	10.91	10.65	10.71	10.96	11.15	11.42
	60	5.59	0.69	5.54	5.41	5.44	5.57	5.27	5.65
	90	4.61	0.77	4.45	4.40	4.41	4.45	4.14	4.33
	120	6.01	0.89	6.82	6.83	6.83	6.81	6.86	6.72
	150	11.11	1.47	9.55	9.58	9.57	9.51	9.93	9.52
$18\lambda^{-2}d\sigma^0/d\omega$	30	15.86	2.53	14.52	16.43	16.32	14.66	15.07	14.48
	60	12.09	2.01	11.23	11.78	11.55	11.23	12.10	10.97
	90	13.15	2.15	12.73	12.33	12.21	12.65	13.19	12.31
	120	17.48	2.92	18.19	17.52	17.69	18.06	17.69	17.73
	150	24.41	4.05	23.60	22.99	23.43	23.50	22.20	23.15
$4\lambda^{-2}\sigma_{\gamma\gamma^+}$	···	84.83	2.43	85.89	84.92	85.00	85.86	84.30	86.38
$36\lambda^{-2}\sigma_{\gamma\gamma^-}$	···	273.83	6.41	274.02	276.48	276.24	273.94	276.49	271.46

[a] Values given here were used in the machine calculation and differ in minor ways from the values given in the tables above.

and where the derived quantities have a linear dependence on the measured quantities in the vicinity of the solution, the expectation value of M is 11 for fitting 17 independent data with 6 parameters. In the present case these conditions were not well satisfied. An effort was made not to overestimate the errors and thereby exaggerate the goodness of fit. However, the errors do include contributions due to uncertainties in the measurements, not purely statistical in nature. Moreover, the errors quoted for the cross sections are not all independent. The error which occurs in N, the number of hydrogen atoms per cm², is common to all the measurements. Errors which appear in the efficiency for detecting gamma rays are common to all the charge exchange cross sections. For these reasons the expectation value should be considerably less than 11. It was not surprising that the solutions found had values of M near 6.

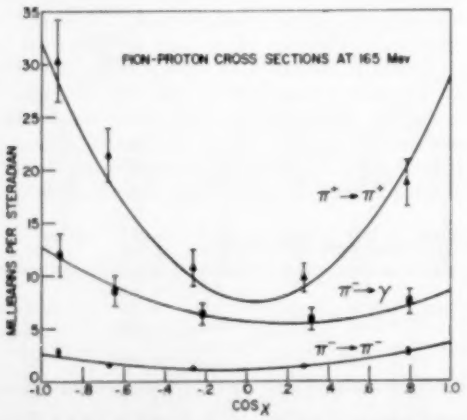

FIG. 4. Scattering of pions by protons at 165 Mev. The curves correspond to solution 1.

It is very difficult to distinguish from these experiments alone, which of the solutions found is the correct one. The values of M found were between 5.21 and 6.25, a variation small compared to the expected rms deviation $\langle(M-\bar{M})^2\rangle_{\text{Av}}^{\frac{1}{2}}=(2\bar{M})^{\frac{1}{2}}=3.5$. This is also made clear in Table XI where the values of the cross sections found by the machine for the various solutions are compared with the input values. Study of this table shows that the machine-found values tend to cluster together, indicating that a considerable improvement in the precision of the measurements would be required to make a clear decision in favor of any one of the possible solutions. A comparison of the experimental data with that of solution 1 is given in Fig. 4.

The reason for the multiplicity of solutions which occurs at 165 Mev can be understood, in part, by examining the Ashkin diagram shown in Fig. 5. In Ashkin's procedure the solutions for α_3 are obtained from the intersection of two circles. In the present case, these circles are almost tangent to one another so that the two solutions marked a and b come close together. In fact, all values of α_3 which lie within the shaded region give almost equally good fits to the experimental data. The corresponding values of α_{31} and α_{33} are also shown shaded. Solutions 1, 2, and 8 all fall within the shaded region. The corresponding Yang forms of these are those which fall between the dashed lines of the diagram and include solutions 4, 6, and 11.

SENSITIVITY OF THE PHASE SHIFTS

In order to obtain a better idea as to how well the phase shifts are determined by the experiments, the machine was started with the phase shifts of solution 1 and the phase shifts were then varied either single or in pairs until the value $M=8$ was reached. This made it possible to draw the contours shown in Fig. 6. In first order, these contours should form a 6-dimensional hyper-

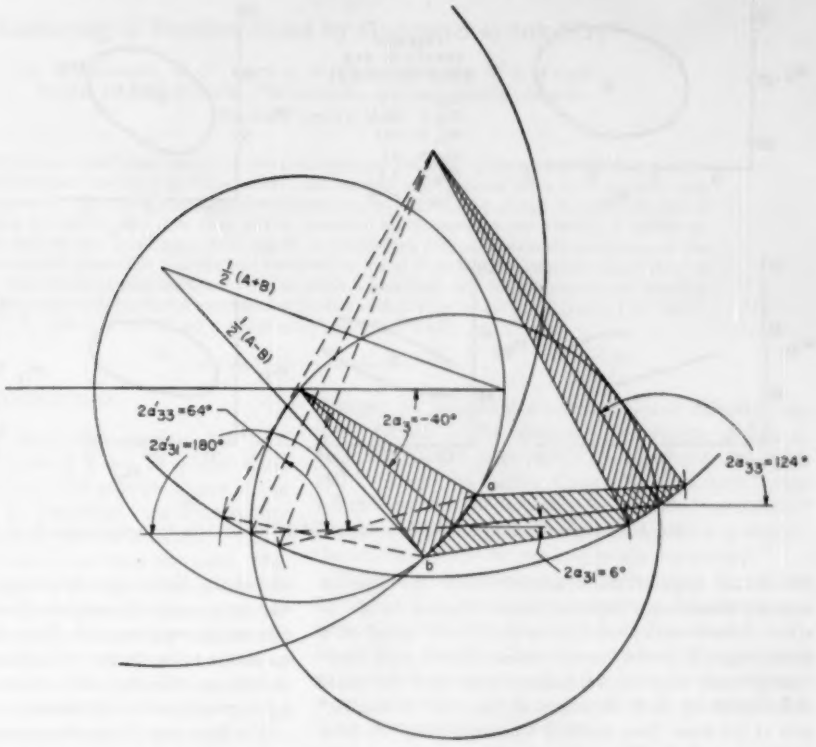

FIG. 5. Ashkin diagram showing spread of possible solutions for α_3. Fermi-type solutions for α_{33} and α_{31} are included in shaded area. Yang-type solutions for α_{33} and α_{31} are included within the dashed lines.

ellipsoid and any set of phase shifts lying within this figure should be acceptable according to the experiments. Figure 6 attempts to show some of the projections of this hyperellipsoid. It shows, in orthographic projection, the ellipsoid corresponding to the isotopic spin $\frac{3}{2}$ state, and separately, that for the isotopic spin $\frac{1}{2}$ state. The elongated form of the ellipses for α_3 and α_{33}, and for α_{31} and α_{33} is due to degeneracy of the solutions for α_3 already referred to.

DISCUSSION

For purposes of discussion, it seems desirable to concentrate the attention on the solutions of the Fermi type, and set aside the solutions of the Yang type. This step receives some justification based on simplicity. The Yang-type solutions have α_{13} and α_{31} both large, instead of just α_{33} large for the Fermi type. When the Yang-type solutions are followed to higher energy, as has been done by de Hoffmann, Metropolis, Alei and Bethe,[4] and by Martin,[5] they lead to three resonances instead of one for the Fermi-type solution.

Our solution 1 is quite close to the one which de Hoffmann, Metropolis, Alei, and Bethe[4] believe to be the correct one. They analyzed the available negative pion data between 120 and 217 Mev and selected those solutions which varied continuously with energy, and gave positive pion total cross sections in agreement with the experimental values. In their preferred solution, α_{33} goes through 90° at about 195 Mev while the other p phase shifts are small. The same solution was also found by Glicksman[6] by setting $\alpha_{11}=\alpha_{13}=\alpha_{31}=0$.

The choice of interaction corresponding to α_{33} dominant and resonant is the one first proposed by Breuckner[17] to account for the early pion scattering results. The same choice has provided the basis for a successful interpretation of a number of the features of the process of pion production by nucleons as well as by gamma rays. Thus, Brueckner and Watson[18] have pointed out that the angular distribution observed[19] for the reaction $p+p\rightarrow\pi^{+}+d$ is not very different from the form $0.3+\cos^2\chi$ which it would have with the $p_{\frac{1}{2}}$ state of the pion-nucleon system dominant. Subsequently, a more detailed study by Rosenfeld[20] and a general review by Gell-Mann and Watson[14] have reaffirmed this point of view. A similar argument operates in the photoproduction process, where again the emission of the pion in the $p_{\frac{1}{2}}$ state would give an isotropic distribution whereas

[17] K. A. Brueckner, Phys. Rev. **86**, 106 (1952).
[18] K. A. Brueckner and K. M. Watson, Phys. Rev. **86**, 923 (1952).
[19] Cartwright, Richman, Whitehead and Wilcox, Phys. Rev. **91**, 677 (1953).
[20] A. H. Rosenfeld, Phys. Rev. **96**, 139 (1954).

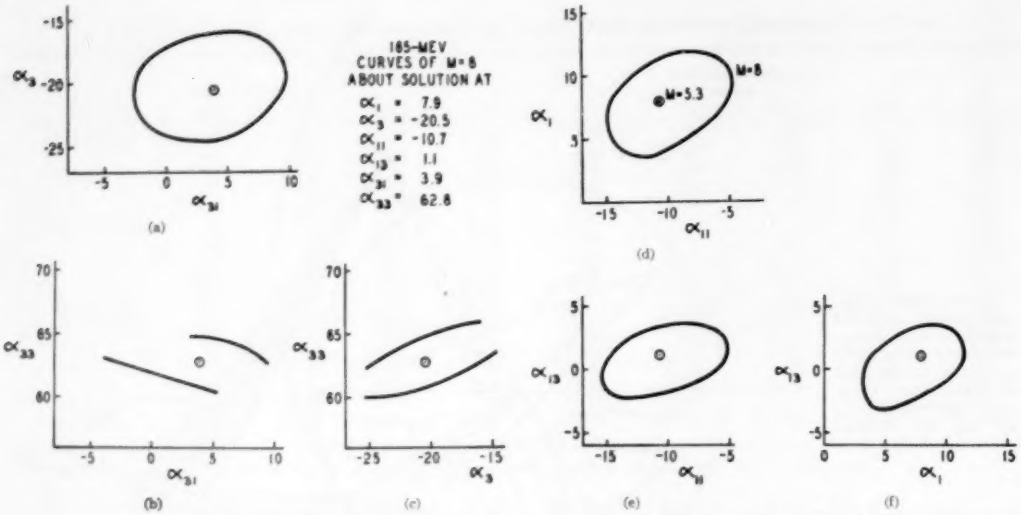

FIG. 6. Orthographic projection of error ellipses of the phase shifts for isotopic spin states $\frac{3}{2}$ and $\frac{1}{2}$.

the actual angular distributions[21] show the marked angular dependence expected from emission in the p_1 state. A noteworthy calculation by Chew[22] based on a static, cut-off, pseudo-vector meson theory, with moderately weak coupling, reproduces quite well the phase shifts given by de Hoffmann *et al.*,[4] and by Glicksman,[6] and at the same time, much of the available photo-pion production data. These qualitative arguments make plausible the choice of solution 1, but they do not finally rule out the other possibilities.

The behavior of α_{33} and of α_3 found by de Hoffmann, Metropolis, Alei, and Bethe[4] is confirmed at 165 Mev by our value for these phase angles. The same can be said of the Fermi-type solutions arrived at by Martin[5] who set $\alpha_{11}=\alpha_{13}=0$, and also the solution of Glicksman[6] who set $\alpha_{11}=\alpha_{13}=\alpha_{31}=0$. Thus the general behavior of α_{33} seems to be rather well determined, at least in the vicinity of 165 Mev and below. This is because the $\frac{3}{2},\frac{3}{2}$ interaction is so dominant.

The behavior of the other phase shifts has been less well established by the analyses carried out thus far. They all have the defect of having neglected the possible effect of d waves. We hope to improve this situation in our future work.

[21] A. Silverman and M. Stearns, Phys. Rev. **88**, 1228 (1952); G. Cocconi and A. Silverman, Phys. Rev. **88**, 1230 (1952); Goldschmidt-Clermont, Osborne, and Scott, Phys. Rev. **89**, 329 (1953); Walker, Oakley, and Tollestrup, Phys. Rev. **89**, 1301 (1953).

[22] G. F. Chew, Phys. Rev. **95**, 1669 (1954).

ACKNOWLEDGMENTS

We wish to thank Mr. Tadao Fujii and Mr. Joseph Fainberg for helping to carry out the measurements and Dr. William C. Davidon and Dr. Ulrich Kruse for helping to analyze the data.

Scattering of Positive Pions by Hydrogen at 189 Mev*

H. L. ANDERSON, W. C. DAVIDON, M. GLICKSMAN,† AND U. E. KRUSE
Institute for Nuclear Studies, The University of Chicago, Chicago, Illinois

(Received April 13, 1955)

The differential and total cross section of pions on hydrogen has been measured for 189 Mev positive pions. Liquid hydrogen was used as the scatterer; the incident and scattered pions were detected with scintillation counters. The angular distribution was fitted by: $\sigma = (7.24 \pm 0.76) + (3.1 \pm 1.3) \cos\chi + (25.6 \pm 2.6) \cos^2\chi$ millibarns per sterad. The total cross section measured by transmission was 194.1 ± 5.2 millibarns. A phase shift analysis was made using these results in conjunction with data obtained previously on the scattering of negative pions. The analysis was restricted to S and P waves and assumed conservation of isotopic spin. Four solutions were obtained. The one which is consistent with the requirements of causality and which corresponds to the preferred solution of de Hoffmann *et al.* is $\alpha_1 = -2.8° \pm 4.5°$, $\alpha_3 = -11.3° \pm 3.2°$, $\alpha_{11} = -2.6° \pm 7.5°$, $\alpha_{13} = -2.1° \pm 3.8°$, $\alpha_{31} = -11.6° \pm 5.1°$, $\alpha_{33} = 98.8° \pm 3.6°$.

INTRODUCTION

THE scattering of pions with nucleons has been interpreted in terms of a set of phase shifts specifying the interaction in the possible states of the pion-nucleon system. In particular, the high-energy data have been analyzed by several authors,[1–3] and a preferred set of phase shifts has been proposed. This set has a resonance behavior for the state of isotopic spin $\frac{3}{2}$ and total angular momentum $\frac{3}{2}$. These analyses were based primarily on measurements of π^- differential cross sections, supplemented to some extent by some data on π^+ total cross sections. The present experiments were undertaken to complement the π^- scattering data at 191 Mev[4] with the corresponding π^+ data, and in this way improve the knowledge of the phase shifts at this energy. The present work extends that carried out at 165 Mev and reported in a companion paper.[5]

Due to the low intensity of positive pions available, a rather poor geometry was used. This necessitated special corrections in analyzing the data. The same corrections were used to reanalyze the previous negative pion data. A separate experiment to determine the efficiencies of the counters used in the charge exchange reactions led to a reanalysis of this reaction. All the results of counter measurements were then used as a basis for a new phase-shift analysis. The accuracy of the phase-shift solutions was also explored.

EXPERIMENTAL ARRANGEMENT

The experimental arrangement was essentially the same as that used in previous work from the laboratory.[6] A larger liquid hydrogen target of 6-inch diameter was used. Details of the geometry are shown in Fig. 1. Counters 1 and 2 were plastic scintillators $\frac{1}{4}$-inch thick and 2 inches$\times 2\frac{1}{16}$ inches. Counters 3, 4, 5, and 6 were 4-inch$\times$6-inch liquid scintillators described previously.[6] The use of four such counters made it possible to observe the scattered pions at two angles simultaneously.

Transmission measurements were made to obtain the total cross sections independently. Measurements were taken with the 4-inch$\times$6-inch counters set at 0°. In addition, 8-inch diameter liquid scintillation counters were used in the geometry of Fig. 2. A similar arrangement with the 8-inch counters was employed for range measurements in copper.

PION BEAMS

A beam of positive pions was obtained by bombarding a copper target in the cyclotron. Pions created in the backward direction emerged from the cyclotron and passed through a channel in the shielding to the experimental area. After passing through an analysing magnet and a proton filter of polyethylene, the pion flux was determined by counters 1 and 2. The flux available was roughly 300 pions/min. This was considerably greater than what could be obtained using a beryllium target.

The energy of the pions was determined from a range measurement in copper. The mean range corre-

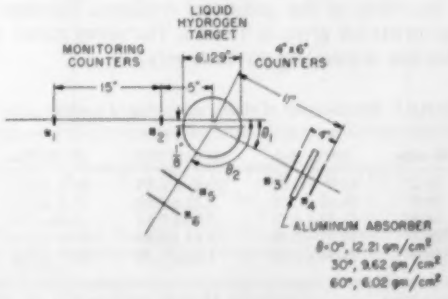

FIG. 1. Arrangement for observing the scattering of positive pions in hydrogen.

* Research supported by a joint program of the Office of Naval Research and the U. S. Atomic Energy Commission.

† Now at David Sarnoff Research Center, RCA Laboratories, Princeton, New Jersey.

[1] Fermi, Metropolis, and Alei, Phys. Rev. **95**, 158 (1954).

[2] de Hoffmann, Metropolis, Alei, and Bethe, Phys. Rev. **95**, 1586 (1954).

[3] R. L. Martin, Phys. Rev. **95**, 1606 (1954).

[4] M. Glicksman, Phys. Rev. **95**, 1045 (1954).

[5] H. L. Anderson and M. Glicksman, preceding paper [Phys. Rev. **100**, 268 (1955).

[6] Anderson, Fermi, Martin, and Nagle, Phys. Rev. **91**, 155 (1953).

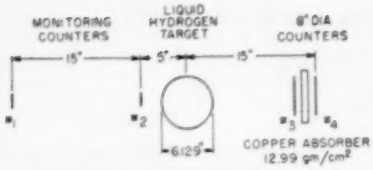

FIG. 2. Arrangement for making transmission measurements on positive pions in hydrogen.

sponded to 90.68 g/cm². Corrections for multiple scattering in the copper and counters and for energy loss in the target walls and counters gave a mean range at the center of the empty target of 97.33 g/cm². From the range curves of Aron[7] the corresponding energy of the pions at the center of the hydrogen filled target was 188.5 Mev. The effective energy spectrum had a full width at half maximum of 13.2 Mev. The fraction of muons in the beam was determined from the range curve; 2.2 percent of the beam were muons that had come through the analyzing magnet. A further 1.9 percent decayed in flight so as to be included by the monitoring counters. Thus 4.1 percent of the number of counts in counters 1 and 2 were due to muons.

In order to determine the distribution of the beam in the hydrogen target, the horizontal intensity distribution at the target position was measured directly with a scintillator $\frac{1}{4}$ inch wide and 2 inches high. The results were used to obtain the effective number of hydrogen scatterers and to correct for their finite extension.

ELASTIC SCATTERING OF POSITIVE PIONS

The differential cross section for the scattering of positive pions was measured at five angles. At 30° and 60°, aluminum absorbers were placed between the counters to eliminate all recoil protons. Measurements were taken simultaneously at two scattering angles, and with the target alternately filled with liquid hydrogen or containing only hydrogen gas at near liquid hydrogen temperature. These measurements are recorded as the ratio Q/D, quadruple coincidences divided by the double coincidences observed in the incident beam monitors. The simple differences in this ratio, Q/D, were taken as the effect of the additional hydrogen introduced. The results are given in Table I. The errors stated are those due to counting statistics only.

TABLE I. Measurement of elastic scattering of positive pions.

Lab angle	$10^4\,(Q/D)_H$	$10^4\,(Q/D)_{No\,H}$	$10^4\,(Q/D)_{net}$
31.2°	45.0 ±1.33	10.9 ±0.93	34.1 ±1.6
60.9°	14.64±0.76	3.37±0.50	11.3 ±0.9
90.6°	14.54±0.74	5.86±0.54	8.68±0.9
120.3°	14.58±0.80	3.11±0.50	11.5 ±0.95
150.0°	21.54±0.92	4.69±0.59	16.9 ±1.6

[7] W. A. Aron, University of California Radiation Laboratory Report, UCRL-1325 (unpublished).

TRANSMISSION EXPERIMENTS

The total cross section was separately determined by transmission measurements. Two measurements were made using the 8-inch counters. A copper absorber of 12.99 g/cm² was used between counters 3 and 4 to discriminate against recoil protons. A third measurement was made with the 4-inch×6 inch counters, with an aluminum absorber of 12.21 g/cm².

Under the assumption that muons in the beam do not interact, the cross section is given by

$$\sigma = -\frac{1}{N}\ln\left[R-\frac{r}{T}(1-R)\right].$$

R is $(Q/D)_H/(Q/D)_{No\,H}$, where N is the number of hydrogen atoms/cm², r is the ratio of muons to pions at the center of the target, and T is the fraction of pions at the center of the target which are detected in counters 3 and 4 (regardless of whether or not they decay on the way). Q/D measures the cross section for scattering greater than θ_{max}, the half-angle subtended by counter 4 at the center of the target. The total cross section is obtained by adding the cross section up to θ_{max}; this

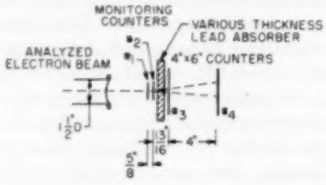

FIG. 3. Arrangement for measuring electron detection efficiencies of counters used in charge-exchange measurements.

was estimated from the angular distribution measurements. The final results are in Table II.

The weighted mean of all the transmission measurements was 194.1±5.2 mb, including a two percent error in the value of N.

GAMMA EFFICIENCIES

A measurement was made to determine the energy dependence of the gamma efficiencies of the counter arrangement used in the earlier charge exchange scattering experiment.[4] The efficiencies for the detection of pairs produced at different depths in the lead radiator were derived from measurements on the transmission of electrons of different energies through various thicknesses of lead. These results were then combined with known pair production cross sections[8,9] to give the gamma efficiencies of the counters. The experimental arrangement used is shown in Fig. 3.

The dimensions and relative positions of the lead and counters 3 and 4 were the same as in the charge exchange measurement. Counters 1 and 2 were $\frac{1}{2}$-inch ×$\frac{1}{2}$-inch plastic scintillators and served to define and

[8] De Wire, Ashkin, and Beach, Phys. Rev. **83**, 505 (1951).
[9] J. L. Lawson, Phys. Rev. **75**, 433 (1949).

TABLE II. Measurement for the total cross section of positive pions.

Counter No. 3 and No. 4	θ_{max}	Absorber	$R=\frac{(Q/D)n}{(Q/D)_{No\ n}}$	γ/T	$\sigma_T-\int_1^{\theta_{max}} d\Omega\frac{d\sigma}{d\Omega}$	$\int_1^{\theta_{max}} d\Omega\frac{d\sigma}{d\Omega}$	σ_T
8 in.	15.2°	12.99 g/cm² Cu	0.9038±0.0051	0.052±0.01	167.2±9.1 mb	12.1±2.5 mb	179.3±9.4 mb
8 in.	15.2°	12.99 g/cm² Cu	0.8945±0.0024	0.052±0.01	184.3±4.5 mb	12.1±2.5 mb	196.4±5.2 mb
4 in.×6 in.	14.1°[a]	12.21 g/cm² Al	0.8924±0.0023	0.053±0.01	188.4±4.4 mb	10.5±3.0 mb	196.5±5.3 mb

[a] Angle for circular counter of area equal to 4 in.×6 in.

monitor the incident beam. Wire measurements were used to determine the electron energies, which ranged from 10 to 75 Mev. At each energy the ratio of triple coincidences in counters 1, 2, and 3, to the double coincidences in 1 and 2, gave the fraction of incident electrons which traversed the lead. The quadruples to triples rate, gave the fraction which was not scattered out of the No. 4 counter. The results are summarized in Table III.

To obtain the gamma efficiencies of the counters, the probability was determined for a photon to traverse various thicknesses of lead, produce a pair, and have at least one of the pair detected. Numerical integrations were made over the counter dimensions, lead thickness, and energy division of the pair produced. The average efficiencies for gammas produced anywhere in the target are presented in Fig. 4. The dependence on the angle at which the detector was set was small and was neglected here.

TABLE III. Measurement of attenuation and scattering of electron beams in lead.

Lead (g/cm²)	Energy (Mev)	T/D	Q/T Position[a] 1	2	3	4
0	8.7	0.98	0.88	0.45	0.77	0.34
	18.2	0.98	0.93	0.62	0.86	0.47
	37.2	0.99	0.98	0.68	0.97	0.69
	56.2	0.99	0.98	0.78	0.99	0.75
	75.2	0.99	0.97	0.81	0.97	0.75
2.76	8.7	0.17	0.24	0.088	0.076	0.065
	18.2	0.70	0.36	0.26	0.29	0.28
	37.2	0.90	0.71	0.46	0.66	0.42
	56.2	0.93	0.86	0.53	0.73	0.45
	75.2	0.93	0.88	0.59	0.86	0.61
5.55	8.7	0.00	...	...	...	...
	18.2	0.22	0.17	0.16	0.19	0.11
	37.2	0.67	0.45	0.31	0.45	0.34
	56.2	0.81	0.61	0.42	0.56	0.36
	75.2	0.89	0.71	0.44	0.57	0.41
7.41	8.7	0.00	...	...	...	...
	18.2	0.15	0.19	0.14	0.23	0.00
	37.2	0.50	0.46	0.27	0.34	0.15
	56.2	0.69	0.52	0.42	0.46	0.29
	75.2	0.78	0.65	0.53	0.61	0.31

[a] Position of beam on first 4 in.×6 in. counter (No. 3).
1. Center.
2. 2 in. from center along 6 in. axis.
3. 1½ in. from center along 4 in. axis.
4. 2 in. from center along 6 in. axis and 1½ in. from center along 4 in. axis.

Calculations were also made in which the Monte Carlo results of Wilson[10,11] were used for the electron scattering. These gave smaller efficiencies as shown in Fig. 4. The uncertainties involved in deducing these efficiences were such that we assigned an error of 15 percent and included this in all the errors stated.

The experimental determination of the gamma efficiency was subject to two tests. First, using the computed results, a determination was made of the efficiency to be expected in a measurement of the Panofsky effect. The results of this calculation gave 54.3±8.1 percent as compared to 58±6 percent obtained directly in a previous measurement.[6] The other test was a comparison between the total cross section for π^- and the sum of integrated differential cross sections for $\pi^-\to\pi^-$, $\pi^-\to\pi^0$, and $\pi^-\to\gamma$. The total cross section was (63.5±1.6 mb) whereas the sum of integrated cross sections was 68.0±3.5 mb. The difference is not outside the experimental error in both cases.

DATA ANALYSIS

Elastic Scattering

The data analysis of the elastic scattering experiment was complicated by the poor geometries used to obtain reasonable counting rates with the weak incident beam. Thus, a number of corrections were needed to

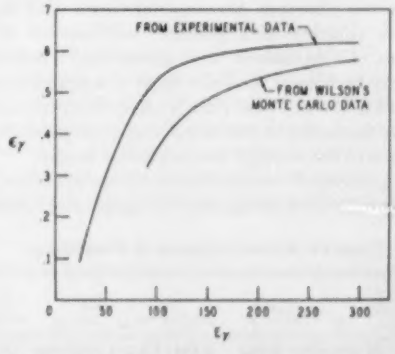

FIG. 4. Gamma detection efficiencies of counters used in charge exchange measurements. E_γ is the gamma energy, ϵ_γ the detection efficiency.

[10] R. R. Wilson, Phys. Rev. **84**, 100 (1951).
[11] R. R. Wilson, Phys. Rev. **86**, 261 (1952).

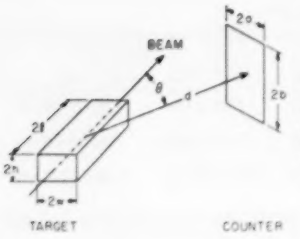

FIG. 5. Idealized target and counter geometry used as basis for geometry corrections.

obtain the scattering cross section from the experimental data. Accordingly, corrections were made for the finite range of scattering angles allowed by the detector and target, each angle being weighted by its own solid angle. Further corrections for thick targets were made to take into account the attenuation of the incident and scattered beams in the target and the multiple scattering in the target. Besides these, the usual corrections for efficiencies of the counters and muon contamination of the beam were made. The cross section for poor geometries was, therefore, taken to be

$$\frac{d\sigma}{d\Omega}=\left(\frac{Q}{D}\right)_{\text{net}}\frac{1}{N\Omega}\frac{1}{f\epsilon GM},$$

where $(Q/D)_{\text{net}}$ as above represents the net quadruples rate, H-liquid minus H-gas, divided by the doubles rate of the incident beam monitor. The mean number of hydrogen scatterers/cm² seen by the actual beam distribution is N; Ω is the solid angle of the fourth counter averaged over the target; f is the fraction of the doubles counts which actually correspond to pions at the center of the target, omitting however possible attenuation in the hydrogen. Thus, fD is the number of pions at the center of the target with no hydrogen in the target; ϵ is the efficiency of counting pions which are scattered toward the counters. This efficiency takes into account nuclear absorption in the third counter and in the absorber between the third and fourth counters together with possible inefficiencies in the counters. G represents the geometrical corrections necessary because of the finite range of scattering angles observed in the detector. Finally, M is the correction for multiple scattering in the target and attenuation in the hydrogen of the incident and scattered beams.

The quantity N was determined from the beam scan together with the dimensions of the target and difference in density of liquid hydrogen and hydrogen gas. The mean path length was 5.96 inches and the net density, 0.070 g/cm³, therefore $N=6.39\times10^{22}$ atoms/cm². The uncertainty in N was estimated to be two percent. The quantity f was 0.947 as determined from the muon contamination of 4.1 percent, obtained from the range curve, and the 1.2 percent absorption of pions in the second counter and front target wall. The accuracy of f was estimated to be ±1 percent.

TABLE IV. Factors in analysis of π^+ scattering.

Lab angle (degree)	N	f	ϵ	M	Ω	G
31.2	6.39×10^{22}	0.947	0.854	0.932	0.1936	0.934
60.9			0.891	0.974	0.1792	1.054
90.6			0.962	0.974	0.1728	1.048
120.3			0.962	0.954	0.1796	0.982
150.0			0.962	0.965	0.1936	0.987

The correction M for attenuation and multiple scattering took into account the energy and angular dependence of the scattering cross section. However, the following approximations were made to obtain a simple formula. The scattering volume was assumed to be spherical, and all the first scatterings were assumed to occur at the center of this sphere. Only double scatterings were considered and these were taken to occur as the particle left the center of the sphere. Attenuations were assumed to occur on the way into the center and on the way out from the center. With these assumptions the single scattering s per unit solid angle is given by

$$\frac{s}{fD\Omega}=e^{-\frac{1}{2}N\sigma_T(0)}N\sigma(\theta)e^{-\frac{1}{2}N\sigma_T(\theta)}$$
$$=N\sigma(\theta)\{1-\tfrac{1}{2}N[\sigma_T(0)+\sigma_T(\theta)]\},$$

to first order in $N\sigma$. Here $\sigma(\theta)$ is the differential cross section for scattering into θ, $E(\theta)$ is the energy of the meson scattered into the angle θ and $\sigma_T(\theta)$ is the total cross section for pion scattering at this energy. The ratio of double scattering to single scattering into a counter at angle θ is given by

$$\frac{d}{s}=\frac{N}{2\sigma_1(\theta)}\int d\phi d(\cos\alpha)\sigma_2(\chi)\sigma_1(\alpha,\phi),$$

where α and ϕ are the polar and azimuthal angles of the first scattering given by $\sigma_1(\alpha,\phi)$. The plane formed by the incident beam and the center of the counter is taken as $\phi=0$. The cross section for second scattering is $\sigma_2(\chi)$ where χ is the angle between the initial scattering and the direction of the counter at θ. To obtain an integrable form, the laboratory differential cross section for second scattering, $\sigma_2(\chi)$ was expanded in terms of Legendre polynomials; the coefficients in the expansion depend on the energy of the pion after the first scattering and hence on α. Thus,

$$\sigma_2(\chi)=\sum a_l(\alpha)P_l(\chi).$$

With the use of the addition theorem for spherical harmonics,

$$P_l(\chi)=\frac{4\pi}{2l+1}\sum_{m=-l}^{l}\gamma_l^{m*}(\alpha,\varphi)\gamma_l^{m}(\theta,0),$$

and after an integration over ϕ, the ratio of double to

TABLE V. Estimated standard errors in π^+ cross section.

Lab angle (degree) \ Quantity	N_{cal} %	M %	Ω %	G %	$\Delta\theta$ %	ΔE %	Subtotal %	Subtotal mb	Statistical mb	Total estimate mb
31.2	3.0	3.9	2.3	1.1	2.0	2.1	6.2	2.4	1.8	3.0
60.9	3.0	1.3	2.5	2.2	2.5	1.1	5.4	0.62	0.9	1.06
90.6	3.0	1.3	2.7	1.2	0.5	0.7	4.5	0.38	0.9	0.98
120.3	3.0	2.3	2.5	0.9	0.8	0.3	4.7	0.55	1.0	1.4
150.0	3.0	1.9	2.3	0.2	0.3	0.1	4.2	0.66	1.5	1.64

single scattering becomes

$$\frac{d}{s}=\frac{\pi N}{\sigma_1(\theta)}\sum_l P_l(\theta)\int_{-1}^{+1} dt a_l(t)\sigma_1(t)P_l(t),$$

where $t=\cos\alpha$. The coefficients $a_l(t)$ were evaluated from the scattering data at lower energies, terms up to $l=2$ only were included. Therefore

$$(s+d)/fD\Omega=N\sigma_1(\theta)[1-\tfrac{1}{2}N\sigma_T(0)-\tfrac{1}{2}N\sigma_T(\theta)+(d/s)]$$

and the correction M to the cross section because of attenuation and double scattering in the target is

$$M=1-\tfrac{1}{2}N\sigma_T(0)-\tfrac{1}{2}N\sigma_T(\theta)+(d/s).$$

The uncertainties in M vary with the scattering angle, from four percent at 31.2° to 1.9 percent at 150°.

The geometrical corrections appear in terms of the two quantities Ω, the corrected solid angle, and G a correction factor for the variations of the cross section over the range of angles detected at one counter setting. If $\sigma(\phi)$ represents the true scattering cross section in the laboratory system, then for a counter at θ,

$$\frac{(Q/D)_{\rm net}(\theta)}{\epsilon fNM}=\frac{1}{V}\int\int_A d\tau da\sigma(\phi)\frac{\cos\delta}{r^2},$$

where $d\tau$ is an element of the target volume V, da is an element of the counter area A, and $\mathbf{r}$ is a vector connecting $d\tau$ with da. The angle between $\mathbf{r}$ and the direction of the incident beam is ϕ, and δ is the angle between $\mathbf{r}$ and the normal to the counter.

Let the counter be of width $2a$ and height $2b$ centered at a scattering angle θ a distance d from the center of the target of width $2w$, height $2h$, and length $2l$ as in Fig. 5. When $\sigma(\phi)$ is expanded in a Taylor series about θ, then in terms of

$$(d\sigma/d\phi)|_\theta=\sigma'(\theta) \quad \text{and} \quad (d^2\sigma/d\phi^2)|_\theta=\sigma''(\theta),$$

$$\frac{\left(\frac{Q}{D}\right)_{\rm net}(\theta)}{\epsilon fNM}=\frac{A}{d^2}[\sigma(\theta)(1+\alpha)+\beta\sigma'(\theta)+\tfrac{1}{2}\gamma\sigma''(\theta)].$$

To second order in a/d, b/d, etc., α, β, and γ are

$$\alpha=\frac{1}{d^2}\left[-\frac{a^2}{2}-\frac{b^2}{2}-\frac{h^2}{2}+\frac{l^2}{2}(3\cos^2\theta-1)+\frac{w^2}{2}(3\cos^2\theta-1)\right]$$

$$\beta=\frac{1}{d^2}\left[\frac{b^2}{6}\cot\theta+\frac{h^2}{6}\cot\theta+l^2\cos\theta\sin\theta-w^2\cos\theta\sin\theta\right]$$

$$\gamma=\frac{1}{d^2}\left[\frac{a^2}{3}+\frac{l^2}{3}\sin^2\theta+\frac{w^2}{3}\cos^2\theta\right].$$

The higher order terms cannot be neglected for small θ.

If the dependence on σ' and σ'' is included in a factor G, then

$$\frac{\left(\frac{Q}{D}\right)_{\rm net}(\theta)}{\epsilon fNM}=\frac{A}{d^2}\sigma(\theta)(1+\alpha)G,$$

with

$$G=1+\beta\sigma'(\theta)+\tfrac{1}{2}\gamma\sigma''(\theta).$$

A further small correction is made for scattering angles near 90°. For these angles, the extremities of the target do not see all of the fourth counter, a fraction λ is cut off by the third counter. The final value for Ω therefore is

$$(A/d^2)(1+\alpha)(1-\lambda).$$

The uncertainty in Ω is estimated at two percent and in G as two percent.

The values of the various quantities for the 189 Mev positive pion scattering are given in Table IV.

In addition to the uncertainties in the various constants of Table IV, the uncertainty in the angle is estimated as $\pm0.7°$ and the uncertainty in the energy, estimated as ±2 Mev, can contribute to the uncertainties in the final cross sections. The estimated standard errors in each cross section are given in Table V, divided

TABLE VI. Cross section for π^+ scattering.

Lab angle (degree)	C. M. angle	$10^{28}(Q/D)_{\rm net}$	$(d\sigma/d\Omega)_{\rm lab}$ in mb	$(d\sigma/d\omega)_{\rm c.m.}$ in mb
31.2	40.3	34.1±1.8	39.2±3.0	25.0±1.9
60.9	75.7	11.3±0.9	11.4±1.1	9.2±0.8
90.6	106.6	8.7±0.9	8.5±1.0	9.1±1.0
120.3	133.4	11.5±1.0	11.7±1.1	16.4±1.6
150.0	157.1	16.9±1.6	15.8±1.6	26.6±2.8

TABLE VII. Factors in analysis of elastic π^- scattering.

Lab angle	N	f	ϵ	M	Ω	G	ϵ_γ^-
25.7	3.59×10^{23}	0.97	0.858	0.975	0.112	0.974	0.025
51.4			0.938	0.985	0.111	0.991	0.025
77.1			0.968	0.986	0.109	1.040	0.024
102.8			0.968	0.987	0.109	1.009	0.024
128.6			0.968	0.987	0.111	1.004	0.024
154.3			0.968	0.988	0.112	1.003	0.024

into contributions from statistics and all other sources. The errors estimated were combined quadratically to give the over-all error estimate. The final cross sections are then given in Table VI.

The elastic negative pion experiments previously performed[4] were reanalyzed in the same way as the positive pion experiments. In this experiment, part of the counting rate is due to gamma rays from the charge exchange reaction. Therefore

$$\sigma_{\pi^-}=\left[\left(\frac{Q}{D}\right)^- - \frac{\epsilon_\gamma^-}{\epsilon_\gamma^0}\left(\frac{Q}{D}\right)^0_{\text{net}}\right]\frac{1}{N\epsilon fGM\Omega},$$

where ϵ_γ^- and ϵ_γ^0 are the average efficiencies for γ detection in the elastic scattering and charge exchange measurements; $(Q/D)_{\text{net}}^-$ and $(Q/D)_{\text{net}}^0$ are the net quadruples to doubles observed in the two arrangements. The quantity $\epsilon_\gamma^-/\epsilon_\gamma^0$ is roughly 4.5 percent.

The numerical values of the terms are given in Table VII, $(Q/D)^0_{\text{net}}$ is given in Table IX.

The cross sections are given in Table VIII and differ only slightly from the previous results.

The charge exchange scattering previously determined was also reanalyzed in terms of the efficiencies given in the section on gamma efficiencies. The analysis is the same as the one given by Bodansky, Sachs, and Steinberger.[13] and in the companion paper.[5]

The number of γ-ray counts due to the charge exchange reaction is converted to the center-of-mass system. The resulting number of counts per unit solid angle and per incident π^- is

$$n_\gamma=\frac{(Q/D)_{\text{net}}^0}{Nf\Omega}\frac{\Delta\Omega}{\Delta\omega}-n'.$$

TABLE VIII. Cross sections for elastic π^- scattering.

Lab angle	C. M. angle	$10^4\,(Q/D)_{\text{net}}$	$(d\sigma/d\Omega)_\gamma$	$(d\sigma/d\Omega)_{\text{tot}}$	$(d\sigma/d\omega)_{\text{c.m.}}$
25.7	33.3	207.5±19.9	13.19±0.82	6.11±0.68	3.85±0.42
51.4	64.7	72.6± 8.8	7.56±0.53	1.85±0.26	1.38±0.20
77.1	93.0	38.6± 6.4	5.02±0.52	0.90±0.18	0.85±0.17
102.8	118.0	48.8± 6.5	5.73±0.52	1.20±0.19	1.45±0.23
128.6	140.3	58.7± 7.0	5.66±0.52	1.44±0.20	2.14±0.30
154.3	160.7	74.9± 9.4	6.13±0.69	1.86±0.26	3.16±0.45

[13] Bodansky, Sachs, and Steinberger, Phys. Rev. **93**, 1367 (1954).

TABLE IX. Factors in analysis of π^- charge exchange scattering.

θ	χ	$(Q/D)_{\text{net}}$	N	f	Ω	n'	n_γ
25.7	32.3	285.6±16.6	3.59×10^{23}	0.97	0.107	0.03	4.93±0.79
51.4	62.8	157.0±10.4			0.107	0.03	3.23±0.53
77.1	90.7	99.4±10.1			0.106	0.03	2.53±0.45
102.8	115.6	109.4± 9.8			0.106	0.03	3.45±0.60
128.6	138.4	106.0± 9.6			0.107	0.03	3.93±0.69
154.3	159.6	115.1±12.8			0.107	0.03	4.77±0.88

$\Delta\Omega/\Delta\omega$ is the ratio of solid angles in the laboratory and center of mass systems and n' is the corresponding number of counts due to the reaction $\pi^-+p\rightarrow n+\gamma$.

Table IX gives the experimental results for n_γ. The 15 percent uncertainty for the efficiencies has been added to the statistical uncertainties.

With the π^0 distribution $\sum a_l P_l$ we have for n_γ

$$n_\gamma=\sum k_l\bar{\epsilon}_l a_l P_l.$$

The values of $\bar{\epsilon}_l$ are given in Table X. For this energy, $k_0=2$, $k_1=1.414$, and $k_2=0.937$.

Figure 6 is a plot of the differential cross sections. For $\pi^-+p\rightarrow\pi^0+n$, the effective γ ray cross section n_γ/ϵ_0 is plotted. The curves represent the cross sections calculated from the first phase-shift solution. The cross sections for positive pion scattering determined by Homa, Goldhaber, and Lederman[12] are in rough agreement with the present measurements.

LEAST SQUARES FIT AND PHASE-SHIFT ANALYSIS

In order to provide a summary of the angular distribution measurements, to integrate the angular distributions, and to prepare an Ashkin diagram,[14] a least squares fit was made to the differential cross section by expressions of the form $a+b\cos\chi+c\cos^2\chi$.

In this least squares fit, and in the determination of the phase shifts, the quantity $M=\sum_i(\Delta_i/\epsilon_i)^2$ is minimized. The quantity Δ_i is the difference between the calculated and experimental cross sections, and ϵ_i is the experimental standard deviation. In the vicinity of the best fit, we consider M to depend quadratically on the parameters. This is exact in the case of the a, b, and c's. For the phase shifts, a fit was made to the actual dependence on M by a function of this type. Under these conditions, if the parameters are changed from

TABLE X. Efficiencies and coefficients in π^- charge exchange scattering.

C. M. angle χ	$\bar{\epsilon}_0$	$\bar{\epsilon}_1$	$\bar{\epsilon}_2$
32.3	0.57	0.60	0.63
62.8	0.53	0.59	0.63
90.7	0.51	0.58	0.63
115.6	0.48	0.57	0.62
138.4	0.47	0.56	0.62
159.6	0.45	0.55	0.62

[12] Homa, Goldhaber, and Lederman, Phys. Rev. **93**, 554 (1954).
[14] J. Ashkin and S. H. Vosko, Phys. Rev. **91**, 1248 (1953).

TABLE XI. Summary of least squares fit at 189 Mev.

Scattering process	Coefficients in fit: $d\sigma/d\omega = a + b\cos\chi + c\cos^2\chi$ (mb/sterad) a	b	c	$4\pi(a+c/3)$ (mb) σ_T	Error matrix G^{-1} (mb/sterad)^2			M_0
$\pi^+ \to \pi^+$	7.24±0.76	3.1 ±1.3	25.6 ±2.6	198.3±8.5	a 0.5775	−0.1362	− 1.297	0.869
					b	1.7853	0.9993	
					c		6.689	
$\pi^- \to \pi^-$	0.79±0.14	0.26±0.22	3.10±0.42	23.0±1.4	a 1.904	−0.7784	− 4.065	2.46
					b	5.028	3.936	
					c		17.81	
$\pi^- \to \pi^0$	1.91±0.53	−0.33±0.60	5.1 ±1.6	45.3±3.2	a 0.2834	−0.0417	− 0.7274	0.78
					b	0.3600	0.1529	
					c		2.408	

their best values by x_i, then

$$M = M_0 + \sum_{ij} x_i x_j G_{ij}.$$

G is a real, symmetric matrix with positive eigenvalues. The errors in the experimentally determined differential and total cross sections are assumed to be independent and normally distributed. This neglects the correlations introduced by such common factors as N, the number of hydrogen atoms per unit area, and also assigns a normal distribution to the systematic errors. With these assumptions, the probability for having obtained the experimental results when any set of x_i are chosen for the parameters is proportional to $e^{-M/2}$. The accuracy with which the parameters have been determined can then be expressed by the error matrix, G^{-1}, with the property

$$(G^{-1})_{ij} = \langle x_i x_j \rangle = \frac{\int dx_1 \cdots dx_n e^{-M/2} x_i x_j}{\int dx_1 \cdots dx_n e^{-M/2}}.$$

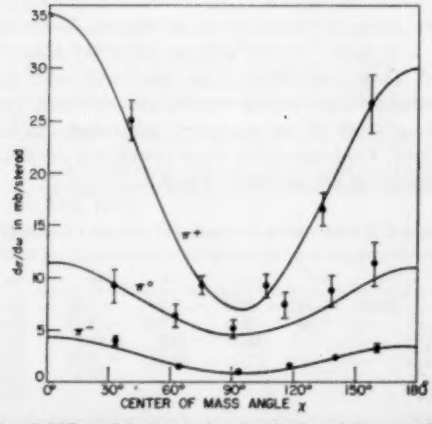

FIG. 6. Differential cross sections for elastic and charge-exchange scattering of 189-Mev pions by hydrogen. The curves correspond to the phase-shift solution 1.

The square root of the diagonal elements of G^{-1} gives the standard deviations for each of the parameters. The off-diagonal elements are the product of the correlation coefficients with the two corresponding standard deviations.

The results of the least squares fit of the form $a+b\cos\chi+c\cos^2\chi$ appear in Table XI, together with the integrated differential cross section, $\sigma_T = 4\pi(a+c/3)$. The errors stated on a, b, and c are the roots of the diagonal elements of G^{-1}. The errors on σ_T include the effects of the negative correlation between a and c.

A phase-shift analysis of the data was carried out in the manner described in the earlier work from this laboratory.[5,6] The cross sections were expressed in terms of six phase shifts, assuming conservation of isotopic spin and limiting the analysis to S and P waves. The AVIDAC at the Argonne National Laboratory was used to seek the phase shifts giving the best fit to the transmission as well as angular distribution measurements.

Figure 7 shows the initial values of the phase shifts obtained from the Ashkin diagrams together with the final values obtained by the AVIDAC.

The twelve initial sets of phase shifts converged to four distinct types. The first and third were of the Fermi type ($\alpha_{33} > \alpha_{31}$), with the α_3 of the first greater

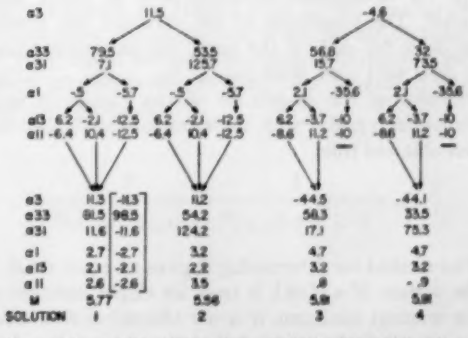

FIG. 7. Phase-shift solutions from Ashkin's diagram together with final values obtained with the AVIDAC.

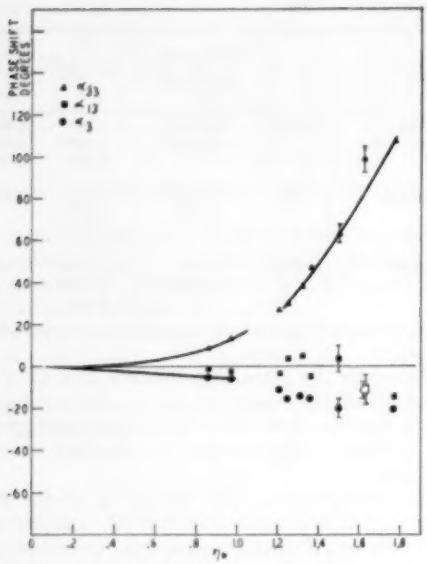

FIG. 8. Dependence of the phase shifts, α_{33}, α_{13}, and α_{31} on η_b, the center of mass pion momentum in units of μc.

than that for the third. The second and fourth are the corresponding Yang types. The significance of these results is discussed in the next section.

To determine the accuracy with which the phase shifts were determined, G^{-1} was evaluated using the AVIDAC. Since the region in which $M=M_0+1$ is the most significant in the integrals involving $e^{-M/2}$, G^{-1} was determined by fitting an ellipsoid to the surface $M=M_0+1$ in the phase angle space. All the angles were varied individually and in pairs until a value of $M=M_0+1$ was reached. With the notation $S_{i+}(S_{i-})$ equal to the increase (decrease) in α_i necessary to change M by one, G_{ii} was evaluated from

$$G_{ii}=4/(S_{i+}+S_{i-})^2.$$

For the off-diagonal elements, pairs of angles were varied. The magnitude of the variation was always the same for each of the pairs, but all combinations of signs were used. With $S_{i+,\,j+}$, $S_{i+,\,j-}$, $S_{i-,\,j+}$, $S_{i-,\,j-}$ representing the magnitude of the change in each the angles i and j with the signs indicated, then G_{ij} was obtained from

$$G_{ij}=\frac{1}{(S_{i+,\,j+}+S_{i-,\,j-})^2}-\frac{1}{(S_{i+,\,j-}+S_{i-,\,j+})^2}.$$

This method for determining G gives an exact result if the surface $M=M_0+1$ is truly an ellipse centered at the nominal minimum. G is not affected to first order by a small displacement of the ellipse in any direction. The elements of the error matrix, G^{-1}, in (degrees)^2 for the solution 1, are listed in Table XII. From this, the standard deviations on the phase shifts are:

$$\alpha_1=-2.8^\circ\pm4.5^\circ,\ \alpha_3=-11.3^\circ\pm3.2^\circ,\ \alpha_{11}=-2.6^\circ\pm7.5^\circ,$$
$$\alpha_{13}=-2.1^\circ\pm3.8^\circ,\ \alpha_{31}=-11.6^\circ\pm5.1^\circ,\ \alpha_{33}=\ 98.8^\circ\pm3.6^\circ.$$

In this determination of the errors in the phase shifts, all the experimental data have been used including the total cross sections from the transmission measurements. These errors are, however, only approximate, since the errors assigned to the cross sections are not independent and normally distributed, nor does M depend quadratically on the phase shifts.

The presence of D waves may introduce further uncertainties in the S and P phase shifts obtained above.[15] To test the possible effects of D wave phase shifts, Ashkin diagrams were drawn treating the D wave phase shift as a perturbation on the least squares values of $a+$, $b+$, and $c+$. With no D wave the solution was $\alpha_3=-13$, $\alpha_{33}=95^\circ$, and $\alpha_{31}=-13^\circ$; with the $T=\frac{3}{2}$ and $J=5/2$ D wave phase shift $\alpha_{35}=-5^\circ$, the solution was only slightly different with $\alpha_3=-12$, $\alpha_{33}=96.5^\circ$ and $\alpha_{31}=-12^\circ$. The present data were not sufficiently accurate to warrant an explicit solution including D waves. Previous estimates by Henley and Ruderman[16] would yield -2.8°, Orear's estimate[15] would yield -6.8° for α_{35}. However, the rapid fall of the total π^+ cross section above 200 Mev makes a sizeable D wave contribution seem unlikely.

DISCUSSION

Four sets of phase shifts have been found which fit the scattering data at 189 Mev. The data are fitted equally well if in any given set the signs of all the phase shifts are reversed. Moreover, it is always permissible to add 180° to any phase shift without altering the scattering amplitudes. Our solution 1 with signs reversed and 180° added to α_{33} corresponds quite closely to the choice preferred by de Hoffmann, Metropolis, Alei, and Bethe in their analysis of earlier scattering data.[2] Thus, our result is in agreement with their preferred solution, except that the present result would have α_{33} cross 90° at an energy somewhat less than 189 Mev. The phase shifts which correspond to solution 1 (resonance) are plotted in Fig. 8.

TABLE XII. Error matrix for phase shift solution 1 (degrees)^2.

	α_1	α_3	α_{11}	α_{13}	α_{31}	α_{33}
α_1	20.3	−6.84	− 7.01	− 5.15	7.32	− 2.16
α_3		9.93	2.18	0.791	− 3.92	− 0.957
α_{11}			56.7	−13.9	−14.3	1.59
α_{13}				14.6	− 2.74	1.33
α_{31}					25.7	− 8.66
α_{33}						13.2

[15] J. Orear, Phys. Rev. **98**, 1155(A) (1955).
[16] E. M. Henley and M. Ruderman, Phys. Rev. **90**, 719 (1953).

Recently Chew[17] has proposed a theory which gives a particularly simple behavior for α_{33}. In his model

$$\frac{k^3}{\omega_q^*}\cot\alpha_{33}=\frac{1}{\lambda_a}\left(1-\frac{\omega_q^*}{\omega_{res}}\right)$$

where k is the momentum of the meson, ω_q^* is the total energy minus the proton rest mass, and λ_a is related to the coupling constant. The results of the scattering experiments are plotted according to this scheme in Fig. 9. It is seen that the agreement is remarkably good. A similar dependence is predicted for the other P wave phase shifts, except that the plot for these must have a slope opposite to that given for α_{33}. The experimental data are not inconsistent with this in view of the small values of α_{31}, α_{13}, and α_{11} in the preferred solution. However, the value $\alpha_{31}=236°$ from solution 2 with signs reversed would be hard to reconcile with Chew's theory.

The choice of solution 1 with signs reversed is also in agreement with requirements from causality. Karplus and Ruderman[18] and also Goldberger, Oehme, and Miyazawa[18] have derived dispersion relations based on the condition that signals cannot propagate faster than the speed of light. Through these, the real part of the forward scattering amplitude can be calculated from the knowledge of the total scattering cross sections for negative as well as positive pions by protons. These data now extend up to 1.9 Bev[19,20] and so permit a reliable evaluation of the dispersion integrals to be made. It is a striking result of this calculation that for the isotopic spin $\frac{3}{2}$ state the real part of the forward scattering amplitude changes sign abruptly between 165 Mev and 189 Mev. In terms of the phase shifts up to P waves the real part of the forward scattering amplitude is given by

$$R(f_3)=(k_L/2k_b^2)(\sin2\alpha_3+2\sin2\alpha_{33}+\sin2\alpha_{31}),$$

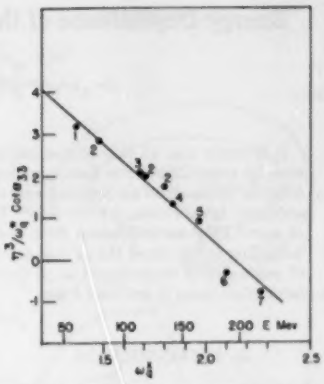

FIG. 9. Plot of $k^3/\omega_q^*\cot\alpha_{33}$ against ω_q^* for comparison to theory of G. Chew: R is the center of mass momentum of the pion, and ω_q^* is the center of mass energy minus the proton rest mass. 1. B. S. S., Columbia, reference 12; 2. A. F. M. and N., Chicago, reference 6; 3 Chicago, [J. Orear, Phys. Rev. **96**, 1417 (1954)]. 4. Washington University, J. J. Lord and A. B. Weaver (private communication). 5. A. and G., Chicago, reference 5; 6. A. D. G. and K., Chicago (present data); 7.Chicago, [M. Glicksman, Phys. Rev. **94**, 1335 (1954)].

where k_b and k_L are the wave numbers of the pions in the center of mass and laboratory systems, respectively.

The dispersion relations gave $R(f_3)$ positive and in good agreement with the experimentally determined phase shifts below 180 Mev. Above 180 Mev, $R(f_3)$ becomes abruptly negative in agreement with the phase shifts listed in Fig. 7 provided the phase shifts are taken with signs reversed. This makes solution 1 with signs reversed the solution of choice. Solutions 3 and 4 now have $\alpha_3=+44°$ and seem most unlikely in view of $\alpha_3=-20°$ or less at 165 Mev.[6] In solution 2, α_{33} goes over to 126° and α_{31} goes over to 236° implying rather large changes in two of the phase shifts. This seems unlikely on grounds of simplicity. Further details and other implications of these dispersion relations for the pion scattering will be published shortly.

ACKNOWLEDGMENTS

It is a pleasure to acknowledge the contributions of Joseph Fainberg and Tadao Fujii to the running of the equipment. We are grateful to Dr. Donald Flanders and Jean Hall of the Argonne National Laboratory for making available the AVIDAC for computing the phase-shift solutions.

[17] G. F. Chew, Fifth Annual Rochester Conference, 1955 (Interscience Publishers, Inc., New York, 1955).

[18] R. Karplus and M. Ruderman, Proceedings of Fifth Annual Rochester Conference, 1955 (Interscience Publishers, Inc., New York, 1955); Goldberger, Oehme, and Miyazawa, Phys. Rev. **99**, 986 (1955).

[19] Ashkin, Blaser, Feiner, Gorman, and Stern, Phys. Rev. **96**, 1104 (1954).

[20] S. J. Lindenbaum and L. C. Yuan; Cool, Clarke, and Piccioni, Fifth Annual Rochester Conference, 1955 (Interscience Publishers, Inc., New York, 1955).

Energy Dependence of the Phase Shifts in Pion-Proton Scattering*

JAY OREAR
Columbia University, New York, New York
(Received June 27, 1955)

It is shown that all pion-proton scattering data up to 300 Mev can be fit within limits of experimental error by using the s-waves linearly extrapolated from the low-energy slopes of $\alpha_1=0.16\eta$ and $\alpha_3=-0.11\eta$. All other phase shifts are assumed zero except α_{33} which is given the energy dependence proposed by Chew and Low, $(\eta^3/\omega^*)\cot\alpha_{33}=8.05-3.8\omega^*$. The two constants in the α_{33} energy dependence fit the initial slope of $\alpha_{33}=0.235\eta^3$ as determined from low-energy experiments and make α_{33} go through 90° at 192 Mev. According to the cutoff theory this determines a $k_{max}\approx 6\mu c/\hbar$, corresponding to a pion-nucleon interaction of much shorter range than $\hbar/\mu c$. A theoretical implication of the fit proposed here is that also the s-wave interaction range is less than $\hbar/\mu c$

A. INTRODUCTION

IN the last year pion-proton scattering angular distributions have been obtained at higher energies and with increased accuracy. New results most pertinent to this paper are the 165 Mev,[1] 189 Mev[2], and 217 Mev[3] Chicago experiments and the Brookhaven 300 Mev π^+ cloud chamber results.[4]

In each case the individual experimenter has solved his data for the best fit s- and p-wave phase shifts. Figure 1 is a plot of recent best fit values of α_1, α_3, and α_{33} as a function of η, the center-of-mass momentum in units of μc.

The curve for α_{33} is the revised energy dependence proposed by Chew and Low[5] of

$$(\eta^3/\omega^*)\cot\alpha_{33}=8.05-3.8\omega^*. \quad (1)$$

ω^* is the total energy minus the proton rest energy.

The constants used here are those which fit the low-energy slope,[6] $\alpha_{33}=0.235\eta^3$, and the value $\alpha_{33}=90°$ at 192 Mev. According to Chew and Low this fit determines the two parameters in the cut-off theory of $f^2=0.08$ and $k_{max}=6(\mu c/\hbar)$. It is seen that the best fit values of α_{33} fit this two parameter curve within the experimental errors.

The energy dependence of the two s-waves is not as clear. De Hoffmann *et al.*[7] have proposed a smoothing-out as shown by the dotted lines in Fig. 1. Glicksman has made good fits to the Chicago data by setting $\alpha_{31}=\alpha_{13}=\alpha_{11}=0$ and using values for α_1 and α_3 close to those of the dotted lines.[8] Here again α_1, α_3, and α_{33} are treated as independent variables until a best fit is obtained. He and others have observed that in the energy region above 130 Mev α_1 and α_3 may be changed with considerable freedom while still maintaining a good fit to the data.

The question arises whether there is enough freedom for α_1 and α_3 to permit their linear extrapolation from the low-energy best fit slopes of $\alpha_1=0.16\eta$ and $\alpha_3=-0.11\eta$.[6] It will be shown in the following section that the linear extrapolations do indeed give a reasonable fit to the data when used with the values of α_{33} given by Eq. (1), and all other phase shifts set equal to zero. Such an energy dependence for the s-waves is what would be expected of a simple short-range potential and should at least be given a try. It also has the advantage of being consistent with the interaction range indicated by the cutoff theory in its rather successful application to the calculation of the p-wave interaction.[6]

B. DISCUSSION

1. Reasons for Choice of Linear s-Waves

Perhaps the best justification for this linear extrapolation is curiosity and simplicity. In addition there is some theoretical basis for expecting a short-range interaction. The cutoff theory as applied by Chew and Low gives a value $k_{max}\sim 6(\mu c/\hbar)$ which corresponds to a pion-nucleon interaction range not much greater than $1/k_{max}$. Another indication of a short-range interaction is the effective range of $\sim\frac{1}{2}\hbar/\mu c$ obtained by Brueckner from the energy dependence of α_{33}.[8] An experimental indication of the extent of the proton virtual meson cloud is given by the Stanford high-energy electron scattering results on hydrogen which imply an rms radius of $\sim\frac{1}{2}\hbar/\mu c$.[9] Even if the virtual meson cloud were of greater extent, the main interaction of the external pion might be with the core. Of course there is the possibility that the s-wave interaction range be different from that of the p-wave. However, the γ_5-theory would suggest a shorter range for the s-wave interaction than for the p-wave.

Ranges even as large as $\hbar/\mu c$ would rule out the

*This research was supported in part by the joint program of the Office of Naval Research and the U. S. Atomic Energy Commission.

[1] H. L. Anderson and M. Glicksman, this issue [Phys. Rev. **100**, 268 (1955)].
[2] Anderson, Davidon, Glicksman, and Kruse, this issue [Phys. Rev. **100**, 279 (1955)].
[3] M. Glicksman, Phys. Rev. **94**, 1335 (1954).
[4] R. Margulies, Phys. Rev. **99**, 673(A) (1955).
[5] G. F. Chew and F. E. Low, Proceeding of the Fifth Rochester Conference on High-Energy Nuclear Physics (Interscience Publishers, Inc., New York, 1955).
[6] J. Orear, Phys. Rev. **96**, 176 (1954).
[7] de Hoffmann, Metropolis, Alei, and Bethe, Phys. Rev. **95**, 1586 (1954).
[8] K. Brueckner, Phys. Rev. **87**, 1026 (1952).
[9] R. Hofstadter and R. W. McAllister, Phys. Rev. **98**, 217 (1955).

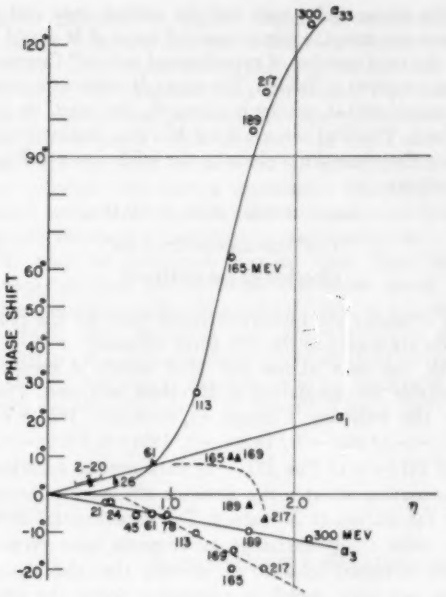

FIG. 1. Phase shifts as a function of pion momentum. The α_{33} curve is the "straight line" energy dependence proposed by Chew and Low.[8] The α_1 and α_3 solid lines are extrapolations of $\alpha_1=0.16\eta$ and $\alpha_3=-0.11\eta$. The dashed lines are proposals of de Hoffmann *et al.*[7] Triangles are best fit values of α_1 (circles for α_3) obtained by experimenters at the indicated energies.

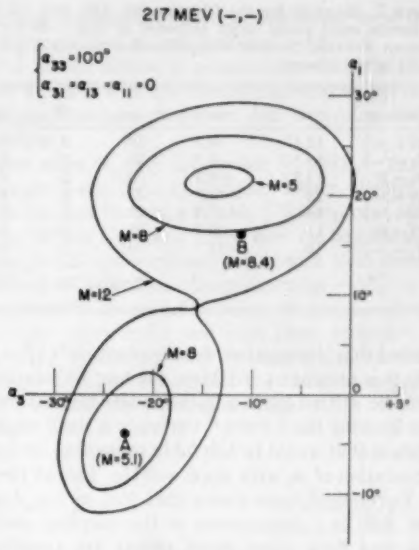

FIG. 2. M-values for 217-Mev π^- elastic scattering as a function of α_1 and α_3. α_{33} is held constant at 100°. All other phase shifts are zero. Point A is the minimum found by Glicksman in his three phase shift solution.[9] Point B is from the linear extrapolation of $\alpha_1=0.16\eta$ and $\alpha_3=-0.11\eta$ and lies near a second minimum. Contours of $M=5$, 8, and 12 are shown.

behavior of α_1 where it rather suddenly changes sign at about 180 Mev. This can be seen from the causality condition that a scattered wave cannot reach an observer before the original wave.[10] This condition requires for individual phase shifts that

$$d\alpha/dk > -r_0,$$

where r_0 is the interaction range. The Chicago values of $\alpha_1=10°$ at 165 Mev and $-2.7°$ at 189 Mev make $d\alpha/dk=-1.85\hbar/\mu c$. If α_1 truly behaved this way the s-wave interaction would have to remain strong for a distance greater than $1.85\hbar/\mu c$.

We rely mainly on this argument to discard the α_1 energy dependence proposed by de Hoffmann *et al.*[7] Furthermore, it will be shown in the next section that there are two equally good Fermi-type solutions to the 217-Mev data: the solution given by Glicksman where α_1 is negative, and a solution where $\alpha_1\sim+20°$ and $\alpha_3\sim-10°$ (see Fig. 2).

Choosing an energy dependence for α_3 is a more difficult problem. De Hoffmann *et al.*[7] and Dyson *et al.*[11] have proposed a slope $\alpha_3=-0.3\eta$ for the region above 100 Mev as shown by the dashed line in Fig. 1. In order not to violate low-energy data it is necessary for α_3 to start off with a slope not nearly so steep. One way of overcoming this difficulty is to propose a short-range repulsive potential with a longer-range attractive part.[12] Then one would expect to observe a change in slope in α_3 between zero and 80 Mev. However the recent low-energy results at (2.5–20) Mev π^-,[13] 21 Mev π^+,[14] 24 Mev π^+,[15] and the pi-mesonic atom K-level shifts[16] give no indication of requiring a change in slope. They confirm the earlier choice of $\alpha_1=0.16\eta$ and $\alpha_3=-0.11\eta$ with greater accuracy.

The main evidence for the steeper slope of $\alpha_3=-0.3\eta$ consists of some of the pion-proton scattering experiments above 120 Mev. In the half-dozen or so experiments which have been performed between 120 and 165 Mev, all of them give best fit values for α_3 below $-10°$. However the most recent α_3 best-fit values at 189 Mev[2] and 300 Mev[4] fall rather close to the curve $\alpha_3=-0.11\eta$. Perhaps a choice of a linear α_3 with a somewhat steeper slope might give a slightly better fit, although with the existing data it is seen that the choice made here does quite well.

One possible effect to explain low α_3 best-fit values would be the presence of some d-wave. It has been

[10] E. Wigner, Phys. Rev. **98**, 145 (1955).
[11] Dyson, Ross, Salpeter, Schweber, Sundaresan, Visscher, and Bethe, Phys. Rev. **95**, 1644 (1954).
[12] R. Marshak, Phys. Rev. **88**, 1208 (1954).
[13] Rinehart, Rogers, and Lederman, Phys. Rev. **99**, 673(A) (1955).
[14] S. Whetstone and D. Stork, Phys. Rev. **99**, 673(A) (1955).
[15] J. Orear, Phys. Rev. **98**, 239(A) (1955).
[16] Sterns, Stearns, De Benedetti, and Leipuner, Phys. Rev. **97**, 240 (1955).

TABLE I. M-values for the Chicago 165, 189, and 217-Mev experiments using phase shifts proposed in Fig. 1 or Eq. (2). The mean M-value (number of experimental points) is given in the next to last column.

Experiment	α_1	α_3	α_{33}	$\bar{M}$	M
165(+,+)	13.5°	−9.3°	70°	5	3.0
165(−,−)	13.5	−9.3	70	5	4.7
165(−,0)	13.5	−9.3	70	5	0.3
189(+,+)	15	−10.3	89	5	4.1
189(−,−)	15	−10.3	89	6	7.4
189(−,0)	15	−10.3	89	6	3.8
217(−,−)	16	−11	101	6	8.4
			Total	38	31.7

observed that if a negative d-wave phase shift ($T=3/2$, $J=5/2$) is present at 165 Mev, the best fit solution of α_3 will be shifted more negative when the analysis is made ignoring the d-wave.[17] Certainly a small negative D_{35} phase shift would be helpful in promoting the linear extrapolation of α_3 with slope -0.11η. Indeed Henley and Ruderman[18] have shown that just such a d-wave phase shift is a consequence of the coupling used by Chew and Low when recoil effects are considered. Their calculations give $D_{35}=-2.1°$ at 165 Mev and $-7°$ at 300 Mev.[18] Their other d-wave phase shifts are smaller and such as to give no effect in the π^- elastic scattering. Their values should be reduced about a factor two if the revised coupling constant of Chew and Low is used.

The other p-waves α_{31}, α_{13}, and α_{11} have been set equal to zero in all the attempts to fit the data. Experimentally the best-fit values for these phase shifts are always small with larger errors. Also no trend for any of them in either magnitude or sign has shown up.

Chew has calculated values for these 3 p-wave phase shifts using the same coupling which gives his α_{33} results. He finds that they must all be small. He believes α_{13} and α_{31} are equal, but is not sure of their sign or magnitude. He believes α_{11} should be small and negative but is not sure of its magnitude.[19]

2. Comparison with Experiment

If the proposed phase shifts are to make sense, they should not give a large M-value or least squares deviation from any pion-proton scattering experiment which has been performed.

$$M=\sum_{i=1}^{N}\left[\frac{y_i-\bar{y}_i(\alpha_1,\alpha_3,\alpha_{33})}{\Delta y_i}\right]^2.$$

y_i = experimental cross section at angle x_i.
$\bar{y}_i(\alpha_1,\alpha_3,\alpha_{33})$ = cross section calculated from Eq. (2).
Δy_i = standard deviation given by experimenter for his determination of y_i.

[17] J. Orear, Phys. Rev. **98**, 1155(A) (1955).
[18] E. M. Henley and M. A. Ruderman, Phys. Rev. **90**, 719 (1953).
[19] G. Chew (private communication).

If the phase shifts used are the correct ones and all others are zero, the mean expected value of M would be N, the total number of experimental points.[20] Comparisons are given in Table I. The mean M value or number of experimental points is given in the next to last column. The final column is the M value obtained when using the phase shifts given by the solid curves in Fig. 1 which are

$$\tan\alpha_1=0.16\eta,\quad \tan\alpha_3=-0.11\eta,$$
$$(\eta^3/\omega^*)\cot\alpha_{33}=8.05-3.8\omega^*, \qquad (2)$$
$$\text{all other phase shifts}=0.$$

For reference the numerical values used for the phase shifts are shown in the first three columns.

All the data above 140 Mev which is presently available for calculation of M values was used. These are the following Chicago experiments: 165(++),[1] 165(−−),[1] 165(−0),[1] 189(++),[2] 189(−0),[2] 189(−−),[2] and 217(−−).[3] The 217(−0) data require additional information about γ-ray detector efficiency *vs* energy for calculation of M values. The experimental errors for these charge-exchange experiments have recently been increased by such an amount that this data is now not very useful in narrowing down the phase shifts.

It is seen from Table I that all the M-values are statistically reasonable. This is most surprising for the 217-Mev data. Here the best-fit phase shifts depart appreciably from the s-wave lines in Fig. 1. The explanation is the existence of a Fermi-type solution other than that used by Glicksman. The s-waves proposed here happen to fall into the region of this equally good solution as can be seen from Fig. 2. Figure 2 is a plot of M-values obtained from the 217(−−) data as a function of α_1 and α_3. α_{33} is held constant at 100°. Glicksman's three-phase shift solution is at point A. The fit to the 217(−0) data should not be much different from that obtained by Glicksman since the quantity $(\alpha_1-\alpha_3)$ is not very different in the two cases.

Other experiments not listed in Table I tend to fit the proposed phase shifts in the sense that the proposed phase shifts are usually within the errors of the experimental phase shifts whenever such errors are given.

C. CONCLUSIONS

One concludes that the energy dependence of phase shifts proposed in Eq. (2) consistently fits all present pion-nucleon experimental knowledge almost as well as any other possible proposal for pion-nucleon phase

[20] In this case where there are no free parameters, the least squares theory does not require that the cross sections be linear in the phase shifts over the region involved. All we are doing here is comparing experiment with a 'known' curve. In the cases where 3 or 6 phase shifts are adjusted to minimize M, the mean M value should be considerably less than the number of experimental points.

shifts. However a higher degree of experimental accuracy is needed in order to conclude whether these are the correct phase shifts. The proposal here has the advantage of simplicity and agreement with meson theory calculations. Up to 300 Mev it is not necessary to use d-wave phase shifts although the small d-waves predicted by recoil corrections to the cutoff theory are welcome. The energy dependence proposed here would arise from a pion-nucleon interaction whose interaction range is on the order of $\frac{1}{2}\hbar/\mu c$ or less.

It may be significant that at least three other approaches lead to this same conclusion about the meson nucleon range. First, that Chew and Low in analysing pion scattering and photoproduction data are led to a $k_{\max}\sim 6\mu c/\hbar$. Second, that an effective-range analysis of the energy dependence of α_{33} by Brueckner gives an effective range of $\frac{1}{2}\hbar/\mu c$.[8] Third, that the Stanford high-energy electron scattering experiments on hydrogen give an rms radius of $\sim\frac{1}{2}\hbar/\mu c$.[9]

The author wishes to acknowledge the help of Mrs. Enid Bierman with the calculations and is indebted to Professor Herbert Anderson for supplying detailed preprints.

Note added in proof (*September 18, 1955*).—The final Carnegie Tech data of Ashkin, Blaser, Feiner, and Stern has just become available ["Pion-proton scattering at 150 and 170 Mev," Phys. Rev. (to be published)]. They give 57 experimental points with total errors for each point (including charge-exchange)$\sim$5% or less. Their best-fit phase shifts ($\alpha_3=-8°$ and $\alpha_1=+10°$ at 170 Mev) agree quite well with those proposed here. Electronic computers can show whether this data is accurate enough to establish the linear extrapolation of α_1 and α_3 as the preferred solution.

PHYSICAL REVIEW VOLUME 100, NUMBER 1 OCTOBER 1, 1955

Range-Energy Relation and Masses of the New Particles*†

DAVID O. CALDWELL
Department of Physics and Laboratory for Nuclear Science, Massachusetts Institute of Technology, Cambridge, Massachusetts

(Received June 17, 1955)

The accuracy to which the masses of most of the new unstable particles can be determined is now limited principally by the uncertainty in the range-energy relations at large velocities. The extent of this uncertainty is indicated, and the available data are re-examined to try to find the best relations to use. In particular, shell corrections are applied to the Sachs-Richardson data, and the mean excitation potentials for 9 elements are determined. The evidence for Al, Cu, and emulsion indicates that the mean excitation potentials are not velocity dependent, and that they may be considerably larger than the values commonly used.

I. INTRODUCTION

MASS values for the new unstable particles generally depend upon a measurement of the range of either the particle itself or its secondaries. These determinations are now of sufficient accuracy so that it is necessary to be quite concerned about the uncertainty in the relations available for converting a measured range into energy or momentum. For instance, the range-energy curve for copper most commonly used for such mass determinations is not based on any direct experimental results.

The experimental data which do exist are correlated by using them to determine, for a given element, the mean excitation potential, I, which appears in the familiar energy-loss equation[1]:

$$-\frac{dE}{dx}=\frac{4\pi e^4 z^2 N}{mc^2\beta^2}\left\{Z\left[\ln\frac{2mc^2\beta^2}{I(1-\beta^2)}-\beta^2\right]-\sum_i C_i\right\}, \quad (1)$$

where ez is the charge of the incident particle, and β its velocity relative to that of light, c; m is the electronic mass; N is the number of stopping atoms of atomic number Z per unit volume; and C_i is the correction for nonparticipating electrons of the ith shell.

II. POSSIBLE VARIATION OF I WITH ENERGY

Since I is determined by measurements of energy and either energy loss or range, which depend only logarithmically on I, it is not too surprising that there has been considerable disagreement in the values for I found in different experiments. However, as was first pointed out by Sachs and Richardson,[2] if one plots the experimental I values for a given element against the logarithm of the energy, instead of scattering badly, the points are seen to lie on a steeply sloping straight line. While an I value which is determined by an energy-loss measurement should be plotted against the incident energy, one which is determined by a range measurement should be plotted at some lower, "effective" energy, if I is not constant. In the latter case, the effective energy, ϵ, should be[2] about 0.6 of the incident

* This work was supported in part by the joint program of the Office of Naval Research and the U. S. Atomic Energy Commission.

† A shortened version of some of this work has appeared in Nuovo cimento **2**, 183 (1955).

[1] M. S. Livingston and H. A. Bethe, Revs. Modern Phys. **9**, 264 (1937).

[2] D. C. Sachs and J. R. Richardson, Phys. Rev. **89**, 1163 (1953).

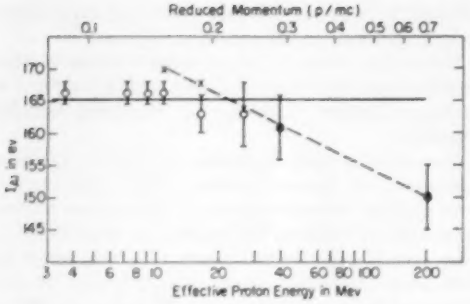

FIG. 1. Experimental values for the mean excitation potential of aluminum as a function of the "effective" proton energy. Old or uncorrected values are indicated by x's and the data available at present, by circles.

energy if $I=a-b\log\epsilon$. This plot of Al I values from reference 2 has been reproduced in Fig. 1, where the measurements available then are shown as x's and are connected by a dashed line.

The work of Lindhard and Scharff[3] gave additional support to the idea that I may be velocity dependent. They plotted stopping number per electron vs $\log(\beta\hbar c)^2/(e^4Z)$, and found that data taken for different elements and at different energies lay on a smooth, nonlinear curve. This curve is the heavy one shown in Fig. 2, and the data on which it is based are indicated by triangles. Lindhard and Scharff were able to reproduce the general form of this curve by a calculation of stopping power based on a Fermi-Thomas model of the atom.

There is a direct correspondence[3,4] between the shape of the Lindhard-Scharff curve and the energy dependence of I for Al over the energy region shown in Fig. 1. According to the Lindhard-Scharff plot, I should have a maximum value at intermediate energies, then drop with energy about as in Fig. 1, but finally level off at higher energies. This variation with energy can be seen qualitatively by following along the curve of Fig. 2, and noting that the change in I is perpendicular to the dashed line.

A variation of I with energy would indicate a fundamental defect in the stopping theory. Also, from the point of view of the experimentalist, this variation leaves the choice of I and hence of the range-energy relation, very uncertain for high velocities. Seemingly one can choose the high value found at low energy, the low value found at high energy, or one can assume I varies logarithmically with energy, or in the manner indicated by the Lindhard-Scharff plot. As an example, this uncertainty is roughly $\pm 15\%$ in the I value for Cu at $p/mc\sim 1$, and of course gets much worse at higher velocities. Therefore it is desirable to re-examine the available data to try to determine the best range-energy relation to use at present.

[3] J. Lindhard and M. Scharff, Kgl. Danske Videnskab. Selskab, Mat.-fys. Medd. **27**, No. 15 (1953).
[4] S. K. Allison and S. D. Warshaw, Revs. Modern Phys. **25**, 779 (1953).

III. RE-EXAMINATION OF THE I-VALUE DATA

A. Sachs-Richardson Data

Since I is most readily and unambiguously determined from an absolute energy-loss experiment, let us consider first the only measurement of this type available in the energy region under consideration, that of Sachs and Richardson,[5,6] using 18-Mev protons. Their results, which have been amended[6] for the difference between the mean and most probable energy loss, can now be corrected for the fact that bound electrons cannot participate fully in the stopping. This correction is designated as $\sum C_i$ in Eq. (1). Due to the work of Walske, corrections for the K shell[7] and for the L shell[8] are now available. For the usually less important higher shell corrections, one can employ the form of the L-shell result,[8] which is a function of η_L and θ_L, by using for the ith shell, $\theta_i=n_i^2I_i/[(Z-\sigma_i)^2\mathrm{Ry}]$ and $\eta_i=mc^2\beta^2/[2(Z-\sigma_i)^2\mathrm{Ry}]$, where the ionization potentials, I_i, have been taken from Hill *et al.*[9]; n_i is the principal quantum number; Ry, the Rydberg constant; and σ_i, the screening constants as given by Slater.[10] The corrected I values, computed according to Eq. (1) above, are given in Table I.

B. Other Measurements for Metals

The I values (at 44 and 66 Mev for Al, and at 64 and 100 Mev for Cu) obtained from the range measurements of Bloembergen and Van Heerden[11] have been changed slightly by employing an energy-dependent multiple scattering correction, and in the case of Al, where the C_k used was known, also by introducing better shell

TABLE I. Mean excitation potentials corrected for shell effects.

Element	Uncorrected stopping power per electron	Mean excitation potential (ev)	Standard deviation (ev)	I/Z
Al	5.365	163.1[a]	3	12.6
Ni	4.538	363	19	13.0
Cu	4.486	377.5	8	13.0
Rh	3.870	656	45	14.6
Ag	3.894	659	50	14.0
Cd	3.903	654	41	13.6
Sn	3.827	708	59	14.2
Ta	3.525	962	54	13.2
Au	3.356	1136	100	14.4

[a] Obtained using an L-shell correction found by Bichsel to fit his experimental results; if instead C_L is determined from an extrapolation of Walske's calculations, I is about 0.5 ev lower.

[5] D. C. Sachs and J. R. Richardson, Phys. Rev. **83**, 834 (1951).
[6] D. O. Caldwell and J. R. Richardson, Phys. Rev. **94**, 79 (1954).
[7] M. C. Walske, Phys. Rev. **88**, 1283 (1952).
[8] M. C. Walske (to be published), and private communications.
[9] Hill, Church, and Mihelich, Rev. Sci. Instr. **23**, 523 (1952).
[10] J. C. Slater, Phys. Rev. **36**, 57 (1930).
[11] N. Bloembergen and P. J. Van Heerden, Phys. Rev. **83**, 561 (1951).

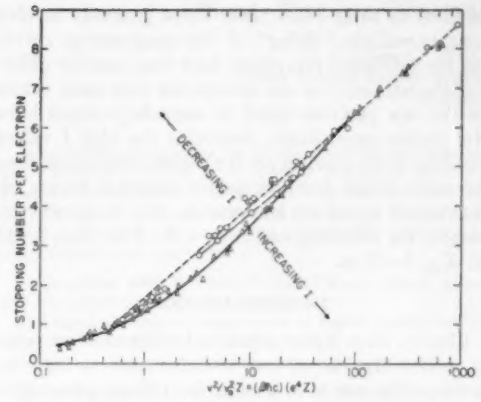

FIG. 2. Experimental stopping power per electron as a function of $(\beta\hbar c)^2/(e^4Z)$. The old data (indicated by triangles) and the solid curve have been taken from reference 3, while the new data (circles) have been taken mainly from plots in references 4 and 18.

corrections. In addition, some excellent range measurements have been made recently by Bichsel and Mozley[12] for 6-, 12-, 15-, and 18-Mev protons in Al and 10- and 18-Mev protons in Cu.

The data available now for Al and Cu appear as circles in Figs. 1 and 3, plotted as a function of the "effective"[12] energy. It is apparent that, except for the 340-Mev range measurements of Mather and Segrè,[13] there is good agreement among the data and no longer any need for assuming that I is energy dependent.

Furthermore, if one adds new or previously unused stopping power measurements[11,14–19] (the circles in Fig. 2), the shape of the Lindhard-Scharff plot is entirely changed. The two sets of circles connected by straight lines represent absolute stopping power data,[17,19] while the other circles are for stopping powers relative to Al. For each set of relative data the Al point has been placed arbitrarily on the dashed straight line representing the Bloch equation,[20] $I \propto Z$. While the ordinate for the relative points from any one experiment can be multiplied by a constant, this does not alter the conclusion that these additional data are represented better by a line of the same *slope* as the dashed line shown than they are by the original (solid) curve. A straight line of this slope represents I values which are independent of velocity and proportional to Z. Actually, since shell corrections are not made for this plot, one should not expect the data to lie strictly on such a line.

The one disturbing feature remaining is that the only absolute high-energy range measurement[13] does not agree with the lower energy data. In order to obtain agreement, Mather's measurement of the angle of Čerenkov radiation would have to be altered by about 25 minutes, which is much in excess of the stated error. Although there is no reason to expect any discrepancy, it is interesting to note that the theoretical Čerenkov relation apparently has otherwise never been checked experimentally to better than $1-2°$.[21]

C. $K_{\mu 2}$ Mass Measurements

Some evidence favoring a larger I value for Cu than that found by Mather and Segrè,[13] and at even higher velocities ($p/mc \gtrsim 1$), is provided by the measurements of the mass of the $K_{\mu 2}$ meson made with magnet and multiplate cloud chambers by the Ecole Polytechnique group. By determining the momentum and range in Cu of the primary $K_{\mu 2}$, and by using a range-energy curve[22] computed for $I_{Cu}=333.5$ ev, they[23] found a mass of 921 ± 16 m.[24] A second mass determination was made by measuring the range in Cu of the μ-meson secondary. An average of the secondary ranges obtained at E.P. and M.I.T. (which are in excellent agreement) gives a mass of 942 ± 8 m,[25] when using the same range-energy curve. Since these two mass measurements are affected oppositely by changing I_{Cu}, it is possible to bring them into agreement. If one assumes only that I_{Cu} is constant from $p/mc \sim 1$ to 2.2, one can solve for that value of I

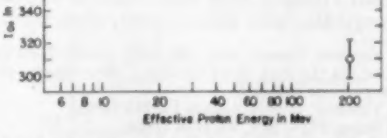

FIG. 3. Experimental values for the mean excitation potential of copper as a function of the "effective" proton energy (0.6 of the incident energy for range measurements, or the incident energy for energy-loss determinations).

[12] H. Bichsel and R. F. Mozley, Phys. Rev. **94**, 764(A) (1954), and private communications. Note that their I values and errors as used here are still preliminary, but it is not expected that their results will change significantly.
[13] R. Mather and E. Segrè, Phys. Rev. **84**, 191 (1951).
[14] E. L. Kelly, Phys. Rev. **75**, 1006 (1949).
[15] J. G. Teasdale, Office of Naval Research Technical Report No. 3, University of California at Los Angeles, 1949 (unpublished).
[16] T. Thompson, University of California Radiation Laboratory Report UCRL-1910, University of California, 1952 (unpublished).
[17] Chilton, Cooper, and Harris, Phys. Rev. **93**, 413 (1954).
[18] C. P. Sonett and K. R. MacKenzie, Phys. Rev. **98**, 280(A) (1955), and private communications. The author is grateful for being allowed to use these results prior to publication.
[19] J. E. Brolley, Jr., and F. L. Ribe, Phys. Rev. **98**, 1112 (1955). The author wishes to thank Dr. Brolley for making this information available before publication.
[20] F. Bloch, Ann. Physik **16**, 285 (1933).
[21] H. O. Wycoff and J. E. Henderson, Phys. Rev. **64**, 1 (1943).
[22] Aron, Hoffman, and Williams, Atomic Energy Commission Report AECU-663, 1949 (unpublished).
[23] Armenteros, Gregory, Hendel, Lagarrigue, Leprince-Ringuet, Muller, and Peyrou, Nuovo cimento **1**, 915 (1955).
[24] This value is obtained for those K's which have secondaries of range greater than those of a τ, and which do not have an associated electron cascade.
[25] Armenteros, Gregory, Hendel, Lagarrigue, Leprince-Ringuet, Muller, Peyrou, Bridge, DeStaebler, Rossi, and Sreekantan, Nuovo cimento (to be published).

which makes equal the mass values determined by the two methods. One gets $I_{Cu}=383\pm43$ ev, which gives a unique mass of 933 m. This I value is in excellent agreement with the low-energy measurements, but nearly two standard deviations from the value determined in reference 13 at a somewhat lower p/mc. Of course, if there were some large systematic error in the magnetic field, this conclusion could be invalidated.

D. Emulsion Data

Additional evidence that I is not velocity dependent is furnished by the work of Vigneron,[26,27] who fitted essentially all the emulsion range data from 1 to 40 Mev, using a constant I value. In his earlier work,[26] Vigneron took the emulsion composition as given by the manufacturer and adjusted I to get the best fit to the data. The value he found, ~396 ev, is in good agreement with that which one obtains for the same composition by using I values similar to those given in Table I (i.e., assuming $I\sim13Z$ for the medium and heavy elements). In order to lower I to correspond to values then available, he assumed in his later work[27] that the emulsion composition was in error by 3% (the maximum amount he thought possible), giving a fit to the data with $I=332$ ev. Even this lower I value is not consistent with the determinations of reference 13.

The range-energy relation at high velocities for emulsion is much more in doubt than is that for Al or Cu. Not only do uncertainties in the composition and density (particularly as affected by humidity) of the emulsion cause additional difficulties, but also the only high-energy emulsion range or energy-loss measurements[28,29] have been made relative to Cu. The energy values associated with these measurements are based on the Mather-Segrè[13] I value for Cu of 310 ev. If instead we take the value of 377.5 ev from Table I, then Heinz's range measurement[28] would be for 335.9 Mev (instead of 342.5) and that of deCarvalho and Friedman[29] would be for 203.9 Mev (instead of 208).

Various attempts have been made to reconcile the low-energy data with Heinz's point, when the latter is assumed to be at 342.5 Mev. These generally involve some unrealistic "tilting" of the range-energy curve, and since different procedures have been used by different laboratories, it is not unexpected that mass values for the new particles based on secondary ranges have been rather inconsistent. Indeed, if the high I values found for lower energies are the correct ones to use, then the mass values from secondary emulsion ranges, as determined at various laboratories, may be in error by roughly the following amounts: τ, 2–8 m; $K_{\tau 2}$, 5–12 m; $K_{\mu 2}$, 5–25 m.

IV. CONCLUSIONS

Clearly, there is great need for further absolute range or, preferably, energy-loss measurements at high velocities. The use of μ mesons for this purpose seems attractive, first, because the nuclear collision loss for these particles would be small. Secondly, since for a given velocity a μ meson has a much lower momentum than a proton, it would be more practicable to determine the momentum in a magnetic field.

Concerning the information available at present, the results in Al, Cu, and emulsion all seem to indicate that each I is constant (and of much higher value than that commonly used) over more than a decade in energy. If the empirical I were suddenly to start dropping off above, say, $p/mc\sim0.5$, this would indicate something radically wrong with the energy loss theory. There is some evidence against this unlikely occurrence furnished by the measurements of the $K_{\mu 2}$ mass.[30] It therefore seems safest at the present time to take I as determined by the low-energy data, and use range-energy relations based on that result. The masses of some of the K particles computed on this basis have been presented elsewhere.[25]

V. ACKNOWLEDGMENTS

The author wishes to thank Professor Bruno Rossi and Dr. Bernard Gregory for many helpful discussions, and Dr. Herbert Bridge for constant aid and encouragement. He is also grateful to Dr. M. C. Walske and Dr. Hans Bichsel for not only providing their results prior to publication, but also for supplying much advice.

[26] L. Vigneron, Compt. rend. **232**, 1199 (1951). Note that this treatment fits the data down to only 5 Mev because shell corrections were not included.

[27] L. Vigneron, J. phys. radium **14**, 145 (1953).

[28] O. Heinz, Phys. Rev. **94**, 1728 (1954).

[29] H. G. deCarvalho and J. I. Friedman, Rev. Sci. Instr. **26**, 261 (1955).

[30] *Note added in proof.*—Stronger evidence is furnished by the measurements of energy loss of 15.7-Mev electrons reported by Goldwasser, Mills, and Robillard in Phys. Rev. **98**, 1763 (1955). At very high velocity ($p/mc=32$), they find $I/Z\sim14$ for Z of 8–10, which is consistent with the values given in Table I.

Cloud-Chamber Observations on Charged *V* Particles*

W. H. Arnold, J. Ballam, and George T. Reynolds
Palmer Physical Laboratory, Princeton University, Princeton, New Jersey

(Received June 20, 1955)

In an experiment utilizing the double cloud-chamber technique at an altitude of 10 600 ft, 46 charged *V* particles have been observed. Where possible these have been classified according to the value, p^*, of the momentum of the charged decay particle in the rest system of the primary particle. On this basis decaying particles have been classed as:

1. Consistent with two-body decay of known heavy mesons and not consistent with known hyperons.
2. Consistent with two-body decay of heavy mesons but also consistent with two-body decay of hyperons.
3. Not consistent with two-body decay of heavy mesons.

In the first group it is generally not possible to distinguish between the possibilities $\theta \to \pi+\pi^0$, on the one hand and $K_{\mu 2} \to \mu+\nu$ on the other. However, several cases suggest strongly the θ particle and yield an average mass $953\pm 18 m_e$. Several other special decay events are reported. After classification by p^*, lifetime measurements are made on groups consistent with two-body heavy meson decay. The nine positive events in this class give a lifetime $3.7\times10^{-10}<\tau<8.5\times10^{-10}$ sec with 50% confidence limits, and 7% probability that $\tau>5\times10^{-9}$ sec. The six negative events in this class give a lifetime $3.0\times10^{-10}<\tau<8.0\times10^{-10}$ sec with 50% confidence limits and 11% probability that $\tau>5\times10^{-9}$ sec. Effects of possible biases are discussed and it is concluded that these lifetimes characterize the charged θ meson. No unambiguous examples of the $K_{\mu 3}$ or K_{e3} heavy mesons were observed.

I. APPARATUS AND METHOD

THE results to be described were obtained by means of a double cloud-chamber arrangement located at the Echo Lake Laboratories of the Inter-University High Altitude Laboratories situated in Colorado at an altitude of 10 600 ft.

Double cloud chambers have been used first by the Paris group[1] in the analysis of heavy unstable particles. In this arrangement, a cloud chamber in a magnetic field is placed above another cloud chamber containing plates of dense material. The upper chamber is referred to as the momentum chamber, the lower as the plate chamber. The momentum chamber in the present disposition has been described previously,[2] being approximately 16 in.×16 in.×6 in. illuminated volume, in a magnetic field averaging 5500 gauss. The plate chamber is approximately 20 in.×20 in.×7 in. illuminated volume. This chamber has contained seven lead plates, 0.5 in. thick (through run 176); and seven copper plates of the same thickness (runs 177 through 241). More recently 11 tungsten plates each 0.6 in. thick have been installed. The results reported here are mainly from the momentum chamber data.

The chambers are triggered simultaneously by means of a penetrating shower detector consisting of lead and geiger counters above the top chamber, proportional counters between the chambers, and proportional counters and lead below the chambers. The general disposition is shown in Fig. 1. The counting rate of the detector is $\frac{1}{4}$20 per hour. The recycling time of the chambers is three minutes.

The quantities that can be measured are indicated in Fig. 2. P is the momentum of a primary track, p the momentum of a secondary track, θ the laboratory angle between the direction of the primary and secondary. The range R of a particle is measured in the plate chamber. Measurement techniques for P, p and θ have been described previously.[2] The errors in the measured momenta are made up essentially of three parts: measurement errors, including errors in reconstruction, curve plotting and magnetic field measurement; mul-

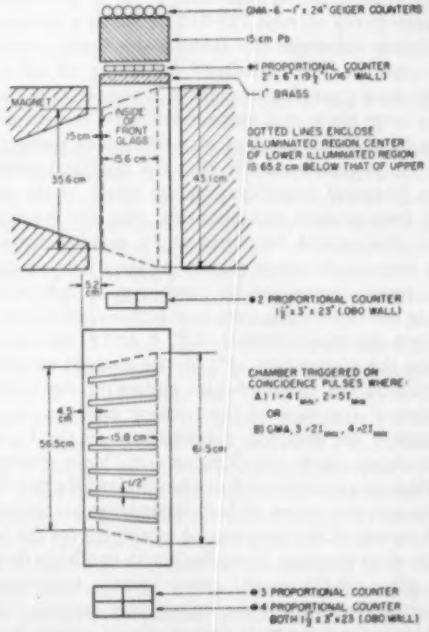
GMA-6 — 1" x 24" GEIGER COUNTERS
15 cm Pb
#1 PROPORTIONAL COUNTER
2" x 6" x 19½" (1/16" WALL)
1" BRASS
MAGNET
INSIDE OF FRONT GLASS
15 cm
15.6 cm
35.6 cm
43.1 cm
DOTTED LINES ENCLOSE ILLUMINATED REGION CENTER OF LOWER ILLUMINATED REGION IS 65.2 cm BELOW THAT OF UPPER
5.2 cm
#2 PROPORTIONAL COUNTER
1½" x 3" x 23" (.080 WALL)
CHAMBER TRIGGERED ON COINCIDENCE PULSES WHERE:
A) I > 4I min., 2 > 5I min.
OR
B) GMA, 3 > 2I min., 4 > 2I min.
4.5 cm
56.5cm
15.8 cm
61.9cm
1/2"
#3 PROPORTIONAL COUNTER
#4 PROPORTIONAL COUNTER
BOTH 1½" x 3" x 23" (.080 WALL)

FIG. 1. Experimental arrangement for dual cloud chambers. This is presented as a typical arrangement. However, the counter disposition and depth of illumination has been varied during the course of the experiment.

* Supported by the Office of Naval Research and the U. S. Atomic Energy Commission.

[1] Gregory, Lagarrigue, Leprince-Ringuet, Muller, and Peyrou, Nuovo cimento **11**, 292 (1954).

[2] Hodson, Ballam, Arnold, Harris, Rau, Reynolds, and Treiman, Phys. Rev. **96**, 1089 (1954).

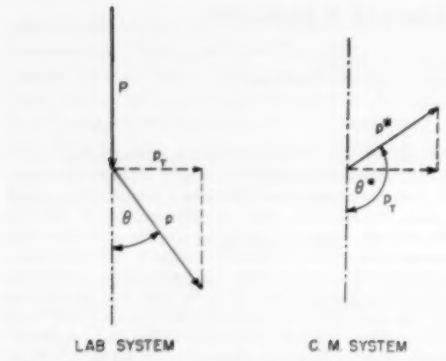

FIG. 2. Representation of a charged V decay in the laboratory and center-of-mass systems. In the laboratory system P and p are the momenta of the primary and secondary particles respectively and θ is the angle of emission of the secondary with respect to the primary. In the c.m. system p^* is the momentum of the secondary and θ^* is the angle of emission of the secondary with respect to the direction of motion of the center of mass. Pt is the transverse component of the momentum of the charged secondary and is the same in both systems.

tiple gas scattering; and random distortion due to gas motion. For all particles except the slow ones the random distortion error predominates. This was estimated by a direct measurement of proton masses by the momentum-range method. For these cases the range error could be neglected. From 17 proton mass measurements on runs 143–176 we found a systematic distortion curvature of -0.020 meter^{-1} and a random curvature of ± 0.012 meter^{-1} for tracks 40 cm long. After these runs, improvements in temperature conditions were made and measurements on 13 protons in runs 183–225 gave values of -0.01 ± 0.01 meter^{-1}. It was found experimentally that the random curvature error increased inversely with the length of the track and, from no-field measurements, that the systematic error disappeared for horizontally moving particles. The momentum errors quoted in this article are probable errors determined by combining as independent errors the three main components described above.

From the measurements of P, p, and θ, one can calculate the momentum (p^*) of the charged secondary particle in the center-of-mass system of the primary particle if the mass of the primary and the charged secondary are assumed. Alternatively on the basis of a two-body decay the Q value (i.e., Mass (primary) $-$ Mass (secondaries) $= Q$) can be obtained if a two-body decay and the nature of both secondaries are assumed.

A survey of the data can be attempted on the basis of the p^* or Q values. If one deals with two-body decays, the p^*'s and Q's should group (within experimental uncertainties) around the appropriate central values. Evidence for three-body decays should appear in distributed values of p^* and Q when these quantities have been calculated on an assumed two-body decay scheme. There is a limit to the usefulness of the p^* method beyond the survey stage unless one resorts to selections that yield statistically significant averages. This limitation is due to the fact that from measurements of P, p, and θ one must assume a primary mass in order to calculate p^*. If then an individual p^* is not consistent with the assumed decay scheme, then there is no quantitative deduction immediately possible from this particular p^*. However, both p^* and Q values are useful in ruling out specific decay schemes as possibilities in particular events.

TABLE I. Decay constants of K mesons and charged hyperons.

Particle	Mass (electron masses)	Decay scheme	Q (Mev)	p^* (Mev/c)
$\tau^\pm$	965.5	$\pi^\pm+\pi^+ +\pi^-$	74.7	<125
		$\pi^\pm+2\pi^0$	84.1	<133
θ^0	966	$\pi^+ +\pi^-$	214	204
$\theta^\pm$	953	$\pi^\pm+\pi^0$	213	202
$K_{\mu 2}$	930	$\mu^+ +\nu$	371	226
κ	~1000	$\mu^\pm+2?$		$\lesssim$250
K_e	~1000	$e^\pm+2?$		$\lesssim$250
$\Sigma^\pm$	2329	$p+\pi^0$	117	196
		$n+\pi^\pm$	111	190
Ξ^-	2583	$\Lambda^0+\pi^-$	66	138

The decay schemes and their resultant p^* and Q values which were used for comparison purposes in this paper are listed in Table I for certain K mesons and hyperons. These are in all cases in close agreement with those presented by Rossi[3] at the Fifth Rochester Conference on Nuclear Physics held in February, 1955. One of the outstanding questions in this field has been that concerning the possibility that the $K_{\mu 2}$, θ^+, and τ^+ might be alternate decay schemes of the same particle. This possibility suggested itself because the measured masses were not clearly different, and has remained because there has been no compelling evidence for differences in lifetimes. The important work of Dalitz[4] has indicated strongly that the θ^+ and τ^+ are not alternate decay modes of the same particle, but there is no similar argument with respect to $K_{\mu 2}$. Evidence has been presented recently[5,6] indicating that the mass of the $K_{\mu 2}$ may be less than that of the τ. The results to be described in the present paper indicate that the lifetime of the θ^+ particle is shorter than that of the $K_{\mu 2}$.

II. EXPERIMENTAL DATA

The methods described above have been applied to a study of 46 charged decays of which 44 could be determined as to sign. One of the positive decays was that

[3] See summary by B. Rossi, Proceedings of the Rochester Conference, February, 1955 (Interscience Publishers, Inc., New York, 1955).
[4] R. H. Dalitz, Proceedings of the Rochester Conference, February, 1955 (Interscience Publishers, Inc., New York, 1955).
[5] Ballam, Hodson, and Reynolds, Phys. Rev. **99**, 1038 (1955); Armenteros, Gregory, Hendel, Lagarrigue, Leprince-Ringuet, Muller, and Peyrou, Nuovo cimento **I**, 915 (1955); Bridge, De-Staebler, Rossi, and Sreekantan, Nuovo cimento, **I**, 874 (1955).
[6] G. T. Reynolds and W. Aron, Phys. Rev. **99**, 1038 (1955).

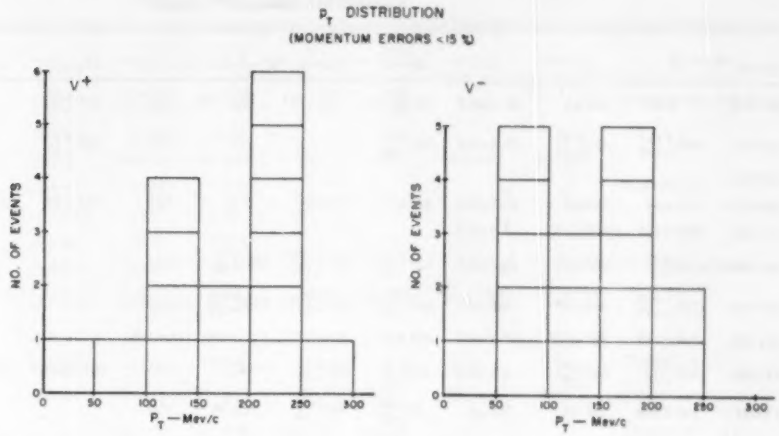

FIG. 3. Transverse momentum distribution of the charged secondary for both V^+ and V^- events.

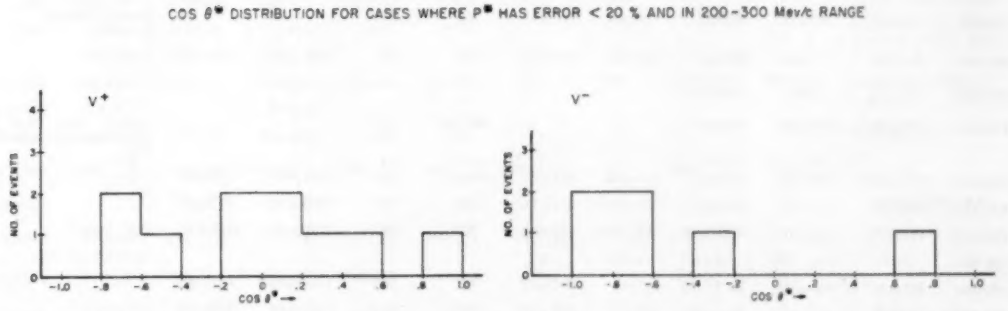

FIG. 4. Distribution of the cosine of the angle of emission of the charged secondary in the c.m. system for both V^+ and V^- events.

of a $\tau^+ \rightarrow \pi^+ + \pi^+ + \pi^-$ and will not be discussed further. Of the remaining 43 events, all of the charged V type, 21 were positive and 22 were negative. These events were obtained in runs during which about 48 000 pictures were taken, including approximately 300 V^0. The measurements on these events are shown in Table II.

Of the 21 positive events, one appears to have mass greater than $1000m_e$ on the basis of a primary momentum of 510±40 Mev/c and ionization 2–5 times minimum. The p^* on the assumption of $\Sigma^+ \rightarrow \pi^+ + n$ is 170±75 Mev/c.

One other event had a p^* consistent with that of a hyperon and not with a K meson. Of the remaining 19 V^+ events, 16 allowed a measurement of the transverse momentum p_T (15 of these have smaller than 15% probable error), 13 have p^* determined to better than 20% probable error.

The distribution of the p_T values is shown in Fig. 3. Figure 4 shows the distribution of $\cos\theta^*$ for these events, where θ^* is the angle of emission of the charged secondary in the c.m. system. The distribution of p_T is consistent with that expected for a two-body decay process, and the $\cos\theta^*$ distribution is consistent with isotropic decay, within the limitations of the statistics due to the number of events. Figure 5 shows the p^* values obtained. Of the 13 p^*'s two could be due to hyperons, in the sense that when they were analyzed as hyperons, the value obtained for p^* was within $1\frac{1}{2}$ probable errors of the accepted value. Thus 11 of the events can be K mesons, but not hyperons. One low p^* value was found, which was consistent with the decay $\tau^+ \rightarrow \pi^+ + \pi^0 + \pi^0$. One high value, 271±20 was found. These two values have been omitted from subsequent analysis. Of the 11 events that could be K mesons and are not consistent with hyperons, two show evidence for π secondaries. One of these, shown in Fig. 6, shows a star in the gas made by the charged secondary particle. Consideration of the laboratory momentum of the secondary, as well as the visible energy in the star indicates that this decay is not that of $\tau^+ \rightarrow \pi^+ + \pi^0 + \pi^0$. Thus it has been analyzed as the decay $\theta^+ \rightarrow \pi^+ + \pi^0$. On this basis the mass obtained is 947_{-44}^{+75}. A second event previously reported[3] yields evidence for a π^0 secondary. On the basis of this θ^+ decay mode, the mass of the primary in this event was found to be 954_{-90}^{+80}. The p^* distribution is seen to be consistent with either θ^+ or $K_{\mu 2}$ decay, or a mixture of the two.

TABLE II(A). Data on V^+ events.[a]

Event	P	p	θ	$p^*_{965\to\pi}$	$p^*_{912\to\mu}$	$Q_{\Sigma^+\to n+\pi^+}$	$Q_{\Sigma^+\to p+\pi^0}$	$M(\pi,\pi^0)$	$M(\mu,\nu)$	Remarks
137–629	(0.8)	153±8	55.7±0.7	201^{+9}_{-6}		NO	NO	954^{+30}_{-20}		$\theta^+\to\pi^++\pi^0$ (See reference 2)
164–818	658^{+125}_{-100}	373^{+95}_{-70}	32.3±0.5	200^{+50}_{-45}		NO	NO	947^{+75}_{-55}		Secondary forms star in gas
176–213										$\tau^+\to\pi^++\pi^-+\pi^+$
136–315	374±64	146±9	86.5±0.5	202±21	198±21	NO	NO	958±50	843±50	
137–834	1065±160	(1000±400)	5.0±0.7							
146–599	$3.8^{+2^\circ}_{-1}$	346±30	24.3±0.5	450^{+235}_{-120}	390^{+200}_{-100}	109^{+95}_{-30}	NO			Possibly $a\Sigma^+\to n+\pi^+$
150–149	1130^{+560}_{-460}	842±95	13.5±1	210^{+85}_{-30}	209^{+85}_{-30}	430^{+225}_{-190}	142±35			Possibly $\Sigma^+\to p+\pi^0$
151–616	794±140	816±125	18.3±0.5	289±50	285±50	511±140	224±100			Possibly $\Sigma^+\to p+\pi^0$
157–566	671^{+85}_{-75}	680^{+80}_{-65}	7.6±0.5	210^{+35}_{-30}	205^{+35}_{-30}	NO	NO	1047±300	787±280	
170–157	600±300	245±9	9.5±1	55^{+60}_{-10}	68^{+60}_{-10}	32±30	NO			V^0 in same picture. Possibly 3-body
178–888	$2^{+1^\circ}_{-0.6}$		20.0±1.5							
179–446	104±12	139±14	63.0±1	126±13	127±13	NO	NO			Possibly 3-body $I=6$–10
180–899	392±30	317±62	50.7±1	245±48	245±48	NO	NO	1100±150	980±140	$I=2.5$–4.5
183–883	$4^{+2.5^\circ}_{-1.5}$	>300	23.8±1							
191–672	515±40	(200±80)	58.0±1			89±65	NO			$1=2$–5 more than 2 probable errors from K mass
192–289	820±300	524±50	23.5±1	211±25	211±25	299±60	NO	993±65	886±60	
195–815	480±55	371±17	36.4±0.5	225±11	225±11	NO	NO	1029±35	917±35	
198–745	437±70	250±15	69.5±0.5	271±20	271±20	NO	NO	1140±50	1049±55	High mass ?
201–564	>4°	916±100	8.5±0.3	>150	>162					Probably not τ'
201–663	481±55	382±20	33.8±0.5	217±13	217±13	NO	NO	1014±50	882±50	
204–042	100±14	220±18	66.1±0.7	205±18	205±18	NO	NO	980±55	850±50	$I=5$–10
214–928	885^{+135}_{-85}	239^{+75}_{-65}	66.8±0.3	373^{+100}_{-85}	367^{+100}_{-85}	175^{+75}_{-65}	NO			Possibly Σ^+; V^0 in same picture

[a] Masses are in electron masses; $M(\pi\pi^0)$ means the mass of K obtained by assuming scheme $K\to\pi+\pi^0$. Momenta are in Mev/c, except for * values which are in Bev/c. Lower limits on P were obtained by using MDM, or setting upper limit of 2 on relative ionization. Lower limits on p^* were obtained by using lower limit on P and one probable error down on p. A NO has been placed in the hyperon columns where the momenta had to be changed more than 1½ probable errors to accord with ionization. Parentheses have been used in the hyperon column either because of a NO or because the calculated Q is more than 1½ probable errors from the accepted value. Where the secondary was heavily ionizing, the remarks column has "L-meson." Ionization is given in multiples of I_{min}.

In a similar way it is not possible to distinguish between the two possibilities on the basis of Q values. The weighted mean of the p^* values on the basis of a θ decay is 208±5 Mev/c. The mean of the basis of a $K_{\mu 2}$ decay omitting the two cases of known π secondaries is 216±8 Mev/c.

Of the 22 negative decay events, one is the cascade type $\Xi^-\to\Lambda^0+\pi^-$, already reported,[7] giving a Q value of 63±9 Mev. Of the remaining 21 negative decay events, 17 have measurements of the transverse momentum to better than 15%. The distribution is shown in Fig. 3, and is seen to be consistent with a three-body distribution. However, the distribution of $\cos\theta^*$ for this particular sample, shown in Fig. 4, indicates an anisotropic distribution in the center of mass.

[7] Arnold, Ballam, Lindeberg, and van Lint, Phys. Rev. **98**, 838 (1955).

As will be discussed below, the p^* values for the negative K's appear to be consistent with a two-body decay process. The consistency of the p_T distribution with a three-body process is due in this case to the anisotropic decay in the center-of-mass system for our particular sample of particles. It is thus apparent that the use of p^* in the investigation of decay schemes offers a distinct advantage over the use of p_T, and that in fact the p_T plots may in particular cases be misleading. In the present analysis, classification of decay events has been on the basis of p^* values.

Of the 21 negative V decays, 10 allow measurement of p^* to within 35%. Of these 10, only two could be known hyperons within 1½ probable errors. Of the remaining eight, only one has a value of p^* below 150 Mev/c. Thus an appreciable component of V^- observed in our apparatus are neither hyperons nor alternate τ decays. It is quite unlikely that all seven p^* values

TABLE II(B). Data on V^- events.

Event	P	p	θ	$\rho^*_{965\to\pi}$	$\rho^*_{912\to\mu}$	$Q_{\Sigma^-\to n+\pi^-}$	$Q_{\Sigma^-\to\Lambda^0+\pi^-}$	$M(\pi,\pi^0)$	$M(\mu,\nu)$	Remarks
122–267	1180^{+420}_{-230}	22±5	62.2±1	312^{+110}_{-60}	245^{+85}_{-45}	128^{+45}_{-20}	115^{+42}_{-25}			L meson sec.; possibly Σ
124–681	>1.2*	480±40	15.3±0.7	>116	>116					
126–637	355±35	110±9	143±1	243±20	243±20	NO	NO	1045±45	941±50	
128–690	>300	51±6	132.4±1	>135	>120					L meson sec.
132–197	>2.5*	585±45	8.2±0.5	>98	>83					
146–745	>300	90±8	84.7±1	>121	>113					
148–972	>2.5*	1250±175	6.6±0.5	>130	>130					V^0 in same picture
151–544	740^{+180}_{-160}	630^{+95}_{-75}	13.7±0.5	201^{+45}_{-40}	211^{+45}_{-40}	279^{+90}_{-75}	356^{+90}_{-75}	942^{+250}_{-200}	767^{+225}_{-190}	
163–068	>1.2*		21.0±1							
164–496	>1.2*	470±75	21.1±0.5	>163	>145					Probably not τ'
168–758	390^{+80}_{-75}	187±9	83.9±1	245±25	241±25	NO	NO	1065±55	986^{+60}_{-55}	$I=2$–4
169–212	1360^{+400}_{-300}	560^{+100}_{-75}	21.3±1	213^{+40}_{-30}	208^{+40}_{-30}	180^{+70}_{-60}	192±70			Possibly Σ^-
170–837	498±75	126±20	29.7±1	69±10	63±10	NO	NO			Sec. L meson; 3-body
173–480	>400	531±75	15.5±0.7	>122	>122					Secondary has deflection with $\rho\tau=18$ Mev/c ($\pi-\mu$)?
173–885	746±65	184±13	60.3±0.7	244±18	231±16	NO	NO	1049±40	936±30	V^0 in same picture
176–200	>2.5*		9.8±0.5							
190–080	>2*	354±16	20.0±0.7	>165	>195					Probably not τ'
195–488	620^{+190}_{-140}	700±50	18.3±1	278^{+100}_{-75}	275^{+100}_{-75}	450±120	NO	1350^{+350}_{-320}	1210^{+330}_{-280}	
198–149		114±6	41.3±0.3				63±9			Σ^-. (See reference 7.)
222–873	1000±160	824^{+240}_{-180}	18.6±0.5	270^{+80}_{-65}	266^{+80}_{-65}	454^{+220}_{-180}	477^{+220}_{-180}	1154^{+320}_{-220}	1158^{+320}_{-220}	
223–284	759±55	78.2±4	60.0±0.5	200±18	166±18	NO 35±4	NO	954±30	790±25	
223–890	>1.4*	637^{+60}_{-45}	17.5±0.5	>180	>180					Probably not τ'

which are neither hyperons nor below 150 Mev/c are due to a three-body decay because of the strongly peaked distribution, although of course some could represent three-body decays. Some could be of the type $\theta^-\to\pi^-+\pi^0$, although no strong evidence exists for this particle. In fact, the average of the p^* values is high, being 231±10 Mev/c.

The uncertainty with regard to the identification of the negative decays is consistent with the observations of some other workers.[8] However, one event is of interest in this regard. Event 223–284 is not consistent with known hyperon decay. It yields a mass $954_{-20}{}^{+30}\ m_e$ when interpreted as a $\theta^-\to\pi^-+\pi^0$ and a mass of $790_{-25}{}^{+25}\ m_e$ when interpreted as a $K_{\mu 2}{}^-\to\mu^-+\nu$. Although the possibility of $K_{\mu 2}{}^-\to\mu+?+?$ cannot be rules out, we have assumed the event as θ^- in analogy with observed θ^+. When this mass is averaged with the two θ^+ events described above, the resulting mass is 953±18 m_e. This may be compared with the value 952±11 m_e obtained by the M.I.T. group[9] by means of range measurements of the charged secondaries.

In comparing the two groups, K^+ and K^-, it can be noted that the average primary momentum of the K^+ events whose p^*'s were determined was 575 Mev/c, and that of the K^-'s whose p^*'s were determined was 750 Mev/c. The total number of K^+ was about equal to the total number of K^-. However, the number of slow K^+ was about twice that of slow K^-. This is also consistent with the experience of other groups.[10] The secondaries of the K^+ events have traversed 225 g/cm² of lead in the lower chamber without observed interactions. (Recall, however, that one K^+ secondary produced a star in the gas of the upper chamber.) No similar information exists for the secondaries of the K^- events, although one such secondary shows a $\pi-\mu$ decay.

III. LIFETIME ANALYSIS

Lifetime measurements were undertaken on the groups of decay events described below. For this purpose it was necessary to establish in advance fiducial planes limiting the volume of observation in the chamber.

[8] B. Gregory (private communication).

[9] H. De Staebler, Jr., and B. V. Sreekantan, Phys. Rev. **98**, 1520 (1955).

[10] Proceedings of the Rochester Conference, 1955 (Interscience Publishers, Inc., New York, 1955).

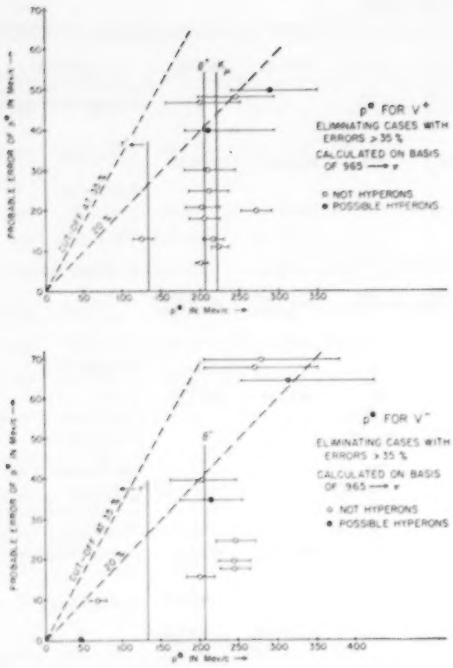
p* FOR V+
ELIMINATING CASES WITH ERRORS > 35 %
CALCULATED ON BASIS OF 965 → ν
○ NOT HYPERONS
● POSSIBLE HYPERONS
p* FOR V−
ELIMINATING CASES WITH ERRORS > 35 %
CALCULATED ON BASIS OF 965 → ν
○ NOT HYPERONS
● POSSIBLE HYPERONS

FIG. 5. Momenta of the charged secondaries in the c.m. system for V^+ and V^- events. These are plotted in order of increasing probable error in the momenta. The cut-off lines determine quickly how many events are eliminated by making the percentage error requirements more stringent.

FIG. 6. Cloud-chamber photograph of a V^+ event in which the secondary creates a star in the argon gas of the chamber. The primary, track 1, decays at point A into the secondary, track 2, which forms a star at point B having a proton, track 3, and an L meson, track 4. There is also a blob due to a heavy recoil. The analysis is given in Table II under event 164–818.

These planes were chosen in such a way that within them there was no dependence of detection efficiency upon the point of decay. The planes chosen in the present experiment are shown in Fig. 7. This figure also includes the projection of each decay on the plane of the front glass. Also for the purpose of lifetime analysis, it is best to deal with homogeneous groups. It is therefore necessary to classify events according to the nature of the decay schemes indicated and thus to be able to make a statement as to the possible identities of the particles. With two exceptions all V^+ events within the planes allowed some measurements of p^* and therefore some statement as to possible identity. In the case of the V^- events, seven decays within the planes did not yield p^* values. Lowering the upper fiducial plane to a distance 12.5 cm above the center plane eliminated five of these. This procedure does not introduce bias, being only analogous to a shift in the zero of time in more conventional lifetime measurements; it allows a better identification of the nature of the sample.

The lifetime planes then contained 20 V^+ and 12 V^-, which were divided into three groups:

Group A: Particles which could not be two-body K decays, but could be $K_{\mu 3}$'s, τ's, or hyperons. These include the cascade event; a particle whose ionization and momentum indicate a mass >965 by more than two probable errors; and low and high p^*'s more than $1\frac{1}{2}$ probable errors from accepted θ^+ and K_μ p^* values. In this group were 7 V^+, 2 V^-.

Group B: Particles which could be two-body decays but which also could be hyperons, due either to the calculated p^*'s, or due to inability to measure p^*. In this group were 4 V^+ and 4 V^-.

Group C: Particles which could be two-body K decays and could not be hyperons or low p^* (i.e., three-body decays). In this group were 9 V^+ and 6 V^-, which are interpreted on the basis of known particles, as a possible mixture of θ and $K_{\mu 2}$.

The events in group A are obviously not a homogeneous group and are disregarded in further analysis.

The lifetime of groups B and C have been calculated using the method of maximum likelihood described by Bartlett.[11] For this purpose actual and potential path lengths X and D are measured and converted into corresponding proper times t and T according to

$$t=(x/v)(1-\beta^2)^{\frac{1}{2}}=x/\eta c, \quad \text{where} \quad \eta=P/M.$$

On the assumption of a single lifetime, τ, for a given group, it is possible to develop a function:

$$S=\frac{\sum_{i=1}^{M}\left[\frac{t_i}{\tau}-1+\frac{T_i}{\tau}\frac{\exp(-T_i/\tau)}{1-\exp(-T_i/\tau)}\right]}{\frac{1}{\tau}\left\{\sum_{i=1}^{M}\left[1-\frac{T_i^2}{\tau^2}\frac{\exp(-T_i/\tau)}{[1-\exp(T_i/\tau)]^2}\right]\right\}^{\frac{1}{2}}}.$$

[11] M. S. Bartlett, Phil. Mag. **44**, 249 (1953).

This function has zero value for the most probable lifetime and unit standard deviation. For a given set of M decay events. S is evaluated for various values of $1/\tau$. If S is then plotted against $1/\tau$ the maximum likelihood value of τ is given by the point at which S is zero, and the value of S at any other value of $1/\tau'$, is the probability, in standard deviations, that τ is farther from the central value than τ'.

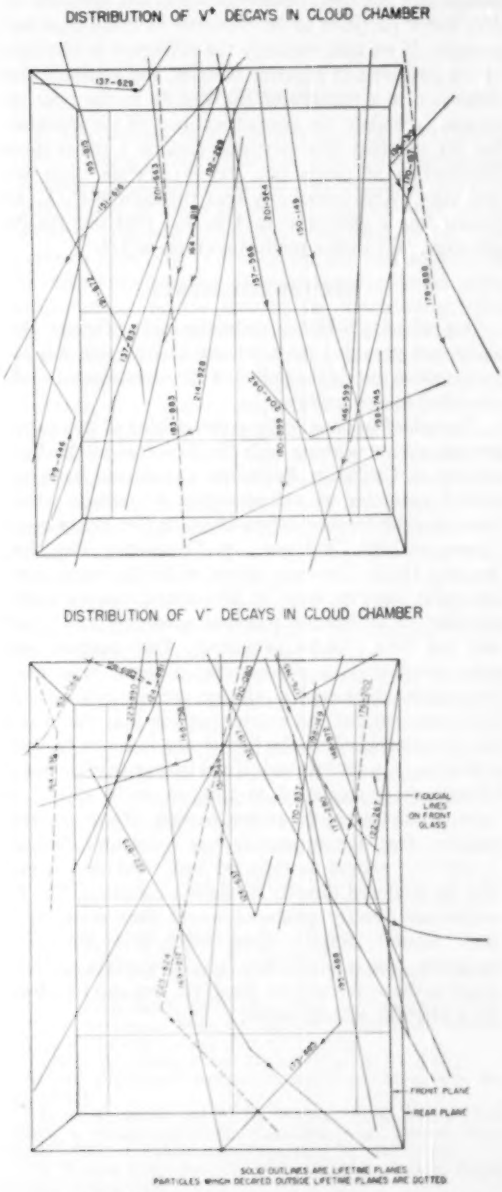
DISTRIBUTION OF V⁺ DECAYS IN CLOUD CHAMBER
DISTRIBUTION OF V⁻ DECAYS IN CLOUD CHAMBER
FIDUCIAL LINES ON FRONT GLASS
FRONT PLANE
REAR PLANE
SOLID OUTLINES ARE LIFETIME PLANES
PARTICLES WHICH DECAYED OUTSIDE LIFETIME PLANES ARE DOTTED

FIG. 7. Fiducial planes used for lifetime measurements.

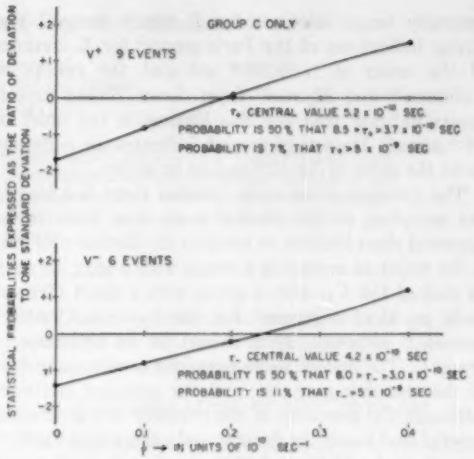
GROUP C ONLY
V⁺ 9 EVENTS
τ₊ CENTRAL VALUE 5.2 x 10⁻¹⁰ SEC.
PROBABILITY IS 50% THAT 8.5 > τ₊ > 3.7 x 10⁻¹⁰ SEC
PROBABILITY IS 7% THAT τ₊ > 5 x 10⁻⁹ SEC
V⁻ 6 EVENTS
τ₋ CENTRAL VALUE 4.2 x 10⁻¹⁰ SEC
PROBABILITY IS 50% THAT 8.0 > τ₋ > 3.0 x 10⁻¹⁰ SEC
PROBABILITY IS 11% THAT τ₋ > 5 x 10⁻⁹ SEC
STATISTICAL PROBABILITIES EXPRESSED AS THE RATIO OF DEVIATION TO ONE STANDARD DEVIATION
1/τ → IN UNITS OF 10⁻¹⁰ SEC⁻¹

FIG. 8. The function S plotted against the reciprocal of the assumed lifetime for group C events. These events are those in which possible hyperons have been excluded.

The results of these measurements are shown in Figs. 8 and 9. From Fig. 8, the indicated lifetime of group C of the positive sample is 5.2×10^{-10} second with 50% probability for the interval $3.7<\tau<8.5\times10^{-10}$ second. The probability that τ is greater than 10^{-9} second is 20% and that τ is greater than 5×10^{-9} second is 7%. For the negative sample, the maximum likelihood value is 4.2×10^{-10} second with 50% probability limits for the interval $3.0<\tau<8.0\times10^{-10}$ second. The probability that τ is greater than 10^{-9} second is 20% and that τ is greater than 5×10^{-9} second is 11%.

These results are to be compared with emulsion[12] and other cloud-chamber work[13–15] that indicates

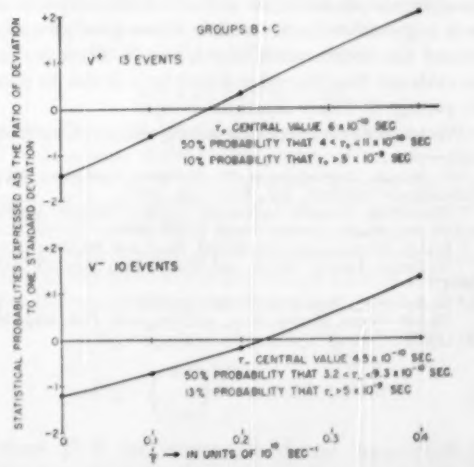
GROUPS B + C
V⁺ 13 EVENTS
τ₊ CENTRAL VALUE 6 x 10⁻¹⁰ SEC
50% PROBABILITY THAT 4 < τ₊ < 11 x 10⁻¹⁰ SEC
10% PROBABILITY THAT τ₊ > 5 x 10⁻⁹ SEC
V⁻ 10 EVENTS
τ₋ CENTRAL VALUE 4.5 x 10⁻¹⁰ SEC.
50% PROBABILITY THAT 3.2 < τ₋ < 9.3 x 10⁻¹⁰ SEC.
13% PROBABILITY THAT τ₋ > 5 x 10⁻⁹ SEC
STATISTICAL PROBABILITIES EXPRESSED AS THE RATIO OF DEVIATION TO ONE STANDARD DEVIATION
1/τ → IN UNITS OF 10⁻¹⁰ SEC⁻¹

FIG. 9. The function S plotted against the reciprocal of the assumed lifetime for group $B+C$ events. These include possible hyperons.

generally longer lifetimes for K meson decays. The strong indications of the Paris group[13] for K lifetimes of the order of $>5\times10^{-9}$ sec and the results of Robinson[16] and Hyams[17] from direct timing experiments indicate that the $K_{\mu 2}$ lifetime is the order of 10^{-8} second. The emulsion work indicates the τ lifetime to be the order of 5×10^{-9} second or longer.

The question arises as to whether there is a bias in the sampling of the present work that leads to an apparent short lifetime, or whether the lifetime obtained is the result of averaging a group with a long life such as that of the $K_{\mu 2}$ with a group with a short lifetime, such as that suggested for the hyperon (5×10^{-11} second),[12] although there should be no hyperons in group C. The first of these questions concerns the bias of the chamber geometry and the selection criterion. Although the geometry of the chamber and generating layer of lead favors the detection of a lifetime of 5×10^{-10} over that of a lifetime of 10^{-8}, this fact in itself would not simulate a short lifetime. The p^* selection criterion should favor longer lifetime, since, if biased at all in application, it tends to select slower, longer living particles. We can investigate the effects of the p^* criterion by mixing the groups referred to above. In the first place, group A is obviously not homogeneous and in fact gives a negative value of $\Sigma_i(T_i/2-t_i)$. The effect of mixing groups B and C is shown in Fig. 9, where essentially the same results as before are obtained. In fact group B alone gives no indication of a shorter lifetime, and this group contains our "possible" hyperons.

The possibility that the lifetime found could result from an average of a group with a short lifetime and a group with a long lifetime can be investigated by calculating a lifetime for each event. Although each event has a very small statistical weight in itself, nevertheless such a procedure in our sample shows good grouping around the median result on a $1/\tau$ scale. There is thus no evidence that the value found for τ is due to such an average of widely separated groups.

We conclude therefore that among charged K mesons, there is a group with a lifetime which has about 90% probability of being shorter than 5×10^{-9} second. In view of the results of our group and other groups mentioned above, which indicate the $K_{\mu 2}$ lifetime to be 10^{-8} second, and in view of the p^* results of the present sample, we conclude that the shorter lifetime is to be attributed to the $\theta^{\pm}$ particle.

It is of course possible that our particular small sample has not been representative of the mixtures of $K_{\mu 2}$ and θ particles to be expected in cloud-chamber samples. If we take seriously the difference in lifetimes of the positive and negative samples, and attribute the difference to a mixture of $K_{\mu 2}$ and θ's in the positive sample; calculate the geometrical bias of the chamber for the different lifetimes; and assume a momentum distribution at production $p\eta d\eta=(K/\eta^2)d\eta$, then we find about 90% probability that the ratio of θ^+/K_μ at production is greater than 1/6, and that our results are consistent with a production ratio of 1/1.

ACKNOWLEDGMENTS

One of us (W.H.A.) gratefully acknowledges the assistance provided by a fellowship from the I.B.M. Corporation during the period of the experimental work described in this paper.

Note added in proof.—Since the writing of this paper several groups working with the Bevatron at the University of California Radiation Laboratory have reported examples of well-identified θ^+ mesons which have lived 10^{-8} second before decaying (see Preliminary Report of Pisa Conference on Elementary Particles, August, 1955). This is a factor of 15–20 longer than the value reported here. In this connection we might consider an interesting proposal made by T. D. Lee and Jay Orear (to be published). They suggest that only two K-mesons of somewhat different mass need be postulated to explain all our present information. They suppose that the heavier particle (e.g. the τ) can decay radiatively into the lighter one (e.g. the θ), with a lifetime of $\sim10^{-8}$ second. If the lighter particle has a lifetime short compared to this, it would *appear* to have the lifetime of the parent particle. We might then imagine that the θ particle has a natural lifetime ($\sim5\times10^{-10}$ second as reported here) and that it can also be produced directly in nuclear collisions. The θ's which are directly produced would then decay with their natural lifetime; those which arise from the radiative τ decay would then have an apparent lifetime equal to the τ. We wish to thank Dr. Lee and Dr. Orear for a preprint of their paper.

[13] G. Menon, Proceedings of the Rochester Conference, 1955 (Interscience Publishers, Inc., New York, 1955).
[14] Armenteros, Gregory, Lagarrigue, Leprince-Ringuet, Muller, and Peyrou, Nuovo cimento, Suppl. 2, 324 (1954).
[15] Bridge, Peyrou, Rossi, and Safford, Phys. Rev. **90**, 921 (1953).
[16] Buchanan, Cooper, Millar, and Newth, Phil. Mag. **45**, 1025 (1954).
[16] K. Robinson, Phys. Rev. **99**, 642(A) (1955).
[17] Barker, Binnie, Hyams, Rout, and Shepherd, Phil. Mag. **46**, 307 (1955).

Pion Production in Proton-Proton Collisions*†

D. B. LICHTENBERG‡
University of Illinois, Urbana, Illinois

(Received June 24, 1955)

The cut-off form of the Yukawa theory is applied to the reaction $p+p\rightarrow\pi^{+}+d$. Using the Low-Wick formulation of field theory, an expression is obtained for the appropriate matrix element in terms of the wave functions of a physical deuteron and diproton. Approximations are made for these wave functions and the matrix element is evaluated. The resulting cross section agrees semiquantitatively with that part of the observed cross section due to pions emitted in a p-state.

I. INTRODUCTION

THE success of the cut-off form of the Yukawa theory[1] in correlating a variety of phenomena involving pions and nucleons has led us to apply it here to the problem of pion production in nucleon-nucleon collisions. Previous treatments[2-7] of this problem have been of two types. The first approach is to make a strictly field theoretical perturbation calculation of the matrix element for the reaction. This approach suffers from the usual difficulties of perturbation theory when applied to meson phenomena. There is an additional difficulty if the final state contains a deuteron, since present perturbation methods are not adequate to treat bound state problems. The second approach tries to avoid these troubles by treating the interaction between the two nucleons by means of a phenomenological potential. There is a practical disadvantage to this method in that the results are very sensitive to the details of the wave functions chosen for the initial and final nucleon systems. Even more important from a fundamental point of view, it has not been adequately shown under what approximations this treatment follows from field theory.

However, two recent developments have put the second approach to the pion production problem on a much sounder footing. The recent work of Low and Wick[8] in reformulating field theory in terms of physical nucleons has enabled us to show that the treatment with nuclear wave functions is indeed consistent with the prescriptions of field theory. And the work of Gartenhaus[9] in obtaining nuclear potentials from the cut-off theory has permitted us to use wave functions in the matrix element which are probably better than wave functions chosen phenomenologically.

II. FORMULATION OF THE PROBLEM

We restrict ourselves to consideration of the reaction

$$p+p\rightarrow\pi^{+}+d, \tag{1}$$

although the methods developed here are more generally valid. The differential cross section is given by the formula (we choose as units $\hbar=c=1$):

$$\frac{d\sigma}{d\Omega}=\frac{1}{(2\pi)^{2}}\frac{M}{2p}q\omega_{q}\sum|T_{qp}|^{2} \tag{2}$$

subject to the condition that energy be conserved. The initial protons each have momentum $\mathbf{p}$ (in the center-of-mass system), and the pion is emitted with momentum $\mathbf{q}$ and energy $\omega_{q}=(q^{2}+\mu^{2})^{\frac{1}{2}}$. The quantity T_{qp} is the appropriate matrix element for the transition, $\sum$ indicates an average and sum over initial and final spin states, and M and μ are respectively the nucleon and pion mass. The recoil of the deuteron is neglected in obtaining Eq. (2).

The problem is to find an adequate estimate for the matrix element T_{qp}. To do this, we first write down an expression for the total Hamiltonian H:

$$H=T_{N}+T_{\pi}+H_{1}'+H_{2}',$$

where T_{N} is the kinetic energy of the two nucleons, $T_{\pi}=\sum_{k}a_{k}^{\dagger}a_{k}\omega_{k}$ is the kinetic energy of the pion field, and $H_{j}'(j=1,2)$ is the interaction between the pion field and the jth nucleon. The quantities a_{k} and $a_{k}^{\dagger}$ are the usual annihilation and creation operators for a pion of type k, where k is a generalized index referring to both the momentum and charge state of the pion. For the cut-off theory, the interaction H_{j}' is given by[1]

$$H_{j}'=\sum_{k}(a_{k}V_{jk}^{0}+a_{k}^{\dagger}V_{jk}^{0\dagger}),$$

$$V_{jk}^{0}=\left(\frac{4\pi}{2\omega_{k}}\right)^{\frac{1}{2}}\frac{f^{0}}{\mu}v(k)\boldsymbol{\sigma}_{j}\cdot i\mathbf{k}\tau_{jk}e^{i\mathbf{k}\cdot\mathbf{r}_{j}}, \tag{3}$$

where f^{0} is the unrationalized and unrenormalized coupling constant, $v(k)$ is the cutoff, $\boldsymbol{\sigma}_{j}$ and $\boldsymbol{\tau}_{j}$ are the usual spin and isotopic spin operators for the jth nucleon at position $\mathbf{r}_{j}$.

* Based on a dissertation submitted in partial fulfillment of the requirements for the Ph.D. degree at the University of Illinois.
† Work supported in part by the Office of Naval Research.
‡ Now at Indiana University, Bloomington, Indiana.
[1] G. F. Chew, Phys. Rev. **95**, 1669 (1954).
[2] C. Morette and H. W. Peng, Proc. Roy. Irish Acad. **A51**, 217 (1948).
[3] L. L. Foldy and R. E. Marshak, Phys. Rev. **75**, 1493 (1949).
[4] K. A. Brueckner, Phys. Rev. **82**, 599 (1951); K. M. Watson and K. A. Brueckner, Phys. Rev. **83**, 1 (1951).
[5] Yoshio Yamaguchi, Progr. Theoret. Phys. **6**, 772 (1951).
[6] Chew, Goldberger, Steinberger, and Yang, Phys. Rev. **84**, 581 (1951).
[7] K. A. Brueckner and K. M. Watson, Phys. Rev. **86**, 923 (1952); S. Matsuyama and H. Miyazawa, Progr. Theoret. Phys. **9**, 492 (1953); A. Aitken *et al.*, Phys. Rev. **93**, 1349 (1954).
[8] F. E. Low, Phys. Rev. **97**, 1392 (1955); G. C. Wick (letter to G. F. Chew, 1954).
[9] Solomon Gartenhaus (to be published).

Following the formalism of Low and Wick, we let $\Psi_q^{D(+)}$ be an eigenfunction of the *total* Hamiltonian H with eigenvalue E_q. This function represents a physical deuteron interacting with its cloud of virtual mesons, and satisfying the boundary condition of a pion at infinity with momentum q, plus outgoing spherical waves. The eigenvalue equation satisfied by this function is

$$H\Psi_q^{D(+)}=E_q\Psi_q^{D(+)}=(E_0+\omega_q)\Psi_q^{D(+)}, \quad (4)$$

where E_0 is the energy of the deuteron when the pion is far away, and ω_q is the pion energy. We now introduce another eigenfunction Ψ_0^D of the total Hamiltonian which satisfies the equation

$$H\Psi_0^D=E_0\Psi_0^D. \quad (5)$$

This eigenfunction Ψ_0^D is the lowest state of the system, and represents the ground state of the deuteron interacting with a virtual meson cloud, but with no real pions in the field. We can produce a real pion of type q by acting on this state with the creation operator $a_q^\dagger$. The function $a_q^\dagger\Psi_0^D$ is not an eigenfunction of H, but we can write

$$\Psi_q^{D(+)}=a_q^\dagger\Psi_0^D+\Psi_s, \quad (6)$$

where Ψ_s is defined by Eq. (6) plus the outgoing wave condition.

To find an expression for Ψ_s, we substitute (6) into (4), obtaining

$$Ha_q^\dagger\Psi_0^D+H\Psi_s=(E_0+\omega_q)(a_q^\dagger\Psi_0^D+\Psi_s). \quad (7)$$

Then, noting that

$$Ha_q^\dagger\Psi_0^D=a_q^\dagger H\Psi_0^D+[H,a_q^\dagger]\Psi_0^D,$$

and

$$[H,a_q^\dagger]=a_q^\dagger\omega_q+V_{1q}^0+V_{2q}^0,$$

Eq. (7) becomes

$$(V_{1q}^0+V_{2q}^0)\Psi_0^D+H\Psi_s=(E_0+\omega_q)\Psi_s.$$

This can be written

$$\Psi_s=[1/(E_0+\omega_q-H+i\epsilon)](V_{1q}^0+V_{2q}^0)\Psi_0^D, \quad (8)$$

where the $+i\epsilon$ signifies that we have chosen the outgoing wave solution.

We now expand (8) in a complete set of eigenfunctions $\Psi_n^{(-)}$ of H which satisfy the incoming wave boundary condition:

$$\Psi_s=\sum_n \Psi_n^{(-)}\frac{(\Psi_n^{(-)},\,(V_{1q}^0+V_{2q}^0)\Psi_0^D)}{E_0+\omega_q-E_n+i\epsilon}.$$

From scattering theory, the transition matrix from the state q to the state n is given by

$$T_{nq}=(\Psi_n^{(-)},\,(V_{1q}^0+V_{2q}^0)\Psi_0^D). \quad (9)$$

In particular, if the state n consists of two protons with no real mesons (this diproton state will be denoted by $\Psi_0^{P(-)}$), we have the appropriate transition matrix for reaction (1) except that the initial and final states are reversed.

III. APPROXIMATION FOR THE MATRIX ELEMENT

For reasons of invariance,[10] if Ψ_j^A and Ψ_j^B are two different states of a *single physical* nucleon, then

$$(\Psi_j^B,V_{jq}^0\Psi_j^A)=(u_j^B,V_{jq}u_j^A), \quad (10)$$

where u_j^A and u_j^B are the corresponding states of the bare nucleon. The quantity V_{jq} has the same form as V_{jq}^0 except that the unrenormalized coupling constant f^0 is replaced by the renormalized coupling constant f.

As our first approximation, we make the assumption that Eq. (10) is valid even if the nucleon is bound. This is equivalent to saying that even in a deuteron, mesons which are emitted and absorbed by the same nucleon will contribute only to renormalization. As our second approximation, we make the assumption that the effect of the mesons which are exchanged between the two nucleons can be replaced by an effective potential between them. Gartenhaus[9] has in fact found a way to calculate approximately this effective potential from the cut-off theory.

With these two approximations, the matrix element can be written

$$T_{pq}=(\Psi_0^{P(-)},\,(V_{1q}^0+V_{2q}^0)\Psi_0^D)$$
$$\simeq(\psi_P^{(-)},\,(V_{1q}+V_{2q})\psi_D), \quad (11)$$

where $\psi_P^{(-)}$ and ψ_D are now the bare diproton and deuteron wave functions. These functions can be found by solving the Schroedinger equation using the effective nuclear potential.

It is possible to make a further simplification by considering the problem at an energy just above threshold for pion production. Then we can set $\exp(i\mathbf{q}\cdot\mathbf{r}_j)=1$ in the interaction, and V_{jq} becomes independent of spatial variables. With this restriction, the square of the matrix element, appropriately summed and averaged, reduces to the form previously found by Chew, Goldberger, Steinberger, and Yang[6]:

$$\sum|T_{pq}|^2=(4\pi)^2\frac{f^2}{\mu^2}\frac{v^2(q)}{\omega_q}q^2\{F_0^2+\sqrt{2}\cos(\delta_0-\delta_2)$$
$$\times F_0F_2(3\cos^2\theta-1)+\tfrac{1}{2}F_2^2(3\cos^2\theta+1)\}, \quad (12)$$

where

$$F_0=\int_0^\infty u_0(r)u_D(r)dr, \quad F_2=\int_0^\infty u_2(r)w_D(r)dr,$$

u_D and w_D being the radial parts of the deuteron S and D functions, and u_0 and u_2 being the radial diproton S and D functions. Here δ_0 and δ_2 are the S and D phase shifts for the diproton. The normalization for the deuteron and diproton wave functions is shown in Figs. 1 and 2.

[10] T. D. Lee, Phys. Rev. **95**, 1329 (1954).

Gartenhaus, using his triplet potential, has computed the S and D functions for the deuteron. Using the Gartenhaus singlet potential, we have calculated the S and D diproton wave functions at the pion production threshold energy of 138 Mev in the center-of-mass system. The phase shifts turn out to be small and attractive ($\delta_0=3°$, $\delta_2=9°$).

The diproton and deuteron wave functions are not as accurate as one would hope. The reason is that the Gartenhaus potentials were calculated using the approximation that the kinetic energy of the nucleons is small compared to the pion mass. This condition is clearly not fulfilled for the diproton. The deuteron wave function also is affected, as can be seen by considering this wave function in momentum space representation. Then it is the high momentum components of the deuteron wave function which are the most inaccurate. But it is just these high momentum components which give the greatest contribution to the overlap integrals F_0 and F_2, since the diproton wave function consists chiefly of high momentum parts.

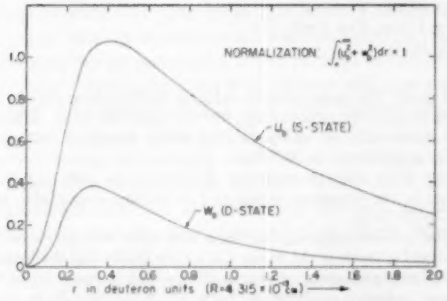

FIG. 1. Deuteron S- and D-state wave functions.

A mitigating circumstance is that the high momentum components of phenomenologically chosen wave functions are likely to be even more uncertain.

IV. RESULTS AND DISCUSSION

The cross section for reaction (1) can be expressed at low energy by the following semiempirical formula of Watson and Brueckner[4,11]:

$$4\pi(d\sigma/d\Omega)=aq+b[(c+\cos^2\theta)/(c+\tfrac{1}{3})]q^3. \qquad (13)$$

The quantities a, b, and c are slowly varying functions of the energy and are usually taken as constant in the energy region under consideration. The term proportional to q is due to pions emitted in an s-state, and the term proportional to q^3 is due to p-wave pions. Crawford and Stevenson[12] compared formula (13) with experiment in the energy range from $q=0.38$ to $q=0.58$ (in units of the pion mass). Their values of the parameters a, b, and c together with our calculated values are given in Table I.

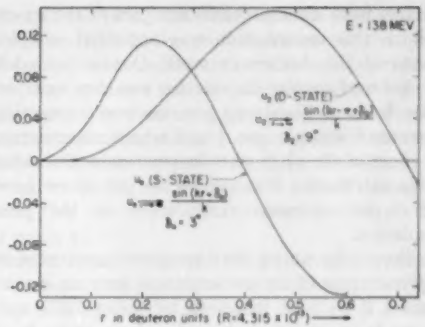

FIG. 2. Diproton S- and D-state wave functions.

The calculated constant $a=0$ because at threshold, the cutoff theory cannot lead to production of pions in the s-state unless nuclear recoil is taken into account. This has not been attempted, since it is not clear how to go about it within the framework of the cutoff theory. However, as has been pointed out by Crawford and Stevenson,[12] a simple theoretical estimate indicates that the ratio of s- to p-state production should be of the order of the ratio of the mass of the pion to the mass of the nucleon. Experiment indicates that this is indeed the case.

The calculated value of the p-wave part of the cross section depends upon the magnitude of the overlap integrals F_0 and F_2. These were found by a numerical integration using the wave functions shown in Fig. 1 and Fig. 2, with the result

$$F_0\simeq 0, \quad F_2=0.08\mu^{-1}.$$

The value zero for the integral F_0 arises from the approximate cancellation of large positive and negative terms. In view of the approximations made in obtaining the wave functions, even the sign of F_0 is uncertain. The quantity F_2 is much more accurate, not only because there is little cancellation from negative terms, but also because the centrifugal barrier prevents the D-state wave functions from being too sensitive to the details of the potential.

Our result that the major part of the p-wave cross section can be accounted for by the contribution from

TABLE I. A comparison of experimental and calculated values of the parameters appearing in the semiempirical formula for the cross section for the reaction $p+p\to\pi^++d$.

Parameter	Crawford and Stevenson	Calculated
a (millibarns)	0.138 ± 0.015	0
b (millibarns)	$1.01\ \pm0.08$	0.6
c	0.082 ± 0.034	$\frac{1}{3}$

[11] This notation, slightly modified, is due to A. H. Rosenfeld, Phys. Rev. **96**, 139 (1954).

[12] F. S. Crawford and M. L. Stevenson, Phys. Rev. **97**, 1304 (1955).

F_2 differs from some previous analyses of the reaction[7] in which this contribution was neglected completely because of the deuteron's small D-state probability. The observed angular distribution was then interpreted on the basis of the strong pion-nucleon interaction in the state of isotopic spin $\frac{3}{2}$ and angular momentum $\frac{3}{2}$. The effect of the $(\frac{3}{2},\frac{3}{2})$ state interaction is not included in this calculation because we do not know how to take it into account consistently in the present formulation.

It should be noted that complete agreement with the p-wave part of the semiempirical formula would be obtained if F_2 were increased by about 20% and F_0 were made positive and about $\frac{1}{4}$ as large as F_2. In view of the approximation made in obtaining formula (12) for the matrix element, this seems as satisfactory a situation as one can expect. Further refinements of this calculation along the lines outlined in this work will depend upon better expressions for the physical deuteron and diproton wave functions.

The author wishes to express his deepest appreciation to Professor Geoffrey F. Chew for suggesting this problem and for his continued aid. This work would not have been possible without his guidance. The author is also grateful to Professor Francis E. Low, Dr. Yoshio Yamaguchi, and especially Dr. Freda Salzman for many stimulating discussions and to Dr. Solomon Gartenhaus for helpful information about the nuclear force problem. He is indebted to Mrs. Marjorie Larson for assistance in the numerical computations.

PHYSICAL REVIEW VOLUME 100, NUMBER 1 OCTOBER 1, 1955

Total Cross Section of Hydrogen for 150- to 750-Mev Positive and Negative Pions*

S. J. LINDENBAUM AND LUKE C. L. YUAN
Brookhaven National Laboratory, Upton, New York
(Received June 10, 1955)

The total cross section of hydrogen for positive and negative pions of 150–750 Mev has been determined.

An early preliminary survey using polyethylene-carbon differences is reported and indicated a resonance in the state of isotopic spin and angular momentum equal to $\frac{3}{2}$ (i.e., $T=J=\frac{3}{2}$).

A more recent precision determination (~3–5%) of the total hydrogen cross section for positive pions in the presumed resonance region (140–340 Mev) has been performed using liquid hydrogen transmission measurements.

A theoretical analysis of the results in conjunction with other available data strongly supports the hypothesis of a resonance.

The behavior of the phase shift of the $T=J=\frac{3}{2}$ state is deduced and given. The most probable solution for the phase shift in this state is found to pass through 90° at ~175–180 Mev, although one cannot rule out the possibility of the resonance (90° phase shift) occurring up to 200 Mev.

The $T=\frac{1}{2}$ state cross section is found to be zero within the errors in the resonance region and to become appreciable only above 300 Mev.

The present experimental data and other relevant work are analyzed in terms of the recent Chew-Low theory and the Brueckner phenomenological resonance theory and is found to fit the general behavior predicted by both, which incidentally is shown to be of similar form.

I. INTRODUCTION

SINCE the original prediction by Yukawa of the meson as the particle responsible for the force field between nucleons, a considerable body of experimental evidence and theoretical speculations thereon relative to the nature of the pion-nucleon interaction have ensued. The early cosmic ray discovery of a meson[1] which is now known to be a moun favored the very weak coupling theories. Later the discovery of the pion[2] gave new impetus to the possibility of strong coupling. However, later experimental work[3] shed considerable doubt on whether the interaction was indeed strong.

The first clear picture of the nature of the pion-nucleon interaction began to emerge as a result of the study of the pion-hydrogen cross sections as a function of energy with the FM cyclotrons at Columbia and Chicago. In particular, the first really definitive work was performed by Anderson, Fermi *et al.*[4] in their measurement of the total hydrogen cross section for positive and negative pions from low energy to 135 and 200 Mev, respectively. The sharp rise of the cross sections with energy from very low values at low energies strongly suggested a gradient coupling with the P-wave predominantly responsible for the interaction.

The first successful quantitative attempt to explain the variation of the total cross sections with energy was proposed by Brueckner.[5] He employed the concept of a nucleon isobar of isotopic spin $T=\frac{3}{2}$ and angular momentum $J=\frac{3}{2}$ as first predicted for the pseudoscalar

* Work performed under the auspices of the U. S. Atomic Energy Commission.

[1] S. H. Neddermeyer and C. D. Anderson, Phys. Rev. **51**, 884 (1937) and J. C. Street and E. C. Stevenson, Phys. Rev. **52**, 1003 (1937).

[2] Lattes, Muirhead, Occhialini, and Powell, Nature **159**, 694 (1947).

[3] W. B. Fretter, Phys. Rev. **76**, 511 (1949).

[4] Anderson, Fermi, Long, Martin, and Nagle, Phys. Rev. **85**, 934 (1952) and Anderson, Fermi, Nagle, and Yodh, Phys. Rev. **86**, 793 (1952).

[5] K. A. Brueckner, Phys. Rev. **86**, 106 (1952).

meson field with strong coupling by Pauli and Dancoff in 1942.[6] Brueckner essentially assigned the resonance level parameters for a resonance in the state with angular momentum and isotopic spin equal to $\frac{3}{2}$ phenomenologically using the methods of Wigner and Eisenbud and imposing charge symmetry to fit approximately the total cross section data. Subsequent more complete total cross section data and extensive negative pion on hydrogen differential data obtained by Anderson and Fermi *et al.*[7] were carefully analyzed by Fermi *et al.*[8] It was concluded that these results could best be explained by a large $T=\frac{3}{2}$ $J=\frac{3}{2}$ phase shift ($\sim 50°$) which did not go through a resonance accompanied by a rather large S-wave phase shift toward the high-energy end. Further support for this type of phase shift behavior was given by an intermediate coupling extended source theory by Chew[9] which was able to fit the then known total cross-section variation with energy reasonably well without going through a resonance.

High-energy meson beams became available for experiments at the Brookhaven Cosmotron in the spring of 1953. At that time the latest Chicago π^--hydrogen total cross sections exhibited a sharp rise with increasing energy and then a broad plateau to 220 Mev, while the π^+-hydrogen cross sections were still increasing sharply with energy to 135 Mev (the highest energy then available at Chicago). It became clear that the general energy dependence of π^+ and π^- hydrogen cross sections from about 150 to 750 Mev would shed considerable light on the nature of the pion nucleon interaction and in particluar whether there was a resonance or not.

In the early stages of Cosmotron operation the beam intensity was low and a liquid hydrogen target was not available so a poor-resolution (± 25 Mev) general survey of the π^+ and π^- hydrogen total cross sections from 150 to 750 Mev was made[10] using rather thick polyethylene and carbon absorbers to obtain the difference. A prominent peak at about 180–200 Mev and a rapid decrease at higher energies was observed.[10] Particularly for positive pions, the decrease after the peak was considerably faster than λ^2. The behavior was very suggestive of a resonance, and as a matter of fact, an extension by the present authors of the Brueckner calculations fit the data crudely. Although the absolute magnitude of the raw peak cross section was below $8\pi\lambda^2$ [11] by approximately 15%, it was then felt that within the errors of the experiment $8\pi\lambda^2$ was probably reached at the peak. The sharp energy dependence of the cross sections in the peak region meant that these poor resolution measurements could not be expected to be very accurate and in particular should give a considerably lower value at the peak point. Furthermore, the muon and electron contamination was quite high ($\sim 30\%$ near the peak) since the Cosmotron was only run at the highest energy of 2.3 Bev[12] during this period. This introduced a contamination uncertainty of as much as 10%.

When a liquid hydrogen target became available, and the beam contamination was reduced to $\sim 10\%$ or less by running the Cosmotron at 0.8 Bev, a precision high resolution measurement of the resonance region (140 to 340 Mev) of the π^+-hydrogen cross section was undertaken. In the π^+-hydrogen cross section only the isotopic spin $\frac{3}{2}$ state (presumed resonance state) can contribute whereas in the π^--hydrogen cross section both isotopic spin $\frac{3}{2}$ and $\frac{1}{2}$ can enter. Therefore, it is of obvious advantage to concentrate on the π^+ cross sections to study the resonance phenomenon. These measurements which will be described and analyzed, clearly seem to indicate the existence of a resonance and give an accurate description of its energy dependence.

Recently, Ashkin *et al.*[13] made a detailed study of the peak region of the π^--p total cross section and also a less complete π^+-p total cross section study. A comparison of these results and ours will be made in Sec. IV D. Same recent π^+-p differential cross section data by Kruse, Anderson, Davidon, and Glicksman,[14] will also be discussed. All of these data are now most consistent with the concept of a resonance.

A detailed phase shift analysis of available data (at that time) by Bethe and his co-workers[15] indicates a resonance solution is most likely.

II. EXPERIMENTAL ARRANGEMENT

A. General Description of Beam Source

The pion beams used for the experiment were obtained from the Brookhaven Cosmotron[16] in the manner shown in Fig. 1. The internal proton beam was allowed to collapse inward onto a beryllium target 2×2×6 in. long which was placed in one of the four straight sections of the Cosmotron. A thin window on the side of the straight section allowed a direct beam at 32° from the forward direction to pass through it, and out of the Cosmotron without passing through any appreciable magnetic field. This direct 32° beam

[6] W. Pauli and S. M. Dancoff, Phys. Rev. **62**, 85 (1942).
[7] Anderson, Fermi, Martin, and Nagle, Phys. Rev. **91**, 155 (1953); Fermi, Glicksman, Martin, and Nagle, Phys. Rev. **92**, 161 (1953).
[8] Fermi, Metropolis, and Alei, Phys. Rev. **95**, 1581 (1954).
[9] G. F. Chew, Phys. Rev. **89**, 591 (1953); **95**, 286 (1954).
[10] S. J. Lindenbaum and Luke C. L. Yuan, Phys. Rev. **92**, 1578 (1953) and **93**, 917 (1954).
[11] $8\pi\lambda^2$ is the predicted theoretical value for the total cross section at the resonant energy, due to a P-wave resonance with $T=J=\frac{3}{2}$.
[12] As will be explained later, the beam contamination for low-energy pion beams increases with the energy of the primary proton beam.
[13] Ashkin, Blaser, Feiner, Gorman, and Stern, Phys. Rev. **96**, 1104 (1954).
[14] Kruse, Anderson, Davidon, and Glicksman, Phys. Rev. **98**, 1188(A) (1955).
[15] de Hoffmann, Metropolis, Alei, and Bethe, Phys. Rev. **95**, 1586 (1954).
[16] M. H. Blewett, Rev. Sci. Instr. **24**, 725 (1953).

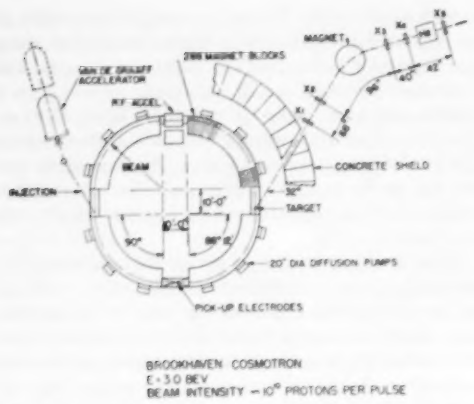

FIG. 1. Experimental arrangement for obtaining pion beams from the Brookhaven Cosmotron.

contained all the reaction products emanating from the target in that direction, and was principally composed of a wide energy range of positive and negative pions, protons, electrons, positrons, neutrons, γ rays, and small amounts of other particles. The beam was allowed to pass through the ten-foot iron oxide-loaded concrete shield of the Cosmotron by imbedding a 3-in. diameter lead collimator in the median plane of the shield.

B. Counter Telescope and Associated Electronics

The charged particle beam was magnetically analyzed by a momentum selective quintuple fast scintillation counter telescope.[17] The experimental arrangement of the telescope is also shown in Fig. 1. The first two counters were placed in line with the 32° beam. Then an 18 in. wide × 36 in. long analyzing magnet was placed behind the second counter. The third, fourth, and fifth counters were placed behind the magnet displaced by an angle of approximately 45°[18] and located along a true magnetic trajectory found by current-carrying wire techniques. Thus by varying the polarity and current through the magnet only charged particles of the desired sign and momentum range were counted by the telescope. High resolution circuitry (2–3×10^{-9} second) rejected protons and other heavy particles so that only pions, muons, and electrons were counted.

The first four counters (X_1, X_2, X_3, and X_4) were similar and each consisted of a diphenyl acetylene crystal of $2\frac{1}{2}$-in. diameter and approximately $\frac{1}{4}$ in. thick. The scintillators were imbedded in a Lucite light pipe which channeled the light to two 1P21 photomultiplier tubes whose outputs were connected in parallel. The light pipes and crystals were surrounded by reflecting aluminum foil which was light sealed by black electrical Scotch tape. Silicone grease was used to couple the light pipe to the glass covering the cathode of the 1P21. Stabilizing condensers were used on the last few dynodes of the photomultipliers. Selected tubes and voltage balancing were employed to achieve a pulse uniformity of the order of 15% or less which is comparable with the statistical fluctuations inherent in the pulse height due to the uncertainty of δ-ray energies. The last counter, X_5, was a large liquid scintillation counter of 6-in. diameter and 1 in. thick. Three 1P21 photomultipliers were symmetrically immersed in the liquid and their outputs paralleled to improve uniformity. Both an aluminum-lined copper and brass container, and in some later work a Lucite container were used with satisfactory results. Either terphenyl-xylene-diphenolhexatriene or phenol-cyclohexane-terphenyl-diphenolhexatriene solutions were found equally satisfactory as scintillators. A block diagram of the electronics system employed is shown in Fig. 2.

The output of each counter was fed directly into a 125-ohm impedance coaxial cable (RG63/U) which was then matched to and connected to the input of a wideband 200 ohm distributed amplifier. The amplifiers were modified to direct dc coupling between stages to avoid large pulse grid current overloading and the resultant long deadtime. The counter pulses were amplified and limited by the distributed amplifiers with a resultant rise time of 2.6×10^{-9} second and an amplitude of about 7 volts positive. Pairs of these counter signals were then fed to 6BN6 dual control grid coincidence tubes, carefully constructed with shielded cables direct to each grid. This results in singles to doubles ratios of three or more and gives a large plateau range in the double output. Shorted clipping lines of length $1\frac{1}{2}$ or 3 feet (depending on the resolution desired in each double channel) were attached in parallel at each grid and gave resolutions of 2–3 millimicroseconds for the shorter lines. The reflected negative pulse from the clipping line is internally absorbed in the terminated plate line of the last stage of the distributed amplifier and hence causes no trouble. The efficiencies of the counters and doubles circuit were found to be greater than 95% in all cases.

The output from each doubles circuit was amplified by 0.03 microsecond rise time linear (feedback-stabilized) amplifiers and followed by 0.1-microsecond discriminators to eliminate singles. The output of the EFP60 secondary emission discriminator tube used, is a shaped square pulse of 10- to 15-volt amplitude and 0.1-μsec width. The various doubles outputs were independently monitored through isolating cathode followers by 10-mc scalers. These double outputs were mixed in crystal diode multiple-coincidence circuits of 100% efficiency with a resolution and recovery time of less than 0.1 microsecond. These

[17] A four element quadruple telescope was used in the earlier carbon-polyethylene difference experiments.

[18] The angle of magnetic displacement was 30° in the earlier measurements. A description of the arrangement used is given in S. J. Lindenbaum and L. C. L. Yuan, Phys. Rev. **92**, 1578 (1953); and **93**, 917 (1954).

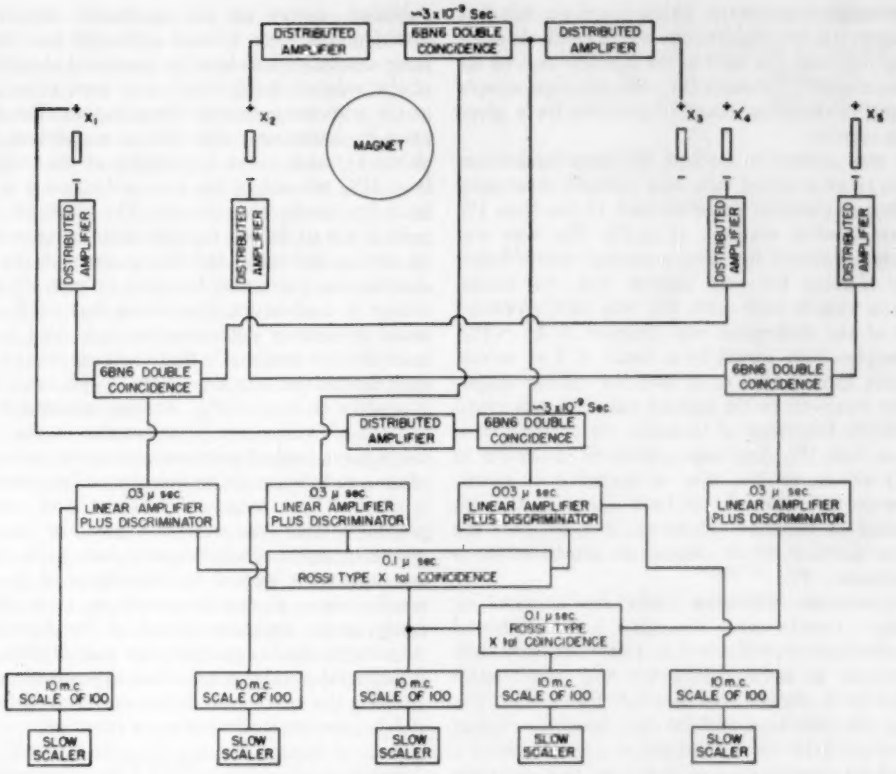

FIG. 2. A block diagram of the electronics system.

multiple slower coincidences compounded of the proper combinations of fast doublets allowed multi-counter coincidences (triples, quadruples, quintuples) to be made with the effective high resolution of the doublets.

The advantages of this type of system are the following:

(a) The same high resolution and the same doubles to singles ratio for each doublet are maintained independent of the multiplicity of coincidence required.

(b) A high degree of flexibility is available in selecting various combinations of multiple coincidences at will, by simply flipping the switches for the desired doublets in the 0.1-microsecond coincidence circuits.

(c) Simultaneous monitoring of any or all double coincidences can be made enabling the detection of any possible circuitry failure or change in beam conditions.

(d) The accidentals of each doublet can be checked independently as a check on operating conditions.

(e) The resolution of each doublet can be independently varied without affecting the over-all singles to doubles ratio.

Of course, the main disadvantage of a compounded doublet system is the requirement for considerably more electronic equipment.

Regulated dc power supplies and regulated ac filament power were employed for most critical circuits. This reduced long time drifts to a minimum. The 1P21 photomultipliers were run with about 1500–1800 volts on the tubes, and large plateaus (~100 to 200 volts) were obtained on all counting rates. The over-all performance of the system was extremely stable and no drifts of any kind were detectable during the compilation of data for this experiment.

C. Determination of the Momentum of the Incident Pions and Other Beam Particles

As previously described the counter telescope includes a magnet between the second and third counters which introduces a magnetic deflection of 45°. The telescope was carefully positioned along a true magnetic trajectory passing through the geometric center of each counter. The true magnetic trajectory was found by current-carrying wire techniques. It was further observed that varying the magnet current to cover the range of momenta used in this experiment did not affect the position of this trajectory or the

relative magnetic geometry. This is due to the fact that the magnet is a very efficient one with a relatively small fringing field and was used in the low field regions far from saturation. Obviously then the telescope accepts a unique[19] momentum range of particles for a given magnet current.

The wire calibration for both the mean momentum and the range accepted were very carefully done using a calibrated precision ammeter read to less than $\frac{1}{4}\%$ with an absolute accuracy of $\pm\frac{1}{2}\%$. The wire was carefully positioned by using a marked mirror below it and aligning the wire shadow with the marks. Precision weights were used. The long term reproducibility of the calibration was observed to be $\sim\frac{1}{2}\%$. The weights were varied by a factor of 5 at several momenta through the range and the current appropriately increased to the balance value. It was found that within this range of variation the absolute error was less than 1%. Any large systematic errors due to gravity effects on the wire or excessive or erratic friction on the pulley should have shown up through this range of variation. Therefore, it is felt that the absolute precision of the momentum determination is approximately 1%.

A momentum calibration curve was obtained by drawing a smooth curve through a large number of these determinations obtained as a function of incident momentum. It is, therefore, felt that the relative calibration is accurate to a small fraction of 1%. During the calibration and the experiment the magnet current was kept constant to within a few tenths of a percent by observing a precision potentiometer (with an internal standard cell) placed across a precision shunt in series with the magnet. Actually, an automatic servo control system was used on the generator to maintain a constant current through the magnet. However, a technician checked with the bridge every few minutes and continually corrected any slow long term drifts.

It is obvious that this kind of high-accuracy absolute and relative momentum determinations are not obtained in other similar experiments which depend primarily on range curve determinations. The accuracy of a range curve determination of the mean momentum is generally limited by the following factors:

(1) Uncertainties in the basic range energy relation which probably cannot be trusted to better than 1–2%.

(2) Uncertainties in determining the mean range due to the following:

(a) Experimentally deciding the precision of the mean range from the observed curve.

(b) Multiple scattering corrections.

It is our opinion that a very careful determination of (a) and (b) still leads to at least a 1–2% uncertainty. However, one might point out that many of the published curves do not necessarily involve this precision. Therefore, it is our conclusion that the usual range determinations have an associated absolute error of the order of $\pm 2\%$ which is at least twice as poor as the wire measurement determination. The relative error in determining the relative momentum of two points by range curve is probably of the order of at least $1\frac{1}{2}\%$ whereas in the wire calibration it is felt to be a few tenths of a percent. The emphasis on this point is due to the fact that the observed cross sections on the rapidly rising and falling parts of the $\pi^+ + p$ cross-section curve vary by about at least 1% per 1% change in momentum. This means that a 2% error in mean momentum determination could lead to a 2% error in cross section. Or that two near relative points each determined with a precision of $1\frac{1}{2}\%$ could exhibit a relative error of $\sim 2\%$. Another advantage of our method of momentum determination is that in the range curve method an experiment is run over a period of time, and then at a later time the incident momentum is checked by a range curve. There is of course the possibility that the cyclotron field, or the target geometry, might change slightly during the course of the experiment without the knowledge of the experimenter, since a constant check on these effects is rarely under complete control of the experimenter. Admittedly this is expected to be a small effect, but it is nevertheless ruled out in these experiments so far as affecting the momentum determination since the selection is done externally inside our telescope.

It is of interest to note here that several careful determinations of the incident mean momentum were made by range curve techniques and were found to agree within 1% with the wire calibration prediction. However, we have used the wire calibration in assigning incident energies in all cases as in our opinion it is the more accurate.

The half-width of the incident momentum range selected by the telescope was also determined by wire calibration and was found to be $\pm 2\%$. A range curve estimate was in reasonable agreement with this figure. Since both the magnetic and physical geometry were maintained constant throughout the experiment, both the percentage of the mean momentum accepted by the telescope and the shape of the momentum resolution function were essentially constant over the range of momenta used. This means that all geometry and resolution corrections are slowly varying functions for neighboring points of the observed curve.

Several other advantages of this method in combination with time of flight discrimination to obtain exceedingly clean meson beams will be pointed out in the following section.

D. Analysis of Beam

The quadruple coincidence of the first four counters was used to monitor and define the incident beam.

[19] This would be exactly true for an incident parallel beam. The mean angular width of the incident beam was $\pm 0.3°$ and this small effect was included in the estimates.

The magnet current selected the desired momentum interval ($\sim\pm 2\%$). The time of flight resolution[20] of $\sim$3 millimicroseconds in a 20-foot long telescope gave, when adjusted for pions, an effective discrimination width in velocity of $\pm 15\%$. Three long (15 ft or more) fast time-of-flight circuits were compounded in the telescope. A typical coincidence rate curve obtained by delaying one pulse in a single doublet coincidence is given in Fig. 3. The compounding of three such doublets yields an over-all resolution curve which is the product of the three and hence much sharper. This completely excluded, with a large factor of safety, incident beam protons and other heavy charged particles.

For example, the highest velocity incident proton in the liquid hydrogen results occurred at 335-Mev incident pion energy. The corresponding time-of-flight delay in millimicroseconds for this proton is 20 millimicroseconds, or over six times the effective resolution. The number of protons in this momentum range was measured to be comparable to the number of positive pions.

However, it is estimated by a very careful study of the tails of the over-all time-of-flight resolution function that even an incident flux of protons 1000 times more would have a negligible result on these measurements.

Although heavy mesons are present in only negligibly small amounts, they too would have been excluded.

This telescope has been used in other applications to incident momenta of at least 1 Bev/c. At this momentum protons are at least ten times as abundant as pions. The difference of time-of-flight for a 1-Bev/c proton compared to a pion is 8 millimicroseconds or almost 3 times the resolution. It was impossible to detect any protons when the time of flight was adjusted for pions. Hence, it is evident that primary beam protons are not counted in these experiments.

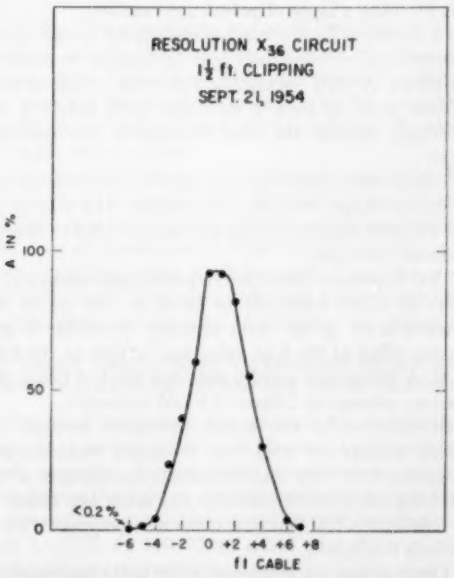

FIG. 3. A typical resolution curve of a 6BN6 fast doublet coincidence. One foot of cable equals 1.2 millimicroseconds.

[20] The resolution is defined as that time delay for which the coincidence counting rate drops to ½ the peak value. In general, the coincidence rate dropped to background levels for delays approximately twice the resolution.

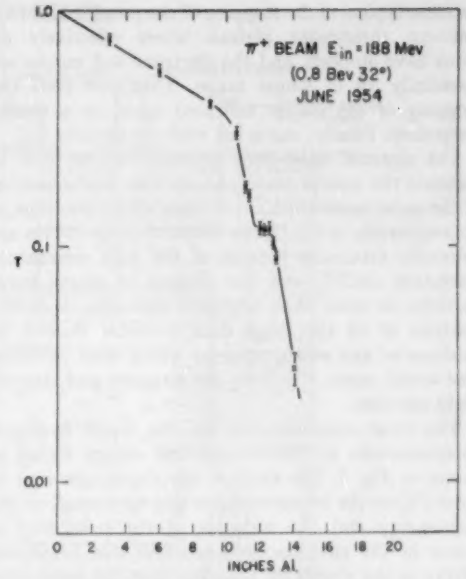

FIG. 4. A typical integral range curve.

Hence, the counted beam consisted of pions, muons, and electrons[21] in the momentum interval selected by the magnetic geometry. This is not strictly true as some small percentage of pions can decay to muons after or even during magnetic analysis, and some secondaries can be generated in the back counters. The second effect is entirely negligible since thin counters were used and the very good geometry and fast time-of-flight discrimination employed make the contribution of the small number of secondaries negligible. The first effect is made quite small by the fact that the angle of μ decay is large enough to make most of these decay muons miss the last counter. However, of the order of 2% of the wrong momentum muons can still be present and this effect has been corrected for throughout.

Aluminum range curves were taken by inserting aluminum directly before the last counter to analyze the beam at the various energies. A typical integral range curve is shown in Fig. 4. This curve plotted on semilog paper shows the typical approximately constant nuclear attenuation of the incident pions, the rapid

[21] Positrons for positive pion and electrons for negative pion beams.

decrease typical of the stopping of the pions, and then a clear-cut three-point plateau where effectively all pions have stopped, and the electrons and mouns are essentially all of longer range. Then one finds the stopping of the muons indicated again by a second steep drop. Finally, one is left with the electron tail.

The clearcut three-point plateaus can be used to estimate the sum of muon and electron contamination of the same momentum as the pion, with a precision of approximately $\pm 1\%$. These cleancut range curves are primarily attainable because of the high momentum resolution ($\pm 2\%$) and the absence of wrong range particles in other than negligible amounts. A careful analysis of all the range data available showed no evidence of any wrong range or wrong mass particles. One would expect this from the magnetic and time-of-flight selection.

The total contamination for the liquid hydrogen determinations at 0.8-Bev machine energy varied as shown in Fig. 5. The electron contaminations were at most 2% at the lowest energies and very small at the high-energy end. An estimate of the possibility of errors in the electron contamination due to shower effects in the aluminum absorber gave the result that these effects are entirely negligible.

In the early $C-CH_2$ difference work when the machine was run at 2.3 Bev, the contaminations were of the order of $2\frac{1}{2}$ times higher (30% at 150 Mev). The much poorer magnetic resolution used, and other differences made the contamination estimate much more uncertain so that an error of $\sim 10\%$ at (150 Mev) was possible.

The increase of contamination with machine energy is caused by the fact that electron and muon contamination in general comes mostly from decay of higher energy pions than those selected for the experiment. This means that if the pion energy selected is near the pion energy spectrum cutoff, there is less contamination. Therefore, as one would expect and as has indeed been observed, if at any particular pion energy, one reduces the machine energy sufficiently, the tails of the pion spectrum move in and reduce the decay contamination.

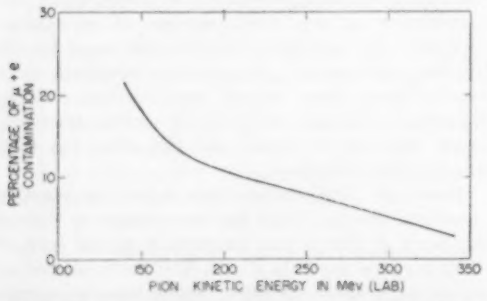

FIG. 5. The sum of muon and electron percentage contamination as a function of positive pion energy for the positive pion beams obtained from the 32° direct beam in the experimental arrangement used. The incident proton energy was 0.8 Bev.

E. Details of Liquid Hydrogen Target and Geometry

A diagram of the liquid hydrogen target used is given in Fig. 6. The target consisted primarily of two hollow Styrofoam rectangular boxes one inside the other. The outer box was $24\frac{3}{4}$ in. long (in beam direction) by 27 in. high by 18 in. wide, and the walls were $1\frac{1}{2}$ in. thick (in the beam direction). The inner box was $17\frac{1}{2}$ in. long (in beam direction) by $12\frac{3}{4}$ in. high by 5 in. wide, and the walls were $\frac{1}{2}$ in. thick (in the beam direction).

A liquid nitrogen jacket surrounded most of the inner box and was located in the space between the two boxes. This whole assembly was placed in a large wooden box to supply a rigid outer container. Inside the inner Styrofoam box was placed a rectangular copper container 12.5 in. long, 5 in. wide and 10 in. high in which the liquid hydrogen was placed. Thin 1-mil copper windows were placed in the inner copper container near the bottom over a 5 in.$\times$5 in. area located symmetrically around the beam center during the running of the experiment. The part of the outer wooden container facing the windows was cut out and the Styrofoam was narrowed so that only 0.1 g of Styrofoam preceded each window. The top of the Styrofoam box was removable and was sealed to the box by using a layer of petroleum vaseline.

In the top a Lucite window was placed so that visual observations on the liquid hydrogen could be made at all times. A level measuring rod with a disk shaped bottom plate to form a meniscus when touching the hydrogen surface was used to monitor the hydrogen level.

Tubes were inserted in the top of the Styrofoam box to fill the target with liquid hydrogen and also to fill the nitrogen jacket. An exhaust was provided to remove gaseous hydrogen.

The hydrogen chamber required approximately 5 liters of liquid hydrogen to fill it to the top of the window level (5 in. from bottom). Actually it was usually filled to the 8-in. level and refilled at the 6-in. level. A filling was usually required every 3 hours and used an average of 2 liters of liquid hydrogen.

Observation of the liquid hydrogen through the Lucite window revealed that the liquid was clear and quiescent with very little bubbling. An estimate of the bubbling effect on the density was made and found to be less than a fraction of a tenth of a percent which is entirely negligible.

The length of the hydrogen in the beam was carefully determined by measuring the distance between the two windows in a hydrogen filled target using a theodolite. The length value obtained was 12.55 in.$\pm$0.03 in. which is accurate to within $\frac{1}{4}\%$. A comparison measurement with the target empty gave a larger length

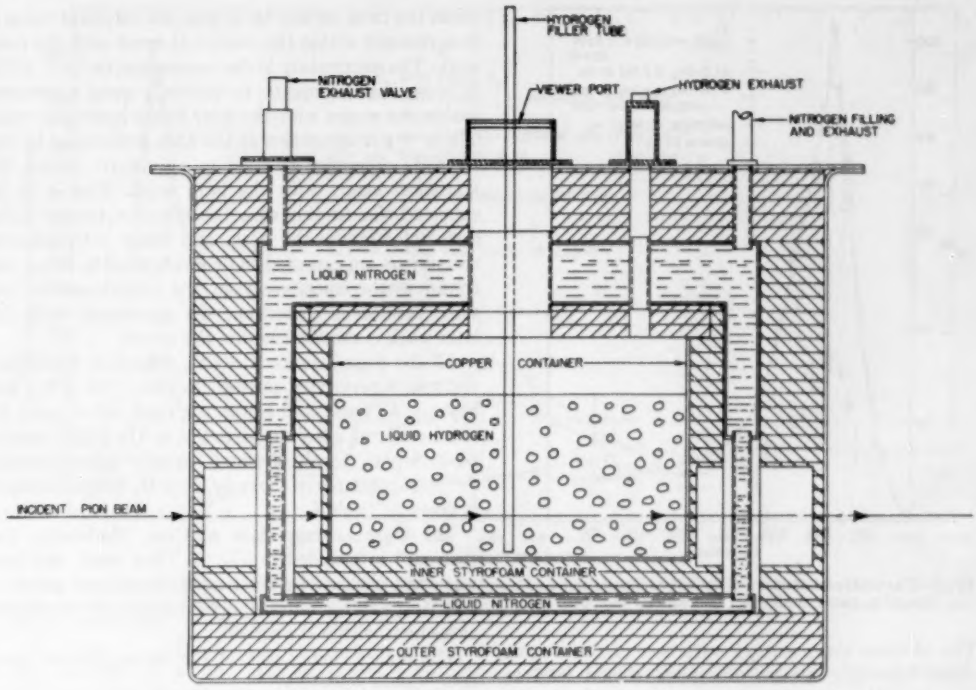

FIG. 6. A schematic diagram of the liquid hydrogen target.

by 0.2%. This means that the total shrinkage is 0.2% which is of the order of one tenth or less than the shrinkage in Styrofoam. This was primarily effected by allowing the copper container to be somewhat spaced from the Styrofoam so that only the shrinkage in copper was involved.

An equivalent[22] empty dummy target was used in the experiments alternately with the filled target, so that the difference due to the hydrogen could be ascertained. The data of Woolley *et al.*[23] for the density of liquid hydrogen at its boiling point was used. The value given is 0.7088 g/cm³. The possible effects of normal variations of atmospheric pressure on this density are negligible.

III. EARLY PRELIMINARY CARBON-POLYETHYLENE RESULTS FOR TOTAL HYDROGEN CROSS SECTIONS

The total hydrogen cross sections for positive and negative pions were in all cases obtained by determining good geometry transmission measurements for the pion beams through an absorber containing hydrogen. In the early work only low-intensity pion beams with a high (~30% at 150 Mev) muon and electron contamination were available. Liquid hydrogen was not available. Therefore, rather thick polyethylene and carbon absorbers were utilized to obtain a quick survey of the general energy dependence of the hydrogen cross section for negative and positive pions. The energy resolution of these experiments varied from about ±25 Mev in the peak region to about ±50 Mev at the higher energies. Polyethylene and carbon absorbers with the same number of carbon atoms per cm² transverse to the beam were alternately placed between the last large liquid counter and the monitor telescope. The carbon was composed of several independent rectangular slabs spaced so as to cover the same volume as the polyethylene.

The geometry was characterized by a mean half angle of 6°. The Coulomb scattering out was negligible, and the required geometry corrections were 3% or less. The background corrections required were of the order of 1%. The major correction applied was the muon and electron contamination of the beam. This was particularly high near the peak (30 percent at 150 Mev, 20 percent at 200 Mev) but dropped rapidly to a few percent at higher energies (5 percent at 500 Mev). The uncertainty in the contamination determination was of the order 20–30% of the contamination in these early measurements, and hence could lead to systematic errors of as high as 10 percent in the peak region. At the higher energies the uncertainty was only about 2–3%. The corrected results are shown in Fig. 7.

[22] The nitrogen jacket was omitted, but this makes no practical difference as it is completely out of the beam.

[23] Woolley, Scott, and Brickwedde, J. Research Natl. Bur. Standards 41, 379 (1948).

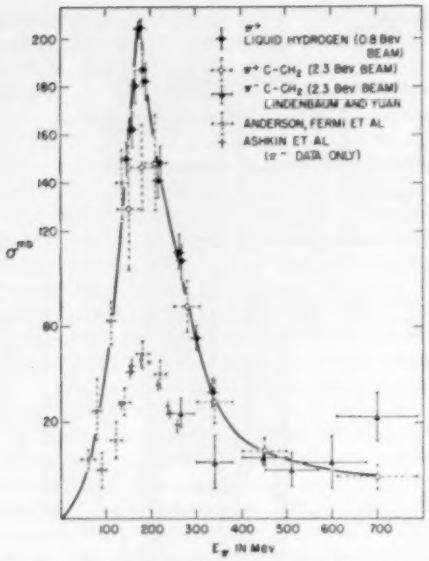

FIG. 7. The total cross section of hydrogen for positive and negative pions of 150–750 Mev kinetic energy.

The obvious sharp energy variation of these cross sections especially around the peak should lead to rather severe resolution corrections considering the ±25-Mev width of the determinations. To a first-order approximation the resolution correction is zero for a straight line energy variation of the cross section. Hence, one expects the high-energy side of the curves to be more accurate. However, around the peak region the resolution corrections can be expected to raise the cross section considerably. An estimate based on the later work shows that approximately 25 mb should be added to the positive pion cross section at 180 Mev (the peak point).

The errors shown are only statistical (rms). The major source of systematic error is the uncertainty in contamination which is high below 200 Mev (7 to 10 percent) and drops rapidly at the higher energies. Hence, since both the systematic errors and resolution corrections are high below 200 Mev, these cross sections measurements were considered to have an associated absolute error of 15–20% and were expected to be low in value since both the resolution corrections and the contamination uncertainty were expected to raise the cross sections. In the region above 200 Mev, both the contamination uncertainty and the resolution corrections drop very rapidly, and these cross sections have an associated absolute error of ±5–7%.

As is evident from Fig. 7, the higher energy $E_{\pi^+} \geq 210$ Mev $C-CH_2$ positive pion cross sections agree very well with the later liquid hydrogen work. The peak point at 180 Mev is considerably lower. However, if one applies the estimated resolution correction which raises the cross section by 25 mb, the resultant value is in agreement within the statistical errors with the later work. The uncertainty in the contamination (~7–10%) is more than adequate to obtain a good agreement within the errors with the later liquid hydrogen work. The $\pi^+ + p$ cross section at 150 Mev determined by the $C-CH_2$ difference is close to agreement within the statistical errors with the later work. This is to be expected, for in this case the effective energy width does not straddle the peak, and hence the resolution corrections are expected to be much smaller. When one considers the uncertainty in the contamination and some resolution correction, the agreement with the later work is excellent within the errors.

All the negative-pion $C-CH_2$ difference determinations were performed at energies ($E_{\pi^-} \geq 265$ Mev) well beyond the peak, and hence, are expected to have the same order of absolute accuracy as the higher-energy positive-pion cross sections, namely approximately 5–7%. A summary of the early $C-CH_2$ determinations[24] is given in Table I.

The higher energy data of Cool, Madansky, and Piccioni[25] is included in Fig. 8. Their work and ours was cross checked by their repetition of our points at 450 Mev, and we found all determinations in reasonable agreement within the errors.

The higher energy part of the curves fits our lower energy data smoothly.

IV. TOTAL CROSS SECTION OF HYDROGEN FOR POSITIVE PIONS FROM 140–340 MEV DETERMINED BY LIQUID HYDROGEN TRANSMISSION

A. Experimental Procedure

The transmission of the liquid hydrogen was determined at various energies by alternately placing the full hydrogen target or the empty dummy between the fourth and fifth (last) counter. The experimentally determined transmission is defined as

$$T_e = \frac{\text{(quintuple/quadruple) hydrogen}}{\text{(quintuple/quadruple) dummy}}.$$

The standard geometry employed is given in Fig. 9.

TABLE I. The total interaction cross section of hydrogen for positive and negative pions obtained by measuring the difference in transmission of carbon and polyethylene.

Mean pion energy in Mev	Total π^+ cross section in mb	Total π^- cross section in mb
210	148 ±20	
265		44±6
280	88 ±11	
340	48 ±9	23±11
450	27.5±6	25±3
510		20±7
600		23±11
700	17 ±3	42±10

[24] Except for the positive pion results at 150 and 180 Mev which require rather large corrections as previously discussed.

[25] Cool, Madansky, and Piccioni, Phys. Rev. **93**, 249 (1954) and **93**, 637 (1954).

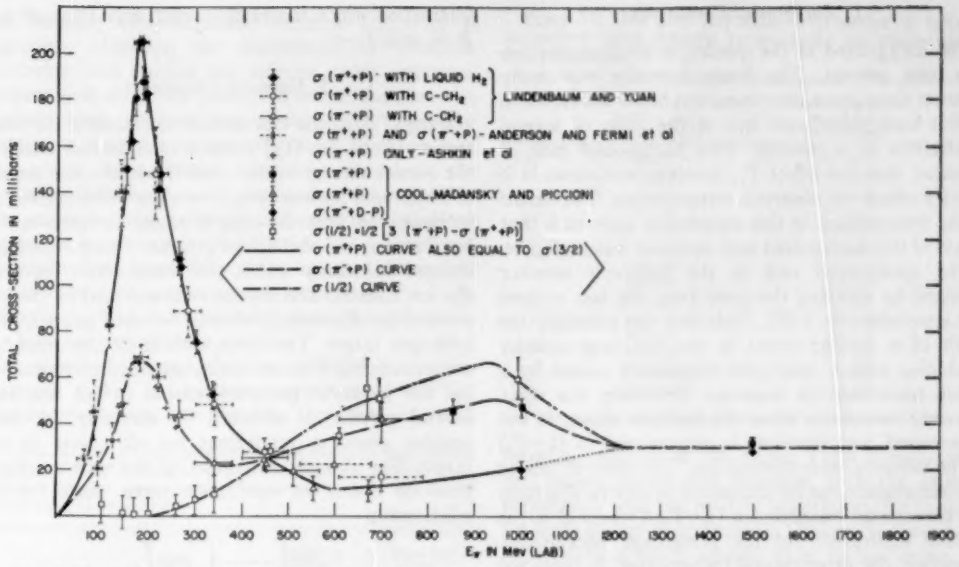

FIG. 8. The total cross section of hydrogen for positive and negative pions from 0 to 1500 Mev. The curves also include some cross sections (at the higher energy end) which are equal to deuterium-hydrogen differences. The deduced values for $\sigma(\frac{1}{2})$ and $\sigma(\frac{3}{2})$ are also shown.

The background in the quadruple and quintuple coincidences was determined by placing a 15 millimicrosecond delay in the respective signal cable after each run.

Before each run a careful check on the operation and rates of the various doubles and multiple coincidences was made. Time resolution, background conditions, and counting efficiencies in each circuit were checked.

As previously described (Sec. II C) the magnet current which determined the incident pion momentum was kept constant to within a few tenths of a percent.

The beam intensity was nearly constant during most of these runs, and the equipment was found to be very stable. No drifts of any kind were detectable during these runs, even when the beam intensity was occasionally observed to change by large factors.

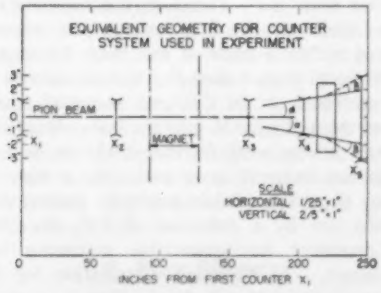

FIG. 9. The standard geometry for the liquid hydrogen measurements.

Each transmission measurement was composed of several cycles of hydrogen target and dummy determinations. In all cases the relative agreement of these successive cycles was reasonable within expected statistical limits.

The discriminator output stage for each doublet coincidence contained a gating tube which was normally gated off. A timing pulse from the Cosmotron master timer was used to open the gate for 50 milliseconds. This period started about 10 milliseconds before the beginning of a gradual reduction in rf voltage, which caused the beam to strike the internal target over a 40 millisecond interval. This procedure ensured that counts recorded on all scalers occurred only when the full energy beam struck the internal target. Hence, spill-out beam conditions which might tend to be erratic were eliminated.

B. Calculation of Cross Sections

The nuclear cross section of an absorber is related to the true transmission due ohly to nuclear attenuation by the relationship

$$\sigma = (1/N) \log(1/T^*), \qquad (1)$$

where N is the surface density of nuclei per cm² of surface transverse to the beam direction.

The experimentally determined transmission T, of the positive pion beams is related to T^* by a series of corrections the most important of which are the beam contamination, geometry, and background.

1. *Background Corrections*

The background in the quadruple monitor was less than one percent. The beam intensity was fairly constant throughout these runs, and hence the variation in this background rate was of the order of several hundredths of a percent. This background rate, if constant, does not affect T_e; however, variations in it directly affect the observed transmissions. The values of the transmission in this experiment were such that effects of this background rate variation was negligible.

The background rate in the quintuple monitor obtained by delaying the pulse from the last counter was approximately 1–2%. This rate was primarily the result of a random count in the last large counter combining with a quadruple coincidence caused by a meson traversing the telescope. Obviously this effect can only contribute when the incident meson is not transmitted, and therefore is proportional to $(1-T_e)$ or the effective beam attenuation. The effect of this on the transmission can be eliminated by subtracting from the uncorrected transmission $(1-T_e)B$ where B is the decimal equivalent[28] of the percentage background. Therefore, the experimental transmission T_e corrected for background is given by:

$$T_e'=T_e-(1-T_e)B. \tag{2}$$

2. *Contamination Correction*

The sum of muon and electron contamination of the same momentum as the incident pions is given as a function of energy in Fig. 5. It was determined by range curve techniques as described in Sec. (II D) to within an uncertainty of approximately ±1%.

The nuclear and also Coulomb scattering out of muons and electrons in the geometry used is negligible, and hence these components of the beam are essentially transmitted without attenuation through the hydrogen. The transmission corrected for this contamination effect is exactly given by the following formula:

$$T_e''=(T_e'-\epsilon)/(1-\epsilon), \tag{3}$$

where ϵ is the decimal equivalent of the percentage muon and electron contamination of the beam. In terms of the experimentally observed transmission

$$T_e''=\frac{T_e(1+B)-B-\epsilon}{1-\epsilon}, \tag{4}$$

where T_e'' is the transmission obtained after correction for both beam contamination and background. The above expression is an exact one applicable for even large ϵ and B and hence is a more accurate method of applying these corrections than the usual one of simply correcting the cross sections by adding a percentage equal to background and a percentage equal to contamination which is strictly correct only for $\epsilon\to 0$ and $B\to 0$ or if $T_e\to 1$.

[28] Decimal equivalent of 1% is defined as 0.01.

3. *Geometry Corrections*

Using T_e'' of the last section to calculate the cross section [from Eq. (1)] yields a cross section which is the correct average nuclear plus Coulomb cross section of a hydrogen nucleus for all processes which remove an incident pion from the cone of angles accepted by the last counter, and also do not generate a time-coincident charged secondary within that cone which traverses the last counter. The angular cone accepted by the last counter is, of course, different for each point in the hydrogen target. The characteristics of the geometry are given in Fig. 9. A reasonably accurate representation for the resultant geometry effects (which are only several percent) is obtained by assuming the same angular geometry equivalent for all points in the target. For an extended target of the type employed here we define an equivalent mean angle by the relationship

$$\bar{\theta}=\left[\frac{1}{\theta_2-\theta_1}\int_{\theta_1}^{\theta_2}\theta^2 d\theta\right]^{\frac{1}{2}},$$

where θ_1 is the half angle of the cone formed by the last counter and the point on the counter system axis at the end of the liquid hydrogen furthest from the last counter.

θ_2 is the half angle of the cone formed by the last counter and the point on the counter system axis at the end of the liquid hydrogen nearest to the last counter. For the present case $\theta_1=5.4°$, $\theta_2=8.6°$, $\bar{\theta}=6.6°$.

$\bar{\theta}$ thus defined would give an exact equivalent for the extended geometry employed if the beam were all concentrated along the axis and all (nuclear and Coulomb) cross sections were isotropic, within the angular range involved. An estimate of the possible error introduced by this assumption for an equivalent geometry is a fraction of 1% and is included in the over-all uncertainty.

The effective angular divergence of the beam issuing from the counter directly before the hydrogen is defined by the counter system including the magnet to be less than ±1°. Therefore, the extremes of the shadow circle on the last counter are essentially contained within a circle of less than 1.9-in. radius. The additional angle δ through which an extreme angle beam particle must be Coulomb scattered from the center of the hydrogen to miss the last counter is 2.5°. Since only a very small fraction of the incident beam particles are extreme rays, and only a very small fraction of the available azimuth corresponds to scattering out by a deflection of 2.5°, the effective angle necessary for appreciable scattering out is much larger. The Gaussian distribution for multiple scattering in the hydrogen has a root mean square angle of 0.6° or less, and hence, the scattering

out resulting from Coulomb multiple scattering is negligible. However, the interference of Coulomb scattering with nuclear can amount to an estimated correction of about one percent or less in the observed nuclear cross sections under the given geometry conditions, and this uncertainty must be taken into account in the geometry corrections. Based on the available differential cross section data[14] for positive pion scattering from hydrogen, it appears that geometry correction by an angular distribution of $1+3\cos^2\theta$ is a reasonable best guess. This is the expected theoretical distribution for a pure resonance in the state $T=J=\frac{3}{2}$. That this is close to the probable case will be shown in the later analysis of these results.

It should be noted that in addition to mesons scattered within the angular acceptance of the last counter, one must also consider the effect of recoil protons from the hydrogen which enter the last counter within this angular range. Actually, an appreciable fraction of these are rejected by time-of-flight discrimination due to their much slower velocity, and some are stopped in the hydrogen.

TABLE II. Absolute and relative errors in the total cross section determination of hydrogen for positive pions of 140–350 Mev. Liquid hydrogen transmission measurements were utilized to obtain these cross sections.

Source of error	Absolute rms percentage error	Relative rms percentage error
(1) Muon and electron contamination correction (3–12%)	1%	¼%
(2) Geometry correction (3–4%)	1%	¼–½%
(3) Hydrogen content of target	½%	0
(4) Background correction (1–2%)	½%	½%
(5) Double scattering, changes in π-μ decay due to energy loss in hydrogen, additional Coulomb scattering in H_2, and other small effects	1%	½%
(a) Total rms absolute error $=[1^2+1^2+(\frac{1}{2})^2+(\frac{1}{4})^2+1^2]^{\frac{1}{2}}\approx 2\%$.		
(b) Total rms relative error $=[(\frac{1}{4})^2+(\frac{1}{2})^2+(\frac{1}{4})^2+(\frac{1}{2})^2]^{\frac{1}{2}}\approx 1.1\%$.		
(c) The linear addition of all absolute errors $=3\frac{1}{2}\%$.		
(d) The linear addition of all relative errors $=2\%$.		

The over-all geometry corrections used to convert the experimental results to an estimated total nuclear cross section amount to approximately 3 to 4% with an estimated uncertainty of $\pm 1\%$. It should be further noted that if an isotopic angular distribution were used instead of the $1+3\cos^2\theta$ distribution, the change in final results would be less than 2%, and hence, the final results are not very sensitive to the small geometry corrections required.

C. Error Estimates

The major individual sources of error in this experiment have been discussed in detail in various of the preceding sections of this paper. Table II summarizes the various errors and indicates both the absolute uncertainty and the relative uncertainty for points in the same energy neighborhood. Obviously, the relative uncertainty is much smaller since certain errors (for example the hydrogen content of the target) are constant and others are only slowly varying functions of energy. The rms absolute error is approximately $\pm 2\%$. However, with a limited number of systematic errors, it is perhaps safer to consider the linear addition of the errors as an upper limit on the absolute error. In this case the maximum estimated absolute error is $3\frac{1}{2}\%$. Therefore, perhaps a mean value of $\pm 3\%$ or less is a quite conservative estimate for the absolute error. The rms value of the relative absolute error is $\pm 1\%$. The linear addition of the relative absolute errors yields $\pm 2\%$ as an upper limit on the relative absolute error. A mean value of 1.5% or less is a quite conservative estimate for the relative absolute error.

One should note that the above error estimates are for the cross section determined for the particular momentum interval of pions selected. These errors do not include possible resolution corrections or possible errors in the mean momentum determination. The mean momentum determination has an absolute error of $\pm 1\%$ (see Sec. II D), and a relative absolute error of a few tenths of a percent. The possible effects of the momentum uncertainty and the resolution corrections will be considered in a later section.

TABLE III. The total interaction cross section of hydrogen for positive pions obtained by measuring the transmission of liquid hydrogen.

Positive pion energy in Mev	Total cross section of hydrogen in millibarns
146±7	150±7
157±7	162±7
166±8	182±6
166±8	176±7
171±8	204±6
173±8	205±6
181±8	187±7
189±8	182±7
214±8	141±7
222±8	148±7
262±9	111±7
263±9	107±7
298±10	75±5
335±10	53±5

D. Results

The results obtained for the total cross section of hydrogen for positive pions are given in Table III and plotted in Fig. 10. The solid curve drawn through them is a best fit by French curve and has no other significance. The errors shown are predominantly statistical (rms) although they also include the relative absolute error.

The theoretical value of the cross section at a

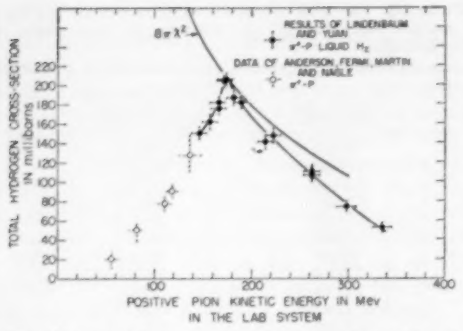
$8\pi\lambda^2$
RESULTS OF LINDENBAUM AND YUAN
π^+-p LIQUID H_2
DATA OF ANDERSON, FERMI, MARTIN AND NAGLE
π^+-p
TOTAL HYDROGEN CROSS-SECTION IN millibarns
POSITIVE PION KINETIC ENERGY IN Mev IN THE LAB SYSTEM

FIG. 10. The total cross section of hydrogen for positive pions of 140–350 Mev kinetic energy. Only our data obtained by using the liquid hydrogen target are shown.

resonance in the $T=\frac{3}{2}$, $J=\frac{3}{2}$ state is $8\pi\lambda^2$[27] and is plotted as a solid line for comparison. A detailed analysis of these results will be presented in Sec. V.

Both the $C-CH_2$ and liquid hydrogen results are plotted in Fig. 7 together with some relevant work of other laboratories.

The positive pion cross sections of Ashkin *et al.*[13] are compared in greater detail to our results in Fig. 11 which is a larger scale graph of the peak region.

It is evident from Fig. 7, that except for the positive pion cross sections at 150 Mev and 180 Mev, the early $C-CH_2$ results agree very well with the later much more accurate liquid hydrogen data. As previously remarked (Sec. III) even these points can be brought into agreement if resolution corrections and contamination uncertainties are considered.

From Figs. 7 and 10 it is evident that the presently determined hydrogen cross sections for positive pions join the lower energy data of Anderson and Fermi[4] smoothly.

The data of Ashkin *et al.*[13] seems to scatter considerably more than our own. However, the over-all agreement is quite good except for their highest energy point at 196 Mev. This one point disagrees well outside of the error with our curve. One should note here that this is their least accurate point and has a much larger error than their preceding point at 185 Mev which falls almost directly on our curve. If one accepts the point at 196 Mev as correct, one must conclude that their preceding higher accuracy point at 185 Mev which also fits our curve very well is too low. Therefore, it is felt that the point at 196 Mev is too high. Although the statistical accuracy in the two experiments is about the same, the absolute errors, the relative errors for neighboring points, and the energy determination errors, are considerably lower in our experiment, and therefore, the observed greater consistency of the data is to be expected.

[27] Assuming all other states do not contribute.

V. ANALYSIS OF RESULTS

A. General Considerations

One of the basic characteristics of the pseudoscalar meson field with strong coupling is the prediction[6] of nucleon isobars characterized by an isotopic spin T and an angular momentum J and such that $T=J$ is most likely required.

For the π^+-p scattering only the isotopic spin $T=\frac{3}{2}$ state is present, and therefore, the first isobar should have $J=\frac{3}{2}$ or involve a P-wave interaction which should for strong enough coupling go through resonance (i.e., the phase shift phasses through 90°).

An extensive theoretical analysis of the expected characteristics of this resonance phenomenon has been made by Brueckner,[5] Chew,[9] Chew and Low,[28] and others and will be discussed more thoroughly in Sec. V C.

The essential common conclusion is that a strong interaction (probably resonant) is expected in the $T=J=\frac{3}{2}$ state with little or no interaction expected in the other P states or S states.

The contribution of D wave and higher states is expected to be less important in the range of energies here considered due to the fact that $\lambda \gtrsim \hbar/2\mu c$.

B. Phase Shift Analysis

Fermi introduced the phenomenological approach of analyzing the experimental data, using charge independence, in terms of the six S and P state phase shifts δ_{33}, δ_{31}, δ_{13}, δ_{11}, δ_3, δ_1. The first index is twice the isotopic spin and the second[29] is twice the angular

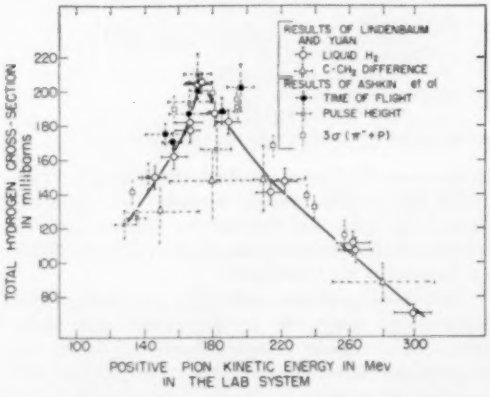
RESULTS OF LINDENBAUM AND YUAN
LIQUID H_2
C-CH_2 DIFFERENCE
RESULTS OF ASHKIN et al
TIME OF FLIGHT
PULSE HEIGHT
3σ (π^++P)
TOTAL HYDROGEN CROSS-SECTION IN millibarns
POSITIVE PION KINETIC ENERGY IN Mev IN THE LAB SYSTEM

FIG. 11. A comparison of the presently reported results with those of Ashkin *et al.* Earlier results of Homa, Goldhaber, and Lederman [Phys. Rev. **93**, 554 (1954)] were 151±31 mb and 159±34 mb at 151±7 and 188±8 Mev, respectively, which agree with our curve. Recent results of Anderson *et al.* [this issue, Phys. Rev. **100**, 268, 279 (1955)] are 188±5.4 mb and 194±5.2 mb at 165 and 189 Mev, respectively, which are also in agreement.

[28] G. E. Chew and F. E. Low (private communication), and *Proceedings of the Fifth Annual Rochester Conference on High-Energy Nuclear Physics* (Interscience Press, New York, 1955).

[29] Omitted for S waves.

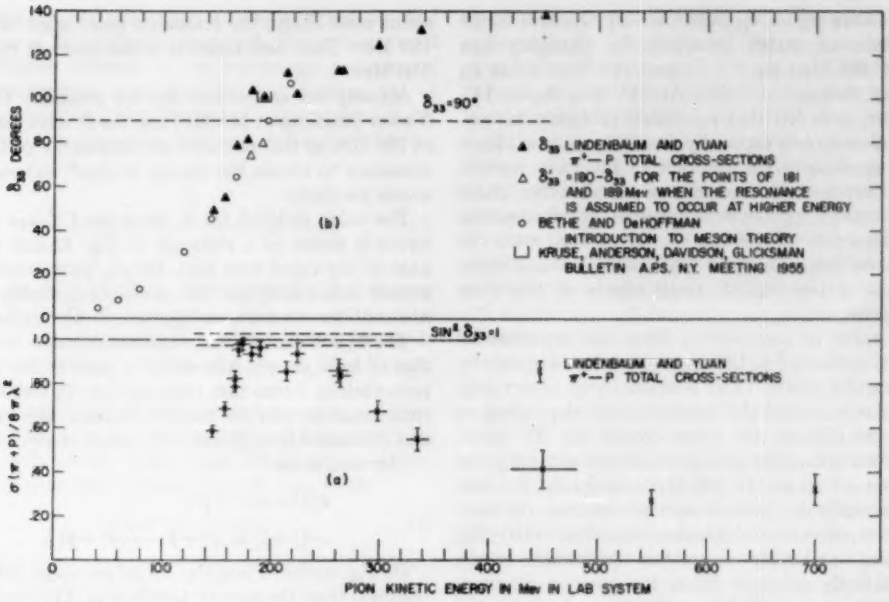
δ33 DEGREES
δ33=90°
▲ δ33 LINDENBAUM AND YUAN π+—P TOTAL CROSS-SECTIONS
△ δ'33=180−δ33 FOR THE POINTS OF 181 AND 189 Mev WHEN THE RESONANCE IS ASSUMED TO OCCUR AT HIGHER ENERGY
○ BETHE AND DeHOFFMAN INTRODUCTION TO MESON THEORY
□ KRUSE, ANDERSON, DAVIDSON, GLICKSMAN BULLETIN A.P.S. N.Y. MEETING 1955
(b)
SIN² δ33=1
LINDENBAUM AND YUAN π+—P TOTAL CROSS-SECTIONS
σ(π+P)/8πλ²
(a)
PION KINETIC ENERGY IN Mev IN LAB SYSTEM

FIG. 12. (a) The ratio of the total cross section of hydrogen for positive pions to $8\pi\lambda^2$ is plotted *versus* incident pion kinetic energy. λ is the De Broglie wavelength of the pion in the c.m. system. (b) The phase shift deduced for the state with isotopic spin and angular momentum equal to $\frac{3}{2}$ is plotted *versus* incident pion kinetic energy.

momentum. The latest and most extensive phase shift analysis of the previously available total differential cross section data (mostly π^-+p) has been performed by de Hoffmann *et al.*[15] Their result is somewhat uncertain, providing several possible solutions; however, the most likely solution is that only δ_{33} is large and probably goes through resonance at 195 Mev.

The π^++p cross section is given in terms of S and P wave phase shifts by:

$$\sigma(\pi^++p)=8\pi\lambda^2[\sin^2\delta_{33}+\tfrac{1}{2}\sin^2\delta_{31}+\tfrac{1}{2}\sin^2\delta_3]. \quad (1)$$

Hence, it follows that if $\alpha_{33}=90°$ that

$$\sigma(\pi^++p)\geq 8\pi\lambda^2. \quad (2)$$

From Fig. 10, it is apparent that the experimental π^++p cross section appears within the errors to equal or exceed $8\pi\lambda^2$ at 173 Mev.

However, the higher energy points (notably that at 189 Mev) stay close enough to $8\pi\lambda^2$ so that especially, if the absolute cross-section uncertainty, $\pm 3\%$, is taken into account, the cross section could possibly exceed $8\pi\lambda^2$ at higher energies up to 200 Mev.

A more critical comparison can be made by plotting $\sigma/8\pi\lambda^2$ *versus* energy as in Fig. 12(a). The resonance condition is indicated by the solid line at $\sigma/8\pi\lambda^2=1$. In comparing the observed cross sections to $8\pi\lambda^2$ one is uncertain within the experimental absolute error in the cross section of $\pm 3\%$. Therefore, the two dotted accompanying lines 1.03 and 0.97 are plotted to define a band of absolute uncertainty for the comparison of the cross section to $8\pi\lambda^2$. The relative absolute uncertainty of two points is much less than this and is equal to approximately 1%.

There is a definite systematic trend in the data to favor a high point relative to $8\pi\lambda^2$ at 173 Mev, although within the relative errors this is not definitely established. If one considers the possible effect of resolution corrections due to the width (± 8 Mev) of the observed energy band on this sharp curve, the following is expected to happen.

(1) The points on both sides of the peak fall on approximately straight lines over the energy band measured. Hence, the first-order resolution correction is zero. The curvature of the curve appears to be concave upwards; hence, the second-order resolution correction probably slightly depresses these points.

(2) The peak points at 171 and 173 Mev have an appreciable first-order resolution correction which of course depends on the exact shape of the curve.

Reasonable estimates place an increase in cross section of probably at least ~ 5 millibarns as the correction. Hence, this makes it more likely that the resonance occurs near that energy region.

Since the maximum cross section is very close to $8\pi\lambda^2$, and it is highly probable that α_{33} goes through 90°, it is obvious that all other phase shifts except α_{33} are probably very small and do not contribute appreciably to the cross section. According to the most acceptable prior solution of Bethe and de Hoffmann, δ_3 contributed approximately 2% to the cross section in

the resonance region. δ_{31} ,which is very sensitive to the data, behaved rather peculiarly by changing sign between 169 Mev ($\delta_{31}=+3°$) and 194 Mev where δ_{31} suddenly changed to $-16°$. At 217 Mev $\delta_{31}=-14°$. Therefore, it is felt that δ_{31} should probably be considered close to zero expecially since there is no evidence for an appreciable contribution to the cross section. The apparent total contribution of all other phase shifts except δ_{33} appears to be less than the experimental errors involved. Therefore, we will proceed with the analysis on the assumption that only $\delta_{33}\neq 0$ and make estimates of the possible small effects of the other phase shifts.

The value of δ_{33} deduced from the experimental results is given in Fig. 12(b) as a function of energy by the triangular points. There is obviously an uncertainty in the shape around the resonant point depending on where one assumes the curve crosses the 90° point. The closed triangular points are drawn assuming the resonance occurs at 175–180 Mev. Obviously, for each experimentally determined cross section near the resonant point, there are two solutions δ_{33} and $\delta_{33}'=180-\delta_{33}$, depending on whether one assumes the resonant energy is respectively above or below the point in question. If the resonance is placed at 195 Mev, the points at 181 and 189 are still below the resonant line and are indicated by the open triangular points.

The overall uncertainty of the resonant point seems to be confined within the region 175 to 195 Mev. The systematic trend of our data implies a lower resonant resonant energy ~175–180 Mev, whereas a straight line drawn through the resonance gives a resonance energy of 195 which agrees with the Bethe-de Hoffmann estimate. This solution is certainly acceptable within the limits of error but is less probable than the former one.

It is really just this selection of the resonant energy which determines the shape of the phase shift curve at the resonant point.

The subtraction of appreciable amounts ~5 to 10% of the contribution of other waves to the cross section will also tend to reduce the knee in the phase-shift curve and place the resonance at ~195 Mev. However, it has been previously concluded that there is no good evidence to support this amount of other waves.

It should be noted that our phase shift curve smoothly joins that deduced by Bethe and de Hoffmann[15] at energies below 160 Mev.

In the resonant region one limit of our data is the Bethe and de Hoffmann curve. However, the most probable guess based on the data alone and not relying on any theoretical prejudices is represented by the curve passing through resonance at ~175–180 Mev.

The latest differential $\pi^+ + p$ cross-section data from Kruse *et al.*[14] at 165 and 189 Mev show a shift from backward peaked to forward peaked scattering in going from 165 to 189 Mev. If the observed asymmetry is due to P wave interference with S wave alone (which seems most likely) the resonance point must be below 189 Mev. Their best estimate of the resonant energy is 180 Mev.

Actually one cannot rule out the possiblity that the S wave interferes at 165 Mev and the D wave interferes at 189 Mev so that one need not necessarily go through resonance to obtain the change in sign[30] although this seems less likely.

The value deduced for δ_{33} from the Chicago experiments is shown as a rectangle in Fig. 12 and fits the knee of our curve very well. Hence, there seems to be several indications that the resonance probably occurs at a considerably lower energy than previously believed.

The hypothesis of charge independence or conservation of isotopic spin allows us to analyze the present pion-nucleon interaction cross sections in terms of the total cross section for the two isobaric spin states $\frac{3}{2}$, and $\frac{1}{2}$ denoted by $\sigma(\frac{3}{2})$ and $\sigma(\frac{1}{2})$, respectively.

The results are:

$$\sigma(\tfrac{3}{2})=\sigma(\pi^+ + p), \tag{3}$$

$$\sigma(\tfrac{1}{2})=\tfrac{1}{3}[3\sigma(\pi^- + p)-\sigma(\pi^+ + p)]. \tag{4}$$

On Fig. 10 the rectangular points represent $3\sigma(\pi^- + p)$ obtained from the data of Ashkin *et al.* The total errors (statistical and absolute) are shown. Half the difference between the $3\sigma(\pi^- + p)$ curve and the $\sigma(\pi^+ + p)$ curve is equal [see Eq. (4)] to $\sigma(\frac{1}{2})$ which is obviously small in the resonance region. However, it appears that if one takes the data literally $\sigma(\frac{1}{2})$ seems to be about 10 mb on both the low and high side of the resonance, disappear between 170 and 180 Mev, reappear and then disappear again at about 260 Mev.

The absolute experimental errors involved could certainly make these small effects (~5–7% or less) consistent with $\sigma(\frac{1}{2})=0$ for any one point. However, the systematic tendency for this peculiar behavior, if attributed to the errors, would imply a peculiar type of systematic distortion in either the negative data, or the positive data, or both. Since our positive pion data is the most precise experimentally and is also in agreement (except for one point) with the positive pion data of Ashkin *et al.*,[13] it follows that probably either $\sigma(\frac{1}{2})$ behaves in a peculiar fashion or that the negative pion data of Ashkin *et al.* exhibit a peculiar type of systematic distortion. The best guess appears to be the latter, and therefore one concludes that within the errors $\sigma(\frac{1}{2})$ is probably equal to zero in the resonance region. A plot of $\sigma(\frac{3}{2})$ and $\sigma(\frac{1}{2})$ as a function of energy is given in Fig. 8.

C. Theoretical Predictions for Pion-Nucleon Interaction

As previously stated Pauli and Dancoff[8] predicted the existance of a series of nucleon isobars characterized by $T=J$, and for which $T=J=\frac{3}{2}$ is the lowest in the $(\pi^+ + p)$ scattering interaction.

[30] This was pointed out by R. Serber.

Brueckner first investigated the expected detailed behavior of this isobar by essentially fitting a one level Breit-Wigner formula to the low-energy behavior of the pion-nucleon cross sections and making use of charge symmetry. The Brueckner[5] type of results can by some minor operations best be stated in the following form:

$$\frac{\sigma}{8\pi\lambda^2}=\sin^2\delta_{33}=\frac{\rho^2}{\rho^2+\epsilon^2}+\text{small terms} \tag{5}$$

where $\rho=A\bar{P}^3/(1+\bar{P}^2a^2)$. a is essentially the channel radius in units of $\hbar/\mu c$, $\epsilon=1-\tilde{\omega}_t/\omega_0$, $\tilde{\omega}_t$ is the total energy of the meson plus the nucleon kinetic energy in the center-of-mass system, and ω_0 is its value at resonance.

Chew and Low[28] recently solved an exact equation deduced by Low for the meson-nucleon interactions which included the meson cloud effects in the nucleon wave function and obtained the following result.

$$\rho\cot\delta_{33}=Af(\tilde{\omega}_t). \tag{6}$$

The experimental data and other reasons lead them to assume $f(\tilde{\omega}_t)\sim 1-\tilde{\omega}_t/\omega_0$.

Hence, the Chew-Low equation can be stated in the following simple form:

$$\rho\cot\delta_{33}=A\epsilon, \tag{7}$$

where

$$\rho=\bar{P}^3/\tilde{\omega}_t,$$
$$\epsilon=1-\tilde{\omega}_t/\omega_0,$$
$$A=\tfrac{3}{4}(f^2/\hbar c)^{-1}.$$

It is apparent that if $\rho\cot\delta_{33}$ is plotted *versus* $\tilde{\omega}_t$ a straight line is predicted by the theory.

Although the Brueckner form of the resonance theory appears quite different, it will be shown that the following simple trigonometric transformation can be used to put it in the same form as the Chew-Low predictions.

$$\sin\delta_{33}=\frac{\rho}{[\rho^2+\epsilon^2]^{\frac{1}{2}}};\quad \cos\delta_{33}=\frac{\epsilon}{[\rho^2+\epsilon^2]^{\frac{1}{2}}}. \tag{8}$$

Hence,

$$\rho'\cot\delta_{33}=A'\epsilon, \tag{9}$$

where $\rho'=\bar{P}^3/(1+\bar{P}^2a^2)$; for $a=1$, the channel radius $=\hbar/\mu c$; and hence $\rho'=\bar{P}^3/\omega_\pi^2$.

Therefore, except for the denominator of ρ' which depends on ω_π, which is equal to ω_t minus the proton kinetic energy in the c.m. system, the two forms of the theory are now of similar form.

The Chew-Low type of plot is made in Fig. 13 where $(\bar{P}^3/\tilde{\omega}_t)\cot\delta_{33}$ is plotted on the y-axis *versus* $\tilde{\omega}_t$ on the x-axis. It is apparent that the high (till 335 Mev) and low-energy points fall reasonably well on a straight line. The resonant point is characterized by $\cot\delta_{33}=0$ and hence is determined by the point where the ordinate of the graph is zero. The straight line determined by the high and low-energy points passes through resonance at approximately 195-Mev pion kinetic energy in the lab system. Again, as in the phase shift plot, a departure from a straight line is indicated if one assumes the resonance is at the lower energy (~175–180 Mev). The points at 181 and 189 Mev are plotted below the resonant line for the assumption of a lower energy resonance. Their shadow is plotted above the line for the higher energy resonance assumption. The band of uncertainty in the resonance energy is 175 to 195 Mev, and this at the higher energy limit gives a straight line plot. The lower energy limit which seems most probable from the data leads to the dotted line.

Again as in the phase-shift curve the subtraction of 5 to 10% of higher waves (for which there is no good evidence) would tend to straighten out the curve before the resonant point and place the resonance at higher energy. The curve would however tend to break downward past resonance. It is also possible that the curve dips downward at the resonant point following the slope shown by the broken line, and that the apparent return to the original straight line is an accident caused by the onset of higher waves or meson production.[31]

The difficulty in deciding exactly where the resonance lies with precision is essentially caused by the rapid momentum dependence of $\rho=\bar{P}^3/\tilde{\omega}_t$ in the resonance formula $\sin^2\delta_{33}=\rho^2/(\rho^2+\epsilon^2)$. A little reflection will convince one that a rapidly increasing ρ with increasing momentum will tend to make $\sin^2\delta_{33}$ approach the neighborhood of 1 rapidly and then to level off and have a horizontal tangent at the resonance, and decrease very slowly thereafter. This behavior is well illustrated in Fig. 12(a). Therefore, it requires a very high precision in the total cross-section measurements to accurately fix the resonance point. A small constant contribution to the cross section by other waves will not change the fact that at the resonant point $\sigma/8\pi\lambda^2$ will be a maximum. However, a small variation in the cross-section contribution of other waves in the neighborhood of the resonant region can affect the location of the peak point of this rather flat topped curve.

It follows from Eq. (7) that the coupling constant in terms of $f^2/\hbar c$ can be determined from the Chew-Low plot by the y intercept at $\tilde{\omega}_t=0$.

The value obtained from the present plot is $f^2/\hbar c=0.076$.

The higher energy points (not shown) at 450, 550, and 750 Mev depart from the essentially straight line plot and exhibit too high a cross section, the increase growing with increasing energy. This behavior is very suggestive of the onset of appreciable contributions of

[31] The energy threshold for meson production is coincidentally at about the resonant point.

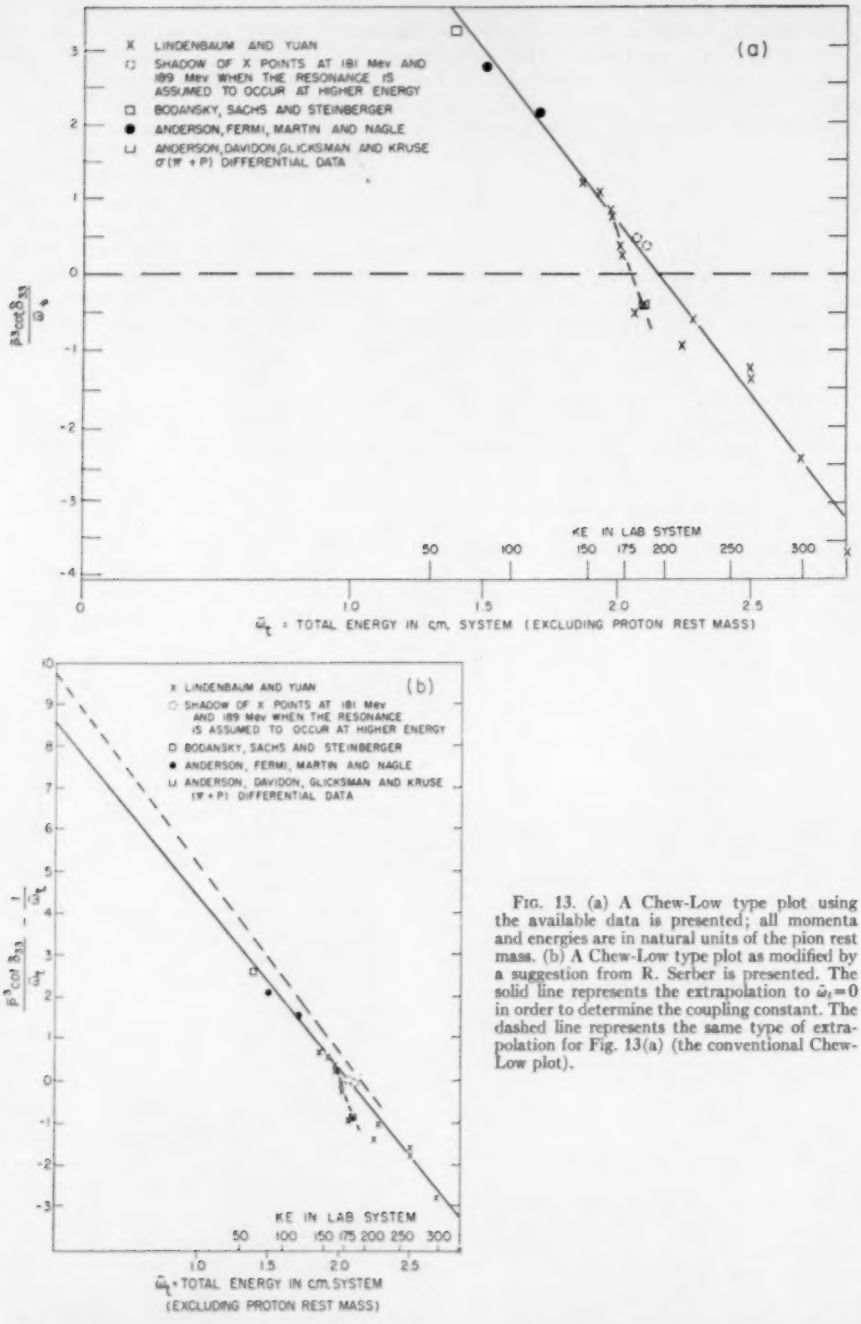
X LINDENBAUM AND YUAN
SHADOW OF X POINTS AT 181 Mev AND 189 Mev WHEN THE RESONANCE IS ASSUMED TO OCCUR AT HIGHER ENERGY
BODANSKY, SACHS AND STEINBERGER
ANDERSON, FERMI, MARTIN AND NAGLE
ANDERSON, DAVIDON, GLICKSMAN AND KRUSE σ(π⁺ + P) DIFFERENTIAL DATA
(a)
KE IN LAB SYSTEM
50 100 150 175 200 250 300
ω̃ₜ = TOTAL ENERGY IN cm. SYSTEM (EXCLUDING PROTON REST MASS)
(b)
KE IN LAB SYSTEM
50 100 150 175 200 250 300
ω̃ₜ = TOTAL ENERGY IN cm SYSTEM
(EXCLUDING PROTON REST MASS)

FIG. 13. (a) A Chew-Low type plot using the available data is presented; all momenta and energies are in natural units of the pion rest mass. (b) A Chew-Low type plot as modified by a suggestion from R. Serber is presented. The solid line represents the extrapolation to $\tilde{\omega}_t=0$ in order to determine the coupling constant. The dashed line represents the same type of extrapolation for Fig. 13(a) (the conventional Chew-Low plot).

higher waves or inelastic meson production effects above 335 Mev. This effect is more clearly demonstrated in Fig. 13 where $\sigma(\pi^+ + p)/8\pi\lambda^2$ suddenly changes slope beyond 350 Mev and passes through a minimum at about 550–600 Mev and increases again beyond 600 Mev.

Serber[32] has found that the proper solution of the Chew-Low equation is

$$\rho \cot\delta_{33} - \frac{1}{\omega} = AF(\omega),$$

where

$$A = \tfrac{2}{3}(f^2/\hbar c)^{-1}.$$

Letting

$$F(\omega) \sim A\epsilon$$

as previously, the corresponding plot suggested by Serber is shown in Fig. 13(b).

Actually, the major change is that $f^2/\hbar c = 0.087$ instead of the previous value of 0.076.

It appears to be a rather interesting coincidence that the kinetic energy in the center-of-mass system at resonance is equal to 144 Mev which is approximately one pion rest mass. If one thinks in terms of the possible states of the nucleon and pion system this is just the point where a real second pion could be created.

The fact that $\sigma(\frac{1}{2})$ is close to or equal to zero in the resonance region can be explained in terms of a calculation performed by Henley and Lee.[33] They found that in the energy region here considered, the overlap between the initial state of meson and nucleon and the $\sigma(\frac{1}{2})$ scattering state is quite small, and hence, a small $\sigma(\frac{1}{2})$ cross section is to be expected. As evidenced in Fig. 8 the $\sigma(\frac{1}{2})$ cross section increases at higher energies, and based on the data of Cool and Piccioni[34] above 700 Mev seems to reach a broad peak in the region of 1 Bev. To explain this peak in terms of elastic scattering in only one state would require $J \approx 5$,[35] which is quite unlikely. Furthermore, the cross section is largely inelastic,[36] and hence, the picture is therefore not easily analyzed. However, one can conclude that higher waves and inelastic processes are involved in the $\sigma(\frac{1}{2})$ cross section. The $\sigma(\frac{3}{2})$ cross section is zero within the errors in the resonance region but becomes important at $\gtrsim$300 Mev (see Fig. 8). It is perhaps reasonable to assume that the energy dependence of higher waves and inelastic processes in the $\sigma(\frac{3}{2})$ state might generally follow that for the $\sigma(\frac{1}{2})$ state. Therefore, one should expect that higher waves and inelastic processes begin to contribute to $\sigma(\frac{3}{2})$ appreciably in the region of $\gtrsim$300 Mev.

This has previously been deduced from the Chew-Low plot and the variation of $\sigma(\pi^+ + p)/8\pi\lambda^2$ *versus* energy.

[32] R. Serber (private communication).
[33] E. Henley and T. D. Lee (private communication).
[34] The curves shown in Fig. 8 and the deduction of $\sigma(\frac{1}{2})$ at the higher energies are based on the points shown plus some recent data of Cool, Clark, and Piccioni, to whom we are indebted for making these data available prior to publication.
[35] M. Gell-Mann and K. M. Watson, Ann. Rev. Nuc. Sci. **4**, 219 (1954).
[36] Eisberg, Fowler, Lea, Shephard, Shutt, Thorndike, and Whittemore, Phys. Rev. **97**, 797 (1955).

VI. ACKNOWLEDGMENTS

The authors are indebted to Dr. R. Serber for many valuable suggestions and discussions pertaining to the theoretical aspects of the problem.

We are also indebted to Dr. E. O. Salant for many valuable discussions.

We particularly wish to acknowledge the invaluable assistance rendered by Mr. E. Rappe and Mr. A. Roesch in the construction, and setting up of the equipment, and also their generous cooperation in assisting with the experimental runs.

The authors wish to thank the Cosmotron staff for their generous cooperation which made this experiment possible.

We are particularly indebted to Mr. A. Schlafke who developed and constructed the Styrofoam liquid hydrogen target.

The authors are indebted to Mr. J. Dominy and the cryogenic staff of the Chemistry Department for providing us with liquid hydrogen.

We also wish to acknowledge the helpful assistance of Mr. L. Landovitz and Mr. B. McIlwain in some of the experimental runs during their stay at the Laboratory last summer.

Note added in proof.—Some recent work by Pontecorvo and his collaborators on pion-proton total cross sections in the energy range of 140 to 400 Mev has been published after this article was submitted. [Ignatenko, Muchin, Ozerov, and Pontecorvo, Doklady Akad. Nauk SSSR **103**, 45 (1955)].

Energy Distribution of K Mesons Produced in Nuclei

M. M. BLOCK,* *Naval Research Laboratory, Washington, D. C.*, E. M. HARTH,†‡ *Duke University, Durham, North Carolina,*

AND

R. M. STERNHEIMER,§ *Brookhaven National Laboratory, Upton, New York*

(Received June 13, 1955)

K mesons produced by internal target bombardment at the Brookhaven Cosmotron and Berkeley Bevatron are assumed to be made by the reaction: $p+N\rightarrow Y+N+K$, where N = nucleon, Y = hyperon. The expected energy distribution of the K particles is calculated for several laboratory angles at proton bombarding energies of 2.9 Bev and 4.8 Bev, assuming various angular and energy distributions of the K mesons in the center-of-mass system of the incoming proton and target nucleon. The internal motions of the target nucleons were taken into account by using both the Gaussian and the Fermi momentum distributions.

I. INTRODUCTION

IN view of the recent Cosmotron[1–3] and Bevatron[4] experiments on the production of K mesons by internal proton bombardment of heavy nuclei targets, it seems of interest to calculate the expected laboratory energy distribution of the K particles as a function of laboratory angle and beam energy, making suitable assumptions about the center-of-mass system (c.m.) energy and angular distribution of the K mesons. A comparison of the calculated laboratory energy distributions with the experimental spectra from heavy nuclei should give information about the mode of production and the angular and energy distribution in the c.m. system for the individual nucleon-nucleon collisions.

Associated production[5] in nucleon-nucleon collisions[6,7] has been assumed, and computations have been made for the following typical reactions:

$$p+p\rightarrow\Sigma^{+}+K^{+}+n, \tag{1}$$

$$p+p\rightarrow\Lambda^{0}+K^{+}+p, \tag{2}$$

where the Σ^{+} is the charged hyperon of mass 2340 m_e, and Λ^{0} is the neutral hyperon of mass 2180 m_e, and the K mass is taken to be 975 m_e. Using either a Fermi or Gaussian internal momentum distribution, an average has been taken over the motion of the target nucleons; the results should be applicable to all but the lightest nuclei, since the internal momentum distribution is approximately independent of atomic number. The procedure of the calculation is essentially that employed by Block, Passman, and Havens[8] to deduce pion emission spectra from targets bombarded by 381-Mev protons.

II. METHOD

For a given beam kinetic energy T_p, the total energy $\bar{W}$ available in the c.m. system can be shown to be dependent primarily on u, the component of the target nucleon velocity parallel to the incident beam. For a particular u, the differential cross section in the c.m. system (of the beam proton and target nucleon) is given by[9]

$$\frac{d^2\bar{\sigma}}{d\bar{\omega}d\bar{T}}=\frac{2\pi}{\hbar}\frac{|\bar{H}|^2}{\bar{v}_r}\frac{d^2\bar{\rho}(u)}{d\bar{\omega}d\bar{T}}, \tag{3}$$

where $\bar{H}$ is the matrix element for production, $\bar{\omega}$ and $\bar{T}$ are the K meson solid angle and kinetic energy, $d\bar{\rho}^2(u)/d\bar{\omega}d\bar{T}$ is the phase space factor for the 3-body final state, and $\bar{v}_r$ is the relative velocity of the colliding nucleons. The laboratory differential cross section is obtained by transforming (3) and averaging over u, and is

$$\frac{d^2\sigma}{d\omega dT}=\int_{u_{\min}}^{u_{\max}}\frac{d^2\bar{\sigma}(u)}{d\bar{\omega}d\bar{T}}JP(u)du, \tag{4}$$

where J is the Jacobian of the transformation, given by $p/\bar{p}$, and p is the K meson momentum. $P(u)du$ is the probability that u lies in du and is obtained from the assumed internal momentum distribution. It can be shown that the exact relativistic 3-body phase

---

* On military leave of absence from Duke University, Durham, North Carolina.

† On leave of absence from the Naval Research Laboratory, Washington, D. C.

‡ The work performed at Duke University was partially supported by a joint ONR-AEC contract.

§ The work performed at Brookhaven National Laboratory was carried out under the auspices of the U. S. Atomic Energy Commission.

[1] Hill, Salant, and Widgoff, Phys. Rev. **94**, 1794 (1954); **95**, 1699 (1954); **99**, 230 (1955). We are indebted to Dr. Hill, Dr. Salant, and Dr. Widgoff for showing us this paper before publication.

[2] J. Hornbostel and E. O. Salant, Phys. Rev. **93**, 902 (1954); Phys. Rev. **98**, 1202(A) (1955).

[3] G. G. Harris, Phys. Rev. **98**, 1202(A) (1955).

[4] Goldhaber, Goldhaber, Heckman, and Smith, Phys. Rev. **98**, 1202, 1203(A) (1955).

[5] A. Pais, Phys. Rev. **86**, 663 (1952); M. Gell-Mann, Phys. Rev. **92**, 883 (1953).

[6] Block, Harth, Fowler, Shutt, Thorndike, and Whittemore, Phys. Rev. **98**, 248(A) (1955); Phys. Rev. **99**, 262 (1955).

[7] Walker, Preston, Fowler, and Kraybill, Phys. Rev. **97**, 1086 (1955).

[8] Block, Passman, and Havens, Phys. Rev. **88**, 1239 (1952); Passman, Block, and Havens, Phys. Rev. **88**, 1247 (1952)

[9] Barred quantities, throughout, will be in the c.m. system, while unbarred symbols will refer to the laboratory system.

space factor is[10]

$$\frac{d^3\bar{p}(u)}{d\bar{\omega}d\bar{T}}=\frac{\pi}{6(2\pi\hbar)^6}\bar{p}\bar{E}\times\left[1-2\frac{(m_1^2+m_2^2)}{(\bar{W}-\bar{E})^2-\bar{p}^2}+\left(\frac{m_1^2-m_2^2}{(\bar{W}-\bar{E})^2-\bar{p}^2}\right)^2\right]^{\frac{1}{2}}\times\left\{3(\bar{W}-\bar{E})^2\left[1-\left(\frac{m_1^2-m_2^2}{(\bar{W}-\bar{E})^2-\bar{p}^2}\right)^2\right]-\bar{p}^2\left[1-2\frac{(m_1^2+m_2^2)}{(\bar{W}-\bar{E})^2-\bar{p}^2}+\left(\frac{m_1^2-m_2^2}{(\bar{W}-\bar{E})^2-\bar{p}^2}\right)^2\right]\right\}, \quad (5)$$

where $\bar{E}$ and $\bar{p}$ are the K particle total energy and momentum, respectively, and m_1 and m_2 are the rest masses of the other two reaction products.

In (3), we will ignore the slow variation of $\bar{v}_r$ with u, and will make various assumptions about the dependence of $|\bar{H}|^2$ on the K meson momentum $\bar{p}$ and angle of emission $\bar{\theta}$. In particular, we assume the following cases:

(1) $|\bar{H}|^2=1$, i.e., isotropic and energy independent.

(2) $|\bar{H}|^2=\cos^2\bar{\theta}$.

(3) $|\bar{H}|^2=\bar{\gamma}^2-1$, where $\bar{\gamma}=\bar{E}/m_K$.

(4) $|\bar{H}|^2=(\bar{\gamma}^2-1)\cos^2\bar{\theta}$.

The normalization constants arising from the above cases were chosen so that the c.m. cross section $d\bar{\sigma}/d\bar{\omega}$ at 0° was equal to 1 mb/sterad for a bombarding energy $T_p=2.9$ Bev.

The momentum distributions employed were:

(1) The Fermi degenerate gas model, which yields

$$P_F(u)=\frac{3}{4u_F}\left(1-\frac{u^2}{u_F^2}\right)=3.4-67.9u^2, \quad (6)$$

where $u_F=0.22$ is the value of u corresponding to the cutoff kinetic energy (22 Mev);

(2) The Gaussian distribution,

$$P_G(u)=\left(\frac{\alpha}{\pi}\right)^{\frac{3}{2}}\exp(-\alpha u^2)=3.41\exp(-36.4u^2), \quad (7)$$

which corresponds to an average kinetic energy of 19.3 Mev.[11]

III. RESULTS

$A\cdot T_p=2.9$ Bev

Using reaction (1), and Eqs. (3)–(7), we have numerically calculated curves for a proton beam energy of 2.9 Bev. Figure 1 shows the normalized energy

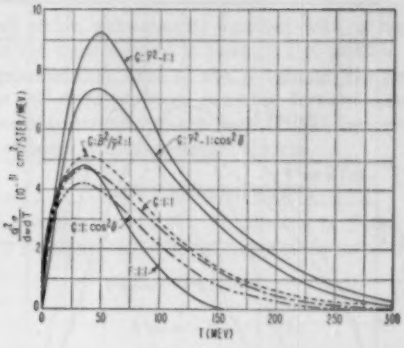

FIG. 1. Laboratory differential cross section $d^2\sigma/d\omega dT$ as a function of the K meson laboratory kinetic energy T, at a 90° laboratory angle and proton beam energy $T_p=2.9$ Bev, for various matrix elements and internal momentum distributions.

distributions $d^2\sigma/d\omega dT$ at a laboratory angle of 90°. The notation in this and the succeeding figures is as follows. In the labeling triplet $\xi:\eta:\zeta$ the first symbol ξ refers to the momentum distribution employed (F for Fermi, G for Gaussian), while η is the energy dependence of $|\bar{H}|^2$, being 1 if independent of $\bar{T}$, or $\bar{\gamma}^2-1$, or $\bar{\beta}^2/\bar{\gamma}^2$, where $\bar{\beta}=(\bar{\gamma}^2-1)^{\frac{1}{2}}/\bar{\gamma}$. The last symbol, ζ, represents the angular dependence of $|\bar{H}|^2$ and is $\cos^2\bar{\theta}$, or 1 for isotropic. In Fig. 1, the spectral shapes are roughly independent of the choice of matrix elements, all curves giving a maximum in the neighborhood of 40 Mev. The principal difference between the Gaussian and Fermi distributions is reflected in the high-energy end of the spectrum, where the Gaussian has a long tail in contrast to the sharp cutoff of the Fermi distribution. Further, there is also little difference in *magnitude*, as well as shape, between for example, $G:1:1$ and $G:1:\cos^2\bar{\theta}$, which is due to the fact that the K mesons emitted at a laboratory angle of 90° are emitted at angles of $\bar{\theta}$ in the c.m. system near 180°, so that $\cos^2\bar{\theta}\approx 1$. The cases where $\eta=\bar{\gamma}^2-1$ and $\bar{\beta}^2/\bar{\gamma}^2$ correspond to matrix elements behaving like $\bar{p}$ for low velocities, which might be expected of gradient coupling. By contrast, the energy independent matrix element may be applicable if the K meson is scalar. Also, this case corresponds to the Fermi theory[12] of meson production. The case of $\eta=\bar{\beta}^2/\bar{\gamma}^2$ was included because this matrix element decreases for large energies, and this compensates in part for the rapid increase of the phase space factor with increasing beam energy.

Figures 2 and 3 indicate the results for laboratory angles of 0° and 45°, respectively. The most striking feature of the 0° spectra is the presence of a minimum near 300 Mev for the energy dependent cases, in contrast to the smooth rise of the energy independent spectra. Thus, one may be able to distinguish experimentally between scalar and gradient coupling by observing the spectrum in the forward direction in the

[10] The units are chosen so that $c=1$.

[11] H. York, Phys. Rev. **75**, 1467 (1949); E. M. Henley and R. H. Huddlestone, Phys. Rev. **82**, 754 (1951).

[12] E. Fermi, Progr. Theoret. Phys. (Japan) **5**, 570 (1950).

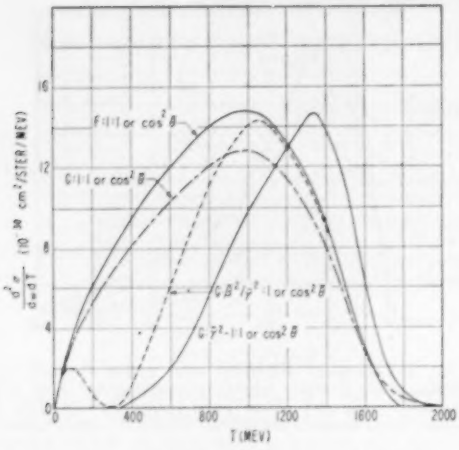

FIG. 2. Laboratory differential cross section $d^2\sigma/d\omega dT$ at $\theta=0°$ for beam energy $T_p=2.9$ Bev for various matrix elements and internal momentum distributions.

low-energy region ($T<800$ Mev). The presence of a minimum in $d^2\sigma/d\omega dT$ would indicate that the matrix element is energy dependent, going to zero as $\bar{p}\to 0$. The shapes and magnitudes of the 45° spectra are most sensitive to the choice of angular distribution, since the K particles emitted at 45° in the laboratory typically arise from c.m. angles $\bar{\theta}\sim 110$–$140°$, where $\cos^2\bar{\theta}$ is markedly different from unity.

$B \cdot T_p = 4.8$ Bev.

Using reaction (1), and Eqs. (3)–(7), the energy spectra were numerically evaluated for a beam energy of 4.8 Bev, and are shown in Fig. 4 for a 90° laboratory

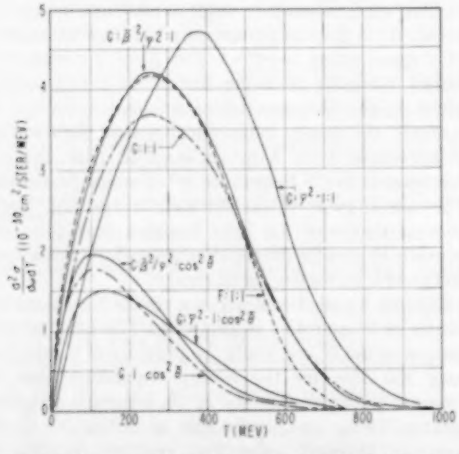

FIG. 3. Laboratory differential cross section $d^2\sigma/d\omega dT$ at $\theta=45°$ for beam energy $T_p=2.9$ Bev for various matrix elements and internal momentum distributions.

angle. The general features are quite similar to the 2.9-Bev results. The curves are normalized by the same procedure as the 2.9-Bev results; thus, a by-product of the calculation is the excitation function of the total cross section. Numerical integration of (4) gives the ratio of the *total* cross section at 4.8 Bev to that at 2.9 Bev as: (a) 9.1 for G:1:1, (b) 23.4 for $G:\bar{\gamma}^2-1$:1, (c) 8.3 for $G:\bar{\beta}^2/\bar{\gamma}^2$:1.

IV. COMPARISON WITH EXPERIMENT

Using nuclear emulsions, Hill, Salant, and Widgoff[1] have observed K mesons produced by internal proton bombardment of a copper target, at laboratory angles of 45° and 90° from the 3-Bev Cosmotron beam. The ratio of K particles at 90° to 45°, was given as $\rho=N(90°)/N(45°)=1.8_{-1.2}^{+0.4}$, where the energy intervals observed were 80 to 145 Mev at 90° and 260 to

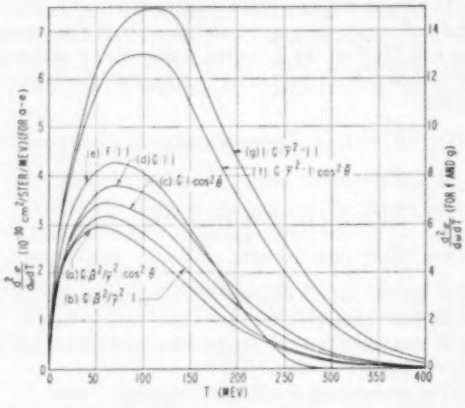

FIG. 4. Laboratory differential cross section $d^2\sigma/d\omega dT$ at $\theta=90°$ for beam energy $T_p=4.8$ Bev for various matrix elements and internal momentum distributions.

300 Mev at 45°. The corresponding calculated results, obtained from numerically integrating the appropriate energy regions in Figs. 1 and 3, are:

(i) $\rho_1=0.11$ for $|\bar{H}|^2=1$,

(ii) $\rho_2=0.31$ for $|\bar{H}|^2=\cos^2\bar{\theta}$,

(iii) $\rho_3=0.21$ for $|\bar{H}|^2=\bar{\gamma}^2-1$,

(iv) $\rho_4=0.63$ for $|\bar{H}|^2=(\bar{\gamma}^2-1)\cos^2\bar{\theta}$.

Only ρ_4 appears to be included within the experimental limits. However, ρ is very sensitive to the kinetic energy available in the c.m. system. The calculations were repeated for reaction (2) in which the K meson is created together with a Λ^0, and a bombarding energy of 3 Bev, which is probably closer to the experimental value, was used. Both the larger energy and smaller rest mass of the Λ^0 act to increase the value of ρ. Recalculating using these assumptions and the same

choice of matrix elements as above, we find: $\rho_1=0.18$, $\rho_2=0.44$, $\rho_3=0.39$, and $\rho_4=0.98$. Thus we conclude that $|\bar{H}|^2=1$ (isotropic and energy independent) appears to be ruled out by experiment, whereas the other choices of matrix elements are probably not inconsistent with the observations, considering the limited statistics of the experiment and the approximations made in the calculations. In this connection, we note that some of the K mesons emitted from a heavy nucleus may have been produced in a secondary reaction, i.e., pions were formed which subsequently collided with a nucleon within the same nucleus to produce a K particle. It is also possible that some of the K mesons emerging at 45° or 90° were produced near the forward direction but were scattered through large angles by collision with nucleons within the target nucleus.

V. ACKNOWLEDGMENTS

We are indebted to Mr. M. Blevins of Duke University for his aid in the initial stages of the calculations.

PHYSICAL REVIEW VOLUME 100, NUMBER 1 OCTOBER 1, 1955

High-Energy Electromagnetic Phenomena in Cosmic Radiation*

M. KOSHIBA AND M. F. KAPLON
Department of Physics, University of Rochester, Rochester, New York
(Received June 1, 1955)

Isolated high-energy electron showers in photographic emulsion have been investigated and have yielded the following conclusions: (1) out of 16 cases of isolated electron showers observed to originate from single electron pairs of energy greater than 1 Bev, 2 cases have been found to be anomalous in the sense that they seem to have been initiated by more than 2 photons; one of the two has been analyzed in detail. (2) The discrepancy between the experimental observations and theoretical predictions on the trident process found in a previous work has been obtained again with the additional experimental data of this experiment.

1. INTRODUCTION

SINCE the work of Schein *et al.*[1] in 1954 on an anomalous electron shower pointed to some possible difficulties in high-energy cascade showers, it has been felt that this field requires a more detailed survey. The purpose of this work is twofold; to check the results obtained previously[2] pertaining to the trident process with additional experimental data and to investigate the high-energy cascade shower development in emulsion under the more favorable experimental conditions of single γ-ray initiated showers to see whether there actually exists some anomaly or not. It seems pertinent, however, to give some general comments on the difficulties inherent in this field before the presentation and discussion of this experiment.

First of all, it must be emphasized that in the development of individual electron-photon cascades, the fluctuations in the numbers of electrons and photons (referred to as number fluctuations) from the average value can be enormously large. In fact, the number fluctuations in the cascade process were, under some simplified assumptions, shown to be similar to that of the Polya distribution, instead of the familiar Poisson distribution of random events. This means that the number fluctuation from the average can be as large as the average itself. In order to illustrate the situation more clearly the results of a Monte Carlo calculation[3] on cascade showers have been given in the Appendix. The original results on 100 showers with a single photon primary were obtained by one of us (M.F.K.) in collaboration with D. M. Ritson, using the cross sections of Approximation A of Rossi and Greisen.[4] The other results with different initial conditions were derived from the original results by a change of shower origin or by a superposition of different initial conditions. As can be seen from these results the number fluctuations are quite large compared with those encountered in random processes.

There is another difficulty which arises when we attempt to measure electron energies. The available methods of energy measurement for electrons or photons, by determination of the multiple Coulomb scattering or of the opening angle of a converted electron pair, have, when applied to high-energy electrons or photons, some defects which usually lead to an underestimation of the energy. That is, in the conventional method of multiple Coulomb scattering, no account is taken of the bremsstrahlung energy loss of the electron. Also, in the energy estimation of a γ ray from the opening angle of its converted electron-positron pair, some care must be

* This research was supported in part by the U. S. Air Force through the Office of Scientific Research, Air Research and Development Command.
[1] Schein, Haskin, and Glasser, Phys. Rev. **95**, 855 (1954); A. Debenedetti *et al.*, Nuovo cimento **12**, 954 (1954); N. Dallaporta (private communication).
[2] M. Koshiba and M. F. Kaplon, Phys. Rev. **97**, 193 (1955), hereafter referred as I.
[3] This method was first proposed by S. Ulam and J. Von Neumann, Bull. Am. Math. Soc. **53**, 1120 (1947).
[4] B. Rossi and K. Greisen, Revs. Modern Phys. **13**, 240 (1941).

FIG. 1. Condition of exposure of emulsion stack; the events labeled *A*, *B*, and *E* characterize the observational origin of the electron showers.

given to the effect of the scattering of the electrons as well as to the energy loss due to bremsstrahlung; for high-energy electron pairs we have to go several millimeters away from the pair origin to measure the opening angle and in this distance the separation due to the scattering cannot, *a priori*, be neglected.[5]

In Sec. 2, the experimental results on isolated showers[6] in the cosmic radiation observed in photographic emulsion will be presented and discussed. In Sec. 3, an apparently anomalous case of an electron shower is analyzed in detail and in Sec. 4 some additional results on the trident process, direct pair production by an electron, will be given. Finally, in Sec. 5 the results of this work are summarized and the possible inferences of the results are discussed.

2. ISOLATED ELECTRON SHOWERS

A stack of 49 stripped emulsions (Ilford G–5) were flown in Sky Hook Balloons at 41° Geomagnetic latitude. These emulsions were processed and aligned by the method described by Crussard *et al.*[7] and the condition of exposure is shown in Fig. 1.

In order to see whether there are cases of electron showers with anomalously large numbers of electrons occurring more frequently than predicted by the Monte Carlo calculation, these plates were scanned for parallel tracks of minimum grain density (hereafter these tracks will be referred simply as minimum tracks). The parallel minimum tracks thus found were followed from plate to plate to find their origin. This tracing was done with a 40× immersion objective and 10× eyepiece. Target diagrams including neighboring tracks were drawn at each emulsion surface to insure correct tracing, which otherwise would be quite difficult, especially when the number of minimum tracks becomes small.

In the process of tracing showers back to an origin, some of them were found to have come from outside the emulsion stack either via the brass plates used to press the stack tightly together during the exposure or directly from the air, passing through a very small quantity of packing material (wood and foam rubber). These cases were classified as *B* (brass) and *A* (air), respectively. In addition, some were found to originate from a pair of minimum tracks and some from nuclear interactions in the emulsion. The latter cases were classified as *N* (nuclear) and are omitted from this analysis. When a pair of minimum tracks starting in the emulsion was found to be the origin of the shower under consideration, scanning for further minimum tracks parallel to this pair was done within 150 μ from the pair (this is an experimental criterion imposed by the limitation of the field of view). If such additional tracks were found they were traced further in the same manner until no further possibly associated tracks in the above specified vicinity of the pair were found. These cases were then classified as *E* (emulsion). Among these *E* cases, the origin of which are most probably electron-positron pairs converted in the emulsion, those cases in which the first pair energy was lower than 1 Bev have been discarded from the later analysis. The reason for doing this is that because of the poor scanning efficiency for low-energy cases we have to expect a considerable number of them to be missed in the initial scan. Only those *E* cases with the first pair energy greater than 1 Bev were used for the study of the cascade development. As for the *B* cases, we cannot be sure about their initial conditions at the entrance point to the sensitive volume. Some of the *A* cases might actually have originated in the emulsion, for in the *A* cases we can trace them only up to a few millimeters from the outer emulsion edge, the vicinity of which is usually quite distorted and blackened by the excess deposit of silver grains. *B* and *A* cases were therefore omitted from the detailed analysis due to the uncertainty in initial conditions. Finally, some cases of unsuccessful tracing are designated as *U*. The appearance in the stack of these various cases, *A*, *B*, and *E*, is illustrated in Fig. 1.

TABLE I. Classification of results of scanning and tracing of electron showers. The numbers represent the number of cases of showers of a given origin (*B*, *A*, *E*, or *U* defined in the test) having 1, 2, 3, or ≥4 minimum tracks at the observational shower origin.

	No. of initial tracks				
Class	1	2	3	4	≥1
B	8	15	2	5	30
A	4	4	0	1	9
E	0	16	0	0	16
U	7	1	0	1	9
Total					64

[5] These points will be discussed in a forthcoming paper in which an improvement of the scattering method for high-energy electrons will be presented with experimental data (if available).

[6] By an isolated electron shower in this paper, we mean a shower of high-energy electrons in emulsion, which, under our experimental conditions, is not obviously associated with any other types of particles or events.

[7] Crussard, Kaplan, Klarmann, and Noon, Phys. Rev. **93**, 253 (1954).

TABLE II. Summary of results of *E*-type shower analysis. The first column gives the shower designation, the second the cosine of its zenith angle, the third the longitudinal distance of observation from the initiating pairs, the fourth the designation of individual pairs, tridents and compton electrons observed within the first 0.5 radiation length, the fifth the distance of the event in column 4 from the first observed pair, the sixth gives the energies of the corresponding events of column 4 (for the tridents the energy is the sum of the two lowest energy electrons) and the 7th column summarizes the information obtained after the first 0.5 radiation length.

Shower No.	Cosine of the zenith angle	Total distance followed in mm	Pair No.	Distance (mm.) from first pair	Energy (Bev)	Secondaries after 0.5 rad. unit
P-1*	0.22	100.0	P_1	0	7.0	* See II–3
			T_1	2.5	1.4	
			T_2	7.6	0.79	
			P_2	9.0	1.7	
			T_3	11.8	0.23	
P-7*	0.80	36.7	P_1	0	1.9	Total opening angle 3×10^{-3} radian P_2 (4.0 Bev) P_3 (0.23 Bev) P_4 (5.3 Bev) T_1 (1.2 Bev) and P_5 (?) are observed after 0.5 rad. length * See the text
P-10	0.88	18.9	P_1	0	15.0	T_2 (1.4 Bev) and
			T_1	12.3	0.96	T_3 (0.14 Bev)
P-12	0.90	15.0	P_1	0	3.3	
			P_2	6.4	0.38	
P-15	0.51	16.1	P_1	0	48.0	P_2 (0.20 Bev) and
			P_3	5.4	0.07	P_4 (0.70 Bev)
P-25	0.995	23.5	P_1	0	1.7	P_2 (0.16 Bev)
			P_3	13.8	0.24	
L-5	0.27	34.1	P_1	0	13.0	2 more T's and
			T_1	5.0	6.0	2 more P's
			P_2	10.0	0.03	
			T_2	12.0	23.0	
L-12	0.82	16.9	P_1	0	6.3	P_2 (0.11 Bev)
			T_1	3.3	1.3	
			T_2	5.5	0.8	
SH-6	0.88	19.4	P_1	0	90.0	T_2 (0.07 Bev)
			T_1	12.6	10.0	
SH-7	0.91	23.0	P_1	0	30.0	P_4 (0.02 Bev),
			T_1	4.2	0.07	P_5 (0.4 Bev) and
			T_2	9.5	1.6	P_6 (0.05 Bev)
			P_3	12.5	0.05	
SH-15	0.93	26.0	P_1	0	4.7	T_1 (0.33 Bev) and
						K_1 (or C_1)
SH-17	0.82	21.8	P_1	0	10.0	
			P_2	4.0	0.092	
			P_3	11.1	0.018	
SH-23	0.97	21.6	P_1	0	3.0	P_4 (0.58 Bev)
			T_1	9.7	0.15	
			P_2	13.0	0.18	
			P_3	13.3	0.15	
SH-27	0.93	29.1	P_1	0	2.9	P_3 (0.25 Bev),
			P_2	10.4	0.90	P_4 (0.021 Bev),
						P_5 (0.074 Bev),
						P_6 (0.10 Bev) and C_1
SH-29*	0.75	19.0	P_1	0	24.0	P_2 (0.11 Bev) and
			P_2	4.6	24.0	P_3 (0.042 Bev)
			P_3	9.8	0.45	* See the text
			P_4	14.3	1.5	
SH-35	0.045	15.4	P_1	0	1.0	
			P_2	3.4	0.15	
			P_3	4.6	0.085	
			P_4	11.7	0.86	
			C_1	12.4	?	
			P_5	12.5	0.02	
SH-22	0.89	13.8	P_1	0	0.65	P_2 (0.25 Bev)
			C_1	5.9	?	* See the text
			P_3	8.7	0.34	
			P_4	9.2	8.0	
			T_1	10.2	0.4	

The results of scanning, tracing and classification are presented in Table I and Fig. 2. In Table I, cases in each classification are tabulated according to their initial number of minimum tracks and in the last column the total number of cases in each class are given.

The angular distribution of the showers (θ is the zenith angle) is given in Fig. 2 and is not corrected for the geometrical factor; the reference axis was taken to be the vertical axis of the stack. There is possibility of different scanning efficiencies for different angles which is rather hard to estimate. It does not seem that much information is obtainable from the angular distribution in this type of experiment except for one feature relevant to the origin of the showers. It may be noticed that there are cases of showers coming upwards which are not observed for the high-energy nuclear showers in the same stack. This presumably indicates the secondary nature of the isolated electron showers (say, γ rays from locally produced π^0's). In 1950 the Bristol group[8] concluded from their experiment on electron pairs in emulsions exposed to the high altitude cosmic radiation that the observed γ rays of energy up to around 800 Mev could be interpreted as due to the π^0 meson-2γ decay. Though our γ-ray energy is appreciably greater than theirs, it seems reasonable to assume that our high-energy γ rays arise also mainly from the π^0 decay process.

The cases classified as *E* were then traced from their origin to follow their development in detail up to at least a half-radiation length. (This minimum observational distance is a function of the shower geometry and energy.) The energies of the secondary pairs as well as of the initial pair were estimated from their opening angles using Borsellino's[9] formula. The results are summarized in Table II, where *P*'s are pairs, *T*'s are apparent tridents, and *C*'s are Compton electrons. These secondaries were found within a cone having an opening angle of 10^{-2} radian in each case. In Table II, the first, second, and third columns give the shower number, cosine of the zenith angle and the total observed distance from the initiating pair origin. In the fourth column, pairs, tridents, and Compton electrons observed within 0.5 radiation unit are given with their distances from the first pair and their energies in the fifth and sixth columns, respectively. In the last column, the development after 0.5 radiation length is given. (1 radiation length in emulsion is 2.9 cm.)

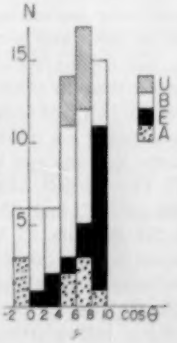

FIG. 2. Angular distribution (not corrected for geometrical bias) of electron showers. θ is the zenith angle. The labelings *U*, *B*, *E*, and *A* characterize the observational origin of the showers and are defined in the text.

[8] A. G. Carlson *et al.*, Phil. Mag. **41**, 701 (1950).
[9] A. Borsellino, Phys. Rev. **89**, 1023 (1953).

TABLE III. Comparison of observed cascade development of *E*-type showers with results of a Monte Carlo calculation. The first row represents the number of additional electrons, N_e, within 0.5 radiation length of the initiating pair origin. The rows labeled *A* and *B* represent respectively the number of observed cases having a given N_e with the convention of counting only ordinary pair electrons (*A*) or ordinary pair electrons plus trident electrons (*B*). Row *C* represents the results of the Monte Carlo calculation. The numbers in parentheses represent relative frequency.

N_e	0	1 and 2	3 and 4	5 and 6	7 and 8	≥0
A	7 (0.50)	5 (0.36)	1 (0.07)	0 (0.00)	1 (0.07)	14 (1.00)
B	3 (0.21)	5 (0.36)	3 (0.21)	1 (0.07)	2 (0.15)	14 (1.00)
C	25 (0.71)	7 (0.20)	3 (0.09)	0 (0.00)	0 (0.00)	35 (1.00)

We now compare these cascade developments with the results of the Monte Carlo calculation given in the Appendix. Table III was prepared from Table II, using secondary electrons of energy greater than 10^{-2} of the initiating pair energy. In this way, we can be fairly sure of a uniform detection efficiency for various degrees of electron number multiplication, because those electrons with energy lower than 10^{-2} of the initiating energy serve only for the purpose of efficient detection. In Table III the first row, N_e, is the number of additional electrons observed within 0.5 radiation length from the initiating pair origin and of energy specified above. The second and third rows, (*A*) and (*B*), give the number of cases having a given N_e with the respective conventions of counting only (*A*) ordinary pair electrons and (*B*) trident secondary electrons as well as the ordinary pair electrons. The fourth row, (*C*), gives the results of the Monte Carlo calculation. The Monte Carlo calculation to be compared with our data was taken from Table A-2-C of the Appendix for the following reasons. The minimum opening angle of the two γ rays from a π^0 meson is equal to $2/\gamma\beta$ (γ and β refer to the primary π^0 meson); this means, for example, that the minimum lateral separation of the two γ rays from a 14 Bev π^0 meson at a distance of 1 cm from the decay (the conversion length in the emulsion is 3.75 cm) is 200 μ and is even larger for lower energy π^0's. By our tracing conventions, it seems appropriate to assume that the other γ ray is outside the investigated area. In fact, the observed energy distance relations in each shower are quite consistent with this assumption except for two cases which were not included in Table III. They are *SH*-22 and *SH*-29 of Table II. In *SH*-22, both pairs *P*1 and *P*3 must be of a primary nature and in *SH*-29 pairs *P*1 and *P*2 must also be of such a nature because the latter pair is greater in energy than the corresponding first pair (*P*1) in each case. We also note that the further development of shower *P*-7 beyond a half-radiation length seems to indicate the existence of at least three photons initially present for similar reasons. *SH*-22 and *SH*-29 can be understood as originating from the 2γ decay of a single π^0 meson and in these two cases both γ rays contribute to the development. The energies of the two high-energy γ rays in *SH*-29 and their angular separation are quite consistent with this assumption; in *SH*-22, no accurate measurement of the angular separation can be made. As to the shower *P*-7, the existence of more than two photons will be discussed later in connection with the similar nature of shower *P*-1.

The results given in Table III seem to indicate agreement between the observed development and the Monte-Carlo calculation if we take only pairs (*A*) and not apparent tridents. If we include the apparent tridents (*B*) the distribution seems to extend too far in favor of large electron numbers. The assumption of a low shower detection efficiency, as low as $\frac{2}{3}$ which is rather improbable in the procedure described above, does not seem to alter this conclusion. Even though the statistics are poor in both the experimental data and the Monte Carlo results, they seem to indicate that the majority of the apparent tridents may actually be genuine tridents which were not included in the Monte-Carlo calculation. This result was suggested by a similar analysis in a previous experiment[2] (referred to as I).

It is instructive at this point to comment about the cascade development observed in I. The situation there is rather different because of the much higher shower energies and the fact that it occurs in a penetrating shower. When we see a high-energy electron pair in the narrow cone of a penetrating shower, the most reasonable assumption is to assume that this arises from the conversion of a γ ray from the decay of a π^0 meson produced in the primary act. The very high energy of these π^0 mesons as estimated from the opening angle of the cone and the rather short observational length at our disposal requires us to assume that another high-energy γ ray is most probably spatially associated with this high-energy electron pair. (The opening angle of 2 γ rays from a 200-Bev π^0 meson is $\sim 1.4\times 10^{-3}$ radian.) The energy-distance relations of the actually observed cascade development are quite consistent with this idea. Therefore, the initial conditions for these electron cascade showers should be taken as one converted electron pair plus one photon incident at the first high-energy pair origin. Further decomposition into single-photon-initiated showers was not possible in I due to the high degree of the two γ-ray collimation.

The cascade development with the above initial conditions was studied using 8 groups of electron pairs in I which were so located that they could be followed at least 0.5 radiation length from the first pair in each group. The results are given in Table IV and are compared with the results of the Monte Carlo calculation given in the Appendix for the same initial conditions. The numbers in parentheses in the second, third, and fourth rows represent the percentage occurrences. In the second row, Case *A*, only the electrons of the ordinary pairs were taken whereas in Case *B* all electrons

(ordinary pair electrons and secondary electrons from apparent tridents) were counted. The cut-off energy for acceptance ($10^{-2}E_0$) was chosen to insure good detection efficiency and to agree with the conventions taken in the Monte Carlo calculation.

Because of the small sampling, we cannot obtain any firm conclusions except that the inclusion of the apparent trident electrons, Case *B*, seems to make the distribution extend to larger electron numbers, slightly more than expected from the Monte Carlo results in which the trident processes were not taken into account. The poor statistics in the experimental results come from the superposition of the two photon showers while for the Monte Carlo results they arise from the fact that the given initial conditions could only be met by superimposing the results from 100 single-photon-initiated showers, since the original calculation had been done only to this extent.

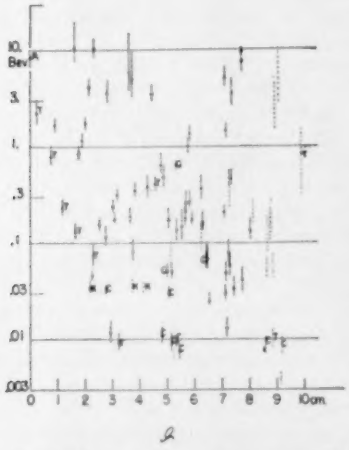

FIG. 3. Energy-distance plot of electron secondaries from shower *P*–1. Unlabeled points are pairs. *T* means trident, *K*, knock-on and *C*, Compton electron. *Q* is a pair conversion in the field of an atomic electron.

The problem of the trident process and its relationship to the general question of the validity of the Bethe-Heitler[10] high-energy quantum electrodynamics will be discussed later.

3. ANALYSIS OF SHOWER *P*–1

Because of the anomaly in the energy-distance relation exhibited in Table IV for showers *P*–1 and *P*–7, one of them, *P*–1, due to its very favorable geometry, was investigated in more detail. This shower is inclined at 78° with respect to the vertical axis of the stack and lies almost parallel to the emulsion surface. The beginning of this shower consists of two electrons entering plate *S*104 from the glass side at a point 8.25 mm from its edge. After 48.1 mm traversal in the same plate it entered plate *S*103, which was the neighboring quarter of the same emulsion before cutting, and then entered plate *S*93 which is part of the next emulsion. Every effort to trace these two electrons back into *S*114 (their continuation from *S*104) failed. A detailed investigation of the emulsion showed that the portion of tracks in the upper layer of the emulsion was removed in the process of wiping off the surface silver deposit after development. This layer is about 5μ in depth and because of the very good parallelism between this shower and the emulsion plane, this depth gives a projected length of about 1.8 mm. Therefore, it is almost certain that the pair was created in the upper layer of *S*114 and entered into *S*104 as two separated tracks. The portion of the track thus wiped out should be less than 1.8 mm in length. There is another fact which supports this assumption; that is, there was no appreciable amount of matter before the entrance to the emulsion except for a negligible quantity of wood and foam rubber.

In order to insure good efficiency for detecting secondary events in following the development of this shower, scanning was done at every 1 mm for tracks of minimum grain density using 40× immersion objective and diagrams were made at these points. Every minimum track thus found and recorded in the diagrams was now traced back and forth to get a one to one correspondence between the tracks in each diagram. In this way, all minimum tracks were identified with respect to their origin and their genetic relation to the others. The energies of these identified tracks were measured by their multiple Coulomb scattering. When there was any possibility of noise or distortion, the relative scattering method described in I[11] was used. The results of these measurements are given in Fig. 3. The abscissa is the distance from the entrance point of the first two electrons to *S*104 and the ordinate is the γ-ray energy of each pair or the electron energy in the case of a

TABLE IV. Comparison of observed cascade development of showers from I with results of a Monte Carlo calculation. The first row represents the number of additional electrons, N_s, within 0.5 radiation length of first pair. The rows labeled *A* and *B* represent respectively the number of observed cases having a given N_s with the convention of counting only ordinary pair electrons (*A*) or ordinary pair electrons plus trident electrons (*B*). Row *C* represents the results of the Monte Carlo calculation with appropriate boundary conditions (1 pair plus an incident γ ray). The numbers in parentheses represent relative frequency.

	No. of additional electrons $E \geq 10^{-2}E_0(\gamma)$ within 0.5 rad. unit						
	0	1	2	3	4	>4	≥0
Case *A*	3 (0.38)	0 (0)	3 (0.38)	1 (0.12)	1 (0.12)	0 (0)	8 (1.00)
Case *B*	3 (0.38)	0 (0)	0 (0)	2 (0.25)	2 (0.25)	1 (0.12)	8 (1.00)
Table A–3–C	1625 (0.46)	195 (0.06)	1010 (0.29)	295 (0.08)	244 (0.07)	131 (0.04)	35 ×100 (1.00)

[10] H. Bethe and W. Heitler, Proc. Roy. Soc. (London) **A146**, 83 (1934).

[11] This method was first used by Lord, Fainberg, and Schein, Phys. Rev. **80**, 970 (1950).

Compton or knock-on electron. The trident energy has been taken to be the sum of the energies of the two lower energy electrons of the emerging electrons. The statistical probable errors in the scattering measurements are indicated by vertical lines. Some of the low-energy electrons were not measured and in these cases rough estimates were made on the basis of the opening angle and are indicated by vertical dotted lines with the estimates obtained by using Borsellino's[9] and Stearns'[12] formula as end points.

In addition, a survey was made to find any possible event associated with this shower. For this purpose, scannings were made across the shower axis for tracks parallel to the shower at distances 1 cm apart longitudinally and up to 1.2 cm in width on both sides of the shower axis using a 40× objective. In this scanning a high-energy pair was found which originated in the same emulsion ($S104$) 5332 μ away from the shower axis. The opening angle and the projected inclination of this pair with respect to the shower axis of P–1 were found to be 0.82×10^{-3} and $(1.30\pm0.04)\times10^{-2}$ radian, respectively. This pair is also almost parallel to the emulsion plane and its opening angle gives an energy estimate of 1.8 or 5.9 Bev using Bosellino's or Stearns' formula, respectively. If we admit that this pair comes from the same primary event which gave rise to shower P–1, we can estimate the position of this primary event as 41.0 ± 1.0 cm away from the entrance point of shower P–1 to plate $S104$.

The total opening angle of shower P–1 as viewed from the entrance point to $S104$ is 2.8×10^{-3} radian for all pairs and 0.82×10^{-3} radian for pairs of energy greater than 1 Bev observed within four cm from the entrance point. The total visible energy of this shower up to 10 cm from the origin is 80 Bev. This value is obtained by adding the energies of individual pairs as measured by scattering or by opening angle and hence does not include the energy loss of electrons after the terminal points of the scattering measurements. This procedure overestimates the instantaneous visible energy but may be compensated for by the invisible energy carried in the form of γ rays and the actual total energy will not be much different from ~100 Bev.

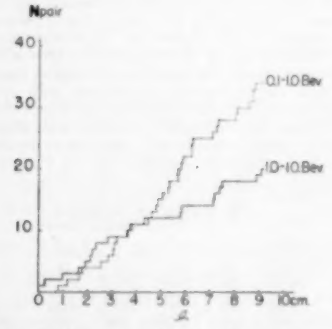

FIG. 4. Integral electron numbers for shower $P-1$ as a function of distance from the origin for electrons in the energy intervals 0.1–1 Bev and 1–10 Bev.

[12] M. Stearns, Phys. Rev. 76, 836 (1949).

The anomaly in the energy-distance relation exhibited in Fig. 3 seems to suggest that at least 4 γ rays were present initially. This conclusion should not and does not rest upon the large number of electrons observed, because, as was seen in the previous section, as far as the number of electrons is concerned, this shower is well inside the fluctuation tail if the initial energy is large enough (at least around 100 Bev). The energy of the initial pair give in Fig. 3 has been estimated in the following way. One of its electrons ($P1^2$) was measured directly by the scattering method using 500 and 1000 μ cells, both giving quite consistent energies, their mean being $1.30_{-0.28}^{+0.48}$ Bev. The other track of the initial pair ($P1^1$) made a trident after 2.46 mm. The scattering measurements on the portion of $P1^1$ before producing $T1$ gave a lower limit of 5 Bev. The energies of $T1^1$ and $T1^3$ were measured to be $0.93_{-0.20}^{+0.34}$ and $0.45_{-0.11}^{+0.12}$ Bev, respectively, by the relative scattering method,[11] using 250 and 500 μ cells. The energy of $T1^2$ was still too high to be estimated and it gave rise to a further trident, $T2$, after 5.117 mm traversal. $T2^1$ and $T2^3$ were measured in a similar way; $T2^2$ was found to be about 5 Bev and it gave still a third trident, $T3$, after 4.13 mm. The highest-energy track of $T3$, $T3^3$, was consistently measured to be 4.9, 4.0, and 4.9 Bev using 500, 1000, and 2000 μ cells, respectively. The energy of $P1^1$ was considered to be the sum of all these secondaries (tridents) and is thus $7.1_{-1.1}^{+1.4}$ Bev. Of course, there is a possibility that electron $P1^1$ had initially an energy of about 100 Bev and became an electron of about 5 Bev by emitting quite a number of γ rays including those higher energy ones of from 5 to 10 Bev whose conversion to pairs accounts for the energy distance anomaly. However, this is a very drastic behavior when we recall that the available distance is about 0.3 radiation length for the electron energy to go from 100 Bev to 5 Bev and that this is not accomplished by the emission of single γ ray of about 95 Bev but by the emission of a number of γ rays of rather small energy as compared with the initial energy. Therefore, it seems more likely to assume that there were at least 4 γ rays of energy around 10 Bev present initially. We also note here that the direction and the energy of the pair found about 5 mm away from shower P–1 would give about 22 Bev or less for the initial single γ-ray energy of shower P–1 if we assume these two pairs are due to the two γ rays from the same π^0-meson decay. This possibility is thus excluded and we must consider that they (pair P–1 and the separated correlated pair) are due to different γ-ray sources, possibly different π^0 mesons.

Let us now ask about the meaning of this event. For the sake of illustration, imagine that we had observed the shower discussed in I without any associated charged penetrating particles. Then we would have concluded

from Fig. 2 of I, by arguments similar to those presented above, that there must have been at least several γ rays present initially on the basis of the energy distance relation and the total energy of this apparently anomalous shower would have been estimated to be around 1000 Bev. However, when we look at the total opening angle of this shower it is found to be 1.1×10^{-2} radian as compared with 2.8×10^{-3} radian for shower P–1 whose total energy is one order of magnitude less than that of this fictitious anomalous shower. Therefore, even if we could explain this fictitious anomalous shower in terms of a fluctuation from the average prediction of charge independence as applied to multiple meson production, the fluctuation giving rise to multiple production of neutral mesons without charged ones, it is much more difficult to apply this kind of argument to shower P–1. The angle of the cone including electron pairs of energy higher than 1 Bev in shower P–1 was 0.82×10^{-3} radian. Since the minimum opening angle of two γ rays from a 20-Bev π^0 meson is 1.4×10^{-3} radian, such a source for these γ rays does not seem quite compatible with the observed data. This argument, however, does not hold if the actual energy of the initiating pair was much higher than that estimated and a fluctuation of the type mentioned previously in the number of emitted γ rays within the first $\frac{1}{4}$ of a radiation length had occurred; this is not entirely impossible. However, when we recall the existence of another possibly anomalous case, P–7, this latter explanation seems less probable. (Shower P–7 exhibits the same anomaly in the energy distance relationship and in the total opening angle as does shower P–1.)

Next, we consider the other features of the shower development of P–1. In Fig. 4, the numbers of electrons of energies from 1 to 10 Bev and from 0.1 to 1 Bev are plotted against their distances from the initial observation point of the first two electrons. What we can say from this figure is that the effect of pairs of the third generation seems to become important at about 5 cm (1.7 radiation lengths) and this is a quite reasonable behavior in view of the ordinary cascade shower theory. We might also notice that there is a bump in the curve of the 1.0–10 Bev electrons over that of 0.1–1.0 Bev group at small distances, where we should expect the same behavior for the two curves if the electrons of both categories are cascade secondaries of the same original electron of much higher energy. The electron pairs, tridents, and Compton electrons of energy smaller than 0.1 Bev were not considered here because the detection efficiency for these low-energy electrons is thought to be poorer than for the higher energy ones. However, from Fig. 3 we can safely say that we cannot neglect the Compton electrons when we are dealing with γ rays of energy smaller than 100 Mev. In addition, the photonuclear reaction will not be negligible if we have to take the Compton effect into account because of the so-called giant dipole maximum of the photonuclear reaction around 20 Mev. To see the effect of this, a strip of 500 μ width with shower P–1 as its central axis was scanned for stars, including low-energy one-prong proton stars and this scan was compared with the background taken from randomly chosen strips of the same width. The results obtained were 4.4 ± 1.7 and 10.8 ± 4.1 stars per 1 cm length of the strip for the regions 0 to 4 and 4 to 8 cm from the origin compared with 5.3 ± 1.0 for background stars in an equal random area. Even though the statistics are poor the low-energy photonuclear effect seems to be observable and this is consistent with the conclusions drawn from Fig. 4. The projected lateral distributions of electrons of energy greater than 100 Mev at 0.5, 1.0, 1.5, 2.0, 2.5, and 3.0 radiation lengths from the observational origin of the shower ($\sim$0.06 radiation length from the first pair origin: see the beginning of this chapter) are presented in the form of histograms in Fig. 5 (parts 1, 2, 3, 4, 5, and 6, respectively). The two-dimensional projection of shower P–1 on a plane parallel to the emulsion surface (which is approximately parallel to the shower axis) was divided into strips of equal width (24.3μ) parallel to the projected shower axis, and the number of electrons of energy greater than 100 Mev in each strip is indicated by the number of blocks (the width 24.3μ was taken for observational convenience). The horizontal lines at the bottom of these histograms indicate the scanned area at each distance. Numbers in parentheses in each of the figures are the number of electrons of energy greater than 100 Mev which were produced within the observed area but were scattered out of it before reaching the distance under consideration. These numbers give a crude

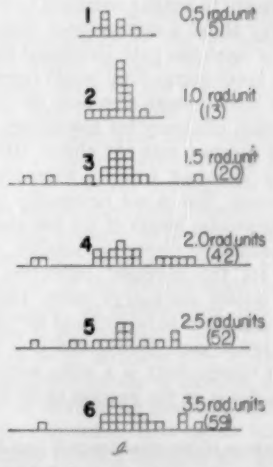

FIG. 5. Lateral distribution of electrons from shower $P-1$ with energy >0.1 Bev. Each histogram is labeled with the longitudinal distance in radiation units from the origin. The numbers in parentheses refer to the number of electrons of energy >100 Mev produced in observed area but scattered out before reaching distance given above. Each block in the histogram is 24.3 μ wide perpendicular to the shower axis.

idea of the extent that the lateral spread of the cascade development is affected by the electron scattering and the emission angle of γ rays of a tertiary nature.

4. TRIDENT PROCESS

The importance of the trident process in the high-energy region was suggested in I. We will consider the problem again in this chapter with the additional data obtained from the analysis of isolated showers.

From the isolated nonanomalous showers investigated in Sec. 2, we get

$$\sum t_i = 20.6 \text{ radiation lengths.}$$
$$\langle t \rangle = 0.395 \text{ radiation length.}$$
$$\langle E_i \rangle = \sum t_i E_i / \sum t_i = 8.0 \text{ Bev } (E_i \geqq 1.0 \text{ Bev}),$$

where t_i and E_i are the track length and the energy of individual electrons of energy greater than 1 Bev. The results on trident formation from these showers are presented in Table V. Here E in Column 1 is the energy of the pair or of the trident (the sum of the two lower energy electrons of the emerging three is taken for the trident energy). Column 2 gives the number of observed apparent tridents, 3 the number of observed bremsstrahlung pairs, 4 the corrected number of tridents by the method described in Appendix B of I, and 5 the resulting mean free path in radiation lengths (2.92 cm in emulsion) for trident production.

It must be emphasized that in the type of correction we have applied to the data, the low detection efficiency for low-energy pairs, the inadequacy of the assumption of complete screening and asymptotic conversion length for low-energy photons and the intervention of other effects, e.g., Compton scattering or photonuclear effects, make it necessary to restrict ourselves to those electron pairs of energy above a certain lower limit. One might think that the mean free path for trident production for a sufficiently lower energy limit would represent a lower limit for the trident mean free path on the basis of a poorer detection efficiency for low-energy bremsstrahlung pairs in contrast with the almost 100% detection efficiency for apparent tridents irrespective of their energy. However, this is not necessarily true, because the longer conversion length of the low-energy photons makes the calculated correction smaller, which would compensate for the increased correction due to the inclusion of missed low-energy pairs. The lower limit in this table was taken to be 10^{-2} and 10^{-3} of the initiating pair energy in each shower and it is felt that the former lower energy limit is a more suitable one. (In energy units this is on the average of 80 Mev.)

TABLE V. Results on trident mean free path from E-type showers.

1 Energy lower limit	2 No. of apparent tridents	3 No. of B. S. pairs	4 Corrected No. of tridents	5 m.f.p. for trident production
$E \geq 10^{-2}E_0$	11	10	6.7	$3.1_{-0.8}^{+1.4}$
$E \geq 10^{-3}E_0$	12	15	5.6	$3.7_{-1.0}^{+2.0}$

Additional data can be obtained from shower P–1. We use the first 4.8 cm of this shower development (the reason for the restriction to this portion is twofold; this part is the most thoroughly measured and if we take too long a path we cannot use the energy values determined by scattering measurements performed on the first 1 or 2 cm of each electron track and would have to take into account the electron energy degradation due to bremsstrahlung), and find:

$$a\begin{cases}\sum t_i = 5.85 \text{ radiation lengths,}\\ \langle t \rangle = 0.835 \text{ radiation length,}\\ \langle E_i \rangle = 4.75 \text{ Bev } (E_i \geqq 2.5 \text{ Bev}),\end{cases}$$

or

$$b\begin{cases}\sum t_i = 14.2 \text{ radiation lengths,}\\ \langle t \rangle = 0.65 \text{ radiation length,}\\ \langle E_i \rangle = 3.3 \text{ Bev } (E_i \geqq 1.0 \text{ Bev}).\end{cases}$$

The results are presented in Table VI which is similar in nature to Table V. The difference between a and b in Table VI is due to the difference in the lower limit of electron energies accepted as a primary track for trident production, consequently the difference in the average electron energy of the primary electrons, $\langle E_i \rangle$.

All the results on tridents are presented in Fig. 6, in which the data from I is also given as well as the results of Bhabha's[13] calculation. The results obtained in Appendix B of I (the correction for B.S. pairs) were revised in the following way. The electron deflection at the instant of bremsstrahlung has been neglected and this amounts to dividing B–9 of I by $\sqrt{2}$. The numerical factor to be used in B–9 was taken to be the one corresponding to the average γ-ray energy for $E\gamma \geq 10^{-2}E_0$. This leads to a change of the factor given in I–B from 0.67 to 0.72. After these revisions we obtain $5.4_{-1.9}^{+8.2}$ and $2.2_{-0.7}^{+2.0}$ radiation lengths for average energies of 4.2 and 50 Bev, respectively of I. The previous results in I were 4.5 and 1.1 radiation lengths, respectively. The revised curves are given in Fig. 7.

Figure 6 seems to indicate a systematic deviation of the experimental mean free path for trident production below that of Bhabha's result which gives the shortest mean free path among all the theoretical calculations of this process. Let us now investigate the situation more closely. First of all, we must recognize that the calculated correction of B.S. pairs in Appendix B of I after the above revision is an overestimate in that the deflection of the primary electron at the instant of γ-ray

TABLE VI. Results on trident mean free path obtained from electrons of shower P–1.

1 Energy lower limit	2 No. of apparent tridents	3 No. of B. S. pairs	4 Corrected No. of tridents	5 m.f.p. for trident production
$E \geq 10^{-2}E_0$	4	13	2.4	$2.4_{-1.0}^{+4.3}$
$E \geq 10^{-3}E_0$	5	14	3.2	$4.4_{-1.5}^{+4.3}$

[13] H. Bhabha, Proc. Roy. Soc. (London) **A152**, 559 (1935).

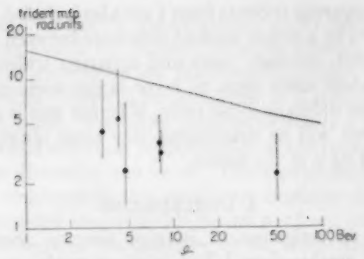

FIG. 6. Experimental results on trident mean free path as a function of energy. The solid line is that calculated by Bhabha.

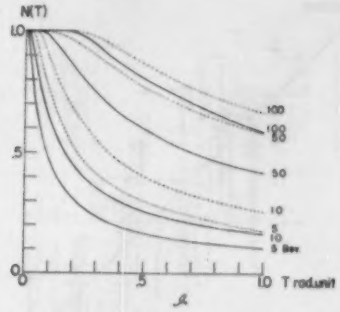

FIG. 7. Calculated correction curves for the trident process (solid curves obtained using the rms emission angle of Stearns: dotted curves represent a zero emission angle). Details of the calculation appear in the Appendix of I.

emission and the energy loss of this electron have not been included. The latter effect, the energy loss of the primary electron, can, within the portion of the electron track on which the energy measurements have been made, partially be taken into account. That is, we use the energy value as estimated by the scattering measurement in choosing a particular correction curve from Fig. 7, since the magnitude of the correction is determined by both the average γ-ray emission angle and the average electron scattering over the observed distance and not directly by the initial instantaneous energy of the primary electron. This argument also applies roughly to the energy estimation by the opening angle determination together with the assumption of energy equipartition, because the separation of the two electrons at a certain distance includes the effect of the electron scattering and the electron energy loss up to this distance. Now, there may be an argument against the use of a Gaussian distribution with the root-mean-square angle of emission as calculated by Stearns for the angular distribution of the emitted γ ray. It is true that there is no direct experimental verification of Stearns' results, while the most probable opening angle of a converted pair as given by Borsellino has been verified experimentally for energies up to 800 Mev.[14] However, in our problem of the bremsstrahlung pair correction to the trident process, we are dealing with the behavior of an ensemble of electrons and photons as a whole and the root mean square angle is better suited for the purpose of representing the whole distribution. As for the approximate use of a Gaussian distribution for the true angular distribution of emitted γ rays we have the following considerations. Although there is no direct calculation of this distribution, we can attempt an estimate of how well its salient features are accounted for by a Gaussian by considering the similarity of bremsstrahlung to pair production together with the results given by Borsellino and Stearns. The true angular distribution would probably be similar to that given by Borsellino for the opening angle distribution of converted pairs. The errors introduced by the use of a Gaussian distribution can be estimated in the following way. We can calculate the mean distance which the emitted γ ray has traveled before it is converted into an electron pair within the observational distance of t radiation lengths and from equation B–4 of I we find it to be about $0.3t$ in the approximation of small t. This means that the important contribution comes from angles smaller than 0.43×10^{-4} radian for an observational distance of 0.5 radiation length and an observational accuracy of 0.2 μ. The percentages of the distributions below this angle are 37% for a Gaussian-type and 40% for a Borsellino-type distribution for an electron energy of 50 Bev. For electron energies smaller than 50 Bev, the Gaussian-type distribution has more percentage within the above angle than the Borsellino-type distribution does; this is because the Guassian type distribution has a nonzero valve at zero angle while the Borsellino type distribution goes to zero with zero angle. Therefore, in our energy region, it seems almost certain that the use of a Gaussian function for the angular distribution of emitted γ rays does not cause an underestimation of the bremsstrahlung correction to the trident process. We also note that the root-mean-square angle for our energy region is much smaller, by at least a factor of 10, than the angle in which our observations have been restricted, so that the number of γ rays converted outside the observed area would not be sufficient to affect the magnitude of the correction appreciably. (See Appendix B of I.)

The remaining problem is to what extent we can trust the energy values as determined by scattering measurements, or by the opening angle determination of converted pairs, as representing the true initial energy. Figure 6 shows that if we want the experimental data to be in harmony with Bhabha's results, an over-all underestimation of electron energy by at least a factor of 30 must be assumed. Although this is not absolutely impossible, it is rather hard to admit that all of these electron energies are systematically underestimated by a factor of $\sim$30 when we consider that our lower energy limit is 1 Bev. We cannot attribute the energy underestimation to a few electron tracks, for we have seen in Table II that the tridents are rather uniformly distributed among the isolated showers considered there and the short observational

[14] K. Hintermann, Phys. Rev. 93, 898 (1954).

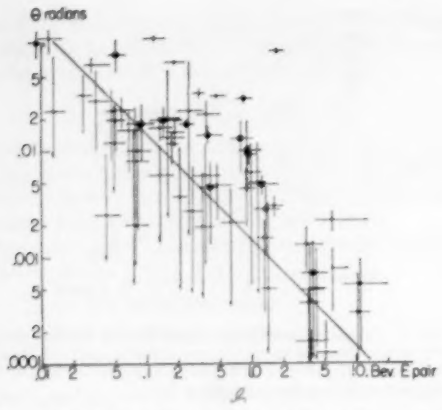

FIG. 8. Opening angles of pairs (solid circles) and tridents (open circles) plotted against their energy as determined by multiple scattering.

length makes it difficult for this discrepancy to be due to a few cases of very high-energy showers. Therefore, it seems rather more probable to conclude that there actually exists a discrepancy of a factor of about 2.5 between the experimental data and the theoretical mean free path for trident production (as calculated by Bhabha).

Additional information is obtained from the opening angle distribution of electron pairs and tridents. This is presented in Figs. 8 and 9. In Fig. 8, the opening angles of individual pairs are plotted against their energies as determined by the scattering measurement. The horizontal lines indicate the statistical probable errors in the scattering measurements while the vertical lines give the uncertainties in the opening angle determination which have been taken to be due to the root-mean-square deviation of the electrons from their original directions as determined by scattering measurements. In Fig. 9, the results are presented following Hintermann[14] in a form directly comparable to Borsellino's calculation: that is, individual cases have been expressed in terms of Borsellino's characteristic angle $W_0=4km c^2/(E_+E_-)$ where k, E_+, E_-, and mc^2 are the energies of primary photon, positive electron, negative electron and the rest mass of the electron respectively. The good agreement with Borsellino's results, which has been verified previously by K. Hintermann for energies below some 800 Mev, is thus apparently extended to the higher energy region of around 10 Bev. This, however, does not necessarily imply that both types of energy measurements give an accurate initial energy, for the effect of bremsstrhalung would be expected to cause a systematic error in favor of an energy underestimation in the high-energy region for both types of measurements. In Figs. 8 and 9, the apparent trident cases, of which a considerable fraction are expected to be genuine ones (from the preceding analysis), are also plotted considering the lower energy two of the emerging electrons as the produced pair. (The apparent tridents from I are also included.) There seems to be a rather marked difference between the two categories, ordinary pairs and apparent tridents; i.e., the trident cases seem to favor larger opening angles than the ordinary γ-ray pairs. Whether this is actually so or not will be determined only upon obtaining increased data in the future.

5. CONCLUSIONS

The investigation of isolated electron showers of energy greater than 1 Bev in photographic emulsions exposed to the high-altitude cosmic rays has revealed the following results.

(1) Out of 16 isolated electron showers with an initial pair energy $\geqq 1$ Bev, 12 cases were found to be consistent with the assumption that they originated from a single γ ray (most probably from a locally produced π^0 meson), and 2 cases were consistent with the assumption that both γ rays from the π^0 decay contributed to the observed development.

In 2 cases, however, it seems quite difficult to reduce the required number of primary photons down to 2. One of them in fact seems to require at least 4 incoming γ rays of comparable energy ($\sim$10 Bev). The very narrow angular spread of these γ rays for their energy makes it difficult to explain this event as due to a nuclear production mechanism for π^0 mesons as the γ-ray source. There might be raised the question of whether this apparently anomalous electron shower could be interpreted in terms of the decay of a long lived neutral particle into several π^0 mesons: e.g., $\tau^0 \rightarrow 3\pi^0$ or $\theta^0 \rightarrow 2\pi^0$. In this way, we could explain the isolation of this event from other charged particles as well as the number of initial γ rays responsible for the event. However, the lower limit of the angular spread of the electron shower is fixed by the spread of the 2 γ rays from the π^0 decay rather than that of the π^0's from the decaying neutral particle (no known particle has been observed decaying directly into γ rays other than the π^0 meson). The minimum angular separation of 2 γ rays from a 20-Bev π^0 meson is 1.4×10^{-2} radian compared with the observed 0.82×10^{-3} radian. Therefore, the production of γ rays through the intermediary of π^0 mesons seems to be excluded.[15]

(2) The experimental mean free path in emulsion for the trident process, direct pair production by an electron, seem to be smaller by a factor of at least 2.5 than that predicted theoretically by Bhabha. In order to bring the experiment into harmony with his calculation, it would be necessary to admit a systematic underestimation, by a factor of about 30, of the initial electron energies by the scattering method, or by opening angle determination in the energy region observed (1 Bev to 15 Bev). There are two kinds of possible

[15] A mechanism proposed by S. Hayakawa in 1949, radiation accompanying the deceleration of primary charged particles [Phys. Rev. 75, 1760 (1949)], may be recalled in this connection. A charge exchange scattering of a very high-energy proton ($\sim$1000 Bev) with a neutron, or a π^- with proton, would probably give rise to this kind of event by his mechanism.

sources of error leading to a systematic under-estimation of energies. One is the inadequacy in the formula which relates the experimentally observed quantities to the energy value. This will be considered in a forthcoming paper in detail. The other possible source is a purely experimental one; that is, calibration of eyepiece scales, emulsion distortion and so on. The experimental procedures employed in this work were carefully checked and no possible source of this nature has been found to affect the results. Furthermore, if we admit that the majority of the energies were underestimated by a large factor, say 15, we should have observed the two photon primary nature in most of the isolated electron showers in Sec. 2 whereas it was observed in only 2 out of 14 cases. Therefore, it seems rather difficult to accept an explanation in terms of an overall energy underestimation by a large factor.

If this discrepancy is confirmed by increased experimental data with improved techniques of energy measurement, its inference would be quite embarrassing. Namely, we have assumed the validity of the Bethe-Heitler conversion length[10] and the angular distribution of emitted γ rays in deriving the correction to be applied to the observed number of apparent tridents; the result obtained is incompatible with Bhabha's calculation which had been carried out in the same theoretical framework as the Bethe-Heitler theory.[10] Thus in order to obtain agreement between the experimental data and the perturbational calculation, it would be necessary to admit a shorter conversion length or a smaller root mean square emission angle than those calculated on the above basis. This would probably mean that the assumption that the lowest order processes pertaining to the phenomena under consideration (bremsstrahlung and pair production in the cascade development) are larger than the higher order processes (such as trident process, simultaneous two γ-ray emission in bremsstrahlung or pair production with the emission of additional γ rays) by the appropriate factors in the perturbation expansion coefficient is no longer well justified in the high-energy region. In fact, if the trident cross section is larger than estimated by the perturbation calculation, there is no *a priori* reason for neglecting, for example, radiative electron-pair production (production of an electron-positron pair with an accompanying photon by an incident photon) as compared with ordinary pair production since this process is of the same order in the perturbation expansion as that of the trident process. In addition, if radiative pair production is not entirely negligible in the high-energy region, it will make the observable γ-ray conversion length shorter and tend to bring the experimental trident cross section in conformity with Bhabha's result.

There is another possible source which might lead to a shorter γ-ray conversion length; that is, if by any reason the screening by atomic electrons is not complete, the lowest order cross sections would increase with energy instead of approaching a constant value.

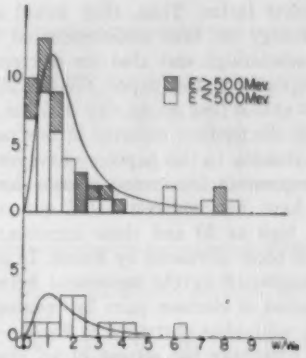

FIG. 9. Comparison of theoretical and experimental opening angle distributions for pairs (upper) and tridents (lower). W/W_0 is the pair energy in units of $W_0=4km_0c^2/(E_+E_-)$, Borsellino's characteristic angle.

We find approximately that in order to have an agreement between the experimental data on the trident process and the results given by Bhabha, it would be necessary to have a smaller conversion length than that given by the Bethe-Heitler theory by a factor of about 1.5 if the angular distribution is unchanged.

All these considerations, however, are tentative in that they require further experimental data with increased statistics combined with more refined techniques of energy measurement for high-energy electrons.

(3) Some additional information was obtained about the opening angle of electron paris and the verification of Borsellino's results was apparently extended up to around 10 Bev. The trident process seems to favor opening angles larger than those characteristic of ordinary electron pairs of equal energy.

In conclusion, almost all the difficulties will be avoided if we can obtain a more reliable method of energy estimation than available at the present time.

We wish to thank Professor K. Greisen for some discussions concerning the trident process and our method of correction; we also would like to express our appreciation to Miss B. Hull and to Mrs. J. Rutherford, Jr. for their scanning assistance, and to thank the Aero Medical Field Laboratory, Holloman Air Force Base for arranging the balloon flight.

Note added in proof.—Recently Peters and his coworkers (private communication) have investigated the limitations of the multiple Coulomb scattering method as applied to nuclear emulsions. They report the existence of an inherent emulsion noise, independent of distortion, presumably arising from small scale dislocations, that gives rise to a spurious scattering which sets an effective upper limit of approximately 1 Bev for the meaningful measurement of momenta of singly charged particles. They would thus ascribe the values of energy determined by the application of the conventional method (their criticism does not apply to the relative scattering method) as spurious and having no meaningful relation to the true energy, the true energy of a given track in general being higher by some

indeterminate factor. Thus, they would say that in fact the energy has been underestimated (due to the spurious scattering) and that no discrepancy exists such as reported in this paper. We feel however that we cannot at this time accept this criticism as a resolution of the discrepancy reported in this paper for the following reasons. In this paper we have set forth some general arguments concerning reasons for our belief that we have not underestimated our energy by a factor as high as 30 and these arguments are independent of those advanced by Peters. In addition this view is supported by the agreement between energy determination of electron pairs by opening angle and scattering method as portrayed in Fig. 8—though this does not constitute the setting of an absolute scale, we believe it is a strong indication of the fact that the scattering measurements are not subject to the random uncertainties implied by Peters' work. In addition we have done some preliminary work on this (spurious scattering) problem in our laboratory and we do not find the effects described by Peters and his co-workers.

APPENDIX. MONTE CARLO CALCULATION OF CASCADE SHOWERS

We present here a set of tables representing the results of a Monte Carlo calculation on the one-dimensional number development of the electron-photon cascade. The original results, the cascade development of 100 single γ-ray initiated showers was done by one of us (MFK) in collaboration with Dr. D. M. Ritson under approximation A of Rossi and Greisen.[4] 100 showers were constructed and tabulations made of the number of showers having a given number of electrons, N_e, of energy greater than αE_0, E_0 = initial photon energy, in intervals of 0.1 radiation length from the origin to 1 radiation length. The results for the single photon initiated showers are presented in Tables A–1–a, A–1–b, and A–1–c, where a, b, and c mean respectively $\alpha = 10^{-4}$, 10^{-3}, and 10^{-2}.

Tables A–2–a, A–2–b, and A–2–c represent the development for two incident electrons and were obtained from Tables A–1 by using those cases in which the primary photon was converted within 0.5

TABLE A–1–a. ($E \geq 10^{-4}E_0$).

t \ N_e	0	1	2	3	4	5	6	7	8	9	10	11	12	13	14	15	16	17	18	19	20	21	22
1.0	47	0	20	1	8	1	3	2	5	3	2	2	0	1	2	0	1	1	0	0	0	1	0
0.9	52	0	17	2	6	3	5	3	1	4	2	0	2	1	1	1	0	0	0	0	0	0	0
0.8	57	0	18	1	6	3	5	3	2	1	2	1	0	0	1	0	0	0	0	0	0	0	0
0.7	61	0	16	3	7	1	3	3	3	0	1	1	1	0	0	0	0	0	0	0	0	0	0
0.6	62	0	19	3	7	2	1	3	1	0	2	0	0	0	0	0	0	0	0	0	0	0	0
0.5	65	0	23	3	2	2	2	0	2	0	1	0	0	0	0	0	0	0	0	0	0	0	0
0.4	72	0	19	1	5	1	1	0	1	0	0	0	0	0	0	0	0	0	0	0	0	0	0
0.3	77	0	19	1	3	0	0	0	0	0	0	0	0	0	0	0	0	0	0	0	0	0	0
0.2	79	0	20	0	1	0	0	0	0	0	0	0	0	0	0	0	0	0	0	0	0	0	0
0.1	87	0	13	0	0	0	0	0	0	0	0	0	0	0	0	0	0	0	0	0	0	0	0

TABLE A–1–b. ($E \geq 10^{-3}E_0$).

t \ N_e	0	1	2	3	4	5	6	7	8	9	10	11	12	13
1.0	47	0	23	2	8	3	5	4	4	1	1	1	1	0
0.9	52	0	20	3	8	7	6	0	1	1	2	0	0	0
0.8	57	0	21	2	11	6	1	1	1	1	0	0	0	0
0.7	60	0	21	3	6	6	3	0	0	1	0	0	0	0
0.6	62	0	23	2	7	3	2	0	1	0	0	0	0	0
0.5	65	0	27	0	3	3	2	0	0	0	0	0	0	0
0.4	72	0	21	1	6	0	0	0	0	0	0	0	0	0
0.3	77	0	20	1	2	0	0	0	0	0	0	0	0	0
0.2	79	0	20	0	1	0	0	0	0	0	0	0	0	0
0.1	87	0	13	0	0	0	0	0	0	0	0	0	0	0

TABLE A–1–c. ($E \geq 10^{-2}E_0$).

t \ N_e	0	1	2	3	4	5	6	7
1.0	47	1	28	6	11	4	3	0
0.9	52	0	29	6	11	1	2	0
0.8	57	0	30	4	7	2	0	0
0.7	60	0	28	4	6	2	0	0
0.6	62	0	30	2	4	2	0	0
0.5	65	0	30	3	2	0	0	0
0.4	72	0	25	1	2	0	0	0
0.3	77	0	22	0	1	0	0	0
0.2	79	0	20	0	1	0	0	0
0.1	87	0	13	0	0	0	0	0

TABLE A–2–a. ($E \geq 10^{-4}E_0$).

t \ N_e	0	1	2	3	4	5	6	7	8	9	10	11
0.5	10	2	8	2	4	3	2	0	1	2	1	0
0.4	16	4	3	2	5	2	1	0	2	0	0	0
0.3	19	4	6	3	1	0	2	0	0	0	0	0
0.2	24	3	7	0	1	0	0	0	0	0	0	0
0.1	33	0	2	0	0	0	0	0	0	0	0	0

TABLE A–2–b. ($E \geq 10^{-3}E_0$).

t \ N_e	0	1	2	3	4	5	6	7	8
0.5	14	4	6	5	4	0	1	1	0
0.4	20	1	6	5	2	0	1	0	0
0.3	24	0	3	2	1	0	0	0	0
0.2	28	2	5	0	0	0	0	0	0
0.1	33	0	2	0	0	0	0	0	0

TABLE A–2–c. ($E \geq 10^{-2}E_0$).

t \ N_e	0	1	2	3	4	5
0.5	25	3	4	2	1	0
0.4	26	3	5	1	0	0
0.3	30	1	4	0	0	0
0.2	32	2	1	0	0	0
0.1	33	1	1	0	0	0

TABLE A-3-a. ($E \geq 10^{-4}E_0$).

t \ N_e	0	1	2	3	4	5	6	7	8	9	10	11	12	13	14	15	16	17	18	19	20	21
0.5	650	130	750	206	470	289	268	105	168	158	132	65	51	17	16	9	6	4	3	2	1	0
0.4	1152	288	520	236	501	221	204	60	211	22	53	7	16	4	3	0	2	0	0	0	0	0
0.3	1463	308	823	326	252	75	194	10	41	2	6	0	0	0	0	0	0	0	0	0	0	0
0.2	1896	237	1033	60	243	3	27	0	1	0	0	0	0	0	0	0	0	0	0	0	0	0
0.1	2871	0	603	0	26	0	0	0	0	0	0	0	0	0	0	0	0	0	0	0	0	0

TABLE A-3-b. ($E \geq 10^{-3}E_0$).

t \ N_e	0	1	2	3	4	5	6	7	8	9	10	11	12	13	14
0.5	910	260	768	433	464	189	231	106	66	49	11	6	5	2	0
0.4	1440	72	852	401	391	117	155	32	33	1	6	0	0	0	0
0.3	1848	0	1096	178	285	48	38	5	2	0	0	0	0	0	0
0.2	2212	158	955	40	128	2	5	0	0	0	0	0	0	0	0
0.1	2871	0	603	0	26	0	0	0	0	0	0	0	0	0	0

TABLE A-3-c. ($E \geq 10^{-2}E_0$).

t \ N_e	0	1	2	3	4	5	6	7	8	9
0.5	1625	195	1010	295	244	78	44	7	2	0
0.4	1872	216	1010	173	180	36	11	2	0	0
0.3	2310	77	968	22	118	1	4	0	0	0
0.2	2528	158	719	40	52	2	1	0	0	0
0.1	2871	87	516	13	13	0	0	0	0	0

radiation length and taking the point of conversion as the origin. The letters a, b, c here again refer to $\alpha = 10^{-4}$, 10^{-3}, and 10^{-2} respectively where now E_0 = initial pair energy. Here N_e is the number of additional electrons formed in the distance t radiation lengths from the first pair origin and the numbers in the rows opposite t represent the number of cases.

Tables A-3-a, A-3-b, and A-3-c represent the development for the initial condition of one electron pair and one photon of equal energy, E_0, incident at the origin and were made by a superposition of Tables A-1 and A-2. Here again a, b, c, refer respectively to $\alpha = 10^{-4}$, 10^{-3}, and 10^{-2} and N_e is the number of additional electrons made in the distance t radiation lengths from the origin and the numbers in the rows opposite t represent the number of cases.

With these results we clearly see the large fluctuations in electron numbers in the cascade development. As a matter of fact, these fluctuations can cover almost all anomalies in electron numbers in cascade showers thus far observed if the initial energy is sufficiently high.

PHYSICAL REVIEW VOLUME 100, NUMBER 1 OCTOBER 1, 1955

Causality in the Pion-Proton Scattering*

H. L. ANDERSON, W. C. DAVIDON, AND U. E. KRUSE
Institute for Nuclear Studies, The University of Chicago, Chicago, Illinois

(Received May 11, 1955)

Dispersion relations applicable to particles with mass and charge have been used for analyzing pion-proton scattering data. In these relations, experimental values of the total cross sections for π^+ and π^- from 0 to 1.9 Bev were used to calculate the real part of the forward scattering amplitudes, and these were compared with the results of phase-shift analyses. With suitable choice of the pion-nucleon coupling constant, good agreement can be obtained for the phase-shift solutions with a resonant behavior for α_{33}.

INTRODUCTION

A RELATION between the real and imaginary parts of the forward scattering amplitude for the scattering of light on atoms has been known for some time. The relation, known as the Kramers-Kronig dispersion relation[1,2] is derived from the condition that the scattered wave should have zero amplitude until the incident wave reaches the scatterer. Following a suggestion by Kronig[3] that such a causality condition might be extended to apply to the scattering of particles

* Research supported by a joint program of the Office of Naval Research and the U. S. Atomic Energy Commission.

[1] R. Kronig, J. Opt. Soc. Am. **12**, 547 (1926).
[2] H. A. Kramers, Atti congr inter fisici Como **2**, 545 (1927).
[3] R. Kronig, Physica **12**, 543 (1946).

with mass, a generalized dispersion relation for Bose particles with finite rest mass has now been obtained by Goldberger.[4] Goldberger's derivation uses the formalism of quantum field theory. The demand that waves do not propagate faster than the velocity of light is expressed by requiring that measurements of two observable quantities made at space like points, should not interfere. Thus, the causality condition is imposed by setting the commutator of two Heisenberg operators for the boson field equal to zero when these are taken at space like points.

Application of such a dispersion relation to the pion-proton scattering was first made by Karplus and Ruderman[5] who were able to show that the causality condition required a positive sign for the real part of the forward scattering amplitude of the low-energy pion-proton scattering. This was in agreement with the result of the study of the effect of the Coulomb interference.[6,7]

Our interest was to make use of the causality condition in the phase-shift analysis of the pion-proton scattering, following a suggestion by Wigner.[8] Wigner had found a lower limit for the derivative of the phase shifts with momentum. This made clear the relevancy of causality for the phase-shift analysis, but seemed less useful than a dispersion relation. The dispersion relation obtained by Karplus and Ruderman applies to the scattering of π^0 by protons. The formula obtained by Goldberger, Miyazawa, and Oehme[9] applies explicitly to the scattering of charged pions by protons and was used in the present work.

DISPERSION RELATION

In a dispersion relation, the real part of the forward scattering amplitude is calculated from a knowledge of the imaginary part over the entire energy range, from $-\infty$ to $+\infty$. For any given scattering process, it is of course possible to measure the total cross section and hence the imaginary part of the forward scattering amplitude, only at energies above μ, the rest energy. According to Goldberger, the usual assumptions made in field theory have the consequence that the cross sections for the charge conjugate particle may be used for energies more negative than $-\mu$. For this reason, both the cross sections $\sigma_+(\omega)$ for π^+ as well as $\sigma_-(\omega)$ for π^- contribute in the dispersion formulas.

There is an additional contribution which occurs at energy $\omega=\mu^2/2M$ for π^+ or $\omega=-\mu^2/2M$ for π^- scattering, where M is the nucleon rest energy. This is the only contribution in the energy range between $-\mu$ and $+\mu$ and arises from the fact that the neutron can be a possible intermediate state in the scattering. This contribution may be expressed in terms of the small coupling constant characteristic of the pseudovector interaction, and is numerically very important. An important object of an experimental check of the dispersion relations is to test the correctness of these ideas.

We reproduce below the formulas given by Goldberger, Miyazawa, and Oehme[9] for the scattering of positive and negative pions by protons.

$$D_+(k)-\tfrac{1}{2}\left(1+\frac{\omega}{\mu}\right)D_+(0)-\tfrac{1}{2}\left(1-\frac{\omega}{\mu}\right)D_-(0)$$
$$=\frac{k^2}{4\pi^2}\int_\mu^\infty\frac{d\omega'}{k'}\left[\frac{\sigma_+(\omega')}{\omega'-\omega}+\frac{\sigma_-(\omega')}{\omega'+\omega}\right]+\frac{2f^2}{\mu^2}\frac{k^2}{\omega-\dfrac{\mu^2}{2M}},\quad(1)$$

$$D_-(k)-\tfrac{1}{2}\left(1+\frac{\omega}{\mu}\right)D_-(0)-\tfrac{1}{2}\left(1-\frac{\omega}{\mu}\right)D_+(0)$$
$$=\frac{k^2}{4\pi^2}\int_\mu^\infty\frac{d\omega'}{k'}\left[\frac{\sigma_-(\omega')}{\omega'-\omega}+\frac{\sigma_+(\omega')}{\omega'+\omega}\right]-\frac{2f^2}{\mu^2}\frac{k^2}{\omega+\dfrac{\mu^2}{2M}},\quad(2)$$

where k is the wave number of the pion and ω its total energy, both in the laboratory system.

The formulas have been written to give the difference between the real part of the forward scattering amplitude $D_+(k)$ for positive pions of wave number k, or $D_-(k)$ for negative pions and the values for these quantities taken at $k=0$. Both integrals contain the total cross sections for π^+ and π^- and it is the principal part of the integral which is to be evaluated. The final term in both expressions gives the contribution of the bound state.

It is well known that in the pion-nucleon scattering, the state of isotopic spin $T=\frac{3}{2}$ is dominant. For this reason, we preferred to calculate the quantity $D_3(k)$ corresponding to this state. This is identical to $D_+(k)$ given in (1).

$$D_3(k)=D_+(k).\quad(3)$$

However, the corresponding quantity for the state $T=\frac{1}{2}$ is given by the linear combination

$$D_1(k)=\tfrac{3}{2}D_-(k)-\tfrac{1}{2}D_+(k).\quad(4)$$

These quantities are readily expressed in terms of the phase shifts which are determined from the angular distribution measurements. We have up to terms including p waves,

$$D_3(k)=(k/2k_b^2)(\sin2\alpha_3+2\sin2\alpha_{33}+\sin2\alpha_{31}+\cdots),\quad(5)$$

and

$$D_1(k)=(k/2k_b^2)(\sin2\alpha_1+2\sin2\alpha_{13}+\sin2\alpha_{11}+\cdots).\quad(6)$$

[4] M. L. Goldberger, Phys. Rev. **99**, 979 (1955).
[5] R. Karplus and M. Ruderman, Proceedings of the Fifth Annual Rochester Conference (Interscience Publishers, Inc., New York, 1955). We thank these authors for a preprint of their paper.
[6] J. Orear, Phys. Rev. **96**, 1417 (1954).
[7] G. Puppi, Proceedings of the Fifth Annual Rochester Conference (Interscience Publishers, Inc., New York, 1955).
[8] E. P. Wigner, Phys. Rev. **98**, 145 (1955). H. L. Anderson, Proceedings of the Fifth Annual Rochester Conference (Interscience Publishers, Inc., New York, 1955).
[9] Goldberger, Miyazawa, and Oehme, Phys. Rev. **99**, 986 (1955).

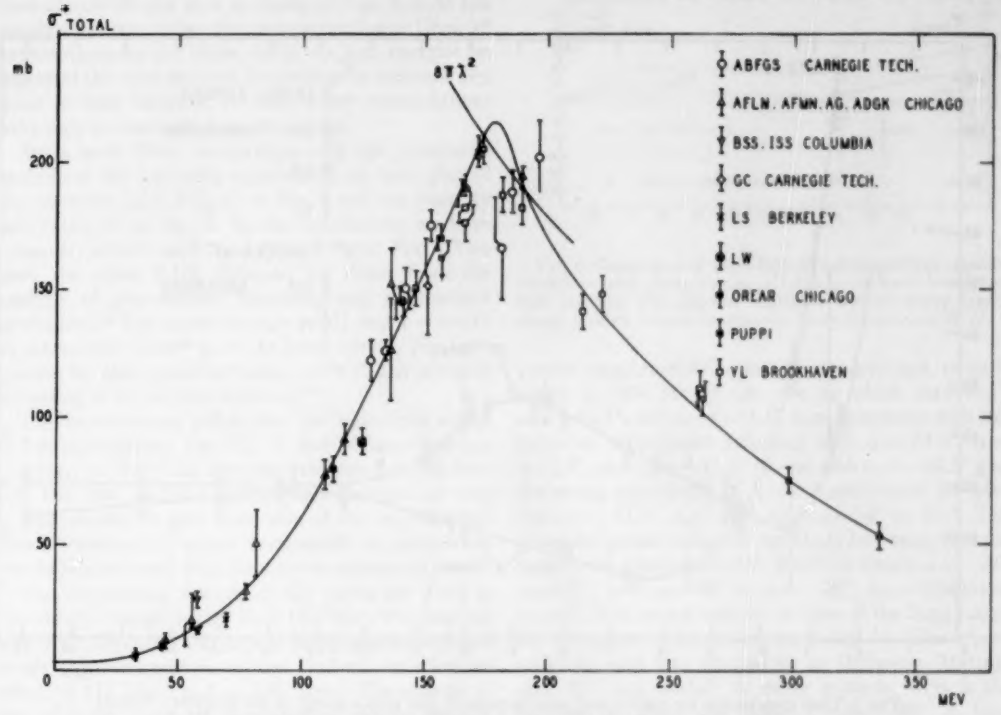

FIG. 1. Total cross section for positive pions on protons *vs* pion kinetic energy in the laboratory system; energy range from 0-350 Mev. Sources for data are listed in references 11–27.

Here k_b is the pion wave number in the center-of-mass system. The transformation from the center of mass to the laboratory system is carried out by recognizing that the ratio $D(k)/k$ is an invariant.

The connection between k_b and k is

$$k_b = k\left(1+\frac{2\omega}{M}+\frac{\mu^2}{M^2}\right)^{-\frac{1}{2}}. \tag{7}$$

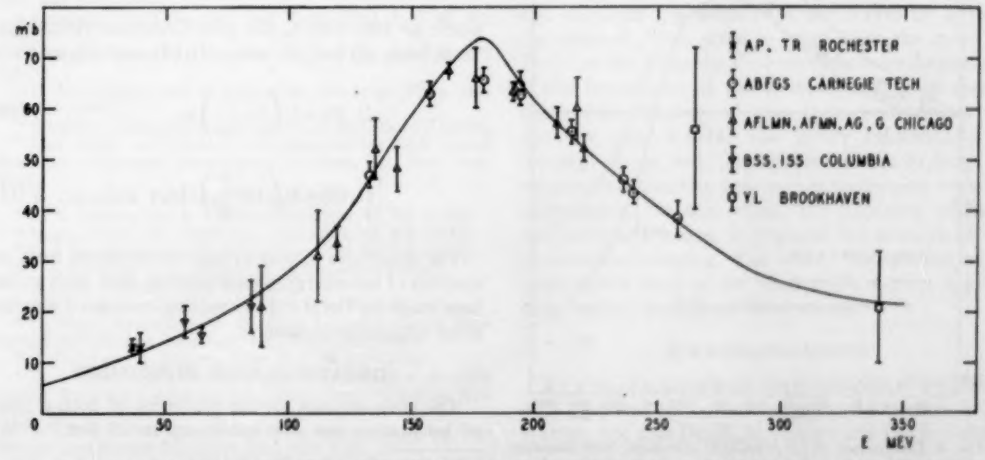

FIG. 2. Total cross section for negative pions on protons *vs* pion kinetic energy in the laboratory system; energy range from 0-350 Mev. Sources for data are listed in references 11–27.

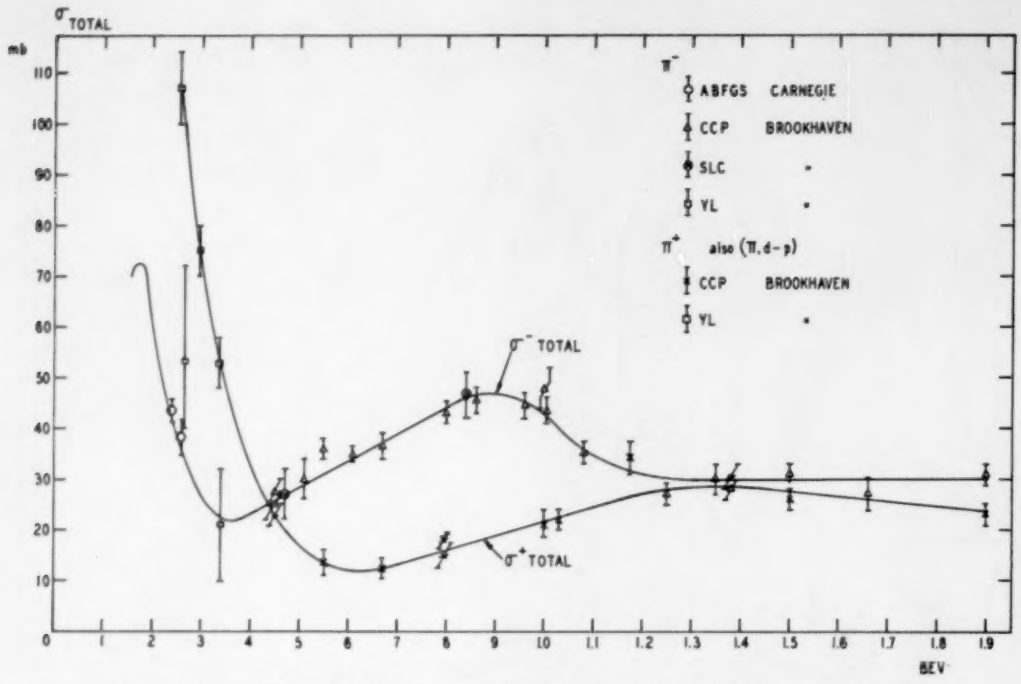

FIG. 3. Total cross section for positive and negative pions *vs* pion kinetic energy in the laboratory system; energy range from 0.25 to 1.9 Bev. Sources for data are listed in references 11–27.

The quantities $D_+(0)$ and $D_-(0)$ may be evaluated from the low-energy behavior of the phase shifts. As is well known, the phase shift corresponding to the state of angular momentum l varies asymptotically as k_b^{2l+1}. Thus, in the limit as $k_b \to 0$, only the s wave phase shifts contribute. These are written:

$$\alpha_3 = a_3\eta, \tag{8}$$

$$\alpha_1 = a_1\eta, \tag{9}$$

where $\eta = k_b\lambda_c$ with λ_c the pion Compton wavelength. Thus, from (5) and (6) using (3), (4), and (7), we write

$$D_+(0) = \lambda_c\left(1+\frac{\mu}{M}\right)a_3, \tag{10}$$

$$D_-(0) = \lambda_c\left(1+\frac{\mu}{M}\right)(\tfrac{2}{3}a_1+\tfrac{1}{3}a_3). \tag{11}$$

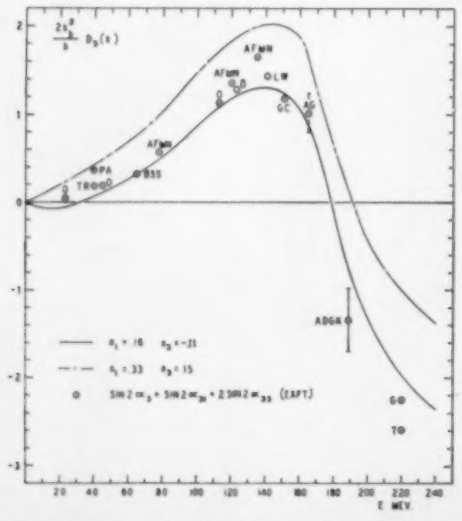

FIG. 4. Comparison of $(2k_b^3/k)D_3(k)$ calculated from causality conditions with $\sin 2\alpha_3 + \sin 2\alpha_{31} + 2\sin 2\alpha_{33}$ obtained from phase-shift analysis. The abscissa represents the laboratory kinetic energy in Mev. Sources for data are listed in references 11–27.

The quantities a_3 and a_1 may be obtained from an analysis of low-energy pion scattering data such as has been made by Orear.[10] The coupling constant f remains as an adjustable parameter.

COMPARISON WITH EXPERIMENT

The cross sections for the scattering of both π^- and π^+ by protons are now known up to 1.9 Bev.[11–27] We

[10] J. Orear, Phys. Rev. **96**, 176 (1954).

[11] Ashkin, Blaser, Feiner, Gorman, and Stern, Phys. Rev. **96**, 1104 (1954).

have plotted all this data as shown in Figs. 1–3. At low energies we have drawn the curve according to Orear's[10] prescriptions for the phase shifts. At high energies we supposed the cross sections to continue as constant and equal to their values at 1.9 Bev. These extrapolations have only a minor effect on the results.

For a more direct comparison with the phase-shift analysis of the scattering experiments we have plotted the quantity $(2k_b^3/k)D_3(k)$ in Fig. 4 and the quantity $(2k_b^3/k)D_1(k)$ in Fig. 5. In the calculations we have taken $M/\mu=6.73$ and $\lambda_c=1.42\times10^{-13}$ cm. For $2f^2$ we used the value 0.161 obtained by Chew from the analysis of pion-nucleon scattering and photomeson production.[24] The quantities $a_3=-0.11$ and $a_1=+0.16$ as taken from Orear[10] gave the lower curves. For comparison we also calculated using $a_3=0.15$ and $a_1=0.33$ according to Noyes and Woodruff.[29]

The experimental points are the quantities $\sin2\alpha_3+2\sin2\alpha_{33}+\sin2\alpha_{31}$ for Fig. 4 and $\sin2\alpha_1+2\sin2\alpha_{13}+\sin2\alpha_{11}$ for Fig. 5. In the case of the points at 165 Mev and 189 Mev an error analysis was available so that it was possible to give some idea of the experimental error. Presumably, errors comparable in magnitude should be associated with the other experimental points.

The outstanding feature of the curve for $T=\frac{3}{2}$ is the abrupt change in sign near 180 Mev. The positive sign of $D_+(k)$ below 180 Mev is in agreement with the result of measurements of the Coulomb interference effect at 113 Mev[6] and at 126 Mev.[7] The change in sign of $D_+(k)$ above 180 Mev implies that the forward scattering should be augmented rather than diminished by the Coulomb interference. This effect has now been observed by Taft[30] with positive pions at 220 Mev.

The abrupt change in sign for $D_3(k)$ has made possible a rather unambiguous choice of one out of several possible sets of phase shifts which fit the pion-proton angular distribution of the solutions recently found at 189 Mev;[12] the one in which $\alpha_{33}=98.5°$, $\alpha_3=-11.3°$, and $\alpha_{31}=-11.6°$ is in agreement with this behavior. Alternative solutions with $\alpha_{33}=81.5°$, $\alpha_3=+11.3°$, and $\alpha_{31}=+11.6°$ or one with $\alpha_3=-44.5°$ give the wrong sign for $D_3(k)$. A fourth solution at 189 Mev has $\alpha_3=-11.6°$, $\alpha_{33}=126°$, and $\alpha_{31}=56°$ or 236°. This gives the proper behavior for $D_3(k)$ but must be compared with solutions at 165 Mev[15] in which $\alpha_3=-20°$, $\alpha_{33}=34°$, and $\alpha_{31}=94°$ or $\alpha_3=-20°$, $\alpha_{33}=+63°$, and $\alpha_{31}=4°$. This seems unlikely in view of the large jumps for two phase shifts which are called for. The choice coincides with that selected by de Hoffmann, Metropolis, Alei, and Bethe[31] on other grounds. This is the solution in which α_{33} passes through 90°. A nonresonant behavior for α_{33} seems excluded by causality.

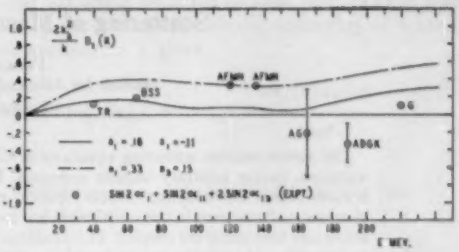

FIG. 5. Comparison of $(2k_b^3/k)D_1(k)$ calculated from causality conditions with $\sin2\alpha_1+\sin2\alpha_{11}+2\sin2\alpha_{13}$ obtained from phase shift analysis. The abscissa represents the laboratory kinetic energy in Mev. Sources for data are listed in references 11–27.

The general fit of the experimental data is surprisingly good in view of the rather considerable experimental errors. Neglect of the presence of d waves in the analysis of the scattering may be responsible for part of the discrepancy which occurs at the higher energies. The agreement with Orear's prescription for a_3 and a_1 is noticeably better than that using the values of Noyes and Woodruff. Adjustment of the curves by altering the value of f^2 can serve to bring down the curve for $T=\frac{3}{2}$ but this raises the $T=\frac{1}{2}$ curve by twice the amount.

The importance of the neutron term is of special significance. Neglect of this term would have the quantity $(2k_b^3/k)D_1(k)$ rise rather substantially at the high-energy end. Its inclusion serves to keep the value of this quantity near zero in conformity with the experiments. For this reason, the dispersion relations can serve as a means to evaluate the strength of the pion-nucleon coupling. The role of the neutron as an intermediate state of the pion-proton system is made more evident because of these results.

ACKNOWLEDGMENTS

We wish to acknowledge the helpfulness of discussions with Professor M. L. Goldberger and Professor K. M. Watson, and also Dr. H. Miyazawa and Dr. R. Oehme.

[12] Anderson, Davidon, Glicksman, and Kruse, this issue [Phys. Rev. **100**, 279 (1955)].
[13] Anderson, Fermi, Lundby, and Nagle, Phys. Rev. **85**, 936 (1952).
[14] Anderson, Fermi, Martin, and Nagle, Phys. Rev. **91**, 155 (1953).
[15] H. L. Anderson and M. Glicksman, this issue [Phys. Rev. **100**, 268 (1955)].
[16] Bodansky, Sachs, and Steinberger, Phys. Rev. **93**, 1367 (1954).
[17] Cool, Clark, and Piccioni, Proceedings of the Fifth Annual Rochester Conference (Interscience Publishers, Inc., New York, 1955).
[18] M. Glicksman, Phys. Rev. **94**, 1335 (1954).
[19] R. A. Grandey and A. F. Clark, Phys. Rev. **97**, 791 (1955).
[20] Isaacs, Sachs, and Steinberger, Phys. Rev. **85**, 803 (1952).
[21] S. J. Leonard and D. H. Stork, Phys. Rev. **93**, 568 (1954).
[22] J. J. Lord and A. B. Weaver (private communication).
[23] J. Orear, Phys. Rev. **96**, 176 (1954).
[24] J. P. Perry and C. E. Angell, Phys. Rev. **91**, 1289 (1953).
[25] G. Puppi, Proceedings of the Fifth Annual Rochester Conference (Interscience Publishers, Inc., New York, 1955).
[26] J. Tinlot and A. Roberts, Phys. Rev. **95**, 137 (1954).
[27] L. C. Yuan and S. J. Lindenbaum, Proceedings of the Fifth Annual Rochester Conference Inc., (Interscience Publishers, New York, 1955).
[28] G. Chew, Proceedings of the Fifth Annual Rochester Conference (Interscience Publishers, Inc., New York, 1955).
[29] H. P. Noyes and A. E. Woodruff, Phys. Rev. **94**, 1401 (1954).
[30] H. Taft (to be published).
[31] de Hoffmann, Metropolis, Alei, and Bethe, Phys. Rev. **95**, 1586 (1954).

Scattering of Mesons by a Fixed Scatterer

FREEMAN J. DYSON
Institute for Advanced Study, Princeton, New Jersey
(Received May 9, 1955)

The meson-nucleon scattering equations of Chew and Low are generalized to the case of mesons and scatterers having arbitrary angular momenta. In consequence, the algebraic structure of the equations is made clearer. Two coupling schemes for the angular momenta are studied, the J-scheme in which momenta of meson and scatterer in the initial state are coupled, and the N-scheme in which the meson momenta in initial and final states are coupled. The condition of unitarity of the S-matrix is simple only in the J-scheme, the condition of causality is simple only in the N-scheme. The interlock between the two schemes gives rise to the peculiar linking of different J-values in the Chew-Low equations. The linkage coefficients are shown to be ordinary Racah coefficients.

I. INTRODUCTION

CHEW[1] has introduced the so-called "fixed-source model" as an approximate model for the meson-nucleon interaction, and has found remarkably good agreement between this model and the experimental data on photo-production and meson-proton scattering. Low[2] has discovered a new type of scattering equation which greatly simplifies the mathematical analysis of the Chew model. Low has also proved[3] a theorem which states that his scattering equation is in a certain sense equivalent to the requirement that the meson-nucleon interaction satisfy the two conditions of causality and unitarity of the S-matrix. This means that the consequences of the Low scattering equation are to some extent independent of the details of the model, and therefore to be taken more seriously than the model itself.

The present paper contains a simple generalization of the Chew-Low analysis to the scattering of mesons by a fixed scatterer, the mesons and the scatterer having arbitrary angular momenta. The treatment is general enough so that scattering matrix elements which are mixtures of different multipole orders can be included. It is found that the essential features of the Chew-Low theory are entirely unchanged by the generalization. In particular, the Low theorem about unitarity and causality still holds.

The purpose of this generalization of the theory was to understand the algebraic structure of the scattering equation [Eq. (3.11) of reference 2], particularly the linkage between scattering amplitudes of different total angular momentum. The generalized equations make the structure clear. The essential results thus obtained are two.

(i) The linkage coefficients are Racah coefficients, which enter here for the same reason that they occur in the theory of angular correlations of successive nuclear radiations.[4]

(ii) The unitarity and causality conditions can be simply formulated in terms of two different coupling schemes for the angular momenta, and it is only in the transformation between the two coupling schemes that the Racah coefficients make an appearance.

The discussion in this paper is intentionally confined to the algebraic properties of the scattering equations. Concerning the physical meaning of the equations, we have nothing to add to what Chew and Low have said.

II. THE SCATTERING EQUATION

We shall consider the interaction of mesons with a heavy scatterer to be a particular case of the following general situation. There is a scatterer whose states are represented by $|S\sigma\rangle$, $|T\tau\rangle$, where σ or τ is the z-component of the angular momentum, and S or T denotes the total angular momentum together with any other variables needed to specify the state completely. There is a neutral spin-zero meson field $\phi(\mathbf{r})$. States of the scatterer plus one meson are denoted by $|S\sigma L\lambda x\rangle$, where L is the orbital angular momentum of the meson, λ is the z-component of L, and x is the magnitude of the meson momentum at infinite distance from the scatterer. The states are normalized by the convention

$$\langle T\tau M\mu y|S\sigma L\lambda x\rangle=\delta_{TS}\delta_{\tau\sigma}\delta_{LM}\delta_{\lambda\mu}\delta(x-y). \quad (1)$$

The Hamiltonian of the whole system is

$$H=H_0+H'+H_m, \quad (2)$$

where H_0 is the energy of the scatterer alone, H_m is that of the free meson field, and H' is the interaction

$$H'=\int U(\mathbf{r})\phi(\mathbf{r})d\mathbf{r}, \quad (3)$$

where $U(\mathbf{r})$ is a Hermitian matrix operating on the states of the scatterer.

The Fourier transform of the operator $U(\mathbf{r})$ may be expressed as a sum of multipoles:

$$U(\mathbf{k})=\int U(\mathbf{r})e^{i\mathbf{k}\cdot\mathbf{r}}d\mathbf{r}=\sum_{L\lambda}(-1)^{\lambda}Y_{-\lambda}{}^{L}(\mathbf{k})U_{\lambda}{}^{L}(\mathbf{k}),$$

[1] G. F. Chew, Phys. Rev. **89**, 591 (1953); **94**, 1748 and 1755 (1954); **95**, 1669 (1954).
[2] F. Low, Phys. Rev. **97**, 1392 (1955).
[3] G. F. Chew (unpublished communication).
[4] G. Racah, Phys. Rev. **84**, 910 (1951).

where $Y_{-\lambda}{}^{L}(\hat{k})$ is a normalized surface harmonic, and $U_{\lambda}{}^{L}(k)$ is an operator depending on the magnitude of k only. The basic hypothesis of the fixed-scatterer model is that the $U_{\lambda}{}^{L}(k)$ be factorizable. That is to say, for each multipole separately we have

$$U_{\lambda}{}^{L}(k)=u_{L}(k)O_{\lambda}{}^{L}, \tag{4}$$

where $u_L(k)$ is a c-number function of $|k|$, and $O_{\lambda}{}^{L}$ is an operator independent of k. The $O_{\lambda}{}^{L}$ are irreducible tensor operators in the sense of Racah.[5] According to Eq. (29) of reference 5, the matrix elements of $O_{\lambda}{}^{L}$ are given by

$$\langle R\rho|O_{\lambda}{}^{L}|S\sigma\rangle=(-1)^{R+\rho}V(RSL,-\rho\sigma\lambda)\langle R\|O^{L}\|S\rangle, \tag{5}$$

where V is a Wigner coefficient, and the reduced matrix elements $\langle R\|O^{L}\|S\rangle$ express the physical properties of the scatterer.

The interaction operator is subject to the further conditions that it be Hermitian and invariant under time reversal. The first condition gives

$$(R\|O^{L}\|S)^{*}u_{L}{}^{*}(k)=(-1)^{S-R+L}(S\|O^{L}\|R)u_{L}(k). \tag{6}$$

The second condition, using the conventions of Coester[6] to define the time-reversal operator, gives

$$(R\|O^{L}\|S)=\eta(-1)^{R-S+L}(S\|O^{L}\|R), \tag{7}$$

where $\eta=\pm1$ expresses the intrinsic parity of the meson field under time-reversal. According to (6), the phase of $u_L(k)$ is independent of k. We may therefore choose the phase of $O_{\lambda}{}^{L}$ in (4) so that $u_L(k)$ is real for $\eta=+1$ and pure imaginary for $\eta=-1$. Then (6) and (7) imply that every $(R\|O^{L}\|S)$ is real.

Consider the part of the S-matrix for which the initial state $|S\sigma L\lambda x\rangle$ is a state of the scatterer with one meson of momentum x, while the final state $|R\rho\rangle$ is any state of the complete system of scatterer plus meson field. For the final state, R represents the total angular momentum and any other variables needed to specify the state, while ρ is the z-component of angular momentum. Let E_R be the energy of the final state, E_S that of the scatterer in the initial state, and $\Delta_R=E_R-E_S$. Let $\omega_x=(\mu^2+x^2)^{\frac{1}{2}}$ be the energy of the meson with momentum x. According to Low [Eq. (3.6) of reference 2], this part of the S-matrix may be written

$$S=I+2i(x/\omega_x)\delta(\omega_x-\Delta_R)F(x), \tag{8}$$

where $F(x)$ is an operator whose relevant matrix elements are given by

$$\langle R\rho|F(x)|S\sigma L\lambda\rangle=-\tfrac{1}{4}(\omega_x/\pi)^{\frac{1}{2}}u_L(x)\langle R\rho|O_{\lambda}{}^{L}|S\sigma\rangle. \tag{9}$$

This $F(x)$ is the scattering amplitude operator for a meson of momentum x. In a scattering state which is an eigenstate of $F(x)$, the eigenvalue will be $e^{i\delta}\sin\delta$, where δ is the phase shift.

[5] G. Racah, Phys. Rev. **62**, 438 (1942).
[6] F. Coester, Phys. Rev. **89**, 619 (1953).

The scattering equation of Low [Eq. (3.7) of reference 2], for the case of elastic scattering of a meson with momentum x, gives

$$\langle T\tau M\mu|F(x)|S\sigma L\lambda\rangle=(-1)^{M+\mu}\frac{xu_L(x)u_M(x)}{16\pi^3}$$
$$\times\sum_{R\rho}\left[\frac{1}{\Delta_R-\omega_x-i\epsilon}\langle T\tau|O_{-\mu}{}^{M}|R\rho\rangle\langle R\rho|O_{\lambda}{}^{L}|S\sigma\rangle\right.$$
$$\left.+\frac{1}{\Delta_R+\omega_x}\langle T\tau|O_{\lambda}{}^{L}|R\rho\rangle\langle R\rho|O_{-\mu}{}^{M}|S\sigma\rangle\right]. \tag{10}$$

Here it is supposed that the initial and final states of the scatterer have equal energy E_S. Equation (10) is exact and depends only on the hypothesis of factorizability of the interaction. The approximation of neglecting states $|R\rho\rangle$ containing more than one meson will not be made anywhere in this paper.

III. THE TWO COUPLING SCHEMES

The usual method of eliminating the magnetic quantum numbers τ, μ, σ, λ from Eq. (10) is to use the fact that the total angular momentum J of the system, and its z-component j, are constants of the motion. Thus we may write

$$\langle T\tau M\mu|F(x)|S\sigma L\lambda\rangle=\sum_{J}(2J+1)V(TMJ,\tau\mu-j)$$
$$\times V(SLJ,\sigma\lambda-j)\langle TM|F_J(x)|SL\rangle. \tag{11}$$

Substituting Eqs. (5) and (11) into (10) gives the Low equation in the J-coupling scheme

$$\langle TM|F_J(x)|SL\rangle=\frac{xu_L(x)u_M(x)}{16\pi^2}\sum_{R}\left[\frac{(-1)^{M+T-R}}{\Delta_R-\omega_x-i\epsilon}\right.$$
$$\times\langle T\|O^{M}\|R\rangle\langle R\|O^{L}\|S\rangle\frac{1}{2J+1}\delta_{JR}+\frac{(-1)^{M+S-R}}{\Delta_R+\omega_x}$$
$$\left.\times\langle T\|O^{L}\|R\rangle\langle R\|O^{M}\|S\rangle W(LSTM,JR)\right]. \tag{12}$$

Here W is the Racah coefficient defined in reference 5. This Eq. (12) is the direct generalization of Low's equation (3.11) in reference 2, and it shows how the coupling between different J-values in Low's equation comes about. The numerical factors 8/3, 2/9, etc., in Low's equation are products of Racah coefficients, as shown explicitly in Eq. (33) below.

An alternative way of eliminating the magnetic quantum numbers from Eq. (10) is to couple together the initial and final angular momenta of the meson; thus we couple together (LM,ST) instead of (TM,SL). We write

$$\langle T\tau M\mu|F(x)|S\sigma L\lambda\rangle=\sum_{N\nu}(2N+1)V(LMN,-\lambda\mu\nu)$$
$$\times V(STN,\sigma-\tau\nu)(-1)^{\sigma+\nu-S-N}\langle TM|G_N(x)|SL\rangle. \tag{13}$$

Substituting Eqs. (5) and (13) into (10) gives the Low equation in the N-coupling scheme

$$\langle TM|G_N(x)|SL\rangle=\frac{xu_L(x)u_M(x)}{16\pi^2}\sum_R\Big[\frac{(-1)^L}{\Delta_R-\omega_x-i\epsilon}\times\langle T\|O^M\|R\rangle\langle R\|O^L\|S\rangle W(TMSL,RN)+\frac{(-1)^{M+N}}{\Delta_R+\omega_x}\times\langle T\|O^L\|R\rangle\langle R\|O^M\|S\rangle W(TLSM,RN)\Big]. \quad (14)$$

For given L, M, S, T, the number of possible values of N is always equal to the number of values of J. From the symmetry of the Racah coefficients, Eqs. (12) and (14) imply

$$\begin{aligned}\langle TM|F_J(x)|SL\rangle&=\langle SL|F_J(x)|TM\rangle,\\ \langle TM|G_N(x)|SL\rangle&=(-1)^{S-T}\langle SL|G_N(x)|TM\rangle.\end{aligned} \quad (15)$$

Thus the S-matrix is symmetric in both J and N coupling schemes, in accordance with the general theorem of Coester.[6]

Equation (14) has in addition a property of symmetry[7] with respect to the interchange of L and M. Thus for $\alpha=0$, 1, we consider the sum or difference defined by

$$\langle TM|G_{N\alpha}(x)|SL\rangle=[\langle TM|G_N(x)|SL\rangle+(-1)^\alpha\langle TL|G_N(x)|SM\rangle]. \quad (16)$$

For this quantity, Eq. (14) gives

$$\begin{aligned}&\langle TM|G_{N\alpha}(x)|SL\rangle\\ &=\frac{xu_L(x)u_M(x)}{16\pi^2}\sum_R\Big[\frac{1}{\Delta_R-\omega_x-i\epsilon}+\frac{(-1)^{N+\alpha}}{\Delta_R+\omega_x}\Big]\\ &\times\{(-1)^L\langle T\|O^M\|R\rangle\langle R\|O^L\|S\rangle W(TMSL,RN)\\ &+(-1)^{M+\alpha}\langle T\|O^L\|R\rangle\langle R\|O^M\|S\rangle\\ &\times W(TLSM,RN)\}. \quad (17)\end{aligned}$$

The F_J and G_N are linear combinations of each other according to Eqs. (11) and (13),

$$\begin{aligned}F_J&=\sum_N(2N+1)(-1)^{M+T-L-J}W(TMSL,JN)G_N,\\ G_N&=\sum_J(2J+1)(-1)^{M+T-L-J}W(TMSL,JN)F_J.\end{aligned} \quad (18)$$

Substituting Eq. (18) into (14) reproduces Eq. (12) by virtue of the Racah sum-rule [Eq. (43) of reference 5]

$$\sum_N(2N+1)(-1)^{L+M+S+T+J+R+N}W(TMSL,JN)\times W(TLSM,RN)=W(LSTM,JR). \quad (19)$$

The physical meaning of the amplitudes $\langle TM|G_N\times(x)|SL\rangle$ is not very clear. They are the "tensor parameters" of the S-matrix, according to the definition of Fano.[8] The following seems to be their most concrete interpretation. For any direction $\hat{p}$, let $|L0_p\rangle$ be the state of the meson having total angular momentum L and zero component of angular momentum about $\hat{p}$. Then Eq. (13) implies

$$\begin{aligned}&\langle T\tau M0_p|F(x)|S\sigma L0_p\rangle\\ &=\sum_N[4\pi(2N+1)]^{\frac{1}{2}}V(LMN,000)V(STN,\sigma-\tau\tau-\sigma)\\ &\times(-1)^{\sigma-S+L+M}\langle TM|G_N(x)|SL\rangle Y_{\sigma-\tau}^N(\hat{p}).\end{aligned} \quad (20)$$

This exhibits the G_N as coefficients of Legendre polynomials in the angular distribution of a scattering amplitude.

IV. UNITARITY AND CASUALITY

Every quantity appearing on the right of Eqs. (10), (12), (14), and (17) is real, except for the infinitesimal $(-i\epsilon)$ in the denominators. Therefore the imaginary part on the right side of these equations comes only from states $|R\rho\rangle$ with $\Delta_R=\omega_x$. Using (9), the imaginary part of (10) becomes

$$\begin{aligned}\mathrm{Im}\langle T\tau M\mu|F(x)|S\sigma L\lambda\rangle&=(x/\omega_x)\sum_{R\rho}\langle T\tau M\mu|F^*(x)|R\rho\rangle\\ &\times\delta(\Delta_R-\omega_x)\langle R\rho|F(x)|S\sigma L\lambda\rangle,\end{aligned} \quad (21)$$

which is simply a statement that the S-matrix (8) is unitary. Since Eqs. (12), (14), and (17) are all equivalent to (10), the imaginary parts of these equations are also equivalent to the unitarity of the S-matrix. For example, the imaginary part of (12) is

$$\begin{aligned}\mathrm{Im}\langle TM|F_J(x)|SL\rangle&=\frac{xu_L(x)u_M(x)}{(2J+1)16\pi}(-1)^{M+T-J}\\ &\times\sum_R\delta_{RJ}\delta(\Delta_R-\omega_x)\langle T\|O^M\|R\rangle\langle R\|O^L\|S\rangle,\end{aligned} \quad (22)$$

and this is another statement of the unitarity condition.

We may now use Eq. (22) in order to simplify (12), following the ideas of Low.[3] The contribution to the right side of (12) from all states R with $\Delta_R=\omega_x>\mu$ may be expressed by (22) in terms of $\mathrm{Im}F_R(z)$. Thus (12) becomes

$$\begin{aligned}\langle TM|F_J(x)|SL\rangle&=\frac{xu_L(x)u_M(x)}{16\pi^2}\sum_R{}'\Big[\frac{(-1)^{M+T-R}}{\Delta_R-\omega_x}\\ &\times\langle T\|O^M\|R\rangle\langle R\|O^L\|S\rangle\frac{1}{2J+1}\delta_{JR}+\frac{(-1)^{M+S-R}}{\Delta_R+\omega_x}\\ &\times\langle T\|O^L\|R\rangle\langle R\|O^M\|S\rangle W(LSTM,JR)\Big]\\ &+\frac{1}{\pi}\int_0^\infty\frac{dz}{\omega_x}\frac{xu_L(x)u_M(x)}{u_L(z)u_M(z)}\Big[\frac{\mathrm{Im}\langle TM|F_J(z)|SL\rangle}{\omega_z-\omega_x-i\epsilon}\\ &+\sum_R\frac{\mathrm{Im}\langle TL|F_R(z)|SM\rangle}{\omega_z+\omega_x}(-1)^{M+S-L-T}\\ &\times(2R+1)W(LSTM,JR)\Big]. \quad (23)\end{aligned}$$

[7] The extra symmetry is related to the Gell-Mann and Goldberger "crossing theorem" [the theorem is mentioned by H. W. Wyld, Phys. Rev. **96**, 1661 (1954), end of Sec. III, but is otherwise unpublished]. The purpose of introducing the quantum-number N is to make this symmetry evident in the equations.

[8] U. Fano, Phys. Rev. **90**, 577 (1953).

Here the first sum extends only over the states R of the system for which $\Delta_R<\mu$, and is in most cases a discrete sum over a finite number of states. The integral has the appearance of a dispersion formula, except that the amplitudes for different angular momenta R are mixed together in the last term.

To obtain a true dispersion formula, we must use the N-coupling scheme and apply the same argument to the real and imaginary parts of Eq. (17). Let $Q_{N\alpha}(R)$ be the quantity in curly brackets on the right of (17). Let the function $g_{N\alpha}(\omega)$ be defined by

$$g_{N\alpha}(\omega_k)=[16\pi^2/xu_L(x)u_M(x)]\langle TM|G_{N\alpha}(x)|SL\rangle. \quad (24)$$

Then using the unitarity of the S-matrix to simplify the right side, Eq. (17) becomes

$$g_{N\alpha}(\omega)=\sum_R{}' Q_{N\alpha}(R)\left[\frac{1}{\Delta_R-\omega}+\frac{(-1)^{N+\alpha}}{\Delta_R+\omega}\right]$$
$$+\frac{1}{\pi}\int_\mu^\infty[\mathrm{Im}g_{N\alpha}(\omega')]d\omega'\left[\frac{1}{\omega'-\omega-i\epsilon}+\frac{(-1)^{N+\alpha}}{\omega'+\omega}\right]. \quad (25)$$

This is a dispersion formula of the customary kind, expressing the fact that $g_{N\alpha}(\omega)$ is an analytic function of ω for complex ω in the upper half-plane, and is an even or odd function according as $(N+\alpha)$ is even or odd. We may call Eq. (25) a causality condition, since it is formally similar to the dispersion formulas which have been deduced from requirements of causality.[9] The fact that the linear transformation (18), (16) from F_J to $G_{N\alpha}$ diagonalizes the Eqs. (23) is due directly to the Racah sum-rule (19).

These results may be summed up in the statement that the Low scattering equation is equivalent to a unitarity condition (22) which is simple in the J-coupling scheme, together with the causality condition (25) which is simple in the N-coupling scheme. The interlock between the two conditions is given by the transformation formulas (18).

When the meson energy is below the threshold for inelastic processes, the unitarity condition is particularly simple. In this case the only states $|R\rho\rangle$ which contribute to (21) are one-meson states $|P\pi K\kappa x\rangle$, and Eq. (22) reduces to

$$\mathrm{Im}\langle TM|F_J(x)|SL\rangle$$
$$=\sum_{PK}\langle TM|F_J^*(x)|PK\rangle\langle PK|F_J(x)|SL\rangle,$$

or simply

$$\mathrm{Im}F_J(x)=F_J^*(x)F_J(x), \quad (26)$$

where $F_J(x)$ is considered as a matrix in the indices $TMSL$.

The "one-meson approximation" of Low[2] means that inelastic processes are neglected and so (26) is assumed to hold for all energies. We shall not make this approximation, but we shall specialize the system slightly in order to bring the dispersion formula (25) into a very simple form. We suppose that the scatterer has a ground state with spin S, and no other state with energy below $E_S+\mu$. We consider the amplitude $\langle SM|G_N|SL\rangle$ for elastic scattering which leaves the scatterer in the ground state, not assuming that competing inelastic processes are absent or unimportant. In this case the causality condition can be deduced directly from (14) instead of from (17), and the sum over states R in (25) reduces to the single term $R=S$ with $\Delta_R=0$. If we write

$$\langle SM|G_N(x)|SL\rangle=[Q_N/16\pi^2]xu_L(x)u_M(x)g_N(\omega_k),$$
$$Q_N=(-1)^L\langle S\|O^M\|S\rangle\langle S\|O^L\|S\rangle W(SMSL,SN), \quad (27)$$

the unitary condition applied to Eq. (14) gives the result

$$g_N(\omega)=[(-1)^N-1]\frac{1}{\omega}$$
$$+\frac{1}{\pi}\int_\mu^\infty[\mathrm{Im}g_N(\omega')]d\omega'\left[\frac{1}{\omega'-\omega-i\epsilon}+\frac{(-1)^N}{\omega'+\omega}\right]. \quad (28)$$

This equation is precisely equivalent to the following four statements:

(a) $g_N(\omega)$ is an analytic function of ω in the whole complex plane with cuts from μ to $+\infty$ and from $-\mu$ to $-\infty$.
(b) $g_N(\omega)$ is real for real ω in the range $-\mu<\omega<\mu$.
(c) $g_N(\omega)$ is even or odd according as N is even or odd.
(d) $g_N(\omega)$ has only a simple pole with residue -2 at $\omega=0$ when N is odd, and it has no pole when N is even.

The fact that these conditions, together with the unitarity condition (21), are equivalent to the scattering Eq. (10), is the theorem of Low which was mentioned in Sec. I.

V. EXTENSION TO CHARGED MESONS. THEORY OF MESON-NUCLEON SCATTERING

The theory which has been developed for neutral mesons can be extended immediately to mesons which possess a total isotopic spin L' and a charge quantum-number λ', scattered by a scatterer possessing total isotopic spin S' and charge quantum-number σ', provided the interaction is invariant under rotations in isotopic space. Particles having several values L', M' of total isotopic spin may also be included. The resulting equations will be the same as for the neutral case, except that each Racah coefficient is replaced by a product of two Racah coefficients operating independently on the angular momentum and isotopic spin quantum numbers. For example in Eq. (12), $W(LSTM,JR)$ is replaced by $W(LSTM,JR)W(L'S'T'M',J'R')$.

The Chew model of p-wave meson-nucleon scattering is the special case of this theory in which always

[9] Gell-Mann, Goldberger, and Thirring, Phys. Rev. **95**, 1612 (1954); M. L. Goldberger, Phys. Rev. **97**, 508 (1955); M. L. Goldberger, Phys. Rev. **99**, 979 (1955); Goldberger, Miyazawa, and Oehme, Phys. Rev. **99**, 986 (1955).

$L=L'=M=M'=1$, $S=S'=T=T'=\frac{1}{2}$. The possible values of J, J', R, R' are $\frac{1}{2}$, $\frac{3}{2}$, and the possible values of N, N' are 0, 1. We write

$$W_{JR}=W(1\tfrac{1}{2}\tfrac{1}{2}1,JR),$$
$$V_{RN}=W(\tfrac{1}{2}1\tfrac{1}{2}1,RN), \tag{29}$$

so that W and V are numerical 2×2 matrices

$$W_{JR}=\frac{1}{12}\begin{bmatrix}-2 & 4\\ 4 & 1\end{bmatrix},\quad V_{RN}=\frac{1}{6}\begin{bmatrix}-\sqrt{6} & 2\\ +\sqrt{6} & 1\end{bmatrix}. \tag{30}$$

The physical properties of the scatterer are expressed only in the form-function $u_1(x)$ and in the single reduced matrix element

$$f=\langle\tfrac{1}{2}\tfrac{1}{2}\|O^{11}\|\tfrac{1}{2}\tfrac{1}{2}\rangle, \tag{31}$$

which fixes the strength of the interaction. We may identify f with the renormalized coupling constant of the Chew theory. The scattering amplitude

$$F_{JJ'}(x)=\langle\tfrac{1}{2}\tfrac{1}{2}11\,|\,F_{JJ'}(x)\,|\,\tfrac{1}{2}\tfrac{1}{2}11\rangle \tag{32}$$

is equal to $e^{i\delta}\sin\delta$, where δ is the phase-shift for a meson of momentum x in the state (J,J') of the system meson-plus-scatterer. In general δ will be complex; it is real below the threshold for inelastic processes, in the range where (26) holds.

The scattering Eq. (23) for the Chew model becomes

$$\begin{aligned}F_{JJ'}(x)=&-(f^2/16\pi^2)\{x[u_1(x)]^2/\omega_x\}\\ &\times[\tfrac{1}{4}\delta_{J\frac{1}{2}}\delta_{J'\frac{1}{2}}-W_{J\frac{1}{2}}W_{J'\frac{1}{2}}]\\ &+\frac{1}{\pi}\int_0^\infty\frac{dz}{\omega_z}\frac{x[u_1(x)]^2}{[u_1(z)]^2}\Big[\frac{\mathrm{Im}F_{JJ'}(z)}{\omega_z-\omega_x-i\epsilon}\\ &+\sum_{RR'}\frac{\mathrm{Im}F_{RR'}(z)}{\omega_z+\omega_x}(2R+1)(2R'+1)W_{JR}W_{J'R'}\Big].\end{aligned} \tag{33}$$

This is identical with Low's equation (3.11) of reference 2 if we choose[10]

$$u_1(x)=(48\pi)^{\frac{1}{2}}(x/\mu), \tag{34}$$

corresponding to the conventional point-source charge-symmetric pseudovector interaction, and assume (26) to hold for all x (one-meson approximation).

If, however, we make the substitution

$$F_{JJ'}(x)=(f^2/16\pi^2)x[u_1(x)]^2\sum_{NN'}Z_{JN}Z_{J'N'}g_{NN'}(\omega_x), \tag{35}$$

$$Z_{JN}=(-1)^{J-\frac{1}{2}}(2N+1)V_{\frac{1}{2}N}V_{JN}, \tag{36}$$

which is the analog of (18), (27) for the Chew model, then the functions $g_{NN'}(\omega)$ satisfy the simple dispersion formula

$$g_{NN'}(\omega)=[\pm1-1]\frac{1}{\omega}+\frac{1}{\pi}\int_\mu^\infty[\mathrm{Im}g_{NN'}(\omega')]d\omega'\Big[\frac{1}{\omega'-\omega-i\epsilon}\pm\frac{1}{\omega'+\omega}\Big]. \tag{37}$$

The ambiguous sign is plus for $N=N'$ and minus for $N\neq N'$. By (30), the numerical values of the coefficients Z_{JN} in (35) are

$$Z_{JN}=\frac{1}{6}\begin{bmatrix}1 & 2\\ 1 & -1\end{bmatrix}. \tag{38}$$

The relations (35) can be inverted to give

$$(f^2/16\pi^2)x[u_1(x)]^2g_{NN'}(\omega_x)=\sum_{JJ'}X_{NJ}X_{N'J'}F_{JJ'}(x), \tag{39}$$

with

$$X_{NJ}=2\begin{bmatrix}1 & 2\\ 1 & -1\end{bmatrix}. \tag{40}$$

It is the $g_{NN'}$, and not the usual scattering amplitudes $F_{JJ'}$, which obey causality relations of the form (37). It happens that the $g_{NN'}$ for the Chew model have a direct interpretation in terms of observable processes. Let $a^\pm(0)$ be the amplitude for elastic scattering without charge exchange of a positive or negative meson by a proton, without changing the proton spin state. Let $a^\pm(1)$ be the amplitude for scattering a positive or negative meson, with change of the proton spin state. Then g_{N0} is proportional to

$$[a^-(N)+a^+(N)],$$

and g_{N1} is proportional to

$$[a^-(N)-a^+(N)].$$

The fact that it is these combinations of the amplitudes which have a simple causal behavior has been already pointed out by Low and by Goldberger.[9]

The causality relations of Goldberger refer always to forward scattering amplitudes, which are expressions of the form (20). The coefficient $V(LMN,000)$ is zero when $(L+M+N)$ is odd, therefore in the case of the Chew model the right side of (20) brings in only the amplitudes with $N=0$ and not those with $N=1$. For this reason the argument of Goldberger demonstrates a causal behavior only for the no-spin-flip amplitudes, which are those with $N=0$. The causal behavior of the spin-flip $N=1$ amplitudes is thus a prediction of the Chew model which is not required (so far as we know) by general principles of field-theory, and may therefore serve as a test of the model.

ACKNOWLEDGMENTS

In conclusion, the author would like to thank Professor Chew and Professor Goldberger for very helpful discussions and for communications in advance of publication.

[10] According to (6) and (7) the time parity of the meson field must be odd, and the $u_L(k)$ pure imaginary, for neutral pseudoscalar mesons. In the charge-symmetric theory the meson field also has odd parity under inversion in isotopic space. This makes the $u_L(k)$ real when the charge variables are inserted in (6) and (7).

Renormalization of Derivative Coupling Theories

R. ARNOWITT AND S. DESER*
The Institute For Advanced Study, Princeton, New Jersey
(Received June 24, 1955)

The method of functional integrals is applied to the problem of meson theories with derivative couplings. In the static limit, solutions in closed form can be exhibited. The infinities occurring in the theory are found to be removable in terms of Z_2 and mass renormalizations, contrary to the conclusions of perturbation analysis. The divergences occurring here have the form of essential singularities, in contradistinction to the branch-point behavior of the usual "renormalizable" theories. The lack of validity of the perturbation expansion is thereby accounted for. These techniques can be extended to treat the full recoil neutral $ps(pv)$ problem omitting closed loops. The theory is represented in terms of an exponential coupling which permits a nonperturbation series solution for the various propagators. Two infinite renormalizations are again required. The resultant functions are given meaning by analytic continuation procedures which are adapted to the four-dimensional nature of the problem. The form of the effective coupling suggests a rearrangement of the answer in terms of exponentials of the meson propagator. As a result mass operator-like structures can be defined. These explicitly exhibit the transcendental nature of the coupling and generalized equivalence theorems with $ps(ps)$ theory can be generated. In a similar fashion, effective interaction operators for the two-nucleon and meson-nucleon Green's functions are derived. The possible applicability of these quantities to questions of physical interest such as nuclear potentials and multiple meson production is briefly mentioned.

In an appendix, a model of beta coupling is discussed in connection with the renormalization question there.

1. INTRODUCTION

FOLLOWING the success of the renormalization program in electrodynamics, the same methods and concepts have been brought to bear on the various types of meson theories. The success in this region, however, has not been universal. The applicability of perturbation renormalization techniques has become a criterion dividing these theories into two classes.

The most salient characteristic of many of the "unrenormalizable" theories is that they involve gradients of the meson field in the interaction. Upon examination of the radiative corrections occurring in these cases, one discovers that the infinities appearing in successive orders become more violent, due to the linear (or higher) dependence upon momentum transfer of the elementary vertex. Further, the infinities appear in such a way that an infinite number of observables would have to be renormalized. Such effects would correspond, in terms of a cut-off picture, to a theory entirely dependent upon the details of the structure of the elementary particles.[1] These derivative interaction theories, whose coupling constants have dimensions of reciprocal length, were thought to require, along with other so-called theories of the second kind, the existence of a fundamental length to give them meaning.[2] The possibility has always remained open, however, that the series of divergences might, in reality, sum to a more tractable form.

The meson theories of most current interest are, of course, the pseudoscalar ones. Although the pseudoscalar theory with pseudovector coupling has long seemed to be physically attractive, it has been neglected in recent years because of the above troubles. It is the purpose of the earlier sections of the paper to treat the problems involved in some simple nonrecoil models of derivative coupling theories. Already in these examples will be found many of the basic difficulties and divergences which beset the complete $ps(pv)$ theory.

By means of the functional integral formulation of field theory, one can obtain closed-form solutions in these cases. In this procedure (which will be the basic tool employed throughout) the complete, radiatively corrected, nucleon Green function, for example, is obtained by considering the propagation of a bare particle in an arbitrary external field distribution averaged over all such possible fields. This process represents the emission and subsequent absorption of the virtual meson field. The problem is thereby divided into two separate parts: that of finding a first quantized nucleon propagator in an arbitrary external field and that of averaging with the appropriate weight factor over this field (the functional integration). Perturbation theory corresponds to a Born approximation solution of the first problem. For the initial cases to be considered, the static, nonrecoil limit will be taken, which is equivalent to having the first quantized kernel satisfy a one dimensional equation. The latter can be solved rigorously and the functional integrations performed for the structures obtained. The steps then necessary to give these theories meaning will be clarified, as will the concept of renormalization. It will be seen in precisely what respects the perturbation analysis of renormalization fails; in addition, the infinities to be deleted from the theory will be exhibited explicitly.

Another set of unrenormalizable theories, not directly related to the above, consists of the so-called direct interactions, exemplified by the Fermi couplings. In Appendix A, a simple model (in that the heavy particles, though not the leptons, are taken as static) of

* F. B. Jewett Fellow. Now at the Institute for Theoretical Physics, Copenhagen, Denmark.
[1] Sakata, Umezawa, and Kamefuchi, Progr. Theoret. Phys. 7, 377 (1952).
[2] W. Heisenberg, Ann. Physik 32, 20 (1938).

scalar beta coupling is considered and the problems of renormalization discussed in the light of our methods.

In the meson case, the chief problem of physical interest must take fully into account all the degrees of freedom of the nucleon field, both the particle and spin motion. To treat the full recoil theory for neutral mesons, omitting closed loop diagrams, the method of functional integration is again the basic technique employed. The procedure used in this problem is to note that the ostensibly linear pseudovector coupling is equivalent to a pseudoscalar coupling exponential in the boson field. This fact allows the functional integrations to be performed and the infinite renormalizations separated. In this representation, the solutions are themselves exponential in the coupling constant. Thus structures similar to those obtained in the simpler models appear again in the complete problem, though in a more complicated context.

Another similarity to the problems noted in the nonrecoil cases is the necessity for giving definition to the propagators by means of analytic continuation. The apparatus developed here extends the treatment required for the case of branch points first considered in the simple renormalizable theory to the more singular derivative coupling four dimensional problems. There is actually a qualitative difference between the role played by the continuation procedure in these two cases due to the more violent nature of the essential singularities. This is true even for the null $s(v)$ theory with recoil, treated in Appendix D.

The expansion appropriate for performing the renormalizations is perhaps not that most suited to display the physical content of the theory. Since the effective coupling structure is transcendental, a natural series in such problems to obtain physical results would seem to involve exponentials in the coupling constant rather than merely the coupling constant itself. One finds many generalized equivalence theorems between the $ps(ps)$ and $ps(pv)$ theories in this process. By this analysis, the consequencies of the theory can be couched in diagrammatic language which displays how the natural exponential structure in the meson propagator replaces the perturbation form. Thus one can speak of an effective mass operator upon which can perhaps be based a reasonable approximation scheme. The above procedure is, of course, applicable to the more complex Green functions such as the meson-nucleon and two-nucleon ones. In both cases interaction operators can be defined; in view of some of the attractive properties of $ps(pv)$ theory, particularly at low energies and (in this formulation) with regard to multiple production, these quantities are briefly investigated.

2. FUNCTIONAL INTEGRAL FORMULATION

Throughout this work we shall employ the functional formulation of field theory to discuss the quantities of interest.[3,4] We consider a Lagrangian of the form[5]

$$\mathfrak{L}(x)=-\tfrac{1}{2}\bar{\psi}(x)(\gamma p+m)\psi(x)+\text{herm conj}$$
$$-\tfrac{1}{2}\phi(x)(k^2+\mu^2)\phi(x)-g\bar{\psi}(x)\Gamma f[\phi(x)]\psi(x), \quad (1)$$

where Γ represents the fundamental vertex ($\Gamma\phi=\phi$ for neutral scalar theory, $\gamma_5\tau^i\phi^i$ for $ps(ps)$ symmetric theory, $i\gamma_5\gamma_\mu\partial_\mu\phi$ for neutral $ps(pv)$ theory, etc.) and $f(\phi)$ equal $\phi(x)$ for a linear coupling, $\phi^2(x)$ for a pair theory, etc. The one-nucleon propagator with all radiative corrections (but omitting vacuum polarization) may be obtained from the functional integral

$$G_+'(x,x')=N^{-1}\int \exp\left[-\tfrac{1}{2}i\int\phi(\xi)\Delta_+^{-1}(\xi,\xi')\phi(\xi')d\xi d\xi'\right]$$
$$\times G_+(x,x';\phi)\delta\phi; \quad (2)$$
$$N=\int\exp\left[-\tfrac{1}{2}i\int\phi\Delta_+^{-1}\phi d\xi d\xi'\right]\delta\phi,$$

where $\phi(\xi)$ is a c-number over which the functional integration is carried out, Δ_+ obeys the equation $(-\partial_x^2+\mu^2)\Delta_+(\xi,\xi')=\delta(\xi-\xi')$ and $G_+(\phi)$ is the bare Green's function in the external field ϕ, satisfying

$$\{\gamma p+m+g\Gamma f[\phi(x)]\}G_+(x,x';\phi)=\delta(x-x'). \quad (3)$$

The "+" subscript indicates the usual outgoing wave boundary conditions. We also shall have occasion to use the free particle Green's function $G_+^{(0)}(x-x')=(x|(\gamma p+m)^{-1}|x')$.

Similarly, the general Green's function governing the propagation of n nucleons and m mesons is given by

$$G_{nm}'(x_1\cdots x_n,x_1'\cdots x_n';\xi_1\cdots\xi_m)$$
$$=N^{-1}i^{[m/2]}\int\exp\left[-\tfrac{1}{2}i\int\phi\Delta_+^{-1}\phi d\xi d\xi'\right]$$
$$\times G_+(x_1x_1')\cdots G_+(x_n,x_n')\phi(\xi_1)\cdots\phi(\xi_m)\delta\phi, \quad (4)$$

where $[m/2]$ means "integral part of $m/2$" and the nucleon coordinates are to be suitably antisymmetrized.

3. DERIVATIVE COUPLING THEORIES IN THE NONRECOIL LIMIT

Although our chief interest will center around the renormalization difficulties appearing in the derivative coupling theories, we first indicate how even so simple an example as neutral scalar theory without recoil exhibits one kind of problem we shall encounter in further work. For this case, in the Dirac Lagrangian, $\gamma p+m$ is replaced by $-p_0+m$.[6] In this approximation

[3] S. F. Edwards and R. E. Peierls, Proc. Roy. Soc. (London) **A224**, 24 (1954).
[4] S. Deser, Phys. Rev. **99**, 325 (1955).
[5] Our γ_μ are defined by the relation $\{\gamma_\mu,\gamma_\nu\}=-2\delta_{\mu\nu}$ and $\gamma_5^2=-1$.
[6] This treatment of the nucleons is equivalent to the usual fixed source approximation.

the solution to $G_+'(t-t')$ is given in reference 3; the relevant point here is that the renormalized Green function behaves at small times as

$$G_c \sim \exp[-(g^2/\pi^2)\ln\mu(t-t')] \quad t>t'$$
$$0 \quad t<t'. \tag{5}$$

The existence of a Fourier transform of the convergent propagator is necessary in order to maintain the quantum mechanical transformation theory for finite times. Further, in momentum space, the Green function must behave appropriately to meet the usual physical requirements on the theory. It is clear, from Eq. (5), that a critical coupling strength occurs at $g^2/4\pi=\pi/4$, above which rigorously no transform exists. Since physically such a limitation on the size of g^2 would appear to have no meaning, we proceed to remove it by one of the various mathematical techniques invented for this purpose.[7] In particular, the method that we will adopt here and elsewhere will be that of an analytic continuation of g^2/π^2 from below the critical value of unity to above it. Specifically we consider the function $G_c(t-t', g^2)$ for values of $g^2/\pi^2<1$. Here we may evaluate its transform $G_c(p_0,g^2)$ which is analytic in g^2 for $g^2/\pi^2<1$. Such a function will have a continuation to values above unity (though poles will occur when $g^2/\pi^2=1, 2, 3, \cdots$). Thus meaning has been given for G_c beyond the barrier that the particular representation in Eq. (5) seemed to impose. Insofar as the resultant behavior in momentum space is concerned, the results of reference 3 should hold for the larger coupling constants.

We now consider a set of examples which both involve derivatives of the meson field in the coupling term and are simple enough to be solved exactly. These will arise from various approximations to be made on the nucleon's motion as represented in Eq. (3) in the case where the coupling is pseudovector. Such approximations do not involve the exponential weight factor in the functional integration which represents the radiative corrections due to the boson field. We begin with a somewhat artificial limit in which both the nucleon recoil and the gradient parts of the coupling have been dropped:

$$(-p_0+m-ig\gamma_4\partial_4\phi)G_+(t,t';\phi)=\delta(t-t'), \tag{6}$$

where $G_+(t,t')$ actually includes a $\delta(r-r')$. The γ_4 has been retained in Eq. (6) in order to include one feature of γ_4 couplings: $\gamma_4^2=-1$. (Terms linear in γ_4 will, of course, turn out to vanish in the solution since negative energy states have been otherwise neglected.)

Equation (6) may easily be integrated to yield

$$G_+(t,t';\phi)=i\theta(t-t')e^{-im(t-t')} \times\exp\left[-g\gamma_4\int_{t'}^{t}\partial_4\phi(\tau)d\tau\right], \tag{7}$$

where $\theta(x)$ is 1 or 0 as x is greater or less than zero (which enforces the nonrelativistic boundary conditions). The functional integration may be performed via the formula

$$N^{-1}\int\exp\left[-\tfrac{1}{2}i\int\phi(\xi)\Delta_+^{-1}(\xi,\xi')\phi(\xi')d\xi d\xi' + \int\phi(\xi)f(\xi)d\xi\right] = \exp\left[-\tfrac{1}{2}i\int f(\xi)\Delta_+(\xi,\xi')f(\xi')d\xi d\xi'\right]. \tag{8}$$

In Eq. (7), $f(\xi)=-g\gamma_4\partial_4 H(\xi_0;t,t')\delta^3(\xi)$, where $H(\xi_0;t,t')=\theta(t-\xi_0)\theta(\xi_0-t')$. The presence of γ_4 in the exponential is not troublesome since it commutes with all other quantities involved. The total Green function is then

$$G_+'(t-t')=i\theta(t-t')e^{-im(t-t')} \times\exp\{-ig^2[\Delta_+(t-t')-\Delta_+(0)]\}. \tag{9}$$

All that is necessary to renormalize the theory, therefore, is to identify $\exp ig^2\Delta_+(0)$ with Z_3, no mass renormalization being required.[8] The form $\Delta_+(t-t')-\Delta_+(0)$ appearing in Eq. (9) arises since

$$\text{disc } G_+'(0)=i\langle\{\bar{\psi}(t),\psi(t)\}\rangle=i. \tag{10}$$

The renormalization just performed is qualitatively different from those needed in a "renormalizable" theory such as the neutral scalar one quoted above. In particular, the infinity appears as an essential singularity rather than as a branch point (the latter manifesting itself in perturbation theory as a series of logarithms). If Eq. (6) and hence G_+' were solved in a perturbation fashion, one would have found the usual "unrenormalizable" results: The higher and higher diagrams would have higher and higher infinities in them, leading one to believe that an infinite number of renormalizations were necessary. Actually, as can be seen in Eq. (9), the infinities sum to an essential singularity which, however, is a harmless multiplicative factor. Indeed, if $G_+'(t)$ is only a function of $\Delta_+(t)-\Delta_+(0)$, the condition that theory be renormalizable in the usual way,

$$G_+'[\Delta_+(t)-\Delta_+(0)]=Z_2[\Delta_+(0)]G_c[\Delta_+(t)] \tag{11}$$

forces an exponential solution like Eq. (9) and hence an essential singularity.

The renormalized one-particle Green function in its dependence on time is everywhere finite and does not even exhibit the difficulties in Fourier analysis discussed for the neutral scalar theory. The higher Green's functions [which may be obtained from Eq. (4)], such

[7] F. J. Dyson has pointed out in conversation that methods of L. Schwartz may also be applied to this problem.

[8] It is interesting to note that this theory formally has a Ward identity. This appears to be the case whenever there are no commutation problems for a nonrecoil meson theory.

as the two-nucleon propagator, may all be renormalized in an analogous fashion. However, in both theories analytic continuation must be applied to Fourier analyze these more complex functions. In the neutral scalar case it is again a matter of branch points while here an essential singularity on the light cone must be treated. The requisite technique for such problems will be introduced later.

As can be seen by inspecting the various Green functions, the theory we have been considering here produces no observable effects in the S-matrix. In this it resembles the situation encountered in $s(v)$ coupling. Indeed the latter's nonrelativistic $\Gamma\phi$ is $\partial_0\phi$. Similar statements can be made about the renormalization and lack of physical effects for theories of the type $\Gamma\phi=\partial_0{}^n\phi$.[9] While all such examples make no physical predictions, they do retain enough of the dynamical structure to illustrate the type of renormalization and the analytic continuation problems that will arise in the physically interesting cases. In Appendix B, a static approximation involving gradient coupling and having observable consequences is discussed.

4. THE NONRECOIL APPROXIMATION AND TRANSCENDENTAL COUPLING

The first approximation scheme considered, Eq. (6), neglected anticommutativity of γ_5 with γ_0 while including the fact that $\gamma_5{}^2=-1$. A scheme that embodies part of this effect starts from the equation

$$(-\gamma_0 p_0+m+ig\gamma_5\gamma_\sigma\partial_\sigma\phi)G_+(t,t';\phi)=\delta(t-t'). \quad (12)$$

We now make a transformation analogous to that introduced by Dyson[10]:

$$G_+(t,t';\phi)=\exp[-g\gamma_5\phi(t)]H_+(t,t';\phi)\times\exp[-g\gamma_5\phi(t')]. \quad (13)$$

The equation obeyed by H_+ is

$$\{-\gamma_0 p_0+m\exp[-2g\gamma_5\phi(t)]\}H_+(t,t';\phi)=\delta(t-t'). \quad (14)$$

Having used the fact that $\{\gamma_0,\gamma_5\}=0$, which is essential in arriving at Eq. (14), we now make the approximation of setting $\gamma_0=1$.[11] As will be seen later, this step changes considerably the predictions of the theory which therefore differs from the true nonrecoil limit of $ps(pv)$. The approximation is simple enough, however, to enable us to justify expansions that will later be generalized to more complicated cases.

Within this framework, then, Eq. (14) may be integrated to yield

$$H_+(t,t';\phi)=i\theta(t-t')\exp\left[-im\int_{t'}^{t}e^{-2g\gamma_5\phi(\tau)}d\tau\right]. \quad (15)$$

In order to perform the functional integral it is necessary to expand H_+ in a power series in m. This expansion, which should be valid at small times, will be justified later. The resulting exponentials may be functionally integrated term by term to yield

$$G_+'(t-t')=Z_2 i\theta(t-t')\times\exp[ig^2\Delta_+(tt')]\sum_{n=0}^{\infty}\frac{(-im')^n}{n!}\int_{t'}^{t}dt_1\cdots dt_n\times\exp[2ig^2\sum_{i=1}^{n}\{\Delta_+(t_it)+\Delta_+(t_it')\}]\times\exp[4ig^2\sum_{i>j=1}^{n}\Delta_+(t_it_j)], \quad (16)$$

where Z_2 and the renormalized mass m' are given by

$$Z_2=\exp[ig^2\Delta_+(0)],\qquad m'=m\exp[2ig^2\Delta_+(0)]. \quad (17)$$

It is interesting that Z_2 here is formally greater than unity if, in the spirit of a static theory, one sets $\mathbf{r}$ to zero in $\Delta_+(0)$ before t. The fact that all signs in the exponentials are positive is explicitly due to the dropping of γ_0 in Eq. (14) and also entails that disc $G_+'(0)$ in Eq. (16) does not reduce to i. Thus this approximation destroys the canonical commutation relations.

Although the infinities obtained here are similar to those arising in previous approximations where the functional integral could be done rigorously, it may be asked whether this theory is indeed infinite or whether the difficulties actually come from the small time expansion and the subsequent functional integration of the series. To consider this question, we first obtain an expression for $G_+(t,t';\phi)$ which is rigorously correct at small times. In general one has

$$G_+(t,t';\phi)=i\theta(t-t')\exp[-g\gamma_5\{\phi(t)+\phi(t')\}]\times\exp\left[-im\int_{t}^{t'}d\tau\{\cos 2g\phi(\tau)-\gamma_5\sin 2g\phi(\tau)\}\right]. \quad (18)$$

We may replace the integrals occurring in Eq. (18) by the integrands evaluated at some mean value since the ϕ's are real functions. Denoting below by t_1 and t_2 the mean value points for the cosine and sine integrals respectively, Eq. (18) may be written

$$G_+(t,t';\phi)=i\theta(t-t')\cos[g\{\phi(t)+\phi(t')\}-im(t-t')\sin 2g\phi(t_2)]\times\exp[-im(t-t')\cos 2g\phi(t_1)], \quad (19)$$

where terms odd in ϕ have been dropped, since they vanish in the subsequent integration. The functional

[9] That nonrecoil theories of the type $\Gamma\phi=\partial_0{}^n\phi$ are renormalizable has also been discovered by L. Cooper, following paper [Phys. Rev. **100**, 362 (1955)].

[10] F. J. Dyson, Phys. Rev. **73**, 929 (1948).

[11] An approximation substantially equivalent to this has been discussed by R. J. Glauber, Phys. Rev. **84**, 395 (1951). In that paper the fact that the scheme was renormalizable was observed and the S-matrix obtained. Our Eq. (16) differs from Glauber's result by the inclusion of the first two exponentials and the existence of Z_2. In the transition from the finite times Green's function to the renormalized S-matrix, these terms disappear.

integral, $\int\delta\phi$, may be viewed as an infinite product of ordinary integrals, $\prod_i\int d\phi(s_i)$, over all cells in space. The range of each integration is from $-\infty$ to $+\infty$. As $\phi(t_1)$ and $\phi(t_2)$ cover this range, $(t-t')\cos 2g\phi(t_1)$ and $(t-t')\sin 2g\phi(t_2)$ remain bounded and tend to zero as $t\to t'$. Thus in the entire range of functional integration the usual power series in $t-t'$ is uniformly convergent. Hence if the functional integral of (19) exists, then the integral of the power series in $t-t'$ exists. To first order one may write

$$G_+(t,t';\phi)\cong i\theta(t-t')[\cos g\{\phi(t)+\phi(t')\}+im(t-t')\{\sin 2g\phi(t_2)\sin g\{\phi(t)+\phi(t')\}-\cos 2g\phi(t_1)\cos g\{\phi(t)+\phi(t')\}], \quad (20)$$

which gives upon functional integration

$$G_+'(t-t')\cong Z_2 i\theta(t-t')\exp[ig^2\Delta_+(t-t')][1-im'(t-t')\times\{\cos 2g^2(\Delta_+(t_1-t)+\Delta_+(t_1-t'))+i\sin 2g^2(\Delta_+(t_2-t)+\Delta_+(t_2-t'))\}]. \quad (21)$$

This is equal, of course, to the first two terms in the expansion (16) when the mean value condition is used at sufficiently small times. The important point is that the series expansion of Eq. (19) when integrated has the same infinities as Eq. (16), and thus the infinite renormalizations are not due to the process of expansion but are intrinsic properties of the theory.

5. SOLUTION AND RENORMALIZATION OF THE THEORY WITH RECOIL

The radiatively corrected one-nucleon propagator for the full recoil neutral $ps(pv)$ theory is given by the same formal functional integral as in the no-recoil cases, Eq. (2). Now, however, $G_+(xx';\phi)$ obeys the more complicated equation

$$[\gamma p+m+ig\gamma_5\gamma_\mu\partial_\mu\phi]G_+(xx';\phi)=\delta(x-x'). \quad (22)$$

One can again bring this into the form in which the transcendental aspect of the coupling is emphasized by the same substitution as was made in Sec. 4:

$$G_+(xx';\phi)=\exp[-g\gamma_5\phi(x)]\times H_+(xx';\phi)\exp[-g\gamma_5\phi(x')]. \quad (23)$$

$H_+(xx';\phi)$ now obeys the equation

$$\{\gamma p+m\exp[-2g\gamma_5\phi(x)]\}H_+(xx';\phi)=\delta(x-x'). \quad (24)$$

A closed form solution here would require the disentangling of even more complicated ordered operator expressions than in the nonrelativistic case. However, the analysis there given of the convergence of a series development of the corresponding equation in powers of the mass times the propagation time, $t-t'$, would seem to sanction a similar expansion in this case. We therefore obtain the operator equation

$$H_+=\frac{1}{\gamma p}\sum_{n=0}^{\infty}\left(\exp[-2g\gamma_5\phi]\frac{-m}{\gamma p}\right)^n. \quad (25)$$

$m/\gamma p$ thus plays the role of $-m/p_0$ in the no-recoil case; hence one is making an expansion in large momenta or small space-time intervals. Defining the neutrino-like free propagator, $H_0(xx')=(x|(\gamma p)^{-1}|x')$, Eq. (25) becomes in the coordinate representation

$$H_+(xx';\phi)=\sum_{n=0}^{\infty}(-m)^n\int\cdots\int dy_1\cdots dy_n H_0(xy_1)\times\exp[-2g\gamma_5\phi(y_1)]H_0(y_1y_2)\times\exp[-2g\gamma_5\phi(y_2)]\cdots H_0(y_nx'). \quad (26)$$

With the exponentials in the positions above, the functional integration cannot be explicitly performed. Now, however, that the operator form of Eq. (25) has been expressed in coordinate functions, the exponentials can be freely commuted past the H_0's to the extreme right by noting that

$$\exp[-2g\gamma_5\phi(y)]H_0(y'y'')=H_0(y'y'')\exp[2g\gamma_5\phi(y)]. \quad (27)$$

One obtains then for $G_+(xx';\phi)$ the structure

$$G_+(xx';\phi)=\sum_{n=0}^{\infty}(-m)^n\int dy_1\cdots dy_n H_0(xy_1)\cdots H_0(y_nx')\times\exp\left\{-2g\gamma_5\int d\xi\phi(\xi)\left[\frac{\delta(\xi-x')}{2}+\frac{(-)^{n+1}\delta(\xi-x)}{2}-\delta(\xi-y_n)+\delta(\xi-y_{n-1})+\cdots+(-)^n\delta(\xi-y_1)\right]\right\}. \quad (28)$$

The usefulness of the neutrino Green's function expansion is now clear; had one attempted to expand Eq. (24) in a series of $G_+^{(0)}$'s by artifically adding and subtracting m, one would have encountered considerably more difficulty in moving the exponentials to one side. A more important problem than this combinatorial one, however, would have been the extraction of the infinite mass renormalization which will turn out to be trivial for the form of Eq. (28). After the renormalization we shall indeed proceed to restate (in Sec. 7) the answer in terms of propagators with masses. Equation (28) more clearly exhibits the fact that we are here dealing with an expansion about the origin in coordinate space; the first term is just $H_0(xx')$ which has the same leading singularity at small times as the rigorous $G_+(xx';\phi)$.[13]

The functional integral can now be performed to

[13] These singularities are, of course, just those of $G_+^{(0)}(x,x')$. The infrared divergences which exist in Eq. (28) due to the fact that we have formally expanded a problem with recoil about $m=0$, will, of course, disappear as the series is recombined into propagators with mass.

yield for the one-nucleon Green function

$$G_+'(xx')=Z_2\sum_{n=0}^{\infty}(-m')^n\exp[-ig^2(-)^n\Delta_+(xx')]$$
$$\times\int dy_1\cdots dy_nH_0(xy_1)\cdots H_0(y_nx')$$
$$\times\exp\{2ig^2\sum_{i=1}^{n}(-)^i[\Delta_+(xy_i)+(-)^{n+1}\Delta_+(y_ix')]\}$$
$$\times\exp\{4ig^2\sum_{i>j=1}^{n}(-)^{i+j}\Delta_+(y_iy_j)\},\quad(29)$$

where

$$Z_2=\exp[ig^2\Delta_+(0)];\quad m'=m\exp[2ig^2\Delta_+(0)].\quad(30)$$

It is shown in Appendix C that the result (29) is formally equivalent to the perturbation one.

The sign of the leading singularity at $x_\mu=0$ of $\Delta_+(0)$ is ambiguous, depending on whether the limit is taken in a space- or time-like fashion. In order to determine whether Z_2 is to be considered greater or less than unity one must insist on the preservation of the boundary condition that

$$\text{disc}\,G_+'(\mathbf{r}-\mathbf{r}',0)=i\langle\{\bar{\psi}(\mathbf{r}),\psi(\mathbf{r}')\}\rangle=i\gamma_0\delta(\mathbf{r}-\mathbf{r}').\quad(31)$$

That this condition is built into G_+' can most easily be seen from Eq. (24). For any reasonably behaved $\phi(x)$, $\gamma_0\rho_0$ is responsible for producing the singularity of Eq. (31) and, since the functional integral of Eq. (2) leaves this leading term unaffected, the desired result is guaranteed. In Eq. (29) the limiting procedure is not so transparent. However, as will become apparent after the process of analytic continuation has rendered the exponentials more meaningful near their singularities, the term linear in H_0 will still be chiefly responsible for producing the characteristic discontinuity. Since this term has for coefficient $\exp[-ig^2\{\Delta_+(x-x')-\Delta_+(0)\}]$ which must approach unity as $x_\mu\to x_\mu'$ in the space-like sense of Eq. (31), the sign of $\Delta_+(0)$ is thus determined to be the "space-like" one. That is, Z_2 for this theory has the physically desirable property of being <1 in magnitude.

6. ANALYTIC CONTINUATION PROCESS

While the renormalizations performed in Eq. (29) extract the appropriate infinite parts of the theory, the intermediate integrals as well as the Fourier analysis of the propagator must be given meaning. In this, the theory is akin to the simplest example of the static neutral scalar theory discussed in Sec. 3. Here, however, the procedures required are complicated by both the four-dimensional nature of the problem and the essential singularities in the functions being considered.

The formal Fourier transform of $G_c(x-x')$, assuming for the moment that all functions are well-behaved, may be written as

$$G_c(p)=\sum_{n=0}^{\infty}(-m')^n\int\cdots\int H_0(p-\sum_{i=1}^{n+1}k_{i,0})\cdots$$
$$\times H_0(p-\sum_{i=0}^{n-1}k_{n+1,i}-\sum_{i=0}^{n-1}k_{n,i})$$
$$\times H_0(p-\sum_{i=0}^{n}k_{n+1,i})\prod_{i>j=0}^{n+1}\lambda_{ij}(k_{ij})dk_{ij},\quad(32)$$

where

$$\lambda_{ij}(k_{ij})=(2\pi)^{-4}\int\exp[ik_{ij}(y_i-y_j)]$$
$$\times\exp[4ig^2a_{ij}\Delta_+(y_iy_j)]d(y_i-y_j)\quad(33)$$

and $a_{ij}=(-1)^{i+j}$ times 1, $\frac{1}{2}$ or $\frac{1}{4}$ depending whether none, one, or both y_i and y_j take on the value 0 or $n+1$. The Fourier variables k_{ij} are defined in the following fashion: Labeling the points x and x' in coordinate space by y_0 and y_{n+1} respectively, the momentum variable k_{ij} is chosen for the λ which connects the points y_i and y_j. Thus diagrammatically, there are n λ's "emitted" from the lowest point x' "propagating" to the remaining n points. The point y_n "reabsorbs" one and in turn emits $n-1$ others, etc.

The problem of giving meaning to the Fourier transformed propagator is essentially, therefore, transferred to that of defining $\lambda(k)$, provided, as will then be the case, the k integrations converge. Since $\lambda(y)$ has as leading singularity near the light cone the form $\exp(\pm g^2/y_\mu^2)$, we consider first a simple one-dimensional example of the same structure. The function $g(x)=x^{-2}\exp(g^2/x^2)$ has the transform

$$g(k)=\int[\exp(g^2/x^2)]e^{ikx}x^{-2}dx.\quad(34)$$

Obviously the difficulties in this integration occur for small x. It will suffice here, therefore, to discuss the analytic continuation procedure for the quantity[18]

$$f(g^2)=\int_0^1[\exp(g^2/x^2)]x^{-2}dx.\quad(35)$$

In the physically interesting case of λ_{ij} when one approaches the light cone from that direction, either space-like ot time-like, such that the exponent approaches $+\infty$, integrals of the type (35) appear.

The function $f(-g'^2)$ exists and is perfectly well behaved. To analytically continue to the region $g'^2<0$ one notes that

$$f(-g'^2)=\frac{1}{2}\left(\frac{g'^2}{\pi}\right)^{-\frac{1}{2}}-{}_1F_1(\tfrac{1}{2},\tfrac{3}{2},-g'^2),\quad g'^2>0.\quad(36)$$

When $g'^2=-g^2(g^2>0)$, Eq. (36) has a quite finite analytic continuation. Using the integral representation

[18] The analytic properties of the more general function $g(k)$ has been considered by L. Cooper.

for ${}_1F_1$, one obtains the defining equation for $f(g^2)$[14,15]:

$$f(g^2)=\frac{-i}{2}\left(\frac{g^2}{\pi}\right)^{-1}-\int_1^\infty[\exp(g^2/z^2)]z^{-3}dz. \quad (37)$$

In the physically significant problem, one must Fourier analyze quantities of the type $\lambda_+(x)=\exp[4ig^2\Delta_+(x)]$. The exponent may be written as

$$4ig^2\Delta_+(x)=ig^2/\pi\delta(x_\mu^2)-g^2/\pi^2(x_\mu^2)^{-1}-g^2\mu^2/2\pi^2F(x^2), \quad (38)$$

where $F(x^2)$ near the light cone behaves as $\ln\mu|x|$ plus a finite but discontinuous function. To treat the δ function part we note that

$$\exp[ig^2/\pi\delta(x_\mu^2)]=1+\frac{\delta(x_\mu^2)}{\delta(0)}\{\exp[ig^2/\pi\delta(0)]-1\}=1, \quad (39)$$

since the second term vanishes everywhere but on the light-cone and is bounded on the cone. Thus the pulse part of the Δ_+ function does not contribute.

The remaining part of $\lambda(x)$ to be analyzed has as its leading singularity $(x_\mu^2)^{-1}$ (which is analogous to our one-dimensional example in the foregoing) and the logarithmic term (which resembles the neutral scalar no-recoil structure treated in 3). The fact that we now have a four dimensional problem manifests itself through the possibility that $1/x^2$ changes sign across the light-cone whereas in one dimension there can be no change of sign. Thus in the Fourier analysis of $\exp[-g^2/\pi^2(x_\mu^2)^{-1}]$ there is no singularity outside the light-cone while in the regions of x_μ^2 time-like analytic continuation as in the one-dimensional example defines that portion of the integration in the transform. When g^2 is large enough, the logarithmic part of $F(x^2)$ will correspond to a branch point in the usual fashion. Thus there will be an analytic continuation required from small g^2 to large g^2 even for the regions outside the light cone.

The other type of function whose Fourier analysis must be defined is $\lambda_-(x)=\exp[-4ig^2\Delta_+(x)]$. The only difference in treating this function from the procedure just outlined lies in the interchange of the space-like and time-like regions. Hence all exponentials must be analytically continued, though each in a separate domain.

The statement made above that $\lambda(k)$ will vanish sufficiently rapidly for large k is now seen to hold, since the continuation has ensured that as a function of x, λ vanishes adequately at the origin.[16]

[14] In obtaining Eq. (37), the usual convention that $(-1)^{\frac{1}{2}}=+i$ has been followed.

[15] The fact that the definition of $f(g^2)$ by continuation results in a complex form [Eq. (37)] for the apparently real integral of Eq. (35) may perhaps be a manifestation of a "charge renormalization" akin in this respect to that required in the theory of T. D. Lee [Phys. Rev. **95**, 1329 (1954)].

[16] An alternate method of obtaining the finite result of Eq. (37) consists of introducing a "structure" or cutoff function $\phi_\lambda(x)$ into the integrand of Eq. (35). $\phi_\lambda(x)$ is taken to have the properties that $\phi_\lambda\to 1$ as $\lambda\to\infty$ and that convergence of the integral (35) is assured. Equation (37) then results when the transformation $x^2=-y^2$ (or more precisely $x=iy$) is made, followed by rotation of the contour onto the x axis. However, in what follows the continuation viewpoint will be adhered to since no additional physical end is gained by introducing a cut-off function of the type required.

It must be remembered that while mathematical meaning has now been given to the theory, the method employed does not necessarily entail that the Fourier transforms so defined behave in momentum space in accordance with physical criteria such as causality and unitarity. These questions require further investigation.

7. THE EFFECTIVE INTERCCTION SERIES FOR THE RENORMALIZED GREEN'S FUNCTIONS

The now well-defined series, Eq. (32), aside from being a high-momentum expansion, may also be classified by the number of λ_{ij}'s in each term. Since the transformation of the theory to the effective transcendental coupling (as reflected in the structure of the λ's) has presumably regrouped the interaction of the fields into more natural units than the perturbation forms, it appears desirable to re-express the solutions in terms of quantities closely related to the λ's but in addition vanishing when the interaction is turned off. When g^2 equals zero, $\lambda_{ij}(x)=1$ or $\lambda_{ij}(k_{ij})=\delta(k_{ij})$. Equation (32) immediately becomes

$$G_+(p)=\sum_{n=0}^{\infty}(-m)^n(\gamma p)^{-n-1}\equiv G_+^{(0)}(p). \quad (40)$$

On the other hand, since $\Delta_+(x)\to 0$ as $x_\mu\to\infty$ (for x_μ not on the light-cone) $\lambda_{ij}(x)\to 1$ in this limit. Since the light-cone is a hypersurface in the volume integration performed on Fourier analyzing, and since further the analytic continuation makes $\lambda_{ij}(x)$ well behaved on the cone, $\lambda_{ij}(k_{ij})$ will have the term $\delta(k_{ij})$ arising in a natural fashion. This result could not have been inferred from a perturbation expansion of λ_{ij} since the latter is not permissible. Indeed the $\delta(k_{ij})$ part of λ_{ij} just accounts for the fact that the nucleon has mass, as may be seen from Eq. (40), while the remainder, $\Lambda_{ij}(k_{ij})=\lambda_{ij}(k_{ij})-\delta(k_{ij})$ represents the interaction of the massed nucleon with the meson field. It is in powers of Λ_{ij} then, that we shall expand our Green's functions. In the process, the H_0's will be replaced by $G_+^{(0)}$'s as this argument leads one to expect.

To this end, we write the product occurring in Eq. (32) as

$$\prod_{i>j=1}^{n}\lambda_{ij}(k_{ij})=\prod_{i>j}\delta(k_{ij})+\sum_{k>l}\Lambda_{kl}(k_{kl})\prod_{i>j}{}'\delta(k_{ij})+\tfrac{1}{2}\sum_{\substack{k>l\\ s>t}}{}'\Lambda_{kl}(k_{kl})\Lambda_{st}(k_{st})\prod_{i>j}{}''(k_{ij})+\cdots, \quad (41)$$

where primes on the $\prod$'s denote omission of indices appearing in the accompanying $\sum$'s while those on the $\sum$'s imply that no two Λ's are to have the same indices.

In Eq. (41) we have considered the product to be only from 1 to n. All terms with end points at either x or x' were thus neglected. In the S-matrix limit when $x, x' \to \pm\infty$ these terms will vanish naturally and hence have been dropped for simplicity.

The first term of Eq. (41) leads to Eq. (40) with the renormalized mass (of course only m' appears henceforth). The second term yields

$$G_c^{(1)} = \sum_{n,\alpha,\beta,\gamma} (-m')^n \int H_0^\alpha(p)\Lambda_\beta(k) \times H_0^\beta(p-k)H_0^\gamma(p)dk, \quad (42)$$

where

$$\Lambda_\beta(x) = \exp[(-)^\beta 4ig^2\Delta_+(x)] - 1. \quad (43)$$

The structure of Eq. (42) arises from Eq. (32) since for this term there is only one nonzero intermediate momentum, or, diagrammatically, one "emission" or "absorption" which spans β of the H_0's. Here and subsequently Λ plays the role of the meson propagator. The summation over α, β and γ extends from 1 to ∞ since only internal Λ's are being retained. In order that there be $n+1$ H_0's, α, β, and γ are restricted by the condition $\alpha+\beta+\gamma=n+1$. The n summation then runs from 2 to ∞ so that at least three H_0's occur, one on each edge and one spanned by the Λ. By straightforward expansion, remembering that $-(p-k)^{-2} = H_0^2(p-k)$, one easily sees that

$$G_c^{(1)}(p) = -G_+^{(0)}(p) \times \left[m'^2 \int dk \gamma_5 \frac{m'\Lambda_0(k) + \gamma(p-k)\Lambda_1}{(p-k)^2 + m'^2} \gamma_5 \right] G_+^{(0)}(p). \quad (44)$$

The Λ_0 and Λ_1 which have opposite signs in their exponents are generalizations of the fact that in $G_+^{(0)}(p-k)$ the numerator would have the form $m-\gamma(p-k)$. Indeed a perturbation expansion of the Λ's to lowest order yields the familiar equivalence result between $ps(ps)$ and $ps(pv)$ with $g_{ps} = 2mg$. Of course, such an expansion should not be made and Eq. (44) represents a more general equivalence relation between the two theories when the full interaction unit, $\Lambda(k)$, rather than just the one meson part, is used.

The expansion for G_c has been recast into the form

$$G_c = G_+^{(0)} - G_+^{(0)}\delta M^{(1)} G_+^{(0)} + \cdots. \quad (45)$$

The quantity in the bracket of Eq. (44) may then be associated with an effective first-order "mass operator," orders meaning now powers of Λ. Every order of this mass operator is, of course, finite now because of analytic continuation and the fact that the explicit infinities have been previously extracted.

The parts quadratic in Λ in Eq. (41) give, along with irreducible second-order diagrams, the iterate of $\delta M^{(1)}$. To arrive at the latter, we consider the terms in Eq. (41) where $l > s$ and the symmetric ones where $l > k$. The portion of $G_c^{(2)}$ thus generated has the form

$$\sum (-m')^n \int H_0^\alpha(p)H_0^\beta(p-k)H_0^\gamma(p)H_0^\delta(p-k') \times H_0^\epsilon(p)\Lambda_\beta(k)\Lambda_\delta(k')dkdk'. \quad (46)$$

All Greek indices but γ sum from 1 to ∞, the latter from 0 to ∞. It may be verified that (46) reduces to

$$m'^4 G_+^{(0)}(p) \int dk \gamma_5 \frac{m'\Lambda_0(k) + \gamma(p-k)\Lambda_1(k)}{(p-k)^2 + m'^2} \times \gamma_5 \{G_+^{(0)}(p) + G_+^{(0)}(0)\} \int dk' \gamma_5 \times \frac{m'\Lambda_0(k') + \gamma(p-k')\Lambda_1(k')}{(p-k')^2 + m'^2} \gamma_5 G_+^{(0)}(p). \quad (47)$$

The first term of the brace gives the iterate of $\delta M^{(1)}$. The $G_+^{(0)}(0) = 1/m'$ term forms a new second order structure characteristic of $ps(pv)$ theory. Diagrammatically, the latter may be viewed as a coalescence of the first term in which the two central vertices coincide. In general, to nth order, one will obtain terms corresponding to every diagram of the normal perturbation type with $\Lambda_{0,1}$ playing the role of the meson propagator, plus all diagrams derived from these by allowing any number of interior $G_+^{(0)}$'s to be replaced by $G_+^{(0)}(0)$ (as long as no two Λ's coincide). Statements similar to those made for $\delta M^{(1)}$ about equivalence relations hold in these higher terms.[17]

The existence of a mass operator brings with it the possibility of further, but finite, renormalizations. These would have to be evaluated in obtaining physical results, but in principle no difficulty should arise in such a calculation.

Turning to the two-nucleon Green function, $G_{12}'(x_1x_2,x_1'x_2')$ the functional integral to be performed is now

$$G_{12}'(x_1x_2,x_1'x_2') = N^{-1} \int \delta\phi \times \exp\left[-\tfrac{1}{2}i \int \phi(\xi)\Delta_+^{-1}(\xi\xi')\phi(\xi')d\xi d\xi' \right] \times \sum_{s,t=0}^{\infty} (-m)^{s+t} \int dy_1 \cdots dy_s H_0(x_1y_1) \cdots H_0(y_sx_1') \times \int dz_1 \cdots dz_n H_0(x_2z_1) \cdots H_0(z_tx_2') \times \exp\left[-2g\gamma_5^1 \int \phi(\xi)f_1(\xi)d\xi - 2g\gamma_5^2 \int \phi(\xi)f_2(\xi)d\xi \right], \quad (48)$$

[17] The formulation of the total mass operator in terms of a suitably defined "vertex operator" may be of interest. It must be remembered that the appearance of Λ_0 or Λ_1 depends upon the specific structure to be spanned by the Λ's.

where $f_i(\xi)$ is the series of δ functions appearing in Eq. (28) and depending parametrically on the y's and z's, respectively. Equation (48) may be suitably antisymmetrized at any stage of the calculation, a procedure which need not be considered here. The γ_5's of each particle commute with any γ's of the other, of course. One aspect of isotopic spin which may be included if desired, is the use of $\tau_3{}^i$ rather than unity to describe the neutral mesons; these matrices may be assumed to have been incorporated into the γ_5's. Use of τ_3's only modifies the n-p forces and would not in any case alter the one-nucleon results. The functional integral is performed in the usual fashion to yield

$$G_{12}'(x_1x_2,x_1'x_2')=Z_2{}^2\sum_{s,t=0}^{\infty}(-m')^{s+t}\int dy_1\cdots dy_s dz_1\cdots dz_t$$
$$\times\exp[-4ig^2\gamma_5{}^1\gamma_5{}^2\sum_{i,j=1}^{s,t}(-)^{i+j}\Delta_+(y_iz_j)]$$
$$\times\exp[4ig^2\sum_{i>j=1}^{s}(-)^{i+j}\Delta_+(y_iy_j)]H_0(x_1y_1)\cdots H_0(y_sx_1')$$
$$\times\exp[4ig^2\sum_{i>j=1}^{t}(-)^{i+j}\Delta_+(z_iz_j)]$$
$$\times H_0(x_2z_1)\cdots H_0(z_tx_2'). \quad (49)$$

Once again all meson terms leading to either edge of both particles have been omitted. The second and third exponentials are each nucleon's radiative corrections. These will, of course, modify the effects of the first exponential which gives the interaction between the nucleons due to the exchange of mesons. To go over to the more physical form, in terms of $G_+{}^{(0)}$ one again would express each exponential in powers of Λ. The analog of the basic Møller interaction can be obtained, however, by dropping all the self-terms and merely expanding the first term:

$$\exp[-4ig^2\gamma_5{}^1\gamma_5{}^2\sum_{i,j=1}^{s,t}(-)^{i+j}\Delta_+(y_iz_j)]$$
$$=1+\sum_{i,j}\Lambda_{ij}{}^{12}(y_iz_j)+\cdots$$
$$\Lambda_{ij}{}^{12}=\exp[-4ig^2\gamma_5{}^1\gamma_5{}^2(-)^{i+j}\Delta_+(y_iz_j)]-1. \quad (50)$$

The unity in Eq. (50) leads to the product of the noninteracting Green functions, $G_+{}^{(0)}(x_1x_1')G_+{}^{(0)}(x_2x_2')$, while the second term produces in momentum space

$$G_c{}^{(1)}(p_1p_2k)=\sum_{s,t=1}^{\infty}(-m')^{s+t}\sum_{i,j=1}^{s,t}\Lambda_{ij}{}^{12}(k)$$
$$\times H_0{}^i(p_1)H_0{}^j(p_2)H_0{}^{s-i+1}(p_1-k)H_0{}^{t-j+1}(p_2+k), \quad (51)$$

where k is the momentum transfer between the nucleons. The $\Lambda_{ij}{}^{12}(k)$ may be brought past the first two H_0 factors where it becomes $\Lambda_{00}{}^{12}$. The sum may then be easily performed to yield

$$G_c{}^{(1)}(p_1p_2k)=G_+{}^{(0)}(p_1)G_+{}^{(0)}(p_2)[m'^2\Lambda_{00}{}^{12}(k)]$$
$$\times G_+{}^{(0)}(p_1-k)G_+{}^{(0)}(p_2+k), \quad (52)$$

and hence the effective lowest order interaction structure becomes

$$I_{12}(k)=m'^2\Lambda_{00}{}^{12}(k) \quad \text{or}$$
$$I_{12}(x_1-x_2)=m'^2\{\exp[-4ig^2\gamma_5{}^1\gamma_5{}^2\Delta_+(x_1x_2)]-1\}, \quad (53)$$

which displays the usual equivalence relation upon perturbation expansion.

In coordinate space, the γ_5 dependence of I_{12} can be brought out of the exponent as $(i\gamma_5{}^1\gamma_5{}^2)^2=-1$:

$$I_{12}(x_1-x_2)=m'^2[\{\cos 4g^2\Delta_+(x_1x_2)-1\}$$
$$-i\gamma_5{}^1\gamma_5{}^2\sin 4g^2\Delta_+(x_1x_2)]. \quad (54)$$

This interaction is, of course, complex, the imaginary part being related to the elastic scattering potential while the real part corresponds to decay out of the two nucleon state, that is to meson and pair production. The adiabatic potential is the time integral of the imaginary part of I_{12}. A preliminary analysis indicates that for p-p forces the central potential has a repulsive core. Of course, the validity of an adiabatic approximation is questionable in a theory involving γ_5's,[18] and more detailed analysis is required to obtain a meaningful result.

The meson-nucleon Green's function may be obtained either by straightforward functional integration by way of Eq. (4) or more easily from the expression

$$G_{MN}'(x\eta,x'\eta')=2\int\Delta_+(\eta\xi)\left[\frac{\delta}{\Delta_+(\xi\xi')}G_+'(xx')\right]$$
$$\times\Delta_+(\xi'\eta')d\xi d\xi'. \quad (55)$$

One can thus get directly the result to first order in Λ from Eq. (44)[19]:

$$G_c{}^{(1)}(x\eta,x'\eta')=\int\Delta_+(\eta\xi)G_+{}^{(0)}(x-\xi)$$
$$\times\{-4ig^2m'^2\gamma_5[m'\lambda_0(\xi-\xi')\Delta_{m'}(\xi\xi')$$
$$-\lambda_1(\xi-\xi')\gamma\partial_\xi\Delta_{m'}(\xi\xi')]\gamma_5\}$$
$$\times G_+{}^{(0)}(\xi'x')\Delta_+(\xi'\eta')d\xi d\xi', \quad (56)$$

where $\Delta_{m'}$ is Δ_+ with mass m'. When $\lambda_{0,1}$ is replaced by unity, one again recognizes the characteristic equivalence with $ps(ps)$ theory, the process of differentiation having replaced Λ by λ in the interaction structure. The approximation of Eq. (56) may be of use for low-energy scattering since a single λ already involves many virtual mesons.[20]

[18] R. Arnowitt and S. Gasiorowicz, Phys. Rev. **94**, 1057 (1954).

[19] We have omitted differentiations of m' and Z_2 which would lead to terms with two meson vertices coinciding.

[20] The behavior of the theory at low energy can also be inferred from threshold theorems. These may be derived by inserting an external meson field into the Lagrangian. A constant pseudoscalar field produces no effects, indicating that, aside from μ/m corrections, the cross section goes to zero at threshold. To arrive at the p-shift one must insert a field $g\phi(x)=a_\mu x_\mu$ where a_μ is a constant vector. The vertex can then be generated by the operation $\Gamma'(p,p+k)\cong k_\mu\partial/\partial a_\mu G^{-1}(p,a)$.

Production processes in both meson-nucleon and nucleon-nucleon collisions can be calculated from the real part of the respective interaction structures. The exponential dependence upon the meson field in these terms should imply that multiple meson production is favored. Such questions have been discussed by Glauber[31] in the semiclassical approximation which is closely related to the first term in our expansion in Λ. The conclusions there seem to support such a conjecture.

8. CONCLUSION

In the early examples of this paper a number of more or less severe approximations were made in order to obtain closed form solutions. The aim in so doing was to exhibit the salient differences between "renormalizable" and "unrenormalizable" theories, rather than to obtain physical predictions at this juncture. Although the examples discussed varied considerably in aspect, the fundamental derivative nature of the coupling produced the striking essential singularity behavior both of the renormalization constants and of the renormalized kernels. When one uses a nonperturbation approach to even the renormalizable theories (such as neutral scalar), another phenomenon arises in that a critical coupling constant exists above which analytic continuation must be performed if the transformation theory is to be maintained. Rigorously, in the gradient theories, the essential singularity causes the critical coupling constant to be zero.

The perturbation renormalization procedure would seem, in view of the above, to require of the theories to which it is applied a certain structure such that though an expansion near the origin (i.e., around a branch point) is not permitted, meaning can still be given to the individual terms. Even if the theory is mild enough so that such a technique is feasible, the perturbation approach would still not tell one of the existence of the critical coupling value and the need for analytic continuation. In the unrenormalizable case the situation is more serious still. Assuming one had been able to extract the explicitly infinite terms order by order (via some prior knowledge of the exact results) the ostensibly renormalized perturbation expansion would still be divergent in a really intractable manner, as analytic continuation, of its very nature, can only give meaning to the closed form expression.

In the beta-decay example treated in the appendix the difficulties encountered in attempting to render the theory finite are of a different nature since here one is dealing with something resembling a vacuum polarization effect. Insofar as one can learn from the perturbation expansion (to which our own criticisms above may apply) the renormalization in the S-matrix limit seems perhaps possible, unlike the finite-times Green's functions. There is perhaps an alternate way of treating the problem. In view of the equivalence between a sufficiently heavy intermediate meson field and a direct interaction, the beta coupling could have been discussed as the limiting case of normal meson couplings. Since now a number of these may be renormalized, then at least in the case of such couplings, the problem is reduced to the consideration of whether the infinite meson mass limit leaves the renormalized structure finite.

The specific approximations which have been made in Secs. 3 and 4 were two in number. The first, the no recoil assumption, reduced the partial differential equation for $G_+(\phi)$ to an ordinary first-order equation.[31] The second approximation used consists in neglecting the commutator of the various Dirac matrices. The use of these assumptions cannot only change the numerical validity of the results (which would not concern us here) but in some cases can destroy the basic requirements that these results must obey. An example of this was seen in Sec. 4. Such questions are perhaps most significant in theories involving γ_5 since this matrix does not have an unambiguous nonrelativistic reduction. For these reasons, it is only insofar as the above results agree with the full recoil theory that they are trustworthy. For the relativistic case, however, it was seen that the infinities are again of the essential singularity type. These can then be removed in the physically acceptable way of the renormalization philosophy. Within the framework of our solution, these strong divergences imply that the remainder after this first renormalization must have equally virulent behavior in the zero time limit of the kernels since the canonical commutation relations are preserved. Hence a further definition is necessary at this point, a process which in "renormalizable" theories is required only in certain domains of the coupling constant (above a critical size) and, hence, there for a much milder problem. As in other examples of redefinition of a theory, it seems reasonable to judge the procedure by the physical usefulness of the results; in particular, the fundamental requirements on the analytic behavior in momentum space must be maintained.

The approximate forms specifically exhibited for several physically important interaction operators of the theory seem promising in those aspects where $ps(pv)$ has always been thought to be of interest, such as multiple meson production and nuclear forces. However, before any predictions (even rigorous ones) can be taken as more than indicative, it should be remembered that several important qualifications apply. The most physical of these has been the neglect of the charged mesons. Had the latter been included none of the steps of this method could have been performed, and in particular no definite statement of renormalizability been made.[32] Analogies from perturbation theory here

[31] When recoil is dropped, vacuum polarization effects automatically vanish, of course.

[32] Inclusion of charged mesons presents many of the same problems as are encountered in treating the spin if one does not make the assumption of commutativity. Such an approximation may correspond to a weak coupling one and not be as serious as in

do not seem of much aid. At the moment then, charge symmetry can only be discussed in an *ad hoc* fashion. The other major omission is concerned with closed loop effects. The problem here is again one of the continued applicability of the renormalization approach. Since the only methods known at present to deal with vacuum polarization are at least of a quasi-perturbation nature, no conclusions can be drawn.

ACKNOWLEDGMENTS

We wish to thank Dr. J. R. Oppenheimer for several interesting conversations and for the hospitality extended us at The Institute for Advanced Study.

APPENDIX A. THE FERMI INTERACTION IN THE STATIC LIMIT

A second class of "unrenormalizable" theories consists of the beta interactions. We consider here the nucleon static limit for the scalar coupling.[23] The Lagrangian for such a system may be written in a unified notation as

$$\mathfrak{L}=-\tfrac{1}{2}\bar{\psi}(-p_0+m)\psi-\tfrac{1}{2}\bar{\phi}(\gamma p+\lambda m_e) -g\bar{\psi}\alpha_1\psi\bar{\phi}\alpha_2\phi+\bar{\eta}\phi+\text{herm conj}, \quad \text{(A1)}$$

where ψ represents the nucleon field, ϕ the lepton field (which is, of course, kept relativistic),

$$\psi=\begin{pmatrix}\psi_p\\ \psi_n\end{pmatrix}, \quad \phi=\begin{pmatrix}\phi_e\\ \phi_\nu\end{pmatrix} \quad \text{(A2)}$$

λ is a lepton mass matrix (unity when acting on electron functions, zero when on neutrino functions) and α_1 and α_2 are the matrices [in the spaces defined by Eq. (A2)] required to allow the appropriate processes to take place. For simplicity, however, we shall in what follows set λ, α_1 and α_2 to unity. η and $\bar{\eta}$ are external spinor sources which are assumed to anticommute with all other fermion amplitudes. By use of these external sources, the functional differential equation for the one-nucleon Green's function may be obtained in a fashion analogous to the case in which the ϕ field is a boson, though slightly more care must be taken due to the anticommutativity of the fermion sources:

$$\left[-p_0+m-g\left\{\frac{1}{i}\frac{\delta_l}{\delta\bar{\eta}(t)}+\phi(t)\right\}\left\{\frac{1}{i}\frac{\delta_r}{\delta\eta(t)}+\bar{\phi}(t)\right\}\right] \times G_+'(t,t';\bar{\phi}\phi)=\delta(t-t'). \quad \text{(A3)}$$

Here subscripts "l" and "r" mean left and right derivatives respectively, that is, in performing the functional differentiations indicated, one takes the variation with respect to the source, and commutes it to the extreme left or right in the expression before dividing by it.

From Eq. (A3) one may again follow the usual procedure[3,4] to arrive at the result

$$G_+'(t-t')=N^{-1}\int\exp\left[-i\int\phi(\xi)G_0^{-1}(\xi-\xi')\phi(\xi')\right] \times G_+(t,t';\bar{\phi}\phi)\delta\bar{\phi}\delta\phi, \quad \text{(A4)}$$

where $(\gamma p+m_e)G_0=1$ and

$$[-p_0+m+g\bar{\phi}(t)\phi(t)]G_+(t,t';\bar{\phi}\phi)=\delta(t-t'). \quad \text{(A5)}$$

In the functional integral of Eq. (A4) it must be remembered that the ϕ's and $\delta\phi$'s still anticommute among themselves.[24] Equation (A5) may be integrated to yield the familiar exponential form but bilinear in the lepton variables. The functional integration may still be performed, however, since the integrand is just a Gaussian with a modified propagator:

$$G_+'(t-t')=i\theta(t-t')e^{-im(t-t')} \times\exp[-\mathrm{Tr}\ln(1+gPG_0)], \quad \text{(A6)}$$

where in coordinate space $P(\xi,\xi')=H(\xi_0,t,t')\delta^3(\xi)\delta^4(\xi-\xi')$. The Tr above refers to a trace both over the spinor indices and coordinates of the leptons. The nucleon variables, t and t', still enter parametrically in $P(\xi,\xi')$. Structures similar to the above appear in the usual vacuum polarization effects. This is not surprising since one is here dealing with a spinor pair theory coupled to a heavy source, which may be likened to vacuum polarization in an external field.

The logarithm in Eq. (A6) may be expanded in a perturbation series in g to yield

$$-\mathrm{Tr}\ln(1+gPG_0)=-\int d\xi \times(\xi|gPG_0-\tfrac{1}{2}g^2(PG_0)^2+g^3/3(PG_0)^3-\cdots|\xi). \quad \text{(A7)}$$

If ξ is a representation which diagonalizes the operator PG_0, then Eq. (A7) may easily be rewritten as[25]

$$-\mathrm{Tr}\ln(1+gPG_0)=-\delta(0)\int d\xi\ln[1+gf(\xi)], \quad \text{(A8)}$$

where $(\xi|PG_0|\xi')=f(\xi)\delta(\xi-\xi')$. While to find the diagonalizing representation in general would be very difficult, when $t-t'\equiv T$ is very large (the S-matrix limit), PG_0 is diagonal in the p_0 part of the usual momentum representation. For this partial diagonalization,

---

the spin reduction since there is no question of a γ_5-like fourth component in this three-dimensional isotopic space.

[23] Such an approximation is actually valid for allowed beta transitions with this coupling.

[24] For a detailed discussion of functional integrals over fermion variables see P. T. Matthews and A. Salam (to be published).

[25] If, for example, ξ were momentum variables, then $\delta(0)$ is to be regarded as VT. In our case, the $\delta(0)$ actually cancels at finite times in the term by term intregation of the perturbation series.

an equation similar to (A8) can be written

$$-\mathrm{Tr}\ln(1+gPG_0)=-iT\int dp_0/iT\,\mathrm{Tr}'\times\ln[(1+gPG_0(p_0)], \quad \text{(A9)}$$

where Tr′ is the trace over all remaining eigenvalues. The integral in Eq. (A9) is thus the mass renormalization (or zero-point energy in fixed source language). In the large time limit, therefore, the Green's function reduces to the unperturbed one with renormalized mass and Z_2 (the latter not appearing in the above calculation). The lepton-nucleon Green function in the same limit exhibits, in addition to these, a coupling constant renormalization.

When the times are not infinite, these simplifications are lost and one must have recourse to the perturbation expansion of Eq. (A7). To first order in g one obtains $-i(t-t')4mg(-i)\Delta_+(0)$ which is a mass renormalization. The second term displays both Z_2 and mass renormalization as well as a finite function of $(t-t')$ (which vanishes at infinity). However, the g^2 term involves, aside from finite terms and a Z_2 renormalization, the product of infinite terms and finite functions of time (which also go to zero at infinity). These presumably would represent g renormalizations but there appear to be terms beyond those necessary to renormalize the second order structure.[26] Thus to renormalize the theory for finite times it may be necessary to obtain a nonperturbation solution or perhaps to introduce other counter terms. However, even within the S-matrix renormalization program, it should be checked whether a unique charge renormalization suffices there in treating all the higher Green functions.

APPENDIX B. STATIC APPROXIMATION WITH GRADIENT COUPLING

A more complex approximation to the full $ps(pv)$ theory than the example of Sec. 3 involves the gradient part of the coupling term:

$$(-p_0+m-ig\sigma\cdot\nabla\phi)G_+(t,t';\phi)=\delta(t-t'), \quad \text{(B1)}$$

where $\sigma_k=\gamma_5\gamma_0\gamma_k$. Equation (B1) can be formally integrated in terms of time-ordered exponentials. However, the evaluation of such a structure in closed form is, of course, an insoluble mathematical problem. We consider here only the simplified approximation in which the σ's are taken to commute.[27] With this assumption the ordered exponentials are equivalent to ordinary ones, allowing the functional integral to be performed.

$$G_+'(t-t')=i\theta(t-t')\exp[(-im(t-t')]\times\exp\left[-\tfrac{1}{2}ig^2\int_{t'}^{t}\int_{t'}^{t}d\tau d\tau'\nabla^2\Delta_+(0,\tau-\tau')\right]. \quad \text{(B2)}$$

The exponential is similar to the result of neutral scalar theory except for the Laplacian. The latter raises the order of infinity of the renormalization constants to be extracted. By use of the equation obeyed by Δ_+, G_+' may be rewritten as

$$G_+'(t-t')=i\theta(t-t')e^{-im(t-t')}\times\exp\left[-ig^2\left\{\Delta_+(t-t')-\Delta_+(0)\right\}-\tfrac{1}{2}ig^2\mu^2\int_{t'}^{t}\int_{t'}^{t}d\tau d\tau'\times\Delta_+(\tau-\tau')+\tfrac{1}{2}ig^2\delta^2(0)(t-t')\right]. \quad \text{(B3)}$$

Again essential singularities of the type encountered in the $\gamma_5\partial\phi\phi$ approximation arise through the first part of the exponent. The second term is equivalent to the no-recoil scalar theory [with $(ig)^2\mu^2$ playing the role of g_s^2] which again is equal to the adiabatic limit of the $ps(ps)$ case.[4] This will produce a further Z_2 as well as a mass renormalization. The third term is the usual contact structure that occurs in $ps(ps)-ps(pv)$ equivalence transformations and is absorbed into the mass term. Physical effects will arise in the higher Green functions from the scalar part of the interaction.

Interactions involving higher powers of the gradient ($\Gamma\phi\sim\nabla^{2n}\phi$) can similarly be handled.

APPENDIX C. FORMAL EQUIVALENCE OF THE SOLUTION WITH PERTURBATION THEORY

In this appendix we show that the solution given in Eq. (29) is formally equivalent to the usual perturbation expansion. It will suffice to consider here only the terms of order g^2. Equation (29), when expanded gives

$$G_{\mu\nu}'(xx')=ig^2\sum_{n=0}^{\infty}(-m)^n\int dy_1\cdots dy_n H_0(xy_1)\cdots\times H_0(y_nx')[(1+2n)\Delta_+(0)-(-)^n\Delta_+(xx')+2\sum_{i=1}^{n}(-)^i[\Delta_+(xy_i)+(-)^{n+1}\Delta_+(y_ix')]+4\sum_{i>j=1}^{n}(-)^{i+j}\Delta_+(y_iy_j)]. \quad \text{(C1)}$$

This is to be compared with

$$-(x|G_+^{(0)}\delta M_\mu{}^\nu G_+^{(0)}|x')=-ig^2\int dydy'G_+^{(0)}(xy)\times\gamma_5\gamma_\mu G_+^{(0)}(yy')\gamma_5\gamma_\nu[i\partial_\mu i\partial_\nu'\Delta_+(yy')]G_+^{(0)}(y'x'). \quad \text{(C2)}$$

[26] For the scalar pair theory, whose charge renormalization has been treated by A. Klein and B. McCormick [Phys. Rev. **98**, 1428 (1955)] in the S-matrix limit, one obtains a linear and logarithmic divergence at finite times. The linear divergence correctly renormalizes the g^2 term, while the logarithm fails to do so.

[27] This might be viewed as a semiclassical approximation to the cutoff theory considered by G. Chew, Phys. Rev. **94**, 1749 (1954).

The two derivatives on $\Delta_+(yy')$ due to the vertices are integrated by parts to act on the appropriate $G_+^{(0)}$'s. Using the defining equation for $G_+^{(0)}$ one then obtains

$$ig^2\Big[\Delta_+(0)\Big\{G_+^{(0)}(xx')-2m\int dy G_+^{(0)}(xy)G_+^{(0)}(yx')\Big\}$$
$$-\Delta_+(xx')\gamma_\delta G_+^{(0)}(xx')\gamma_\delta$$
$$+2m\int dy\Delta_+(xy)\gamma_\delta G_+^{(0)}(xy)\gamma_\delta G_+^{(0)}(yx')$$
$$+2m\int dy\gamma_\delta G_+^{(0)}(xy)\gamma_\delta G_+^{(0)}(yx')\Delta_+(yx')$$
$$-4m^2\int dydy'\Delta_+(yy')G_+^{(0)}(xy)$$
$$\times\gamma_\delta G_+^{(0)}(yy')\gamma_\delta G_+^{(0)}(y'x')\Big]. \quad \text{(C3)}$$

In the derivation of Eq. (C3) a term having as coefficient $\partial_\mu\Delta_+(y)]_{y=0}$ has been dropped since this factor vanishes by oddness. Equation (C3) need only be expanded in a power series in m to prove it equivalent to (C1).

The terms in which either of the arguments of Δ_+ is x or x' vanish in S-matrix limit. The last term is the usual $ps(ps)$ lowest order correction. The coefficient of the remaining $G_+^{(0)}(xx')$ is recognizable even in the perturbation expansion as a Z_2 renormalization while the other $\Delta_+(0)$ term is similarly a mass renormalization. The $ps(ps)$ structure produces its own infinities. However in the rigorous form terms of this sort add back in such a way that the $\Delta_+(yy')$ is replaced by $\exp[\pm 4ig^2\Delta_+(yy')]$. When analytic continuation is employed, what remains is finite, which is necessary since higher powers of $\Delta_+(yy')$ appear in subsequent orders and would not be renormalizable.

It may be noted that the formal equivalence with perturbation theory is demonstrable for higher Green's functions as well. However, as was pointed out in Eq. (39), the $\delta(x_n^2)$ part of $\Delta_+(x)$ does not contribute to $\exp[4ig^2\Delta_+(x)]$ but would produce effects in the expanded forms.

APPENDIX D. NEUTRAL $S(V)$ THEORY

The relativistic counterpart of the nonrecoil case with $\partial_\delta\phi$ coupling is, of course, the $s(v)$ theory which will be considered here. The equation for $G_+(\phi)$ is

$$(\gamma p+m+g\gamma_\mu\partial_\mu\phi)G_+(x,x';\phi)=\delta(x-x'). \quad \text{(D1)}$$

Letting $G_+(x,x';\phi)=e^{-ig\phi(x)}H_+(xx';\phi)e^{+ig\phi(x')}$ one easily finds that

$$(\gamma p+m)H_+(x,x';\phi)=\delta(x-x') \quad \text{(D2)}$$

or $H_+(x,x')=G_+^{(0)}(x,x')$. The functional integral is trivial to perform here, yielding

$$G_+'(x,x')=Z_2\exp[-ig^2\Delta_+(x,x')]G_+^{(0)}(x,x'), \quad \text{(D3)}$$

where $Z_2=\exp[ig^2\Delta_+(0)]$. The structure indicates the well-known fact that the $s(v)$ theory has no physical effects.

Z_2 in this case is less than unity according to the interpretation given to $\Delta_+(0)$ in Sec. 5. In order to give meaning to $G_c(p)$, however, analytic continuation is still required just as in the $ps(pv)$ theory.

Some Notes on Nonrenormalizable Field Theory

LEON N. COOPER*†
Institute for Advanced Study, Princeton, New Jersey
(Received June 24, 1955)

Some nonrecoil, derivative coupling theories, which are exactly soluble, are analyzed in order to discover what it is that produces the nonrenormalizable behavior typical of derivative coupling. This behavior is found to arise as the result of an essential singularity which the operators of the derivative theories possess at the origin in coordinate space and the resulting branch point the Fourier transforms of these operators possess at the origin in the complex coupling constant domain. This branch point causes the breakdown of the expansion of the Fourier transform of the operators in powers of the coupling constant and introduces the nonrenormalizable infinities. It is shown that a coordinate space coupling constant expansion is possible, and that a Fourier transform of the operators of the derivative theories may be defined by analytic continuations and made finite by renormalization.

I. INTRODUCTION

THE success of the renormalization program in identifying all of the infinite parts of quantum electrodynamics with a renormalization of the charge and mass of the electron has led to many attempts to duplicate this procedure with less tractable theories. Although these have sometimes succeeded, it has become clear that for many field theories it is not possible, with the usual methods, to remove the ambiguities by identifying the infinities with empirical constants. In particular, for derivative coupling theories, one finds that the usual renormalization procedure cannot be carried through because, no matter what subset of graphs is chosen as primitive, the degree of divergence increases indefinitely as one goes to higher order processes.

In what follows, several simple nonrecoil derivative coupling theories (all but one of which is nonrenormalizable by the usual methods) are analyzed in order to discover what it is that produces the nonrenormalizability which is characteristic of derivative coupling and whether, in spite of their very bad behavior in the power series expansion, something can still be done to make these theories finite and unambiguous. Perhaps the most striking result is that these theories in a sense are renormalizable; that is, it is possible to make all the operators of the theories finite by mass, Z_1 and Z_2 renormalizations.

The distinction between the renormalizable and nonrenormalizable theories considered occurs as follows: for the renormalizable theory, the renormalized propagator in coordinate space is analytic (in the finite plane) in the coordinate difference everywhere except at the origin, where it has a branch point. For small enough values of the coupling constant its Fourier transform exists and is analytic in the coupling constant in the neighborhood of $g^2/4\pi^2=0$. The renormalized propagators of all the nonrenormalizable theories, in coordinate space, are also analytic in the coordinate difference, in the finite plane, everywhere except at the origin. At the origin, however, they have essential singularities. Because of these essential singularities, the Fourier transform of the propagators for the nonrenormalizable theories exists only in one half of the complex coupling constant plane, and it sometimes turns out to be that half of the plane for which the Hamiltonian cannot be Hermitian. However, a Fourier transform can be defined by analytic continuation from the non-Hermitian half of the coupling constant plane. The Fourier transform in any case has a branch point at $g^2/4\pi^2=0$ which makes it a many-valued function of the coupling constant.

It then results that the set of progressively worse infinities, which in the power series expansion is associated with nonrenormalizability, is due solely to the failure of the expansion of the momentum space propagator about a branch point in coupling constant space.

The infinities which occur in the simple theories treated here, therefore, fall into two distinct classes: those which have nothing to do with the power series expansion and which occur in a similar fashion in both renormalizable and nonrenormalizable cases (renormalization constants), and those whose existence is due entirely to the coupling constant expansion (the nonrenormalizable infinities). This suggests that the behavior of the momentum space propagator, in the coupling constant, may divide field theories into three classes: those for which the propagator is analytic at the origin and is renormalizable; those for which the propagator is not analytic in the coupling constant at the origin, but a formal expansion of which gives an asymptotic series which is renormalizable; and those for which the behavior in the coupling constant at the origin is such that an expansion cannot be made at all.

It also turns out that the solutions of the nonrenormizable theories are so singular that it is not possible to freely interchange the order of such operations as differentiation and integration. The momentum space perturbation expansion sometimes implicitly interchanges these operations and, in so doing, may add

* National Science Foundation Postdoctoral Fellow.
† Present address: Department of Physics, University of Illinois, Urbana, Illinois.

spurious (sometimes infinite) terms to the correct solution, depending on the method of calculation. In the renormalizable case, the solutions are not so singular so that this difficulty does not occur, and the usual momentum space perturbation expansion gives the correct result.

In the second section, the propagators for several simple nonrecoil theories are obtained exactly by functional methods and are renormalized. The difference between the renormalizable and nonrenormalizable theories is then discussed in Sec. III. A perturbation method suitable for calculation with the nonrenormalizable theories is outlined in Sec. IV. In Sec. V, the operators of a nonrenormalizable theory are defined by analytic continuation. Appendix A gives the details of these analytic continuations and considers the multivalued behavior of the propagator as a function of the coupling constant. In Appendix B, the accuracy of a cutoff approximation to the nonrenormalizable theories is discussed.

II. THE PROPAGATOR FOR A CLASS OF NONRECOIL THEORIES

We shall, to illustrate the method, first obtain the propagator for a simple class of theories which has the following equations of motion for the nuclear field ψ, and the meson field ϕ:

$$\{-i(\partial/\partial t)+m+\delta m-g(\partial^n\phi/\partial t^n)\}\psi=0$$
$$\{\Box^2-\mu^2\}\phi=0. \tag{1}$$

This can be thought of as a spinor field in the nonrecoil limit interacting with the nth derivative of a boson field with no vacuum polarization.[1] When $n=0$ we have the neutral scalar theory previously solved.[2,3] It will be seen that the method of solution would permit us to work out in a similar fashion any nonrecoil theory with a coupling term of the form $g\bar{\psi}^*\alpha_i(D_i{}^n\phi)\psi$ where D^n is a differential operator and α is a commuting vector.

Since the technique used below is relatively new, it will be explained in some detail. Later, when the solutions are examined, it will be seen that a certain kind of perturbation expansion is possible even in the nonrenormalizable cases. This gives a series which can be summed when the α's commute. The reader who is not willing to follow the first method is referred to the second.

To find the propagator we employ the functional integral formulation of field theory first proposed by Feynman[4] and exploited recently by Edwards and Peierls[2] and Matthews and Salam.[5] Using this formulation the nucleon propagator for the fields above can be written as

$$S_{(n)}'(t-t')=\frac{\int\delta\phi\delta\bar{\psi}\delta\psi\psi(t)\bar{\psi}(t')\exp\{i\int\int\mathfrak{L}^{(n)}(x_1)\delta(x_1-x_2)dx_1dx_2\}}{\int\delta\phi\delta\bar{\psi}\delta\psi\exp\{i\int\int\mathfrak{L}^{(n)}(x_1)\delta(x_1-x_2)dx_1dx_2\}}$$
$$=\langle T(\psi(t)\bar{\psi}(t'))\rangle_0, \tag{2}$$

where

$$\mathfrak{L}^{(n)}=\frac{1}{2}\Big[\bar{\psi}\Big\{-i\frac{\partial}{\partial t}+m+\delta m-g\frac{\partial^n\phi}{\partial t^n}\Big|\psi$$
$$+\text{Herm. conj.}-\{(\Box\phi)^2+\mu^2\phi^2\}\Big].$$

Following Matthews and Salam the integration over ψ and $\bar{\psi}$ is performed, and, neglecting the effects of vacuum polarization, one gets an equation which (except for the factor $-i$) is identical to Eq. (21) of Edwards and Peierls:

$$S_{(n)}'(t-t')=-iN\int\delta\phi G_4{}^{(n)}(t,t';\phi)$$
$$\times\exp\Big\{-\frac{i}{2}\int\int\phi(\xi)\Delta^{-1}(\xi,\xi')\phi(\xi')d\xi d\xi'\Big\}, \tag{3}$$

where

$$\Delta^{-1}(\xi,\xi')=\delta(\xi-\xi')(-\Box^2+\mu^2)_{\xi'},$$
$$N^{-1}=\int\delta\phi\exp\Big\{-\frac{i}{2}\int\int\phi(\xi)\Delta^{-1}(\xi,\xi')\phi(\xi')d\xi d\xi'\Big\},$$

and $G_4{}^{(n)}(t,t';\phi)$ is the solution of the equation

$$\Big\{-i\frac{\partial}{\partial t}+m+\delta m-g\frac{\partial^n\phi}{\partial t^n}\Big\}G_4{}^{(n)}(t,t';\phi)=\delta(t-t') \tag{4}$$

and is a functional of ϕ. The symbol $\int f[\phi]\delta\phi$ means a functional integration over all functions ϕ. This integral is still to be precisely defined, but in the simple cases considered it will be seen that the method of solution is to manipulate the variable function ϕ by linear transformations until the functional integration cancels out.

The solution of Eq. (4) is

$$G_4{}^{(n)}(t,t';\phi)=i\theta(t-t')\exp\Big\{-i(m+\delta m)(t-t')$$
$$+ig\int_{t'}^{t}\frac{\partial^n\phi}{\partial\xi^n}d\xi\Big\} \tag{5}$$

where

$$\theta(t-t')\begin{cases}=1 & t-t'>0\\ =0 & t-t'<0\end{cases}$$

[1] Equations of this form have been solved and renormalized also by R. Arnowitt and S. Deser, preceding paper [Phys. Rev. **99**, 349 (1955)].

[2] S. F. Edwards and R. E. Peierls, Proc. Roy. Soc. (London) **A224**, 24 (1954).

[3] T. D. Lee, Phys. Rev. **95**, 1329 (1954).

[4] R. P. Feynman, Revs. Modern Phys. **20**, 376 (1948).

[5] P. Matthews and A. Salam, Nuovo cimento **II**, 120 (1955).

Putting this into Eq. (3) one has, with $\tau \equiv t-t'$

$$S_{(n)}'(\tau)=\theta(\tau)e^{-i(m+\delta m)\tau}N\int\delta\phi\,\exp\left\{ig\int_{t'}^{t}\frac{\partial^n\phi(\xi)}{\partial\xi^n}d\xi\right.$$
$$\left.-\frac{i}{2}\int\int\phi(\xi)\Delta^{-1}(\xi,\xi')\phi(\xi')d\xi d\xi'\right\}. \quad (6)$$

Now let

$$\phi(\xi)=\phi'(\xi)+g\int_{t'}^{t}\Delta^{(n)}(\xi,\eta)d\eta; \quad \delta\phi'=\delta\phi,$$

where

$$\int_{-\infty}^{\infty}d^4\xi\Delta^{-1}(x,\xi)\Delta^{(n)}(\xi,x')=\delta^{(n)}(t-t')\delta(\mathbf{r}-\mathbf{r}').$$

This gives

$$S_{(n)}'(\tau)=\theta(\tau)\exp\left\{-i(m+\delta m)\tau\right.$$
$$\left.+\frac{ig^2}{2}\int_{t'}^{t}d\xi\int_{t'}^{t}d\xi'\frac{\partial^n}{\partial\xi^n}\Delta^{(n)}(\xi,\xi')\right\} \quad (7)$$

as the functional integral just cancels out.

$\Delta^{(n)}(\xi,\xi')$ can be represented by

$$\Delta^{(n)}(\xi,\xi')=\frac{\partial^n}{\partial\xi_0'^n}\Delta^{(0)}(\xi,\xi'). \quad (8)$$

Then the second part of the exponential of Eq. (7) becomes

$$\frac{ig^2}{2}\int_{t'}^{t}d\xi_0\int_{t'}^{t}d\xi_0'\frac{\partial^n}{\partial\xi_0^n}\frac{\partial^n}{\partial\xi_0'^n}\Delta^{(0)}(\xi,\xi'), \quad (9)$$

which at $\xi=\xi'$ is [letting $\omega=(p^2+\mu^2)^{\frac{1}{2}}$]

$$\frac{-g^2}{8\pi^2}\int_{t'}^{t}d\xi_0\int_{t'}^{t}d\xi_0'\int_0^{\infty}\omega^{2n-1}p^2dp$$
$$\times\left(e^{-i\omega|\xi_0-\xi_0'|}+\begin{matrix}0\\ i\omega\delta(\xi_0-\xi_0')+\cdots\end{matrix}\right)\begin{matrix}n=0\\ n>0\end{matrix} \quad (10)$$

where

$\Delta^{(0)}(\xi,\xi')$ at $\xi=\xi'$ is $\Delta^{(0)}(0,\xi_0;0,\xi_0')$

$$=\frac{i}{4\pi^2}\int_0^{\infty}p^2dp\frac{e^{-i\omega|\xi_0-\xi_0'|}}{\omega},$$

and the terms omitted in (10) are derivatives of $\delta(\xi_0-\xi_0')$ which give zero when integrated from t' to t.

Doing the ξ_0 and ξ_0' integrations, (10) becomes

$$\frac{g^2}{4\pi^2}\int_0^{\infty}p^2dp\omega^{2n-4}\left[\frac{1}{\omega^2}(e^{-i\omega\tau}-1)+\begin{matrix}i\tau/\omega\\ 0\end{matrix}\right]\begin{matrix}n=0\\ n>0.\end{matrix} \quad (11)$$

This gives for the propagator:

$$S_{(n)}'(\tau)=\theta(\tau)e^{-im\tau}R^{(n)}(\tau),$$

where

$$R^{(n)}(\tau)=\exp\left\{\frac{g^2}{4\pi^2}\int_0^{\infty}p^2dp\omega^{2n-3}(e^{-i\omega\tau}-1)\right\} \quad (12)$$

and

$$\delta m=\frac{g^2}{4\pi^2}\int_0^{\infty}p^2dp\omega^{-2} \quad \text{for} \quad n=0; \quad \delta m=0 \quad \text{for} \quad n>0.$$

The propagator is renormalized by a multiplicative constant $Z_2^{(n)}$:

$$S_{(n)}'(\tau)=Z_2^{(n)}S_c^{(n)}(\tau), \quad (13)$$

where

$$Z_2^{(n)}=\exp\left\{-\frac{g^2}{4\pi^2}\int_0^{\infty}p^2dp\omega^{2n-3}\right\}.$$

The Z_2 renormalization makes $S_c^{(n)}(\tau)$ finite for $\tau>0$. We see that this multiplication shifts the value of the propagator so that where the unrenormalized function is finite for $\tau=0$ and zero for $\tau\neq0$, the renormalized function is finite for $\tau>0$ and infinite for $\tau=0$.[6]

For $n>0$ it is convenient to investigate the behavior of the renormalized radiative correction term $R_c^{(n)}(\tau)$ for meson mass $\mu=0$, as this does not change the behavior of the function at its singularities. Then $R_c^{(n)}(\tau)$ becomes:

$$R_c^{(n)}(\tau)=\exp\left\{\frac{g^2}{4\pi^2}\int_0^{\infty}p^{2n-1}dpe^{-ip\tau}\right\}.$$

The integral in the exponent is well defined for τ in the lower half plane and can be continued to all points in the complex τ plane, except $\tau=0$, to give[7]:

$$R_c^{(n)}(\tau)=\exp\{(g^2/4\pi^2)(-1)^n(2n-1)!\tau^{-2n}\}.$$

Letting $\gamma=(-1)^n(g^2/4\pi^2)$, we have for $n>0$, the radiative correction term

$$R_c^{(n)}(\tau)=\exp\{\gamma(2n-1)!\tau^{-2n}\}, \quad (14)$$

where $(-1)^n\gamma=(-1)^n\gamma^*\geq0$ for Hermitian Hamiltonians.

With the interaction term $g\psi^*\alpha_s(D_s^n\phi)\psi$ (where $\alpha_i\alpha_j-\alpha_j\alpha_i=0$; $\alpha_1\alpha_1=\alpha_2\alpha_2=\cdots=1$), everything goes through almost exactly as above (except that one gets

[6] Although $Z_2^{(n)}$ above appears always to be smaller than one, actually this depends upon the way the limit $\tau\to0$ is taken. Since $Z_2^{(n)}$ in the $n>0$ cases is

$$Z_2^{(n)}=\lim_{\tau\to0}\exp(\gamma\tau^{-2n}),$$

the value of a function at its essential singularity, this value depends upon the path by which it was reached.

[7] If the meson mass was kept unequal to zero, the singular functions in the exponential would be Hankel functions of argument $\mu\tau$ and their derivatives.

a mass renormalization). Equation (7) becomes

$$S'(\tau)=\theta(\tau)\exp\left\{-i(m+\delta m)\right.$$
$$\left.+\frac{ig^2}{2}\alpha_i\alpha_j\int\int_{\nu'}^{\nu}d\xi_0'd\xi_0D_\xi{}^iD_{\xi'}{}^j\Delta^0(\xi,\xi')\right\}. \quad (7a)$$

For $D=\nabla$, (11) becomes

$$\frac{g^2}{4\pi^3}\int_0^\infty k^4dk\omega^{-3}(e^{-i\omega\tau}-1+i\omega\tau) \quad (11a)$$

and so, after renormalization—for meson mass $\mu=0$, this is just identical to $R_\epsilon{}^{(1)}(\tau)$ above. In general any differential operator D^n will give results which, with respect to the singularities of the solutions, are identical to those above.

III. COMPARISON OF THE RENORMALIZABLE AND NONRENORMALIZABLE THEORIES

The differences between the theories with interaction terms of the form $g\psi^*\alpha_i(D_i{}^n\phi)\psi$, which we shall designate as nonrenormalizable or $n>0$ theories, and the renormalizable or $n=0$ theory (with the interaction term $g\psi^*\phi\psi$), result almost entirely from the type of singularity the operators of these theories possess at the origin in coordinate space.

For $n=0$ the renormalized propagator is singular at $\tau=0$ for Hermitian Hamiltonians, but it is summable at this point for any complex value of γ, $|\gamma|<1$. For $n=0$, $S_\epsilon{}^{(0)}(\tau)$ is[8]

$$S_\epsilon{}^{(0)}(\tau)=\theta(\tau)\exp\left\{-im\tau+\gamma\int_0^\infty\frac{p^2dp}{\omega^3}e^{-i\omega\tau}\right\}. \quad (15)$$

In order to find the behavior at $\tau=0$ we write

$$\int_0^\infty dp\frac{p^2}{\omega^3}e^{-i\omega\tau}=\frac{\pi i}{2}H_0{}^{(1)}(\mu\tau)-\mu^2\int_0^\infty\frac{dp}{\omega^3}e^{-i\omega\tau}. \quad (16)$$

For $\tau\ll1$ the second term can be neglected as we are interested only in the singular part at $\tau=0$. Then (16) becomes

$$\int_0^\infty dp\frac{p^2}{\omega^3}e^{-i\omega\tau}\sim-\ln\bar{\gamma}(\mu\tau)+\ln2$$

where

$$\ln\bar{\gamma}=C\simeq0.577\cdots.$$

Thus $R_\epsilon{}^{(0)}(\tau)$ for $\tau\ll1$ is

$$R_\epsilon{}^{(0)}(\tau)\sim(\text{const})(\mu\tau)^{-\gamma}. \quad (17)$$

In coordinate space, for $\gamma>0$, $R_\epsilon{}^{(0)}(\tau)$ is singular at $\tau=0$. However, for $|\gamma|<1$, the Fourier transform of $S_\epsilon{}^{(0)}(\tau)$ exists and is analytic in γ at $\gamma=0$. One can reproduce the renormalized perturbation series by expanding $R_\epsilon{}^{(0)}(\tau)$ in powers of γ. Then each term of the expansion converges (involving integrals like $\int_0\log^n\tau d\tau$) and, for $|\gamma|<1$, the series itself converges.

For $n>0$, as can be seen from Eq. (14), the radiative correction term $R_\epsilon{}^{(n)}(\tau)$ has an essential singularity at $\tau=0$. As a consequence of this, the propagator $S_\epsilon{}^{(n)}(\tau)$ is not summable at $\tau=0$ for γ in the right half plane and thus the Fourier transform of $S_\epsilon{}^{(n)}(\tau)$ is defined only for γ in the left half complex plane. The fact that the Fourier transform of the propagator exists for certain complex values of γ, however, suggests that a Fourier transform could be defined over the entire domain of γ by an analytic continuation. This possibility is exploited, in Sec. V, in order to define the momentum space operators of the $n>0$ theories. However, the Fourier transform of the propagator so defined has a branch point at $\gamma=0$. It is just this that makes the momentum space coupling constant expansion impossible and introduces a nonrenormalizable set of infinities into these theories. For the characteristic nonrenormalizability in which the degree of divergence at infinity (in the Fourier transform space) increases with each term of the series is reflected in the breakdown of the expansion $\int_0\exp[-(\gamma/\tau^{2n})-i(q+m)\tau]d\tau$ in powers of γ. The expansion, of course, breaks down independent of the sign of γ.

Another consequence of the high degree of singularity possessed by the $n>0$ theories, is the fact that in the calculation of the operators of these theories spurious terms may arise if the order of the operations of differentiation and integration are interchanged. This arises, in particular, for the nonrecoil theories treated above when the differential operators involve the time. In the nth derivative theories each meson propagation line is operated on to give

$$-\frac{1}{4\pi^3}\int_0^\infty p^2dp\frac{d^n}{d\xi_1{}^n}\frac{d^n}{d\xi_2{}^n}\int_{C_F}\frac{e^{+iE(\xi_1-\xi_2)}}{(E-\omega)(E+\omega)}dE.$$

Putting $(\pm i)^ng^nE^n$ at each vertex, as one would do in the usual perturbation expansion, is equivalent to reversing the orders of the operations and could introduce spurious terms even if the entire expansion did not break down.

In all the theories, infinite constants appear which can be absorbed by Z_2, Z_1 and mass renormalizations and whose existence is independent of the method of calculation. These "traditional" divergences do not arise because of the power series expansion, but their identification and absorption into physical constants is made difficult by the expansion. The nonrenormalizable divergences associated with the derivative coupling theories are produced by the incorrect expansion and thus disappear when the method of calculation is changed.

[8] The meson mass μ cannot be set equal to zero in the $n=0$ case because a logarithmic infrared divergence would result.

IV. A PERTURBATION EXPANSION FOR THE NONRENORMALIZABLE THEORIES

Because of the behavior of the momentum space propagator at $\tau=0$ for the $n>0$ theories, the usual coupling constant expansion becomes impossible. However, since the propagator in coordinate space for $\tau\neq 0$ is analytic in γ, it is possible to obtain all the operators even for the $n>0$ theories by a power series expansion in γ as long as one remains in coordinate space and keeps $\tau\neq 0$. The fact that such an expansion does exist for the nonrenormalizable cases would make it possible to explore more complicated theories for which it is not such a trivial matter to obtain an exact solution.[9] Also, this provides an alternative derivation of the results of Sec. II.

We will consider a general nonrecoil theory, with an interaction term $g\psi^*\alpha\cdot(D^n\phi)\psi$, in which the nucleon propagator (everything will be in coordinate space) is given by

$$S_F(t_2-t_1)=\theta(t_2-t_1)e^{-i\omega(t_2-t_1)}, \tag{18}$$

the meson propagator by

$$\Delta_F(x_2-x_1)=\frac{1}{16\pi^3}\int_0^\infty d^3p e^{-ip(r_2-r_1)}\frac{e^{-\omega|t_2-t_1|}}{\omega}, \tag{19}$$

and the vertex operators by

$$g\alpha_i D_i^n. \tag{20}$$

Then the $2l$-order propagator is given by a sum of diagrams in which a nucleon line, beginning at x' and ending at x, emits and absorbs mesons at the $2l$ points $x_1\cdots x_{2l}$, where the meson lines connect all permutations of the coordinate pairs $(x_1x_2)(x_3x_4)\cdots(x_{2l-1}x_{2l})$. $S^{(2l)}(\tau)$ is

$$S^{(2l)}(\tau)=\int_{-\infty}^{+\infty}dt_{2l}\cdots\int_{-\infty}^{+\infty}dt_1\theta(t_1-t')\cdots\theta(t-t_{2l})$$
$$\times(-1)^l\frac{g^{2l}}{l!2^l}e^{-i\omega(t_1-t')-i\omega(t_2-t_1)-\cdots-i\omega(t-t_{2l})}$$
$$\times\alpha_{\mu 1}D_{\mu 1}^n\alpha_{\mu 2}D_{\mu 2}^n\cdots\alpha_{\mu 2l}D_{\mu 2l}^n\sum_{\substack{\text{Permutations}\\ \text{of } x_1\cdots x_{2l}}}\Delta_F(x_2-x_1)$$
$$\times\Delta_F(x_4-x_3)\cdots\Delta_F(x_{2l}-x_{2l-1}). \tag{21}$$

Here $D_{\mu j}^n$ is a differential operator which acts on the coordinate x_j. The factor $1/2^l l!$ is introduced because we sum over all permutations of the coordinates $x_1\cdots x_{2l}$ rather than all pairings. This just duplicates $l!2^l$ identical diagrams.

The θ functions combine to give limits of integration over the t variables:

$$t'\leqslant t_1\leqslant t_2\leqslant\cdots\leqslant t_{2l}\leqslant t,$$

and the exponentials give $e^{-i\omega(t-t')}$. Associating the differential operators $D_{\mu j}^n$ with the coordinates on which they operate, $S^{(2l)}(\tau)$ becomes

$$S^{(2l)}(\tau)=(-1)^l\frac{g^{2l}}{2^l l!}\theta(\tau)e^{-i\omega\tau}\int_{t'}^{t}dt_{2l}\int_{t'}^{t_{2l}}dt_{2l-1}\cdots$$
$$\times\int_{t'}^{t_2}dt_1\alpha_{\mu 1}\alpha_{\mu 2}\cdots\alpha_{\mu 2l}\sum_{\text{Permutations}}D_{\mu 1}^n D_{\mu 2}^n\Delta_F(x_2-x_1)\cdots$$
$$\times D_{\mu 2l}^n D_{\mu(2l-1)}^n\Delta_F(x_{2l}-x_{2l-1}). \tag{22}$$

If the α's commute the integrand is symmetric in $t_1\cdots t_{2l}$ and we may change the limits of integration to get,

$$S^{(2l)}(\tau)=\frac{g^{2l}}{2^l l!}\frac{(-1)^l}{(2l)!}\theta(\tau)e^{-i\omega\tau}\alpha_{\mu 1}\alpha_{\mu 2}\cdots\alpha_{\mu 2l}$$
$$\times\sum_{\text{Permutations}}\int_{t'}^{t}dt_{2l}\int_{t'}^{t}\cdots\int_{t'}^{t}dt_1 D_{\mu 1}^n D_{\mu 2}^n\Delta_F(x_2-x_1)\cdots$$
$$\times D_{\mu 2l}^n D_{\mu(2l-1)}^n\Delta_F(x_{2l}-x_{2l-1}). \tag{23}$$

Using the representation (19) for $\Delta_F(x_2-x_1)$ and assuming for an explicit example that $D^n=\nabla$, we can do the t integrations. Then we have for $S^{(2l)}(\tau)$:

$$S^{(2l)}(\tau)=\frac{g^{2l}}{l!}\frac{1}{(2l)!}\theta(\tau)e^{-i\omega\tau}Q^l\alpha_{\mu 1}\cdots$$
$$\alpha_{\mu 2l}\sum_{\text{Permutations}}\delta_{\mu 1,\mu 2}\delta_{\mu 3,\mu 4}\cdots\delta_{\mu(2l-1),\mu 2l}, \tag{24}$$

where

$$Q=\frac{1}{16\pi^3}\int\frac{k_{\mu i}k_{\mu j}d^3k}{\omega^3}\{e^{-i\omega\tau}-1+i\omega\tau\}$$
$$=\frac{1}{4\pi^2}\frac{1}{3}\int\frac{k^4dk}{\omega^3}\{e^{-i\omega\tau}-1+i\omega\tau\}$$

at $\mathbf{x}=\mathbf{x}'$ and is diagonal because of the antisymmetry of $k_{\mu i}k_{\mu j}$. Since the α's commute the sum over permutations gives $(2l)!$ identical factors $(\alpha_\mu\alpha_\mu)^l=3^l$ for a three dimentional ∇. Therefore, we have

$$S^{2l}(\tau)=g^{2l}3^lQ^l/l!\theta(\tau)e^{-i\omega\tau} \tag{25}$$

and

$$S_F'(\tau)=\sum_{l=0}^{\infty}S^{(2l)}(\tau)=\theta(\tau)e^{-i\omega\tau}$$
$$\times\exp\left\{\frac{g^2}{4\pi^2}\int_0^\infty\frac{k^4dk}{\omega^3}(e^{-i\omega\tau}-1+i\omega\tau)\right\},$$

which checks with Eqs. (7a) and (11a). Other operators of the theory such as the vertex function and the meson-nucleon Green function can be calculated in a similar fashion by inserting one or more external lines into the propagator and again summing over all possible permutations.

[9] Arnowitt and Deser (reference 1) have investigated the $\rho s(p\pi)$ theory, including recoil, with the use of an expansion in a parameter which is not related to the coupling constant but is proportional to the proper distance Mx_μ.

The crucial point in the calculation is the assertion that the α's commute. If they did not, then each pairing of the coordinates would have a different weight and there would no longer be symmetry in the $t_1 \cdots t_{2l}$ variables. Then the t integrations cannot be done so easily, and the problem is no longer trivial.

It is of interest to inspect this perturbation expansion of the propagator for the nonrenormalizable theories. For $t \neq 0$ it is clear that term by term the infinite parts can be removed by mass and Z_2 renormalizations. For $t=0$ the renormalized expansion breaks down and this just is due to the singularity of the exact solution at this point. One also sees that the terms of the series correspond, as they must, to an expansion of the exact propagator in powers of γ.

V. DEFINITION OF THE OPERATORS FOR THE NONRENORMALIZABLE THEORIES

In order that the nonrenormalizable theories treated above be physically meaningful, it is at least necessary that the Fourier transforms of the various operators of the theories be defined, as these Fourier transforms are closely related to quantities, such as the scattering amplitudes, which are comparable with experiments. The scattering due to the diagram in Fig. 1, for example, is proportional to the Fourier transform of the propagator; more generally, the meson-nucleon scattering amplitude is given by the Fourier transform of the meson-nucleon Green's function which will involve, with other quantities, the Fourier transform of the propagator.

The renormalized propagators, for the n larger than zero theories, are given by

$$S_c^{(n)}(\tau)=\theta(\tau)e^{-im\tau}\exp\{\gamma(2n-1)!\tau^{-2n}\}, \quad (26)$$

and the Fourier transform of $S_c^{(n)}(\tau)$ is (suppressing the superscript n)

$$S(q)=\int_0^\infty e^{-i(m+q)\tau}\exp\{\gamma(2n-1)!\tau^{-2n}\}d\tau. \quad (27)$$

This is defined for $m+q$ in the lower half plane ($m+q-i\epsilon$) and for γ in the left half plane. We want to extend the domain of definition of Eq. (27) to all complex values of γ. When this is done the Fourier transform of the propagator can be defined for those theories (n even; $n>0$) for which the requirement that the Lagrangian be Hermitian would place γ in the right half plane; also the singularity that the Fourier transform of the propagator possesses at $\gamma=0$ can be examined. This turns out to be a logarithmic branch point and introduces an ambiguity into the theory because the Fourier transforms of the operators become many-valued functions of the coupling constant.

$S(q)$ can be analytically continued from the left half plane into the entire domain of γ by the procedure given in Appendix A. Equation (A2) of this appendix

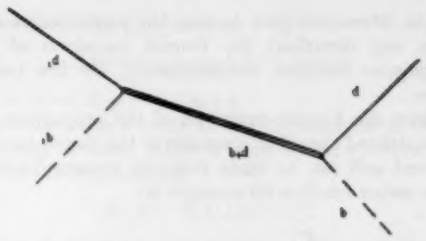

FIG. 1. A Feynman diagram for the scattering of a meson by a nucleon. The double line represents the nucleon propagator with all radiative connections: $S_c(p+q)$.

gives a representation of $S(q)$

$$S(q)=\int_{C_\theta}\exp\{-i(m+q)\tau-\lambda(2n-1)!\tau^{-2n}e^{i\theta}\}d\tau, \quad (28)$$

where $\gamma=-\lambda e^{i\theta}$ and $\lambda=\lambda^*\geqslant 0$, which is defined for the entire domain of γ. From Eq. (28) one can see that $S(q)$ is a many valued function of γ, as there will be an infinite number of contours $C_{\theta+2l\pi}$ which correspond to a given $\gamma=-\lambda e^{i\theta}e^{i2l\pi}$, $l=0\pm1\pm2\cdots$.

In the $n=1$ case, where γ must be real and smaller than zero for the physically interesting Hamiltonians, the values of θ are restricted to even multiples of π, $\theta=2l\pi$, where $l=0, \pm1, \pm2\cdots$. We can define $S_0(q)$ (that function of q for which $l=0$) as the principle value of $S(q)$. It is $S_0(q)$ that would be reached in a "natural" way beginning with a cut-off theory and permitting the cutoff to go to infinity. (See Appendix B.) $S_l(q)$ is the sum of $S_0(q)$ and terms which are the contributions of the integrand of Eq. (28) when integrated over a contour which encloses the point $\tau=0$.

In a theory which contained scattering, if the same general results were valid, the extra terms, while not changing the residue of the propagator at $q+m=0$, would give an additional contribution to the scattering which did not necessarily have the same energy dependence as the scattering due to the principal value. Some explicit evaluations of these terms are given in Appendix A.

In the $n=2$ case γ must be real and larger than zero for Hermitian Lagrangians. Then θ is an odd multiple of π, $\theta=(2l+1)\pi$, where $l=0, \pm1, \pm2\cdots$. Again one gets a many-valued propagator but here the principal value $S_0(q)$ would not be approached by a cut-off solution. (The cut-off solution diverges as the cutoff approaches infinity.) The fact that two such cases occur seems to be a peculiarity of the nonrecoil theories. In the four-dimensional case, the results obtained by Arnowitt and Deser[1] show that due to the presence of functions like $\exp(-g^2/x^2)e^{-ik\cdot x}$ which must be integrated over all of space-time—positive and negative values of x^2—no cut-off solution would approach the continuation which gives the finite Fourier transform.

The point $\gamma=0$ is a finite branch point, for any value of n, and is shared by all the Riemann surfaces. Thus,

as the interaction goes to zero (as γ approaches zero from any direction) the Fourier transform of the propagator becomes, unambiguously, the free propagator.

Once the Fourier transform of the propagator has been defined the other operators of the theory are also defined and can be made finite by renormalizations. The vertex function for example is:

$$\Gamma^{(n)}(t,t';\xi)=N\int\delta\phi\phi(\xi)G_4^{(n)}(t,t';\phi)$$

$$\times\exp\left\{-i/2\int\int\phi(\xi)\Delta^{-1}(\xi,\xi')\phi(\xi')d\xi d\xi'\right\}, \quad (29)$$

where $\Gamma^{(n)}$ is related to the usual vertex function by

$$\int\Delta^{-1}(\xi,\xi')S^{-1}(y,t')S^{-1}(x,t)\Gamma^{(n)}(x,y;\xi')dxdyd\xi'$$
$$=\Gamma^{(n)}(t,t';\xi). \quad (30)$$

By a procedure entirely analogous to that of Sec. II, one gets for $\Gamma^{(n)}$

$$\Gamma^{(n)}(t,t';\xi)=gS_{(n)}'(\tau)\int_{t'}^{t}\Delta^{(n)}(\xi,\eta_0)d\eta_0. \quad (31)$$

The Fourier transform of this operator is well defined if the Fourier transform of $S'(\tau)$ is defined, and there are no additional ambiguities. Let

$$\Gamma_e^{(n)}=Z_1^{(n)}\Gamma^{(n)}. \quad (32)$$

Then $\Gamma_e^{(n)}$ will be finite if

$$Z_1^{(n)}=Z_2^{(n)}. \quad (33)$$

The same kind of argument is applicable to the meson-nucleon Green function

$$G(t,t';\xi,\xi')=g^2\int_{t'}^{t}\Delta^{(n)}(\xi,\eta_0)d\eta_0$$
$$\times\int_{t'}^{t}\Delta^{(n)}(\xi',\eta_0')d\eta_0'S_{(n)}'(\tau) \quad (34)$$

and to the other operators of these theories.

The matrix elements between free particle states of the operators which describe scattering amplitudes [such as the meson-nucleon Green function, Eq. (34)] are all zero. This is because the interactions of the theories treated can be transformed away and contain no scattering of mesons by nucleons.[10] The procedure outlined in the foregoing, however, makes it possible to define finite matrix elements for virtual transitions and thus to make all the operators finite for any value of n, in spite of the fact that for $n>0$ the operators, from the usual perturbation series point of view, are not renormalizable.

[10] G. Wentzel, *Quantum Theory of Fields* (Interscience Publishers, Inc., New York, 1949), p. 47.

The author wishes to express his gratitude to Dr. J. R. Oppenheimer and to the Institute for Advanced Study for their hospitality. He also would like to thank the members of the Institute for many helpful conversations.

APPENDIX A. BEHAVIOR OF THE PROPAGATOR IN THE γ DOMAIN

The existence of the Fourier transform of $S_e^{(n)}(\tau)$ for part of the complex γ plane makes possible the definition of a Fourier transform of $S_e^{(n)}(\tau)$, for the entire domain of γ, by the process of analytic continuation.[11] If $-\gamma=\lambda e^{i\theta}$ where $\lambda=\lambda^*\geq 0$, the Fourier transform of $S_e^{(n)}(\tau)$ is

$$S(q)=\int_0^\infty\exp\{-i(m+q)\tau-\lambda(2n-1)!\tau^{-2n}e^{i\theta}\}d\tau, \quad (A1)$$

and this is well defined for $m+q$ in the open lower half plane and for γ in the left half plane $(-\pi/2\leq\theta\leq\pi/2)$. If the contour of integration in the τ plane is now deformed to C_θ, as shown in Fig. 2, we obtain the analytic continuation of Eq. (A1) into the entire domain of γ. $S(q)$ is then

$$S(q)=\int_{C_\theta}\exp\{-i(m+q)\tau-\lambda(2n-1)!\tau^{-2n}e^{i\theta}\}d\tau. \quad (A2)$$

This is a many-valued function of γ since there are an

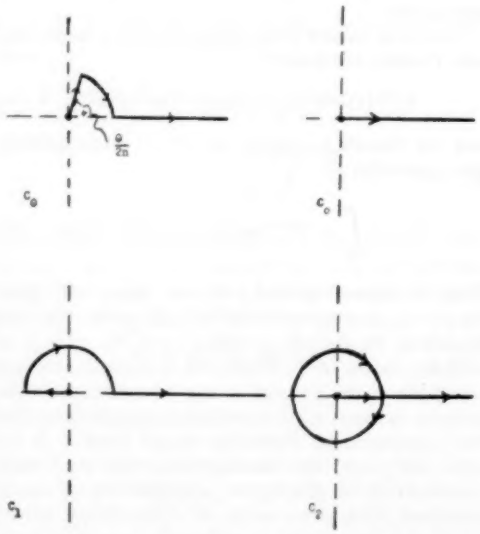

FIG. 2. Contours in the τ plane which define the Fourier transform of the propagator in various regions of the γ domain. C_θ applies for any value of n. C_0, C_1, and C_2 are the contours which give $S_0(q)$, $S_1(q)$, and $S_2(q)$ for the case $n=1$.

[11] The author wishes to acknowledge some very helpful discussions on this point with Professor A. Beurling and Dr. P. Malliavin of the Institute for Advanced Study.

infinite number of values of θ which correspond to a given γ and each of these give a different $S(q)$ due to the contour C_θ. Some of the contours that arise are shown in Fig. 2.

As an example of the kind of behavior $S(q)$ exhibits let us investigate in detail the case $n=1$. For this case $\gamma=-g^2/4\pi^2$ (in order that the Hamiltonian be Hermitian) so that the relevant values of θ are $\theta=2l\pi$ where $l=0, \pm1, \pm2\cdots$. Let $S_l(q)$ be the function $S(q)$ when $\theta=2l\pi$. Then

$$S_l(q)=S_0(q)+T_l(q), \tag{A3}$$

where $S_0(q)$ is defined as the principal value of $S(q)$ and $T_l(q)$ is the contribution that arises due to integrations, such as those in Fig. 2, which surround the point $\tau=0$. The procedure outlined above would also be applicable if the meson mass μ were not set equal to zero. However, the explicit evaluation of $T_l(q)$ then becomes much more difficult.

$T_2(q)$, which is the contribution of the integrand of Eq. (A2) in a complete, clockwise circuit of the origin, is (for $n=1$)

$$T_2(q)=2\pi\sum_{r=1}^{\infty}\frac{(\lambda)^r(m+q)^{2r-1}}{r!(2r-1)!}. \tag{A4}$$

$T_2(q)$ goes to zero as $(m+q)\to0$ and as $\lambda\to0$. As $m+q$ or λ become infinite along the real axis $T_2(q)$ also becomes infinite. This latter behavior is true for all odd n while for n even ($n>0$) $T_2(q)$ oscillates and goes to zero as λ or $(m+q)$ become infinite. For the meson mass unequal to zero $T_2^a(q)$ remains finite as $m+q\to0$ and is zero for $\lambda=0$. However, the explicit form of $T_2^a(q)$ would be much more complicated than that of Eq. (A4) and its dependence as $q\to\infty$ has not been ascertained as yet.

A peculiarity of the meson mass zero case is the logarithmic branch point $S(q)$ possesses, in the q domain, at the point $m+q=0$. This corresponds to the production of mesons with arbitrary energy. The value at $S(q)$ in the $m+q$ domain differs from branch to branch of the Riemann surface by just $T_2(q)$.

In examining the behavior of $S_l(q)$ for the various values of l it is convenient to separate off the singular part of $S_l(q)$ at $m+q=0$. We then have (for $n=1$)

$$S_0(q)=\frac{-i}{m+q}+\int_0^\infty e^{-i(m+q)\tau}h(\tau)d\tau, \tag{A5}$$

where $h(\tau)=\exp(-\lambda/\tau^2)-1$. The second term of Eq. (A5) contains the radiative correction to the propagator; it is finite for all values of q and goes to zero as $\lambda\to0$. For $l\neq0$ we get

$$\begin{aligned}S_1(q)&=\frac{-i}{m+q}-\int_0^\infty e^{+i(m+q)\tau}h(\tau)d\tau+\theta(m+q)T_2(q)\\ S_2(q)&=\frac{-i}{m+q}+\int e^{-i(m+q)\tau}h(\tau)d\tau+T_2(q), \text{ etc.}\end{aligned} \tag{A6}$$

As $m+q\to0$, $S(m+q)$ becomes

$$S_l(q)=-i/m+q+\text{finite terms}, \tag{A7}$$

and for $\lambda=0$, $S_l(q)=-i/m+q$.

We can obtain a crude idea of the behavior of these functions, for small values of $m+q$ and λ, by replacing $h(\tau)$ by the step function

$$h(\tau)\simeq-\theta[3/2(\lambda)^{\frac{1}{3}}-\tau]. \tag{A8}$$

Then neglecting terms of order $m+q$ or higher we have,

$$\begin{aligned}S_0&\simeq-i/m+q-3/2\sqrt{\lambda}+\cdots\\ S_1&\simeq-i/m+q+3/2\sqrt{\lambda}+\cdots\\ S_2&\simeq-i/m+q-3/2\sqrt{\lambda}+\cdots, \text{ etc.}\end{aligned} \tag{A9}$$

For larger values of $m+q$, $T_2(q)$ becomes dominant except in the odd l cases where the step function $\theta[\pm(m+q)]$ cuts off $T_2(q)$ as $m+q$ changes sign.

APPENDIX B. CUT-OFF APPROXIMATION

In spite of the impossibility of making a coupling constant expansion for the Fourier transforms of the $n>0$ theories discussed above, it is possible to approximate the exact theory by a cut-off theory, the error term which can be estimated when the solutions are known. The Fourier transform of the operators of the cutoff theory can be calculated in a perturbation expansion and this expansion will be practical if the coupling constant and cutoff are small enough.

As an example let us consider the $n=1$ theory with an interaction term $g\psi^*(\alpha\cdot\nabla\phi)\psi$. Then the renormalized propagator is

$$S_c(\tau)=\theta(\tau)e^{-im\tau}\exp\left\{\frac{g^2}{4\pi^2}\int_0^\infty\frac{k^4dk}{\omega^3}e^{-i\omega\tau}\right\}. \tag{B1}$$

A theory which cuts off the meson momentum at K would give for the renormalized propagator,

$$S_c^K(\tau)=\theta(\tau)e^{-im\tau}\exp\left\{\frac{g^2}{4\pi^2}\int_0^K\frac{k^4dk}{\omega^3}e^{-i\omega\tau}\right\}. \tag{B2}$$

The cut-off solution above is analytic in $g^2/4\pi^2$ for all values of τ and thus the Fourier transform is analytic in $g^2/4\pi^2$ at $g^2/4\pi^2=0$ and can be expanded in the coupling constant at the origin. As K increases and the cutoff solution approaches the $K=\infty$ solution the terms of the expansion of the Fourier transform of $S_c^K(\tau)$ grow increasingly large and oscillate. Thus the expansion appears to be completely dependent on the cutoff.

This is not necessarily so, however, for an examination of the exact solutions shows that the cutoff and $K=\infty$ theories differ mostly in the region where $\tau\to0$, but this region itself contributes very little to the Fourier transform of the propagator because of the radiative correction:

$$R_c(\tau)=\exp\{-(g^2/4\pi^2)\tau^{-2}\} \quad \text{as} \quad \tau\to0.$$

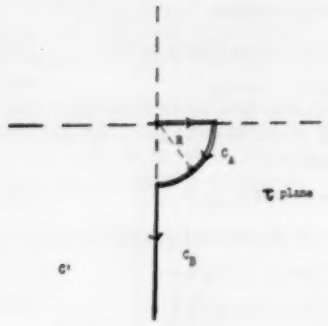

FIG. 3. Contour used in evaluating the error term $E(K,q)$.

To make this more precise we will examine the Fourier transform of $S_\epsilon(\tau)-S_\epsilon^K(\tau)$ and show that, for a large enough cutoff, the error term is small and, for a small coupling constant, a perturbation expansion of the Fourier transform of $S_\epsilon^K(\tau)$ can be made.

The Fourier transform of $S_\epsilon^K(\tau)$ is

$$S^K(q)=\int_0^\infty \exp\left\{-i(m+q)\tau + \frac{g^2}{4\pi^2}\int_0^K \frac{k^4dk}{\omega^3}e^{-i\omega\tau}d\tau\right\} \quad \text{(B3)}$$

and the principal value of that of $S_\epsilon(\tau)$ is

$$S(q)=\int_0^\infty \exp\left\{-i(m+q)\tau+\frac{g^2}{4\pi^2}\int_0^\infty \frac{k^4dk}{\omega^3}e^{-i\omega\tau}d\tau\right\}. \quad \text{(B4)}$$

Define the error term $E(K,q)$ to be

$$E(K,q)=[S(q)-S^K(q)]/S^K(q). \quad \text{(B5)}$$

If the contour of integration is shifted to C', shown in Fig. 3, we can divide the contribution to the error term into a portion which comes from the neighborhood of the origin C_A and that which comes from the major part of the path C_B. The contribution to $E(K,q)$ which results from C_B is

$$E^B(k,q)\simeq(\lambda/R)e^{-KR}\{1/R+K\} \quad \text{(B6)}$$

where $\lambda=g^2/4\pi^2$, while the contribution from C_A is of the order of

$$E^A(K,q)\simeq\exp(-\lambda/R^2)R + \frac{\pi R}{2}\lambda\exp(\lambda/R^2-KR)[KR-1]\frac{1}{S^K(q)}. \quad \text{(B7)}$$

Letting $R=r\sqrt{\lambda}$ and $K=k/\sqrt{\lambda}$, one can choose values of r and k so that the error term becomes arbitrarily small. However, this is limited in practice by the requirement that K be kept reasonably small in order that a perturbation expansion of $S^K(q)$ be possible. In any case one gets a better approximation close to the poles of $S^K(q)$ since the major contribution at the singularities comes from large values of r where $S_\epsilon^K(\tau)$ is a very good approximation to $S_\epsilon(\tau)$.

PHYSICAL REVIEW VOLUME 100, NUMBER 1 OCTOBER 1, 1955

Agreement of Classical and Quantum Coulomb Excitation Integrals*

JOHN P. LAZARUS AND S. SACK†
Yale University, New Haven, Connecticut

(Received June 13, 1955)

A comparison is made between classical and quantum Coulomb excitation integrals. Use is made of a relation due to Breit and Daitch concerning close equality of classical and quantum density integrals. It is shown that the indefinite Coulomb excitation integrals show agreement at nearly the same distances as the corresponding density integrals. The agreement of the Coulomb excitation integrals for small excitations is therefore believed to be caused at least partly by the agreement of the density integrals.

THE fact that semiclassical and quantum calculations of Coulomb excitation are in close agreement has been discussed by Breit and Daitch,[1] by Daitch, Lazarus, Hull, Benedict and Breit,[2] and by Biedenharn and Class.[3] In a note to appear shortly, Breit and Daitch[4] show that there is a close agreement between integrals of classical and quantum densities integrated from $r=0$ to r. They show that if the integrals are taken to a node of the radial wave function F/r and if the JWKB approximation holds at the point r, there is an exact agreement between the two integrals. A redistribution of densities occurs as a result of going from the classical to the quantum theories. It is reasonable to expect, therefore, that the calculation of radial

* This research was supported by the United States Air Force, through the Office of Scientific Research of the Air Research and Development Command.

† Now at University of California, Livermore, California.

[1] G. Breit and P. B. Daitch, Phys. Rev. **96**, 1447 (1954).

[2] Daitch, Lazarus, Hull, Benedict, and Breit, Phys. Rev. **96**, 1449 (1954).

[3] L. C. Biedenharn and C. M. Class, Phys. Rev. **98**, 691 (1955).

[4] G. Breit and P. B. Daitch, Proc. Natl. Acad. Sci. (to be published).

integrals having the form $\int_0^\infty (F^2/r^3)dr$ which occur in the theory of Coulomb excitation will show related similarities between the classical and quantum values. The classical density which enters in this connection is according to[1] the quantity $1/(2Q)$ where

$$Q=\left[1-\frac{2\eta}{\rho}-\frac{L(L+1)}{\rho^2}\right]^{\frac{1}{2}}.$$

Here $\rho=kr$ in the usual notation and F is normalized so as to be a sine function of unit amplitude at infinity. It has been thought of interest, therefore, to compare $\int^\rho(1/2Q)d\rho$ with $\int_0^r F^2dr$ and also to compare $\int^\rho(1/2Q)\rho^{-3}d\rho$ with $\int_0^\rho(F^2/\rho^3)d\rho$. The lower limit in the integrals involving Q is the classical turning point. The comparison shows that the indefinite integrals considered as functions of ρ are very similar to each other and that the quantum integral oscillates about the value of the classical integral. Such a behavior can be expected as a consequence of the redistribution theorem.[4]

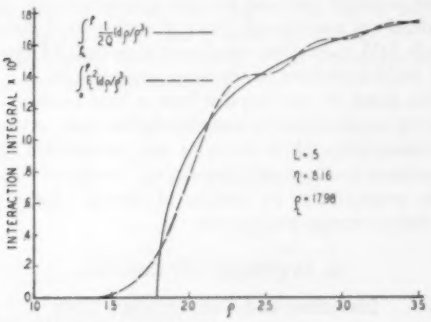

FIG. 1. Interaction integrals in quantum mechanical and semi-classical treatments of Coulomb excitation. The quantity ρ_L is the value of ρ at the classical turning point.

The present calculations have been carried out in order to see more quantitatively how the compensations of positive and negative deviations of the quantum density from the classical density affect the integrals which enter the problem of Coulomb excitation. The comparison is presented in Figs. 1 and 2. Figure 1 shows the integrals involving the factor $1/\rho^3$ as a function of ρ. Figure 2 shows the corresponding density integrals. In Fig. 2 there are marked the positions of maxima, minima and nodes of the function F. It is seen that the integrals of the density are indeed closely equal to each other at the nodes. There are also points in between at which the two integrals are equal to each other in agreement with the considerations of Breit and Daitch.[1,4] As a result the quantum integrated density

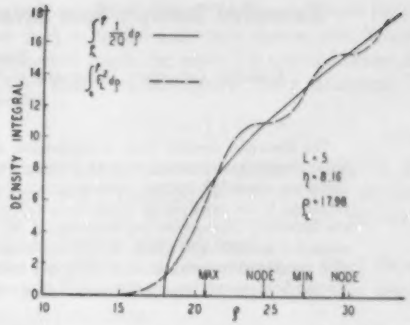

FIG. 2. Density integrals in quantum mechanical and semi-classical treatments of Coulomb excitation. Values of the abscissa corresponding to maxima, minima, and nodes of $F_L(\rho)$ are indicated by arrows at the appropriate values of ρ.

curve intersects the classical curve at frequent intervals. This circumstance contributes to the relative insignificance of the variation of $1/\rho^3$ in its effect on the location of points of compensation (intersections between quantum and classical curves). The relatively rapid oscillation makes the difference between quantum and classical integrands consist of alternatively positive and negative parts so that the variation of $1/\rho^3$ is not very important. A contributing factor is the fact that the Coulomb wave function F vanishes rather rapidly as one proceeds to the left of the classical turning point. The contribution of the region to the left of the classical turning point to the Coulomb excitation integral is thus not very important since the distance within which the function F becomes negligible as one proceeds to the left of the classical turning point is relatively small in comparison with the value of ρ at the turning point. There is a good chance of compensation of the contribution to the quantum integral to the left of the turning point by the difference between the classical and quantum densities just to the right and it is seen that this as well as succeeding points of compensation occur at nearly the same values of ρ.

The present considerations have been made only for zero excitation energy. Unpublished work by Benedict, Daitch, Lazarus, and Breit indicates similar compensation under more general conditions.

The authors wish to express their appreciation to Professor G. Breit for suggesting this investigation and to him and Dr. P. B. Daitch for helpful discussions throughout the work. They also would like to express their indebtedness to Dr. P. Rabinowitz and Dr. M. Abramowitz of the National Bureau of Standards for the computation of Coulomb Functions by means of the SEAC which proved useful in this work.

Extended Isotopic Spin Invariance and Meson-Nucleon Coupling*

SIDNEY A. BLUDMAN
Radiation Laboratory, Department of Physics, University of California, Berkeley, California
(Received April 22, 1955)

The identities derived from a Lagrangian density that is invariant under transformations that depend on arbitrary functions are used to develop the restrictions on allowed forms of coupling that follow from assuming extended isotopic spin invariance. A proof is given that invariance under local isotopic spin rotations is not possible for pions and nucleons alone. The relations between the transformation law and the invariant Lagrangian are developed if (a) the pion-nucleon system is allowed to admit a more general extended isotopic spin group, or (b) additional fields are admitted in order to maintain the local isotopic spin rotational invariance. In either case, definite restrictions on the permissible transformation properties for the field quantities are obtained if pion-nucleon isotopic spin conservation is to be maintained.

I. INTRODUCTION

IN the isotopic spin formalism, nucleons and pions are described by spinors and vectors in isotopic spin space. Pion-nucleon phenomena and the charge independence of nuclear forces (at least at energies corresponding presumably to interactions via pions alone) suggest that if electromagnetic interactions are neglected, total isotopic spin is conserved in interactions involving pions and nucleons alone. This situation is described formally by stating that the pion-nucleon interaction is invariant with respect to the three-parameter group of rotations of the isotopic spin coordinate system.

This paper is concerned with the possibility of extending this invariance to isotopic spin rotations which are local in the sense that at different points in space-time different isotopic spin rotations are permitted. Such an extension is motivated[1] by the possibility that the meson-nucleon coupling may be suggested by some such extended physical symmetry principle. This is the case in electrodynamics where the assumption of local gauge invariance suggests the coupling between charged particles and the electromagnetic field, and in general relativity where general covariance leads to Bianchi identities which suggest how other fields are coupled into the gravitational field.

The principle to be emphasized here is that certain identities are present whenever the equations of motion are derived from a Lagrangian density that is invariant under transformations depending on arbitrary functions rather than arbitrary parameters. This important theorem, due originally to Noether,[2] is briefly derived in the next section: the new idea here consists in recognizing that these identities are applicable to coupled fields. The central results needed are Eqs. (17), (18), and (19).

In the third section, these identities are used to show that local isotopic spin rotational invariance is not possible for nucleons and scalar or pseudoscalar mesons. The possibility of allowing an additional "**b** field" in order to maintain local isotopic spin rotational invariance, as Yang and Mills have recently done,[3] is considered in the fourth section. It is shown that, as a consequence of the local isotopic spin invariance, independently of any special choice of equations of motion, this **b** field must obey nonlinear equations of motion and must contribute to the total isotopic spin.

The point of view implied here is that isotopic spin may be explicable as a consequence of some extended invariance principle in the same way as extended gauge invariance and general coordinate covariance illuminate, respectively, the nature of electric charge and the role of energy-momentum.

II. EXTENDED INVARIANCE

Identities and Conservation Laws

Suppose the equations of motion are obtained by the variation of an action integral

$$I=\int_\Omega \mathfrak{L}(y^A(x),y^A{}_{,\mu}(x))d^4x. \tag{1}$$

The $,_\mu$ designate differentiation with respect to the coordinates x^μ. Y^A is the Ath field variable. The summation convention is assumed. Under the transformation considered, let the coordinates change by

$$\delta x^\mu=x^{\mu\prime}-x^\mu, \tag{2}$$

where x' designates the point x in the transformed system, and let

$$\delta\mathfrak{L}=\mathfrak{L}(y'^A(x'),y^A{}_{,\mu}{}'(x'))-\mathfrak{L}(y^A(x),y,_\mu{}^A(x)) \tag{3}$$

be the local variation in the integrand $\mathfrak{L}$. Then the change in the action integral is

$$\delta I=\int_\Omega[\delta\mathfrak{L}+\mathfrak{L}(\delta x^\mu),_\mu]d^4x, \tag{4}$$

* This work was performed under the auspices of the U. S. Atomic Energy Commission.

[1] See, for example, the interchange between W. Pauli and A. Pais, Physica **19**, 887 (1953).

[2] E. Noether, Nachr. Akad. Wiss. Göttingen, Math.-physik. Kl. **235** (1918). See also E. Bessel-Hagen, Math. Ann. **84**, 258 (1921); P. G. Bergmann and R. Schiller, Phys. Rev. **89**, 4 (1953).

[3] C. N. Yang and R. L. Mills, Phys. Rev. **96**, 191 (1954).

where $(\delta x^\mu)_{,\mu}$ is the term in the Jacobian brought about by the transformation from x to x' coordinates. For the equations of motion to be invariant, the action integral must change at most by a boundary term on which the variations performed in obtaining the equation of motion vanish. Since the volume V is arbitrary, this requires[4] that the integrand in Eq. (4) change at most by a divergence:

$$\delta\mathfrak{L}+\mathfrak{L}(\delta x^\mu)_{,\mu}=(\delta\Omega^\mu)_{,\mu}. \tag{5}$$

Then $\mathfrak{L}-\Omega^\mu{}_{,\mu}$ would be an invariant Lagrangian density, since

$$\delta(\mathfrak{L}-\Omega^\mu{}_{,\mu})+(\mathfrak{L}-\Omega^\mu{}_{,\mu})(\delta x^\mu)_{,\mu}=0. \tag{6}$$

In the following, Ω^μ is dropped and it is assumed that one always has to do with an invariant Lagrangian density. This possibility of changing the Lagrangian density by a suitable divergence can introduce a certain ambiguity in the densities that are differentially conserved, but will not affect the conclusions of this paper about the possibility of admitting a local isotopic spin group for the pion-nucleon system. If the substantial change in the form of y^A as a function of its argument is designated by

$$\delta^* y^A=y'^A(x)-y^A(x), \tag{7}$$

then

$$\delta\mathfrak{L}=\delta^*\mathfrak{L}+\mathfrak{L}_{,\mu}\delta x^\mu, \tag{8}$$

and

$$\delta^*\mathfrak{L}=\mathfrak{L}^A\delta^* y^A+\left(\frac{\partial\mathfrak{L}}{\partial y^A{}_{,\mu}}\delta^* y^A\right)_{,\mu}. \tag{9}$$

The Lagrangian derivative,

$$[\mathfrak{L}]_A\equiv\partial\mathfrak{L}/\partial y^A-(\partial\mathfrak{L}/\partial y^A{}_{,\mu})_{,\mu}, \tag{10}$$

vanishes where the field equations hold.

Equation (6), the invariance of the Lagrangian density, gives

$$[\mathfrak{L}]_A\delta^* y^A+\left(\frac{\partial\mathfrak{L}}{\partial y^A{}_{,\mu}}\delta^* y^A+\mathfrak{L}\delta x^\mu\right)_{,\mu}=0. \tag{11}$$

This is Noether's first result: If the equations of motion are invariant under the variations (2) and (7), $[\mathfrak{L}]_A\delta^* y^A$ must be of the form of a divergence.

Now suppose that the transformation is described by p arbitrary parameters or functions of the coordinates ξ^i $(i=1, 2\cdots p)$ and that the transformation induces the change

$$\delta x^\mu=c_i{}^\mu\xi^i \tag{12}$$

in the coordinates and the change

$$\delta^* y^A=a_i{}^A\xi^i+b_i{}^{A\mu}\xi^i{}_{,\mu} \tag{13}$$

in the field variables. The $a_i{}^A$, $b_i{}^{A\mu}$ are definite functions of the field variables and their derivatives. Where no confusion will result the index i is omitted below. Since $[\mathfrak{L}]_A\delta^* y^A$ must be a divergence, the p identities

$$[\mathfrak{L}]_A a_i{}^A\equiv([\mathfrak{L}]_A b_i{}^{A\mu})_{,\mu} \tag{14}$$

must obtain among the field equations $[\mathfrak{L}]_A=0$. These identities, which characterize theories that depend on arbitrary functions rather than arbitrary parameters, constitute Noether's second result.

Since the field quantities need not all be of the same kind, these identities can be used to obtain relations among coupled fields.

Equation (11) now states that

$$(T^\mu\xi+U^{\mu\lambda}\xi_\lambda)_{,\mu}=0, \tag{15}$$

where

$$\begin{aligned}-T^\mu&\equiv[\mathfrak{L}]_A b^{A\mu}+(\partial\mathfrak{L}/\partial y^A{}_{,\mu})a^A+\mathfrak{L}c^\mu,\\ -U^{\mu\lambda}&\equiv(\partial\mathfrak{L}/\partial y^A{}_{,\mu})b^{A\lambda}.\end{aligned} \tag{16}$$

Since ξ, $\xi_{,\mu}$, and $\xi_{,\mu\lambda}$ may each have arbitrary values, Eq. (15) implies

$$U^{\mu\lambda}+U^{\lambda\mu}=0, \tag{17}$$

$$T^\mu=U^{\mu\lambda}{}_{,\lambda}, \tag{18}$$

$$T^\mu{}_{,\mu}=0. \tag{19}$$

Now a conservation law like Eq. (19) could be obtained directly from Eq. (11) by using the equations of motion $[\mathfrak{L}]_A=0$, even if the ξ^i were arbitrary parameters rather than arbitrary functions. The crucial point is, however, that when as in this paper there is an *extended* invariance, Eqs. (17)–(19) are obtained as identities in form which which are not dependent on the applicability of the field equations.

The next two subsections illustrate these identities, briefly for the gravitational field, and in more detail for the electromagnetic field, which bears a closer resemblance to the meson-nucleon application to be made.

Gravitational Field

The four (Bianchi) identities (14) which follow in general relativity from the assumed covariance of the theory with respect to arbitrary transformations on the four coordinates, make $R_{\mu\nu}-\frac{1}{2}g_{\mu\nu}R$ have vanishing covariant divergence. (The $R_{\mu\nu}$ and R are the contractions of the curvature tensor.) This suggests that in the presence of nongravitational fields described by an energy-momentum tensor $T_{\mu\nu}$, the field equations be taken to be

$$R_{\mu\nu}-\tfrac{1}{2}g_{\mu\nu}R=-kT_{\mu\nu}. \tag{20}$$

In fact, in simple enough field theories, this principle that a field's energy-momentum density should be capable of being the source of the gravitational field does away with any ambiguity in the definition of the energy-momentum density.

[4] R. Courant and D. Hilbert, *Methoden der Mathematischen Physik* (Verlag Julius Springer, Berlin, 1931), second edition, p. 165.

Electromagnetic Field

Consider from now on transformations on the field variables alone

$$\delta x^\mu = 0. \tag{21}$$

Generalizing a nomenclature of Pauli,[5] one might now define transformations of the first kind for which $\delta y^A = a^A \xi$ ($b^{A\mu}=0$), and transformations of the second kind for which $\delta y^A = b^{A\mu}\xi_{,\mu}$ ($a^A=0$). Then Eq. (19) states that a "current" $J^\mu \equiv -T^\mu$ of fields undergoing transformations of the first kind is conserved. Equations (18) and (17) state that this current is the divergence of an antisymmetric "superpotential"[6] $U^{\mu\lambda}$ consisting of fields undergoing transformations of the second kind.

The assumption of extended gauge invariance,

$$\delta \mathfrak{L} = 0 \tag{22}$$

for

$$\delta\psi = ie\xi\psi, \quad \delta\bar{\psi} = -ie\xi\bar{\psi}, \quad \delta A_\mu = \xi_{,\mu}, \tag{23}$$

requires by Eq. (19) that the charged-particle current

$$J_\mu = ie\left(\bar{\psi}\frac{\partial \mathfrak{L}}{\partial \bar{\psi}_{,\mu}} - \frac{\partial \mathfrak{L}}{\partial \psi_{,\mu}}\psi\right) \tag{24}$$

be conserved. Equation (17) in this case requires

$$\frac{\partial \mathfrak{L}}{\partial A_{\mu,\nu}} + \frac{\partial \mathfrak{L}}{\partial A_{\nu,\mu}} = 0, \tag{25}$$

namely that the derivatives of the vector potential occur only in the antisymmetric combination $F_{\mu\nu} = A_{\mu,\nu} - A_{\nu,\mu}$. Equation (18) requires that

$$J_\mu = (\partial \mathfrak{L}/\partial A_{\mu,\nu})_{,\nu} = \partial \mathfrak{L}/\partial A_\mu, \tag{26}$$

or that the vector potential occur in the Lagrangian density only through an interaction term $J_\mu A_\mu$. In this way the assumption of extended gauge invariance leads to the form of coupling between the charged-particle and electromagnetic fields.

III. PION-NUCLEON SYSTEM

Under infinitesimal rotations of the isotopic-spin coordinate system, described by the three parameters ξ^i, the nucleon and (pseudoscalar) meson variables transform as isotopic spinors and vectors:

$$\begin{gathered}\delta\psi = \tfrac{1}{2}i\xi^i\tau^i\psi, \quad \delta\bar{\psi} = -\tfrac{1}{2}i\bar{\psi}\xi^i\tau^i, \\ \delta\phi^i = \epsilon^{ijk}\phi^j\xi^k.\end{gathered} \tag{27}$$

Here the τ^i are the Pauli matrices in isotopic spin space and the ϵ^{ijk} are the alternating symbols. It is natural to assume that the Lagrangian density $\mathfrak{L}$ is invariant even when the ξ^i in Eq. (27) are allowed to be arbitrary functions of space-time. Defining this as local isotopic rotational spin invariance for the nucleon isotopic spinors and meson isotopic vectors,

$$\begin{aligned}0 = \delta\mathfrak{L} = &\left(\frac{\partial \mathfrak{L}}{\partial \phi^i_{,\mu}}\delta\phi^i + \frac{\partial \mathfrak{L}}{\partial \psi_{,\mu}}\delta\psi + \delta\bar{\psi}\frac{\partial \mathfrak{L}}{\partial \bar{\psi}_{,\mu}}\right)_{,\mu} \\ &+ [\mathfrak{L}]_{\phi^i}\delta\phi^i + [\mathfrak{L}]_\psi\delta\psi + \delta\bar{\psi}[\mathfrak{L}]_{\bar{\psi}}.\end{aligned} \tag{28}$$

The identities (14) in this theory are

$$\tfrac{1}{2}i([\mathfrak{L}]_\psi \tau^i\psi - \bar{\psi}\tau^i[\mathfrak{L}]_{\bar{\psi}}) = \epsilon^{ijk}\phi^j[\mathfrak{L}]_{\phi^k}. \tag{29}$$

The existence of these three identities is connected with the assumption that the local isotopic-spin coordinate system can be chosen arbitrarily.

Substituting from Eq. (27) into Eq. (28), one obtains, from the vanishing of the coefficient of ξ^i,

$$J_\mu{}^i{}_{,\mu} = 0, \tag{30}$$

where

$$J_\mu{}^i = -\tfrac{1}{2}i\left(\frac{\partial \mathfrak{L}}{\partial \psi_{,\mu}}\tau^i\psi - \bar{\psi}\tau^i\frac{\partial \mathfrak{L}}{\partial \bar{\psi}_{,\mu}}\right) + \epsilon^{ijk}\phi^j\frac{\partial \mathfrak{L}}{\partial \phi^k_{,\mu}} \tag{31}$$

is an isotopic spin current consisting of spinor and orbital parts. However, from the vanishing of the coefficient of $\xi^i_{,\mu}$,

$$J_\mu{}^i = 0. \tag{32}$$

If the meson and the nucleon fields transform locally as isotopic vectors and spinors, then all components of the isotopic-spin current vanish everywhere. This result follows whenever the two fields ψ and ϕ both undergo transformations of the first kind only: a coupling between pions and nucleons cannot be brought about as a consequence of local isotopic spin invariance.

In the face of this result, two possibilities present themselves:

(1) According to Eqs. (18) and (19) if the nucleon and pion fields transformed by

$$\begin{aligned}\delta\psi &= \tfrac{1}{2}i\xi^i\tau^i\psi + b_\psi{}^\mu\,\xi_{,\mu} \\ \delta\bar{\psi} &= -\tfrac{1}{2}i\bar{\psi}\xi^i\tau^i + b_{\bar{\psi}}{}^\mu\,\xi_{,\mu} \\ \delta\phi^i &= \epsilon^{ijk}\phi^j\xi^k + b_{\phi^i}{}^\mu\,\xi_{,\mu}\end{aligned} \tag{33}$$

and

$$\begin{aligned}J_\mu &= U^{\mu\lambda}{}_{,\lambda}, \\ U^{\mu\lambda} &= -U^{\lambda\mu} \equiv \frac{\partial \mathfrak{L}}{\partial \psi_{,\lambda}}b_\psi{}^\mu + b_{\bar{\psi}}{}^\mu\frac{\partial \mathfrak{L}}{\partial \bar{\psi}_{,\lambda}} + \frac{\partial \mathfrak{L}}{\partial \phi^i_{,\lambda}}b_{\phi^i}{}^\mu,\end{aligned} \tag{34}$$

the current $J_\mu{}^i$ in Eq. (31) would be conserved and nonvanishing. This possibility of extending the constant isotopic spin rotations to something *different* from the local rotations (27) is being investigated.

(2) Alternatively one might insist on the local isotopic spin invariance of this section, i.e., $\xi^i = \xi^i(x)$ but no $\xi^i{}_{,\mu}$ appearing in the transformation law (27). Then the result of this section leads one to maintain this invariance by introducing additional fields which transform suitably. The addition of new fields does not,

[5] W. Pauli, Revs. Modern Phys. **13**, 203 (1941).
[6] P. G. Bergmann and R. Schiller, reference 2.

however, illuminate in any simple way phenomena between pions and nucleons for which isotopic spin invariance was demanded in the first place.

IV. ADDITIONAL FIELDS

Yang and Mills[3] have recently sought to maintain local isotopic spin invariance by positing the existance of a certain "**b** field." This field is a vector in space-time and in isotopic spin space, and transforms according to the law

$$\delta b_\mu{}^i=\epsilon^{ijk}b_\mu{}^j\xi^k+\frac{1}{2\epsilon}\xi^i{}_{,\mu}. \tag{35}$$

It is not difficult to show from the identities (17)–(19) that this field carries isotopic spin itself and obeys nonlinear equations of motion. These properties (which correspond to no field yet observed) cannot then be avoided, as one might conceivably have hoped, by employing a different Lagrangian than the one used by Yang and Mills.

The identities corresponding to Eqs. (17) and (18) are

$$(\partial\mathfrak{L}/\partial b_\mu{}^i{}_{,\nu})+(\partial\mathfrak{L}/\partial b_\nu{}^i{}_{,\mu})=0, \tag{36}$$

$$\epsilon^{ijk}b_\lambda{}^j(\partial\mathfrak{L}/\partial b_\lambda{}^k{}_{,\mu})=\partial\mathfrak{L}/\partial b_\mu{}^i. \tag{37}$$

These relations indicate that the derivatives of the **b** field occur in the Lagrangian only in the antisymmetric combination $b_\mu{}^i{}_{,\nu}-b_\nu{}^i{}_{,\mu}$ and that the $b_\mu{}^i$ themselves occur only via the combination $f_{\mu\nu}{}^i=b_\mu{}^i{}_{,\nu}-b_\nu{}^i{}_{,\mu}-2\epsilon\epsilon^{ijk}b_\mu{}^jb_\nu{}^k$. Since the Lagrangian is to be a scalar in space-time and in isotopic spin space, the most general form for the **b** field Lagrangian is

$$\mathfrak{L}=\mathfrak{L}(f_{\mu\nu}{}^if_{\mu\nu}{}^i). \tag{38}$$

Corresponding to Eq. (19), a current

$$J_\mu{}^i=\epsilon^{ijk}b_\lambda{}^j(\partial\mathfrak{L}/\partial b_\lambda{}^k{}_{,\mu}) \tag{39}$$

is conserved. This isotopic spin current contributed by the **b** field violates, wherever real **b** quanta are involved, the observed conservation of isotopic spin for pions and nucleons alone.

That the equations of motion of the **b** field are nonlinear follows, for example, from the observation that for an extended isotopic spin vector like $f_{\mu\nu}{}^i$, the covariant derivative is

$$D_\nu f_{\mu\nu}{}^i\equiv\partial_\nu f_{\mu\nu}{}^i+2\epsilon\epsilon^{ijk}b_\nu{}^jf_{\mu\nu}{}^k.$$

These consequences can be avoided by conceiving of a field which undergoes transformations of the second kind only, so that according to Eq. (16) it makes no contribution to the isotopic current, yet does act as a right-hand side in Eq. (18).

The formalism of this paper is useful in deriving identities and conservation laws in more general situations. If the **b** field is coupled to nucleons and pions transforming according to Eq. (27), then from Eqs. (14) and (16) the three identities

$$\frac{1}{2\epsilon}([\mathfrak{L}]_{b_\mu{}^i})_{,\mu}=\tfrac{1}{2}i([\mathfrak{L}]_{\psi}\tau^i\psi-\bar{\psi}\tau^i[\mathfrak{L}]_{\bar{\psi}})-\epsilon^{ijk}(\phi^j[\mathfrak{L}]_{\phi^0}+b_\lambda{}^j[\mathfrak{L}]_{b_\lambda{}^k}) \tag{40}$$

must hold among the equations of motion, and the conserved current is

$$J_\mu{}^i=-\frac{i}{2}\left(\frac{\partial\mathfrak{L}}{\partial\psi_{,\mu}}\tau^i\psi-\bar{\psi}\tau^i\frac{\partial\mathfrak{L}}{\partial\bar{\psi}_{,\mu}}\right)+\epsilon^{ijk}\left(\phi^j\frac{\partial\mathfrak{L}}{\partial\phi^k{}_{,\mu}}+b_\lambda{}^j\frac{\partial\mathfrak{L}}{\partial b_\lambda{}^k{}_{,\mu}}\right). \tag{41}$$

V. CONCLUSIONS

The admissible couplings between meson-nucleon fields have been investigated from the invariant Lagrangian point of view. A distinction has been made between transformations linear in the arbitrary functions and transformations linear in the gradients of the arbitrary functions. Fields transforming in the first way contribute to a current which is conserved; fields transforming in the second way contribute to the superpotentials from which this current is obtained.

Assuming invariance under local isotopic spin rotations for the pion-nucleon system leads to the result that the total isotopic current density must vanish identically. Since this is inadmissible physically, one is led to consider (a) more general extended isotopic spin invariance principles for pions and nucleons, or (b) additional fields constructed to maintain invariance under local isotopic spin rotations. In either case, if the ordinary pion-nucleon isotopic current density is to be conserved, the most general extension of the restricted transformation law (27) admits only transformations of the second kind on the field variables. For the pion-nucleon fields this leads to relations (34) between the extended transformation contemplated and the invariant Lagrangian.

The **b** field introduced by Yang and Mills, on the other hand, since it undergoes in part transformations of the first kind, contributes to the isotopic spin current. This result, which prevents conservation of isotopic spin between nucleons and pions whenever the **b** field is present, is not avoidable by conceiving of different equations of motion.

I am indebted to Dr. J. V. Lepore for several stimulating discussions on isotopic spin and coupling.

Quantum Calculation of Coulomb Excitation. I*

L. C. BIEDENHARN, *The Rice Institute, Houston, Texas*

AND

J. L. MCHALE AND R. M. THALER, *University of California, Los Alamos Scientific Laboratory, Los Alamos, New Mexico*

(Received May 4, 1955)

A complete quantum mechanical treatment for Coulomb excitation is presented. Angular correlations as well as total cross section are developed. The reduction to a form suitable for computation of the radial Coulomb integrals which are needed to evaluate the transition matrix elements is discussed in detail. The relation of the quantum mechanical treatment to the classical treatment is established, and it is shown that the results may be presented as the classical result plus a quantum mechanical correction.

INTRODUCTION

COULOMB excitation of nuclear levels is an old concept in nuclear physics which was first considered in the pioneer work of Cockcroft and Walton. The study of this process has advanced considerably both experimentally[1] and theoretically[2] since that time. Interest in Coulomb excitation was further stimulated by the work of Bohr and Mottelson[3] who indicated the importance of the role played by electric quadrupole excitation. Numerous experiments have since verified this conclusion.

The increase in the number and accuracy of the experiments has brought about an increased need for accurate theoretical discussion of Coulomb excitation. Ter-Martirosyan[5] has treated the problem from the classical point of view. In this work the charged particles are considered as traveling in definite Kepler orbits with the Coulomb field causing the nuclear transition. To be valid this approximation requires that[4]

$$\eta \equiv z_1 z_2 e^2/\hbar v \gg 1.$$

For many experiments, however, $\eta \sim 3$. This approximation further requires that the energy absorbed by the nucleus be small compared to the energy of the incident particles. The second requirement results from the fact that $\hbar \to 0$ implies $\hbar\omega = E \to 0$, so that no energy loss is considered in the classical treatment. For both large and small bombarding energies, therefore, the classical approximation fails.[5]

The present experimental results on the total cross section have, nevertheless, been in agreement with the classical predictions. Not only is the shape of the excitation function reproduced, but in several cases the absolute cross section has been measured and found to be in excellent agreement.[6] It should be noted, however, that the agreement exceeds the accuracy ($\sim 10\%$) of the experiments.

In addition to measurements on the total cross section, one may also measure angular distributions to obtain further information concerning the Coulomb excitation process. A particularly desirable measurement considers the directional correlation with incident beam of the gamma rays emitted by the excited nuclei, averaging over emergent particle directions. Calculations on this process have been made using Ter-Martirosyan's methods.[7] Although there are still only a few experiments of this type, the results seem to be clear cut. It is found that the measured results[8] deviate quite significantly ($\sim 20\%$) from the classical predictions, in a region where the total cross section shows good agreement. For some cases the anisotropy measured is *larger* than predicted. Since external influences always tend to diminish the anisotropy, this may indicate that the classical approximation is at fault.

Several quantum calculations[9,10] have been made to test the classical approximation. However, these calculations have neglected energy loss. Breit and collaborators[9] numerically calculated the total cross section for $\eta = 8.156$ and found excellent agreement between the quantum and classical result. Biedenharn

* Work performed under the auspices of the U. S. Atomic Energy Commission.

[1] Lark-Horowitz, Risser, and Smith, Phys. Rev. **55**, 878 (1939); C. McClelland and C. Goodman, Phys. Rev. **91**, 760 (1953); T. Huus and C. Zupančič, Kgl. Danske Videnskab. Selskab, Mat-fys. Medd. **28**, No. 1 (1953); G. M. Temmer and N. P. Heydenburg, Phys. Rev. **93**, 351, 906 (1954), among others more recently. See also a forthcoming review article by A. Bohr and B. R. Mottelson.

[2] L. Landau, Physik Z. U.S.S.R. **1**, 88 (1932); V. Weisskopf, Phys. Rev. **53**, 1018 (1938); E. Guth, Phys. Rev. **68**, 280 (1945); R. Huby and H. C. Newns, Proc. Phys. Soc. (London) **A64**, 619 (1951); C. Mullin and E. Guth, Phys. Rev. **82**, 141 (1951); K. A. Ter-Martirosyan, J. Exptl. Theoret. Phys. (U.S.S.R.) **22**, 284 (1952).

[3] A. Bohr and B. R. Mottelson, Kgl. Danske Videnskab. Selskab, Mat-fys. Medd. **27**, No. 16 (1953).

[4] N. Bohr, Kgl. Danske Videnskab. Selskab, Mat-fys. Medd. **18**, No. 8 (1948).

[5] K. A. Ter-Martirosyan [J. Exptl. Theoret. Phys. (U.S.S.R.) **22**, 284 (1952)], has also given classical calculations that apply for the case where $\Delta E \sim E$, but numerical results are not available. The statement is meant to apply only to calculations based upon no energy loss as given in extensive tabulations of the report by K. Alder and A. Winther, CERN/T/KA-AW-1, October, 1954 (unpublished).

[6] F. K. McGowan and P. H. Stelson, Oak Ridge National Laboratory Report, ORNL 1798, December, 1954 (unpublished); Phys. Rev. **99**, 112 (1955).

[7] K. Alder and A. Winther, Phys. Rev. **91**, 1578 (1953).

[8] P. H. Stelson and F. K. McGowan, Phys. Rev. **98**, 249(A) (1955); F. K. McGowan and P. H. Stelson, Phys. Rev. **99**, 127 (1955).

[9] G. Breit and P. B. Daitch, Phys. Rev. **96**, 1447 (1954); Daitch, Lazarus, Hull, Benedict, and Breit, Phys. Rev. **96**, 1449 (1954); K. Alder and A. Winther, Phys. Rev. **96**, 237 (1954).

[10] L. C. Biedenharn and C. M. Class, Phys. Rev. **98**, 691 (1955).

and Class[10] employed the exact Coulomb integrals for no energy loss, given in Sec. II, and found that the classical approximation was in excellent agreement with the exact results for $\eta>3$. For the directional correlations, however, this calculation predicted larger anisotropies than the classical treatment.

Since these considerations indicate that the classical approximation is inadequate, it appeared reasonable to attempt to take the Coulomb field rigorously into account in a quantum mechanical treatment.[11] In this connection it is of interest to note that for dipole transitions, the problem was effectively solved in parabolic coordinates by Sommerfeld[12] many years ago. The cases of greatest interest are, however, the more complicated quadrupole transitions. For multipoles higher than the dipole it appears futile to attempt the integrations in parabolic coordinates, and recourse to the spherical representation is indicated.

In the following, therefore, the problem is formulated in the spherical representation and expressions for both the total cross section and angular correlations are obtained. The formulation of the angular correlation problem is considerably simplified by recognition of the formal analogy to the correlation problem in the internal conversion process.[13] For internal conversion, transitions between a bound state and a continuum state must be considered, whereas here the transitions are between two continuum states. Moreover, for the final state, there is no coherent mixing of different angular momenta because it is assumed that this state is not observed experimentally.

The second part of this paper is concerned with the problem of evaluating the radial Coulomb integrals. Since the excitation and correlation involve infinite sums over angular momenta, of the radial Coulomb matrix elements, it is necessary to estimate the number of L's which enter in a significant way. To a sufficient approximation this can be done as follows. For the quadrupole case the radial Coulomb matrix element is of the form $[\int_0^\infty dr r^{-3}F_L(\eta_1,k_1r)F_L(\eta_2,k_2r)]^2$. For large values of L, the magnitude of the Coulomb function $F_L(\eta,kr)$ at the classical turning point, $kr\sim L$, varies as $L^{1/6}$.[14] Because of this slow variation the crude estimate is made that the amplitude of F_L is unity for all L beyond the turning point. Inside the turning point, the functions F_L behave roughly as $(r/L)^{L+1}$. Thus, the contribution to the integral from $r<L$ is of the order of L^{-3}. Outside the turning point, the Coulomb functions F_L oscillate. If one neglects the phase difference between the two F_L's and takes their product to be of the order of unity everywhere, one obtains an overestimate of the outside contribution to be of the order of L^{-3}. Thus one gets as a rough estimate that the integrals are, in general, of the order of L^{-2}. Using this estimate in the summation for the total cross section, it is clear that the sum will involve, in the limit of large L, a summation over terms of the order of $L[\int_0^\infty dr \times r^{-3}F_L(\eta_1,k_1r)F_L(\eta_2,k_2r)]^2\sim L^{-3}$, and thus this part of the sum will be of the order of L^{-2}. For good accuracy one, therefore, needs about one hundred terms and it is clearly essential to simplify the work as far as possible. Direct numerical integration of the radial integrals does not appear feasible, since the Coulomb functions oscillate and many oscillations must be integrated before asymptotic formulas are applicable. It would thus seem most desirable to use the properties of the Coulomb functions to cast the required integrals into a more tractable form.

This is, however, not a very straightforward task. The range of physical interest has the parameter $\rho\equiv k_e/k_f$ of the order of unity. Typical experimental values are $1<\rho<1.1$. But for $\rho\sim1$ the integrals do not have simple properties. A simple example of such behavior is afforded by the related spherical Bessel function integrals, to which the desired integrals reduce in the limit of zero nuclear charge. These are cases of the Sonine-Schafheitlin discontinuous integral.[15] It is possible, nonetheless, to get useful rapidly converging series in the region of $\rho\sim1$. The necessary development for such results are presented in this paper. In addition, various recursion relations are also presented. The use of the recursion relations makes it unnecessary to compute the integrals for all values of L. Rather, the integrals may be computed at appropriate intervals in L and the recursion relations used to bridge the gaps. However, repeated application of these relations causes great loss in numerical accuracy, so that they can only be used over a very limited range of L.

The classical orbit calculation results from the present quantum treatment under the simultaneous limiting process $\eta\to\infty$; $\rho\to1$; $\eta(1-\rho)\to\xi=$finite. From the series results for the Coulomb integrals one gets in this limit confluent forms, which are the series form of the classical integrals. It is interesting also to obtain this result in a more elementary fashion without the necessity of using series, and this is done in the concluding section. Sommerfeld[12] has discussed a closely related limiting form for the electric dipole case to obtain Kramer's approximate bremsstrahlung formula.[16]

The radial Coulomb matrix elements should be valuable in problems other than Coulomb excitation and it is hoped that the present discussion will be of more general interest.

Numerical calculations of electric quadrupole excitation have been completed and submitted for publication.

[11] A preliminary account was given by L. C. Biedenharn and M. E. Rose, Oak Ridge National Laboratory Report, ORNL 1789, September 1954 (unpublished).

[12] A. Sommerfeld, *Wellenmechanik* (F. Ungar Publishing Company, New York, 1947).

[13] Rose, Biedenharn, and Arfken, Phys. Rev. **85**, 5 (1952).

[14] Biedenharn, Gluckstern, Hull, and Breit, Phys. Rev. **97**, 542 (1955).

[15] W. Magnus and F. Oberhettinger, *Special Functions of Mathematical Physics* (Chelsea Publishing Company, New York, 1949), p. 35.

[16] H. A. Kramers, Phil. Mag. **46**, 836 (1923).

I. FORMAL DEVELOPMENT

The Coulomb excitation problem can be schematically described as the following process. A (Coulomb-distorted) plane wave of spinless particles, of wave vector $\mathbf{k}_1$ and charge z_1 is incident upon a nucleus of charge z_2. By means of the electromagnetic coupling between the nucleus and incident particles, the nucleus undergoes a a transition from a state $J_i\pi_i$ to a state $J_f\pi_f$, and the incident particles emerge at infinity as a (Coulomb distorted) plane wave of wave vector $\mathbf{k}_2$. Here J, π represent the nuclear angular momentum and parity. We seek to find first: the total cross section for this process, averaged over the directions of $\mathbf{k}_2$, and second: the directional correlation with respect to the incident direction $\mathbf{k}_1$ of a subsequent nuclear radiation, again averaging over the directions of the emergent particles, $\mathbf{k}_2$. The center of mass of the system is considered to be at the nucleus.

Total Cross Section

The electromagnetic coupling can be expressed in terms of the interaction energy density between the two transition charge and current systems (nuclear and bombarding particles), that is:

$$H_{\text{int}}=(\mathbf{j}_N\cdot\mathbf{G}\cdot\mathbf{j}_P+\rho_N\cdot\rho_P g). \tag{1}$$

Here $\mathbf{j}_N$ and $\mathbf{j}_P$ are the current operators for the nuclear and particle systems, respectively, and similarly the ρ's are charge density operators. The $\mathbf{G}$ and g are dyadic and scalar Green's functions for the infinite domain with outgoing waves at infinity. Introducing a multipole expansion for the Green's functions,[17] and assuming that the bombarding particles always remain exterior to the nucleus, one may write for the Lth magnetic multipole the interaction energy density,

$$H_L^{(m)}=4\pi\sum_M(-ik)\mathbf{j}_N\cdot[L(L+1)]^{-\frac{1}{2}}\times j_L(kr_N)[\mathbf{L}Y_L^{M*}(\theta_N,\phi_N)]\times\mathbf{j}_P\cdot[L(L+1)]^{-\frac{1}{2}}h_L^{(1)}(kr)\mathbf{L}Y_L^M(\theta,\phi)$$

and for the Lth electric multipole,

$$H_L^{(e)}=4\pi\sum_M i[L(L+1)]^{-\frac{1}{2}}j_L(kr_N)\mathbf{j}_N\cdot\boldsymbol{\nabla}\times\mathbf{L}Y_L^{M*}(\theta_N,\phi_N)k^{-1}[L(L+1)]^{-\frac{1}{2}}\times h_L^{(1)}(kr)\mathbf{j}_P\cdot\boldsymbol{\nabla}\times\mathbf{L}Y_L^M(\theta,\phi). \tag{2}$$

Here the $j_L(kr)$ are spherical Bessel functions, the $h_L^{(1)}(kr)$ are spherical Hankel functions, and k is the wave number for the virtual gamma quantum absorbed by the nucleus. The operator $\mathbf{L}$ is the rotation operator, $\mathbf{L}=-i\mathbf{r}\times\boldsymbol{\nabla}$. The coordinates r_N, θ_N, ϕ_N refer to the nucleus and r,θ,ϕ are the coordinates of the bombarding particle.

The usual perturbation treatment then leads immediately to the result for the total cross section for excitation by electric (e) or magnetic (m) multipole of order L.

$$\sigma_L^{(e,m)}=4\pi\frac{k_2}{k_1}\left(\frac{2m}{\hbar^2}\right)^2\mathfrak{S}\int d\mathbf{f}_2|\langle\psi_2(\mathbf{k}_2,\mathbf{r})\Psi_f|\times H_L^{(e,m)}|\Psi_i\psi_1(\mathbf{k}_1,\mathbf{r})\rangle|^2. \tag{3}$$

In Eq. (3), $\mathfrak{S}$ denotes the appropriate summation over final states, and averaging over initial states for the nucleus (wave functions Ψ_f and Ψ_i, respectively), and $\mathbf{f}$ is a unit vector in the $\mathbf{k}$ direction. The (Coulomb-distorted) plane waves for the bombarding particles are, for the incident state:

$$\psi_1(\mathbf{k}_1,\mathbf{r})=\left(\frac{2\pi\eta_1}{e^{2\pi\eta_1}-1}\right)^{\frac{1}{2}}e^{i\mathbf{k}_1\cdot\mathbf{r}}\,{}_1F_1(-i\eta_1,1;i(k_1r-\mathbf{k}_1\cdot\mathbf{r})), \tag{4}$$

with $\eta_1\equiv z_1z_2e^2/\hbar v_1$, and for the emergent state:

$$\psi_2(\mathbf{k}_2,\mathbf{r})=\left(\frac{2\pi\eta_2}{e^{2\pi\eta_2}-1}\right)^{\frac{1}{2}}e^{i\mathbf{k}_2\cdot\mathbf{r}}\,{}_1F_1(i\eta_2,1;-i(k_2r+\mathbf{k}_2\cdot\mathbf{r})), \tag{5}$$

with η_2 defined analogously.

These latter wave functions are exact wave functions for a particle of charge z_1 in the field of a fixed charge z_2 as discussed in detail by Sommerfeld.[12] They reduce to distorted plane waves at infinity, with the appropriate outgoing and incoming spherical parts respectively. The wave function ψ_2 will be observed to be the time and space-reversed emergent wave, so as to have an incoming scattered spherical component.[12]

The integral over the nucleus is evaluated formally in terms of reduced matrix elements.[18] That is, for magnetic multipoles,

$$\langle\Psi_f|[L(L+1)]^{-\frac{1}{2}}j_L(kr_N)\mathbf{j}_N\cdot\mathbf{L}Y_L^{M*}(\theta_N,\phi_N)|\Psi_i\rangle\equiv C(J_iLJ_f;M_iMM_f)(f\|mL\|i), \tag{6}$$

and for electric multipoles,

$$\langle\Psi_f|k^{-1}[L(L+1)]^{-\frac{1}{2}}j_L(kr_N)\mathbf{j}_N\cdot\boldsymbol{\nabla}\times\mathbf{L}Y_L^{M*}(\theta_N,\phi_N)|\Psi_i\rangle\equiv C(J_iLJ_f;M_iMM_f)(f\|eL\|i). \tag{7}$$

The projectile wave functions are expanded in the spherical representation, with the result[12]:

$$\psi_1(\mathbf{k}_1,\mathbf{r})=\sum_{l,m}[4\pi(2l+1)]^{\frac{1}{2}}\frac{e^{i(\sigma_l-\sigma_0)}}{k_1r}\times F_l(\eta_1,k_1r)D_{m0}^l(\mathbf{f}_1)i^lY_l^m(\theta,\phi) \tag{8}$$

and

$$\psi_2(\mathbf{k}_2,\mathbf{r})=\sum_{l',m'}[4\pi(2l'+1)]^{\frac{1}{2}}\frac{e^{-i(\sigma_{l'}-\sigma_0)}}{k_2r}\times F_{l'}(\eta_2,k_2r)D_{m'0}^{l'}(\mathbf{f}_2)^*i^{l'}Y_{l'}^{m'}(\theta,\phi). \tag{9}$$

Here D_{mn}^l are rotation matrices.[19]

It is useful now to introduce the reduced matrix elements for the transition multipole between the

[17] J. M. Blatt and V. F. Weisskopf, *Theoretical Nuclear Physics* (John Wiley and Sons, Inc., New York, 1952), Appendix B.

[18] S. P. Lloyd, Phys. Rev. **81**, 161 (1951).

[19] E. P. Wigner, *Gruppentheorie* (Friedrich Vieweg und Sohn, Braunschweig, 1931).

various angular momenta of the bombarding particles. For magnetic transitions, we have:

$$\left\langle \frac{F_{l'}(\eta_2,k_2r)}{k_2r} Y_{l'}^{m'}(\theta,\phi) \times |[L(L+1)]^{-\frac{1}{2}} h_L^{(1)}(kr)\, \mathbf{j}_P \cdot \mathbf{L} Y_L^M(\theta,\phi)| \times \frac{F_l(\eta_1,k_1r)}{k_1r} Y_l^m(\theta,\phi) \right\rangle \equiv Q(l',l,Lm) C(Ll l'; Mmm'), \quad (10)$$

and for electric transitions:

$$\left\langle \frac{F_l(\eta_2,k_2r)}{k_2r} Y_{l'}^{m'}(\theta,\phi) | k^{-1}[L(L+1)]^{-\frac{1}{2}} h_L^{(1)}(kr) \times \mathbf{j}_P \cdot \nabla \times \mathbf{L} Y_L^M(\theta,\phi) | \frac{F_l(\eta_1,k_1r)}{k_1r} Y_l^m(\theta,\phi) \right\rangle \equiv Q(l',l;Le) C(Ll l'; Mmm'). \quad (11)$$

The evaluation of these reduced matrix elements is given in Appendix I.

The indicated operations in Eq. (3) can now be carried out. After some manipulation, the total cross section is found to be:

$$\sigma_L^{(e,m)} = \left(\frac{k_2}{k_1}\right) \frac{2J_f+1}{2J_i+1} \frac{(f\|(e,m)L\|i)^2}{2L+1} \cdot \left(\frac{32\pi^2 mk}{h^2}\right)^2 \times \sum_{l,l'} (2l'+1) |Q(l'l; L(e,m))|^2. \quad (12)$$

In the long-wavelength approximation the reduced multipole matrix elements assume a simple form. The total cross section has a more recognizable form in this limit, and for the electric quadrupole transitions we have the explicit result that:

$$\sigma_2^{(e)} = 4\pi \left(\frac{k_2}{k_1}\right) \left(\frac{2J_f+1}{2J_i+1}\right) (f\|r^2\|i)^2 \left(\frac{8\pi z_1 z_2 e^2}{5k_1k_2h^2}\right)^2 \times \sum_l \left\{ \frac{l(l+1)(2l+1)}{(2l-1)(2l+3)} \left[\int_0^\infty r^{-3} dr F_l(\eta_1,k_1r) F_l(\eta_2,k_2r) \right]^2 + \frac{3l(l-1)}{2(2l-1)} \left[\int_0^\infty r^{-3} dr F_l(\eta_1,k_1r) F_{l-2}(\eta_2,k_2r) \right]^2 + \frac{3(l+1)(l+2)}{2(2l+3)} \left[\int_0^\infty r^{-3} dr F_l(\eta_1,k_1r) F_{l+2}(\eta_2,k_2r) \right]^2 \right\}. \quad (13)$$

Directional Correlation

If the nuclei excited by the bombarding particles upon returning to their ground states emit gamma rays with a half-life short compared to the reorientation times of external perturbing fields, these gamma rays will be correlated with the direction of the incident beam, and the emergent beam as well. In practice this latter direction is unobserved and corresponds to the directional correlations averaged over this direction. Calculations for such correlations, using classical trajectories, were given by Alder and Winther.[7]

The calculation of this directional correlation is greatly facilitated by the result[20] that if one knows the $\gamma-\gamma$ correlation for the nuclear transitions characterized by the angular momenta $J_1 \to J_2 \to J_3$ to be,

$$W(\theta) = \sum_\nu A_\nu P_\nu(\cos\theta),$$

then the directional correlation for particle emission replacing the γ transition $J_1 \to J_2$ is given by

$$W(\theta) = \sum_\nu A_\nu a_\nu P_\nu(\cos\theta),$$

where the a_ν are "particle parameters" independent of the nuclear transitions. The problem for the directional correlation is thus reduced to solution by standard techniques. The solution is, however, even more immediate if one notes the close formal similarity between this Coulomb excitation problem and the internal conversion problem. Except for the fact that the present problem involves both initial and final particle states in the continuum, the two problems are precisely the inverse of each other. The calculation given below exploits this similarity, and does not reproduce details given by Biedenharn and Rose.[20] As discussed there, the particle parameters are the ratio of the tensor parameters of the projectile to the tensor parameters of the gamma ray it replaces, normalized so that $a_0=1$. To obtain the tensor parameters of the projectile we couple the tensor parameters of the observed initial state and the tensor parameters of the unobserved final state. The latter, being random, are scalar.

The tensor parameters of the initial state[21] are:

$$R_i(\nu q; ll') = 4\pi[(2l+1)(2l'+1)]^{\frac{1}{2}} (-)^{l-q} i^{l-l'} \times C(ll'\nu; 000) e^{i(\sigma_l - \sigma_{l'})} D_{q0}^{\nu}(\mathbf{f}_i). \quad (14)$$

For the final state we have the simple result:

$$R_f(\nu q) = \delta_{0\nu}\delta_{0q}.$$

Using the previous definition, Eq. (10), for the reduced multipole matrix elements, one finds that the coupled tensor parameters, for a pure multipole transition are:

$$R(\nu q) = \sum_{ll'L} Q(ll'; L\pi) Q^*(l'l; L\pi) [(2l+1)(2l'+1)]^{\frac{1}{2}} \times W(ll\nu L; Ll') R_i(\nu q; ll'). \quad (15)$$

[20] L. C. Biedenharn and M. E. Rose, Revs. Modern Phys. **25**, 729 (1953). This result is originally due to S. P. Lloyd, thesis, University of Illinois, 1951 (unpublished).

[21] *Note added in Proof.*—In the preliminary work of Biedenharn and Rose[11] the phase factor $i^{l-l'}$ in Eq. (14) was accidentally omitted. This error was propagated in the work of Biedenharn and Class[20] but affected only Eq. (6) and Fig. 2 of that paper (an erratum has been submitted). The equations in this paper have been corrected accordingly.

Unfortunately an equivalent error (of different origin, however) was contained in the calculations of Alder and Winther[4,7] invalidating their results for a_2 and a_4 (but not δ_0). This led to a spurious agreement between the classical limit for a_2 in reference 10 and the no energy loss result for a_2 in reference 7.

The tensor parameters of the gamma transition whose observation is replaced by the particle transition are:

$$R_\gamma(\nu q)\sim(-)^{q+L+1}C(L\,L\,\nu;1\,-1\,0)D_{q0}^{\nu}(\mathbf{f}). \quad (16)$$

Thus one immediately obtains for the particle parameters, the result:

$$a_\nu(L,\pi)=\{\sum_{ll'l}(2l+1)(2l'+1)(-)^l C(ll'\nu;000)i^{l-l'}\times e^{i(\sigma_l-\sigma_{l'})}Q(ll';L\pi)Q^*(l'l;L\pi)W(ll'\nu L;Ll')\}\times\{(-)^{L+1}C(LL\nu;1-10)\sum_{ll}(2l+1)|Q(ll;L\pi)|^2\}^{-1}. \quad (17)$$

The index π denotes the type of multipole, i.e., electric (e) or magnetic (m).

By virtue of the vector coupling relationship, the values of l, l' are restricted to lie between $l+L$ and $|l-L|$. Hence in the triple sum over l, l' and l only one of these represents an infinite summation. Moreover, parity eliminates approximately half of the values available for l or l'. Since the total cross section itself was a singly infinite summation, it follows that both the total cross section and the directional correlation are tasks of about the same level of difficulty, with the primary task the rapid evaluation of the reduced multipole matrix elements for Coulomb waves.

For the long wavelength limit, the particle parameters assume a much simpler form. Confining attention to the experimentally interesting electric quadrupole case, the explicit results are found to be

$$a_2(2e)=b_2/b_0, \quad (18)$$

$$a_4(2e)=b_4/b_0, \quad (19)$$

with

$$b_0=\sum_l\left[\frac{l(l+1)(2l+1)}{(2l-1)(2l+3)}I^2(l,l)+\frac{3l(l-1)}{2(2l-1)}I^2(l-2,l)+\frac{3}{2}\frac{(l+1)(l+2)}{2l+3}I^2(l+2,l)\right], \quad (20)$$

$$b_2=\sum_l\left[\frac{3(l-2)(l-1)(l)}{(2l-1)^2}I^2(l-2,l)-\frac{l(l+1)(2l+1)(2l-3)(2l+5)}{(2l-1)^2(2l+3)^2}I^2(l,l)+\frac{3(l+1)(l+2)(l+3)}{(2l+3)^2}I^2(l+2,l)-6\cos(\sigma_l-\sigma_{l-2})\frac{l(l-1)(l+1)}{(2l-1)^2}I(l-2,l)I(l,l)-6\cos(\sigma_l-\sigma_{l+2})\frac{l(l+1)(l+2)}{(2l+3)^2}I(l+2,l)I(l,l)\right], \quad (21)$$

$$b_4=-\frac{1}{16}\sum_l\left[\frac{9l(l-1)(l-2)(l-3)}{(2l+1)(2l-1)^2}I^2(l-2,l)+\frac{36(2l+1)(l+2)(l+1)(l)(l-1)}{(2l+3)^2(2l-1)^2}I^2(l\,\cdot\right.$$
$$+\frac{9(l+4)(l+3)(l+2)(l+1)}{(2l+1)(2l+3)^2}I^2(l+2,l)$$
$$-60\cos(\sigma_{l-2}-\sigma_l)I(l,l)I(l-2,l)\times\frac{(l+1)(l)(l-1)(l-2)}{(2l-1)^2(2l+3)}+210\cos(\sigma_{l-2}-\sigma_{l+2})\times\frac{(l+2)(l+1)(l)(l-1)}{(2l-1)(2l+1)(2l+3)}I(l-2,l)I(l+2,l)$$
$$\left.-60\cos(\sigma_l-\sigma_{l+2})\frac{(l+3)(l+2)(l+1)(l)}{(2l-1)(2l+3)^2}\times I(l,l)I(l+2,l)\right]. \quad (22)$$

The σ_l in Eqs. (20)–(22) are the Coulomb phase shifts, $\sigma_l=\arg[\Gamma(l+1+i\eta_1)]$, and the radial integrals are defined as

$$I(l,l')\equiv\int_0^\infty r^{-3}dr F_l(\eta_1,k_1r)F_{l'}(\eta_2,k_2r). \quad (23)$$

The sums are over all positive values of l including zero, with the understanding that $I(l,l')=0$ if $l+l'<1$.

Limitations of the Present Treatment

In this treatment there are several approximations, and it is essential to make clear the errors involved. First there is the question of replacing the multipole moments by the long-wavelength approximation. The parameter involved here can, for an order of magnitude orientation, be taken to be $(r_{t.p.}/\lambda_{rad})$, where $r_{t.p.}$ is the classical turning point radius given approximately by $(L^2+\eta^2)^{\frac{1}{2}}$. For low angular momenta, this parameter ranges from $\sim 1/100$ (for 4-Mev protons exciting 100-kev radiation on $Z=50$) to $\sim 1/5$ (for 4-Mev alphas exciting 500-kev radiation on $Z=50$). Except for the radial current contributions in electric multipoles, this parameter enters as the square; it is clear, however, that there will exist cases where the error is not negligible. For sufficiently high angular momentum the error is always large, but since the dominant contributions are from $L\sim\eta$ (except for $E1$) this need not introduce appreciable error. For cases where retardation is appreciable, the contribution of the higher terms gives rise to matrix elements which can be evaluated by the methods given below, and, in fact, these corrections are generally simpler to evaluate than the lower order terms. Because retardation effects may be

important, the accurate form for the multipoles has been given in Appendix I.

The neglect of electronic shielding is another possible source of error. The parameter involved here is the ratio of the Bohr K shell radius to the turning point radius. For 2-Mev protons on $Z=50$, this parameter is $\sim 1/30$ for $L=0$. For increasing L, however, the comparison is less favorable, and, in fact, becomes sizable for $L\sim 20$. Drell and Huang[22] have carried out an estimate of the screening effect for 2-Mev proton bremsstrahlung on $Z=50$ and find the correction negligible (<0.1 percent). Since the large angular momenta contribute far more prominently to dipole bremsstrahlung than for quadrupole excitation[23] their result indicates that shielding may be safely neglected.

The effects of penetration of the nucleus have been neglected, and this is possibly important for S wave particles. For 5-Mev protons on $Z=50$, the nuclear radius is about one half the turning point radius and the penetration of the order of a few percent or less. This is a rather extreme case, but it indicates that, in the vicinity of resonances at least, the $L=0$ contributions might have to be altered by the addition of irregular components. This constitutes a refinement of the theory that seems somewhat premature, but it is well to bear in mind the possibility of such effects.

The assumption that the nucleus defines the center of mass may be a serious source of error. Although it is easy to calculate the particle multipole moments in terms of the true center of mass, this is no real help since the nuclear absorption takes place with multipoles based upon its own center of mass, and the error caused by the non-coincidence of these two centers still arises. The effect is particularly bad for alpha particles on light nuclei. For such cases, in the center-of-mass system, the effective dipole moment will almost vanish, yet the translation of the remaining multipoles to the nuclear center-of-mass system will reintroduce dipole terms. The approximation is thus poor in some cases of interest. Although corrections can be made for this effect, attention will be restricted to larger $A(\sim 100)$ where the error should be of the order of one percent or less.

Finally it should be mentioned, for completeness, that spinless particles have been assumed. For the case of protons, the spin magnetization should enter the magnetic multipoles significantly; for electric multipoles the change is generally insignificant. This effect may be treated by using the spin magnetization current in the magnetic multipoles, as discussed in reference 17.

II. RADIAL COULOMB INTEGRALS

In this section, explicit integration of the general Coulomb radial matrix element $(m,n;L)$ is discussed. $(m,n;L)$ is defined as

$$(m,n;L)\equiv\int_0^\infty dr r^{-n}F_L(\eta_1,k_1r)F_{L+m}(\eta_2,k_2r), \quad (24)$$

where k_1 and k_2 are respectively the "incoming" and "outgoing" wave numbers. The parameter η is given by

$$\eta\equiv z_1z_2e^2/\hbar v,$$

and the Coulomb wave function[24] is defined in terms of the confluent hypergeometric function to be

$$F_L(\eta,r)=C_L(\eta)r^{L+1}e^{-ir}\,{}_1F_1(L+1-i\eta;2L+2;2ir),$$

with the normalizing factor

$$C_L(\eta)=2^Le^{-\pi\eta/2}|\Gamma(L+1+i\eta)|/\Gamma(2L+2).$$

A more convenient form in which to treat the integral of Eq. (24) is

$$(m,n;L)=k_2^{n-1}\int_0^\infty dr r^{-n}F_L(\eta,\rho r)F_{L+m}(\rho\eta,r), \quad (25)$$

where $0<\rho\equiv k_1/k_2<\infty$, and $\eta=\eta_1$. Although on physical grounds ρ is restricted to values greater than or equal to unity, it is convenient to discuss also cases with ρ less than unity. This enables one to restrict m to be zero or a positive integer. Since the integral must converge at the origin, the inequality $2L+3+m-n>0$ must hold. In addition from the vector addition rule one has generally that $m\leqslant n-1$, but if retardation corrections enter, m may exceed $n-1$.

In order to transform the integral into more useful forms, it is necessary at this point to introduce explicitly into the integral the convergence factor e^{-sr}. For all values of s such that $\mathrm{Re}\,s>0$, the resulting integral is then uniformly convergent. The limit $s\to 0$ will be taken in the final answer, and it is this limiting operation that introduces the discontinuous behavior at $\rho=1$ discussed in the introduction. The integral with the convergence factor s is denoted by $(m,n;L;s)$. Employment of the Euler-type integral representation for the confluent hypergeometric functions,[25] interchange of the order of integration, and integration over the r-coordinate yields a double contour integral form for the matrix element:

$$(m,n;L;s)=K\int_0^{(1+)}du\int_0^{(1+)}\times dv[s+i(1+\rho)-2i(v+\rho u)]^{n-2L-m-3}\times u^{L-in}(u-1)^{L+in}v^{L+m-i\rho\eta}(v-1)^{L+m+i\rho\eta}, \quad (26)$$

[22] S. D. Drell and K. Huang, Phys. Rev. **99**, 686 (1955). A preliminary account of this work appears in Bull. Am. Phys. Soc. **30**, No. 3, 28 (1955).

[23] Similar considerations show that estimating errors in WKB calculations by comparison to the Sommerfeld bremsstrahlung results [see K. Alder and A. Winther, Phys. Rev. **96**, 237 (1954)] should not necessarily be conclusive.

[24] *Tables of Coulomb Wave Functions*, U. S. National Bureau of Standards, Applied Mathematics Series 17 (U. S. Government Printing Office, Washington, D. C., 1952).

[25] Erdelyi, Magnus, Oberhettinger, and Tricomi, *Higher Transcendental Functions* (McGraw-Hill Book Company, Inc., New York, 1953), Vol. 1, p. 272. We shall in the sequel denote this reference as HTF-1.

with

$$K=(-1)^m k_2^{n-1}\rho^{L+1}2^{2L+m-2}e^{-\frac{1}{2}\pi\eta(1+\rho)} \times\frac{\Gamma(2L+3+m-n)}{\sinh\pi\eta\,\sinh\pi\rho\eta\,|\Gamma(L+1+i\eta)|\,|\Gamma(L+m+1+i\rho\eta)|}.$$

The many-valued functions appearing in the integrand are made analytic by taking their principal values. The symbol $\int_0^{(1+)}$ signifies a loop which begins and ends at the origin and encircles the point 1 counter-clockwise. In the case at hand, both loops can be considered closed contours encircling the points 0 and 1 of the integration variables.

The double integral appearing in Eq. (26) is readily expressed in terms of Appell's double hypergeometric series[26] $F_2(\alpha,\beta,\beta';\gamma,\gamma';x,y)$.

The result is

$$(m,n;L;s)=-(k_2^{n-1}/4\pi^2)\rho^{L+1}C_L(\eta)C_{L+m}(\rho\eta) \times\Gamma(2L+m+3-n)[s+i(1+\rho)]^{n-2L-m-3} \times F_2(\alpha,\beta,\beta';\gamma,\gamma';x,y), \quad (27)$$

where $\alpha=2L+m+3-n$, $\beta=L+1-i\eta$, $\beta'=L+m+1-i\rho\eta$, $\gamma=2L+2$, $\gamma'=2L+2m+2$, $x=2i\rho/[s+i(1+\rho)]$ and $y=2i/[s+i(1+\rho)]$. For calculational purposes, the double series (see Appendix II) for F_2 might be thought to be useful. Since the series form of F_2 converges absolutely only for

$$|x|+|y|=|2i\rho/[s+i(1+\rho)]|+|2i/[s+i(1+\rho)]|<1,$$

it is evident, however, that the limit $s\to 0$ can never taken and the series is, therefore, only of formal interest. Any transformation of the series which does not have the character of an analytic continuation cannot alter this conclusion.

For analytic continuation in a single variable, e.g., y, the theory of the Gauss hypergeometric function can be used to advantage. Such transformations, however, are insufficient to treat the case $\rho\sim 1$. For the parameters given in Eq. (27) with the specialization $m=n-1$, the desired analytic continuation has been given by Appell and Kampe de Feriet.[27] It will be shown below that the specialization, $m=n-1$, is not necessary, and that all cases of interest for Coulomb excitation can be worked out directly.

The special case $m=n-1$ with $m=0$, was treated by Sommerfeld,[12] who obtained the result:

$$(0,1,L;s) =-\frac{1}{4\pi^2}C_L(\eta)C_L(\rho\eta)\Gamma(2L+2)[s+i(1+\rho)]^{-2L-2} \times\left(\frac{s+i(1-\rho)}{s+i(1+\rho)}\right)^{-L-1+i\eta}\left(\frac{s+i(\rho-1)}{s+i(\rho+1)}\right)^{-L-1+i\rho\eta} \times\rho^{L+1}{}_2F_1\left(\beta,\beta';\alpha;\frac{-4\rho}{s^2+(1-\rho)^2}\right). \quad (28)$$

[26] HTF-1, p. 224. Some properties of the Appell functions are given in Appendix II.

[27] P. Appell and M. J. Kampe de Feriet, *Fonctions hypergeometriques et hyperspheriques* (Gauthier-Villars, Paris, 1926), p. 43.

Here α, β, β', are as defined in Eq. (27), with $m=n-1=0$. For $\rho\sim 1$ the usual theory of the hypergeometric function can be used to obtain series in the variable $1-\rho$.

Series Applicable for Small Energy Loss

The analytic continuation of Eq. (27) is now obtained in a form which readily permits the confluences required in the classical limit. For convenience the order of integration in Eq. (26) is inverted. It is seen that the integrand as a function of u has branch points at 0 and 1, and a pole at $[s+i(1+\rho)]/2i\rho-(v/\rho)$. For $m<n-1$ there is also a pole at $u=\infty$. The integral over u can be evaluated in the usual way in terms of the two poles outside the original contour encircling the singularities at $u=0$ and $u=1$. The contribution due to the pole at infinity is called $f_1(v)$, while the contribution of the other pole is called $f_2(v)$. Thus,

$$\int_0^{(1+)}du u^{L-i\eta}(u-1)^{L+i\eta} \times[s+i(1+\rho)-2i(v+\rho u)]^{-2L-m-3+n} \equiv f_1(v)+f_2(v). \quad (29)$$

The evaluation of $f_1(v)$ yields

$$f_1(v)=2\pi i(2i\rho)^{n-2L-m-3} \times\frac{\Gamma(L+1+i\eta)}{\Gamma(L+m+3-n+i\eta)\Gamma(n-m-1)} \times\sum_\lambda\frac{(2L+m+3-n)_\lambda(m+2-n)_\lambda}{\lambda!(L+m+3-n+i\eta)_\lambda} \times\left[\frac{s+i(1+\rho)-2iv}{2i\rho}\right]^\lambda. \quad (30)$$

The notation

$$(a)_q\equiv a(a+1)(a+2)\cdots(a+q-1)=\Gamma(a+q)/\Gamma(a)$$

is used in the series above. It will be noted that $f_1(v)=0$ for $n\leq m-1$, and is a terminating series for $n>m-1$.

The integration over v (for the $f_1(v)$ contribution) is carried out next. This is found to be

$$\int_0^{(1+)}dv f_1(v)v^{L+m-i\rho\eta}(v-1)^{L+m+i\rho\eta} =4\pi i(-)^{L+m}\sinh\pi\rho\eta(2i\rho)^{n-2L-m-3} \times\frac{\Gamma(L+1+i\eta)|\Gamma(L+m+1+i\rho\eta)|^2}{\Gamma(L+m+3-n+i\eta)\Gamma(n-m-1)\Gamma(2L+2+2m)} \times\sum_{\lambda,\mu}\frac{(2L+m+3-n)_\lambda(m+2-n)_\lambda(L+m+1-i\rho\eta)_\mu}{\mu!(\lambda-\mu)!(L+m+3-n+i\eta)_\lambda(2L+2+2m)_\mu} \times\left(\frac{s+i(1+\rho)}{2i\rho}\right)^\lambda\left(\frac{-2i}{s+i(1+\rho)}\right)^\mu. \quad (31)$$

The double series in Eq. (31) is a terminating series in both λ and μ with $0\leqslant\mu\leqslant\lambda$ and $0\leqslant\lambda\leqslant n-2-m$.

The evaluation of the contribution due to the remaining pole is somewhat more difficult, and, in contrast to the foregoing, does not lead solely to a polynomial. It is readily shown that

$$f_2(v)=(2\pi i)(2i\rho)^{n-2L-m-1}\times\frac{\Gamma(L+1-i\eta)}{\Gamma(2L+3+m-n)\Gamma(-L-i\eta+n-m-1)}\times\left[\frac{s+i(1+\rho)-2iv}{2i\rho}\right]^{-L-m+n-2-i\eta}\times\left[\frac{s+i(1-\rho)-2iv}{2i\rho}\right]^{-L-m+n-2+i\eta}\times{}_2F_1\left(-m+n-1,\,-2L-2-m+n;\,-L-i\eta-m+n-1;\,\frac{s+i(1+\rho)-2iv}{2i\rho}\right). \quad (32)$$

For $m<n-1$, the ${}_2F_1$ function above is represented by a terminating series consisting of $(2L+3+m-n)$ terms. In the special case $m=n-1$ the series consists of a single term equal to one.

In order to carry out the remaining integration over v, it proves useful to employ the series form of Eq. (32):

$$\int_0^{(1+)}dv f_2(v)v^{L+m-i\rho\eta}(v-1)^{L+m+i\rho\eta}\equiv\sum_\lambda P_\lambda J_\lambda, \quad (33)$$

where

$$P_\lambda=\pi(2i)^{n-2L-m-2}\rho^{m+1-n-\lambda}(-)^\lambda\times\frac{\Gamma(L+1-i\eta)}{\Gamma(2L+3+m-n)\Gamma(-L-i\eta+n-m-1)}\times\frac{(n-m-1)_\lambda(n-2L-m-2)_\lambda}{\lambda!(n-L-i\eta-m-1)_\lambda} \quad (34)$$

and

$$J_\lambda=\int_0^{(1+)}dv v^{L+m-i\rho\eta}(v-1)^{L+m+i\rho\eta}\times\left(v-\frac{1+\rho}{2}+\frac{is}{2}\right)^{-L-m-2+n-i\eta+\lambda}\times\left(v-\frac{1-\rho}{2}+\frac{is}{2}\right)^{-L-m-2+n+i\eta}. \quad (35)$$

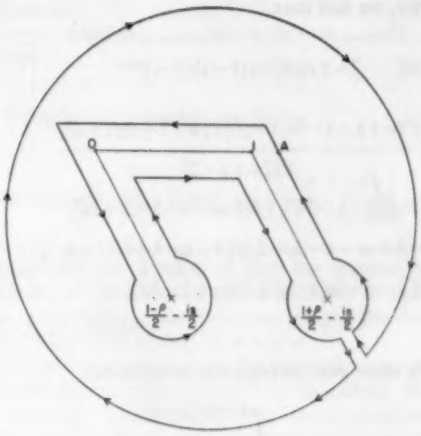

FIG. 1. The null contour D on which J_λ is defined. At the point A, $\arg v=0$. The outer portion of the contour schematically represents a circle of infinite radius.

The contour on which J_λ is defined is a loop encircling the points $v=0$ and $v=1$ in the positive sense. Consideration of the null contour D illustrated in Fig. 1 shows that the integral J_λ may be expressed in the form,

$$e^{-\pi\eta}\left(\frac{\sinh\pi\eta(\rho-1)}{\sinh\pi\eta\rho}\right)J_\lambda=\oint_\infty dv[\cdots]-\int_0^{[(\frac{1}{2}-\frac{1}{2}\rho-\frac{1}{2}is)+]}dv[\cdots]-\int_1^{[(\frac{1}{2}+\frac{1}{2}\rho-\frac{1}{2}is)+]}dv[\cdots], \quad (36)$$

where

$$[\cdots]=v^{L+m-i\rho\eta}(v-1)^{L+m+i\rho\eta}\times\left(v-\frac{1+\rho}{2}+\frac{is}{2}\right)^{-L-m-2+n-i\eta+\lambda}\times\left(v-\frac{1-\rho}{2}+\frac{is}{2}\right)^{-L-m-2+n+i\eta}. \quad (37)$$

The first integral on the right-hand side of Eq. (36) is understood to be a positive circle of large radius. The phases are determined by the requirement that the integrand be real and positive as v approaches infinity along the positive real axis, with the cuts as shown in Fig. 1. The second and third contours on the right-hand side of Eq. (36) terminate at 0 and 1, respectively.

Evaluation of the integral over the infinite circle is readily accomplished, and leads to a polynomial. Writing the result in terms of an Appell function for

brevity, we find that

$$\oint_{\infty} dv[\cdots]=2\sinh[\pi\eta(1-\rho)](-)^{n+\lambda}$$
$$\times\frac{\Gamma(n+\lambda-1-i\eta(1-\rho))\Gamma(n-1+i\eta(1-\rho))}{\Gamma(2n+\lambda-2)}$$
$$\times F_2([3-\lambda-2n],[L+m-n-\lambda+2+i\eta],$$
$$[L+m-n-i\eta+2];[2-n-\lambda+i\eta(1-\rho)],$$
$$[2-n-i\eta(1-\rho)];[\tfrac{1}{2}is+\tfrac{1}{2}-\tfrac{1}{2}\rho],$$
$$[-\tfrac{1}{2}is+\tfrac{1}{2}-\tfrac{1}{2}\rho]). \quad (38)$$

We must now perform the integrations

$$\int_{0,1}^{[(\frac{1}{2}\pm\frac{1}{2}\rho-\frac{1}{2}is)+]}.$$

A simplification results from the fact that

$$\int_{0}^{[(\frac{1}{2}-\frac{1}{2}\rho-\frac{1}{2}is)+]} dv f_2(v)v^{L+m-i\rho\eta}(v-1)^{L+m+i\rho\eta}$$
$$=\text{complex conjugate}$$
$$\int_{1}^{[(\frac{1}{2}+\frac{1}{2}\rho-\frac{1}{2}is)+]} dv f_2(v)v^{L+m-i\rho\eta}(v-1)^{L+m+i\rho\eta}. \quad (39)$$

It is, therefore, necessary to perform only one of these integrations, e.g., $\int_0^{[(\frac{1}{2}-\frac{1}{2}\rho-\frac{1}{2}is)+]}$, which we shall denote as $J_\lambda^{(2)}$. In a straightforward manner we finally arrive at the result:

$$J_\lambda^{(2)}=2\pi i(-)^{\lambda+1}\left(\frac{\rho-1}{2}+\frac{is}{2}\right)^{n-1+i\eta(1-\rho)}$$
$$\times\frac{\Gamma(L+m+1-i\rho\eta)}{\Gamma(L+m+2-n-i\eta)\Gamma[n+i\eta(1-\rho)]}$$
$$\times F_2(\alpha,\beta,\beta';\gamma,\gamma';x,y), \quad (40)$$

where

$$\alpha=2-n-\lambda+i\eta(1-\rho),\quad \beta=L+m+2-n+i\eta-\lambda,$$
$$\beta'=L+m+1-i\rho\eta,\quad \gamma=2-n-\lambda+i\eta(1-\rho),$$
$$\gamma'=n+i\eta(1-\rho),\quad x=\tfrac{1}{2}-\tfrac{1}{2}\rho+\tfrac{1}{2}is,\quad y=\tfrac{1}{2}-\tfrac{1}{2}\rho-\tfrac{1}{2}is.$$

In passing to the limit $s\to 0$ in the integrals obtained above only $J_\lambda^{(2)}$ need be examined critically. In this case, the factor $(\frac{1}{2}\rho-\frac{1}{2}+\frac{1}{2}is)^{n-1+i\eta(1-\rho)}$ has a different limit for $\rho>1$ than for $\rho<1$. The two limits are:

$$\lim_{s\to 0}(\tfrac{1}{2}\rho-\tfrac{1}{2}+\tfrac{1}{2}is)^{n-1+i\eta(1-\rho)}$$
$$=\begin{cases}|\frac{1}{2}\rho-\frac{1}{2}|^{n-1+i\eta(1-\rho)}, & \text{for } \rho>1\\ |\frac{1}{2}\rho-\frac{1}{2}|^{n-1+i\eta(1-\rho)}(-)^{n+1}e^{-\pi\eta(1-\rho)}, & \text{for } \rho<1.\end{cases} \quad (41)$$

The polynomials given by Eqs. (31) and (38), together with the nonterminating double series given by Eq. (40) constitute, when introduced into Eqs. (26), (33) through (36), the desired results for $(m,n;L)$ valid in the vicinity of $\rho\sim 1$. Before explicitly exhibiting this final result, it is useful to note that the polynomials of Eqs. (31) and (38) are not, however, expressed in the most convenient form (although the present form does have the advantage of a more straightforward derivation). The present form, for example, does not exhibit the barrier penetration in a simple way.

A more useful result is obtained by utilizing in the integral over the infinite circle, Eq. (38), not the function $f_2(v)$ alone, but rather the sum $f_1(v)+f_2(v)$. The latter function is expressible as a hypergeometric function regular in the vicinity of infinity, and thus greatly simplifies the results. To compensate for the addition of the term in $f_1(v)$, we must alter the coefficient of the polynomial, Eq. (31), into which this term integrates.

It is convenient to give separate designations to these various contributions to the matrix element $(m,n;L)$. Let us define:

$$(m,n;L)=A(m,n;L)+B(m,n;L)+C(m,n;L), \quad (42)$$

where A and B are the polynomials discussed above. A arises from $f_1(v)$ and B arises from $f_1(v)+f_2(v)$. C is the nonterminating series part. Collecting the various constants that enter, one finds explicitly that:

$$A(m,n;L)=\pi i^{n-m}2^{n-3}\rho^{n-L-m-2}k_2^{n-1}\frac{e^{\frac{1}{2}\pi\eta(\rho-1)}}{\sinh\pi\eta(\rho-1)}\left|\frac{\Gamma(L+m+1+i\rho\eta)}{\Gamma(L+1+i\eta)}\right|$$
$$\times\frac{\Gamma(L+1+i\eta)}{\Gamma(L+m+3-n+i\eta)}\frac{\Gamma(2L+3+m-n)}{\Gamma(2L+2m+2)\Gamma(n-m-1)}$$
$$\times\sum_{\lambda,\mu}\frac{(2L+m+3-n)_\lambda(m+2-n)_\lambda(L+m+1-i\rho\eta)_\mu}{\mu!(\lambda-\mu)!(L+m+3-n+i\eta)_\lambda(2L+2m+2)_\mu}\left(\frac{1+\rho}{2\rho}\right)^\lambda\left(\frac{-2}{1+\rho}\right)^\mu. \quad (43)$$

$$B(m,n;L)=\pi k_2^{n-1}e^{\frac{1}{2}\pi\eta(1-\rho)}\left|\frac{\Gamma(L+1+i\eta)}{\Gamma(L+m+1+i\rho\eta)}\right|\rho^{L+1}2^{n-2}i^{n-m}\frac{\Gamma(L+1+m-i\rho\eta)}{\Gamma(L+3-n-i\rho\eta)}\frac{\Gamma(2L+m+3-n)}{\Gamma(2L+2)\Gamma(m-1+n)}$$
$$\times\frac{1}{\sinh\pi\eta(\rho-1)}\sum_{\lambda,\mu}\frac{(L+1-i\eta)_\lambda(2L+m+3-n)_{\lambda+\mu}(2-m-n)_{\lambda+\mu}}{\lambda!(2L+2)_\lambda\mu!(L+3-n-i\rho\eta)_{\lambda+\mu}}\rho^\lambda\left(\frac{1-\rho}{2}\right)^\mu. \quad (44)$$

$$C(m,n;L)=\frac{\pi(k_2-k_1)^{n-1}\rho^{L+m+2-n}e^{-\frac{1}{2}\pi\eta|1-\rho|}}{2\sinh\pi\eta(\rho-1)}\times\mathrm{Re}\left\{\frac{i^{n-m}|(\rho-1)/2|^{i\eta(1-\rho)}}{\Gamma(n+i\eta(1-\rho))}\exp i\{2\sigma_{L+m+1-n}(\eta)-\sigma_L(\eta)-\sigma_{L+m}(\rho\eta)\}\right.$$

$$\times\sum_\lambda\frac{(n-m-1)_\lambda(n-2L-m-2)_\lambda}{\lambda!(n-L-i\eta-m-1)_\lambda}\rho^{-\lambda}\times F_2\Big(2-n-\lambda+i\eta(1-\rho),\ L+m+2-n-\lambda+i\eta,$$

$$\left.L+m+1-i\rho\eta;\ 2-n-\lambda+i\eta(1-\rho),\ n+i\eta(1-\rho);\ \frac{1-\rho}{2},\frac{1-\rho}{2}\Big)\right\}. \quad (45)$$

It will be noted that although $A(m,n;L)$ and $B(m,n;L)$ are written in the form of terminating double series, $C(m,n;L)$ is in the form of a *triple* series, except in the case $m=n-1$, when the terminating sum over λ reduces to a single term. The advantage of the triple series form is that it permits the confluence required to obtain the classical limit. This point will be discussed in detail in a later section. An alternate expansion for $f_2(v)$ leads to a *double* series for $C(m,n;L)$, which does not, however, exhibit the confluence required for the classical limit. Since the procedure is very similar to that already used, we give only the result, Appendix III. For cases where L, η are not too large, this double series form is of value for computational purposes.

Results for Special Cases

The polynomials $A(m,n;L)$, $B(m,n;L)$ defined by the terminating series given in Eqs. (43) and (44) are much simpler than would at first appear. Consider, for example, the terms that enter in the quadrupole excitation. Here $n=3$ and $m=0$ or 2. For $m=2$ and $n=3$, the term $A(2,3;L)$ vanishes, and we have only $B(2,3;L)$ entering. This is found to be

$$B(2,3;L)=\frac{k_2^2}{6}\left|\frac{\Gamma(L+1+i\eta)}{\Gamma(L+3+i\rho\eta)}\right|e^{\frac{1}{2}\pi\eta(1-\rho)}\frac{\pi\eta(1-\rho^2)\rho^{L+2}}{2\sinh\pi\eta(\rho-1)}. \quad (46)$$

For the matrix element with $m=0$, $n=3$ both A and B enter. These are found to be

$$A(0,3;L)=k_2^2\rho^{1-L}e^{-\frac{1}{2}\pi\eta(1-\rho)}\left|\frac{\Gamma(L+1+i\rho\eta)}{\Gamma(L+1+i\eta)}\right|$$

$$\times\frac{\pi\eta}{\sinh\pi\eta(\rho-1)}\frac{1}{2L(L+1)(2L+1)}, \quad (47)$$

$$B(0,3;L)=-k_2^2e^{\frac{1}{2}\pi\eta(1-\rho)}\left|\frac{\Gamma(L+1+i\eta)}{\Gamma(L+1+i\rho\eta)}\right|$$

$$\times\frac{\pi\eta\rho^{L+2}}{\sinh\pi\eta(\rho-1)}\frac{1}{2L(L+1)(2L+1)}. \quad (48)$$

The special case for no energy loss ($\rho=1$) is a limit that is of some interest.[9,10] Unfortunately, however, it is apparently not possible to sum the required series (which are ${}_3F_2$ functions of unit argument) in general. It is, nevertheless, relatively easy to get the desired results for definite choices of m and n.

The particular case $m=n-1$ is, as usual, exceptional. Here the general result for $\rho=1$ is immediate. If one puts $\rho=1$ into the arguments (but not the parameters) of the equation for B, then the required sums can be done by the Gauss formula for the hypergeometric function. The result is:

$$\lim_{\rho\to1}(n-1,n;L)=k^{n-1}\cdot2^{n-3}$$

$$\times\frac{[\Gamma(n-1)]^2}{\Gamma(2n-2)}\left|\frac{\Gamma(L+1+i\eta)}{\Gamma(L+n+i\eta)}\right|. \quad (49)$$

In the remaining cases where $m<n-1$, the result for $\rho=1$ must be obtained by a limiting process. This can be illustrated by the example for the matrix element $(0,3;L)$. The terms A and B, given above in Eqs. (47) and (48), cancel for $\rho=1$, if the $\sinh\pi\eta(1-\rho)$ in the denominator is disregarded. The required limit then yields:

$$\lim_{\rho\to1}(0,3;L)=\frac{k^2}{2L(L+1)(2L+1)}[2L+1-\pi\eta$$

$$+i\eta\Psi(L+1-i\eta)-i\eta\Psi(L+1+i\eta)], \quad (50)$$

where $\Psi(x)=d/dx[\log\Gamma(x)]$.

It should be pointed out that the use of the recursion formulas given below provides an alternative procedure for obtaining explicit results for $\rho=1$.

As will be shown in general in the concluding section, the Coulomb matrix elements go over into the classical orbit integrals in the limit $\eta,\ L\to\infty$, $\rho\to1$, $\eta(1-\rho)\to\xi=$finite. The results given for the quadrupole matrix elements provide a nice example of this. Thus:

$$4(\eta/k)^{-2}(2,3;L)\to\epsilon^{-2}/6,$$

$$4(\eta/k)^{-2}(0,3;L)\to$$

$$\tfrac{1}{2}(\epsilon^2-1)^{-1}[1-(\epsilon^2-1)^{-1}\tan^{-1}(\epsilon^2-1)^{\frac{1}{2}}], \quad (51)$$

where $\epsilon=[1+L^2/\eta^2]^{\frac{1}{2}}=$eccentricity of the Kepler orbits. The terms on the right side are exactly the classical orbit integrals for $\xi=0$.[6,7]

The electric quadrupole matrix elements may be given in the following form suitable for calculation in

the vicinity of no energy loss:

$$(2,3;L)=\frac{\pi\eta k_2^2\rho^{L+2}(1-\rho^2)e^{\frac{1}{2}\pi\eta(1-\rho)}}{12\sinh\pi\eta(1-\rho)}\left|\frac{\Gamma(L+1+i\eta)}{\Gamma(L+3+i\rho\eta)}\right|$$
$$+\frac{\pi k_2^2(1-\rho)^2\rho^{L+1}e^{-\frac{1}{2}\pi\eta|1-\rho|}}{2\sinh\pi\eta(1-\rho)}$$
$$\times\mathrm{Im}\left\{\frac{|\frac{1}{2}\rho-\frac{1}{2}|^{i\eta(1-\rho)}}{\Gamma[3+i\eta(1-\rho)]}\exp[i\sigma_L(\eta)\right.$$
$$-i\sigma_{L+2}(\rho\eta)]\times F_2(-1+i\eta(1-\rho),$$
$$L+1+i\eta\ L+3-i\rho\eta;-1+i\eta(1-\rho),$$
$$\left.3+i\eta(1-\rho);\tfrac{1}{2}-\tfrac{1}{2}\rho,\tfrac{1}{2}-\tfrac{1}{2}\rho)\right\},\quad(52)$$

and

$$(0,3,L)=\frac{\pi\rho\eta k_2^2}{2L(L+1)(2L+1)\sinh\pi\eta(1-\rho)}$$
$$\times\left[\rho^{-L}e^{-\frac{1}{2}\pi\eta(1-\rho)}\left|\frac{\Gamma(L+1+i\rho\eta)}{\Gamma(L+1+i\eta)}\right|\right.$$
$$\left.-\rho^{L+1}e^{\frac{1}{2}\pi\eta(1-\rho)}\left|\frac{\Gamma(L+1+i\eta)}{\Gamma(L+1+i\rho\eta)}\right|\right]$$
$$-\frac{\pi(k_2-k_1)^2e^{-\frac{1}{2}\pi\eta|1-\rho|}}{2\sinh\pi\eta(1-\rho)}$$
$$\times\mathrm{Im}\left\{\frac{\rho^{-i\eta}|\frac{1}{2}\rho-\frac{1}{2}|^{i\eta(1-\rho)}\exp\{i\sigma_L(\eta)-i\sigma_L(\rho\eta)\}}{\Gamma(3+i\eta(1-\rho))}\right.$$
$$\times F_2\left(-L+i\eta,-L-i\rho\eta,L+1+i\eta,\right.$$
$$\left.\left.L+1-i\rho\eta;3+i\eta(1-\rho);\frac{\rho-1}{2\rho},\frac{1-\rho}{2}\right)\right\}.\quad(53)$$

Equation (53) uses the double series form given in Appendix III. This form is most useful for values of L and η which are not too large. (A rough criterion is that $|L+i\eta|^2(1-\rho)/2\sim1$.) For larger values of L and η the triple series form given by Eq. (45) is to be preferred.

Recursion Relations for the Radial Matrix Elements

Recursion relations in the variable L are of great value both as a primary means of generating radial matrix elements from a few initial values, and, in cases when such a procedure is not advisable because of cumulative error, in checking values obtained by other methods. One can obtain recursion relations in many ways, either from the power series or from the various integral representations given earlier.[28] It proves most convenient to use the basic defining relation, Eq. (24), directly. The fundamental relations for the Coulomb wave functions[24] are:

$$Ld/d\rho[F_L(\eta,\rho)]=[L^2+\eta^2]^{\frac{1}{2}}F_{L-1}(\eta,\rho)$$
$$-[(L^2/\rho)+\eta]F_L(\eta,\rho),\quad(54)$$

$$(L+1)\frac{d}{d\rho}F_L(\eta,\rho)=\left(\frac{(L+1)^2}{\rho}+\eta\right)F_L(\eta,\rho)$$
$$-[(L+1)^2+\eta^2]^{\frac{1}{2}}F_{L+1}(\eta,\rho).\quad(55)$$

These relations imply the three-term recursion relation for the $F_L(\eta,\rho)$, and thus the three-term relation provides no new information. By partial integration of Eq. (24), and the use of Eqs. (54) and (55), four equations satisfied by the $(m,n;L)$ are obtained. Only three of these are independent and one thus obtains:

$$(2-m-n)(m,n;L)+k_1\eta_1\left(\frac{1}{L+1}-\frac{1}{L+m}\right)(m,n-1;L)$$
$$+\frac{k_2}{L+m}[(L+m)^2+\eta_2^2]^{\frac{1}{2}}(m-1,n-1;L)$$
$$-\frac{k_1}{L+1}[(L+1)^2+\eta_1^2]^{\frac{1}{2}}(m-1,n-1;L+1)=0,\quad(56)$$

$$(2+m-n)(m,n;L)$$
$$+k_1\eta_1\left(\frac{1}{L+m+1}-\frac{1}{L}\right)(m,n-1;L)$$
$$+\frac{k_1}{L}[L^2+\eta_1^2]^{\frac{1}{2}}(m+1,n-1;L-1)$$
$$-\frac{k_2}{L+m+1}[(L+m+1)^2+\eta_2^2]^{\frac{1}{2}}$$
$$\times(m+1,n-1;L)=0,\quad(57)$$

and

$$(2L+3+m-n)(m,n;L)$$
$$+k_1\eta_1\left(\frac{1}{L+1}+\frac{1}{L+m+1}\right)(m,n-1;L)$$
$$=\frac{k_1}{L+1}[(L+1)^2+\eta_1^2]^{\frac{1}{2}}(m-1,n-1;L+1)$$
$$+\frac{k_2}{L+m+1}[(L+m+1)^2+\eta_2^2]^{\frac{1}{2}}(m+1,n-1;L).\quad(58)$$

In obtaining Eqs. (56) to (58), the integrated contribution from both the origin and infinity has been discarded. This implies that $2L+m+1-n>0$.

One may regard Eqs. (56) to (58) as expressing inter-relations among the three operations of changing the indices, m, n and L by integers. The desired recursion relations will result upon suitably eliminating the

[28] P. Appell and M. J. Kampe de Feriet (reference 27), give various contiguous relations for the Appell functions, from which recursion relations may be derived.

unwanted changes in the indices m and n. Two general relations involving a common value of n, but different values of m and L, may be obtained immediately from these equations. These relations are:

$$\frac{k_2(1+m-n)}{L+m}[(L+m)^2+\eta_2^2]^{\frac{1}{2}}(m-1,n;L)$$
$$-\frac{k_1(1+m-n)}{L+1}[(L+1)^2+\eta_1^2]^{\frac{1}{2}}(m-1,n;L+1)$$
$$+k_1\eta_1\left[\frac{(2L+1)(1-n)-m}{L(L+1)}\right.$$
$$\left.-\frac{(2L+2m+1)(1-n)-m}{(L+m)(L+m+1)}\right](m,n,L)$$
$$+\frac{k_2(1-m-n)}{L+m+1}[(L+m+1)^2+\eta_2^2]^{\frac{1}{2}}(m+1,n;L)$$
$$-\frac{k_1(1-m-n)}{L}[L^2+\eta_1^2]^{\frac{1}{2}}(m+1,n;L-1)=0, \quad (59)$$

and

$$\frac{k_2}{L+m}[(L+m)^2+\eta_2^2]^{\frac{1}{2}}\left[\frac{1+m-n}{L+1}+\frac{2L+2+m-n}{L}\right.$$
$$\left.-\frac{2L+1}{L+m+1}\right](m-1,n;L)-\frac{k_1}{L+1}[(L+1)^2+\eta_1^2]^{\frac{1}{2}}$$
$$\times\left[\frac{1+m-n}{L+m}+\frac{2L+2m+1}{L}-\frac{2L+m+n}{L+m+1}\right]$$
$$\times(m-1,n;L+1)-\frac{k_1}{L}[L^2+\eta_1^2]^{\frac{1}{2}}$$
$$\times\left[\frac{1-m-n}{L+m+1}+\frac{2L+2+m-n}{L+m}-\frac{2L+2m+1}{L+1}\right]$$
$$\times(m+1,n;L-1)+\frac{k_2}{L+m+1}[(L+m+1)^2+\eta_2^2]^{\frac{1}{2}}$$
$$\times\left[\frac{1-m-n}{L}+\frac{2L+1}{L+m}-\frac{2L+m+n}{L+1}\right]$$
$$\times(m+1,n;L)=0. \quad (60)$$

The latter relation is of particular interest for Coulomb excitation since it relates matrix elements differing by two units in m, which is just the condition imposed by conservation of parity.

Consider now some special cases of the above relations. For $m=0$, Eq. (58) gives a relation for $(0,n;L)$ and $(0,n-1;L)$ in terms of $(\pm1,n-1;L)$. But introducing $m=1$ into Eq. (56) and $m=-1$ into Eq. (57) enables one to eliminate the $(\pm1,n-1,L)$ elements in terms of elements with $m=0$. That is, elements with $m=0$ can be expressed in terms of other elements with $m=0$, but differing in n and L. Two independent relations can thus be obtained by this type of procedure, namely:

$$(2-n)^2(0,n;L)+\frac{(n-2)k_1\eta_1}{L(L+1)}(0,n-1;L)$$
$$=\frac{k_1k_2}{(L+1)^2}[(L+1)^2+\eta_1^2]^{\frac{1}{2}}[(L+1)^2+\eta_2^2]^{\frac{1}{2}}$$
$$\times(0,n-2;L+1)-\left[k_1^2+k_2^2\right.$$
$$\left.+k_1^2\eta_1^2\left(\frac{1}{L^2}+\frac{1}{(L+1)^2}\right)\right](0,n-2;L)$$
$$+\frac{k_1k_2}{L^2}[L^2+\eta_1^2]^{\frac{1}{2}}[L^2+\eta_2^2]^{\frac{1}{2}}(0,n-2;L-1), \quad (61)$$

and

$$(2-n)(2L+3-n)(0,n;L)+\frac{2k_1\eta_1(2-n)}{L+1}(0,n-1;L)$$
$$=\frac{2k_1k_2}{(L+1)^2}[(L+1)^2+\eta_1^2]^{\frac{1}{2}}[(L+1)^2+\eta_2^2]^{\frac{1}{2}}$$
$$\times(0,n-2;L+1)$$
$$-\left(k_1^2+k_2^2+\frac{2k_1^2\eta_1^2}{(L+1)^2}\right)(0,n-2;L). \quad (62)$$

For the particular case of $n=3$, it will be noted that the left-hand sides of Eqs. (61) and (62) are the same to within a factor. In this case, one therefore finds the three terms recursion relation:

$$\frac{2k_1k_2}{L+1}[(L+1)^2+\eta_1^2]^{\frac{1}{2}}[(L+1)^2+\eta_2^2]^{\frac{1}{2}}(0,1;L+1)$$
$$-\frac{2L+1}{L(L+1)}[(k_1^2+k_2^2)(L)(L+1)+2k_1^2\eta_1^2](0,1;L)$$
$$+\frac{2k_1k_2}{L}[L^2+\eta_1^2]^{\frac{1}{2}}[L^2+\eta_2^2]^{\frac{1}{2}}(0,1;L-1)=0. \quad (63)$$

This simple relation merely expresses the fact that this matrix element may be written in terms of an ordinary hypergeometric function. This is the Sommerfeld result given previously. The above recursion relation will prove useful in the work that follows.

For $n>3$, Eqs. (61) and (62) in general yield a complicated five-term recursion formula, which, however, will not be given here.

In the electric dipole case the matrix elements that enter are $(\pm1,2;L)$. Although it might at first appear

that these are also Appell functions, Eqs. (56) and (57) show they are expressible in terms of ordinary hypergeometric functions. For example, Eq. (56) with $m=1$ and $n=2$ gives:

$$(1,2;L)=\frac{k_2}{L+1}[(L+1)^2+\eta_2^2]^{\frac{1}{2}}(0,1;L) \\ -\frac{k_1}{L+1}[(L+1)^2+\eta_1^2]^{\frac{1}{2}}(0,1;L+1). \quad (64)$$

The case $(-1,2;L)$ is obtained by interchanging k_1 and k_2 in Eq. (64). Once again the electric dipole case shows great simplicity.

For the electric quadrupole case one has in addition to the $(0,3;L)$ matrix element discussed above, the matrix elements $(\pm 2,3;L)$. A four-term recursion relation can be found in this case. Since the subsidiary relations that lead to this result are also of interest, the derivation will be given in more detail than would otherwise be the case. The desired element has $m=2$ and $n=3$ and if these values are introduced into Eq. (56) terms with $n=2$ but $m=2$ or 1 arise. Equation (57) shows that $m=2$, $n=2$ is expressible in terms of $m=1$, $n=2$ which, as given in Eq. (64) above, thus implies that the desired element can be related to the $(0,1;L)$ element. This relation is found to be

$$4(L+1)k_2[(L+2)^2+\eta_2^2]^{\frac{1}{2}}\{k_2[(L+3)^2+\eta_2^2]^{\frac{1}{2}}(2,3;L+1) \\ -k_1[(L+1)^2+\eta_1^2]^{\frac{1}{2}}(2,3;L)\} \\ =(k_1^2-k_2^2)\{[2k_1^2\eta_1^2+k_1^2(L+1)(2L+3) \\ -k_2^2(L+1)](0,1;L+1)-2k_1k_2[(L+1)^2+\eta_1^2]^{\frac{1}{2}} \\ \times[(L+1)^2+\eta_2^2]^{\frac{1}{2}}(0,1;L)\}. \quad (65)$$

This result is itself of interest. For the special case $k_1=k_2$ (no energy loss) the right hand side vanishes and the resulting two term relation for $(2,3;L)$ can be solved to give, within a constant, the result previously obtained in Eq. (49). For $k_1\neq k_2$ the relation yields $(2,3;L)$ in terms of a finite sum over L of the $(0,1;L)$. Since the latter are more readily calculated than the $(2,3;L)$ themselves, this may provide a useful calculational procedure.

Using Eq. (63) in Eq. (65) yields the desired four term relation satisfied by the $(2,3;L)$:

$$2k_1k_2^2[(L+3)^2+\eta_1^2]^{\frac{1}{2}}[(L+4)^2+\eta_2^2]^{\frac{1}{2}} \\ \times[(L+5)^2+\eta_2^2]^{\frac{1}{2}}(2,3;L+3)-k_2[(L+4)^2+\eta_2^2]^{\frac{1}{2}} \\ \times[6k_1^2\eta_1^2+3(k_1^2+k_2^2)(L+3)^2 \\ +(k_1^2-k_2^2)(L+3)(L+4)](2,3;L+2) \\ +k_1[(L+2)^2+\eta_1^2]^{\frac{1}{2}}[6k_1^2\eta_1^2+3(k_1^2+k_2^2)(L+3)^2 \\ -(k_1^2-k_2^2)(L+2)(L+3)](2,3;L+1) \\ -2k_1^2k_2[(L+1)^2+\eta_1^2]^{\frac{1}{2}}[(L+2)^2+\eta_1^2]^{\frac{1}{2}} \\ \times[(L+3)^2+\eta_2^2]^{\frac{1}{2}}(2,3;L)=0. \quad (66)$$

The result for $(-2,3;L)$ is obtained by interchanging k_1 and k_2 in Eq. (66).

An equation for $(0,3;L)$ that is the analog of Eq. (65) can be obtained. The result is

$$(L+1)(L+3)(2L+5)k_1k_2[(L+2)^2+\eta_1^2]^{\frac{1}{2}} \\ \times[(L+2)^2+\eta_2^2]^{\frac{1}{2}}(0,3;L+2) \\ -(2L+3)[k_1^2\eta_1^2((L+1)^2+(L+2)^2) \\ +(k_1^2+k_2^2)(L+1)^2(L+2)^2](0,3;L+1) \\ +L(L+2)(2L+1)k_1k_2[(L+1)^2+\eta_1^2]^{\frac{1}{2}} \\ \times[(L+1)^2+\eta_2^2]^{\frac{1}{2}}(0,3;L) \\ =-(3/4)(L+1)(L+2)(2L+3)(k_1^2-k_2^2)^2 \\ \times(0,1;L+1). \quad (67)$$

This agrees with the earlier results obtained in Eq. (50) for the special case $k_1=k_2$, and, just as mentioned in connection with Eq. (65), may provide the basis for a useful calculational procedure.

It is clear that the relations, Eqs. (56) to (58), provide a basis for determining recursion relations in L for the $(m,n;L)$. The above results, however, are sufficient for the electric dipole and electric quadrupole cases. As a calculational tool the recursion relations are only useful over a limited spread in L, since the unavoidable cumulative error will eventually dominate. For good accuracy in the final result contributions for $L\sim 100$ may be expected to enter, so that it is clear that a straightforward use of recursion relations is inadvisable.

Classical Limit and Quantum Corrections

It is obvious that classical results will be obtained from the quantum results given above by letting $\hbar\to 0$. In the case at hand, this reduction applies not only to the complete answer but termwise to the various parts of the calculation as well. This is not unexpected since it is well known that the various Racah functions that enter the formulas for the a_r go over into the Legendre polynomials of the classical result. The limit $\hbar\to 0$ which carries the Coulomb integrals into the classical Fourier integrals over the orbits appears here as the limiting process $1-\rho\to 0$, $L,\eta\to\infty$ and $\lim\eta(1-\rho)\equiv\xi$ is finite. This limit process cannot be carried out directly for the Coulomb integrals in the form given by Eq. (24); rather it requires the use of the analytic continuation into the region $\rho\sim 1$. By utilizing Eqs. (43)–(45), the limit process can be carried out immediately, to yield series which can be identified as the classical orbit integrals. These series, which are confluent forms of the Appell functions, are given in Appendix IV.

It is more direct, however, to proceed from the double integral Eq. (26) and thus obtain an expression for the complete classical limit[29] which is readily generalized to include first order quantum corrections. Instead of expanding the u contour to infinity in Eq. (26) and considering the contributions from the two poles as was done earlier, the u integration is performed

[29] Sommerfeld, reference 12, Appendix 16, has carried out a similar transformation (employing steepest descents) to compare proton bremsstrahlung with Kramer's semiclassical calculation (reference 16).

on the original contour to give

$$(m;n;L;s)=(-)^L 2\sinh\pi\eta(-2i)^{n-2L-m-1}K$$
$$\times\frac{|\Gamma(L+i\eta+1)|^2}{\Gamma(2L+2)}\sum_{\lambda=0}\frac{(-\rho)^\lambda(L+1+i\eta)_\lambda(n-m-1)_\lambda}{\lambda!(2L+2)_\lambda}$$
$$\times\int_0^{(1+)}dv\,v^{L+m-i\rho\eta}(v-1)^{L+m+i\rho\eta}$$
$$\times\left[v+\frac{is}{2}-\tfrac{1}{2}(1+\rho)\right]^{-L-1-\lambda-i\eta}$$
$$\times\left[v+\frac{is}{2}-\tfrac{1}{2}(1-\rho)\right]^{-L+i\eta-m+n-2} \quad (69)$$

with the use of a Kummer transformation. In order to obtain an expression suitable for the confluences required in the classical limit, the v contour is transformed to a contour starting at infinity and encircling the origin counterclockwise by the substitution $v=1/(z+1)$, with the result

$$\int_0^{(1+)}dv(\cdots)$$
$$=-(2)^{2L+m-n+2+\lambda}\int_\infty^{(0+)}dz(-z)^{L+m+i\rho\eta}$$
$$\times(z+1)^{1-m-n+\lambda}[1-\rho+is-z(1+\rho-is)]^{-L-i\eta-1-\lambda}$$
$$\times[1+\rho+is-z(1-\rho-is)]^{-L+i\eta-m+n-2}. \quad (70)$$

Since there is no pole at the origin and $(-z)$ is taken real and positive on the negative real axis, this integral is immediately expressible as a real integral,[30] *viz.*,

$$\int_\infty^{(0+)}dz(\cdots)$$
$$=(-)^{m-\lambda}2e^{\pi\eta}\sinh\pi\rho\eta(1+\rho-is)^{-L-i\eta-1-\lambda}$$
$$\times(1+\rho+is)^{-L+i\eta-m+n-2}\int_0^\infty dz\,z^{-i\eta(1-\rho)-1-\lambda+m}$$
$$\times(z+1)^{1-m-n+\lambda}\left[1-\frac{1-\rho+is}{1+\rho-is}\frac{1}{z}\right]^{-L-i\eta-1-\lambda}$$
$$\times\left[1-\frac{1-\rho-is}{1+\rho+is}z\right]^{-L+i\eta-m+n-2}. \quad (71)$$

The phase $e^{\pi\eta}$ is determined by the cut

$$|\arg[1-\rho+is-z(1+\rho-is)]|\leqslant\pi.$$

The integral (71) is now in a form for confluence to the classical limit. Equations (70) and (71) are substituted in (69) and, since (71) converges uniformly in λ for the classical limit, the summation and integration in (69) may be interchanged in the limit.

[30] See, for example, Hankel's contour for the Γ function, E. T. Whittaker and G. N. Watson, *A Course of Modern Analysis* (Cambridge University Press, London, 1945), p. 244.

There results,

$$(m,n;L;s)=(-i)^{n-m-1}k_2^{n-1}2^{n-3}e^{\frac{1}{2}\pi\eta(1-\rho)}\rho^{L+1}$$
$$\times\left|\frac{\Gamma(L+i\eta+1)}{\Gamma(L+m+1+i\rho\eta)}\right|\frac{\Gamma(2L+m-n+3)}{\Gamma(2L+2)}2^{2L+m-n+3}$$
$$\times(1+\rho-is)^{-L-i\eta-1}(1+\rho+is)^{-L+i\eta-m+n-2}$$
$$\times\int_0^\infty dz\,z^{-i\eta(1-\rho)-1+m}(z+1)^{1-m-n}$$
$$\times\left[1-\frac{1-\rho+is}{1+\rho-is}\frac{1}{z}\right]^{-L-i\eta-1}\left[1-\frac{1-\rho-is}{1+\rho+is}z\right]^{-L+i\eta-m+n-2}$$
$$\times\sum_\lambda\frac{(L+1+i\eta)_\lambda(n-m-1)_\lambda}{\lambda!(2L+2)_\lambda}$$
$$\times\left[\frac{\rho(z+1)}{z-(1-\rho+is)/(1+\rho-is)}\right]^\lambda\left[\frac{2}{1+\rho-is}\right]^\lambda. \quad (72)$$

In the limit L, η very large, $\eta(1-\rho)\equiv\xi$ finite, and $s\to 0$, the series can be summed if $(L+1+i\eta)_\lambda$ is replaced by the first term in the expansion,

$$(L+1+i\eta)_\lambda=(L+1+i\eta)^\lambda+(L+1+i\eta)^{\lambda-1}\sum_1^{\lambda-1}j$$
$$+(L+1+i\eta)^{\lambda-2}\sum_1^{\lambda-1}j\sum_1^{j-1}i+\cdots, \quad (73)$$

with unity neglected in comparison with $L+i\eta$. The expression $(2L+2)_\lambda$ is treated similarly, with the result that

$$\sum_\lambda(\cdots)\sim\left[\frac{(L-i\eta)z-(L+i\eta)}{2Lz}\right]^{-n+m+1}$$
$$\times\left[1+\frac{L(1-\rho)(z-1)}{(L-i\eta)z-(L+i\eta)}\Big/1-\frac{1-\rho}{2}\frac{1}{z}\right]^{-n+m+1}. \quad (74)$$

The second factor on the right in Eq. (74) is a quantum correction and is neglected in the passage to the classical limit. In the classical limit the integral becomes

$$\int_0^\infty dz(\cdots)=\left(\frac{L-i\eta}{2L}\right)^{-n+m+1}\int_0^\infty dz\,z^{-i\xi+n-2}$$
$$\times(z+1)^{1-m-n}\left(z-\frac{L+i\eta}{L-i\eta}\right)^{-n+m+1}$$
$$\times\exp\left[(L+i\eta)\left(\frac{1-\rho}{2}\right)\frac{1}{z}+(L-i\eta)\left(\frac{1-\rho}{2}\right)z\right]. \quad (75)$$

The exponentials result from expanding the factors concerned and approximating by the first term in expansions of the type given in Eq. (73).[31] If the classical

[31] It is not obvious that this procedure is valid, but it may in fact be justified by a more detailed argument employing Hankel's form for the gamma function.

variables

$$1+(iL/\eta)=\epsilon e^{i\phi} \tag{76}$$

are introduced in Eq. (75), there results

$$\int_0^\infty dz(\cdots)=\left(\frac{-i\epsilon\eta}{2L}\right)^{-n+m+1}\int_0^\infty dz z^{-i\xi+n-2}\times(z+1)^{1-m-n}(ze^{i\phi}+e^{-i\phi})^{-n+m+1}\times\exp\left[\frac{i\epsilon\xi}{2}\left(\frac{e^{-i\phi}}{z}-e^{i\phi}z\right)\right]. \tag{77}$$

The substitution $z\rightarrow 1/z$ in the integral is equivalent to complex conjugation, hence the integral is real. When Eq. (77) is substituted into Eq. (72) and the limit is taken for the coefficient, the classical answer is obtained. Thus,

$$\lim(m,n;L)=\frac{1}{4}\left(\frac{2k}{\epsilon\eta}\right)^{n-1}e^{t\phi}\int_0^\infty dz z^{-i\xi+n-2}\times(1+z)^{2-2n}\left[\frac{ze^{i\phi}+e^{-i\phi}}{1+z}\right]^{-n+m+1}\times\exp\left[\frac{i\epsilon\xi}{2}\left(\frac{e^{-i\phi}}{z}-e^{i\phi}z\right)\right]. \tag{78}$$

Equation (78) can be put in a more recognizable form by making the substitution $z=e^{t-i\phi}$, and noting that

$$\frac{e^{t-i\phi}}{(1+e^{t-i\phi})^2}=\frac{\epsilon}{2}\frac{[\epsilon+\cosh t+i(\epsilon^2-1)^{\frac{1}{2}}\sinh t]}{[\epsilon\cosh t+1]^2}, \tag{79}$$

and

$$\frac{(e^t+e^{-i\phi})}{(1+e^{t-i\phi})}=\frac{\epsilon+\cosh t+i(\epsilon^2-1)^{\frac{1}{2}}\sinh t}{\epsilon\cosh t+1}. \tag{80}$$

As a result of these considerations, Eq. (78) becomes

$$\lim(m,n;L)=\frac{1}{4}\left(\frac{k}{\eta}\right)^{n-1}\int_{-\infty}^{+\infty}dt e^{-i\xi(\epsilon\sinh t+t)}\times\frac{[\epsilon+\cosh t+i(\epsilon^2-1)^{\frac{1}{2}}\sinh t]^m}{[\epsilon\cosh t+1]^{m+n-1}}. \tag{81}$$

Here, the substitution $t\rightarrow -t$ results in complex conjugation. This integral, to within the factor $\frac{1}{4}(k/\eta)^{n-1}$, is the general Fourier integral over classical orbits of the multipole matrix elements as given, for example, by Ter-Martirosyan and by Alder and Winther.[8]

The advantage of the procedure outlined above is that it enables one to obtain easily integral forms for the first order quantum correction to the classical limit. In order to avoid undue complication, the quantum correction is illustrated only for the case $m=n-1$. It is clear, however, that the procedure for the general case $m\leqslant n-1$ is the same except for additional corrections arising from summing the series [see Eqs. (73) and (74)].

For the special case $m=n-1$, Eq. (72) gives the result,

$$(n-1,n;L)=k_2^{n-1}2^{n-2}\left[\frac{4\rho}{(1+\rho)^2}\right]^{L+1}e^{\frac{1}{2}\pi\eta(1-\rho)}\times\left|\frac{\Gamma(L+1+i\eta)}{\Gamma(L+n+i\rho\eta)}\right|\int_0^\infty dz z^{-i\eta(1-\rho)+n-2}\times(z+1)^{2-2n}\left[1-\frac{1-\rho}{1+\rho}\frac{1}{z}\right]^{-L-i\eta-1}\times\left[1-\frac{1-\rho}{1+\rho}z\right]^{-L+i\eta-1}. \tag{82}$$

The first-order quantum corrections for this integral arise from neglect of the second term in expansions of the form of Eq. (73) in the approximation by exponentials, and the neglect of unity compared with $L+i\eta$ and $L-i\eta$. If the first two terms in expansion of $(-1)^\lambda(L+i\eta+1)_\lambda$ and of $(-1)^\lambda(L-i\eta+1)_\lambda$ are kept one obtains,

$$\left[1-\left(\frac{1-\rho}{1+\rho}\right)z\right]^{-L+i\eta-1}=\exp\left[(L+1-i\eta)\left(\frac{1-\rho}{1+\rho}\right)z\right]\times\left\{1+\frac{1}{2}\frac{\left[(L+1-i\eta)\left(\frac{1-\rho}{1+\rho}\right)z\right]^2}{L+1-i\eta}+\cdots\right\}, \tag{83}$$

and

$$\left[1-\left(\frac{1-\rho}{1+\rho}\right)\frac{1}{z}\right]^{-L-i\eta-1}=\exp\left[(L+i\eta+1)\left(\frac{1-\rho}{1+\rho}\right)\frac{1}{z}\right]\times\left\{1+\frac{1}{2}\frac{\left[(L+i\eta+1)\left(\frac{1-\rho}{1+\rho}\right)\frac{1}{z}\right]^2}{L+i\eta+1}+\cdots\right\}, \tag{84}$$

Thus, it is found that the desired Coulomb integral, accurate through terms of order $(1-\rho)$, is given by

$$(n-1,n;L)=k_2^{n-1}2^{n-2}\left[\frac{4\rho}{(1+\rho)^2}\right]^{L+1}e^{\frac{1}{2}\pi\eta(1-\rho)}\times\left|\frac{\Gamma(L+1+i\eta)}{\Gamma(L+n+i\rho\eta)}\right|\int_0^\infty dz z^{-i\eta(1-\rho)+n-2}(z+1)^{2-2n}\times\exp\left[(L+1-i\eta)\left(\frac{1-\rho}{1+\rho}\right)z+(L+i\eta+1)\left(\frac{1-\rho}{1+\rho}\right)\frac{1}{z}\right]\times\left\{1+\frac{1}{2}\frac{z^2}{L-i\eta+1}\left[(L-i\eta+1)\left(\frac{1-\rho}{1+\rho}\right)\right]^2+\frac{1}{2}\frac{z^{-2}}{L+i\eta+1}\left[(L+i\eta+1)\left(\frac{1-\rho}{1+\rho}\right)\right]^2\right\}. \tag{85}$$

As it is written, the classical variables ξ and ϵ have not been introduced above, since their introduction complicates the formulas.

For the cases of physical interest, $(1-\rho)/(1+\rho)$ is generally small, $\sim 1/20$. The difference between $(1-\rho)/(1+\rho)$ and $\frac{1}{2}(1-\rho)$ is hence insignificant. On the other hand, η is not too large, since $3 \leqslant \eta \leqslant 8$ is usual. Since the quantum correction is most significant for the low angular momenta, it is thus seen from Eq. (85) that the zeroth order (classical) approximation should be improved by the use of $\epsilon^2 = 1+(L+1)^2/\eta^2$ to replace $\epsilon^2 = 1+L^2/\eta^2$.

ACKNOWLEDGMENTS

The authors are indebted to Dr. F. K. McGowan and Dr. P. H. Stelson for many helpful discussions, which in large part stimulated the present work. In addition, the help and encouragement of Dr. R. A. Charpie and Dr. M. E. Rose and the courtesies extended by the Oak Ridge National Laboratory to one of the authors (L.C.B.) while he was a visitor during the summer of 1954 are gratefully acknowledged.

APPENDIX I. REDUCED COULOMB MULTIPOLE MATRIX ELEMENTS

Magnetic Multipoles

$$Q(l'l;Lm)C(Ll';Mmm') \equiv \left\langle \frac{F_{l'}(\eta_2,k_2r)}{k_2r} Y_{l'}^{m'}(\theta,\phi) \middle| [L(L+1)]^{-\frac{1}{2}} h_L^{(1)}(kr) \times \mathbf{j}_P \cdot \mathbf{L} Y_L^M(\theta,\phi) \middle| \frac{F_l(\eta_1,k_1r)}{k_1r} Y_l^m(\theta,\phi) \right\rangle. \quad (86)$$

Introducing the definition of the current operator, in spherical coordinates, one finds two terms, of which the first is

$$[L(L+1)]^{-\frac{1}{2}} \frac{\hbar z_1 e}{2imc} \times \left\langle \frac{F_{l'}}{k_2r} Y_{l'}^{m'} \middle| h_L^{(1)}(\mathbf{L}Y_L^m) \cdot \frac{\mathbf{r}\times\mathbf{L}}{r^2} \middle| \frac{F_l}{k_1r} Y_l^m \right\rangle.$$

The second term has the $\mathbf{r}\times\mathbf{L}$ operator acting on the $F_{l'}Y_{l'}^{m'}$, and can be shown to be equal to the term above. The angular function $\mathbf{L}Y_L^m$ and $\mathbf{r}\times\mathbf{L}Y_l^m$ can be expressed as vector spherical harmonics[32] and this facilitates performing the angular integrals.

The result, after some manipulation, is found to be

$$Q(l'l;Lm) = \left(\frac{\hbar z_1 e}{imc}\right) \frac{(2L+1)(2l+1)}{\sqrt{(4\pi)}} \left[\frac{(l+1)(2l+3)}{2l'+1}\right]^{\frac{1}{2}} \times C(Ll+1l';000) W(LLl l+1;1l') \frac{1}{k_1k_2} \times \int_0^\infty r^{-1} dr F_l(\eta_1,k_1r) F_{l'}(\eta_2,k_2r) h_L(kr). \quad (87)$$

[32] H. C. Corben and J. Schwinger, Phys. Rev. 58, 967 (1940).

Electric Multipoles

$$Q(l'l;Le)C(Ll';Mmm') \equiv \left\langle \frac{F_{l'}(\eta_2,k_2r)}{k_2r} Y_{l'}^{m'}(\theta,\phi) \middle| k^{-1}[L(L+1)]^{-\frac{1}{2}} h_L(kr) \times (\mathbf{j}_P \cdot \nabla \times \mathbf{L} Y_L^M(\theta,\phi)) \middle| \frac{F_l(\eta_1,k_1r)}{k_1r} Y_l^m(\theta,\phi) \right\rangle. \quad (88)$$

The matrix element on the right can be put in an alternative, more convenient, form by using the expansion for $\nabla\times\mathbf{L}$ and partial integration. One finds that:

$$\langle \cdots \rangle = [L(L+1)]^{-\frac{1}{2}} \left\langle \frac{F_{l'}(\eta_2,k_2r)}{k_2r} Y_{l'}^{m'} \times \left| \varrho_P \frac{d}{dr}(rh_L) Y_L^M + ikY_L^M h_L \mathbf{r}\cdot\mathbf{j}_P \right| \frac{F_l}{k_1r} Y_l^m \right\rangle. \quad (89)$$

Hence the reduced matrix element is

$$Q(l'l;Le) = \left[\frac{(2L+1)(2l+1)}{4\pi(L)(L+1)(2l'+1)}\right]^{\frac{1}{2}} \times C(Ll';000)(k_1k_2)^{-1} z_1 e \times \int_0^\infty dr \left\{ F_l(\eta_1,k_1r) F_{l'}(\eta_2,k_2r) d/dr[rh_L(kr)] + \frac{\hbar k}{2mc} h_L(kr)(k_1r F_{l'}(\eta_2,k_2r) F_l'(\eta_1,k_1r) - k_2r F_l(\eta_1,k_1r) F_{l'}'(\eta_2,k_2r) \right\}. \quad (90)$$

The long wavelength limit for these reduced matrix elements replaces $h_L(kr)$ by $-i(2L-1)!!(kr)^{-L-1}$, and discards the radial current in the electric multipoles. For the electric quadrupole case we obtain:

$$Q(l'l;2e) \to ik^{-3} z_1 e [30(2l+1)/4\pi(2l'+1)]^{\frac{1}{2}} \times C(2l';000) \frac{1}{k_1k_2} \int_0^\infty r^{-3} dr F_l F_{l'}. \quad (91)$$

APPENDIX II

The Appell functions used in this report have the series definitions:

$$F_1(\alpha,\beta,\beta';\gamma;x,y) = \sum \frac{(\alpha)_{m+n}(\beta)_m(\beta')_n}{(\gamma)_{m+n} m!\,n!} x^m y^n, \quad (92)$$

$$F_2(\alpha,\beta,\beta';\gamma,\gamma';x,y) = \sum \frac{(\alpha)_{m+n}(\beta)_m(\beta')_n}{(\gamma)_m(\gamma')_n m!\,n!} x^m y^n, \quad (93)$$

$$F_3(\alpha,\alpha',\beta,\beta';\gamma;x,y) = \sum \frac{(\alpha)_m(\alpha')_n(\beta)_m(\beta')_n}{(\gamma)_{m+n} m!\,n!} x^m y^n. \quad (94)$$

The series for F_1 and F_3 are absolutely convergent for $|x|, |y|<1$, while F_2 is absolutely convergent for $|x|+|y|<1$.

The confluent function Ψ_2 is given by the series:

$$\Psi_2(\alpha;\gamma,\gamma';x,y)=\sum\frac{(\alpha)_{m+n}}{(\gamma)_m(\gamma')_n m!n!}x^m y^n. \quad (95)$$

The transformations and reductions that are useful for the present work are

$$F_2(\alpha,\beta,\beta';\alpha,\alpha;x,y)=(1-x)^{-\beta}(1-y)^{-\beta'}\times{}_2F_1\left(\beta,\beta';\alpha;\frac{xy}{(1-x)(1-y)}\right). \quad (96)$$

[This is the reduction used in obtaining Sommerfeld's integral, Eq. (28).]

$$F_2(\alpha,\beta,\beta';\alpha,\gamma';x,y)=(1-x)^{-\beta}F_1[\beta',\alpha-\beta,\beta;\gamma';y,(y/1-x)]. \quad (97)$$

[This transformation reduces the case with $m=n-1$ to a single contour integral.]

$$F_3(\alpha,\alpha',\beta,\beta';\alpha+\alpha';x,y)=(1-y)^{-\beta'}F_1[\alpha,\beta,\beta';\alpha+\alpha';x,(y/y-1)]. \quad (98)$$

APPENDIX III

A double series formulation is derived here for $C(m,n;L)$ in the general case where $m\neq n-1$.

$$C(m,n;L)=\frac{2Ke^{\pi\eta}\sinh\pi\rho\eta}{\sinh\pi\eta(1-\rho)}\operatorname{Re}\int_0^{[(\frac{1}{2}-\frac{1}{2}\rho-\frac{1}{2}i\eta)+]}dv\times v^{L+m-i\rho\eta}(v-1)^{L+n+i\rho\eta}f_2(v). \quad (99)$$

If the alternative form for $f_2(v)$ is employed, *viz.*,

$$f_2(v)=2\pi i(-2i\rho)^{n-2L-m-2}\times\frac{\Gamma(L+1+i\eta)}{\Gamma(2L+m+3-n)\Gamma(-L+i\eta+n-m-1)}\times\left(\frac{s+i(1-\rho)-2iv}{2i\rho}\right)^{-L-m+n-2+i\eta}\times{}_2F_1\left(-L+i\eta,L+1+i\eta;-L+i\eta-m+n-1;\frac{s+i(1-\rho)-2iv}{-2i\rho}\right), \quad (100)$$

one finds, using now the series for the ${}_2F_1$ function, that:

$$C(m,n;L)=\frac{\pi}{2}\frac{e^{-\frac{1}{2}\pi\eta|1-\rho|}}{\sinh\pi\eta(1-\rho)}(k_2-k_1)^{n-1}\times\operatorname{Re}\left\{i^{m-n}\rho^{-i\eta}\left|\frac{\rho-1}{2}\right|^{i\eta(1-\rho)}\times\exp[i\sigma_L(\eta)-i\sigma_{L+m}(\rho\eta)]\frac{1}{\Gamma(n+i\eta(1-\rho))}\times F_3\left(-L+i\eta,-L-m-i\rho\eta,L+1+i\eta,L+m+1-i\rho\eta;n+i\eta(1-\rho);\frac{\rho-1}{2\rho},\frac{1-\rho}{2}\right)\right\}. \quad (101)$$

By using the reduction formulas given in Appendix II, one can show that in the particular case $m=n-1$ this reduces properly to a single F_2, as given in Eq. (45).

APPENDIX IV

A series representation for the integrals in the classical limit can be obtained by taking the appropriate limit for $A(m,n;L)$, $B(m,n;L)$, and $C(m,n;L)$, as given in Eqs. (43)–(45), respectively. Consider first $C(m,n;L)$. In the classical limit, one finds that

$$F_3(2-n-\lambda+i\eta(1-\rho),L+m+2-n-\lambda+i\eta,L+m+1-i\rho\eta;2-n-\lambda+i\eta(1-\rho),n+i\eta(1-\rho);\tfrac{1}{2}(1-\rho),\tfrac{1}{2}(1-\rho))\to\psi_2(2-n-\lambda+i\xi;2-n-\lambda+i\xi,n+i\xi;\tfrac{1}{2}i\epsilon\xi e^{-i\phi},-\tfrac{1}{2}i\epsilon\xi e^{i\phi}), \quad (102)$$

where[25]

$$\psi_2(\alpha;\gamma,\gamma';x,y)\equiv\sum\{(\alpha)_{m+n}/(\gamma)_m(\gamma')_n m!n!\}x^m y^n,$$

and

$$\exp[i(2\sigma_{L+m+1-n}(\eta)-\sigma_L(\eta)-\sigma_{L+m}(\rho\eta))]\to(\eta\epsilon)^{i\xi}e^{i\phi(2n-2-m)}(-)^{n-m-1}i^{-m},$$

with the final result that

$$C(m,n;L)\to\frac{\pi}{2}\left(\frac{k\xi}{\eta}\right)^{n-1}\frac{e^{-\epsilon\xi\sin\theta-\frac{1}{2}\pi|\xi|}}{\sinh\pi\xi}\times\operatorname{Re}\left\{i^{n-m}\left|\frac{\epsilon\xi}{2}\right|^{i\xi}\frac{e^{i\phi(2n-2-m)}}{\Gamma(n+i\xi)}\sum_\lambda\frac{(n-m-1)_\lambda}{\lambda!}\times(1-e^{-2i\phi})^\lambda\psi_2(\alpha;\gamma,\gamma';x,y)\right\}, \quad (103)$$

where the parameters of ψ_2 are the same as those occurring in Eq. (102).

To obtain the limiting forms for $A(m,n;L)$ and $B(m,n;L)$ it is most expedient to use alternative forms of Eqs. (43)–(44), which are obtained by Kummer transformations of $f_1(v)$ and $f_2(v)$ in the integrands.

The result is

$$A(m,n;L)=k_2^{n-1}\left[\frac{4\rho}{(1+\rho)^2}\right]^{L+1}\left(\frac{2}{1+\rho}\right)^{m-n}(1+\rho)^{n-4}$$
$$\times i^{-1-m-n}\frac{e^{\frac{1}{2}\pi\xi}}{\sinh\pi\xi}\left|\frac{\Gamma(L+m+1+i\rho\eta)}{\Gamma(L+1+i\eta)}\right|$$
$$\times\frac{\Gamma(2L+3+m-n)}{\Gamma(2L+2m+2)}\sum_\lambda\frac{(m+n-1)_\lambda}{\lambda!}$$
$$\times\frac{(L+m+1+i\rho\eta)_\lambda}{(2L+2m+2)_\lambda}\left(\frac{2}{1+\rho}\right)^\lambda\oint_{-1}dww^{n-2-i\xi}$$
$$\times[1+w]^{m+1+\lambda-n}\left[1+\frac{1-\rho}{1+\rho}w\right]^{-L-m-1-i\rho\eta-\lambda}$$
$$\times\left[1+\frac{1-\rho}{1+\rho}w^{-1}\right]^{-L-2+n+i\rho\eta}. \quad (104)$$

The limiting form is then found to be

$$A(m,n;L)\to-\frac{1}{8}\left(\frac{2k}{\eta\epsilon}\right)^{n-1}\frac{e^{\pi\xi-\xi\vartheta}}{\sinh\pi\xi}\oint_{-1}dww^{n-2-i\xi}$$
$$\times[we^{-i\vartheta}+e^{i\vartheta}]^{2-2n}\left[\frac{1+w}{we^{-i\vartheta}+e^{i\vartheta}}\right]^{m+1-n}$$
$$\times\exp\left[-\frac{i\epsilon\xi}{2}(we^{-i\vartheta}-w^{-1}e^{i\vartheta})\right]$$
$$=(-)^{m+1}\frac{\pi i}{4}\left(\frac{2k}{\eta\epsilon}\right)^{n-1}(2i\sin\vartheta)^{1-m-n}$$
$$\times\frac{e^{-\xi\vartheta}}{\sinh\pi\xi}\sum_{\lambda,\mu,\nu}\frac{(m+n-1)_\lambda}{\lambda!\mu!\nu!}$$
$$\times\frac{\Gamma(n-1-i\xi+\mu-\nu)}{\Gamma(n-m-1-\lambda)\Gamma(m+1-i\xi+\mu+\lambda-\nu)}$$
$$\times(1-e^{2i\vartheta})^{-\lambda}\left(\frac{i\xi\epsilon}{2}e^{-i\vartheta}\right)^\mu\left(\frac{-i\xi\epsilon}{2}e^{i\vartheta}\right)^\nu. \quad (105)$$

Similarly, the results for B are

$$B(m,n;L)=k_2^{n-1}\left[\frac{4\rho}{(1+\rho)^2}\right]^{L+1}\left(\frac{2}{1+\rho}\right)^{m-n}(1+\rho)^{n-4}$$
$$\times i^{m+1-n}\frac{e^{-\frac{1}{2}\pi\xi}}{\sinh\pi\xi}\left|\frac{\Gamma(L+1+i\eta)}{\Gamma(L+m+1+i\rho\eta)}\right|$$
$$\times\frac{\Gamma(2L+m+3-n)}{\Gamma(2L+2)}\sum_\lambda\frac{(m+n-1)_\lambda}{\lambda!}$$
$$\times\frac{(L+m+1+i\rho\eta)_\lambda}{(2L+2m+2)_\lambda}\left(\frac{2}{1+\rho}\right)^\lambda\oint_{-1}dww^{n-2-i\xi}$$
$$\times[1+w]^{m+1+\lambda-n}\left[1-\frac{1-\rho}{1+\rho}w\right]^{-L-m-1-i\rho\eta-\lambda}$$
$$\times\left[1+\frac{1-\rho}{1+\rho}w^{-1}\right]^{-L-2+n+i\rho\eta}. \quad (106)$$

The above results show the symmetry between A and B, namely that $A\rightleftharpoons B$ under the interchange of (k_1,η_1,L_1) with (k_2,η_2,L_2). The limiting form of B is then

$$B(m,n;L)\to\frac{1}{8}\left(\frac{2k}{\epsilon\eta}\right)^{n-1}\frac{e^{-\xi(\pi-\vartheta)}}{\sinh\pi\xi}\oint_{-1}dww^{n-2+i\xi}$$
$$\times\exp\left[\frac{i\xi\epsilon}{2}(e^{i\vartheta}w-e^{i\vartheta}w^{-1})\right]$$
$$\times[1+w]^{2-2n}\left[\frac{we^{-i\vartheta}+e^{i\vartheta}}{1+w}\right]^{m+1-n}$$
$$=(-)^m\frac{1}{8}\left(\frac{2k}{\epsilon\eta}\right)^{n-1}(2i\sin\vartheta)^{1+m-n}$$
$$\times\frac{e^{i\vartheta}}{\sinh\pi\xi}\sum_{\lambda,\mu,\nu}\frac{(n-m-1)_\lambda}{\lambda!\mu!\nu!}$$
$$\times\frac{\Gamma(n-1+i\xi+\mu-\nu)}{\Gamma(m-n-1-\lambda)\Gamma(1-m+i\xi+\lambda+\mu-\nu)}$$
$$\times(e^{2i\vartheta}-1)^{-\lambda}\left(\frac{-i\xi\epsilon}{2}e^{-i\vartheta}\right)^\mu\left(\frac{i\xi\epsilon}{2}e^{i\vartheta}\right)^\nu. \quad (107)$$

Structure of Green's Functions in Quantum Field Theory*

YOICHIRO NAMBU†
Institute for Nuclear Studies, University of Chicago, Chicago, Illinois
(Received June 8, 1955)

The Green's functions are vacuum expectation values of time ordered products of field operators in the Heisenberg representation. They give us vital information about the nature of the interacting particles and quanta represented by these field operators. It is shown that the Fourier transforms of the Green's functions (for up to four operators) are expressible as parametric integrals involving invariant energy denominators and real, scalar weight functions which are termed the spectral functions. Relativity, causality, and some other fundamental assumptions of field theory are required to derive the result.

The spectral functions have a simple physical interpretation, and completely specify the structure of the Green's functions. The equations of motion which hold between Green's functions of different order can be translated into the corresponding relations between the spectral functions. Renormalization can be carried out explicitly, bringing the equations for the spectral functions into a manifestly renormalized form. The causality condition also serves as a means of obtaining renormalized quantities without recourse to the usual subtraction procedure. The observed masses and coupling constants occur in the equations for the spectral functions as external parameters fixing the boundary condition. No unobservable bare masses and couplings, nor the (infinite) renormalization constants ever appear in the equations. These quantities, however, are shown to be expressible in terms of the spectral functions.

The Green's functions involving more than four field operators are not considered in this paper.

1. INTRODUCTION

IN the quantum theory of interacting fields the nature of field operators in the Heisenberg representation seems to be of interest and importance, since these operators correspond to physically observable quantities, and there have been various attempts at the study of the Heisenberg operators which are free from the limitations of perturbation theory. Källén,[1] Lehmann,[2] and Gell-Mann and Low[3] have studied the structure of the Green's functions like Δ_F', which is defined for a scalar field by

$$\Delta_F'(x-x')=\langle 0|P(\varphi(x),\varphi(x'))|0\rangle, \tag{1.1}$$

where $|0\rangle$ is the actual vacuum state and P the time ordering operator; they have been able to show that Δ_F' can be expressed, quite independently of the details of interaction, in the form

$$\Delta_F'(x-x')=\frac{1}{(2\pi)^4}\int e^{ip(x-x')}\Delta_F'(p)(dp)^4,$$
$$\Delta_F'(p)=-i\int_0^\infty \frac{1}{p^2+m^2-i\epsilon}\nu(m^2)dm^2, \tag{1.2}$$

where the function ν satisfies certain conditions. In deriving this result, two physical requirements are to be made: (1) the theory is Lorentz invariant, and (2) positive energy states form a complete system in the Hilbert space.

A generalization of the above idea was attempted in a previous paper[4] where the Fourier component of a quantity which is related to the scattering matrix for a meson and a particle, was expressed in the form

$$M(x,x')\equiv\langle q|P(j(x),j(x'))|p\rangle$$
$$=\frac{1}{(2\pi)^4}\int e^{-ikx'+ilx}\delta(p+k-q-l)\times M(k+l,p,q)(dk)^4(dl)^4, \tag{1.3}$$
$$M(k+l,p,q)$$
$$=\int\int\int\frac{\nu_1+(k+l,p)\nu_2+(k+l,q)\nu_3}{(k+l+\alpha p+\beta q)^2+m^2-i\epsilon}dm^2d\alpha d\beta,$$

$|p\rangle$ or $|q\rangle$ being the one-particle state of momentum p or q which is assumed to have no spin. In achieving this, the causality principle was emphasized in addition to the above two conditions. It is characterized by the requirement that two observables (Heisenberg operators) must commute outside of each other's light cones.

It can be seen, however, that the tools used in deriving Eq. (1.3) are essentially equivalent to those for Eq. (1.2). Indeed, the causality requirement, as in the case of the Kramers-Kronig relation,[5] should generally manifest itself in a relation between real and imaginary components of matrix elements, or between quantities like $\langle m|\{A(x),A(x')\}|n\rangle$ and $\langle m|[A(x),A(x')]|n\rangle\epsilon(x-x')$ which compose the matrix element $\langle m|P(A(x),A(x'))|n\rangle$. For the Green's function Δ_F' the relation followed automatically from the two conditions mentioned above, but in the case of M it had to be recognized as such.

It is a very interesting question to ask whether one can analyze, along a similar line, the structure of a more

* This work was supported by a grant from the U. S. Atomic Energy Commission.
† On leave from Osaka City University, Osaka, Japan.
[1] G. Källén, Helv. Phys. Acta **25**, 417 (1952); Kgl. Danske Videnskab. Selskab, Mat.-fys. Medd. **27**, No. 12 (1953).
[2] H. Lehmann, Nuovo cimento **11**, 342 (1954).
[3] M. Gell-Mann and F. Low, Phys. Rev. **95**, 1300 (1954).
[4] Y. Nambu, Phys. Rev. **98**, 803 (1955). This will be referred to as NI.
[5] R. de L. Kronig, J. Opt. Soc. Am. **12**, 547 (1926), H. A. Kramers, Atti congr. intern. fisici, Como **2**, 545 (1927).

general variety of quantities, namely matrix elements of time-ordered products of more than two Heisenberg operators. These quantities play an important role in a covariant description of quantum states in field theory, and the renormalization problem can best be treated in this way.

In fact, it has been pointed out in NI that the renormalization not only secures finite results but also satisfies causality requirements, and that conversely by demanding causality in a certain way one could automatically remove divergences.[6] The point is that in the lowest approximation, the imaginary part of a self-energy or a scattering matrix (the damping term) turns out to be finite although the real part without renormalization may be divergent. The causality relation between the two parts will force the latter to be finite and well determined.

In pursuing this end, one finds that the method followed in NI is not quite sufficient for our purposes, and more physical insight is needed. It seems thus worth while, as an orientation to the solution of the problem, to point out here the following observation. Let us consider the relation between the real and imaginary part of a matrix element using the fundamental formula of perturbation theory. Suppose we want to calculate the matrix element $\langle b|S|a\rangle$ of a certain scattering process. This will be given by

$$\langle b|S|a\rangle=\langle b|H|a\rangle+\sum_n \frac{\langle b|H|n\rangle\langle n|H|a\rangle}{E_a-E_n+i\epsilon}+\cdots, \quad (1.4)$$

where H is the interaction Hamiltonian, and the E_n are the free energy eigenvalues. The small imaginary quantity $i\epsilon$ indicates how to handle the poles of S in accordance with the boundary condition. If the particles concerned can be described by real fields (no spin, no charge), we may take the individual elements $\langle n|H|m\rangle$ to be real (for the interactions allowed in field theory). Thus the imaginary part of S will appear if and only if there occur intermediate states with the same energy as the initial state, or in other words, only if competing real processes, which may be the same as the initial or final state, are possible in the intermediate stage.[7]

The above formula does not show immediately the relation between the real and imaginary components since $\langle n|H|m\rangle$ may depend on energy and momentum in general; nor is it of a relativistically covariant form which one would desire. Nevertheless, it is interesting to see that these ideas, which have a definite physical meaning, can be carried over to a relativistic formulation, partly thanks to the "simplicity" of quantum field theory.

In the next section we shall first give the definition of the quantities which we are going to study, and the equations of motion satisfied by these quantities. In Sec. 3 we write down explicit formulas expressing the Green's functions of the first few orders in terms of certain real functions which may be called the spectral functions. Relativity, causality, and some other properties of field theory will be exploited to determine the general character of the spectral functions without going into the details of the interaction. In Sec. 4, we then translate the equations of motion holding for the Green's function into those for the spectral functions. Divergences will arise during this procedure, and it will be shown how the causality consideration again enables one to get the correct manifestly renormalized equations of motion which involve no formal infinities and could in principle be solved without fear of encountering divergences of the usual kind. Formulas giving the relation between the various renormalization constants and the spectral function will be found in the Appendix.

2. GREEN'S FUNCTIONS AND RELATED QUANTITIES

In the present paper, we treat the symmetrical pseudoscalar field coupled to the Dirac nucleon field, although this does not mean any restriction on the theory itself. The Lagrangian density of the meson-nucleon system is

$$\begin{aligned} L=&-\bar{\psi}\gamma_\mu\partial_\mu\psi-\kappa\bar{\psi}\psi \\ &-\tfrac{1}{2}(\partial_\mu\varphi_i\partial_\mu\varphi_i+\mu^2\varphi_i\varphi_i) \\ &-g i\bar{\psi}\gamma_5\tau_i\psi\varphi_i. \end{aligned} \quad (2.1)$$

We have adopted natural units $\hbar=c=1$, and $x_\mu \equiv (x, y, z, it=ix_0)$. ψ stands for the Dirac nucleon field with two isotopic spinor components. τ_i are the usual three vector components of the isotopic spin operator, and φ_i the corresponding ones of the meson field.

The Hamiltonian density of the system easily follows from the Lagrangian (1) by introducing the canonical variables and the commutation relations in the usual way:

$$\begin{aligned} H=&\sum_{k=1}^{3}\bar{\psi}\gamma_k\partial_k\psi+\kappa\bar{\psi}\psi \\ &+\tfrac{1}{2}(\pi_i\pi_i+\sum_{k=1}^{3}\partial_k\varphi_i\partial_k\varphi_i+\mu^2\varphi_i\varphi_i)+g_i\bar{\psi}\gamma_5\tau_i\psi\varphi_i, \end{aligned} \quad (2.2)$$

$$\{\psi_\alpha(\mathbf{x}), \bar{\psi}_\beta(\mathbf{y}')\}=(\gamma_4)_{\alpha\beta}\delta_{st}\delta(\mathbf{x}-\mathbf{y}'),$$

$$[\varphi_i(\mathbf{x}), \pi_j(\mathbf{y}')]=[\varphi_i(\mathbf{x}), \partial\varphi_j(\mathbf{y}')/\partial x_0']=i\delta_{ij}\delta(\mathbf{x}-\mathbf{y}'),$$

where α, β refer to the spinor components and s, t to the isotopic spin components. The Heisenberg equations

[6] It is true that a convergent theory does not always satisfy causality as in the case of the so-called damping theory, which gives rise to singularities of matrix elements not allowed in a causal theory. But the previous paper suggests the possiblity of finding a convergent and causal theory which will coincide with the orthodox renormalization theory.

[7] Rigorously speaking, there will be, of course, energy shifts of the particles due to interaction (self-energy) so that we have to interpret E_n as the energy of the observed free particles.

of motion for the field operators are

$$\begin{aligned}&\gamma_\mu\partial_\mu\psi+\kappa\psi+gi\gamma_5\tau_i\varphi_i\psi=0,\\&-\partial_\mu\bar\psi\gamma_\mu+\kappa\bar\psi+gi\bar\psi\gamma_5\tau_i\varphi_i=0,\\&(\Box-\mu^2)\varphi_i=gi\bar\psi\gamma_5\tau_i\psi.\end{aligned}\tag{2.3}$$

The nature of the Heisenberg operators is the main subject of our concern. Let us introduce the following quantities which give us vital information about these operators.[8]

$$\begin{aligned}T(x\alpha s,y\beta t)&\equiv\langle0|T(\psi_{\alpha s}(x),\bar\psi_{\beta t}(y))|0\rangle\\&=\epsilon(xy)\langle0|P(\psi_{\alpha s}(x),\bar\psi_{\beta t}(y))|0\rangle,\\T(zi,z'j)&\equiv\langle0|T(\varphi_i(z),\varphi_j(z'))|0\rangle\\&=\langle0|P(\varphi_i(z),\varphi_j(z'))|0\rangle,\\T(xyz)&\equiv\langle0|T(\psi(x),\bar\psi(y),\varphi_i(z))|0\rangle\\&=\epsilon(xy)\langle0|P(\psi(x),\bar\psi(y),\varphi_i(z))|0\rangle,\\T(xyzz')&\equiv\langle0|T(\psi(x),\bar\psi(y),\varphi_i(z),\varphi_j(z'))|0\rangle\\&=\epsilon(xy)\langle0|P(\psi(x),\\&\qquad\bar\psi(y),\varphi_i(z),\varphi_j(z'))|0\rangle,\\T(x_1x_2y_1y_2)&\equiv\langle0|T(\psi(x_1),\psi(x_2),\bar\psi(y_1),\bar\psi(y_2))|0\rangle\\&=\epsilon(x_1x_2y_1y_2)\langle0|P(\psi(x_1),\\&\qquad\psi(x_2),\bar\psi(y_1),\bar\psi(y_2))|0\rangle.\end{aligned}\tag{2.4}$$

Here $|0\rangle$ is the vacuum or the lowest energy state of the total interacting meson nucleon field; P means the time ordering of the operators, and $\epsilon(x,y)$, etc., is the sign function which takes the values ±1 according as the permutation $(x_0,y_0)\to P(x_0,y_0)$ is even or odd; the spin and isotopic spin indices of the operators may be suppressed when not necessary. Alternatively we may write

$$\begin{aligned}T(xy)&=\theta(x-y)\langle0|\psi(x)\bar\psi(y)|0\rangle\\&\quad-\theta(y-x)\langle0|\bar\psi(y)\psi(x)|0\rangle\\&=\theta(x-y)\textstyle\sum_n\langle0|\psi(x)|n\rangle\langle n|\bar\psi(y)|0\rangle\\&\quad-\theta(y-x)\sum_n\langle0|\bar\psi(y)|n\rangle\langle n|\psi(x)|0\rangle,\\T(zz')&=\theta(z-z')\langle0|\varphi(z)\varphi(z')|0\rangle\\&\quad+\theta(z'-z)\langle0|\varphi(z')\varphi(z)|0\rangle\\&=\theta(z-z')\textstyle\sum_n\langle0|\varphi(z)|n\rangle\langle n|\varphi(z')|0\rangle\\&\quad+\theta(z'-z)\sum_n\langle0|\varphi(z')|n\rangle\langle n|\varphi(z)|0\rangle,\\T(xyz)&=\theta(x-y)\theta(y-z)\langle0|\psi(x)\bar\psi(y)\varphi(z)|0\rangle\\&\quad-\theta(y-x)\theta(x-z)\langle0|\bar\psi(y)\psi(x)\varphi(z)|0\rangle\\&\quad+\theta(x-z)\theta(z-y)\langle0|\psi(x)\varphi(z)\bar\psi(y)|0\rangle+\cdots\\&=\theta(x-y)\theta(y-z)\textstyle\sum_{n,m}\langle0|\psi(x)|n\rangle\\&\quad\times\langle n|\bar\psi(y)|m\rangle\langle m|\varphi(z)|0\rangle-\cdots,\end{aligned}\tag{2.5}$$

$$\theta(x-y)=\frac{1+\epsilon(x-y)}{2}=\begin{cases}1 & x_0-y_0>0\\ 0 & x_0-y_0<0,\end{cases}$$

where n, m run through a complete set of states of the meson-nucleon field.

The T's give, so to speak, a measure of the correlation of field quantities at different space-time points. In the absence of interaction, $T(x,y)$ and $T(z,z')$ are the Feynman propagation functions $S_F(x,y)$ and $\Delta_F(z,z')$ for the nucleon and meson respectively; in the presence of interaction, they are the quantities $S_F'(x,y)$ and $\Delta_F'(z,z')$ which were originally defined by Dyson[9] in the perturbation theory. The T's of higher orders describe more complicated correlations of more than two field quantities, and are closely related to what Schwinger[8] has generally termed Green's functions.

A higher order T contains a part which derives from lower order correlations, so that it is convenient to introduce further the irreducible correlations ρ[10]:

$$\begin{aligned}\rho(xy)&=T(xy),\quad\rho(zz')=T(zz'),\\\rho(xyz)&=T(xyz),\\\rho(xyzz')&=T(xyzz')-T(xy)T(zz'),\\\rho(x_1x_2y_1y_2)&=T(x_1x_2y_1y_2)+T(x_1y_1)T(x_2y_2)\\&\quad-T(x_1y_2)T(x_2y_1),\text{ etc.}\end{aligned}\tag{2.6}$$

We shall refer to all the quantities introduced in this section simply as Green's functions when no confusion arises.

If we make use of the interaction representation and Feynman graphs, the meaning of the ρ's is clear. $\rho(x_1\cdots x_ly_1\cdots y_mz_1\cdots z_n)$ corresponds to the totality of graphs in which there are $l+m+n$ external lines starting at $x_1,x_2,\cdots z_n$, and all these lines are connected with each other through the network of internal lines.

The Green's functions of different order are related by equations of motion which are obtained by differentiating them and making use of Eq. (2.3):

$$\begin{aligned}&(\gamma\partial+\kappa)_{\alpha\rho}(xy)\\&\quad=-i\delta(xy)-ig\gamma_5\tau_j\int\rho(xyz'j)\delta(x-z')(dz')^4,\\&(-\gamma^T\partial+\kappa)_{\alpha\rho}(xy)\\&\quad=-i\delta(xy)-ig\int\rho(xyz'j)\gamma_5\tau_j\delta(y-z')(dz')^4,\\&(\Box-\mu^2)_{ik}\rho(zz')\\&\quad=i\delta(zz')-ig\int\mathrm{tr}(\gamma_5\tau_i\rho(xyz'))\\&\qquad\qquad\times\delta(x-z)\delta(y-z)(dx)^4(dy)^4,\\&(\gamma\partial+\kappa)_{\alpha\rho}(xyz)\\&\quad=-ig\int\gamma_5\tau_j[\rho(xy)\rho(zz'j)+\rho(xyzz'j)]\delta(x-z')(dz')^4,\\&(\Box-\mu^2)_{ik}\rho(xyz)\\&\quad=ig\int\{-\rho(xy)\,\mathrm{tr}[\gamma_5\tau_i\rho(x'y')]+\rho(xy')\gamma_5\tau_i\rho(x'y)\\&\qquad+\rho(xx'\alpha s,yy'\beta t)(\gamma_5\tau_i)_{\beta t,\alpha s}\}\\&\qquad\times\delta(x'-z)\delta(y'-z)(dx')^4(dy')^4.\end{aligned}\tag{2.7}$$

[8] G. C. Wick, Phys. Rev. **80**, 268 (1950); J. Schwinger, Proc. Natl. Acad. Sci. U. S. **27**, 452 and 455 (1951). See also E. Freese, Z. Naturforsch. **8a**, 776 (1953); P. T. Matthews and A. Salam, Proc. Roy. Soc. (London) **A221**, 128 (1953); K. Nishijima, Progr. Theoret. Phys. **10**, 549 (1953); **12**, 279 (1954). The notations do not necessarily agree with those used by these authors.

[9] F. J. Dyson, Phys. Rev. **75**, 486 and 1736 (1949).

[10] E. Freese, Nuovo cimento **2**, 50 (1955).

Under the assumption of adiabatic switching at $t=\pm\infty$, and the boundary condition for the vacuum, they can be converted into integral equations:

$$\begin{aligned}
\rho(xy)&=S_F(xy)+g\int S_F(xx')\gamma_5\tau_j\rho(x'yz'j)\\
&\qquad\times\delta(x'-z')(dx')^4(dz')^4,\\
\rho(zi,z'j)&=\delta_{ij}\Delta_F(zz')-g\int\Delta_F(zz'')\ \mathrm{tr}[\gamma_5\tau_\varphi\rho(xyz'j)]\\
&\qquad\times\delta(x-z'')\delta(y-z'')(dx)^4(dy)^4(dz'')^4,\\
\rho(xyz)&=g\int S_F(xx')\gamma_5\tau_j[\rho(x'y)\rho(zz'j)\\
&\qquad+\rho(x'yzz'j)]\delta(x'-z')(dx')^4(dz')^4\\
&=g\int\Delta_F(zz')\{-\rho(xy)\ \mathrm{tr}[\gamma_5\tau_\varphi\rho(x'y')]\\
&\qquad+\rho(xy')\gamma_5\tau_i\rho(x'y)+\rho(xx'\alpha s,yy'\beta t)(\gamma_5\tau_i)_{\beta t,\alpha s}\}\\
&\qquad\times\delta(x'-z')\delta(y'-z')(dx')^4(dy')^4(dz')^4.
\end{aligned}\tag{2.8}$$

It is to be noted that the ρ functions of higher order than the first do not have inhomogeneous terms in their equations of motion.

In the following sections we shall analyze the nature of the T's and ρ's up to four external lines. These are of particular interest since it is they that cause infinities in the actual calculation, and also because $\rho(xyzz')$, for example, describes the scattering of a nucleon and a meson which has direct physical significance.[11]

The problem of renormalization, which has not been discussed so far, is usually dealt with by starting from renormalized fields and a renormalized Lagrangian:

$$\begin{aligned}
L=&-Z_2[\bar\psi\gamma_\mu\partial_\mu\psi+\kappa\bar\psi\psi]+Z_2\delta_k\bar\psi\psi\\
&-\tfrac{1}{2}Z_3[\partial_\mu\varphi_i\partial_\mu\varphi_i+\mu^2\varphi_i\varphi_i]-\tfrac{1}{2}Z_3\delta\mu^2\varphi_i\varphi_i\\
&-Z_1 g i\bar\psi\gamma_5\tau_i\psi\varphi_i-Z_4\tfrac{1}{4}\lambda\varphi_i\varphi_i\varphi_k\varphi_k.
\end{aligned}\tag{2.9}$$

We will not describe this procedure in detail here since we approach the problem in a different fashion. In fact, we shall be treating physically significant renormalized quantities only, and we need not be meticulous about the distinction between renormalized and unrenormalized quantities since the infinite constants which characterize their difference will not occur explicitly in our equations. We shall regard all the Green's functions and operators as renormalized ones, but treat them as if they obeyed the equations of motion for canonical observables, with, however, observed masses and couplings.

[11] The scattering matrix is obtained essentially by the adiabatic limiting process

$$\lim_{\substack{x_0,\,z_0\to\infty\\ y_0,\,z_0'\to-\infty}}\rho(xyzz').$$

See reference 20.

3. REPRESENTATION OF THE GREEN'S FUNCTIONS BY MEANS OF SPECTRAL FUNCTIONS

In accordance with the ideas outlined in the introduction, we start out with the following fundamental assumptions.

(I) Lorentz invariance and other invariances which are inherent in the theory. As was discussed in NI, it is important to note that the Green's functions, which are T-products of operators, should not depend on the choice of the time axis used for the time ordering. This is guaranteed by causality (to be mentioned below) which insures the independence of field quantities (commutability or anticommutability) for spacelike points.

(II) Completeness of the positive energy states. In addition, we will also assume naturally that the one-nucleon or meson state is stable. But we do not necessarily exclude the existence of bound states.

(III) The adiabatic switching of interaction. This has always been necessary if one wants at all to talk about interaction between particles. It must be recognized, however, that its exact meaning is not a uniquely defined one, and one will get different connections between the perturbed and unperturbed field quantities according to different definitions of the adiabatic process. We want to use it in the simple physical sense that the field variables behave as *essentially* free when they are far apart from one another, and these essentially free fields should serve to *define* the physical constants (the "observed" masses and coupling constants). This should be enough for our purpose of finding relations between observable quantities only. On the other hand, the connection between unrenormalized and renormalized quantities is in principle to be obtained by the unrealistic process in which the coupling constant itself is turned on and off instead of separating the particles from each other. It is also to be noted that the bound states do not cause any difficulty since we are not asked to treat them by perturbation once the physical constants are fixed.

(IV) Causality. This will be the main tool in deriving our results. But we use it here in a disguised way which is not immediately recognizable as such. We postulate namely that, apart from spin and isotopic spin matrices, the imaginary part of the Green's functions arises through vanishing denominators which occur if energy-conserving processes are possible in the intermediate stages appearing in Eq. (2.5). The conditions I and II then say that the energy-momentum of such an intermediate state must form a timelike four-vector with positive time component. This suggests that the relativistically invariant form of the energy denominator and the nature of its singularity are determined by the time-ordered character of the Green's functions. Causality is reflected in all these points in an implicit fashion: The timelike energy-momentum vector will guarantee the noninterference of measurements outside

the light cone; and the positive energy condition and the time-ordering will fix the analytic behavior of the function with regard to each energy denominator.

The implication of these arguments will become clear as we go over to the actual application below.

A. Modified Propagation Functions $\rho(xy)$ and $\rho(zz')$

We begin with the simplest cases of $\rho(xy)$ and $\rho(zz')$ as an illustration though the result is already known.[1] We observe that, in the first place, the invariance under the inhomogeneous Lorentz transformation, charge conjugation, and isotopic transformation requires the Fourier transforms

$$\rho(pq)=\frac{1}{(2\pi)^8}\int e^{-ipx-iqy}\rho(xy)(dx)^4(dy)^4,$$
$$\rho(kk')=\frac{1}{(2\pi)^8}\int e^{-ikz-ik'z'}\rho(zz')(dz)^4(dz')^4, \tag{3.1}$$

to be of the form

$$\rho(p\alpha s,q\beta t)=i\delta(p+q)\delta_{st}[ip\gamma\rho_1(p^2)+\rho_0(p^2)]_{\alpha\beta},$$
$$\rho(ki,k'j)=-i\delta(k+k')\delta_{ij}\rho(k^2), \tag{3.2}$$

where the spin (α,β) and isotopic spin (s,t,i,j) indices are explicitly written down. The graphs corresponding to these quantities are of course two external nucleon or meson lines of energy-momenta p, $q=-p$ or k, $k'=-k$ which we measure for convenience always in the "out" direction.

Following the assumption (IV) let us next ask the question: under what conditions will they give rise to real processes?

(1) If the incident particle is a real particle, it can go through the same real state without interaction. In this case

$$p^2+\kappa^2=0, \quad k^2+\mu^2=0,$$

where κ and μ are the masses of the real nucleon and meson respectively. (2) If the energy $|p_0|$ or $|q_0|$ of the incident virtual nucleon is large enough, it can split into a real nucleon and at least one real meson[12]; similarly if $|k_0|$ or $|k_0'|$ is large enough, the incident pseudoscalar meson can split into at least three mesons. The condition for this to happen can be written in an invariant way as

$$p^2+(\kappa+\mu)^2\leq 0,$$
$$k^2+(3\mu)^2\leq 0.$$

We thus conclude, according to (IV), that the ρ's must have terms of the form

$$1/(p^2+m^2), \quad m=\kappa \text{ or } m\geq\kappa+\mu,$$
$$1/(k^2+n^2), \quad n=\mu \text{ or } n\geq 3\mu, \tag{3.3}$$

which become singular in case a real process (1) or (2) is possible. To determine the character of the singularity precisely, we invoke the assumption (II) together with the decomposition (2.5). Since the energy of the intermediate states is positive definite, the Fourier component of a function $\rho(x,y)$ must behave like $\exp(-i|k_0(x_0-y_0)|)$. So we conclude, just as in the case of S_F and Δ_F, that Eq. (3.3) should actually contain $1/(p^2+m^2-i\epsilon)$ and $1/(k^2+n^2-i\epsilon)$. Thus we can write

$$\rho_\lambda(p^2)=\int_0^\infty \frac{\nu_\lambda(u)}{p^2+u}du, \quad \lambda=0,1$$
$$\rho(k^2)=\int_0^\infty \frac{\nu(w)}{k^2+w}dw, \tag{3.4}$$
$$u\equiv u-i\epsilon, \quad w\equiv w-i\epsilon,$$

where the real functions ν have the property[12]

$$\nu_\lambda(u)=\nu_\lambda{}^0\delta(u-\kappa^2)+f\lambda(u)\theta(u-(\kappa+\mu)^2),$$
$$\nu(w)=\nu^0\delta(w-\kappa^2)+g(w)\theta(w-(3\mu)^2). \tag{3.5}$$

We also note that

$$\nu_\lambda(u)=\frac{1}{\pi}\operatorname{Im}\rho_\lambda(-u),$$
$$\nu(w)=\frac{1}{\pi}\operatorname{Im}\rho(-w). \tag{3.6}$$

On the other hand, from the decomposition (2.5) and (II) and (IV) it is again easy to see that

$$\delta_{st}(ip\gamma_{\alpha\beta}\operatorname{Im}\rho_1(p^2)+\delta_{\alpha\beta}\operatorname{Im}\rho_0(p^2))$$
$$=\sum\langle 0|\psi_{\alpha s}|p\rangle\langle p|\bar\psi_{\beta t}|0\rangle\theta(p)$$
$$-\sum\langle 0|\bar\psi_{\beta t}|-p\rangle\langle -p|\psi_{\alpha s}|0\rangle\theta(-p), \tag{3.7}$$
$$\delta_{ij}\operatorname{Im}\rho(k^2)=\sum\langle 0|\varphi_i|k\rangle\langle k|\varphi_j|0\rangle\theta(k)$$
$$+\sum\langle 0|\varphi_j|-k\rangle\langle -k|\varphi_i|0\rangle\theta(-k),$$

where the summation extends over all the spin states with the momentum $\pm p$ or $\pm k$. The second equation indicates[2]

$$\nu(w)\geq 0. \tag{3.8}$$

For ν_1 and ν_0 we observe that $\bar\psi=\psi^*\gamma_4$, and

$$(1/\pi)\{\sum|\langle 0|\psi_{\alpha s}|p\rangle|^2\theta(p)-\sum|\langle -p|\psi_{\alpha s}|0\rangle|^2\theta(-p)\}$$
$$=p_0\nu_1(p^2)-(\gamma_4)_{\alpha\alpha}\nu_0(p^2),$$

choosing the rest system for p. Thus both sides must have the same sign as p_0:

$$\epsilon(p)[p_0\nu_1(p^2)-(\gamma_4)_{\alpha\alpha}\nu_0(p^2)]\geq 0,$$

which means[2]

$$\nu_1(u)\geq 0, \quad |p_0|\nu_1(u)=u^{\frac{1}{2}}\nu_1(u)\geq|\nu_0(u)|, \tag{3.9}$$

since the expectation value of γ_4 lies always between -1 and $+1$.

[12] We excluded here the existence of a bound meson-nucleon system. In case such a bound system exists, $\nu_\lambda(u)$ will have an additional point spectrum between κ^2 and $(\kappa+\mu)^2$.

More information on ν is to be obtained by considering the boundary conditions. If we assume, according to (III), that the interaction can be switched off adiabatically at $t=\pm\infty$, then $\rho(xy)$ and $\rho(zz')$ should go in this limit over to the propagation functions for free incoming and outgoing fields:

$$\lim_{\substack{x_0\to\infty\\ y_0\to-\infty}}{}^{*}\ \langle 0|\psi(x)\bar{\psi}(y)|0\rangle = \lim_{\substack{x_0\to\infty\\ y_0\to-\infty}} \langle 0|\psi_{\text{out}}{}^{0}(x)\bar{\psi}_{\text{in}}{}^{0}(y)|0\rangle, \text{ etc.}^{13} \quad (3.10)$$

On the other hand, the initial condition on the behavior of the ρ's for equal times may be checked by the relation

$$\begin{aligned}&\epsilon(xy)\rho(xy)\,|_{x_0=y_0}=\langle 0|\,\{\psi(x),\bar{\psi}(y)\}\,|0\rangle\,|_{x_0=y_0},\\ &\epsilon(zz')\frac{\partial}{\partial z_0}\rho(zz')\Big|_{z_0=z_0'}\\ &\quad=\left\langle 0\left|\left[\frac{\partial\varphi(z)}{\partial z_0},\,\varphi(z')\right]\right|0\right\rangle\Big|_{z_0=z_0'},\end{aligned} \quad (3.11)$$

since the right-hand side is the commutation relation for the field variables.

Although we have thus two conditions at hand, we should primarily use the condition at infinity since our derivation of the ν's was based on the over-all behavior of incoming or outgoing waves. Consequently we assume that the asymptotic fields ψ^0, $\bar{\psi}^0$ and φ^0 are normalized in the usual way so that

$$\begin{aligned}\epsilon(xy)\langle 0|\,T(\psi^0(x),\bar{\psi}^0(y))\,|0\rangle&=S_F{}^{(\kappa)}(xy),\\ \langle 0|\,T(\varphi_i(z),\varphi_j(z'))\,|0\rangle&=\delta_{ij}\Delta_F{}^{(\mu)}(zz'),\end{aligned} \quad (3.12)$$

where the right-hand sides are the ordinary Feynman functions with mass κ and μ, respectively. This leads to

$$\begin{aligned}&\nu_1{}^0=1,\quad \nu_0{}^0=-\kappa,\\ &\nu^0=1.\end{aligned} \quad (3.13)$$

The field operators being thus normalized, Eq. (3.11) is no more the commutation relation for canonical variables since the adiabatic process is in general not a unitary transformation. Indeed we must conclude from Eqs. (3.11) and (2.9) that

$$\begin{aligned}&\langle 0|\,\{\psi_{\alpha s}(x),\bar{\psi}_{\beta t}(y)\}\,|0\rangle\,|_{x_0=y_0}=Z_2{}^{-1}\delta_{st}(\gamma_4)_{\alpha\beta}\delta(\mathbf{x}-\mathbf{y}),\\ &\left\langle 0\left|\left[\frac{\partial\varphi_i(z)}{\partial z_0},\,\varphi_j(z')\right]\right|0\right\rangle\Big|_{x_0=y_0}=Z_3{}^{-1}\delta_{ij}\delta(\mathbf{z}-\mathbf{z}'),\end{aligned} \quad (3.14)$$

where

$$\begin{aligned}Z_2{}^{-1}&=\int\nu_1(u)du=1+\int_{(\kappa+\mu)^2}^{\infty}f_1(u)du\geq 1,\\ Z_3{}^{-1}&=\int\nu(w)dw=1+\int_{2\mu}^{\infty}g(w)dw\geq 1,\end{aligned} \quad (3.15)$$

which are the renormalization constants introduced by Dyson in relation to the unrenormalized fields ψ_u, $\bar{\psi}_u$, and φ_u obeying the proper commutation relations:

$$\begin{aligned}&\psi_u=Z_2{}^{\frac{1}{2}}\psi,\quad \bar{\psi}_u=Z_2{}^{\frac{1}{2}}\bar{\psi},\\ &\varphi_u=Z_3{}^{\frac{1}{2}}\varphi.\end{aligned}$$

It is clear from the above result that the boundary condition at infinity is more convenient than the initial condition since we can deal with the renormalized quantities directly and thus the functions ν should be finite. They should also satisfy

$$\begin{aligned}&\int\frac{\nu_i(u)}{u}du<\infty,\\ &\int\frac{\nu(w)}{w}dw<\infty,\end{aligned} \quad (3.16)$$

without which Eq. (3.4) would be meaningless.

Mathematically speaking, Eq. (3.4) expresses the fact that $\rho(k^2)\equiv\rho(-\zeta)$, etc., have no poles in the upper half of the complex plane as functions of ζ:

$$\rho(-\zeta)=\frac{1}{2\pi i}\int_{-\infty}^{\infty}\frac{\rho(-\zeta')}{\zeta'-\zeta-i\epsilon}d\zeta',\quad \zeta \text{ real}, \quad (3.17)$$

since $\mathrm{Im}\rho(-\zeta)=\pi\nu(\zeta)=0$ for real $\zeta<0$ (or $\zeta_{\min}$). In case the condition (3.16) is not satisfied, we can still take, for example, a function

$$f(-\zeta)\equiv\rho(-\zeta)/(\zeta-a)^n,\quad n=\text{positive integer},\quad a<\zeta_{\min},$$

such that

$$\int_{-\infty}^{\infty}\frac{\nu(\zeta)}{(\zeta-a)^n}\frac{d\zeta}{\zeta}<\infty, \quad (3.18)$$

and express it as

$$f(-\zeta)=\frac{1}{2\pi i}\int_{-\infty}^{\infty}\frac{1}{\zeta'-\zeta-i\epsilon}f(-\zeta')d\zeta',$$

or

$$\begin{aligned}\rho(k^2)=&\int\frac{\nu(w)}{k^2+w}\left(\frac{a+k^2}{a-w}\right)^n dw\\ &+\frac{(a+k^2)^n}{(n-1)!}\left(-\frac{\partial}{\partial a}\right)^{n-1}\left[\frac{\rho(a)}{a+k^2}\right].\end{aligned} \quad (3.19)$$

Thus $\rho(k^2)$ is not completely determined by the imaginary part alone; the second term on the right is a polynomial in k^2, and to omit (or separate) this term

[13] lim* means the switching off of the interaction at $+\infty$; in other words, $\langle n|\bar{\psi}|0\rangle$, etc., should vanish for all n except for the one-particle states. We do not mean, however, that the particles turn into "bare" particles. The incoming and outgoing waves are equal since they are renormalized waves without the self-energy effect.

physically means some sort of renormalization of ρ. In our formalism the boundary condition for ν will serve to fix it. The "renormalized" ρ has a factor $(k^2+a)^n$, and behaves as $O(k^{2n})$ for large k^2. In other words, $\rho(zz')$ has derivatives (of order $\leq 2n$) of the delta function at the origin.

The Green's functions $\rho(xy)$ and $\rho(zz')$ do not have singularities of the above kind. But the quantity

$$M(zz')\equiv\langle 0|T(ig\bar{\psi}\gamma_5\tau_i\psi(z),ig\bar{\psi}\gamma_5\tau_i\psi(z'))|0\rangle, \quad (3.20)$$

which is related to $\rho(zz')$ by

$$(\Box-\mu^2)^2\rho(zz')=i(\Box-\mu^2)\delta(zz')+M(zz'), \quad (3.21)$$

has the representation

$$M(k^2)=-\delta_{ij}i(k^2+\mu^2)^2\int\frac{1}{k^2+w}\frac{\nu^*(w)}{(w-\mu^2)^2}dw, \quad (3.22)$$

$$\nu^*(w)=(w-\mu^2)^2\nu(w)=-\frac{1}{\pi}\mathrm{Im}M(-w).$$

This corresponds to the choice $a=\mu^2$, $n=2$ in Eq. (3.19). We shall also meet with this situation later.

B. Three-Body Green's Functions

Let us take the three-body Green's function

$$\rho(xyz)=\langle 0|T(\psi(x),\bar{\psi}(y),\varphi_i(z))|0\rangle, \quad (3.23)$$

and define its Fourier transform

$$\rho(pqz)=\frac{1}{(2\pi)^{12}}\times\int e^{-ipx-iqy-ikz}\rho(xyz)(dx)^4(dy)^4(dz)^4. \quad (3.24)$$

Because of the conservation law

$$p+q+k=0, \quad (3.25)$$

$\rho(pqk)$ is a function of three scalars p^2, q^2, k^2 in addition to the spin functions γ_5, $(p\gamma)\gamma_5$, $\gamma_5(q\gamma)$, and τ_i. γ_5 reflects here the pseudoscalar nature of the field φ_i. We may thus generally write

$$\rho(p\alpha s,q\beta t,k_i)=i\delta(p+q+k)\sum_{\lambda,\lambda'=0,1}[(ip\gamma)^\lambda\gamma_5(-iq\gamma)^{\lambda'}]_{\alpha\beta}\times(\tau_i)_{st}\rho_{\lambda\lambda'}(p^2,q^2,k^2). \quad (3.26)$$

Under the extended charge conjugation $\psi\rightarrow C\bar{\psi}$, $\bar{\psi}\rightarrow C^{-1}\psi$, $\varphi_i\rightarrow-\varphi_i$, $\rho(xyz)$ goes into $-(C^{-1}\rho(yxz)C)^T$; this means for $\rho(pqk)$[14] the invariance under $p\leftrightarrow q$, $\gamma\rightarrow-\gamma$ so that $\rho_{\lambda\lambda'}$ must be symmetric:

$$\rho_{\lambda\lambda'}(p^2,q^2,k^2)=\rho_{\lambda'\lambda}(q^2,p^2,k^2). \quad (3.27)$$

[14] The spin matrices are transformed according to $O\rightarrow C^{-1}OC$, with $C^{-1}\gamma_\mu C=-\gamma_\mu^T$, $C^{-1}\tau_i C=-\tau_i^T$, etc.

Next we ask, as before, for the condition of producing a real process. In the first place, an incoming external line p, q, or k by itself can give rise to such a process just as in the case A. This means that $\rho_{\lambda\lambda'}$ must have factors of the form

$$\frac{1}{p^2+m_1^2-i\epsilon},\quad\frac{1}{q^2+m_2^2-i\epsilon},\quad\frac{1}{k^2+m_3^2-i\epsilon},$$

where

$$m_1,\ m_2=\kappa\quad\text{or}\quad\geq\kappa+\mu,\qquad m_3=\mu\quad\text{or}\quad\geq 3\mu \quad (3.28)$$

(again excluding bound states). Next, it is possible that any two of the incoming particles together produce a real process by interaction (scattering). This would mean that there should be factors of the form

$$\frac{1}{(p+q)^2+m_4^2-i\epsilon},\quad\frac{1}{(p+k)^2+m_5^2-i\epsilon},\quad\frac{1}{(q+k)^2+m_6^2-i\epsilon}.$$

But the conservation law (3.25) just reduces these factors to those in Eq. (3.28) so that we get no new ones.

In order to proceed further, it is necessary to consider the equations of motion for $\rho(xyz)$: By differentiating it with respect to x, y, and z successively, we obtain

$$\begin{aligned}&(\gamma\partial+\kappa)_x(-\gamma^T\partial+\kappa)_y(\Box-\mu^2)_z\rho(xyz)\\&=-ig\gamma_5\tau_i\delta(x-y)\delta(x-z)\\&\quad+ig^2\gamma_5\tau_j\langle 0|T(\psi\varphi_j(x),\bar{\psi}(y))|0\rangle\gamma_5\tau_i\delta(y-z)\\&\quad+ig^2\gamma_5\tau_i\langle 0|T(\psi(x),\bar{\psi}\varphi_k(y))|0\rangle\gamma_5\tau_k\delta(x-z)\\&\quad-ig^2\gamma_5\tau_j\langle 0|T(\varphi_j(x),\bar{\psi}\gamma_5\tau_i\psi(z))|0\rangle\delta(x-y)\\&\quad+ig^3\gamma_5\tau_j\langle 0|T(\psi\varphi_j(x),\bar{\psi}\varphi_k(y),\bar{\psi}\gamma_5\tau_i\psi(z))|0\rangle\gamma_5\tau_k.\end{aligned} \quad (3.29)$$

Now we could apply the same argument as above to the T products appearing on the righthand side, and could conclude that they must contain the same factors as Eq. (3.28). Hence the original $\rho_{\lambda\lambda'}$ must necessarily contain the three factors simultaneously. In other words,

$$\rho_{\lambda\lambda'}(p^2q^2k^2)=\int\frac{\nu_{\lambda\lambda'}(uvw)}{(p^2+u)(q^2+v)(k^2+w)}dudvdw, \quad (3.30)$$

which is the desired spectral decomposition.

According to Eq. (3.28), $\nu_{\lambda\lambda'}$ has a point spectrum at the masses for real particles, and a continuous spectrum extending upward from the thresholds for various reactions. By Eq. (3.27), it satisfies the symmetry condition

$$\nu_{\lambda\lambda'}(uvw)=\nu_{\lambda'\lambda}(vuw). \quad (3.31)$$

To see the implication of the boundary condition at infinity, we again let the fields ψ, $\bar{\psi}$, and φ go separately to $+\infty$ or $-\infty$, and suppose that they turn into almost free fields there. In this case the only interaction which can be measured by these waves will be that of the type $ig\bar{\psi}\gamma_5\tau_i\psi\varphi_i$, where g *defines* the observed coupling constant. To be more precise, we mean by the adiabatic

procedure that only the first term of the right-hand side of Eq. (3.29) remains (understanding that contributions of the same type from the rest have been incorporated into it). Thus

$$\lim^{*}\rho(pqk)=-igS_F(p)i\gamma_5\tau_3 S_F(-q)\Delta_F(k), \quad (3.32)$$

from which it follows that

$$\nu_{\lambda\lambda'}(uvw)=g\nu_{\lambda\lambda'}{}^{0}\delta(u-\kappa^2)\delta(v-\kappa^2)\delta(w-\mu^2)+\cdots,$$

with

$$\nu_{\lambda\lambda'}{}^{0}=\begin{pmatrix}\kappa^2 & -\kappa\\ -\kappa & 1\end{pmatrix}. \quad (3.33)$$

To find the relation between renormalized and unrenormalized quantities a systematic study is needed since it is more complicated than in the previous case. Deferring the details to the Appendix, we quote here only the main result which gives the unrenormalized charge g_0:

$$\int\nu_{11}(uvw)dudvdw=gZ_1Z_2^{-2}Z_3^{-\frac{1}{2}}=g_0Z_2^{-1}Z_3^{-\frac{1}{2}}. \quad (3.34)$$

As is well known, there is in general an arbitrariness in defining the observed coupling constant, so that the above definition of g, Eq. (3.33), is not the only possibility, though it seems to be the most natural one in our scheme. A different quantity could be obtained, for example, in the following way. Suppose we take the equation of motion

$$(\Box-\mu^2)_2\rho(xyz)=\langle 0|T(\psi(x),\bar\psi(y),ig\bar\psi\gamma_5\tau_i\psi(z))|0\rangle, \quad (3.35)$$

and let $\psi(x)$ and $\bar\psi(y)$ recede to $+\infty$ and $-\infty$, respectively. We then get the relation

$$\langle p|ig\bar\psi\gamma_5\tau_i\psi|-q\rangle=\frac{k^2+\mu^2}{4\kappa^2}\int\frac{(-\kappa)^{\lambda}(-\kappa)^{\lambda'}}{k^2+w}\nu_{\lambda\lambda'}{}^{0}(\kappa\kappa w)\times dw\langle p|i\gamma_5\tau_i|-q\rangle, \quad (3.36)$$

where $|p\rangle$ and $|-q\rangle$ represent one-nucleon states and $\nu_{\lambda\lambda'}{}^{0}(\kappa\kappa w)$ the magnitude of ν at the point spectrum $u=v=\kappa^2$. This is nothing but the matrix element for the "current" $ig\bar\psi\gamma_5\tau_i\psi$, and we may define the charge as the coefficient of $i\gamma_5\tau_i$ in the static limit $p=-q$, $k=0$:

$$g'\equiv\int\frac{(-\kappa)^{\lambda+\lambda'}}{4\kappa^2}\frac{\mu^2}{w}\nu_{\lambda\lambda'}{}^{0}(\kappa\kappa w)dw=g+\int_{(2\kappa)^2}^{\infty}\frac{(-\kappa)^{\lambda+\lambda'}}{4\kappa^2}\frac{\mu^2}{w}\nu_{\lambda\lambda'}{}^{0}(\kappa\kappa w)dw. \quad (3.37)$$

g' is thus directly related to an ideal measurement whereas g does not allow such an interpretation, since a real nucleon cannot absorb or emit a real meson. The customary definition of renormalization due to Dyson[8] gives g'.

C. Four-Body Green's Functions

There are three four-body functions which do not vanish identically. They correspond to meson-nucleon, nucleon-nucleon, and meson-meson scattering respectively.

As the first example, we take

$$\rho(xyzz')=T(xyzz')-T(xy)T(zz'), \quad (3.38)$$

and its Fourier transform

$$\rho(pqkk')=\frac{1}{(2\pi)^{16}}\int e^{-ipx-iqy-ikz-ik'z'}\rho(xyzz')\times(dx)^4(dy)^4(dz)^4(dz')^4. \quad (3.39)$$

In view of the conservation law[18]

$$p+q+k+k'=0, \quad (3.40)$$

we have six independent scalars of the momenta, for which we adopt

$$p^2,\ q^2,\ k^2,\ k'^2,\quad (p+q)^2=(k+k')^2,$$
$$(p+k)^2=(q+k')^2 \quad\text{or}\quad (p+k')^2=(q+k)^2,$$

as will be found convenient below. In addition, there are three scalars formed with the Dirac matrices, which may be chosen as

$$ip\gamma,\ -iq\gamma,\ i(p+k,\gamma) \quad\text{or}\quad i(p+k',\gamma),$$

and the two isotopic tensors δ_{ij} and $\tau_{ij}=[\tau_i,\tau_j]/2i$. ρ should be invariant under charge conjugation C: $p\leftrightarrow q$, $\gamma\rightarrow-\gamma$, $\tau_{ij}\rightarrow-\tau_{ij}$; obviously it is also invariant against the interchange C': $k\leftrightarrow k'$, $i\leftrightarrow j$, but we can easily see that $CC'=1$. Thus we may write the general form of ρ as

$$\rho(pqkk')=i\delta(p+q+k+k')(1+C')\times\sum_{\lambda=0,1}(ip\gamma)^{\lambda_1}(i\overline{p+k}\gamma)^{\lambda_2}(-iq\gamma)^{\lambda_3}(i\tau)^{\lambda_4}\times\rho_{\lambda_1\lambda_2\lambda_3\lambda_4}(p^2,q^2,k^2,k'^2,(p+q)^2,(p+k)^2). \quad (3.41)$$

We can then apply the argument of real processes to $\rho_{\lambda_1\cdots\lambda_4}$ and conclude that it must have factors

$$\frac{1}{p^2+u},\ \frac{1}{q^2+v},\ \frac{1}{k^2+w},\ \frac{1}{k'^2+w'},$$
$$\frac{1}{(p+q)^2+s_1},\ \frac{1}{(p+k)^2+s_2},\ \text{or}\ \frac{1}{(p+k')^2+s_2'}, \quad (3.42)$$
$$u,\ v=\kappa^2\ \text{or}\ \geq(\kappa+\mu)^2,\quad w,\ w'=\mu^2\ \text{or}\ \geq(3\mu)^2,$$
$$s_1\geq(2\mu)^2,\quad S_2=\kappa^2\ \text{or}\ \geq(\mu+\kappa)^2.^{18}$$

[18] Since ρ represents the irreducible correlation, no subdivision like $p+q=0$, $k+k'=0$ can occur, which is the reason for taking ρ rather than T.

[18] The thresholds for w, w', and s_1 are characteristic of the pseudoscalar meson theory.

The indicated behavior of the denominators at a singularity is universal. To show this for $1/(p+k)^2+\bar{s}_2$, for example, we may choose $x_0, z_0 > y_0, z_0'$ or $x_0, z_0 < y_0, z_0'$, so that

$$T(xyzz') = \sum_n \langle 0|T(\psi(x)\varphi_i(z))|n\rangle\langle n|T(\bar{\psi}(y)\varphi_j(z')|0\rangle, \quad x_0, z_0 > y_0, z_0'$$

$$= -\sum_n \langle 0|T(\bar{\psi}(y)\varphi_j(z'))|n\rangle\langle n|T(\psi(x)\varphi_i(z))|0\rangle, \quad x_0, z_0 < y_0', z_0'$$

which gives a factor $\exp[-i|(p_0+k_0)(x_0+z_0-y_0-z_0')|]$ similar to the previous cases.

Since $\rho(xyzz')$ obeys an equation of motion

$$(\gamma\partial+\kappa)_x(-\gamma^T\partial+\kappa)_y(\Box-\mu^2)_z(\Box-\mu^2)_{z'}\rho = g^2\{\delta(x-z)\delta(y-z')\gamma_5\tau_i\rho(xy)\gamma_5\tau_j + (z\leftrightarrow z', i\leftrightarrow j)\}+\cdots, \quad (3.43)$$

the first four factors always occur simultaneously, but the last one is missing for the first term on the right of Eq. (3.43). At any rate we may write

$$\rho_{\lambda_1\cdots\lambda_4} = \int \frac{\nu_{\lambda_1\cdots\lambda_4}(uvu'v's_1s_2)\,du\,dv\,du'\,dv'\,ds_1\,ds_2}{(p^2+\bar{u})(q^2+\bar{v})(k^2+\bar{w})(k'^2+\bar{w}')((p+q)^2+\bar{s}_1)((p+k)^2+\bar{s}_2)}, \quad (3.44)$$

if we understand that $\nu_{\lambda_1\cdots\lambda_4}$ may have delta functions at infinity: $s_1\delta(s_1-\infty)=\delta(1-\infty/s_1)$ and/or $s_2\delta(s_2-\infty)=\delta(1-\infty/s_2)$.

On the other hand, the boundary condition for $\rho(xyzz')$ should enable one to define the direct four-body interaction of the form $f_1\bar{\psi}\psi\varphi_i^2+if_2\bar{\psi}\gamma_\mu\tau_i\psi\varphi_i\partial_\mu\varphi_j+\cdots$ as the value of ν at the point spectrum u, $v=\kappa^2$, w, $w'=\mu^2$, s_1, $s_2=\infty$. Since we exclude the existence of such an interaction, however, ν is zero at this point.[17]

The other four-body functions may be treated in a similar way. $\rho(z_1z_2z_3z_4)$ is simpler since no γ matrices are involved. The result is

$$\rho(k_1k_2k_3k_4) = -i\delta(\textstyle\sum k_i)\frac{1}{8}\sum_P \delta(i_1i_2)\delta(i_3i_4) \times\rho(k_1^2,k_2^2,k_3^2,k_4^2,(k_1+k_2)^2,(k_1+k_3)^2), \quad (3.45)$$

where $\rho(k_1^2\cdots)$ has the same structure as Eq. (3.44):

$$\rho = \int \frac{\nu(w_1w_2w_3w_4s_1s_2)}{\prod_i (k_i^2+w_i)\cdot[(k_1+k_2)^2+\bar{s}_1][(k_1+k_3)^2+\bar{s}_2]} \times\prod_i dw_i\cdot ds_1 ds_2, \quad (3.46)$$

and $\sum_P$ runs over the permutations of 1, 2, 3, 4. In this case ν does not have the delta functions $\delta(1-\infty/s_1)$ and $\delta(1-\infty/s_2)$ provided that the meson-meson direct interaction $(\lambda/4)\varphi_i^2\varphi_j^2$ does not really exist (which means that the renormalized λ is zero). In case λ is finite, ν should have a point spectrum

$$\nu = \nu^0(w_i)\delta(1-\infty/s_1)\delta(1-\infty/s_2)+\cdots, \quad \nu^0(w_i) = 2\lambda\textstyle\prod_i \delta(w_i-\mu_i^2)+\cdots, \quad (3.47)$$

whereby λ is exactly defined. On the other hand, the unrenormalized λ_0 is expressed by (see Appendix)

$$\int \nu^0(w_i)\prod_i dw_i = 2\lambda Z_4 Z_3^{-4} = 2\lambda_0 Z_3^{-2}. \quad (3.48)$$

As for $\rho(xx'yy')$, we have two sets of γ matrices and three independent momenta which give $2\times3=6$ scalars of the form $(p\gamma)$; in addition, five scalars may be formed out of the γ's as is familiar in the β-decay theory. In the isotopic space, there are two scalars 1 and $\tau\cdot\tau'$. We put accordingly

$$\rho(pp'qq') = \delta(p+p'+q+q') \times\tfrac{1}{4}(1+C)(1-P)\sum_{i=1}^{5}(ip\gamma)^{\lambda_1}(ip'\gamma')^{\lambda_2}O_i \times\{[i(p+p',\gamma+\gamma')]^{\lambda_3},[i(p+q,\gamma-\gamma')]^{\lambda_4}\}O_i' \times(-iq\gamma)^{\lambda_5}(-iq'\gamma')^{\lambda_6}(\tau\cdot\tau')^{\lambda_7} \times\rho_{\lambda_1\cdots\lambda_7}(p^2,p'^2,q^2,q'^2,(p+p')^2,(p+q)^2). \quad (3.49)$$

$O_i\cdot O_i'$ stands for the five scalars $1\cdot1$, $\gamma_\mu\gamma_\mu'$, etc.; P means the permutation $p\alpha s\leftrightarrow p'\alpha's'$, and C the charge conjugation $p\leftrightarrow q$, $p'\leftrightarrow q'$, $\gamma\to-\gamma$, $\gamma'\to-\gamma'$, $O_i\leftrightarrow O_i'$. $\rho_{\lambda_1\ldots\lambda_7}$ may be written as before

$$\rho_{\lambda_1\cdots\lambda_7} = \int \frac{\nu_{\lambda_1\cdots\lambda_7}(uu'vv's_1s_2)\,du\,du'\,dv\,dv'\,ds_1\,ds_2}{(p^2+\bar{u})(p'^2+\bar{u})(q^2+\bar{v})(q'^2+\bar{v})[(p+p')^2+\bar{s}_1][(p+q)^2+\bar{s}_2]}, \quad (3.50)$$

with similar point spectra as in the case of $\rho(xyzz')$, namely $\delta(u-\kappa^2)$, $\delta(u'-\kappa^2)$, $\delta(v-\kappa^2)$, $\delta(v'-\kappa^2)$, and $\delta(1-\infty/s_1)$.

4. RELATION BETWEEN THE SPECTRAL FUNCTIONS

So far the structure of the Green's functions has been determined in a way which reflects to a large extent only the fundamental assumptions of field theory. Now we are going to take full account of the equations of motion and see how they are translated into relations

[17] We can also show, on the basis of Eq. (3.43), that $\delta(1-\infty/s_1)$ does not occur at all, and at u, $v=\kappa^2$, w, $w'=\mu^2$, $s_1=\infty$, $s_2=\kappa^2$, ν is exactly given by the lowest perturbation result:

$$\nu_{\lambda_1\cdots\lambda_4} = g^8\nu_{\lambda_1\cdots\lambda_4}{}^0\delta(u-\kappa^2)\delta(v-\kappa^2)\delta(w-\mu^2) \times\delta(w'-\mu^2)\delta(1-\infty/s_1)\delta(s_2-\kappa^2),$$

$$\nu_{\lambda_1\cdots\lambda_4}{}^0 = (-\kappa)^{2-\lambda_1-\lambda_2}\kappa^{\lambda_3+\lambda_4},$$

where g is the constant defined in (ii). But this will need a detailed analysis of Eq. (3.43) (or the relation between different ν functions to be discussed later), and is not of the nature of a boundary condition for ν that can be imposed at our choice.

between the various spectral functions introduced in the last section.

According to Sec. 2, there are a set of equations which connect the Green's functions of different order. If we substitute the parametric representation of the Green's functions developed in the last section in these equations, we should be able to obtain the corresponding equations of motion for the spectral functions ν. In explicitly carrying this out, we naturally meet with divergences due to the singularities of the Green's functions, making the results meaningless unless they are renormalized. Since in our representation of the Green's functions their dependence on the relative coordinates or momenta is clearly exhibited by the energy denominators, such a renormalization procedure can be carried through explicitly without tampering with the ν functions, and the ensuing relation between the ν functions will be in a manifestly renormalized, divergence-free form. We will discuss this procedure for each equation successively.

(i) Let us begin with one of the lowest order equations:

$$(\gamma_\mu\partial_\mu+\kappa)\rho(xy) = -i\delta(xy)-ig\gamma_\delta\tau_j\int\rho(xyz_j')\delta(x-z')(dz')^4. \quad (4.1)$$

Going to the momentum representation and using the formulas Eqs. (3.2), (3.4), (3.26), and (3.30), we get

$$\begin{aligned} &i\int(ip\gamma+\kappa)\frac{(ip\gamma)^\lambda\nu_\lambda(u)}{p^2+u}du \\ &=-i+\frac{g}{(2\pi)^4}\int\delta(p'+k-p)dp'dk \\ &\times\int\frac{\gamma_\delta\tau_j(ip'\gamma)^\lambda\gamma_\delta\tau_j(-iq\gamma)^{\lambda'}\nu_{\lambda\lambda'}(uvw)}{(p'^2+u)(q^2+v)(k^2+w)}dudvdw \\ &=-i+\frac{3g}{(2\pi)^4}\int dk \\ &\times\int\frac{[-i(p-k,\gamma)]^\lambda(-iq\gamma)^{\lambda'}\nu_{\lambda\lambda'}(uvw)}{[(p-k)^2+u](q^2+v)(k^2+w)}dudvdw. \quad (4.2)\end{aligned}$$

Assuming that the integrations in k and the other variables can be interchanged in order freely, we may first carry out the integration

$$I_\lambda(p)\equiv\frac{-i}{(2\pi)^4}\int\frac{(-i(p-k,\gamma))^\lambda}{[(p-k)^2+u](k^2+w)}dk, \quad \lambda=0,1, \quad (4.3)$$

which is obviously divergent logarithmically. It is formally equivalent to the lowest order self-energy

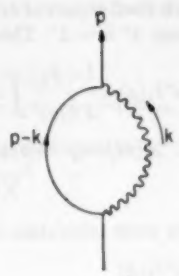

FIG. 1. A self-energy diagram corresponding to Eq. (4.3).

(Fig. 1)

$$\begin{aligned}\sum(p)&=\frac{g^2i}{(2\pi)^4}\int\gamma_\delta\tau_jS_F(p-k)\gamma_\delta\tau_j\Delta_F(k)dk \\ &=-\frac{3g^2i}{(2\pi)^4}\int\frac{i(p-k,\gamma)+\kappa}{[(p-k)^2+\bar\kappa^2](k^2+\bar\mu^2)}dk,\end{aligned}$$

if we put $u=\kappa^2$, $w=\mu^2$, so that the renormalization could be carried out by the standard methods. Instead of doing this, however, we will again make use of the causality requirement in a trick originally due to Lehmann.[2]

$I_\lambda(p)$ is the Fourier component of the function

$$I_\lambda(x)=i[(-\gamma_\mu\partial_\mu)^\lambda\Delta_F^{(u)}(x)]\Delta_F^{(w)}(x), \quad (4.4)$$

where $\Delta_F^{(u)}$, $\Delta_F^{(w)}$ are the Feynman propagation functions with the masses $\sqrt{u}$ and $\sqrt{w}$, and are defined conveniently as

$$\begin{aligned}(-\gamma_\mu\partial_\mu)^\lambda\Delta_F^{(u)}(x)&=\theta(x)(-\gamma_\mu\partial_\mu)^\lambda\Delta^{(u)+}(x) \\ &\quad+\theta(-x)(-\gamma_\mu\partial_\mu)^\lambda\Delta^{(u)-}(x), \quad (4.5)\\ \Delta_F^{(w)}(x)&=\theta(x)\Delta^{(w)+}(x)+\theta(-x)\Delta^{(w)-}(x),\end{aligned}$$

$\Delta^\pm(x)$ being a function containing only positive or negative frequency part:

$$\Delta^{(u)\pm}(x)=\frac{1}{(2\pi)^3}\int\theta(\pm k)\delta(k^2+u)e^{ikx}dk. \quad (4.6)$$

We now ask for the "imaginary part" of $I_\lambda(p)$ which expresses possible real processes. In the present case, a real process would mean that the incident wave of four-momentum $p(p_0>0)$ splits up into two "particles" of mass $\sqrt{u}$ and $\sqrt{v}$, four-momentum $p-k$ $(p_0-k_0>0)$, and $k(k_0>0)$. Such a process certainly corresponds to the first term of

$$\begin{aligned}&\theta(x)[(-\gamma_\mu\partial_\mu)^\lambda\Delta^{(u)+}(x)]\theta(x)\Delta^{(w)+}(x) \\ &=\theta(x)[(-\gamma_\mu\partial_\mu)\Delta^{(u)+}(x)]\Delta^{(w)+}(x) \\ &=\tfrac{1}{2}[(-\gamma_\mu\partial_\mu)\Delta^{(u)+}(x)]\Delta^{(w)+}(x) \\ &\quad+\frac{\epsilon(x)}{2}[(-\gamma_\mu\partial_\mu)^\lambda\Delta^{(u)+}(x)]\Delta^{(w)+}(x),\end{aligned}$$

which itself is part of $I_\lambda(x)$. If $p_0<0$, we have simply to change Δ^+ into Δ^-. Thus

$$\text{"Im"}I_\lambda(p)=\frac{1}{2}\frac{1}{(2\pi)^2}\int(-i\gamma,\,p-k)^\lambda \times[\theta(p)\theta(p-k)\theta(k)+\theta(-p)\theta(k-p)\theta(-k)] \times\delta((p-k)^2+u)\delta(k^2+v)dk. \quad (4.7)$$

After some calculation (see Appendix 2) it leads to

$$\text{"Im"}I_\lambda(p) =\frac{1}{8\pi}\frac{S(u,w,-p^2)}{-p^2}[C(u,w,-p^2)(-ip\gamma)]^\lambda$$

$$2S(u,w,-p^2) =\{[(\sqrt{u}+\sqrt{w})^2+p^2][(\sqrt{u}-\sqrt{w})^2+p^2]\}^{\frac{1}{2}}, \quad \sqrt{-p^2}\geq\sqrt{u}+\sqrt{w} \quad (4.8)$$

$$=0, \quad \text{otherwise}$$

$$C(u,w,-p^2)=(-u+w+p^2)/2p^2.$$

$S/2$ is the area of a non-Euclidean triangle formed with the three sides of length $\sqrt{u}$, $\sqrt{w}$, $\sqrt{-p^2}$, and C is the ratio of the projection of the side $\sqrt{u}$ onto $\sqrt{-p^2}$ to $\sqrt{-p^2}$.

Once the imaginary part has been calculated, it is now easy to obtain the whole "renormalized" I_λ by means of the formula (3.19):

$$I_\lambda^{(n)}(p)\equiv\frac{1}{8\pi^2}\int\frac{\bar{u}}{p^2+\bar{u}}\left(\frac{a+p^2}{a-u'}\right)^n\frac{S(uwu')}{u'} \times[C(uwu')(-ip\gamma)]^\lambda du'. \quad (4.9)$$

Since $S/u'\sim1$, $C\sim1$ for large u', n must be ≥1, and $a<\sqrt{u}+\sqrt{w}$. We put the result into the righthand side of Eq. (4.2). Remembering that $p=-q$, we have now a product of two factors

$$\frac{1}{p^2+\bar{u}'}\frac{1}{p^2+\bar{v}}=\frac{1}{v-u'}\left(\frac{1}{p^2+\bar{u}'}-\frac{1}{p^2+\bar{v}}\right).$$

As the last step, we divide Eq. (4.2) by $(ip\gamma+\kappa)$, and again the "imaginary parts" of both sides may be compared for a given p, and thus the relation between the ν's obtained except at the point $u=\kappa^2$. At $u=\kappa^2$, instead, we have to invoke the boundary condition (3.13) to renormalize ν correctly. Thus

$$\nu_\lambda(u)=\delta(u-\kappa^2)+\frac{3g}{8\pi^2}\frac{1}{u-\kappa^2}\int\frac{1}{u-v} \times\left[\frac{S(u'wu)}{u}K_{1\lambda\lambda'}(u'wu)\nu_{\lambda\lambda'}(u'vw) +\left(\frac{u-\kappa^2}{v-\kappa^2}\right)^2\frac{S(u'wv)}{v}K_{1\lambda\lambda'}(u'wv) \times\nu_{\lambda\lambda'}(u'uw)\right]du'dvdw,$$

$$\nu_0(u)=-\kappa\delta(u-\kappa^2)+\frac{3g}{8\pi^2}\frac{1}{u-\kappa^2}\int\frac{1}{u-v} \times\left[\frac{S(u'wu)}{u}K_{2\lambda}{}'(u'wu)\nu_{\lambda\lambda'}(u'vw) +\left(\frac{u-\kappa^2}{v-\kappa^2}\right)^2\frac{S(u'wv)}{v}K_{2\lambda\lambda'}(u'wv) \times\nu_{\lambda\lambda'}(u'uw)\right]du'dvdw, \quad (4.10)$$

$$K_{1\lambda\lambda'}(u'wu)=\begin{pmatrix}-1 & \kappa\\ -C(u'wu)\kappa & C(u'wu)u\end{pmatrix},$$

$$K_{2\lambda\lambda'}(u'wu)=\begin{pmatrix}\kappa & -u\\ C(u'wu)u & -C(u'wu)u\kappa\end{pmatrix}.$$

It has been so designed that, with $a=\kappa^2$ and $n=1$ or 2 depending on the individual term, the integrals in Eq. (4.10) are convergent, reduce to zero for $u=\kappa^2$, and that ν_λ satisfies the condition (3.16) if a similar condition holds for $\nu_{\lambda\lambda'}$. The second point is essential for the correct renormalization according to Eq. (3.13). The factor $1/(u-v)$ in the integrands is to be interpreted as the principal value.

The equation of motion for $\rho(zz')$ may be treated in a similar way. We have namely

$$(\Box-\mu^2)_z\rho(zz')=i\delta(zz')-gg\int\text{tr}[\gamma_5\tau_r\rho(xyz')] \times\delta(x-z)\delta(y-z)(dx)^4(dy)^4, \quad (4.11)$$

or substituting the parametric representation,

$$i\int\frac{k^2+\mu^2}{k^2+v\bar{v}}\nu(w)dw=i-\frac{ig}{(2\pi)^4}\int\delta(p+q+k)dpdq \times\int\frac{\text{tr}[i\gamma_5\tau_s(ip\gamma)^\lambda\gamma_5\tau_j(-iq\gamma)^{\lambda'}]}{(p^2+\bar{u})(q^2+\bar{v})(k^2+v\bar{v})} \times\nu_{\lambda\lambda'}(uvw)dudvdw, \quad (4.12)$$

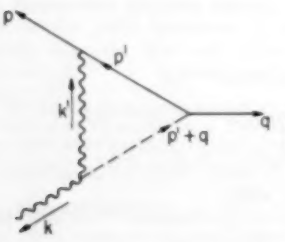

FIG. 2. A vertex part diagram corresponding to Eq. (4.18).

which is of the same nature as Eq. (4.2). We quote the final result only.

$$\nu(w)=\delta(w-\mu^2)+\frac{1}{w-\mu^2}\frac{3g^2}{2\pi^2}\int\frac{1}{w-w'}\times\left[\frac{S(uvw)}{w}H_{\lambda\lambda'}(uvw)\nu_{\lambda\lambda'}(uvw')+\left(\frac{w-\mu^2}{w'-\mu^2}\right)^2\frac{S(uvw')}{w'}H_{\lambda\lambda'}(uvw')\times\nu_{\lambda\lambda'}(uvw)\right]dudvdw', \tag{4.13}$$

$$H_{\lambda\lambda'}(uvw)=\begin{pmatrix}1 & 0\\ 0 & \frac{1}{2}(w-u-v)\end{pmatrix}.$$

(ii) The three-body Green's function $\rho(xyz)$ obeys the equations of motion

$$(\gamma\partial+\kappa)_{\alpha}\rho(xyzi)=-ig\int\gamma_{\delta}\tau_j[\rho(xy)\rho(zix'j)+\rho(xyzix'j)]\delta(x-x')(dx')^4,$$

$$(\Box-\mu^2)_{\alpha}\rho(xyzi)=ig\int[-\rho(xy)\,\mathrm{tr}[\gamma_{\delta}\tau_{\epsilon}\rho(x'y')]+\rho(xy')\gamma_{\delta}\tau_{\epsilon}\rho(x'y)+\rho(xx'\alpha s,yy'\beta t)(\gamma_{\delta}\tau_i)_{\beta t,\alpha s}]\times\delta(x'-z)\delta(y'-z)(dx')^4(dy')^4, \tag{4.14}$$

of which we will consider here only the first equation. Going over to the Fourier component, we get

$$(ip\gamma+\kappa)\rho(pqk)=-ig\gamma_{\delta}\tau_j\left[\rho(q)\rho_{ij}(k)\delta(p+q+k)+\frac{1}{(2\pi)^4}\int\rho(p'qkik'j)\delta(p'+k'-p)dp'dk'\right]. \tag{4.15}$$

We may divide ρ into ρ_a and ρ_b, corresponding respectively to the two terms on the right-hand side. Inserting the expression for $\rho(q)$ and $\rho_{ij}(k)$, Eqs. (3.2) and (3.4), we find easily

$$\rho_a(pqk)=-ig\delta(p+q+k)\frac{ip\gamma-\kappa}{p^2+\kappa^2}\gamma_{\delta}\tau_i\times\int\frac{(-iq\gamma)^{\lambda}\nu_{\lambda}(v)\nu(w)}{(q^2+\bar{v})(k^2+w)}dvdw, \tag{4.16}$$

or using the representation Eqs. (3.26) and (3.30) for $\rho(pqk)$,

$$\nu_{a\lambda\lambda'}(uvw)=g(-\kappa)^{1-\lambda}\delta(u-\kappa^2)\nu_{\lambda'}(v)\nu(w). \tag{4.17}$$

As for ρ_b, it may further be divided into two corresponding to the two terms of Eq. (3.41):

$$\rho(p'qkk')=\delta(p'+q+k+k')(1+C)(ip'\gamma)^{\lambda_1}\times(i(p'+k,\gamma))^{\lambda_2}(-iq\gamma)^{\lambda_3}(\tau)^{\lambda_4}\rho_{\lambda_1\cdots\lambda_4},$$

which we call ρ_b' and ρ_b''. Let us first consider ρ_b''. We have to carry out the integration[18]

$$I_{\lambda}(pqk)\equiv\frac{-i}{(2\pi)^4}\times\int\frac{(ip'\gamma)^{\lambda}\delta(p'+k'-p)}{(p'^2+\bar{u})(k'^2+w)((p'+q)^2+\bar{s}_1)}dp'dk', \tag{4.18}$$

which is similar to the lowest order vertex part represented by the Feynman diagram Fig. 2, so that we would expect to find I_{λ} in the form

$$I_{\lambda}=\int\frac{[i(ap+bq),\gamma]^{\lambda}}{(p+\bar{u}_1)(q^2+\bar{v}_1)(k^2+w_1)}\times f(u_1v_1w_1)du_1dv_1dw_1. \tag{4.19}$$

To obtain directly the renormalized finite expression for I_{λ}, we again avail ourselves of the method used in connection with (i). I_{λ} is the Fourier component of the quantity

$$I_{\lambda}(xyz)=-[(\gamma_{\mu}\partial_{\mu})^{\lambda}\Delta_{F^{(w)}}(x-y)]\times\Delta_{F^{(s)}}(x-z)\Delta_{F^{(s_1)}}(y-z). \tag{4.20}$$

Let us then ask for that part of I_{λ} where all the three internal lines p', k', p', $+k$ contribute to real processes. Suppose that $p_0>0$, $k_0<0$ (or $p_0<0$, $k_0>0$), and large enough to create real processes. In this case the internal "real" particles must be moving in the direction (or opposite) indicated in Fig. 2. Since p' and $p'+q$ point to opposite directions seen from the external line q, q cannot create a real process under such circumstances. This means that when the two denominators p'^2+u, k'^2+w become zero, the third does not, which amounts to a certain restriction on the range of the values of u, w, and s_1. At any rate, the "imaginary part" of I_{λ} arising from the above mentioned process comes, using Eq. (2.5), from the ϵ-independent part of

$$-\sum_{\pm}\theta(\pm(x-y))\theta(\pm(x-z))\theta(\pm(y-z))\times[(\gamma_{\mu}\partial_{\mu})^{\lambda}\Delta^{(w)\pm}(x-y)]\Delta^{(w)\pm}(x-z)\Delta^{(s_1)\pm}(y-z)$$

$$=-\sum_{\pm}\frac{1\pm\epsilon(x-y)}{2}\frac{1\pm\epsilon(y-z)}{2}[(\gamma_{\mu}\partial_{\mu})^{\lambda}\Delta^{(w)\pm}(x-y)]\times\Delta^{(w)\pm}(x-z)\Delta^{(s_1)\pm}(y-z), \tag{4.21}$$

[18] In case $s_1=\infty$, it reduces to the type of Eq. (4.3).

which leads to

$$-\frac{1}{2\pi}\frac{1}{4}\int[\theta(p)\theta(-k)\theta(p')\theta(p'+q)\theta(k')$$
$$+\theta(p)\theta(k)\theta(-p')\theta(-p'-q)\theta(-k')]$$
$$\times(ip'\gamma)^\lambda\delta(p'^2+u)\delta((p'+q)^2+s_1)$$
$$\times\delta(k'^2+w)\delta(p'+k-p)dp'dk'. \quad (4.22)$$

This must be equated to the corresponding "imaginary part" of Eq. (4.19):

$$\text{"Im"}I_\lambda=(i\pi)^2\int\frac{[i(ap+bq,\gamma)]^\lambda}{q^2+v_1}f(u_1v_1w_1)dv_1,$$
$$u_1=-p^2,\quad w_1=-k^2. \quad (4.23)$$

Evaluating Eq. (4.22), we get (see Appendix 2):

$$\text{"Im"}I_\lambda=-\tfrac{1}{16}(\theta(k)\theta(-p)$$
$$+\theta(-k)\theta(p))\frac{[i(a'p+b'q,\gamma)]^\lambda}{S(u_1,w_1,-q^2)}, \quad (4.24)$$
$$4S^2a'=2(u_1+u-w)q^2+(u_1-q^2-w_1)(u-q^2-s_1),$$
$$4S^2b'=2(u-q^2-s_1)u_1+(u_1+u-w)(u_1-q^2-w_1).$$

S is defined in Eq. (4.8), and the arguments u_1, w_1, $-q^2$ subject to the condition

$$\sqrt{u_1}\geq\sqrt{u}+\sqrt{w},\quad \sqrt{w_1}\geq\sqrt{s_1}+\sqrt{w},$$
$$-q^2\leq(\sqrt{s_1}-\sqrt{u})^2. \quad (4.25)$$

Equation (4.23) is still of an integral form, and we do not know the domain of v_1 yet. But if we make an analytic continuation of $-q^2$ to the unknown domain of v_1, Eq. (4.24) should acquire an imaginary part due to the pole at $v_1-i\epsilon$. On the other hand, Eq. (4.24) becomes imaginary only if $-q^2$ is such as to make the factor under the root sign in S [Eq. (4.8)] negative, or

$$(\sqrt{u_1}+\sqrt{w_1})^2\geq-q^2\geq(\sqrt{u_1}-\sqrt{w_1})^2. \quad (4.26)$$

Hence the domain of v_1 should agree with that of $-q^2$ above, and comparing these new "imaginary parts" we finally get

$$f(u_1v_1w_1)=\frac{1}{16\pi^3}\frac{1}{S^*(u_1v_1w_1)},$$
$$S^*(u_1v_1w_1)=[(\sqrt{u_1}+\sqrt{v_1}+\sqrt{w_1})$$
$$\times(\sqrt{u_1}+\sqrt{v_1}-\sqrt{w_1})$$
$$\times(\sqrt{u_1}-\sqrt{v_1}+\sqrt{w_1}) \quad (4.27)$$
$$\times(-\sqrt{u_1}+\sqrt{v_1}+\sqrt{w_1})]^{\frac{1}{2}},$$
$$4S^{*2}a=2(u_1+u-w)v_1-(u_1+v_1-w_1)(u+v_1-s_1),$$
$$4S^{*2}b=-2(u+v_1-s_1)u_1$$
$$-(u_1+u-w)(u_1+v_1-w_1).$$

$S^*/2$ is the area of an Euclidean triangle with the familiar relations

$$\sqrt{u_1}+\sqrt{v_1}\geq\sqrt{w_1}\geq|\sqrt{u_1}-\sqrt{v_1}|,$$
$$\sqrt{v_1}+\sqrt{w_1}\geq\sqrt{u_1}\geq|\sqrt{v_1}-\sqrt{w_1}|, \quad (4.28)$$
$$\sqrt{w_1}+\sqrt{u_1}\geq\sqrt{v_1}\geq|\sqrt{w_1}-\sqrt{u_1}|,$$

which limit the domain of the variables together with the restriction

$$\sqrt{u_1}\geq\sqrt{u}+\sqrt{w},\quad \sqrt{w_1}\geq\sqrt{s_1}+\sqrt{w},$$
$$\sqrt{v_1}\geq\sqrt{u}+\sqrt{s_1}. \quad (4.29)$$

The last condition simply indicates the threshold values of $-p^2$, $-k^2$, and $-q^2$ for creating real processes.

We thus obtain

$$I_\lambda(pqk)=\frac{1}{16\pi^3}$$
$$\times\int\frac{[i(ap+bq,\gamma)]^\lambda}{(p^2+\bar{u}_1)(q^2+\bar{v}_1)(k^2+\bar{w}_1)}\frac{du_1dv_1dw_1}{S^*(u_1v_1w_1)}, \quad (4.30)$$

which is certainly convergent [without use of the modified formula (3.19)] because of the triangular relation (4.28). The θ factors in Eq. (4.24) have dropped out also because of the triangular relation which effectively takes care of them. I_λ being thus determined, we substitute it into the equation for

$$(ip\gamma+\kappa)\rho_b''(pqk)=g\gamma_s\tau_f\frac{1}{16\pi^3}\int\frac{[i(ap+bq,\gamma)]^{\lambda_1}(ip\gamma)^{\lambda_2}(-iq\gamma)^{\lambda_3}(\tau)^{\lambda_4}}{(p^2+\bar{u}_1)(q^2+\bar{v}_1)(k^2+\bar{w}_1)(p^2+\bar{s}_2)(q^2+\bar{v})(k^2+\bar{w}')}$$
$$\times\frac{\nu_{\lambda_1\cdots\lambda_4}(uvww's_1s_2)}{S^*(u_1v_1w_1)}du_1dv_1dw_1dudvdwdw'ds_1ds_2. \quad (4.31)$$

We put the representation (3.30) for $\rho_b''(pqk)$ on the left-hand side, divide the whole thing by $ip\gamma+\kappa$, transform products of factors like $1/(q^2+\bar{v}_1)(q^2+\bar{v})$ on the right into partial fractions, and compare both sides (or their imaginary parts) for a given set of p^2, q^2 and k^2. We shall not write down the ensuing relation between $\nu_{b\lambda\lambda'}''(u_1v_1w_1)$ and $\nu_{\lambda_1\cdots\lambda_4}(uvww's_1s_2)$ since it is too complicated due to the spin matrices.

We are left with ρ_b' that corresponds to the first term of Eq. (3.41). The integral to be considered is now[19]

$$I_{\lambda_1\lambda_2}(pqk)\equiv\frac{-i}{(2\pi)^4}\int\frac{(ip'\gamma)^{\lambda_1}[i(p'+k,\gamma)]^{\lambda_2}\delta(p'+k'-p)}{(p'^2+\bar{u})(k'^2+\bar{w}')[(p'+q)^2+\bar{s}_1][(p'+k)^2+\bar{s}_2]}dp'dk', \tag{4.32}$$

which contains four denominators. A Feynman diagram for this is given in Fig. 3, where four external lines p, k, k, and $-p-2k=q-k$ come in. We assume the representation

$$I_{\lambda_1\lambda_2}''=\int\frac{[i(ap+bq,\gamma)]^{\lambda_1}[i(cp+dq,\gamma)]^{\lambda_2}-\Lambda\delta(2-\lambda_1-\lambda_2)}{(p^2+\bar{u}_1)(k^2+\bar{w}_1)(q^2+\bar{v}_1)}g(u_1v_1w_1)du_1dv_1dw_1. \tag{4.33}$$

To the simultaneous "imaginary part" for the three denominators of Eq. (4.33) with $p_0>0$, $k_0<0$, $(p+k)_0=-q_0>0$, for example, corresponds the following part of Eq. (4.32):

$$\begin{aligned}
&\text{"Im"}I_{\lambda_1\lambda_2}\\
&=-\frac{2(\pi i)^4}{(2\pi)^4}\int(ip'\gamma)^{\lambda_1}[i(p'+k,\gamma)]^{\lambda_2}\delta(p'^2+\bar{u})\delta(k'^2+\bar{w}')\\
&\quad\times\delta((p'+q)^2+s_1)\delta((p'+k)^2+s_2)\theta(p')\theta(k')\\
&\quad\times\{\theta(p'+k)\theta(p'+q)+\theta(-p'-k)\theta(-p''-q)\}\\
&\qquad\qquad\times\delta(p'+k'-p)dp'dk'.
\end{aligned}\tag{4.34}$$

By a procedure similar to that for Eq. (4.22) as explained in the Appendix, this yields

$$\begin{aligned}
&\text{"Im"}I_{00}=g(u_1v_1w_1)\\
&\quad=\frac{1}{64}\frac{1}{|S^*(u_1v_1w_1)|}\\
&\quad\times\delta(u+w'+v_1+w_1-s_1-s_2-u_1)\\
&\quad\times\theta(\sqrt{u_1}-\sqrt{u}-\sqrt{w'})\\
&\quad\times[\theta(\sqrt{w_1}-\sqrt{s_1}-\sqrt{w'})\theta(\sqrt{v_1}-\sqrt{w'}-\sqrt{s_2})\\
&\quad+\theta(\sqrt{w_1}-\sqrt{u}-\sqrt{s_2})\theta(\sqrt{v_1}-\sqrt{s_1}-\sqrt{u})],\\
&4S^{*2}a=2(u_1+u-w')v_1\\
&\qquad-(u_1+v_1-w_1)(u+v_1-s_1),\\
&4S^{*2}b=-2(u+v_1-s_1)u_1\\
&\qquad-(u_1+u-w)(u_1+v_1-w_1),\\
&4S^{*2}c=-2v_1(w_1+w'-v_1-u)\\
&\qquad-(u_1+v_1-w_1)(s_1+u_1-2v_1-w_1-u),\\
&4S^{*2}d=2u_1(s_1+u_1-2v_1-w_1-u)\\
&\qquad-(u_1+v_1-w_1)(w_1+w'-v_1-u),\\
&2\Lambda=-(u+u_1+v_1-w'-s_1-s_2)+2acu_1\\
&\qquad+2bdv_1-(ad+bc)(u_1+v_1-w_1).
\end{aligned}\tag{4.35}$$

[19] In case $s_1=\infty$, the integration reduces to the type of Eq. (4.18).

Finally, we piece together the equations for ν_a, ν_b', and ν_b'' to get one for the total $\nu_{\lambda\lambda'}$. The renormalization has not been completely taken into account since $\nu_{\lambda\lambda'}$ may not yet satisfy the required boundary condition (3.33). If we "correct" it to the value Eq. (3.33) we get the properly renormalized equation. The remaining part of the spectrum is already correct, and will not be affected.

5. DISCUSSION

The significance of what we have achieved here seems to lie in several points. To begin with, the Green's functions which have rather complicated transformation properties have been expressed in terms of the ν functions, or spectral functions, which are real scalar functions depending on scalar variables only. The Green's functions thus obtained satisfy the various requirements of field theory, including relativity and causality. It can easily be seen that the formulas given in NI for some scattering matrices are compatible with the present results. Our new representations are more general in the sense that they show the complete dependence of

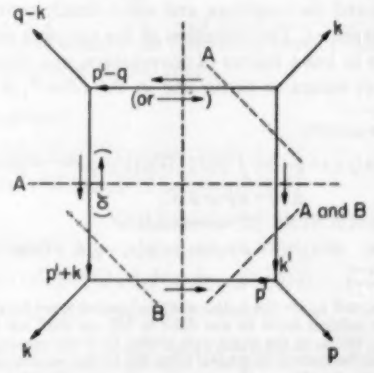

FIG. 3. A Feynman diagram corresponding to Eq. (4.32). The arrows beside the lines indicate the direction of motion of the "free" particles when the real processes corresponding to the "imaginary" part considered in the text are realized. These real processes occur across either set, A or B, of broken lines (intermediate states).

the matrix on all the variables. The results of NI follow from the present ones, but the converse is not true.[20]

As a matter of fact, our derivation of the formulas in Sec. 3 is not to be regarded as a proof; if we start from the fundamental assumptions I to IV, we do not know *a priori* whether we may use Eq. (3.17) rather than Eq. (3.19) to express the general Green's functions in terms of the ν functions. Thus in order to confirm our formulas we would have to show that they are actually consistent with the equations of motion connecting different Green's functions. This was done in our paper up to the four-body functions.

One undesirable character of the old formulas was that the density functions ρ introduced there did not seem to be uniquely defined, and there was no physical reason to prefer one over the other. In the present case, on the other hand, the ν functions have a well-defined meaning since they may be related directly to matrix elements of the "real processes."

As for the problem of renormalization, we have attained two remarkable results. One is that the equations of motion for the ν functions are in a manifestly renormalized form, and involve only renormalized constants. The other is that renormalization can be performed by making use of causality, together with the boundary condition for the field operators at infinity,[21] instead of going through the usual subtraction procedure. To put it more precisely, the real (or dispersive) part of a renormalized Green's function is determined from the imaginary (or absorptive) part via causality. Part of the imaginary part is connected with the corresponding part of different Green's functions via the equations of motion; the rest is theoretically at our disposal, being of the nature of a boundary condition (or inhomogeneous terms in the equation) which is fixed by the given fundamental constants, namely the masses and the couplings, and which finally controls all the quantities. The definition of the coupling constant is more or less a matter of convenience, and there is no absolute reason to prefer one to the other[22]; it would be sufficient if the relation between different coupling constants were known.

The equations of motion for the ν functions are the fundamental relations in our theory, which should provide us with all the necessary information about the system, though we do not know yet whether they have meaningful solutions at all. Neither are we quite sure whether the present renormalization is completely equivalent with the usual one. In the lowest approximation it seems to be the case (except for the slightly different definition of g), but it is well known that a self-energy operator calculated to a certain approximation can give rise to spurious singularities of $\rho(xy)$ or $\rho(zz')$ which may violate causality. It would thus seem that causality is necessary as an additional requirement to perform a consistent calculation if one believes in microscopic causality at all.

Källén[17] has investigated the nature of the renormalization constants, and has shown in particular that we run into contradiction if all the constants are assumed to be finite. In the present paper, not much attention has been focused on this problem since we have been trying to do away with unobservable quantities. The relation of the ν functions to the renormalization constants is discussed briefly in the Appendix.

To make a complete study of all these points mentioned above, it would be necessary to extend our formulation to the Green's functions of all orders which are connected by the equations of motion. This will be done in a separate paper. Though somewhat complicated, there seems to be no essential difficulty. It would also seem possible to give a similar formulation for the relativistic wave functions such as $\langle 0|T(\psi(x),\varphi(z),\cdots)|P\rangle$ which have been studied extensively.[8] Among other things, the bound state or scattering problems may be handled conveniently in our formulation, and a new insight into the boundary condition may be obtained.

The author would like to acknowledge his gratitude to Professor Goldberger and Dr. Freese for their interest and enlightening discussions.

APPENDIX

1. Renormalization Constants

In order to study the various renormalization constants we must start from the renormalized Lagrangian (2.9) which leads to the equations of motion

$$\begin{aligned}(\gamma\partial+\kappa)\psi &= -igZ_2^{-1}Z_1\gamma_5\tau_i\varphi_i\psi-\delta_2\psi,\\ (\Box-\mu^2)\varphi_i &= igZ_2^{-1}Z_1\bar{\psi}\gamma_5\tau_i\psi \\ &\qquad -\delta\mu^2\varphi_i-\lambda Z_3^{-1}Z_4\varphi_i\varphi_k^2,\end{aligned} \tag{A1}$$

and the commutation relations

$$\begin{aligned}\{\psi_{\alpha s}(r),\bar{\psi}_{\beta t}(r')\} &= Z_2^{-1}(\gamma_4)_{\alpha\beta}\delta_{st}\delta(r-r'),\\ [\varphi_i(r),\partial\varphi_k(r')/\partial t] &= iZ_3^{-1}\delta_{ik}\delta(r-r').\end{aligned} \tag{A2}$$

---

[20] The quantity

$$M(k,l)\delta(p+k-q-l)=\int\langle p|T(j_i(x)j_i(x'))|q\rangle e^{ikx'-ilx}(dx)^4(dx')^4,$$
$$j_i(x)=ig\bar{\psi}\gamma_5\tau_i\psi(x),$$

introduced in NI Eq. (17) corresponds to

$$\lim_{\substack{ip_\gamma+\kappa=0\\ iq_\gamma+\kappa=0}}(k^2+\mu^2)(l^2+\mu^2)\bar{u}_p(ip_\gamma+\kappa)\rho(p,-q,k,-l)(iq_\gamma+\kappa)u_q,$$

where u_q and v_p are the initial and final spinor wave functions. If we take spinless fields as was done in NI, we shall see that the terms ρ_2 and ρ_3 in the numerator of Eq. (1.3) are missing, which could not be derived in general from the earlier considerations.

[21] Ideas related to ours have also been developed by H. Lehmann[2] and W. Zimmermann, Nuovo cimento **11**, 416 (1952), Lehmann, Symanzik, and Zimmermann, Nuovo cimento **1**, 205 (1955). The significance of causality in the problem of renormalization has been noticed by Stueckelberg. See for example, E. C. G. Stueckelberg and T. A. Green, Helv. Phys. Acta **24**, 153 (1951).

[22] G. Källén, Nuovo cimento **12**, 217 (1954).

The equations of motion for the Green's functions become thus

$$\begin{aligned}(\gamma\partial+\kappa_0)\rho(xy)&=-iZ_2^{-1}\delta(x-y)-igZ_2^{-1}Z_1\gamma_\delta\tau_\epsilon\\&\quad\times\langle 0|T(\varphi_\epsilon\psi(x),\bar\psi(y))|0\rangle,\\(\Box-\mu_0^2)\rho(zz')&=iZ_3^{-1}\delta(z-z')+igZ_3^{-1}Z_1\\&\quad\times\langle 0|T(\bar\psi\gamma_\delta\tau_\epsilon\psi(z),\varphi_j(z'))|0\rangle\\&\quad-\lambda Z_3^{-1}Z_4\langle 0|T(\varphi_i\varphi_k^2(z),\varphi_j(z'))|0\rangle\text{ etc.},\end{aligned}\tag{A3}$$

where we have put

$$\kappa_0\equiv\kappa+\delta\kappa,\quad \mu_0^2\equiv\mu^2+\delta\mu^2,\tag{A4}$$

denoting the mechanical masses.

We will treat all the constants Z_i^{-1}, $\delta\kappa$, and $\delta\mu^2$ as if they were finite quantities. Taking the Fourier transforms, we substitute the parametric representation on the left-hand side. But this time we rewrite

$$\begin{aligned}i(ip\gamma+\kappa)\int\frac{(ip\gamma)\nu_1+\nu_0}{p^2+u}du&\\=-i\int\nu_1du&\\+i\int\frac{(ip\gamma)(\kappa\nu_1+\nu_0)+(u\nu_1+\kappa\nu_0)}{p^2+u}du,&\\i(k^2+\mu^2)\int\frac{\nu}{k^2+w}dw=i\int\nu dw+i\int\frac{\mu^2-w^2}{k^2+w}\nu dw,&\end{aligned}\tag{A5}$$

pretending convergence of each integral on the right. Comparing this with the right-hand side of Eq. (A3), we see that the first terms of Eq. (A5) must correspond to the first terms of Eq. (A3) since the other terms would have no singularities of the delta-function type if they were finite. Thus

$$\int\nu_1(u)du=Z_2^{-1},\quad\int\nu(w)dw=Z_3^{-1}.\tag{A6}$$

Next we differentiate Eq. (A3) once more and obtain

$$\begin{aligned}&(\gamma\partial+\kappa_0)_\epsilon(-\gamma^\tau\partial+\kappa_0)_\eta\rho(xy)\\&\quad=-iZ_2^{-1}(-\gamma^\tau\partial+\kappa_0)\delta(x-y)\\&\qquad-(gZ_2^{-1}Z_1)^2\langle 0|T(\gamma_\delta\tau_\epsilon\varphi_\epsilon\psi(x),\bar\psi\gamma_\delta\tau_j\varphi_j(y))|0\rangle,\\&(\Box-\mu_0^2)_\epsilon(\Box-\mu_0^2)_{\epsilon'}\rho(zz')\\&\quad=i(\Box-\mu^2)\delta(z-z')\\&\qquad-(gZ_3^{-1}Z_1)^2\langle 0|T(\bar\psi\gamma_\delta\tau_\epsilon\psi(z),\bar\psi\gamma_\delta\tau_{\epsilon'}\psi(z'))|0\rangle\\&\qquad-i\lambda Z_3^{-2}Z_4\delta_{ij}\delta(z-z')[\langle 0|\varphi_k^2(z)|0\rangle\\&\qquad\qquad+2\langle 0|\varphi_i\varphi_k(z)|0\rangle]\\&\qquad-i\lambda gZ_3^{-2}Z_1Z_4[\langle 0|T(\varphi_i\varphi_k^2(z),\bar\psi\gamma_\delta\tau_{\epsilon'}\psi(z'))|0\rangle\\&\qquad\qquad+\langle 0|T(\bar\psi\gamma_\delta\tau_\epsilon\psi(z),\varphi_j\varphi_k^2(z'))|0\rangle]\\&\qquad+(\lambda Z_3^{-1}Z_4)^2\langle 0|T(\varphi_i\varphi_k^2(z),\varphi_j\varphi_l^2(z'))|0\rangle.\end{aligned}\tag{A7}$$

The equations corresponding to Eq. (A5) become

$$\begin{aligned}-i(ip\gamma+\kappa_0)^2\int\frac{(ip\gamma)\nu_1+\nu_0}{p^2+u}du&=i\int(ip\gamma+\kappa_0)\nu_1du+i\int(\kappa\nu_1+\nu_0)du\\&\quad-i\int\frac{(ip\gamma)\{(\kappa^2+u)\nu_1+2\kappa\nu_0\}+\{2\kappa u\nu_1+(\kappa^2+u)\nu_0\}}{p^2+u}du,\\-i(k^2+\mu_0^2)\int\frac{\nu}{k^2+w}dw&=-i\int(k^2+\mu_0^2)\nu dw-i\int(\mu_0^2-w)\nu dw-i\int\frac{(\mu_0^2-w)^2}{k^2+w}\nu dw.\end{aligned}\tag{A8}$$

Comparison with Eq. (A7) leads to

$$\begin{aligned}&\int(\kappa\nu_1+\nu_0)du=0,\quad\text{or}\quad\kappa_0Z_2^{-1}=-\int\nu_0(u)du,\\&\int(\mu_0^2-w)\nu dw=5c\lambda Z_3^{-2}Z_4,\\&\text{or}\\&\mu_0^2Z_3^{-1}=\int\nu(w)wdw+5c\lambda Z_3^{-2}Z_4,\\&c\equiv\tfrac{1}{5}\langle 0|\varphi_i(x)\varphi_i(x)|0\rangle=\int\int\frac{\nu(w)}{k^2+w}dwdk.\end{aligned}\tag{A9}$$

If we take beforehand the Wick product[8]

$$\begin{aligned}\frac{\lambda}{4}:\varphi_i^2\varphi_k^2:=\frac{\lambda}{4}[&\varphi_i^2\varphi_k^2-2\varphi_i^2\langle\varphi_k^2\rangle-4\varphi_i\varphi_k\langle\varphi_i\varphi_k\rangle\\&+\langle\varphi_i^2\rangle\langle\varphi_k^2\rangle+2\langle\varphi_i\varphi_k\rangle^2],\end{aligned}$$

in the Lagrangian, the term with c will be absent.

Now let us consider the three-body Green's functions. The equations of motion read

$$\begin{aligned}&(\gamma\partial+\kappa_0)\rho(xyz)\\&\quad=-igZ_2^{-1}Z_1\langle 0|T(\gamma_\delta\tau_j\varphi_j\psi(x),\bar\psi(y),\varphi_i(z))|0\rangle\\&\quad=-igZ_2^{-1}Z_1[\gamma_\delta\tau_j\langle 0|T(\varphi_j(x),\varphi_i(z))|0\rangle\\&\qquad\times\langle 0|T(\psi(x),\bar\psi(y)|0\rangle+\cdots],\\&(\Box-\mu_0^2)\rho(zz')\\&\quad=igZ_3^{-1}Z_1\langle 0|T(\psi(x),\bar\psi(y),\bar\psi\gamma_\delta\tau_\epsilon\psi(z))|0\rangle\\&\quad=igZ_3^{-1}Z_1[\langle 0|T(\psi(x),\bar\psi(z))|0\rangle\gamma_\delta\tau_\epsilon\\&\qquad\times\langle 0|T(\psi(z),\bar\psi(y))|0\rangle+\cdots],\\&(\gamma\partial+\kappa_0)_\epsilon(-\gamma^\tau\partial+\kappa_\tau)_\eta\rho(xyz)\\&\quad=(gZ_2^{-1}Z_1)^2\gamma_\delta\tau_j\langle 0|T(\bar\psi\varphi_j(x),\bar\psi\varphi_k(y),\varphi_i(z))|0\rangle\gamma_\delta\tau_k\\&\qquad+gZ_2^{-2}Z_1\gamma_\delta\tau_\eta\delta(x-y)\\&\qquad\times\langle 0|T(\varphi_j(x),\varphi_k(x))|0\rangle,\text{ etc.}\end{aligned}\tag{A10}$$

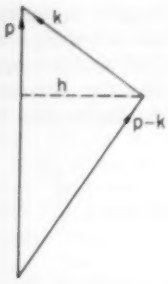

FIG. 4. Vectorial relation for the integral (A15).

$$
\begin{aligned}
&(\gamma\partial+\kappa_0)_x(-\gamma^7\partial+\kappa_0)_y(\Box-\mu_0^2)_z\rho(xyz)\\
&=i(gZ_2^{-1}Z_1)^2(gZ_3^{-1}Z_1)\gamma_5\tau_j\\
&\quad\times\langle 0|T(\psi\varphi_j(x),\bar\psi\varphi_k(y),\bar\psi\gamma_5\tau_i\psi(z))|0\rangle\gamma_5\tau_k\\
&+i(gZ_2^{-1}Z_1)^2Z_3^{-1}\gamma_5\tau_j\\
&\quad\times\langle 0|T(\psi\varphi_j(x),\bar\psi(y))|0\rangle\gamma_5\tau_i\delta(y-z)\\
&+i(gZ_2^{-1}Z_1)^2Z_3^{-1}\gamma_5\tau_i\\
&\quad\times\langle 0|T(\psi(x),\bar\psi\varphi_k(y))|0\rangle\gamma_5\tau_k\delta(x-z)\\
&-i(gZ_2^{-1}Z_1)(gZ_3^{-1})\gamma_5\tau_j\\
&\quad\times\langle 0|T(\varphi_j(x),\bar\psi\gamma_5\tau_i\psi(z))|0\rangle\delta(x-y)\\
&-igZ_2^{-2}Z_3^{-1}Z_1\gamma_5\delta(x-y)\delta(x-z).
\end{aligned}
$$

Substituting the representation for $\rho(xyz)$, we proceed as before. For example

$$
\begin{aligned}
&i(ip\gamma+\kappa_0)\int\frac{(ip\gamma)^\lambda\gamma_5\tau_i(-iq\gamma)^{\lambda'}}{(p^2+u')(q^2+v')(k^2+w)}\nu_{\lambda\lambda'}dudvdw\\
&\quad=-i\int\frac{\gamma_5\tau_i(-iq\gamma)^{\lambda'}}{(q^2+v)(k^2+w)}\nu_{1\lambda'}dudvdw+\cdots. \qquad \text{(A11)}
\end{aligned}
$$

This, being dependent only on q^2 and k^2, must correspond to the first term on the right of the first of Eq. (A10). Thus

$$\int\nu_{1\lambda'}(uvw)du=gZ_2^{-1}Z_1\nu_{\lambda'}(v)\nu(w).$$

In a similar way we get the following set of relations

$$
\begin{aligned}
&\int\nu_{\lambda 1}(uvw)dv=gZ_2^{-1}Z_1\nu_\lambda(u)\nu(w),\\
&\qquad\text{(equivalent to the above)}\\
&\int\nu_{\lambda\lambda'}(uvw)dw=gZ_3^{-1}Z_1\nu_\lambda(u)\nu_{\lambda'}(v),\\
&\int\nu_{\lambda 1}(uvw)dvdw=gZ_2^{-1}Z_3^{-1}Z_1\nu_\lambda(u), \qquad \text{(A12)}\\
&\int\nu_{11}(uvw)dudv=gZ_2^{-1}Z_1\nu(w),\\
&\int\nu_{11}(uvw)dudvdw=gZ_2^{-2}Z_3^{-1}Z_1,
\end{aligned}
$$

which are consistent with Eq. (A6).

Finally we take $\rho(z_1\cdots z_4)$ which obeys the equation

$$
\begin{aligned}
&(\Box-\mu_0^2)\rho(z_1\cdots z_4)\\
&=\lambda Z_3^{-1}Z_4\langle 0|T(\varphi_1\varphi_2^2,\varphi_2,\varphi_3,\varphi_4)|0\rangle\\
&\qquad+ig\langle 0|T(\bar\psi\gamma_5\tau_i\psi(z_1),\varphi_2,\cdots\varphi_4)|0\rangle+\cdots\\
&=\lambda Z_3^{-1}Z_4[2\langle 0|T(\varphi_1\varphi_2)|0\rangle\langle 0|T(\varphi_i\varphi_3)|0\rangle\\
&\qquad\qquad\times\langle 0|T(\varphi_i\varphi_4)|0\rangle+\cdots]\\
&\quad+ig\langle 0|T(\bar\psi\gamma_5\tau_i\psi(z_1),\varphi_2,\cdots\varphi_4)|0\rangle+\cdots. \qquad \text{(A13)}
\end{aligned}
$$

Substituting the representation Eq. (3.46), we conclude that

$$
\begin{aligned}
&\int\nu^0(w_i)dw_1=2\lambda Z_4Z_3^{-1}\nu(w_2)\nu(w_3)\nu(w_4),\ \text{etc.}\\
&\int\nu^0(w_i)dw_1dw_2=2\lambda Z_4Z_3^{-2}\nu(w_3)\nu(w_4),\ \text{etc.} \qquad \text{(A14)}\\
&\int\nu^0(w_i)dw_1dw_2dw_3=2\lambda Z_4Z_3^{-3}\nu(w_4),\ \text{etc.}\\
&\int\nu^0(w_i)\prod dw_i=2\lambda Z_4Z_3^{-4},
\end{aligned}
$$

ν^0 being defined in Eq. (3.47).

2. Evaluation of Some Integrals

There is an easy way of evaluating the integrals in Sec. 4. First let us take Eq. (4.7). Let

$$
\begin{aligned}
\vartheta_\lambda\equiv\sum_\pm\int&(ip'\gamma)^\lambda\theta(\pm p)\theta(\pm p')\theta(\pm k)\delta(p'^2+u)\\
&\times\delta(k^2+w)\delta(p'+k-p)dp'dk. \qquad \text{(A15)}
\end{aligned}
$$

The three vectors are related to each other as shown in Fig. 4. The delta functions in the integrand demand that the length of the vectors p' and k be kept fixed as well as the vector p itself, so that the triangle pkp' has a fixed shape and can rotate in the four-dimensional space around the vector p. We may thus write Eq. (A15) as

$$
\begin{aligned}
\vartheta_\lambda=\sum_\pm\frac{\theta(\pm p)}{4(uw)^{\frac12}}\int&(ip'\gamma)^\lambda\theta(\pm p')\theta(\pm k)\\
&\times\delta(|p'|-\sqrt{u})\delta(|k'|-\sqrt{w})dP, \qquad \text{(A16)}
\end{aligned}
$$

where P is the apex of the triangle opposite the vector p. The integration may be factorized into two, namely that within the plane of the triangle and that resulting from the rotation of the triangle (or the point P) in a two-dimensional (space-like) space orthogonal to it.

For $\lambda=0$, the first integration gives the Jacobian

$$(uw)^{\frac12}/S,$$

which is the ratio of the area of a square with the sides $\sqrt{u}$ and $\sqrt{w}$ to that of the parallelogram (denoted by S)

formed with the vectors p' and k. The second integration gives the surface area of a sphere

$$4\pi h^2,$$

where h is the height of the triangle seen from the base p. Thus

$$g_0=\frac{1}{4(uw)^{\frac{1}{2}}}\frac{(uw)^{\frac{1}{2}}}{S}4\pi h^2=\frac{\pi h^2}{S}=\frac{\pi h^2}{h\sqrt{-p^2}}=\frac{\pi S}{\sqrt{-p^2}}, \quad \text{(A17)}$$

and S may be expressed in terms of the three sides of the triangle:

$$S^2=\begin{vmatrix} p'^2 & (p'k) \\ (p'k) & k^2 \end{vmatrix}=p'^2k^2-\frac{(p'^2+k^2-p^2)^2}{4}. \quad \text{(A18)}$$

We have not been careful about the indefinite character of the metric in Minkowski space, but g_0 is obviously a positive definite quantity. From physical consideration, on the other hand, we must have $\sqrt{-p^2}\geq\sqrt{u}+\sqrt{w}$ which is contrary to the usual relation for the three sides of a triangle. S must then be

$$S=\{[(\sqrt{u}+\sqrt{w})^2+p^2][(\sqrt{u}-\sqrt{w})^2+p^2]\}^{\frac{1}{2}}. \quad \text{(A19)}$$

For $\lambda=1$, the vector p' in $ip'\gamma$ gets simply projected onto the axis p as a result of the second integration, so that we get

$$g_1=c(ip\gamma)g_0,$$

$$c=(pp')/p^2=\frac{p^2+p'^2-k^2}{-2p^2}=\frac{p^2+w-u}{-2p^2}. \quad \text{(A20)}$$

Next take the integral in Eq. (4.22),

$$g_\lambda'\equiv\sum_{\pm}\int\theta(\pm p)\theta(\mp k)\theta(\pm p')\theta(\pm p'\pm q)\theta(\pm k')\times(ip'\gamma)^\lambda\delta(p'^2+u)\delta((p'+q)^2+s)\times\delta(k'^2+w)\delta(p'+k'-p)dp'dk'$$

$$=\sum_{\pm}\frac{1}{8(uws)^{\frac{1}{2}}}\theta(\pm p)\theta(\mp k) \quad \text{(A21)}$$

$$\times\int(ip\gamma)^\lambda\delta(|p'|-\sqrt{u})\delta(|p'+q|-s)\times\delta(|k'|-w)\delta(p'+k'-p)dp'dk'.$$

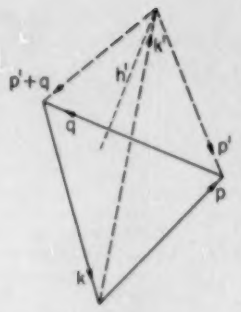

FIG. 5. Vectorial relation for the integral (A21).

The vectorial relations are shown in Fig. 5. This time the three vectors p, q, k and the lengths of the vectors p', k', $p'+q$ are fixed, so that the shape of the tetrahedron in Fig. 5 and its base pqk are fixed, while the apex P is movable with one degree of freedom in the four-dimensional space. The integration may be factorized into that within the space of the tetrahedron and that in the complementary (space-like) space. The first yields the Jacobian

$$(uws)^{\frac{1}{2}}/\Delta$$

where Δ is the volume of the parallelopiped formed with the vectors p', k', $p'+q$. The second gives the perimeter of a circle

$$2\pi h',$$

where h' is the distance between P and the base plane pqk. Thus

$$g_0'=\frac{\sum}{8(uws)^{\frac{1}{2}}}\frac{(uws)^{\frac{1}{2}}}{\Delta}2\pi h'=\frac{\sum h'}{4\Delta}=\frac{\sum h'}{2Sh'}=\frac{\sum}{2S}, \quad \text{(A22)}$$

$$\sum\equiv\sum_{\pm}\theta(\pm p)\theta(\mp k),$$

S being the area of the base triangle.

The factor $ip'\gamma$ in g_1' goes, as before, into its projection onto the plane pqk, so that

$$g_1'=[i(ap+bq,\gamma)]g_0. \quad \text{(A23)}$$

a and b are determined from

$$(pp')=ap^2+a(pq), \quad (qp')=a(pq)+bq^2,$$

together with

$$(pp')=(p^2+p'^2-k'^2)/2=(p^2+w-u)/2,$$
$$(p'q)=-(p'^2+q^2-(p'+q)^2)/2=(-q^2+u-s)/2, \quad \text{(A24)}$$
$$(pq)=-(p^2+q^2-k^2)/2.$$

Connection Between the *S*-Matrix and the Tensor Force

ROGER G. NEWTON*†
Institute for Advanced Study, Princeton, New Jersey
(Received April 21, 1955)

The present paper is a study of the radial Schrödinger equations for the case of an interaction between the lth and the $(l+2)$nd angular momentum, produced by the tensor force in the presence of spin-orbit coupling. It contains a number of theorems, known for central potentials, concerning the low-energy behavior of the S-matrix, bound states, and zero-energy resonance. The construction, in two stages, of all potentials belonging to a given S-matrix and given bound states, is described. The step from the spectral function to the potential involves the generalization of the Gel'fand Levitan equation given in a recent paper; that from the S-matrix to the spectral function, a procedure due to Plemelj also outlined in that paper. The latter procedure leads to a restriction on the S-matrix necessary for a short range potential to exist. If there is such a potential, it is uniquely determined by the S-matrix, the binding energies, and as many real, symmetric, positive semidefinite matrices as there are bound states.

1. INTRODUCTION

IN the work of Bargmann,[1,2] Jost and Kohn,[3–5] and Levinson,[6,7] it was shown that the scattering phase shift of one angular momentum, l, given as a function of the energy, if caused by a short-range central potential, together with the L_l bound state energies and a set of L_l positive parameters C_n, uniquely determines that potential. Moreover, the latter can be constructed from the former by solving a Fredholm integral equation first derived by Gel'fand and Levitan.[5,7,8] It is the primary purpose of the present paper to generalize the work of the above authors to such noncentral potentials as that of a combination of spin-orbit coupling and the tensor force.[9,10] As a first step in that direction, the author and Res Jost have recently extended the construction procedure to the (physically fictitious) case of a finite number of coupled radial Schrödinger equations for S-states.[11] The then neglected centrifugal barrier is now fully taken into account.

In addition to the construction of the potential from the S-matrix, the bound states, and as many matrices as there are bound states, a number of generalizations of theorems, known for central potentials, concerning bound states and the low-energy behavior of the S-matrix are proved.

Section 2 contains several kinds of solutions of the radial Schrödinger equation with coupling between the lth and the $(l+2)$nd angular momentum, and their properties as functions of the distance and of the energy. The S-matrix is defined and shown to be unitary and symmetric. At the end of the section a theorem is proved concerning the low-energy behavior of the S-matrix, being the generalization of the statement that for a large class of potentials the lth phase shift goes as k^{2l+1} near $k=\sqrt{E}=0$. Section 3 deals with the bound states and the special possibility of a resonance with no bound state at zero energy for $l=0$. While the former are independent of the S-matrix (except for their total number), the latter is not. Subsection 3*a* treats the bound states for negative energy; 3*b* that of zero energy and $l\geqslant 1$; 3*c* the bound state and resonance for zero energy and $l=0$ (coupled with $l=2$); 3*d* the generalization of the theorem at the end of Sec. 2 to the case of bound states or resonance at $E=0$; 3*e* the only connection between bound states and the S-matrix for short range potentials.

Section 4 contains the completeness relation and the definition of the spectral function. The generalization of the Gel'fand Levitan equation derived in (I) connects the latter directly with the potential. In Sec. 5 the construction of the spectral function from the S-matrix, the bound state energies, and a set of real, symmetric, positive semidefinite matrices is described. In contrast to the case of a central potential, this step in the construction is rather involved and, as in (I), leads to certain restrictions on the S-matrix necessary for the existence of a short-range potential.

There are three appendices. The first supplies all the convergence and existence proofs as well as a number of inequalities necessary for the work; Appendix B contains the proof of an ideal-theoretic theorem needed for the existence of an "irregular solution" of the Schrödinger equation as an entire function of the energy. Appendix C proves a special theorem about matrix functions needed for the completeness relation in the case of coupling between S- and D-states.

* Frank B. Jewett Fellow.
† Now at Indiana University, Bloomington, Indiana.
[1] V. Bargmann, Phys. Rev. **75**, 301 (1949).
[2] V. Bargmann, Revs. Modern Phys. **21**, 488 (1949).
[3] R. Jost and W. Kohn, Phys. Rev. **87**, 977 (1952).
[4] R. Jost and W. Kohn, Phys. Rev. **88**, 382 (1952).
[5] R. Jost and W. Kohn, Kgl. Danske Videnskab. Selskab, Mat.-fys. Medd. **27**, No. 9 (1953).
[6] N. Levinson, Kgl. Danske Videnskab. Selskab, Mat.-fys. Medd. **25**, No. 9 (1949).
[7] N. Levinson, Phys. Rev. **89**, 755 (1953).
[8] I. M. Gel'fand and B. M. Levitan, Doklady Akad. Nauk. S.S.S.R., Ser. **77**, 557 (1951), and Izvest. Akad. Nauk. S.S.S.R., **15**, 309 (1951).
[9] W. Rarita and J. Schwinger, Phys. Rev. **59**, 436 (1941).
[10] J. M. Blatt and V. F. Weisskopf, *Theoretical Nuclear Physics* (John Wiley and Sons, Inc., New York and London, 1952), pp. 94 ff.
[11] R. G. Newton and R. Jost, Nuovo cimento **1**, 590 (1955), hereafter referred to as (I).

The general position- and spin-dependent potential between two particles is of the form[10]

$$\mathcal{V}(r)=v_d(r)+v_\sigma(r)\boldsymbol{\sigma}_1\cdot\boldsymbol{\sigma}_2+v_t(r)S_{12}. \quad (1.1)$$

When this is applied to the wave function of two spin $\frac{1}{2}$ particles in a triplet state, whose two relevant radial components, of the lth and the $(l+2)$nd angular momentum, may be combined in the row-matrix or vector

$$U=(u,w),$$

and whose spin-angle components are

$$Y=(Y_{j,l,s}{}^M, Y_{j,l+2,s}{}^M),$$

then, in matrix notation,

$$\mathcal{V}UY^T=UVY^T.$$

Here V is a real, symmetric (2×2)-matrix whose elements are functions of r alone. For $l=0$,

$$V=\begin{pmatrix} v_c & 2\sqrt{2}v_t \\ 2\sqrt{2}v_t & v_c-2v_t \end{pmatrix},$$

where[10] $v_c=v_d+v_\sigma$. Only *two* of the elements in the matrix V are independent.

From the point of view of the S-matrix any restriction on V beyond symmetry and reality is unnatural. No criterion is known for the scattering to arise from a potential V that satisfies the condition necessary to be associated with the $\mathcal{V}$ of (1.1). In order to remove this restriction, a spin-orbit potential of the form $v_o(r)\mathbf{S}\cdot\mathbf{L}$ must be added to (1.1). Such a potential has the property

$$v_o(r)\mathbf{S}\cdot\mathbf{L}UY^T = \tfrac{1}{2}v_o(r)U\begin{pmatrix} J^2-l^2-S^2 & 0 \\ 0 & J^2-(l+2)^2-S^2 \end{pmatrix}Y^T.$$

Consequently, the potential

$$\mathcal{V}'=v_d(r)+v_\sigma(r)\boldsymbol{\sigma}_1\cdot\boldsymbol{\sigma}_2+v_t(r)S_{12}+v_o(r)\mathbf{S}\cdot\mathbf{L}, \quad (1.2)$$

when applied to a triplet state wave function, manifests itself as a matrix-multiple of the radial part, UV (the spin-angle matrix that always multiplies from the right being neglected), where V is a real, symmetric (2×2)-matrix function of r and otherwise unrestricted. The matrix V and the set of three potentials v_c, v_t, and v_o stand in one-to-one correspondence to each other. Among the latter it is the tensor force alone that produces coupling between the lth and the $(l+2)$nd angular momentum.

2. SOLUTIONS AND THE S-MATRIX

In view of the statements in the introduction, the Schrödinger equation for the radial part of the wave function containing the components of angular momentum l and $l+2$ can, in the presence of the potential $\mathcal{V}'$ of (1.2), be written as follows[12]:

$$\psi''(E,r)+E\psi(E,r)=\psi(E,r)[r^{-2}l(l+1)(\mathbf{1}-P) + r^{-2}(l+2)(l+3)P+V(r)], \quad (2.1)$$

where

$$P=\begin{pmatrix} 0 & 0 \\ 0 & 1 \end{pmatrix}, \quad (2.2)$$

and $V(r)$ is a real symmetric (2×2)-matrix function of r; $\psi(E,r)$ is a (2×2)-matrix whose rows are individually vector solutions of (2.1). "A solution of (2.1)" will always mean such a square matrix of two vector solutions.

In the space of (2×2)-matrices it will be useful to define a norm:

$$|M|\equiv 2\max_{\alpha,\beta=1,2}(|M_{\alpha\beta}|), \quad (2.3)$$

which obeys both the triangle and Schwarz's inequalities. Furthermore, we use the notation $\mathfrak{M}(s)$ for the class of (matrix valued) functions whose sth absolute moment exists[13]:

$$M(r)\epsilon\mathfrak{M}(s) \text{ if } \int_0^\infty dr\, r^s|M(r)|<\infty. \quad (2.4)$$

The assumptions on the potential will not be entirely fixed. For the main purpose it will be assumed that $V\epsilon\mathfrak{M}(0)\bigcap\mathfrak{M}(5)$, although for $l=0$ it will suffice that $V\epsilon\mathfrak{M}(0)\bigcap\mathfrak{M}(4+\delta)$, $\delta>0$. For the purpose of one theorem concerning the behavior of the S-matrix at low energies (see the end of this section) we will need $V\epsilon\mathfrak{M}(0)\bigcap\mathfrak{M}(2l+6)$. The only other assumption, needed in Sec. 5, will be

$$\int_0^\infty dr\, r|V(r+R)-V(r)|<CR^\delta, \text{ for some } \delta>0. \quad (2.5)$$

Several different kinds of solutions of (2.1) will be used. The first is $G(k,r)$, $(k^2=E)$, which vanishes at[14]

[12] Differentiation with respect to r will be indicated by a prime; r is the radial distance in units of $\hbar/mc\sqrt{2}$, E the energy in units of mc^2, V the potential in units of mc^2; m is the reduced mass if (2.1) describes the interaction between two particles. The first derivative with respect to k, where $k^2=E$, is denoted by a dot, the second by a dash.

[13] The symbolism customary in mathematics is used: "ϵ" stands for "is a member of;" "$\bigcap$" stands for the intersection of two classes, i.e., the members of $\mathfrak{M}_1\bigcap\mathfrak{M}_2$ are all elements which are both in $\mathfrak{M}_1$ and in $\mathfrak{M}_2$.

[14] It is well known that, in contrast to the scalar case (i.e., with no coupling between different angular momenta) in general no "regular" solution can be defined for the tensor force without interference with the logarithmic term. (There is one regular vector solution without a logarithm, but the second row of the matrix solution generally contains $\log r$.) It is correspondingly difficult to define this solution by a boundary condition. The obvious integral equation for this solution diverges at $r=0$ unless the existence of large negative moments of the potential is assumed. If to the inhomogeneity of this integral equation, however, a judicious (*V-dependent*) multiple of the solution of (2.1) with $V=0$ is added, the integral is made to converge. The result is (2.6).

$r=0$. It is defined by the integral equation

$$G(k,r)=G_0(k,r)+(2l+3)\int_1^r dt\, t^{-1}(1-P)V(t)G_0(k,r)$$
$$+\int_0^r dt[G(k,t)V(t)\mathcal{G}(k;t,r)$$
$$-(2l+3)t^{-1}(1-P)V(t)PG_0(k,r)], \quad (2.6)$$

which, if $V\epsilon\mathfrak{M}(0)$, has a unique solution obtainable by successive approximations.[15] The following functions occur in (2.6): the free solution

$$G_0(k,r)=\begin{pmatrix} k^{-(l+1)}u_l(kr) & 0 \\ 0 & k^{-(l+3)}u_{l+2}(kr)\end{pmatrix}, \quad (2.7)$$

and the Green's function

$$\mathcal{G}(k;t,r)=\begin{pmatrix} g_l(k;t,r) & 0 \\ 0 & g_{l+2}(k;t,r)\end{pmatrix}, \quad t\leqslant r, \quad (2.8)$$

where

$$g_l(k;t,r)=k^{-1}[u_l(kt)v_l(kr)-u_l(kr)v_l(kt)],$$
$$=\tfrac{1}{2}i(-1)^l k^{-1}[w_l(kr)w_l(-kt)$$
$$-w_l(-kr)w_l(kt)], \quad (2.9)$$

$$u_l(x)=xj_l(x),$$
$$v_l(x)=xn_l(x), \quad (2.10)$$
$$w_l(x)=i(-1)^{l+1}xh_l^{(1)}(-x)=-[v_l(x)+iu_l(x)],$$

and j_l, n_l, $h_l^{(1)}$ are the customary[16] spherical Bessel functions, spherical Neumann functions, and spherical Hankel functions of the first kind, respectively. The solution $G(k,r)$ of (2.6) and (2.1) is[15] an even, entire function[17,18] of k for all r. If $V\epsilon\mathfrak{M}(0)\bigcap\mathfrak{M}(1)$, then,[15,19] with $\nu=\mathrm{Im}k$,

$$(1-P)G(k,r)=(1-P)[k^{-(l+1)}\sin(kr-\tfrac{1}{2}\pi l)\mathbf{1}$$
$$+O(k^{-(l+2)}e^{|\nu|r})], \text{ as } |k|\to\infty,$$
$$PG(k,r)=P[-k^{-(l+3)}\sin(kr-\tfrac{1}{2}\pi l)\mathbf{1} \quad (2.11)$$
$$+O(k^{-(l+4)}e^{|\nu|r})], \text{ as } |k|\to\infty,$$

and

$$(1-P)G(k,r)=(1-P)\{[(2l+1)!!]^{-1}r^{l+1}\mathbf{1}$$
$$+O(r^{l+2})\}, \text{ as } r\to 0,$$
$$PG(k,r)=P\{[(2l+5)!!]^{-1}r^{l+3}\mathbf{1} \quad (2.12)$$
$$+O(r^{l+4})\}, \text{ as } r\to 0.$$

If we define a Wronskian matrix[20]

$$[\Phi;\Psi]\equiv\Phi(r)\Psi^{T'}(r)-\Phi'(r)\Psi^T(r), \quad (2.13)$$

which is independent of r if both Φ and Ψ satisfy (2.1) (due to the symmetry of V), then

$$[G;G]=0. \quad (2.14)$$

An "irregular" solution $I(k,r)$ of (2.1) that for all $r>0$ is an entire function of k and satisfies the equations

$$[I;G]=\mathbf{1}, \quad (2.15)$$

$$[I;I]=0, \quad (2.16)$$

can be defined as follows. Let $\psi_1(k,r)$ and $\psi_2(k,r)$ be two solutions of (2.1) fixed by the boundary conditions

$$\psi_1(k,1)=\psi_2'(k,1)=\mathbf{1}, \quad \psi_1'(k,1)=\psi_2(k,1)=0.$$

They are entire functions of k for all $r>0$. Let

$$G(k,r)=M_1^T(k)\psi_1(k,r)+M_2^T(k)\psi_2(k,r),$$
$$I_1(k,r)=-N_2(k)\psi_1(k,r)+N_1(k)\psi_2(k,r).$$

In order for $I_1(k,r)$ to obey (2.15), N_1 and N_2 must satisfy

$$N_1(k)M_1(k)+N_2(k)M_2(k)=\mathbf{1}. \quad (2.17)$$

Both M_1 and M_2 are entire functions of k. Moreover, (2.12) shows that, for every k_0, the only vector a with the property $M_1(k_0)a=M_2(k_0)a=0$ is $a=0$. It is proved in Appendix B that under these circumstances there exist two matrices N_1 and N_2 which solve (2.17) and which are entire functions of k. Because of (2.14), the solution

$$I(k,r)=[-N_2(k)+A(k)M_1^T(k)]\psi_1(k,r)$$
$$+[N_1(k)+A(k)M_2^T(k)]\psi_2(k,r),$$

where

$$A(k)=-N_2(k)N_1^T(k)+B(k),$$

and $B(k)$ is symmetric and an entire function of k, is then an entire function of k for all $r>0$ and it satisfies both (2.15) and (2.16).

A further solution of (2.1) is defined by the boundary condition

$$\lim_{r\to\infty}\exp[i(kr-\tfrac{1}{2}\pi l)]\mathcal{S}F(k,r)=\mathbf{1}, \quad (2.18)$$

where

$$\mathcal{S}=\begin{pmatrix}1 & 0\\ 0 & -1\end{pmatrix}. \quad (2.19)$$

If $V\epsilon\mathfrak{M}(3)$, $F(k,r)$ is[15] an analytic function of k in $\mathrm{Im}k<0$, continuous for $\mathrm{Im}k\leqslant 0$, except at $k=0$; at the latter point,

$$\mathcal{K}_l(k)F(k,r)\equiv F_e(k,r), \quad (2.20)$$

with

$$\mathcal{K}_l(k)=k^l(1-P)+k^{l+2}P, \quad (2.21)$$

[15] See Appendix A for the proof.

[16] See, for example L. I. Schiff, *Quantum Mechanics* (McGraw-Hill Book Company, Inc., New York, 1949), pp. 77 ff. The functions u_l and v_l are identical with those used by Walter Kohn, Revs. Modern Phys. **26**, 292 (1954) and are called j_l and n_l in reference 6.

[17] The notions analyticity, continuity, etc., when applied to a matrix valued function, are always meant to hold for each matrix element.

[18] Such a regular solution can presumably be defined under the weaker assumption $V\epsilon\mathfrak{M}(1)$ for which (2.6) in general, diverges. It will, however, in the following be convenient to have an equation for G whose series of successive approximations converges. Therefore it was assumed that $V\epsilon\mathfrak{M}(0)$.

[19] Throughout this paper, the notations O and o will be used to mean a *matrix* all of whose elements are $O(\cdots)$ or $o(\cdots)$.

[20] A superscript T will stand for transposition, an asterisk for complex conjugation.

is continuous. The asymptotic behavior in $\mathrm{Im}k\leqslant 0$ is the following[18]:

$$F(k,r)=\exp[-i(kr-\tfrac{1}{2}\pi l)]\mathcal{S}+O(r^{-1}e^{-|\kappa|r}),\quad \text{as } r\to\infty,\ k\neq 0, \tag{2.22}$$

$$F_e(0,r)=(2l-1)!!(\mathbf{1}-P)[r^{-l}\mathbf{1}+o(r^{-l-2})]+(2l+3)!!P[r^{-l-2}\mathbf{1}+o(r^{-l-4})],\quad r\to\infty, \tag{2.23}$$

$$F(k,r)=\exp[-i(kr-\tfrac{1}{2}\pi l)]\mathcal{S}+O(|k|^{-1}e^{-|\kappa|r}),\quad \text{as } |k|\to\infty,\ r>0. \tag{2.24}$$

If[15] $V\epsilon\mathfrak{M}(2)$, then[12] $P\dot{F}_e(0,r)$ exists (for $r>0$); if $V\epsilon\mathfrak{M}(4)$, so does $(\mathbf{1}-P)\dot{F}_e(0,r)$. If $V\epsilon\mathfrak{M}(3)$, then $P\dot{F}_e(0,r)\equiv 0$ and[12] $P\ddot{F}_e(0,r)$ exists; if $V\epsilon\mathfrak{M}(5)$, then, for $l\geqslant 1$, $(\mathbf{1}-P)\dot{F}_e(0,r)\equiv 0$ and $(\mathbf{1}-P)\ddot{F}_e(0,r)$ exists. The same is true for the first derivative of F with respect to r.

The solution $F(k,r)$ satisfies, for $\mathrm{Im}k\leqslant 0$,

$$[F(k,r);F(k,r)]=0, \tag{2.25}$$

and for $\mathrm{Im}k=0$,

$$[F(k,r);F(-k,r)]=2i(-1)^l k\mathbf{1}; \tag{2.26}$$

for real k it also has the property

$$F(-k,r)=(-1)^l F^*(k,r). \tag{2.27}$$

By means of the definitions[21]

$$F(k)\equiv[F(k,r);G(k,r)]\mathcal{K}_l(k), \tag{2.28}$$

$$F'(k)\equiv-[F(k,r);I(k,r)]\mathcal{K}_l(k^{-1}), \tag{2.29}$$

$G(k,r)$ can readily be expressed in terms of $F(k,r)$ and $F(-k,r)$, for $\mathrm{Im}k=0$:

$$G(k,r)=(2ik)^{-1}\mathcal{K}_l(k^{-1})[(-1)^l F^T(k)F(-k,r)-F^T(-k)F(k,r)]. \tag{2.30}$$

Similarly, $F(k,r)$ can be expressed in terms of G and I, for $\mathrm{Im}k\leqslant 0$:

$$F(k,r)=F'(k)\mathcal{K}_l(k)G(k,r)+F(k)\mathcal{K}_l(k^{-1})I(k,r). \tag{2.31}$$

The function $F(k)$ is of fundamental importance in the following. It is analytic in $\mathrm{Im}k<0$, continuous for $\mathrm{Im}k\leqslant 0$, except possibly at $k=0$, where

$$F_e(k)\equiv\mathcal{K}_l(k)F(k)\mathcal{K}_l(k^{-1}), \tag{2.32}$$

however, is continuous. The statements following (2.24) apply to $F_e(0)$: If $V\epsilon\mathfrak{M}(0)\bigcap\mathfrak{M}(2)$, then $P\dot{F}_e(0)$ exists; if $V\epsilon\mathfrak{M}(0)\bigcap\mathfrak{M}(4)$, so does $(\mathbf{1}-P)F_e(0)$; if $V\epsilon\mathfrak{M}(0)\bigcap\mathfrak{M}(3)$, then $P\dot{F}_e(0)=0$ and $P\ddot{F}_e(0)$ exists; if $V\epsilon\mathfrak{M}(0)\bigcap\mathfrak{M}(5)$, then, for $l\geqslant 1$, $(\mathbf{1}-P)\dot{F}_e(0)=0$ and $(\mathbf{1}-P)\ddot{F}_e(0)$ exists. Furthermore, if $V\epsilon\mathfrak{M}(0)\bigcap\mathfrak{M}(1)$, then

$$F(k)=\mathbf{1}+O(k^{-1}),\ \text{as } |k|\to\infty \text{ in } \mathrm{Im}k\leqslant 0. \tag{2.33}$$

In contrast to (2.27), $F(k)$ has the property that for real k

$$F(-k)=F^*(k). \tag{2.34}$$

[21] The functions $F(k)$ and $F'(k)$ of (I) although *definad* differently, satisfy (2.28) and (2.29) *mutatis mutandis*.

Finally, insertion of (2.30) and (2.26) in (2.14) yields the relation

$$F^T(k)F(-k)=F^T(-k)F(k). \tag{2.35}$$

The S-matrix[22] is obtained from (2.30) and (2.35) as

$$S(k)=F(k)F^{-1}(-k). \tag{2.36}$$

Owing to (2.35) it is symmetric, and due to (2.34),

$$S(-k)=S^*(k)=S^{-1}(k), \tag{2.37}$$

which, together with its symmetry, demonstrates its unitarity.

It is well known that for central potentials sufficiently small at infinity, the asymptotic phase ($\frac{1}{2}\log$ ImS) of the lth angular momentum tends to zero at $k=0$ as k^{2l+1}, provided there is no bound state (of angular momentum l) with zero binding energy.[23] The generalization of this theorem to the present case is given in the remainder of this section.

It is proved in Appendix A that, if $V\epsilon\mathfrak{M}(0)\bigcap\mathfrak{M}(2l+6)$, then

$$\mathrm{Im}F_e(k)=(\mathbf{1}-P)O(k^{2l+1})+PO(k^{2l+6}),\ \text{as } k\to 0. \tag{2.38}$$

Suppose now that $\det F_e(0)\neq 0$. Then, owing to (2.36) and (2.34)

$$\begin{aligned}S(k)&=\mathcal{K}_0(k^{-1})[\mathbf{1}+i\mathrm{Im}F_e(k)(\mathrm{Re}F_e(k))^{-1}\\&\quad\times[\mathbf{1}-i\mathrm{Im}F_e(k)(\mathrm{Re}F_e(k))^{-1}]^{-1}\mathcal{K}_0(k)\\&=\mathbf{1}+\begin{pmatrix}O(k^{2l+1}) & O(k^{2l+3})\\ O(k^{2l+3}) & O(k^{2l+6})\end{pmatrix},\quad \text{as } k\to 0.\end{aligned} \tag{2.39}$$

The modification of this statement in case $\det F_e(0)=0$ will be given in part (*d*) of the next section.

3. BOUND STATES AND RESONANCE

a. $k\neq 0$.—Suppose that for $k=k_0$, $\mathrm{Im}k<0$, $\det F(k)=0$, so that there exists a vector $a\neq 0$ for which (2.31) yields

$$aF(k_0,r)=aF'(k_0)\mathcal{K}_l(k_0)G(k_0,r). \tag{3.1}$$

The vector solution $aF(k_0,r)$ of (2.1) thus vanishes both at $r=0$ and $r=\infty$; at the latter point exponentially. This means that $-k_0^2$ in an eigenvalue of (2.1), or the energy of a bound state. One can show from (2.15), via (2.12) and similar estimates for G', that

$$I(k,r)=(\mathbf{1}-P)[(2l-1)!!r^{-l}\mathbf{1}+o(r^{-l})]+P[(2l+3)!!r^{-(l+2)}\mathbf{1}+o(r^{-(l+2)})],\quad \text{as } r\to 0; \tag{3.2}$$

consequently,

$$\lim_{r\to 0} bI(k,r)=0 \text{ implies } b=0. \tag{3.3}$$

[22] See C. Møller, Kgl. Danske Videnskab. Selskab, Mat.-Fys. Medd. **22**, No. 19, 19 (1946).

[23] This theorem was proved rigorously for central potentials in $\mathfrak{M}(2l+2)$, by David S. Carter in a Ph.D. thesis at Princeton University, 1952 (unpublished).

It follows, therefore, from the fact that $\det\mathfrak{K}_l(k_0^{-1})\neq 0$, by (2.31), that if $-k_0^2$, $\mathrm{Im}k_0\leq 0$, is a bound state energy, then there must exist a vector $a\neq 0$ so that $aF(k_0)=0$, and hence $\det F(k_0)=0$. Thus the nonzero eigenvalues of (2.1) correspond exactly to the points in the lower half plane where $F(k)$ is a singular matrix. It is proved in the standard fashion that these eigenvalues are all real. The functions $F(k)$ and $F^{-1}(k)$ are therefore both analytic for $\mathrm{Im}k<0$, except at a finite number[24] of points on the negative imaginary axis, $k=-iK_i$, $K_i>0$, where $F^{-1}(k)$ has poles. As in (I), we shall now prove that at $k=-iK_i$, $F^{-1}(k)$ has exactly a *simple* pole.

Since[12] $[\dot{G};G]$ vanishes at $r=0$, one obtains, as in (I), (3.1),

$$[\dot{G}(k,r);G(k,r)]=2k\int_0^r dtG(k,t)G^T(k,t). \tag{3.4}$$

On the other hand, (2.14), (2.16), (2.28), and (2.31) lead to

$$\begin{aligned}[\dot{F}(k,r);G(k,r)]=&\dot{F}(k)\mathfrak{K}_l^{-1}-F(k)\dot{\mathfrak{K}}_l\mathfrak{K}_l^{-2}\\&+F'(k)\mathfrak{K}_l[\dot{G}(k,r);G(k,r)]\\&+F(k)\mathfrak{K}_l^{-1}[\dot{I}(k,r);G(k,r)].\end{aligned} \tag{3.5}$$

Now suppose that the vectors a and b solve

$$aF(-iK)=0, \tag{3.6a}$$

$$a\dot{F}(-iK)+bF(-iK)=0. \tag{3.6b}$$

Substitution of (2.31) in (2.25) yields, for $\mathrm{Im}k\leq 0$:

$$F(k)F'^T(k)-F'(k)F^T(k)=0. \tag{3.7}$$

Equations (3.6a) and (3.6b) therefore imply

$$\begin{aligned}&a\dot{F}(-iK)F'^T(-iK)a^T\\&\quad=-bF(-iK)F'^T(-iK)a^T\\&\quad=bF'(-iK)F^T(-iK)a^T=0.\end{aligned} \tag{3.8}$$

Multiplication of (3.5), taken at $k=-iK$, by a on the left and by $\mathfrak{K}_l(-iK)F'^T(-iK)a^T$ on the right then leads, via (3.1) and (3.4), to

$$\begin{aligned}&a[\dot{F}(-iK,r);F(-iK,r)]a^T\\&\quad=-2iK\int_0^r dtaF(-iK,t)F^T(-iK,t)a^T.\end{aligned} \tag{3.9}$$

The function $F(-iK,r)$ being real, the absolute value of the right-hand side increases monotonely, while that of the left vanishes at $r=\infty$. It follows that $a=0$ and, according to (I), Appendix A, therefore that $F^{-1}(k)$ has a simple pole at $k=-iK$.

We can now reduce the case of bound states to that without bound states. For that purpose we need for every bound state a real, symmetric projection P_n which satisfies[25]

$$\mathrm{range}P_n\equiv\mathrm{kernel}(\mathbf{1}-P_n)\equiv\mathrm{kernel}F(-iK_n). \tag{3.10}$$

It describes the mixture of angular momenta for which K_n^2 is a bound state energy, in the sense that if the ratio of the two components of the bound state wave function is asymptotically equal to c, then

$$P_n=(1+c^2)^{-1}\begin{pmatrix}1 & -c\\ -c & c^2\end{pmatrix}. \tag{3.10'}$$

This is not directly related to the probability ratio of the two states in the sense in which the ground state of the deuteron is a 4% D-state. The connection between the two strictly speaking, involves the potential.

If $\{-K_n^2\}$, $n=1,\cdots,L$, $0<K_1<\cdots<K_L$, are the bound state energies and P_n the corresponding projections fulfilling (3.10), then one defines a matrix $R\equiv R_L(k)$ as follows:

$$\begin{aligned}&R_0=\mathbf{1},\\&R_n(k)=\left(\mathbf{1}-P_n'\frac{2iK_n}{k+iK_n}\right)R_{n-1}(k),\quad n=1,\cdots,L,\end{aligned} \tag{3.11}$$

where P_n' is again a real, symmetric projection, related to P_n by

$$\begin{aligned}\mathrm{range}P_n'&\equiv\mathrm{kernel}(\mathbf{1}-P_n')\\&\equiv\mathrm{range}[R_{n-1}(-iK_n)P_nR_{n-1}^{-1}(-iK_n)].\end{aligned} \tag{3.12}$$

One then forms

$$F_N(k)\equiv R(k)F(k), \tag{3.13}$$

and

$$S_N(k)\equiv R(k)S(k)R^{-1}(-k)=F_N(k)F_N^{-1}(-k). \tag{3.14}$$

It was proved in (I), Sec. 3, that F_N and S_N have all the relevant properties of F and S: $F_N(k)$ is analytic for $\mathrm{Im}k<0$, continuous for $\mathrm{Im}k\leq 0$, except at $k=0$, $\lim F_N(k)=\mathbf{1}$ as $|k|\to\infty$; S_N is unitary and symmetric and satisfies (2.37). In addition, however, $F_N^{-1}(k)$ is also analytic for $\mathrm{Im}k<0$.

b. $k=0$, $l\geq 1$.—It is evident from (2.23) that for $l\geq 1$, $F_e(0,r)$ is always square integrable at infinity. It is therefore again clear from (2.31) that a necessary and sufficient condition for $k^2=0$ to be the energy of a bound state, is that $\det F_e(0)=0$; i.e., that there exist a vector $a\neq 0$ so that $aF_e(0)=0$ and therefore

$$aF_e(0,r)=aF_e'(0)G(0,r). \tag{3.15}$$

It is now, however, not true that $kF_e^{-1}(k)$ is continuous at $k=0$. We shall prove that $k^2F_e^{-1}(k)$ exists at $k=0$ and, if and only if $k^2=0$ is an eigenvalue, it does not vanish there.[26]

---

[24] See (I), reference 19.

[25] As in (I), we mean by the range of a matrix M the set of all vectors x for which there exist vectors y so that $x=yM$; the kernel of M is the set of all x so that $xM=0$. By a projection we mean merely an idempotent matrix, $P^2=P$.

[26] We assume in the following that $V\in\mathfrak{M}(0)\cap\mathfrak{M}(5)$.

Consider the system

$$aF_\epsilon(0)=0, \quad a\dot{F}_\epsilon(0)+bF_\epsilon(0)=0. \tag{3.16}$$

By (3.15) both $aF_\epsilon(0,r)$ and $aF_\epsilon'(0,r)$ vanish at $r=0$. Moreover, since $\dot{F}_\epsilon(0)=0$, by (2.31),

$$bF_\epsilon(0,r)=bF_\epsilon'(0)G(0,r)+bF_\epsilon(0)I(0,r), \tag{3.17}$$

$$a\dot{F}_\epsilon(0,r)=a\frac{\partial^2}{\partial k^2}[F_\epsilon'(k)G(k,r)]_{k=0}+a\dot{F}_\epsilon(0)I_\epsilon(0,r). \tag{3.18}$$

The second equation in (3.16) then shows that $a\dot{F}_\epsilon(0,r)+bF_\epsilon(0,r)$ vanishes at $r=0$ and so does its derivative. Consequently

$$f(r)\equiv[aF_\epsilon(0,r);\, a\dot{F}_\epsilon(0,r)+bF_\epsilon(0,r)]\to 0, \quad r\to 0. \tag{3.19}$$

The differential equation (2.1), on the other hand, yields[27]

$$f'(r)=-2aF_\epsilon(0,r)F_\epsilon{}^T(0,r)a^T, \tag{3.20}$$

which is certainly nonpositive (a and $F_\epsilon(0,r)$ being real). Now, as $r\to\infty$

$$[aF_\epsilon(0,r);\, a\dot{F}_\epsilon(0,r)]\to[aF_{\epsilon 0}(0,r);\, a\dot{F}_{\epsilon 0}(0,r)]\to 0,$$

and similarly,

$$[aF_\epsilon(0,r);\, b\dot{F}_\epsilon(0,r)]\to 0.$$

Therefore $f(0)=f(\infty)=0$. Since (3.20) states that $f(r)$ is monotonic, it follows that $f'(r)\equiv 0$ and hence by (3.20),

$$aF_\epsilon(0,r)=0.$$

As $r\to\infty$, (2.23) shows that

$$\det F_\epsilon(0,r)\to(2l-1)!!(2l+3)!!\,r^{-l-2},$$

and therefore $a=0$. The theorem of (I), Appendix A, then states that the inverse of

$$M(k)\equiv F_\epsilon(0)+\tfrac{1}{2}k^2\dot{F}_\epsilon(0)$$

has exactly a double pole at $k=0$. Since $\dot{F}_\epsilon(0)=0$, and

$$F_\epsilon{}^{-1}(k)=[\mathbf{1}+M^{-1}(k)\mathcal{R}(k)]^{-1}M^{-1}(k), \tag{3.21}$$

where

$$\mathcal{R}(k)=o(k^2) \quad \text{as} \quad k\to 0,$$

it follows that

$$Q_0\equiv\lim_{k\to 0}k^2F_\epsilon{}^{-1}(k) \tag{3.22}$$

always exists and

$$E=0 \text{ is an eigenvalue if and only if } Q_0\neq 0. \tag{3.23}$$

(The sufficiency follows clearly from the fact that $\dot{F}_\epsilon(0)=0$.)

The bound state at $k=0$ can now be removed as in the previous procedure. Let P_0' be a projection that satisfies (3.10) with respect to $F_\epsilon(0)$. Then

$$R_{00}(k)=(\mathbf{1}-P_0'ik^{-1})^2 \tag{3.24}$$

will be used in the same way as the other R_n's. We form

$$F_{\epsilon 1}(k)=R_{00}(k)F_\epsilon(k) \tag{3.25}$$

and find that $F_{\epsilon 1}(k)$ and $F_{\epsilon 1}{}^{-1}(k)$ both exist at $k=0$. One can then write

$$F(k)=R_0{}^{-1}(k)F_1(k), \tag{3.26}$$

where

$$R_0(k)=\mathfrak{K}_0(k^{-1})R_{00}(k)\mathfrak{K}_0(k), \tag{3.27}$$

$$F_1(k)=\mathfrak{K}_0(k^{-1})F_{\epsilon 1}(k)\mathfrak{K}_0(k). \tag{3.28}$$

Instead of choosing P_0' symmetric, we make it such that

$$(\mathbf{1}-P)P_0'P=0, \tag{3.29}$$

which is always possible.[28] With that choice of P_0'

$$R_0(\infty)=\mathbf{1}, \tag{3.30}$$

and consequently $F_1(\infty)=\mathbf{1}$. Equation (3.27) with (3.24) now replaces the first line in (3.11). The matrix S_N of (3.14) will, if $k^2=0$ is a bound state energy, in general not be unitary or symmetric. It will be noticed that in contrast to the discussion in (I), Sec. 3, P_0' is independent of the S-matrix. For $l\geqslant 1$ one always has

$$S(0)=\mathbf{1}. \tag{3.31}$$

c. $k=0$, $l=0$.—Contrary to the case of no coupling between angular momenta, where $E=0$ never is a bound state energy for $l=0$ [if $V\epsilon\mathfrak{M}(2)$],[29] and for $l\geqslant 1$ it is a bound state if and only if $f(0)=0$, in the present case $E=0$ may or may not be an eigenvalue if $F_\epsilon(0)$ is a singular matrix. Equation (2.23) shows that, while $PF_\epsilon(0,r)$ is always square integrable, $(\mathbf{1}-P)F_\epsilon(0,r)$ is not. The criterion for a bound state at $E=0$ is therefore that $PF_\epsilon(0,0)=0$. As before, it follows from (2.31) that a necessary and sufficient condition for the existence of a bound state of zero binding energy is that $F_\epsilon(0)=0$.

If $\det F_\epsilon(0)=0$ we distinguish three cases:

(1) The case of a bound state[30] and no resonance; by this we mean $(\mathbf{1}-P)F_\epsilon(0)\neq 0$, $PF_\epsilon(0)=0$;
(2) The case of a bound state and a resonance at the same time; then $F_\epsilon(0)=0$;
(3) The case of a resonance and no bound state, i.e., $PF_\epsilon(0)\neq 0$, $\det F_\epsilon(0)=0$.

In the following we assume that $V\epsilon\mathfrak{M}(0)\bigcap\mathfrak{M}(4)$, in which case $\dot{F}_\epsilon(0)$ exists, $P\dot{F}_\epsilon(0)=0$, and $P\ddot{F}_\epsilon(0)$ exists. We now wish to prove that Q_0, (3.22), exists.

---

[27] As (I), (3.1).

[28] If the kernel of $F_\epsilon(0)$ is represented by $(1,C)$, then

$$P_0'=\begin{pmatrix}0 & 0\\ C^{-1} & 1\end{pmatrix};$$

if it is $(1,0)$, then $P_0'=\mathbf{1}-P$; if it is the whole space, then $P_0'=\mathbf{1}$.

[29] See V. Bargmann, Proc. Natl. Acad. Sci. U. S. **38**, 961 (1952).

[30] This occurs in the lower row of F_0, if $l=0$. It must be remembered, though, that the first *column* refers to S-components and the second *column* to D-components.

Consider the system

$$aF_e(0)=0, \quad a\dot{F}_e(0)+bF_e(0)=0, \tag{3.32a}$$

$$a\bar{F}_e(0)+b\dot{F}_e(0)+cF_e(0)=0. \tag{3.32b}$$

Insertion of (2.31) in (2.26) yields

$$F(k)F'^{T}(-k)-F'(k)F^{T}(-k)=2ik\mathbf{1}. \tag{3.33}$$

If this is multiplied by $\mathcal{K}_l(k)$ on the left, $\mathcal{K}_l(-k)$ on the right, and differentiated, it becomes for $l=0$, $k=0$,

$$\dot{F}_e(0)F_e'^{T}(0)-F_e(0)\dot{F}_e'^{T}(0)-\dot{F}_e'(0)F_e^{T}(0)+F_e'(0)\dot{F}_e^{T}(0)=2i(\mathbf{1}-P). \tag{3.34}$$

Multiplication by a on the left and by a^T on the right leads, by (3.32a) and (3.7), to

$$2ia(\mathbf{1}-P)a^T=-2bF_e(0)F_e'^{T}(0)a^T=-2b\dot{F}_e'(0)F_e^{T}(0)a^T=0.$$

This means that

$$\text{Eqs. (3.32a) imply } a(\mathbf{1}-P)=0. \tag{3.35}$$

Consequently $a\bar{F}_e(0)$ exists. Now consider separately the three cases distinguished above.

(1) $PF_e(0)=0$, $(\mathbf{1}-P)F_e(0)\neq 0$. Then $b(\mathbf{1}-P)=0$ and (3.32) becomes

$$aF_e(0)=0, \quad a\bar{F}_e(0)+cF_e(0)=0. \tag{3.32'}$$

The arguments following (3.16) apply equally here and show that (3.32) implies $a=0$.

(2) $F_e(0)=0$. In that case (3.32b) reduces to

$$a\bar{F}_e(0)+b\dot{F}_e(0)=0. \tag{3.32b''}$$

Similarly as (3.18) we obtain

$$b\dot{F}_e(0,r)=b\frac{\partial}{\partial k}[F_e'(k)G(k,r)]_{k=0}+b\dot{F}_e(0)I(0,r), \tag{3.36}$$

while (3.18) still holds. One now uses (3.36) in place of (3.17) to prove, quite as before, that $a=0$.

(3) $\det F_e(0)=0$, $PF_e(0)\neq 0$. In that case the first line of (3.32a) and (3.35) imply $a=0$.

This completes the proof that the system (3.32) implies $a=0$. That statement, however, is a necessary and sufficient condition[31] for the inverse of

$$M(k)=F_e(0)+k(\mathbf{1}-P)\dot{F}_e(0)+\tfrac{1}{2}k^2P\bar{F}_e(0) \tag{3.37}$$

to have at most a double pole at $k=0$. We now write

$$F_e(k)=M(k)+\mathfrak{R}(k), \quad \mathfrak{R}(k)=(\mathbf{1}-P)o(k)+P\,o(k^2),$$

and

$$\mathfrak{R}_1(k)\equiv F_e^{-1}(k)-M^{-1}(k)=-[M^{-1}\mathfrak{R}(\mathbf{1}+M^{-1}\mathfrak{R})^{-1}]M^{-1}. \tag{3.38}$$

It is proved in Appendix C that, since $M(k)$ has at most a double pole at $k=0$, (3.35) is a necessary and sufficient condition for $M^{-1}(k)(\mathbf{1}-P)$ to have at most a *simple* pole at $k=0$. Therefore $M^{-1}\mathfrak{R}=o(1)$ as $k\to 0$ and we can write

$$F_e^{-1}(k)=[\mathbf{1}+o(1)]M^{-1}(k), \quad \text{as} \quad k\to 0; \tag{3.39}$$

hence Q_0 of (3.22) exists.

Moreover, neither in case (1) nor in case (2) can $M^{-1}(k)$ have a *simple* pole at $k=0$, because then (3.32a) would, by (I), Appendix A, imply $a=0$; in both cases, however, the second component of a is quite undetermined by (3.32a). Conversely, if $M^{-1}(k)$ has a simple pole at $k=0$, then (3.32a) must force $a=0$. But since $P\dot{F}_e(0)=0$, the lower row of $F_e(0)$ can then not be zero and $PF_e(0)\neq 0$; we are then in case (3) and $E=0$ is not an eigenvalue. Consequently, (3.23) holds also for $l=0$. In addition, in view of the statement following (3.38),

$$\lim_{k\to 0} kF_e^{-1}(k)(\mathbf{1}-P) \text{ exists for } l=0. \tag{3.40}$$

We are now in a position to remove the singularity of F_e^{-1} at $k=0$ as before. Again one forms $F_{e1}(k)$ by (3.25), but now

$$R_{00}(k)=\begin{cases}(\mathbf{1}-Pik^{-1})^2, \text{ in case (1)},\\ (1-ik^{-1})(\mathbf{1}-Pik^{-1}), \text{ in case (2)},\\ (\mathbf{1}-P_0'ik^{-1}), \text{ in case (3)},\end{cases} \tag{3.41}$$

where

$$\text{range}P_0'\equiv\text{kernel}(\mathbf{1}-P_0')\equiv\text{kernel}F_e(0), \tag{3.42}$$

and

$$(\mathbf{1}-P)P_0'=0. \tag{3.43}$$

The proof that $F_{e1}(0)$ and $F_{e1}^{-1}(0)$ both exist is straight forward and analogous to the previous proof in (I), Sec. 3. R_0 of (3.27) with R_{00} of (3.41) again satisfies (3.30).

In case (3), there is a connection between the kernel of $F_e(0)$ and the S-matrix. One can write

$$F_e(k)=F_e(0)+k(\mathbf{1}-P)\dot{F}_e(0)+\tfrac{1}{2}k^2P\bar{F}_e(0)+(\mathbf{1}-P)o(k)+P\,o(k^2),$$

$$F_e^{-1}(k)=N_{-1}k^{-1}+\mathfrak{R}(k), \quad \mathfrak{R}(k)=o(k^{-1}),$$

where N_{-1} and $\mathfrak{R}$ must satisfy (even if $\mathfrak{R}(0)$ does not exist),

$$N_{-1}F_e(0)=F_e(0)N_{-1}=0,$$

$$\mathfrak{R}(0)F_e(0)+N_{-1}(\mathbf{1}-P)\dot{F}_e(0)=F_e(0)\mathfrak{R}(0)+(\mathbf{1}-P)\dot{F}_e(0)N_{-1}=\mathbf{1},$$

where $\mathfrak{R}(0)F_e(0)=\lim\mathfrak{R}(k)F_e(0)$ as $k\to 0$. For a modified S-matrix one then obtains

$$S_e(0)=F_e(0)\mathfrak{R}(0)-(\mathbf{1}-P)\dot{F}_e(0)N_{-1}=\mathbf{1}-2(\mathbf{1}-P)\dot{F}_e(0)N_{-1}\equiv\mathbf{1}-2P_0'', \tag{3.44}$$

where

$$S_e(k)=\mathcal{K}_0(k)S(k)\mathcal{K}_0(k^{-1}), \tag{3.45}$$

and P_0'' is a projection which satisfies (3.42) and, in addition

$$PP_0''=0.$$

[31] The proof of this is entirely parallel to that of (I), Appendix A.

The equality of the ranges of P_0 and P_0'', together with (3.43), determines the former uniquely. For the S-matrix itself, therefore

$$S(k)=\mathfrak{K}_0(k^{-1})[\mathbf{1}-2P_0''+o(1)]\mathfrak{K}_0(k)$$
$$=\mathbf{1}-2(\mathbf{1}-P)P_0''(\mathbf{1}-P)+(\mathbf{1}-P)o(1)(\mathbf{1}-P)$$
$$+P\,o(1)P+(\mathbf{1}-P)o(k^2)P+P\,o(k^{-2})(\mathbf{1}-P),$$

and thus, because it is symmetric,[32]

$$S(0)=-\mathcal{E}. \tag{3.46}$$

d. Generalization of (2.39).—In case $\det F_e(0)=0$ we now write, for $l\geqslant 1$ and case (1) of $l=0$:

$$S(k)=\mathfrak{K}_0^{-1}(\mathbf{1}-k^{-2}P_0')^{-1}[\mathbf{1}+iR_{00}{}^*\,\mathrm{Im}F_e(\mathrm{Re}F_{e1})^{-1}]$$
$$\times[\mathbf{1}-iR_{00}\,\mathrm{Im}F_e(\mathrm{Re}F_{e1})^{-1}]^{-1}(\mathbf{1}-k^{-2}P_0')\mathfrak{K}_0$$
$$=\mathfrak{K}_0^{-1}[\mathbf{1}+2i\,\mathrm{Im}F_e(\mathrm{Re}F_{e1})^{-1}(\mathbf{1}-k^{-2}P_0')$$
$$+\cdots]\mathfrak{K}_0, \tag{3.47}$$

where $P_0'=P$ for $l=0$. This leads, for $l\geqslant 1$, to

$$S(k)=\mathbf{1}+\begin{pmatrix}O(k^{2l-1}) & O(k^{2l+1})\\ O(k^{2l+1}) & O(k^{2l+3})\end{pmatrix},\quad \text{as}\quad k\to 0, \tag{3.48}$$

and for $l=0$, since it is symmetric, to

$$S(k)=\mathbf{1}+\begin{pmatrix}O(k) & O(k^3)\\ O(k^3) & O(k^3)\end{pmatrix}. \tag{3.48'}$$

In case (2) of $l=0$, one writes

$$R_{00}(k)=(\mathbf{1}-k^2P)(\mathbf{1}-ik^{-1}(\mathbf{1}-P))[\mathbf{1}-2i(k/k^2-1)P]$$

and proves similarly as in (3.47), if $V\in\mathfrak{M}(4+\delta)$, $0<\delta\leqslant 1$, that

$$S(k)=-\mathcal{E}+\begin{pmatrix}O(k) & O(k^2)\\ O(k^2) & O(k^2)\end{pmatrix}; \tag{3.48''}$$

in case (3), $l=0$, finally

$$S(k)=-\mathcal{E}+\begin{pmatrix}O(k^3) & O(k^{3+\delta})\\ O(k^{3+\delta}) & O(k^4)\end{pmatrix}. \tag{3.48'''}$$

e. The Determinant.—Consideration of the determinants leads to a connection between the S-matrix and the number of bound states. If one defines an asymptotic phase continuously between $k=\infty$ and $k=0$, as

$$\tfrac{1}{2}\log\det S(k)\equiv i\eta(k), \tag{3.49}$$

then it is shown as in (I), end of Sec. 3, that if m is the number of bound states (counted twice if more than one mixture has a bound state at the same energy), then

$$\eta(0+)-\eta(\infty)$$
$$=\begin{cases}\pi(m+\tfrac{1}{2}), \text{ for } l=0, \text{ if } k=0 \text{ is a resonance,}\\ \pi m, \text{ otherwise.}\end{cases} \tag{3.50}$$

[32] $\mathcal{E}$ is defined in (2.19).

4. SPECTRAL FUNCTION AND POTENTIAL

The completeness relation is derived as in (I), Sec. 4. We shall give here only the necessary changes for the present case of the admixture of higher angular momenta. In the integral on the left hand side of (I), (4.2), the contribution due to the small semicircle in (I), Fig. 1, will now not vanish. Equation (I), (4.13) will therefore be modified to read

$$\mathfrak{F}(r)=2\pi^{-1}\mathcal{P}\int_{-\infty}^{\infty}k^2dk\int_{r-\epsilon}^{r}dt\mathfrak{F}(t)G^T(k,t)$$
$$\times[F_e^T(k)\mathfrak{K}_l^{-2}(k)F_e(-k)]^{-1}G(k,r)$$
$$-2\int_{r-\epsilon}^{r}dt\mathfrak{F}(t)G^T(0,t)Q_0F_e(0,r)$$
$$+2\sum_{n=1}^{L}\int_{r-\epsilon}^{r}dt\mathfrak{F}(t)G_n{}^T(t)C_nG_n(r), \tag{4.1}$$

where $\mathcal{P}$ denotes the principal value of the integral, $G_n(r)\equiv G(-iK_n,r)$, and

$$C_n\equiv -Q_nF_e'(-iK_n)=\int_0^{\infty}drC_nG_n(r)G_n{}^T(r)C_n$$
$$=\int_0^{\infty}drQ_nF_{en}(r)F_{en}{}^T(r)Q_n{}^T, \tag{4.2}$$

with

$$Q_n\equiv\lim_{k\to -iK_n}(k^2+K_n^2)F_e^{-1}(k), \tag{4.3}$$

$$F_e'(k)\equiv\mathfrak{K}_l(k)F'(k)\mathfrak{K}_l(k).$$

The matrix C_n is real, symmetric and positive semi-definite. Equation (4.2) also holds for $K_0=0$ and defines C_0. From (2.31) one obtains

$$Q_0F_e(0,r)=-C_0G(0,r),$$

so that the last two terms in (4.1) can be combined into one sum of the form of the last term, n running from 0 to L. In view of (3.23), C_0 has the same connection with a bound state at $k=0$ as C_n has with one at $k=-iK_n$.

In the first term of (4.1),

$$k^2[F_e^T(k)\mathfrak{K}_l^{-2}(k)F_e(-k)]$$
$$=[kF_e^{-1}(-k)\mathfrak{K}_l(k)][kF_e^{-1}(k)\mathfrak{K}_l(k)]^T.$$

For $l\geqslant 1$ this obviously exists at $k=0$; owing to (3.40), it also does for $l=0$. The principal value sign can therefore be dropped in (4.1). As a result the completeness relation becomes

$$\int G^T(\sqrt{E},t)d\mathrm{P}(E)G(\sqrt{E},r)=\delta(t-r), \tag{4.4}$$

or

$$\int_0^\infty dr\mathfrak{F}(r)\mathfrak{F}^T(r)=\int\Big[\int_0^\infty dr\mathfrak{F}(r)G^T(\sqrt{E},r)\Big]\times d\mathrm{P}(E)\Big[\int_0^\infty dr\mathfrak{F}(r)G^T(\sqrt{E},r)\Big]^T,$$

where the spectral function $\mathrm{P}(E)$ is defined by

$$\mathrm{P}(-\infty)=0,$$

$$d\mathrm{P}(E)/dE=\begin{cases}\pi^{-1}E^{l+\frac{1}{2}}\mathfrak{K}_0(\sqrt{E})[F^T(\sqrt{E})\\ \quad\times F(-\sqrt{E})]^{-1}\mathfrak{K}_0(\sqrt{E}), & E>0,\\ \sum_{n=0}^{L}C_n\delta(E-E_n), & E_0=0, \quad E\leqslant 0.\end{cases}\tag{4.5}$$

It is a real, symmetric, positive semidefinite matrix function of E.

It was shown in (I), Sec. 4, that one can write, for $n>0$,

$$C_n=Q_n\mathfrak{K}_l(-iK_n)A_n\mathfrak{K}_l(-iK_n)Q_n{}^T,\tag{4.6}$$

where

$$A_n=\int_0^\infty P_nF_n(r)F_n{}^T(r)P_ndr\tag{4.7}$$

is a real, symmetric, positive-semidefinite matrix with the property that

$$\mathrm{kernel}A_n\equiv\mathrm{kernel}P_n.\tag{4.8}$$

In fact, with the notation (3.10′) we can write (in the case of no degeneracy; if $F(-iK_n)=0$, then $P_n=\mathbf{1}$ and *three* parameters are needed to fix A_n).

$$A_n=(1+c^2)^{-1}dP_n,\tag{4.9}$$

where[22]

$$d=\int_0^\infty dr\{[F_{n11}(r)+cF_{n21}(r)]^2+[F_{n12}(r)+cF_{n22}(r)]^2\}.\tag{4.10}$$

For $n=0$, the projection P_0 to be used in (4.7) must be a real, symmetric projection, with

$$\mathrm{range}P_0\equiv\mathrm{range}P_0',\tag{4.11}$$

i.e., the projection of (3.10′) rather than that of reference 28.

The connection between the spectral function and the potential via the generalized Gel'fand Levitan equation is precisely the same as in (I), Sec. 4. If the subscript 1 denotes quantities belonging to a suitable comparison potential V_1, and

$$\mathfrak{G}(s,r)=-\int G_1{}^T(\sqrt{E},s)\times d[\mathrm{P}_1(E)-\mathrm{P}(E)]G_1(\sqrt{E},r),\tag{4.12}$$

then there exists a matrix function $\mathfrak{K}(s,r)$ which is the unique solution of the integral equation

$$\mathfrak{K}(s,r)+\mathfrak{G}(s,r)+\int_0^r dt\mathfrak{G}(s,t)\mathfrak{K}(t,r)=0, \quad s\leqslant r,\tag{4.13}$$

and satisfies

$$2(d/dr)\mathfrak{K}(r,r)=V(r)-V_1(r),\tag{4.14}$$

5. CONSTRUCTION OF V FROM S

The potential $V(r)$ can now be constructed from a given S-matrix, L bound state energies, K_n^2, and L real, symmetric, positive-semidefinite matrices A_n. Except for (3.50), all these quantities are independent of each other. From A_n one obtains, via (4.8) or (4.9), P_n; by means of the procedures of Sec. 3 one then removes from S the bound states and, for $l=0$, the resonance at $k=0$ if $S(0)=-\mathcal{S}$, forming S_N. We then define

$$F_{N0}(k)=\mathfrak{K}_0\Big(\frac{-ik}{k-i}\Big)F_N(k)\mathfrak{K}_0{}^{-1}\Big(\frac{-ik}{k-i}\Big),\tag{5.1}$$

and

$$S_{N0}(k)=\mathfrak{K}_0\Big(\frac{-ik}{k-i}\Big)S_N(k)\mathfrak{K}_0{}^{-1}\Big(\frac{-ik}{k+i}\Big).\tag{5.2}$$

The functions $F_{N0}(k)$ and $F_{N0}{}^{-1}(k)$ are analytic for $\mathrm{Im}k<0$ and continuous for $\mathrm{Im}k\leqslant 0$. Moreover,

$$F_{N0}(\infty)=\mathbf{1}.\tag{5.3}$$

The new S-matrix can be written

$$S_{N0}(k)=F_{N0}(k)\mathfrak{K}_0\Big(\frac{k+i}{k-i}\Big)F_{N0}{}^{-1}(-k),\tag{5.4}$$

and, although in general not unitary or symmetric, it satisfies

$$S_{N0}(k)S_{N0}(-k)=\mathbf{1},\tag{5.5}$$

and

$$S_{N0}(\infty)=\mathbf{1},\tag{5.6}$$

$$S_{N0}(-k)=S_{N0}{}^*(k).\tag{5.7}$$

After the transformation

$$z=(k+i)/(k-i),\tag{5.8}$$

which takes the lower half plane into the interior of the unit circle, (5.4) becomes, in the notation of (I), Sec. 5,

$$M(t)=\Phi_+(t)N(t)\Phi_+{}^{-1}(t^{-1}),\tag{5.9}$$

where, with $t=z$ for $|z|=1$,

$$M(1)=\mathbf{1}, \quad M(t)M(t^{-1})=\mathbf{1}, \quad M(t^{-1})=M^*(t),\tag{5.10}$$

[22] The relative probability for the $(l+2)$-state is

$$p=d^{-1}\int_0^\infty dr(F_{n12}+cF_{n22})^2,$$

and depends both on c and d. It can be obtained from the latter two variables only via $F(k,r)$.

and

$$N(z)=(1-P)+Pz^2. \tag{5.11}$$

It is proved in Appendix C that if $V\in\mathfrak{M}(4+\delta)$ and (2.5) is satisfied, then M fulfills a Hölder condition. The Plemelj theorem,[34,35] quoted at the end of (I), Sec. 5, is therefore applicable. Accordingly, Eq. (5.9) can always be satisfied with a matrix $N(z)$,

$$N_{ij}(z)=\delta_{ij}z^{\mu_i}, \tag{5.12}$$

the integers μ_i, or "indices," being uniquely (up to permutations) determined by $M(l)$. The solution $\Phi_+(l)$ as well as the indices are obtainable by solving a Fredholm equation. Since the present situation is in general not the "normal case" of (I), Sec. 5, the reader is referred to references 34 and 35 for the procedure of solving (5.9) and obtaining the indices. If the latter have the values 0 and 2, (5.9) and (5.11) together have a solution and one obtains $F_{N0}(k)$, $F_N(k)$, and $F(k)$.

Once $F(k)$ is obtained, the spectral function is formed via (4.5), (4.6), and (4.3). Equations (4.12) to (4.14) then lead to the potential. The latter will automatically be symmetric, since $P(E)$ is so.[36] If the potential so constructed is in $\mathfrak{M}(0)\bigcap\mathfrak{M}(5)$ (for $l=0$, $\mathfrak{M}(0)\bigcap\mathfrak{M}(4+\delta)$ is sufficient), then it will have $S(k)$ as an S-matrix and K_n^2, P_n as bound state energies and projections.

If the indices do not have the values 0 and 2, then there exists no "short range" potential (i.e., $\epsilon\mathfrak{M}(5)$) as either $F_{N0}(k)$ or $F_{N0}^{-1}(k)$, or both, will be forced to have a singularity at $k=0$.[37] So long as $F_{N0}^{-1}(k)$ is continuous at $k=0$, the Gel'fand Levitan equation can be solved and a potential found. If, however, $F_{N0}^{-1}(k)$ has a singularity at $k=0$, then one has to shift the latter, if necessary, to several different points on the negative imaginary k-axis (so that at each point $F_{N0}^{-1}(k)$ has exactly a simple pole), where they produce bound states; at the same time $F_{N0}(k)$ will become infinite at $k=0$.

One can, in such a manner, always find an $F(k)$ for which the Gel'fand Levitan equation (4.13) can be solved and a potential constructed. Unless the S-matrix is such that the indices are 0 and 2, that potential will not be of short range and, in addition, it may produce more bound states than were originally contemplated.[38]

The author takes great pleasure in thanking Dr. Res Jost for many fruitful and stimulating conversations. Appendix B, indeed, is entirely his work.

[34] J. Plemelj, Monatshefte Math. und Physik, **19**, 211 (1908).
[35] N. I. Muskelishvili, *Singular Integral Equations* (Croningen, Holland, 1953), pp. 381 ff.
[36] See (I) for the proof.
[37] One writes

$$z=\frac{z}{z+1}\,\frac{z^{-1}+1}{z^{-1}},$$

and thus distributes the extra powers of z onto $\Phi_+(l)$ and $\Phi_+^{-1}(l^{-1})$.
[38] If $F_s(k)$ is $O(k^{-n})$ at $k=0$, then more bound states will not alter (3.50).

APPENDIX A

The purpose of this appendix is to supply a number of existence proofs and inequalities that are essential to the support of the body of the paper. All of the estimates below will rest on inequalities satisfied by the solutions of (2.1) with $V=0$. We shall list the essential properties of these functions first.

The following are well known[16]:

$$\left.\begin{aligned} u_l(x)&=[(2l+1)!!]^{-1}x^{l+1}+O(x^{l+3}),\\ v_l(x)&=-(2l-1)!!x^{-l}+O(x^{-l+2}),\\ w_l(x)&=(2l-1)!!x^{-l}+O(x^{-l+2}),\quad l>0;\end{aligned}\right\}\text{as } x\to 0, \tag{A.1}$$

$$\left.\begin{aligned} u_l(x)&=\sin(x-\tfrac{1}{2}\pi l)+O(x^{-2}e^{|\mathrm{Im}x|}),\\ v_l(x)&=-\cos(x-\tfrac{1}{2}\pi l)+O(x^{-2}e^{|\mathrm{Im}x|}),\\ w_l(x)&=i^le^{-ix}+O(x^{-1}e^{\mathrm{Im}x}).\end{aligned}\right\}\text{as } |x|\to\infty. \tag{A.2}$$

If $\nu=\mathrm{Im}k$, one then easily obtains the following inequalities[6]:

$$|u_l(kr)|\leqslant Ce^{|\nu|r}\left(\frac{|k|r}{1+|k|r}\right)^{l+1}, \tag{A.3}$$

$$|v_l(kr)|\leqslant Ce^{|\nu|r}\left(\frac{1+|k|r}{|k|r}\right)^{l}, \tag{A.4}$$

$$|w_l(kr)|\leqslant Ce^{\nu r}\left(\frac{1+|k|r}{|k|r}\right)^{l}. \tag{A.5}$$

The Green's function obeys the following[6]:

$$|g_l(k;t,r)|\leqslant Ce^{|\nu|(r-t)}\frac{r}{1+|k|r}\left(\frac{r}{1+|k|r}\,\frac{1+|k|t}{t}\right)^{l},$$
$$\text{for}\quad t\leqslant r. \tag{A.6}$$

In addition we require an estimate for $\dot g_l$. By considering separately the cases where $|k|t\leqslant 1$ and $|k|t\geqslant 1$, one obtains in a straightforward manner, for $\mathrm{Im}k=0$,

$$|\dot g_l(k;t,r)|\leqslant C\frac{|k|r^3}{(1+|k|r)^2}\left(\frac{r}{1+|k|r}\,\frac{1+|k|t}{t}\right)^{l},$$
$$t\leqslant r. \tag{A.7}$$

For the purpose of proving the convergence of the successive approximations [Liouville-Neumann series, or Born expansion] to (2.6) and estimates on G, we rewrite (2.6):

$$\Delta G(k,r)=\phi(k,r)+\int_0^r dt\Delta G(k,t)V(t)\mathcal{G}(k;t,r), \tag{A.8}$$

where

$$\Delta G(k,r)=G(k,r)-G_0(k,r),$$

and

$$\begin{aligned}\phi(k,r)=\int_0^r dt[&G_0(k,t)V(t)\mathcal{G}(k;t,r)\\ &-(2l+3)^{-1}(1-P)V(t)PG_0(k,r)]\\ &+(2l+3)\int_1^r dt\,t^{-1}(1-P)V(t)PG_0(k,r).\end{aligned} \tag{A.9}$$

The only part of the estimate on ϕ that requires detailed consideration is the (12)-term, containing

$$\mathfrak{f}(k;t,r)=kg_{l+2}(k;t,r)u_l(kt) - (2l+3)(kt)^{-1}u_{l+2}(kr), \quad t\leqslant r. \quad \text{(A.10)}$$

For $|k|t\leqslant 1$ one may use both terms in g separately, its second part together with the second term on the right of (A.10); for $|k|t\geqslant 1$ one estimates both terms on the right of (A.10) separately. In either case one readily obtains

$$|\mathfrak{f}(k,t,r)|\leqslant Ce^{|r|r}\left(\frac{|k|r}{1+|k|r}\right)^{l+1}\left(\frac{|k|t}{1+|k|t}\right).$$

Accordingly, the (12)-element of the first integral in (A.9) is, in absolute value,

$$\leqslant Ce^{|r|r}\left(\frac{r}{1+|k|r}\right)^{l+2}\int_0^r dt|\,V_{12}(t)\,|.$$

The (12)-element of the second integral in (A.9), its only nonzero one, is in absolute value

$$\leqslant Ce^{|r|r}\left(\frac{r}{1+|k|r}\right)^{l+2}\left(\frac{1+r}{1+|k|r}\right)\int_0^\infty dt|\,V_{12}(t)\,|,$$

and one easily obtains

$$|\phi_{11}|\leqslant Ce^{|r|r}\left(\frac{r}{1+|k|r}\right)^{l+2}\int_0^r dt|\,V_{11}(t)\,|.$$

Under the assumption, then, that $V\in\mathfrak{M}(0)$,

$$|(\mathbf{1}-P)\phi(k,r)| \leqslant Ce^{|r|r}\left(\frac{r}{1+|k|r}\right)^{l+2}\left(1+\frac{r}{1+|k|r}\right). \quad \text{(A.11a)}$$

Similarly, one obtains,

$$|P\phi(k,r)| \leqslant Ce^{|r|r}\left(\frac{r}{1+|k|r}\right)^{l+3}\int_0^r dt\frac{t}{1+|k|t}|\,V(t)\,|. \quad \text{(A.11b)}$$

If we now write

$$\Delta G(k,r)=\sum_{n=0}^{\infty}G^{(n)}(k,r),$$

where

$$G^{(0)}(k,r)=\phi(k,r),$$

$$G^{(n)}(k,r)=\int_0^r dtG^{(n-1)}(k,t)V(t)\mathfrak{S}(k;t,r), \quad n\geqslant 1,$$

and define

$$\Xi^{(n)}(k,r)\equiv e^{-|r|r}\left(\frac{1+|k|r}{r}\right)^{l+3}\left[\left(1+\frac{r}{1+|k|r}\right)^{-1}(1-P) +\left(\frac{1+|k|r}{r}\right)^{2}P\right]G^{(n)}(k,r),$$

then (A.6) and (A.11) show that the series $\sum\Xi^{(n)}$ is dominated by $\sum h_n$, where

$$h_0(r)=C(|k|+r^{-1}),$$

$$h_n(r)=C\int_0^r dth_{n-1}(t)|\,V(t)\,|t(1+|k|t)^{-1}, \quad n\geqslant 1,$$

which, in turn, is dominated by the series $\sum\xi^{(n)}$, where

$$\xi^{(0)}=C(|k|+r^{-1}),$$

$$\xi^{(n)}=C\left[\int_0^r dt(1+t)|\,V(t)\,|\right]^n\Big/n!, \quad n\geqslant 1.$$

Then

$$\sum\xi^{(n)}=C(|k|+r^{-1}-1)+C\exp\left[C\int_0^r dt(1+t)|\,V(t)\,|\right].$$

It follows that if $V\in\mathfrak{M}(0)$, then $\sum\Xi^{(n)}$ and hence the Born series of (A.8) converges for all k and r. Furthermore, if $V\in\mathfrak{M}(0)\bigcap\mathfrak{M}(1)$, then ΔG satisfies a set of inequalities, which, when resubstituted in (A.8) yield, for all k and all r,

$$|(\mathbf{1}-P)\Delta G(k,r)|\leqslant Ce^{|r|r}\left(\frac{r}{1+|k|r}\right)^{l+2}\left(1+\frac{r}{1+|k|r}\right),$$

$$|P\Delta G(k,r)|\leqslant Ce^{|r|r}\left(\frac{r}{1+|k|r}\right)^{l+3}\int_0^r dt\frac{t}{1+|k|t} \times\left(1+\frac{t}{1+|k|t}\right)^{2}|\,V(t)\,|. \quad \text{(A.12)}$$

Since G is now defined by a series of entire functions of k which converges for all finite k, it is itself an entire function of k. Moreover, (A.2) and (A.12) show that for every $r<\infty$, as $|k|\to\infty$,

$$\begin{aligned}(\mathbf{1}-P)G(k,r)&=(\mathbf{1}-P)[k^{-(l+1)}\sin(kr-\tfrac{1}{2}\pi l)\mathbf{1} +O(k^{-(l+2)}e^{|r|r})],\\ PG(k,r)&=P[-k^{-(l+3)}\sin(kr-\tfrac{1}{2}\pi l)\mathbf{1} +O(k^{-(l+4)}e^{|r|r})].\end{aligned} \quad \text{(A.13)}$$

Also, for every k, as $r\to 0$,

$$\begin{aligned}(\mathbf{1}-P)G(k,r)&=(\mathbf{1}-P)[((2l+1)!!)^{-1}r^{l+1}\mathbf{1} +O(r^{l+2})],\\ PG(k,r)&=P[((2l+5)!!)^{-1}r^{l+3}\mathbf{1}+o(r^{l+4})].\end{aligned} \quad \text{(A.14)}$$

One now readily verifies that G satisfies the differential equation (2.1). Equation (A.8) also shows that, as $r\to 0$, $\lim[G'(k,r)-G_0'(k,r)]=0$, and therefore, with

(A.14),

$$[G;G]=0. \tag{A.15}$$

For later purposes we need an estimate on $\dot{G}(k,r)$, where k is real. Differentiation of (A.8) with respect to yields

$$\Delta\dot{G}(k,r)=\Psi(k,r)+\int_0^r dt\Delta\dot{G}(k,t)V(t)\mathcal{G}(k;t,r), \tag{A.16}$$

where

$$\Psi(k,r)=\dot{\phi}(k,r)+\int_0^r dt\Delta G(k,t)V(t)\mathcal{G}^{\cdot}(k;t,r). \tag{A.17}$$

One obtains from (A.10) that

$$|\mathfrak{f}^{\cdot}(k,t,r)|\leqslant Cr\left(\frac{|k|t}{1+|k|t}\right)\left(\frac{|k|r}{1+|k|r}\right).$$

As a result of this and similar estimates on the other integrals in (A.9), it is easily found that, for $\mathrm{Im}k=0$,

$$\begin{aligned}|(1-P)\dot{\phi}(k,r)|&\leqslant C|k|^{-1}r\left(\frac{r}{1+|k|r}\right)^{l+1}\left(1+\frac{r}{1+|k|r}\right),\\ |P\dot{\phi}(k,r)|&\leqslant C|k|^{-1}r\left(\frac{r}{1+|k|r}\right)^{l+3}.\end{aligned} \tag{A.18}$$

The second term on the right of (A.17) is estimated by means of (A.7) and (A.12). If $V\in\mathfrak{M}(0)$, then

$$\left|\int_0^r dt(1-P)\Delta G(k,t)V(t)\mathcal{G}^{\cdot}(k;t,r)\right|\leqslant C|k|^{-1}r\left(\frac{r}{1+|k|r}\right)^{l+2}\left(1+\frac{r}{1+|k|r}\right)^{2}, \tag{A.19}$$

$$\left|\int_0^r dtP\Delta G(k,t)V(t)\mathcal{G}^{\cdot}(k;t,r)\right|\leqslant C|k|^{-1}r\left(\frac{r}{1+|k|r}\right)^{l+4}\left(1+\frac{r}{1+|k|r}\right). \tag{A.19}$$

The integral equation (A.16) leads from (A.18) and (A.19) to (A.20) in the same fashion as (A.8) does from (A.11) to (A.12).

$$\begin{aligned}|(1-P)\Delta\dot{G}(k,r)|&\leqslant C|k|^{-1}r\left(\frac{r}{1+|k|r}\right)^{l+1}\left(1+\frac{r}{1+|k|r}\right)^{4},\\ |P\Delta\dot{G}(k,r)|&\leqslant C|k|^{-1}r\left(\frac{r}{1+|k|r}\right)^{l+3}\left(1+\frac{r}{1+|k|r}\right)^{3}.\end{aligned} \tag{A.20}$$

This completes the inequalities needed from $G(k,r)$.

For the purpose of estimating $F(k,r)$, we write

$$F_s(k,r)=F_{s0}(k,r)+\int_r^\infty dtF_s(k,t)V(t)\mathcal{G}(k;r,t), \tag{A.21}$$

or

$$\Delta F_s(k,r)=\varphi(k,r)+\int_r^\infty dt\Delta F_s(k,t)V(t)\mathcal{G}(k;r,t), \tag{A.21'}$$

where

$$\Delta F_s(k,r)=F_s(k,r)-F_{s0}(k,r),$$

$$\varphi(k,r)=\int_r^\infty dtF_{s0}(k,t)V(t)\mathcal{G}(k;r,t),$$

$$F_{s0}(k,r)=k^l[(1-P)w_l(kr)+Pk^2w_{l+2}(kr)].$$

According to (A.5) and (A.6), for $\nu=\mathrm{Im}k\leqslant 0$,

$$\begin{aligned}|(1-P)\varphi(k,r)|&\leqslant Ce^{-|\nu|r}\left(\frac{1+|k|r}{r}\right)^{l+2}\times\int_r^\infty dt\left(\frac{t}{1+|k|t}\right)^{2}|V(t)|,\\ |P\varphi(k,r)|&\leqslant Ce^{-|\nu|r}\left(\frac{1+|k|r}{r}\right)^{l+2}\times\int_r^\infty dt\left(\frac{t}{1+|k|t}\right)|V(t)|.\end{aligned} \tag{A.22}$$

If we now write

$$\Delta F_s(k,r)=\sum_{n=0}^{\infty}F^{(n)}(k,r),$$

where

$$F^{(0)}(k,r)=\varphi(k,r),$$

$$F^{(n)}(k,r)=\int_r^\infty dtF^{(n-1)}(k,t)V(t)\mathcal{G}(k;r,t),\quad n\geqslant 1,$$

and

$$\begin{aligned}\mathfrak{T}^{(n)}(k,r)=e^{|\nu|r}&\left(\frac{r}{1+|k|r}\right)^{l+2}\times\left\{\left[\int_r^\infty dt\left(\frac{t}{1+|k|t}\right)^{3}|V(t)|\right]^{-1}(1-P)\right.\\&\left.+\left[\int_r^\infty dt\left(\frac{t}{1+|k|t}\right)|V(t)|\right]^{-1}P\right\}F^{(n)}(k,r),\end{aligned}$$

then $\sum\mathfrak{T}^{(n)}$ is dominated by the series $\sum\xi_n$, where

$$\xi_0(r)=C,\quad \xi_n(r)=C\int_r^\infty dt|V(t)|t\xi_{n-1}(t),\quad n\geqslant 1.$$

Then $\xi_n(r)=C[C\int_r^\infty dt\,t|V(t)|]^n/n!$ and $\sum\xi_n\leqslant C'$, if $V\in\mathfrak{M}(1)$. Consequently the Born series of (A.21) converges for all $r>0$ and all k for which $\mathrm{Im}k\leqslant 0$. (For

$k=0$, it is required that $V\in\mathfrak{M}(3)$.) Thus, $F_e(k,r)$ is, for all $r>0$, an analytic function of k for $\mathrm{Im}k<0$, continuous for $\mathrm{Im}k\leqslant 0$. Moreover, it satisfies the following inequalities:

$$\begin{aligned}|(\mathbf{1}-P)\Delta F_e(k,r)| &\leqslant Ce^{-|\kappa|r}\left(\frac{1+|k|r}{r}\right)^{l+2}\\ &\quad\times\int_r^\infty dt\left(\frac{t}{1+|k|t}\right)^3|V(t)|,\\ |P\Delta F_e(k,r)| &\leqslant Ce^{-|\kappa|r}\left(\frac{1+|k|r}{r}\right)^{l+2}\\ &\quad\times\int_r^\infty dt\left(\frac{t}{1+|k|t}\right)|V(t)|.\end{aligned}\tag{A.23}$$

For $\mathrm{Im}k\leqslant 0$, therefore, as $r\to\infty$,

$$\begin{aligned}F_e(k,r) &= F_{e0}(k,r)+o(r^{-2}e^{-|\kappa|r})\\ &= (ik)^l e^{-ikr}\mathfrak{K}_0(k^2)\mathcal{S}+O(r^{-1}e^{-|\kappa|r}),\quad k\neq 0,\\ F_e(0,r) &= (2l-1)!!\{(\mathbf{1}-P)[r^{-l}\mathbf{1}+o(r^{-l-2})]\\ &\quad+(2l+3)(2l+1)P[r^{-l-2}\mathbf{1}+o(r^{-l-4})]\},\end{aligned}\tag{A.24}$$

where $\mathcal{S}$ is defined by (2.19).

For every $r>0$, as $|k|\to\infty$, $\mathrm{Im}k\leqslant 0$,

$$F(k,r)=i^l e^{-ikr}\mathcal{S}+O(|k|^{-1}e^{-|\kappa|r}).\tag{A.25}$$

We now wish to prove the existence of $\dot{F}_e(k,r)$ and estimate it, for real k. Accordingly we differentiate (A.21) with respect to k:

$$\dot{F}_e(k,r)=\dot{\psi}(k,r)+\int_r^\infty dt\dot{F}_e(k,t)V(t)\mathcal{G}(k;r,t)\tag{A.26}$$

$$\dot{\psi}(k,r)=\dot{F}_{e0}(k,r)+\int_r^\infty dtF_e(k,t)V(t)\dot{\mathcal{G}}(k;r,t).\tag{A.27}$$

Now

$$\left.\begin{aligned}|(\mathbf{1}-P)\dot{F}_{e0}(k,r)| &\leqslant \begin{cases}Cr, & l=0,\\ Cr|k|(|k|+r^{-1})^{l-1}, & l\geqslant 1,\end{cases}\\ |P\dot{F}_{e0}(k,r)| &\leqslant Cr|k|(|k|+r^{-1})^{l+1}.\end{aligned}\right\}\tag{A.28}$$

The inequalities (A.7) and (A.23) yield for $r\geqslant r_0>0$, $|k|\leqslant k_0<\infty$,

$$\begin{aligned}&\left|\int_r^\infty dt(\mathbf{1}-P)F_e(k,t)V(t)\dot{\mathcal{G}}(k;r,t)\right|\\ &\leqslant C\left(\frac{1+|k|r}{r}\right)^{l+2}\int_r^\infty dt\,t^4|V(t)|\left(\frac{|k|t}{1+|k|t}\right)\\ &\left|\int_r^\infty dtPF_e(kt,)V(t)\dot{\mathcal{G}}(k;r,)t\right|\\ &\leqslant C\left(\frac{1+|k|r}{r}\right)^{l+2}\int_r^\infty dt\,t^3|V(t)|\left(\frac{|k|t}{1+|k|t}\right).\end{aligned}\tag{A.29}$$

Therefore, for $r\geqslant r_0>0$, $|k|\leqslant k_0<\infty$,

$$\left.\begin{aligned}&|(\mathbf{1}-P)\dot{\psi}(k,r)|\\ &\leqslant\begin{cases}Cr, & l=0, \quad \text{if } V\in\mathfrak{M}(4) \text{ and if } V\in\mathfrak{M}(5),\\ Cr(|k|+r^{-1})^{l-1}, & \text{if } V\in\mathfrak{M}(4),\\ Cr(|k|+r^{-1})^{l-1}|k|, & \text{if } V\in\mathfrak{M}(5),\end{cases}\Bigg\}\ l\geqslant 1,\\ &|P\dot{\psi}(k,r)|\\ &\leqslant\begin{cases}Cr(|k|+r^{-1})^{l+1}, & \text{if } V\in\mathfrak{M}(2),\\ Cr(|k|+r^{-1})^{l+1}|k|, & \text{if } V\in\mathfrak{M}(3).\end{cases}\end{aligned}\right\}\tag{A.30}$$

The inequalities (A.30) lead to estimates on $\dot{F}_e(k,r)$, via (A.26) in the same way as (A.22) leads to (A.23). For the existence of $P\dot{F}_e(0,r)$ it is sufficient that $V\in\mathfrak{M}(2)$, while for that of $(\mathbf{1}-P)\dot{F}_e(0,r)$ we require $V\in\mathfrak{M}(4)$. If $V\in\mathfrak{M}(3)$, then $P\dot{F}_e(0,r)\equiv 0$ and $P\ddot{F}_e(0,r)$ exists; if $V\in\mathfrak{M}(5)$, then, for $l\geqslant 1$, $(\mathbf{1}-P)\dot{F}_e(0,r)\equiv 0$ and $(\mathbf{1}-P)\ddot{F}_e(0,r)$ exists. The same is true for $F_e(k,r)$ and therefore for $F_e(k)$, if in addition $V\in\mathfrak{M}(0)$.

For the purpose of further estimates it is convenient to introduce an integral representation for $F(k)$. We write

$$F_e(k)=[F_{e0}(k,r);G(k,r)]+[\Delta F_e(k,r);G(k,r)].$$

The last term vanishes as $r\to\infty$. Since, moreover,

$$[F_{e0}(k,r);\mathcal{G}(k;t,r)]=F_{e0}(k,t),$$

and

$$[F_0(k,r);Pu_{l+2}(kr)]=kP,$$

one obtains from the integral equation for G, (2.6),

$$\begin{aligned}F_e(k) &= \mathbf{1}+\int_0^\infty dt[F_{e0}(k,t)V(t)G^T(k,t)\\ &\quad-(2l+3)t^{-1}PV(t)(\mathbf{1}-P)]\\ &\quad+(2l+3)\int_1^\infty dt\,t^{-1}PV(t)(\mathbf{1}-P),\end{aligned}\tag{A.31}$$

or

$$\begin{aligned}F(k)-\mathbf{1} &= \int_0^\infty dt[F_0(k,t)V(t)G_0^T(k,t)\mathfrak{K}_l(k)\\ &\quad-(2l+3)k^{-2}t^{-1}PV(t)(\mathbf{1}-P)]\\ &\quad+(2l+3)k^{-2}\int_1^\infty dt\,t^{-1}PV(t)(\mathbf{1}-P)\\ &\quad+\int_0^\infty dtF_0(k,t)V(t)\Delta G^T(k,t)\mathfrak{K}_l(k).\end{aligned}\tag{A.31'}$$

(For the convergence of the last integral we require $V\in\mathfrak{M}(0)$.) If $V\in\mathfrak{M}(1)$, then (A.12) shows that the last term in (A.31′) is $O(k^{-2})$ as $|k|\to\infty$. The first term is $O(k^{-1})$ as $|k|\to\infty$, if $V\in\mathfrak{M}(0)$. Therefore, if $V\in\mathfrak{M}(0)$

$\bigcap \mathfrak{M}(1)$, then

$$F(k)=1+O(k^{-1}), \text{ as } |k|\to\infty \text{ in } \mathrm{Im}k\leqslant 0. \quad (A.32)$$

We further wish to estimate the derivative of $F(k)$. The first term in (A.31′) contains expressions such as $k^{-1}\varphi_{22}(k)$, where

$$\varphi_{22}(k)=\int_0^\infty dt V_{22}(t)w_{l+2}(kt)u_{l+2}(kt).$$

The boundedness of φ_{22} is readily proved. For the derivative we write

$$u_l(x)=\begin{cases}(-1)^{l/2}\left(\dfrac{x}{1+x}\right)^l \sin x+\alpha_l(x), & l \text{ even}\\ (-1)^{(l+1)/2}\left(\dfrac{x}{1+x}\right)^{l+1} \cos x+\alpha_l(x), & l \text{ odd},\end{cases}$$

$$w_l(x)=e^{-ix}\beta_l(x),$$

and easily prove the following inequalities (for real x) from (A.2) and (A.5):

$$|\alpha_l(x)|\leqslant C\frac{x^{l+1}}{(1+x)^{l+2}}, \quad |\beta_l(x)|\leqslant C\left(\frac{1+x}{x}\right)^l,$$

$$|\alpha_l'(x)|\leqslant C\frac{x^l}{(1+x)^{l+1}}, \quad |\beta_0'(x)|=0,$$

$$|\beta_l'(x)|\leqslant C\frac{(1+x)^{l-1}}{x^{l+1}}, \quad l\geqslant 1.$$

We now have

$$\dot\varphi_{22}(k)=\int_0^\infty dt\, tV_{22}(t)\left\{\frac{\partial}{\partial kt}[\alpha_{l+2}(kt)w_{l+2}(kt)]\right.$$
$$-(-1)^{l/2}e^{-2ikt}\left(\frac{kt}{1+kt}\right)^{l+2}\beta_{l+2}(kt)$$
$$\left.-(-1)^{l/2}e^{-ikt}\sin kt\frac{\partial}{\partial kt}\left[\left(\frac{kt}{1+kt}\right)^{l+2}\beta_{l+2}(kt)\right]\right\}$$

for even l, and a similar expression for odd l. The first and third terms are $O(k^{-1})$ as $|k|\to\infty$ if $V\in\mathfrak{M}(0)$ $\times(O(k^{-\delta})$ if $V\in\mathfrak{M}(1-\delta))$. Consider the second;

$$\chi_l(x)\equiv\beta_l(x)[x/(1+x)]^l$$

is bounded, and

$$|\chi_l'(x)|\leqslant c/(1+|x|)^2.$$

Therefore, with $\pi|k|^{-1}=\xi$,

$$|\chi_l(k(t+\xi))-\chi_l(kt)|$$
$$=\pi|\chi_l'(kt')|\leqslant c/(1+|k|t)^2\leqslant c/(t|k|).$$

One then proves precisely as in (I). (C.5) to (C.7), from (2.5) that the second term in $\dot\varphi_{22}$ is $O(k^{-\delta})$ as $|k|\to\infty$. Therefore

$$\dot\varphi_{22}(k)=O(k^{-\delta}) \text{ as } |k|\to\infty.$$

One proceeds similarly for

$$\varphi_{00}(k)=\int_0^\infty dt V_{11}(t)w_1(kt)u_1(kt),$$

$$\varphi_{02}(k)=\int_0^\infty dt V_{12}(t)w_1(kt)u_{l+2}(kt),$$

$$\varphi_{20}(k)=\int_0^\infty dt V_{21}(t)[w_{l+2}(kt)u_1(kt)-(2l+3)(kt)^{-1}],$$

φ_{20} requires a little extra care; there one sets

$$u_l(x)=[(2l+1)!!]^{-1}\left(\frac{x^{l+1}}{1+x^{l+2}}\right)+\gamma_l(x),$$

$$w_l(x)=(2l-1)!!x^{-l}+e^{-ix}\zeta_l(x),$$

and obtains

$$w_{l+2}(x)u_l(x)-(2l+3)x^{-1}=-(2l+3)\frac{x^{l+1}}{1+x^{l+2}}$$
$$+(2l+3)!!x^{-l}\gamma_l(x)+\zeta_{l+2}(x)e^{-ix}u_l(x),$$

whose integrals exist separately. The first two terms contribute $O(k^{-1})$ to the k-derivative, and the last $O(k^{-\delta})$.

Consequently, the first integral in (A.31) yields, when differentiated with respect to k, $O(k^{-\delta})$ as $|k|\to\infty$. The derivative of the second is clearly $O(k^{-2})$; that of the last consists of two parts:

For $|k|\geqslant k_0>0$, by (A.5) and (A.12),

$$\left|\int_0^\infty dt\dot F_0(kt)V(t)\Delta G^T(k,t)\right|$$
$$\leqslant C\int_0^\infty dt|V(t)|(t+|k|^{-1})|k|^{-2}\leqslant C'|k|^{-2}$$

if $V\in\mathfrak{M}(0)\bigcap\mathfrak{M}(1)$;

$$\left|\int_0^\infty dt F_0(kt)V(t)\Delta\dot G^T(k,t)\right|\leqslant C|k|^{-2},$$

by the use of (A.20). Therefore it follows that

$$\dot F(k)=O(k^{-1-\delta}), \text{ as } |k|\to\infty \text{ in } \mathrm{Im}k\leqslant 0. \quad (A.33)$$

The function $F_{N0}(k)$ of (5.1) combines the features of $F_s(k)$ at the origin with those of $F(k)$ at infinity. It is continuous and has a continuous derivative for all real k, and it satisfies (A.32) and (A.33). It was proved in (I), Appendix C, that therefore $F_{N0}(k)$, when transformed to the unit circle, satisfies a Hölder condition, (I), (C.15).

Finally, the behavior of $\dot{F}_e(k,r)$ near $k=0$ must be examined. From (A.21) we obtain

$$\dot{F}_e(k,r)-\dot{F}_e(0,r)=\dot{F}_{e0}(k,r)-\dot{F}_{e0}(0,r)$$
$$+\int_r^\infty dt F_e(0,t)V(t)[\mathcal{G}^-(k;r,t)-\mathcal{G}^-(0;r,t)]$$
$$+\int_r^\infty dt[F_e(k,t)-F_e(0,t)]V(t)\mathcal{G}^-(k;r,t)$$
$$+\int_r^\infty dt\dot{F}_e(0,t)V(t)[\mathcal{G}(k;r,t)-\mathcal{G}(0;r,t)]$$
$$+\int_r^\infty dt[\dot{F}_e(k,t)-\dot{F}_e(0,t)]V(t)\mathcal{G}(k;r,t). \quad \text{(A.34)}$$

We use this equation for $l=0$ only, and multiplied on the left by $(\mathbf{1}-P)$. Regarding (A.34) as an integral equation for $\dot{F}_e(k,r)-\dot{F}_e(0,r)$, we estimate first the inhomogeneity. For $r\geqslant r_0>0$, $|k|\leqslant k_0<\infty$, if $V\in\mathfrak{M}(4+\delta)$,

$$|(\mathbf{1}-P)[\dot{F}_{e0}(k,r)-\dot{F}_{e0}(0,r)]|\leqslant Cr|\sin kr|\leqslant Cr^{1+\delta}|k|^\delta,$$

$$\left|\int_r^\infty dt(\mathbf{1}-P)F_e(0,t)V(t)[\mathcal{G}^-(k;r,t)-\mathcal{G}^-(0;r,t)]\right|$$
$$\leqslant C\int_r^\infty dt|V(t)|\frac{|k|t^\delta}{(1+|k|t)^4}\leqslant C'|k|^\delta,$$

$$\left|\int_r^\infty dt(\mathbf{1}-P)[F_e(k,t)-F_e(0,t)]V(t)\mathcal{G}^-(k;r,t)\right|$$
$$\leqslant C|k|\int_r^\infty dt|V(t)|\frac{|k|t^\delta}{(1+|k|t)^4}\leqslant C'|k|^\delta,$$

$$\left|\int_r^\infty dt(\mathbf{1}-P)\dot{F}_e(0,t)V(t)[\mathcal{G}(k;r,t)-\mathcal{G}(0;r,t)]\right|$$
$$\leqslant C\int_r^{1/|k|}dt|V(t)|t\frac{|k||k'|t^\delta}{(1+|k'|t)^4}$$
$$+C\int_{1/|k|}^\infty dt|V(t)|t\left(\frac{t}{1+|k|t}\right)^3$$
$$\leqslant C\int_r^{1/|k|}dt\,t^{4+\delta}|V(t)||k|^\delta$$
$$+C\int_{1/|k|}^\infty dt\,t^{4+\delta}|V(t)||k|^\delta\leqslant C'|k|^\delta,$$

where we have used the mean value theorem and (A.6), (A.7), and (A.30). In the same manner as previously, one then obtains from (A.34) by successive approximations, that, if $V\in\mathfrak{M}(4+\delta)$, then

$$|(\mathbf{1}-P)[\dot{F}_e(k,r)-\dot{F}_e(0,r)]|\leqslant C|k|^\delta, \quad \text{(A.35a)}$$

for $l=0$. It follows from (A.30) and (A.26) that $V\in\mathfrak{M}(4+\delta)$ also implies (A.35a) for $l\geqslant 1$, and

$$|P[\dot{F}_e(k,r)-\dot{F}_e(0,r)]|\leqslant C|k|^\delta \quad \text{(A.35b)}$$

for all l. As a consequence,

$$S_{N0}(k)=\mathbf{1}+O(k^\delta), \text{ as } k\to 0$$

and then, as in (I) Appendix C, after the transformation (5.8) to the unit circle, S_{N0} satisfies a Hölder condition:

$$|M(t_1)-M(t_2)|\leqslant A|t_1-t_2|^\mu \quad \text{(A.36)}$$

provided that $V\in\mathfrak{M}(4+\delta)$ and V obeys (2.5).

A further theorem is obtained by taking the imaginary part of (A.31):

$$\mathrm{Im}F_e(k)=-k^{2l+1}\mathfrak{K}_0^2(k)\int_0^\infty dtG_0(k,t)V(t)G^T(k,t). \quad \text{(A.37)}$$

If $V\in\mathfrak{M}(0)\bigcap\mathfrak{M}(2l+4)$, then it follows that

$$(\mathbf{1}-P)\,\mathrm{Im}F_e(k)=O(k^{2l+1}), \text{ as } k\to 0, \quad \text{(A.38a)}$$

and if $V\in\mathfrak{M}(0)\bigcap\mathfrak{M}(2l+6)$, then

$$P\,\mathrm{Im}F_e(k)=O(k^{2l+3}), \text{ as } k\to 0. \quad \text{(A.38b)}$$

APPENDIX B

In this Appendix, we shall prove an ideal-theoretic theorem which is needed for the purpose[39] of defining an "irregular" solution of (2.1) as an entire function of E.

All matrices in the following are understood to be matrices over the ring of entire functions of a complex variable z (i.e., all elements are entire functions). The subsequent three theorems were proved by O. Helmer.[40]

Theorem 1.—Every finitely generated ideal (in the ring of entire functions) is a principal ideal[41]:

$$[\![\alpha_1,\alpha_2,\cdots\alpha_r]\!]=[\![\mu]\!].$$

The function μ is the "largest common divisor" of the set $\{\alpha_1,\cdots,\alpha_r\}$ and we also use the notation $[\![\alpha_1,\cdots,\alpha_r]\!]=\mu$. The common zeros of $\{\alpha_1,\cdots,\alpha_r\}$ and their multiplicities determine μ.

Theorem 2.—If $[\![\alpha_1,\cdots,\alpha_n]\!]=\mu$, then there exists an $(n\times n)$-matrix with the vector $(\alpha_1,\cdots,\alpha_n)$ as its first row and whose determinant is μ.

Corollary.—Every matrix $A=\|\alpha_{ik}\|$ can be made triangular by means of a left multiplication by an

[39] See the paragraph after (2.14).

[40] O. Helmer, Duke Math. J. **6**, 351 (1940); and Bull. Am. Math. Soc. **49**, 225 (1943).

[41] Here is a reminder of the definitions: An ideal is a set with the property that if it contains α, and β is any member of the ring, then it also contains $\beta\alpha$; it is generated by the set $\{\alpha_1,\cdots,\alpha_r\}$ if every member of the ideal is a "linear combination" of $\alpha_1,\cdots,\alpha_r$ with coefficients in the ring. A principal ideal is an ideal generated by a single element. We use the notation $[\![\alpha_1,\cdots,\alpha_r]\!]$ for the ideal generated by the functions $\{\alpha_1,\cdots,\alpha_r\}$. The ideal generated by the unity is, of course, the whole ring.

invertible[42] matrix T:

$$B=TA=\begin{pmatrix}\beta_{11} & \beta_{12} & \cdots & \beta_{1n}\\ 0 & \beta_{22} & \cdots & \beta_{2n}\\ \vdots & \vdots & & \vdots\\ 0 & 0 & \cdots & \beta_{nn}\end{pmatrix}.$$

Proof.—We prove this by induction. For $n=1$ the statement is trivial. Let $[\alpha_{11},\alpha_{21},\cdots,\alpha_{n1}]=\mu$ and $\sum\alpha_{k}\alpha_{k1}=\mu$, with $[\alpha_1,\cdots,\alpha_n]=1$, which is always possible; let T_1 have the vector $(\alpha_1,\cdots,\alpha_n)$ as its first row and let T_1 be invertible. The matrix T_1A has then in its left upper corner a divisor of all elements of its first column. By means of a subtraction of suitable multiples of the first row from the other rows (which can be accomplished by left multiplication by an invertible matrix), a matrix of the following kind can be obtained:

$$\begin{pmatrix}\mu & ** & \cdots & *\\ 0 & & & \\ \vdots & & A_1 & \\ 0 & & & \end{pmatrix}.$$

One then applies the induction hypothesis to A_1.

Remark.—If the first column of A vanishes, then there exist invertible matrices T and T' so that

$$B=TA=\begin{pmatrix}0 & \beta_{12} & \beta_{13} & \cdots & \beta_{1n}\\ 0 & 0 & \beta_{23} & \cdots & \beta_{2n}\\ \vdots & \vdots & \vdots & & \vdots\\ 0 & 0 & 0 & \cdots & 0\end{pmatrix},$$

and

$$B'=T'A=\begin{pmatrix}0 & 0 & 0 & \cdots & 0\\ 0 & \beta_{22}' & \beta_{23}' & \cdots & \beta_{2n}'\\ 0 & 0 & \beta_{33}' & \cdots & \beta_{3n}'\\ \vdots & \vdots & \vdots & & \vdots\\ 0 & 0 & 0 & & \beta_{nn}'\end{pmatrix}.$$

Theorem 3 (*Elementary divisor theorem*).—To every matrix A there exist two invertible matrices T_1 and T_2 so that

$$T_1AT_2=N=\begin{pmatrix}\epsilon_1 & & & & & & \\ & \epsilon_2 & & & 0 & & \\ & & \ddots & & & & \\ & & & \epsilon_k & & & \\ & 0 & & & 0 & & \\ & & & & & \ddots & \\ & & & & & & 0\end{pmatrix},$$

where ϵ_i is a divisor of ϵ_{i+1}.

We can now prove the following

Theorem.—Let M_1 and M_2 be two $(n\times n)$-matrices with the property that for every z_0 it follows from

$$M_1(z_0)a=0 \quad \text{and} \quad M_2(z_0)a=0$$

that $a=0$. Then there exist two matrices N_1 and N_2 so that

$$N_1M_1+N_2M_2=\mathbf{1}.$$

In other words: the left ideal $\mathfrak{M}=[M_1,M_2]$ generated by M_1 and M_2 is the entire ring.

Proof.—Again we proceed by induction. For $n=1$, the theorem is equivalent to Theorem 1.

Clearly, $[T_1M_1S,T_2M_2S]=\mathfrak{M}S$, if T_1 and T_2 are invertible. We assume the same about S. Due to Theorem 3 and the corollary to Theorem 2 we may, then, assume that the generators of $\mathfrak{M}S$ are of the form

$$M_1'=\begin{pmatrix}\epsilon_1 & & & & & & \\ & \epsilon_2 & & & 0 & & \\ & & \ddots & & & & \\ & & & \epsilon_k & & & \\ 0 & & & & 0 & & \\ & & & & & \ddots & \\ & & & & & & 0\end{pmatrix},\quad M_2'=\begin{pmatrix}\alpha_{11} & \alpha_{12} & \cdots & \alpha_{1n}\\ 0 & \alpha_{22} & \cdots & \alpha_{2n}\\ \vdots & \vdots & & \vdots\\ 0 & 0 & \cdots & \alpha_{nn}\end{pmatrix}.$$

The hypothesis of our theorem evidently still holds for M_1 and M_2. If it is applied to a column vector whose only nonzero component is the first, it follows that $[\epsilon_1,\alpha_{11}]=1$, i.e., there exist α and β so that $\alpha\epsilon_1+\beta\alpha_{11}=1$. With these one constructs the matrices

$$A_{11}=\begin{pmatrix}\alpha & 0 & \cdots & 0\\ 0 & & & \\ \vdots & & \mathbf{1} & \\ 0 & & & \end{pmatrix},\quad A_{12}=\begin{pmatrix}\beta & 0 & \cdots & 0\\ 0 & & & \\ \vdots & & 0 & \\ 0 & & & \end{pmatrix},$$

$$A_{21}=\begin{pmatrix}-\alpha_{11} & 0 & \cdots & 0\\ 0 & & & \\ \vdots & & 0 & \\ 0 & & & \end{pmatrix},\quad A_{22}=\begin{pmatrix}\epsilon_1 & 0 & \cdots & 0\\ 0 & & & \\ \vdots & & \mathbf{1} & \\ 0 & & & \end{pmatrix}.$$

The matrices

$$M_1''=A_{11}M_1'+A_{12}M_2',\quad M_2''=A_{21}M_1'+A_{22}M_2',$$

for which

$$M_1'=A_{22}M_1'-A_{12}M_2'',\quad M_2=-A_{21}M_1''+A_{11}M_2'',$$

generate the same left ideal as M_1' and M_2'. Both are triangular:

$$M_1''=\begin{pmatrix}1 & \beta\alpha_{12} & \beta\alpha_{13} & \cdots & \beta\alpha_{1n}\\ 0 & \epsilon_2 & 0 & \cdots & 0\\ 0 & 0 & \epsilon_3 & \cdots & 0\\ \vdots & \vdots & \vdots & & \vdots\\ 0 & 0 & 0 & \cdots & 0\end{pmatrix},$$

$$M_2''=\begin{pmatrix}0 & \alpha_{12}'' & \alpha_{13}'' & \cdots & \alpha_{1n}''\\ 0 & \alpha_{22}'' & \alpha_{23}'' & \cdots & \alpha_{2n}''\\ 0 & 0 & \alpha_{33}'' & \cdots & \alpha_{3n}''\\ \vdots & \vdots & \vdots & & \vdots\\ 0 & 0 & 0 & \cdots & \alpha_{nn}''\end{pmatrix}.$$

[42] We call a matrix T invertible if T^{-1} exists and is a matrix over the ring of entire functions.

In both matrices one now subtracts the first column multiplied by $\beta\alpha_{1k}$ from the kth column, which corresponds to an allowed right multiplication. This diagonalizes M_1'', does not change M_2'', and transforms the ideal $\mathfrak{M}S$ into $\mathfrak{M}S_1$. Finally one transforms M_2'', according to the remark after the corollary to Theorem 2, in such a way that $\mathfrak{M}S_1$ is generated by

$$\begin{pmatrix} 1 & 0 \\ 0 & M_1^{(0)} \end{pmatrix} \quad \text{and} \quad \begin{pmatrix} 0 & 0 \\ 0 & M_2^{(0)} \end{pmatrix}.$$

The $[(n-1)\times(n-1)]$-matrices $M_1^{(0)}$ and $M_2^{(0)}$ again satisfy the hypothesis of the theorem and the latter thus follows by induction.

APPENDIX C

Theorem.—Let $M(z)$ be an $(n\times n)$-matrix valued function, analytic in a neighborhood of the origin and $\det M(z)\neq 0$ for all z in that neighborhood, except possibly at $z=0$; furthermore, let $M^{-1}(z)$ have at most a double pole at $z=0$; and let T be a constant $(n\times n)$-matrix. Then a necessary and sufficient condition for $M^{-1}(z)T$ to have at most a simple pole at $z=0$ is that the system

$$aM_0=0, \quad aM_1+bM_0=0, \tag{C.1}$$

where $M_0=M(0)$, $M_1=(\partial M/\partial z)_{z=0}$, implies $aT=0$.

Proof.—If we expand

$$M(z)=M_0+M_1z+\cdots,$$
$$M^{-1}(z)=N_{-2}z^{-2}+N_{-1}z^{-1}+N_0+\cdots,$$

then the matrices M_i and N_i must satisfy

$$\begin{gathered} M_0N_{-2}=0, \quad M_0N_{-1}+M_1N_{-2}=0, \\ M_0N_0+M_1N_{-1}+M_2N_{-2}=\mathbf{1}, \end{gathered} \tag{C.2}$$

and the same equations with the order of M and N reversed.

Suppose that $M^{-1}T$ has a simple pole at $z=0$. Then $N_{-2}T=0$. Multiplication of the last equation in (C.2) by a on the left and T on the right then yields, by (C.1) and the second and first equation in (C.2),

$$aT=aM_1N_{-1}T=-bM_0N_{-1}T=bM_1N_{-2}T=0.$$

This proves the necessity. The sufficiency is obtained immediately from the first two equations in (C.2) with the order of M and N reversed.

Letters to the Editor

PUBLICATION of brief reports of important discoveries in physics may be secured by addressing them to this department. The closing date for this department is five weeks prior to the date of issue. No proof will be sent to the authors. The Board of Editors does not hold itself responsible for the opinions expressed by the correspondents. Communications should not exceed 600 words in length and should be submitted in duplicate.

Angular Distribution of Gamma Rays in Coulomb Excitation*

G. BREIT, M. E. EBEL, AND F. D. BENEDICT

Sloane Physics Laboratory, Yale University, New Haven, Connecticut

(Received August 2, 1955)

DISAGREEMENT of the angular correlation coefficient $a_2(\xi)$ of Alder and Winther[1] (AW) with experiment has been recently reported.[2] By means of improvements it has proved possible to remove most of the discrepancy. The work made use of the following steps.

The correspondence[3] between the semiclassical (SCT) and the quantum mechanical theories (QM) combined with numerical agreement[4] for zero excitation indicated the likelihood of a similar connection of QM and SCT radial matrix elements (RME) for finite excitation. It has been ascertained that QM and SCT values of the RME are nearly the same, provided SCT values for mean energies and only the integrals of Eq. (2′) of reference 3 are used.

On account of the disagreement between the signs of cross product terms in the AW formula with their numerical work and with a published[5] quantum formula for a_2, the SCT and QM formulas have been rederived. The AW formula was confirmed except for a sign in front of the whole coefficient of P_4. Calculations have been carried out for Pt employing the excitation energy $\Delta E = 330$ kev of Pt^{194}. The combined effect of Rutherford scattering and of admixture of Pt^{196} with $\Delta E = 358$ kev was inferred to be small by comparison of SCT calculations employing the signs of AW's numbers with calculations of McGowan and Stelson[2] on the effect of Rutherford scattering in which they use the sign just mentioned. The agreement with experiment is usually within the combined spread of statistical errors and differences between multichannel and single-channel values, as shown in Table I.

TABLE I. Comparison of angular factor a_2 with experiment for Pt for three proton energies E_p.

E_p Mev	a_2 Theory	a_2 Experiment
3.0	0.72	0.71 ±0.03
4.0	0.56	0.59 ±0.03
5.0	0.44	0.472±0.012

The somewhat arbitrary exaggeration of the experimental error appears justifiable in view of the absence of corrections for $\Delta E = 358$ kev and Rutherford scattering corrections with cross term sign opposite to that of AW formula. Agreement with experiment regarding the slope of the (a_2, E_p) curve is improved mainly by the correct cross term sign; agreement with the absolute value of the experimental a_2 is improved by the change to the QM formula. After the present work was completed, the authors were kindly informed by Dr. L. C. Biedenharn of a slip in his derivation found independently and agreeing with the signs used here.

* This research was supported by the Office of Ordnance Research, U. S. Army.

[1] K. Alder and A. Winther, Phys. Rev. **91**, 1578 (1953).

[2] P. H. Stelson and F. K. McGowan, Phys. Rev. **98**, 249 (1955); F. K. McGowan and P. H. Stelson, Phys. Rev. **99**, 127 (1955).

[3] G. Breit and P. B. Daitch, Phys. Rev. **96**, 1447 (1954).

[4] Daitch, Lazarus, Hall, Benedict, and Breit, Phys. Rev. **96**, 1449 (1954).

[5] L. C. Biedenharn and C. M. Class, Phys. Rev. **98**, 691 (1955); Biedenharn, McHale, and Thaler, "Quantum Calculation of Coulomb Excitation" (preliminary version).

14-Mev (n,α) Cross-Section Measurements

H. G. BLOSSER, C. D. GOODMAN, T. H. HANDLEY, AND M. L. RANDOLPH

Oak Ridge National Laboratory, Oak Ridge, Tennessee

(Received July 27, 1955)

MEASUREMENTS have been made of the 14-Mev (n,α) cross sections of the isotopes Zn^{68}, Zr^{90}, Zr^{94}, and In^{115}. The results obtained differ radically from the trend reported in a previous survey of (n,α) reactions[1] and, in contrast with the earlier work,[1] are in order-of-magnitude agreement with the predictions of the statistical theory of nuclear reactions.[2] The agreement with statistical theory is (on the basis of these four measurements) of approximately the same degree as was found in a survey of (p,α) reactions[3] done at this Laboratory. Measurements of additional (n,α) cross sections are being made to ascertain the range of validity of the trend indicated by the four measurements reported here. Results of these additional measurements along with a more complete account of the present work will appear in another paper.

Cross sections were measured by a comparison technique in which the activity resulting from the reaction to be measured is compared with the activity resulting from a reaction of known cross section. For the known cross section, the value of 110 mb[4] for the 14-Mev (n,p) reaction on Fe^{56} was used. Targets consisted of a sandwich formed from a foil of zinc (or Zr, In, etc.) between two 1-mil iron foils. The activities of the front and back iron foils, which were equivalent to within about 2%, were averaged to determine the neutron flux passing through the target material in the center of the sandwich. After bombardment, the target material (atomic number Z) and the material

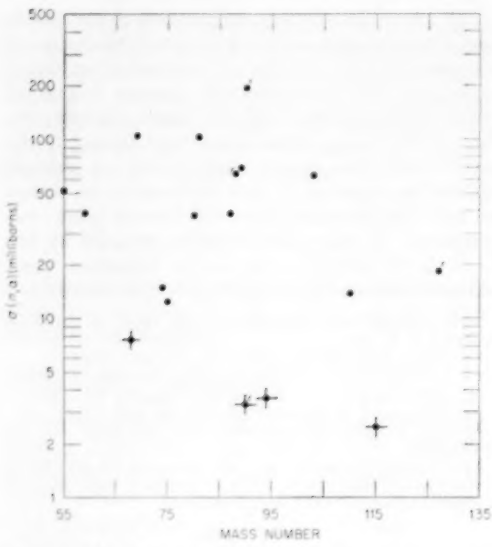

FIG. 1. (n,α) cross sections in millibarns. +—(n,α) cross sections observed in present experiment; ●—(n,α) cross sections observed in reference 1 for this mass region; '—partial (n,α) cross section leading to an isomeric state.

of atomic number $Z-1$ were removed from the sample by radiochemical techniques. Samples were then counted under end-window Geiger counters and the induced (n,α) activities were determined by analysis of decay curves. In the case of zirconium, the decay curves were analyzed with the Oracle, the Laboratory's digital computer.

The cross section values obtained were: Zn^{65}, 7.6 ± 0.8 mb; Zr^{89}, 3.3 ± 0.6 mb; Zr^{94}, 3.6 ± 0.5 mb; and In^{115}, 2.5 ± 0.4 mb. In Fig. 1, these results are plotted along with the results from reference 1 for this mass region; the distinct difference between these results and the trend indicated by reference 1 may be seen. Zr^{89} is the only isotope included in both sets of measurements. For this isotope reference 1 reports a cross section of 194 ± 107 mb. It should be noted that our value for the cross section on this isotope is in agreement with the results of recent measurements at Los Alamos by Brolley *et al.*[6] In view of the fact that chemical separations were not performed in the work of reference 1, it seems quite likely that the reported large (n,α) cross section on Zr^{89} is in considerable measure a result of (n,p) reaction on Zr^{92} which leads to a similar half-life. Examination of the (n,α) cross sections reported in that work indicates the possibility of a similar error in a number of the measurements so that the indicated trend is perhaps also in error. It is hoped that additional measurements now being undertaken will clarify this situation.

The authors which to express their deep indebtedness to Dr. B. L. Cohen for suggesting this experiment and for much useful discussion. The Cockcroft-Walton accelerator of the ORNL Biology Division provided the neutron source for these experiments.

[1] E. B. Paul and R. L. Clarke, Can. J. Phys. **31**, 267 (1953).
[2] J. M. Blatt and V. F. Weisskopf, *Theoretical Nuclear Physics* (John Wiley and Sons, Inc., New York, 1952).
[3] D. J. Coombe (to be published).
[4] *Neutron Cross Sections*, U. S. Atomic Energy Commission Report AECU-2040 (Technical Information Division, Department of Commerce, Washington, D. C., 1952), Supplement 2.
[5] Brolley, Bunker, Cochran, Henkel, Mize, and Starner, Phys. Rev. **99**, 330 (1955).

Mass Values of the K Mesons*

R. W. BIRGE, J. R. PETERSON, D. H. STORK, AND M. N. WHITEHEAD
Radiation Laboratory, University of California, Berkeley, California

(Received July 25, 1955)

ADDITIONAL data have been obtained from the stack of emulsions[1] exposed to 114-Mev K mesons at the Bevatron and from another stack exposed to 170-Mev K mesons. Both exposures were made with the use of the strong-focusing magnetic spectrometer.[2]

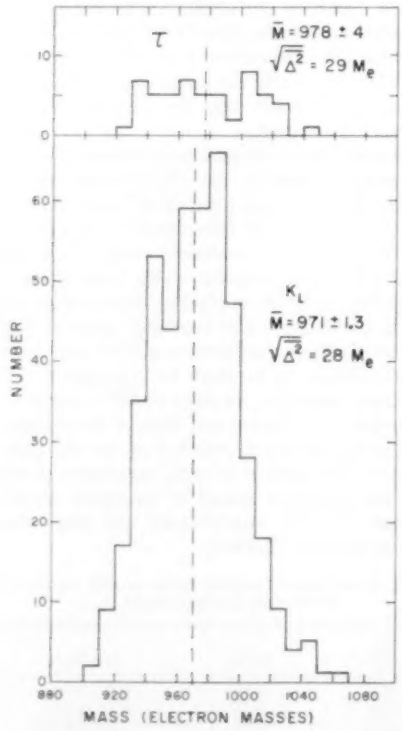

FIG. 1. Masses of 459 K_L and 55 τ mesons found in stack 16.

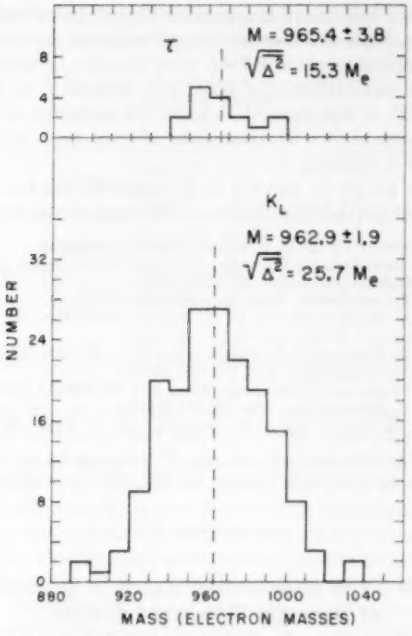

FIG. 2. Masses of 177 K_L and 16 τ mesons found in stack 17.

In the preliminary report, the stopping point of each K meson was used to determine its lateral position, and hence its momentum. We have now calculated the masses of all the K mesons in the first stack (stack 16), using the lateral position where the track was first picked up (about 3 cm from the end) to determine the momentum of the particle. The results plotted separately for K_L and τ mesons are shown in Fig. 1. The distribution includes 459 K_L mesons, 42 τ mesons, and 13 alternate decays of τ mesons into one charged pion.

Of the fifteen τ mesons in the preliminary report, three were found to have large angle scatters causing a large error in the projected range. These few events caused most of the apparent mass difference between the τ and K_L mesons. These events represent a large statistical deviation from the number of scatterings predicted using nuclear area for the interaction cross section. In the much larger sample of K_L mesons, such a fluctuation is unlikely.

In the emulsion exposed to 170-Mev K mesons (stack 17), each K meson track has been followed back to the stopping proton position to determine its momentum. The results shown in Fig. 2 include 177 K_L mesons, 12 τ mesons, and four alternate decays of τ mesons.

The mass values obtained in units of the electron mass are

	Stack 16	Stack 17
K_L	971±1.3	962.9±1.9
τ	978±4	965.4±3.8

The uncertainties given are $\sigma/\sqrt{N}$, where $\sigma=(\langle\Delta^2\rangle_{\text{Av}})^{\frac{1}{2}}$ is the root-mean-square deviation from the average mass and N is the total number of events in the distribution.

The absolute values for the masses include systematic errors due to uncertainties in measurement of the momentum of the K particles, to the errors in the proton range measurement, and to scattering and ionization loss in the air path. In addition, the resolution is somewhat broadened from that expected, by multiple scattering in the window of the Bevatron tank and in the emulsions and by aberrations of the strong focusing lens. Relative masses of the mesons should not be affected by the above errors. However, a different interaction cross section for the τ and K_L particles could cause a range shortening of one with respect to the other and hence an apparent mass shift.

A more complete report of this work will appear in the summary of the International Conference on Elementary Particles held in Pisa, Italy, in June, 1955.

* This work was performed under the auspices of the U. S. Atomic Energy Commission.

[1] Birge, Haddock, Kerth, Peterson, Sandweiss, Stork, and Whitehead, Phys. Rev. **99**, 329 (1955).
[2] Kerth, Stork, Birge, Haddock, and Whitehead, Phys. Rev. **99**, 641(A) (1955).

New Radioactive Isotope Scandium-42†

H. MORINAGA*
Department of Physics, Purdue University, Lafayette, Indiana
(Received August 12, 1955)

THE nuclide Sc^{42} is of interest for several reasons: (1) Because of its probable configuration, Ca^{40} plus one neutron and one proton, a reliable theoretical treatment should be possible. (2) In analogy with three known 0^+-0^+ transitions in the positron decay of Al^{26}, Cl^{34}, and K^{38},[1-3] it may also decay by a 0^+-0^+ transition. (3) From the analogy to Li^6 and F^{18} the lowest $T=0$ state may be expected to have spin 1^+, if one extends the prediction of King and Peaslee.[4]

It cannot be predicted, however, whether the $T=0$ or the $T=1$ state would be the ground state since these states lie very close in neighboring similar nuclides. The separate positron decay of these states, which occurs in Al^{26}, Cl^{34}, and K^{38}, is rather unlikely because of the small spin difference. So the lower level will determine the half-life of the positron decay. If the 0^+ state ($T=1$) is lower, the decay will proceed by a pure Fermi-type super-allowed transition and its half-life will be about 0.6 sec.[2] But if the 1^+ state is lower, the half-life of 0.6 sec is expected only under the assumption of perfect LS coupling which is more or less unrealistic for such a heavy nucleus. Therefore, a somewhat longer half-life is expected from the 1^+ ground state. A $T=0$ state with higher spin is safely rejected since it would

result in a longer-lived activity which would have been detected during the course of many other studies.

In order to search for a short half-life due to Sc^{42}, potassium metal was bombarded repeatedly with alpha particles of energy of ~18 Mev and the activity was counted with anthracene crystal. The counts were started about $\frac{1}{4}$ sec after the bombardments and displayed with the aid of a relay circuit on nine scalers each counting a period of 32/60 sec. A strong activity with a half-life of 0.62 ± 0.05 sec (error limit) was found. It is due to high-energy positrons since it was found with a bias of several Mev and the annihilation peak observed with a NaI crystal showed the same decay. The intensity of this radiation was several times stronger than the intensity of the activity due to Ti^{42} ($t_{\frac{1}{2}}$~0.6 sec) produced by alpha particles on calcium and measured with the same arrangement.

The activity is concluded to be due to Sc^{42} because of the following reasons: (1) From its intensity, it must be due to one of the major reactions from alpha particles on potassium. No possible impurity or minor reaction like $(\alpha,n\alpha)$ on potassium can produce higher activity due to the reaction $Ca^{40}(\alpha,n)Ti^{42}$, although there is strong competition between the latter reaction and the (α,p) reaction.[5] (2) The threshold for producing Sc^{41} (0.87 sec) by an $(\alpha,2n)$ reaction is higher than 20 Mev. (3) High-energy positrons are expected from Sc^{42}. (4) The half-life lies in the range of values expected.

In Fig. 1, the half-life of Sc^{42} is plotted together with

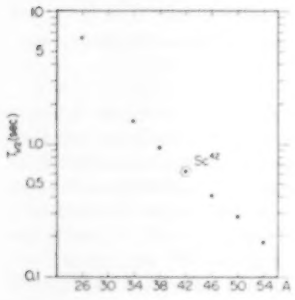

FIG. 1. Half-lives of the 0^+-0^+ transitions in $A=4n+2$ positron emitters.

the half-lives of known 0^+-0^+ positron transitions in the nuclides of this type. The observed half-life lies right on the curve, strongly suggesting that the 0^+ state is the ground state. This indicates that the energy suppression due to the spin interaction of the proton and neutron outside of the core is smaller than the energy suppression due to the configuration mixing in the 0^+ state.[6]

No attempt has been made yet to measure the positron end point, but according to the semiempirical formula given by Peaslee[7] it should be 5.70 Mev. This energy together with the measured half-life gives a logft of 3.6, which is considerably higher than in the cases of Al^{26}, Cl^{34}, and K^{38}. Actually, Peaslee's formula gives much higher logft for higher A, in which cases only the half-life of the possible 0^+-0^+ transition[8] is known. Since this increase in logft value, or the failure of complete overlap of $T=1$ wave function, is noticed in the measurements of Hunt and Zaffarano[9] on Cl^{34} and K^{38}, it is of interest to know the end point of the positrons of 0^+-0^+ transitions of this type in the higher-A region.

The author is grateful to Professor E. Bleuler for his kind help and discussions in the course of this study.

† Supported by the U. S. Atomic Energy Commission.

* On leave from the University of Tokyo, Tokyo, Japan.

[1] P. Stähelin, Phys. Rev. **92**, 1076 (1953).
[2] O. Kofoed-Hansen, Phys. Rev. **92**, 1075 (1953).
[3] S. A. Moszkowski and D. C. Peaslee, Phys. Rev. **93**, 455 (1954).
[4] R. W. King and D. C. Peaslee, Phys. Rev. **90**, 1001 (1953).
[5] H. Morinaga, Phys. Rev. **97**, 1185 (1955).
[6] E. Bleuler and H. Morinaga, Phys. Rev. **99**, 658(A) (1955).
[7] D. C. Peaslee, Phys. Rev. **95**, 717 (1954).
[8] W. M. Martin and S. W. Breckon, Can. J. Phys. **30**, 643 (1952).
[9] W. A. Hunt and D. J. Zaffarano, U. S. Atomic Energy Commission Ames Laboratory Report ISC-469, 1954 (unpublished).

New Type of Selection Rules in β Decay of Strongly Deformed Nuclei

G. ALAGA*

CERN, Theoretical Study Division at the Institute for Theoretica Physics, University of Copenhagen, Copenhagen, Denmark

(Received July 25, 1955)

IT is well known that in regions between closed shells (especially in the region $150<A<190$) the nuclei have deformed equilibrium shapes.[1] A classification of the nuclear ground state and excited states in this region has been recently suggested by Mottelson and Nilsson.[2] They assume essentially a single particle moving in a spheroidal harmonic potential well with appropriate spin-orbit coupling.

It is instructive to study the limiting case of very large deformations, because then there is an approximate separation of the motion, into oscillations along the symmetry axis and oscillations in the plane perpendicular to this axis.[2] For a classification of the states, one can then use the quantum numbers N, μ_z, Λ, and Ω. N is the principal quantum number of the oscillator, μ_z the quantum number of the oscillations along the asymmetry axis, Λ the component of the particle orbital angular momentum along the symmetry axis, and Ω the projection of the total particle angular momentum on the symmetry axis.

TABLE I. Selection rules for allowed transitions.

Operators	Selection rules				
1	$\Delta N=0$,	$\Delta\mu_z=0$,	$\Delta\Lambda=0$,	$\Delta\Omega=0$,	No
σ	$\Delta N=0$,	$\Delta\mu_z=0$,	$\Delta\Lambda=0$,	$\Delta\Omega=0,\pm1$	No

TABLE II. Selection rules for first forbidden transitions.

Operators	Selection rules			
$\sigma\cdot\mathbf{r}$	$\Delta N=\pm1$	$\Delta\mu_s=\pm1$, $\Delta\Lambda=0$	$\Delta\Omega=0$	Yes
$\sigma\cdot\nabla$		$\Delta\mu_s=0$, $\Delta\Lambda=\pm1$		
$\mathbf{r}$	$\Delta N=\pm1$	$\Delta\mu_s=\pm1$, $\Delta\Lambda=0$, $\Delta\Omega=0$		Yes
		$\Delta\mu_s=0$, $\Delta\Lambda=\pm1$, $\Delta\Omega=\pm1$		
$\sigma\times\mathbf{r}$	$\Delta N=\pm1$	$\Delta\mu_s=\pm1$, $\Delta\Lambda=0$, $\Delta\Omega=\pm1$		Yes
$\sigma\times\nabla$		$\Delta\mu_s=0$, $\Delta\Lambda=\pm1$, $\Delta\Omega=0,\pm1$		
B_{ij}	$\Delta N=\pm1$	$\Delta\mu_s=\pm1$, $\Delta\Lambda=0$, $\Delta\Omega=0,\pm1$		Yes
		$\Delta\mu_s=0$, $\Delta\Lambda=\pm1$, $\Delta\Omega=0,\pm1,\pm2$		

The list of selection rules for allowed and first forbidden β transitions associated with these quantum numbers is given in Tables I and II.[3] We confine ourselves to the transitions with $\Delta I=\Delta\Omega$, i.e., we omit rotational branchings and K-forbidden transitions.[4] It is seen that besides the selection rules on $\Omega(=K)$ there are also selection rules on the other quantum numbers. We shall refer to those transitions which are permitted with respect to the selection rules of all quantum numbers as unhindered transitions, "u." The transitions which are permitted by the selection rules on Ω and I, but forbidden because of selection rules on other quantum numbers we shall call hindered transitions, "h."

In Tables III and IV, we list the data for allowed and first forbidden transitions in odd-A nuclei in the region $150<A<190$. The classification is that given by Mottelson and Nilsson[2] where one also can find the references to the experimental literature.

From Tables III and IV one can see that the hindered or unhindered nature of the transition is clearly reflected in the experimental ft value.[5] For allowed transitions the unhindered group (only two examples) have $\log ft<5.5$, while the hindered group have $6.0<\log ft<6.8$. The first forbidden transitions with $\Delta I=0$, or 1 have $6.0<\log ft<7.7$ if unhindered, while $7.2<\log ft<8.3$ if hindered. The one example of an unhindered first forbidden $\Delta I=2$ transition has $\log ft=8.2$, while the single hindered transition of this type has $\log ft\geqq8.7$.

The selection rules here discussed may also be of help in the discussion of electron-capture transitions where often the disintegration energy is not known and therefore the ft value may not be available. Thus in the electron capture decay of Hf^{175} ($I=5/2-$) to Lu^{175}, the transition to the excited ($I=5/2+$) configuration at 342 kev is found to compete successfully with the higher energy transition to the $I=7/2+$ ground state.[6] This may be understood in terms of the nucleonic states involved which are for Hf^{175} (5,1,2,5/2) and for the Lu^{175} ground state and excited state (4,0,4,7/2) and (4,0,2,5/2), respectively. Thus, the ground-state transition is hindered while the excited-state transition is not.

It is a pleasure for me to thank Dr. Aage Bohr and Dr. Ben R. Mottelson for suggesting this problem and for their continuous interest and advice. Further, I wish to thank Dr. K. Alder and Dr. S. G. Nilsson for many helpful discussions.

TABLE III. The table lists the experimental ft values and theoretical classification of the allowed β transitions in the region of strongly deformed nuclei. In columns 1, 2, and 3 are listed the isotopes of parent and daughter nucleus, and the excitation energy of the level populated in the daughter. The asymptotic quantum numbers (N, μ_s, Λ, Ω) corresponding to the orbital assignments of reference 2 are given in columns 4 and 5; the number in brackets is the identifying number for these orbits employed in the same reference. Column 6 gives the hindered or unhindered classification of the transitions resulting from these quantum numbers. The experimental ft value is given in the last column.

Parent	Daughter	Excit. of final	Orbit Parent	Orbit Daughter	Add. class.	(ft) exp.
$_{63}Sm^{150}$	$_{63}Eu^{150}$	~0.60	5,2,1,3/2(52)	5,3,2,5/2(36)	h	~6.5
$_{63}Eu^{156}$	$_{64}Gd^{156}$	0.106	4,1,3,5/2(27)	6,4,2,5/2(55)	h	6.6
$_{68}Er^{175}$	$_{69}Tm^{175}$	0.426	5,1,2,5/2(44)	5,2,3,7/2(35)	h	6.5
$_{70}Yb^{174}$	$_{71}Lu^{174}$	0.395	5,1,4,7/2(41)	5,1,4,9/2(32)	u	4.8
$_{70}Yb^{177}$	$_{71}Lu^{177}$	0	6,2,4,9/2(49)	4,0,4,7/2(25)	h	6.2
$_{71}Lu^{177}$	$_{72}Hf^{177}$	0.321	4,0,4,7/2(25)	6,2,4,9/2(49)	h	6.3
$_{76}Os^{191}$	$_{77}Ir^{191}$	0.171	5,0,5,9/2(40)	5,0,5,11/2(28)	u	5.3

TABLE IV. The table lists the experimental ft value and theoretical classification of the first forbidden transition in the region of strongly deformed nuclei. The material is arranged in the same manner as in Table III. The first part of the table corresponds to the $\Delta I=0$ or 1 transitions: the last two transitions listed have $\Delta I=2$.

Parent	Daughter	Excit. of final	Orbit Parent	Orbit Daughter	Add. class.	(ft) exp.
$_{63}Sm^{150}$	$_{63}Eu^{150}$	0	5,2,1,3/2(52)	4,1,3,5/2(27)	h	7.4
$_{63}Sm^{150}$	$_{63}Eu^{150}$	0.103	5,2,1,3/2(52)	4,1,1,3/2(33)	u	6.8
$_{63}Eu^{155}$	$_{64}Gd^{155}$	0	4,1,3,5/2(27)	5,2,1,3/2(52)	h	8.2
$_{63}Eu^{157}$	$_{64}Gd^{157}$	0	4,1,3,5/2(27)	5,2,1,3/2(52)	h	8.0
$_{64}Gd^{159}$	$_{65}Tb^{159}$	0	5,2,3,5/2(44)	4,1,1,3/2(33)	h	7.3
$_{66}Dy^{165}$	$_{67}Ho^{165}$	0	6,3,3,7/2(54)	5,2,3,7/2(35)	u	6.2
$_{68}Er^{169}$	$_{69}Tm^{169}$	0	5,2,1,1/2(63)	4,1,1,1/2(43)	u	6.1
$_{69}Tm^{171}$	$_{70}Yb^{171}$	0	4,1,1,1/2(43)	5,2,1,1/2(63)	u	6.4
$_{70}Yb^{175}$	$_{71}Lu^{175}$	0	5,1,4,7/2(41)	4,0,4,7/2(25)	u	6.3
$_{70}Yb^{177}$	$_{71}Lu^{177}$	0.146	6,2,4,9/2(49)	5,1,4,9/2(32)	u	7.0
$_{71}Lu^{177}$	$_{72}Hf^{177}$	0	4,0,4,7/2(25)	5,1,4,7/2(41)	u	6.8
$_{73}Ta^{180}$	$_{74}W^{180}$	0.453	4,0,4,7/2(25)	5,0,3,7/2(48)	u	6.8
$_{73}Ta^{186}$	$_{74}W^{186}$	0	4,0,4,7/2(25)	5,1,4,7/2(41)	u	6.3
$_{74}W^{186}$	$_{75}Re^{186}$	0	5,1,4,7/2(41)	4,0,2,5/2(31)	h	7.5
$_{74}W^{187}$	$_{75}Re^{187}$	0	5,1,4,7/2(41)	4,0,2,5/2(31)	h	8.0
$_{68}Er^{171}$	$_{69}Tm^{171}$	0	5,1,2,5/2(50)	4,1,1,1/2(43)	u	8.2
$_{73}Ta^{180}$	$_{74}W^{180}$	0.209	4,0,4,7/2(25)	5,1,2,3/2(62)	h	8.7

* At present at the Institute R. Bosković, Zagreb, Yugoslavia.

[1] A. Bohr and B. R. Mottelson, *Beta and Gamma Ray Spectroscopy*, edited by K. Siegbahn (North Holland Publishing Company, New York, 1955), Chap. 17 and the references given there.

[2] S. G. Nilsson, Kgl. Danske Videnskab. Selskab, Mat-fys. Medd. **29**, No. 16 (1955); B. R. Mottelson and S. G. Nilsson, Phys. Rev. **99**, 1615 (1955). See also the more detailed report of this work to appear in *Kongelige Danske Videnskabernes Selskab, Matematisk-fysiske Meddelelser*.

[3] A more detailed report on the calculation of ft values for strongly deformed nuclei is in preparation; see also G. Alaga, dissertation, University of Zagreb, 1955 (unpublished).

[4] Alaga, Alder, Bohr, and Mottelson, Kgl. Danske Videnskab. Selskab, Mat.-fys. Medd. **29**, No. 9 (1955).

[5] Similar selection rules for certain γ transitions have been found by S. G. Nilsson (private communication).

[6] Burford, Perkins, and Haynes, Phys. Rev. **99**, 3 (1955).

Inelastic Scattering of Neutrons from Iron by Time-of-Flight*

L. Cranberg and J. S. Levin

University of California, Los Alamos Scientific Laboratory, Los Alamos, New Mexico

(Received August 5, 1955)

A SYSTEM of fast-neutron spectroscopy has been developed using the time-of-flight principle and a pulsed-beam technique.[1] Protons from the large Los Alamos Van de Graaff are swept across the target by applying sinusoidal voltage of frequency 3.7 Mc/sec to a pair of deflector plates, so that the target current consists of 7.4×10^6 bursts per second, each of about 2 millimicroseconds duration and 30 μa amplitude. Monoenergetic neutrons are produced by the reaction $T(p,n)He^3$ in a tritium-filled gas target. The scattering samples consist of tubes 2 inches long, with an outside diameter which is 1 inch or less and an inside diameter $\frac{3}{8}$ inch or less, depending on the material. The detector, which is 1.2 meters from the scatterer, is a hydrogenous scintillator coupled to an RCA-5819 photomultiplier, and is enclosed in a shield of lithium carbonate, paraffin, and lead, to reduce background from room- and air-scattered neutrons and gamma rays. A cone of polyethylene shields the detector from the direct neutrons from the target. Detector, shield, and cone assembly may be rotated about the axis of the scatterer.

The spectrum of arrival times of the scattered neutrons at the detector is measured by converting elapsed time to pulse height,[2] and displaying the pulse-height spectrum on a 100-channel analyzer of the Hutchinson-Scarrott type.[3] Elapsed time is measured between a fiducial pulse generated once per rf cycle and the signals obtained from the neutron detector.

The time spectra shown in Figs. 1 and 2 were obtained for a 71.5-gram iron scatterer viewed at 90 degrees, and a 2.2-gram polyethylene scatterer viewed at 37 degrees from the direction of the primary neutrons, which have an energy of 2.45 Mev, and a spread of 125 kev. The backgrounds obtained with the sample removed are also shown. Each channel corresponds to a time interval of 2.3 mμsec. The energy scale has been inferred from the known features of the spectra. The double presentation of the data arises from the fact that in each rf cycle two bursts of target current and neutrons are produced whereas only one fiducial pulse is generated. Each run required about five minutes.

In Fig. 1, one notes structures readily identified as gamma rays, primarily due to inelastic scattering, elastically scattered neutrons, and inelastically scattered neutrons corresponding to excitation of the known levels[4] in Fe^{56} at 850 kev, and in Fe^{54} at 1.4 Mev. In Fig. 2, the elastically scattered neutrons from hydrogen and carbon are clearly resolved. The peak at the end of each run is instrumental.

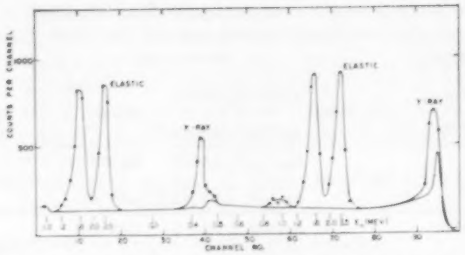

FIG. 1. The time spectrum resulting from the scattering of primary neutrons of 2.45-Mev energy by iron at 90°.

The cross section for inelastic scattering to a particular level may be determined by comparison with the differential (n,p) scattering cross section. This is accomplished by using a polyethylene scatterer viewed at such an angle that the energy of the neutrons elastically scattered from hydrogen is the same as the energy of the inelastic group of interest. Thus, for primary neutrons of 2.45-Mev energy used in the measurements reported here, the elastic scattering from hydrogen at 37 degrees gives neutrons of the same energy as those scattered inelastically from the 850-kev level in Fe^{56}.

To a first approximation, the corrections to the inelastic scattering cross section for multiple scattering and beam attenuation in the samples may be balanced out by proper choice of the dimensions of the iron and polyethylene scatterers. Assume that elastic scattering in iron and carbon does not change the average path length of a neutron in the iron and polyethylene scatterers. Then the corrections may be made approximately by equating the transmission of the iron sample, taking account only of inelastic scattering and absorption, to the transmission of the polyethylene, taking account only of the scattering by hydrogen. In the runs for cross-section determination, these transmissions were each 93 percent. This method of compensation is

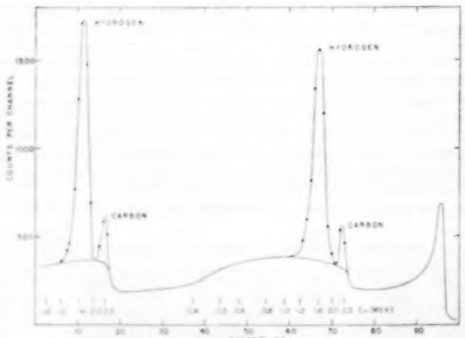

FIG. 2. The time spectrum resulting from the scattering of primary neutrons of 2.45-Mev energy by polyethylene at 37°.

thought to leave no more than 2 or 3 percent uncertainty in the cross section obtained directly from the comparison.

The cross section obtained from many runs for excitation of the 850-kev level in Fe^{56} by neutrons of 2.45-Mev energy scattered at 90 degrees is 0.085 ± 0.003 barn/steradian, taking account of the relative abundance of Fe^{56} in natural iron.

Thanks are due J. L. McKibben, R. K. Smith, and R. Hood for help and suggestions in various phases of this work.

* Work performed under the auspices of the U. S. Atomic Energy Commission.

[1] Earlier measurements using this technique with oscillographic recording of the data are described by the author [L. Cranberg, Los Alamos Report LA-1654, April, 1954 (unpublished)].

[2] An early application of this principle to millimicrosecond techniques is described by N. F. Moody, Elec. Engr. **24**, 289 (1952). The circuit used in this work was designed and built by C. W. Johnstone, W. Weber, and H. Lang, Los Alamos Scientific Laboratory, following suggestions by J. L. McKibben, Los Alamos Scientific Laboratory, and J. H. Fraser, Chalk River Laboratory.

[3] G. W. Hutchinson and G. G. Scarrott, Phil. Mag. **42**, 792 (1951). A modified model due to J. D. Gallagher, following suggestions by J. L. McKibben, Los Alamos Scientific Laboratory, was used in this work.

[4] R. Sinclair, Phys. Rev. **98**, 1147 (1955).

Scattering of 30- to 95-Mev Photons by Protons*

C. L. Oxley and V. L. Telegdi

Institute for Nuclear Studies, The University of Chicago, Chicago, Illinois

(Received August 5, 1955)

We have measured the elastic scattering of gamma rays by hydrogen, a process which has received theoretical attention[1] as a source of information regarding the proton. The source was the 98-Mev bremsstrahlung from the betatron with beam pulse stretched to 100 microseconds. The collimated beam was brought in vacuum through a heavy shielding wall with an inset electron-sweep magnet. The target was styrofoam-walled, with thickness 0.18 g/cm^2 or 0.0043 radiation length. The liquid hydrogen was in a cylindrical container five inches in diameter, with axis perpendicular to the three-inch diameter gamma beam. The hydrogen was 0.84 g/cm^2 or 0.014 radiation length thick.

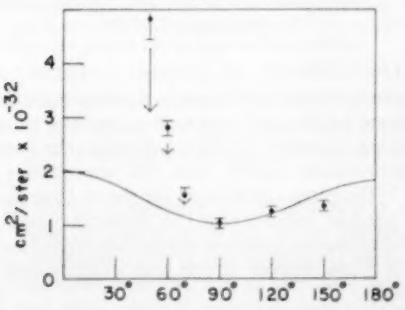

Fig. 1. Experimental points and theoretical curve of differential cross sections.

The detector was a converter-telescope. A 2.1-g/cm^2 carbon filter preceded the anticoincidence plastic scintillation counter which was then followed by a 7.4-g/cm^2 lead converter and a threefold telescope with 5.2 g/cm^2 of aluminum absorber interspersed. The central efficiency of the counter was calculated using the measured electron efficiencies at several energies and partial thicknesses of lead. Edge effects were accounted for by comparing the efficiency of the counter with over-all and central illumination by the 98-Mev bremsstrahlung.

The bremsstrahlung flux from the nickel target was put on an absolute scale with the induced C^{11} activity in polyethylene foils and the data of Barber, George, and Reagen.[2]

Data were collected at angles from 50–150 degrees. Approximate counting rates were three per minute with target full and two with target empty. The resulting cross sections are shown in Fig. 1. The counter efficiency has been adjusted for the energy loss to proton recoil. This correction is substantially independent of gamma energy and ranges from -13 percent at 150 degrees to -3 percent at 50 degrees. The product of efficiency and number of quanta in the bremsstrahlung spectrum rises from a threshold near 20 Mev to a value which remains constant within 20 percent from 40 to 89 Mev, so the cross section reported is approximately evenly weighted over this range with mean energy of 64 Mev.

At small angles, multiple effects will become evident. Of these, the conversion of gammas and subsequent large-angle bremsstrahlung is expected to be most important. Scattered-electron counts at most are three times the gamma counts and the anticoincidence is more than 98 percent effective. Shower effects may be distinguished experimentally by their quadratic dependence upon target thickness. We have not varied the hydrogen thickness, but have used carbon targets of several thicknesses. The effects thus observed have been transposed for hydrogen and result in the correction indicated by the downward arrows in Fig. 1. The correction is uncertain on this basis and its angular dependence is more rapid than is expected for large-angle bremsstrahlung. We plan experiments with variable hydrogen thickness to clarify the small angle data.

Shown in the figure is the theoretical scattering from a point proton with the static anomalous moment.[3] Deviations are expected, and these are calculated to be a decrease in the cross section due to the interference between the Thomson scattering and the scattering from the proton's meson cloud. These are of the order of 15 percent at 64 Mev. Our absolute error is estimated as about 15 percent. From our measurements, we

conclude that any deviations from the Powell cross section do not greatly exceed the expected amounts and that in the range of angles 90 degrees and above, where our measurements should be valid, there is no marked change in the angular distribution from that of Powell.

* Research supported by a joint program of the Office of Naval Research and the U. S. Atomic Energy Commission.

[1] For example, M. Gell-Mann and M. L. Goldberger, Phys. Rev. **96**, 1433 (1954); and R. H. Capps and W. G. Holladay, Phys. Rev. **99**, 931 (1955) with previous references of these papers.
[2] Barber, George, and Reagen, Phys. Rev. **98**, 73 (1955).
[3] J. L. Powell, Phys. Rev. **75**, 32 (1949).

Angular Distributions of Protons from $Be^9(He^3,p)B^{11}$

H. D. Holmgren, M. L. Bullock, and W. E. Kunz
Naval Research Laboratory, Washington, D. C.
(Received August 5, 1955)

WHEN nuclei are bombarded with heavy particles, the resulting nuclear reactions may take place by the formation of a compound nucleus or by some direct process such as stripping or possibly by a combination of these processes. Alpha particles, being tightly bound, tend to form a compound nucleus when they are the incident particles, but deuterons, being more loosely bound, generally enter into (d,p) and (d,n) reactions by a stripping process.[1] It is of considerable interest, therefore, to determine whether particles with intermediate binding energies such as H^3 and He^3 nuclei will enter into reactions by a direct process or by compound nucleus formation. Studies of the angular distributions of tritons from (d,t) reactions on Be^9 and C^{13} seem to indicate that H^3 particles can be formed by a direct process.[2] Similarly, the angular distributions of the protons from (He^3,p) reactions may be useful in determining the mechanism of He^3-induced reactions.

Proton groups from the $Be^9(He^3,p)B^{11}$ reaction have been previously observed.[3] The angular distributions of these protons have been investigated at this laboratory using a multiplate scattering chamber with the Naval Research Laboratory 2-Mev Van de Graaff generator. A thin beryllium target evaporated on a 10-microinch nickel backing was bombarded with the 2-Mev He^3 beam, and the reaction protons from the ground state and the first excited state of Be^{11} were detected in 200-micron Ilford C-2 emulsions. Slits subtending a 0.12-degree angle from the target were placed in front of each emulsion, and the total number of tracks for each proton group was counted in each plate.

Figure 1 represents the center-of-mass angular distributions of the protons which leave B^{11} in the ground state (curve p_0) and the first excited state (curve p_1). Interpretation of these curves awaits theoretical analysis, but it is to be noted that the curves exhibit a lack

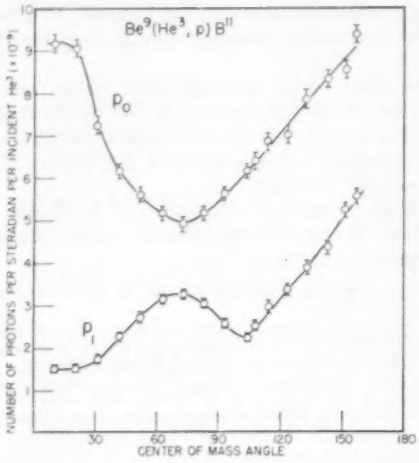

FIG. 1. The angular distributions of ground-state proton (p_0) and first excited state protons (p_1) from the $Be^9(He^3,p)B^{11}$ reaction for 2-Mev He^3 particles.

of symmetry about 90 degrees, indicating that the reactions do not proceed exclusively through the formation of a compound nucleus unless levels of opposite parity contribute.

The angular distributions of the protons for the second and third excited states of B^{11} are also being investigated.

[1] W. Tobocman and M. H. Kalos, Phys. Rev. **97**, 132 (1955).
[2] F. A. El-Bedewi, Proc. Phys. Soc. (London) **A64**, 947 (1951); Holmgren, Blair, Simmons, Stratton, and Stuart, Phys. Rev. **95**, 1544 (1954).
[3] Moak, Good, and Kunz, Phys. Rev. **95**, 614(A) (1954).

Coulomb Excitation Directional Correlation*

M. Goldstein, J. L. McHale, and R. M. Thaler, *University of California, Los Alamos Scientific Laboratory, Los Alamos, New Mexico*
and
L. C. Biedenharn, *The Rice Institute, Houston, Texas*
(Received August 1, 1955)

CALCULATIONS of Coulomb excitation using classical trajectories[1,2] are in good agreement with experiment for the total cross section; for the directional correlation,[2] however, significant discrepancies between this approximate theory and the experiments are found.[3,4] Quantum calculations for the limiting case of no energy loss[5] indicate that this discrepancy might be resolved by similar quantum calculations for the general case. It is the purpose of this note to show that this the case.

Utilizing the formalism and mathematical techniques given elsewhere,[6] the Coulomb excitation gamma corre-

lation for Cd^{114} has been calculated. This case provides a clear-cut test of the theory, since the transition is pure electric quadrupole, the lifetime of the excited state is very short, the energy loss is large, and the experiments used separated isotopes. The particle parameters,[7] a_ν, which enter into the directional correlation has been calculated and the results are shown in Fig. 1. Curves (*a*) and (*b*) are for thin targets, whereas the data shown were obtained with thick targets. An approximate thick-target correction has been applied, curves (*a'*) and (*b'*), using the method discussed in reference 4. The present calculations are less reliable

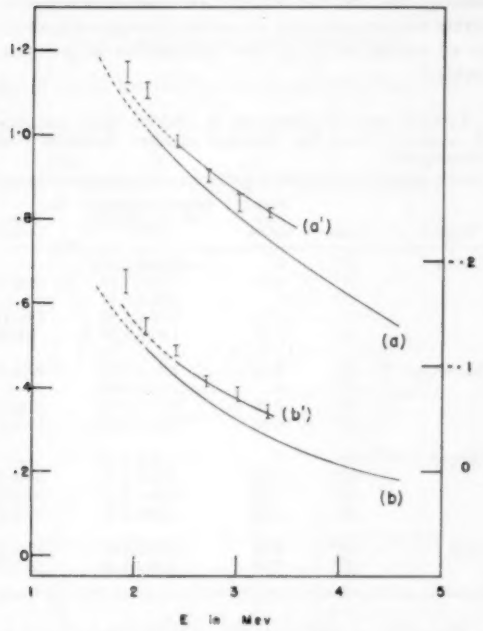

FIG. 1. Cd^{114} particle parameters a_2 and a_4 *versus* energy of the incident proton. The scale for the curves (*a*), representing the parameter a_2, appears on the left; that for the curves (*b*), representing a_4, appears on the right. The data are due to McGowan and Stelson, and are for thick targets. The unprimed curves are for thin targets; the primed curves include approximate thick-target corrections. The dashed portions of the curves show the region where the present calculations are least reliable.

for the lower proton energies; the curves are shown dashed in this region. Accurate results near threshold require other techniques, and such calculations are in progress.

In the course of analyzing this experiment, an error in the literature became apparent. In the calculations of both references 2 and 5, the cross terms for a_2 and two of the three cross terms in a_4 were used with the wrong sign. (The correct formulas are given in reference 6.) Because this error introduces large changes in previous results, no comparison with the classical case will be made here.

The good agreement between theory and experiment illustrated in the accompanying figure is encouraging for the use of Coulomb excitation correlations in nuclear spectroscopy. To this end, tables of particle parameters are being prepared to assist in analyzing such data.

The authors would like to extend to Dr. McGowan and Dr. Stelson their thanks for permission to use their data in advance of publication. Thanks are due to Mrs. Bertha Fagan and Mr. John T. Mann for assistance in coding and running this problem.

* Work performed under the auspices of the U. S. Atomic Energy Commission.

[1] K. A. Ter-Martirosyan, J. Exptl. Theoret. Phys. (U.S.S.R.) **22**, 284 (1952).
[2] K. Alder and A. Winther, Phys. Rev. **91**, 1578 (1953); **96**, 237 (1954); CERN Report T/KA–AW–1, October, 1954 (unpublished).
[3] P. H. Stelson and F. K. McGowan, Phys. Rev. **98**, 249(A) (1955).
[4] F. K. McGowan and P. H. Stelson, Phys. Rev. **99**, 127 (1955).
[5] L. C. Biedenharn and C. M. Class, Phys. Rev. **98**, 691 (1955).
[6] Biedenharn, McHale, and Thaler, Phys. Rev. **100**, 376 (1955).
[7] L. C. Biedenharn and M. E. Rose, Revs. Modern Phys. **25**, 729 (1953).

Polarization of 350-Mev Neutrons Elastically Scattered from Nuclei*

ROBERT T. SIEGEL
Carnegie Institute of Technology, Pittsburgh, Pennsylvania
(Received July 25, 1955)

THE large polarization observed in the elastic scattering of protons from nuclei[1] is fairly well explained by the spin-orbit potential predicted by the shell model of the nucleus.[2] Therefore, one expects similar polarization effects to be present when high-energy neutrons are scattered in the same way. This report describes such an experiment performed with the 350-Mev, sixteen percent polarized neutron beam[3] of the Carnegie cyclotron.

Figure 1 shows the apparatus for detecting the scattered neutrons. (Actually two such counter arrays were used on opposite sides of the beam). Counter *A* was in anticoincidence with the triple telescope *BCD*. Neutrons converted in the eight-inch polythene block were counted if the recoil protons penetrated the copper absorber, which was thick enough to stop 320-Mev protons originating at the center of the CH_2. The uncertainty in the neutron energy caused by the thickness of the converter and the broadness of the incident spectrum resulted in a rather poor separation of elastic from inelastic scattering events. However, the thick converter was necessary to bring the counting rate up to a reasonable level.

The scatterers were 3½ inch diameter cylinders, 1½ inches thick, mounted with their axes parallel to the

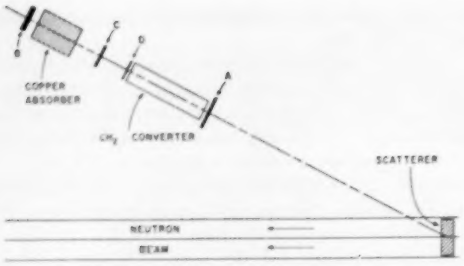

FIG. 1. Apparatus for detecting the neutrons scattered from nuclei at 350 Mev. *A*, *B*, *C*, and *D* are scintillation counters.

beam. The neutron flux was most intense over a $3\frac{3}{4}$ inch circular region; its intensity pattern was studied with a probe counter as described previously.[3] An unpolarized beam proceeding along the same axis was used to look for spurious asymmetries.

Table I shows the asymmetry *vs* angle for neutrons scattered from C, Al, Cu, and Pb. The last column of this table displays the corresponding polarizations. In Fig. 2, the results for carbon are shown for both the polarized and unpolarized beams; also plotted are the experimental results for protons as obtained by the Berkeley group.[4] The neutron and proton results agree fairly well for the elements investigated, though details of the proton results, such as the dip in the Al polarization at 16°, were not observable with the limited angular resolution and accuracy of the neutron data.

The magnitudes of the observed cross sections at 10° were consistent with the measured values for proton cross sections, though the efficiency of the neutron detector was somewhat uncertain. Also significant were the angular variations of these cross sections, which indicated that for light nuclei the neutrons detected at 10° and 15° were mostly those which had been elastically scattered, with a larger proportion of inelastic events entering at 20°. For example, the neutron counting rates from carbon at 10°, 15°, and 20° were in the ratios of 1.00:0.30:0.13, while the proton results[4] gave 1.00:0.25:0.06 at 313 Mev.

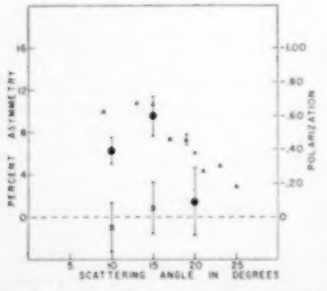

FIG. 2. Asymmetry *vs* angle for neutrons scattered from carbon. Large crosses = unpolarized beam. Large circles = polarized beam. Triangles are data from protons scattered by carbon at 313 Mev, with representative error at 19°. (See reference 4.)

Since the magnitudes of the polarization of neutrons elastically scattered from light nuclei agree with those for protons, it is reasonable to suppose that the signs also agree, especially in view of the spin-orbit origin of these effects. Our observation was that the neutron intensity scattered to the right (as seen by the incident beam) is greater than that scattered left when the beam has been produced at 20° to the right in a *p-n* exchange reaction. One concludes that the sign of the polarization of such a neutron beam is the same as that of a proton beam elastically scattered to the right, i.e., the average spin is downward ($P<0$).[5] This polarization direction would also confirm an earlier assumption[3] that the neutron polarization in *n-p* scattering has the same sign (as well as the same magnitude at all angles) as the proton polarization in *p-n* scattering.[6,7]

TABLE I. Data on polarization in 350-Mev elastic scattering of neutrons. Errors are statistical standard deviations from counting only.

Scatterer	Angle	Beam polarization	Percent asymmetry $[(R-L)/(R+L)]\times 100$	Polarization
Carbon	10°	0	$-(0.99\pm 2.31)$	...
	10°	0.16	6.22 ± 1.29	38 ± 8
	15°	0	0.82 ± 2.45	...
	15°	0.16	9.56 ± 1.95	59 ± 12
	20°	0.16	1.47 ± 3.20	9 ± 19
Aluminum	10°	0.16	7.98 ± 0.83	49 ± 5
	15°	0	$-(2.17\pm 4.07)$	...
	15°	0.16	8.17 ± 2.98	50 ± 18
	20°	0.16	2.39 ± 3.39	15 ± 21
Copper	10°	0	$-(1.24\pm 1.53)$	...
	10°	0.16	5.56 ± 1.27	34 ± 8
	15°	0.16	8.09 ± 2.22	50 ± 14
	20°	0.16	5.33 ± 2.45	33 ± 15
Lead	15°	0.16	6.03 ± 4.07	37 ± 25
	20°	0.16	3.54 ± 4.84	22 ± 30

We wish to thank G. Hinman, B. Bloch, and R. Zener for aid in taking data, and many members of the laboratory for helpful discussions.

* Supported in part by the U. S. Atomic Energy Commission.

[1] Chamberlain, Segrè, Tripp, Wiegand, and Ypsilantis, Phys. Rev. **93**, 1430 (1954).

[2] See, for example, Fernbach, Heckrotte, and Lepore, Phys. Rev. **97**, 1059 (1955).

[3] Siegel, Hartzler, and Love, Phys. Rev. (to be published). The scattering table and method of measuring asymmetries are described in this paper.

[4] R. D. Tripp, thesis, University of California Radiation Laboratory UCRL-2975 (unpublished).

[5] L. Marshall and J. Marshall, Phys. Rev. **98**, 1398 (1955). We use the same convention as these authors, namely, that positive polarization has the sense of $\mathbf{k}_f\times\mathbf{k}_i$.

[6] However, the signs of the beam polarization and of the *n-p* polarization assumed in reference 3 should both be reversed, so that P_{np} is negative for small c.m. scattering angles, as is P_{pn}.

[7] J. Tinlot, E. M. Hafner, *et al.* have performed an experiment similar to the one reported here, but with a neutron energy of ~200 Mev. See E. M. Hafner, *Proceedings of the Fifth Annual Rochester Conference* (Interscience Publishers, Inc., New York, 1955), p. 148.

Nuclear Hartree-Fock Calculations*

M. ROTENBERG
Department of Physics, Massachusetts Institute of Technology, Cambridge, Massachusetts
(Received August 15, 1955)

TWO self-consistent calculations for 184 nucleons ($N=Z=92$) have been carried out. The assumed two-body internucleon interactions were Gaussian and Yukawa, plus exchange. The Hartree-Fock equations were solved by assuming square-well wave functions and iterating as shown below.

If the potential between two nucleons is of the form

$$f(r_{12})[1+xP(r_1r_2)+yP(s_1s_2)+zP(t_1t_2)],$$

and if $N=Z$, the Hartree-Fock equations read

$$\left\{\nabla^2+\frac{2M}{\hbar^2}(4-x-2y+2z)\sum_j\int\varphi_j^*(2)f(12)\varphi_j(2)d\tau_2 - \frac{2M}{\hbar^2}(1-4x+2y-2z) \times\frac{\sum_{kj}\int\varphi_j^*(2)\varphi_k^*(1)f(12)\varphi_j(1)\varphi_k(2)d\tau_2}{4\sum_k|\varphi(1)|^2}\right\}\varphi_i(1) = E_i\varphi_i(1), \quad (1)$$

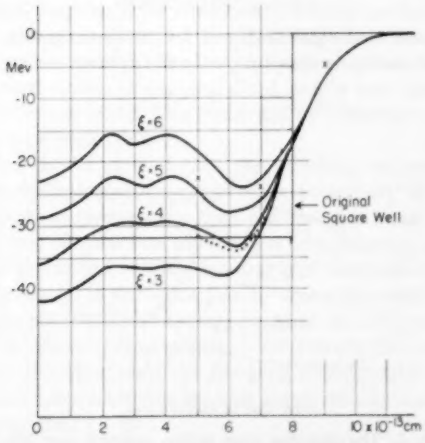

FIG. 1. Collective potentials using various amounts of exchange, ξ, with Gaussian interactions. In actual calculation, $\xi=x$, $y=z=0$ [see Eq. (1)]. The solid lines represent potentials calculated using square-well wave functions. The dotted line is the $\xi=4$ potential calculated from the eigenfunctions of the $\xi=4$ solid-line potential well. The x's are points on the $\xi=5$ potential calculated from the eigenfunctions of the $\xi=5$ solid-line potential well. The self-consistent potential is evidently closer to $\xi=4$ than $\xi=5$.

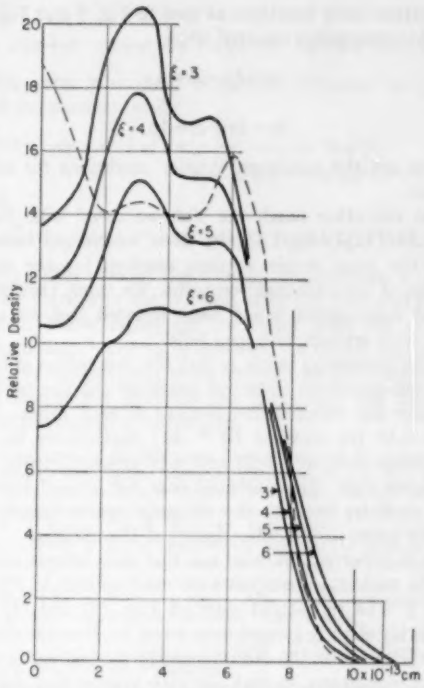

FIG. 2. Density of nuclear matter in the various potential wells of Fig. 1. The dashed line is the density distribution of 186 non-interacting nucleons (four particles to each state) placed in a square-well 32-Mev deep and 8.2×10^{-13} cm radius.

where x, y, and z are the strengths of the position-, spin-, and charge-exchange operators, respectively, and r, s, and t are the position, spin, and charge coordinates. Magnetic and Coulomb interactions have been neglected and the last term in Eq. (1) is the Slater[1] average of the usual exchange term. The φ_i's are the spatial part of the single-particle wave functions.

Equations (1) were solved by first using square-well wave functions to compute the integrals. The square-well radius used was $1.4A^{\frac{1}{3}}\times10^{-13}$ cm and the depth was adjusted so that the top particle, the $3s$ state, was bound by 10 Mev. New wave functions were found by assuming the form of a polynomial times an error function, and minimizing the Hamiltonian by varying the coefficients in the error function. The coefficients in the polynomial were determined by orthogonality conditions. These new wave functions were used to recompute the potential, and so on. The Massachusetts Institute of Technology high-speed digital computer was used.

In the Gaussian case,[2] with

$$f(r_{12})=-55.6\exp(-r_{12}^2/2)\ \text{Mev}$$

(radial distances in units of 10^{-13} cm), square-well wave functions seem to be a good approximation to the self-

consistent wave functions as seen in Fig. 1 and Fig. 2. Rapid convergence resulted when

$$x+2y-2z=4 \tag{2}$$

and

$$4x-2y+2z=16. \tag{3}$$

These are the minimum Wigner conditions for saturation.

On the other hand, the Yukawa case,[2] with $f(r_{12})=-35.6[\exp(-r_{12}/1.4)]/r_{12}$ Mev, converged slowly, but the most stable solution resulted for the same values of the exchange strengths. We think that more rapid convergence would have resulted had we used primitive orbitals with long tails.

The interesting result is that the rms radius of both the self-consistent collective potential and the particle density are within a few percent of each other: 6.44 and 6.23 (in units of 10^{-13} cm) respectively in the Gaussian case, and 5.90 and 6.16 respectively in the Yukawa case. The potential does not extend beyond the particles because the exchange forces cancel the direct forces in the outer regions of the nucleus.

It is important to point out that only integer values of the exchange strengths were used, as seen in Figs. 1 and 2. The right-hand sides of Eqs. (2) and (3) are probably slightly greater than 4 and 16. For this reason the difference in the radii quoted in the last paragraph is not significant, so that one may assume that matter and potential radius are the same.

If the rms radii of the particle densities are compared to the uniform density model, $R=r_0A^{\frac{1}{3}}$, we obtain $r_0=1.37\times10^{-13}$ and 1.31×10^{-13} cm for the Gaussian and Yukawa cases, respectively.

The 90 to 10 percent fall-off distance of the matter density, r_{90-10}, obtained for the Gaussian case is about 2.7×10^{-13} cm which is compatible with the fall-off obtained by Hofstadter *et al.*[3] for gold, about 2.4×10^{-13} cm. The value of r_{90-10} obtained with Yukawa interactions was 3.1×10^{-13} cm.

Drell[4] has offered an argument in favor of long-range attractive and short-range repulsive forces in order to account for the discrepancy between neutron and electron measurements of the nuclear radius, yet preserve a homogeneous mixture of neutrons and protons. In our calculations, we used repulsions (exchanges) of the same range as the attractions and obtained the same radius for matter and potential. This is in agreement with Drell's result.

The author wishes to extend his appreciation to Professor S. D. Drell, Professor V. F. Weisskopf, and Professor P. M. Morse for their encouragement and advice during the course of this problem.

* This work was supported in part by the Office of Naval Research.

[1] J. C. Slater, Phys. Rev. **81**, 385 (1951).
[2] J. Blatt and J. D. Jackson, Phys. Rev. **76**, 18 (1949).
[3] Hofstadter, Hahn, Knudsen, and McIntyre, Phys. Rev. **95**, 512 (1954).
[4] S. D. Drell, this issue [Phys. Rev. **100**, 97 (1955)].

Strong Pion-Pion Interaction Model Applied to Pion-Nucleon Scattering in the 1-Bev Region*

GYO TAKEDA†
Department of Physics, University of Wisconsin, Madison, Wisconsin
(Received August 9, 1955)

THE total cross section for scattering of pions by protons has been measured using high-energy pion beams at Brookhaven.[1] The π^-+p cross section shows a pronounced maximum at about 900 Mev, while the π^++p cross section shows a minimum at about 600 Mev. (See Fig. 1.) Here we discuss the qualitative aspects of the $\pi^\pm+p$ cross section in the 1-Bev region based on a strong pion-pion interaction model.

(1) A nucleon is a compound system of a nucleon core and a virtual pion cloud, whose probability of having more than one pion is neglected.

(2) There is a strong interaction between the incident pion and a pion in the cloud. In particular we assume the presence of a resonance state of the two pions, when they make the isotopic spin $T=1$ state.[2]

(3) The incident pion and the nucleon core do not interact strongly, because the wavelength of the incident pion is very small and the nucleon core is localized in a small region.

Using the impulse approximation for the pion-pion interaction and assuming the charge independence of our system, the total cross sections are given by

$$\sigma(p,\pi^-)=\mathcal{P}\{(2/9)\bar{\sigma}_0+\tfrac{1}{2}\bar{\sigma}_1+(5/18)\bar{\sigma}_2\} \tag{1}$$

and

$$\sigma(p,\pi^+)=\mathcal{P}\{\tfrac{1}{6}\bar{\sigma}_1+\tfrac{5}{6}\bar{\sigma}_2\}, \tag{2}$$

where $\mathcal{P}$ is the probability of the one-pion state in the cloud and σ_T is the pion-pion collision cross section for

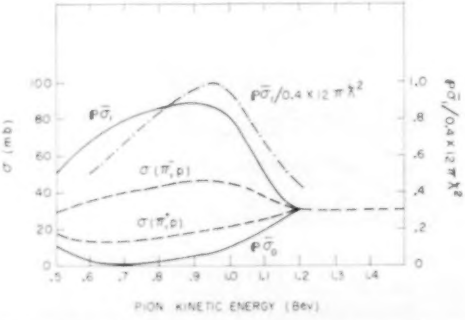

FIG. 1. The pion-pion cross section averaged over the momentum distribution of the bound pion. The dashed curves $\sigma(\pi^-,p)$ and $\sigma(\pi^+,p)$ are experimentally measured curves of $\pi^\pm$ cross sections by protons. (See reference 1.) The solid curves $\mathcal{P}\bar{\sigma}_1$ and $\mathcal{P}\bar{\sigma}_0$ are obtained from the $\sigma(\pi^\pm,p)$ curves by using Eqs. (1) and (2) and the assumption $\bar{\sigma}_0=\bar{\sigma}_2$. The dot-dashed curve is the ratio of $\mathcal{P}\bar{\sigma}_1$ to $\mathcal{P}\times12\pi\lambda^2$ ($\mathcal{P}=0.40$), the maximum P-wave collision cross section of the incident pion with the bound pion neglecting the internal motion of the bound pion.

an isotopic spin T (=0, 1, or 2) state of the two pions. $\bar{\sigma}_T$ is the average of σ_T over the momentum distribution of the pion cloud.

Since the wavelength of the incident pion in the center-of-mass system of the two pions is still large ($\sim 2\hbar/m_\pi c$) even at 900-Mev incident energy, only S and P wave interactions of the two pions are sufficiently strong to explain the large pion-nucleon cross sections in the 1-Bev region.

Assuming $\bar{\sigma}_0 = \bar{\sigma}_2$, we obtained $\mathcal{P}\bar{\sigma}_1$ and $\mathcal{P}\bar{\sigma}_0$ from the experimental values of $\sigma(p,\pi^\pm)$. (See Fig. 1.) $\mathcal{P}\bar{\sigma}_1$ is much larger than $\mathcal{P}\bar{\sigma}_0$ and shows a pronounced peak at about 900 Mev.[3] Applying the one-level formula to the p-wave pion-pion scattering ($T=1$),

$$\sigma_1 = 12\pi\lambda^2(\Gamma/2)^2/[(\epsilon-\epsilon_0)^2+(\Gamma/2)^2], \qquad (3)$$

where λ and ϵ are the wavelength and the energy of the incident pion in the center-of-mass system of the two pions, and neglecting the internal motion of the pion cloud, we can reproduce the $\mathcal{P}\bar{\sigma}_1$ curve between 500 Mev and 1100 Mev, if $\mathcal{P}\approx 40\%$, $\epsilon_0 \approx 155$ Mev, and $\Gamma = 50$–90 Mev.

The Doppler effect due to the internal motion of the pion cloud brings an additional width into the $\mathcal{P}\bar{\sigma}_1$ curve. For simplicity, we consider the case where the width due to this Doppler effect is larger than Γ, replacing Eq. (3) by

$$\sigma_1 = 12\pi\lambda_0^2(\pi\Gamma/2)\delta(\epsilon-\epsilon_0), \qquad (3')$$

where λ_0 is the wavelength corresponding to the resonance energy ϵ_0. $\mathcal{P}\bar{\sigma}_1$ is given by averaging Eq. (3′) over the momentum distribution of the pion cloud. If we take a momentum distribution of the form[4] $q^2\exp(-\alpha q^2/m_\pi^2)$, the experimental $\mathcal{P}\bar{\sigma}_1$ can be obtained by taking $\alpha = 6$–10 and $\Gamma = 55$–40 Mev with $\epsilon_0 \approx 155$ Mev and $\mathcal{P}\approx 40\%$. Because of the large effect of the internal motion of the pion cloud, only a very narrow distribution of the pion cloud can be consistent with the experimental $\mathcal{P}\bar{\sigma}_1$.[5]

Our model predicts also the following features of pion-nucleon scattering. Since the probability of the pion cloud having more than one meson is small, the inelastic pion-nucleon scattering is predominantly one-pion production until the incident pion energy becomes high enough to produce a pion by a pion-pion collision. If the latter becomes appreciable when the pion energy in the center-of-mass system of the two pions is larger than 340 Mev, then the two-pion production in the pion-nucleon scattering becomes appreciable for a larger energy than 1.7 Bev.

If the pion-nucleon scattering occurs only through the $T=1$ state of the two pions, the ratios of the various types of inelastic scattering are

$$\sigma(p+\pi^-\to p+\pi^-+\pi^0):\sigma(p+\pi^-\to n+\pi^-+\pi^+):\sigma(p+\pi^-\to n+2\pi^0) = 1:1:0$$

and

$$\sigma(n+\pi^-\to n+\pi^-+\pi^0):\sigma(n+\pi^-\to p+2\pi^-) = 1:0$$

when there is no final interaction between the pions and the nucleon, while

$$\sigma(p+\pi^-\to p+\pi^-+\pi^0):\sigma(p+\pi^-\to n+\pi^-+\pi^+):\sigma(p+\pi^-\to n+2\pi^0) = 17:26:2$$

and

$$\sigma(n+\pi^-\to n+\pi^-+\pi^0):\sigma(n+\pi^-\to p+2\pi^-) = 13:2$$

when either one of the two pions composes a $T=\frac{3}{2}$ isobar state with the nucleon after the two-pion interaction. These ratios are consistent with the experimental data.[6] The ratio between the elastic scattering and the inelastic scattering depends on the strength of the interaction between the pions and the nucleon after the two-pion interaction.

* Supported by the Wisconsin Alumni Research Foundation.

† Now at Brookhaven National Laboratory, Upton, New York.

[1] Cool, Madansky, and Piccioni, Phys. Rev. **93**, 637 (1954); Shapiro, Leavitt, and Chen, Phys. Rev. **92**, 1073 (1953).

[2] F. J. Dyson [Phys. Rev. **99**, 1037 (1955)] has proposed independently a similar model which assumed the presence of a resonance state of the two pions in $T=0$ state. We are obliged to him for sending us his manuscript before publication and for comments he made on this paper. Also we are very grateful to Dr. M. Ross who informed us about Dyson's work.

[3] The arbitrariness of the assumption $\bar{\sigma}_0 = \bar{\sigma}_2$ does not change these qualitative conclusions about $\mathcal{P}\bar{\sigma}_1$ as long as only S and P wave interactions are considered.

[4] This is proportional to the probability of a pion in the cloud for having a momentum between q and $q+dq$. The momentum distribution can be taken to be spherically symmetric, since the direction of spin of the nucleon is averaged out.

[5] This difficulty was pointed out to the author by Dr. O. Piccioni, who had suggested a similar model several years ago, and by Dr. M. Ross. If the strong pion-pion interaction works only when the bound pion has a very small momentum, this difficulty might be solved. This possibility was suggested to the author by Professor F. J. Dyson.

[6] W. D. Walker (private communication).

Spatial Extension of the Proton Magnetic Moment from the Hyperfine Structure of Hydrogen

W. M. Moellering, *Physikalische Institut, Heidelberg, Germany*
A. C. Zemach and A. Klein,* *Harvard University, Cambridge, Massachusetts*
and
F. E. Low, *University of Illinois, Urbana, Illinois*

(Received July 18, 1955)

UNTIL recently the measurement of the hyperfine splitting of the ground state of hydrogen, used in conjunction with the theoretical formula,[1] has provided the most accurate means of ascertaining the value of the fine structure constant, $\alpha = e^2/\hbar c$. In this note, we propose to employ the formula, together with an independent measurement[2] of α, to estimate a "magnetic radius" for the proton.

The doublet separation, $\Delta\nu_H$, can be represented to

within a few parts per million by the equation

$$\Delta\nu_H=\frac{16}{3}\alpha^2cR_\infty\frac{\mu_p}{\mu_0}\left\{1+\frac{m}{M}\right\}^{-3}\left\{1+\frac{\alpha}{2\pi}-2.97\frac{\alpha^2}{\pi^2}\right\}$$
$$\times\{1+\tfrac{3}{2}\alpha^2\}\left\{1-\alpha^2\left(\frac{5}{2}-\ln 2\right)\right\}\left\{1-\frac{\alpha}{\pi}\frac{m}{M\mu_p}\right.$$
$$\times\{[3-\tfrac{3}{4}(\mu_p-1)^2]\ln\frac{M}{m}-\tfrac{1}{8}(\mu_p-1)^2\}$$
$$\left.-\frac{9}{4}\frac{\alpha}{\pi}\frac{m}{M\mu_p}(\mu_p-1)^2\ln\frac{2k_0}{M}\right\}\{1-\delta\}, \quad (1)$$

where μ_p is the proton magnetic moment and μ_0 the the electron Bohr magneton.

The leading factor is the Fermi formula,[1] whereas the factors in brackets represent successively the reduced mass correction, half the gyromagnetic ratio of the electron, the Breit correction, the term which takes account of the distributed character of electrodynamic effects, the contribution of proton recoil, and finally, a hitherto unknown fractional correction, $-\delta$, arising from the structure of the proton. The calculation of the penultimate factor[1] presupposed that the proton is characterized as a point charge with an anomalous point magnetic moment. The result depends, although not sensitively, on structure in that a cutoff, k_0, is required for the terms in which the proton interacts exclusively via the anomalous part of its moment. Equation (1) is a double power series in α and m/M, in which the corrections of relative order α, α^2, and m/M can be certified.[4] On the other hand, previous treatments have lacked the criteria for determining the accuracy of the term of relative order $\alpha m/M$ and for distinguishing recoil and structure effects.

By employing an approach in which the electron-proton system is studied by means of the relativistic two-body equation and all the interactions of the proton, other than with the electromagnetic field, are treated phenomenologically, we have been able to justify the use of Eq. (1). In particular we have been able to demonstrate that the proton recoil factor of Eq. (1) contains the only term of relative order $\alpha(m/M)\ln(M/m)$, although there may be additional terms of order $\alpha(m/M)$ too small to worry us here. Moreover, we have established that the main contribution to δ is obtained by considering the proton as a distributed source of magnetic dipole field with magnetization $\mu_p f(r)$, where $f(r)$ is a spherically symmetric function with total strength unity,

$$\int d\mathbf{r}\, f(r)=1, \quad (2)$$

to insure the correct value of the magnetic moment. It follows that δ has the value

$$\delta=2\bar{r}/a_0, \quad (3)$$

where $a_0=\alpha(\hbar/mc)$ is the Bohr radius and

$$\bar{r}=\int d\mathbf{r}\, r f(r) \quad (4)$$

is the first moment of the distribution of magnetization.

In general, we may expect $\bar{r}$ to lie between the nucleon and meson Compton wavelengths. Thus the relative correction to Eq. (1) may be as large as 5×10^{-5}. On the other hand the direct measurement of fine structure has yielded a value of $\alpha^{-1}=137.0365\pm0.0012$, accurate to 1×10^{-5}. If we remark that $\alpha(m/M)\ln(M/m)$ is of relative order 3×10^{-5}, we realize that Eq. (1) is sufficiently precise to permit an estimate of $\bar{r}$. Inserting the recent experimental value of $\Delta\nu_H$,[5] the value of α^2cR_∞ from the fine structure measurement,[2] and all other atomic constants from the review article of DuMond and Cohen,[6] we obtain

$$(3.26\times10^{-6})\ln(2k_0/M)-2\alpha\bar{r}/a_0=(2.6\pm20.0)\times10^{-6}, \quad (5)$$

where the uncertainty follows from the error in α^2. For any reasonable value of k_0, say $k_0\sim M$, we may assert that the value of $\bar{r}$ is bounded from above by the inequality

$$\bar{r}\leq 2.5(\hbar/Mc), \quad (6)$$

as determined by the experimental error in Eq. (5). The upper bound thus established lies barely within the limits of error for the proton "size" deduced from the electron-scattering result of Hofstadter and McAllister.[7] It should be recalled, however, that the latter experiment measures $\langle r^2\rangle_{Av}$ for a combination of the charge and magnetization distributions.

A detailed account of the calculations is in preparation and will be submitted later for publication.

* Currently at the University of Pennsylvania, Philadelphia, Pennsylvania.

[1] R. Arnowitt, Phys. Rev. **92**, 1002 (1953); W. A. Newcomb and E. E. Salpeter, Phys. Rev. **97**, 1146 (1955).

[2] Dayhoff, Triebwasser, and Lamb, Phys. Rev. **89**, 106 (1953).

[3] References to all significant previous work will be found in reference 1.

[4] Corrections of relative order $\alpha^2\ln\alpha$ of purely electrodynamic origin have been omitted. These may be expected to be of the same order as $\alpha(m/M)$.

[5] J. P. Wittke and R. H. Dicke, Phys. Rev. **96**, 530 (1954).

[6] J. W. DuMond and E. R. Cohen, Revs. Modern Phys. **25**, 691 (1953).

[7] R. Hofstadter and R. McAllister, Phys. Rev. **98**, 217 (1955).